PERIODICAL Woods Hole Oceanog. Inst.
Collected Reprints

1959 1959

GD
2
8

LIBRARY
NOV 25 1960
FISH & WILDLIFE SERVICE

WOODS HOLE
OCEANOGRAPHIC INSTITUTION

COLLECTED REPRINTS

1959

JULY, 1960

LIBRARY
BUREAU OF COMMERCIAL FISHERIES
U. S. FISH AND WILDLIFE SERVICE
P. O. BOX 3830
HONOLULU 12, HAWAII

WOODS HOLE
OCEANOGRAPHIC INSTITUTION

COLLECTED REPRINTS

1959

JULY, 1960

This volume contains contributions from the WOODS HOLE OCEANOGRAPHIC INSTITUTION which were published in 1959; also the Annual Report of the Director for the year 1959.

TABLE OF CONTENTS

Contribution No.

AYERS, JOHN C.
The Hydrography of Barnstable Harbor, Massachusetts.......... 995

BARAKAT, RICHARD
A Note on the Transient Stage of the Random Dispersal of Logistic Populations 1020

BARNES, H. and MARGARET BARNES
A Comparison of the Annual Growth Patterns of *Balanus balanoides* (L.) with Particular Reference to the Effect of Food and Temperature.......... 950

BARNES H. and MARGARET BARNES
Note on Stimulation of Cirripede Nauplii.......... 1037

BAYLOR, EDWARD R.
The Responses of Snails to Polarized Light.......... 996

BOLIN, BERT
On the Use of Tritium as a Tracer for Water in Nature.......... 1006

BOLIN, BERT and ERIK ERIKSSON
Changes in the Carbon Dioxide Content of the Atmosphere and Sea due to Fossil Fuel Combustion.......... 1025

BUTLER, PATRICK
Palynological Studies of the Barnstable Marsh, Cape Cod, Massachusetts..... 1024

CHASE, JOSEPH
Wind-Induced Changes in the Water Column along the East Coast of the United States.......... 1032

CLARKE, GEORGE L. and CHARLES J. HUBBARD
Quantitative Records of the Luminescent Flashing of Oceanic Animals at Great Depths.......... 1019

CLARKE, GEORGE L. and LLOYD R. BRESLAU
Measurements of Bioluminescence off Monaco and Northern Corsica......... 1043

CONOVER, JOHN T.
Seasonal Growth of Benthic Marine Plants as Related to Environmental Factors in an Estuary.......... 1038

FALLER, ALAN J. and WILLIAM S. VON ARX
The Modeling of Fluid Flow on a Planetary Scale.......... 987

GIBBS, ROBERT H., JR., and BRUCE B. COLLETTE
On the Identification, Distribution, and Biology of the Dolphins, *Coryphaena hippurus* and *C. equiselis*.......... 961

GORDON, MALCOLM S.
Osmotic and Ionic Regulation in Scottish Brown Trout and Sea Trout (*Salmo trutta* L.).......... 927

GORDON, MALCOLM S.
Ionic Regulation in the Brown Trout (*Salmo trutta* L.).......... 989

Contribution No.

GRAHAM, JOHN W.
Metabolically Induced Precipitation of Trace Elements from Sea Water 1011

GRAHAM, JOHN W. and SUSAN C. COOPER
Biological Origin of Manganese-rich Deposits of the Sea Floor 1017

HART, J. S. and LAURENCE IRVING
The Energetics of Harbor Seals in Air and in Water with Special Consideration of Seasonal Changes 1030

HAURWITZ, BERNHARD, HENRY STOMMEL and WALTER H. MUNK
On the Thermal Unrest in the Ocean 954

HERSEY, J. B., ELIZABETH T. BUNCE, R. F. WYRICK and F. T. DIETZ
Geophysical Investigation of the Continental Margin between Cape Henry, Virginia, and Jacksonville, Florida 973

KANWISHER, JOHN
Histology and Metabolism of Frozen Intertidal Animals 1013

KANWISHER, JOHN
Polarographic Oxygen Electrode 1014

LEVINE, JOSEPH
Spherical Vortex Theory of Bubble-Like Motion in Cumulus Clouds 1012

MALKUS, JOANNE S. and GEORG WITT
The Evolution of a Convective Element: A Numerical Calculation 967

MALKUS, W. V. R.
Magnetoconvection in a Viscous Fluid of Infinite Electrical Conductivity 1021

McGILL, DAVID A., NATHANIEL CORWIN and BOSTWICK H. KETCHUM
The Temperature Correction of Oceanic Inorganic Phosphorus Analyses 1047

McLACHLAN, JACK
The Growth of Unicellular Algae in Artificial and Enriched Sea Water Media 993

McLACHLAN, JACK and CHARLES S. YENTSCH
Observations on the Growth of *Dunaliella euchlora* in Culture 1010

McLACHLAN, JACK and GUY C. McLEOD
The Use of Conversion Factors for the Determination of the Concentration of Nutrients in Culture Media 975

McLEOD, GUY C. and JACK McLACHLAN
The Sensitivity of Several Algae to Ultraviolet Radiation of 2537 Å 997

MORDY, W. A.
Computations of the Growth by Condensation of a Population of Cloud Droplets 1028

NICHOLLS, G. D., HERBERT CURL, JR., and V. T. BOWEN
Spectrographic Analyses of Marine Plankton 980

Contribution No.

OFFICER, C. B.
On some Offshore Seismic Refraction Profiles in the Cook Strait, Tasman Bay, and Golden Bay Areas of New Zealand 738

OFFICER, C. B., J. I. EWING, J. F. HENNION, D. G. HARKRIDER and D. E. MILLER
Geophysical Investigations in the Eastern Caribbean: Summary of 1955 and 1956 Cruises 999

PARKER, FRANCES L. and WILLIAM D. ATHEARN
Ecology of Marsh Foraminifera in Poponesset Bay, Massachusetts 971

ROBINSON, ALLAN and HENRY STOMMEL
Amplification of Transient Response of the Ocean to Storms by the Effect of Bottom Topography 1004

ROBINSON, ALLAN and HENRY STOMMEL
The Oceanic Thermocline and the Associated Thermohaline Circulation 1003

RYTHER, JOHN H.
Potential Productivity of the Sea 1016

RYTHER, JOHN R.
Light Adaptation by Marine Phytoplankton 1039

RYTHER, JOHN H. and R. R. L. GUILLARD
Enrichment Experiments as a Means of Studying Nutrients Limiting to Phytoplankton Production 1026

SCHLEICHER, KARL E.
A Note on the Constancy of the T/S Relationship in a Water Mass 1060

SCHELL, IRVING I.
On a Criterion of Representativeness of Sea Surface Temperature Data 1029

SCHROEDER, ELIZABETH, HENRY STOMMEL, DAVID MENZEL and WILLIAM SUTCLIFFE, JR.
Climatic Stability of Eighteen Degree Water at Bermuda 992

SCHROEDER, WILLIAM C.
The Lobster, *Homarus americanus*, and the Red Crab, *Geryon quinquedens*, in the Offshore Waters of the Western North Atlantic 947

SMAYDA, THEODORE J.
The Seasonal Incoming Radiation in Norwegian and Arctic Waters, and Indirect Methods of Measurement 964

STERN, MELVIN E.
The Moving Flame Experiment 974

STOMMEL, HENRY

Florida Straits Transports: June 1956–July 1958 1008

Contribution No.

SUGIHARA, T. T., H. I. JAMES, E. J. TROIANELLO and V. T. BOWEN
Radiochemical Separation of Fission Products from Large Volumes of Sea Water. Strontium, Cesium, Cerium, and Promethium 982

TSCHIEGG, CARL E. and EARL E. HAYS
Transistorized Velocimeter for Measuring the Speed of Sound in the Sea 1022

TURNER, HARRY J., JR. and JAMES E. HANKS
Infestation of *Pecten irradians* by *Polydora* 1022

VERONIS, G.
Cellular Convection with Finite Amplitude in a Rotating Fluid 985

WIESER, WOLFGANG and JOHN KANWISHER
Respiration and Anaerobic Survival in some Sea Weed-Inhabiting Invertebrates 1061

WORTHINGTON, L. V.
The 18° Water in the Sargasso Sea 1015

YENTSCH, CHARLES S. and JOHN H. RYTHER
Relative Significance of the Net Phytoplankton and Nanoplankton in the Waters of Vineyard Sound 984

YENTSCH, CHARLES S. and JOHN H. RYTHER
Absorption Curves of Acetone Extracts of Deep Water Particulate Matter 1027

ZEIGLER, JOHN M.
Origin of the Sea Islands of the Southeastern United States 988

ZEIGLER, JOHN M., CARLYLE R. HAYS and SHERWOOD D. TUTTLE
Beach Changes during Storms on Outer Cape Cod, Massachusetts 956

ZEN, E-AN
Mineralogy and Petrography of Marine Bottom Sediment Samples off the Coast of Peru and Chile 1036

ZEN, E-AN
Clay Mineral — Carbonate Relations in Sedimentary Rocks 962

THE WOODS HOLE OCEANOGRAPHIC INSTITUTION
Report for the Year 1959

LIST OF CONTRIBUTIONS

The following contributions are not included in this volume:

BARNES, H.
Temperature and the Life Cycle of *Balanus balanoides* (L.) 937

BARNES, H. and MARGARET BARNES
The Effect of Temperature on the Oxygen Uptake and Rate of Development of

Contribution No.

the Egg-Masses of Two Common Cirripedes, *Balanus balanoides* (L.) and *Pollicipes polymerus* J. B. Sowerby 1075

DAY, C. GODFREY
Oceanographic Observations, 1957, East Coast of the United States 986

DAY, C. GODFREY
Oceanographic Observations, 1958, East Coast of the United States 1048

REDFIELD, A. C.
Physical and Chemical Properties of Sea Water: Biological Considerations — The Fourth Phase 1041

SCHOLANDER, P. F. and JOHN KROG
Countercurrent Heat Exchange and Vascular Bundles in Sloths (Published in 1957) 872

SCHOLANDER, SUSAN I. and JOAN T. KANWISHER
Latitudinal Effect on Respiration in Some Northern Plants 948

Contribution No. 738

Reprinted from the New Zealand Journal of Geology and Geophysics, *Vol. 2, No. 2, May, 1959.*

Contribution No. 738, Woods Hole Oceanographic Institution.

ON SOME OFFSHORE SEISMIC REFRACTION PROFILES IN THE COOK STRAIT, TASMAN BAY, AND GOLDEN BAY AREAS OF NEW ZEALAND

By C. B. Officer, Fulbright Research Fellow*, Geophysics Division, Department of Scientific and Industrial Research, Wellington

(Submitted for publication, 15 November 1954. Received by Editor, 1 December 1958)

Summary

Marine seismic profiles show that the thickness of unconsolidated sediments varies from a few hundred feet in the Cook Strait to Golden Bay areas to 2,300 ft in the vicinity of Marlborough Sounds. The Tertiary geosynclinal sediments of N.W. Nelson thicken northwards beneath Golden Bay. The maximum recorded velocities are consistent with the basement rock mapped in neighbouring land areas.

Introduction

During the summer of 1953-54 the author had the opportunity to be in New Zealand on a Fulbright Research Fellowship and to be able to work with the scientists of the Geophysics Division, D.S.I.R. Largely through the efforts of Dr E. I. Robertson Director of the Geophysics Division, and the co-operation of the New Zealand Naval Board, a programme in marine geophysics was carried out. The purpose of this programme was both to add, however slightly, to the general geophysical and geological knowledge of New Zealand and to enable the exchange of information on offshore seismic techniques for future geophysical investigations and for research and development in the allied field of underwater sound transmission. The original intention was to map the seaward extension of the large Tertiary basin that covers the south-west portion of the North Island. However, due to poor weather during the period the ships were available, it was not possible to work in this area; a smaller scale investigation was carried out in the relatively sheltered area of Golden Bay, Tasman Bay, and the northern Sounds area of the South Island. These results did bring out some interesting features and are reported briefly here.

Equipment and Techniques

Two ships took part in the operation. The larger ship, H.M.N.Z.F.A. *Isa Lei* served as the receiving ship. The recording gear was a truck-mounted 24-channel seismic exploration equipment, which was placed in the forward hold of the ship. A geophone and a hydrophone, suitably sealed, were placed on the bottom as the detecting elements. In deep water the hydrophone was suspended on a long cable and floated away from the ship so that during the reception of the shot the hydrophone and cable system was neutrally buoyant beneath the surface or slowly sinking. The smaller ship, SML 3355B, a converted HDML attached to the survey ship *Lachlan,* served as the shooting ship. The shots were fired electrically from a long cable off the stern of the SML and transmitted by radio and recorded on the photographic record of the receiving equipment. Distances were determined from the time of arrival of the water wave.

---

*Now of Rice Institute, Houston, Texas, U.S.A.

Geophysical Interpretation

The locations of the several refraction profiles are shown in Fig. 1. Profiles A, B, C, and D all showed a simple structure of a layer identified as the unconsolidated sediment, the velocity in which is only slightly greater than that in water, overlying a high velocity basement. Profile B was made from Okepuka Bay out through Tory Channel. Profiles A and C from Makara to Mana Island, and Profile D north of Queen Charlotte Sound. Profile E consisted of two legs nearly at right-angles. Velocities along the north-east leg indicated unconsolidated sediment overlying a layer of velocity 13,900 ft/sec. in turn overlying a basement of velocity 19,200 ft/sec. On the south-east leg the 13,900 ft/sec layer is much thicker; and the basement, if present at all, was not indicated.

LOCATION OF OFFSHORE SEISMIC REFRACTION STATIONS

(Geology taken from Geol map N.Z. Geol Surv. 1947)

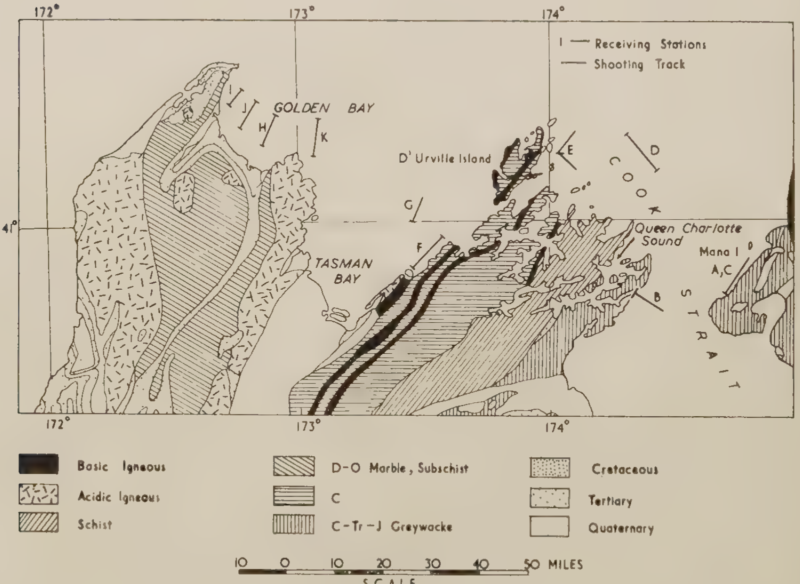
172°
173°
174°
41°
I — Receiving Stations
— Shooting Track
GOLDEN BAY
I
J
H
K
D' Urville Island
E
D
G
F
Queen Charlotte Sound
Mana I
A,C
B
TASMAN BAY
STRAIT
Basic Igneous
Acidic Igneous
Schist
D-O Marble, Subschist
C
C-Tr-J Greywacke
Cretaceous
Tertiary
Quaternary
10 0 10 20 30 40 50 MILES
SCALE

Fig. 1.

Profile F showed a complicated structure. The reversed profile (i.e. shooting north-eastwards) revealed a 10,700 ft/sec layer beneath the unconsolidated sediment and a displaced 15,600 ft/sec basement toward the north; shooting south-eastwards showed only the 15,600 ft/sec basement. The profile is interpreted as indicating that the 10,700 ft/sec layer pinches out toward the north with a possible fault present. Profile G was shot in Tasman Bay and had to be terminated due to inclement weather after measuring a layer of intermediate velocity below the unconsolidated sediment. Profiles H, I, and J were all made in Golden Bay and showed unconsolidated sediment overlying two sedimentary layers, with velocities in the neighbourhood of 8000 ft/sec and 11,000 to 12,000 ft/sec, respectively, overlying a high velocity basement. Profile K was made off Separation Point. Shooting south indicated a section similar to that from the Golden Bay stations. Shooting north gave less detailed results but these indicated a maximum thickness for the sedimentary layers.

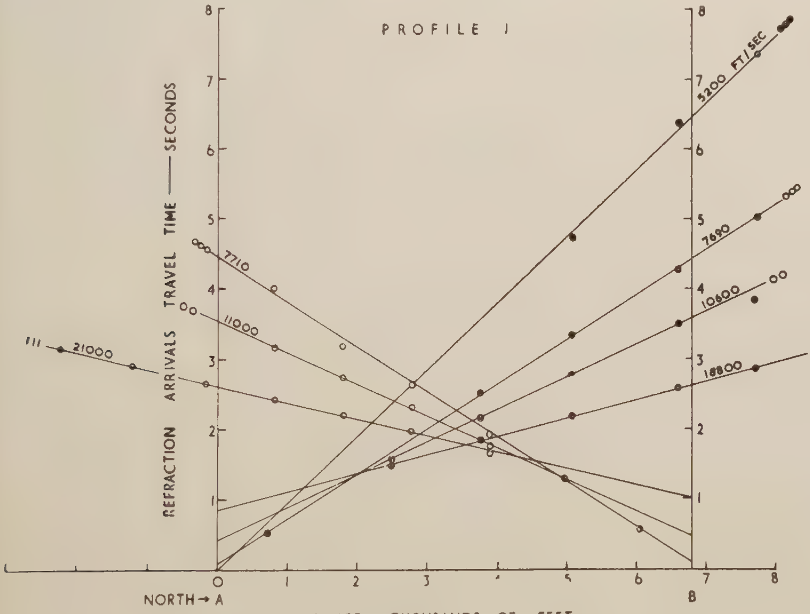

FIG. 2.

A sample travel time graph for one of the more complex stations is shown in Fig. 2. The abscissa is the range as determined from the travel time of the sound wave in the water channel. (A) is the location of the receiving ship for the northwards shooting and (B) the location for the southwards shooting. The ordinate is the travel time refractions from the various sub-bottom layers. The numbers on the refraction lines are the apparent velocities along the north- and south-for the refraction arrivals, and the plotted points are the observed shooting lines.

Geophysical and Geological Results

A summary of the thicknesses and seismic velocities along each profile is shown in Fig. 3. Three features are of interest.

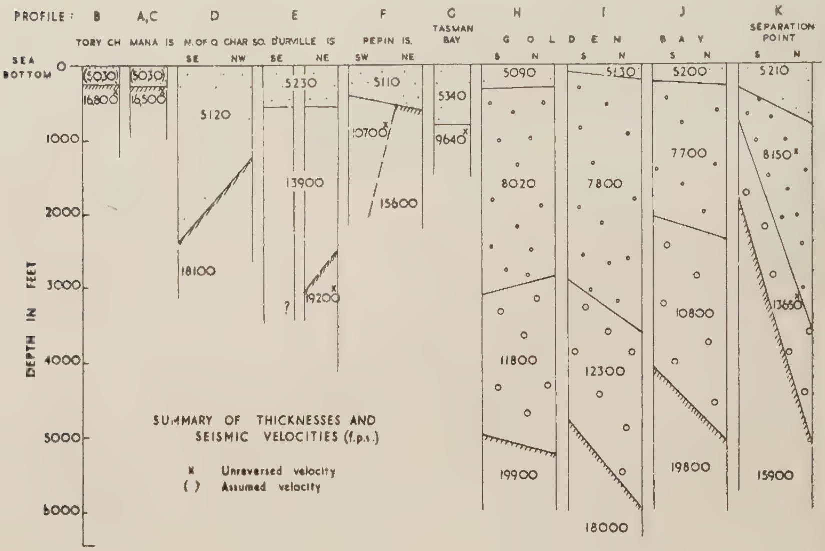
PROFILE: B A,C D E F G H I J K
TORY CH
MANA IS
N. OF Q. CHAR. SD.
D'URVILLE IS
PEPIN IS.
TASMAN BAY
G O L D E N B A Y
SEPARATION POINT
SE NW SE NE SW NE S N S N S N S N
SEA BOTTOM 0
1000
2000
3000
4000
5000
6000
DEPTH IN FEET
(5030)
16800
(5030)
16500
5120
18100
5230
13900
19200
?
5110
10700
15600
5340
9640
5090
8020
11800
19900
5130
7800
12300
18000
5200
7700
10800
19800
5210
8150
13650
15900
SUMMARY OF THICKNESSES AND SEISMIC VELOCITIES (f.p.s.)
x Unreversed velocity
( ) Assumed velocity

Fig. 3.

(1) *Thickness of unconsolidated sediment.* On the two profiles, B and A, C, near land in the Cook Strait area the unconsolidated sediment is thin, being only 250 ft thick. Similarly, on the profiles in Golden Bay, I, J, H, and K(S), the sediment is again thin, being 100 to 300 ft in thickness. Off Pepin and D'Urville Islands the thickness of sediment is 500 ft, increasing to 800 ft in Tasman Bay (Profiles G and K(N)). The thickest unconsolidated sediment, 1200 to 2300 ft, is measured on the most exposed profile, D, north of the Sounds area. All show the same pattern of thicker sediment away from the land areas.

(2) *Synclinal sediments in Golden Bay.* The geologic map of New Zealand shows that the southern shore of Golden Bay traverses a tertiary geosyncline which includes a Miocene mudstone more than 1000 ft thick underlain by an Oligocene limestone. The Golden Bay profiles measure the seaward extension of this syncline. Two sedimentary layers were observed, the contact between the two seismic layers probably corresponding to that between the mudstone and limestone. All four profiles, I, J, H, and K shows the synclinal sediments thickening toward the north, with maximum thicknesses of the order of 5000 ft.

(3) *Basement velocities*. The several profiles were made over widly differing basement types. It is interesting to compare the seismic velocities with rock types. Higher seismic velocities will be measured in the less compressible rocks. For sedimentary rocks the velocity increases progressively through the sequence, compaction, lithification, metamorphism. For igneous rocks the velocity is higher in the basic rocks than in the acidic rocks. In general the velocity is higher in the basic igneous and metamorphosed rocks than in the acidic igneous and sedimentary rocks. It is not unreasonable to identify the basement rocks at each profile by extension of the neighbouring land geology (Fig. 1). If this is done, then the basement under A, C, and B is greywacke and that under D schist. The upper layer of E is the Maitai-Te Anau limestone, mudstone, sandstone group; and the lower layer can be identified only with the ultrabasic to basic plutonic-volcanic sequences associated with the Maitai-Te Anau. Te upper layer of F is difficult to identify but may be granite; the lower basement is the Maitai-Te Anau. The basement under K is granite. For the Golden Bay area the basement under H and J is marble and that under I the subschistose core of the syncline. Table 1 is a comparison of rock type and seismic velocity. It shows the expected gradation. The ultrabasic to basics and the marble have the highest velocities of 19,000 to 20,000 ft/sec, the schist and subschist next with 18,000 ft/sec, then the greywacke with 16,500 ft/sec, the limestone, mudstone, sandstone with 14,000 to 15,500 ft/sec and the granites with 16,000 ft/sec and possibly lower.

TABLE 1.—Correlations of Seismic Velocities with Assumed Rock Types.

Basement Type (Nos from N.Z. Geol. map 1947)	Rock Description	Seismic Velocity
3	peridotites, serpentines, basaltic lavas	E 19,200 ft/sec
7	marble	H 19,900, J 19,800
7	subschistose conglomerates, breccia, greywacke	I 18,000
6	schist	D 18,100
9A	greywacke	B 16,800, AC 16,500
8	limestone, mudstone, sandstone	F 15,600, E 13,900
2	biotite granites	K 15,900, F 10,700

ACKNOWLEDGEMENTS

The author wishes to thank Dr E. I. Robertson and the New Zealand Naval Board for their considerable help in making the expedition possible and to those at the Geophysics Division and the Dominion Physical Laboratory who assisted in the operations. Particular appreciation is due to those who took part in the expedition, Dr Robertson, Messrs W. I. Reilly, F. E. Studt, Jenkins, R. A. Wooding, Burr, and Kusabs and to the personnel of the *Isa Lei* and the *SML 3355B*.

HARRY H. TOMBS LTD, THE WINGFIELD PRESS, WELLINGTON

Contribution No. 927

REPRINTED FROM THE JOURNAL OF EXPERIMENTAL BIOLOGY,
VOL. 36, NO. 2, pp. 253–260, JUNE 1959.
[*All rights reserved*] PRINTED IN GREAT BRITAIN

OSMOTIC AND IONIC REGULATION IN SCOTTISH BROWN TROUT AND SEA TROUT (*SALMO TRUTTA* L.)

BY MALCOLM S. GORDON*

Department of Zoology, Yale University, and Woods Hole Oceanographic Institution†

(*Received* 11 *July* 1958)

The brown trout (*Salmo trutta* L.) was originally a Palearctic fish, widely distributed in Europe and western Asia from the Mediterranean to the Arctic. Many river drainage systems in this area contained, and still contain, two or even three more or less morphologically and behaviourally recognizable forms of this species. These forms are the 'lake trout', living in fresh-water lakes, the 'brown trout', living in fresh-water streams, and the 'sea trout', an anadromous form. The question of whether or not these forms, especially the brown trout and the sea trout, are 'really' (equals genetically) different from one another has been debated by fishermen and others for centuries.

Trewavas (1953) reviewed the most significant portions of the voluminous literature on this subject. She concluded that average differences in some characters (meristic characters, age at maturity and frequency of spawning) do separate some populations of the two types, but these do not separate all brown trout from all sea trout. Trewavas favoured the view that the forms are ecotypes of a single species, although there are difficulties attendant on the application of even this generalized term.

The results of hatchery breeding experiments carried out under fairly uniform conditions by Skrochowska (1951) were unknown to Trewavas at the time she wrote her paper, but confirm her view. This also is the case with tagging experiments reported by Skrochowska (1953), though these latter data are not as numerous as one might wish. Svärdson (1955) further supports Trewavas and presents an ingenious hypothesis explaining the existence of the two forms on the basis of responses of individual fish to environmental changes.

The morphological, behavioural and genetic evidence thus seems to indicate very strongly that brown trout and sea trout are at most morphotypes of a single species. Alm (1949), however, described morphological differences between the brown trout and the lake trout which seem to be genetically determined. Further, a very closely related form, the rainbow trout (*Salmo gairdneri*), shows what appear to be genetically determined differences in lateral line scale-counts between sea-run and fresh-water populations (Neave, 1944).

---

* Present address: Department of Zoology, University of California, Los Angeles 24, California.

† Contribution number 927 from the Woods Hole Oceanographic Institution.

That a polymorphic species differentiated into three more or less equally morphologically distinct forms, say *A*, *B* and *C*, would have *A* and *B* genetically different from one another, but *B* and *C* not so, would seem unlikely. It also seems doubtful that the rainbow trout is significantly older than the brown trout in an evolutionary sense. It would therefore be surprising if the brown trout, faced with environmental stresses identical to those faced by the rainbow trout, has not made genetic rearrangements similar to those made by the rainbow. One might also expect that such rearrangements would be reflected in the osmotic and ionic regulatory abilities of the fish.

During the course of a detailed study of osmotic and ionic regulation in an American hatchery population of *Salmo trutta* the writer observed several instances of variable behaviour between individual fish subjected to the same strong osmotic stress for long periods of time (Gordon, 1959). American brown trout are derived from European brown trout, and no one knows whether or not, or how many, European sea trout were included in the original *Salmo trutta* shipments sent to the United States. This fact, combined with the considerations mentioned above, made it seem reasonable to interpret the variability noted in the American fish as being a result of their being hybrid fish descended from physiologically distinct ancestors.

To test this hypothesis arrangements were made to obtain blood serum samples from known Scottish sea and brown trout subjected to osmotic stresses similar to those used on the American fish. The results of the analyses for freezing-point depression, chloride, sodium, and potassium that were carried out on these samples, the implications of these analyses for the brown trout or sea trout problem, and some comparisons of these data with material obtained from American fish form the basis for this paper.

MATERIALS AND METHODS

Known Scottish sea trout and brown trout were obtained from the area around Aberdeen between November 1956 and May 1957 by Dr Isabel W. Smith of the Marine Laboratory, Aberdeen. The fish were all sexually mature and varied in size from 18 to 55 cm. standard length. Temperature throughout was 10 ± 2° C. Fish were sampled as follows:

Sea trout. In November 1956 three sea trout were sampled after unknown, but perhaps quite short, periods in fresh water while on the upstream phase of their spawning migration. Two sea trout caught similarly were sampled 24 hr. after having been transferred to full sea water (salinity 32·6‰). Five more sea trout were sampled after having been maintained in full sea water for 5 months at the Marine Laboratory aquarium. In May 1957 seven sea trout were sampled after having been captured in commercial nets in an estuary containing water varying tidally in salinity from about 2–32‰.

Brown trout. In March 1957 a number of fish locally considered to be *Salmo levenensis*, or fresh-water brown trout, were removed from a reservoir near Aberdeen in which they had been stocked either 12 or 20 years earlier. Eleven of these were sampled while still in fresh water (some of them twice), then were transferred to one-half sea water (salinity 16‰) where they were kept for 10 days. Several of them were then sampled and all were transferred to full sea water. Additional samples were taken from varying numbers of these fish after 2 days in sea water, 10 days in sea water and 64 days in sea water (three survivors).

Blood samples were taken from the fish by Dr Smith by either heart or caudal artery puncture using a syringe with a fine needle. The samples were allowed to clot and the serum was pipetted off and placed in acid-cleaned vials. The vials were then tightly stoppered with paraffined corks, the samples frozen on dry ice and shipped in the frozen state by air express to the United States. Analyses for freezing-point depression (Δ), chloride (Cl), sodium (Na) and potassium (K) were then carried out by the author using methods described elsewhere (Gordon, 1959).

The multiple sampling of single brown trout in the present work is similar to the procedure used with Arctic char (*Salvelinus alpinus*) by Gordon (1957). It did not seem to cause any shock effects in the char.

Table 1. *Serum Δ in Scottish brown and sea trout*

State of acclimatization	N	Serum Δ (° C.) ($\bar{x}$ ± S.E.)
Brown trout		
F.W.	11	0·607 ± 0·011
½ S.W., 240 hr.	5	0·622 ± 0·038
½ S.W., 240 hr.–S.W., 48 hr.	4	0·748 ± 0·030
½ S.W., 240 hr.–S.W., 240 hr.	8	0·674 ± 0·021
½ S.W., 240 hr.–S.W., 64 days	3	0·637 ± 0·022
Sea trout		
F.W.	3	0·653 ± 0·045
S.W., 24 hr.	2	0·79, 0·81
S.W., 5 months	5	0·662 ± 0·014
Brackish, indefinite	7	0·666 ± 0·015

RESULTS

The data on serum Δ, Cl, Na and K in the sea and brown trout are presented in Tables 1–4. Gordon (1959) has shown that neither sex of the fish nor season (during the sampling periods involved here) have any significant effect on these concentrations.

The main point demonstrated by these data is that, with only one exception, the concentrations studied were insignificantly different (at the $P = 0{\cdot}05$ level by 't' test) in the brown trout and the sea trout when the fish were acclimatized to full sea water for long periods (10 days to 5 months). The one exception was serum Cl in brown trout acclimatized to sea water for 10 days as compared with sea trout in sea water for 5 months. These two means are highly significantly different ($P \ll 0{\cdot}01$). This exception is discussed below.

Similar agreement between the two forms occurred for their fresh-water concentrations as well, though the sample size of only two fish for most of the sea trout concentrations makes this point less certain.

Table 2. *Serum chloride in Scottish brown and sea trout*

State of acclimatization	N	Serum Cl (m-equiv./l.) ($\bar{x}$ ± S.E.)
Brown trout		
F.W.	11	133·3 ± 3·1
½ S.W., 240 hr.	5	131·4 ± 7·8
½ S.W., 240 hr.–S.W., 48 hr.	4	185·2 ± 4·5
½ S.W., 240 hr.–S.W., 240 hr.	8	168·9 ± 6·1
½ S.W., 240 hr.–S.W., 64 days	3	150·0 ± 9·5
Sea trout		
F.W.	2	110, 137
S.W., 24 hr.	2	186, 196
S.W., 5 months	5	138·4 ± 0·8
Brackish, indefinite	7	121·7 ± 1·6

Table 3. *Serum sodium in Scottish brown and sea trout*

State of acclimatization	N	Serum Na (m-equiv./l.) ($\bar{x}$ ± S.E.)
Brown trout		
F.W.	5	149·8 ± 3·1
½ S.W., 240 hr.	5	139·0 ± 10·7
½ S.W., 240 hr.–S.W., 240 hr.	6	179·7 ± 6·9
½ S.W., 240 hr.–S.W., 64 days	3	163·0 ± 6·5
Sea trout		
F.W.	2	141, 168
S.W., 24 hr.	2	203, 206
S.W., 5 months	5	165·8 ± 2·2
Brackish, indefinite	1	144

Table 4. *Serum potassium in Scottish brown and sea trout*

State of acclimatization	N	Serum K (m-equiv./l.) ($\bar{x}$ ± S.E.)
Brown trout		
F.W.	5	2·7 ± 0·5
½ S.W., 240 hr.	5	5·1 ± 0·8
½ S.W., 240 hr.–S.W., 240 hr.	6	1·5 ± 0·2
½ S.W., 240 hr.–S.W., 64 days	3	3·1 ± 0·3
Sea trout		
F.W.	2	4·0, 6·6
S.W., 24 hr.	2	0·5, 1·3
S.W., 5 months	5	3·5 ± 1·5
Brackish, indefinite	1	> 10

DISCUSSION

It seems reasonable to conclude from this that, at least for the populations of sea and brown trout near Aberdeen and for the concentrations measured, there are no significant osmotic or ionic regulatory differences between the two forms. However, the implications of the somewhat anomalous behaviour of serum chloride concentration complicate the situation.

The serum Na:Cl ratios for all groups of brown trout are in the range 1·07–1·13. Excepting the two fish sampled after only 24 hr. in sea water (and therefore probably not in states of internal ionic equilibrium) all groups of sea trout had Na:Cl ratios of 1·18–1·28. This difference in ratios is perhaps indicative of a larger contribution of alkaline reserve to total serum concentration in the sea trout than in the brown trout. Such a difference in alkaline reserve could account for the statistically significant difference found between the mean serum chloride concentrations of brown trout in sea water for 10 days as compared with sea trout in sea water for 5 months. It also might indicate a real difference between sea and brown trout with respect to mechanisms for control of blood acid-base balance.

If correct, this interpretation would perhaps not be in agreement with the results of work on the eel (*Anguilla*) done by Boucher-Firly (1935). Boucher-Firly found consistent decreases of alkaline reserve (to about 40% of mean fresh-water levels) in all life-history stages of the eel following long-term acclimatizations to sea water (more than 12 days). The relative constancy of the Na:Cl ratios in brown trout and sea trout in both fresh and sea water argues against the occurrence of such changes in *Salmo trutta*. However, the actual concentration changes involved would be small (on the order of 10 m-equiv./l.) and may have been masked in the present material by other effects. Direct measurements of alkaline reserve in brown and sea trout are obviously needed.

The only previously published data on osmotic and ionic concentrations in *Salmo trutta* that the writer is aware of are given by Dekhuyzen (1905), Spalding, in Jones (1956), and Phillips & Brockway (1958). Dekhuyzen lists serum Δ for one brown trout in fresh water in the Amsterdam aquarium (−0·57° C.), and a mean for six dead, or nearly dead, sea trout from sea water at Bergen, Norway (−0·78° C.). Spalding lists mean serum Na and K concentrations for brown trout in fresh water during the winter (Na: 144·2 m-equiv./l.; K: 8·9 m-equiv./l.). Phillips & Brockway (1958) present figures for the means and ranges of Cl, Na and K concentrations (also concentrations of several other ions) in the serum of brown trout in fresh water in summer. These values are: Cl: 119 m-equiv./l. (range: 118–124 m-equiv./l.); Na: 156 m-equiv./l. (range: 151–162 m-equiv./l.); K: 5·2 m-equiv./l. (range: 4·3–6·6 m-equiv./l.).

The present data on serum Δ and Na in fresh water agree well with the figures of Dekhuyzen and Spalding, the K data do not. The cause of the discrepancy is unknown. The Δ from dying or dead sea trout is probably unreliable.

The figures given by Phillips & Brockway (1958) are different from both the present data and those of Spalding, probably primarily as a result of having been obtained from summer fish. Brown trout in summer are quite different from brown trout during the rest of the year (Gordon, 1959, for details).

The patterns of variation in serum concentrations indicated here for Scottish brown trout are similar to those found in American brown trout. The latter are discussed in detail elsewhere (Gordon, 1959). However, there are several points which should be made here concerning comparisons between the two groups of fish.

As noted, the overall patterns of variation of the different serum components are very similar in the two groups, though there are small quantitative differences. This may be seen for serum Cl by comparing Table 5 with Table 2. Table 5 presents serum Cl data for brown trout from a hatchery in Massachusetts acclimatized in the ways noted. The experiments were carried out during the same times of year as the experiments with Scottish fish. The only significant difference between the two series is that the American experiments were done at 20° C., the Scottish at 10° C. Additional data on the American fish show that this temperature difference results in the American figures averaging 10 m-equiv./l. higher than they would have been if the experiments had been carried out at 10° C.

Table 5. *Serum chloride in American brown trout*

State of acclimatization	N	Serum Cl (m-equiv./l.) ($\bar{x}$ ± S.E.)
F.W.	14	140·5 ± 1·1
½ S.W., 240 hr.	12	148·2 ± 2·3
S.W., 21–30 hr.	15	203·6 ± 3·3
½ S.W., 240 hr.–S.W., 47 hr.	5	170·4 ± 1·6
½ S.W., 240 hr.–S.W., 240 hr.	7	179·1 ± 11·5

This agreement in overall patterns of regulation indicates that conclusions concerning mechanisms of ionic regulation in the brown trout reached on the basis of the American experiments are very likely valid for the species as a whole. The quantitative differences between the two groups indicate that their many generations of genetic isolation from one another have resulted in small amounts of divergence, but not in any basic changes.

The two groups of data also demonstrate that the brown trout is an almost perfect osmotic and ionic regulator. With long-term acclimatizations over the range of salinities from fresh water to full sea water (again excepting serum Cl after 10 days in sea water) all internal concentrations were either statistically insignificantly different from the fresh-water levels or were within 10 % of the fresh-water levels. Many individual trout were completely homoiosmotic. *Salmo trutta* is the first salmonid known to possess such excellent regulatory abilities (cf. Gordon, 1957).

Finally, there is a small but interesting point of difference between American and Scottish fish with regard to the degree of parallelism shown between changes in serum Δ and changes in serum Cl and Na. In American brown trout under all the conditions studied serum Cl contributed 40–45 %, serum Na 45–49 % of the Δ (assuming unit activities for the ions). Much the same was true for the Scottish fish, but with one clear exception. This was the group of sea trout sampled from brackish water in an estuary. In these fish ion concentrations were significantly below the range to be expected from the Δ measurements (only enough material for one Na determination was available). Cl made up only 35 %, Na only about 41 % of the total concentration.

It might be worthwhile investigating the possibility that, in fish subjected to continually and widely varying salinities, some blood component other than Na and Cl becomes important in regulation of total osmotic pressure. The one serum K value from a fish in brackish water was well above the calibration range of the analyses. Perhaps K is the other component varied (though this would seem unlikely on the basis of known depressant effects of high external K concentrations on nerve and muscle function). This situation may be similar to the differential behaviour of serum Δ and serum Cl noted in shallow-water fishes in Hebron Fjord, Labrador, in winter by Scholander *et al.* (1957).

SUMMARY

1. Adult brown trout (*Salmo trutta* L.) of both sea-run (sea trout) and fresh-water stream (brown trout) forms were captured in the vicinity of Aberdeen and acclimatized to full-strength sea water for periods of up to 5 months.

2. Blood serum samples from these fish were analysed for freezing-point depression, chloride, sodium and potassium concentrations.

3. The patterns of regulation of these concentrations are very nearly the same in both forms. Brown trout and sea trout, at least in eastern Scotland, thus appear to be virtually identical in osmotic and ionic regulatory abilities. However, there is a possibility that there is a difference between the two forms with respect to mechanisms controlling blood acid-base balance.

4. The patterns of regulation shown by Scottish fish are the same as those shown by American hatchery fish treated similarly. The different populations of the species seem not to have diverged significantly from one another in this regard after many generations of more or less complete genetic isolation.

5. The species *Salmo trutta* is strongly homoiosmotic. Internal concentrations are either unchanged or increase by less than 10% above fresh-water levels with long-term acclimatizations to half and full sea water. The brown trout is the first salmonid species known to regulate so well.

These studies were aided by National Science Foundation Predoctoral Fellowships for 1954–57 and a grant from the Higgins Fluid Research Fund, Yale University. This paper is a portion of a dissertation presented to the faculty of the Graduate School of Yale University in candidacy for the degree of Doctor of Philosophy. Contribution number 927 from the Woods Hole Oceanographic Institution.

The author's thanks for aid and advice are due to the following: Drs E. J. Boell, T. H. Waterman, G. E. Pickford and L. M. Passano, Yale University; Drs C. O'D. Iselin, B. H. Ketchum and A. C. Redfield, Woods Hole Oceanographic Institution; Dr H. Barnes, Marine Laboratory, Millport, Scotland; Mr K. A. Pyefinch, Brown Trout Research Laboratory, Pitlochry, Scotland; Dr I. W. Smith, Marine Laboratory, Aberdeen, Scotland; Dr H. O. Werntz, Harvard University; and Mr H. Robbins, Wareham, Mass.

REFERENCES

ALM, G. (1949). Influence of heredity and environment on various forms of trout. *Rep. Inst. Freshw. Res. Drottning.* **29**, 29–34.

BOUCHER-FIRLY, S. (1935). Recherches biochimiques sur les teleostéens apodes (Anguille, Congre, Murène). *Ann. Inst. oceanogr. Monaco,* **15**, 217–327.

DEKHUYZEN, M. C. (1905). Sur la pression osmotique dans le sang et dans l'urine des poissons. *Arch. néerland. Sci.* **10**, 121–36.

GORDON, M. S. (1957). Observations on osmoregulation in the Arctic Char (*Salvelinus alpinus* L.). *Biol. Bull., Woods Hole,* **112**, 28–33.

GORDON, M. S. (1959). Ionic regulation in the brown trout (*Salmo trutta* L.). *J. Exp. Biol.* **36**, 227–52.

JONES, I. C. (1956). The role of the adrenal cortex in the control of water and salt-electrolyte metabolism in vertebrates. *Mem. Soc. Endocrin.* no. 5, 102–20.

NEAVE, F. (1944). Racial characteristics and migratory habits in *Salmo gairdneri*. *J. Fish. Res. Bd., Can.* **6**, 245–51.

PHILLIPS, A. M., JR. & BROCKWAY, D. R. (1958). The inorganic composition of brown trout blood. *Progr. Fish Cult.* **20**, 58–61.

SCHOLANDER, P. F., VAN DAM, L., KANWISHER, J., HAMMEL, T. & GORDON, M. S. (1957). Supercooling and osmoregulation in Arctic fish. *J. Cell. Comp. Physiol.* **49**, 5–24.

SKROCHOWSKA, S. (1951). The rearing of sea trout, *Salmo trutta* L., in artificial ponds. *Bull. Int. Acad. Polon. Sci. Lett., Classe Sci. Math. Nat.* Ser. B (II), no. 4–6, 179–226.

SKROCHOWSKA, S. (1953). The migrations of sea trout (*Salmo trutta*) and other salmon fishes bred in ponds. *Polsk. Arch. Hydrobiol.* **1**, 89–135 (in Polish, English summary).

SVÄRDSON, G. (1955). Salmon stock fluctuations in the Baltic Sea. *Rep. Inst. Freshw. Res. Drottning.* **36**, 226–62.

TREWAVAS, E. (1953). Sea-trout and brown trout. *Salmon and Trout Mag.* **139**, 199–215.

Contribution No. 947

Deep-Sea Research, 1959, Vol. 5, pp. 266 to 282. Pergamon Press Ltd., London. Printed in Great Britain

The lobster, *Homarus americanus*, and the red crab, *Geryon quinquedens*, in the offshore waters of the western North Atlantic

WILLIAM C. SCHROEDER

(*Received 7 October* 1958)

Abstract—A population of lobsters, large enough to support commercial fishing, is present off the east coast of the United States along the outer shelf and upper slope between the eastern part of Georges Bank and the offing of Delaware Bay. This area at depths of roughly 60-250 fm (110-450m), is about 400 miles long and 5-10 miles wide. Lobsters are more plentiful along the eastern half of this stretch than to the west and south. Although there are all sizes from " shorts " to very large, a much greater percentage than in the shoal water populations are large.

Prior to 1953, the New England trawler fleet took only small numbers of lobsters, incidental to their catch of fish, in deep water, but since then several otter trawlers have been fishing offshore exclusively for lobsters and have made substantial catches. However, the recorded total annual catch in deep-water up to 1956 has not exceeded 1 per cent of the total annual catch taken by the inshore pot fishery.

The otter-trawl catch of lobsters off New York and New Jersey, small prior to 1947, now exceeds the catch taken with pots, but the fishery as a whole is of small magnitude compared with that to the north and east.

There is no evidence thus far of a definite migration of lobsters between inshore and offshore areas but no doubt most of them wander from time to time in search of food (or perhaps for no particular reason).

A deep-water crab (*Geryon quinquedens*), as yet unexploited, might become the source of a commercial fishery along the North and Middle Atlantic coast. It inhabits depths between 150-700 fm (275-1280 m), or more, and ranges from the offing of Nova Scotia to Virginia and southward, perhaps in diminishing numbers, at least to Cuba.

THE LOBSTER, *Homarus americanus*

EVER since the introduction by the commercial fishery of the beam trawl in 1891 and of the otter trawl in 1905* in American waters, lobsters have been taken with this gear as an incidental part of the fish catch along our North Atlantic coast. The beam trawl long ago ceased to be an important adjunct to our fisheries but the number of otter trawlers operating off New England has steadily increased from 7 vessels in 1912 to 44 in 1920 (RADCLIFFE, 1922, p. 51) and to 603 vessels of 5 tons or over in 1955. As a rule the catch of lobsters taken by trawlers per trip has been very small, ranging from a few individuals to about a hundred pounds, and occasionally to a thousand pounds or more, as for example the 1850 lb landed by *Cap'n Bill II*, April 3, 1952, fishing for fluke (*Paralichthys*) in 60-65 fm (110-120 m) south-west from No Mans Land. On some trips none are caught. The aggregate annual lobster catch by all trawlers engaged primarily in fishing, not lobstering, is probably substantial although amounting to but a very small percentage of that taken by the regular lobster trap fishery.†

---

*For a discussion of the earliest fishing in our waters, see ALEXANDER *et al.*, 1915.

†There are no adequate statistical records of these incidental catches made by otter trawlers, for it has been customary, when enough lobsters are brought in to warrant selling, to divide the proceeds among the crew, apart from their share in the sale of fish. These lobsters are not reported in the vessel's catch.

Most of the early otter-trawl fishing was not much deeper than about 80 fm (146 m) and many of the lobsters caught were very large. More recently depths down to 125 fm (228 m), and beyond, have been trawled by part of the fishing fleet and increasing amounts of lobsters have been taken along with the fish catch, not only very large ones, but also medium-sized and small ones as well. A large proportion of these offshore lobsters are caught in depths well beyond the realm of the pot fishery.

One of the earliest, if not the first, published statistical record of otter-trawl caught lobsters landed along our coast was for 7985 lb listed for New York in 1921 (U.S. Bureau of Fisheries, 1924, p. 85). Fishery statistics for the Middle Atlantic and New England states are not available for all years since 1921. Thus, the next records available are for 1440 lb landed in Connecticut in 1925 and for 3465 lb in 1926, part of them by the shore fishery and part by the so-called vessel fishery.

Table 1. *Catch of lobsters for the New England States, from* 1928 *to* 1956 *with a comparison between the inshore pot fishery and offshore otter trawling**

Year	lb		*Percentage of total catch taken by trawls*	*No. of pots*	lb *Aver. per pot*
	Pots	*Otter trawls*			
1928	11,603,328	351	†	334,574	34·6
1929	10,322,262	204	†	345,824	29·8
1930	12,356,121	1201	0·01	332,791	37·1
1931	11,311,985	34	†	357,704	31·6
1932	10,278,272	85	†	341,595	30·0
1933	9,086,243	1882	0·02	319,460	28·5
1935	10,847,300	5000	0·05	289,437	37·5
1937	10,931,400	4500	0·05	306,130	35·7
1938	11,397,100	10,700	0·10	302,510	37·6
1939	11,303,600	7900	0·07	330,246	34·3
1940	11,157,900	7400	0·07	328,988	33·9
1942	11,791,300	200	†	267,342	44·2
1943	15,650,800	400	†	290,649	53·7
1944	17,203,400	13,300	0·08	312,934	55·0
1945	22,237,800	29,100	0·13	464,826	47·8
1946	22,819,300	4500	0·02	572,098	39·9
1947	23,310,900	5500	0·03	660,961	35·3
1948	20,206,800	19,500	0·10	598,425	33·8
1949	23,980,500	14,000	0·06	601,786	39·8
1950	22,546,700	12,000	0·05	570,635	39·5
1951	25,528,100	6000	0·02	507,927	50·3
1952	24,309,800	13,100	0·05	540,216	45·0
1953	27,032,100	103,600	0·40	564,665	47·9
1954	26,273,000	167,600	0·60	618,279	42·5
1955	27,510,500	107,500	0·39	665,269	41·4
1956	24,932,100	227,500	0·91	648,337	38·5

*Based on annual reports of the U.S. Bureau of Fisheries published from 1929 to 1941 for the years 1928-1938 and the U.S. Fish and Wildlife Service published from 1942 to 1956 for the years 1939 to 1954. Statistics for 1955 and 1956 are based on data furnished by Mr. Dwight L. Hoy of the U.S. Fish and Wildlife Service.

†Less than 1 one-hundreth of 1 per cent.

Beginning in 1928, the catch statistics were entered regularly for otter-trawl caught lobsters landed in New England (Table 1) and in 1929 in New York and New Jersey (Table 3) (U.S. Bureau of Fisheries, 1931), although in some years the amounts were trifling. If the reported landings of otter-trawl caught lobsters, prior to 1953, were multiplied by say 10 or 20 they would more closely approximate the actual quantities brought to port (Footnote 2, p. 266). Even if corrected in this way, the trawl catch would scarcely amount to 1 per cent of the total catch in most years.

It is of interest to find that an average annual catch of 42·5 lb of saleable lobsters per pot was recorded for the 14 years from 1943 to 1956 as compared with 34·4 lb for the 12 years for which statistics are available for the period from 1928 to 1942 (Table 1). While some unknown factors are involved in this comparison, such as the number of days the pots may have fished during each of these periods, the effects of economic conditions, etc., nevertheless there appears to be no indication that the population suffered from overfishing. Similarly, TAYLOR *et al.* (1957, p. 325) in discussing the fluctuations in lobster landings, which in Maine increased from 7·6 million to 19·1 million lb per year between 1940 and 1945, concluded " that the increased catch was caused by an increase in abundance rather than by an increase in the amount of fishing", possibly due to the warming of the coastal waters north of Cape Cod since 1940. Increased landings occurred not only along the coast of Maine but also in Massachusetts and Nova Scotia.

The first evidence that lobsters inhabit depths well beyond 100 fm (183 m) along our coast was furnished by a catch of 3 small ones trawled in 195-210 fm (356-384 m) by the *Caryn* of the Woods Hole Oceanographic Institution, on June 29, 1948, about 85 miles SSW of Martha's Vineyard (lat. 39° 55′N., long. 70° 39′W.). This was followed by a catch taken nearby on October 16, of 23 lobsters, 5½ to 9 in. long (measured from the end of the rostrum to the end of the tail) in 167-250 fms (305-456 m) and by 13 others, 7 to 14 in. long, trawled September 10, 1949, in 100-150 fm (183-274 m).

On a cruise of the *Albatross III*, May 11-17, 1950, a number of hauls* were made in depths beyond 100 fm (183 m), several of which yielded fair numbers of lobsters. Of particular interest are the following :

No. of lobsters	*Wt.* (lb)	*Locality*	*Depths* (fm)	(m)	*Duration of drag* (hr)
26	2–18	39° 42′N, 71° 57′W	145–210	265–384	1
6	1½–6	39° 50′N, 71° 44′W	107–137	196–250	½
11	1½–7	39° 54′N, 71° 35′W	112–142	205–260	½

In June–July 1952 and 1953, during the course of deep-water exploratory fishing with the chartered trawler *Cap'n Bill II*, the author discovered off southern New England areas that gave promise of yielding substantial numbers of lobsters and of supporting an offshore otter-trawl fishery. On July 8, 1954, *Atlantis* made several good hauls of lobsters, followed by 6 hauls made by *Caryn*, September 2–3, 1956, in the same general area trawled by *Cap'n Bill II* in 1952 and 1953†.

---

*An Iceland trawl with a 78 ft head-rope and 114 ft foot-rope, but without rollers, was used on this cruise.

†Most of these hauls fished at the bottom for about 30-40 min with a towing speed of 2·5 knots. In 1952 the trawls used measured 35 and 50 ft respectively at the foot-rope and in 1953-1956, 50 and 60 ft, the head-rope being about 18 per cent shorter in each case. The body and wings were of 3 in. and the cod end of 1½ in. stretched mesh.

Table 2. Catches of lobsters made by Cap'n Bill II, Atlantis *and* Caryn *during 1952-1956 along the outer shelf and upper continental slope from the offing of Georges Bank to Virginia, arranged by longitude*

Station	*Date*	*Lat.*	*Long.*	(fm)	*Lobsters*		*Bottom*† *Temp* (°F)
					No.	*Length** *(in.)*	
200	July 25, 1953	40° 46′	66° 48′	100–105	1	18	53
201	July 25, 1953	40° 45′	66° 51′	85–87	2	14–16	52
116	July 29, 1952	40° 46′	66° 53′	85–87	1	14	
117	July 29, 1952	40° 46′	66° 55′	67–71	1	11½	
194	July 24, 1953	40° 41′	67° 15′	52–55	4	12–18	
209	July 26, 1953	40° 15′	68° 28′	85–92	1	8	50
54	July 10, 1952	39° 55′	69° 25′	185–235	24	8–13	
81	July 16, 1952	39° 55′	69° 25′	190–220	1	10	
82	July 16, 1952	39° 58′	69° 28′	105–135	6	6–9½	
83	July 16, 1952	39° 59′	69° 32′	87–90	7	7–13	
84	July 16, 1952	39° 59′	69° 35′	82–85	14	8–17	
85	July 16, 1952	40° 02′	69° 37′	75–90	30	6–18	
45	June 26, 1952	39° 52′	69° 43′	180–260	5	7¼–12	
217	July 28, 1953	39° 57′	69° 51′	90–100	30	7¼–17	
218	July 28, 1953	39° 59′	69° 54′	80–87	16	6¼–20¾	53
219	July 28, 1953	39° 55′	70° 03′	110–115	4	9–9½	52
38	June 25, 1952	40° 04′	70° 12′	190–225	3	7½–13	
37	June 25, 1952	40° 01′	70° 18′	160–170	3	6–10	
35	June 25, 1952	40° 02′	70° 24′	105–110	1	7½	
34	June 25, 1952	40° 03′	70° 25′	110–125	1	7¾	
33	June 25, 1952	40° 00′	70° 30′	160–200	1	7½	
255	July 8, 1954	40° 06′	70° 31′	100	4	**	57
254	July 8, 1954	40° 04′	70° 33′	70–85	16	**	54
256	July 8, 1954	40° 04′	70° 33′	70–73	64	**	60
264	Sept. 2, 1956	40° 04′	70° 33′	65–80	9	**	
221	July 29, 1953	40° 04′	70° 34′	70–75	57	7–16¼	54
32	June 24, 1952	39° 58′	70° 36′	150–160	10	6½–12½	
252	July 8, 1954	40° 04′	70° 37′	70–72	64	**	58
253	July 8, 1954	40° 05′	70° 37′	70	24	**	59
222	July 29, 1953	40° 03′	70° 39′	80–93	36	7–20½	52
260	Sept. 2, 1956	40° 04′	70° 39′	70	14	**	
251	July 8, 1954	40° 04′	70° 41′	75	38	**	58
223	July 29, 1953	40° 00′	70° 42′	150–155	18	6½–9¾	46
227	July 29, 1953	40° 02′	70° 42′	110	5	7–9	49·5
261	Sept. 2, 1956	40° 04′	70° 42′	75	15	**	
266	Sept. 3, 1956	40° 04′	70° 44′	70–80	24	**	
267	Sept. 3, 1956	40° 04′	70° 47′	81–83	10	**	
268	Sept. 3, 1956	40° 04′	70° 50′	75	17	**	
19	June 23, 1952	39° 57′	71° 13′	175–180	6	8–11	
15	June 22, 1952	39° 56′	71° 22′	175–200	8	6½–9½	
14	June 22, 1952	39° 56′	71° 26′	150	8	7¾–16	
13	June 22, 1952	39° 55′	71° 27′	180–190	13	6¾–11½	
4	June 21, 1952	39° 32′	72° 01′	185–225	4	8–11½	
162	July 1, 1953	39° 36′	72° 04′	81–83	5	9–13	
161	July 1, 1953	39° 34′	72° 05′	120–135	8	9–16	
155	July 1, 1953	39° 22′	72° 22′	76–79	2	12–13	53
130	June 27, 1953	38° 45′	73° 08′	50–55	15	9–16	
150	June 30, 1953	38° 38′	73° 10′	190–200	9	6½–19	42·4
149	June 30, 1953	38° 37′	73° 12′	145–165	2	18½–21	46·4
147	June 30, 1953	38° 36′	73° 14′	95–100	10	8–21	51·4
146	June 29, 1953	38° 33′	73° 18′	63–65	10	7–13	54
131	June 28, 1953	38° 13′	73° 40′	145–160	1	19	45·2
137	June 28, 1953	38° 10′	73° 45′	72–73	9	9–16	54·5
140	June 29, 1953	37° 38′	74° 14′	230–265	1	13½	41·4
139	June 29, 1953	37° 38′	74° 15′	120–130	2	15½	46·4

*From tip of rostrum to end of tail.

†On the three cruises made in 1953, from June 26 to July 29, and for the several hauls made July 8, 1954, temperatures were obtained for most of the hauls with a maximum-minimum thermometer attached to an otterboard. It may be presumed that these minimum temperatures, in most cases at least, were those prevailing at or very close to the bottom, at about deepest part of haul.

**In the 6 hauls made July 8, 1954, by *Atlantis* the 210 lobsters caught fell in the following size groups : 79 were 7 to 8¾ in. ; 97 were 9 to 12 in. ; 29 were 12¼ to 15 in. and 5 were 15½ to 17½ in. measured from end of rostrum to end of tail. In the 6 hauls made September 2-3, 1956, by *Caryn*, the 89 lobsters caught fell in the following size groups : 51 were 6¼ to 8¾ in. ; 24 were 9 to 12 in. ; 11 were 12¼ to 15 in. and 3 were 15¼ to 19¼ in.

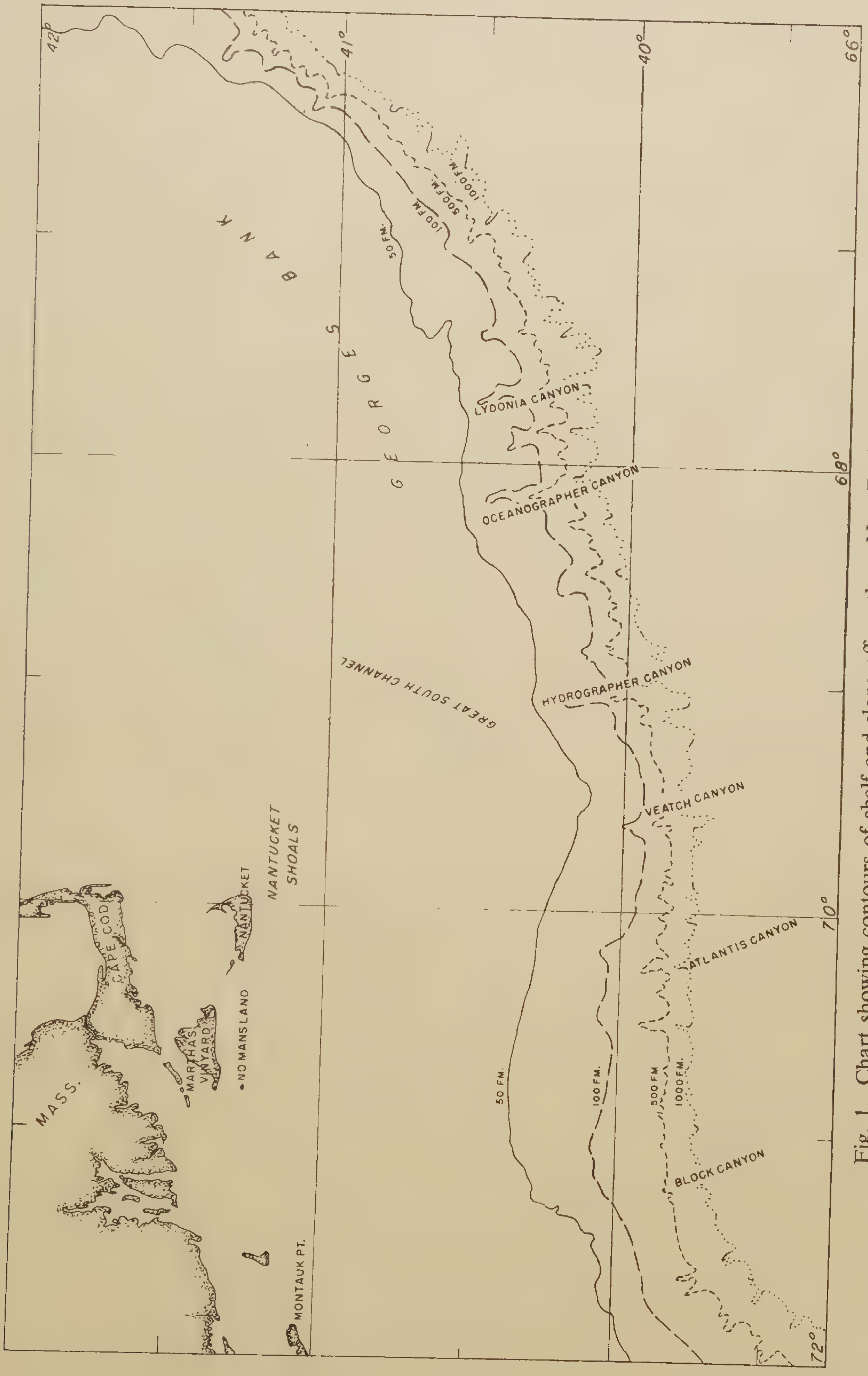
42°
41°
40°
66°
68°
70°
72°
GEORGES BANK
50 FM.
100 FM.
500 FM.
1000 FM.
LYDONIA CANYON
OCEANOGRAPHER CANYON
HYDROGRAPHER CANYON
VEATCH CANYON
ATLANTIS CANYON
BLOCK CANYON
GREAT SOUTH CHANNEL
NANTUCKET SHOALS
NANTUCKET
CAPE COD
MARTHAS VINYARD
NO MANS LAND
MASS.
MONTAUK PT.

Fig. 1. Chart showing contours of shelf and slope off southern New England and Georges Bank.

The area explored, although only about 5 to 20 miles wide, extends some 600 miles – or from the offing of La Have Bank to that of Cape Charles, Virginia, from long. 63° 17′ to 74° 15′W – and with few exceptions, the depths ranged from 70 to 730 fm (128-1340 m). Of the 217 hauls in which no apparent mishap to the gear occurred (including 15 made by *Atlantis* in 1954 and 9 by *Caryn* in 1956) 181 were deeper than 100 fm (183 m).

It should be emphasized that the purpose of our exploratory fishing was chiefly an attempt to determine the identity, distribution and relative abundance of the fishes living in this region. Therefore, lobster catches (Table 2) for the most part were incidental and the numbers taken would have been substantially greater if our efforts had been directed chiefly to seeking and exploring the most productive lobster grounds (SCHROEDER, 1955).

While several sizes of trawls were used, the hauls were too few in number to reveal any significant correlation between the width of foot-rope and the quantities of lobsters caught. Although the best catches were between depths of 70-100 fm (128-183 m), the number of lobsters taken deeper suggests that commercial fishing might also prove successful well beyond 100 fm (183 m). Such was the case, for, as a result of reports* released by the Woods Hole Oceanographic Institution, one trawler (*Sonia*) began fishing offshore for lobsters during the fall of 1953. The next year other boats joined in this fishery which has proven to be a successful one†.

The *Delaware* has reported a number of substantial catches of lobsters, mostly large in size, along the southern slope of Georges Bank. Catches per trip ranging up to 7000 lb or more were taken between long. 66° 45′ and 67° 20′W and between 69° 10′ and 69° 30′W., chiefly in depths of 175-275 fm (320-503 m), during January and November 1955 and January, March and May 1956 on those cruises when lobsters were especially sought. Thus this is conclusive evidence that large numbers of lobsters are to be found in these depths at least as far eastward as the vicinity of Lydonia Canyon (Fig. 1).

There are but few records of sizable catches of lobsters taken offshore in winter, a season when the lobster trawlers either lay up their boats or find it more profitable to seek fish. Hence, it is of interest to report 800 lb of lobsters trawled in 55-65 fm (101-119 m) SSW from No Mans Land, landed by *Cap'n Bill II* February 3, 1956 along with a fare of fluke, and 400 lb in about 76 fm (139 m) from between Hydrographer and Oceanographer Canyons, landed February 29.

To the west and south of New England, landings of lobsters taken offshore with otter trawls have shown a steady increase in the New York-New Jersey region during the past few years. These catches, compared with those taken inshore with pots, are listed in Table 3.

New Jersey landings account for the greater part of the recent large increase in the otter-trawl catch (Table 3). Thus, for the years 1950 to 1956 these catches amounted to 28·2, 29·8, 36·0, 43·6, 53·0, 61·7 and 48·4 per cent, respectively, of the total catch landed in both New York and New Jersey taken by trawls and pots. The New York landings for the same years were 14·0, 15·9, 11·4, 7·1, 12·8, 9·8 and 17·7 per cent,

---

*Published in *Atlantic Fisherman*, September and October 1952 ; *Maine Coast Fisherman*, October 1952 ; *Boston Traveler*, December 1, 1952 ; *Boston Globe*, December 28, 1952, January 25, 1953 ; *New Bedford Standard Times*, January 18, 1953.

†An account of some of the trips is given in the Appendix, p. 279.

respectively. Thus, percentagewise, the New Jersey landings of trawl caught lobsters have been tending sharply upwards while those for New York have shown but little increase during this period.

In 1955, 14 otter-trawlers from New Jersey fished 4 to 5 months for lobsters and their catch represented about 75 per cent of the total poundage for that state, the remainder being taken with lobster and fish pots, while in 1956 there were 16 lobster trawlers operating from May to September. Some of the catches were made as deep as 100-250 fms (183-457 m) (E. A. LOVERDE, private communication).

*Table 3. Lobster catch landed in New York and New Jersey for certain years from 1929 to 1956**

Year	*Pots* (lb)	*Otter trawls* (lb)	*Total catch* (lb)	*Percentage of total catch taken by otter trawls*
1929	1,386,343	26,285	1,412,628	1·8
1930	1,544,370	2600	1,546,970	0·2
1931	1,125,443	12,038	1,137,481	1·0
1932	866,641	570	867,211	
1933	703,546	6470	710,016	0·9
1935	633,100	6200	639,300	1·0
1937	625,200	10,400	635,600	1·6
1938	543,200	28,100	571,300	5·0
1939	644,400	22,000	666,400	3·3
1940	560,200	32,800	593,000	5·6
1942	460,500	43,200	503,700	8·5
1943	704,100	64,100	768,200	8·3
1944	652,000	68,500	720,500	9·6
1945	408,800	46,900	455,700	10·3
1947	502,800	106,300	609,100	17·4
1948	503,300	255,400	758,700	33·6
1949	552,900	106,400	659,300	16·1
1950	367,500	267,800	635,300	42·2
1951	221,800	186,800	408,600	45·7
1952	371,200	335,200	706,400	47·4
1953	475,800	489,500	965,300	50·7
1954	354,450	680,900	1,035,350	65·8
1955	374,370	939,170	1,313,540	71·5
1956	448,740	874,820	1,323,560	66·1

*Based on annual reports of the U.S. Bureau of Fisheries published from 1931 to 1941, for the years 1929-1938, and the U.S. Fish and Wildlife Service published from 1942 to 1956 for the years 1939 to 1954. Statistics for 1955 and 1956 are based on data furnished by Mr. E. A. LoVerde and Mr. C. T. Smith, of the U.S. Fish and Wildlife Service.

Further south small amounts of lobsters are taken by otter-trawls along with catches of fish. Such catches as entered in the published statistics include, for Maryland, 100 to 1500 lb and, for Virginia, 300 to 10,500 lb per year for the period 1944-1953. The present known southerly range of this lobster is North Carolina.

The most northerly range of the American lobster, on the other hand, is the Strait of Belle Isle. At the northern extreme, large catches of lobsters are taken off the Maritime Provinces of Canada, Quebec and Newfoundland, the landed catch there for 1950 amounting to nearly 40 million lb*. Up to the present time, however, there is no otter-trawl lobster fishery in that region. Newfoundland trawlers fishing in moderately deep and deep water seldom catch a lobster. Dr. W. TEMPLEMAN†

*For an excellent account of the fishery and habits of the lobster in Canadian waters, see WILDER, (1954).

†Private communication.

states that the *Investigator II* operating offshore all over the Newfoundland Banks and in deep water down to 400 fm (730 m), since 1946, has never caught a lobster. Furthermore, the only records which have come to his attention are :

No. of lobsters	*Locality*	*Depth*		*Date*	*Boat*
		(fm)	(m)		
1 male, $3\frac{1}{2}$ lb	46° 50′N, 57° 04′W (St. Pierre Bank)	90	165	20/3/54	*Gaultois*
1 female, $3\frac{1}{2}$ lb	46° 46′N, 56° 22′W (W of Miquelon Is.)	30	55	16/1/55	*Gaultois*
1 female, total length 14 in.	6 miles off Cape Race	24–30	44–55	18/10/54	*Blue Spray*
1 female, $12\frac{5}{16}$ in.	44° 00′N, 51° 40′W	43	79	7/5/57	

MIGRATIONS

Marking experiments indicate that lobsters, with few exceptions, do not make long migrations but tend to stay within a limited area, at least during the year or so that their marks can be recognized or their tags remain attached.

In the Magdalen area in the southern part of the Gulf of St. Lawrence (Templeman, 1936, p. 43) the greatest distances travelled by tagged lobsters were only 5 or 6 miles in 9 to 11 months, while two tagged at Prince Edward Island were recaptured about 20 and 30 miles away, as measured along an uneven shore line. Thus, in both localities, the population as a whole appears to be more or less local in character with no definite migrations, but rather a scattering and wandering of some individuals.

" From favourable warm water areas (in the vicinity of Newfoundland) where many young survive, lobsters wander slowly during their lifetime of 20 years or more and come to occupy many areas around the coast unsuitable for the survival of the young and many miles distant from the point where they originally settled at the bottom. These are the first areas to be fished out, since once lobsters are caught it takes many years for other lobsters to wander in to take their places, migration being only on the average about 2 miles a year (according to our tagging investigations in St. George's Bay, 1938-39) " (Templeman, 1941, p. 14).

Of about 100,000 lobsters tagged in Canadian waters in the past 25 years more than half were recaptured but only 3 of these had moved as much as 60 miles (Wilder, 1957 ; also 1950). From this and other evidence he concluded that the Canadian lobster population " is made up of a series of separate, independent stocks with very little mixing between areas " (Wilder, 1957, p. 7). Again, of a 1000 lobsters tagged for the Maine Department of Sea and Shore Fisheries at Monhegan, about 25 per cent were recaptured but only 9 were caught as far as 2 to $2\frac{1}{2}$ miles from the place of liberation (Harriman, 1957).

Offshore, in depths from about 100 to 275 fm (183-457 m) along the southern slope of Georges Bank and offing of Nantucket Shoals, about 2250 lobsters have been tagged* as a result of exploratory trawling by the U.S. Fish and Wildlife Research

*The tag, stamped with number and return address, was a stainless steel strip bent on one end to hook on the posterior edge of the carapace and fastened to the rostrum by a rubber band.

Vessel *Delaware* in co-operation with the Department of Natural Resources of the Commonwealth of Massachusetts :

Locality where tagged	*Date*	*No. tagged*	*No. recovered*	*Remarks*
15-30 miles E of Lydonia Canyon 67° 06′-67° 21′W	Nov. 1955	786	6*	3 nearby within few days 3 after 168-255 days, 12-25 miles N
App. 15-30 miles E of Lydonia Canyon	Jan. 1956	115	2	1 nearby 105 days later 1 after 166 days 40 miles to NE
E of Lydonia Canyon	May 1956	825	7	5 within 25-38 miles N 36-102 days later 2 within 12-23 miles W after 62-449 days
Veatch Canyon 69°14′-69° 25′W	Jan. 1956	350	7	All within 10 miles after 117-207 days
Veatch Canyon	May 1956	177	5	4 within 10 miles after 7-104 days 1 about 45 miles NE after 53 days

*In addition, a tag, but no lobster was found in the stomach of a cod taken on Nantucket Shoals in Nov. 1957, two years after the lobster was liberated.

Of the 27 recaptured (4 by the *Delaware*, 23 by fisherman), 15 were taken within a few miles of the tagging locality and 12 were more than 10 miles away. Of the latter, 9 had moved northward onto Georges Bank, a distance of about 11 to 40 miles and in depths of about 30 to 50 fm. One was taken about 45 miles to the north-east or about 60 miles south-east of Nantucket, in 38 fm. Two wandered to the west.

The paucity of recaptures from shoaler water on nearby Georges Bank, where many otter trawlers operate, indicates that relatively few of the offshore lobsters wander far from their deep water habitat, if it can be assumed that a substantial mortality and/or loss of tags* did not ensue soon after they were released. Nor is there any indication that many of them migrate or wander far to the west in either deep water (beyond 100 fm) or shoal, for none were reported west of Veatch Canyon, where, in addition to the many trawlers seeking fish, much of the commercial offshore otter trawling for lobsters occurs.

Experiences of fishermen trawling offshore have shown that an area yielding a good catch one week may be sparsely populated the next, but soon thereafter may again be productive. In such a case the poor fishing might be due to the large catches of the previous trip, but if so, certain areas, at least, soon become repopulated by lobsters which shift ground presumably from close by.

Thus far, no significant differences, either racial or subspecific, have been found to separate the inshore from the offshore stocks of lobsters. Dr. FENNER A. CHACE, Jr. of the U.S. National Museum compared several lobsters taken beyond 100 fm with shoal water specimens and found no constant differences between the two. My comparison of several specimens taken in February 1958 near Veatch Canyon, in about 60 fm, with others from close inshore substantiate this. However, Dr. CHACE points out that a large series from the two regions should be compared. If it can be determined that the inshore and offshore populations differ racially this would give added weight to the present opinion that the two populations are for the most part distinct with relatively little intermigration.

---

*Deep water lobsters, if uninjured, survive the ordeal of being hauled along in the trawl while fishing and being brought aboard from depths well beyond 100 fm, for a large percentage reach the market in lively condition. Hence, it is probable that the attachment of tags and the return of the lobsters to the sea bottom does not entail a heavy mortality. Presumably, relatively few tags are lost within the first six months or so by individuals which molt, for large lobsters are believed to shed their shells infrequently and many of those tagged ranged in weight from 5 to 7 or 8 lbs. Some were much larger. However, after the lapse of about a year the loss of the tags from this cause would become increasingly great.

While the offshore population comprises lobsters of all sizes, individuals of 2 lb or more make up a much larger percentage of the population than in inshore waters where the fishery has been intensive for many years. Lobsters are believed to grow to be very old but there appears to be no reliable data for estimating the maximum age. Individuals of 15 to 25 lb are not rare in offshore waters while the largest one recorded (WILDER, 1954, p. 5) weighed 45 lb. It is probable that these very large lobsters are more than 15 years of age and it seems logical that during such a life span some of them may wander many miles.

The early development of the lobster has long been known (HERRICK, 1896 ; 1911). The larvae have a free-swimming stage of one to two months before they settle to the bottom at a length of a little more than ½ in. and " since larvae are hatched over wide areas, and since there is yet no practical way of marking them, it is extremely difficult to determine the direction, speed and extent of their surface drift " (WILDER, 1957, p. 24). Thus we have yet to determine the origin of the larvae which take to the bottom offshore and the destination of the larvae which hatch in deep water off our coast*.

THE DEEP-WATER RED CRAB, *Geryon quinquedens*

Off the east coast in deep water, there is a species of crab (*Geryon quinquedens*), which is very good to eat, reaches a fair size, up to 2 lb or a little more, with a large one yielding 4 ounces of meat. Although it soon dies if exposed to air or water temperatures much above about 45°F (7·2°C), it will stay alive for several days if buried in ice. As otter trawlers become equipped for fishing in greater depths, this species may some day become the source of a commercial fishery, if a market for the canned meat can be established.

This crab, first described (SMITH, 1879, p. 35) from a number of very small specimens taken off Casco Bay, Maine, and off Massachusetts Bay, in about 100-160 fm (183-292 m) was later taken by the *Albatross* between the offings of Martha's Vineyard and Chesapeake Bay in depths of 535-1043 fm (980-1906 m) (SMITH, 1886). The range of *quinquedens* extends from south of Halifax (lat. 42° 37′N) to South Carolina in 100-1000 fm (183-1828 m) (RATHBUN, 1929, p. 35) and possibly to Brazil in depths of 22-1178 fm (40-2153 m) (RATHBUN, 1937, pp. 266-270)†. More recently limits given for *quinquedens* are from the offing of Nova Scotia (42° 46′N, 63° 22′W, *Cap'n Bill II* Sta 88) southward to at least the north coast of Cuba (CHACE, 1940, p. 38).

---

*For a list of references on the biology of the lobster and on the lobster fishery, see DAWSON, (1954).

†Dr. FENNER A. CHACE (private communication) points out that Miss RATHBUN evidently included two species in her *quinquedens*, the other being *G. affinis*. The specimen figured by Miss RATHBUN as *quinquedens* is really *affinis* (CHACE, 1940, p. 39). The two species are alike in general appearance and grow to about the same size. Living or fresh specimens may be readily identified by colour : *quinquedens* is red or deep orange, *affinis* creamy buff. Anatomical differences are noted by CHACE (1940, p. 40).

G. affinis probably does not occur much north of the offing of Chesapeake Bay, but is widely distributed in the lower latitudes of the Atlantic and Indian Oceans.

A brief account of the relative abundance of the red crab by depths and geographic areas, as a result of exploratory otter-trawling during 1952 and 1953, is given by SCHROEDER (1955, p. 371). Some of the figures in the latter report have been modified in the more detailed summary given in Table 4 which also includes 12 hauls made by the *Caryn* in 1948 and 1949.

Table 4. *Composite catch of deep water red crabs taken along the continental slope between the offings of Nova Scotia and of Virginia from* 1948 *to* 1953 *by the* Caryn *and the* Cap'n Bill II *arranged by depths and geographic areas. Egged females are not included*

	Area A		*Area B*		*Area C*		*Area D*	
	Long. 63° 17′-65° 59′W		*Long.* 66°00′-69° 59′W		*Long.* 70° 00′-71° 59′W		*Long.* 72° 00′-74° 15′W	
Depth (fm)	*Number of hauls*	*Average no. of crabs per haul*	*Number of hauls*	*Average no. of crabs per haul*	*Number of hauls*	*Average no. of crabs per haul*	*Number of hauls*	*Average no. of crabs per haul*
50-100	1	0	10	0	2	0	7	1
101-150	0		5	0	7	0	6	3
151-200	0		2	1	8	2	3	126
201-250	2	0	7	35	11	29	2	210
251-300	8	16	4	79	4	12	3	245
301-350	12	49	3	38	5	50	1	68
351-400	6	26	4	45	2	80	4	118
401-450	6	23	5	12	6	80	2	69
451-500	6	52	11	11	2	29	2	60
501-550	4	115	1	5	1	34	2	14
551-600	0		1	33	0		2	22
601-650	1	18	1	2	0		2	14
651-730	1	30	0		1	9	2	6

†All of the catches were made in June and July excepting a few hauls by the *Caryn* in September. The quantities listed are adjusted to represent one hour's fishing of the net on bottom. Obviously the small mesh of the trawls used was not necessary to capture red crabs and it should be emphasized again that the nets were designed to explore the fish population and that crustaceans formed but an incidental part of the catch. Furthermore, the catches of red crabs would have totalled considerably more if trawling had always been concentrated in those areas where crabs were found in greatest abundance. The larger trawls yielded, on the average, more crabs than the smaller one, as was to be expected, but no attempt was made to compensate for these differences in evaluating the results in this table.

Red crabs were so generally distributed throughout the region explored that they were caught in all but 10 of the 140 hauls made deeper than 200 fm in Areas *A* to *C* and deeper than 150 fm in Area *D* (Table 4). The most productive region was found in Area *D* in depths of 150 to 400 fm, but deeper than this all Areas, *A* to *D*, appeared to have a crab population of about the same magnitude. In the 150-200 fm zone of Area *D* (between 38° 13′-38° 44′N, 73° 01′-73° 40′W), the 3 hauls made in late June 1953 and averaging 126 crabs (Table 4) yielded 176, 152 and 44, respectively.

On the basis of our present knowledge, no explanation can be offered as to why crabs were so scarce in the 150-200 fm zones of Areas *B* and *C* as compared with Area *D* or why the latter region was the most productive one down to about 400 fm. However, it is probable that crabs are more plentiful a little shoaler than 200 fm in Areas *B* and *C* than our records indicate for Capt. Warren Vincent, while trawling lobsters to the east of Veatch Canyon (Area *B*) in the vicinity of 39° 55′N, 69° 20′W, took 12 to 20 red crabs per 1 hr tow in 175-200 fm during May 1956. He also took " many large red crabs " in 260 fm in Area *B* on his first lobster trawling trip (p. 281) in April 1957, where our exploratory trawling found the best average catch of red crabs. But Capt. Vincent and other otter trawl fishermen operating off southern New England seldom catch red crabs shoaler than this.

Most of the crabs taken can be classed as large and medium large, i.e., about 4 to 5½ in. across the widest part of the carapace, with a few reaching 6 in. The smaller ones were chiefly 3 to 4 in. in width, relatively few being less than this. Specimens with a 5½ in. carapace have a leg spread of about 23 in. In a small series of measurements, males averaged 1 in. wider in carapace than females. A male of 5 in. weighed 1 lb 7 oz. and one of 5⅝ in. weighed 2½ lb.

Males outnumbered females and in many of the hauls they comprised the entire catch. Thus, of 115 tows in which the sexes were recorded, 43 contained males only and in the others males were most often in the majority (Table 5).

Table 5. *Average number per haul of male, female, and egged female red crabs taken shoaler and deeper than* 400 fm *between lat.* 42° 46′ *and lat.* 37° 38′N.

	Shoaler than 400 fm				*Deeper than* 400 fm			
	Number of hauls	*Males*	*Females*	*Egged*	*Number of hauls*	*Males*	*Females*	*Egged*
Area *A* Long. 63° 17′-65° 59′W	21	30	9	1	18	41	10	5
Area *B* Long. 66° 00′-69° 59′W	16	38	8	3	10	19	4	0
Area *C* Long. 70° 00′-71° 59′W	16	34	8	1	10	35	10	13
Area *D* Long. 72° 00′-74° 15′W	14	76	51	24	10	30	3	0

In individual tows with a large percentage of females (adjusted to one hour's fishing), there were :

No. of tows	*Area*	*Depth zone* (fm)	*Males*	*Total females*	*Females with eggs*
1	*D*	201-250	226	219	99
2	*D*	351-400	64	226	156
1	*C*	401-450	33	141	117
1	*A*	501-550	75	65	26

These were exceptional, especially in the relatively large number of egged crabs taken, for in many hauls, none of the females carried eggs, although the hauls were all made during June and July.

The majority of the hauls, deeper than about 200 fm, throughout the areas explored, were made on muddy bottom, which was seldom of a consistency to clog the fine meshed nets. Although red crabs were relatively plentiful on this bottom, good catches were also taken on hard bottom. One haul in particular, which contained many stones, yielded 156 crabs averaging about 30 to a bushel (42° 36′N, 64° 15′W).

Bottom temperatures varied little, deeper than 200 fm :

Area	*Depth* (fm)	*Temperature*	*Depth* (fm)	*Temperature*
A	201-250	40·5 (4·7)	701-730	38·0 (3·3)
B	201-250	41·3 (5·2)	701-730	39·0 (3·9)
C	201-250	42·0 (5·5)	701-730	38·5 (3·6)
D	201-250	42·4 (5·8)	701-730	38·8 (3·8)

Thus, temperature *per se* does not appear to afford an explanation of the variations in abundance of crabs that might exist within a given depth zone (see SCHROEDER, 1955, p. 372).

Acknowledgements—Thanks are due to the captains of several otter trawlers for their co-operation in furnishing information of their experiences in the offshore lobster fishery, among them ALBERT DAHL, RUSSELL GRINNELL, JARED VINCENT and, especially, the late WARREN VINCENT* who made available records of his daily catches and other pertinent data ; to A. W. ANDERSON, D. L. HOY, E. A. LOVERDE, C. T. SMITH, R. A. SOULEN and J. L. SQUIRE, Jr., of the U.S. Fish and Wildlife Service for the most recent catch records and other useful information ; to CHARLES L. WHEELER and RICHARD W. BURTON of the Department of Natural Resources of the Commonwealth of Massachusetts for records of lobsters tagged offshore ; to Dr. FENNER A. CHACE, Jr., of the U.S. National Museum for comparing inshore and offshore lobsters for possible racial differences and for data on the deep-sea red crab ; to Dr. D. G. WILDER of the St. Andrews, N. B., Canada, Biological Station for data on tagging and migrations of lobsters in Canadian waters and to Dr. W. TEMPLEMAN for records of deep water catches off Newfoundland.

Woods Hole Oceanographic Institution
Woods Hole, Mass., U.S.A.

Contribution from Woods Hole Oceanographic Institution, No. 947.

REFERENCES

ALEXANDER A. B., MOORE H. F. and KENDALL W. C. (1915) Report on the otter trawl fishery. *Rep. U.S. Comm. Fish and Fisheries for* 1914 App. VI, 97 pp.

CHACE FENNER A. Jr. (1940) Reports on the scientific results of the Atlantis expeditions to the West Indies, under the joint auspices of the University of Havana and Harvard University. The Brachyuran Crabs. *Torreia* No. 4, 67 pp., 22 figs.

CHACE FENNER A. Jr. Private communication.

DAWSON C. E. (1954) A bibliography of the lobster and the spiny lobster. Florida State Board of Conservation 86 pp.

HARRIMAN DONALD (1957) Monhegan fisherman-biologist cooperation proved effective. In : *Maine Coast Fisherman*, Belfast, 1957, pp. 7, 10.

HERRICK F. H. (1896) The American lobster : a study of its habits and development. *Bull. U.S. Fish Comm. for* 1895 **15**, 1-252, 50 pls.

HERRICK F. H. (1911) Natural History of the American lobster. *Bull. U.S. Bur. Fish. for* 1909 **29**, 149-408, pls. 28-47.

LOVERDE E. A. Private communication.

RADCLIFFE LEWIS (1922) Fisheries Industries of the United States. *Rep. U.S. Comm. Fisheries for* 1922 App. IX, Document No. 932, 136 pp., 8 figs.

RATHBUN MARY J. (1929) Canadian Atlantic Fauna. 10. Arthropoda. 10 m. Decapoda. *Biol. Bd. Canada* 38 pp., 53 figs.

RATHBUN MARY J. (1937) The Oxystomatous and allied crabs of America. *Bull.* 166, *U.S. Nat. Mus.* 278 pp., 47 figs., 86 pls.

SCHROEDER W. C. (1955) Report on the results of exploratory otter trawling along the continental shelf and slope between Nova Scotia and Virginia during the summers of 1952 and 1953. *Papers Mar. Biol. and Oceanogr. Deep-Sea Res.*, Suppl. to vol. **3**, 358-372.

*Capt. Warren Vincent was lost at sea in July 1958, when his boat was sunk in a collision.

Smith S. I. (1879) The stalk-eyed crustaceans of the Atlantic Coast of North America north of Cape Cod. *Trans. Conn. Acad. Arts and Sci.* **5**, Art. 2, 27-138, pl. 8-12.

Smith S. I. (1886) Report on the decapod crustacea of the Albatross dredgings off the east coast of the United States during the summer and autumn of 1884. *Rep. U.S. Comm. Fish and Fisheries for* 1885 605-705, pls. 1-20.

Taylor Clyde C., Bigelow H. B. and Graham H. W. (1957) Climatic trends and the distribution of marine animals in New England. *U.S. Fish and Wildlife Service, Fish. Bull.* 115, **57**, i-iii, 293-345, 29 figs.

Templeman W. (1936) Local differences in the life history of the lobster (*Homarus americanus*) on the coast of the maritime provinces of Canada. *Biol. Bd., Canada* **2**, (1), 41-88.

Templeman W. (1941) The Newfoundland lobster fishery ; an account of statistics, methods, and important laws. *Dept. Nat. Res., Res. Bull. St. Johns*, (11), 42 pp., 4 figs.

Templeman W. Private communication.

United States Bureau of Fisheries (1924-1941) Fishery Industries of the United States. Annual reports of the Commissioner of Fisheries for 1924, 1929-1939.

United States Fish and Wildlife Service (1942-1956) Fishery statistics of the United States. Annual reports for 1939-1954.

Wilder D. G. (1954) The lobster fishery of the southern Gulf of St. Lawrence. *Fish. Res. Bd., Canada, General Service Circular* No. 24, 16 pp., 13 figs.

Wilder D. G. (1957) Researchers tag 100,000 lobsters during 25 year migration study. In : *Maine Coast Fisherman*, Belfast, 1957 pp. 7, 24.

APPENDIX

As no detailed report has been published on the methods employed, or the catches made, by the offshore lobster fleet operating off our coast, the accounts furnished through the kindness of several of the otter trawler captains, namely, Albert Dahl of the *Sonia*, Russell Grinnell of the *Metacomet*, Jared L. Vincent of the *Priscilla V* and the late Warren Vincent of the *R. W. Griffin, Jr.* follow :

Sonia. The *Sonia* is a 60 ft dragger, usually fishing with a crew of 4. In 1954, she was equipped with 3 storage containers on deck (two of them 3 ft wide, $2\frac{1}{2}$ ft deep, 12 ft long, each holding about 1600 lb of lobsters ; one 3 ft. × 2 ft × 7 ft holding about 800 lb, or a total of 4000 lb), supplied with running water from two pumps (2 in. and 3 in.). When these were filled, lobsters were packed in the hold on burlap and ice. The trawls used by Capt. Dahl had a 98 ft head rope, 105 ft sweep rope, of 4 in. mesh 24 or 30 thread throughout, boards weighing about 500 lb each and with 340 fm of $\frac{9}{16}$ in. wire on the winch.

Capt. Dahl made 7 trips up to the middle of July in 1954 and returned to New Bedford after each of these with 3500 to 5000 lb of lobsters, or a total of 30,000 lb. An average catch per haul of about $1\frac{1}{2}$ hr was 7-8 bushels in 60-80 fm and 5 bushels in 120-130 fm. Other trips the summer of 1954 were reported by Capt Dahl as follows :

" Left New Bedford July 15 ; arrived back in port, 6 p.m., July 17. Fished in area around 40° 04′N, 70° 34′–70° 37′W, chiefly in 77 fm. Caught 6000 lb of lobsters (excluding shorts, molting, damaged and egged lobsters) in 34 hr fishing ; first haul of $2\frac{1}{2}$ hr took 20 bushels ; after that caught 14-16 bushels per $1\frac{3}{4}$ hr haul. Average weight of lobsters about 2 lb. of which 75 per cent were 3 lb or less, 25 per cent of more than 3 lb but with very few extra large. Short lobsters comprised about 10 per cent by weight of the total catch on the trip ; only 1 out of 30 or so lobsters was egged.

" Arrived on the same ground as on previous trip on the afternoon of July 19. Found but few lobsters and moved eastward to area around Veatch Canyon, 69° 51′ to 69° 54′W, in 80-100 fm. Here only 7 lobsters were caught in a 2 hr drag. Returned to the original ground, vicinity of 70° 34′W, and took 10 bushels in $2\frac{1}{2}$ hr drag first haul. Fished $1\frac{1}{2}$ days on this ground and caught 4500 lb of marketable lobsters, of which about 400 lb died enroute to port.

" Left port, July 25. Arrived on grounds noon July 26. Fished until 6 p.m., July 28. Arrived New Bedford early July 29 for Thursday market. Running time about 11 hr each way. Fished in vicinity of 40° 03′N, 70° 39′W, 80-93 fm. Landed 3500 lb of lobsters in New Bedford. Two sets were negative, one because net fouled and one because sharks attacked cod end and much of the catch was lost. Hauls ran 6-7 bushels in $2\frac{1}{2}$ hr drags."

On August 17, 1954, the *Sonia* landed 4000 lb of lobsters, taken in 48 hr dragging in about 100 fm to the south of No Mans Land. Many " shedders " were returned to the water. The following trip August 22 to the same area, but fishing somewhat deeper, 120-125 fm in rough seas, 3000 lb were landed. Proportionately fewer " shedders " were taken than in the 100 fm area.

Early in July 1955, Capt. Dahl caught 8200 lb of lobsters to the south of No Mans Land in 70-77 fm. At that time 8 draggers were otter trawling for lobsters off southern New England, 1 each from Cape May and Pt. Pleasant, New Jersey, one from Greenport, Long Island, 3 from New Bedford and 1 each from Woods Hole, Massachusetts and Portland, Maine.

Metacomet. About 5000 lb of lobsters were landed on August 15, 1954 taken in the vicinity of 39° 58′N, 69° 25′W, in about 62 fm using a trawl with a 120 ft sweep and 103 ft head-rope of 4 in. stretched mesh. Another trip, of 3500 lb was landed on October 4, 1954.

On June 9, 1955, Capt. Grinnell, at sea 4 days, landed 5080 lb of lobsters at Woods Hole, after fishing in about 75 fm, 15 miles west of Block Canyon (about 71° 20′W) and on June 19, 7000 lb were brought in from the vicinity of 70°35′W, a little farther to the east. On this trip only one soft lobster was caught and very few egg-bearers.

Priscilla V. Two trips the last week of July 1954 to an area fished earlier that month by the *R. W. Griffin, Jr.* resulted in landings of 3000 and 2500 lb after trawling for 2 days and a night in each case. One-hour drags during the day and 1 to 1½ hr at night yielded no significant difference in catch per unit of effort.

Trawling in 85-86 fm to the south of Martha's Vineyard, August 14-15, 1954, in 22 hauls of about 1 hr each, the following estimated numbers and weights of saleable lobsters were taken : 1580 of 1-3 lb (3160 lb) and 150 over 3 lb (840 lb) or a total of 4000 lb. In addition, 1070 lobsters (weight not given) were soft and 900 shorts. In much the same locality, August 18-19, 1954, in 13 hauls of about 1½ hr each, 510 lobsters of 1 to 3 lb (1020 lb) and 100 over 3 lb (550 lb), or a total of 1570 lb was taken in 36 hr fishing. Also caught were 355 soft and 365 short lobsters which were released. Egged lobsters caught on these trips were not recorded.

Early in June, after trawling near Block Canyon in about 75 fm, 7700 lb were landed.

R. W. Griffin, Jr. A catch of 2800 lb of marketable lobsters obtained in the immediate vicinity of the position trawled experimentally (40° 02′N, 70° 35′W, 77 fm) by the Woods Hole Oceanographic Institution on July 8 was landed in Woods Hole, July 12, 1954, after 18 hr dragging. Most were 1-3 lb, a few were very large, but many short lobsters were thrown back.

Twenty-six drags in 44 fm in the vicinity of 40° 18′N, 69° 20′W, yielded 5200 lb of lobsters landed on October 21, 1954.

Capt. Warren Vincent kindly made available his daily records for 1955, 1956 and 1957 (Tables 6-8). " Selects " were lobsters of marketable size up to 4 lb, " large " over 4 lb in weight and " culls " were of various sizes but lacked one or both claws or were otherwise imperfect but saleable. The lobsters were kept alive below decks in tanks with running water.

During 1955 most of the catches (Table 6) were made in the vicinity of Veatch Canyon and to the south of No Mans Land in 55-90 fm, chiefly in 60-80 fm. No records are available as to the number of short, soft or egged lobsters.

During 1956 trawling was chiefly south of No Mans Land and in the vicinity of Veatch Canyon, as in 1955, but some fishing was done to the east between Lydonia and Oceanographer Canyons. On the first two trips in May, catches were made in 165-210 fm (vicinity of Veatch Canyon and to the south of No Mans Land) with fair success (Table 7) when lobsters were scarce in the usual 70-80 fm areas. By the end of May and for the rest of the season, they were taken in shoaler depths (60-80 fm). On September 7-9, however, to the south of No Mans Land, about 800-1000 lb a day were caught in 50 fm or a little more than on September 11-12 in 74-82 fm further offshore. The largest 24 hr catch during 1955-1956, on May 29-30, 1956, was 4480 lb of saleable lobsters.

Although Capt. Vincent made random notes when the proportion of non-saleable lobsters was unusually large, no methodical record was kept of short lobsters, " eggers " or " shedders " in 1956, but many were taken and returned to the water. Thus, in the period; July 22-25, trawling south of No Mans Land in 70-80 fm, in addition to about 4200 lb of saleable lobsters, about 1500 shorts and many soft lobsters and a few eggers were caught. On the July 31-August 5 trip in 58-64 fm near Veatch Canyon, about 500 lb of shorts (probably about 800 individuals) were taken and released in addition to 8070 lb of saleable lobsters landed. On August 27 only about 600 lb of saleable lobsters were caught and nearly ⅓ the total catch were shorts and ⅓ eggers.

During the spring of 1957 Capt. Warren Vincent resumed offshore trawling for lobsters (Table 8).

Table 6. Total lobster catch per trip of the R. W. Griffin, Jr. *taken off southern New England during* 1955

Days fished	lb *selects*	lb *large*	lb *culls*	lb *total*
June 13-16	2985	3990	430	7405
24-28	4400	4300	700	9400
July 4-8	5730	2640	930	9300
25-29	4880	2530	830	8240
Aug. 5-7	4190	3310	935	8435
24-30	3580	4000	1050	8630
Sept. 5-10	2450	3430	590	6470
23-28	3900	1790	1290	6980
Grand total	32,115	25,990	6755	64,860
Percentage	50	40	10	

Table 7. Lobster catch per trip of the R. W. Griffin, Jr. *taken off southern New England during* 1956

Days fished	lb *selects*	lb *large*	lb *culls*	lb *total*
May 6-10	2230	3000	370	5600
18-21	2870	3555	675	7100
27-30	2440	7785	475	10.700
June 5-11	2930	6130	440	9500
June 27-July 1	3930	3170	600	7700
July 6-12	4410	3110	680	8200
19-25	3590	3390	610	7590
July 31-Aug. 5	3800	3440	830	8070
Aug. 12-16	1340	1660	240	3240
23-27	720	810	190	1720
Sept. 7-12	1430	3150	320	4900
Grand total	29,690	39,200	5430	74,320
Percentage	40	52	8	

Table 8. Lobster catch per trip of the R. W. Griffin, Jr. *taken off southern New England and on Georges Bank during* 1957

Days fished	*Trip No.*	lb *selects*	lb *large*	lb *culls*	lb *total*
Apr. 20-25	1	1750	5995	290	8035
May 1-5	2	4130	5720	550	10,400
9-14	3	5105	5770	830	11,705
18-20	4	1575	2350	345	4270
23-30	5	3535	6230	610	10,375
June 5-9	6	1140	1950	170	3260
July 2-7	7	4720	2480	580	7780
11-18	8	2280	2240	235	4755
July 25-Aug. 1	9	860	4315	40	5215
Aug. 13-19	10	440	7685	—	8125
25-31	11	45	1435	—	1480
Grand total		25,580	46,170	3650	75,400
Percentage		34	61	5	

Following are notes concerning the 11 trips made during 1957.

Trip no.	*Vicinity of*	*Depths fished* (fm)	*No. of tows*	*fishing* (hr)	*Remarks*
1	Veatch Canyon	175-260	37	120	about 900 egged and 300 short lobsters
2	Block Canyon	165-300	34	96	at least 1500 egged lobsters (2-15 lb) and about 400 short
3	Block Canyon	160-250	44	120	many egged, few short lobsters
4	Block Canyon	170-270		44	no data on egged or short lobsters
5	Block Canyon	160-300	50	168	about 20 egged, 10 short lobsters per tow (100 egged to State Hatchery)
6	Block Canyon NE Atlantis Canyon	120-175 80-200		48 38	short trip, engine trouble
7	NE Atlantis Canyon	70-80		114	no egged lobsters, about 50 shorts per tow
8	Veatch Canyon NE Atlantis Canyon Block Canyon	55-80 75 50		84 48 48	no egged lobsters, 30-50 shorts per tow
9	Veatch Canyon	42-75		48	some short and egged lobsters
	South Central Georges Bank	30-68		110	no short lobsters, egged females present
10	South Central Georges Bank	29-32		136	large number soft lobsters, no shorts
11	South Central Georges Bank (3 days) Veatch Canyon (4 days)				saleable lobsters scarce. Many small ones a few egged females near Veatch Canyon

Capt. Vincent on July 27 (Trip 9) shifted from Veatch Canyon to south-central Georges Bank on the telephoned advice of a flounder dragger who happened upon a good lobster ground. In the next 5 days he took 4140 lb of lobsters, mostly large, in 29-32 fm, chiefly within an area of about 2-4 miles^2 in an isolated pocket of mud bottom surrounded by an extensive expanse of hard bottom. On the following trip, he landed 8125 lb from the same locality. These catches are of interest, because the regular fleet fishing on Georges Bank in depths of 50-60 fm or so has usually found lobsters to be few in number and scattered. Although this concentration cannot be explained, the locality may merely not have been intensively trawled for a long time, the lobsters may have gathered to mate and some may have wandered in from deeper water. Possibly the character of the bottom may be a factor. Offshore particularly beyond about 60 fms, good catches are made on both hard and soft bottom. This is in contrast to inshore waters, where plentiful catches are taken on hard, especially rocky bottom.

On the final trip (No. 11) in 1957, three days in this same area of Georges Bank, visited only a week earlier, yielded a catch notably smaller, possibly because the population had dispersed or, more likely, because it was decimated on the two previous trips.

Printed in Great Britain by The Salisbury Press Ltd., Publicity House, Wilton Road, Salisbury, Wilts. (15661)

Contribution No. 950

Reprint OIKOS 10:I 1959

A COMPARISON OF THE ANNUAL GROWTH PATTERNS OF *BALANUS BALANOIDES* (L.) WITH PARTICULAR REFERENCE TO THE EFFECT OF FOOD AND TEMPERATURE

BY

H. BARNES and *MARGARET BARNES*[1]

(The Marine Station, Millport, Scotland and the Oceanographic Institution,
Woods Hole[2])

Introduction

The annual growth in temperate waters of a number of cirripedes appears to be very similar: during the first year, rapid growth of the young spat follows the spring settlement and is succeeded by more moderate growth rates as the size increases during the summer; subsequently, in the autumn and winter little further growth takes place. This pattern is repeated annually as long as growth continues. Such a sequence appears to hold for *Balanus balanoides* (L.), *B. balanus* (L.) da Costa, *B. crenatus* Brug. and *Verruca stroemia* (O. Müller) (see Barnes, 1952–53, 1955 and 1958a; Barnes and Barnes 1954; Barnes and Powell 1953) at Millport, Scotland, and similar results have been obtained elsewhere (Runnström 1925; Hatton and Fischer-Piette 1932; Moore 1934; Hatton 1938; Bousfield 1954; Crisp 1954). When the effect of crowding, covering by mud or algae, and extent of intertidal exposure, are eliminated by semi-controlled raft exposures, the growth rate at any time of the year is seen to be particularly under the influence of the amount of food available. Food is particularly abundant during the planktonic phase and during the period when the young spat is growing vigorously. Indeed, it has been shown that in *Balanus balanoides* synchrony of nauplii release and the spring diatom outburst is achieved over the wide range of its distribution and the mechanism has been,

---

[1] We wish to thank Dr. B. H. Ketchum for his encouragement and help during the course of all this work, Mr. H. Turner (Jr.) who frequently made various facilities available, Mr. Dean Bumpus who provided temperature records and Mr. D. Graham who made measurements during the later part of the season.

[2] Contribution No. 950 from the Woods Hole Oceanographic Institution. One of us (H.B.) wishes to acknowledge receipt of a Research Fellowship from the Instution and leave of absence granted by the Council of the Scottish Marine Biological Association.

in part, elucidated (Barnes 1957). One of the most interesting features noted when examining the regional evidence for such synchrony was the apparently anomalous release of nauplii during December, rather than in the spring months, in the Buzzards Bay area of the American coast. However, the anomaly is only apparent; examination of the available literature (see particularly, Fish 1925) indicates that in this region there is a distinct winter diatom increase and that the synchrony is maintained. This has recently been more fully confirmed (Barnes 1958*b*; Barnes and Barnes 1958).

It was, therefore, of great interest to follow the growth of *B. balanoides* in the Buzzards Bay area under semi-controlled experimental conditions similar to those used in previous studies of the species, since synchrony of the diatom increase and planktonic phase has been interpreted to be of survival value both to the planktonic larvae and to the young vigorously growing spat. In addition to determining the growth rates of animals completely submersed, and regularly cleaned, for direct comparison with the previous results, growth of individuals and populations under normal habitat conditions were followed in detail at Woods Hole. General field observations on the growth of the species were also made over a wide extent of the eastern shores of North America for a more restricted period, namely the late summer, autumn, and early winter months.

The Material and Methods

For the estimation of growth rates when totally and continuously submersed, small stones on which *B. balanoides* had settled, were drilled and fastened to a plastic panel by stainless steel bolts; in the absence of a raft, this panel was bolted to a metal frame which was fastened to the Institution pier at Woods Hole so that its upper edge was about 2 ft below extreme low water level. At intervals the stones were brought into the laboratory, the animals cleaned and then measured; all animals had unrestricted growth. For the smaller individuals a binocular microscope with scaled ocular was used for the measurements, and for the larger animals, fine calipers with a millimetre scale. The animals were kept free from mud and sedentary organisms by cleaning carefully each time measurements were made. The stones were returned to the pier as soon as possible.

Several series were exposed; the first set, consisting of a number of different size groups, was put out in September 1956. Newly settled spat was followed from the following February and March through the summer and three size groups were exposed for a month in the following August, 1957. The mean length ($\bar{L}$) and the mean specific growth rate, *i. e.* increase in length per unit length per day ($\Delta l/\bar{l}.n$), were calculated for each series at each inspection.

The growth of shore populations was followed at Woods Hole by measuring individuals on boulders. These animals, measured by calipers and millimetre scale, were also kept free from attached algae. In addition, during a survey of the Atlantic coast large numbers of animals were measured at a number of other places, the measurements being made at various times during the late summer, autumn, and winter. The observations were supplemented by photographs.

Growth under conditions of continuous immersion

The results are shown in Figures 1 and 2. It is evident that when kept clean and totally submersed the animals grow rapidly during the autumn and winter months from September onwards as well as during the early spring. In the course of six months an increment of 9 mm length was added (Fig. 1).

During March, however, there was a slight increase in growth rate that is

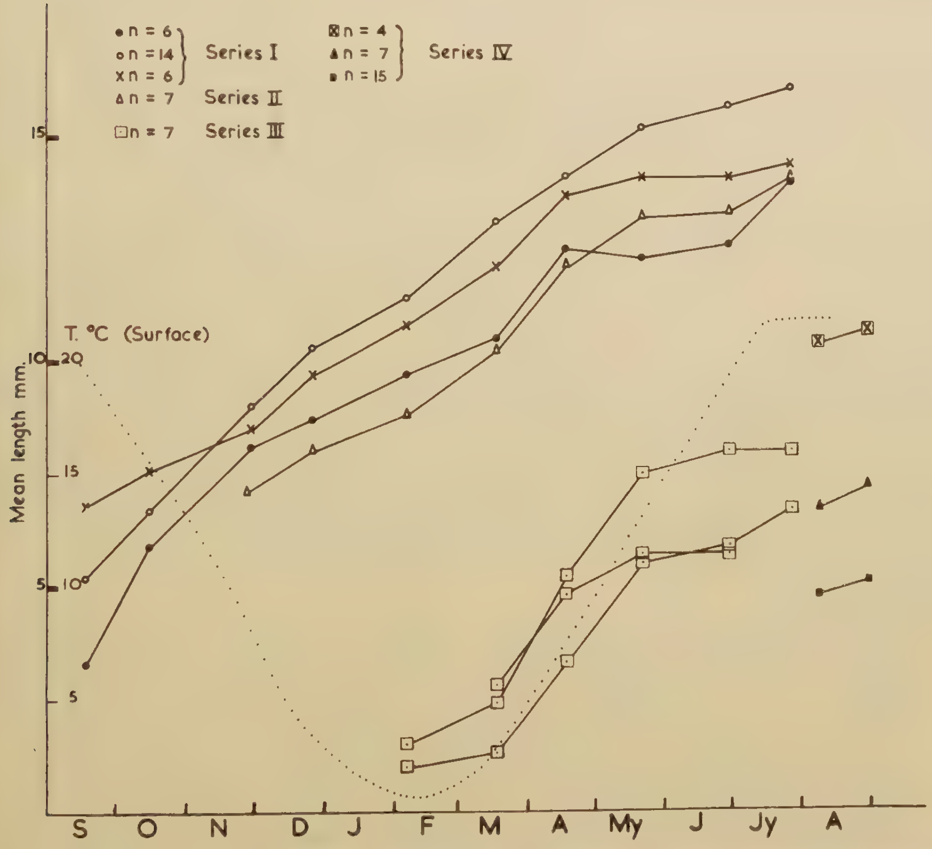

Fig. 1. Growth of *Balanus balanoides* at Woods Hole: animals on panels continuously submerged about 2 ft below extreme low water and cleaned at each inspection: sea surface temperature also shown.

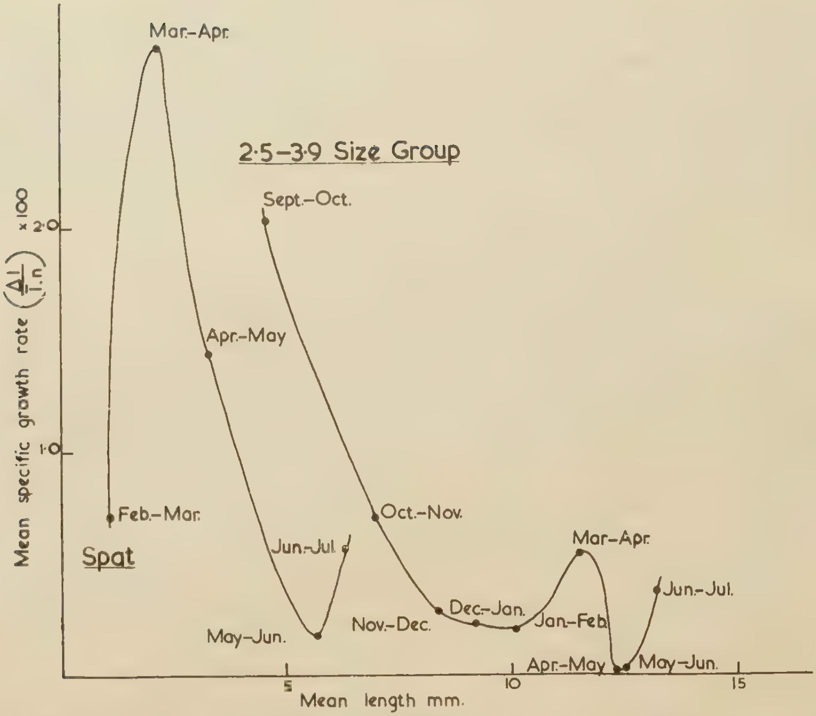

Fig. 2. The mean specific growth rate of *Balanus balanoides*, *i. e.* (increase in length per unit length per day) × 100, plotted against mean length for two series: data taken from Figure 1 for autumn and spring exposures.

somewhat more marked in the smaller animals. Young newly settled spat exposed during February and March likewise grew rapidly during the early spring. The most striking feature of the growth curves is, however, the very distinct arrest in May and June. In most groups—whether they had been growing all winter or only during the current year—there was virtually no increase in size during this period. Subsequently, in July, or in some series rather later, renewed growth takes place. In one year a size of some 14–16 mm is reached.

These changes in growth rate are more clearly brought out by examining the relation between mean specific growth rate and length (Fig. 2). When the conditions of the environment remain constant or above a level adequate for continuous growth the specific growth rate normally falls with increasing size.

It is evident from the curves for the 2.5–3.9 mm size group exposed in September 1956, for example, that after falling with increasing size during the winter months there is a rise in mean specific growth rate during March and April (even though the animals are larger) and that this is followed by a minimum in May–June with a subsequent increase. This can only be explained by either a change in the course of metabolic processes, for example, the laying down of gonads at the expense of growth, or by some considerable change in the conditions of the environment. The changes in the specific growth rate of the spat followed a similar course: a very marked rise in March–April, more marked than in Series I to III probably because of the smaller size, followed by minimum value in May–June and a subsequent rise in July. In order to elucidate these seasonal effects completely it would be necessary to be able to compare the growth rates at the *same* size at all seasons of the year. This would require large numbers of replicate exposures; furthermore, since the species breeds only once a year giving a single spat-fall in the late winter and spring, it is difficult to obtain small individuals throughout the year. However, by plotting all the specific growth rates and then grouping them in size classes it is seen that the same general trend as noted in the previous discussion of particular size groups is found: the 'normal' minimum and accelerated growth occur at the same times, but with relatively lower values as size increases (Fig. 3).

We may now attempt to explain these seasonal changes in growth rate which are in marked contrast to those previously obtained. First, it may be noted that although at the time of the accelerated growth in March and April, water

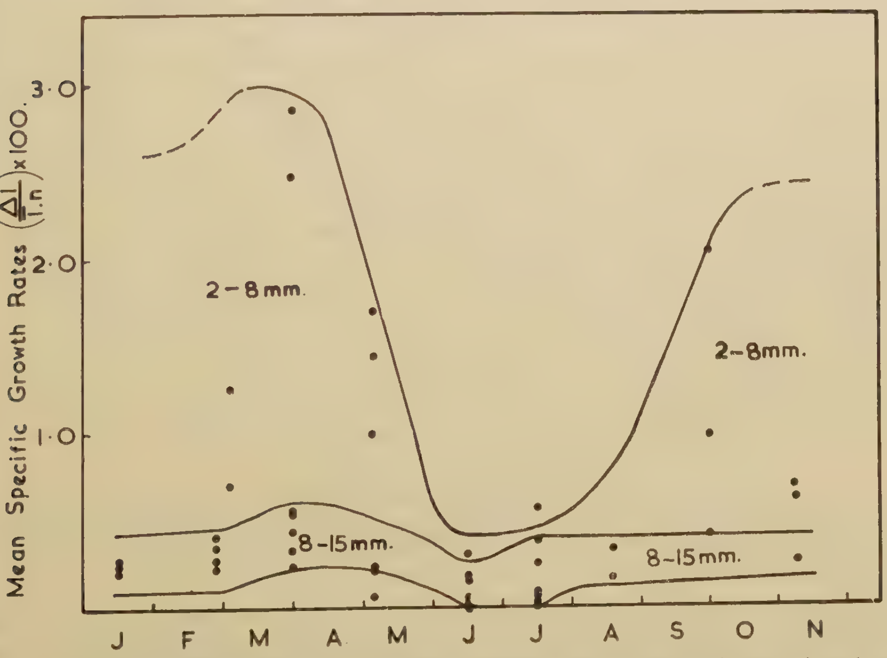

Fig. 3. The mean specific growth rate of *Balanus balanoides* for all data in Figure 1 plotted against season and values grouped into size classes to show fluctuations.

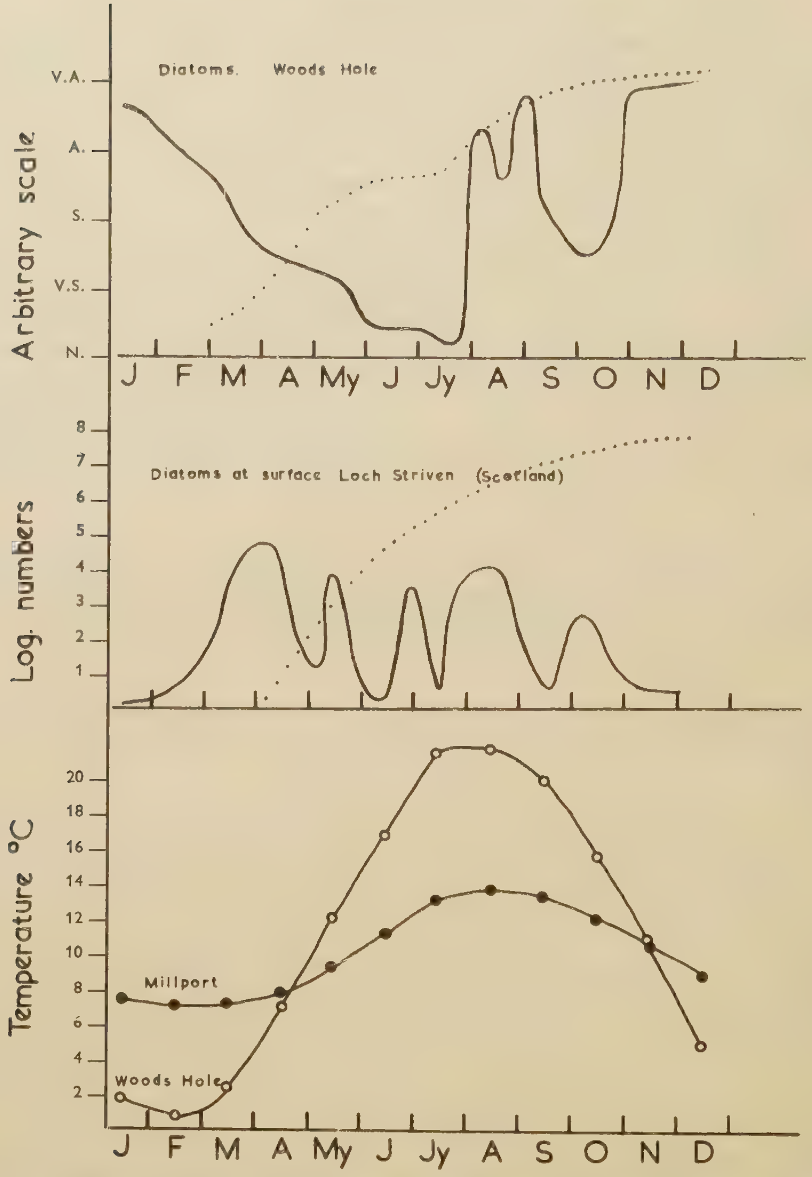

Fig. 4. Generalised form of annual growth curve (arbitrary scales) for *Balanus balanoides* at Millport and Woods Hole, together with course of respective diatom populations taken from Fish (1925) and Marshall and Orr (1927): sea surface temperature shown.

temperatures are relatively low, both the actual temperatures and their rates of change are similar to those earlier in the year when growth was less rapid. Secondly, water temperatures when growth almost ceased in May–June, were not at their highest and were indeed very similar to those during September when the growth rate was relatively high. In the case, therefore, of both acceleration and arrest of growth there is little reason to ascribe the observed effects to temperature, unless it affects the animals differently at different seasons even when they are in the same state of development or unless it has a differential effect according to the state of development of the animal. That the sensitivity to temperature of this species as regards its growth does not vary in either of these respects is suggested by the fact that all size groups are similarly affected, both the larger size groups with well developed gonads and the smaller size groups with little or no gonadal tissue. Furthermore, no such differential effects have been noted with *B. balanoides* elsewhere at various stages of its growth.

There does appear, however, to be a correlation between growth rate and availability of food as indicated by the diatom population. Whether, as seems likely, the diatoms themselves are responsible, or whether it is some associated flora and fauna (other micro-plankton, /μ flagellates, or bacteria, for example) is not known. Ideally it would be desirable to be able to compare the growth rates with the diatom populations of the same period. These data are not available. However, in spite of variations, the same *pattern* of diatom population may be expected to be repeated annually (see p. 14). The data on diatom production given by Fish (1925) may be considered, providing it is stressed that it is the annual pattern of growth that is of interest. Figure 4 shows the seasonal diatom regime at Woods Hole as given by this author and it is clearly very atypical for a north temperate region. Diatoms are present at all times of the year, but there are major outbursts during the winter that fall off somewhat in the early spring. This is followed by a period during the early summer when the standing crop of diatoms is virtually negligible. Subsequently, the standing crop rises to its winter maximum. Diatom production is apparently adequate for steady growth during the autumn and early winter; the increase of the growth rate during March cannot, however, be due to an increased diatom population. The cessation of growth in the summer may be ascribed to the almost complete absence of the appropriate kind of food, and this is followed by a resumption of growth in the late summer and autumn as diatom flowering is renewed.

The growth on the shore

Newly settled spat and young animals in their first year of growth were measured at intervals during the late spring and summer; all were kept free from algae. Although individual animals were followed throughout the observations, from time to time during the latter part of the observations, losses arising from various causes, had to be made good by measuring additional animals from the same original populations; no allowance has been made because of this in calculating the results which may as a consequence be subject to some small bias. Six groups were followed, all on a large boulder some 4 ft high firmly embedded in the sand somewhat below the mid-tide level. Three groups were located on the seaward face of the boulder facing west and three on the side at right angles to this and so running up the beach and facing to the south. This selection was made on the basis of preliminary observations indicating that differences due to scouring and exposure to the sun might be expected. On each of these faces one patch was situated 0.5 ft above the sand, a second 1 ft, and a third at 2 ft. The beach (Rocky Beach, Woods Hole) except from the west, is relatively sheltered being situated about one mile north of Penzance Point at the eastern side of the entrance ot Buzzards Bay. The results are given in Table 1.

The differences with respect to position in regard either to the total increase in size or to seasonal and spatial variations in growth are quite small, and perhaps of little ecological significance at this particular place. However, they form a distinct pattern that can be related to changes in micro-environment, and they indicate how an increase in the stresses, whose effects are here only small, could, and indeed does, affect the distribution of the species. On either the seaward front or the landward side total growth increases from top to bottom of the boulder. On the front this differentiation is most noticeable in the early growing period following settlement, namely April to May. Subsequently the specific growth rates are little different at the three levels. It is suggested that this gradation is the effect of increasing periods of immersion consequent upon decreasing 'height' up the shore and relatively greater access to food; immersion is greatest at the lowest level and this effect might be expected to be more significant when growth is most rapid, that is in the young stages. Barnes and Powell (1953) have shown a marked effect of intertidal position on the same species grown under semi-controlled conditions at Millport, Scotland; between low water and mid-tide level growth rate fell off but little, yet above mid-tide level it was roughly proportional to the hours of submergence. The base of the boulder was somewhat below mid-tide level and the top experimental patch 2 ft higher, and it is considered that differences in the degree of submergence give rise to the differences in growth rate between the top and bottom of the boulder. The fact that below about mid-tide level, the hours of submersion have relatively little effect on the growth rate indicates that there is some form of compensation for duration of submersion; whether this may be considered true acclimation is not known. We have no knowledge at present as to whether *B. balanoides* adjusts its rate of feeding during immersion to its tidal level, or whether below about mid-tide level, sufficient or excess food being available for maximum growth rate, activity is similar at all

Table 1. Growth of *Balanus balanoides* at Rocky Beach, Woods Hole.

Position	Date	Front		Side	
		L mm	$(\Delta l/\bar{l}.n)\times 100$	$\bar{L}$ mm	$(\Delta l/\bar{l}.n)\times 100$
Top	18/4	2.76	–	2.60	–
	31/5	3.92	0.81	3.89	0.92
	27/7	5.99	0.72	5.85	0.71
	28/9	7.08	0.25	6.03	0.05
	Increase	4.32	–	3.43	–
Centre	18/4	2.51	–	2.60	–
	31/5	3.77	0.93	4.76	1.36
	27/7	5.63	0.69	6.88	0.64
	28/9	7.70	0.49	7.44	0.12
	Increase	5.19	–	4.84	–
Low	18/4	2.60	–	2.10	–
	31/5	4.03	1.00	4.07	1.48
	27/7	6.89	0.84	5.83	0.62
	28/9	8.00	0.24	7.00	0.29
	Increase	5.40	–	4.90	–

levels but once the 'appetite' is satisfied feeding ceases or is reduced; the latter could not, of course, be termed acclimation.

On the side of the boulder it is evident that increase in length over the whole period is again greatest at the lowest level although the difference between the early and late part of the season is much more marked. In April and May the mean specific growth rate increases from top to bottom (even though the size is somewhat greater lower down) and this may again be ascribed to the increasing hours of submersion at the lower levels. Towards the end of the season this trend is, however, even more marked. It is considered that the relatively greater reduction in growth rate at the higher levels during the summer is due to the additional deleterious effect of the high air temperatures; these high temperatures (up to 25°C) are responsible for a considerable mortality in the first year group at the higher levels of the shore. Estimations of temperature in the middle of the day *at* the rock surface (which on a hot day may be 5–10°C higher than the free air temperature) have shown values decreasing from top to bottom and, at any given level, higher on the side facing south than on the west-facing seaward front, where this effect is not significant.

The results for the seaward front and landward side at each level may now be compared. Although at each level the total growth during the season is in all cases greater on the seaward side, it is evident that this difference is not uniform over the whole period. During the early months growth rate is higher on the landward side and more so at the lower levels. Later, however, the growth rates are similar and in August the situation is reversed with the higher growth rate on the side of the boulder at the lowest level. The side facing south tends to be warmer than the front of the boulder, and during the cold spring months it is considered that this is favourable and results in greater growth rates on this side at all levels. As already pointed out, air temperatures during August are high enough to be deleterious to the growth of this boreo-arctic species and it is considered that this not only reduces growth rate at all the upper levels but that it is more effective on the landward south-facing side than on the seaward west-facing side.

These micro-climatic effects are more readily appreciated when they are exaggerated; for example summer growth under rock overhangs in this region of high summer temperatures is greater than that on an exposed face and thus conform to this pattern. As the general level of the mean climatic conditions changes and approaches that of an unfavourable macro-climate, the animals may only survive in places where more favourable micro-climates are found (see also SOUTHWARD and CRISP 1954); it is in such places that a species may survive at the limit of its distribution. For example, *B. balanoides* may be completely absent on exposed rocks and yet be present under boulders or artificial structures in the neighbourhood of Sandy Hook, N.J. Even on a larger scale enclaves of a species may be found far more abundant than in the surrounding area due to local as distinct from regional or micro-climatic conditions.

We may now compare the growth rate on the shore with that under the conditions of total submersion on the pier. Only a restricted comparison can be made since growth on the shore was followed for a shorter period, and with longer intervals between readings. It is essential to compare animals of similar size; thus under total immersion Series II grew from 3.3 to 7.7 mm while on the lowest part of the boulder during the same period an increase from 2.6 to 8.0 mm was obtained. Under the less optimal conditions at the upper part of the landward side of the boulder growth was somewhat less, from 2.6 to 6.0 mm. These results are in accord with those found previously and already stressed, namely that, when the animals are kept free from smothering growths, little increase in growth rate is obtained by complete submersion over that at mid-tide level (BARNES and POWELL 1953). Above mid-tide level the degree of submersion has more effect; under moderate temperature conditions the reduced growth may be largely the result of a reduction in the time available for feeding but under more extreme temperature conditions, such as are experienced towards the southern limit of the species, high temperatures are probably effective in further depressing the growth rate on the upper levels of the shore.

The observations on these individuals, the spat of 1957, were made over a short period, namely the late spring and summer and the intervals between measurements were relatively long. The marked reduction in growth rate in mid-summer found with the animals kept completely submerged (see p. 4) was not detected. However, a very distinct increase in growth in the autumn and winter is visually very evident in the shore populations, for during this period new growth in the form of a basal band of white calcareous wall quite free from unicellular algae is present; it forms a striking feature of the whole population of the upper shore. By measuring groups of individuals at the upper and lower diameters of this renewed growth an estimate of the mean increase in size was obtained. At Rocky Beach mid-tide level from a mean size of 4.6 mm in early September (8th) a mean size of 9.6 mm was reached by the end of December 1956. Similar winter growth (September–December) was observed elsewhere in this area as the following measurements on populations at the mid-tide level indicate:—

Wings Neck Point, Buzzards Bay..........	4.9– 8.0 mm
Cannonville, Buzzards Bay	6.8– 8.7 mm
Nausett, Outer Cape Cod.................	10.4–12.9 mm
Narragansett, R. I.	7.5– 9.3 mm

The amount of winter growth as indicated by the striking white basal band varied from place to place and was most marked in the Buzzards Bay region. It appears to depend not only on the regional position but also on local conditions. While some such winter growth was found along the shores of Connecticut southwards into Long Island Sound, north of Cape Cod there was very little, if any; thus at East Dennis and at Provincetown it was not apparent and it is suspected that here the growth pattern was 'normal' (see p. 1).

No measurements were made beyond December—for by this time the shores were ice covered and remained so for many weeks.

The data allow a comparison to be made with the growth under complete submersion during autumn and winter. It may be estimated (see Fig. 1) that animals of the same size completely submersed at Woods Hole would have reached a size of about 9.5 mm by December, not a great deal more than that found on the shore at Rocky Beach. The similarity between winter growth on the shore and completely submersed may be largely ascribed to the relative lack of smothering algae on the shore during the winter months. At Millport, Scotland, growth under conditions of total submergence is far greater than on the shore even at low levels but here the growth is taking place in the spring and summer when the effect of smothering algae is maximal.

Discussion

It is evident that the course of the growth curve at Woods Hole is far different from that at Millport, or any other typical north temperate region (Fig. 4) and it must again be stressed that this is the case with animals grown under what may be termed semi-controlled conditions in which the effects of varying degrees of intertidal exposure and smothering by algae or sediment have been eliminated. The regime at Woods Hole is atypical for the growth curve as well as for some phases of the breeding cycle.

Although the total growth of newly settled spat at the two places during a year is similar, about 15 mm, virtually the whole of this takes place between March and October at Millport, whereas it is spread over much of the year at Woods Hole; the mean specific growth rates at equivalent sizes are, therefore, much higher at Millport where they show no fluctuations during the season but fall steadily with increasing size. There would seem to be two possible explanations for these differences. The *B. balanoides* at Woods Hole may be a genetically distinct race, physiologically adapted to the rather unusual planktonic conditions and higher summer temperatures found there. Alternately, there may be adaptation or acclimation. The first hypothesis is superficially the simpler for the ecologist, since ecologically it is self-sufficient and passes the problem to the geneticist. Such an explanation has been advanced by SOUTHWARD (1955) to explain differences between his results and those of COLE (1929) on the effect of temperature on cirral beat. The British barnacles used by Southward first showed an adverse effect of increasing temperature at 17°C whereas Cole's barnacles from Maine were unaffected up to 23°C. Furthermore, at a given temperature within the optimal range the Maine barnacles showed a frequency of cirral beat some two to three times that obtained by Southward. Now the intrinsic growth rate (under semi-controlled conditions) as measured by the specific growth rate at half maximum size (BARNES 1958) might be expected to be a function of the rate of cirral beat since the latter is in part at least a feeding activity; the order of the intrinsic growth rates of three species namely, *B. balanoides*, *B. crenatus*, *Chthamalus stellatus* has been shown to be the same as that of the order of the rate of cirral beat at any temperature within the optimal range of all three species. It would be expected, therefore, that in view of their reported high cirral beat the Maine barnacles would possess a higher specific growth rate. Neither the results of BOUSFIELD (1954) from St. Andrews, N.B., just north of Maine, nor those of the present investigation at Woods Hole, some three hundred miles to the south indicate that the growth rate of *Balanus balanoides* on the American Atlantic coast is higher than in European waters or elsewhere. The rate of cirral beat is easily affected by changes in the experimental conditions used and it seems most likely that differences in experimental techniques are responsible for the discrepancies between Cole's and Southward's results.

There are, however, further facts not in accord with gross sub-speciation. First, although a detailed morphological and biometrical study is not yet complete there are certainly no gross morphological indications of speciation. Secondly, unpublished work on the metabolism of the species over its range of distribution indicates no differences. Thirdly, the breeding is essentially similar everywhere: unusual conditions merely displace parts of the breeding cycle but only to keep it in phase with other factors. The 'displacement' can be predicted from a knowledge of its behaviour elsewhere in conjunction with the conditions of the new environment (BARNES 1957 and 1958*b*); for example, nauplii release is still synchronised with the diatom increase although the latter takes place in December. Fourthly, the distribution of *B. balanoides* is virtually continuous all along the coast from Labrador as far south as New Jersey wherever suitable substrata exist and to the north the behaviour is known to be 'normal' from the work of BOUSFIELD (1954). There is, however, a minor topographical break; the species is abundant all along the north shore of Cape Cod to Provincetown, but the eastern outer side of the Cape is largely made up of extensive stretches of shifting sand and for considerable distances there are few suitable places for barnacles to settle. Nevertheless, where such places exist, as for example, in the sheltered bay at Nausett (where behind a sand bar is a stoney beach), *B. balanoides* is abundant.

The alternative to accepting sub-speciation is to attempt to explain the changes in the pattern of growth in terms of adaptation to the different environment. This is possible by making appropriate assumptions about the response to the two major variables, namely, temperature and food. This has already been attempted (see p. 6) with regard to the *form* of the growth curve during the year, the availability of food being particularly stressed. However, certain quantitative factors must be considered.

During the autumn and winter at Woods Hole growth was continuous while the surface water temperature was falling from 20°C to 1°C, and at least for the first part of this period the food was apparently abundant as a result of the considerable winter diatom increase. There is no suggestion of any increase in the growth rate with decreasing temperature and it seems unlikely, therefore, that water temperatures of the order of 20°C were having any depressing effect on the growth rate even during early autumn. It may be noted that SOUTHWARD (1955) has indicated no change in the Q_{10} of the cirral beat between temperatures of 5°–20°C, and further unpublished experimental studies on the local (Woods Hole) population substantiate this with respect to other metabolic processes. By the end of October the temperature had fallen to some 12°C—a temperature commonly encountered by the species in many parts of its range. Nevertheless, the specific growth rate at equivalent sizes was only about one-third that observed at Millport during the spring and early summer. In view of the fact that at Millport almost the same growth rate is maintained when the animals are submersed for only half their time, it seems unlikely that during the very intense winter diatom outburst at Woods Hole the quantity of diatoms, in terms of protein, fat, or carbohydrate, was inadequate to support a higher growth rate. For the same reason it would seem that the increased growth rate in the spring cannot be due to an increase in the availability of food. The virtual cessation of growth in May–July when temperatures are similar to those in October and when growth was quite moderate, does seem to be related to the extreme paucity of food during this period; the situation is analogous to that at Millport in late autumn and winter although here the temperatures are somewhat lower.

It is, of course, possible that there is some seasonal variation in hormonal control. However, for much of the year the animals at any given time are in the same state of development at Woods Hole as elsewhere. The major difference is in the earlier 'spawning', i. e. release of nauplii. Thus, if it were assumed, for example, that the absence of winter growth at Millport were only partly due to absence of food, but also dependent upon a change in endocrine control inhibiting growth during the period when the eggs were being incubated, then a similar effect might lead to a relatively lower rate of growth during autumn at Woods Hole even in the presence of food. There is no evidence that such is the case. Thus, if animals carrying embryos during the winter at Millport are transferred to diatom-rich water they feed rapidly for long periods and normal moulting then takes place.

It appears that one must consider not only the quantity but the 'quality' of the food available in any attempt to explain the reduced growth rate. We have only evidence from earlier years. FISH (1925) pointed out that the diatom components at Woods Hole (and similar conditions are found in Long Island Sound) are much different from those present in the Gulf of Maine or further north. The winter maximum is shared by a large number of species (see also LILLICK 1940); *Rhizosolenia alata* is usually early in abundance, later to be replaced by *Leptocylindrus danicus* and *Skeletonema costatum*. Also abundant, and according to Lillick co-dominant, are *Ditylium brightwelli*, *Thallassionema nitzschioides*, *Rhizosolenia setigera*, *R. imbricata* var. *shrubsolei*, and *Chaetoceros sociale*, oceanic forms. In the late spring and early summer it has already been noted that the diatom flora is sparse; it consists largely of neritic and tychopelagic forms and includes, *Guinardia flacada*, *Leptocylindrus danicus*, *Thallassionema nitzschioides*, *Skeletonema costatum*, *Corethron hystix*, *Nitzschia seriata*, and *Chaetoceros* sp. The summer maximum is largely *Rhizosolenia semispina* or *R. calca-avis* and also contains a large number of pigmented flagellates.

As LILLICK (1940) and BIGELOW, LILLICK, and SEARS (1940) have stressed, not only is there a strong resemblance all over the boreal regions as regards the cycle of diatom production, but there are considerable similarities as to the generic and even specific composition of the flora at various points in this cycle; however, compared with western Atlantic waters *Skeletonema costatum* plays a much greater part on the European coast.

At Woods Hole, apart from the very mixed character of the diatom flora, its very different cycle and different composition at any given season compared with a typical boreo-arctic region, it is evident that although many north temperate forms are often present there are also many south temperate and even tropical species particularly during the summer months. The available nutrients are limited and with these mixed floras there can hardly ever be the strong outbursts of a boreo-arctic or north temperate flora type that characterizes such regions.

It is tentatively suggested, therefore, that the nutritional requirements of *Balanus balanoides*—a boreo-arctic species—are most completely (or even *only* completely) met by the seasonal cycle and specific composition with which it is associated in such regions. Elsewhere, although the species survives and may be abundant, the diatom flora is less adequate for growth; to some extent this may be off set by a longer growing period. Indeed it may be put forward as a general principle that lack of the right kind (rather than quantity) of food, namely that with which it is typically associated, may be yet another factor determining the limits of a species.

It is, of course, quite unknown—on the preceeding hypothesis—what form this 'quality' associated with a boreo-arctic fauna and its seasonal cycle takes. It may be nutritional value as regards the general metabolism of the animal; it may be the presence of some micro-nutrient required either in general or specialised metabolic processes. Since the presence of food appears to stimulate cirral activity it is possible that it is an effect associated with external metabolites produced by the appropriate flora.

In the foregoing discussion the emphasis has been laid on the available food —its quantity and quality. In considering the form of the annual growth curve the difficulty of separating the effect of food and that of temperature in observations of this kind was emphasised. The evidence does, however, suggest that in the presence of abundant food temperature has very little effect on specific growth rate. On the other hand it has been shown that over the normal habitat range the frequency of cirral beat has a Q_{10} of about 2 (SOUTHWARD 1955) and one would expect temperature on this evidence to have a considerable effect on feeding and growth. A similar discrepancy has been found for larval activity; the rate of transition of Stage I to Stage II nauplii has a Q_{10} of about 2, and yet the field evidence indicates a similar length of the planktonic phase at different places with widely different temperatures (BARNES and BARNES 1958). This problem may be further considered.

B. balanoides have been grown on the raft at Millport in spring and late

Table 2. Growth rate of *Balanus balanoides* at different seasons at Millport.

Date	$\bar{L}$ mm	Specific Growth Rate × 100	T°C	Date	$\bar{L}$ mm	Specific Growth Rate × 100	T°C
1 May	1.5	–	9.2	11 July.......	2.1	–	12.6
28 May	4.9	3.94	10.7	5 Aug.......	4.7	3.06	13.6
23 June	9.8	2.56		26 Aug.......	9.0	2.40	

summer using small animals of the same size group. The mean length at the beginning of the experiment was about 2 mm and for each exposure 20 animals were followed. The results are given in Table 2.

The temperature differences between the two sets of exposures are not great —only some 3°C—but even so there is no indication of a higher specific growth rate at the higher temperature; the values are very similar. Two periods in which the temperatures were different and in which observations were made on animals of similar size groups are available at Woods Hole. In the autumn a size of 5.9 mm was reached from one of 3.3 mm in a period of 28 days when the mean temperature was 17°C (19° to 15°C) while later in the year 34 days were required for the same increase (read from the graph, Fig. 1) at a mean temperature of 8°C (5° rising to 11°C). Somewhat longer is taken at the lower temperature.

Comparisons on natural populations are less reliable in view of the effects of varying intertidal exposure, smothering by algae, and physical restriction of growth due to crowding. However, the difficulties are minimized by taking only the initial stages. Data, variable as to details, have been given by Runnström (1925) for Herdla, Norway, by Hatton and Fischer-Piette (1932) and Hatton (1938) for St. Malo, by Moore (1934) for Port Erin, by Bousfield (1952-53) for St. Andrews, N.B., and by Feyling-Hanssen (1953) for Spitzbergen. The results are tabulated in Table 3.

In view of the difficulties of interpretation to which reference has already been made, it is hardly profitable to discuss these results individually or in great detail. There is certainly a suggestion of a slightly reduced growth rate in regions of extremely low temperature but no really consistent trend and no indication of a value of Q_{10} approaching 2.

Now it is normal for these early stages to be growing when diatoms are abundant in the plankton and under these conditions temperature appears to have relatively little effect on the growth rate. What form this compensation takes is not known (see p. 10). If the cirral activity follows a pattern required by a Q_{10} of 2 without any acclimation then feeding must cease at the higher temperatures if it is assumed that feeding efficiency is constant and proportional to the rate of cirral beat. Alternately, cirral activity may continue at a rate appropriate to the temperature of the environment but once the appetite is

Table 3. Growth of young spat, *Balanus balanoides*.

Place	Dates	Days	Growth
St. Malo	15/4–15/5	30	1.7–2.7 = 1.0 mm 1.5–2.6 = 1.1 mm
Port Erin................	14/5–19/6	35	1.6–2.4 = 0.8 mm
Spitzbergen..............	28/6–31/7	34	1.5–2.3 = 0.8 mm
Herdla	1/4– 1/5	30	1.4–2.0 = 0.8 mm
St. Andrews, N.B.	1/6– 1/7	30	1.4–2.5 = 1.1 mm

satisfied food may be rejected (BARNES and REESE 1958). Temperature acclimation is an alternative but further details on the type of cirral beat, its relation to macro- and micro-feeding and respiration, and any differential effects of temperature in relation to these two processes would be valuable. It is also hoped that experiments on the effect of temperature on growth rate when the available food is sub-optimal will help to elucidate the factors involved.

Summary

1. The growth pattern of *Balanus balanoides* is discussed: typically growth is rapid during the spring following settlement, slows down during the summer and virtually ceases during the winter.
2. References are made to the unusual conditions at Woods Hole and attention drawn to the fact that synchrony of planktonic phase and diatom abundance is maintained.
3. Growth of marked individuals has been followed on panels kept continuously submerged and on shore populations. In both cases the animals were kept free from algae so that comparisons could be made with the results elsewhere.
4. Growth is moderate and continuous during the autumn and winter, slightly accelerated during the spring and for a short period in the summer almost ceases.
5. Temperature does not appear to be the controlling factor.
6. There is a strong correlation between the course of the diatom population —with a distinct winter maximum—and the course of the growth curves.
7. Some effects of micro-climate are demonstrated.
8. Even at the height of the diatom increase at Woods Hole the specific growth rates, at any particular size, are less than those under similar conditions at Millport. It is suggested that the kind of food as well as the amount must be taken into account. The diatom flora and its sequence at Woods Hole are not typically boreo-arctic in character. The quality of the food may be a factor in limiting a species.
9. The question of acclimation is discussed.

References

Barnes, H., 1952–53: The effect of light on the growth rate of two barnacles *Balanus balanoides* (L.) and *B. crenatus* Brug. under conditions of total submergence. Oikos, *4*: 104–111.

— 1955: The growth rate of *Balanus balanoides* (L.). Oikos, *6*: 109–113.

— 1957: Processes of restoration and synchronization in marine ecology; the spring diatom increase and the 'spawning' of the common barnacle, *Balanus balanoides* (L.). Ann. Biol., *33*: 67–85.

— 1958 a. The growth rate of *Verruca stroemia* (O. Müller). J. Mar. Biol. Ass. U. K., *37*; 427–433.

— 1958 b. Temperature and the life cycle of *Balanus balanoides* (L.). (in press).

— & M. Barnes, 1954: The general biology of *Balanus balanus* (L.) da Costa. Oikos, *5*: 63–76.

— 1958. The rate of development of *Balanus balanoides* larvae. Oceanogr. and Limnol., *3*: 29–32.

— and H. T. Powell, 1953: The growth rate of *Balanus balanoides* (L.) and *B. crenatus* Brug. under varying conditions of submersion. J. Mar. Biol. Ass. U.K., *32*: 107–128.

— and E. S. Reese, 1958: Feeding in the pedunculate cirriped *Pollicipes polymerus* J. B. Sowerby. Proc. Zool. Soc. Lond., (in press).

Bigelow, H. B., L. Lillick and M. Sears, 1940: Phytoplankton and planktonic protozoa of the off shore waters of the Gulf of Maine. Part I. Numerical distribution. Trans. Amer. Phil. Soc., (N.S.), *31*: 149–191.

Bousfield, E. L., 1954: The distribution and spawning seasons of barnacles on the Atlantic coast of Canada. Ann. Rept. Nat. Mus., Canada for year 1952–53, Bull. 132, 112–154.

Cole, W. H., 1929: The relation between temperature and the pedal rhythm of *Balanus*. J. Gen. Physiol., *12*: 599–608.

Crisp, D. J., 1954: The breeding of *Balanus porcatus* (Da Costa) in the Irish Sea. J. Mar. Biol. Ass. U.K., *33*: 473–496.

Feyling-Hanssen, R. W., 1953: The barnacle *Balanus balanoides* (Linné 1766) in Spitzbergen. Norsk Polarinstitutt Skrifter, Nr. 98, 64 pp.

Fish, C. J., 1925: Seasonal distribution of the plankton of the Woods Hole region. Bull. U.S. Bur. Fish. (Washington), *41*: 91–179.

Hatton, H.: 1938: Essais de bionomie explicative sur quelques espèces intercotidales d'algues et d'animaux. Ann. Inst. océanog., N.S., *17*: 241–348.

— & E. Fischer-Piette, 1932: Observations et expériences sur le peuplement des côtes rocheuses par les Cirripèdes. Bull. Inst. océanogr., Monaco, No. 592, 15 pp.

Lillick, L. 1940: Phytoplankton and planktonic protozoa of the off shore waters of the Gulf of Maine. Part II. Qualitative composition of the planktonic flora. Trans. Amer. Phil. Soc. (N.S.), *31*: 193–234.

Marshall, S. M., & A. P. Orr, 1927: The relation of the plankton to some chemical and physical factors in the Clyde Sea Area. J. Mar. Biol. Ass. U.K., *14*: 837–868.

Moore, H. B., 1934: The biology of *Balanus balanoides*. I. Growth rate and its relation to size, season and tidal level. J. Mar. Biol. Ass. U.K., *19*: 851–868.

Runnström, S., 1925: On the biology and development of *Balanus balanoides* (Linné). Bergen Mus. Aarbok, Nr. 5.

Southward, A. J., 1955: On the behaviour of barnacles. I. The relation of cirral beat and other activities to temperature. J. Mar. biol. Ass. U.K., *34*: 4) 3–422.

— & D. J. Crisp, 1954: The distribution of certain intertidal animals round the Irish coast. Proc. Roy. Irish Acad., *57*: 1–29.

Contribution No. 954

Reprinted from THE ATMOSPHERE AND THE SEA IN MOTION
The Rossby Memorial Volume
The Rockefeller Institute Press and Oxford University Press 1959

On the Thermal Unrest in the Ocean

By

Bernhard Haurwitz
New York University

Henry Stommel
Woods Hole Oceanographic Institution[1]

Walter H. Munk
Scripps Institution of Oceanography, La Jolla[2]

Abstract

Rossby (1937, 38) has argued from theoretical grounds that there should be a great deal of thermal unrest in the deep ocean, partly due to variable wind-stresses associated with storms. Defant (1936, 1950, etc.) has suggested that internal tidal waves are a practically ubiquitous feature of the ocean, and has presented many analyses of rather short series of observations in evidence. As Haurwitz (1954) has indicated, the chief uncertainty involved in all discussions to date has been the result of the series of observations being too short: often only a few days. The purpose of this paper is to present a preliminary analysis of portions of temperature data obtained since Dec. 8, 1954 on two resistance thermometers located on the bottom off Bermuda at depths of 50 and 500 meters, the data being recorded regularly for several years now. The analysis for tidal periods, inertial periods, and shorter periods of the Brunt-Väisälä type is described.

I. Introduction

In two pioneer studies of the response of the ocean to transient wind-stresses, Rossby (1937—38) demonstrated theoretically that internal inertial gravity wave motions are induced in the deep stratified layers of the sea, thus suggesting a mechanism for stirring deep water. These theoretical results are of fundamental importance as indicative of a process of mixing which may play a central role in the general circulation of the deep ocean: "—because of the variability of the surface stresses it appears probable that vigorous inertia oscillations must develop in stratified media and express themselves as a marked intensification of the large scale horizontal turbulence..." (Rossby 1938, p. 248). These investigations stimulated theoretical studies by Cahn (1945), and others, the latest being a study by Veronis and Stommel (1956) which contains a summary of other studies.

In addition there is a very large literature concerning internal tidal waves in the ocean, among

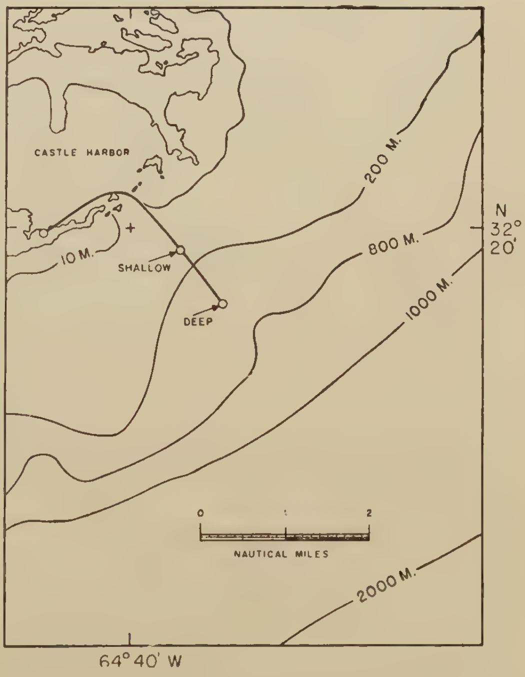

Fig. 1. Bathymetric Chart of Portion of Bermuda showing approximate location of the shallow and deep thermistors, the cable, and of the shore installation.

---

[1] Contribution No. 954 from the Woods Hole Oceanographic Institution and No. 229 from the Bermuda Biological Station.

[2] Contribution from the Scripps Institution of Oceanography, new series.

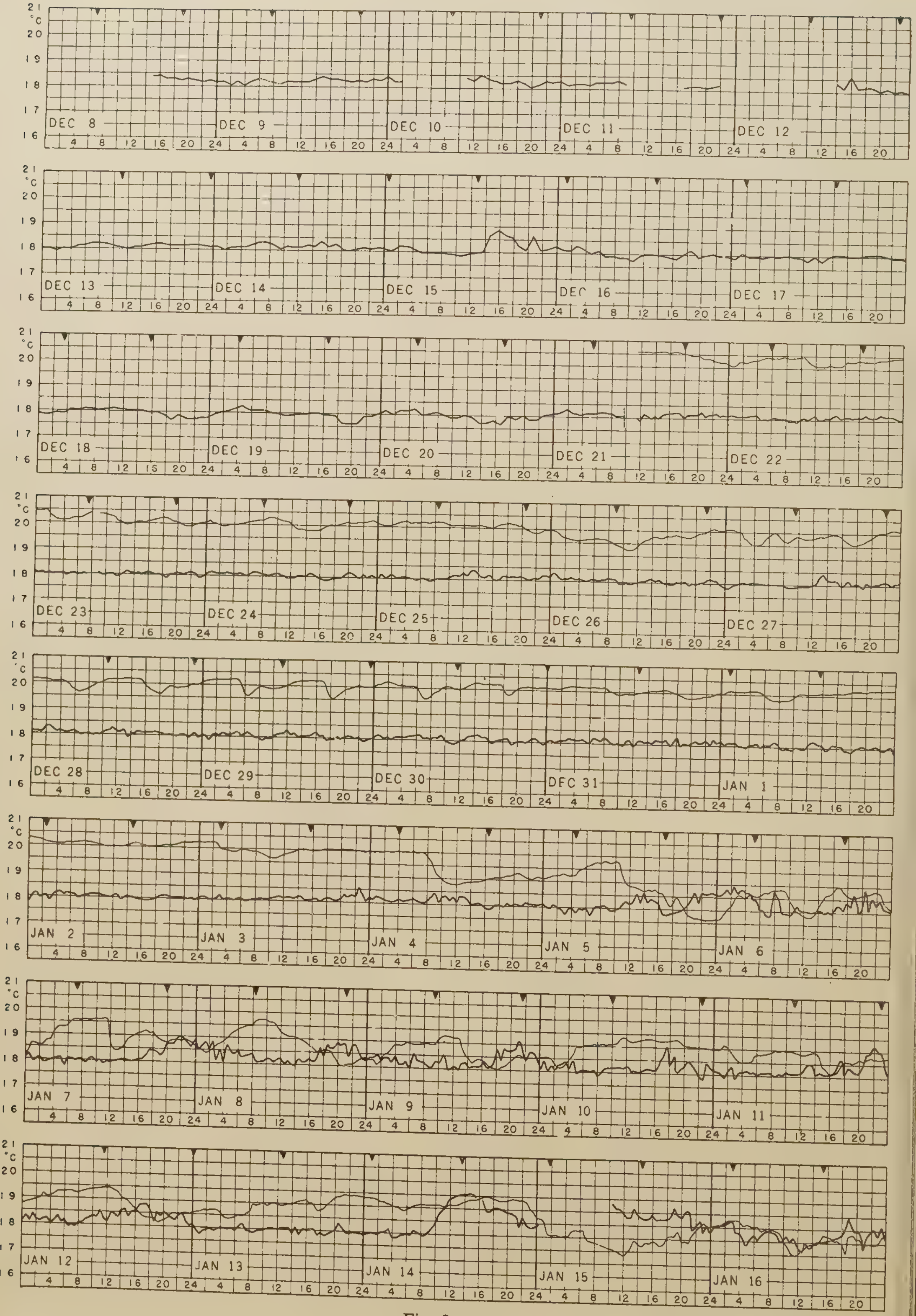
21
°C
20
19
18
17
16
DEC 8
DEC 9
DEC 10
DEC 11
DEC 12
DEC 13
DEC 14
DEC 15
DEC 16
DEC 17
DEC 18
DEC 19
DEC 20
DEC 21
DEC 22
DEC 23
DEC 24
DEC 25
DEC 26
DEC 27
DEC 28
DEC 29
DEC 30
DEC 31
JAN 1
JAN 2
JAN 3
JAN 4
JAN 5
JAN 6
JAN 7
JAN 8
JAN 9
JAN 10
JAN 11
JAN 12
JAN 13
JAN 14
JAN 15
JAN 16
4 8 12 16 20 24

Fig. 2a.

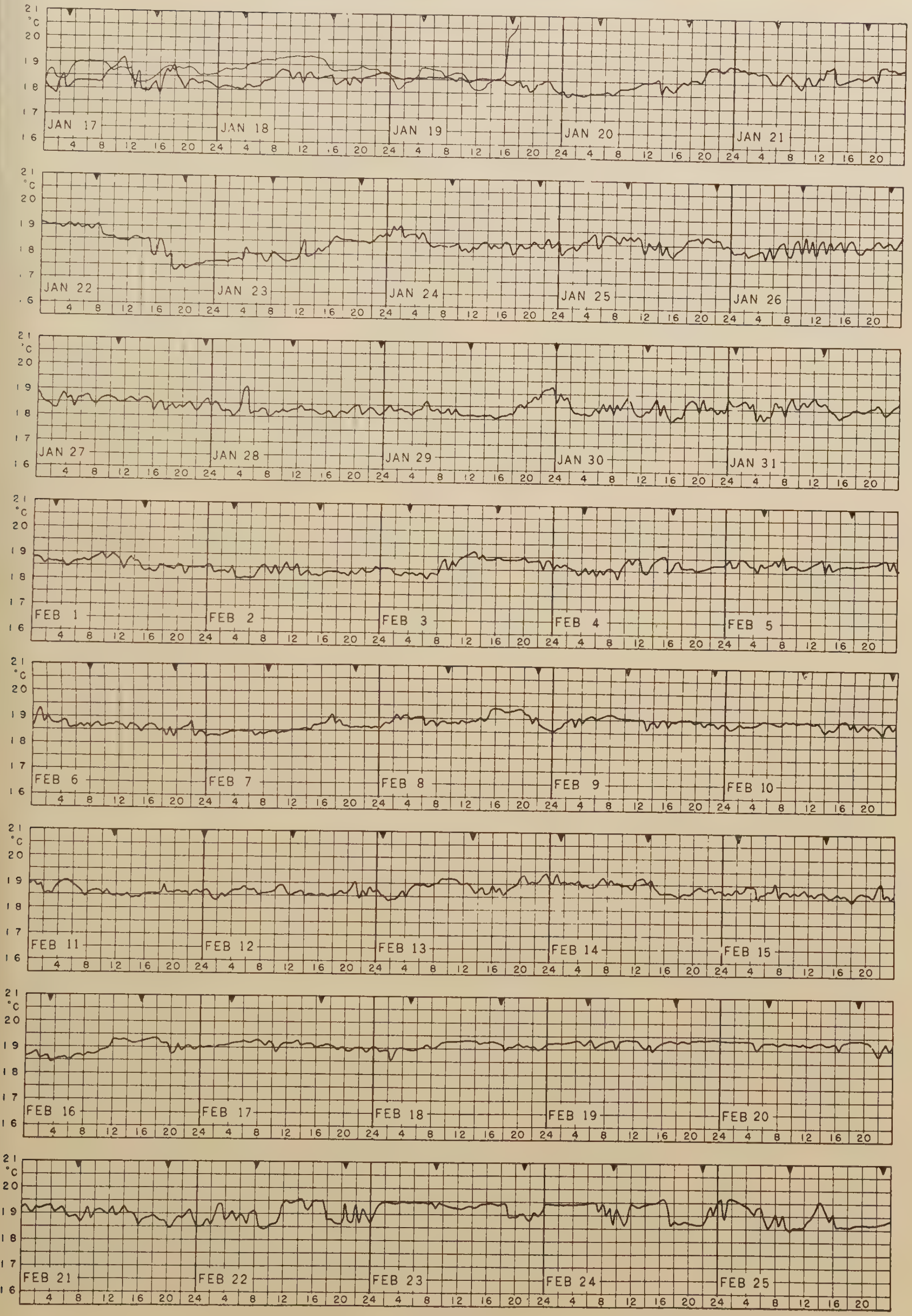
21
°C
20
19
18
17
16
JAN 17
JAN 18
JAN 19
JAN 20
JAN 21
JAN 22
JAN 23
JAN 24
JAN 25
JAN 26
JAN 27
JAN 28
JAN 29
JAN 30
JAN 31
FEB 1
FEB 2
FEB 3
FEB 4
FEB 5
FEB 6
FEB 7
FEB 8
FEB 9
FEB 10
FEB 11
FEB 12
FEB 13
FEB 14
FEB 15
FEB 16
FEB 17
FEB 18
FEB 19
FEB 20
FEB 21
FEB 22
FEB 23
FEB 24
FEB 25
4
8
12
16
20
24

Fig. 2b.

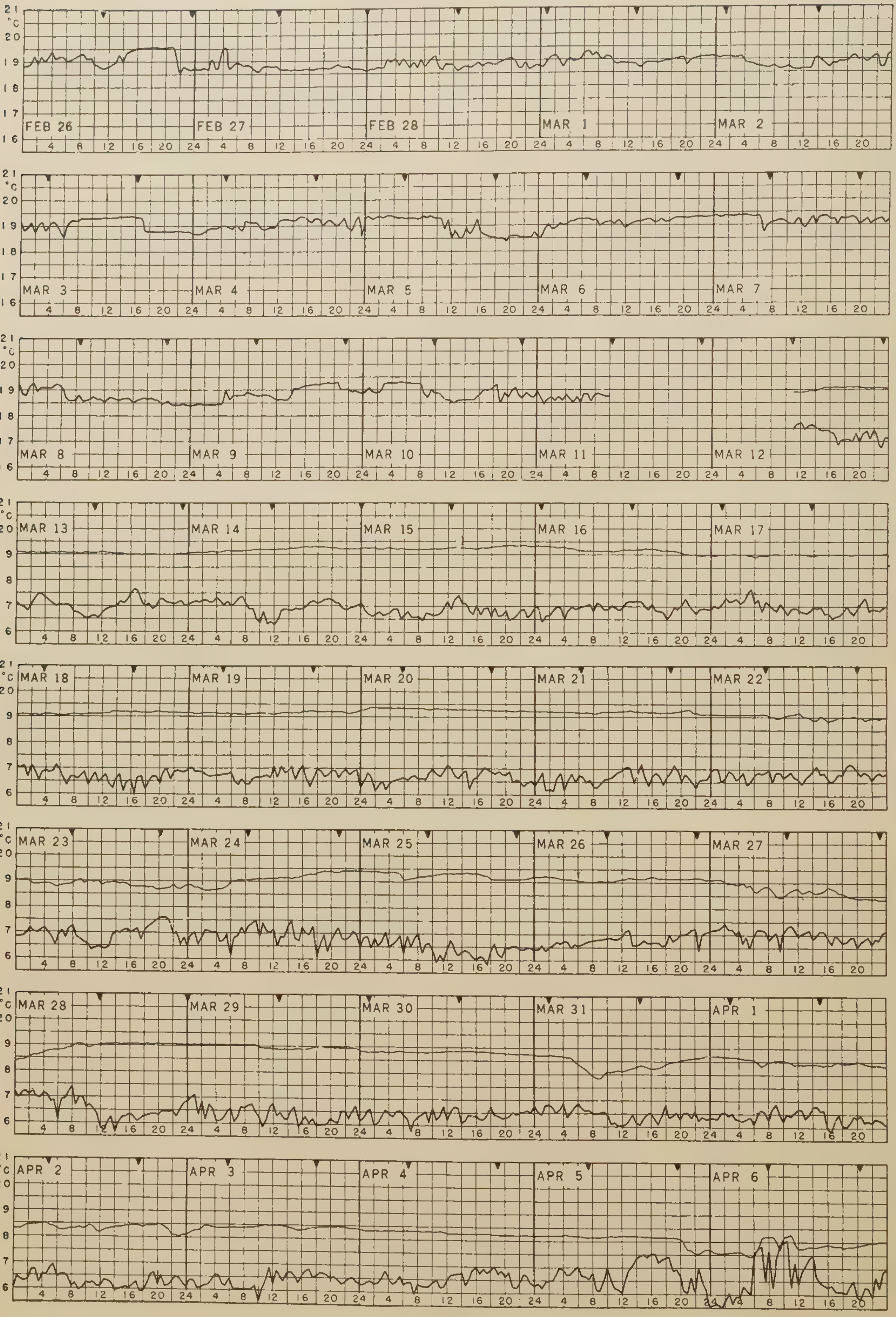
21
°C
20
19
18
17
16
4
8
12
16
20
24
FEB 26
FEB 27
FEB 28
MAR 1
MAR 2
MAR 3
MAR 4
MAR 5
MAR 6
MAR 7
MAR 8
MAR 9
MAR 10
MAR 11
MAR 12
MAR 13
MAR 14
MAR 15
MAR 16
MAR 17
MAR 18
MAR 19
MAR 20
MAR 21
MAR 22
MAR 23
MAR 24
MAR 25
MAR 26
MAR 27
MAR 28
MAR 29
MAR 30
MAR 31
APR 1
APR 2
APR 3
APR 4
APR 5
APR 6

Fig. 2c.

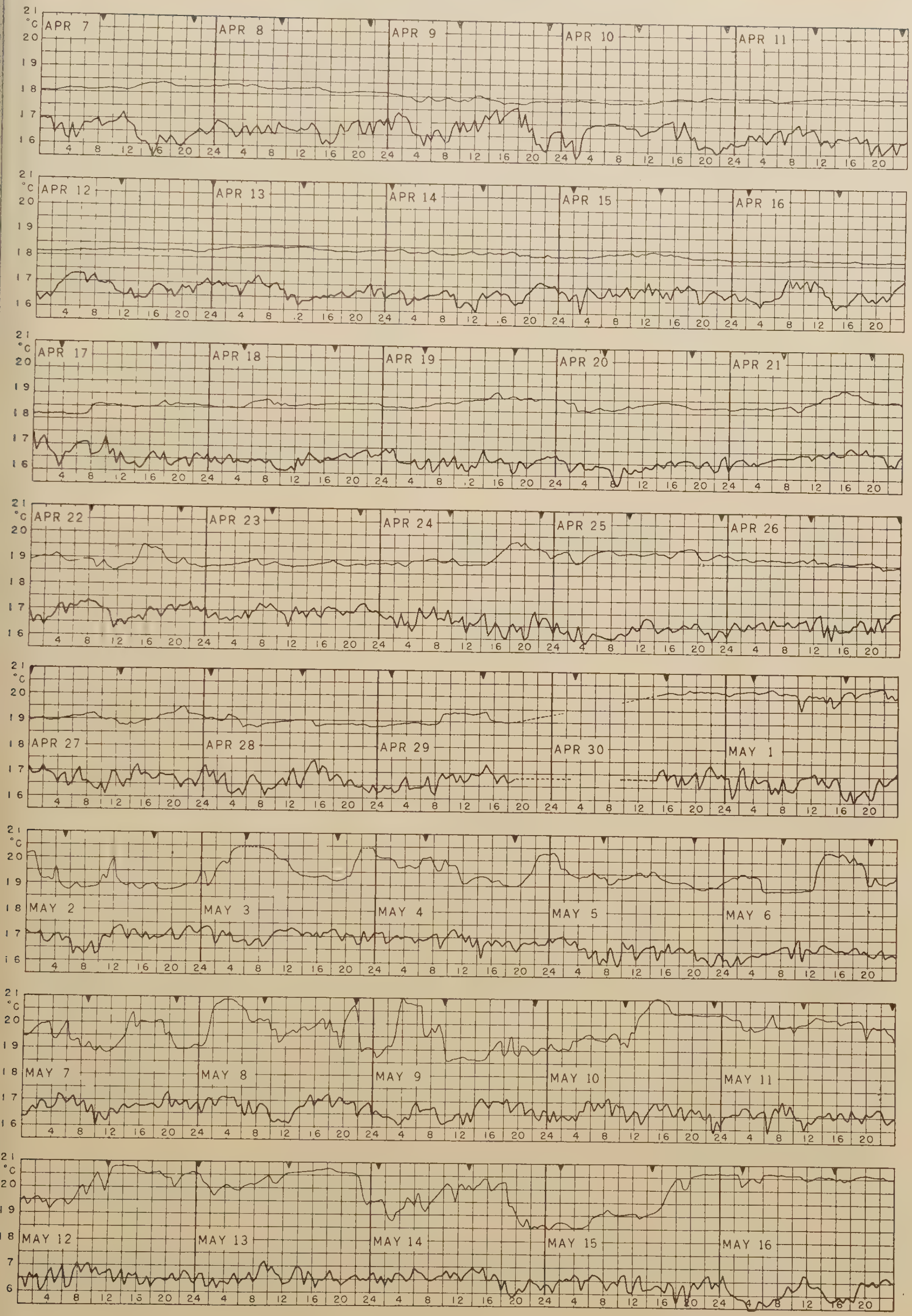
°C
21
20
19
18
17
16
4
8
12
16
20
24
APR 7
APR 8
APR 9
APR 10
APR 11
APR 12
APR 13
APR 14
APR 15
APR 16
APR 17
APR 18
APR 19
APR 20
APR 21
APR 22
APR 23
APR 24
APR 25
APR 26
APR 27
APR 28
APR 29
APR 30
MAY 1
MAY 2
MAY 3
MAY 4
MAY 5
MAY 6
MAY 7
MAY 8
MAY 9
MAY 10
MAY 11
MAY 12
MAY 13
MAY 14
MAY 15
MAY 16

Fig. 2d.

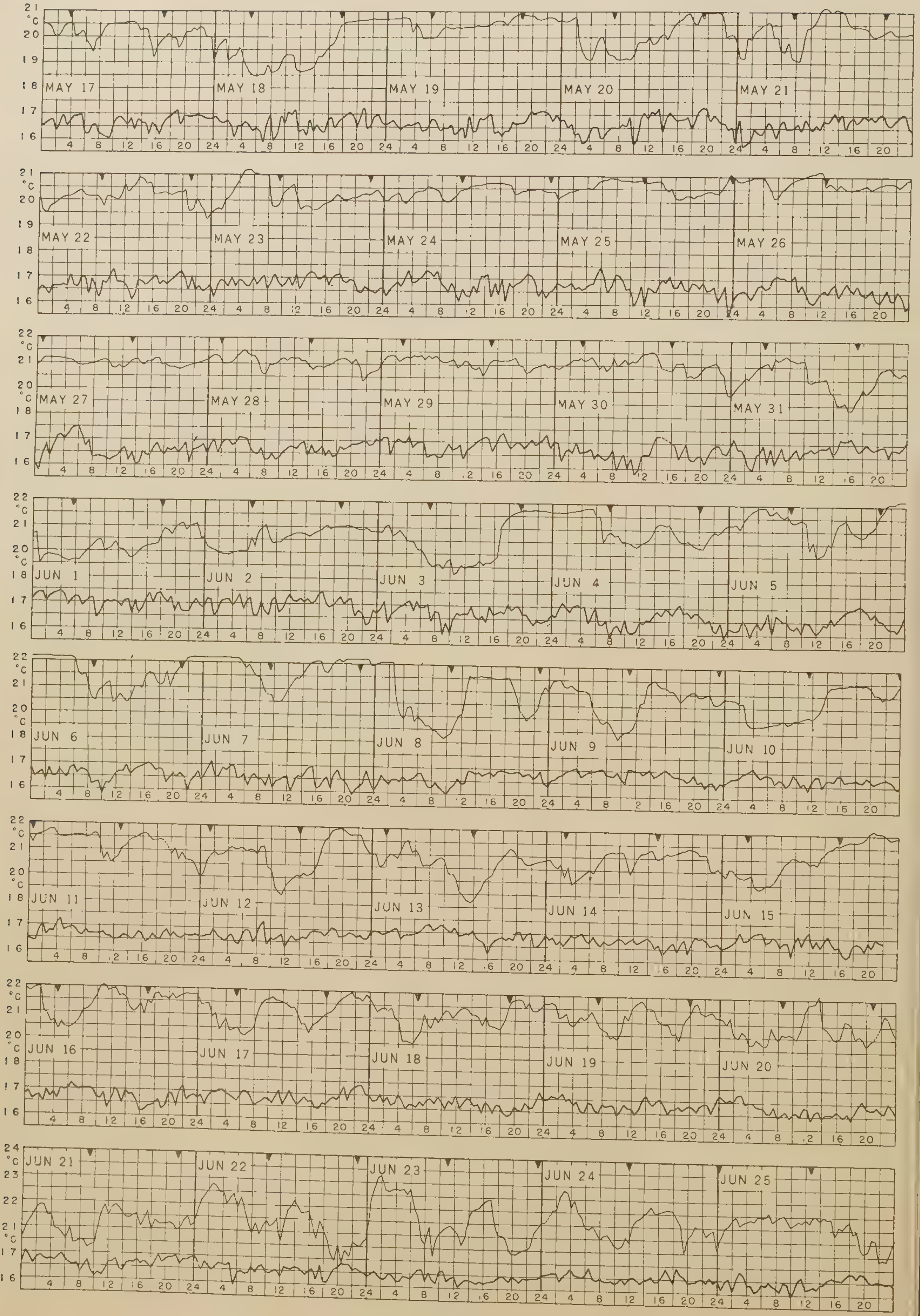
°C
MAY 17
MAY 18
MAY 19
MAY 20
MAY 21
MAY 22
MAY 23
MAY 24
MAY 25
MAY 26
MAY 27
MAY 28
MAY 29
MAY 30
MAY 31
JUN 1
JUN 2
JUN 3
JUN 4
JUN 5
JUN 6
JUN 7
JUN 8
JUN 9
JUN 10
JUN 11
JUN 12
JUN 13
JUN 14
JUN 15
JUN 16
JUN 17
JUN 18
JUN 19
JUN 20
JUN 21
JUN 22
JUN 23
JUN 24
JUN 25
16
17
18
19
20
21
22
23
24
4
8
12
16
20
24

Fig. 2e.

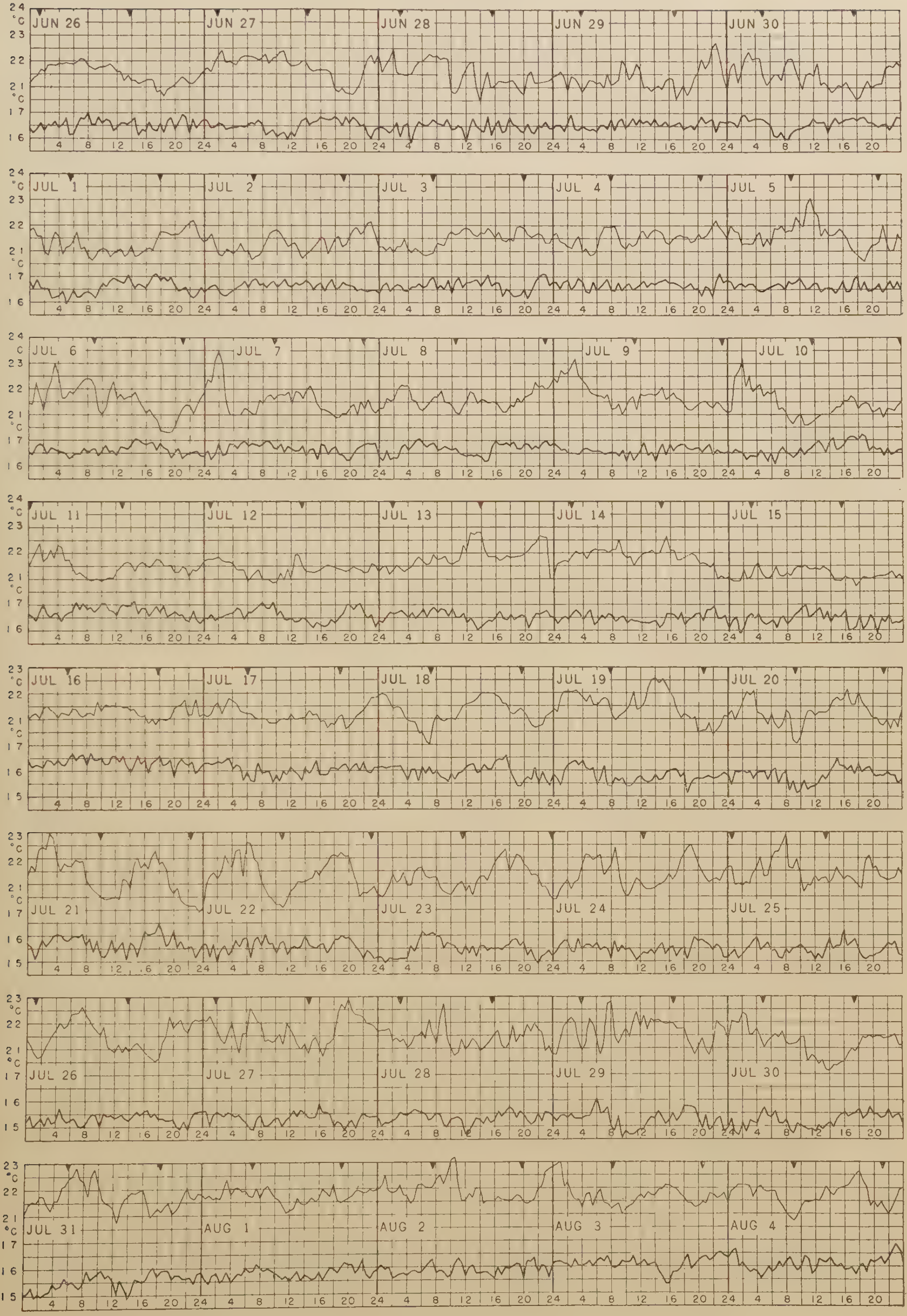
24
°C
23
22
21
°C
17
16
15
JUN 26
JUN 27
JUN 28
JUN 29
JUN 30
JUL 1
JUL 2
JUL 3
JUL 4
JUL 5
JUL 6
JUL 7
JUL 8
JUL 9
JUL 10
JUL 11
JUL 12
JUL 13
JUL 14
JUL 15
JUL 16
JUL 17
JUL 18
JUL 19
JUL 20
JUL 21
JUL 22
JUL 23
JUL 24
JUL 25
JUL 26
JUL 27
JUL 28
JUL 29
JUL 30
JUL 31
AUG 1
AUG 2
AUG 3
AUG 4
4
8
12
16
20
24

Fig. 2f.

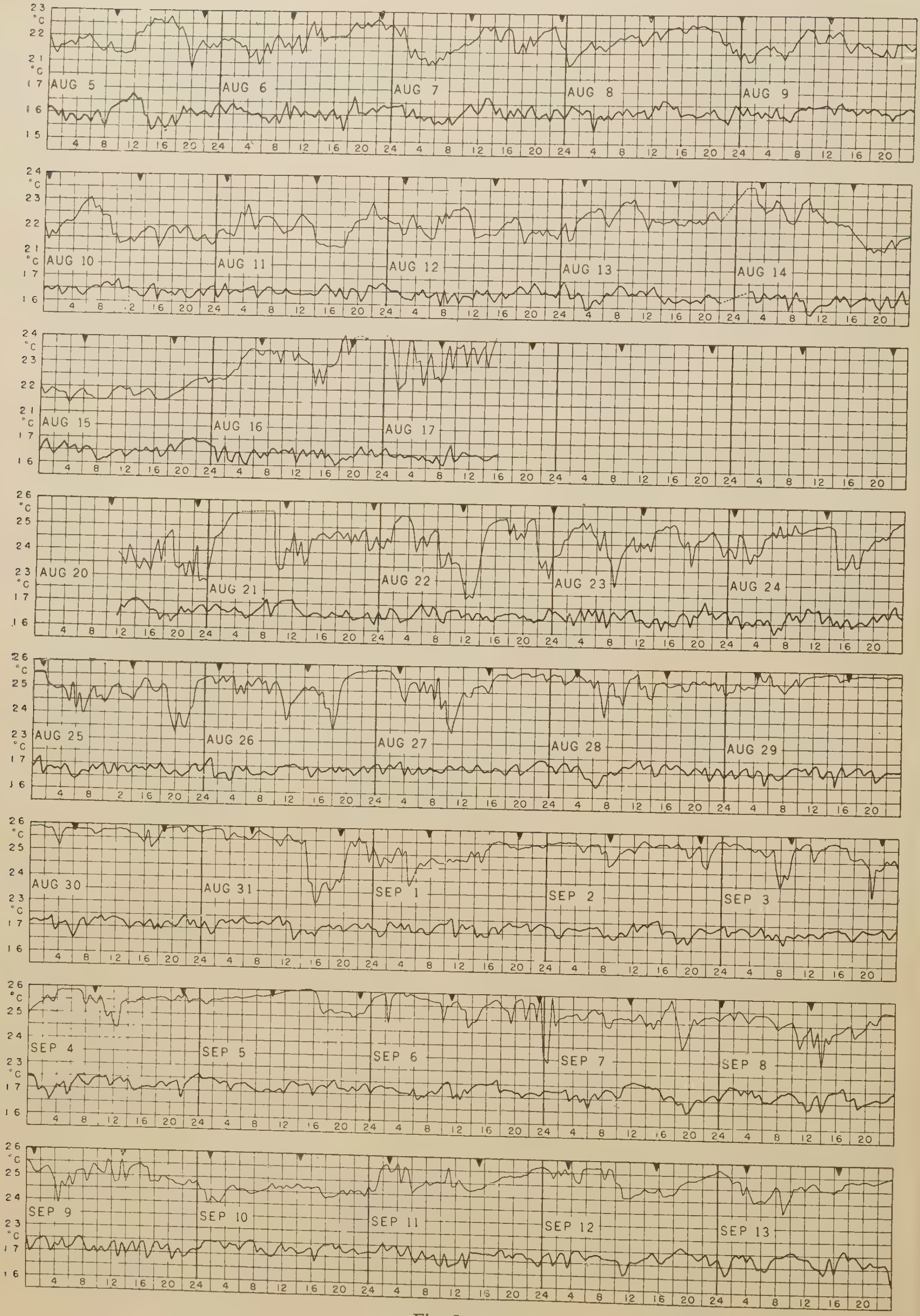
23 °C
22
21 °C
17
16
15
24
26
25
°C
AUG 5
AUG 6
AUG 7
AUG 8
AUG 9
AUG 10
AUG 11
AUG 12
AUG 13
AUG 14
AUG 15
AUG 16
AUG 17
AUG 20
AUG 21
AUG 22
AUG 23
AUG 24
AUG 25
AUG 26
AUG 27
AUG 28
AUG 29
AUG 30
AUG 31
SEP 1
SEP 2
SEP 3
SEP 4
SEP 5
SEP 6
SEP 7
SEP 8
SEP 9
SEP 10
SEP 11
SEP 12
SEP 13
4
8
12
16
20
24

Fig. 2g.

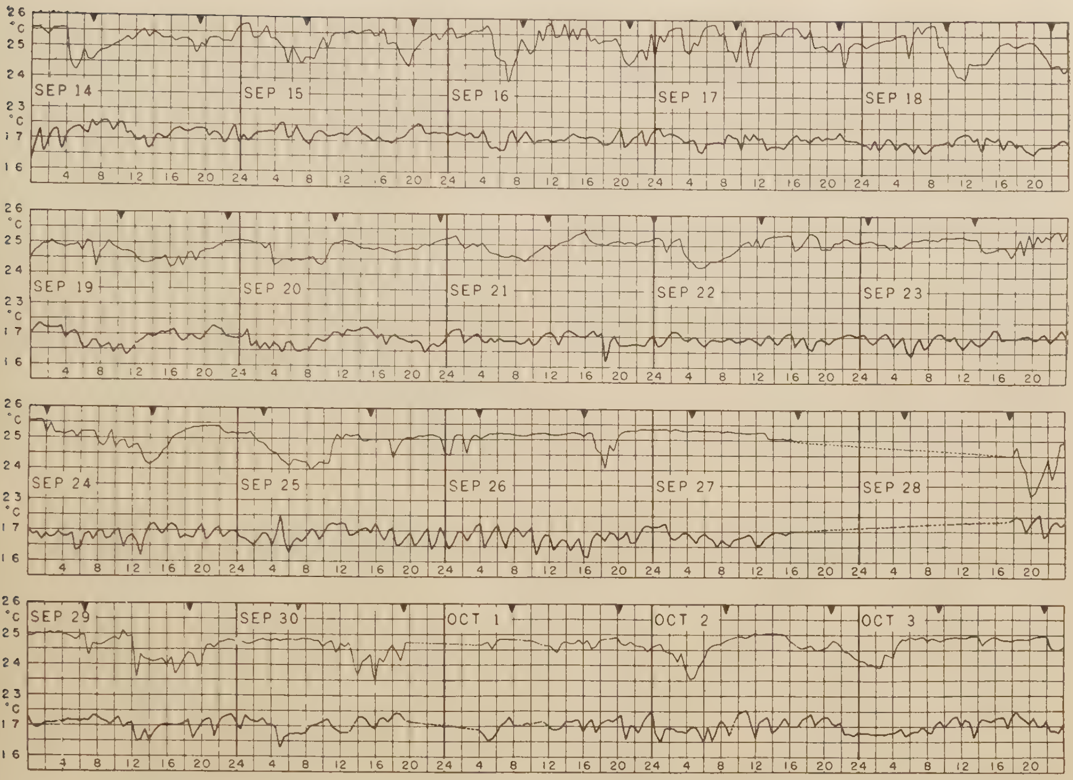

Fig. 2. The thermistor records from Dec. 8, 1954—Oct. 3, 1955 showing temperatures at the shallow and deep thermistors (light and heavy lines respectively). A new cable was installed March 12, with thermistors at slightly different depths. The small black triangles at the top show time of Bermuda high water, the time at the bottom is 60° W meridian time.

the most recent being papers by Defant (1950) and Haurwitz (1954). These studies have been largely based upon the analysis of very short series of data, usually of no more than a few days' duration. As Haurwitz (1954) has pointed out, one of the main obstacles to obtaining a more certain knowledge of the existence of internal waves in the ocean has been the lack of a truly long series of records of temperature in the deep water. As a first attempt to help supply such data, a submarine cable was laid from a recording Wheatstone bridge on the shore at Bermuda to two resistance thermometers offshore: one lying on the bottom at a depth of 50 meters, the other at 500 meters. (See Fig. 1 for location.) The shallow one was therefore approximately at the depth of the seasonal thermocline; the deeper one near the top of the main thermocline. Records have been obtained on this cable from Dec. 8, 1954 to Oct. 3, 1955 at intervals of one-half hour. From October 3, 1955 to May 7, 1957 records were obtained at five minute intervals. Since May 7, 1957 records have also been obtained from another resistance thermometer at 500 meters depth, but located five miles away from the original thermometer at a point further to the southwest along the coast of the island.

II. Qualitative presentation of data for the first period of observation

Portions of the cable data are presented in Fig. 2. The temperatures in degree Centigrade are given as ordinate, the dates and 60° W time are given as abscissa. The heavy line is the temperature as indicated by the deep thermometer: the light line indicates the shallow-element temperature. Occasionally, in order to keep the graph on scale, the origin of the ordinate is shifted (for example, see shift from June 20 to June 21, or July 15 to July 16). Also the scale is often broken in the middle to accommodate both thermistors (the first date at which the broken scale occurs is May 27). The little black triangles indicate time of predicted Bermuda high water. Two cables were used, one from December 8, 1954 to March 11, 1955; the second cable, from March 12 through October 3, 1955. The first cable was unarmored and soon began to fail—the shallow thermistor was lost on January 19, 1955, and it seems likely that the slow increase of the average deep temperature from 18.4° C near December 8 to 19.0° C in March, was also due to progressive cable failure. The deep thermistor of the second cable was placed somewhat deeper than that of the first as can be seen from the lower deep temperature beginning March 12. Readings at first were made every hour, but after December 22 were made every half hour. The readings were scaled off and replotted as shown in Figure 2.

In addition to the cable data, hydrographic data were also obtained over the same period by the PANULIRUS, the research vessel of the Bermuda Biological Station, and these data are exhibited in Figures 3 and 4. The vertical lines represent actual PANULIRUS stations—the rest of the contours are interpolated. Inasmuch as the variations of deep thermal structure indicated by the hydrographic data are no more than the high frequency variations revealed on the cable, it seems probable that the monthly fluctuations implied by the method of contouring in Figures 3 and 4 are simply the result of sampling errors. The seasonal variation above 500 meters is of course real. The main usefulness of the hydro-

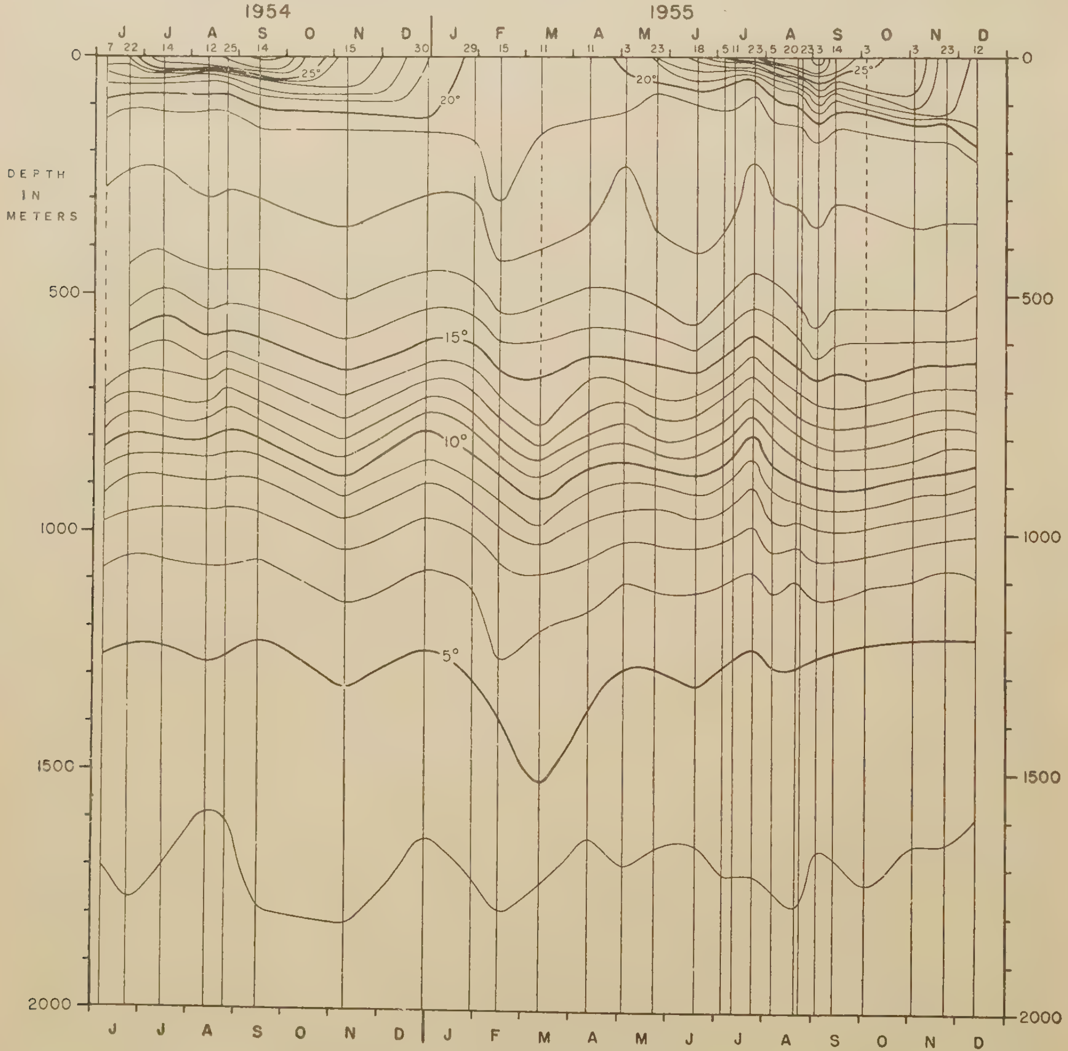

Fig. 3. Temperature as a funtion of time and depth by hydrographic station off Bermuda.

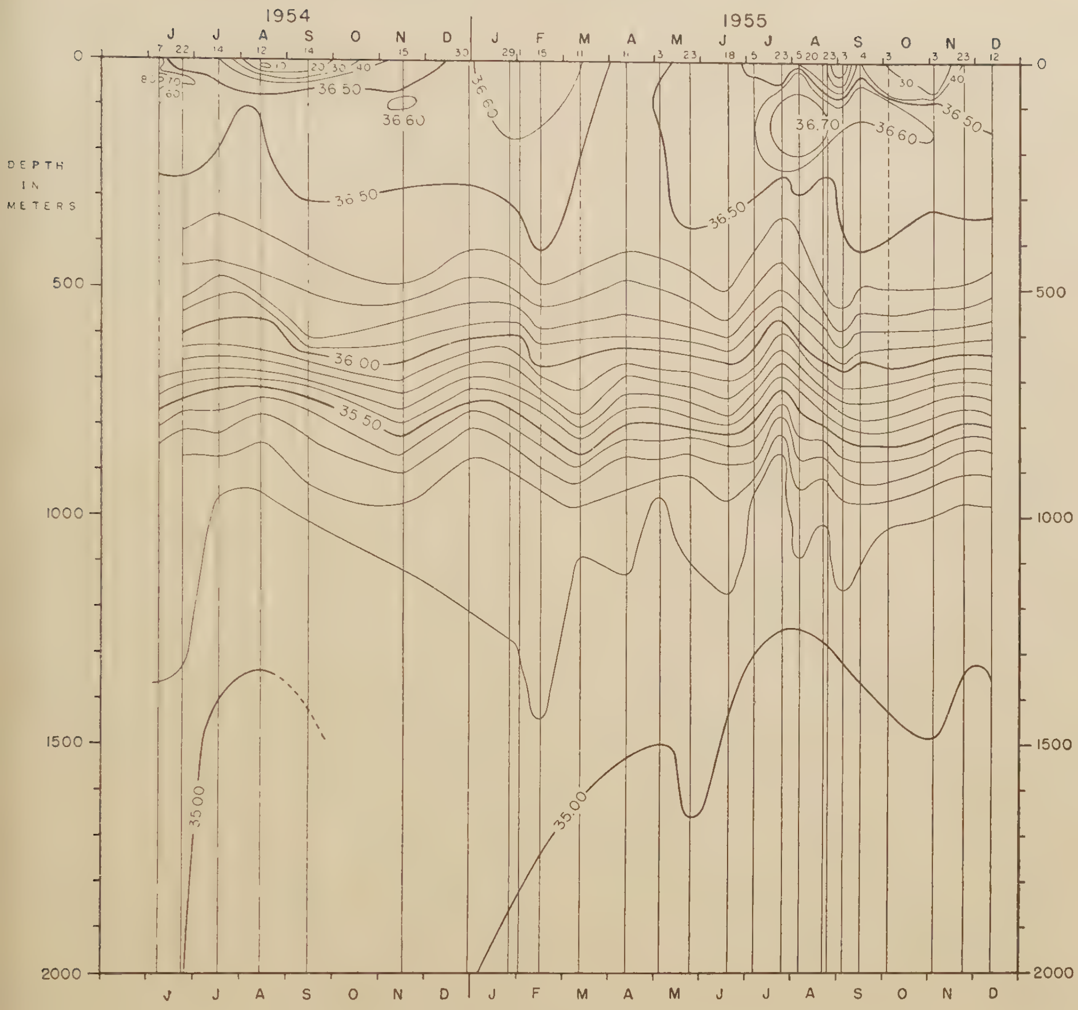

Fig. 4. Salinity corresponding to Fig. 3.

graphic data in Figures 3 and 4 is that it gives an idea of the *mean* vertical distribution of properties at various seasons near the cable, so that a rough estimate of vertical displacements of water can be obtained from the thermistor cable data.

From December 8 to January 3 there are few large disturbances on the shallow or deep thermistor. From December 26 to January 1 there is a slight drop in temperature of the shallow thermistor slightly after low water. Inasmuch as this is unassociated with any similar tidal fluctuation in the deep thermistor, and this is a period when the upper layer is fairly well mixed (Figure 4) we are inclined to explain this as evidence of cascading along the bottom slope of cold water from Castle Harbour (see BODEN 1952, 1953), which just manages to reach the shallow thermistor, but does not penetrate deeply enough to reach the deep one.

On January 2 a violent series of storms commenced over the North Atlantic, and by January 4, major disturbances at both thermistors were evident. During January 6 to 12 a pronounced long period, of somewhat less than 24 hours—perhaps an inertial period—can be seen on the deep thermistor record. Gradually the record becomes more and more confused or jagged—and during the period January 15 to February 15 even longer periods make an appearance. Above all, the deep records do not bear any resemblance to a tidal phenomenon—the phases appear to be quite randomly distributed with respect to time of high water. Isolated portions of the record (say February 24—25) look very much like tides—but they fail to persist and the similarity is doubtlessly fictitious. During this period the upper water became more and more mixed, the shallow thermistor was destroyed, and electrical tests indicated a gradual failure of insulation on the deep thermistor. On March 12 a completely new—and this time armored—cable was put into operation.

The violent temperature oscillations of the deep thermistor, starting on April 5 seem to be related to an intense storm just north of the island. During late April and May the growing amplitude of fluctuation on the shallow element appears to be associated with increasing vernal heating and growth of the seasonal thermocline (Figure 4), and gradually appears to be connected with surface tides. By mid-July there can be no doubt that the shallow temperature fluctuations are tied in with the surface tides. The deep thermistor appears to become more steady as the seasonal thermocline forms above it. Perhaps the seasonal thermocline shelters the main thermocline in some way, from disturbances at the surface—even hurricanes. Very remarkable long period fluctuations in deep temperature are indicated during the summer season, however, for example during July the average deep temperature dropped 1.5° C over a period of about three weeks and then rose again.

The hurricane which passed to the SW of Bermuda August 15th apparently caused the major disturbance at the shallow thermistor on August 16, without having any discernible effect at the deep one. A weak hurricane was passing to the east of Bermuda on August 31.

III. Preliminary search for tidal and inertial periods

A complete analysis of the large amount of data represented by the temperature records obtained off Bermuda is best carried out by cross-spectrum analysis. Such an analysis has been performed on the data obtained from November 1955 through February 1956. Its results are discussed in Section IV. But, since the records show some intervals during which periodicities appear fairly clearly it appeared worth while to make a simple preliminary investigation of the material.

In this section the results will be described which have been found in this manner. Attention has mainly been paid to the time interval up to the summer of 1955 when most of the work was done on which this section is based.

If the inspection of the temperature time graphs indicated that during a certain time interval a period or periods appeared in the data its statistical significance, and hence by inference its physical reality, was studied on the basis of periodogram analysis, harmonic analysis, and expectancy test. For some time intervals the tests for periodicities were made even though an inspection of the curves did not show that the periods to be looked for were present. This was done in particular for the lunar semidiurnal tidal period since it was thought that a demonstration of the presence or absence of this, the tidal period with the largest theoretical amplitude, was of intrinsic interest.

The methods employed here in the investigation of periodicities are all standard statistical procedures. They will therefore be described only very briefly in order to demonstrate specifically how they were used in this study. The temperatures are given at intervals of one-half hour. Since only periods of at least a few hours' duration are to be investigated the data were first smoothed by forming the means for each two-hour period. Only in the analysis of the 500 m records for the period 16—29 March 1955 such a smoothing was not performed.

With a few exceptions to be noted below for each selected record interval a periodogram analysis was first performed to determine the predominant amplitudes. Since no great accuracy was required a simplified method of periodogram analysis was used as a rule, as described by WHITTAKER-ROBINSON (1944, p. 356). In this simplification one takes for a given trial period the difference between the highest and lowest value in the line of mean values and plots this as abscissa.

After the predominant period or periods in the selected record interval have been determined the data were subjected to a harmonic analysis, with the determined period or an integral multiple of it as the analysis interval. Harmonic analysis will, of course, always give an amplitude for an assumed period even if the computation is based on random numbers. It is therefore necessary to ascertain how much larger the actually computed amplitude is than an amplitude resulting from an analysis of random numbers. This can be done by the expectancy test. Let A_i with the components a_i and b_i denote the amplitudes by harmonic analysis of the n individual periods.

Then

$$E^2 = \frac{1}{n^2}\sum_{i=1}^{n} A_i^2$$

the expectancy, is a measure of the amplitude of the mean period which should be expected in random data. Let $\overline{A}$ be the actual mean of the amplitudes,

$$\overline{A}^2 = \frac{1}{n^2}\left[\left(\sum_{i=1}^{n} a_i\right)^2 + \left(\sum_{i=1}^{n} b_i\right)^2\right]$$

Then the probability p that

$$\overline{A} = kE$$

is

$$p = e^{-k^2}$$

If p is small it can be concluded that the computed mean amplitude is not likely to appear in random data; in other words it is likely that $\overline{A}$ is statistically and hence physically significant.

A difficulty in the application of the expectancy test in the present study is that the investigated time intervals are not selected arbitrarily, but because they showed fairly well developed temperature oscillations. This biased selection decreases the probability p, but it is impossible to state to what extent p is affected by this selection. It can only be said that with large p it is highly probable that the data are randomly distributed, and that the computed amplitudes are not significant. To be sure that a low value of p indicates non-random data and significance of the amplitude one would wish to find lower values of p than in those cases when the data are not pre-selected.

In the following the analyses of the various intervals will be discussed briefly.

a) *6—18 January, 1955*

During this time some pronounced oscillations occurred at the 50 m and 500 m recorders. The periodogram analysis for the 50 m record suggested periods of 24 hours and 30 hours, for the 500 m level a period of 23 hours, close to the inertia period. Accordingly expectancy tests were performed for these periods, and also for a 12-hour period because of its proximity to the theoretically largest lunar tidal period. The results are summarized in Table I. An inspection of the harmonic coefficients of the 24-hourly oscillation at both levels for the individual days shows a much greater regularity during the first six days than later. Therefore, the expectancy test was also applied separately to this time interval. None of the computed probabilities is small enough to state that the periods under consideration are not statistical accidents, especially in view of the manner in which this time interval was selected for analysis. In particular the values for the 12-hour period indicate that the 12-hourly tidal period was not contained in the data. Further, the harmonic coefficients for the 12-hourly period, based on the temperature on the individual days, which are not reproduced here did not show the systematic phase change which would be present if a lunar period of 12 hours 25 minutes existed. At 500 meters depth the lower probability associated with the 23 hour period favors an inertial oscillation over a diurnal tide, at least during 6—11 January 1955, but the statistical significance of this result remains in doubt because of the selection of the data.

b) *16—29 March 1955; 1—29 June 1955*

Although the time interval from 6—18 January 1955 did not show either the 12-hourly or 24-hourly lunar tidal period it was thought that statistically significant values for the amplitudes of these two tidal oscillations might perhaps be obtained if a longer series of data were chosen. First, the temperatures registered at 500 meters during the epoch from 16 March to 29 May,

Table I. Expectancy Test, 6—18 January 1955, 50 m and 500 m

Period	50 meters			500 meters		
	Ampl.	Expect.	Prob.	Ampl.	Expect.	Prob.
30 hrs.	0.26° C	0.15° C	0.05	—	—	—
24 hrs.	0.15	0.13	0.33	0.13° C	0.10° C	0.18
12 hrs.	0.09	0.06	0.10	0.08	0.14	0.67
24 hrs.*	0.28*	0.16*	0.05*	0.23*	0.11*	0.013*
23 hrs.*	0.26*	0.17*	0.08*	0.22*	0.10*	0.009*

* First six days.

1955 have been studied. This time interval was chosen because about the middle of March 1955 a new and more satisfactory cable was installed. The data were plotted on a time graph with solar time as the abscissa. On this graph the upper lunar transits (local lunar noon) were marked so that the temperatures for each lunar hour could be read off without difficulty. For this particular computation no smoothing by averaging was performed here. The data were then combined into groups each of which consisted of four consecutive lunar days, in order to reduce the amount of computational work. Altogether 17 such groups were available; the period April 26—30 had to be omitted because of insufficient data.

The 17 four-day mean daily ranges were then harmonically analyzed. The results of the expectancy test for the harmonics 1 and 2 are shown in Table II.

Table II. Expectancy test for time interval 16 March —29 May 1955, 500 meters

Period length	Amplitude	Expectancy	Probability
24 lunar hours	0.038° C	0.026° C	0.10
12 lunar hours	0.034° C	0.020° C	0.27

The probabilities that the 24-hourly and especially the 12-hourly amplitudes are due to random data are large. Thus it must be concluded that these two main lunar periods are not present in these data. Because of the negative result for the 500-m depth the temperature at the 50-m depth has not been studied.

In order to see whether a different result would be obtained for another time interval an expectancy test for the two main lunar tidal periods was also made for 1—19 June 1955, both for the 50 and 500-m depths. The difference between lunar and solar time was allowed for by a rearrangement of the solar hours in the computation schedule. In order to reduce the numerical work the data were averaged in groups of four consecutive lunar days prior to the harmonic analysis. The results are summarized in Table III. Only the semidiurnal lunar period at 50 m can possibly be considered as appearing in the temperature data. The amplitudes of the diurnal lunar period at both depths and of the semidiurnal lunar period at 500 m are not statistically significant.

Table III. Expectancy tests for time interval 1—29 June 1955, 50 m and 500 m

Depth	Period length	Amplitude	Expectancy	Probability
50 m	24 lun. hrs	0.12° C	0.14° C	0.51
50 m	12 lun. hrs	0.28° C	0.13° C	0.01
500 m	24 lun. hrs	0.012° C	0.031° C	0.85
500 m	12 lun. hrs	0.057° C	0.044° C	0.19

During this period the temperature at 500 m depth showed some pronounced oscillations. Therefore a simplified periodogram analysis was performed beginning with a period of 10 hours and extended in steps of two hours, to 42 hours (Fig. 5). The periodogram shows a peak for a period of 20 hours, and another one for 40 hours

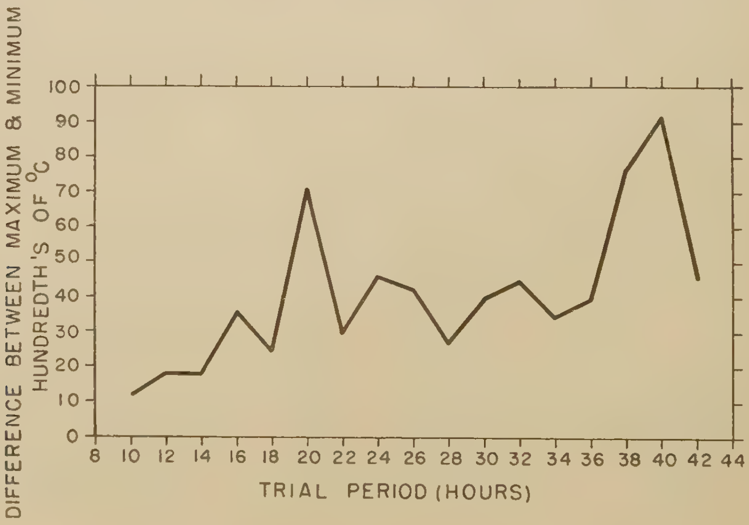

Fig. 5. Periodogram of temperature records at 500 m depth off Bermuda, April 5—13, 1955.

which is a reappearance of the maximum at 20 hours.

This 20-hour period is evidently not of tidal origin. The inertia period at the latitude of Bermuda is 22.4 hours, considerably longer than 20 hours. A direct expectancy test showed furthermore that a period of 22 hours is not indicated in the data (see Table IV below). Thus it must be concluded that the 20-hour period has no connection with the inertial period. It does not appear fruitful at this time to speculate on the physical origin of the 20-hour oscillation; it may be that it is excited by the storm in the vicinity of Bermuda at the beginning of the time interval under investigation, and that the length of its period is determined by the physical state of the waters around Bermuda. But this is admittedly pure speculation.

For the sake of completeness this same time interval has also been searched for periods of 24 and 12 hours because these periods are very close to the lunar tidal periods. The results together with the relevant expectancy test data for all the periods studied for this interval are shown in Table IV. The probabilities that the 24-hour and especially the 12-hour oscillations as expressed by their amplitudes are of real physical significance are evidently very low. Since it is actually the lunar tidal periods which are in general strongest and not the solar tidal periods it might be thought that the test is not conclusive since the analysis has been performed for solar hours. It is possible to apply a correction for the phase shift which arises if a set of data containing the lunar period is analyzed according to 24 solar hours. This has been done but the resulting corrections do not alter the computed probabilities significantly. Hence it appears that the lunar periods are definitely not observable during the time interval under investigation.

Table IV. Expectancy test for time interval 5—13 April 1955, 500 meters

Period length	Amplitude	Expectancy	Probability
20 hours ...	0.31° C	0.13° C	0.003
22 hours ...	0.09° C	0.12° C	0.613
24 hours ...	0.16° C	0.12° C	0.14
12 hours ...	0.05° C	0.09° C	0.70

d) *7—12 May and 3—7 June 1955, 500 m*

These time intervals were investigated because the temperature graphs showed some fairly regular oscillations during these times. Periodogram analyses extending from trial periods of 10 to 42 hours indicated peaks at 12 hours, 24 hours, and 36 hours. The expectancy test was performed only for the 12 and 24 hour periods because its result showed immediately that the periodogram peaks at 24 hours, and by inference those at 36 hours, are merely repetitions of the twelve-hour peak. The results of Table V make it appear possible that the 12-hourly periods are real, but it must be remembered that the time intervals were chosen because they showed regular oscillations. While the analysis was carried out according to solar time it is likely that the 12-hourly periods discussed here are in reality lunar 12-hourly periods, since the lunar tidal force is larger than the solar tidal force. If the lunar tides were more strongly developed and not as much disturbed by superimposed variations it would be possible to differentiate between lunar and solar tidal oscillations by studying the phase shift of the harmonic constants as determined for each day. But the superimposed noise makes this procedure inapplicable.

Table V. Expectancy tests for time intervals 7—12 May and 3—7 June 1955, 500 m

Epoch	Period length	Amplitude	Expectancy	Probability
7—12 May	24 hours	0.03° C	0.06° C	0.80
	12 hours	0.14° C	0.08° C	0.035
3—7 June	24 hours	0.07° C	0.07° C	0.32
	12 hours	0.23° C	0.12° C	0.019

In summary of the discussion in this section it can be said that from time to time periodicities appear in the record with periods whose lengths are 30, 24, 23, 20, and 12 hours. The 24-hourly and 12-hourly oscillations are presumably the lunar tidal periods, the period of 23 hours may be the inertial period (more accurately 22.4 hours at Bermuda). No explanation is offered for the 30 and 20-hourly periods. None of these periods can be regarded as definitely established, except perhaps the 12-hourly lunar tidal period at 50 m depth during June 1955 (Table III) whose chance occurrence has a probability of only one in one hundred. Other periods with equally low or lower probability, 20 hours

(Table IV), 23 hours (Table I) are not as significant because they were found in pre-selected data. Even the 12-hourly period is not always clearly indicated in the data, as shown by the expectancy tests. Physically, it would seem quite plausible that even these periodicities for which causes are known, such as the tidal and inertial periods, are not always clearly shown in the observation material because they may often be completely obscured by other periodic and unperiodic variations.

To make an over-all test concerning the reality of various periodicities in the Bermuda data it is necessary to extend the analysis to a larger body of data. It becomes then desirable to compute cross spectra using high-speed computers. This part of the investigation will now be discussed. The resulting gain of higher resolution and statistical reliability is offset in part by the implied assumption that many months of record can be treated as a "stationary time series".

IV. Spectra of the records

A) THE METHOD

The method is essentially the one given by Tukey (Tukey, 1949; Panofsky and McCormick, 1954). From the cosine transform of the autocorrelations one obtains the spectra S_d and S_s of the deep and shallow temperature records. The cosine and sine transforms of the cross-correlation are the cospectrum C and quadrature spectrum Q. From these we obtain the coherence Co and phase Θ between the two records according to

$$Co^2 = \frac{C^2 + Q^2}{S_d S_s}, \qquad \tan \Theta = \frac{Q}{C},$$

with Θ taken between 0° and 180° for positive Q, and between 180° and 360° for negative Q. With this convention Θ designates the phase *lead* of shallow record with respect to the deep one.

For each of the six analyses the four quantities S_d, S_s, Co^2 and Θ are plotted without smoothing against frequency in cycles per hour. The highest frequency in Fig. 6 is 2.5 c.p.h., exactly half the sampling frequency of 5 readings per hour. The frequency range from 0 to 2.5 c.p.h. is divided into $m = 62$ equal frequency intervals $\triangle f = 2.5/62 = .0432$ c.p.h. (see Table VI). S_d, S_s, Co^2 and Θ are plotted for all but the first of these intervals.

S_d and S_s are in units of °C²/c.p.h. This can be interpreted as follows. The r.m.s. value of the deep record A: 1 is .25 °C (Table VI); the variance thus equals .0625 °C². The plotted values give the contribution towards this variance from a unit frequency band (width 1 c.p.h.) centered at the plotted frequency. The reliability of the plotted values depends on the degrees of freedom, $\gamma = (2\,N/m) - {}^1/_2$, where N is the total number of values used in the analyses. Analyses A: 1, A: 2, and A: 3 are each based on 2,355 readings, thus $\gamma = 75$. The vertical arrows on Fig. 6 and 7 give the 95 per cent confidence limits. For 75 degrees of freedom these are 0.76 to 1.40; i.e., there is one chance in twenty that the correct value be less than 0.76 or larger than 1.40 times the computed value. The logarithmic plot enables one to plot a single "confidence arrow" for all values in an analysis.

The mean phase relation throughout the record length is given by Θ for each of the frequency bands. Co^2 is a measure of the variability in Θ at this frequency. If Θ were constant throughout the analyzed record, then $Co^2 = 1$; if it were randomly distributed, then $Co^2 = \Theta$. Clearly the reliability of the computed Θ depends on coherence. The 95 per cent confidence limits that Θ lies within the limits $\Theta - \Delta\Theta$ and $\Theta + \Delta\Theta$ are as follows (from Goodman, 1957):

Table VI. Information concerning the two charts that were analyzed. Data extend from Nov. 1955 to Feb. 1956

		Prefilter	Δf c.p.h.	E °C		N	v
				deep	shallow		
A: 1	Nov. 9: 0800—Nov. 28: 2200 . . .	12^m H 12^m	.04032	.25	.11	2355	75
A: 2	Nov. 28: 2200—Dec. 18: 1200 . . .	12^m H 12^m	.04032	.31	.15	2355	75
A: 3	Dec. 18: 1200—Jan. 7: 0200	12^m H 12^m	.04032	.32	.22	2355	75
B: 1	Jan. 11: 1300—Feb. 2: 0700	12^m H 12^m	.04032	.25	.20	2610	84
A: 4	Nov. 11: 0500—Jan. 5: 0500	12^m L 48^m H 48^m	.001008	.28	.23	1650	53
B: 2	Jan. 13: 1000—Jan. 31: 1000 . . .	12^m L 48^m H 48^m	.01008	.29	.32	540	17

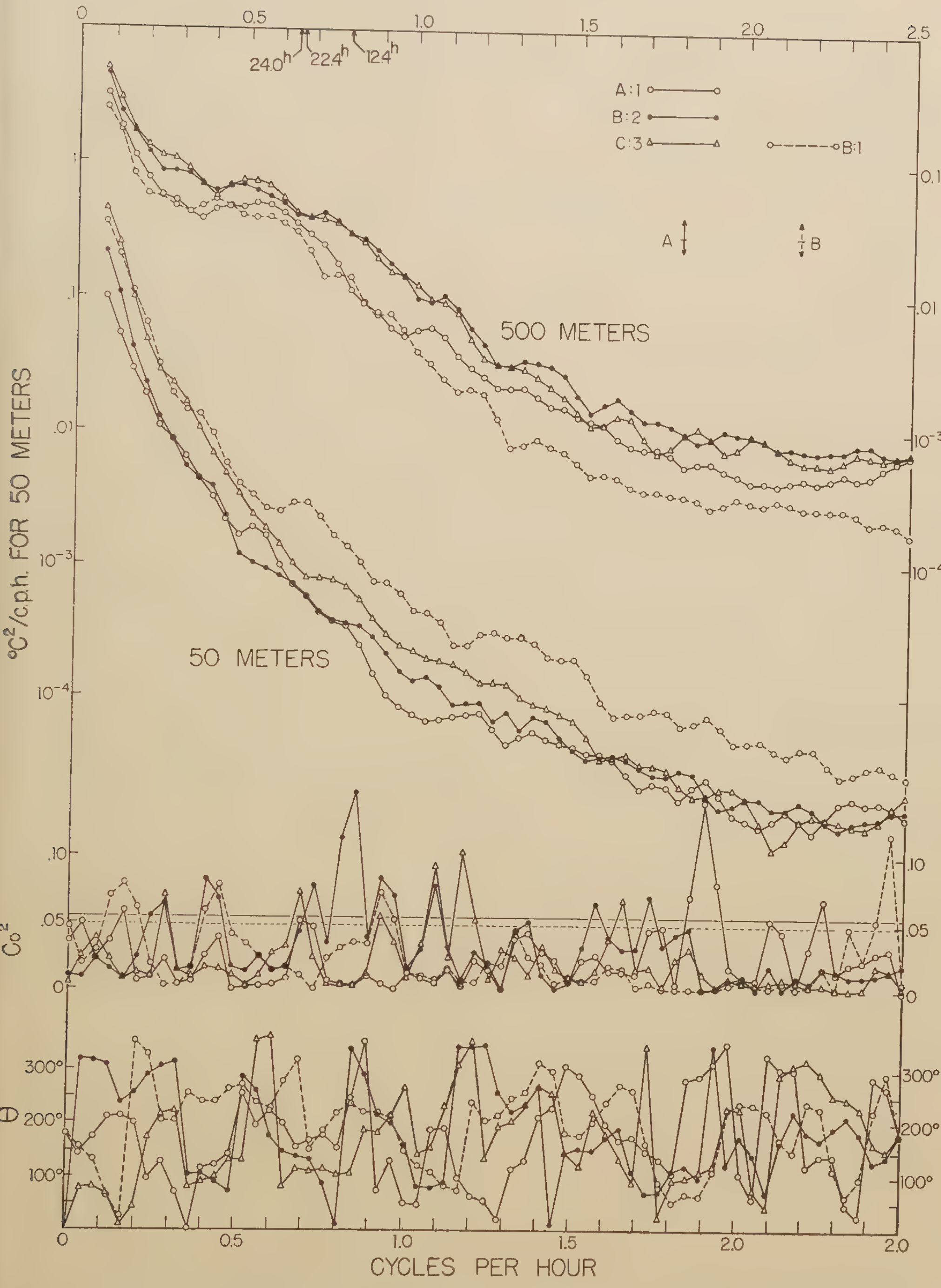

Fig. 6. Four co- and quadrature spectra designated by A: 1, A: 2, A: 3, B: 1 in Table VI. The spectral densities at 500 meters (right scale) and 50 meters (left scale) are displaced relative to one another by a factor 10. The arrows indicate the 95 per cent confidence limits. Approximate confidence limits on the coherence Co² between the records are given by the horizontal lines. Evidently there is no significant coherence, and accordingly the phase relation Θ between the records is not significant.

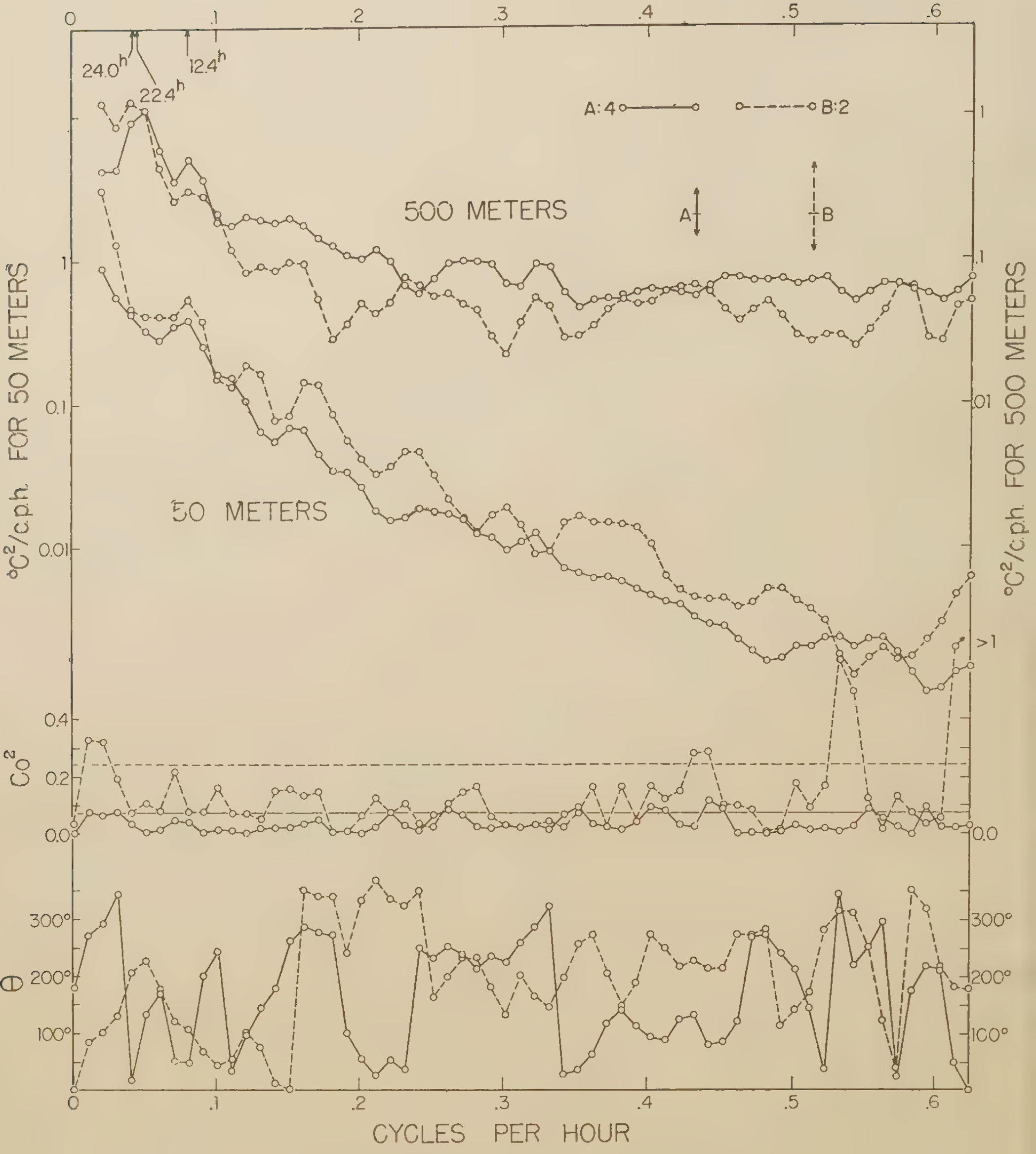

Fig. 7. Similar to Figure 6 except for a lower frequency range.

Table VII. Values of $\Delta\theta$ for stated coherence Co^2 and degrees of freedom

		ν			
		84	75	53	17
Co^2	.50	16°	17°	20°	40°
	.25	28°	30°	37°	—

The corresponding limits on Co^2 are roughly $4/\nu$, so that only the largest values of coherence are significant, and only for those can a meaningful phase relation be inferred.

The procedure adopted was as follows. Record A was read every 12 minutes to the nearest 0.01 chart-inch (0.005° C); each reading is in doubt by something like .02 chart inches (.01° C). The data were put on punchcards and a numerical high-pass filter applies (designated by 12^m H 12^m in Table VI). In this way long-term temperature drifts are suppressed without appreciably affecting the frequencies here under consideration. If the high-pass filtering were not done, then the spectrum would be seriously contaminated by the relatively high "energy" associated with this drift. Fifteen hours of record are lost at each end by virtue of the high-pass filtering. The remaining portion was split up into three equal lengths as shown in Table VI, and the spectrum analysis performed. Prefiltering was done on an IBM 650 computer, the spectrum on a Remington Rand 1103 computer.

In addition, the complete record was analyzed in another way in order to improve the resolution at low frequencies (Table VI, A: 4). By a suitable set of weighting functions the high-frequency wiggles were reduced, and the smoothed record tabulated at an interval of 48^m, four times that of the original record. This low-pass filtering was again performed on an IBM 650 computer. The 48^m readings were then high-passed and analyzed as before. The prefiltering is designated by 12^mL 48^mH 48^m in Table VI. The result is that the smoothed spectra (Fig. 7) extend only over one-fourth the frequency range as compared to the original spectra (Fig. 6), from 0 to 0.625 c.p.h. instead of 0 to 2.5 c.p.h. The reduced frequency range is again divided into 62 intervals, and in this way the frequency resolution is quadrupled. The improved resolution is at the expense of reliability. In the case of record A, the reduction in ν is moderate, from 75 to 53, because A: 4 is based on roughly three times the length of records as the other analysis. In the case of B the length of record was too short for subdivision, and the reduction in ν is severe, from 84 in B: 1 to 17 in B: 2. (Note the uncertainty arrows in Fig. 7.)

In any analyses based on observations at discrete intervals, the "aliasing problem" is severe (Tukey, 1949): frequencies in the vicinity of the sampling frequency appear in the alias of a low frequency. Thus for reading every 12^m a 13^m wave would have the appearance of $13^m \times 12^m = 156^m$ wave. The problem is particularly acute when going from the 12^m readings to the 48^m reading, and the low-pass filter is designed to alleviate the difficulty. First order corrections for aliasing were made for A: 4 and B: 2, and the final results were corrected for slight modifications due to filtering. The procedures are cumbersome and dull. A full discussion is in preparation (Munk, Snodgrass, and Tucker, in press).

B) THE RESULTS

i. *The high frequency cut-off*

For frequencies in excess of 0.75 c.p.h. all spectra drop towards high frequency by something like 10 db per octave, that is, somewhat more sharply than f^{-3}. The computed cut-off is actually weaker than the true cut-off for a number of reasons: (1) In any steep spectrum the calculation leads to a diffusion of spectral energy from the high to the low regions. (2) More important, random errors in chart reading introduce a white noise which materially boosts the high frequency values. Suppose the rms error is .02 chart inches = .01 °C. The error variance is then 10^{-4} °C^2, and if this is uniformly distributed across the entire range of frequencies, from 0 to 2.5 c.p.h., the resulting spectral density is $10^{-4}/2.5 = 4\times 10^{-5}$ °C^2/c.p.h. This is roughly the value reached at the high frequency and by the shallow spectra. The deep spectra at the high frequency end are ten times higher and may be real. A reliable determination of the spectra for $f > 2$ c.p.h. would require some elaboration in the recording scheme.

In all events the monotonic high-frequency cut-off is a real feature and needs to be explained. For each of the four spectra the *trends* are reproducible within the limits of statistical uncertainty. Actual values may vary from record to record by a factor three. B: 1 record has the lowest densities of the deep spectra and the highest of the shallow spectra. A noteworthy feature is that the deep spectrum is ten times the shallow spectrum.

In a general way this can be accounted for in terms of the stability of the water column. A thorough analysis of the internal wave motions possible in the waters around Bermuda does not seem warranted by the available data. But certain conclusions can be drawn by means of the Väisälä (or Brunt) frequency,

$$N = \frac{1}{2\pi}\sqrt{\frac{g}{\varrho}\frac{d\varrho}{dz}}$$

Fig. 8 shows $N(z)$ for winter conditions in 1955. A maximum $N_m = 5.6$ c.p.h. at 200 meters is associated with the seasonal thermocline, a second, weaker maximum at 850 m with the permanent thermocline. N_s and N_d are local values of the frequency at the depths of the shallow and deep instruments, respectively. At any depth we should expect no frequencies larger than N_m; a greatly reduced spectral density for frequencies larger than the local Väisälä frequency, and a relatively large spectral density for frequencies less than the local Väisälä frequency. An extrapolation of the computed curves bears out the first prediction of no significant spectral density at 5.6 c.p.h.; the second prediction might account for the relative absence of high frequencies in the shallow record. The spectral densities at the local Väisälä frequencies is 10^{-3} °C²/c.p.h. for both the deep and shallow records.

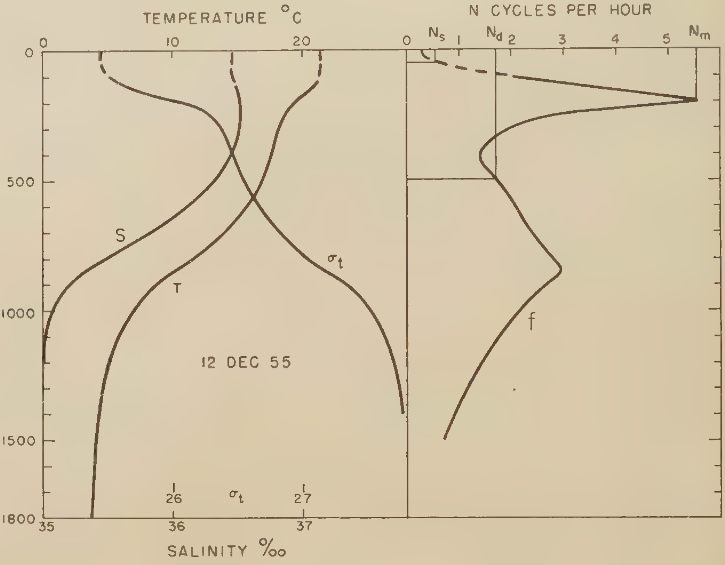

Fig. 8. The Väisäla (or Brunt) frequency $2\pi\,(g\varrho^{-1}\,d\varrho/dz)^{1/2}$ on December 12, 1955. The upper maximum (N_m=5.6 c.p.h.) is associated with the seasonal thermocline; the lower, weaker maximum with the permanent thermocline; N_s and N_d are the local values of this frequency at the depths of the hallow and deep recorders, repectively.

This geometric argument has been developed by Eckart (personal communication) and will be discussed in detail in his forthcoming book.[1] It would be out of place to reproduce the argument here. There is, however, some doubt concerning the applicability of the argument to a situation as complex as the one found at Bermuda, with two maxima of N. Judging by the three-layer case, one expects the oscillations at the two thermoclines to be only weakly coupled, with the shallow instrument responding largely to modes associated with the seasonal thermoclines, and the deep instrument to modes associated with the permanent thermocline. This situation could account for the virtual absence of coherence between the records. At no frequency range is there a significant coherence, and it is significant that this should be so.[2]

ii. *The 0.5 c.p.h. plateau*

All four deep records show a weak maximum (or at least a plateau) of spectral density between 0.4 and 0.6 c.p.h. There is no corresponding feature on the shallow records. The feature can be seen on both the low and high-frequency spectra, and there can be no reasonable doubt of its reality. The surprisingly low frequency involved, 1 cycle in two hours, is an embarrassing aspect of the situation. Nowhere beneath the seasonal thermocline does the Väisälä frequency reach such low values, except depths below 2,000 m. Could it be that the Väisälä frequency associated with the deeper half of the ocean contributes appreciably to the thermal unrest in the permanent thermocline?

iii. *The lunar tide*

Both spectra show a peak for both the shallow and deep records at the frequency of the principal lunar tide (see Fig. 7). For the deep spectrum the area under the peak corresponds to roughly

---

[1] The earliest discussion of the cut-off frequency (as far as we know) has been given by GROEN (1948).

[2] Widely separated low-frequency surface wave records have yielded coherences up to $Co^2=0.9$ (MUNK, SNODGRASS and TUCKER, in press). Two components of currents as determined by a long GEK series taken by J. Reid also had coherences up to 0.9.

.004 °C^2 above background, somewhat more for the shallow spectrum. The corresponding amplitude is $\sqrt{.008} \approx 0.1$ °C, or 10 meters of vertical displacement. The internal tide contributes only a small fraction of the energy in the band centered at .008 c.p.h., and for that reason the coherence must remain low; still a coherent harmonic embedded in an incoherent noise could have been expected to give some enhancement in Co^2 at this frequency. The fact that it is not so indicates that the relative phase of the two instruments for the 12.4^h internal tides does not remain fixed!

With regard to the possible existence of discrete tidal modes, the present method of analyzing into relatively wide frequency bands cannot compete with the resolution obtained by Fourier Series methods employed in earlier parts of this paper.

iv. *Diurnal oscillation*

A significant peak in spectral density for the two shallow records at .04—.05 c.p.h. can be ascribed to either a 24.0^h tide or a 22.4^h inertial oscillation.

Whether or not this is due largely to internal tides could be decided by the use of the expectancy test. If the peak is due chiefly to inertial motion which decays in, say, tenperiods, then the resolution by the present method is adequate.

Remarks

The authors have tacitly assumed an explanation in terms of internal waves rather than drifting convection cells. To settle this point decisively the cross-spectrum of two records at 500 m depth would be required.

Acknowledgements

The authors are greatly indebted to a number of people who generously gave their help to us, in particular: (B.H.) to Mr. Frank Haurwitz for his help in carrying out the harmonic analyses; (H.S.) to Messrs. Brunel Spurling and Sloat Hodgson for collaboration in putting out the thermometric cable at Bermuda and the preliminary preparation of the data; and (W.H.M.) to Mr. Ferber, Mrs. Shumway and Mrs. Covher of Convair Corp. for their help in programming and carrying out the computations involved in the cross-spectrum analysis.

REFERENCES

Cahn, A. J., 1945: An Investigation of the free oscillations of a simple current system. *J. Meteorology*, **2**, p. 113—119.

Defant, A., 1932: Die Gezeiten und inneren Gezeitenwellen des Atlantischen Oceans. *Wissensch. Erg. d. Deutschen Atl. Exp. »Meteor«*, 1925—27, Bd. VII, Teil I, 1—318.

— 1950: On the origin of internal tide waves in the open sea. *J. Mar. Res.* IX, **2**, 111—119.

Goodman, N. R., 1957: On the joint estimation of the spectra, cospectrum and quadrature spectrum of a two-dimensional stationary Gaussian process. *New York University: Scientific Paper* No. 10, Engineering Statistics Laboratory.

Groen, P., 1948: Contribution to the theory of internal waves. *Kon. Ned. Met. Inst. de Bilt. Med. en Verh.*, **2**, 11.

Haurwitz, B., 1954: The occurrence of internal tides in the ocean. *Arch. Meteor. Geophys. und Bioklimat*, **7**, 406—424.

Munk, W. H., Snodgrass, F. E., and Tucker, M. J.' 1959: Spectra of low frequency ocean waves. To be submitted to the *Bulletin of the Scripps Institution of Oceanography* (in press).

Panofsky, H. A., and McCormick, R. A., 1954: Properties of spectra of Atmospheric turbulence at 100 meters. *O., J. Roy. Meteor. Soc.*, **80**, 546—564.

Rossby, C.-G., 1937—38: On the mutual adjustment of pressure and velocity distribution in certain simple current systems. *Jour. Mar. Res.* Part I, **1**, 15—28, Part II, **1**, 239—263.

Tukey, J. W., 1949: The sampling theory of power spectrum estimates. *Symposium on applications of autocorrelation analysis to physical problems*, Woods Hole, Mass., 13—14 June 1949, p. 47—67 (printed by Office of Naval Research).

Veronis, G. and Stommel, H., 1956: The action of variable wind stresses on a stratified ocean. *Journ. Mar. Res.* **15**, p. 43—75.

(Manuscript received 15 March, 1958)

Contribution No. 956

BEACH CHANGES DURING STORMS ON OUTER CAPE COD, MASSACHUSETTS

JOHN M. ZEIGLER, CARLYLE R. HAYES,
AND SHERWOOD D. TUTTLE

Reprinted for private circulation from
THE JOURNAL OF GEOLOGY
Vol. 67, No. 3, May 1959
Copyright 1959 by the University of Chicago
PRINTED IN U.S.A.

BEACH CHANGES DURING STORMS ON OUTER CAPE COD, MASSACHUSETTS[1]

JOHN M. ZEIGLER, CARLYLE R. HAYES, AND SHERWOOD D. TUTTLE
Woods Hole Oceanographic Institution

ABSTRACT

Effects on beaches of nine storms and two hurricanes have been measured on the beaches of Cape Cod. Changes in beach volume and topography take place very rapidly, and vertical cuts of 9 feet in the foreshore and volume changes of as much as 520 cubic feet per linear foot during one tide have been measured. The positions of offshore shoals influence the amounts of beach erosion, with cutting being greater behind openings in the bars. Migration of openings in the bars shifts the locus of maximum cut and fill laterally along the beach. Wave erosion at the base of the cliffs, while occurring irregularly, is important as it increases the rate of mass wastage in the slopes.

INTRODUCTION

A program of beach investigations was initiated in August, 1953, by the Office of Naval Research through the Woods Hole Oceanographic Institution. Periodically, results have been reported to the Office of Naval Research in a series of unpublished manuscripts, which have had very limited distribution. It seems advisable to publish some of the findings even though research is still in progress. Three published reports deal with material gathered in these investigations: Zeigler and Ronne (1957) on the use of time-lapse aerial photography in coastal studies; Miller and Zeigler (1958 and 1958*a*) on the distribution patterns of wave-deposited sediments.

It has long been common knowledge among geologists and engineers that storms produce large waves and that large waves are responsible for rapid and significant shoreline changes. Beach changes during some of the storms which have reached Cape Cod since 1953 have been well documented and therefore can be described in terms of rate and magnitude.

Douglas Johnson (1919, p. 65–72) vividly describes examples of damage done to breakwaters, harbor installations, etc., by storm waves. All these dealt with spectacular instances of storm damage after the fact, so to speak. None of the examples used by Johnson involved measurements before and after storms. Studies similar to those conducted on Cape Cod were made by Shepard and LaFond (1940), who observed the general offshore movement of sand during stormy periods in California. Sand was eroded from the beach and carried seaward at Scripps Institution pier during the stormy season of winter and early spring. Sand was later shifted landward during the calmer weather of summer and early fall. They suggested that cutting was produced by large waves of long period and filling by small waves of short period.

Shepard (1950), Shepard and Inman (1951), and Inman (1953) have described beach changes in the vicinity of La Jolla, California. Profile measurements were made in connection with sediment distribution and movement studies on the beaches and in the shallow water zone offshore. Shepard and Inman (1951) categorized their beach changes as principally alternation between full summer beaches and depleted winter beaches. They used data from eight surveys made between April 12, 1949, and May 10, 1950.

They show seasonal changes in terms of isopleth movements and volume gains and losses. They also point out that storms which arrive on the coast at time of spring tides do considerably more cutting.

There are several distinct differences be-

---

[1] Contribution No. 956 from the Woods Hole Oceanographic Institution. Manuscript received November 2, 1958.

tween Cape Cod beaches and the beaches at La Jolla. The extensive near-shore shoals off all Cape Cod beaches are missing at La Jolla, and the character of storms and storm waves is different. The heavy continuous swells from the Pacific have no counterpart on Cape Cod shores.

A more recent study of storm effects on coasts was reported by Morgan (Morgan, Nichols, and Wright, 1958). This dealt with morphological effects of Hurricane Audrey, June, 1957, on the marginal deltaic plain of southwestern Louisiana. Due to high water and large waves, the beaches were cut back and considerably modified. Large amounts of sediments were shifted and rearranged.

GEOLOGY OF CAPE COD

Works of four men provide the most succinct source of information about the geology of Cape Cod: Henry Marindin (1889 and 1891); W. M. Davis (1896); and Woodworth and Wigglesworth (1934). In addition to their own work, these writers summarized the works of scores of others. Marindin measured the rate of erosion between Chatham and Provincetown on the east coast of Cape Cod. He surveyed a line of levels along the eastern coast and compared the position of the shoreline with an earlier chart made in 1856. Davis attempted to describe the original outline of Cape Cod and the manner in which the present shoreline was developed, and, in so doing, he discussed many of the coastal features of the Cape. Woodworth and Wigglesworth described the geology of the entire Cape and the surrounding islands.

Cape Cod is shaped somewhat like a bent arm; the forearm, or easternmost portion, is locally called the Outer Cape. Insofar as sand or beach detritus is concerned, the Outer Cape is a closed system. All material on its beaches or dunes was derived immediately offshore or from erosion of fluvioglacial material of the Cape itself. Both ends of the Outer Cape terminate in relatively deep water, 180 feet off Race Point and about 50 feet off Monomoy. It seems unlikely that material is moved to the Outer Cape from deep water, either from the north or south, or by littoral drifting from any other part of the New England coast. Drifted detritus would be trapped or obstructed many times before it could reach the beaches of the Outer Cape.

A condition of importance to these beach studies is the abundance of detritus available for beaches which face the open Atlantic on the Outer Cape. High cliffs (60–100 feet) of sands and gravels are exposed to wave attack between Nauset Coast Guard Station and the Highland Light Life Saving Station, a distance of 16 miles (fig. 1). Even moderate rains cause deposition of small fans of clay and gravel on the beach at the foot of these cliffs. The Pleistocene stratigraphy of the cliff section was described by Woodworth and Wigglesworth (1934, pl. 2) as sands, gravels, and scattered boulders forming the Wellfleet plain of Wisconsin age.

Offshore shoals and bars influence the sea state on the eastern coast of the Outer Cape. Peaked Hill Bar (fig. 1), famous in the days of sail, springs from the beach near Highland Light and extends more or less parallel to the beach, a few thousand feet offshore, to Race Point. The wide treacherous shoals east of Nantucket and Monomoy absorb much of the energy of the sea off the southern end of Cape Cod.

STUDY AREAS

Data from five beach locations on the Outer Cape were selected: New Beach, Race Point, High Head, Highland, and Nauset, located clockwise around the end of the Cape (fig. 1). Specific information about each of these study areas is tabulated in table 1.

MEASUREMENT PROCEDURES

Measurements of profile changes on Outer Cape Cod beaches began in August, 1953. Among the areas sampled were Nauset, Highland, and Race Point. The frequency of surveys has generally increased since the beginning. In 1953 they were measured about once a month, and shallow-water soundings on the seaward end of the lines were taken from a dory. By fall, 1955, profiles were measured at least twice each month to low water line. During 1956 and 1957, with several major interruptions, measurements were made more than once a week at Highland, Race Point, and Nauset, and, finally, data were recorded every other low tide (about five times a week), with measurements made every low tide for short periods during storms at New Beach, Race Point, High Head, and Highland from January to June, 1958.

Profile lines were located at right angles to the water line across the beaches to be studied. A suitable point of origin was established well inland on the backshore or at the base of the cliffs or dunes, and elevations of the beach surface were taken along the same profile line each time the beach was measured.

During the first years of the study beach measurements were made with a transit and stadia rod. This procedure needed two people, fair visibility, and moderate weath-

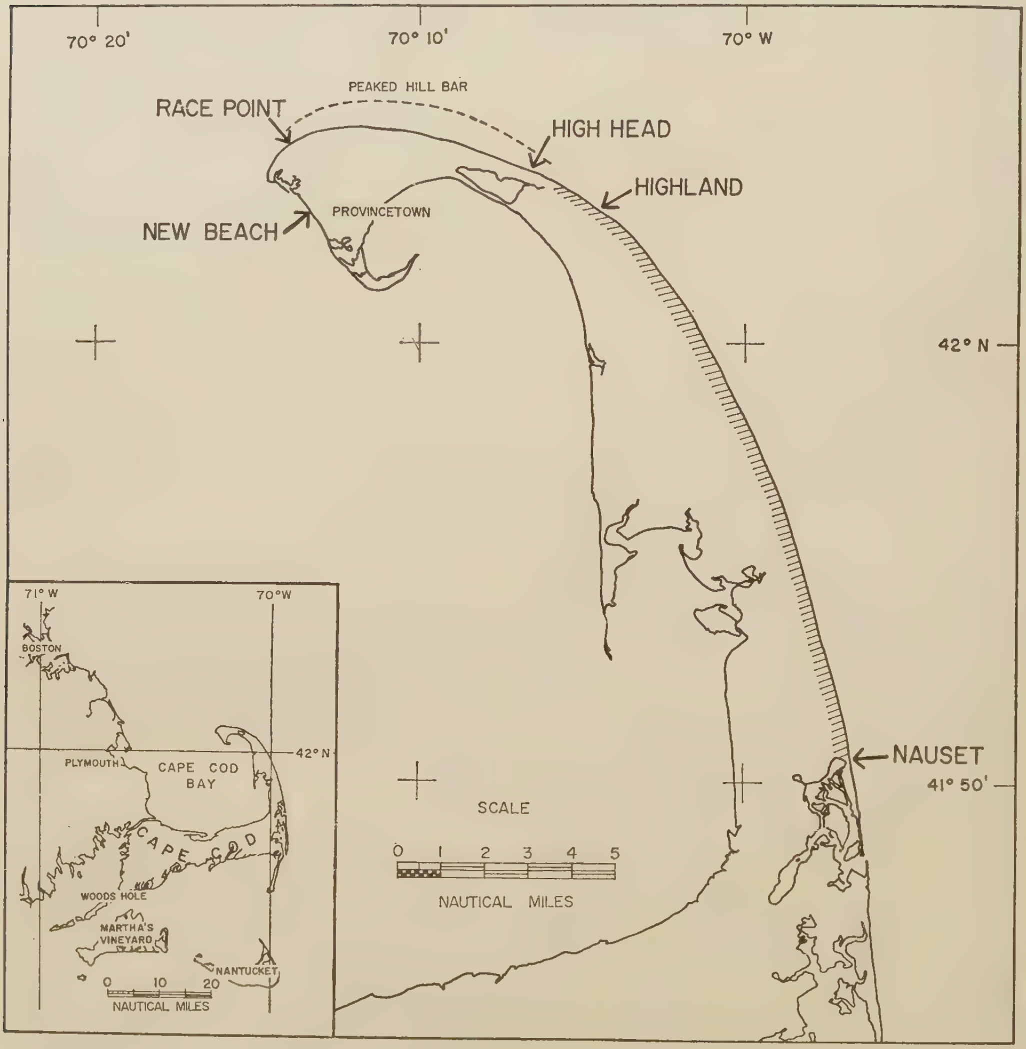
70° 20'
70° 10'
70° W
PEAKED HILL BAR
RACE POINT
HIGH HEAD
HIGHLAND
PROVINCETOWN
NEW BEACH
42° N
NAUSET
41° 50'
SCALE
0 1 2 3 4 5
NAUTICAL MILES
71° W
70°W
BOSTON
PLYMOUTH
CAPE COD BAY
42°N
CAPE COD
WOODS HOLE
MARTHA'S VINEYARD
NANTUCKET
0 10 20
NAUTICAL MILES

FIG. 1.—Index map, Cape Cod, Massachusetts

TABLE 1

Factors Which Affect Topographic Changes on Specific Beaches

	Trend of Coast	Fetch 90° to Coast (Nautical Miles)	Fetch 45° to Coast (Nautical Miles)	Type Coast behind Beach	Source of Sand (Nautical Miles)	Net Direction Long Shore Drift	Open Fetch to Northerly Storms (Nautical Miles)	Proximity of Offshore Bars	Near-Shore Bars
New Beach....	320°–140° T., NW.–SE.	16	17 W., 18 S.	Dune area (Provincelands)	10, Cliffs at Highland	Southeasterly	None	None, or poorly developed	None, or poorly developed
Race Point....	043°–221° T., NE.–SW.	37	100 N.×E., 21 W.×N.	Dune area (Provincelands)	Cliffs at Highland, 8 southeasterly	Northwesterly	Tangent to coastline	Terminus of Peaked Hill Bar	Complex and changing
High Head....	290°–110° T., WNW.–ESE.	150	65 NNW., 220 ENE.	Dune area (Provincelands)	1.5, Cliffs at Highland	Northwesterly	250 (Bay of Fundy)	1,000 feet—origin of Peaked Hill Bar	Complex, migratory
Highland.....	308°–128° T., NW.–SE.	150	100 N., unlimited E.	High cliffs of glacial drift	Cliffs behind beach, O	Northerly	260 (Bay of Fundy)	2,000 feet	Numerous and complex (see fig. 2)
Nauset.......	350°–170° T., N.×W.–S.×E.	Unlimited	180 NE., unlimited SE.	Sand spit in front of marsh	Cliffs near Nauset Light H., 0.5 northerly	Southerly	200 (Nova Scotia)	2,000 feet	700 feet—numerous and complex

er. In order that data could be collected by one man in any condition of visibility and weather, stakes were located 25 feet apart along the profile lines, and the elevations of their tops were determined. Surface heights of the beach could be quickly measured on each stake, and the beach profile was calculated later.

ISOPLETHS AND VOLUME MEASUREMENTS

Some difficulty was encountered in arranging and correlating the voluminous survey data for study. Large diagrams were constructed, with the horizontal axis representing locations of the elevation measurements across the beach and the vertical axis representing dates of successive surveys. On these diagrams, isopleth, or equal value lines, were drawn (figs. 2 and 3). Each line connects points of equal elevation, and each line shifts laterally whenever the beach changes. Shifts in position of the isopleth lines show depletion or replenishment of the beach. Elevations are based on the 1929 datum for mean sea level. The geoid of 1929 upon which bench marks are based does not fit local sea level exactly; therefore, zero elevation based on the 1929 geoid falls almost exactly at mean low water level on Outer Cape Cod. Thus the isopleth elevations used in this report are essentially vertical distances above mean low water level.

Volumes were calculated for each beach every time its profile was surveyed. Volumes were determined as follows: First, the area of a geometric figure was calculated. The figure was bounded by sea level as a base, the elevation of the landward end of a profile as one side, and the beach surface (a series of sloping straight lines) as the top. The area values were converted to cubic measure by multiplying by one foot of width or distance along the beach. Volumes and volume changes in this paper are expressed as cubic feet per linear foot.

Since the different beach profiles vary in length, and the profiles grow or shrink in length with beach cutting and filling, comparisons of volume changes between different beach areas are difficult. A compilation of maximum daily volume changes, showing both cuts and fills, can be used in evaluating beach growth or shrinkage. There are two high and two low tides each day off this coast.

Some of the changes which occurred on beaches can be seen on figure 4 or table 2. Even the daily and every other low tide measurements carried out during winter and spring, 1958, may not be close enough together to record extreme amounts of cut or fill.

STORMS

Storm tracks along the East Coast of the United States are related to the general wind circulation. Storms are associated with low-pressure areas, hence wind circulation is counterclockwise around the center, and wind direction at any specific beach will change as the storm center passes. All these storms have a net easterly movement. Storm tracks shown on figures 7 and 8 refer to storms studied in this report (tables 3A and 3B).

When storm centers pass east of Cape Cod, high-velocity winds come from the east and then shift through northeast to north and northwest. This type of storm creates onshore winds and maximum storm waves on Outer Cape Cod beaches.

When the storm center passes west and northwest of Cape Cod, initial storm winds start from the southeast and veer through south to west. This storm pattern results in alongshore and offshore winds on the Outer Cape beaches and smaller and less-well developed storm waves.

If the forward progress of the storm along its track is delayed by the blocking action of a stalled high-pressure cell, the wind has a longer time to blow from the easterly direction and consequently builds up higher and more damaging waves (Storm 1, Oct. 22–26, fig. 7, *A;* also Storm 3, Oct. 14–17, fig. 7, *C*).

Storm tracks shown in figures 7 and 8 were plotted from the daily U.S. Weather Bureau maps. Wind directions and velocities for the beach-study project starting in

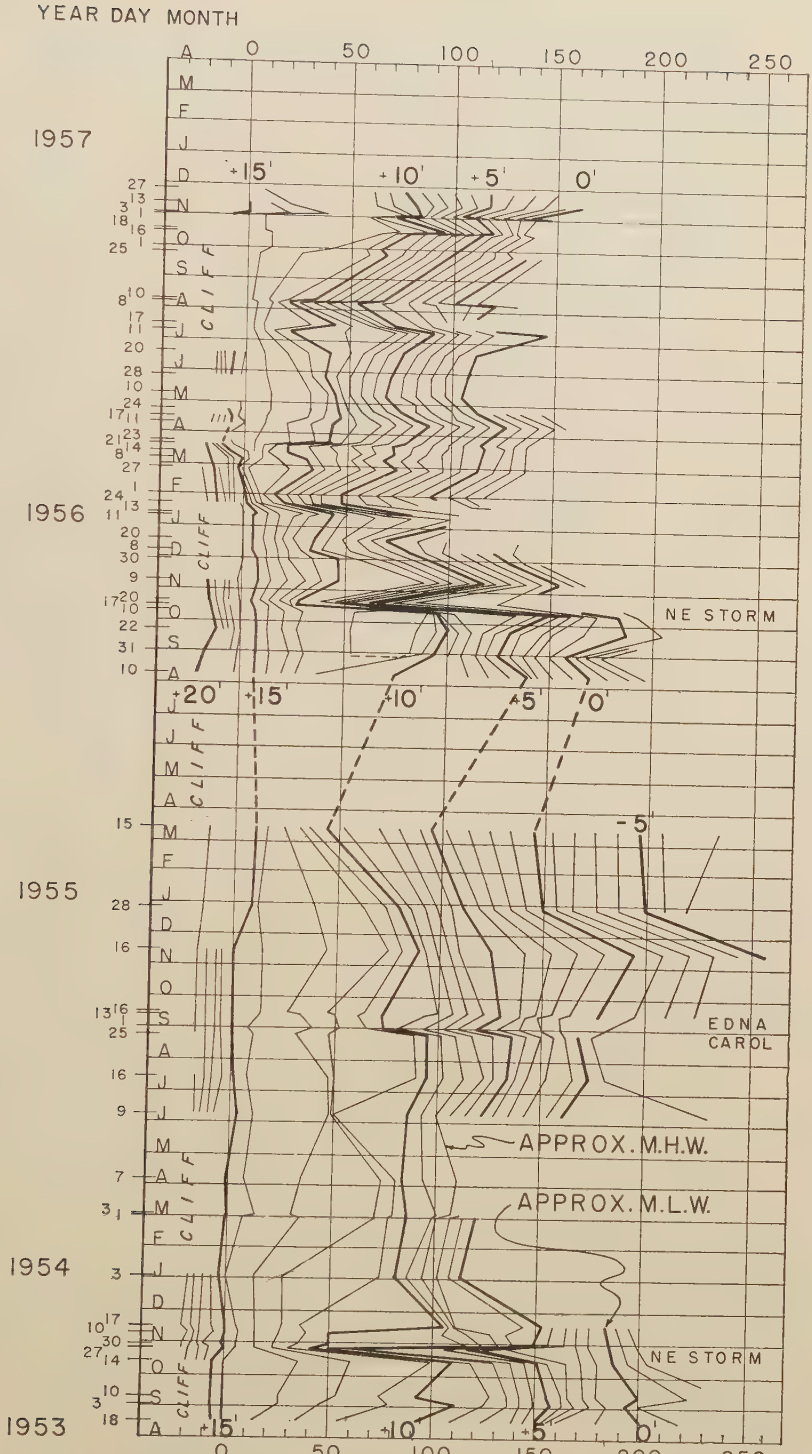

FIG. 2.—Isopleth diagram, Highland A. 0–250, distance from cliff base. Contours connect points of equal elevation.

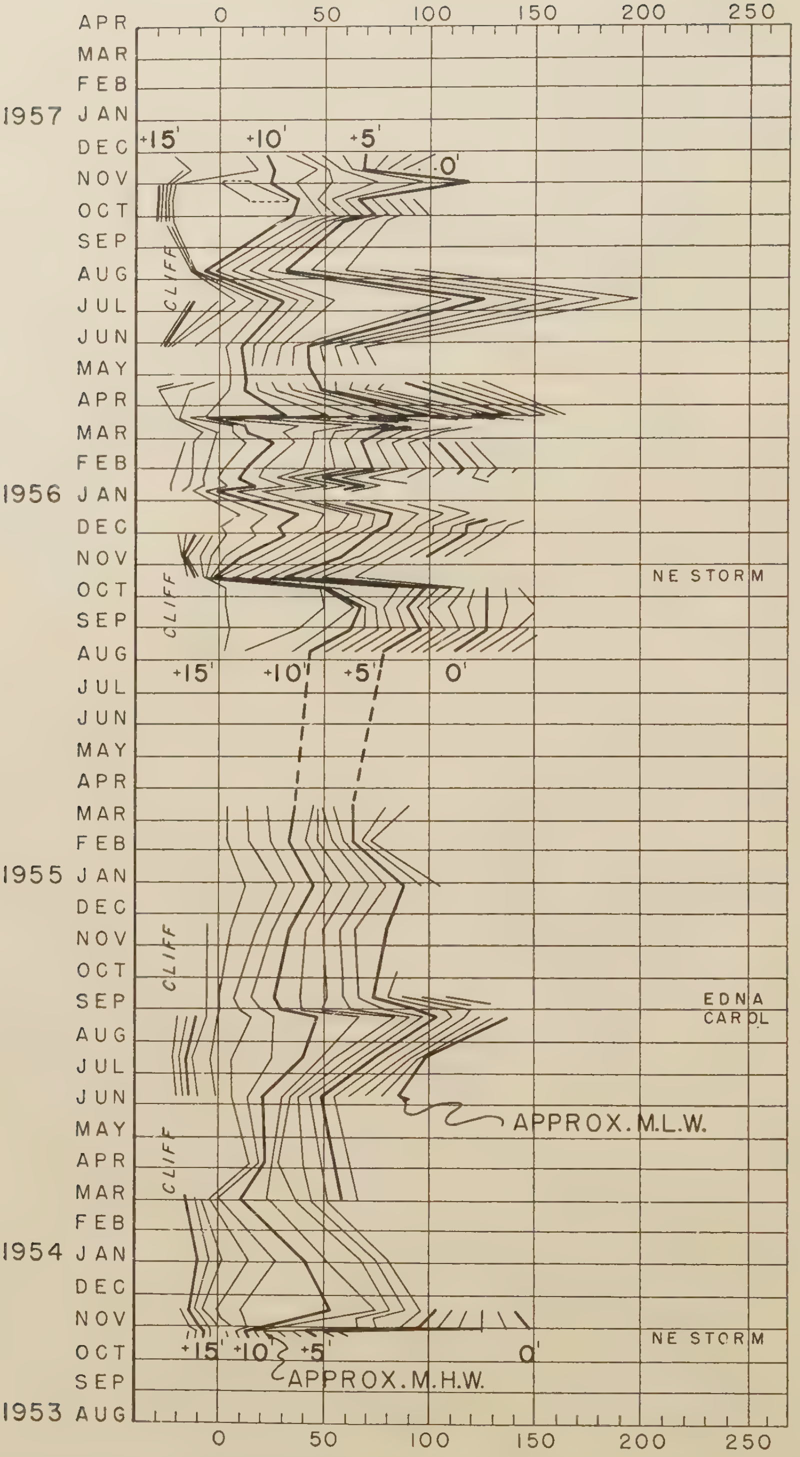

FIG. 3.—Isopleth diagram, Highland B. 0–250, distance from cliff base. Contours connect points of equal elevation.

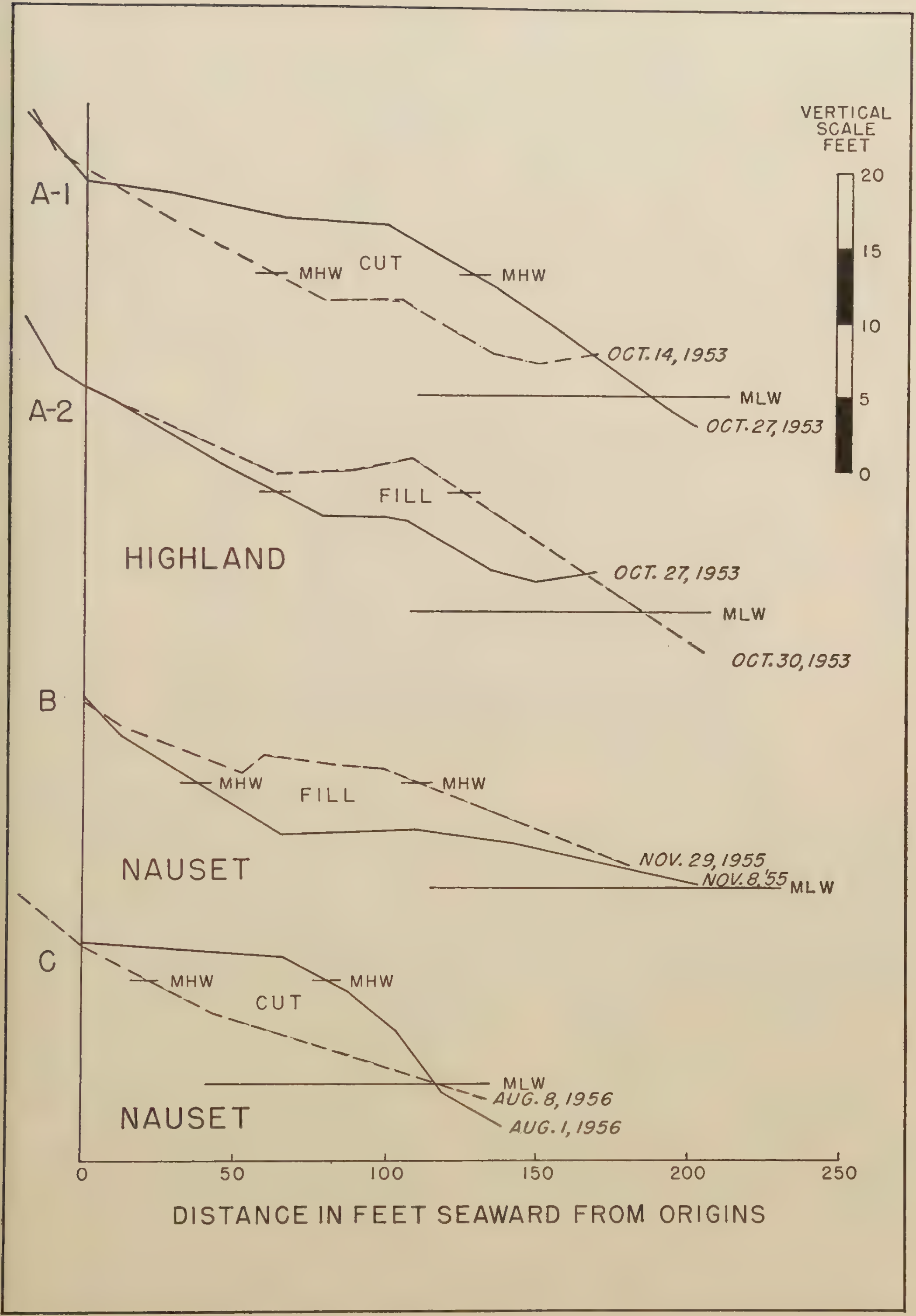

FIG. 4.—Beach profiles, before-after storms

1953 were obtained from the daily weather observations recorded at the Race Point Coast Guard Station near the tip of Cape Cod. Starting in February, 1958, wind direction and velocity were recorded at a station manned by Woods Hole Oceanographic Institution personnel in Provincetown.

Additional information regarding storm tracks, wind directions, and velocities was taken from the Weather Bureau station on Nantucket Island as recorded on daily U.S. Weather Bureau maps. This location is 48 miles south of Provincetown.

TABLE 2*

MAXIMUM CUT AND FILL MEASURED ON BEACHES FOR TWO TIDES AND FOR ONE TIDE

	Maximum Cut (2 tides)	Maximum Fill (2 tides)	Maximum Cut (1 tide)	Maximum Fill (1 tide)
New Beach	106	145	...	79
Race Point	136	177	95	134
High Head	257	154	199	154
Highland A	256	296	223	166
Highland B	...	371	...	...
Nauset A	66	87	81	48
Nauset C	...	192	520	...

* Maximum measured volume changes in cubic feet per linear foot during one day, two tidal cycles, and during one tide for beaches of Outer Cape Cod. The A, B, and C lines refer to different profile lines measured in the same area. New Beach, Race Point, High Head, and Highland had daily measurements taken between January–April, 1958. Race Point, Highland, and Nauset had measurements taken less regularly since 1953.

DESCRIPTION OF STORMS

The following storms plus one extended stormy period were chosen for discussion because they were bracketed with adequate beach surveys (tables 3*A* and 3*B*). The same information, and much more, is shown graphically for Highland on the isopleth diagrams (figs. 2 and 3) and on the diagram for volume changes (figs. 5 and 6).

STORMS DURING THE WINTER AND SPRING OF 1958

During this period the beaches at New Beach, Race Point, High Head, and Highland were surveyed every other low tide. Between the first of the year and the end of April there were approximately 16 storms or stormy days (fig. 8, *F*, *G*, and *H* and table 4).

New Beach.—New Beach grew under conditions of north winds and lost slightly under a variety of other storm conditions.

Race Point.—In general, the beach gained volume under east winds and lost it under northeast and north winds. The pattern of gains and losses is not always the same under similar winds. The differences are probably due to variations in beach drifting.

High Head.—High Head beaches lost volume under most of the storms but gained in the face of an east wind. This situation probably represents a case where more detritus arrives in the area by drifting than is eroded away.

Highland.—The Highland beaches lost volume during most of the storms, especially when the winds came from the northeast or east.

The relationships between the four beach areas and the 16 storms of the winter and spring of 1958 are complex. Since each beach faces a different direction, some may fill while others cut during the same storm. Northwest, west, and southwest winds caused little change at High Head and Highland. Major erosional changes at Race Point, High Head, and Highland occurred with north, northeast, and east winds.

Beaches at Race Point were cut or filled erratically. Amounts of erosion were not as great as at either High Head or Highland, probably due to the protecting effect of Peaked Hill Bar, which lies 1,000 to 2,000 feet offshore. Numerous very large gains in this area are assumed to result from vigorous

TABLE 3A

DATA CONCERNING STORMS AND STORM EFFECTS ON OUTER CAPE COD

SELECTED STORMS

Storm	Track	Period	Av. Max. Velocities (Knots)	Wind Direction	Type of Storm	Remarks (Refer to Table 3B for beach changes)
1........	Fig. 7A	Oct. 22–26, 1953	25–35	N.–E.	A slow northeastward moving coastal storm; a four-day northeaster	Race Point beach volume increase may have been due to loss at Highland
2........	Fig. 7A	Mar. 1–6, 1954	15–25	S.–W. to W.	Two storms from the interior passed on northerly courses 300 miles west of Cape Cod	Outer Cape Cod beaches little affected by the southwest (offshore) winds of this type of storm
3........	Fig. 7C	Oct. 14–17, 1955	24–40	E. to N.–E.	Four days of easterly and northeasterly winds resulted from the stalling of a high over St. Lawrence River mouth and the blocking of two coastal lows	Under the impact of the northeast wind and spring tide, Highland beach was severly cut and Race Point beach gained volume
4........	Fig. 7D	Jan. 5–20, 1956	25–50	N. and E.	A series of five coastal storms passed southeast of Cape Cod causing northeast blizzards	Beach changes were limited by the fact that winter profiles had already been established. Foot of cliffs were exposed to storm-wave attack
5........	Fig. 8E	Mar. 16–17, 1956 Mar. 18–20, 1956	25–50	N.–E.	A complex pattern of lows and highs produced about three days of northeast winds	Storm waves attacked cliffs and dunes on account of beach having winter profile
6........	Fig. 8E	Aug. 7–8, 1956	35–45	E. and N.	A vigorous storm moving easterly from the Great Lakes Region passed out to sea near Delaware Bay, then on a northeast course about 150 miles southeast of Cape Cod	An unusual summer northeaster hit the outer Cape Cod beaches where they were in the well-nourished condition—summer profile

TABLE 3B

DATA CONCERNING STORM EFFECTS ON OUTER CAPE COD BEACHES

Storm	Survey Dates	Volume Change	Race Point	Survey Dates	Volume Change	Highland	Survey Dates	Volume Change	Nauset
1.....	October 15; October 30, 1953	Lost 340 cu. ft.	Lower beach gained; upper beach lost	October 14, October 27, 1953	Lost 540 cu. ft.	Severe displacement of topography: +10 ft. isopleth moved 70 ft. landward	October 14, October 21; October 21, November 3, 1953	Lost 341 cu. ft.; gained 460 cu. ft.	+10 ft. isopleth displaced 70 ft. landward; +5 ft. isopleth 50 ft. seaward
2.....	March 2; March 28, 1954	....	No significant change observed	March 1, March 3, 1954	....	No significant change observed	February 26, March 8, 1954	Gained 102 cu. ft.	Whole foreshore aggraded
3.....	October 11; October 18, 1955	Gained 62 cu. ft.	The foreshore built seaward vigorously: +9 ft. isopleth seaward 60 ft., + 5 ft. isopleth seaward 30 ft., 0 isopleth seaward 5 ft.	October 10, October 17; October 17, October 20, 1955	Lost 262 cu. ft.; gained 167 cu. ft.	Much shifting around of material; beach was cut 9 ft. vertically in middle foreshore; near-shore bar was breached	....	....	Not enough surveys; appeared to be cut similar to Highland
4.....	January 12; February 23, 1956	Lost 379 cu. ft.	Upper foreshore steepened; +4 ft. isopleth moved shoreward 45 ft.	January 11, January 16, 1956	Lost 440 cu. ft.	Beach was wasted (winter profile); slopes changed very little but volume loss was great	Dec. 6, '55, Jan. 6, '56; January 6, January 13; January 13, January 16; January 16, January 24	Lost 253 cu. ft.; gained 215 cu. ft.; lost 93 cu. ft.; lost 72 cu. ft.	Large gains and losses in volume from December, 1955, to January 24, 1956
5.....	March, 1956	....	Insufficient data	March 8, March 21; March 21, March 28, 1956	Gained 6 cu. ft.; gained 104 cu. ft.	Beach was badly depleted (winter profile); storm had almost no effect	March 15, March 20; March 20, March 21, 1956	Lost 86 cu. ft.; lost 41 cu. ft.	Cutting throughout stormy period
6.....	July 19; August 18, 1956	....	No significant change	July 17, August 8; August 8, August 9; August 9, August 10, 1956	Lost 199 cu. ft.; lost 25 cu. ft.; gained 166 cu. ft.	Rapid cutting and filling	August 1, August 8, 1956	Lost 383 cu. ft.	Backshore eroded; lower foreshore aggraded

longshore drifting of eroded material from the High Head and Highland areas.

New Beach, which had undergone considerable erosion in previous years, did not change much in the early months of 1958. The rapid growth on April 2, 1958, was probably due to extensive longshore drifting from Race Point, which underwent cutting before a north wind.

HURRICANES

Hurricanes Edna and Carol were full-fledged hurricanes which did much damage on Cape Cod in the fall of 1954, but they

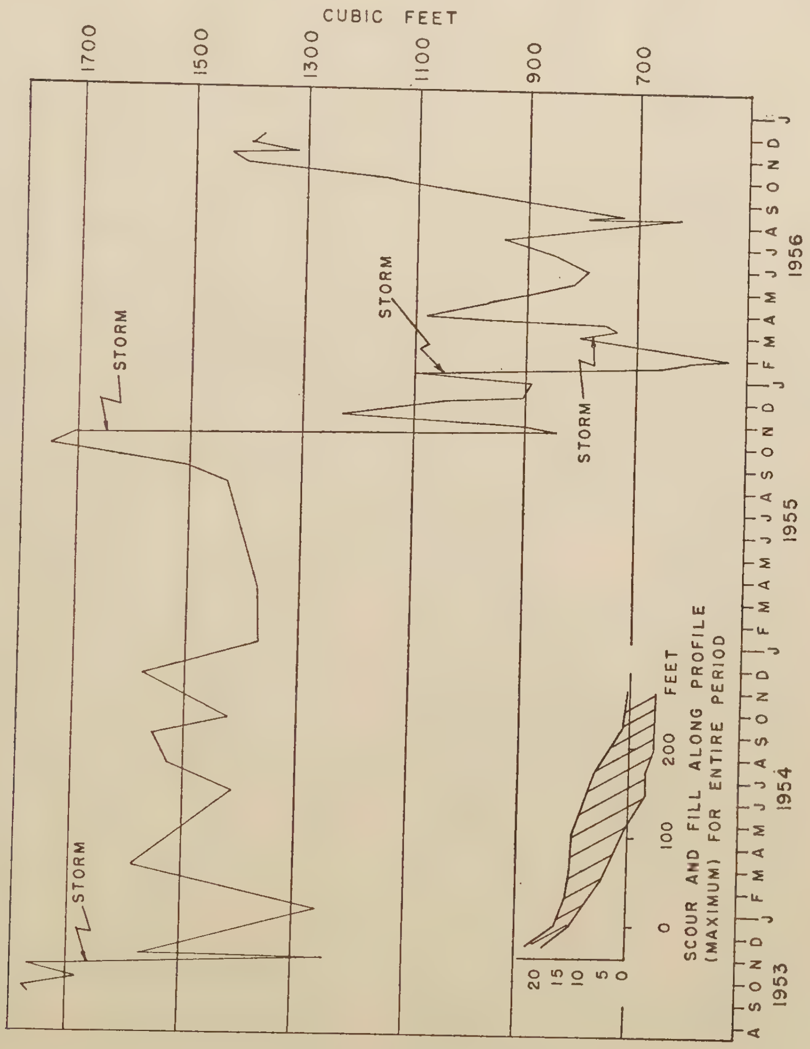

VOLUME OF BEACH BETWEEN TOE OF CLIFF AND APPROXIMATE MLW HIGHLAND "A"

Fig. 5.—Volume of beach, Highland A

moved across the Outer Cape in an offshore direction. Consequently, the seas caused by Hurricanes Edna and Carol never built up on easterly-facing beaches, and their effects on beaches of the Outer Cape were negligible (figs. 2, 3, and 7*b*). However, these same hurricanes caused flooding and severe shore-front erosion in the more enclosed sound and bay areas, such as Narragansett Bay, Buzzards Bay, and Vineyard Sound, and battered the open coasts in the Carolinas. Nichols and Marston (1939) and Chute (1946) have described effects of past hurricanes on the coasts of southern New England, where water levels were raised high above normal.

Cliff erosion.—It is impressive that while

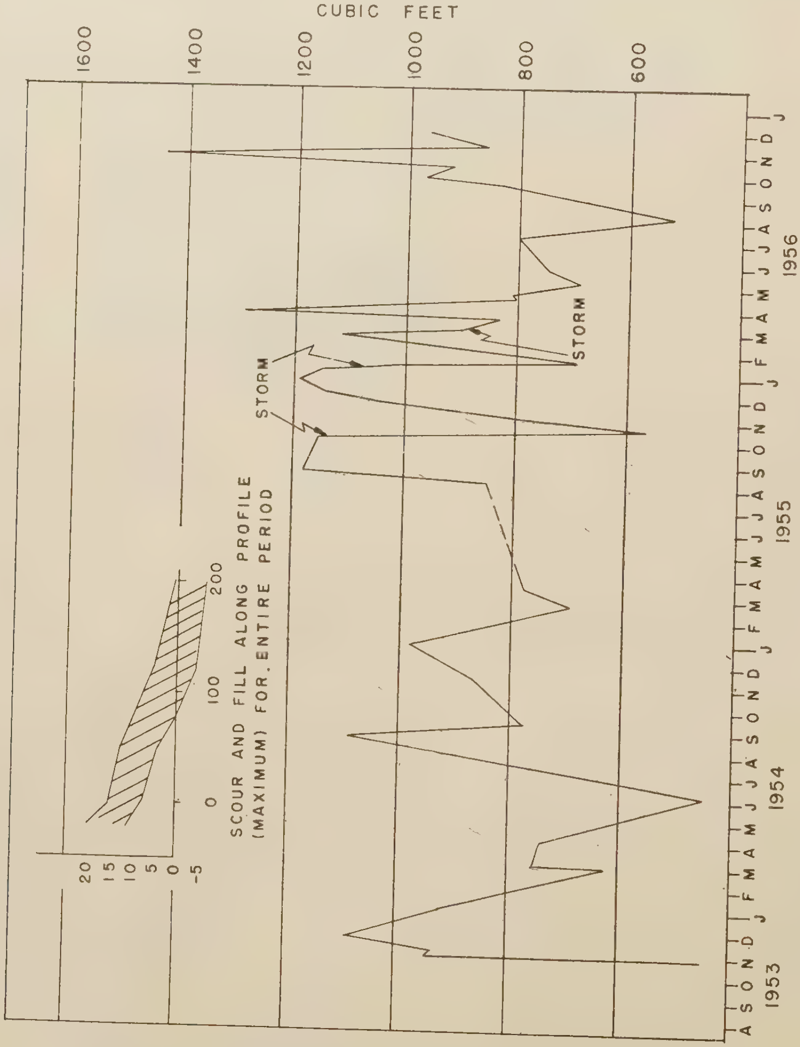

VOLUME OF BEACH BETWEEN TOE OF CLIFF AND APPROXIMATE MLW HIGHLAND "B"

FIG. 6.—Volume of beach, Highland B

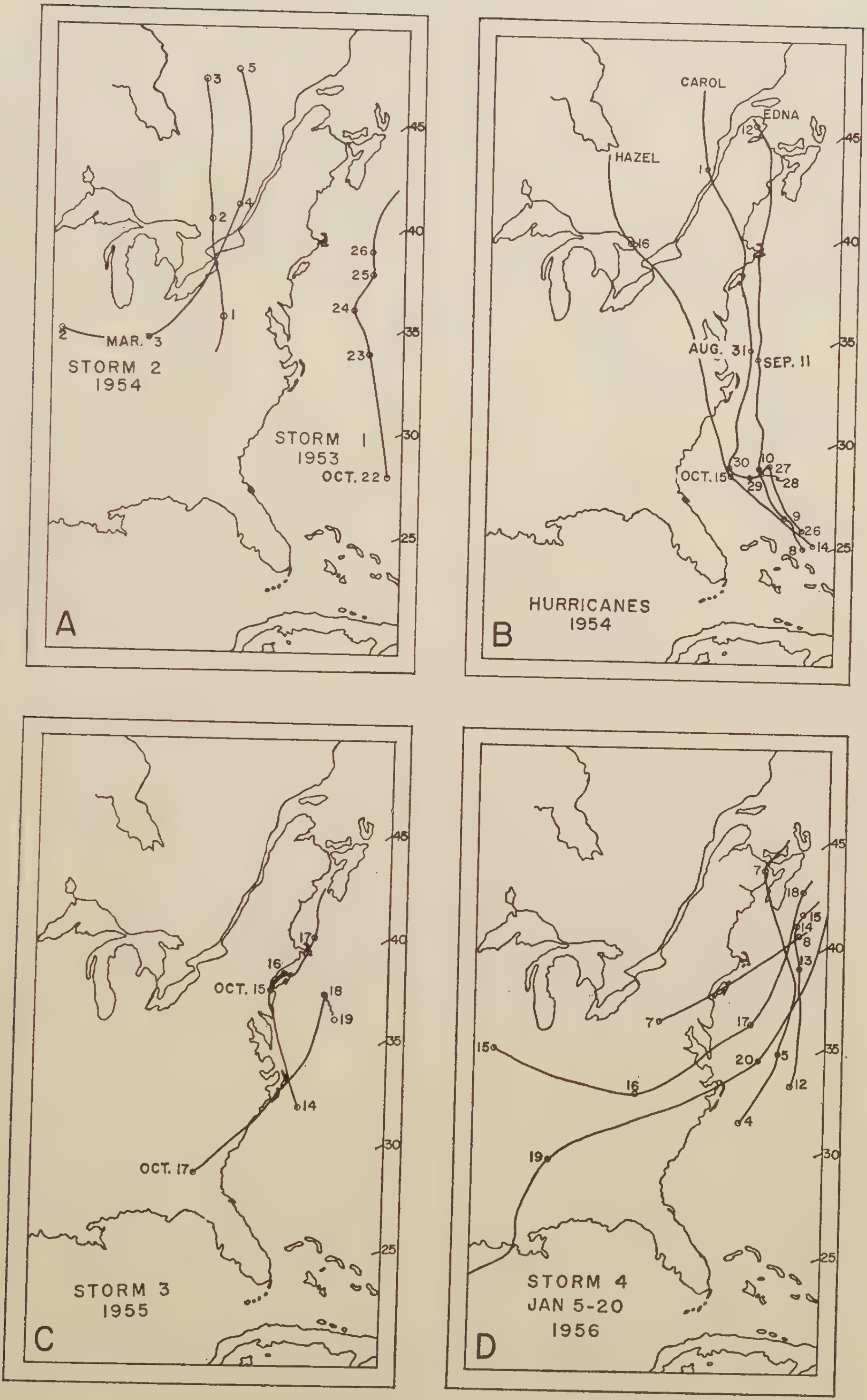
3
5
45
4
2
40
26
25
24
1
2
MAR. 3
35
23
STORM 2
1954
STORM 1
1953
30
OCT. 22
25
A
CAROL
EDNA
12
45
HAZEL
1
16
40
AUG. 31
SEP. 11
35
30
10
27
OCT. 15
30
28
29
9
26
8
14
25
HURRICANES
1954
B
45
17
40
16
OCT. 15
18
19
35
14
30
OCT. 17
25
STORM 3
1955
C
45
7
18
15
14
8
40
13
7
17
15
35
20
5
16
12
4
30
19
25
STORM 4
JAN 5-20
1956
D

FIG. 7.—Selected storm tracks

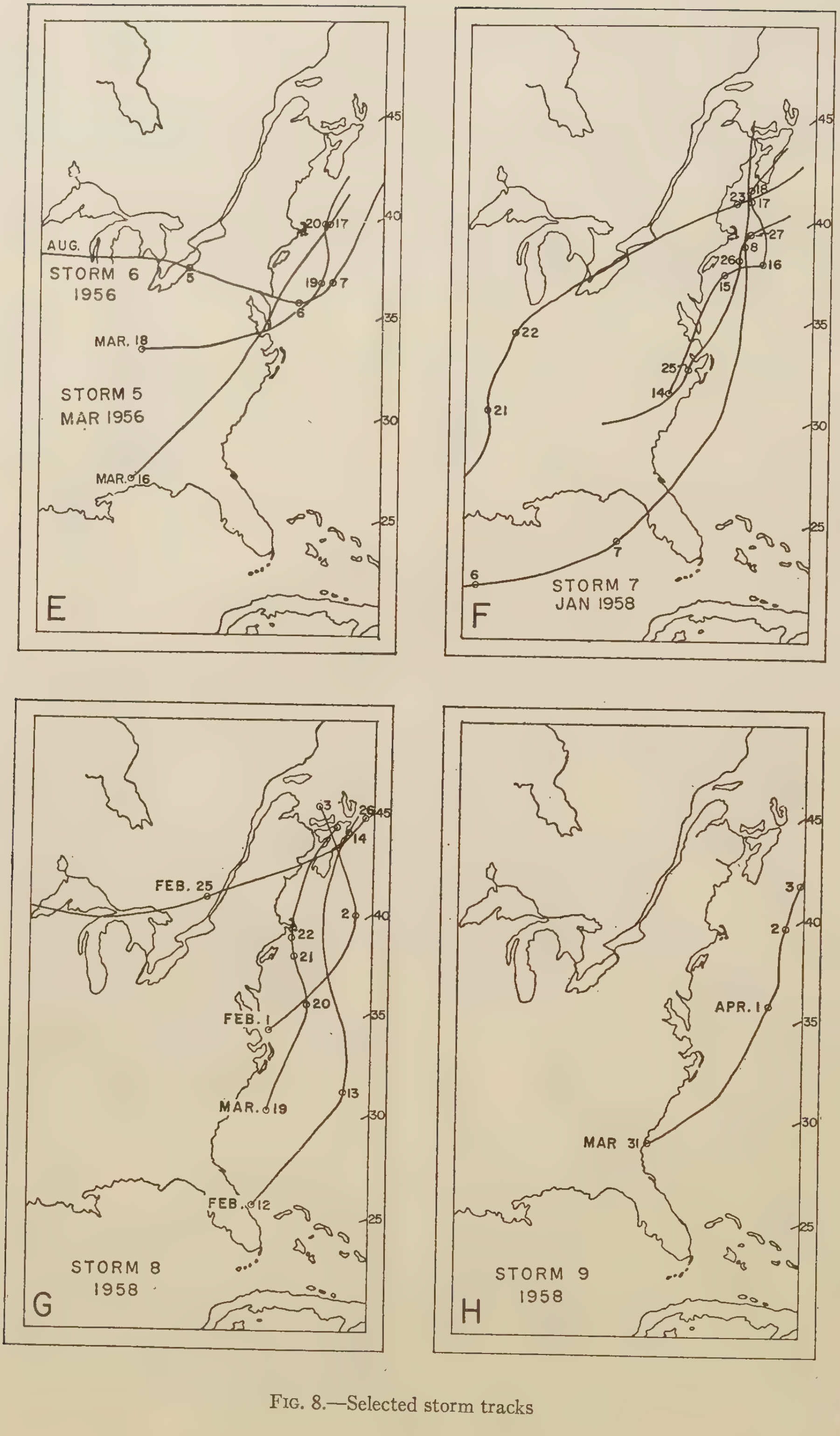
E
AUG.
STORM 6
1956
5
20
17
19
7
6
MAR. 18
STORM 5
MAR 1956
MAR. 16
45
40
35
30
25
F
23
18
17
27
8
26
16
15
22
25
14
21
7
6
STORM 7
JAN 1958
45
40
35
30
25
G
3
26
14
FEB. 25
2
22
21
20
FEB. 1
13
MAR. 19
FEB. 12
STORM 8
1958
45
40
35
30
25
H
3
2
APR. 1
MAR 31
STORM 9
1958
45
40
35
30
25

FIG. 8.—Selected storm tracks

many storms eroded the beaches, the cliffs were untouched by some of these storms, for example, at Highland the toe of the cliff was untouched by storms from August, 1953, until January, 1956. When cutting did take place in January and March, 1956, storm waves eroded the cliff base 20 feet and left a scarp 5 feet high at one profile and 14 feet high on another (pl. 1, *A*). This scarp was slowly buried by the addition of colluvial material from the cliff face and was topographically gone in May, 1956. One could still discern a line in the cliff face marking the top of the scarp in September, 1956 (pl. 1, *B*). The cliff toe at Highland has retreated a net distance of about 4 feet and the top of the cliff about $4\frac{1}{2}$ feet in $4\frac{1}{4}$ years (October, 1953, until January, 1958). Furthermore, it must be remembered that erosion rates on the cliffs differ between Nauset and Highland, being greatest in the center (Marindin, 1889; Davis, 1896). Very spectacular cliff cutting took place in the April storm during 1958, when the entire cliff section from Nauset to Highland was cut. Measurements showed 30 to 50 feet cut away at the Nauset parking lot in front of the coast-guard station. Twelve and one-half feet were cut from a point in the central part of the Cape and 4 feet from Highland. It is estimated that 150,000 cubic yards of material were carried away by this one storm.

TABLE 4*

DATA CONCERNING STORMS AND STORM EFFECTS IN 1958

Date	Direction	Wind Velocity (mph)	New Beach	Race Point	High Head	Highland
Jan. 8......	E.	45–50	....	−124	−150 +158	−86/+10
12......	NW.	25–30	....	+9†	x/−83	x/−55
15......	E.	40–50	....	+91	+49	−124/+25
23......	W.	25–30	....	−7†	+15	0
26......	E.	25–30	....	+98†	+79	+33/+95
Feb. 2......	N.	30–40	....	−49‡	−34†	+29†
14......	W.	25–30	−18	−136	−25	−14/+61
25......	SE.	25–30	−2	+56	+12	+20
28......	E.	25–30	−22	+141	−10/+53	−8
Mar. 20......	NE.	20–25	....	−109†	−3	+31
21......	E.	35–40	....	+65†	+47/+38	−73
27......	NE.	25–30	+4	−22	+69	+3
28......	NE.	35–40	....	+136	+18	−87
Apr. 2......	N.	25–30	+79 +66	−111 +134	−58 −199	+89 −223
3......	N.	25–30	+9 +1	−70 +110	−25 −25	+38 −42
4......	N.	20–25	+35	−95	−71 +46	+133 −127
7......	S.	25–30	−12‡	+142‡ −64	−70†	+38†
Maximum cut and fill changes during one day, 1953–1958			−106 +145	−136 +177	−257 +154	−256 +296

* Daily volume changes during the winter and spring, January–April, 1958. When two numbers are included in one square, one above the other, they indicate changes per tidal cycle for that day. When two numbers in one block are separated by a slant line, they indicate changes for successive days, the left-hand number is for the day indicated.

† Average daily changes for a 2-day period.

‡ Average daily changes for a 3-day period.

Erosion and bar positions.—Behavior of the Highland profile line illustrates the importance of nearshore shoals in absorbing storm energy. The isopleth diagram (fig. 2) indicates that the Highland beach area was eroded severely by the storm which occurred in October, 1955, and that the beach remained in a wasted condition until autumn, 1956, when it began to recover. The profile at the Nauset line showed the same sort of history—erosion, a period of very narrow beach and finally recovery to the prestorm condition. This sequence is well illustrated by figure 5, which shows the volume changes of the beach at Highland.

This erosion and recovery pattern was related directly to the near-shore shoal in front of the beach (pl. 2, *A*). Both at Nauset and Highland the near-shore bars were cut away during the storm which damaged them in October, 1955. As long as the bar protected the beaches, they withstood erosion reasonably well, but, when the bar was cut through, the beach was eroded at once. The bar at Highland gradually began to grow in August, 1956, and by mid-October had practically healed the break. The beach recovered slowly both in width and in volume during this period. Also, it is interesting to note that the toe of the cliff was cut in 1956 when the beach was in a wasted condition. The profile line at Nauset remained unprotected by an offshore bar, i.e., it faced a break-through until summer, 1957. Measurements there were not being made at this time, but it was noticed that when the bar grew in front of the line, the beach recovered in width and volume. The tendency of the beach to be cut away behind openings in the bar is well shown in plate 2, *B*. One can see the scalloped cuts along the entire shore.

It was noted that during the storms prior to April, 1958, the cliffs tended to erode opposite the gaps in the bar. Inasmuch as these near-shore bars and the gaps between them shifted their positions laterally along the coast, the erosive tendency shifted also. The action is like a giant-toothed saw, in which the gaps in the bar represent the cutting teeth. The storm in April, 1958, simply overwhelmed bars and gaps together and cut the cliff along its entire length.

A second example of control by bars was best documented during the storm of April, 1958. Beaches in the lee of Peaked Hill Bar were not damaged by this very violent storm—in fact they grew in width and volume in the face of this storm which blew directly onshore there. Measurements taken at Race Point and Highland in the lee of the bar showed that the beaches filled (table 4), and aerial surveys of the entire strip of coast from Highland Light to Race Point showed general widening of the beach.

COMMENTS AND CONCLUSIONS

Even with the multiplicity of surveys, considerable uncertainty exists regarding rapid changes. Surely large cuts might have been masked by the beginning of filling before the next survey, and, therefore, maximum changes might not have been measured. In some cases changes may be masked by new conditions. These too can take place rapidly enough to escape detection unless continuous observations are taken.

Wave changes may be many hours behind wind changes, and it is sometimes impossible to identify beach changes with specific wind conditions. Also, when large storms pass some distance away, the waves reaching the coast may have no relationship to the local wind conditions on the beach. Only gross changes in beach conditions can be related to the specific wave conditions far offshore; therefore, it is imperative that knowledge of shoaling waves be extended if one is to understand beach regimen.

Uncertainty exists as to the exact whereabouts and movements of the large volume of beach material removed from profile lines. Two possibilities, or combinations of both, are possible. The material may be raked down off the beach and laid to rest in quieter

---

PLATE 1

A, Cliff erosion, Highland B profile, March 22, 1956. 14-foot nearly vertical wave-cut cliff base, the result of storm series 4 and 5, winter, 1956.

B, Cliff erosion, Highland B profile, October 1, 1956. Six months of cliff-face slumping and wind drift have filled in the 14-foot scarp cut into the cliff base during winter of 1956 (see pl. 1, *A*).

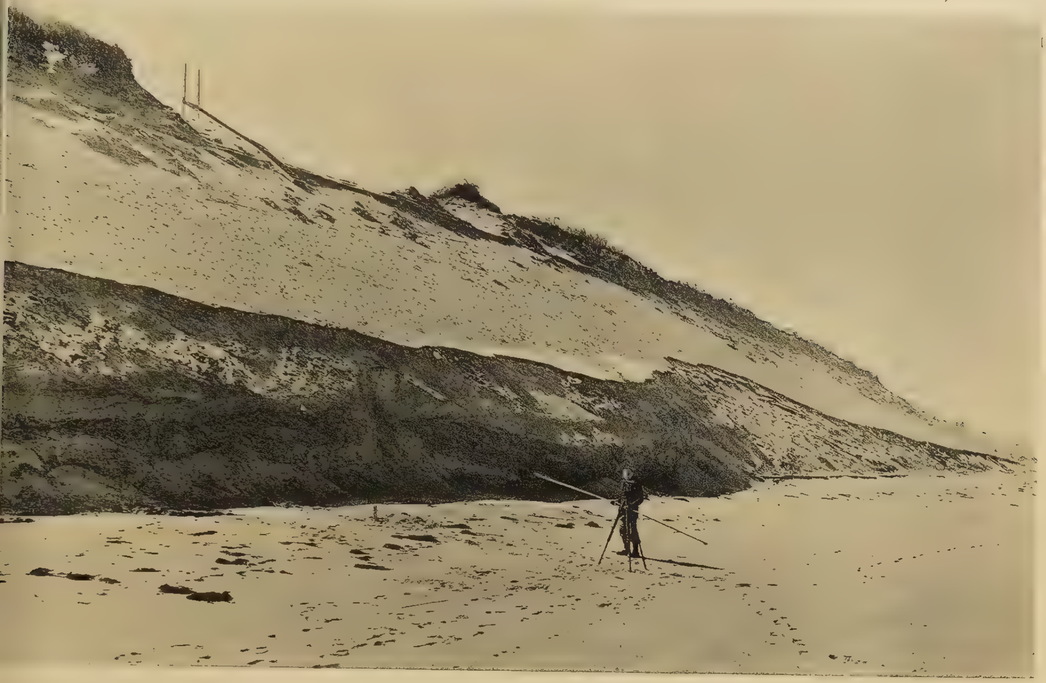

A

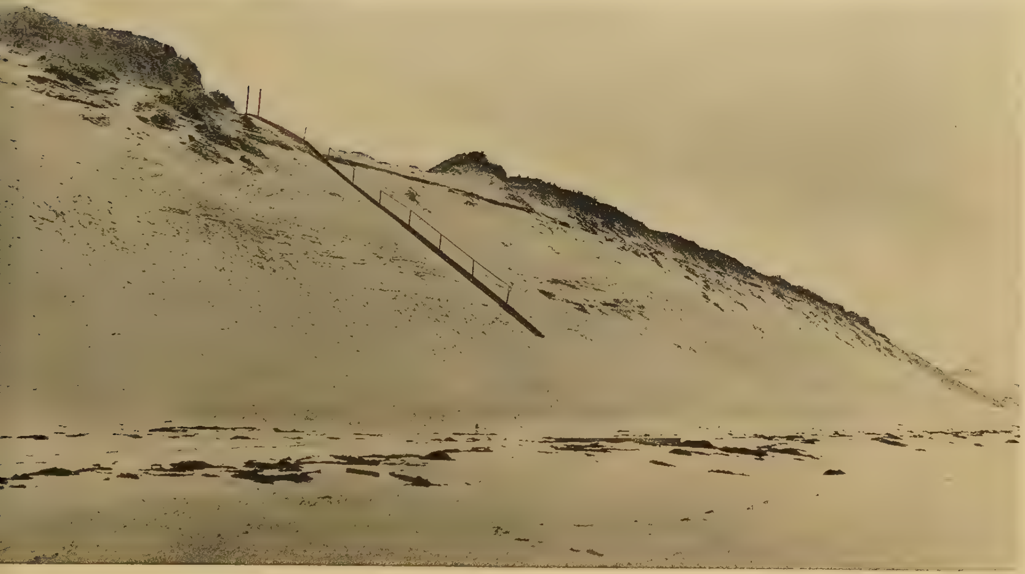

B

Wave-cut cliff base

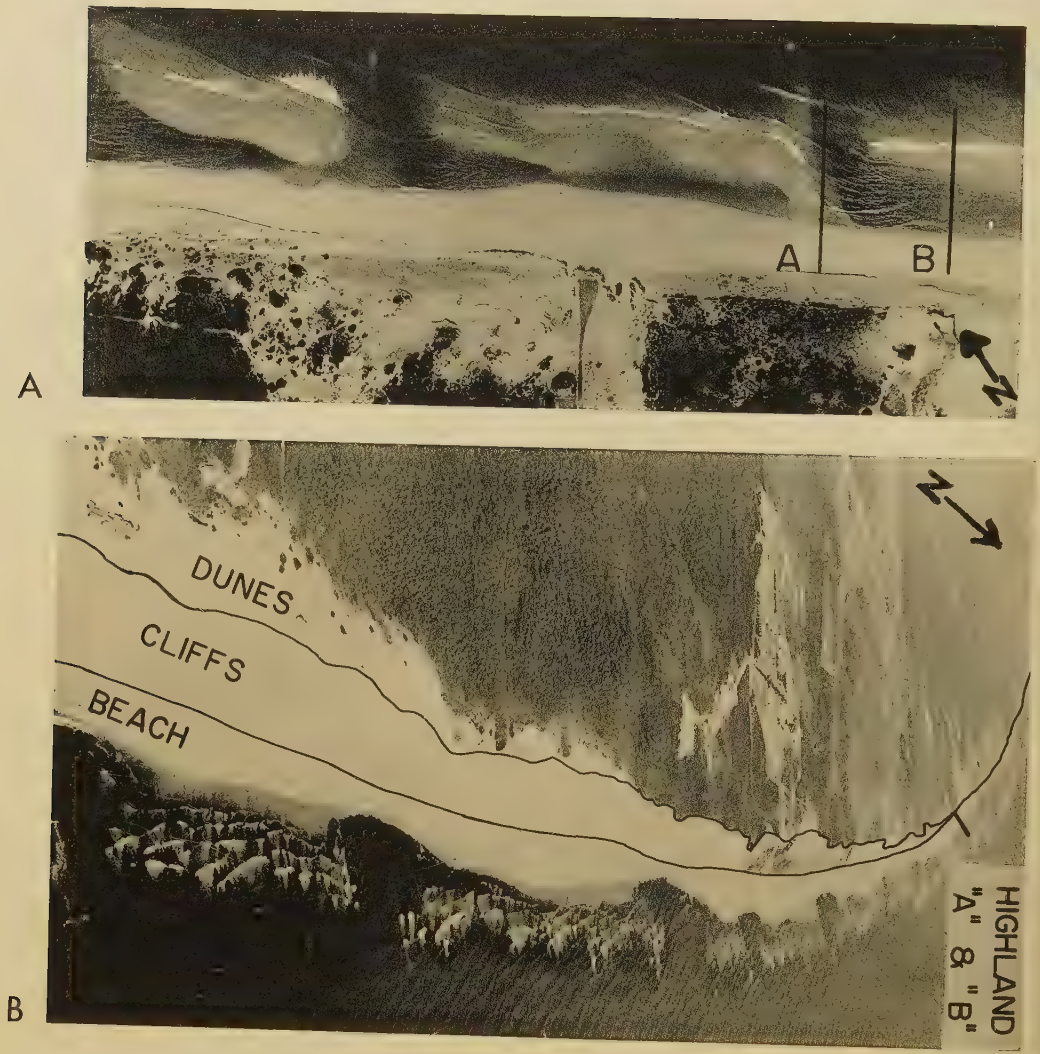
A
B
N
A
N
DUNES
CLIFFS
BEACH
HIGHLAND "A" & "B"
B

Aerial photographs

water offshore, to be returned to the beach after the wave conditions change. The other possibility is that, on the curving shore of the Outer Cape, beach and longshore drifting occurs very rapidly during storms and much of the material eroded from one place is moved laterally along the coast. Continuous profile measurements along miles of beaches would be necessary as well as extremely accurate shallow-water topographic surveys to locate this material without using radioactive tracers.

Examination of cut and fill measurements suggests that beach erosion occurs very rapidly during storms and that recovery to prestorm conditions occurs within a few days. Data are presented in a variety of ways, such as isopleths and volume changes.

Beaches on Cape Cod, at the time of the first low tide following a storm, are smooth with a uniform slope usually less steep than before. Stones and pebbles are rare but they return to the foot of the foreshore within a few tides.

After storms, beach profiles are planar or concave upward. When the beaches are full during nonstormy periods, the beach profiles are convex upward.

Data are presented to show the extent of protection offered by offshore bars. Changes in the bar have been related to changes of the beach.

Data are presented to show the rate of erosion of cliffs on Cape Cod and the rates of recovery of cliffs after cutting.

ACKNOWLEDGMENTS.—Many people have aided in the gathering and processing of the data used in this study; only a few can be mentioned specifically. Surveying and measuring of the profile lines have been done since 1957, by Herman Tasha of Provincetown. The tedious and involved task of assembling, calculating, and plotting the survey data was done in the main by Mrs. Barbara Gill. Aerial photographs were made by members of the Institution's photographic staff from Woods Hole Oceanographic Institution aircraft.

No acknowledgment would be complete which did not point out the stimulus of the late Henry C. Stetson, who initiated the program, and Professor Marshall Schalk, of Smith College, who worked with him. The Geography Branch of the Office of Naval Research through its head, Dr. L. O. Quam, and project supervisor, Miss Evelyn Pruitt, provided financial support which permitted unhurried and flexible research. The work was carried out under ONR-Geography Branch Contract No. Nonr-1254 (00)(NR-388-018). Finally, we are grateful to Professor R. L. Miller, of the University of Chicago, for encouragement in many aspects of our beach-study program.

REFERENCES CITED

CHUTE, N. E., 1946, Shoreline changes caused by hurricane of September 1944: Bull. 9, Mass. Dept. Public Works in co-operation with the U.S. Geol. Survey.

DAVIS, W. M., 1896, The outline of Cape Cod; *in:* D. W. JOHNSON (ed.), Geog. Essays, p. 690–724: New York, Dover Publications, 1909. Also Proc. Am. Acad. Arts & Sci., 1896, v. 31, p. 303–332.

INMAN, D. L., 1953, Areal and seasonal variations in beach and near shore sediments at La Jolla, California: Tech. Memo. no. 39, Beach Erosion Board.

JOHNSON, D. W., 1919, Shore processes and shoreline development: New York, John Wiley & Sons, Inc.

MARINDIN, H. L., 1889, Encroachment of the sea upon the coast of Cape Cod, Massachusetts as shown by comparative studies; cross-sections of

---

PLATE 2

A, Vertical aerial photo of the Highland study area. The offshore bar here is not exactly parallel to the shoreline, and each segment appears to be growing northwestward.

B, Oblique aerial photo of 3 miles of the east coast of Outer Cape Cod south of Highland. Re-entrants are cut in the beach opposite breaks in the offshore bars. The areas of multiple breakers indicate the position of the shallow parts of the bar. Notice also how these openings in the bar have caused wave refraction.

the shore of Cape Cod between Chatham and the Highland Lighthouse: Ann. Rept. U.S. Coast and Geodetic Survey, 1889, app. 12, p. 403–407; app. 13, p. 409–457.

Marindin, H. L., 1891, On the changes in the shoreline and anchorage areas of Cape Cod (or Provincetown) Harbor as shown by a comparison of surveys made between 1835, 1867 and 1890; cross-sections of the shore of Cape Cod, Massachusetts between the Cape Cod and Long Point Lighthouses: *ibid.*, 1891, app. 8, p. 283–287; app. 9, p. 289–341.

Miller, R. L., and Zeigler, J. M., 1958, A study of the relation between dynamics and sediment pattern in the region of shoaling waves, breaker zone and foreshore: Ecol. Helvet. (in press).

——— — ——— 1958*a*, A model relating dynamics and sediment pattern in equilibrium in the region of shoaling water, breaker zone and foreshore: Jour. Geology, v. 66, p. 417–441.

Morgan, I. P., Nichols, L. G., and Wright, Martin, 1958, Morphological effects of Hurricane Audrey on the Louisiana Coast: Coastal Studies Inst., La. State Univ., Tech. Rept. no. 10.

Nichols, R. L., and Marston, A. P., 1939, Shoreline changes in Rhode Island produced by hurricane of September 21, 1938: Geol. Soc. America Bull., v. 50, p. 1357–1370.

Shepard, F. P., 1950, Beach cycles in southern California: Tech. Memo. no. 20, Beach Erosion Board.

——— and Inman, D. L., 1951, Sand movement on the shallow intercanyon shelf at La Jolla, California: *ibid.*, no. 26, Beach Erosion Board.

——— and LaFond, E. C., 1940, Sand movement along the Scripps Institution pier, California: Amer. Jour. Sci., v. 238, p. 272–285.

Woodworth, J. B., and Wigglesworth, Edward, 1934, Geography and geology of the region including Cape Cod, the Elizabeth Islands, Nantucket, Martha's Vineyard, No Mans Land and Block Island: Mus. Comp. Zoöl., Harvard Coll., v. 52.

Zeigler, J. M., and Ronne, F. C., 1957, Time-lapse photography—an aid to studies of shorelines: Res. Rev.

Contribution No. 961

Reprinted from
BULLETIN OF MARINE SCIENCE
OF THE GULF AND CARIBBEAN
Vol. 9, No. 2, pp. 117-152
JUNE, 1959

ON THE IDENTIFICATION, DISTRIBUTION, AND BIOLOGY OF THE DOLPHINS, *CORYPHAENA HIPPURUS* AND *C. EQUISELIS*[1]

ROBERT H. GIBBS, JR.
Department of Biology, Boston University, Boston, Massachusetts

AND

BRUCE B. COLLETTE
Department of Conservation, Cornell University, Ithaca, New York

ABSTRACT

Coryphaena hippurus, the common dolphin, and *C. equiselis,* the pompano dolphin, have been studied. The specific name *equiselis* is considered valid, as opposed to the emended form, *equisetis.* The two species differ markedly in numbers of dorsal and anal rays and lateral-line scales, in morphometric characters which reflect depth, in relative heights of dorsal and anal fins, in the shape of the tooth patch on the tongue, and in the color pattern and head spination of the young. Weights of males and females are similar below about 950 mm, after which males appear heavier. Both species are probably cosmopolitan in warm seas. *C. hippurus* is most often caught in waters over 70°F. Adults of *C. equiselis* are seldom caught and are probably more pelagic and more tropical. *C. hippurus* breeds in summer in the Gulf Stream, earlier in the Caribbean. Young *C. hippurus* are, paradoxically, less abundant than those of *C. equiselis,* particularly in the Gulf of Mexico and Florida Current. The sex ratio of *C. hippurus* is 50:50 in the Gulf Stream, but females apparently predominate in Caribbean sport catches. Stomach analyses show fishes to be the most abundant item in the diet of *C. hippurus,* with no evidence of selectivity. There is some indication that feeding is inhibited at night.

INTRODUCTION

The family Coryphaenidae comprises a single genus, *Coryphaena* Linnaeus, which contains two presently recognized species. *C. hippurus* Linnaeus is cosmopolitan in tropical and subtropical waters and s a well-known food and game fish in much of its range. *C. equiselis* Linnaeus is relatively little known, but is probably also cosmopolitan n much the same waters. The exact distributional status of the latter

---

Work done under National Science Foundation Grant 2102 at the Woods Hole Oceanographic Institution. W.H.O.I. Contribution No. 961.

is difficult to determine because it has been confused with its congener. Those who have purported to recognize two species have either cited poor differentiating characters or have considered as *C. equiselis,* females and young males of *C. hippurus,* which lack the high, vertical forehead, and have relegated to *C. hippurus* only the larger males, which have the vertical head profile. Thus it is difficult to determine whether reports of *C. equiselis* are, indeed, that species. An example is found in Barnhart (1936), in which the illustration of "*Coryphaena equisetis*" shows a *C. hippurus* (possibly a female) without the vertical forehead.

The present paper has the following objectives: to facilitate the identification of the two species of dolphin, at least as they occur in the western north Atlantic, at any size above about ten millimeters (the smallest size at which specimens of both species were available to us), to clarify their nomenclature, to show relative growth patterns of the two species, to indicate the distribution of both young and adult in the Atlantic, and to contribute to the biology of both species by giving data on spawning and food habits. It is hoped that this information will provide a basis for future, more-detailed studies of both species, and of *C. equiselis* in particular.

NOMENCLATURE

Linnaeus described both *Coryphaena hippurus* and *C. equiselis* in the 10th edition of Systema Naturae (1758:261). Whereas other nominal species have been described, at the present time none of these seem justified.

Although the name *equiselis* was used by Linnaeus in his work, this has long been considered a misprint, and *equisetis* has been used instead. Osbeck (1757:308), from whose work the Linnaean description and name were apparently derived, did, indeed, use the name *equisetis*. On the other hand, Linnaeus' "misprint" was not corrected in three editions of Systema Naturae following the tenth. Furthermore, as Fowler (1906:122) pointed out, neither form is incorrect from an etymological standpoint. There is no decisive evidence that the Linnaean form was not intentional. We therefore believe that the name should stand as *Coryphaena equiselis* Linnaeus, 1758.

Coryphaena hippurus is properly termed "dolphin," even though this name is also applied to certain cetaceans. *C. equiselis* may be known as "pompano dolphin," in reference to the deep body of adults.

MATERIALS AND METHODS

Most of our data is derived from material from two regions: from the Gulf of Mexico and the Gulf Stream. Many small specimens were collected by Harvey R. Bullis, Jr. of the U. S. Fish and Wildlife Service and the crew of the M/V OREGON. We are indebted to Mr. Bullis, not only for the specimens, but also for permission to participate personally in a cruise aboard the OREGON. Edgar L. Arnold, Jr. of the Fish and Wildlife Service contributed other Gulf specimens. From the region of the Gulf Stream (*sensu stricto,* cf. Iselin, 1936:74), most of our specimens were collected from the M/V DELAWARE. We are grateful to James L. Squire, of the Fish and Wildlife Service, for allowing us to participate in several cruises. Members of the crews and scientific personnel of the research vessels ATLANTIS, CRAWFORD, BEAR, and CARYN, of the Woods Hole Oceanographic Institution, collected specimens from the Gulf Stream, the Caribbean Sea, and the tropical Atlantic. We are especially grateful to W. Scott Bray, Richard H. Backus, Dana Densmore, Robert A. Lufburrow, and Nicholas Rosa for these specimens. W. W. Anderson and Jack W. Gehringer kindly loaned us the specimens collected in the Florida Current and Bahamas region by the Fish and Wildlife M/V THEODORE H. GILL. We extend our thanks for Rockport, Texas, specimens to Patricia Pew of the Texas Game and Fish Commission; for Woods Hole specimens to Nadine Athearn; and for specimens in their collections, to Reeve M. Bailey of the Museum of Zoology, University of Michigan, Royal D. Suttkus of Tulane University, and ichthyologists at the Museum of Comparative Zoology and the U. S. National Museum. Edward C. Raney and William C. Schroeder critically read the manuscript. We are particularly indebted to Frank J. Mather III, of the Woods Hole Oceanographic Institution, for allowing us to use his unpublished data and preserved material, to Donald S. Erdman of Lajas, Puerto Rico, for information on *C. equiselis* in Puerto Rico, to Donald P. deSylva of the University of Delaware, Bayside Laboratory, for reading the manuscript and contributing information on the coloration of *C. equiselis* and on other phases of the work. All figures are the work of G. G. Pasley.

Five counts (dorsal, anal, pectoral rays, lateral-line scales, gill rakers) were made routinely. The dorsal, anal, and pectoral counts include all elements, both spines and rays. In the dorsal fin, it is difficult to determine how many, if any, of the anterior elements are spines.

In the anal fin, we found one to three spines preceding, and usually considerably shorter than, the rays, although there was usually a single, slightly shorter ray preceding an otherwise rather uniformly graded series. There was one pectoral spine. The pelvic fins were almost constantly I, 5, and we did not enumerate this beyond an initial check. Lateral-line scales are extremely difficult to count, as there is no well-arranged pattern of vertical or horizontal rows. We counted either pores in or scales above or below the lateral line. This count is probably not precise, but even so its value is seen in the species comparison, where it provides almost complete separation. Because of the range, it was necessary to present the results in groups of five, which then show a relatively normal distribution. Gill rakers were counted without including rudiments. Even in the younger specimens (ca. 10 mm) there were rough patches at the ends of the gill bar which could have been construed as remnants. Since these occurred in our smaller specimens, it was concluded they did not represent reduced rakers.

Measurements were taken in accordance with Hubbs and Lagler (1947). Those not listed by them are self-evident or are explained in the appropriate place. Dial calipers were used on all small specimens, and, on large specimens, calipers constructed of specially made headpieces on a meter stick. Most of the latter were measured at sea and the specimens not retained.

Weights were taken by the authors on fresh specimens caught well out at sea. Ship's motion usually prevented precision beyond the nearest pound. Further weights were contributed by Mather, and others were taken from the literature. Preserved specimens were not weighed.

We have routinely used standard length as a basis for comparisons and this is used throughout this paper except where expressly stated otherwise (as in length-weight, where we used the data of others who did not use standard length).

COLORATION

The color of living *C. hippurus* can only be described as superbly beautiful; detailed comments are never quite adequate to convey this impression. Swimming free in the water, *C. hippurus* is commonly a rich, almost turquoise blue in general coloration, with tinges of yellow. Often individuals have been seen which displayed vertical bands, and on occasion this pattern has been observed to disappear and reappear at short intervals. Such a banded pattern has never been noted by us in a landed fish. A freshly-caught specimen changes color very rapidly;

yellow is usually the predominant shade, but much turquoise blue is seen at first. After death, these colors fade to leave the fish uniformly silvery.

The coloration of freshly-caught adults of *C. equiselis* has not been observed by us, but is said to resemble closely that of *C. hippurus,* with more silvery, instead of yellow, hues. The black spots on the sides are supposedly more noticeable in *equiselis,* particularly shortly after death, and the dorsal, anal, and caudal may have more yellow. This does not agree with preserved adults, which are rather uniformly dark, or with the young, which are discussed below.

The young of the two species are distinctively patterned. This enables their identification without reference to counts or measurements in almost all cases, from the smallest we have seen (ca. 9 mm) to about 200 mm, and perhaps larger. The principal differences are in the pattern of the sides and of the dorsal, anal, pelvic, and caudal fins.

Young of *C. hippurus* (see Fig. 1, upper) tend to have the entire sides of the body marked with a pattern of alternating dark and light bars. This is particularly evident at very small sizes (10-20 mm standard length), where specimens with erected dorsal and anal fins resemble miniature feathers. The bars are continued onto the dorsal and anal fins, except for the rear rays of each, where the dark coloration forms a more or less solid patch. We have observed this general pattern in individuals slightly more than 100 mm long. At larger sizes, however, the bars become more obscure, and are lacking in many specimens. Such specimens are similar to *C. equiselis* in this respect.

C. equiselis (see Fig. 1, lower) when very small tends to be uniformly dark on the sides. The fins, while sometimes displaying weak bars, never show these as prominently as *C. hippurus*. Ordinarily the dorsal fin is relatively clear, often having, in addition to any weak bars, a concentration of pigment near the middle of the fin and in the posterior membranes. The anal fin is quite clear except for a posterior darkened area.

The pelvic fin of *C. hippurus* is usually dark, while that of *C. equiselis* is clear.

Most consistent of all is the pattern of the caudal fin. In young of *C. hippurus* the fin is pigmented except for the tips of each lobe. In *C. equiselis* the unpigmented region extends in a band along the entire margin of the fork. In some small specimens of this species almost the entire fin may appear clear, but the pigment present usually has an

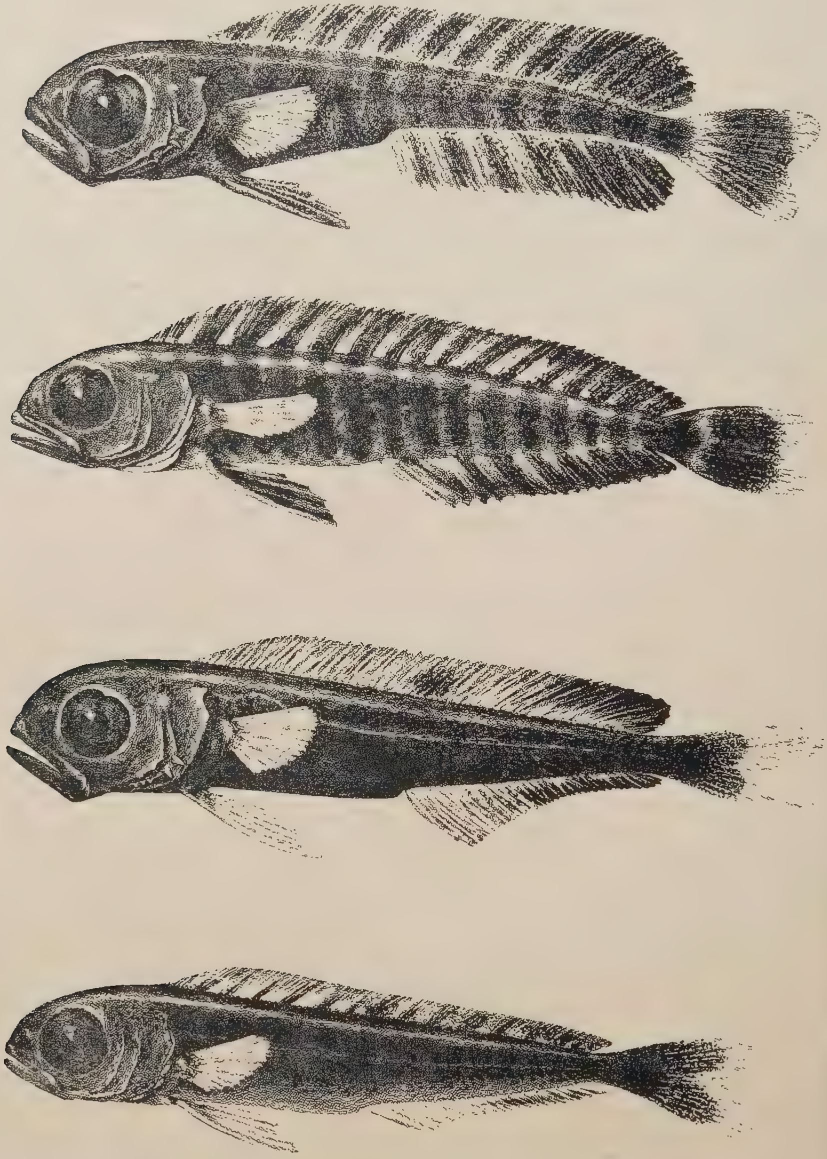

FIGURE 1. Upper 2, *C. hippurus*. Lower 2, *C. equiselis*. Upper figure of each species was drawn with modifications from specimens ca. 15 mm standard length from M/V OREGON station 1298 in the northern Gulf of Mexico; lower figures from specimens ca. 35 mm from OREGON station 1313 in the northern Gulf and from 12°00′ N, 76°00′ W (R/V CRAWFORD collection), respectively.

emarginated posterior border. At around 200 mm this caudal fin pattern becomes obscure, and it is absent from larger adults of both species.

HEAD SPINATION

The head region of both *C. hippurus* and *C. equiselis* is characterized by the presence of sphenotic (SPH) and supratemporal (ST) spines, by a double series of preopercular spines (POPa and POPb), by a mandibular or angular spine (A), and by a supraorbital spine (SO) (Fig. 2).

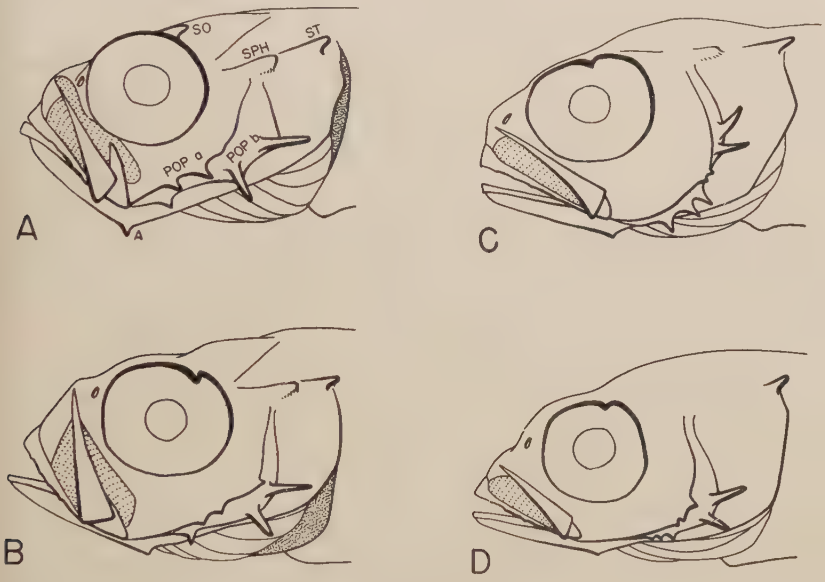

FIGURE 2. Heads of *Coryphaena* showing spination. A and B, *C. hippurus*, standard length 13.8 and 16.6 mm, respectively. C and D, *C. equiselis*, 13.3 and 16.5 mm, respectively.

In *C. hippurus*, the series of spines are all present in a 10.5 mm specimen, the smallest that could be satisfactorily examined. The sphenotic spine is thick and moundlike in appearance. The supratemporal spine is small but sharp, and is located at the angle of the opercular slit. In the anterior preopercular series there are two small spines below the angle, and a third may or may not be present at the angle. In the posterior preopercular series there are two groups. The upper and most prominent is a pair of long, divergent spines which reach well across the opercle. Below these, and anterior to the first series, is a single small spine (sometimes two). The angular spine is blunt and not always prominent. The supraorbital process is quite conspicuous on the upper posterior part of the orbit. The position of these spines remains fairly constant, but their relative size decreases as the size of the fish increases. By 25 mm POPa and the smaller POPb have almost disappeared. SPH is a welt at this size, and ST is very short. At 35 mm the spines may all be observed as tiny points except the larger POPb, which are not considerably less prominent than before. By 38 mm only the larger POPb may be seen, and these are now mere tips. Thus by about 40 mm little or no trace of head spination remains in this species.

The arrangement of spines is similar in *C. equiselis,* but there are differences in number and development. The lower series of small POPb spines usually numbers three, instead of one or two, and SO and SPH are comparatively poorly developed. SO disappears by about 19 mm. POPa and the lower, smaller POPb gradually are reduced and by about 24 mm are no longer evident. ST is no longer observable by about 30 mm, and the strong POPb disappear by about 35 mm.

The fact that the spines lose their identity in *C. equiselis* at a smaller size than in *C. hippurus,* may be correlated with the earlier maturity of the former.

TONGUE TEETH

Nichols (1909) compared the two species and noted differences in the tooth patches on the tongue. Fig. 3 shows the typical situation in intermediate and larger specimens. In *C. hippurus,* the patch is usually ovoid and covers the center half of the width of the tongue. In *C. equiselis,* the patch is somewhat trapezoidal, with angular edges, larger in front than behind, and covers most of the width of the tongue.

In specimens smaller than about 75 mm the patch tends to be less well-defined and is thus no longer reliable as a means of identification.

MERISTIC CHARACTERS

These characters are quite difficult to use, but they provide excellent means for differentiating the species of *Coryphaena.* Table 1 and Figs. 4 and 5 show the frequency distributions.

Dorsal-fin elements (Fig. 4) have usually been the common differentiating character. Obviously, however, few specimens were examined, for the separations were deceptive, of the order of "around 55 vs. around 60." Great care must be taken in counting the most anterior elements, particularly in large specimens, where they must be dissected.

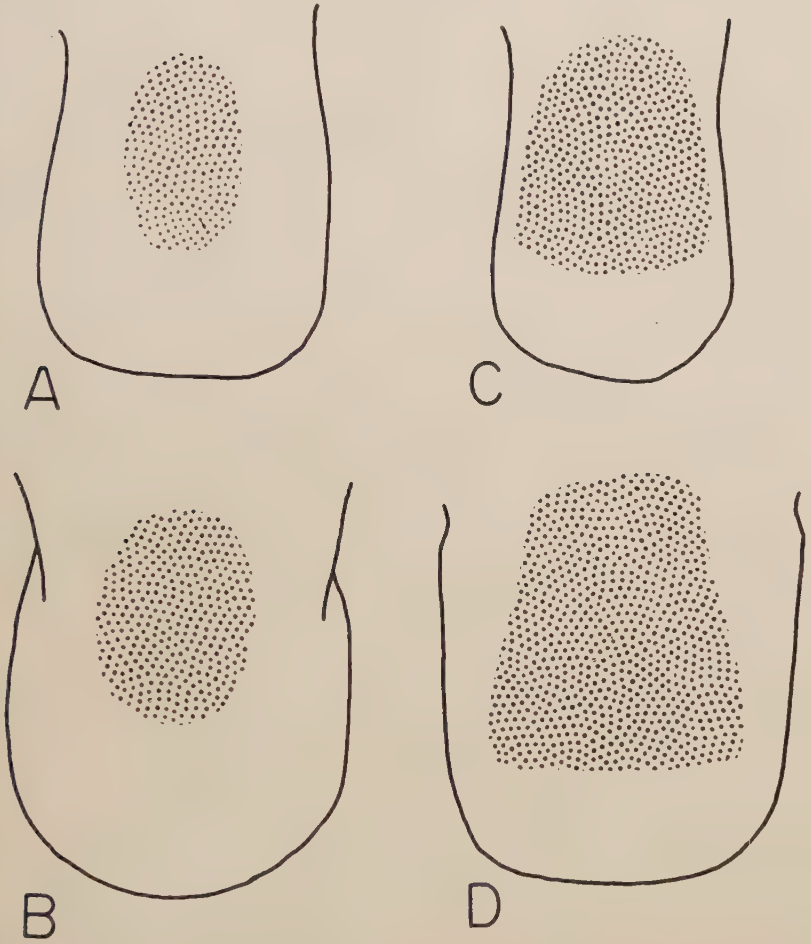

FIGURE 3. Dorsal surface of tongue of *Coryphaena* showing tooth patches. A and B, *C. hippurus,* standard length 223 mm and 420 mm, respectively. C and D, *C. equiselis,* 205 and 435 mm, respectively.

When this precaution is taken, most specimens with 55 or fewer dorsal elements are *C. equiselis,* those with 56 or more, *C. hippurus.* In our study, 87.3% of *C. hippurus* are separable from 94.4% of *C. equiselis* by this count, for an index of divergence (Ginsburg, 1954) of 90.4.

Anal elements (Table 1) are less reliable, although their frequency distributions do not coincide. *C. equiselis* usually has 27 or fewer elements, *C. hippurus* 26 or more, but there is considerable overlap,

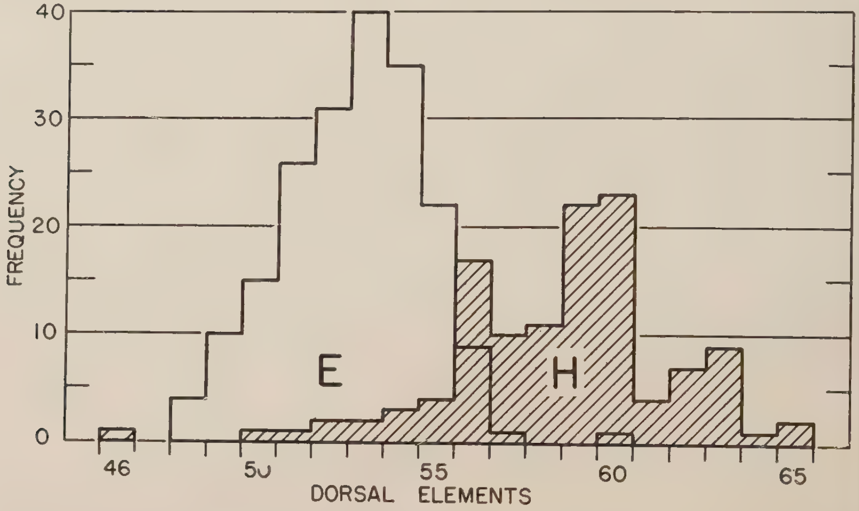

FIGURE 4. Number of dorsal rays in *C. equiselis* (E, open bars) and *C. hippurus* (H, crosshatched bars).

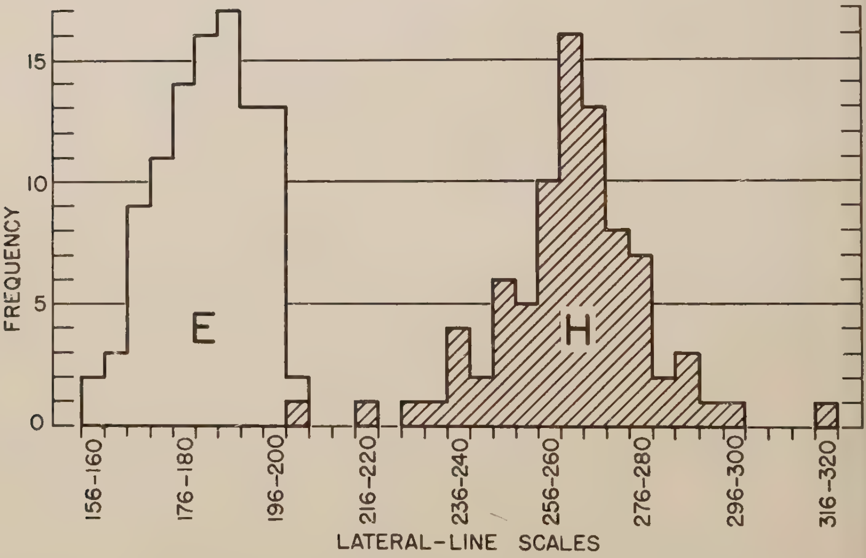

FIGURE 5. Number of lateral-line scales in *C. equiselis* (E, open bars) and *C. hippurus* (H, crosshatched bars).

particularly on 26 and 27 elements. The index of divergence here is only 79.8.

Pectoral rays (Table 1) are usually 19 or 20 in either species. Pelvic elements are almost invariably I, 5.

TABLE 1
Frequency Distribution of some Meristic Characters of Coryphaena in the Atlantic Ocean

C. hippurus Gill Rakers

	upper			lower						total							
	0	1	2	7	8	9	10	11	12	8	9	10	11	12	13	14	15
small	—	36	14	—	1	17	24	7	1	—	—	1	13	22	10	3	1
intermediate	1	2	—	—	3	—	—	—	—	—	1	2	—	—	—	—	—
large	67	3	—	23	42	5	—	—	—	23	40	7	—	—	—	—	—

C. equiselis Gill Rakers

	upper				lower				total					
	0	1	2	3	8	9	10	11	9	10	11	12	13	14
small	3	131	51	1	12	93	67	14	1	11	75	59	33	7
intermediate	—	5	—	—	—	5	—	—	—	—	5	—	—	—
large	4	4	—	—	4	4	—	—	3	3	2	—	—	—

	Anal Elements								Pectoral Elements				
	23	24	25	26	27	28	29	30	17	18	19	20	21
C. hippurus	—	—	2	24	49	42	9	1	1	5	37	76	4
C. equiselis	5	24	62	86	38	6	1	—	—	3	62	124	8

The number of lateral-line scales (Fig. 5), while somewhat difficult to count, affords the best means of differentiation. Of a total of 183 specimens, only three overlap. For practical purposes *C. equiselis* has 200 or fewer scales, *C. hippurus* more than 200. Most *C. equiselis* fall between 170-200 (mean 183.5), most *C. hippurus* between 245-280 (mean 262.8).

The gill-raker counts (Table 1) show no evident species differences except for a slightly lower mode for those on the lower arch of *C. equiselis*. There is, however, an obvious reduction in number with age. This is particularly notable in *C. hippurus,* where enough adult counts are available to afford reliability. There was little question in this study as to which specimens were considered as adults. We have few specimens in a wide gap between small (less than 150 mm) and large (300 mm and over) specimens (see graphs, Figs. 6-9). Most young have one or two rakers on the upper limb of the arch, one in the middle, and nine or ten on the lower limb. The adults have no rakers on the upper limb, one in the middle, and only seven or eight (or nine in *C. equiselis*) on the lower limb. Thus the total raker count is usually 8 or 9 (or 10 in *C. equiselis*) in adults, 11 or 12 in young of both species.

RELATIVE GROWTH

Twenty measurements, in addition to standard and fork lengths, have been used in this study. Of these the ten discussed below and shown in Figs. 6, 7, and 9 indicate species differences in proportions, either as young or adult or both. The remaining ten, which do not show interspecific differences, are shown in Fig. 8. In examining these graphs, it should be remembered that *C. equiselis* presumably does not attain as large a size as *C. hippurus;* our largest specimen of the former was 447 mm standard length, of the latter over 1200 mm. Each graph includes one or more reference lines. These are not intended as regression lines, but partly as indications of the linearity of the plotted points and partly as rough indications of the relative size of the given part. The indicated proportions are that of the part compared to standard length.

Most measurements are quite uniform in their changes with growth. On semi-logarithmic paper, plotted against standard length, their points form a wide hyperbolic curve. On non-logarithmic paper this would in most cases be nearly a straight line. Only orbit length shows appreciable scatter of points. This is probably due to the small magnitude of the dimension, together with the difficulty of accurately measuring the bony orbit.

The following, which show specific distinctions, are considered individually.

Body depth (Fig. 6). Up to about 100 mm both species are similar in this character. At this point, they gradually diverge, so that by about 200 mm the depth in *C. hippurus* is less than 25% of the standard length, that in *C. equiselis* 25% or usually greater. Exactly where the 25% rule can be applied with certainty is not evident, but care should be taken with specimens under 200 mm. Generally we can say that the greatest depth enters the standard length 4 times or more in *C. hippurus* over 200 mm and less than 4 times in *C. equiselis* of the same size.

Depth at vent (Fig. 6). As in body depth, this character shows divergence between the species only in specimens larger than 100 mm. A line indicating a ratio of 1:4.5 separates most of the available specimens of the two species over 100 m., *C. equiselis* being deeper.

Caudal peduncle depth (Fig. 7). There is no sharp demarcation in

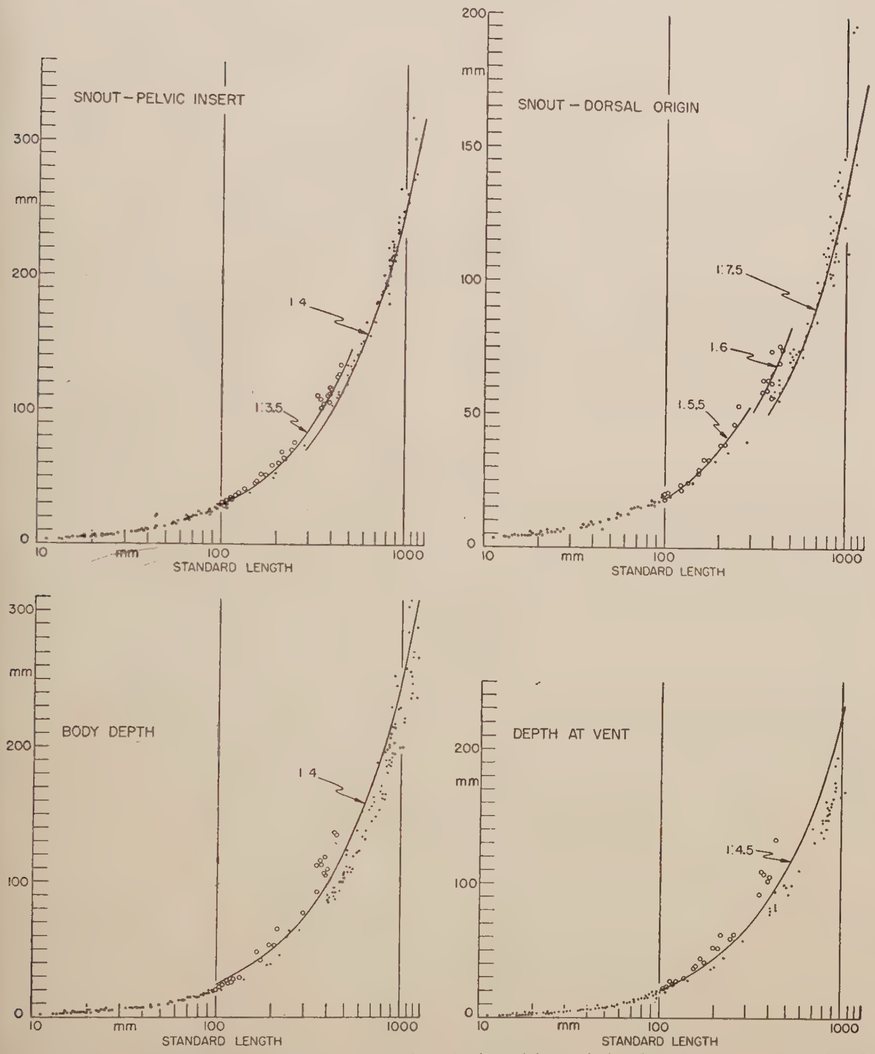

FIGURE 6. Semi-logarithmic plots of relationship of body parts to standard length showing differences in *C. hippurus* (dots) and *C. equiselis* (open circles). Below 100 mm, all specimens are represented by dots. Lines indicate ratio of body part to standard length and are intended as guides, not necessarily as regression lines (see text).

this measurement, but specimens 350-500 mm appear separated. This follows the trend of the first two characters, *C. equiselis* being deeper. *Head depth at occiput* (Fig. 7). This measurement was made on few

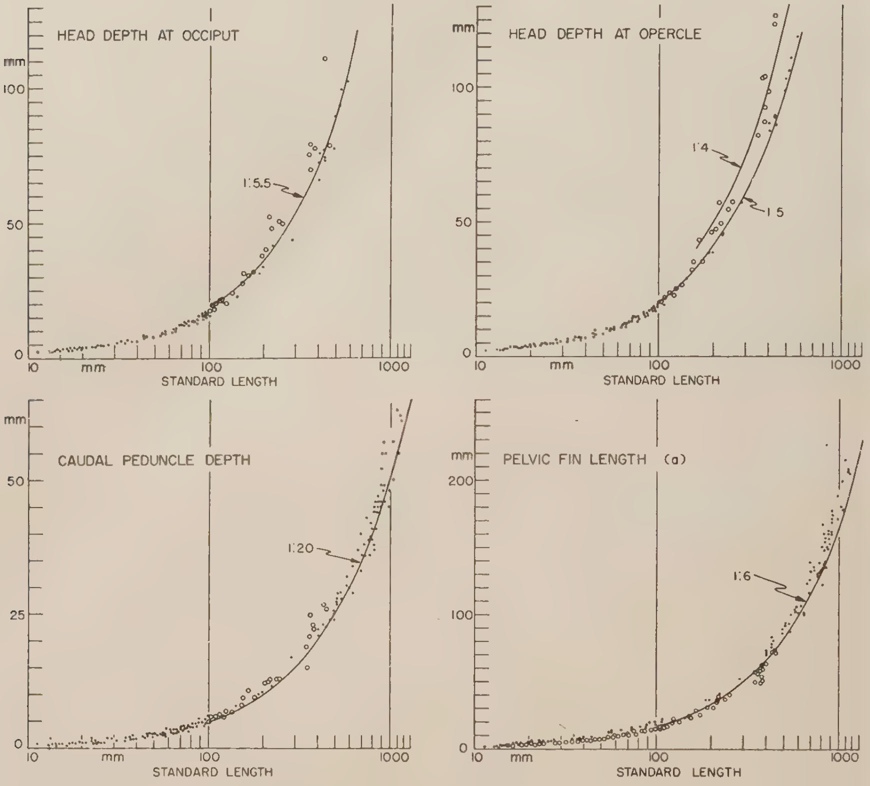

FIGURE 7. See legend for Fig. 6.

and mostly smaller specimens, but it seems to indicate a greater depth of head in larger *C. equiselis*. Again this follows the trend mentioned above. Where mature males of *C. hippurus* with vertical foreheads enter the picture, there is probably a reversal, but such data were, unfortunately, not gathered. Changes in head shape with growth in both species were shown by Lütken (1880).

Depth at opercular margin (Fig. 7). Like the last character, few and mostly small specimens were measured. The opercular margin is near the point of greatest depth in *C. hippurus*, whereas in *C. equiselis* the greatest depth is farther back. Again *C. equiselis* is deeper, but no measurements were made in the size range which would include the bull-headed males.

Snout to dorsal-fin origin (Fig. 6). In part, this is a reflection of depth. In the size range for which specimens of *C. equiselis* are available, this species is deeper than *C. hippurus.* Above that size in *C. hippurus,* most larger measurements are of bull-headed males, which is an indication of the vertical forehead limited to that sex.

Snout to pelvic insertion (Fig. 6). As with the last character, *C. equiselis* is deeper.

It is noteworthy that in measurements of horizontal distance, no differences were found. This was true for head length, snout to pectoral-fin insertion, snout to anal-fin origin, and pectoral-fin insertion to anal origin. Thus the different appearances of *C. equiselis* and *C. hippurus* seem to be due entirely to depth differences, and not at all to elongation.

Pelvic-fin length (Fig. 7). The pectorals appear equal in length in both species. The pelvics, on the other hand, are longer in *C. hippurus* from a standard length of about 20 mm and larger. This is the one differentiating character which holds in both young and adults. A line indicating a fin length: standard length ratio of 1:5.5 is effective in separating specimens less than about 100 mm (Fig. 8). Because of lack of *C. hippurus* of intermediate size, little can be said for the area between 100 and 350 mm. In specimens over 350 mm, a ratio of 1:6 effectively separates the two species.

Dorsal and anal-fin heights (Fig. 10). These characters must be considered from two standpoints: the greatest height of each fin and the relative height of anterior and posterior parts of the same fin. Up to about 20 mm, it is difficult to detect differences in either respect. In larger specimens, *C. hippurus* has a decidedly higher dorsal fin, and a considerably higher anal fin. It is emphasized by the fact that in young of *C. hippurus* the fins tend to be erected in preservation, and are conspicuously marked by bars. In *C. equiselis* the fins more often are prostrate, and seldom have a barred pattern.

The relative heights of the anterior and posterior parts of the fins differ in the two species. *By height, we mean the length of the rays,* not necessarily the vertical height of the fin. Ordinarily the longest posterior rays are inclined rearward, so that the fin may not appear as high posteriorly, but the rays may be longer. The height of the dorsal was the length of the longest ray taken approximately 10-15 rays from the origin.

In *C. hippurus,* there is comparatively little gradation in the height of the dorsal fin, although the posterior part tends to be slightly higher.

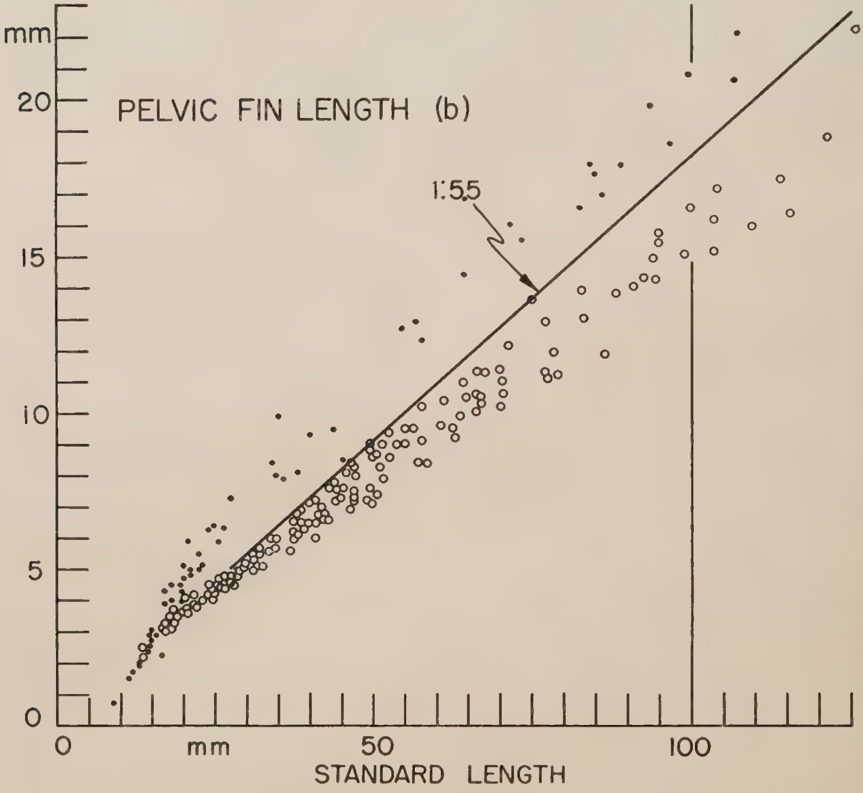

FIGURE 8. Pelvic-fin length shown on a non-logarithmic scale to emphasize completeness of separation at small sizes.

In *C. equiselis,* there is a greater difference in height, the anterior end always being highest.

The anal fin of *C. hippurus* is higher posteriorly and there seems to be a greater difference than in its dorsal. In *C. equiselis,* the anterior end is again higher than the posterior.

Fork length. This measurement, the distance from snout to fork of tail, is rather consistently about 10% greater than standard length.

LENGTH-WEIGHT RELATIONSHIP

The graph (Fig. 11) showing change of weight with length is based not only on our own data, but on that accumulated by Mather, which includes all the *C. equiselis* weights, and that in the literature (Anderson *et al.,* 1956, 1957; Bonham, 1946; Morrow, 1954; Schuck, 1951

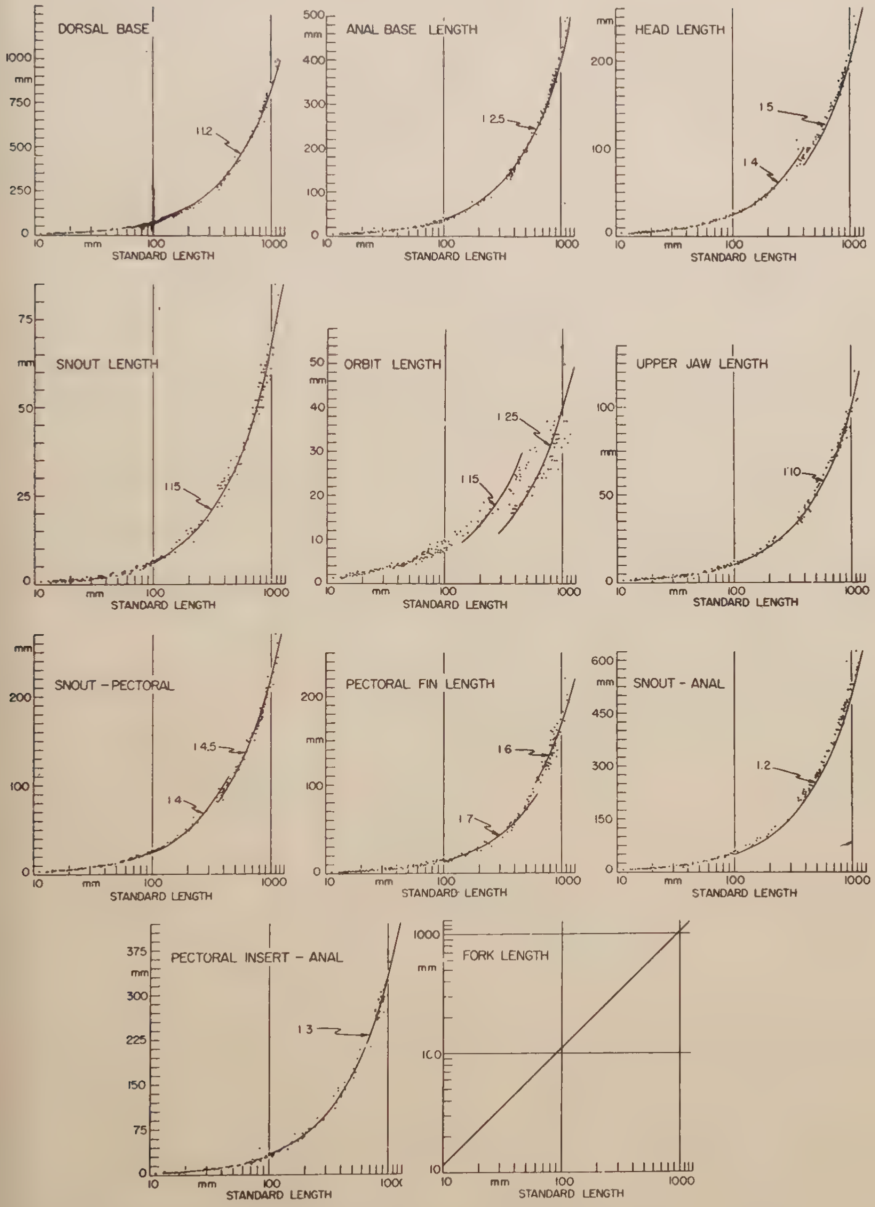

FIGURE 9. Semi-log. plots of body part — standard length relationships not showing differences in dolphin species. Species are not distinguished. Lines are guides, not necessarily regression lines.

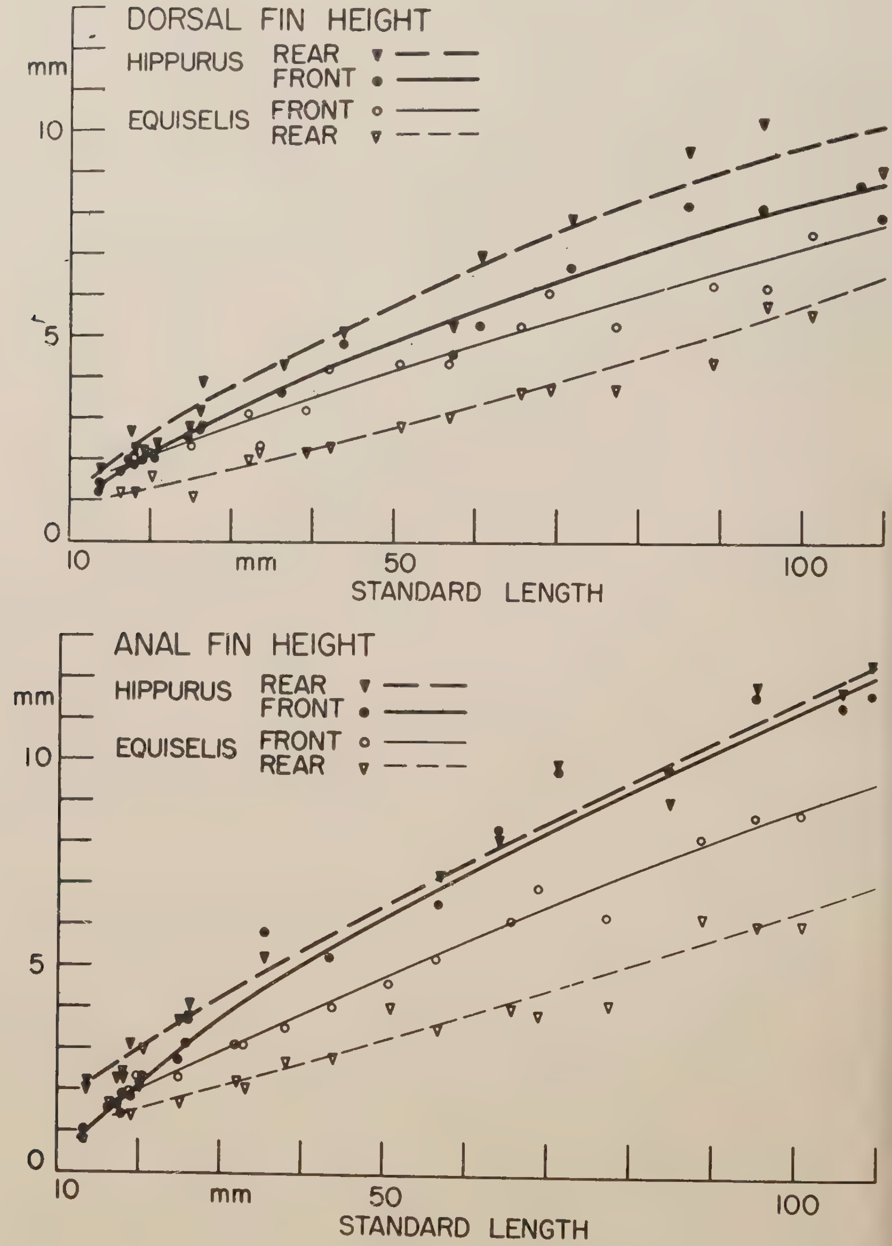

FIGURE 10. Relationship of front and rear heights of dorsal and anal fins in *Coryphaena*.

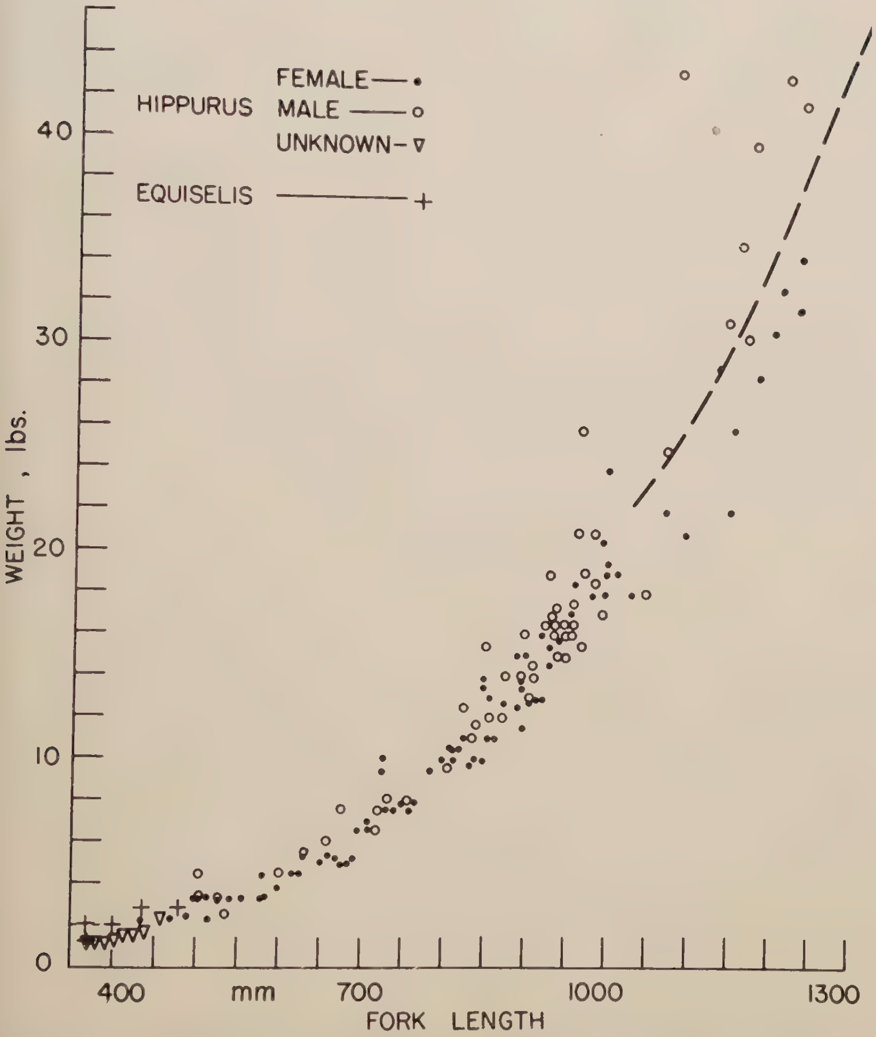

FIGURE 11. Length-weight relationship in *Coryphaena* (principally *C. hippurus*). Dashed line emphasizes the difference in weight of males and females over 1000 fork length.

a and b). Although Morrow was concerned with dolphins off the east coast of Africa and Bonham with those of Hawaii, their data are not out of line with the western North Atlantic data.

In *C. hippurus* up to about 950 mm., there is no apparent sexual difference in weight. Above that size, males appear to be heavier than females. That weight can vary considerably is shown by two large males, 1180 and 1175 mm, which weigh 40 and 30.5 lbs., respectively.

GEOGRAPHIC DISTRIBUTION

Both species appear to be cosmopolitan in warm seas. In reviewing literature records, we found *C. hippurus* recorded very commonly, but since *C. equiselis* may not have been recognized, most of these records are somewhat doubtful.

If identifications are correct, *C. hippurus* is much more abundantly caught by various commercial and sport fisheries than is *C. equiselis*. The extreme published latitudinal records in the Atlantic that have come to our attention are those of Vladykov and McKenzie (1935), who record a specimen ca. 2 feet long in Bedford Basin, Halifax Harbour, Nova Scotia, on August 7, 1901, and of Barnard (1927), who records the species from Cape Seas, Table Bay, and False Bay, on the southern tip of Africa. In a letter to Howard A. Schuck, L. R. Day reports three specimens about 14 inches long salted at North Rustico, Prince Edward Island, in 1945. Roughly, then, the distribution may be said to be limited latitudinally by the 45° line, which corresponds to the poleward limits of the 15°C(59°F) isotherm, as shown in the Meteor Atlas (Böhnecke, 1936). In the northern hemisphere at least, dolphins are rare at the extreme limit, and their general range can probably best be described by the 20°C (68°F) isotherm in the same atlas. Only four records north of Cape Cod, other than those noted above, are known to us (MacCoy, 1931; Schuck, 1951a; Scattergood, 1953; Bigelow and Schroeder, 1953). Most of our own catches have been at temperatures greater than 70°F. In March and April 1957, of fifteen long-line stations occupied by the M/V DELAWARE, the surface temperature was 70°F or higher at only two. One of these (70.0°F) produced a dolphin. The only other dolphin of the trip was caught where the surface temperature was 69.2°F, the third highest of all the stations. We recorded the catch for seven stations in June 1957. At four stations from 72.5° to 79.0°, dolphins were caught; at three from 66.1° to 70.9°, they were not. Of 22 stations in September and October 1957, nine produced dolphins. Surface temperatures at these successful stations ranged from 72.0°F to 81.0°F. The others ranged from 69.5° to 81.5°. The negative results at lower temperatures during the spring and summer trips corroborate our postulated temperature limitation, while the fall results do not contradict it.

In accord with its general propensity for warm waters, *C. hippurus* is quite common at certain times in the Caribbean Sea (Erdman, 1956), in the Gulf of Mexico (Baughman, 1941; Springer and Bullis, 1956), in the Florida Current (Anderson *et al.*, 1956, 1957), and in the Gulf Stream (Schuck, 1951a). Where the Gulf Stream system comes close to land, sport fishermen on the Atlantic coast of the United States are able to catch them in considerable numbers. This is notably true of southern Florida, Cape Hatteras, Ocean City, Maryland, and intercalated areas.

The only reference to relative abundance correlated with depth of water is that of Schuck (1951a) who found, using average miles of surface trolling per fish hooked, the greatest concentrations in water 0-20 fm. and 100-1000 fm. Water 21-100 fm. and greater than 1000 fm. produced relatively few fish. This needs to be corroborated. For example, whereas Schuck caught no dolphins by trolling over more than 1000 fm. of water, the M/V DELAWARE, by longlining and hand lines, caught many over such depths, although no quantitation was attempted.

Coryphaena equiselis is so poorly known that little can be said of its distribution. In addition to a few mid-Pacific records (viz. Kendall and Radcliffe, 1912), Fowler (1928) reports one from between Easter Island and the Galapagos, Nichols (1909) describes one from the eastern Pacific, Snodgrass and Heller (1905) note a record by Jordan and McGregor (1899) from San Benedicto Island, and Deraniyagala (1952) records the species reliably from Gulifalu Island and the Maldive Islands in the Indian Ocean. Specimens have recently been noted by Clemens (1957) for the eastern Pacific.

In the Atlantic, relatively large specimens (over 300 mm) have been reported in various parts of the tropical Atlantic (Mather and Day, 1954; Mezelaar, 1919), and in the Gulf Stream off Cape Hatteras and southern New England (Gudger, 1932; Mather, 1954), and the Fish and Wildlife Service M/V OREGON has taken individuals in the Gulf of Mexico and the Caribbean (see Fig. 12). In the eastern Atlantic, the species is recorded without mention of size from the Azores (Hilgendorf, 1888), the Canaries (Steindachner, 1868), Madeira (Lowe, 1839), and Senegal (Cadenat, 1950).

Young and intermediate-sized specimens have been taken more commonly than larger ones (intermediate, Fig. 12, young, Fig. 13), and they will be discussed in the next section.

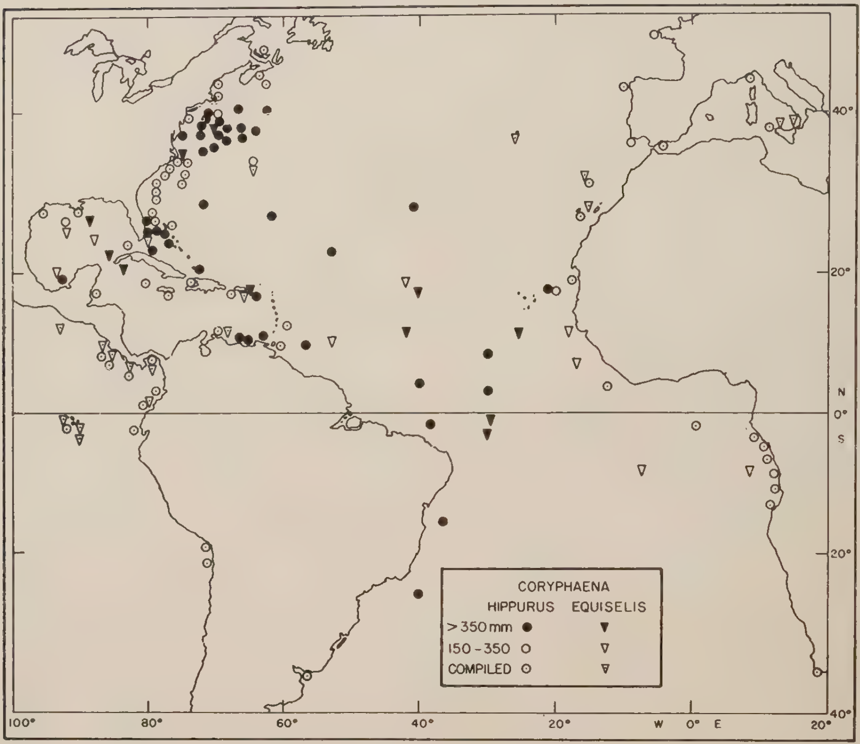

FIGURE 12. Distribution of intermediate-sized and adult dolphins in the Atlantic from specimens examined and from selected references (compiled).

SPAWNING AND SEASONAL DISTRIBUTION

Adults. The actual spawning act of dolphins has, presumably, not been observed. Certain distributional factors correlated with gonad condition give evidence of spawning time and place. Most data concern *C. hippurus.*

Erdman (1956) tabulated by months the distribution of 562 specimens of *C. hippurus* caught in Puerto Rican waters. He found them most abundant in January to March, almost absent in the summer, and moderately common again from October through December. In February, the month of greatest abundance, the ovaries had eggs in the most advanced stage of development. We have no information to explain their relative absence during the summer.

The records of Anderson *et al.* (1956, 1957) for the region of the Florida Current indicate that most of the dolphins caught by trolling

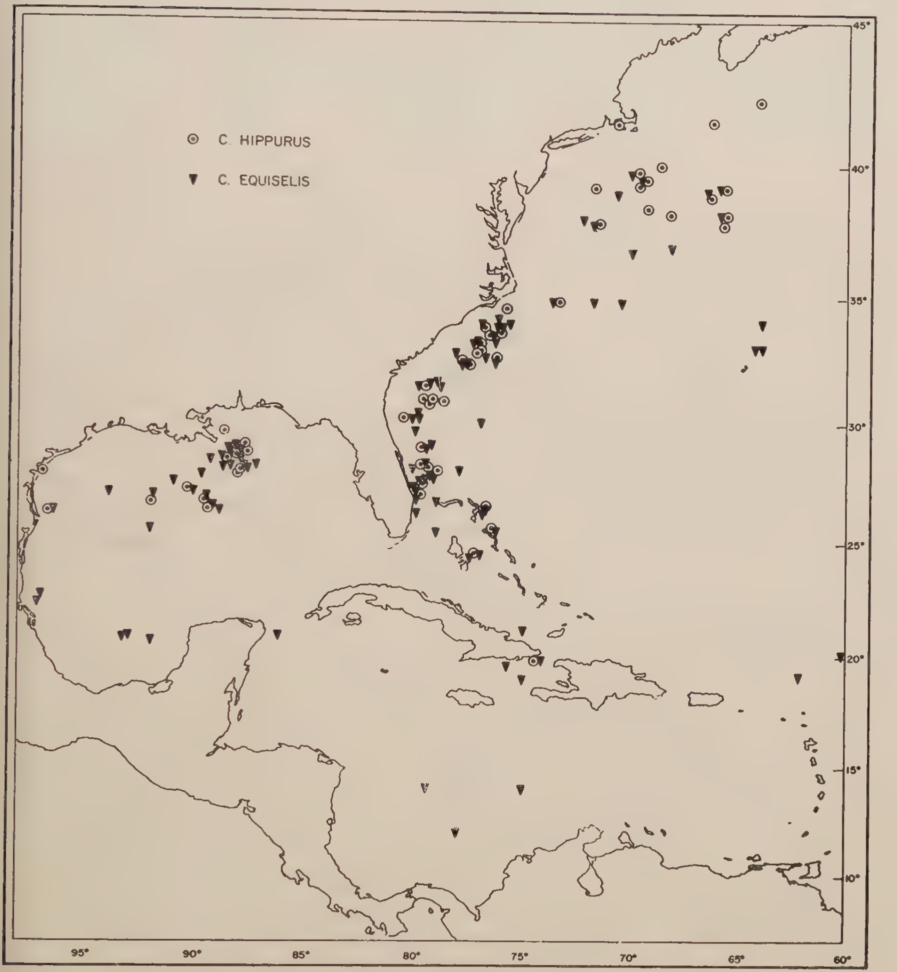

FIGURE 13. Distribution of young (less than 150 mm) dolphins in the western north Atlantic from specimens examined only.

in April and May were either very close to spawning condition or ripe, whereas those caught in July and August were not. The spawning season, therefore, appears to be later here than in the Caribbean.

C. hippurus caught in the vicinity of the Gulf Stream *(sensu stricto)* in June were either ripe or very close to it, and the species was present in large numbers at this time. In March and April, only two dolphins were taken either by long line or hand line. In June they were abundant on long line and not uncommon on incidental hand lines. In September and October, the abundance on long line sets dropped off considerably, though quite a few were caught on hand lines. Fig. 14 indicates the relative seasonal abundance of adults in the Gulf Stream and compares this with Erdman's (1956) Puerto Rico data.

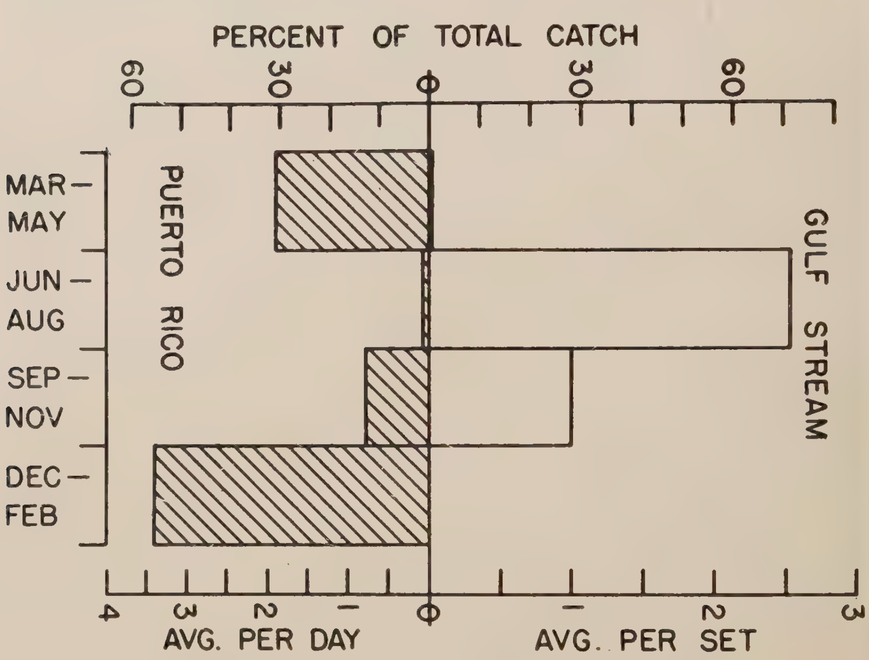

FIGURE 14. Relative seasonal abundance of adults of *C. hippurus* in the Gulf Stream (M/V DELAWARE data) and Puerto Rico (from Erdman, 1956). Gulf Stream data are given as average catch per long-line set. Puerto Rico data are given as average catch per day by sport fishermen. Both are reduced to percentage for comparison.

We have also noted ripe females caught off Ocean City, Maryland, in July and August 1957.

In the Indian Ocean, off the coast of east Africa and in the Mauritius-Seychelles region, Williams (1953) found ripe females in March and suggested a possible shoreward spawning migration there from February to June.

It thus appears that *C. hippurus* may gather in certain broad areas to spawn as the surface temperature rises toward its midsummer maximum. Since a similar temperature is probably reached earlier in the

Caribbean than in the Florida Current or Gulf Stream, this may account for the discrepancy in spawning times between the two areas. Mather, however, reports (pers. comm.) finding ripe fish off the Virgin Islands at late as August, and de Sylva *(in litt.)* has seen them throughout the year at Miami.

Evidence of spawning time and place of *C. equiselis* comes from a specimen 205 mm standard length (ca. 9 inch), collected from the R/V CRAWFORD in March, 1957, which had well-developed eggs. This is far smaller than any *C. hippurus* observed in the same condition. Erdman (1956) reported Puerto Rican specimens 12-14 inches in fork length with well-developed eggs in August and October 1956, and recently told us *(in litt.)* that on September 7, 1957, in the stomach of a blue marlin *(Makaira ampla)* he found three specimens 10-12 inches fork length with orange ovaries and well-formed eggs.

Young. The distribution of young dolphins in time in the various parts of the western Atlantic where dip-net collections have been made corroborates the evidence obtained from the adults and gives further information. However, there exists a seeming paradox. Whereas larger specimens of *C. hippurus* are relatively easy to obtain and those of *C. equiselis* are seldom seen, the young just reverse this picture. In the collections examined in this study, there was a total of 122 young of *C. hippurus* (53 from the Gulf Stream, 48 from the Florida Current, 21 from the Gulf of Mexico) as contrasted to 353 specimens of *C. equiselis* (44 from the Gulf Stream, 152 from the Florida Current, 157 from the Gulf of Mexico). Probably, *C. equiselis* is more a mid-ocean inhabitant than *C. hippurus* and prefers more tropical waters. Most of the few available adults of *C. equiselis* used in this study were, indeed, from equatorial or sub-equatorial Atlantic waters, the exceptions being those from the Gulf Stream. DeSylva has informed us that in southern Florida, *C. hippurus* adults are caught both in the Gulf Stream and at its junction with coastal water, and that they occasionally enter inshore waters of rather high turbidity. *C. equiselis,* however, seems to be strictly oceanic over deeper waters. We have seen small specimens of *C. hippurus* caught in shallow water near docks in Rockport, Texas (cf. Pew, 1957), Woods Hole, Mass., and Biscayne Bay, Fla. No such reports are available for *C. equiselis.* This upholds the contention that *C. hippurus* tolerates coastal waters and breeds farther inshore than *C. equiselis.*

In the Gulf of Mexico, from which specimens of *C. equiselis* are abundant, we have seen specimens taken from April through August and in November and December. The distribution of sizes by season is shown in Fig. 15. In the five spring and summer months, most of the young are between 10 and 50 mm, with no prominent mode. It seems, however, that larger specimens become more common in the later months. This suggests that *C. equiselis* breeds throughout spring and summer in that region. The size distribution in November and December lies principally between 40 and 70 mm, indicating an increase in size and probably also that the breeding season is generally past.

Comparatively few data are available for the young of *C. hippurus*, but a picture for the Gulf similar to that of *C. equiselis* is suggested.

In the Gulf Stream, in spring and summer we have collected only two young *C. equiselis*. In the fall, however, numerous young of this species have been taken, very few of which have been in the very small size classes; most were 40-70 mm, with quite a few larger. This suggests that *C. equiselis* does not breed within the immediate influence of the Gulf Stream, but that the fall influx comes from another breeding ground.

C. hippurus shows a different seasonal pattern. No young were caught in the Gulf Stream in March and April. In June, many were caught, all in the smaller size range. In September and October, again quite a few were collected, and the size range shows a decided increase. It would seem that the species breeds in or near the Gulf Stream, which corroborates our earlier evidence, and that early summer is the most intense breeding period.

The relatively few specimens from the Gulf of Mexico appear to indicate a longer breeding season there, possibly extending from April through July or August, as did that of *C. equiselis*. It is difficult to explain the scarcity of young of *C. hippurus* in the Gulf unless the adults are also somewhat scarce, which, as attested by Springer and Bullis (1956), is surely not the case.

Recently, we have been fortunate in being able to examine the young dolphins collected by the Fish and Wildlife Service in the Florida Current and Bahamas Region. The seasonal distribution of these specimens (Fig. 16) approaches the picture in the Gulf of Mexico far more closely than that of the Gulf Stream. There is no paucity of specimens of *C. equiselis* in spring and summer; rather there is evidence of breeding at all seasons including winter. The obvious difference between the patterns of *C. equiselis* in the Gulf Stream and in the Florida Current is disconcerting, as it would seem logical to expect a more or less continuous phenomenon, whereby considerable

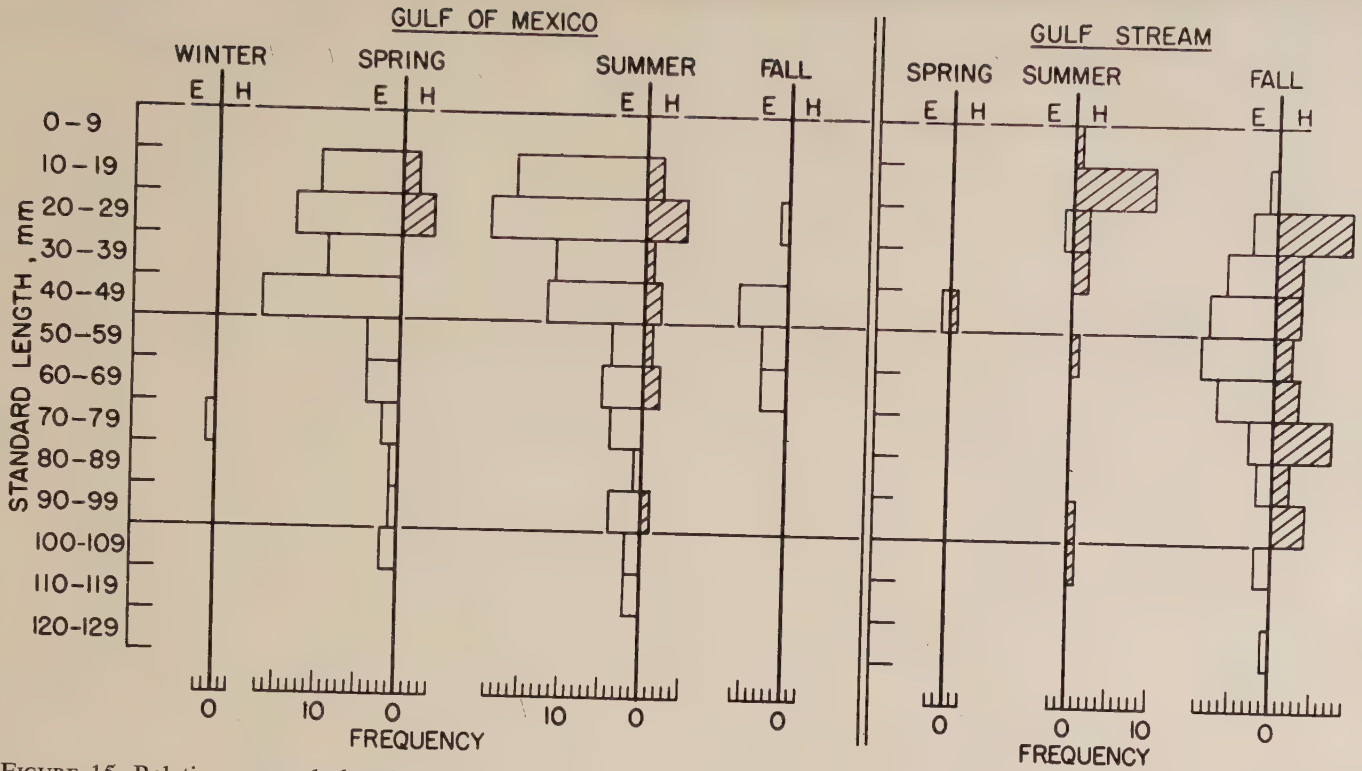

FIGURE 15. Relative seasonal abundance of young of *Coryphaena* in the Gulf of Mexico and the Gulf Stream. E, open bars = *C. equiselis;* H, crosshatched bars = *C. hippurus.*

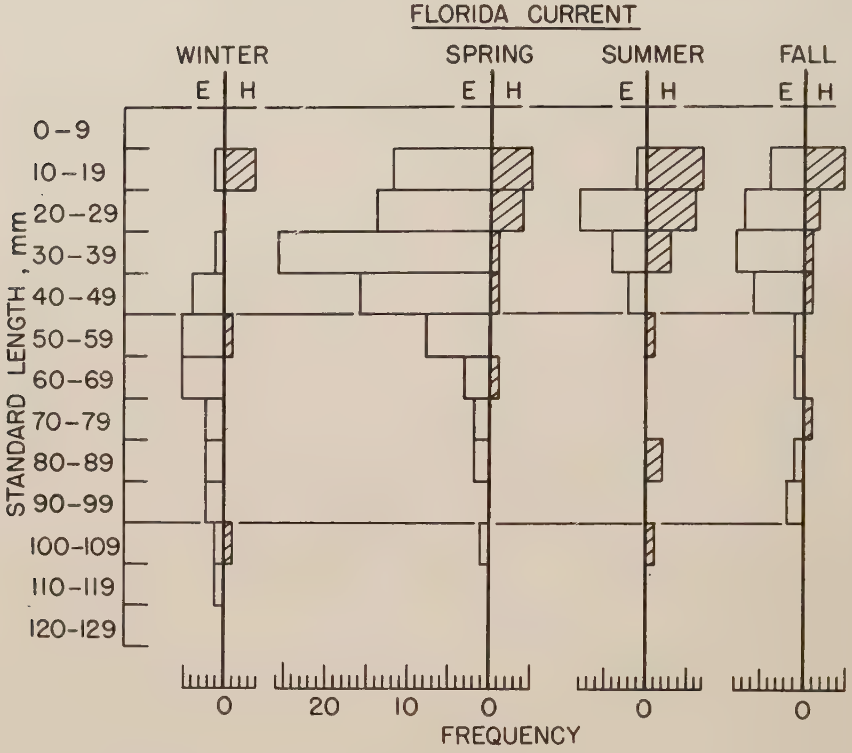

FIGURE 16. Relative seasonal abundance of *C. equiselis* (E, open bars) and *C. hippurus* (H, cross-hatched bars) in the Florida Current.

numbers of specimens would be carried into the Gulf Stream at times when they are abundant in the Florida Current. We are unable to adequately explain this disjunct situation.

SEX RATIO

In the Gulf Stream region sampled by the M/V DELAWARE, we found essentially a 50:50 sex ratio, as shown in Table 2. Data from Mather for the Virgin Islands, consisting largely of winter records, indicates a preponderance of females, about a 65:35 ratio. We are unable to explain satisfactorily the difference between these areas. Assuming that specimens from the Virgin Islands were correctly sexed, the spring abundance in the Caribbean, indicated by Mather's data and that of Erdman (1956), may be a pre-spawning migration, mainly of females.

TABLE 2

SEX RATIOS FOUND AT VARIOUS SEASONS IN THE GULF STREAM (FROM "DELAWARE") AND AT ST. CROIX, VIRGIN ISLANDS (FROM MATHER).

	Males	Females
Gulf Stream Oct. 1956	8	8
Gulf Stream June 1957	17	14
Gulf Stream Fall 1957	5	5
Gulf Stream Total	30	27
St. Croix Oct. 1956- May 1957	25	47

FEEDING HABITS OF *C. hippurus*

Stomachs of 46 adults of *C. hippurus* from the Gulf Stream were analyzed to determine species composition and number of fish eaten. We found a minimum of 32 species of fishes belonging to 19 families, at least one species of crab *(Portunus sayi)*, one shrimp, and four cephalopods, as well as *Sargassum* weed, (Table 3). Empty stomachs have not been considered.

TABLE 3

FOOD ITEMS OF *Coryphaena hippurus* SHOWING NUMBER OF STOMACHS IN WHICH EACH WAS FOUND AND NUMBER OF INDIVIDUAL ITEMS FOUND IN ALL STOMACHS.

	Number of Stomachs	Number of Individuals
Cephalopoda	28	46
Unidentified	23	33
Decapoda		
Illex illecebrosus	1	1
Species?	4	5
Octopoda		
Argonauta argo	4	6
Pterygioteuthis giardi	1	1
Tremoctopus violaceus	1	1
Crustacea	15	18
Crab		
Portunus sayi	7	10
Species?	6	6
Shrimp-Species?	2	2
Fishes	42	342
Scopeliformes-Myctophidae	1	1
Beloniformes		

TABLE 3—*Continued*

FOOD ITEMS OF *Coryphaena hippurus* SHOWING NUMBER OF STOMACHS IN WHICH EACH WAS FOUND AND NUMBER OF INDIVIDUAL ITEMS FOUND IN ALL STOMACHS.

	Number of Stomachs	Number of Individuals
Scomberesocidae-*Scomberesox saurus*	1	1
Syngnathiformes		
Syngnathidae-*Hippocampus hudsonius*	1	1
Beryciformes	4	15
Holocentridae		
Holocentrus ascensionis	1	4
H. bullisi	1	4
H. species?	4	7
Perciformes	16	207
Acanthuridae-*Acanthurus* species?	3	3
Ammodytidae-*Ammodytes americanus*	1	31
Bramidae-species?	1	1
Carangidae	7	15
Caranx crysos	2	2
C. latus	1	1
C. ruber	1	1
C. species?	1	1
Decapterus punctatus	2	4
Selar crumenophthalmus	1	5
unidentified	1	1
Coryphaenidae-*Coryphaena hippurus*	2	2
Gempylidae	3	106
Gempylus serpens	1	1
Nealotus tripes	2	105
Trichiuridae-*Diplospinus multistriatus*	1	2
Scombridae	6	39
Auxis thazard	5	38
Euthynnus alleteratus	1	1
Xiphiidae-*Xiphias gladias*	4	8
Tetraodontiformes	17	65
Balistidae	14	20
Balistes capriscus	1	1
Canthidermis maculatus	2	3
C. sobaco	4	5
Xanthichthys ringens	6	8
unidentified	3	3
Diodontidae-*Diodon hystrix*	3	4
Molidae-species?	1	1
Monacanthidae	8	13
Monacanthus hispidus	7	11
M. tuckeri	1	2
Ostraciidae-*Lactophrys triqueter*	1	1
Tetraodontidae	4	26
Sphaeroides spengleri	1	4
S. species?	3	22
Unidentified fishes	29	51

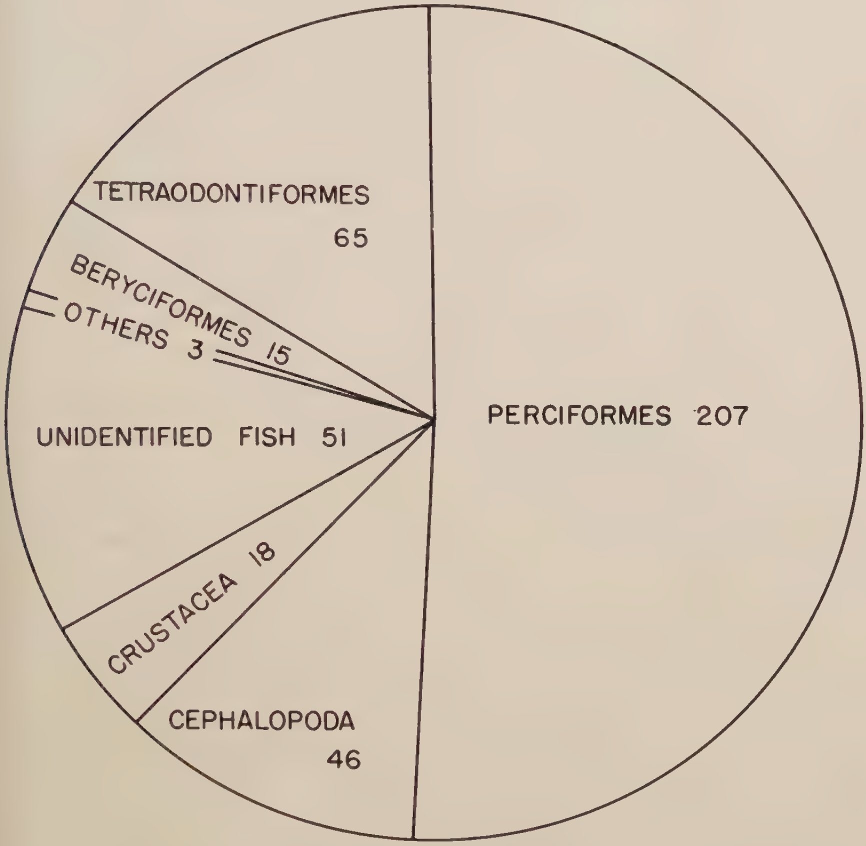

FIGURE 17. Numerical abundance of organisms in stomachs of *C. hippurus* by major categories. Figures represent actual total numbers.

We find fishes the most abundant item, occurring in 42 out of 46 stomachs. Three of the other four contained cephalopods only, the other one both cephalopods and crustacea. The numerical contribution of the various types of animals is shown in Fig. 17. Because numbers of specimens were not recorded for some stomachs examined at sea, each such case was counted as one individual. We thus have a minimum number of individual items. The order Perciformes contributed more than half the total. A little over half of this number was a single species *(Nealotus tripes)* found in stomachs of two fish captured on the same day. One stomach had 29, another 16 specimens of *Auxis,* and the single dolphin examined from Ocean City, Maryland, contained 31

Ammodytes. These represent the only instances where more than ten individuals of a fish species were recorded from a single stomach. Because of these few instances, the evaluation is perhaps biased toward Perciformes; however, the unidentified category probably consists largely of this order.

Considering the number of stomachs in which each category is represented, the order is changed (Fig. 18), the two leading fish orders reversing their positions. The Carangidae (7 stomachs) Balistidae (14) and Monacanthidae (8), which are the three most-frequent families, are the forms most commonly associated with *Sargassum*, as shown by dip-net collections. At least eight stomachs contained *Sargassum*. It appears, therefore, that the dolphins are feeding to a considerable extent on this readily available source of food. There is no apparent selectivity. This point is further borne out by the single fish from Ocean City which contained only *Ammodytes,* a very abundant shallow-water fish.

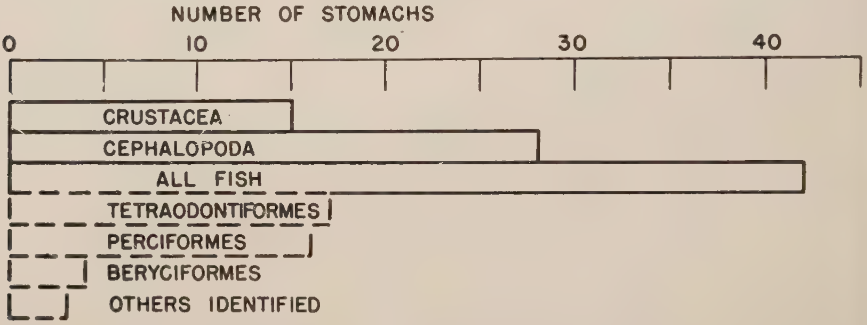

FIGURE 18. Frequency of occurrence of fishes and invertebrates in stomachs of *C. hippurus*. Upper (solid bars): major groups. Lower (dashed bars): orders of identified fishes.

Flying fishes were never identified among the stomach contents, although they were not uncommon in dip-net collections made at a night light. These are reputed to be the favorite food of dolphins, but our evidence points to the contrary, at least in the Gulf Stream. It further corroborates our contention that selectivity is not a major factor in the feeding habits of dolphins, as presumably flying fishes, although available, are more difficult to catch than the relatively sedentary forms inhabiting the *Sargassum*. DeSylva *(in litt.)* has noted that dolphins caught off Miami, Florida, also feed heavily on the *Sargassum*-fauna, but that flying fishes are common in the diet there.

Our findings compare favorably with those of Ronquillo (1954), who studied Philippine dolphins, in which Trichiuridae (closely related to Gempylidae) were most abundant numerically, followed by Tetraodontiformes, *Auxis*, Syngnathiformes, Holocentridae, and Carangidae.

Empty stomachs were found in none of 30 dolphins examined in June 1957; only one of ten in Fall 1957 was empty. These fish were all caught during the morning hours, mostly by long line. Nine of 15 dolphins caught on hand lines at night in October 1956 had empty stomachs. Possibly the species does not feed well in darkness.

LITERATURE CITED

American Fisheries Society
1948. A list of common and scientific names of the better known fishes of the United States and Canada. Amer. Fish. Soc. Spec. Publ. No. 1: 1-45.

Anderson, W. W. and J. W. Gehringer
1957. Physical oceanographic, biological, and chemical data. South Atlantic coast of the United States. Theodore N. Gill Cruise 3. Spec. Sci. Rep. U. S. Fish and Wildl. Serv., 210: 1-208.

Anderson, W. W., J. W. Gehringer, and E. Cohen
1956. Physical oceanographic, biological, and chemical data. South Atlantic coast of the United States. Theodore N. Gill Cruise 2. Spec. Sci. Rep., U. S. Fish and Wildl. Serv., 198: 1-270.

Barnard, K. H.
1927. A monograph of the marine fishes of South Africa. Ann. S. Afr. Mus., *21* (2): 419-1065.

Barnhart, P. S.
1936. Marine fishes of southern California. iv + 209 pp. Univ. Calif. Press., Berkeley.

Baughman, J. L.
1941. On a heavy run of dolphin, *Coryphaena hippurus*, off the Texas coast. Copeia, 1941 (2): 117.
1941. Scombriformes, new, rare, or little known in Texas waters, with notes on their natural history or distribution. Trans. Tex. Acad. Sci., *24:* 14-26.

Beebe, W. and J. Tee-Van
1928. The fishes of Port-au-Prince Bay, Haiti. Zoologica, N. Y., *10* (1): 1-279.

Behre, E. H.
1950. Annotated list of the fauna of the Grand Isle region 1928-1946. Occ. Pap. Mar. Lab. La. Univ., 6: 1-66.

Bigelow, H. B. and W. C. Schroeder
1953. Fishes of the Gulf of Maine. Fish. Bull., U. S., 74: viii + 577 pp.

Böhnecke, G.
1936. Atlas zu: temperatur, salzgehalt und dichte an der oberfläche des Atlantischen Ozeans. Wiss. Ergeb. Deut. Atl. Exp. "Meteor" 1925-1927. Band V. Atlas. vii pp., 74 maps.

BONHAM, K.
1946. Measurements of some pelagic commercial fishes of Hawaii. Copeia, 1946 (2): 81-84.
BREDER, C. M., JR.
1936. Heterosomata to Pediculati from Panama to Lower California. Bull. Bingham oceanogr. Coll. *2* (3): 1-56.
CADENAT, J.
1950. Poissons de Mer du Senegal. Inst. Franc. d'Afr. Noire. Dakar. 345 pp.
CLEMENS, H. B.
1957. Fishes collected in the tropical eastern Pacific, 1954. Calif. Fish Game, *43* (4): 299-307.
DEBUEN, F.
1950. El Mar de Solis y su fauna de peces. II parte. La fauna de peces del Uruguay. Publ. cient. Serv. oceanogr. Montevideo, 2: 47-144.
DERANIYAGALA, P. E. P.
1952. A colored atlas of some vertebrates from Ceylon. *1:* xii + 147, Ceylon Gov. Press.
ERDMAN, D. S.
1956. Recent fish records from Puerto Rico. Bull. Mar. Sci. Gulf & Carib. *6* (4): 315-340.
FOWLER, H. W.
1906. New, rare or little known scombroids, No. 3. Proc. Acad. nat. Sci. Philad., *58:* 114-122.
1915. The fishes of Trinidad, Grenada, and St. Lucia, British West Indies. Proc. Acad. nat. Sci. Philad., *67:* 520-548.
1928. The fishes of Oceania. Mem. Bernice P. Bishop Mus. 10. iii + 540 pp.
GINSBURG, I.
1954. Certain measures of intergradation and divergence. Zoologica, N. Y., *39* (1): 31-35.
GUDGER, E. W.
1932. The abundance of the dolphin, *Coryphaena hippurus,* on the North Carolina coast. J. Elisha Mitchell sci. Soc., *47:* 237-244.
HILGENDORF, F.
1888. Zur kenntniss der Azorenfauna. II. Die fische der Azoren. Arch. Naturgesch. 54. 1 Band: 205-213.
HUBBS, C. L. AND K. F. LAGLER
1947. Fishes of the Great Lakes region. Cranbrook Inst. Sci. Bull. 26: xi + 186 pp.
ISELIN, C. O'D.
1936. A study of the circulation of the western north Atlantic. Pap. phys. Oceanogr. *4* (4): 1-101.
JORDAN, D. S. AND R. C. MCGREGOR
1899. List of fishes collected at Revillagigedo Archipelago and neighboring islands. Rep. U. S. Comm. Fish. 1898: 271-284.
KENDALL, W. C.
1908. Fauna of New England. 8. List of the Pisces. Occ. Pap. Boston Soc. nat. Hist. *7:* vii + 152 pp.
KENDALL, W. C. AND L. RADCLIFFE
1912. Reports on the scientific results of the expedition to the eastern tropical Pacific, in charge of Alexander Agassiz, by the U. S. Fish Commission steamer "Albatross," from October, 1904 to March, 1905, Lieut. Commander L. M. Garrett, U.S.N., commanding. 25. The shore fishes. Mem. Mus. comp. Zool. Harv., *35* (3): 75-172.

LINNAEUS, C.
1758. Systema Naturae. Ed. 10. Facsimile. 824 pp. Brit. Mus. (Nat. Hist.).
LOWE, R. T.
1849. Supplement to "A synopsis of the fishes of Madeira." Trans. zool. Soc. Lond., *3*: 1-20.
LÜTKEN, C.
1880. Spolia Atlantica. Dansk. Vindesk. Selsk. Skr. 5 Raekke. 12 Bind: 409-613.
MACCOY, C. V.
1931. Museum Notes. Bull. Boston Soc. nat. Hist., *58*: 16-18.
MANN, G.
1950. Peces de Chile. Clave de Determinacion. 48 pp. Min. de Agric., Santiago.
MATHER, F. J., III
1954. Northerly occurrence of warm-water fishes in the western Atlantic. Copeia, 1954 (4): 292-293.
MATHER, F. J., III AND C. G. DAY
1954. Observations of pelagic fishes of the tropical Atlantic. Copeia, 1954 (3): 179-188.
MEEK, S. E. AND S. F. HILDEBRAND
1925. The marine fishes of Panama. Part 2 Publ. Field Mus. No. 226. Zool. Ser. 15: xii-xx, 331-707.
METZELAAR, J.
1919. Over tropisch Atlantische visschen. 314 pp. A. H. Kruyt, Amsterdam.
MORROW, J. E.
1954. Data on dolphin, yellowfin tuna, and little tuna from East Africa. Copeia, 1954 (1): 14-16.
NICHOLS, J. T.
1909. A note on the dolphins (*Coryphaena equisetis* and *Coryphaena hippurus*). Bull. Amer. Mus. nat. Hist., *26*: 131-133.
OSBECK, P.
1757. Dagbok ofwer en Ostindisk Resa aren 1750, 1751, 1752, med unmärkningar uti naturkunnigbeten, franimande Folflags, Sprat, Seder, hushallning, mm. Da Fleras astundan. Stockholm. (6) 376 (16) pp.
PELLEGRIN, J.
1914. Missions Gruvel sur la cote occidental d'Afrique (1905-1912). Poissons. Ann. Inst. oceanogr. Monaco, *6* (4): 1-100.
PEW, P.
1957. Occurrence of young dolphin, *Coryphaena hippurus*, in a Texas bay. Copeia, 1957 (4): 300.
POLL, M.
1953. Poissons. III. Teleosteens Malacopterygiens. Res. Sci. Exp. Oceanogr. Belg. dans les Eaux. Cot. Afr. de l'Atl. Sud (1948-1949), Vol. 4. Fasc. 2.
POSTEL, E.
1950. Peche sur les cotes d'Afrique Occidentale. II. Poissons de surface. Rapport et note sur quelques poissons de surface. 77 pp., Gov. Gen. de l'Afr. Occ. Franc. Insp. Gen. de l'Elevage. Dakar.
RIBEIRO, A. DE M.
1918. Fauna Brasiliense, Peixes. Tomo V. (Eleutherobranchios Aspirophores)—Physoclisti. Archiv. Mus. Nac. Rio de Janeiro, *21*: 1-227.
RONQUILLO, I. A.
1954. Food habits of tunas and dolphins based upon examination of their

stomach contents. Philipp. J. Fish. 2 (1): 71-83.

SCATTERGOOD, L. W.

1953. Notes on Gulf of Maine fishes in 1952. Copeia, 1953 (3): 194-195.

SCHUCK, H. A.

1951a. Notes on the dolphin (*Coryphaena hippurus*) in North Carolina waters. Copeia, 1951 (1): 35-39.

1951b. New Gulf of Maine record for occurrence of dolphin, *Coryphaena hippurus,* and data on small specimens. Copeia, 1951 (2): 171.

SNODGRASS, R. E. AND E. HELLER

1905. Papers from the Hopkins-Stanford Galapagos Expedition, 1898-1899. XVII. Shore fishes of the Revillagigedo, Clipperton, Cocos, and Galapagos Islands. Proc. Wash. Acad. Sci. *6*: 333-427.

SPRINGER, S. AND H. R. BULLIS, JR.

1956. Collections by the OREGON in the Gulf of Mexico. Spec. Sci. Rep., U. S. Fish and Wildl. Serv. 196. 134 pp.

STEINDACHNER, F.

1868. Ichthyologischer bericht über eine nach Spanien und Portugal unternommene reise (V. Fortsetzung) Sitzungsber. Kaiserlichen Akad. Wissensch. 57. Band 1. Abt. 351-424.

VLADYKOV, V. D. AND R. A. MCKENZIE

1953. The marine fishes of Nova Scotia. Proc. N. S. Inst. Sci., *19* (1): 17-113.

WILLIAMS, F.

1953. Catches of *Coryphaena hippurus* (L.) in the western Indian Ocean. Nature, London, *171*: 703-704.

WOODS, L. P. AND R. H. KANAZAWA

1951. New species and new records of fishes from Bermuda. Fieldiana, Zool., *31*: 629-644.

Contribution No. 96

[AMERICAN JOURNAL OF SCIENCE, VOL. 257, JANUARY 1959, P. 29-43]

CLAY MINERAL—CARBONATE RELATIONS IN SEDIMENTARY ROCKS*

E-AN ZEN

Department of Geology, University of North Carolina, Chapel Hill, N. C.

ABSTRACT. Mineralogical investigation of modern sediments off the coast of Peru and Chile reveals the presence of volcanic glass in many samples. The glass is commonly devitrified in sea water to fine aggregates of minerals, including calcite and kaolinite. The textural relations of these two phases suggest attainment of chemical equilibrium, and thus a thermodynamic analysis of their relationship is desirable.

A seven-component system, including the phases dolomite, calcite, chlorite, kaolinite, and quartz, is chosen for study. This system may be analyzed graphically if quartz is present in excess and H_2O and CO_2 are taken as "mobile" components. The expected phase associations under a given set of conditions are studied in detail and agree with existing petrographic data; the agreement shows that the hypothesis of chemical equilibrium among these phases in sedimentary rocks should be seriously entertained. The idea of incompatible relationship between calcite and kaolinite is reviewed and the evidences for it are not compelling.

Possible complications due to other clay minerals and other components are briefly considered. The most likely sources of trouble are montmorillonite and the mixed-layer clays. Depending on its composition, the montmorillonite may change the geometry of the phase diagrams but will not affect the calcite-kaolinite binary join. Whether the mixed-layer clays will change the diagrams depends on whether such clays behave as mono- or polyphase systems, about which nothing is as yet known.

INTRODUCTION

The physical-chemical relations among the minerals in sediments and sedimentary rocks have in the past received comparatively little attention. This neglect was probably due in part to difficulties in studying multicomponent systems, and in part to practical difficulties in phase identification, especially for the very fine-grained material. The problem of identification is amended by the rapid improvement of the Geiger-counter diffractometer since the end of World War II. A number of excellent studies are now in the literature.

To comprehend the mutual relations among the minerals, it is not adequate to study the mineral associations from composite samples, nor is it enough to study a few specific minerals in a given sample. Rather, the mineral phases that must be considered depend on the nature of the physico-chemical relations to be examined, and must be decided upon in each case. The present paper deals with certain of the observed mineral assemblages, and also theoretical possibilities and limitations, in systems involving carbonates and some clay minerals.

The clay mineral-carbonate systems are chosen for study, partly because of the data on hand, and partly because these, occurring commonly in fine-grained rocks, have the best chance of attaining chemical equilibrium. It is hoped that elucidation of their relations may also contribute towards a resolution of some controversial questions, for example whether a given clay mineral is an indicator of its environment of deposition or of the source area.

ACKNOWLEDGMENTS

I wish to thank sincerely Professors R. M. Garrels, R. Siever, and J. B. Thompson, Jr., and Mr. R. F. Schmalz for reading the manuscript and making

---

* Contribution no. 388 from the Department of Mineralogy and Petrography, Harvard University; no. 962 from Woods Hole Oceanographic Institution.

many helpful suggestions. To the faculty of the Division of Geological Sciences, Harvard University, I am indebted for the use of the laboratory facilities and for their constant cooperation in all matters. Dr. W. F. Bradley of the Illinois Geological Survey spent much of his time in stimulating discussions on clay mineralogy, and also read the manuscript for which I am grateful.

MINERALOGY

Description of samples and experimental procedure.—Most of the samples studied are modern marine bottom deposits cored from the coast of Peru and Chile, by the research vessel *Atlantis* of the Woods Hole Oceanographic Institution, during the winter of 1955-56 (cruise no. 221). A number of the coring traverses extended from the shallow coastal waters across the Peru-Chile Trench (Zeigler, Athearn, and Small, 1957) to the "plateau" on the seaward side, thus enabling a study of the mineralogy of the cores with respect to their geographical location.

One of the interesting finds of the mineralogical study is the presence, in most of the samples, of variable amounts of volcanic glass mixed with the crystalline phases and fossil fragments. The glass grains are generally no more than 0.02 mm across. By a combination of index-of-refraction ($n \geqslant 1.57$) and density (≈ 2.7-2.8) measurements, most of the fresh fragments, which are olive green, are taken to be basalt (Wahlstrom, 1955, p. 287, 299) although other types, dominantly andesite but ranging to rhyolite, are also found (Zen, 1957b, p. 901). Much of the glass is devitrified to varying degrees with a concomitant decrease in density; in many cases the original glassy state of the grains is inferred when the grains enclose relatively fresh, commonly euhedral phenocrysts, generally hornblende and/or plagioclase in the andesine-labradorite range.

As it has not been practicable so far to separate the devitrified glass from the rest of the sample, due to the extremely fine grain size, x-ray study of the mineralogy is confined to the bulk samples. In these cases, microscopic examination of the samples under high magnification helps in correlating the nature of the x-ray mineralogy with the textural relations.

X-ray studies were made with a Norelco high angle Geiger-counter diffractometer. The techniques adopted have been described elsewhere (Zen, 1957b, p. 890). The -2μ fractions of the samples are prepared in the following way:

The sample (about 5 grams, because of the availability of material) is thoroughly stirred in a 100 ml graduated cylinder filled with distilled water. It is then allowed to settle for about 6 hours, and the top 13 cms of the liquid is decanted. If the sample does not deflocculate, more fresh distilled water is used until it does; no reagent is added. If the density of the grains is taken to be 2.5, Stokes' Law gives a maximum effective settling diameter equal to 1.3 microns for the fraction remaining in suspension. The suspended material is then centrifuged and thoroughly washed with distilled water, finally brought back to a milky suspension, transferred to glass slides and dried. Slides thus prepared show strong orientation of the platy minerals, suitable for x-ray identification. For each sample, four identical slides are made. The first slide is used as such. The second slide is saturated with ethylene glycol. The third slide is heated to

170-200°C for one hour, and the fourth slide heated to 450-500°C for one-half hour.

Criteria of mineral identification.—A large number of minerals encountered in the samples, such as quartz, plagioclase, calcite, dolomite, and halite (due to evaporation of the water trapped in the cores), have clear and distinct x-ray diffraction patterns and their identification and microscopic verification, even for fine-grained material, present little trouble. Such is not the case with the platy minerals. The criteria used for differentiating among the various groups of these have been set out before (Zen, 1957b, p. 890-892) ; since the writing of that paper, however, a number of modifications and improvements have been introduced. These are as follows:

1. Organic swelling of montmorillonite is now done with glycol rather than glycerin. Heating is done in the 450-500°C range rather than 550-600°C.
2. For chlorite-kaolinite differentiation, the criterion of Johns, Grim and Bradley (1954, p. 243) is adopted. The samples are heated to 450-500°C, and if the 7Å line is destroyed, it is taken to be chlorite; if weakened, a mixture of kaolinite and chlorite. This procedure is justified because kaolinite is known to be thermally stable under atmospheric conditions until *ca.* 600°C (Brindley, *in* Brindley, 1951, p. 57). Occasionally, a sharp 14Å line, revealed after glycol treatment has shifted the interfering montmorillonite line, remains after heating (the montmorillonite line is shifted to 10Å after this treatment). Such a line is interpreted as detrital chlorite whose thermal characteristics more nearly correspond to the data of Brindley and Robinson (*in* Brindley, 1951, p. 188) on well-crystallized material. No attempt has yet been made to differentiate non-swelling vermiculite from chlorite.

Phases resulting from devitrification.—With the combined x-ray and microscopic examinations, using the cited criteria, it has been possible to identify a number of phases resulting from the devitrification of glass[1], with varying degrees of confidence. Among the phases thus identified, quartz, calcite, a 10Å mica ("illite"), and an iron oxide (hydrous?) are definite. Microscopically, kaolinite is strongly suggested by a fine-grained, optically negative, platy mineral whose indices of refraction correspond to those of kaolinite (Grim, 1953, p. 279) and are not affected by the immersion media. Chlorite (optically positive) and an alkali feldspar are suspected but not confirmed. In the disaggregated material, there is no doubt of the presence of all the above phases, and in many of the very fine-grained bulk samples there is likewise no doubt of the above mineral assemblage.

PHASE RELATIONS

General considerations.—After a brief, general study of the choice of components and phases, the consideration of the phase relations between clay minerals and carbonates will be taken up in three parts. First, the relation between calcite and kaolinite will be studied in terms of the Phase Rule, and the existing hypothesis on their mutual relations reviewed. This will be followed by a study of a larger, seven-component system, which includes the minerals dolomite and chlorite as well as calcite and kaolinite. Mineral assemblages will be predicted and compared with observations. Finally, the role of some other clay minerals will be briefly considered.

---

[1] The textural relationships of the glass grains form studies by themselves and will not be pursued here.

Gibb's Phase Rule, which relates the number of phases, ϕ, with the number of *independent* components, c, is:

$$w = c + 2 - \phi$$

where w, the variance or degrees of freedom, is the number of independent conditions that must be imposed on the system for its unique description. For a system in which c' components are "mobile" (i.e., values of their chemical activities[2] a are fixed independently of the bulk composition of the system), the variance is reduced,

$$w' = c + 2 - \phi - c'$$

(Korzhinsky, 1950, p. 52; Thompson, 1955, p. 80). For arbitrary values of the temperature and pressure, the maximum number of phases thus is

$$\phi_{\text{max.}} = c - c'$$

In our general four solid-phase system, seven components, reckoned as the oxides, must be considered. These are CaO, MgO, FeO, Al_2O_3, SiO_2, CO_2, and H_2O. As this is too many to treat graphically with convenience, the following simplifications will be used:

First, we may suppose that the chemical activity, a, of H_2O, is independently fixed, i.e., H_2O is a "mobile" component. This is consistent with observations on metamorphic rocks (Thompson, 1957, p. 844). For sediments and sedimentary rocks, the activity might be regarded as fixed by the composition of the sea water or ground water.

Second, we may do the same to the activity of CO_2. One might perhaps consider the value as that in an "average" atmosphere, a situation that would obtain and apply to the sediments if the sea water, say, is saturated with respect to atmospheric CO_2.

Finally, we might limit our study to systems in which some form of pure SiO_2 exists, thus eliminating the need to consider SiO_2 as a component (Turner, 1948, p. 50; Thompson, 1957, p. 843). In most cases this will be quartz. For some sediments, specifically many of the Peruvian samples, the presence of amorphous siliceous microfossil remains suggests that the limiting value of

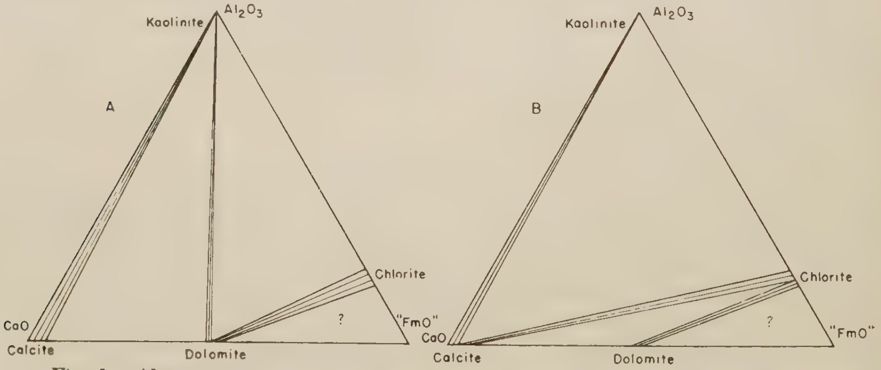

Fig. 1. Alternative assemblages in the system Al_2O_3—CaO—FmO in the presence of quartz and at particular values of T, P, a_{H_2O} and a_{CO_2}.

---

[2] Chemical activity is used in the sense of Lewis and Randall, 1923, p. 255.

a_{SiO_2} may be higher than that of quartz. Although amorphous silica may not have a fixed composition, due to its variable H_2O content and possibly adsorbed material, its fairly constant solubility in water (Siever, 1957, p. 824) indicates a narrow range of variation in a_{SiO_2} and may therefore be used as a metastable but reliable yardstick. It is doubtful that the differences between the solubilities of quartz and amorphous silica (Siever, 1957, p. 825-826), corresponding to a free energy difference of about 2 kcal/mole, will affect the stability of the silicate phases in equilibrium therewith.

We are thus left with four remaining "fixed" components, CaO, FeO, MgO, and Al_2O_3; if FeO and MgO are, for the time being, lumped together as "FmO", the system may be represented, at arbitrary values of T, P, a_{H_2O}, a_{CO_2}, and a_{SiO_2}, by a ternary diagram, figure 1, in which *A* and *B* depict two topologically distinct possibilities.

A few words may be said of the variations shown by the phases. The system calcite--dolomite has been recently studied (Harker and Tuttle, 1955; Graf and Goldsmith, 1955) and the compositions of these phases are extrapolations of the high temperature experimental data. These extrapolations should be qualitatively correct. Little is known of the composition of chlorite in sediments, and what is shown is the range observed in metamorphic rocks (Hey, 1954; Zen, 1955). It is assumed that this applies approximately to sediments. Again, this should be qualitatively correct. Finally, the "FmO" corner is left open as we are not sure of the appropriate phase. It may be siderite, serpentine, greenalite, or some other ferromagnesian phase.

To account for the observed mineral assemblages in terms of the phase diagrams, we presuppose of course that the system is at chemical equilibrium. It may be argued that for sedimentary minerals involving the silicates this does not obtain, and the argument is indeed difficult to reject with certainty. In some cases like the devitrifying glass, the assumption of chemical equilibrium seems justified. In Mesozoic and Paleozoic rocks, time is in favor of attainment of equilibrium, and the mineral associations are consistent with those in metamorphic rocks of comparable composition (Millot, 1950; Grim, Bradley, and White, 1957), where chemical equilibrium may be more completely attained. It is the bulk of the more recent sediments for which doubt is strong. In these cases, accord of petrographic data with the phase diagrams (and perhaps, in lucky instances, textural information) may be the best criteria of chemical equilibrium. If the mineralogy of a series of closely-spaced samples shows consistent correlation with that predicted from phase diagrams for the given chemical compositions, for instance, the suggestion is strong that the minerals in the rocks are in mutual equilibrium. Study of clay minerals by Grim indeed suggests (1958, p. 247, 249, 250) that these commonly adjust themselves to the depositional environment, although this conclusion is by no means held by all (Weaver, 1958, p. 255).

Calcite-kaolinite relationship.—The persistent association of calcite and kaolinite in the South American marine sediments is interesting, particularly as the apparent occurrence, in devitrified glass, excludes any possibility of organic or detrital origin for these phases. Assuming that they crystallized out of the glass *in situ*, in a marine environment, one may then inquire into their equilibrium relationships.

In the literature it is generally suggested (Grim, 1953; Millot, 1950) that kaolinite and calcite form a mutually incompatible pair; their mere co-occurrence is taken by some as sufficient evidence of chemical disequilibrium. Millot states that the presence of calcium ions in solution blocks the formation of kaolinite, and Grim considers that the high pH value necessary for calcite to form causes kaolinite to be unstable, where montmorillonite, illite, or chlorite form in its stead (1953, p. 351). The concepts of Millot and Grim may be discussed along the following lines:

1. Millot (1950, p. 288) considers that the presence of dissolved divalent ions, particularly calcium and magnesium, tends to block the formation of kaolinite. It is not clear whether he refers to a rate or an equilibrium process. It is clear however that dissolved calcium ions may not always be equated with the phase calcite; in fact for a given value of the chemical activity of CO_2 the presence of calcite severely limits the calcium ion concentration in a solution.

2. Although an increase in the pH value of the surrounding solution, *other things being equal*, may increase the solubility of kaolinite, it does not necessarily mean that the phase ceases to be stable, provided that the system is not an open one with respect to the material exchange of interest. We can, for instance, increase the solubility of halite by raising the temperature, but the solid halite remains intrinsically stable in its saturated solution.

3. Millot (1950, p. 284; see also Grim, 1953, p. 351) considers that a given cation concentration causes the flocculation of an alumina sol more readily than it does a silica sol. He uses this concept to predict the formation of kaolinite in an environment of low cation concentration, and of montmorillonite, for example, in one of relatively high concentration, with the ultimate control apparently the concentration of colloidal silica and alumina remaining as sols. In an analogous way (Millot, 1950, p. 283) he considers the effect of pH on the resulting clay mineral phase. It is clear however that these considerations pertain largely to rates of processes, and cannot apply to equilibrium properties. As a matter of fact, reference to figure 2 shows that, accepting the compatibility of kaolinite and quartz, the pair solution—Al montmorillonite (after the formula of Roy and Osborn, 1954, p. 869) cannot be stable at all.

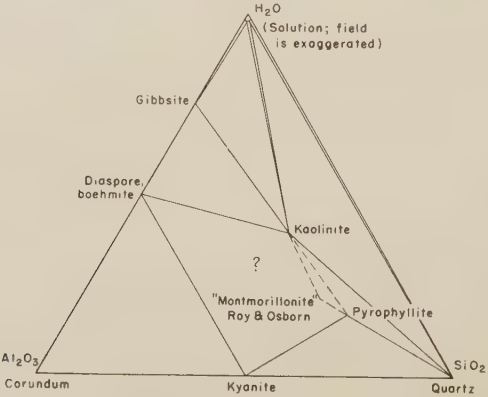

Fig. 2. Schematic and partial representation of the system H_2O—Al_2O_3—SiO_2.

Natural montmorillonites all contain other components in addition to Al_2O_3, SiO_2, and H_2O, and therefore do not necessarily belong to the systems of sols that Millot considers.

4. Phases or groups of phases such as illite, chlorite, and montmorillonite, contain components other than Al_2O_3, SiO_2, CaO, H_2O, and CO_2, and so considerations of the compatibility of calcite and kaolinite as such cannot include these phases as alternatives; much larger and more complex systems must be taken into account. On the other hand, it is true that in the presence of sea water a phase like kaolinite *might* cease to be stable, either due to the desiccating effect of the saline water or due to chemical reactions forming a phase like illite. This point can be settled unequivocally only through laboratory studies; however, petrographic data do not indicate that this is true, at least in all cases.

5. There is a considerable body of petrographic data, both from modern sediments and consolidated rocks, supporting the common co-occurrence of the calcite-kaolinite pair. Of the 19 Mesozoic samples of marine sedimentary rocks studied by Millot (1950, p. 130-173), for example, 16 cases of this pair are reported; of the 18 samples of Mesozoic and Cenozoic lagunal deposits, 8 cases (*ibid*, p. 178-222). Other petrographic data will be presented later.

It is not claimed that calcite and kaolinite, wherever found, are stable together, or that sediments and sedimentary rocks are always equilibrium systems. Rather, it is suggested that existing petrographic evidence is compatible with the hypothesis of equilibrium, and that arguments advanced against this hypothesis might be open to alternative interpretations. In particular, the Peruvian sediments, as a whole, certainly are out of chemical equilibrium, as attested by the existence of volcanic glass; its devitrification nonetheless indicates that chemical reactions are taking place and thus equilibrium is being approached. Moreover, if two phases, here calcite and kaolinite, demonstrably result from devitrification, it is reasonable to suppose that locally, at least, chemical equilibrium is attained. The basic assumption here is that each phase is in equilibrium with its surrounding sea water with which material exchange is known to have occurred, and that diffusion of material in the water phase is sufficiently rapid that no sensible chemical gradient is set up on the scale of a devitrifying grain.

The problem may be alternatively formulated in terms of our general approach outlined earlier. The system involving calcite and kaolinite involves five oxide components, CaO, Al_2O_3, SiO_2, H_2O, and CO_2. Consistent with the simplifying scheme, H_2O and CO_2 are taken to be "mobile" components in a marine environment and need not be considered, and quartz is presumed to be present. Two components, CaO and Al_2O_3, remain, and the corresponding solid phases are calcite and kaolinite. The question then is, are there other phases, within this same binary system, which might be stable under the same conditions of temperature, pressure, and activities of the "mobile" components? Phases that have correct chemical compositions are these: anorthite, zoisite or clinozoisite, lawsonite, pumpellyite, margarite, and probably some of the zeolites like chabazite and scolecite. To the writer's knowledge, no such zeolite is reported from sediments or sedimentary rocks, and it is improbable that the other phases listed above would be stable within the environment of marine sedimentation, even though these minerals occur in many of the heavy mineral suites. Pyrophyllite is a possible alternative phase to kaolinite, but is not known in sediments. There appears to be no alternative to the calcite-kaolinite pair within the five-component system.

System involving the solid phases chlorite-kaolinite-calcite-dolomite.—In addition to the five components just considered, we might consider two additional components, FeO and MgO, thus enabling us to account for two more phases, chlorite and dolomite. H_2O and CO_2 are again taken to be "mobile", and quartz or amorphous silica is taken to be present in excess. By lumping FeO and MgO together—their separate effects will be considered shortly—pseudoternary diagrams may thus be constructed. Two alternative diagrams are presented in figures 1A and 1B; each diagram displays two 3-phase assemblages, separated by 2-phase fields, all in addition to quartz and an aqueous phase. Each of the 3-phase fields is invariant, i.e., the phases at apices of the fields are fixed in compositions, under arbitrary choices of T, P, a_{SiO_2}, a_{H_2O}, and a_{CO_2}, as well as of the bulk Fe:Mg ratio. There is considerable petrographic evidence to support the arrangement of the fields. Thus, in the Peruvian samples, calcite-chlorite-kaolinite (1B), as well as the three bounding 2-phase assemblages, are common. Calcite-dolomite-chlorite (1B) is suspected but as yet unconfirmed. Milliot's study of Mesozoic sedimentary rocks amply substantiates this diagram (1950, p. 130-173); this agrees with the calcite-dolomite-chlorite and calcite-chlorite assemblage from certain Ordovician rocks reported by Weaver and Bates (1952, p. 259) and Weaver (1953, p. 925-929; 935-939). Potter and Glass (1958, p. 35-39) also report the calcite-chlorite-kaolinite association with at least some of the kaolinite authigenic (p. 34). All these are in accord with the writer's study of some slates in Vermont, where the calcite-dolomite-chlorite assemblage is found.

On the other hand, both the works of Grim, Lamar, and Bradley (1937) and of Robbins and Keller (1952) on the clay mineralogy of Paleozoic limestones and dolomites show that the kaolinite-dolomite pair exists, corresponding to figure 1A. Unfortunately, it is not clear what the other mineral phases are in a given sample, for although the dolomite-kaolinite pair indicates *A*, the possible absence of quartz might negate our assumption of fixed a_{SiO_2}. It might also be desirable to apply more modern criteria on chlorite-kaolinite differentiation (W. D. Keller, letter, November, 1957). Among the more modern work, the dolomite-kaolinite association is reported by Bonython (1956, p. 83) and Rogers, Quirk, and Norrish (1956, p. 177-179). The association dolomite-chlorite-kaolinite has also been reported (H. D. Glass, 1957, oral communication).

Figures 1A and 1B are related by a reaction which may be schematically represented as follows.

$$\begin{aligned}&\text{calcite} + \text{chlorite} + \text{carbon dioxide}\\&= \text{dolomite} + \text{kaolinite} + \text{quartz} + \text{water}\end{aligned} \tag{1}$$

In this equation, the bulk Fe:Mg ratio, among other variables, is clearly significant in determining the assemblage, inasmuch as calcite, dolomite, and chlorite all show variability along this coordinate. This shows that to treat Fe and Mg as a single component is incorrect (Thompson, 1957, p. 846). One could show these relations more explicitly yet retain the ternary appearance of the diagram by projecting from one of the phases in figure 1 (for a general discussion of this problem, see Thompson, 1957, p. 847). To aid visualization, a schematic representation of the four-component tetrahedron, A (kaolinite) - C (calcite) - F (siderite?) - M (magnesite?) is shown in figure 3; this is applicable at appropriate values of T, P, a_{H_2O}, a_{CO_2}, and in the presence of free quartz. The 3- and 4-phase assemblages are given, and the letters, a,b,c, etc., indicate their compositional ranges. Chlorite is shown as more ferroferous than the coexisting dolomite; this is extrapolated from evidences found in slates, where chlorite of nearly unit Fe:Mg ratio coexists with nearly pure magnesian dolomite (Zen, unpublished data). At the high iron end, siderite and calcite are shown to coexist; this agrees with existing experimental information (Rosenberg and Harker, 1956, p. 1728) and the scanty petrographic evidence (Lippmann, 1955, p. 485; Potter and Glass, 1958, p. 35-39). Chlorite is assumed to be intrinsically stable over the entire Fe-Mg ratio range. For simplicity, all solid solution series are shown to have only one compositional degree of freedom, although in reality a phase like chlorite is known to show Al: (Fe,Mg) variations as well.

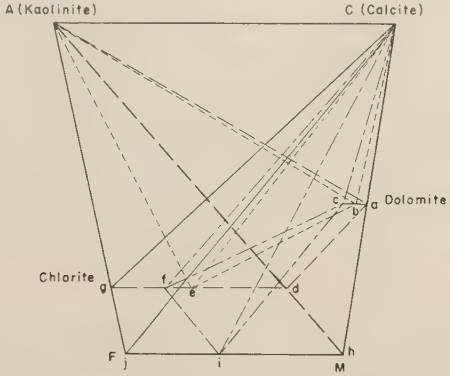

Fig. 3. The system A-C-F-M with quartz at particular values of T, P, a_{H_2O} and a_{CO_2}. The various volumes within the tetrahedron represent the following mineral assemblages:

C-c-i-f : calcite-chlorite-dolomite-siderite (?)
A-C-b-e : kaolinite-calcite-dolomite-chlorite
C-fg-ij : calcite-chlorite-siderite (?)
A-C-eg : calcite-kaolinite-chlorite
C-bc-ef : calcite-dolomite-chlorite
ac-hi-df : dolomite-magnesite-(?)-chlorite
A-C-ab : kaolinite-calcite-dolomite
A-ab-de : kaolinite-dolomite-chlorite

Two ternary projections of the tetrahedron, from calcite and kaolinite, respectively, are given in figure 4, *A* and *B*, on which the four 3-phase fields of figure 1 are indicated. It is evident that *all things being equal*, alternatives 1A and 1B may occur side by side, depending on the bulk Fe:Mg ratio.

We do not know enough about the intrinsic stability of chlorite under the contemplated conditions to warrant a representation of the situation should chlorite fail to show complete solid solution over the entire Fe:Mg range, a situation that might be indicated by the siderite-kaolinite pair reported by Potter and Glass. The necessary modifications to figures 3 and 4 are fairly

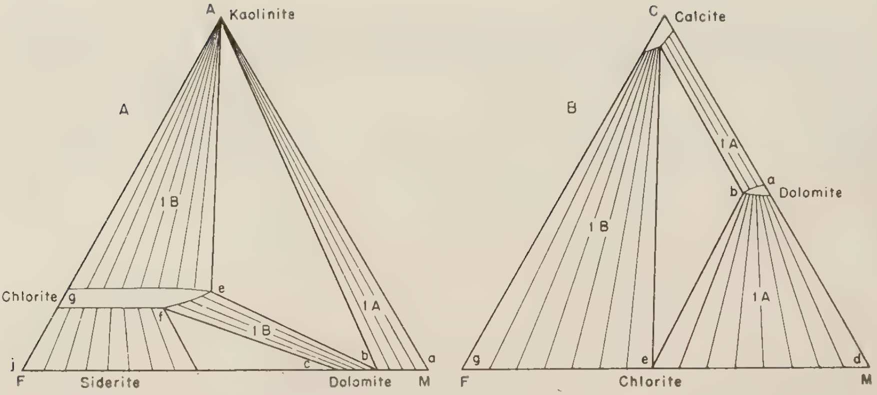

Fig. 4. Projections from the tetrahedron, A-C-F-M. (A), projected from calcite; (B), projected from kaolinite. Diagrams are highly schematic and assume the presence of excess quartz.

straightforward for such a case and the details will not be pursued. The problem is further complicated by the possibility of oxidation of ferrous minerals to form, for instance, oxy-chlorite; for this means that another independent variable, a_{O_2}, is to be introduced without new phases being added to the system. More empirical data, experimental, petrographic, and oceanographic, are needed for specific conclusions.

Finally, a few words may be said of the qualitative effect on the system of changing the values of the physical and chemical variables in addition to the effect of Fe:Mg ratio, just discussed. Reference to equation (1) shows that increases in a_{H_2O}, due, for example, to an influx of fresh water, as well as in a_{SiO_2} (which is assumed to be fixed by quartz, however) favor the calcite-chlorite pair, where increases in a_{CO_2} have the opposite effect, other things being equal. An increase in temperature favors the side of higher entropy content, but as thermochemical data on most of the phases are lacking, this effect cannot be evaluated.

A pressure increase (e.g., different depth of water) favors the side of lesser volume. The numerical values of ΔV, and even its sign, depend strongly on the state of aggregation of CO_2 and H_2O. Without going into the details, it may be said that, as limiting cases, if H_2O is liquid water and CO_2 is a gas (corresponding to a saturated solution of carbon dioxide), the volume of gaseous CO_2 is the predominating term. If the system is closed with respect to CO_2, pressure increases favor the kaolinite-dolomite pair. However, if the system is open to CO_2, whose activity is externally fixed, then an increase in total pressure favors the calcite-chlorite pair instead (Thompson, 1955, p. 80, eq. 19a). On the other hand, for a solution in which all the CO_2 hydrolyzes and dissociates into CO_3^{--}, pressure strongly favors calcite and chlorite due to the negative partial molar volume of H_2CO_3 (Zen, 1957, p. 116).

Role of other clay minerals

A. Montmorillonite.—Montmorillonite presents difficulties in graphical representation, largely because of its variable composition. Published analyses

(Ross and Hendricks, 1945; Kerr et al., 1950; see also Grim, 1953, p. 371) show that what is called montmorillonite may vary along *all* the compositional coordinates, partly through valence-coupled substitution and partly through ion exchange. It definitely does not lie in the seven-component system just considered. Roy and Osborn (1954, p. 869) have synthesized an Al-montmorillonite end member. Sand, Roy, and Osborn (1953, p. 341; see also Roy and Tuttle, 1956, p. 161) also made preliminary studies on the phase relations of Na-montmorillonite, and Roy and Roy (1955) on pure Mg-montmorillonite as well as Mg, Al-montmorillonite. Unfortunately, these do not correspond to natural montmorillonites at least in that alkali and/or alkaline earth elements in the exchange position are absent. The results of their preliminary studies therefore cannot be directly applied to natural systems.

The method of treatment in this paper is as follows. The formula of montmorillonite is taken to be

$$\begin{array}{c}(Al_{1.67}Mg_{0.33})Si_4O_{10}(OH)_2 \\ \downarrow \\ Na_{0.33}\end{array}$$

proposed by Ross and Hendricks (1945, p. 48) where the exchangeable Na position may be more commonly occupied by Ca (*ibid*, p. 40). Two cases may then be distinguished, depending on whether the presence of montmorillonite represents a *net* addition of a phase or not, in our seven-component system.

Case I. Montmorillonite is not a net additional phase. This situation would obtain if the montmorillonite contains appreciable amount of Na, and no other essential Na phase such as albite is present. The added component, Na_2O, is balanced by the added phase, montmorillonite, in the phase rule, and the phase diagrams already considered remain valid.

Case II. Montmorillonite is a net additional phase. This is the case if the system contains essential Na phases like albite, *or* if the montmorillonite has only Ca, Mg, or Fe in its exchangeable position. Graphically this situation can be handled, on the A-C-Fm diagram, by subtracting an amount of Al from the montmorillonite formula equal to the amount of Na (i.e., albite composition, since quartz is present in excess; see, in this connection, Thompson, 1957, p.

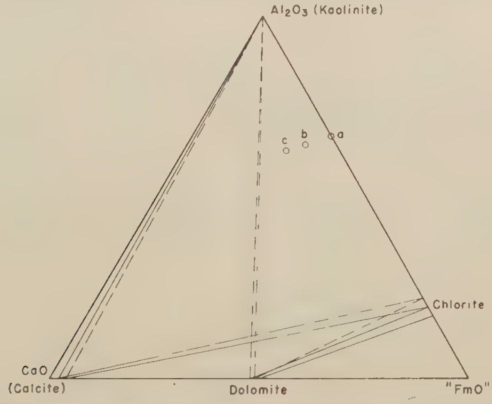

Fig. 5. A-C-Fm diagram showing composition of montmorillonite (points a,b,c) in relation to the system A-C-Fm. See text for explanations.

845) and recalculating the remaining Al_2O_3, CaO, and FmO to 100 percent. This is shown in figure 5, where the points a, b, c correspond to 1:0, 2:1, and 0:1 Na:Ca atomic ratio, respectively. The most notable feature of this diagram is that all the points plot well to the right of the kaolinite-dolomite 2-phase region; it does not at all enter into considerations of the calcite-kaolinite assemblage. Figure 6 gives schematic representations of the successive phase assemblages that must obtain to correspond to figures 1A and 1B. The transitions, from 6A to 6B, and 6B to 6C, are given, respectively, by the following reactions, assuming a 2:1 atomic ratio between Na and Ca:

montmorillonite + calcite + carbon dioxide
= kaolinite + dolomite + quartz + albite + water
(2)

and

montmorillonite + dolomite
= calcite + chlorite + albite + quartz + water
+ carbon dioxide
(3)

Mineral associations which are permitted by figure 1 but which are now in-

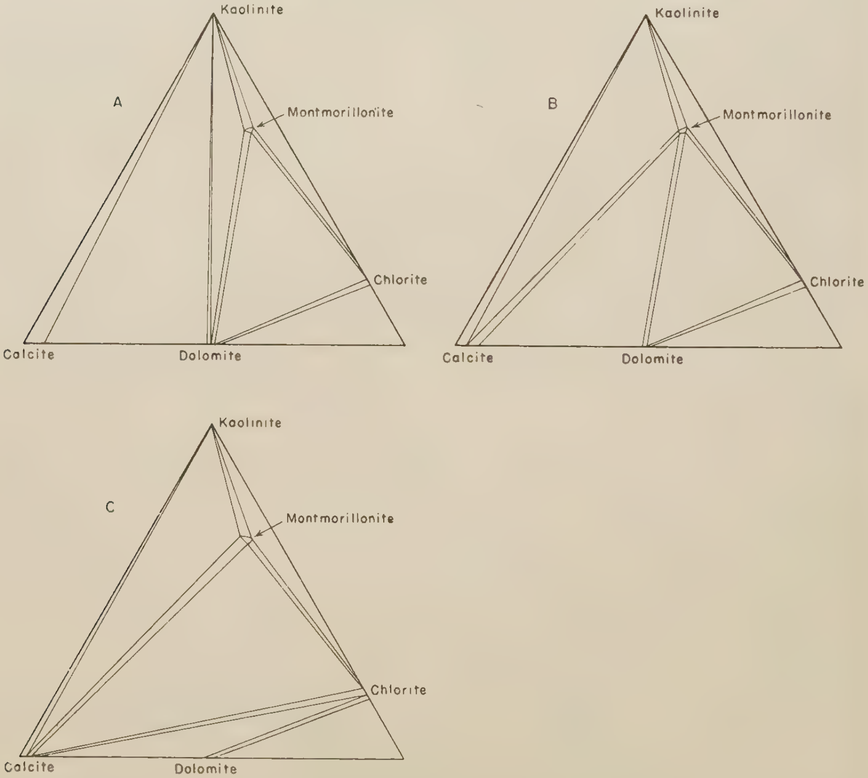
Kaolinite
A
Montmorillonite
Chlorite
Calcite
Dolomite
Kaolinite
B
Montmorillonite
Chlorite
Calcite
Dolomite
Kaolinite
C
Montmorillonite
Chlorite
Calcite
Dolomite

Fig. 6. The system A-C-Fm of figure 1, including montmorillonite. Figures A and C are analogues of figures 1A and 1B, respectively.

compatible are the 3-phase assemblages: dolomite-kaolinite-chlorite and chlorite-kaolinite-calcite. No 2-phase assemblages are affected by the net addition of montmorillonite as a phase in the seven-component system.

B. Other clay-mineral phases.—Illite is a common constituent of sediments and sedimentary rocks. It is, however, a phase in which potassium is an essential component, which is not part of our seven-component system. The equilibrium relationship of potassic phases, which include illite, potash feldspar, and phillipsite, constitute a study by itself and will not be pursued at this point; we only note that the presence of illite does not affect the preceding phase-equilibria considerations as such.

Vermiculite is an important phase in some sediments although it is not yet known from the Peruvian samples. Whatever its mode of origin, vermiculite may best be regarded for our purpose as a solid solution between K-biotite and Mg, Ca-biotite (see Barshad, 1948, p. 670). It therefore is another phase for which potassium is essential, and its discussion will be deferred until a later paper.

Mixed-layer clays pose a special problem. These clays occur commonly in many sediments and the constituent layers are largely montmorillonite, illite, chlorite, and vermiculite (Weaver, 1956). These individual constituents, as distinct phases, have all been referred to; the question is then whether a mixed-layer clay mineral behaves thermodynamically as a mono- or polyphase system. Roy and Roy suggest (1955, p. 173) that the occurrence of the discrete phases means that the appropriate mixed-layer phases must be metastable assemblages. Mixed-layer clays however may merely represent fine mechanical mixtures and connote no metastability, provided that the discrete phases are demonstrably *also* stable under the same physical and chemical conditions. Should some or all of the mixed-layer clays turn out to behave as monophase systems, of course, our phase diagrams will have to be drastically modified.

SUMMARY AND CONCLUSIONS

1. Study of some modern marine bottom samples shows the common coexistence of calcite and kaolinite, in addition to chlorite and quartz. At least some of these associations result from devitrification of volcanic glass and thus their mutual chemical equilibrium is suggested.

2. The arguments against the compatibility of calcite and kaolinite are reviewed. It is felt that these are not compelling, and the existing data are equally explainable in terms of chemical equilibrium as in terms of chance collection of detrital material.

3. An hypothesis of chemical equilibrium carries with it the implication that phase transformations may take place even at near-surface conditions, in a reasonably short time. Such transformations include major structural changes of the clay-mineral lattices. A clay mineral, therefore, may not be a reliable indicator of source material except insofar as the bulk chemical composition of the sediment must in some way reflect the bulk chemical composition of the material supplied. Should a detrital phase happen to be stable in the new environment, of course, it would not have to transform, even if the reactions should take place at rapid rates.

4. A seven-component system, involving the clay minerals chlorite and kaolinite, and the carbonates calcite and dolomite, is discussed in its general aspects, in terms of the Gibbs Phase Rule, and the phase assemblages predicted and compared with petrographical data. Alternative phase associations are shown to occur in sediments and sedimentary rocks, and the causes of the phase shifts are discussed. The possible effects of other clay minerals in this system are also considered.

5. Under favorable conditions, satisfied by many modern sediments, moderately complex, multicomponent systems can be successfully analyzed by thermodynamic methods. To make such an approach useful, however, detailed petrographic data are generally required, not only for specific minerals, but for the mineral *assemblages*. For it is often in the nature of these assemblages, rather than in any one particular mineral, that the clue to the environment of deposition lies. It is, therefore, hoped that in the future, petrographic reports on sediments and sedimentary rocks will emphasize the specific mineral associations, and wherever possible also the detailed mineral compositions and the textural relations among the phases, as these data are essential to a complete discussion of the mutual relations among them.

REFERENCES

Barshad, I., 1948, Vermiculite and its relation to biotite as revealed by base exchange reactions, x-ray analyses, differential thermal curves, and water content: Amer. Mineralogist, v. 33, p. 655-678.

Bonython, C. W., 1956, The salt of Lake Eyre—its occurrence in Madigan Gulf and its possible origin. Roy. Soc. South Australia Trans., v. 79, p. 66-92.

Brindley, G. W., ed., 1951, X-ray identification and crystal structures of clay minerals: London, The Mineralogical Society, 345 p.

Graf, D. L., and Goldsmith, J. R., 1955, Dolomite-magnesian calcite relations at elevated temperatures and CO_2 pressures: Geochim. et Cosmochim. Acta, v. 7, p. 109-128.

Grim, R. E., 1953, Clay mineralogy: New York, McGraw-Hill Book Co., 384 p.

————, 1958, Concept of diagenesis in argillaceous sediments: Am. Assoc. Petroleum Geologists Bull., v. 42, p. 246-253.

Grim, R. E., Lamar, J. E., and Bradley, W. F., 1937, The clay minerals in Illinois limestones and dolomites: Jour. Geology, v. 45, p. 829-843.

Grim, R. E., Bradley, W. F., and White, W. A., 1957, Petrology of the Paleozoic shales of Illinois: Ill. State Geol. Survey Rpt. Inv. 203, 35 p.

Harker, R. I., and Tuttle, O. F., 1955, Studies in the system CaO—MgO—CO_2, part 2, limits of solid solution along the binary join $CaCO_3$—$MgCO_3$: AM. JOUR. SCI., v. 253, p. 274-282.

Hey, M. H., 1954, A new review of the chlorites: Mineralog. Mag., v. 30, p. 277-292.

Johns, W. D., Grim, R. E., and Bradley, W. F., 1954, Quantitative estimations of clay minerals by diffraction methods: Jour. Sed. Petrology, v. 24, p. 242-251.

Kerr, P. F. *et al.*, 1950, Analytical data on reference clay minerals: Am. Petroleum Inst. Project 49, Prelim. Rpt. no. 7, 160 p.

Korzhinsky, D. S., 1950, Phase rule and geochemical mobility of elements: 18th Internat. Geol. Cong. Proc., Section A, Problems of Geochemistry, p. 50-57.

Lewis, G. N., and Randall, M., 1923, Thermodynamics: New York, McGraw-Hill Book Co., 653 p.

Lippmann, F., 1955, Ton, Geoden und Minerale des Barrême von Hoheneggelsen: Geol. Rundschau, v. 43, p. 475-503.

Millot, G., 1950, Relations entre la constitution et la genèse des roches sédimentaires-argilleuses: Thesis, Univ. of Nancy, Fac. of Sciences, 352 p.

Potter, P. E., and Glass, H. D., 1958, Petrology and sedimentation of the Pennsylvanian sediments in southern Illinois: a vertical profile: Ill. State Geol. Survey Rpt. Inv. 204, 59 p.

Robbins, C., and Keller, W. D., 1952, Clay and other non-carbonate minerals in some limestones: Jour. Sed. Petrology, v. 22, p. 146-152.

Rogers, L. E. R., Quirk, J. P., and Norrish, K., 1956, Occurrence of an aluminum-sepiolite in a soil having unusual water relationships: Jour. Soil Sci., v. 7, p. 177-184.

Rosenberg, P. E., and Harker, R. I., 1956, Studies in the system $CaCO_3$—$MgCO_3$—$FeCO_3$. Part I: limits of solid solution along the binary join, $CaCO_3$—$FeCO_3$: Geol. Soc. America Bull., v. 67, p. 1728.

Ross, C. S., and Hendricks, S. B., 1945, Minerals of the montmorillonite group: U. S. Geol. Survey, Prof. Paper 205-B, p. 23-79.

Roy, D. M., and Roy, R., 1955, Synthesis and stability of minerals in the system MgO—Al_2O_3—SiO_2—H_2O: Am. Mineralogist, v. 40, p. 147-178.

Roy, R., and Osborn, E. F., 1954, The system Al_2O_3—SiO_2—H_2O: Am. Mineralogist, v. 39, p. 853-885.

Roy, R., and Tuttle, O. F., 1956, Investigations under hydrothermal conditions: *in* Physics and Chemistry of the Earth, v. 1: New York, McGraw-Hill Book Co., p. 138-180.

Sand, L. B., Roy, R., and Osborn, E. F., 1953, Stability relations of some minerals in the system Na_2O—Al_2O_3—SiO_2—H_2O: Geol. Soc. America Bull., v. 64, p. 1469-1470.

Siever, R., 1957, The silica budget in the sedimentary cycle: Am. Mineralogist, v. 42, p. 821-841.

Thompson, J. B., Jr., 1955, The thermodynamic basis for the mineral facies concept: AM. JOUR. SCI., v. 253, p. 65-103.

————, 1957, The graphical analysis of mineral assemblages in pelitic schists: Am. Mineralogist, v. 42, p. 842-858.

Turner, F. J., 1948, Mineralogical and structural evolution of the metamorphic rocks: Geol. Soc. America, Mem. 30, 342 p.

Wahlstrom, E. E., 1955, Petrographic mineralogy: New York, John Wiley and Sons, 408 p.

Weaver, C. E., 1953, Mineralogy and petrology of some Ordovician K-bentonites and related limestones: Geol. Soc. America Bull., v. 64, p. 921-943.

————, 1956, The distribution and identification of mixed-layer clays in sedimentary rocks: Am. Mineralogist, v. 41, p. 202-221.

————, 1958, Geologic interpretation of argillaceous sediments. Part I. Origin and significance of clay minerals in sedimentary rocks: Am. Assoc. Petroleum Geologists Bull., v. 42, p. 254-271.

Weaver, C. E., and Bates, T. F., 1952, Mineralogy and Petrography of the Ordovician "metabentonites" and related limestones: Clay Minerals Bull., v. 1, p. 258-261.

Zeigler, J. M., Athearn, W. D., and Small, H., 1957, Profiles across the Peru-Chile Trench: Deep-sea Research, v. 4, p. 238-249.

Zen, E., 1955, Metamorphism of sedimentary rocks in the Castleton area, Vermont: Harvard University Thesis, 135 p.

————, 1957a, Partial molar volumes of some salts in aqueous solutions: Geochim. et Cosmochim. Acta, v. 12, p. 103-122.

————, 1957b, Preliminary report on the mineralogy and petrology of some marine bottom samples off the coast of Peru and Chile: Am. Mineralogist, v. 42, p. 889-903.

Contribution No. 964

The Seasonal Incoming Radiation in Norwegian and Arctic Waters, and Indirect Methods of Measurement[1]

By

Theodore J. Smayda

Institute for Marine Biology, Sect. B, University of Oslo, Norway

The importance of light in governing primary production in the sea has been well documented. Furthermore, it is common knowledge that the amount and quality of light reaching a cell surface is a function of many physical determinants which reflect, scatter, or absorb radiation causing an attenuation with depth. Measurements of this energy are easily made by any of a variety of instruments now available (LUND and TALLING, 1957), or indirectly by employing a formula.

KIMBALL (1928) calculated the average daily totals of solar radiation (Q) reaching the sea surface at different latitudes by the formula:

$$Q = Q_0\,(0{\cdot}29 + 0{\cdot}71\,[1{\cdot}0 - C])\ \text{g cal. per cm}^2\ \text{per day} \qquad (1)$$

where Q_0 represents total radiation assuming a clear sky and C is the proportion of the sky covered by clouds.

MOSBY (SVERDRUP, 1953) also derived a formula to estimate incoming radiation ($\bar{I}_0$):

$$\bar{I}_0 = 0{\cdot}026\,(1 - 0{\cdot}075\,\bar{C})\,\bar{h}\ \text{g cal. per cm}^2\ \text{per min.} \qquad (2)$$

where $\bar{C}$ is the average cloud cover on the scale 0–10 and $\bar{h}$ is the average altitude of the sun. The constant (0·026) expresses the atmospheric turbidity at 60°N; at 70°N it becomes 0·027 (SVERDRUP, JOHNSON, and FLEMING, 1942).

Incoming total (global) radiation (G_H^N) can also be calculated by WERNER JOHANNESSEN's (1956) formula:

$$G_H^N = \bar{C}_H \cdot \bar{G}_H\ \ \text{k cal. per m}^2\ \text{per day} \qquad (3)$$

where $\bar{C}_H$ is a cloud factor expressing the relationship between cloud cover and radiation as found at Bergen, Norway and is defined as:

$$\bar{C}_H = 1{\cdot}339 - 0{\cdot}1073 \cdot \bar{N} \qquad (4)$$

---

[1] Contribution No. 964 from the Woods Hole Oceanographic Institution.

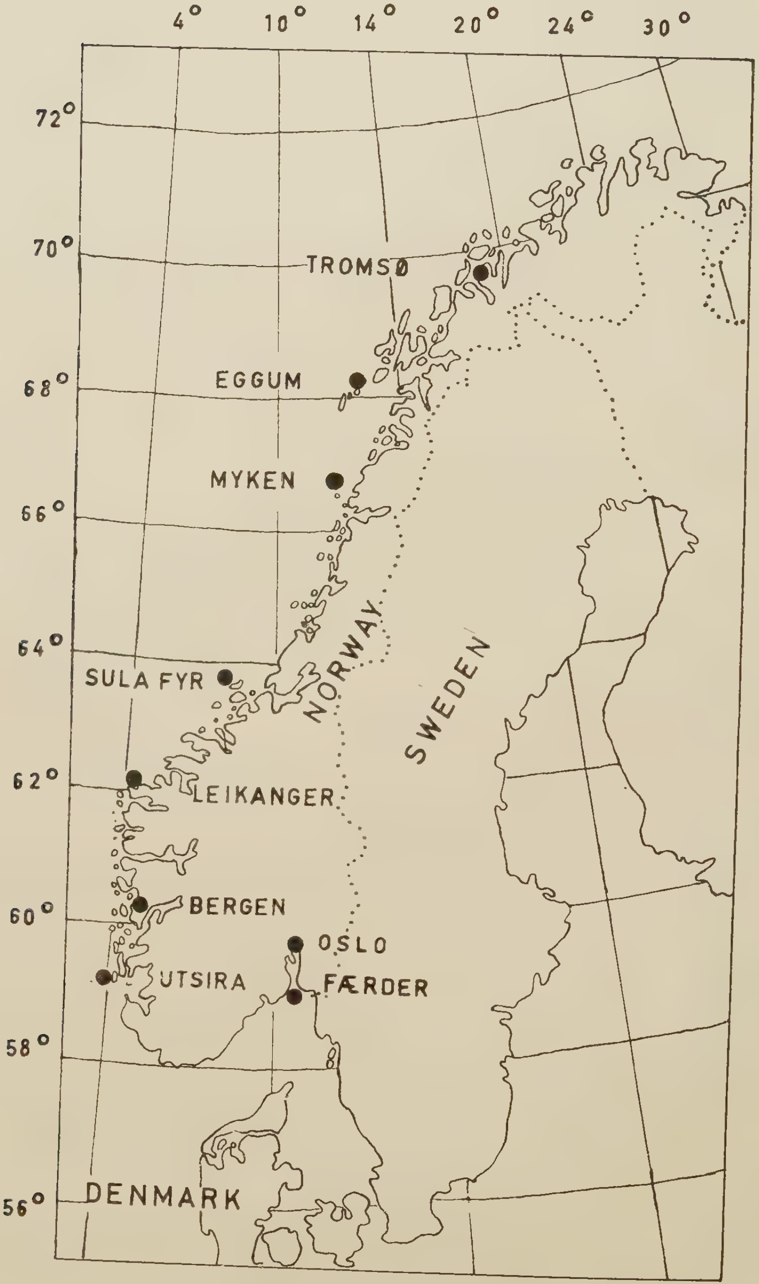
4°
10°
14°
20°
24°
30°
72°
70°
68°
66°
64°
62°
60°
58°
56°
TROMSØ
EGGUM
MYKEN
SULA FYR
LEIKANGER
BERGEN
OSLO
UTSIRA
FÆRDER
NORWAY
SWEDEN
DENMARK

Figure 1. Sites along the Norwegian coast where the seasonal radiation cycle has been calculated.

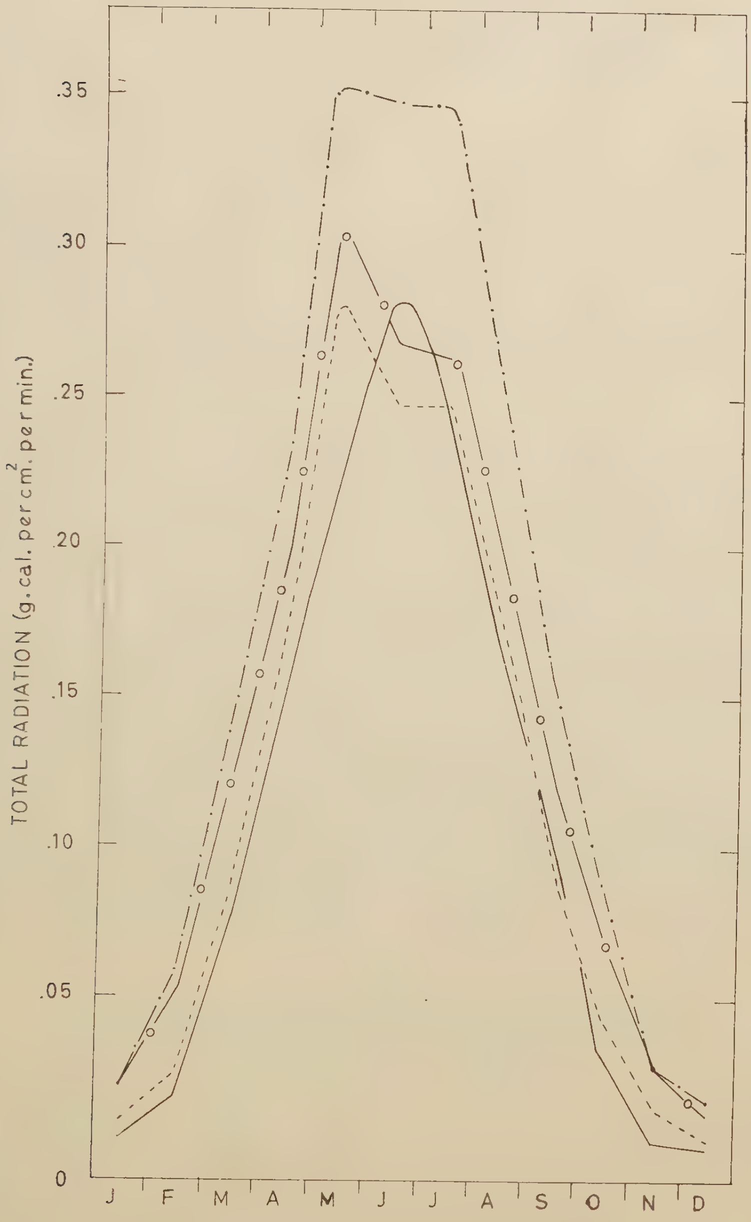

Figure 2. Seasonal radiation cycle at selected points along the Norwegian coast.

——— · ——— Færder 59°N
——— ○ ——— Utsira 59°N
· · · · · · · · · · Sula Fyr 64°N
———————— Eggum 68°N

Table 1

Average daily total radiation (G_H^N) reaching the sea surface at selected points along the Norwegian coast

(g cal. per cm² per min.)

Date	Færder 59°N	Utsira 59°N	Oslo 60°N	Bergen 60°N	Leikanger 62°N	Sula Fyr 64°N	Myken 66°45′N	Eggum 68°N	Tromsø 70°N
19. January	·021	·022	·019	·021	·014	·009	·004	·002	–
13. February	·057	·052	·051	·049	·041	·025	·019	·016	·013
17. March	·144	·119	·132	·119	·121	·083	·078	·076	·069
16. April	·233	·196	·202	·174	·185	·170	·164	·152	·147
15. May	·352	·304	·297	·290	·316	·280	·257	·225	·199
10. June	·347	·268	·293	·277	·305	·248	·279	·281	·278
19. July	·346	·262	·275	·256	·300	·248	·262	·244	·271
17. August	·252	·198	·208	·204	·224	·180	·181	·165	·161
17. September	·157	·126	·128	·118	·121	·098	·095	·107	·095
14. October	·088	·070	·079	·069	·066	·044	·037	·033	·027
15. November	·028	·028	·023	·026	·019	·014	·007	·005	·003
11. December	·016	·013	·011	·012	·008	·004	–	–	–

where $\bar{N}$ is the average monthly cloud cover on the scale 0–10. For any given day the relationship becomes:

$$\bar{C}_H = 0{\cdot}950 - 0{\cdot}0237 \cdot N_d - 0{\cdot}00907 \cdot N_d^2 \qquad (5)$$

where N_d represents the mean cloud cover.

The expression $\bar{G}_H$, in equation (3), represents the mean total daily radiation (direct + diffuse) on a horizontal surface assuming a cloudless sky.

Inserting the mean monthly cloud covers for the period 1941–1950 in WERNER JOHANNESSEN's formula, the seasonal radiation cycle has been calculated for selected points along the Norwegian coast from 59° to 70°N (Figs. 1, 2; Table 1). The values for $\bar{G}_H$, representing those days when the solar declination corresponded to the monthly mean, were abstracted from WERNER JOHANNESSEN's report and are presented here in tabular form (Table 2).

The decrease in radiation with increasing latitude is well defined (Table 1). Comparison of the seasonal cycles at Færder located at the entrance to Oslo-, fjord, and Utsira, on the western coast, both at approximately 59°N (Fig. 1),

Table 2

Daily total radiation (direct + diffuse) ($\bar{G}_H$) received on a horizontal surface in the absence of clouds

(k cal. per m² per day)

Date	59°N	60°N	62°N	64°N	66°N	68°N	70°N
19. January	565	480	325	185	115	40	–
13. February	1305	1210	960	785	575	430	305
17. March	3030	2910	2665	2430	2160	1975	1720
16. April	4895	4785	4610	4400	4210	4100	3885
15. May	6320	6195	6160	6080	5875	5835	5750
10. June	7075	7035	6960	6975	7015	6875	6945
19. July	6550	6390	6310	6320	6180	6205	6195
17. August	5140	5000	4950	4765	4550	4455	4265
17. September	3460	3310	3195	2940	2635	2450	2165
14. October	1970	1890	1650	1405	1175	950	790
15. November	775	660	510	360	205	130	65
11. December	370	320	200	100	25	–	–

reveals the importance of cloud cover in determining the amount of incoming radiation. The occurrence of a maximum energy flux during May between 59° and 64°N (Table 1) results from reduced cloud cover. Although the daily total radiation under cloudless conditions is at a maximum during June (Table 2), the observed cloud cover is from 1·0 to 1·5 units greater than that prevailing during May.

The development of the spring phytoplankton along the Norwegian coast is coincident with the marked increase in radiation occurring during March (Braarud and Bursa, 1939; Braarud, Gaarder, and Nordli, 1959; Føyn, 1929; Gaarder, 1938; Gran, 1927, 1929). This flowering begins approximately a month earlier at 59°–60°N than at 68°–70°N. In general, the radiation is between 0·090–0·100 g cal. per cm^2 per min. at this growth phase, and maximum abundance is not attained until the intensity is approximately 0·150 g cal. per cm^2 per min. As the conditions of turbidity and stability influence the light-phytoplankton relationship, deviations from the above correspondence can be expected.

Using Mosby's formula, results in close agreement with those obtained with Werner Johannessen's formula are found for cloud covers greater than 6·5 on the scale 0–10, the average difference being only 0·005 g cal. per cm^2 per min. At cloud covers less than 6·5, Mosby's formula gives significantly lower results, the divergence being inversely related to the degree of cloud cover. At a cloud cover of 5·0 the difference was 0·030 g cal. per cm^2 per min., and the mean difference between 5·0 and 6·5 was 0·016 g cal. per cm^2 per min. Kimball's formula consistently gave lower results than the other two, especially during the period April–August when differences greater than 0·050 g cal. per cm^2 per min. were common; the mean difference for the other months was only 0·009 g cal. per cm^2 per min.

The purpose of this note is to depict the seasonal radiation cycle along the Norwegian coast, and to present data enabling the calculation of incoming radiation on the sea surface between latitudes 59° and 70°N. Should Mosby's formula be used, the appropriate solar altitude can be obtained from a nautical almanac or through interpolation of the rather incomplete data presented here (Table 3), condensed from Werner Johannessen's tables. Should Werner Johannessen's or Kimball's formula be employed, Table 2 can be consulted

Table 3

Mean solar altitude ($\bar{h}$) on days when solar declination corresponds to monthly means

Date	59°N	60°N	62°N	64°N	66°N	68°N	70°N
19. January	2·0	1·8	1·2	0·9	0·5	0·2	–
13. February	4·2	3·9	3·3	2·8	2·2	1·7	1·2
17. March	9·0	8·7	8·1	7·5	6·9	6·3	5·6
16. April	14·7	14·5	14·3	13·5	13·0	12·4	11·9
15. May	19·8	19·6	19·3	19·0	18·7	18·5	18·4
10. June	22·1	22·4	22·2	22·0	22·0	22·1	22·3
19. July	21·1	21·0	20·7	20·5	20·3	20·3	20·4
17. August	16·7	16·4	16·0	15·5	15·1	14·7	14·2
17. September	10·9	10·7	10·1	9·4	8·9	8·2	7·7
14. October	6·3	6·0	5·3	4·7	4·2	3·5	3·0
15. November	2·6	2·3	1·8	1·4	0·9	0·5	0·2
11. December	1·4	1·1	0·8	0·4	0·06	–	–

to obtain incoming radiation for a *cloudless sky* anywhere between 59°–70°N. These data, then, make it necessary to know only the degree of cloudiness for the area in question.

Although here the data are applied to Norwegian coastal waters, they have also been used to estimate incoming radiation within the Norwegian Sea around Jan Mayen Island (SMAYDA, 1958). SVERDRUP (1953) outlines a procedure to calculate the amount of light reaching any depth after knowing the incoming radiation and extinction coefficient of the water mass. The values obtained by indirect measurements represent total radiation, whereas the radiation active in photosynthesis, that in the spectral region 400–700 mμ, represents an average fraction of 0·46 of the total energy (TALLING, 1957).

While direct measurements of radiation should be made when possible, indirect measurements yield results of considerable accuracy (KIMBALL, 1928) that can be used with profit.

Summary

1. The seasonal radiation cycle along the Norwegian coast has been calculated for nine localities between latitudes 59°–70°N by means of WERNER JOHANNESSEN's formula. It has been found that the incoming radiation amounts to 0·090–0·100 g cal. per cm^2 per min. when the phytoplankton initiate their spring development; maximum abundance is obtained when incident radiation is approximately 0·150 g cal. per cm^2 per min.

2. A comparison has been made of radiation estimates by three different formulae, and data have been presented enabling the calculation of incoming radiation between latitudes 59°–70°N.

References

BRAARUD, T., & BURSA, A., 1939. "The phytoplankton of the Oslofjord 1933–1934". Hvalråd. Skr. norske VidenskAkad., 19: 1–63.

BRAARUD, T., GAARDER, K. RINGDAL, & NORDLI, O., 1959. "Seasonal changes in the phytoplankton at various points off the Norwegian west coast". (In press.)

FØYN, B. R., 1929. "Investigation of the phytoplankton at Lofoten March–April, 1922–1927". Skr. norske VidenskAkad., I mat.-nat. Kl. 1928, 10: 1–71.

GAARDER, K. RINGDAL, 1938. "Phytoplankton studies from the Tromsø district 1930–31". Tromsø Mus. Aarsh., **55**: 1–159.

GRAN, H. H., 1927. "The production of plankton in the coastal waters off Bergen March–April 1922". Rep. Norweg. Fish. Invest., **3** (8): 1–74.

GRAN, H. H., 1929. "Investigation of the production of plankton outside the Romsdalsfjord 1926–27". Rapp. Cons. Explor. Mer, **56**: 1–112.

KIMBALL, H. H., 1928. "Amount of solar radiation that reaches the surface of the earth on the land and on the sea, and methods by which it is measured". Monthly Weather Rev., **56**: 393–98.

LUND, J. W. G., & TALLING, J. F., 1957. "Botanical limnological methods with special reference to the algae". Bot. Rev., **23**: 489–583.

SMAYDA, T. J., 1958. "Phytoplankton studies around Jan Mayen Island, March–April, 1955". Nytt Mag. Bot., **6**: 75–96.

SVERDRUP, H. U., 1953. "On conditions for the vernal blooming of phytoplankton". J. Cons. int. Explor. Mer, **18**: 287–95.

SVERDRUP, H. U., JOHNSON, M. W., & FLEMING, R. H., 1942. "The Oceans". Prentice-Hall Inc., New York.

TALLING, J. F., 1957. "Photosynthetic characteristics of some fresh water plankton diatoms in relation to underwater radiation". New Phytologist, 56: 29–50.

WERNER JOHANNESSEN, T., 1956. "Varmeutvekslingen i bygninger og klimaet". Rapp. Norges Byggforskningsinst., 21.

Contribution No. 967

Reprinted from THE ATMOSPHERE AND THE SEA IN MOTION
The Rossby Memorial Volume
The Rockefeller Institute Press and Oxford University Press 1959

The Evolution of a Convective Element: A Numerical Calculation[1]

By Joanne S. Malkus
Woods Hole Oceanographic Institution

and

Georg Witt
International Meteorological Institute in Stockholm

Abstract

The evolution of a convective element is studied, starting with the introduction of a specified distribution of buoyancy into a resting stratified fluid. Because of the interaction between temperature and motion fields, the differential equations describing the onset of convection are non-linear and usually intractable to analytic solution, but they are well suited to integration in finite time steps on a high speed computer. The results of several cases programmed for one such machine (BESK) are reported here.

We consider two-dimensional motions in vertical planes with central symmetry in a 640 m by 640 m space. A lower unstable or neutral layer is topped by a more stable one. A potential temperature perturbation is introduced at the initial moment, with amplitude 0.5° C, half-width 160 m, slowly decaying with height. We set up in finite difference form equations governing the vorticity, temperature, and motion fields and solve them in a series of time steps. The calculation is ended after a time corresponding to five to seven minutes due to the growth of numerical errors.

Five cases have been computed and compared to date, varying one of four initial or environmental parameters in each, namely instability, horizontal shape, frictional exchange, and the presence of the ground at the lower boundary of the perturbation. It was found that in each of the cases studied the initial perturbation developed into a mushroom-shaped bubble-like element exhibiting a rounded cap with a concentration of isentropes, and a vortex ring circulation at its edges. The early stage of development of the element has been found to consist of two phases. The first of these is an "organization phase", during which the cap and the vortex ring are formed accompanied by only slight upward motion. The second one is the actual ascent of the bubble.

I. Introduction

This is a study of the initiation of convective motions from rest in a stratified fluid. Convective motions are created and maintained by buoyancy or horizontal gradients in density, so that the different parts of the fluid are acted upon differently by gravity, producing vertical accelerations in restricted regions. In this work, we are interested in the formation and structure of the buoyant elements themselves as a function of time, and only less directly in the grosser properties of the convecting fluid and its transports. We introduce an initial, arbitrarily determined distribution of buoyancy into a fluid of given stratification and study the growth of the elements in a series of time steps for about five to seven minutes.

The direct impetus for this undertaking comes from our interest as meteorologists in the development and structure of thermals and cumuliform clouds. The type of questions we raise and hope to answer have thus mainly been formulated from attempts to learn something concerning this kind of atmospheric convection: We seek to discover what factors control the size, shape, velocity and temperature distribution, onset and decay of cumulus-size buoyant elements; and how they interact with their environment and with each other.

---

[1] Contribution No. 967 from the Woods Hole Oceanographic Institution.

Previous quantitative work on cumulus convection has, of necessity, largely been concerned with the mature and decaying phase in the element's life cycle. The main developments in the field leading up to the present inquiry are three:

1) The "entrainment" model of the cumulus, begun by STOMMEL (1947) and carried further by others at Woods Hole (MALKUS 1952, 1954). This model treats the convection element as a steady-state column discontinuously distinct from the surroundings. It has been of value primarily in relating observations of buoyancy, updrafts, and mixing. It has illustrated the effects of environment properties, such as dryness, stability, and wind shear in inhibiting the growth of cumuli and provided considerable advance over the concept of the non-interacting adiabatic parcel. It was able to say little about the mechanism of entrainment and nothing about the very early or late phases of the life cycle.

2) The "bubble" model, first evolved by SCORER and LUDLAM (1953). These authors proposed an analogy between convection element and a buoyant bubble, which was suggested to them by time-lapse cloud films and their comparison with experiments on air bubbles in water. This formulation had the advantage of dealing with individual elements or "building blocks" of convection. Large cumuli were envisaged as composed of an aggregate or succession of a number of these bubbles and their turbulent wakes. A mechanism for entrainment was suggested, namely "erosion" from the bubble cap, its protuberances being shed into the wake behind. A quantitative formulation was only possible, however, for the very final or decay phase of cumulus towers (MALKUS and SCORER, 1955). The organization, early growth, and interaction of bubbles could only be treated descriptively, nor were the conditions prescribing the rate of erosion clarified.

3) Laboratory experiments on bubbles of controllable buoyancy at Imperial College, London, by SCORER and RONNE (1956). By releasing mud slurry bubbles with realistic (2—15 %) density anomalies into a neutrally or stably stratified water tank, these workers attempted to learn more about the processes of erosion and wake formation. It was found that shedding into a wake only occurred with a stably stratified environment. Under conditions of neutral stability, a mushroom-shaped, long stemmed element evolved, with an appearance similar to a typical atomic bomb cloud. These bubbles spread out along a cone and dilution occurred primarily because of the expansion, so that the fluid ahead was engulfed into the circulation. An interesting feature was the vortex ring which appeared at the edge of the element, with up-motions in its center, so that it progressed forward by continually turning inside out, growing wider in the process.

All these studies to date treated bubbles or elements which were already formed and which possessed *ab initio* sharp density gradients at their edges. Although advances from the parcel method were significant, because dilution or mixing with the surroundings was considered, in all cases it was possible to point to a physical entity which existed from the start of the study. Nothing was said about how the bubbles or columns got there in the first place or how the field of motion believed or observed to exist is initially created by buoyancy. The reason for this is obvious, in that the initial organization of convective motions is a basically non-linear process and thus enormously difficult to treat theoretically: Once motions set in, the original temperature field is altered by advection (and also by turbulent transfer). The change in the temperature field creates alterations in the accelerations; the consequent alterations in the motions in turn further alter the temperature field, and so forth. Thus, except in rare and special cases where the thermal field may, to first order, be considered "decoupled" from feedback from the motion field (for example, when a wind blows across a heated island, as studied by MALKUS and STERN, 1953) linearization of the equations to analytically tractable form loses the basic physics of the process. With the advent of high-speed electronic computers to geophysics, however, many problems previously prohibitive due to non-linearity may now be tackled numerically without a stupefying amount of labor. This paper reports a beginning attempt to apply this new technique to convection.

II. The Model

The basis of the enquiry

We consider a resting stratified fluid and impose an initial distribution of buoyancy. Equations describing the subsequent evolution of motion, temperature and vorticity fields are derived and solved numerically under five different sets of conditions each of which differs from the others in only one respect, thus simulating a controlled experiment. We leave aside the important question of how initial buoyancy is brought about, although in one of the five cases we suppose it to be due to the sudden release of condensation heating at a short distance above the ground. In the remaining four cases, the initial density gradient is greatest at ground level; here we attempt to simplify a complex situation in nature by envisaging that the buoyancy is built up by smaller-scale processes prior to the onset of significant convective-sized motions.

The buoyancy is introduced by means of a specified "perturbation" in the undisturbed potential temperature field, which in all cases has a half-width of 160 m, a peak amplitude of 0.5° C, and decays as the cosine squared of elevation to zero in 200 m. There are thus no strong vertical gradients at the outset. The development is studied in a series of finite time steps without, in this preliminary phase of the work, the introduction of any further heat sources.

One of the main questions we sought to answer was whether a concentration of isotherms would develop with time and if so how and under what conditions most favorably. In other words, we wish to know whether a "bubble-like" element with rounded cap and intense packing of isotherms into a "front" at its top will arise spontaneously. We also wish to know whether a vortex ring circulation will develop and at what point, if any, in time it will become closely associated with the buoyant element. We wish to find out whether the element will look like a bubble with a wake, a mushroom, chimney, plume or column, or if all these shapes are possible, what conditions select between them? We wish to enquire about the development of the motion field, the magnitude of the updrafts at various stages, and where they will locate relative to the maximum temperatures. We wish to find out where the air comes from that composes the circulation and how this grows under different initial and environmental conditions.

Equations and assumptions

The basic equations used are those of motion, state, continuity, and heat transfer which have (in order) the following form

$$\frac{d\bar{v}}{dt} = -\frac{1}{\varrho}\nabla p + g + \nabla\cdot(k\nabla\bar{v}) \tag{1}$$

$$p = \varrho RT \tag{2}$$

$$\operatorname{div}\,\bar{v} = -\frac{1}{\varrho}\frac{d\varrho}{dt} \tag{3}$$

$$\frac{d\Theta}{dt} = \nabla\cdot(k'\nabla\Theta) \tag{4}$$

where Θ is potential temperature and the remaining symbols have their usual meaning. The coefficients k and k' refer to eddy transfers of momentum and heat, respectively, the molecular transfer being ignored in comparison.

The simplifying assumptions made are essential in the physical modelling and in the numerical solutions of the equations and are thus stated explicitly as follows:

1) Only two-dimensional fields are treated, due to excessive machine time required by more general cases. The initial stratification and resulting flow are defined in the Cartesian $x-z$ plane and assumed of infinite extent in the normal or y-direction. A trial case of more realistic cylindrical symmetry was begun by hand computation; its development in the first several steps looked sufficiently similar to the two-dimensional results that we feel none of the essentials are lost by this simplification.

2) $\operatorname{div}\,\bar{v} = 0$

Omission of the $\frac{1}{\varrho}\frac{d\varrho}{dt}$ term in similar convection problems in a shallow layer with small velocities has been justified by Malkus and Stern (1953) and Smith (1955). Physically it means that the fluid density is altered only by heating and lifting. It also means that the velocity of sound squared is infinitely larger than the squares of any velocities arising in the problem. The latter is helpful in a numerical approach like the present one since it eliminates difficulties of signal propagation due to sound waves, which is not only irrelevant but if permitted could lead to trouble in achieving computational stability.

3) $k = k'$ or the turbulent exchange coefficients of momentum and heat are equal.

4) $g \gg \left|\frac{d\bar{v}}{dt}\right|, |k\nabla^2\bar{v}|$ so that the latter two terms may be neglected when they appear compared to $\bar{g}$. Physically the neglection here of $\frac{d\bar{v}}{dt}$ means that pressure is to be determined hydrostatically while the important acceleration terms are not neglected. Implicitly we assume that the pressure is constant at the undisturbed upper boundary of the fluid and below this its horizontal gradients are hydrostatically produced. There is no way of evaluating the realism of this view at present. However, neglection of both $\frac{d\bar{v}}{dt}$ and $k\nabla^2\bar{v}$ compared to g was justified retrospectively by calculation of the omitted terms which did not, in fact, contribute in the last decimal place of the computations undertaken.

5) $\frac{k}{\Theta}\nabla^2\Theta = k\nabla^2\varphi$ where $\varphi = \ln\Theta$. It may be demonstrated that the omitted term $\frac{K}{\Theta^2}(\nabla\Theta)^2$ is always more than an order of magnitude smaller than $k\nabla^2\varphi$ when $\Theta \sim 300°$ A.

Introducing these simplifications, taking the curl of equation (1) to obtain a vorticity equation, and defining a stream function ψ such that

$$u = \frac{\partial\psi}{\partial z}; \quad w = -\frac{\partial\psi}{\partial x}$$

we obtain the final set of equations for numerical integration, namely

$$\boxed{\frac{\partial\eta}{\partial t} = \overset{A}{J(\psi, \eta)} - \overset{P}{g\frac{\partial\varphi}{\partial x}} + \overset{T}{k\nabla^2\eta}} \qquad \text{I}$$

$$\boxed{\frac{\partial\varphi}{\partial t} = \overset{A}{J(\psi, \varphi)} + \overset{T}{k\nabla^2\varphi}} \qquad \text{II}$$

$$\boxed{\nabla^2\psi = \eta} \qquad \text{III}$$

where η is the component of vorticity about the y-axis, $\varphi = \ln\Theta$ and the Jacobian $J(a, b) =$

$$= \frac{\partial a}{\partial x}\frac{\partial b}{\partial z} - \frac{\partial b}{\partial x}\frac{\partial a}{\partial z}$$

Physically, equation I discusses the time rate of change of vorticity (rotation in the $x-z$ plane). The local change is determined by the interaction of production by buoyancy (term P), advection (term A) and turbulent transfer (term T).

Equation II describes the time rate of change of potential temperature (logarithm thereof), the local change being determined by advection (term A) and turbulent transfer (term T).

Equation III relates the vorticity and stream function.

III. Solution of the equations

Basic Method

The non-linear character of our system of equations necessitates the use of numerical methods for the solution, either by hand or on a high-speed electronic computer. The equations are set up in finite difference form in time and space. The region is divided into 32 by 32 grid points located at a distance d = 20 m apart so that "walls" are placed at x = 640 m, z = 640 m. Their effect on a 160 m by 200 m disturbance may thus be expected to be rather small during the first 5—7 minutes, as the results will substantiate. Then we proceed to carry out the solution in a series of time steps of length Δt, with $\eta = \psi = 0$ at $t = 0$ where $\varphi(x, z)$ $\left(\text{and } \frac{\partial\varphi}{\partial x}\right)$ has been specified. At the end of the first time interval $\eta = -\Delta t \cdot g\frac{\partial\varphi}{\partial x}$ and thus the initial ψ is determined by a first relaxation step. An advection step is then undertaken using this stream function in equations I and II to obtain the new potential temperature and vorticity distribution whereafter a second relaxation step is performed, and so forth. The distribution of temperature, motion and vorticity may be printed by the machine and plotted after each time-step, if desired, but in most cases the development of the convection proceeds slowly enough so that printing at one minute intervals was sufficient.

Computational stability

In order that small computational errors (arising from the finite difference approximation to derivatives and from round-off) do not grow without bounds and rapidly destroy the validity of the calculation, the length of the time step must be restricted, relative to the grid size and the other physical parameters; neither fluid nor energy can be allowed to propagate across the distance between grid points in a single time step. Now, using the methods[1] of previous workers (for example, CHARNEY, FJØRTOFT, and VON NEUMANN, 1950, and COLLATZ, 1951), we can show that, if we solve an advection equation containing an exchange term by using centered time differences, the solution may become numerically unstable, i.e. the errors may increase exponentially with time, even if the above conditions are fulfilled. This difficulty can be avoided if we replace the exchange term evaluated at $t = \tau$ with the time average of the exchange at $t = \tau - 1$ and $\tau + 1$, respectively. In this case the stability criterion for Δt is

$$|u| + |w| \leq \frac{d}{\Delta t}\sqrt{1-\mu^2}; \quad \mu = \frac{8k\Delta t}{d^2} \tag{5}$$

where u and v are the horizontal and vertical velocities, k is the exchange coefficient, and d is the grid interval. In the present computations we have used centered time steps and the exchange term was evaluated at $t = \tau$; still our solutions remained stable as long as the above criterion was fulfilled, due to the small exchange coefficient and the relatively low number of time steps. Actually our equations also permit gravity waves, but their restriction on Δt can be shown negligible compared to that prescribed by advection and exchange (for the physical ranges of parameters chosen). When $k = 0$, the criterion depends on the advection velocities only. Considering these cases, we found the right side of (5) frequently approached 4 m/sec by 5—7 minutes and thus our initial Δt of 20 secs had to be cut down to 5 secs by the end of the time period of interest. Further reduction of Δt would lead to prohibitive use of machine time in studying bubble growth at 1 min intervals over 5—7 minutes. With time steps in the range 20—5 sec we found criterion (5) could not be satisfied with values of k in excess of 0.5 m^2/sec and thus we restricted k to two values, namely that or zero in this preliminary study. The meaning and effect of this choice of k is discussed later.

In a few of the cases studied, the test for computational stability was made at each grid point after each time step; in the majority it was found sufficient to test at boundaries and points where velocities were known to be maxima.

Procedures and boundary assumptions

After the first time step, central differences in time were used to obtain the ψ, η, and φ fields and central space differences were always used except at certain boundary points where inward differences were the only ones possible. The lower boundary presented difficulties in evaluating vertical gradients. Since in real situations, the lower boundary which may be rough and to some degree conducting exerts a complex and unknown effect, any choice here of evaluation scheme is bound to be arbitrary and unrealistic. Two different procedures were followed in this work, depending on whether k was chosen as zero or as 0.5 m^2/sec. For the cases where $k = 0$, we are concerned only with evaluating u at the lower boundary from $\partial\psi/\partial z$. We chose a constant u from 10 m (one-half grid width) to the surface at one-half the value obtained by central differences for $z = 20$ m. This means that we could use inward differences at these points for the evaluation of the Jacobian (J) terms. Physically we are crudely attempting to simulate a fairly smooth boundary with neither total slip nor complete adhesion. In those cases where $k = 0.5$ m^2/sec, the exchange terms are also evaluated as if the vorticity and the temperature were constant up to 10 m. In these we also arbitrarily reduced the horizontal advection along the lower boundary by one-half in an attempt to model a very rough boundary and to test effect of radically different boundary choices upon bubble development. As will be seen, the different boundary assumptions led to no significant differences in the major features of the convection.

Accuracy of the calculation and numerical errors

The accuracy of the solution of the Poisson equation is determined by the number of iterations carried out in the Liebmann relaxation process. In the actual computations we have continued the iterations until the maximum residual over the entire field remained below a certain tolerance. Assuming that this residual is homogeneously distributed over the entire field (i.e. the most unfavourable case) the corresponding errors in the velocity field can be estimated by conventional methods. The velocity errors can be shown to reach their maximum at the axis of symmetry. According to the tolerance used in the present computations these maximal errors were kept below 10 cm/s and 20 cm/s, respectively.

---

[1] The writers are deeply indebted to Dr. Norman Phillips for his generous and persistent aid in their struggles with computational stability.

The major source of error lies in the so-called "truncation" errors of the finite difference approximations. In approximating the second space derivatives, only terms in d^4 and higher were omitted, but in the finite difference approximation to first derivatives terms in $(\Delta t)^2$ and d^2 are left out by the method (see for example ALLEN, 1954). This means physically that the average values of the first derivatives are taken across distance $2d$ and time $2\Delta t$ which become firsreasingly poor as gradients concentrate and atit derivatives begin to vary (i.e. second derivincves become large) across a grid distance. Since advection velocities are also increasing concurrently, this means that errors will propagate as well as grow. In general, errors showed up as wiggles and bumps at the lower edges of the elements and particularly near the ground, first in the field of vorticity, second in potential temperature, and lastly in stream function and velocity. In the potential temperature field these errors become obvious as impossible non-adiabatic changes which in certain regions reach 0.1 C or 20 % of the initial perturbation after 5 minutes (or somewhat sooner in the case of $k = 0$, smooth boundary). The computation was generally ended shortly after this time, although the major outlines of the elements were still clearly defined and readily analyzable at seven minutes.

IV. Choice of parameters: the cases studied

The initial conditions of the cases studied are summarized in Table 1.

In all examples calculated to date the initial perturbation amplitude was 0.5° C. In each a slightly stable layer was placed at a level 200 m above the initial level of maximum Θ. This was necessary to prevent the velocities from growing too large, requiring a prohibitive shortening of the later time steps. This layer usually had a potential temperature increase of 1° C in 400 m and thus was only slightly stable (lapse rate 75 % adiabatic). We have thus not yet studied the effects of strong stability on a convective element.

It was noted that only two values of eddy transfer coefficients have been considered to date; namely $k = 0$ and $k = 0.5$ m²/sec. The latter corresponds to an "Austausch" of 5 c.g.s. units and may seem very low to meteorologists accustomed to Austausch values of 50—500 c.g.s. units or even larger. The value chosen was specified by Richardson's empirical formula

Table 1. Initial conditions for cases studied

Shape of perturbation	Environment	Remarks
1. $\cos\left(\frac{x}{160}\frac{\pi}{2}\right)\cos^2\left[\frac{(z-100)}{200}\frac{\pi}{2}\right]$	Unstable: $\frac{\partial\Theta}{\partial z}=\frac{-0.25\ ^\circ\mathrm{C}}{100\ \mathrm{m}}$ $k=0.5$ m²/sec	"Up in the air" bubble (100 m) neutral ground layer; slight stability below element's base.
2. $\cos\left(\frac{x}{160}\frac{\pi}{2}\right)\cos^2\left[\frac{z}{200}\frac{\pi}{2}\right]$	Neutral $k=0.5$ m²/sec	Maximum initial perturbation amplitude at ground. "Rough" lower boundary.
3. $\cos^2\left(\frac{x}{160}\frac{\pi}{2}\right)\cos^2\left[\frac{z}{200}\frac{\pi}{2}\right]$	Neutral $k=0.5$ m²/sec	Same as 2, except for initial shape in x.
4. $\cos\left(\frac{x}{160}\frac{\pi}{2}\right)\cos^2\left[\frac{z}{200}\frac{\pi}{2}\right]$	Neutral $k=0$ smooth lower boundary	Same as 2, except no exchange and doubled lower boundary advection.
5. $\cos\left(\frac{x}{160}\frac{\pi}{2}\right)\cos^2\left[\frac{z}{200}\frac{\pi}{2}\right]$	Unstable: $\frac{\partial\Theta}{\partial z}=\frac{-0.5\ ^\circ\mathrm{C}}{100\ \mathrm{m}}$ $k=0.5$ m²/sec	Same as 2, except for environment stability.

$k = 0.2\ L^{4/3}$ using $L = d = 20$ m. The attempt was to parameterize only the turbulent transfers by the scale of motion smaller than that of the convective element studied, or eddies of size comparable to the 20 m grid spacing (whose effects are lost by averaging across it) and not to include transports by the convective scale itself. It will be seen from the results that this small exchange coefficient affected the development of the elements very little; in fact the turbulent transfer term in equations I and II approaches the advective term only in the late time steps and only then in the regions of strong gradients and weak advection, and most pronouncedly in the regions of fictitiously high gradients due to truncation errors. Introduction of $k = 0.5$ m^2/sec, which indeed retarded the growth of fictitious gradients, may thus be regarded primarily as a smoothing device preventing rapid development of numerical errors. We have not yet tested the effects of strong turbulence in inhibiting the growth of convection. Due to the limitation imposed by the computational stability criterion and the questionable physical meaning of larger values of k, we shall probably continue the study of exchange effects by reducing our initial perturbation amplitude rather than by increasing k.

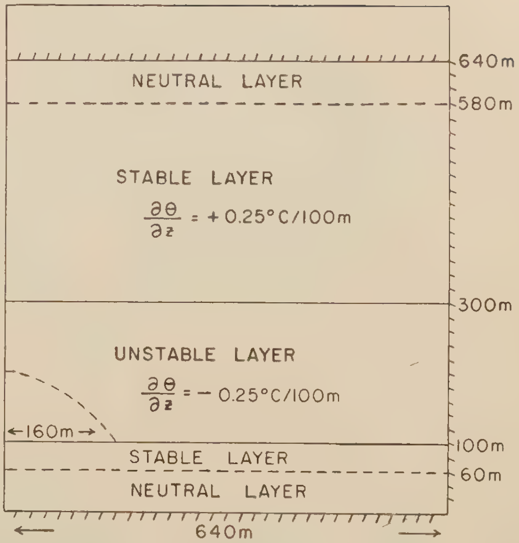
640m
NEUTRAL LAYER
580m
STABLE LAYER
$\frac{\partial\theta}{\partial z} = +0.25°C/100m$
300m
UNSTABLE LAYER
$\frac{\partial\theta}{\partial z} = -0.25°C/100m$
←160m→
100m
STABLE LAYER
60m
NEUTRAL LAYER
640m

Fig. 1. Schematic outline of the initial conditions for "up in the air" (Case 1, Table 1) bubble. The z-axis is vertical, x-axis horizontal with symmetry about $x = 0$ (left vertical line). The upper neutral layer is inserted only for convenience in programming; the slight stable layer at 60—100 m merely smoothly joins the lower neutral layer and the perturbation and thus is most pronounced at $x = 0$, grading off to neutral at $x = 160$ m. The conditions crudely simulate those over the tropical oceans, a breeding ground for convective clouds.

V. Discussion of results

The selection of initial conditions was devised to investigate in a controlled manner the effects of the following four factors on convection growth, namely environment instability, initial shape, small values of exchange and friction (via differing boundary advection) and the presence or absence of the ground at the level of maximum initial temperature perturbation. The cases in Table 1 represent successive alteration of each of these factors in turn. The resulting convection development will now be described, beginning with Case 1, the "up in the air" bubble. This was believed to be the most satisfactory case undertaken, due to the unimportance of choices concerning the lower boundary, the slower growth of numerical errors (in the remaining cases the ground gave rise to stronger concentrations of high horizontal velocities and gradients in the region of closest packed isotherms), and the greater meaningfulness of starting from rest with an initial finite buoyancy distribution, which can be envisaged here as resulting from the sudden release of condensation heating.

Figure 1 illustrates schematically the conditions for this calculation and Fig. 2 shows the resulting growth of the convection element at one minute intervals for the first five minutes. The computation was actually carried to nearly seven minutes but is shown only through five because by this time numerical errors have become visible. Errors in potential temperature as large as 0.1° C both higher and lower than any original values are seen in the last (lower right) drawing.

We note especially the following features of the convection:

1) Intensification of the vertical temperature gradient into a "front" with formation of a bubble "cap". The potential temperature gradient at the element top increases from —0.2° C in 40 m initially to nearly 1° C in that distance at 5 minutes, or a five-fold packing of isotherms.

2) Vortex ring circulation, initially centered at about 160 m elevation, which first remains stationary in height as it intensifies. After the first three minutes, it becomes closely associated with the bubble edge and thereafter moves up with it.

3) Growth of the mushroom shape, with colder air pinching in to form the stem.

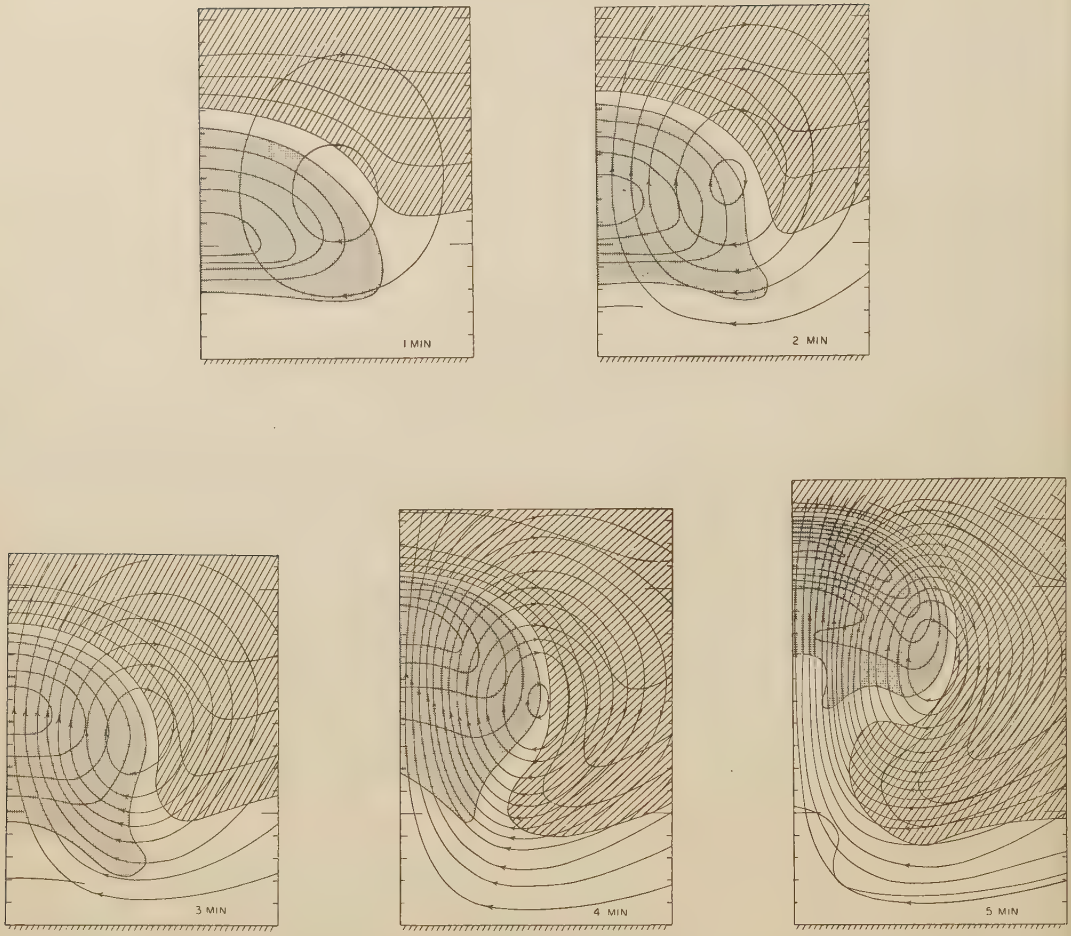

Fig. 2. Growth of "up in the air" bubble (Case 1, Table 1; initial conditions, Fig. 1) at one minute intervals for the first five minutes. The ticks are vertically spaced 20 m apart, with large ticks at $z = 100$ m (initial perturbation base) and $z = 300$ m (beginning of upper stable layer). Potential temperature isopleths (intervals of 0.1° C) are solid lines without arrows; the dotted region includes all potential temperatures higher than 289° A or that characteristic of the lower neutral layer, while the hatched region includes all values lower than 288.9° A. Lines with arrows are streamlines.

4) The changing level of inflow into the element's circulation. During the first two minutes, most of the inflow is from levels near or below 100 m (base of unstable or "cloud" layer). In the later stages, the inflow region rises, so that at five minutes the air entering the circulation comes mainly from levels above 100 m.

5) Favourable conditions at later stages for a new bubble, if available, to follow the first. The stable layer originally below perturbation base has been destroyed and even supplanted by instability. Although the instability is actually greatest in the downdraft zone (where unrealistically the initial stability was weakest) presumably just under the stem region of the element would probably be the most favourable path for a successor in a real cloud case due to moisture shed by passage of the first element.

Figure 3 shows the development of buoyancy (in terms of excess potential temperature over undisturbed environment at same level) and vertical motion at one, three and five minutes. The maximum vertical velocities reach 1 m/sec after three minutes, and 2 m/sec after five (maximum horizontal indrafts attain about 60 % of these values). Maximum downdrafts are about 50 % of the maximum updrafts. Vertical velocities at 100 m (base of unstable layer) are 1 m/sec, diminishing rapidly downward.

It is interesting to note that at five minutes the

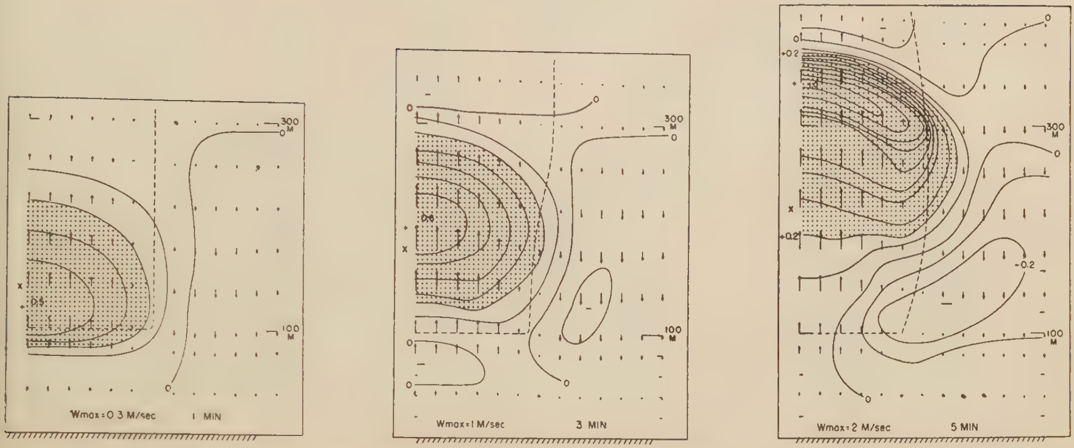

Fig. 3. Development of buoyancy and vertical motion for "up in the air" bubble. Solid lines are isopleths of buoyancy in terms of potential temperature excess $\Delta\Theta$ over the undisturbed environment at the same level. They are drawn at intervals of 0.1° C and the dotted region includes buoyancies of $\Delta\Theta \geq 0.2°$ C. The level of maximum buoyancy is denoted by the "plus" at the right. The arrows are vertical motions: in the left-hand diagram the longest one is 30 cm/sec; in the middle diagram the longest represents 1 m/sec and in the right diagram, 2 m/sec. The level of vertical velocity maximum is denoted by the cross at the right. The dashed line (except horizontal portion along initial element base at 100 m) separates up from down motions.

buoyancy has doubled its original value of $\Delta\Theta = 0.5°$ C by drawing on instability. At five minutes, 20 % of the buoyancy is due to numerical errors and 80 % is real. The center of maximum buoyancy is now concentrated in the lower part of the stable layer, which begins at 300 m, and now has passed and risen much above the center of maximum updraft. The relationship between these various centers and their motions is illustrated further in Figure 4. In Figure 4A the heights of the centers of maximum Θ (closely coincident with maximum buoyancy), maximum w, and of the vortex ring are plotted as a function of time. These reach the same level at just short of three minutes when the bubble appears to begin rising as an entity and we say that its

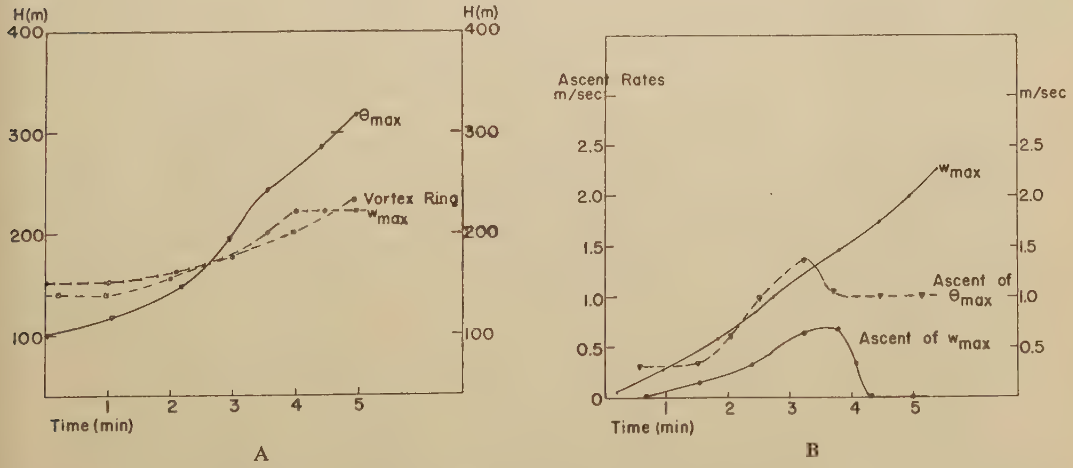

Fig. 4. Behavior of centers for "up in air" bubble. A: Vertical position as a function of time of 1) maximum potential temperature (triangles), 2) maximum vertical velocity (circles) and 3) center of vortex ring (squares). B: Ascent rates as a function of time. The solid curve labelled w_{max} is simply the value of the highest vertical velocity. The dashed curve (triangles) gives the ascent rate of the center of maximum potential temperature, while the lowest solid curve shows the rate of ascent of the center of maximum vertical velocity.

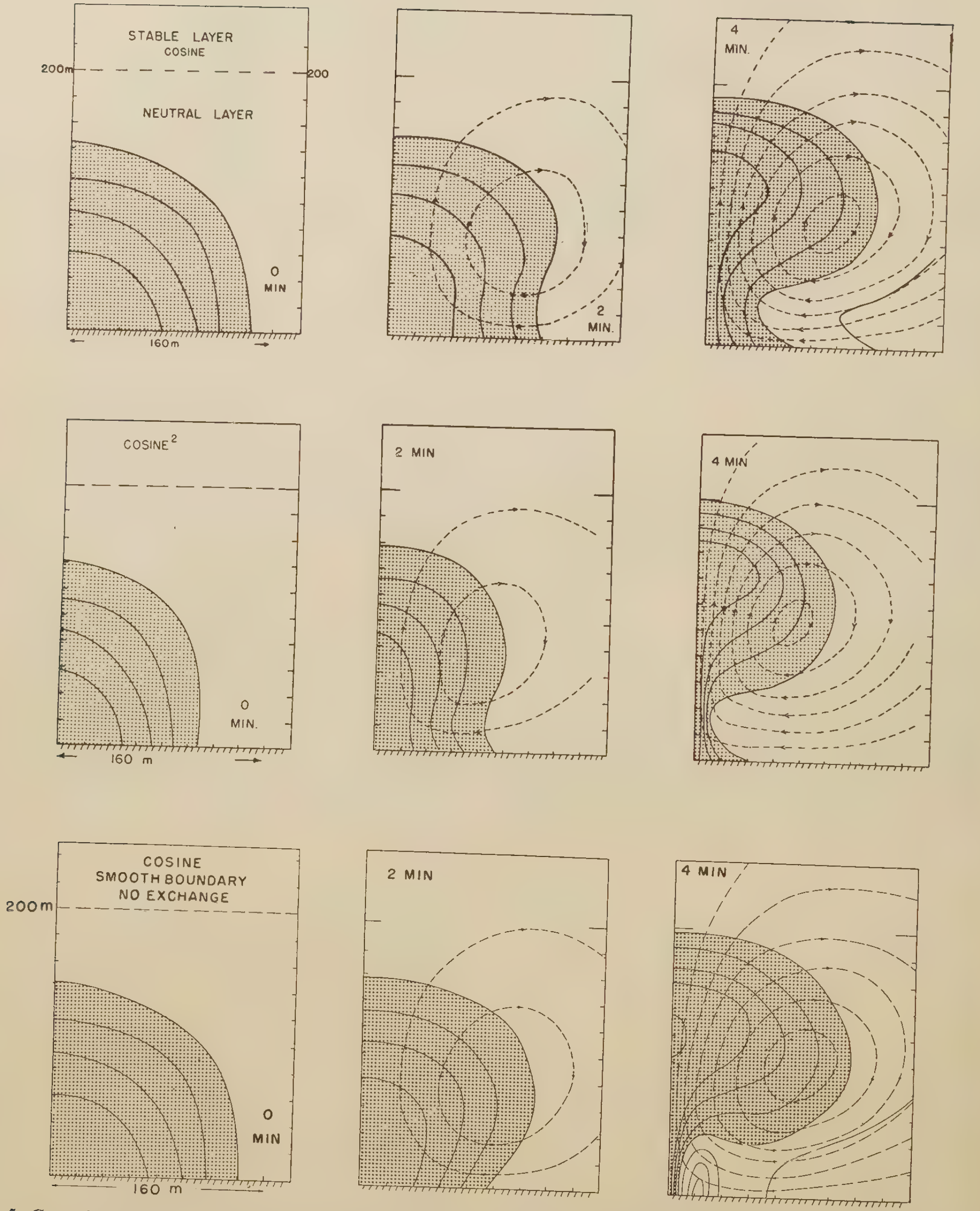
STABLE LAYER
COSINE
200m
200
NEUTRAL LAYER
0 MIN
160m
2 MIN.
4 MIN.
COSINE²
0 MIN.
160 m
2 MIN
4 MIN
COSINE
SMOOTH BOUNDARY
NO EXCHANGE
200m
0 MIN
160 m
2 MIN
4 MIN

Fig. 5. Growth of three different bubbles in neutral environment with maximum initial perturbation at the ground. (Table 1, Case 2 top row, Case 3 middle row, Case 4 bottom.) In all three, potential temperature isopleths (solid lines) are drawn for 0.1° C intervals and the shaded region includes values 0.1° C or more higher than the neutral surroundings. In the upper bubble, the initial perturbation Θ decays to zero in 160 m as cosine of x. In the middle bubble, it decays to zero at 160 m as cosine squared of x, with everything else unaltered from the first. The lowest bubble differs from the topmost only by the removal of turbulent exchange and by the doubling of lower ($z = 0$) boundary advection. Note in the latter the more rapid growth of numerical errors in temperature, evidenced by the small hump of impossibly (lower than any initial) cold values near the stem and the 0.1° C impossibly high region in bubble center.

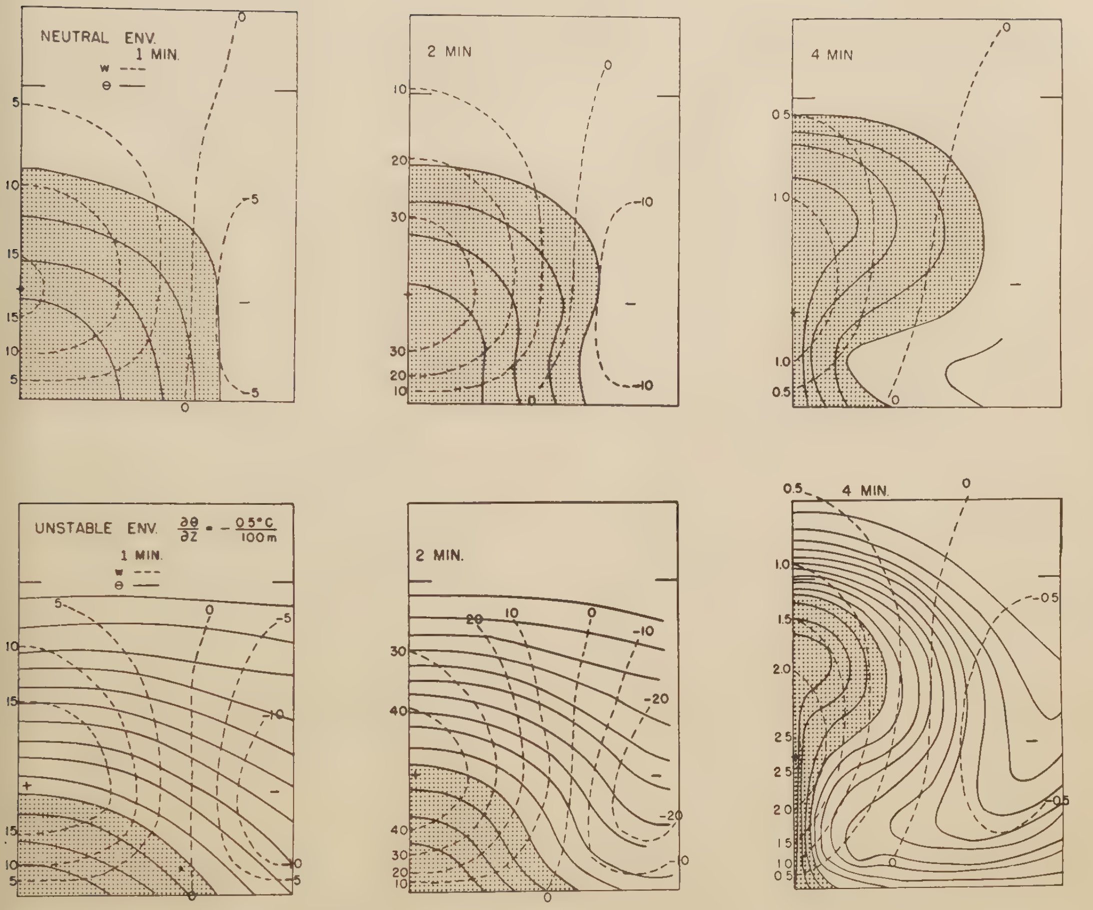

Fig. 6. Comparison of bubble growth in neutral and unstable surroundings (Table 1, Case 2 upper row; Case 5, lower). Potential temperature isopleths are solid lines, drawn for 0.1° C intervals; in the upper bubble the shaded area covers the region of Θ exceeding the neutral environment by 0.1° C or more; in the lower bubble it covers the region exceeding the surface value undisturbed Θ by 0.1° C or more. The dashed lines are vertical velocity isopleths labelled in cm/sec in the two left-hand sets of drawings and in m/sec for the right-hand set. The plus sign denotes the location of maximum w.

"organization phase" is completed. A similar organization phase was experienced by all the other bubbles studied, as will be seen.

After this time the $\Theta_{\max}$ is found increasingly above the level of $w_{\max}$, which appears to have stopped rising in elevation (despite continuously increasing updraft intensity).

Figure 4B shows rates of ascent as a function of time. The strength of the maximum updraft increases continuously and slightly exceeds 2 m/sec after five minutes, while the center of maximum w never rises faster than 70 cm/sec and ceases rising altogether after four minutes. The rate of rise of the center of maximum potential temperature has this same characteristic shape in all cases studied, accelerating to a maximum at the end of the organization phase. The rate of rise of $\Theta_{\max}$ here exceeds $w_{\max}$ by about 10% (the time step was already cut down to 10 secs before two minutes so no computational instability results). Naturally this excess of rise rate of $\Theta_{\max}$ over the maximum advective updrafts can occur only for bubbles with turbulent mixing and comes about because at the "front" or cap region the potential temperature gradients and instability are so great that Θ diffuses upward faster than it is advected, "swallowing" some of the air ahead into the bubble circulation. This effect is slightly more pronounced for the foremost Θ isopleths of the bubble cap and would presumably be even more pronounced (as it was in the Imperial College experiments of SCORER

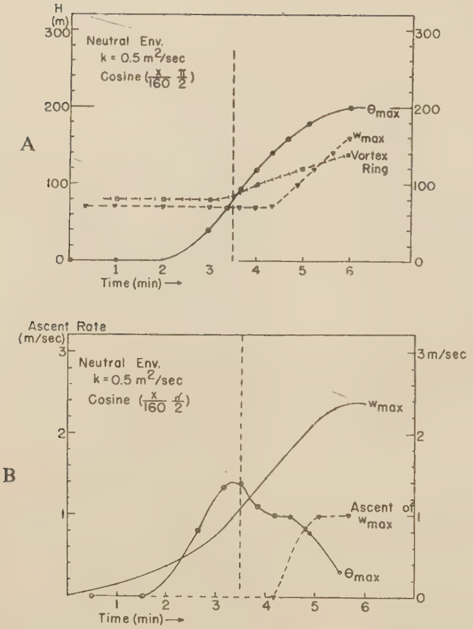

Fig. 7.

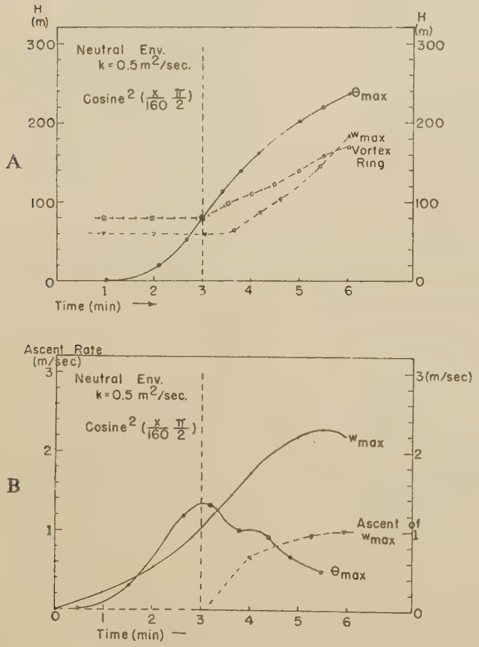

Fig. 8.

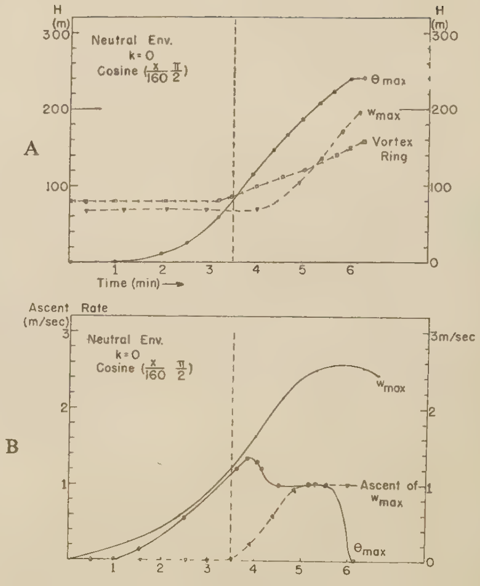

Fig. 9.

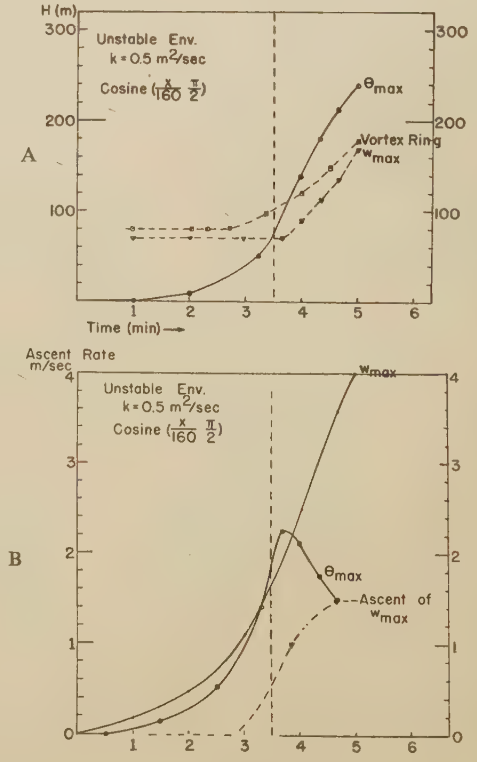

Fig. 10.

Figs. 7—10. Behavior of centers for bubbles starting at ground (Table 1, Cases 2—5 in order). Upper graphs (Figs. 7A—10A) show the heights of the centers as a function of time; the solid curve shows Θ_{max}; the dashed curve with triangles, w_{max}, and the broken curve with squares, the vertical position of the vortex ring.
Lower graphs (Figs. 7B—10B) give the ascent rates as a function of time; the solid curve marked w_{max} gives the actual value of maximum vertical velocity; the dashed curve gives the rate of ascent of its center, and the solid curve marked Θ_{max} gives the rate of rise of the center of highest potential temperature.

and Ronne, 1956) had higher values of exchange relative to buoyancy been used.

Figures 5 and 6 show the development of the remaining bubbles studied, all with the maximum initial potential temperature perturbation at the ground, while Figures 7—10 show the behavior of their various centers and the duration of the organization phase (vertical line). In all these bubbles, the end of the organization phase coincided with the penetration of the maximum vorticity into the central stem region, which could in fact have been used to define it.

In Figure 5 we compare three different bubble developments in a neutrally stratified environment (the only initial instability is contained in the perturbation itself). In the upper two everything is identical except the initial shape of the perturbation which decays to zero in 160 m as the cosine of *x* in the first and as the cosine squared in the second, thus concentrating the strong potential temperature gradient nearer the center. In the cosine squared case, the vortex ring begins closer to the center and by four minutes the bubble has a more concentrated cap, is higher, and has a narrower stem. The suggestion that its organization phase is completed more rapidly is confirmed by comparison of Figures 7 and 8 in which we see the centers reach the same level with each other 30 seconds sooner. The reason is clarified in Figure 11 comparing the early velocity fields in the two cases. In the cosine squared bubble the maximum horizontal velocity develops closer to the center. The vorticity maximum also originates closer to the center and is advected in sooner, marking an earlier close of the organization phase. The bubble stem is formed sooner. The updraft develops faster and so does a more pronounced downdraft. Initial shape (other things being equal) thus appears to play a very important role in the organization phase of a convective element and throughout at least the first four minutes of its lifetime. Since the cosine squared bubble could perhaps be regarded as effectively one of narrower width than the cosine bubble, this suggests that the duration of the organization phase depends on the ratio of bubble diameter to depth of unstable layer and that these perhaps vary directly. We plan to investigate that question further as the study continues. Figures 7—10 show that for all the remaining bubbles studied, the organization phase was the same, that is, it is not affected by variations in turbulent exchange, boundary friction, or stability. Comparing the first and third rows of Figure 5 and Figures 7 and 9, we see the effect of eliminating turbulent exchange and doubling lower boundary advection. The isotherms pinch more rapidly at the stem and numerical errors grow more rapidly but the basic features of the development are unchanged. On Figure 9 compared to Figure 7, the only difference on the "frictionless" case is a slightly augmented (less than 10%) $w_{\max}$ and a rate of rise of $\Theta_{\max}$ which no longer exceeds advection. The choice of assumptions concerning the lower boundary thus seem to affect the convection negligibly which mitigates the arbitrariness and unreality of those used. A value of *k* equal to 0.5 m²/sec serves, under these conditions, only to smooth numerical errors and to permit the bubble to grow upward slightly faster than by advection alone.

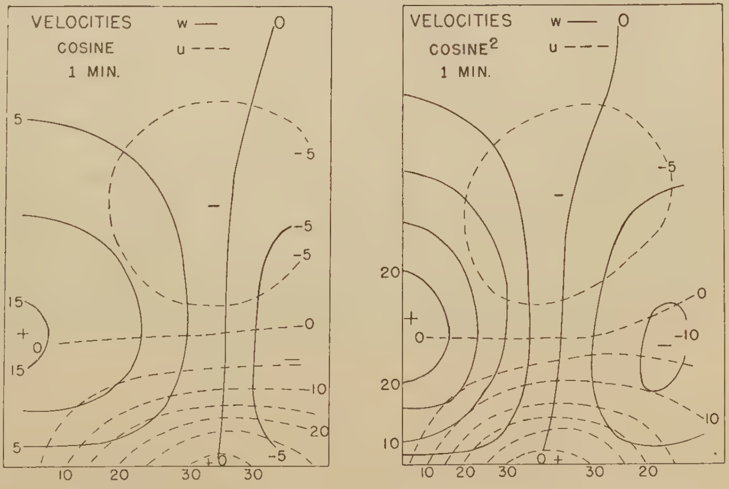

Fig. 11. Comparison of velocities in cm/sec at one minute between cosine bubble (Table 1, Case 2, left diagram) and cosine squared bubble (Table 1, Case 3, right diagram). Vertical velocity isopleths are solid, horizontal dashed. The locations of maxima and minima of each are indicated by the pluses and minuses.

Finally in Figures 6, 7, and 10 we compare the cosine bubble in an unstable and neutral environment to isolate the effect of instability. This produced markedly stronger velocities, with a $w_{\max}$ reaching 4 m/sec at 5 minutes and more rapid ascent rates of all centers, but the duration of organization time is the unaltered and the general character of curves and bubble development resemble the other cases.

VI. Conclusion

In general summary, it may be said that we have investigated the early growth of a convective element under very favorable conditions; with no wind shear or initial vorticity present, with an unstable or at worst neutral early environment, with weak or no turbulent mixing, with probably a favorable initial buoyancy distribution and a somewhat exaggerated initial buoyancy amplitude. Under these conditions it may be considered that a bubble or mushroom-like element spontaneously organizes in about three minutes, developing a rounded cap with a "front-like" concentration of isentropes and a vortex ring circulation at its edges.

More specifically we may conclude:

1) That the early life of the element has two phases: the first is an organization phase lasting a time dependent on the initial buoyancy distribution, or probably on the ratio of the depth of the convective layer to the half-width of the element; in our cases the latter was approximately one to one and the organization phase required about three minutes. During this period the element forms its cap and vortex ring and rises little. The second phase is a rising phase which begins when the vortex ring, maximum updraft and maximum buoyancy have come together at the same level.

2) Turbulent transfer coefficients corresponding to an Austausch of 5 c.g.s. units have little important affect on bubbles of these dimensions and initial buoyancy. Large differences in lower boundary advection affect the development only in minor ways.

3) While environment instability favors high velocities and permits the buoyancy to increase with time, it does not alter the organization phase.

4) Downdrafts outside the element are favored by instability and centrally concentrated isentropes initially.

5) Without condensation, or other continued heat source, these elements acquire a mushroom shape and not that of a plume, jet or column.

6) Without condensation, or other heat source, the vertical velocity maximum remains (subsequent to the organization phase) well below the cap and buoyancy maximum.

The results of these preliminary calculations suggest further directions in which we hope to carry the inquiry with this model. In the next stage envisaged, these are primarily three: First, a further investigation of the organization phase, and especially its suggested dependence upon the ratio of dimensions of convective layer to perturbation width. Second, the introduction of heat sources, either dependent upon the coordinates or upon the vertical motions themselves to simulate condensation; this would be an attempt to discover whether a more column-like "cloud" may organize if new sources of buoyancy are available, and to see whether the centers of maximum vertical motion and potential temperatures will coincide more closely if non-adiabatic heating dependent on the former is introduced.

Finally, we hope to investigate, one at a time, factors believed to be inhibitory to convection, such as wind shear, an upper layer of strong stability, and a larger exchange coefficient relative to initial buoyancy.

Acknowledgments

This work has been supported largely by the United States Office of Naval Research, with an important contribution in the early phases from the Munitalp Foundation.

The writers are deeply grateful to Dr. Bert Bolin for his help, advice, and suggestions throughout all stages of the work and to Dr. Norman Phillips who provided indispensable aid on the problem of computational stability and other phases of the numerical calculation. The original formulation of the problem was instigated and assisted by Dr. R. S. Scorer.

REFERENCES

Allen, D. N. DeG., 1954: *Relaxation methods*. McGraw-Hill. New York. Chaps. 4 and 5.

Charney, J. G., Fjørtoft, R., and von Neumann, J., 1950: Numerical integration of the barotropic vorticity equation. *Tellus*, **2**, 237—254.

Collatz, L., 1951: *Numerische Behandlung von Differentialgleichungen*. Springer-Verlag, Berlin-Göttingen-Heidelberg. Chap. III.

Malkus, J. S., 1952: Recent advances in the study of convective clouds and their interaction with the environment. *Tellus*, **4**, 71—87.

— 1954: Some results of a cumulus cloud investigation. *J. Meteor.*, **11**, 220—237.

Malkus, J. S., and Scorer, R. S., 1955: The erosion of cumulus towers. *J. Meteor.*, **12**, 43—57.

Malkus, J. S., and Stern, M. E., 1953: The flow of a stable atmosphere over a heated island. Part I. *J. Meteor.*, **10**, 30—41.

Scorer, R. S., and Ludlam, F. H., 1953: Bubble theory of penetrative convection. *Quart. J. R. Met. Soc.*, **79**, 94—103.

Scorer, R. S., and Ronne, C., 1956: Experiments with convection bubbles. *Weather*, **11**, 151—154.

Smith, R. C., 1955: Theory of air flow over a heated land mass. *Quart. J. R. Met. Soc.*, **81**, 382—395.

Stommel, H., 1947: Entrainment of air into a cumulus cloud. *J. Meteor.*, **4**, 91—94.

(Manuscript received April 8, 1958)

Contribution No. 971

ECOLOGY OF MARSH FORAMINIFERA IN POPONESSET BAY, MASSACHUSETTS

FRANCES L. PARKER AND WILLIAM D. ATHEARN

Reprinted from
Journal of Paleontology
Vol. 33, No. 2, March, 1959

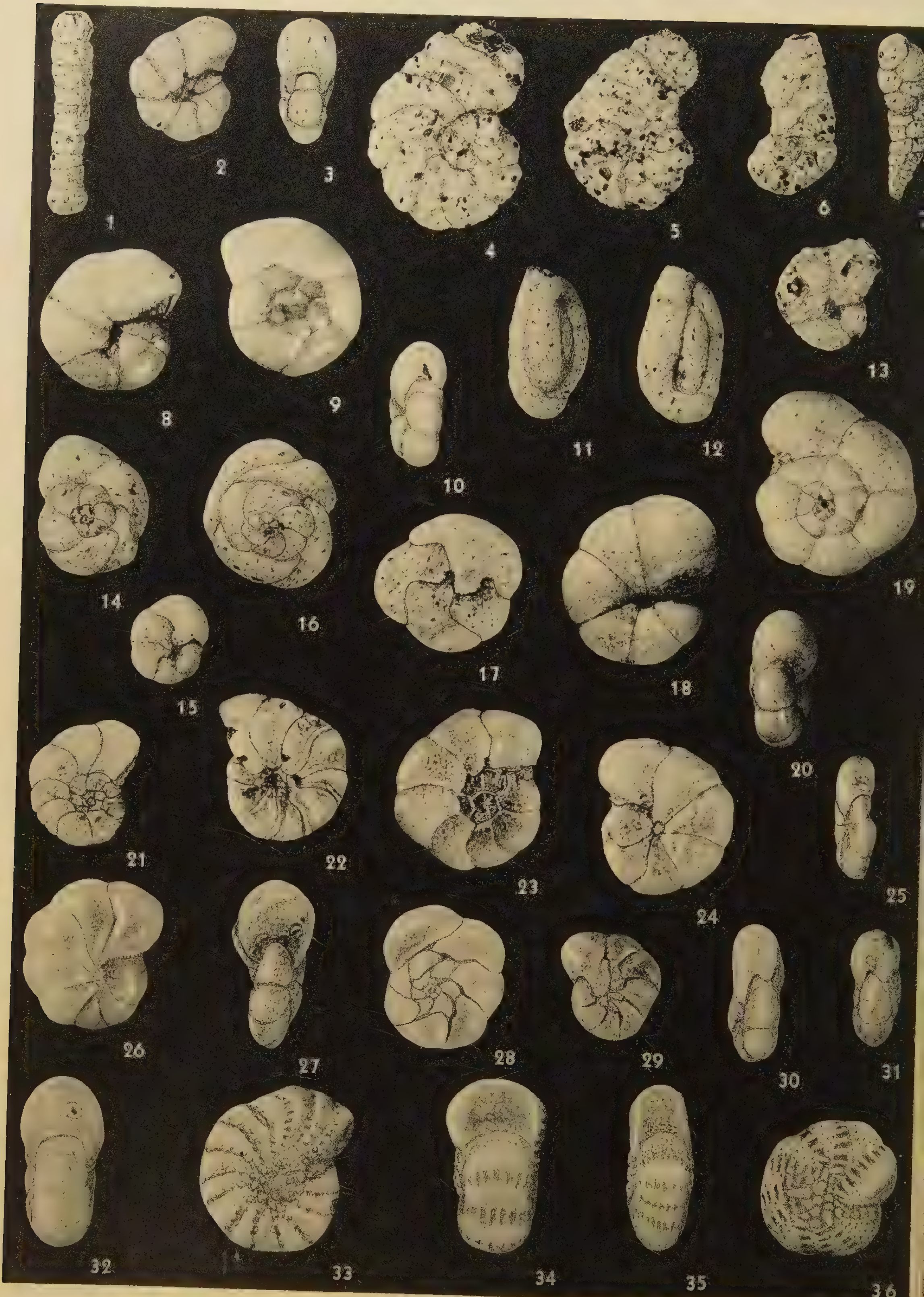
1
2
3
4
5
6
8
9
10
11
12
13
14
15
16
17
18
19
20
21
22
23
24
25
26
27
28
29
30
31
32
33
34
35
36

JOURNAL OF PALEONTOLOGY, v. 33, NO. 2, P. 333–343, PL. 50, 5 TEXT-FIGS., MARCH 1959

ECOLOGY OF MARSH FORAMINIFERA IN POPONESSET BAY, MASSACHUSETTS

FRANCES L. PARKER AND WILLIAM D. ATHEARN
Scripps Institution of Oceanography, La Jolla, Calif., and
Woods Hole Oceanographic Institution, Woods Hole, Mass.

ABSTRACT—Distributions of the species of Foraminifera (living and dead) forming the greater part of the foraminiferal faunas in marshes in Poponesset Bay, Massachusetts, have been studied. Eight stations were sampled bimonthly for one year (August, 1956 to September, 1957). The marsh environments vary from almost non-marine (with tidal influence) to near marine. *Arenoparrella mexicana*, *Haplophragmoides hancocki*, *Tiphotrocha comprimata*, and *Trochammina macrescens* decrease with increasingly marine conditions, whereas *Jadammina polystoma* and *Trochammina inflata* increase. Other species such as *Ammobaculites dilatatus*, *Ammotium salsum*, *Miliammina fusca*, and *Protelphidium tisburyense* fluctuate independently of the degree of brackish or marine conditions. Unknown factors governing micro- and macroenvironments probably play an important part in controlling distributions. Suggested factors are type of vegetation, chemical factors, pH, nutrients and food. Calcareous specimens are rapidly destroyed after death presumably due either to the ability of the living form to resist acidity or to a postulated increase in acidity immediately below the sediment surface, more probably the latter. This destruction of the tests is of importance in the interpretation of ancient marsh environments. Many species, including the calcareous ones, had their largest living populations in June or September and their smallest in December or February. There were some exceptions such as *Miliammina fusca* which showed an increase in winter. The total living populations were greatest in June and lowest in December, which may be related to maximum temperature and time of greatest reduction in temperature respectively. Multiple sampling showed that distributions at any one station were fairly uniform although nearby samples in different microenvironments in some cases vary considerably.

EXPLANATION OF PLATE 50

All illustrations were photographed and retouched by the senior author.

FIG. *1*—*Reophax* sp. Station 7. USNM 626397, ×58.
2,3—*Haplophragmoides hancocki* Cushman & McCulloch. *2*, Side view, USNM 626384; and *3*, apertural view, USNM 626385, ×58. Station 2.
4,5—*Ammobaculites dilatatus* Cushman & Bronnimann. Side views, USNM 626373, 626374, ×45. Station 2.
6,13—*Ammotium salsum* (Cushman & Bronnimann). Side views, USNM 626375, 626376, ×58. Station 8.
7—*Textularia earlandi* Parker. USNM 626398, ×58. Station 6.
8–10—*Arenoparrella mexicana* (Kornfeld). *8,9*, Side views, USNM 626377, 626378; and *10*, apertural view, USNM 626379, ×58. Station 2.
11,12—*Miliammina fusca* (Brady). Side views, USNM 626389, 626390, ×45. Station 1.
14–17—*Tiphotrocha comprimata* (Cushman & Bronnimann). *14,16*, Dorsal view, USNM 626399, 626401; and *15,16*, ventral views, USNM 626400, 626402, ×45. Station 1.
18–20—*Trochammina inflata* (Montagu). *18*, Ventral view, USNM 626404, ×45; *19*, dorsal view, USNM 626403, ×58; and *20*, edge view, USNM 626405, ×45. Station 3.
21,22,27—*Jadammina polystoma* Bartenstein & Brand. *21*, Dorsal view, USNM 626386; *22*, ventral view, USNM 626387; and *27*, edge view, USNM 626388, ×58. Station 8.
23–25—*Trochammina macrescens* Brady. *23*, Dorsal view, USNM 626406; *24*, ventral view, USNM 626407; and *25*, edge view, USNM 626408, ×45. Station 1.
26,32—*Protelphidium tisburyense* (Butcher). *26*, Side view, USNM 626391; and *32*, apertural view, USNM 626392, ×58. Station 2.
28–31—*Pseudoeponides anderseni* Warren. *28*, Dorsal view, USNM 626393; *29*, ventral view, USNM 626394; and *30,31*, edge views, USNM 626395, 626396, ×58. Station 6.
33–35—*Elphidium galvestonense* Kornfeld. *33*, Side view, USNM 626380; and *34,35*, apertural views, USNM 626381, 626382, ×45. Station 5.
36—*Elphidium gunteri* Cole. Side view, USNM 626383, ×58. Station 2.

INTRODUCTION

THE purposes of this study were: 1, to investigate the distribution of Foraminifera in marsh environments of varying salinity from almost fresh (with tidal effect) to nearly normal marine and 2, to study the seasonal numerical variation of living specimens of the various species. Eight stations along the marshy shores of Poponesset Bay from the mouth of the narrow portion of the Cotuit River to Meadow Point were sampled bimonthly from August, 1956, to September, 1957. Duplicate samples were taken occasionally to check the reliability of the samples and triplicate samples were taken at the final collection. Salinity and temperature were measured each time of sampling. This study was supported by the University of California under contract with the Office of Naval Research and by the Woods Hole Oceanographic Institution. James R. Moriarty drafted the text figures. Miss Ruth Todd kindly compared specimens of *Ammobaculites dilatatus* with the types.

This is Marine Foraminifera Laboratory Contribution no. 27, Scripps Institution of Oceanography Contribution, New Series, and Woods Hole Oceanographic Institution Contribution no. 971.

DESCRIPTION OF THE AREA

Poponesset Bay is situated on the south side of Cape Cod, Massachusetts, extending roughly from Lat. 41°35′ N to Lat. 41°37′ N and Long. 70°27′ W to Long. 70°28′ W. The upper part of the bay is charted as the Cotuit River but in this study the river is more rigorously defined as the narrow stream draining into the bay at the northern end. The collecting stations (Text-fig. 1) are situated along the eastern shore of the bay from the river mouth to a small marsh east of Meadow Point. The latter is almost directly exposed to the open water of Nantucket Sound owing to the comparatively recent opening of a large gap through the sand spit (Poponesset Beach) which formerly cut this area off from the open sound to the southeast and east. This sand spit and opening are not illustrated since no accurate survey is available.

STATIONS

Eight stations were sampled at approximately bimonthly intervals from August, 1956, to September, 1957. At various times duplicate samples were taken and, at the last collection, triplicate ones. The following is a general description of the environment of each station, including maximum and minimum temperatures and salinities encountered during the collecting period, and the foraminiferal species comprising the major part of the faunas (living plus dead). These temperature and salinity values may not necessarily reflect the extremes which occurred during this interval since the sampling times may not have coincided with them. At no time of sampling was any locality frozen solid although in February there was a thin skin of ice at stations 4, 5, and 8.

Station 1. In *Zostera* on high marsh submerged only at high tide. Located slightly above the river mouth. 1.5°C. (Feb.) to 24°C. (Aug.), salinity 0.6–21.6 °/₀₀. This maximum salinity was observed only once, salinities otherwise did not exceed 9.9 °/₀₀. *Miliammina fusca, Tiphotrocha comprimata,* and *Trochammina macrescens* comprise 91% of the fauna.

Station 2. Muddy bank at edge of *Zostera* growth, submerged at mid-tide. Located slightly below the river mouth. 4.5°C. (Dec.) to 26°C. (June), salinity 1.8–28.2 °/₀₀. *Ammotium salsum, Arenoparrella mexicana, Miliammina fusca, Protelphidium tisburyense, Tiphotrocha comprimata,* and *Trochammina macrescens* comprise 90% of the fauna.

Station 3. Zostera marsh exposed at low tide. 3°C. (Feb.) to 22°C. (Aug.), salinity 4.2–20.6 °/₀₀. *Arenoparrella mexicana, Miliammina fusca, Tiphotrocha comprimata,* and *Trochammina inflata* comprise 88% of the fauna.

Station 4. Shallow pool in *Zostera* growth about one foot above low tide level. This station was not sampled until December. 1°C. (Feb.) to 22.5°C. (Sept.), salinity 6.2–23.9 °/₀₀. *Ammotium salsum, Arenoparrella mexicana, Miliammina fusca, Protelphidium tisburyense, Tiphotrocha comprimata,* and *Trochammina macrescens* comprise 93% of the fauna.

Station 5. Shallow pool (1–4 inches deep) in high marsh behind *Zostera* growth. 1°C. (Feb.), to 32°C. (June), salinity 4.5–24.2 °/₀₀. *Ammotium salsum, Jadammina polystoma, Protelphidium tisburyense, Tiphotrocha comprimata,* and *Trochammina inflata* comprise 92% of the fauna.

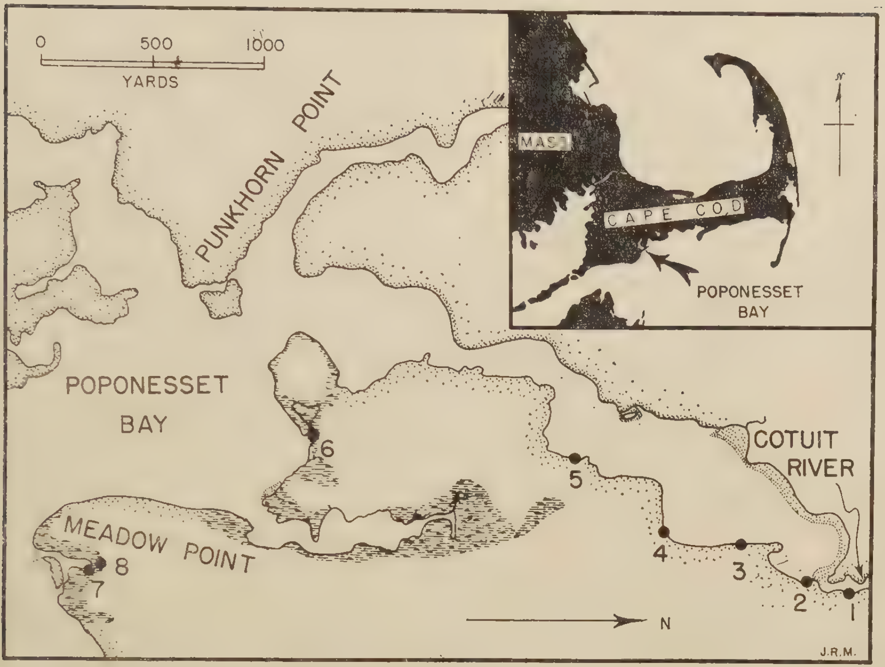

TEXT-FIG. *1*—Location of stations.

Station. 6. High *Spartina* marsh exposed except at high tide. 3.6°C. (Dec.) to 29.5°C. (June), salinity 24.8–28.2 °/₀₀. *Ammotium salsum, Jadammina polystoma, Miliammina fusca,* and *Trochammina inflata* comprise 88% of the fauna.

Station 7. High *Zostera* marsh exposed except at high tide. 0.2°C. (Feb.) to 29°C. (June), salinity 23–34.3 °/₀₀. *Ammotium salsum, Miliammina fusca,* and *Protelphidium tisburyense* comprise 90% of the fauna.

Station 8. Inner (landward) end of long, narrow high marsh in shallow pool or channel (1–6 inches deep), isolated except at high tide and not flushed by every tide. 0.2°C. (Feb.) to 30°C. (Aug., June), salinity 26.5–45.2 °/₀₀. The salinity only reached this high value at one time of sampling, otherwise the maximum was 35.8 °/₀₀. *Ammotium salsum, Jadammina polystoma,* and *Trochammina inflata* comprise 88% of the fauna.

In most places the highest temperatures were registered in June, the lowest in February. The salinity changes did not follow any regular seasonal pattern probably due to the many factors involved such as tidal influence, rainfall, seepage, evaporation, etc. Station 5, which shows a lower salinity minimum than station 4 nearer the river, may be affected by fresh water seepage from the high bank lying behind it. The high salinity registered at station 8 may be due to evaporation since the locality is apparently not reached by all high tides.

METHODS OF STUDY

The samples were collected by pushing a piece of plastic tubing (internal diameter 3.3 cm.) into the sediment. A constant volume sample one centimeter thick was taken from the upper part of the core using the method described by Walton (1955). The fluid condition of the mud in many cases made it difficult to be certain that equal volume samples were obtained by this method. The area of sediment surface collected, however, was constant. The samples were preserved with buffered formalin and a small quantity of sodium bicarbonate was added, since it has been found that buffered formalin and sea water become increasingly acid with time. Occasional samples giving an acid reaction were discarded before laboratory study. The samples were washed through a

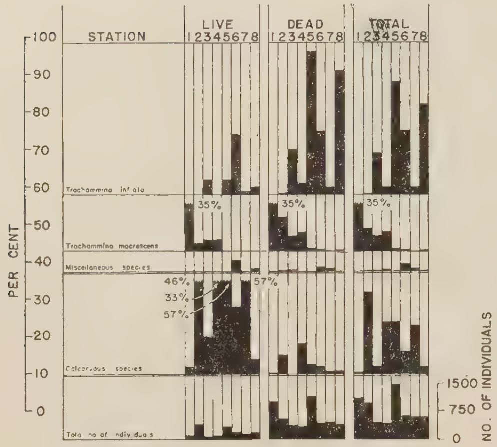

Text-fig. *2*—Average frequency distributions (% of living, dead, and total) of foraminiferal species at each station.

sieve (average openings 0.062 mm.), stained with rose Bengal and examined while wet, which is necessary since many specimens of marsh species are destroyed or badly distorted upon drying. It was found that much of the organic detritus could be eliminated by using a pick and then decanting several times.

To determine distributional patterns at each station (Text-figs. 2–4) all samples, regardless of season, were averaged. Multiple samples at any one station were averaged first. Each species is plotted in percents of living, dead, and total populations. Occurrences of less than 0.1% are omitted so that a species which may occur very rarely appears to be absent. Some of these rare occurrences are mentioned in the "systematic descriptions."

The data for all stations were averaged to determine the seasonal distributions of the living species. These are given (Text-fig. 5) in numbers of specimens since the area of sampling is constant and it is assumed that the living population is sampled *in toto.*

DISTRIBUTION OF SPECIES

Environmental.—By averaging the data for all seasonal samples taken at each station it is believed that any irregularities of collection are smoothed out and a general picture at any locality obtained. The diagrams (Text-figs. 2–4) include species distributions of dead and total populations, which are o the most interest to the paleontologist, a well as the living populations.

The following generalizations can be mad on the distributional patterns, when pro gressing from the least to the most nearl marine conditions. *Arenoparrella mexicana Haplophragmoides hancocki, Tiphotroch comprimata,* and *Trochammina macrescens* which form relatively high percentages o the populations at the lower salinity sta tions, are much rarer at the more marin stations. On the other hand, *Jadammin polystoma, Reophax* sp. and *Trochammina in flata,* which are absent or very rare at th low salinity stations, are abundant at th more marine ones. Whether or not thes

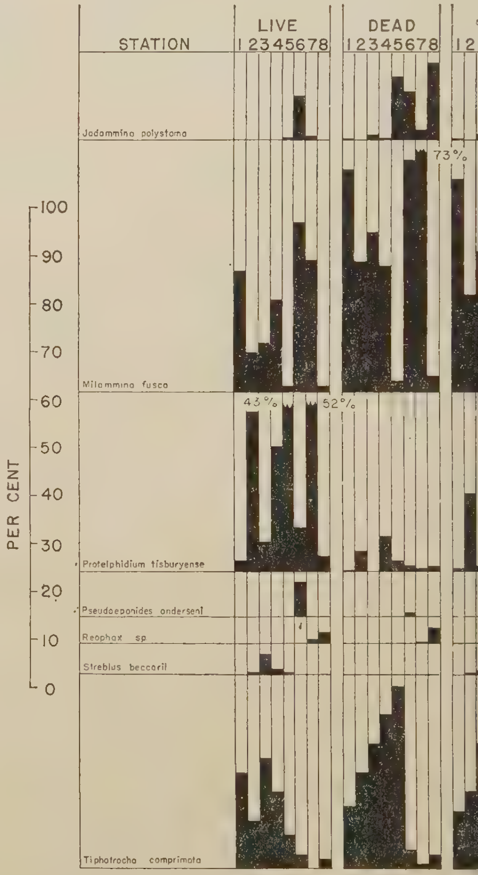

Text-fig. *3*—Average frequency distribution living, dead, and total) of foraminiferal sp each station.

differences in distributions are related to differences in salinity conditions is an open question. Other factors may be involved such as changes in vegetation, differences in pH at the sediment surfaces under varying saline conditions, and chemical nutrients or food introduced by the fresh water.

Ammobaculites dilatatus, *Ammotium salsum*, *Elphidium galvestonense*, *E. gunteri*, *Miliammina fusca*, and *Protelphidium tisburyense* appear to fluctuate, for the most part, independently of the salinity or related factors. *Ammotium salsum*, common at most stations, is very abundant at station 8. Perhaps this is due to its apparently high tolerance of varying conditions. It will be noted that it forms a much higher percent of the living population than of the dead population, whereas *Jadammina polystoma* and *Trochammin inflata*, which are fairly abundant in the dead population, form a very small part of the living one. This leads to the speculation that conditions adverse to the latter two species have occurred and the more tolerant form has flourished. The high salinity of 45.2 °/₀₀ found in April is a clue to what one of these adverse conditions may be. *Miliammina fusca*, which occurs at very low frequencies at stations 5 and 8, apparently prefers an environment which is periodically exposed because of tidal action. The fluctuations of *Ammobaculites dilatatus*, the two species of *Elphidium*, and *Protelphidium tisburyense* are not easily explained by the known characteristics of the

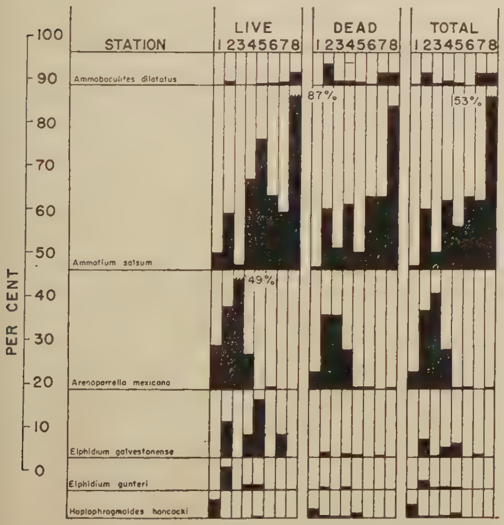

TEXT-FIG. 4—Average frequency distributions (% of living, dead, and total) of foraminiferal species at each station.

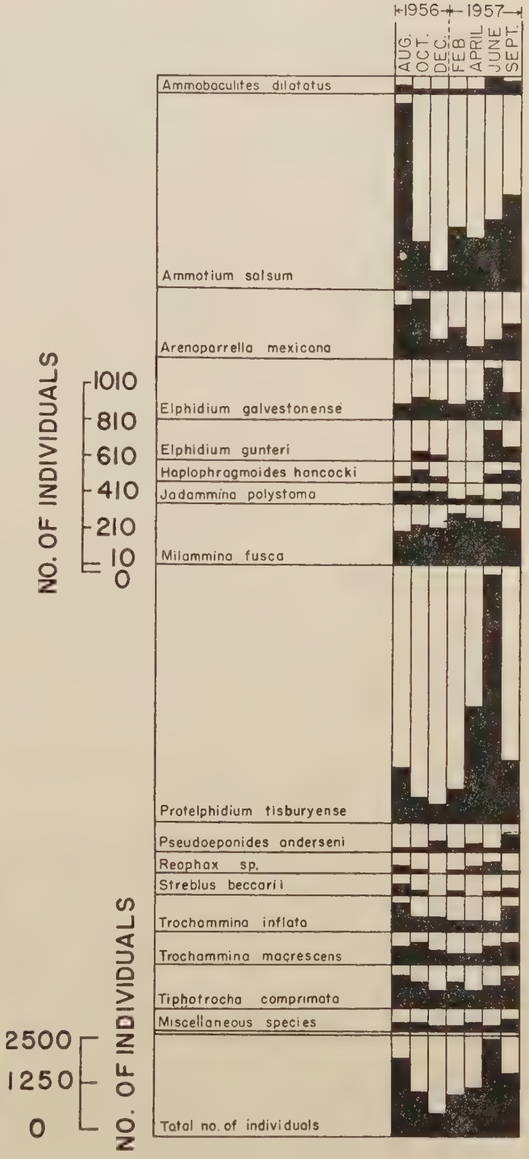

TEXT-FIG. 5—Seasonal frequency distributions (actual number of living specimens) of foraminiferal species at all stations. (Note change of scale after the first 10 individuals.)

environments. In general, the three calcarious species follow the same pattern, being present or most common at stations 2, 4, 5, and 7. Thus, they are adapted to both non-marine and near marine conditions and to environments which may or may not be partly exposed due to tidal action.

Of the remaining two species illustrated in the bar diagrams, *Pseudoeponides anderseni* is confined to station 6 (a few dead specimens at station 4) and is discussed more fully in the systematic section; *Streblus beccarii* is too rare in the area for a reliable analysis of its preferences. It is most common at station 3 and was not found at stations 1 and 6–8 suggesting that it prefers intermediate conditions between non-marine and marine. It is possible, however, that marsh environments are not favorable for this species and its distribution is mainly confined to other environments

In addition, most species appear to favor certain microenvironments. This is discussed further in the section on multiple sampling. The species forming the major part of the faunas at each station are listed in the station descriptions.

Calcareous species.—A study of the bar diagrams (Text-figs. 2–4) shows that the calcareous species are represented for the most part by living specimens. Very few dead ones were observed. This leads to the inference that below the sediment surface, or perhaps even at the sediment-water interface, the pH is sufficiently low to cause the dissolution of the tests. If this condition exists in the "living environment" of the species they must have some mechanism to resist the acidity. Since this implies the expenditure of considerable energy on the part of the organism, it seems more probable that the increase in acidity occurs immediately below the sediment surface, probably due to decaying vegetation, and that it is here that the solution of the tests occurs. It should be remembered that the samples represent only the upper centimeter of sediment so that this supposed acidity increase must occur very near the surface. No reliable measurements have been taken in marsh sediments to show this postulated change in pH across the sediment-water interface. Stewart (1956) found pH values of 7.45 and 6.79 at depths of 15–20 cm. and 23–28 cm. respectively in two marsh cores from San Miguel Lagoon in Baja California. Similar or even lower values have also been observed by others in marsh sediments. Such acidity is more than sufficient to dissolve the calcium carbonate tests.

This rapid solution of the calcareous tests in marsh sediments means that ancient marsh sediments in the sedimentary column may not contain the calcareous species. This must be taken into consideration in interpreting ancient environments by comparison with those of the present day.

Seasonal.—The bar diagram (Text-fig. 5) illustrates the occurrence of living specimens of each species for each season. Some species show a decided increase at certain seasons which suggests that reproduction increases, or mainly occurs, at such times. Examples of this are *Ammotium salsum* (August), *Elphidium galvestonense* (June, September), and *Protelphidium tisburyense* (June). The peak of the standing crop may, of course, have occurred before or after the month where it appears but must have been later than the previous collecting date and before the following one.

Other species such as *Jadammina polystoma*, *Tiphotrocha comprimata*, and *Trochammina macrescens* apparently maintain a fairly steady production, although showing a slight decrease in the winter months. *Miliammina fusca* shows a slight increase in winter. The standing crops taken as a whole are largest in June and lowest in December. An interesting correlation can be made with the temperatures obtaining at these seasons. If the temperatures at the various stations are averaged for each season the results are as follows: August (1956) 24.5°C., October 17.9°C., December 4.9°C., February (1957) 1.6°C., April 17.7°C., June 26.3°C., and September 21.9°C. Thus, during this particular time interval, the standing crop was highest at the time of highest temperature and lowest following the greatest *fall* in temperature, rather than at the time of minimum temperature. Laboratory studies by Myers (1935) and Bradshaw (1955) show that reproduction in certain species increases at higher temperatures and so it may be inferred that the increased standing crop found in summer is due to increased production at that time.

Multiple sampling.—At the final collecting period (September, 1957) triplicate samples were taken at each station, usually within about six inches of each other. This was done to check the reliability of the sampling. The results were very reassuring although occasional discrepancies occurred, usually in the frequency of living specimens of a single species. The total number of living specimens, however, was surprisingly uniform, the larger fluctuations occurring in the numbers of dead specimens. This strengthens the validity of the assumption that the living populations were sampled *in toto.*

A duplicate sample taken near station 5 in December apparently represents a different microenvironment from that of station 5 itself. Unlike the other samples from that station, which were taken in a shallow pool, it was taken from sediment in the *Zostera* growth. The fauna differs in the much larger population of living *Ammotium salsum*, *Haplophragmoides hancocki*, *Miliammina fusca* (previously mentioned as apparently preferring an environment partially exposed during the tidal cycle), and *Trochammina inflata* and the smaller populations of living *Elphidium galvestonense* and *Protelphidium tisburyense.* The environmental factors involved, aside from the partial exposure, may be differences in salinity and other chemical factors (note the unusually low salinity registered at times in the pool at station 5), food supply, competition of rival organisms, etc. A detailed study should be made to define the factors affecting such microenvironmental differences. This would probably involve, in addition to measurements of the physical characteristics, a study of the vegetation and organisms found in the various communities. Bacterial activity is probably of great importance. This particular example also emphasizes the danger of drawing conclusions from isolated samples.

SYSTEMATIC DESCRIPTIONS

Sixteen species which comprise most of the foraminiferal fauna in the area are discussed, together with a brief résumé of the distribution pattern. It should be realized that where the largest living population of any species is said to occur at any given collection it may actually have occurred earlier or later but not as early as the preceding collection or as late as the following one.

In addition, there are a few species (included with "miscellaneous species" in Text-figs. 4, 5) which are worth mentioning. One is a very small, smooth, thin-shelled *Miliolinella* which occurs rarely at stations 3–5 and somewhat more commonly at stations 6 and 8. Like the other calcareous species, most specimens were living. Members of the "*Trochammina squamata*" Parker and Jones group occurred rarely. Occasional specimens of *Saccodendron* were observed in most samples. Thecamoebina were observed at station 1.

The figured specimens have been deposited at the U. S. National Museum, Washington, D. C.

Order FORAMINIFERA
Family REOPHACIDAE
REOPHAX sp.
Pl. 50, fig. 1

This species appears to be new but due to its fragility most of the specimens found were broken. For this reason it is left unnamed until a good suite of material can be obtained. The figured specimen, one of the few unbroken forms, has ten chambers including a relatively large proloculus. The cross section is circular, as is the aperture. The sutures are very slightly depressed and, since the chambers do not increase in size as added, the test is almost straight sided with a bulging proloculus. Length of figured specimen 0.58 mm.

Distribution.—Very rare at many stations but reaches frequencies greater than 0.1% only at stations 7 and 8 (up to 2% of total at station 8). The largest living population appeared to be in June but there were too few living specimens for a reliable statement.

Family LITUOLIDAE
HAPLOPHRAGMOIDES HANCOCKI Cushman & McCulloch
Pl. 50, figs. 2,3

Haplophragmoides hancocki CUSHMAN & MCCULLOCH, 1939, Allan Hancock Pacific Expeds., v. 6, no. 1, p. 79, pl. 6, figs. 5,6.

This species was described from a sample collected from off the wharf at Ketchikan, Alaska, in which numerous representatives of the Thecamoebina also were found, showing that there must have been contamination by river forms. Reported occurrences farther south by Cushman & McCulloch should be viewed with some doubt since this species is probably not a truly marine form.

Distribution.—At stations 1–5, most commonly at station 1 (3% of total). The largest living populations were found in September and October, but so few living specimens occurred that this may not be a reliable observation.

AMMOTIUM SALSUM (Cushman & Bronnimann)

Pl. 50, figs. 6,13

Ammobaculites salsus CUSHMAN & BRONNIMANN, 1948, Cushman Lab. Foram. Research, Contr., v. 24, p. 16, pl. 3, figs. 7–9.

Ammoscalaria fluvialis PARKER, 1952, Mus. Comp. Zoology, Bull., v. 106, no. 10, p. 444, pl. 1, figs. 24,25.

The specimens are slightly thicker than the types from Trinidad. Parker's (1952) observations that the septa are like those of the genus *Ammoscalaria* Höglund (straight, chitinous) are now believed to be erroneous. Further study shows that although very thin when viewed in clarifying oil, the septa are not straight but curved as in the genus *Ammotium* Loeblich & Tappan.

Distribution.—At all stations, most commonly stations 2, 4–8 (up to 17% of total except at station 8, 53%). The largest living population was found in August, the lowest in December.

AMMOBACULITES DILATATUS Cushman & Bronnimann

Pl. 50, figs. 4,5

Ammobaculites dilatatus CUSHMAN & BRONNIMANN, 1948, Cushman Lab. Foram. Research, Contr. v. 24, p. 39, pl. 7, figs. 10,11.

Specimens were compared with the types by Miss Ruth Todd. She reports (personal communication) that the Poponesset specimens are identical with at least one paratype but otherwise are more inflated. This inflation makes the umbilicus more depressed, the sutures more incised, the chambers more distinct, and the periphery more lobulated. The difference, however, is essentially a minor one and does not seem sufficient for specific or subspecific differentiation.

Distribution.—At all stations, most commonly stations 2, 7, and 8 (3% of total). The largest living population was found in June, the lowest in April. Few living specimens were observed at any time at station 7 which is strange in view of the relatively large dead populations found there. These stations, although subject to a high variation of salinity, are all out of water during part of the tidal cycle.

ARENOPARRELLA MEXICANA (Kornfeld)

Pl. 50, figs 8–10

Trochammina inflata (MONTAGU) var. *mexicana* KORNFELD, 1931, Dept. Geology Stanford Univ., Contr., v. 1, no. 3, p. 86, pl. 13, fig. 5.

The specimens are typical.

Distribution.—At all stations except station 7, most common at stations 1–4 (up to 22% of total). This species apparently prefers the less marine localities. The largest living population was found in October, although the numbers for August were almost as high. There was a considerable increase between December and February after which the numbers dropped off again.

Family TEXTULARIIDAE

TEXTULARIA EARLANDI Parker

Pl. 50, fig. 7

Textularia elegans LACROIX, 1932 (*non Plecanium elegans* HANTKEN, 1868), Instit. Ocean., Monaco, Bull., no. 591, p. 8, text-figs. 4–6.

Textularia tenuissima EARLAND, 1933 (*non. T. tenuissima* HÄUSLER, 1881), Discovery Repts., v. 7, p. 95, pl. 3, figs. 21–30.

Textularia earlandi PARKER, 1952, Mus. Comp. Zoology, Bull., v. 106, no. 10, p. 458 (footnote).

This species is included under "miscellaneous species" in the bar diagrams (Text-figs. 4,5). Its occurrence is of interest since it is found only at stations 6–8, indicating that near marine conditions may be required. No living specimens were found except in September and October.

Family RZEHAKINIDAE

MILIAMMINA FUSCA (Brady)

Pl. 50, figs. 11,12

Quinqueloculina fusca BRADY, 1870, *in* BRADY, G. S., & ROBERTSON, Ann. Mag. Nat. Hist., s. 4, v. 6, p. 286, pl. 11, figs. 2a–c, 3.

There is some variation in the smoothness of the test. Smooth-walled individuals, however, are rare.

Distribution.—An ubiquitous marsh form, occurring at all stations at very high frequencies (up to 62% of total) except at stations 5 and 8 (2%). The latter stations are in shallow pools which are never exposed during the tidal cycle suggesting that the species prefers partially exposed environments. The largest living population was found in February, the smallest in August. The production is presumably fairly high throughout the year to account for the large number of living specimens always present.

Family TROCHAMMINIDAE

TIPHOTROCHA COMPRIMATA (Cushman & Bronnimann)

Pl. 50, figs. 14–17

Trochammina comprimata CUSHMAN & BRONNIMANN, 1948, Cushman Lab. Foram. Research Contr., v. 24, p. 41, pl. 8, figs. 1–3.

Adult specimens have very irregular chambers (figs. 16,17) but the juvenile stages are regular (figs. 14,15).

Distribution.—At all stations, most abundantly at stations 1–5 (up to 31% of total) suggesting that marine conditions are adverse. The largest living populations were found in August and September.

TROCHAMMINA INFLATA (Montagu)

Pl. 50, figs. 18–20

Nautilus inflatus MONTAGU, 1808, Test. Brit., Supp., p. 81, fig. 3.

Distribution.—At all stations except station 1. The highest frequencies are at stations 3, 5, 6, and 8 (up to 30% of total). The largest living population was found in August, the smallest in February, although in April and June living populations were almost as low.

TROCHAMMINA MACRESCENS Brady

Pl. 50, figs. 23–25

Trochammina inflata (MONTAGU) var. *macrescens* BRADY, 1870, *in* BRADY, G. S., & ROBERTSON, Ann. Mag. Nat. Hist., s. 4, v. 6, p. 290, pl. 11, figs. 5a–c.

The possible relationship of this species with *Jadammina polystoma* is discussed under the latter.

Distribution.—Occurs at all stations except station 7. The highest frequencies are found at stations 1–4 (up to 35% of total at station 1) suggesting that this species prefers a non-marine environment. The largest living populations were found from August to October.

JADAMMINA POLYSTOMA Bartenstein & Brand

Pl. 50, figs. 21,22,27

Jadammina polystoma BARTENSTEIN & BRAND, 1938, Senckenbergiana, Band 20, n. 5, p. 381, text-figs. 1–3.

It is possible that this species and *Trochammina macrescens* are related or even identical. *J. polystoma* differs in the less massive test, which is usually more compressed, and in the presence of supplementary apertures on the apertural face. Boltovskoy (1958) postulates that the presence of supplementary apertures on the apertural face of *Protelphidium tisburyense* is a modification due to environmental conditions and does not imply specific difference from specimens without these apertures. It is possible that in a similar manner *J. polystoma* may be a modified form of *T. macrescens* although when the two occur together the adults are easily distinguished. This hypothesis may be tested eventually by culturing in the laboratory.

Distribution.—Rare at stations 1, 3, and 4; somewhat more common at station 7; very common at stations 5, 6, and 8 (up to 11% of total). The species apparently prefers the more marine environments. The largest living populations were found from September to December, but since the number of living specimens was very small even at those times this may not be a reliable observation.

Family ROTALIIDAE

PSEUDOEPONIDES ANDERSENI Warren

Pl. 50, figs. 28–31

Pseudoeponides anderseni WARREN, 1957, Cushman Found. Foram Research, Contr., v. 8, p. 39, pl. 4, figs. 12–15.

Valvulineria sp. PHLEGER & WALTON, 1950, Am. Jour. Science, v. 248, p. 285, pl. 2, fig. 22a,b.

Hofker (1958) suggests that the genus *Pseudoeponides* Uchio is closely related to the genus *Streblus* Fischer. In the Poponesset Bay samples care had to be taken not to mistake specimens of this species for some of the variant forms of *Streblus beccarii*. Especially in wet samples, the dorsal openings are not always immediately observed. *Pseudoeponides anderseni* is also distinguishable by the prolongation of the final chamber which forms a lobe over the umbilical region. This resemblance is mentioned here because it seems possible, in view of the few reported occurrences of *E. anderseni*, that it has not been differentiated from *Streblus beccarii* by some workers.

Distribution.—At station 6 (2% of total). A few dead specimens were observed at station 4 (too few to be included in Text-fig. 3). The species seems to prefer environments having near-marine characteristics (minimum salinity at station 6 was 24.8 °/₀₀). Phleger and Walton (1950) found it only in the high marsh at Barnstable, Mass. (minimum salinity 25 °/₀₀). What the other requirements are which confine this species to such a limited occurrence are not known.

STREBLUS BECCARII (Linné)

Nautilus beccarii LINNÉ, 1758, Test. Brit., Supp., p. 710.

Specimens of this species are usually very small, although at station 1 large specimens were found previous to the current collecting period. In general, the marshes in this area do not seem favorable for the development of the species.

Distribution—At stations 2–5 (up to 0.7% of total). The living population was largest in August. Few living specimens were found except in August and September.

Family ELPHIDIIDAE

PROTELPHIDIUM TISBURYENSE (Butcher)

Pl. 50, figs. 26,32

Nonion tisburyensis BUTCHER, 1948, Cushman Lab. Foram. Research, Contr., v. 24, p. 22, text-figs. 1–3.

This species has a radiate wall structure (personal communication, M. N. Bramlette) and sometimes shows rudimentary retral processes. It is referred to *Protelphidium* because of its affinity with many species referrable to that genus. *Protelphidium* is placed in the family Elphidiidae, although it was originally included with the Nonionidae (Haynes, 1956, p. 86), because the structure of the wall appears to be a fundamental character of more importance in the classification of family groups than such morphological characters as sutural pores or retral processes. As pointed out by Boltovskoy (1958, p. 18) specimens sometimes occur with supplementary apertures on the apertural face, although in Poponesset Bay such specimens are rare and none was observed with more than one such aperture. In counting, however, not every specimen was closely examined for this feature.

Distribution.—At all stations, most commonly stations 2, 4, 5, and 7 (up to 16). It appears to be less adapted to extreme salinities (and/or accompanying factors) being less common at stations 1 and 8. The largest living population was in June, the smallest in December.

ELPHIDIUM GALVESTONENSE Kornfeld

Pl. 50, figs. 33–35

Elphidium gunteri COLE var. *galvestonensis* KORNFELD, 1931 (part), Dept. Geology Stanford Univ., Contr., v. 1, no. 3, p. 87, pl. 15, fig. 1 (not figs. 2,3).

Elphidium galvestonense KORNFELD, PARKER, PHLEGER & PEIRSON, 1953, Cushman Found. Foram. Research, Special Pub. 2, p. 7, pl. 3, figs. 15,16.

The specimens are very variable in the amount of inflation of the chambers. In edge view the umbo often appears to be depressed (fig. 34) rather than protruding as in the typical form. Specimens of other species of *Elphidium* may have been included occasionally in the population counts of this species.

Distribution.—At stations 2, 3–5, and 7; most commonly at stations 2, 4, and 5 (up to 4% of total). The largest living population was in June, the smallest in August and February.

ELPHIDIUM GUNTERI Cole

Pl. 50, fig. 36

Elphidium gunteri COLE, 1931, Florida State Geol. Survey, Bull. 6, p. 34, pl. 4, figs. 9,10; PARKER, PHLEGER & PEIRSON, 1953, Cushman Found. Foram. Research, Special Pub. 2, p. 8, pl. 3, figs. 18,19.

The specimens are usually very small although occasionally larger ones (up to 0.47 mm.) occur. Most of them have about ten chambers in the final whorl instead of 14. In other respects they are typical.

Distribution.—At stations 2–5; most commonly at station 2 (2% of total). The largest living population was in June, with few or no living specimens observed during the rest of the year.

REFERENCES

Boltovskoy, Esteban, 1958, The foraminiferal fauna of the Rio de la Plata and its relation to the Caribbean area: Cushman Found. Foram. Research, Contr., v. 9, p. 17–21, pl. 6.

Bradshaw, J. S., 1955, Preliminary laboratory experiments on ecology of foraminiferal populations: Micropaleontology, v. 1, p. 351–358.

Haynes, John, 1956, Certain smaller British Paleocene Foraminifera, Part I: Cushman Found. Foram. Research, Contr., v. 7, p. 79–101, pls. 16–18.

Hofker, Jan, 1958, The taxonomic position of the genus *Pseudoponides* Uchio, 1950: Cushman Found. Foram. Research, Contr., v. 9, p. 46–48.

Myers, E. H., 1935, The life history of *Patellina corrugata* Williamson, a foraminifer: Scripps Instit. Oceanography, Univ. California, Tech. ser., v. 3, no. 15, p. 355–392, pls. 10–16.

Parker, F. L., 1952, Foraminiferal distribution in the Long Island Sound-Buzzards Bay area: Mus. Comp. Zoology, Bull., v. 106, no. 10, p. 428–473, pls. 1–5.

Phleger, F. B. & Walton, W. R., 1950, Ecology of marsh and bay Foraminifera, Barnstable, Mass.: Am. Jour. Science, v. 248, p. 274–294, pls. 1,2.

Stewart, H. B., Jr., 1956, Sediments and the environments of deposition in a coastal lagoon: Doctoral Thesis, Univ. of California, Los Angeles, 355 p.

Walton, W. R., 1955, Ecology of living benthonic Foraminifera, Todos Santos Bay, Baja California: Jour. Paleontology, v. 29, p. 952–1018, pls. 99–104.

Contribution No. 973

BULLETIN OF THE GEOLOGICAL SOCIETY OF AMERICA
VOL. 70, PP. 437-466, 13 FIGS., 2 PLS. APRIL 1959

GEOPHYSICAL INVESTIGATION OF THE CONTINENTAL MARGIN BETWEEN CAPE HENRY, VIRGINIA, AND JACKSONVILLE, FLORIDA

By J. B. Hersey, Elizabeth T. Bunce, R. F. Wyrick, and F. T. Dietz

Abstract

Forty seismic-refraction and reflection profiles on the eastern continental shelf and adjacent deep-water areas of the Atlantic Ocean, from 29°39′ to 36°30′ N. Lat. and 73°30′ to 81°10′ W. Long. trace the transition from deep-oceanic to continental-type structures. The transitional area divides naturally into three parts: the continental shelf, the Blake Plateau, and the adjoining deep-water area.

The results on the continental shelf are correlated with adjacent continental geology. The deepest horizon traced along the shelf is interpreted as granitic basement, which has compressional velocities of 5.82–6.1 km/sec. At the southern extremity it is at a dept of 6 km, shoals to 0.86 km near Cape Fear, and deepens north of Cape Hatteras to more than 3 km. North of Charleston, South Carolina, there is excellent depth correlation with granitic basement in coastal wells; to the south all deep wells are inland. Age correlations are based on well data near the coast, which indicate to us that most of the observed section is Cretaceous.

On the Blake Plateau, several layers (1.83–4.5 km/sec.) are interpreted as sedimentary. A 5.5-km/sec. layer is found only south of a line from 30°30′N., 78°W. to Cape Canaveral. Velocities higher than 5.5 km/sec. have been measured on six profiles on the Blake Plateau. The 5.5-km/sec. layer and a 6.2-km/sec. layer appear to form a positive feature to the south of the above-mentioned line. Higher velocities, 8.0 km/sec. and 7.28 and 7.3 km/sec., which are probably not the same horizon, are found at markedly different depths. Possibly these represent the M layer and ultrabasic material, depending on relations not now known.

The deep-water area is a continental slope and rise modified by the Blake Plateau and by a ridge trending southeastward from Cape Fear and deepening from about the 1500-fathom contour to more than 2000 fathoms (3657 m). The ridge is underlain by thick low-velocity layers (1.83–2.96 km/sec.), interpreted as sediments, and higher-velocity layers which form a distinct linear structure having the same general trend as the ridge. At its northwestern end this trend terminates against a thick lower-velocity section interpreted as a sediment-filled trough. South of the ridge profiles are similar to those of the ocean basins. Excellent seismic-refraction evidence of faulting indicates subsidence of the ridge relative to its surroundings. A hypothesis interprets the ridge as a former chain of islands and reefs on a structural trend colinear with the Cape Fear Arch.

The structural pattern formed by the Piedmont crystallines and the Peninsular Arch of Florida and the Cape Fear Arch and the ridge resembles that formed by the Japanese archipelago, the Ryukyus, and the Bonin ridge. The pattern of the trough of the Blake Plateau and the deep-water area is somewhat similar to such modern features as Exuma Sound and the Tongue of the Ocean in the Bahamas. Such comparisons should not be regarded as strictly homologous but are suggested as possibly reflecting similarities in deep-lying tectonic activity. Similarly it would seem fruitful to consider similarities of deep structure beneath isolated seamounts, chains of seamounts, submerged ridges, island arcs, and mature mountain ranges.

CONTENTS

TEXT

Page
ntroduction.............................. 438
cknowledgments.......................... 439
bservations.............................. 440
General description.................... 440
Methods.................................. 441
Reduction and interpretation of data....... 444
Discussion................................. 445
Continental shelf profiles................. 445
Blake Plateau profiles..................... 448
Deep-water profiles........................ 455
Relationship of adjoining structures........ 460
Relation to the ocean basins............ 460

Page
Relation to other continental slope structures 461
Relation to continental structures 461
Comparison with other regions 461
References cited 462
Appendix: Discussion of data 463
Continental shelf 463
Blake Plateau 463
Outer continental slope and ridge area 464

ILLUSTRATIONS

Figure Page
1. Layers of Tables 2, 3, and 4 444
2. Depths of layer boundaries, continental shelf 446
3. Continental shelf: 29°50′N. to 36°50′N. . . 449
4. Continental shelf: Jacksonville, Florida, section 450
5. Continental shelf: Charleston, South Carolina, section 451
6. Blake Plateau: 28°90′N. to 31°00′N. . . . 452
7. Blake Plateau: 77°W to 81°30′W 453
8. Blake Plateau: 77°30′W to 80°35′W 454
9. Deep-water section along the ridge 455
10. Deep-water section paralleling continental slope 456
11. Deep-water section: Interior basin to ridge 457
12. Speculative history of the ridge 459
13. Comparison of Piedmont, coastal plain, and oceanic structure with western Pacific island arcs 460

Plate Facing page
1. Profile and structure section locations and bathymetry 437
2. Travel-time graphs 466

TABLES

Table Page
1. Receiving positions for seismic-refraction profiles 440
2. Layer velocities and layer thicknesses, continental shelf 441
3. Layer velocities and layer thicknesses, Blake Plateau 442
4. Layer velocities and layer thicknesses, deep-water section 443

Introduction

A geophysical study of the transitional structures between an ocean basin and a continent is presented in this paper. The area studied lies between Cape Henry, Virginia, and Jacksonville, Florida, and extends from the coast to the 73rd meridian. Primary reliance has been placed on the seismic-refraction method, although bathymetric and seismic-reflection evidence has been considered as well. The observations reported form one of several sets taken within the area since Hersey and M. Ewing (1949) reported a bathymetric and seismic and reflection study, and Katz and M. Ewing (1956) reported a reconnaissance seismic-refraction study, each of larger areas which include part of this one. Woollard, Bonini, and Meyer (In preparation) have made a study of continental structures in Georgia, North Carolina, and South Carolina which overlaps ours on the continental shelf, and Nafe and Hennion (In preparation) have studied the ocean area south of the latitude of Jacksonville.

Seismic-refraction investigations made by at least four separate groups of geophysicists since World War II have led to a general picture of the structure of the earth's crust beneath the broad deep areas of the oceans. There is general agreement that the simplest oceanic crustal structure consists of (1) about 5 km of sea water overlying about 1 km of sediments whose compressional wave velocity approximates 1.8 km/sec. near the top of the column, and (2) 4.0–5 km of rock below, which has a compressional wave velocity of about 6.5 km/sec. and overlies the Mohorovic discontinuity (M layer). At the M layer, compressional wave velocities ranging from about 7.8 to 8.2 km/sec. were measured (M. Ewing and Press, 1955). In the vicinity of oceanic islands such as the Bermudas this simple picture appears to be altered by structures resulting from the volcanic activity in the area (Officer, 1955), and in the vicinity of relatively young island-arc structures, such as the Lesser Antilles, even more complicated alterations are found (Officer *et al.*, 1957; J. Ewing *et al.*, 1957). M. Ewing and his co-workers have established several lines of seismic-refraction profiles (M. Ewing *et al.*, 1937; 1939; 1940; 1950; Officer and M. Ewing, 1954; Oliver and Drake, 1951) from North America Basin to the shallow water of the eastern continental shelf of North America north of Cape Hatteras to study the nature and structural arrangement of the changes that take place between the simple, thin crustal section of the ocean basin and the much more complicated, thicker, and deeper continental crust. In all these last studies, the M-layer arrivals that are readily measured in deep water are lost beneath a thick section, which has velocities suggesting thick sediments laid down in a trough more or less parallel to the edge of the continental shelf (*e.g.*, Officer and M. Ewing, 1954; Drake *et al.*, 1957).

The bathymetry of the deep-water area south of Cape Hatteras (Pl. 1) suggests different and more complicated underlying structures than those discussed by Drake *et al.* (1957) for the continental margin to the north. The continental slope is interrupted at 450 fms. by the Blake Plateau, a remarkably smooth and nearly flat area extending north from the Bahamas to Cape Hatteras. The plateau is bounded on the east by a steep escarpment more than a mile high in the southern half, and, within the area of the present study, by irregular slopes dominated by a ridge trending southeastward from Cape Fear. This ridge appears to protrude from below the northern Blake Plateau at a depth of about 1500 fms. To the southeast it deepens irregularly, turns abruptly southwestward toward the Bahamas, and joins Eleuthera at about 2500 fms. It was suspected that here might be a continental-type structure that gradually changes into ocean-basin structure. The trend of the topographic ridge coincides with a prominent continental structure, the Cape Fear Arch, or the Great Carolina Ridge or Carolina Arch. One of the objectives in the present study has been to find out whether a structural connection exists between the Cape Fear Arch and this topographic ridge. Another objective has been to learn what we could about the structures underlying the Blake Plateau and their relationship with known structures both on the continent and under the ocean to the east and north.

In addition to seismic-refraction, seismic-reflection, and echo-sounding studies, we have attempted some core sampling, but this program has not yet been productive; coring should be continued and supplemented by rock dredging. A few dredgings and bottom photographs were made during a recent cruise and will be reported in another paper. J. L. Worzel and his co-workers at the Lamont Geological Observatory have made numerous gravity observations within this area (M. Ewing *et al.*, 1957; Worzel, unpublished data), and M. Davidson has made some magnetic observations there. We have had access to these data during preparation of this paper, but the gravity and magnetic data have not been analyzed entirely at present writing and hence are principally useful as a qualitative guide.

ACKNOWLEDGMENTS

Woods Hole Oceanographic Institution ships participating were ATLANTIS and BEAR with masters W. S. Bray and E. J. Mysona, respectively. Their helpful co-operation throughout is greatly appreciated.

Staff members of the institution who contributed to the observations at sea were: A. C. Vine, R. S. Edwards, and H. R. Johnson as chief scientists, and as members of the scientific party: R. H. Backus, S. W. Bergstrom, H. A. Cain, A. L. Carter, L. C. Davis, W. M. Dunkle, G. Duys, Jr., M. E. Edwards, C. S. Innis, S. T. Knott, D. E. Maddux, M. S. Rutstein, H. Small, G. W. Wheeler, W. E. Witzell.

The following technical assistants helped in reducing the data: J. Dragonette, R. S. Singsaas, N. C. Hickman, R. V. Olson, C. M. Dixon, S. J. Klein, and E. H. Rogers. Charles Innis, J. W. Stimpson, and C. E. Spooner prepared the plates and figures for publication. Peter J. Westervelt of Brown University, J. L. Northrop of Hudson Laboratories, Clifford Parker and J. B. Duchene of the Marine Division, Sperry Rand Corporation, assisted in part of the work at sea.

The co-operative effort at sea in 1955 with Nafe and Hennion on R/V VEMA made possible much of the shallow-water work. The continued co-operation of Nafe and Hennion throughout the analysis of the sea data has contributed much to this study through repeated exchange of ideas. We are most grateful to J. L. Worzel for the opportunity to consult his unpublished gravity data and to Maurice Davidson for his efforts to make his magnetic program as useful as possible in the area of our research. We are grateful to the Bureau of Ships (Contract NObsr-43270) and the Office of Naval Research (Contract Nonr-1367) for support of this work and to the Bureau of Ordnance and the Naval Ammunition Depot, Charleston, South Carolina, for assistance with explosives.

All authors contributed to analysis of the data. Final interpretation and preparation of the manuscript are the responsibility of the first two authors, and the geological speculation was made by the first author.

The base map for Figure 13 is AMS1101 (The World), Army Map Service (SN) Dept. of the Army, Washington, D. C.

Table 1.—Receiving Positions for Seismic-Refraction Profiles

Profile Number	Latitude (N.)	Longitude (W.)
Atlantis 196—Bear 89		
3–54	34°11′	76°59.5′
4–54	30°27.1′	81°00.4′
5–54	30°16′	81°14.8′
9–54	28°48′	77°51′
10–54	32°12.4′	79°24′
11–54	33°14′	78°12′
12–54	33°52′	76°58′
13–54	34°16′	76°15′
14–54	35°47′	75°12′
15–54	36°22′	75°11.5′
Vema 6—Bear 113		
5–55 N.	30°52.5′	80°28′
5–55 S.	30°17′	80°32.8′
6–55 N.	30°37′	78°28′
6–55 S.	30°21.9′	78°19.8′
11–55 N.	30°52.8′	80°13.8′
11–55 S.	30°34.5′	80°18.5′
12–55 E.	31°09.5′	79°57.8′
12–55 W.	31°14.0′	80°16.5′
13–55 N.	31°35.7′	80°15.0′
13–55 S.	31°24.8′	80°21.8′
14–55 E.	32°04.5′	79°16.2′
14–55 W.	32°13.08′	79°24.5′
15–55 E.	32°14.5′	79°27.8′
15–55 W.	32°26′	79°39.5′
17–55 N.	29°58.5′	80°39.7
17–55 S.	29°41.6′	80°40′
18–55 E.	29°43.9′	80°25.6′
18–55 W.	29°41′	80°41.5
Atlantis 213—Bear 113		
29–55 N.	30°56′	78°57.8′
29–55 S.	30°45′	78°40.1′
30–55 N.	30°14′	77°46.5′
30–55 S.	30°01′	77°25′
31–55 E.	29°33.5′	75°01′
31–55 W.	29°40.2′	75°40.6
32–55 N.	30°08.3′	74°39.5′
32–55 S.	29°43′	74°30.6′
33–55 N.	30°13′	73°53′
33–55 S.	29°56′	73°28′
Atlantis 213—Bear 113—*Continued*		
34–55 N.	30°45′	74°33′
34–55 S.	30°30.7	74°11.8′
35–55 E.	31°05.7′	75°03.3′
35–55 W.	31°11.5′	75°30′
36–55 E.	31°11′	77°21′
36–55 W.	31°15.5	78°00′
37–55 E.	31°22′	76°22′
37–55 W.	31°21′	76°57.3′
38–55 E.	31°39.2′	75°30′
38–55 W.	31°29′	75°53′
39–55 N.	32°22.2′	74°41′
39–55 S.	31°52′	74°46′
Atlantis 223—Bear 140		
1A–56	30°22.5′	78°10′
1B–56	29°42.5′	78°14.8′
1C–56	29°56.6′	78°10′
2–56 E.	31°13.5′	77°56.5′
2–56 W.	30°59.4′	78°50′
3–56 N.	30°10.4′	79°04′
3–56 S.	29°44.7′	78°45′
4–56 N.	31°12.3′	76°28.1′
4–56 S.	30°28.0′	76°53.5′
5–56 E.	30°26.5′	75°24.5′
5–56 W.	30°35.4′	75°58.2′
6–56 E.	30°49.8′	74°39′
6–56 W.	30°59.5′	75°44′
7–56 N.	32°18.6′	75°13.2′
7–56 S.	31°50.8′	75°08.2′
8–56 N.	33°19′	74°25′
8–56 S.	32°41.5′	74°36.9′

OBSERVATIONS

General Description

The seismic-refraction program commenced in 1954 when Dietz and Hersey made a series of 15 end-to-end profiles on the continental shelf with Atlantis and Bear. Most of these are in the area of the present study (Pl. 1). In 1955 R. F. Wyrick on Bear and J. E. Nafe of the Lamont Geological Observatory on Vema shot 24 refraction profiles on the coninental shelf and the Blake Plateau. Nafe and Hennion are preparing for publication the profiles south of 30°N.Lat.; the more northerly stations are included in the present study exploit fully the echo sounder as a geological tool; one exception is a brief study of a fault zone in this area, (Hersey and Knott, in preparation).

TABLE 2.—LAYER VELOCITIES AND LAYER THICKNESSES, CONTINENTAL SHELF
(In km and km/sec.) N., S., E., W.: locations of receiving positions relative to each other

	LAYER VELOCITY									LAYER THICKNESS						
PROFILE	WATER	A	B	C	D	E	F	G		WATER	A	B	C	D	E	F
3-54	1.50	1.86		2.48			5.49			0.03	0.22		0.91			
4-54	1.51	1.77			3.25		5.38			0.03	0.20			1.50		
5-54	1.51		1.96	2.66	3.67					0.02		0.13	0.23			
10-54	1.52	1.66		2.71				6.04		0.03	0.47		1.28			
11-54	1.51		2.05	2.26				5.89		0.03		0.06	0.77			
12-54	1.51	1.88		2.46				5.90		0.04	0.36		1.07			
13-54	1.51	1.84		2.41	3.88					0.03	0.50		0.79			
14-54	1.49	1.69		2.85		4.30		6.14		0.03	0.58		1.32		1.31	
15-54	1.48	1.75	1.98	2.79	3.27		5.32			0.02	0.26	0.63	0.59	2.09		
5-55	1.52	1.68		2.57	3.65		5.16	5.82	N S	0.03 0.03	0.23 0.11		0.72 0.34	1.32 1.99		1.44 2.45
11-55	1.52		1.92	2.34/2.85	3.43			5.96	N S	0.04 0.04		0.10 0.22	0.41/0.46 0.29/0.51	2.04 2.04		
12-55	1.52		1.95	2.88				6.30	NW SE	0.04 0.04		0.30 0.40	2.45 2.27			
13-55	1.51	1.83		2.56	3.45			5.95	NE SW	0.03 0.03	0.22 0.28		0.84 0.42	1.18 1.86		
14-55	1.51	1.77		2.65				5.96	NW SE	0.05 0.05	0.57 0.56		1.53 1.79			
15-55	1.51	1.90		2.44				5.98	NW SE	0.03 0.03	0.32 0.45		0.93 1.29			
17-55	1.52	1.76		2.42	3.16	4.26	5.35	6.06	N S	0.03 0.03	0.08 0.08		0.19 0.21	0.94 0.42	1.40 2.95	3.48 2.22
18-55	1.52	1.69		2.25	3.21	4.36	5.52		E W	0.04 0.03	0.13 0.05		0.19 0.28	0.91 0.66	2.56 3.09	

(Pl. 1). Later in 1955, Hersey and others made 15 additional stations with ATLANTIS and BEAR, some on the northern part of the Blake Plateau, but most over the ridge and its surroundings (Pl. 1). Finally, in 1956 Hersey and others made 8 profiles with ATLANTIS and BEAR on the Blake Plateau and over the outer continental slope and ridge area (Pl. 1). Receiving positions for the profiles are listed in Table 1.

Seismic-reflection studies were made concurrently with most of the deep-water refraction profiles of the 1955 and 1956 cruises. Echo-sounding data were taken routinely during all the cruises, but inasmuch as all this work had to be accommodated to other programs, we had limited opportunity to

Methods

The seismic-refraction observational techniques were basically similar to those that have been described in many papers on deep-sea explosion seismology (M. Ewing *et al.*, 1937; 1939; 1950; Officer *et al.*, 1952). We were able to drop very closely spaced charges (about 0.25 mile apart) and paid special attention to doing so at short range on most of the profiles. This practice frequently revealed shallow and intermediate depth layers which could not have been demonstrated without such close spacing.

In the seismic-reflection studies, we followed the method described by Officer (1955) except that we alternated shallow changes (no bubble

TABLE 3.—LAYER VELOCITIES AND LAYER THICKNESSES, BLAKE PLATEAU

(In km and km/sec.) N., S., E., W.: locations of receiving positions relative to each other. Overbar indicates unreversed velocities.

	LAYER VELOCITY												LAYER THICKNESS									
PROFILE	WATER	A	B	C	D	E	F	G	H	I	J		WATER	A	B	C	D	E	F	G	H	I
9-54	1.51	1.83				4.11	5.52						1.01	0.38				1.72				
6-55	1.52	1.83		2.77	3.80	4.54						N	0.84	0.49		0.02	1.01					
												S	0.83	0.52		0.07	0.59					
29-55	1.51	1.83			3.87	4.81		$\overline{6.18}$				NW	0.84	0.55			2.39					
												SE	0.85	0.59			0.75	7.33				
30-55	1.51	1.83				4.30	4.99			$\overline{7.20}$		NW	0.83	0.59				0.90	6.50			
												SE	0.83	0.52				0.94	6.40[a]			
36-55	1.50	1.83			3.61	4.55		$\overline{5.77}$		$\overline{7.28}$		E	0.98	0.66			0.53					
												W	0.84	0.58			1.01	4.45[b]		7.31[b]		
1A-56	1.51	1.83		$\overline{2.61}$		$\overline{4.84}$	$\overline{5.50}$		$\overline{6.70}$			N	0.80	0.31		1.14		0.85	3.84			
1B-56	1.51	1.83		$\overline{2.27/2.80}$		$\overline{4.63}$	$\overline{5.22}$		$\overline{6.66}$			NW[1]	0.81	0.09		0.04/1.30		1.01	3.22			
1C-56	1.51	1.83		$\overline{3.15}$		$\overline{4.45}$	$\overline{5.50}$	$\overline{5.85}$				N	0.81	0.26		1.04		1.31	3.88			
2-56	1.51	1.74			3.84	4.62			6.39		$\overline{8.04}$	E	0.79	0.77			0.52	6.45				
												W	0.77	0.66			1.04	5.91			5.82	
3-56	1.51	1.77				4.36	4.96					NW	0.82	0.69				1.15				
												SE	0.79	0.64				1.38				

[1] *See* Appendix

[a] Velocity line associated with this thickness not observed; assumed from correct reverse point

[b] Thickness obtained by a complex interpretation

TABLE 4.—LAYER VELOCITIES AND LAYER THICKNESSES, DEEP-WATER SECTION

(In km and km/sec.) N., S., E., W.: locations of receiving positions relative to each other. Overbar indicates unreversed velocities.

	LAYER VELOCITY												LAYER THICKNESS									
PROFILE	WATER	A	B	C	D	E	F	G	H	I	J		WATER	A	B	C	D	E	F	G	H	I
31-55	1.51	1.89							6.70	7.85		E	4.50	2.39							4.44	
												W	4.57	2.52							3.99	
32-55	1.51	1.83	2.06						6.55	7.34		N	4.49	0.16	2.46						2.61	
												S	4.49	0.16	2.46						4.20	
33-55	1.51	1.83		2.44			5.67		$\overline{6.90}$		$\overline{8.10}$	NW	3.80	1.12		2.20			1.54		4.90[a]	
												SE	3.80	1.24		2.15			1.10[a]		4.90	
34-55	1.51	1.83	2.20	2.96			5.20		6.33	$\overline{7.36}$		NW	3.69	0.41	1.67	1.39			1.00		3.79[a]	
												SE	3.69	0.41	1.76	1.43			1.14		2.92	
35-55	1.51	1.83	2.17	2.57			5.24		6.69	7.20	$\overline{8.40}$	E	3.43	1.07	0.49	1.97			2.90		0.37	8.00
												W	3.43	1.07	0.63	1.85			1.85		2.55	7.01
37-55	1.50	1.83		2.77	3.89			6.10		7.42		E	2.90	0.93		2.18	3.48			3.21		
												W	2.45	1.32		1.34	5.55			5.01		
38-55	1.51	1.83		2.38	3.98				6.36	7.73		NE	3.05	1.13		1.78	4.16				1.38	
												SW	2.81	1.79		1.55	3.10				5.08	
39-55	1.51	1.83		2.64	3.84				6.45	7.12	$\overline{7.95}$	N	4.17	1.12		1.32	3.53				2.05	
												S	4.11	1.44		1.36	2.08				3.34	8.98
4-56	1.51	1.68		2.43	3.75	4.46			6.70	$\overline{7.64}$		N	2.78	0.83		2.17	1.59	3.55			3.55	
												S	2.90	0.57		1.64	0.62	6.23				
5-56	1.51	1.83	$\overline{2.26}$				$\overline{5.37}$			$\overline{7.16}$		E	4.06	0.22	2.31				1.66			
			$\overline{2.22}$		$\overline{3.94}$				$\overline{6.51}$	$\overline{7.31}$	$\overline{8.60}$	W	3.83	0.75	1.57		2.52				1.29	3.78
6-56	1.51	1.83	$\overline{2.20}$	$\overline{2.78}$	$\overline{3.99}$			$\overline{6.00}$		$\overline{7.37}$		E	3.56	1.12	0.65	0.99	2.40			2.14		
			$\overline{2.15}$	$\overline{2.73}$	$\overline{3.80}$			$\overline{6.00}$		$\overline{7.55}$		W	3.55	0.53	0.51	2.18	1.96			1.58		
7-56	1.51	1.83			3.20	4.26		6.15		7.54		N	3.94	1.09			2.30	3.17		2.71		
												S	3.42	1.86			1.64	2.25		2.71		
8-56	1.51	1.77		2.35	3.71			6.24		7.10	8.43	N	4.34	0.80		1.54	2.31			4.25		4.27
												S	4.45	1.19		0.76	3.10			1.31		4.27

[a] Velocity line associated with this thickness not observed; assumed from correct reverse point

pulse) with deeper charges in order to take advantage of the enhanced low-frequency radiation from the deep charge for very deep reflections. Alternate deep and shallow charges make it possible to trace adequately both the deep and shallow reflecting horizons simply by adjusting appropriately the spacing between charges.

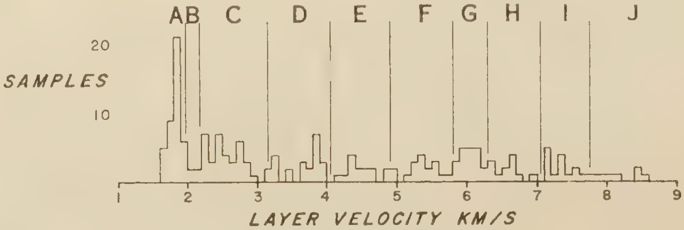

FIGURE 1.—LAYERS OF TABLES 2, 3, AND 4

Throughout all these cruises, ATLANTIS and BEAR were equipped with Edo Corporation UQN-1B echo sounders and Woods Hole precision graphic recorders (PGR) (Knott and Hersey, 1956) for echo sounding. This combination can resolve depth differences of 1 fm in any depth of water; its usefulness in submarine geologic and topographic studies has already been demonstrated (Hersey and Rutstein, 1958). Regrettably the weather was generally so bad that the full potentialities of precision depth recording were not realized most of the time.

Reduction and Interpretation of Data

Reduction of the seismic data was done by the same general method described by Officer and Wuenschel (1951) and Sutton and Bentley (1953). This includes a correction for the time taken for the sound to travel from the shot to the shooting ship (shot-instant correction); a correction reducing the travel times to a surface of reference, taken as sea level; and a correction necessitated by the irregular bottom topography underlying a number of the stations.

Certain departures from the standard procedures were made necessary by gaps in the recorded data. During computation of the shot-instant correction for profiles 4-56 to 8-56, BEAR receiving, it was found that sinking times (time from the moment the charge is thrown over the side to detonation) had not been recorded for the majority of the M-2 shots. Since bubble-pulse intervals (and hence charge depths) from the two ships for the sam charge size and fuse length were nearly identical, it was possible to infer an average valu for the sinking time from data taken by th other ship at the same range. The error thu introduced into the determination of shot-instant correction has been determined as n more than .01 sec. In a few cases, no echo-sounding records were available for both ends of the profile owing to malfunctions of the equipment. In these cases water depths were determined on the basis of the bottom-reflection record taken by the shooting ship. Good agreement was obtained between these and the available echo-sounder records.

Determination of compressional wave velocities and layer thicknesses followed the methods of M. Ewing *et al.* (1939). Individual profiles are discussed in the Appendix, and the refracted-wave travel-time graphs for the three principal regions are reproduced in Plate 2. Layer velocities and layer thicknesses are presented in Table 2, 3, and 4 in km/sec. and km respectively. Layer designations of A, B, C—J are arbitrary and based principally on grouping of the velocities (Fig. 1). These groupings are based on velocity only and do not imply identical horizons.

We have made only a preliminary examination of the reflection data from the 1955 and 1956 deep-water profiles. The results indicate that reflections can be identified from several of the low-velocity layers. The computed layer thicknesses are slightly less than the corresponding ones determined by refraction data. The velocities, however, are closely comparable, and there is only one instance throughout the analysis of a large discrepancy in layer thickness. Deepest reflection penetration was on profile 7–56 where at least a portion of layer E (4.26 km/sec.) was penetrated. There is considerable reflection evidence of multiple layering. Hence it is possible that we have picked travel times of layers with light velocity contrast lying above the bound-ries along which the refracted waves are ransmitted.

Discussion

Continental Shelf Profiles

Continental structures buried beneath the tlantic Coastal Plain sediments are domi-ated by two major positive features, the ape Fear Arch in North Carolina and Penin-ular Arch in Florida. These same structures xtend beneath the continental shelf. The Cape ear Arch trends southeastward from the iedmont Upland to Cape Fear on the southern orth Carolina coast. The Peninsular Arch imilarly trends southeastward underlying and onforming in shape generally to the Florida eninsula. The principal structural trends ave been discussed by Mansfield (1936), Rich-rds (1945), Spangler (1950), and Stephenson 1926; 1928) for North Carolina and South arolina and by Applin and Applin (1944), pplin (1951), and Stephenson (1926; 1928) or Georgia and Florida. The structure con-ours are shown for the top of Cretaceous ver this whole region and on Ocala limestone Eocene) in Florida on the Tectonic Map f the United States (Longwell *et al.*, 1944). il exploration and other geophysical studies long the coastal areas have provided con-iderable structural data, especially on the epth of crystalline basement. Published aterial is discussed by Skeels (1950) and pangler (1950), Applin (1951), Applin and pplin (1944), Mansfield (1936), King (1950), nd Richards (1945). Other excellent data rom seismic studies in shallow water and on he coastal plain were presented at the New rleans meeting (1955) of The Geological ociety of America (Meyer, 1955; Bonini, 955).

The refraction results from the shelf profiles re summarized in Figure 2*a*, *b*, *c*, and *d* for the ur principal higher velocities. Depths are iven in km, and velocities (in parentheses) re in km/sec. We suggest that the velocities hown together in each division of the figure re correlated over the shelf southwest of ape Fear. These are also to be correlated ith the results of Nafe and Hennion (In reparation) south of 30°N. Lat. Correlations f the more northerly structures are discussed elow.

Several dry holes near shore reached granitic asement, the depth of which is shown on Figure 2*d*. These depths, together with the structural trends suggested by Spangler's map (1950), indicate that the horizon having velocity near 6.0 km/sec. is granitic basement, where the wells are close by. This velocity (layer G) is found on all but four profiles; thus we interpret its depths as depths to granitic basement. The possibility that it might be a high-velocity limestone cannot be disproved, but the correlation with the well logs supports the granitic-basement interpretation, and under the Blake Plateau, where there is much more likelihood of a thick limestone section, the velocities at these depths are all appreciably lower. Meyer (Personal communication) found velocities well above granitic which he supposes may be intrusive basalts. We may have a similar instance in the unreversed 6.3 km/sec. of profile 12-55 to the southwest. To the north a 6.0-km/sec.-type layer appears to be replaced by 5.49 and 5.32 km/sec. at 3-54 and 15-54 respectively. M. Ewing *et al.* (1937; 1939; 1950) presented strong arguments for such a low-velocity basement in Virginia and New Jersey. These may be used to explain both 3-54 and 15-54. If so, 12-54 may indicate local variation. We know from good evidence that 5.2 to 5.5 km/sec. onlaps 6.0 km/sec. in the south. This may also be the case near Cape Hatteras. Only closer control in this area can provide proof.

Both north and south of the Cape Fear Arch a lower-velocity, 5.16- to 5.5-km/sec., layer is found on a few stations (Fig. 2*c*). The southern group appear well correlated; they reflect the Peninsular Arch toward Jacksonville and deepen with basement to the south and to the east. This trend is to be seen also in the results of Nafe and Hennion (In preparation) south of 29°30′N. Lat. Thus, this layer appears to onlap the Cape Fear structure to the north. Worzel and Ewing (1948) found this layer at depths in essential agreement with ours in their Jacksonville deep and shoal profiles. They interpreted it as basement. However, it seems clear now that their profiles were too short to bring out the higher velocity (6.06 km/sec.) of 17-55 which is now correlated with other granitic basement-layer velocities. Nafe and Hennion (Personal communication) present evidence for identifying this velocity with the top of lower Cretaceous from its correlation with Big Pine Key (Applin 1951). The northern profiles, 3–54, 12–54, and 15–54 appear to present a different picture, as outlined above.

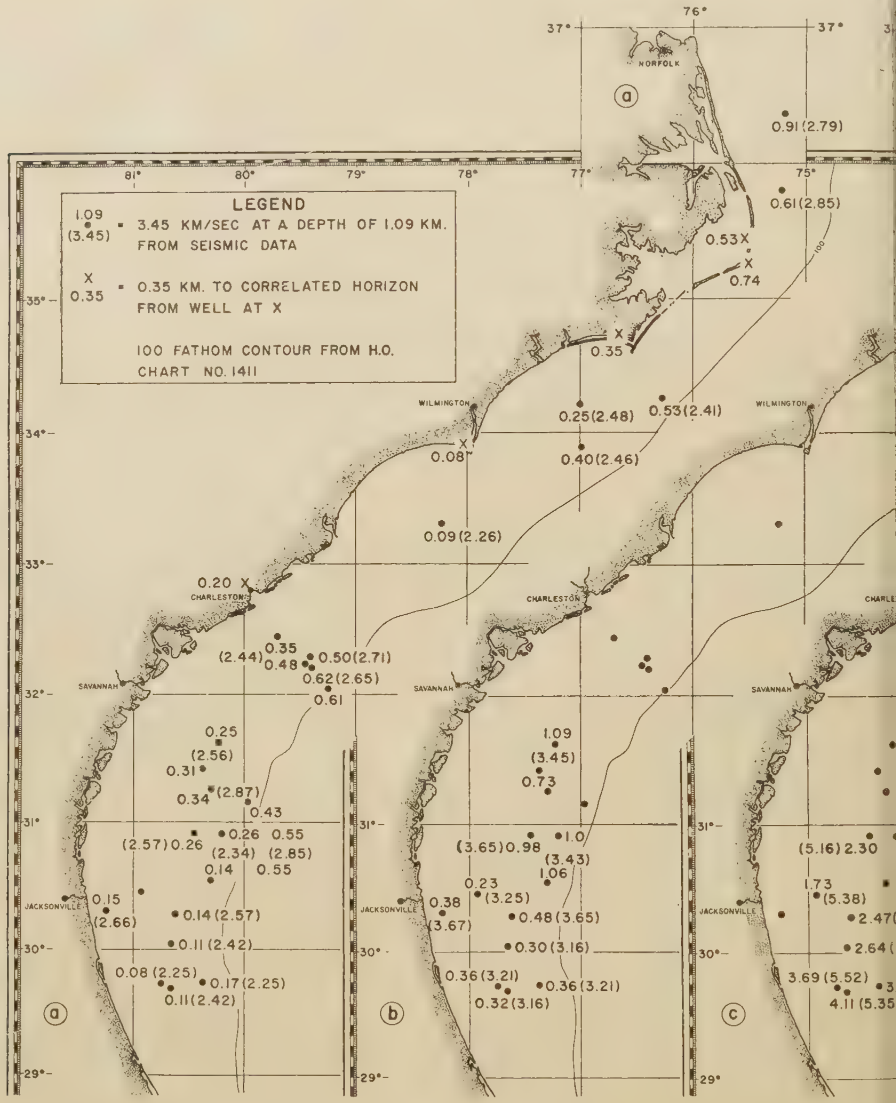
LEGEND
1.09 (3.45) • 3.45 KM/SEC AT A DEPTH OF 1.09 KM. FROM SEISMIC DATA
X 0.35 • 0.35 KM. TO CORRELATED HORIZON FROM WELL AT X
100 FATHOM CONTOUR FROM H.O. CHART NO. 1411
NORFOLK
WILMINGTON
CHARLESTON
SAVANNAH
JACKSONVILLE
81°
80°
79°
78°
77°
76°
75°
37°
35°
34°
33°
32°
31°
30°
29°
a
b
c
0.91 (2.79)
0.61 (2.85)
0.53X
0.74
0.35
0.25 (2.48)
0.53 (2.41)
0.08
0.40 (2.46)
0.09 (2.26)
0.20
(2.44) 0.35
0.48
0.50 (2.71)
0.62 (2.65)
0.61
0.25
(2.56)
0.31
0.34 (2.87)
0.43
(2.57) 0.26
0.26 0.55
(2.34) (2.85)
0.14 0.55
0.15
(2.66)
0.14 (2.57)
0.11 (2.42)
0.08 (2.25)
0.17 (2.25)
0.11 (2.42)
1.09
(3.45)
0.73
(3.65) 0.98
1.0
(3.43)
1.06
0.23
(3.25)
0.38
(3.67)
0.48 (3.65)
0.30 (3.16)
0.36 (3.21)
0.36 (3.21)
0.32 (3.16)
(5.16) 2.30
1.73
(5.38)
2.47(
2.64 (
3.69 (5.52)
4.11 (5.35
3
100

FIGURE 2.—DEPTHS

(a) 2.26–2.85 km/sec. (top of Upper Cretaceous) (b) 3.0–3.9 km/sec. (top of Taylor formatio of Lower Cretaceous, Nafe *et al.*, unpublished) (d) 5.89–6.1 km/sec. (top of granitic basement)

The next lower velocity group lying between 4.26 and 4.36 km/sec. were found on only three profiles: in the north on 14-54 and south on 17-55 and 18-55. More detail is required for the interpretation of these profiles, although their location suggests another onlap to the Cape Fear Arch from both north and south. Nafe and Hennion correlate similar velocities to the south with well data, indicating that this layer may be approximately top of Upper Cretaceous.

The layer (Fig. 2*b*) that has velocities from 3.2–3.9 km/sec. is also missing from the crest of the Cape Fear Arch between Savannah and Cape Lookout. It shoals from Georgia to Florida toward the Peninsular Arch and locally forms a positive feature along a north-north-west south-southeast trend including 4-54, 17-55, and 18-55. Its absence over the Cape Fear Arch and its presence on two stations to the north suggest that it is a sedimentary onlap there. However, it may be present farther

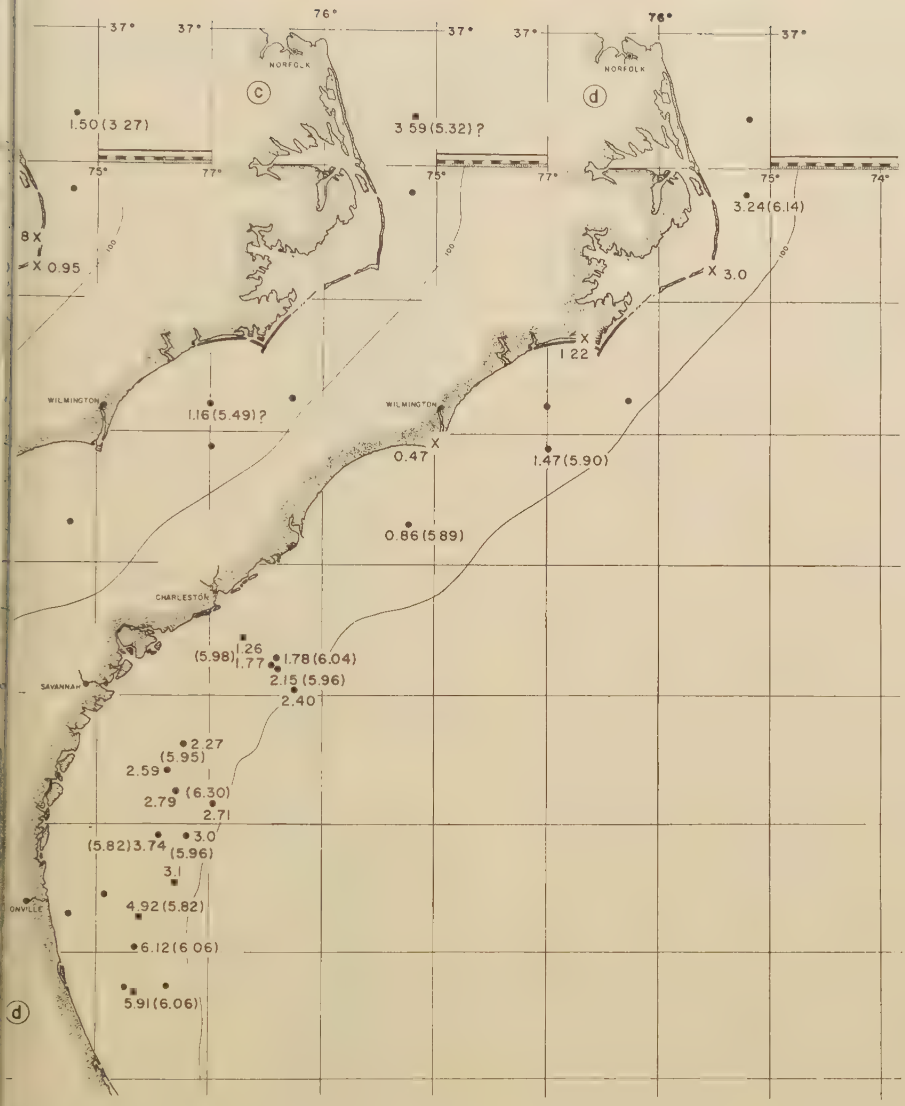
76°
37°
37°
37°
37°
76°
37°
NORFOLK
NORFOLK
c
d
1.50 (3 27)
3 59 (5.32) ?
75°
77°
75°
77°
75°
74°
3.24 (6.14)
8 X
X 0.95
100
100
100
X 3.0
X
1 22
WILMINGTON
WILMINGTON
1.16 (5.49) ?
0.47 X
1.47 (5.90)
0.86 (5 89)
CHARLESTON
(5.98) 1.26
1.77
1.78 (6.04)
2.15 (5.96)
2.40
SAVANNAH
2.27
(5.95)
2.59
2.79
(6.30)
2.71
(5.82) 3.74
3.0
(5.96)
3.1
4.92 (5.82)
6.12 (6 06)
5.91 (6.06)
ONVILLE
d

es, Continental Shelf

gia; top of Black Creek formation, North Carolina and South Carolina) (c) 5.0–5.5 km/sec. (top

p the flanks of the Cape Fear Arch but is a asked arrival on some of the stations there.

A layer of 2.26–2.85 km/sec is found on all rofiles along the shelf (Fig. 2*a*). Its depth eflects both major arches and shows an offhore crest slightly farther east than the 3.5-m/sec. layer. It deepens northeast of Cape Fear, deepens gradually southeast of Charleson, and shows a depth minimum southeast f Jacksonville; Nafe and Hennion's results In preparation) show that it deepens south of 29°30′N. On profile 11-55 velocities of 2.34 and 2.85 km/sec. are found on the same profile; otherwise the seismic data indicate that we are dealing with a single extensive layer. Comparison of the depths of this layer with well logs taken at various points near the coast shows that it agrees well with the depths to the top of Upper Cretaceous from Charleston northeast. Near Jacksonville the only well control is the Hilliard Turpentine Co. No. 1 mentioned in several studies of the region.

(*Cf.* Applin, 1951, well 67.) There the top of Upper Cretaceous is at a depth of 0.8 km, which is considerably deeper than these velocities on the shelf. We have adequate control to indicate correlation of this layer from profile to profile along the shelf south of Charleston but not northeast where well-log correlation is good. Nevertheless we suggest that this layer represents the top of Cretaceous over the entire area because of the depth correspondence with coastal Carolina well data. Applin and Applin (1944) show thickening of Eocene and some Cretaceous formations toward the sea in southeastern Georgia. If the above correlation be true, the shallow-layer depths along the shelf and the greater depth inland imply a partially closed basin for Eocene sediments and for part of Upper Cretaceous as well. A further possible implication of these results is that the presence of the ridge trending from Charleston toward Cape Canaveral may be the reason for the broadening of the continental shelf there. More information is needed both east and west of the present profiles, and detailed information about shallower formations would be needed to assess the effect of the structure on the shelf topography.

Above the 2.5-km/sec. layer we found only one layer, which had velocities from 1.66 to 2.05 km/sec. and lay very close to, if not quite at, the sea bottom. The 2.05 km/sec. layer was measured 25 miles south of Cape Fear at 11-54. Other bottom velocities are all lower, ranging from 1.66 to 1.95 km/sec. We have not studied the bottom sediments along the shelf here except by means of these measurements and by a few scattered reflection measurements made to test the combination of the precision graphic recorder (PGR) and a sparksound source discussed by Knott and Hersey (1956). From the latter, we know that considerable local variation occurs in the first 10–30 meters below the bottom; some sediments have velocities not exceeding that of sea water by more than 1 per cent. Hence it seems useless to speculate about the possible significance of the refraction measurements of bottom velocity until much more detailed information is available.

SUMMARY OF CONTINENTAL SHELF PROFILES: The foregoing discussion of the shelf profiles is summarized by the sections in Figures 3, 4, and 5. The section of Figure 3, taken along line *A-A′* (Pl. 1), shows the granitic basement continuously traced (except at 13-54) from south of Jacksonville to north of Cape Hatteras. The onlapping 5.3-km/sec. layer, possibly the top of Lower Cretaceous, is traced north of Jacksonville to 31°N. Similarly, the 4.3-km/sec. layer appears to onlap from the south and possibly from the north as well. To the south Nafe and Hennion (In preparation) correlate it approximately with the top of Upper Cretaceous. The 3.3-km/sec. layer has been correlated tentatively with Black Creek near Cape Hatteras but is not satisfactorily correlated with well data to the south. The apparent inconsistency with Nafe and Hennion's correlation cannot now be resolved. The 2.5-km/sec. layer is present throughout the section and is thought to correspond with or lie close to the top of Cretaceous throughout. Both these latter surfaces show the structural high east of Jacksonville, whereas the older surfaces do not.

East-west structural trends are indicated by the section roughly east-northeast from Jacksonville along line *B-B′* (Fig. 4; Pl. 1), which shows the high in the Cretaceous rocks and an apparently reverse trend in the basement. A third section, *C-C′* (Fig. 5; Pl. 1), southeast from Charleston shows a seaward deepening of all formations. Thus the high, which appears to trend north-northeast from the offing of Jacksonville, must trend somewhat west of 15-55, probably toward Charleston.

Blake Plateau Profiles

The floor of the central portion of the Blake Plateau is grossly smooth at about 800 meters depth. To the west, it becomes somewhat rough and irregular toward the continental slope, while to the north the smooth topography is interrupted by depressions and ridges with many fluctuations in depth of as much as 100 meters. We know little about the details of the topography, but some consistent trends, which appear to be evidence of faulting, have been found among these apparently irregular features. Between 27° and 30°N. the plateau gradually deepens eastward to its lip at a depth of about 1280 meters, where depths then increase suddenly to the small deep basin in the central part. To the northeast it deepens, as shown in Plate 1, approximately over the submerged ridge and into North America Basin. The topographic forms in this northeastern region suggest complicated underlying structures; this suggestion is borne out in the refraction profiles.

The 11 profiles discussed below are located on the northern part of the central smooth area, on the southern part of the rough terrain, and on the irregular northeastern slope. One

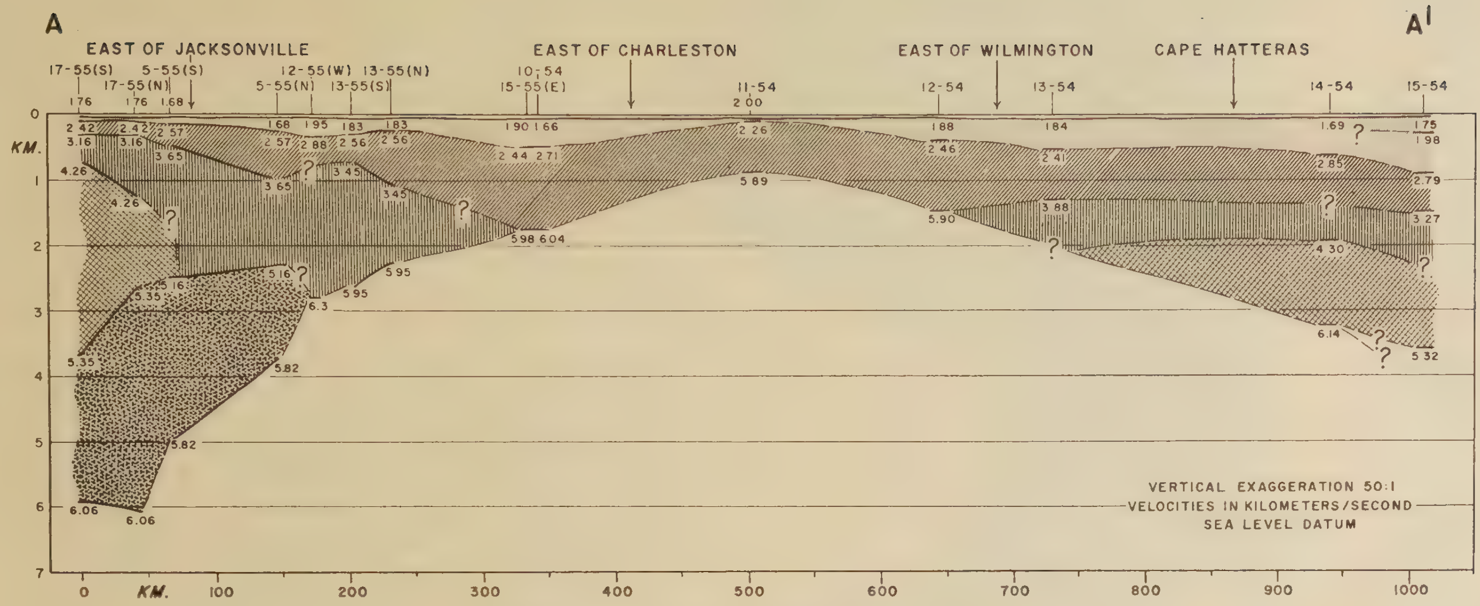
A
A'
EAST OF JACKSONVILLE
EAST OF CHARLESTON
EAST OF WILMINGTON
CAPE HATTERAS
17-55(S)
17-55(N)
5-55(S)
5-55(N)
12-55(W)
13-55(S)
13-55(N)
10-54
15-55(E)
11-54
12-54
13-54
14-54
15-54
KM.
VERTICAL EXAGGERATION 50:1
VELOCITIES IN KILOMETERS/SECOND
SEA LEVEL DATUM
0
1
2
3
4
5
6
7
0
100
200
300
400
500
600
700
800
900
1000
KM.

Figure 3.—Continental Shelf: 29°50′N. to 36°50′N.
Structure section *A-A′* (Pl. 1)

profile, 16-55, on the continental slope could not be interpreted because of drift in the Gulf Stream. The remaining profiles vary in quality because of rough weather that plagued much of the observational program.

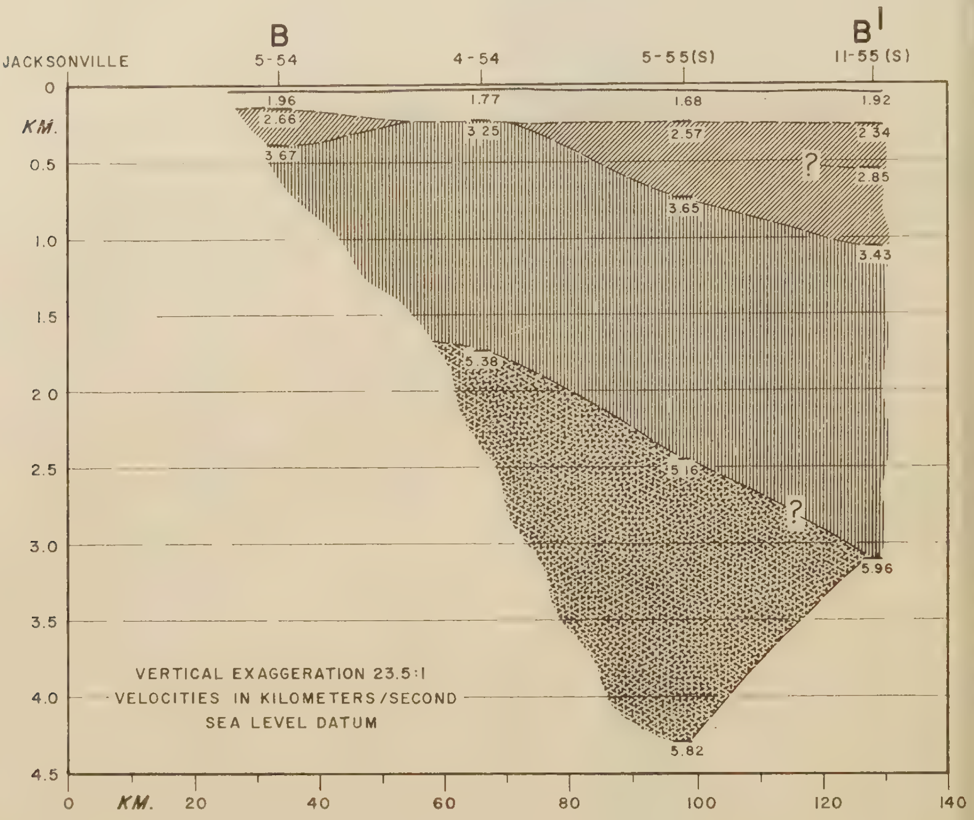

Figure 4.—Continental Shelf: Jacksonville, Florida, Section
Structure section *B-B'* (Pl. 1)

The structures of the Blake Plateau are simplest at shallowest depth and therefore are described from top to bottom.

The surface of the Blake Plateau has been sampled by coring and dredging and has been photographed in a few places. Manganese nodules have been recovered in cores taken on cruises of Atlantis by Edwards and Rutstein (Unpublished) and of Vema by Heezen (Personal communication). Calcareous samples have been recovered from scrapings on the core barrel, bottom cameras, and dredges. In August 1957, Edwards, Graham, and others dredged a considerable sampling of manganese nodules and a friable breccia of coral fragments, Globigerina, pteropods, barnacles, and similar calcareous remains, as well as living bryozoans and tunicates. Photographs indicate that this bottom composition is widespread at least on the northern half of the plateau.

Seismically we have had only modest success in measuring apparent bottom velocities and have assumed 1.83 km/sec. for many of the refraction profiles. Some of these assumptions are taken from the accompanying reflection data. On two profiles 1.77 and 1.74 km/sec. were measured.

The second-layer velocity ranges from 2.27 to 4.6 km/sec., obviously representing different rock surfaces in different places. The slowest velocities, 2.27–3.16 km/sec., are found in a group comprised of 6-55 and 1A-56, 1B-56, 1C-56, all of which are in the central part of the plateau where the bottom is "smooth".

The higher velocities found as the second layer are also found as the third or fourth layers (or are missing) on other stations; thus a layer 3.6-3.87 km/sec. is found at 29-55, 36-55, 2-56, and at 6-55 but not anywhere south of 6-55. A

.1- to 4.68-km/sec. layer is found on all profiles, hereas velocities from 4.96 to 5.5 km/sec. are ound at comparable depths south of 1A-56 nd are tentatively regarded as corresponding.

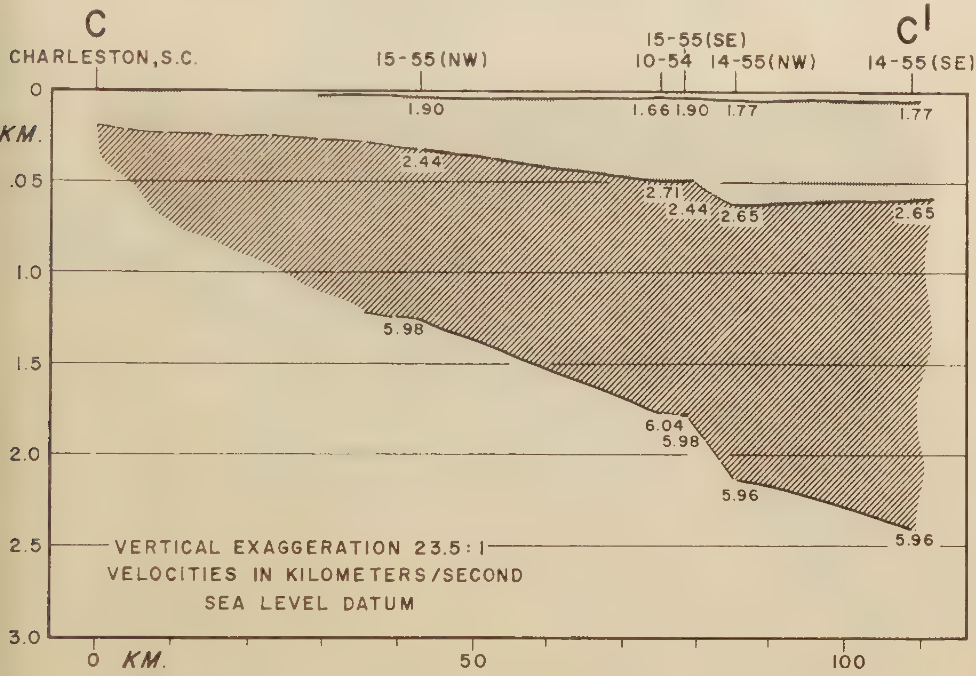

FIGURE 5.—CONTINENTAL SHELF: CHARLESTON SOUTH CAROLINA, SECTION
Structure section *C-C′* (Pl. 1)

ie structures indicated by these layers are all ntly sloping, except for local faulting.

Velocities higher than 5.5 km/sec. were easured on comparatively few profiles because the aforementioned weather difficulties and e available in many instances only as unre- rsed velocity lines. However, with appropri- e reservations, their characteristics are help- l in speculating about deep crustal structure neath the plateau. One velocity group ranges om 6.18 (one profile of poor quality) to 6.33 d 6.7 km/sec. (one good, two poor) which, if ey are correlated, indicate considerable relief the horizon from a possible depth of 5.7 km 1B-56 to 9.4 km at 2-56. The latter profile reversed and of good quality, whereas all the hers are unreversed for this velocity. Higher- locity lines were obtained on one side only of o profiles: 36-55 and 2-56 with apparent locities of 7.28 and 8.0 km/sec., respectively. e former profile is near the edge of the plateau d was made over an irregular surface in an erlying layer. We have shown the depth of the 7.28-km/sec. layer as 14 km, but since the profile is otherwise complicated and is unreversed for this layer, both velocity and depth are at best merely indications. However, the profile 2-56 was placed with considerably more knowledge of probable structure, and its shallower layers show very small slopes. Hence, the unreversed velocity of 8.0 km/sec., depth of 14.5 km, must be given correspondingly more weight. The thickness of 5 km for the 6.3-km/sec. layer is comparable to the corresponding layer in the ocean basins.

GEOLOGICAL INTERPRETATION: The structure of the northern half of the Blake Plateau can be sketched in a tentative way from the available results, but from our own data no age identifications can be made. Coring data reported by Nafe, Hennion, and Ericson (Unpublished) on the steep eastern slope separating the plateau from the deep ocean have led them to deduce that the top of Cretaceous probably corresponds to their 4.2-km/sec. layer there. The character of their coring evidence is such that the layers of 2.3-3.8 km/sec. might also be Cretaceous. This view has some support from comparison with the age correlations on the continental shelf discussed above.

STRUCTURE: Three structure sections (Figs. 6, 7, 8) summarize what we have deduced about the northern half of the plateau.

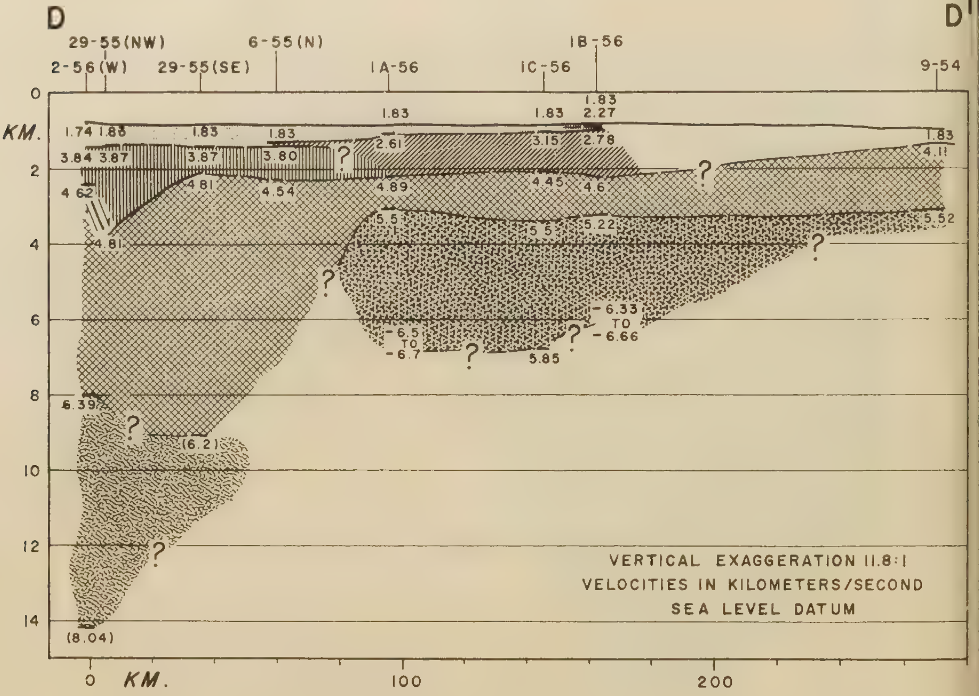
D
D'
29-55 (NW)
6-55 (N)
1B-56
2-56 (W)
29-55 (SE)
1A-56
1C-56
9-54
0
KM.
2
4
6
8
10
12
14
1.74
1.83
1.83
1.83
1.83
1.83
1.83
2.27
1.83
3.84
3.87
3.87
3.80
2.61
3.15
2.78
4.11
4.62
4.81
4.54
4.89
4.45
4.6
5.5
5.5
5.22
5.52
4.81
6.33 TO 6.66
6.5 TO 6.7
5.85
6.39
(6.2)
(8.04)
0 KM.
100
200
VERTICAL EXAGGERATION 11.8:1
VELOCITIES IN KILOMETERS/SECOND
SEA LEVEL DATUM

FIGURE 6.—BLAKE PLATEAU: 28°90′N. to 31°00′N. Structure section *D-D′* (Pl. 1)

In Figure 6 (Pl. 1, *D-D′*), the 3.8-km/sec. layer, which immediately underlies the surface layer, is markedly thinner than for near-by 29-55 and 36-55 to the south and east. The shallow trench found by Hersey and Knott (In preparation) lies just south of 2-56 and trends roughly parallel to it. Because of this relationship we have shown a fault at this point in the section. Farther south the 3.8-km/sec. layer is replaced by layers of lower velocity. From 6-55 we suppose that the 3.8-km/sec. layer extends beneath the lower-velocity layers and may be present but masked to the south.

The interpretation of the low velocities is reasonably based on first arrivals and clearly correlated second arrivals. However, on profiles where, for example, the 3.8-km/sec. layer does not form a first arrival and hence does not appear, the layer should not be regarded as necessarily absent. The same can be said of still lower velocities which generally appear as second arrivals. We have tested the effect on the apparent structure of supposing these intermediate velocities to be present but masked a profiles 2-56, 3-56, and 30-55, which are critica profiles in which the low velocities are missing

It is wholly on the absence of low velocitie in 3-56 and 30-55 that one might interpret th synclinal profile shown in Figure 8. We hav tested these interpretations by supposing tha a 3.8-km/sec. layer is present but just barely masked on the three profiles. On 2-56 possibl second arrivals of about 2.5 km/sec., similar t those observed elsewhere on the plateau, ar present. A similar assumption would mak similar changes in 29-55 and 36-55 (Fig. 7), s that the same interpretation of faulting her would be justified, but the low velocity woul be thickened. With respect to the synclinal section shown in Figure 8, the 3.8-km/sec. laye cannot be present on 3-56 and 30-55, but velocities of about 2.5 km/sec. can be assumed which at most would deepen the 4.4-km/sec horizon by about 250 meters. Hence a synclinal section there is established.

Below the lower-velocity layers the 4.11- t 4.89-km/sec. layer shoals gradually to th south as does the next deeper one of 5.2 to 5. km/sec. This latter layer is well established o

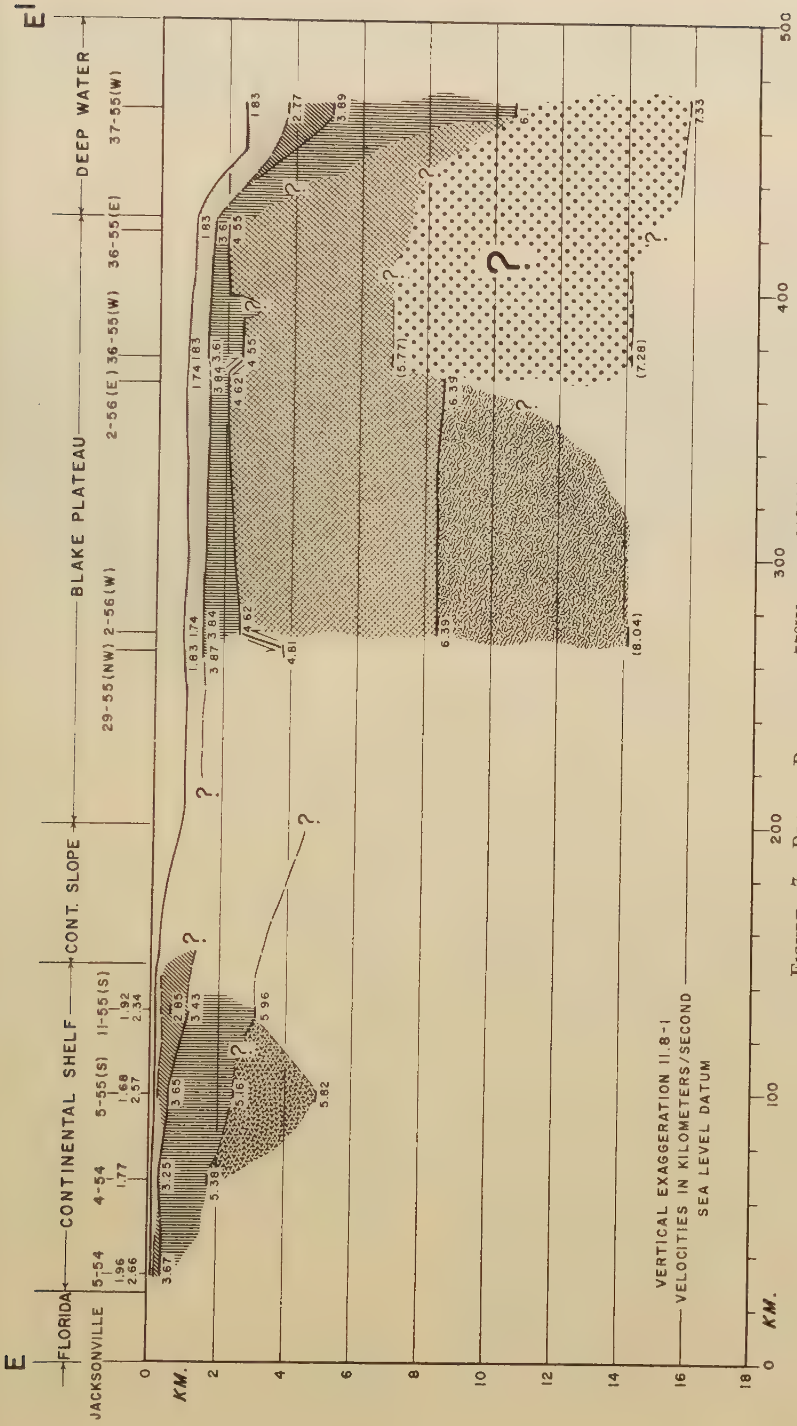
E
E'
JACKSONVILLE
FLORIDA
CONTINENTAL SHELF
CONT. SLOPE
BLAKE PLATEAU
DEEP WATER
5-54
4-54
5-55(S)
11-55(S)
29-55(NW)
2-56(W)
2-56(E)
36-55(W)
36-55(E)
37-55(W)
1.96
2.66
1.77
1.68
2.57
1.92
2.34
3.67
3.25
5.38
3.65
5.16
5.82
2.85
3.43
5.96
1.83
1.74
3.87
3.84
4.62
4.81
6.39
(8.04)
174
183
3.61
3.84
4.62
4.55
(5.77)
(7.28)
6.1
7.33
2.77
3.89
?
0
2
4
6
8
10
12
14
16
18
KM.
100
200
300
400
500
VERTICAL EXAGGERATION 11.8-1
VELOCITIES IN KILOMETERS/SECOND
SEA LEVEL DATUM

FIGURE 7.—BLAKE PLATEAU: 77°W. to 81°30′W.
Structure section *E-E′* (Pl. 1)

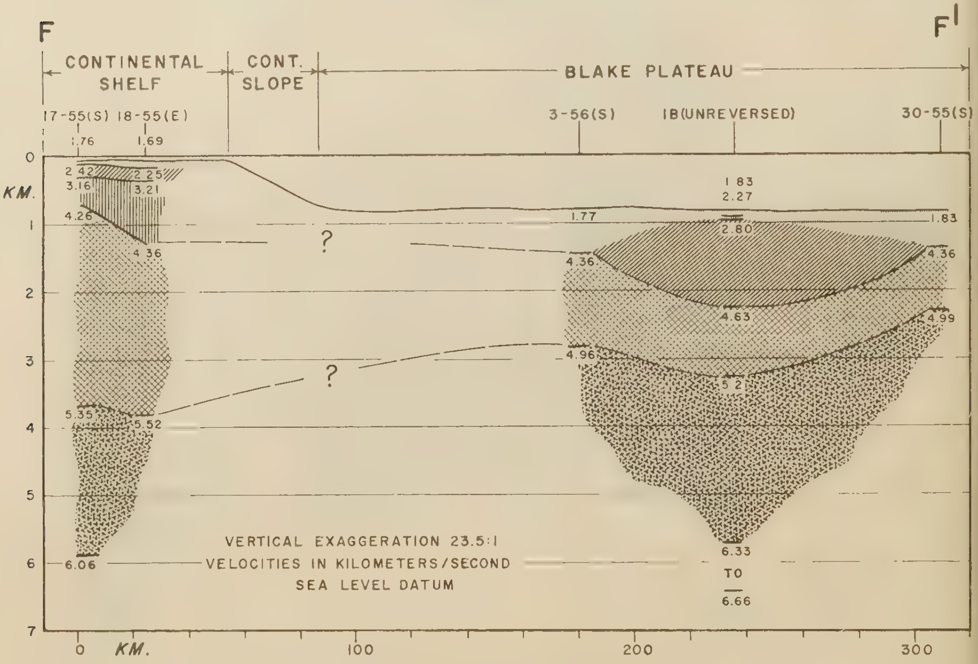
F
F'
CONTINENTAL SHELF
CONT. SLOPE
BLAKE PLATEAU
17-55(S) 18-55(E)
1.76
1.69
3-56(S)
IB(UNREVERSED)
30-55(S)
KM.
0
1
2
3
4
5
6
7
2.42
2.25
3.16
3.21
4.26
4.36
?
1.83
2.27
1.77
2.80
1.83
4.36
4.36
4.63
4.99
4.96
?
5.2
5.35
5.52
6.06
6.33
TO
6.66
VERTICAL EXAGGERATION 23.5:1
VELOCITIES IN KILOMETERS/SECOND
SEA LEVEL DATUM
0 KM.
100
200
300

FIGURE 8.—BLAKE PLATEAU: 77°30′W. to 80°35′W. Structure section *F-F′* (Pl. 1)

9-54, an end-to-end profile, and on 1A-56, 1B-56, 1C-56, all unreversed. On 2-56, the absence of the 5.2-km/sec. layer is based on inadequate travel-time evidence; it is apparently absent on 29-55 and 36-55 as well. Hence we suggest that there is probably a considerable thickness of the 4.4-km/sec. layer beneath these profiles. Test calculations indicate the same beneath 6-55, indicating a major trough structure which, on evidence to be discussed, we suppose trends east-northeast.

Four profiles, three unreversed, show a high velocity, mostly 6.3–6.7 km/sec.; three south of the trough are shallow compared with the fourth, which is over it. The greater depth is the reversed profile (2-56). This large difference in depth corroborates the trough structure discussed above.

The structure section *E-E′* (Fig. 7) crosses and recrosses the fault zone south of 2-56. Recent topographic studies by Hersey and others (Unpublished) have shown that the east-west trench south of 2-56 curves northward near the eastern end of 2-56 and the western end of 36-55, as is also indicated by the occurrence of the 3.8-km/sec. layer and the change in depth of the 4.4-km/sec. layer. Profile 36-55 contains excellent evidence of local depression, possibly faulting, in the 4.55-km/sec. layer as shown. North and northwest of the general vicinity of 2-56 the plateau loses its smooth character and shows complicated relief as the bottom shoals to the continental shelf. From this admittedly scanty evidence we suggest that structures similar to those shown in Figure 7 form the pattern of adjustment between the southern flank of the Cape Fear Arch, the northern wedge of the Blake Plateau, and the deeper ocean area to the east.

The deeper horizons of 2-56, 36-55, and 37-55 are based on data of variable quality, but there can be little doubt that high-velocity layers are present. On 2-56, 6.3 km/sec. is well established, as is 6.1 km/sec. on 37-55, but 5.77 km/sec. on 36-55 is unreversed. It seems plausible that these represent the same horizon. If so, they show much less marked change in depth here than the lower-velocity layers. However, the high relief in the 6.3 km/sec. indicated on section *D-D′* (Fig. 6) and the uniformly great depth on section *E-E′* (Fig. 7) and on profile 30-55 reveal a major depression of this layer trending east-northeast, north of 1A-56. The topographic nose trending east-northeast (Pl. 1) ight represent the extension of the southern nk of this depression, but we were not able investigate this possibility. On 2-56, 8.0 n/sec. is unreversed but is based on high ality data. On 36-55, 7.28 km/sec. is unrersed, whereas 7.4 km/sec. on 37-55 is reversed l shows considerable slope at this interface. these represent the same interface, it must ve considerable relief. We have not meas-d velocities higher than 7 km/sec. elsewhere the Blake Plateau. These high velocities ıld represent either the M layer or possibly tially differentiated ultrabasic material; suggest that either may be the case, dependon locality. In order to determine the depth l velocity of this layer beneath the Blake teau, several critically located long profiles h heavy charges will be needed.

Deep-Water Profiles

ast of the northern part of the Blake Plateau profiles were established in water depths from 0 to 4500 meters with the intention of study-the structures underlying the topographic e extending on a line roughly southeast from e Fear. With a few exceptions the locations orientation of the profiles were determined by weather rather than the problems to be solved. Nevertheless we were able to gather fair to excellent data giving velocities as high as 7.5–8.4 km/sec. on nearly all profiles.

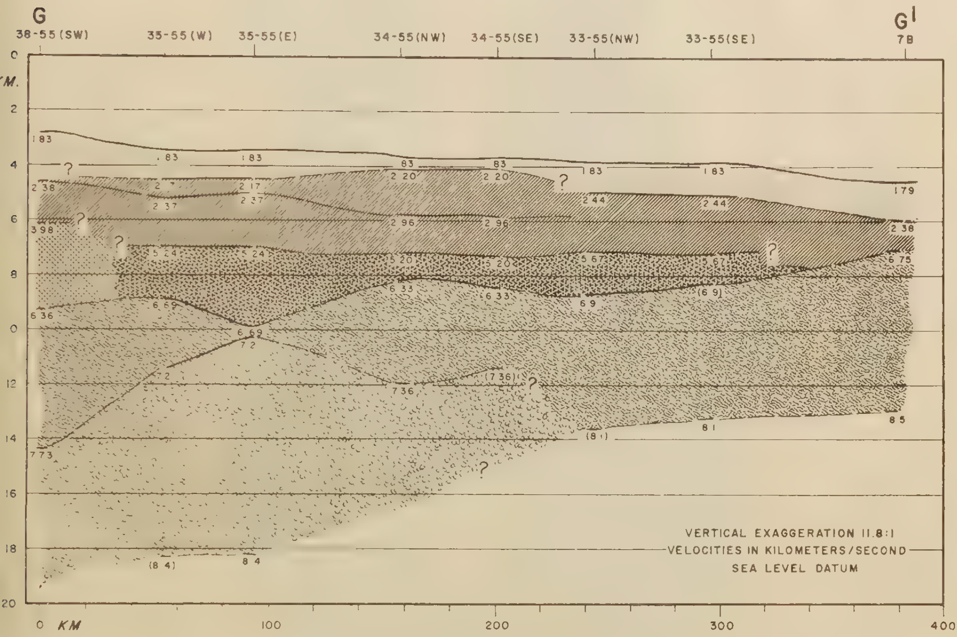
G
G'
38-55 (SW)
35-55 (W)
35-55 (E)
34-55 (NW)
34-55 (SE)
33-55 (NW)
33-55 (SE)
7B
0
KM.
2
4
6
8
10
12
14
16
18
20
1 83
1 79
2 38
2 17
2 37
2 20
2 44
2 96
3 98
5 24
5 20
5 67
6 75
6 36
6 69
6 33
6 9
(6 9)
7 2
7 36
(7 36)
7 73
8 1
(8 1)
8 5
8 4
(8 4)
?
VERTICAL EXAGGERATION 11.8:1
VELOCITIES IN KILOMETERS/SECOND
SEA LEVEL DATUM
0 KM
100
200
300
400

Figure 9.—Deep-Water Section Along the Ridge
Structure section *G-G'* (Pl. 1)

The sections of Figures 9–11 summarize the results. In Figure 9 (Pl. 1, *G-G'*) a section is shown approximately along the crest of the ridge. At the southeastern end is one end of profile 7 of Katz and Ewing (1956) where the section is rather like those representative of deep ocean basins (Ewing and Press, 1955) except that a 2.38-km/sec. layer is shown overlying the layer commonly identified as basaltic. Proceeding northwestward, a 2.5-km/sec. layer is underlain by 5.3 km/sec. which, in turn, overlies 6.6 km/sec., 7.3 km/sec., and 8.4 km/sec. in more or less similar sequences through 35-55. Here the section thickens and the 8.4-km/sec. interface deepens to the northwest. Between 35-55 and 38-55 the section changes abruptly and the 5.3-km/sec. layer is replaced by 3.98 km/sec. Other notable features are the very thick section of low velocities 1.79–2.96 km/sec. and considerable variation in thickness of the 5.3- and 6.6-km/sec. layers.

The sections shown in Figures 10 and 11 are transverse to *G-G'*. Section *H-H'* (Fig. 10) to the northwest indicates that a section some-

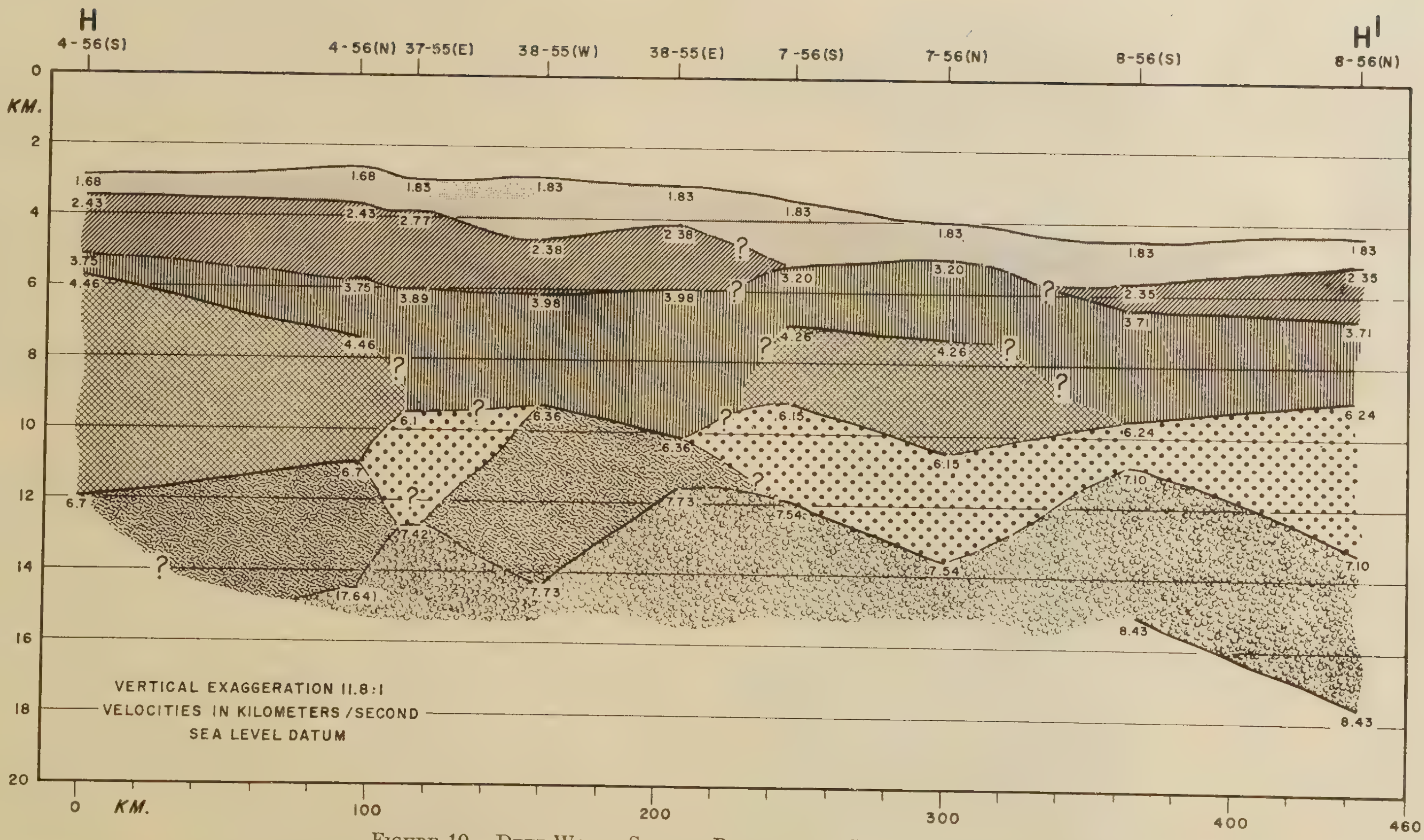
H
H'
4-56(S)
4-56(N)
37-55(E)
38-55(W)
38-55(E)
7-56(S)
7-56(N)
8-56(S)
8-56(N)
KM.
0
2
4
6
8
10
12
14
16
18
20
1.68
1.83
2.43
2.77
2.38
2.35
3.75
3.89
3.98
3.20
3.71
4.46
4.26
6.1
6.36
6.15
6.24
6.7
7.42
7.73
7.54
7.10
(7.64)
8.43
?
VERTICAL EXAGGERATION 11.8:1
VELOCITIES IN KILOMETERS/SECOND
SEA LEVEL DATUM
0
KM.
100
200
300
400
460

FIGURE 10.—DEEP-WATER SECTION PARALLELING CONTINENTAL SLOPE

Structure section *H-H'* (Pl. 1)

at like that of 38-55 persists along this trend, d that the velocities above 10-km depth are ther similar to those in the structural trough the Blake Plateau and could be an extension t. Notable in contrast to section *G-G′* is the ence of any velocity close to 5.3 km/sec. l the variable thickness and velocity of the up lying between 6.1 and 6.7 km/sec. Profile 55 is essentially similar to section *H-H′*.

rofiles 5-56 and 6-56 which lie southwest of ridge are complicated by evidence of fault- which appears as displacement of the high- velocity line. Both lie over structures that partly like those of section *H-H′* and partly the ridge; this indicates that the trough ntioned in connection with section *H-H′* ends southeastward from profile 37-55 be- ween the ridge and the edge of the Blake teau (Fig. 13). The faulting shown in 6-56 lownthrown on the ridge side. We cannot ncile the displacement of the high-velocity because of the difficulty with the low ve- ties discussed in the evaluation of the profile (Appendix). Maximum possible vertical fault throw is 2 km. Profile 5-56 is downthrown to the northwest and appears to overlie different shallow structures at either end; it is like the trough section to the northwest and like the ridge to the southeast.

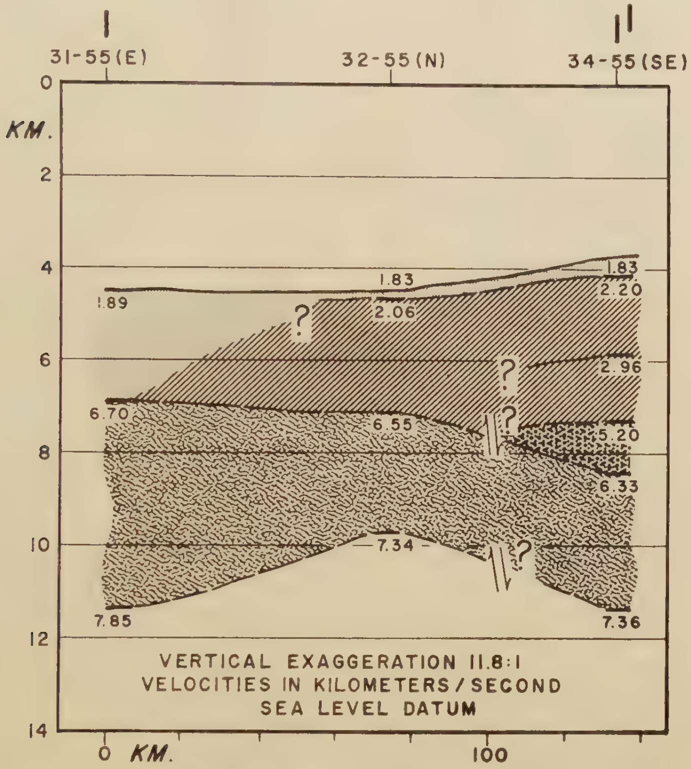

FIGURE 11.—DEEP-WATER SECTION: INTERIOR BASIN TO RIDGE
Structure section *I-I′* (Pl. 1)

The final section *I-I′* (Fig. 11) shows the transition from the nearly ocean-basin type of 31-55 through the slightly more complicated section of 32-55 to the typical ridge section of 34-55. Katz and Ewing's (1956) station 13 (A-164, not shown) lies about halfway between 32-55 and the ridge but is similar to 32-55, which indicates that the change to the ridge section is abrupt on its southwest side.

Gravity measurements were made by J. L. Worzel and his co-workers (1957) on the Blake Plateau and over the deep-water area. Free-air anomalies over the Blake Plateau section of the trough are as great as −47 milligals, compared with 0 to about −20 milligals in the area south of the trough. The thick section of 4.5 km/sec. in the trough compared with 6.2 km/sec. at the same depths to the south results in about this gravity difference using the density/P-wave velocity relationships recently compiled from various sources by Nafe and Drake (Personal communication). The ridge has free-air anomalies from about 0 to 8 milligals compared with about −30 to −50 milligals in surrounding near-by ocean-basin areas. Roughly a 40-milligal gravity excess can be found on the ridge by comparing a velocity section down to the base of the 5.4-km/sec. layer with an assumed ocean-basin section of 5 km of water, 1 km of sediment, and 5 km of 6.5 km/sec. above the M layer. The spread of the density-velocity relations allows considerable choice throughout this section without having an overwhelming effect on the anomaly. However, below the 5.4-km/sec. layer the layer thicknesses are so much greater that slight differences in density choice have a large effect on the computed gravity effect. Hence it seems useless now to speculate about the gravitational effects of the deeper structures.

Air-borne magnetometer observations were made over the area by M. Davidson. These have not been reduced at this writing, but some of their obvious qualitative features indicate that further magnetic observations will be valuable in continued study of this whole area.

GEOLOGIC HISTORY OF THE DEEP-WATER AREA: Even though additional profiles are needed both north and south of the ridge, there are adequate data for a coherent hypothesis about the structure and geologic history. In this section, we present a hypothesis about the structural history of the deep-water area and its relation to the Blake Plateau structures based on our results there.

The structure sections in the deep-water area suggest that three main divisions in the area can be treated as units: (1) the interior-basin type comprising profiles 31-55 and 32-55, (2) the ridge, comprising 33-55, 34-55, 35-55, parts of 5-56 and 6-56, and 7B of Katz and Ewing (1956), and (3) the slope comprising section *H-H'* and parts of 5-56 and 6-56.

(1) The interior-basin-area profiles are somewhat similar to typical deep-ocean-basin sections with low-velocity sediment layers and two higher-velocity layers. The thickness of low-velocity material, thought to be of unconsolidated sediments, is about 2.5 km, or considerably thicker than the 1 km or less of the oceanic section. The basaltic layer taken as 6.4–6.8 km/sec. is somewhat less thick than that of the ocean basins and is underlain by a velocity somewhat lower than the expected 8.0 km/sec. for the M layer, particularly at 32-55. The thicker sedimentary section there is reasonable because of its nearness to the continental slope. The 7.5- to 7.8-km/sec.-layer depths in this area and beneath the ridge suggest a deep-seated structural high just to the southwest of the ridge and parallel to it. Such a velocity at this depth might be due to interaction between the mantle and the basaltic layer which resulted in a material of intermediate composition, as suggested by Officer *et al.* (1957) for portions of the Caribbean. On this supposition, it is reasonable to account for structures restricted to the ridge as consequent to this deep-seated activity.

(2) The ridge structures differ from all others here by containing an appreciable thickness of 5.3 km/sec. overlying the basaltic layer (6.4–6.8 km/sec.) and the intermediate layer (7.3 km/sec.) discussed above. Velocity lines of the M layer, recorded on two profiles beneath the ridge, indicate that the M layer deepens there to the northwest; this is a wholly reasonable expectation. If we suppose it to be igneous rock, the 5.3-km/sec. layer, occurring near the apparent crest of the high in the intermediate layer (7.3 km/sec.), suggests further differentiation which might be consequent to that producing the intermediate layer. Its velocity is low for granite but agrees with oceanic volcanic rocks reported by Raitt *et al.* (1955) west of the Tonga trench.

The top of the 5.3-km/sec. layer under the ridge is at about the same depth as the top of the basaltic layer to the southwest but appreciably shoaler than basaltic velocities everywhere in the slope section. However, profile 6-56 on the southwest flank of the ridge shows a fault downthrown on the ridge side possibly by as much as 2 km. This indicates that the ridge area is one of relative subsidence. The indicated movement may not be the whole subsidence, and thus we suggest that the ridge may once have been as much as 2 km higher; another 2-km elevation would readily allow it to have been a shallow reef or a land area.

(3) The slope structures are distinguished principally by the great thickness of layers having 3.8- to 4.4-km/sec. velocity, by apparently unsystematic variations in the depth of the intermediate layer (7.3 km/sec.), by evidence of faulting on several profiles, and by the persistent occurrence of material with 6.0- to 6.24-km/sec. velocity, apparently in place of adjoining masses which have velocities of 6.34–6.7 km/sec.

rofiles 36-55, on the edge of the Blake Pla- u, and 5-56 and 6-56 contain evidence of lting; *i.e.*, they contain two velocity lines of tical slope but displaced in intercept on the e end of the profile. The faults of 36-55 and and the abrupt contrast between the ridge ion and structures in near-by 6-56 and 38-55 consistent with the notion that a fault- nded trough was formed roughly along the d of section *H-H′* (Fig. 10) before and during formation of the layers which have veloci- 3.8–4.5 km/sec. However, as discussed ve, the fault in 6-56 has the opposite throw; the ridge area has moved downward per- as much or more than 2 km relative to the ining depression.

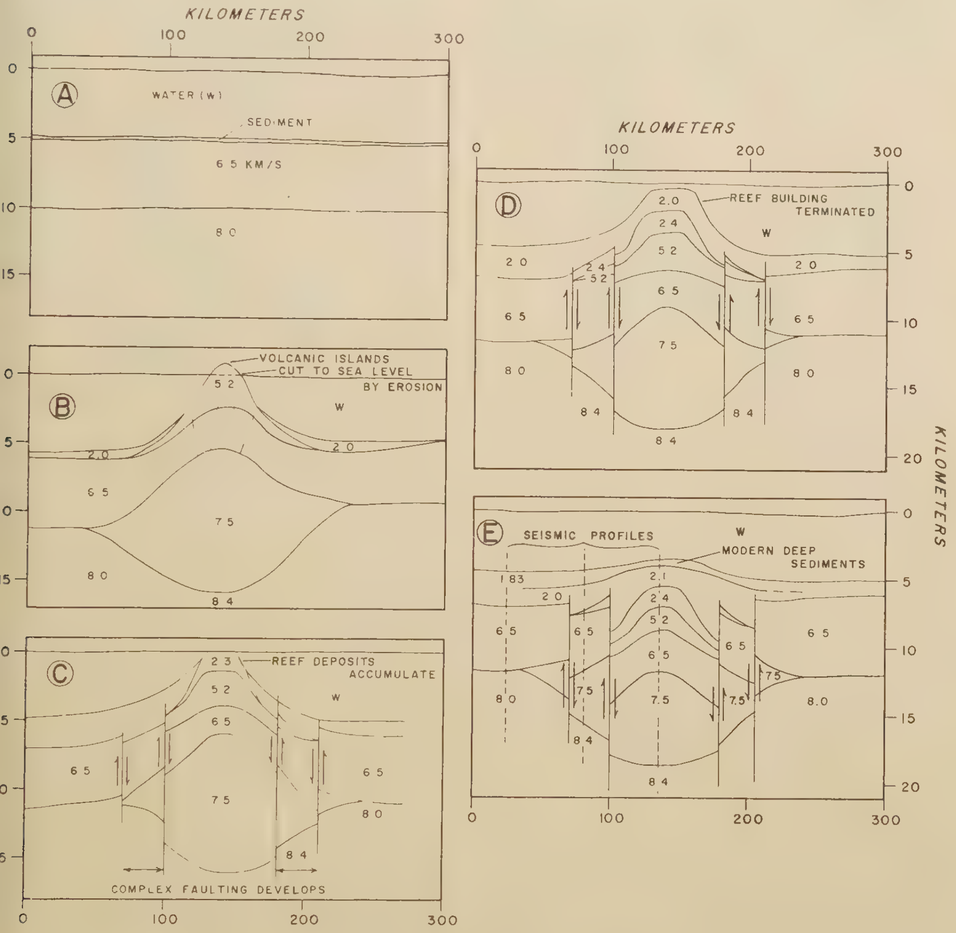
KILOMETERS
0
100
200
300
A
WATER (W)
SEDIMENT
6.5 KM/S
8.0
B
VOLCANIC ISLANDS
CUT TO SEA LEVEL BY EROSION
5.2
W
2.0
6.5
7.5
8.0
8.4
C
2.3
REEF DEPOSITS ACCUMULATE
5.2
6.5
7.5
8.0
8.4
COMPLEX FAULTING DEVELOPS
D
2.0
REEF BUILDING TERMINATED
2.4
5.2
6.5
7.5
8.0
8.4
E
SEISMIC PROFILES
MODERN DEEP SEDIMENTS
1.83
2.1
2.4
5.2
6.5
7.5
8.0
8.4
5
10
15
20

Figure 12.—Speculative History of the Ridge

Section is southwest–northeast across ridge.

light of the facts discussed above we sug- the following speculative hypothesis about the geologic history of the trough and ridge area. The history of the ridge according to this hypothesis is sketched in Figure 12. The horizontal dimensions of the structures are outlined in Figure 13.

If we suppose that all velocities from 1.7 to 4.5 km/sec. represent sediments, then the depths and thicknesses of the corresponding layers can be accounted for by the following sequence: (1) normal ocean structure (Fig. 12*A*); (2) formation of the material of 7.5-km/sec. velocity from interaction between the mantle and the basaltic layer, and accompanying formation of the lower-velocity 5.2 km/sec. above the basaltic layer by extrusion and separation of the lighter materials; during this period the ridge structures may have formed a continuous land area, or a chain of islands and reefs (Fig. 12*B*); (3) downwarping and faulting of the irregular area where the trough structures of the slope are found (outlined in Figure 13), accompanied by deposition of material, the velocity of which is now 3.8–4.5 km/sec; (4) deposition of 2.1- 2.4-km/sec. material accompanied by downward movement of the ridge with accommodation along bordering fault zones (Fig. 12*C*, *D*); (5) downward movement of the whole area relative to the continent accompanied by deposition of the unconsolidated sediments forming the top layer (Fig. 12*E*).

The Blake Plateau structures are consistent with this hypothesis, if one imagines that the considerable thickness of material having velocities of 4.5 km/sec. and less at and north of profiles 6-55 forms a southwesterly extension of the trough interpreted to occupy the slope section. There appear to be far greater thicknesses of material with velocities in the 5.2–5.8 range beneath the Blake Plateau than on the ridge. Nafe and Hennion (In preparation) present evidence that the shallow 6.7-km/sec. layer at 1A-56, 1B-56, and 1C-56 together with the overlying 5.2- to 5.8-km/sec. layer are part of a structure that has irregular relief bu trends beneath the Blake Plateau toward Cap Canaveral. Nafe and Hennion were able to ma the 5.2- to 5.8-km/sec. layer extensively sout of this trend. It is tempting to suppose that this 5.2- to 5.5-km/sec. layer is found only on this trend and south of it. In any event there is no other evidence for such a velocity north of 1A-56 except on the ridge.

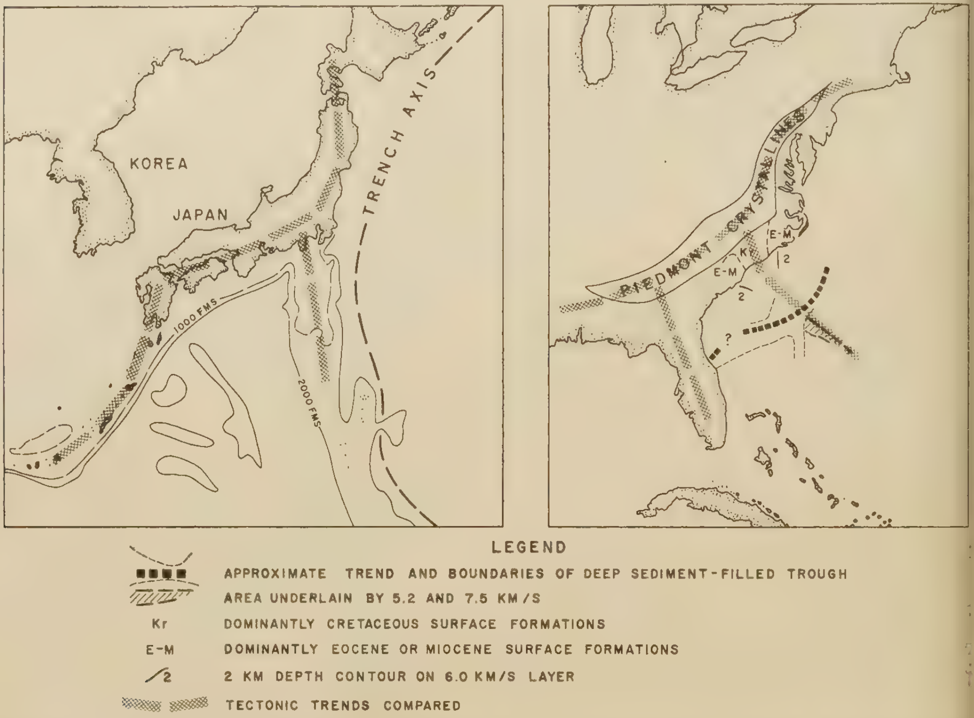
KOREA
JAPAN
TRENCH AXIS
1000 FMS
2000 FMS
PIEDMONT CRYSTALLINES
E-M
Kr
2
E-M
2
?
LEGEND
APPROXIMATE TREND AND BOUNDARIES OF DEEP SEDIMENT-FILLED TROUGH
AREA UNDERLAIN BY 5.2 AND 7.5 KM/S
Kr DOMINANTLY CRETACEOUS SURFACE FORMATIONS
E-M DOMINANTLY EOCENE OR MIOCENE SURFACE FORMATIONS
2 2 KM DEPTH CONTOUR ON 6.0 KM/S LAYER
TECTONIC TRENDS COMPARED

FIGURE 13.—COMPARISON OF PIEDMONT, COASTAL PLAIN, AND OCEANIC STRUCTURE WITH WESTERN PACIFIC ISLAND ARCS

Relationship of Adjoining Structures

Relation to the ocean basins.—The nearest seismic-refraction profiles in North America basin are those of Katz and Ewing (1956), one of which is reproduced here in part (Fig. 9, profile 7B). They are essentially typical ocean-basin profiles with a thin basaltic crust overlain by one or two thin layers of low-velocity sediments. A profound change has occurred between them and the easternmost profiles in deep water here. Assuming the ridge to be an ancient volcanic-island structure, by analogy with modern structures one might expect to find evidence of an ancient foredeep in the deeper water northeast of the ridge. The struc-

e of this area must be known to understand
region as a whole. Similarly, the apparent
ension of the topographic ridge toward
uthera (Pl. 1) and the structure of the in-
ior basin west of it must be better known.

Relation to other continental slope structures.—
ake *et al.* (1957) presented an interpretation
the findings of the Lamont Geological Ob-
vatory group beneath the continental shelf
l slope north of Cape Hatteras to the Grand
nks. They found two roughly parallel sedi-
nt-filled trenches of probable Mesozoic age
ralleling the coast. Possibly the trench of the
pe section in this area is continuous with the
stern one to the north. Again, additional
smic observations should provide the answer.

Relation to continental structures.—The work
Nafe and Hennion (In preparation) on the
ıthern part of the Blake Plateau indicates
ıt the layers of 5.2–5.6 km/sec. and 4.2–4.5
ı/sec. are of Cretaceous age; similarly Upper
etaceous age is indicated for the 2.5-km/sec.
er in the depth relations between the outer-
st profiles on the shelf off Jacksonville and
ofile 29-55 on the Blake Plateau. This implies
etaceous age for the layers 2.8 through 4.5
ı/sec. throughout the area. This further im-
es Cretaceous as the age of the sediment-
ed trough that we have interpreted above as
tting across the northern Blake Plateau and
ng the slope section. This would imply a
e-Upper Cretaceous period of tectonic ac-
ity as the time of formation of the deep-
ıter ridge and the positive feature from pro-
1A-56 south.

The Cape Fear Arch, a positive feature, is a
sement structure which has been traced
utheast from the Piedmont nearly to the edge
the continental shelf. It seems unlikely that
ends abruptly there, and from a very early
ıge in the present study we supposed that the
ep-water ridge might be an extension of it.
e have been unable to make observations in
e obvious gap between the shelf and the
00-fm (2745 m) contour here, but some facts
pport such an interpretation: (1) The ridge
s the same trend as the arch and is approxi-
ately aligned with it. (2) The ridge is the
rface expression of a deep-lying structure
ıceable to activity of the mantle, which has
e same trend. (3) In several profiles of the
pe area there are thin and variable thick-
sses of 6.0- to 6.2-km/sec. velocity. Supposing
is material to be granitic, it seems likely that
re is the edge of continental granitic ma-
rial. Hence the Cape Fear Arch may persist
some form this far from the shelf.

In any event the gap in seismic results between the shelf and 1500 fathoms (2745 m) must be an area of structural adjustment. There are many superficial suggestions of complicated structure in the known topography here, but the topographic picture is not detailed enough to further our understanding at present.

Comparison with Other Regions

The tectonic lineaments suggested by this line of speculation are similar to those of the western Pacific. Thus, the Appalachian Piedmont of late Paleozoic time may be compared with the modern Japanese archipelago, the Cape Fear Arch and ridge structure with the Bonin-Marianas arc, and the Peninsular Arch of Florida described by Applin (1951) with the Ryukyu island chain extending southwestward from Japan (Fig. 13). This comparison rests primarily on the similarity between western Pacific topography and southeastern United States structures. The Cape Fear Arch trends southward from a sharp northward bend in the Piedmont, as do the Honshu-Mariana ridges from a similar northward bend of Honshu; the Peninsular Arch trends sharply away from the Piedmont much as the Ryukyu arc does from Japan. However, there is another point of similarity in the relative ages of the component parts of the two systems: the Japanese and Ryukyu arc structures are thought to be mid-Mesozoic and the Honshu-Mariana ridges Cretaceous to Tertiary (Hess, 1948); Kay (1951, p. 57–60) favors a mid-Paleozoic age for the development of Piedmont structures, and structures on the seaward trend from the Cape Fear Arch appear to have been formed much more recently, possibly in late Mesozoic. The American structures are older than those of the western Pacific, and seismic activity in the former is much less than the latter, thus eliminating present-day dynamics as a means of comparison. Comparative studies in the two regions including seismic and other geophysical exploration techniques are needed for testing further any ideas of tectonic similarity.

The conjectured Cretaceous aspect of the plateau and slope region is strikingly similar to modern land forms in the Bahamas; the plateau-slope trench has a probable shape (not yet completely defined) somewhat similar to the Tongue of the Ocean or Exuma Sound. The latter comparison is consistent with what is known of the Bahamas, where great thicknesses of limestone have been found by drilling, with our hypothesis about the region as a whole, and with modern

Blake Plateau topography. For example, imagine a Cretaceous aspect of the plateau similar to the modern Bahamas. Then during the later history of the trough erosional action, possibly in part by the Gulf Stream and in part by subaerial processes, may have planed the central portion of the Blake Plateau to nearly its present smoothness near sea level. Subsequent subsidence and continued erosion by Gulf Stream-driven currents might then produce the modern aspect of the plateau. Possibly the pattern of Gulf Stream flow may have been deflected easterly and southerly by the ridge when it was partially emerged or at least much shoaler than now. In this event the latter stage of purely submarine erosion was probably most marked to the south and progressed northerly across the plateau as the submarine topography permitted the Gulf Stream thus to alter its course. Such an account of the history of the region would imply that this erosional process continues. This is consistent with what is known of the area and the behavior of the Gulf Stream as far north as Cape Hatteras.

These large-scale comparisons contain obvious pitfalls. However, we have become increasingly convinced in the course of this study that much new understanding of crustal tectonics may be found by comparative study of smaller and probably simpler oceanic structures, such as individual seamounts and their environs, connected chains of seamounts, and relatively minor ridge-like topographic features such as that of the present study. Just as the studies of the Caribbean Island arcs by M. Ewing and Worzel (1954), Officer *et al.* (1957), and J. Ewing *et al.* (1957), and the studies of the Bermuda area (Officer *et al.*, 1952) have suggested large-scale interactions between crust and mantle, it appears likely that lesser oceanic topographic features which probably have simpler structures may be the key to understanding the elements of the larger structures and the antecedent geodynamics.

REFERENCES CITED

Applin, P. L., 1951, Preliminary report on buried pre-Mesozoic rocks in Florida and adjacent States: U. S. Geol. Survey Circ. 91, 28 p.

Applin, P. L., and Applin, E. R., 1944, Regional subsurface stratigraphy and structure of Florida and southern Georgia: Am. Assoc. Petroleum Geologists Bull., v. 28, p. 1673–1753

Bonini, W. E., 1955, Seismic-refraction studies of geologic structure in North Carolina and South Carolina (Abstract): Geol. Soc. America Bull., v. 66, p. 1552

Drake, C. L., Sutton, G. H., and Ewing, M., 1957, Continental margins and geosynclines, east coast of North America north of Cape Hatteras (Abstract): Geol. Soc. America Bull., v. 68, p. 1718

Ewing, J. I., Officer, C. B., Johnson, H. R., and Edwards, R. S., 1957, Geophysical investigations in the Eastern Caribbean and Trinidad Shelf, Tobago trough, Barbados Ridge, Atlantic Ocean: Geol. Soc. America Bull., v. 68, p. 897–912

Ewing, M., and Press, F., 1955, Geophysical contrasts between continents and ocean basins, p. 1–6 *in* Poldervaart, Arie, *Editor*, Crust of the Earth: Geol. Soc. America Special Paper 62, 762 p.

Ewing, M., and Worzel, J. L., 1954, Gravity anomalies and structure of the West Indies, Parts I and II: Geol. Soc. America Bull., v. 65, p. 165–174, 195–200

Ewing, M., Crary, A. P., and Rutherford, H. W., 1937, Geophysical investigations in the emerged and submerged Atlantic Coastal Plain, Part I: Methods and results: Geol. Soc. America Bull., v. 48, p. 753–802

Ewing, M., Woollard, G. P., and Vine, A. C., 1939, Geophysical investigations in the emerged and submerged Atlantic Coastal Plain, Part III: Barnegat Bay, New Jersey, section: Geol. Soc. America Bull., v. 50, p. 257–296

—— 1940, Geophysical investigations in the emerged and submerged Atlantic Coastal Plain, Part IV: Cape May, New Jersey, section: Geol. Soc. America Bull., v. 51, p. 1821–1840

Ewing, M., Worzel, J. L., and Shurbet, G. L., 1957, Gravity observations at sea in U. S. submarines BARRACUDA, TUSK, CONGER, ARGONAUT, and MEDREGAL, p. 50–115 *in* Jubilee Volume in honor of F. A. Vening Meinesz: The Hague, Royal Netherlands Geol. and Min. Soc.

Ewing, M., Worzel, J. L., Steenland, N. C., and Press, F., 1950, Geophysical investigations in the emerged and submerged Atlantic Coastal Plain, Part V: Woods Hole, New York, and Cape May section: Geol. Soc. America Bull., v. 61, p. 877–892

Hersey, J. B., and Ewing, M., 1949, Seismic reflections from beneath the ocean floor: Am. Geophys. Union Trans., v. 30, p. 5–14

Hersey, J. B., and Rutstein, M., 1958, A reconnaissance survey of the Oriente Deep with a precision echo sounder: Geol. Soc. America Bull., v. 69, p. 1297–1304

Hess, H. H., 1948, Major structural features of the western North Pacific; an interpretation of H. O. 5485, bathymetric chart, Korea to New Guinea: Geol. Soc. America Bull., v. 59, p. 417–445

Katz, S., and Ewing, M., 1956, Seismic-refraction measurements in the Atlantic Ocean, Part VII: Atlantic Ocean Basin, west of Bermuda: Geol. Soc. America Bull., v. 67, p. 475–510

Kay, Marshall, 1951, North American geosynclines: Geol. Soc. America Mem. 48, 143 p.

King, P. B., 1950, Tectonic framework of southeastern United States: Am. Assoc. Petroleum Geologists Bull., v. 34, p. 635–671

Knott, S. T., and Hersey, J. B., 1956, Interpretation of high-resolution echo sounding techniques and their use in bathymetry, marine geophysics, and biology: Deep Sea Research, v. 4, p. 36–44

ngwell, C. R., *et al.*, 1944, Tectonic map of the United States: Am. Assoc. Petroleum Geologists

ansfield, W. C., 1936, Some deep wells near the Atlantic coast in Virginia and the Carolinas: U. S. Geol. Survey Prof. Paper 186-I, p. 159–161

yer, R. P., 1955, Seismic studies of offshore geologic structure between Charleston, South Carolina, and Cape Fear, North Carolina (Abstract): Geol. Soc. America Bull., v. 66, p. 1597

icer, C. B., 1955, A deep-sea seismic reflection profile: Geophysics, v. 20, p. 270–282

icer, C. B., and Ewing, M., 1954, Geophysical investigations in the emerged and submerged Atlantic Coastal Plain, Part VII: Continental shelf, continental slope, and continental rise south of Nova Scotia: Geol. Soc. America Bull., v. 65, p. 653–670

icer, C. B., and Wuenschel, P. C., 1951, Reduction of deep-sea refraction data: Palisades, N. Y., Lamont Geol. Observatory Tech. Rept. 1, 12 p.

icer, C. B., Ewing, M., and Wuenschel, P. C., 1952, Seismic refraction measurements in the Atlantic Ocean, Part IV: Bermuda, Bermuda Rise, and Nares Basin: Geol. Soc. America Bull., v. 63, p. 777–808

icer, C. B., Ewing, J. I., Edwards, R. S., and Johnson, H. R., 1957, Geophysical investigations in the eastern Caribbean: Venezuelan basin, Antilles island arc, and Puerto Rico trench: Geol. Soc. America Bull., v. 68, p. 359–378

ver, J. E., and Drake, C. L., 1951, Geophysical investigations in the emerged and submerged Atlantic Coastal Plain, Part VI: The Long Island area: Geol. Soc. America Bull., v. 62, p. 1287–1296

itt, R. W., Fisher, R. L., and Mason, R. G., 1955, Tonga Trench, p. 237–254 *in* Poldervaart, Arie, *Editor*, Crust of the earth: Geol. Soc. America Special Paper 62, 762 p.

hards, H. G., 1945, Subsurface stratigraphy of Atlantic Coastal Plain between New Jersey and Georgia: Am. Assoc. Petroleum Geologists Bull., v. 29, p. 885–955

els, D. C., 1950, Geophysical data in the North Carolina Coastal Plain: Geophysics, v. 15, p. 409–425

ngler, W. B., 1950, Subsurface geology of Atlantic Coastal Plain of North Carolina: Am. Assoc. Petroleum Geologists Bull., v. 34, p. 100–132

phenson, L. W., 1926, Major features in the geology of the Atlantic and Gulf coastal plain: Wash. Acad. Sci. Jour., v. 16, p. 460–480

– 1928, Major marine transgressions and regressions and structural features of the Gulf Coastal Plain: Am. Jour. Sci., ser. 5, v. 16, p. 281–298

ton, G. H., and Bentley, C. R., 1953, Topographic correction curves: Palisades, N. Y., Lamont Geol. Observatory Tech. Rept. 3, 5 p.

stoy, I., 1951, Submarine topography in the North Atlantic: Geol. Soc. America Bull., v. 62, p. 440–451

S. Hydrographic Office, 1948, North America, East Coast and West Indies: Halifax to Hispaniola including the Bahamas and Greater Antilles: H. O. Chart No. 1411

Worzel, J. L., and Ewing, M., 1948, Explosion sounds in shallow water, p. 1–53 *in* Ewing, M., Worzel, J. L., and Pekeris, C. L., Propagation of sound in the ocean: Geol. Soc. America Mem. 27, 205 p.

Woods Hole Oceanographic Institution, Woods Hole, Mass.; Woods Hole Oceanographic Institution, Woods Hole, Mass.; General Electric Company, Syracuse, N. Y.; University of Rhode Island, Kingston, R. I.

Manuscript Received by the Secretary of the Society, April 24, 1958

Woods Hole Oceanographic Institution Contribution No. 973

Appendix: Discussion of Data

I. *Continental Shelf—Plate 2A*

Profiles 3-54 to 5-54 and 10-54 to 15-54

(a) Atlantis 196—Bear 89

Bear acted throughout as receiving ship, while Atlantis closed and opened range, using Bear as center. The velocity and layer-thickness determinations based on these data are reasonable interpretations of the profiles obtained and will not be discussed in detail. Comparatively small charges (up to 20 pounds) were used, the profiles were short, and the depth of penetration modest.

Profiles 5-55 and 11-55 to 18-55

(b) Vema 6—Bear 113

With the exception of the profiles discussed in more detail below, all the reversed data are in good agreement. Velocities that range from 1.68 to 1.92 km/sec. (indicative of sediments) are found on almost all the travel-time plots as second and third arrivals and at short range as first arrivals.

Profile 17-55:

All the lower velocities are relatively well established. The 5.35 km/sec. horizon has few points because of the relatively wide shot spacing in this range. The 6.06 km/sec. horizon occurs as strong first arrivals over the last three seconds on Vema and last 4.5 seconds on Bear.

Profile 18-55:

Vema receiving end of this profile indicates a velocity of 1.69 km/sec. which is apparently masked by 2.25-km/sec. arrivals on Bear. It has been assumed present on Bear from Vema evidence and an equivalent velocity on Profile 17. Vema has only slight substantiation of the 4.36-km/sec. velocity found on Bear. Some evidence suggests a horizon of velocity 5.55 km/sec. on Bear only.

II. *Blake Plateau—Plate 2B*

Profiles 9-54, 6-55, 29-55, 30-55, 36-55; 1A-56, 1B-56, 1C-56, 2-56, and 3-56

(a) Atlantis 196—Bear 89

Profile 9-54: The velocities determined on this profile are well established by the data. There is no refraction evidence for any horizon of velocity higher than 4.11 km/sec., but the profile is short, and 20 pounds was the largest charge used.

(b) Vema 6—Bear 113

Profile 6-55: These velocities are well established. There is no evidence for any horizon of velocity higher than 4.54 km/sec. This is a short profile with 20-pound maximum charge.

(c) Atlantis 213—Bear 113 (Profiles 29-55, 30-55, and 36-55)

Profile 29-55: This profile station was made before the structure of the area was known. The travel-time data suggest a complicated structural problem. The determination of the 3.8-km/sec. velocity is excellent. On the southeast end (Atlantis), there is strong evidence for a layer of 4.81 km/sec. velocity which overlies one of 6.18 km/sec. A few arrivals on the northwest (Bear) end of the profile substantiate this 4.81-km/sec. layer. A horizon with compressional velocity of greater than 4.68 km/sec. is suggested but not established by some arrivals received at distances greater than 9 seconds on the Bear end.

Profile 30-55: The determination of 4.30- and 4.99-km/sec. horizons is straightforward. A few poor arrivals at distances greater than 15 seconds on Atlantis end indicate a higher-velocity horizon but do not determine it. On Bear end there is evidence (indicated by the dashed line) for a high-velocity horizon. This can be interpreted as 6.9 km/sec., at 8.5 km below sea level or as high as 7.2 km/sec., 8.8 km below sea level. Possibly the 5.5-km/sec. horizon found throughout this region of the Blake Plateau is present but masked by the Bear high velocity and by poor data on the reverse.

Profile 36-55: The 3.61-km/sec. horizon is well established. The lines having approximately 4.5 km/sec. indicate that it is deeper at the northwest end than at the southeast end, but that in between it is depressed still farther, possibly by local faulting, over about 12 km. The depression amounts to about 0.5 km relative to the southeast end (Fig. 7). An excellent line with an apparent velocity of 7.33 km/sec. is found on the Bear profile (northwest); no data on Atlantis end.

(d) Atlantis 223—Bear 140 (Profiles 1A-56 1B-56, 1C-56, 2-56, and 3-56)

Refraction arrivals on Profiles 1A-56, 1B-56, 1C-56, and 3-56 substantiate the reflection evidence for sedimentary horizons varying in velocity from 1.6 to 1.9 km/sec. In computing velocities for the profiles having no refraction evidence for these sedimentary horizons a value of 1.83 km/sec. obtained from reflection data has been used.

Profiles 1A-56, 1B-56, and 1C-56: These three unreversed profiles are from the same general vicinity (Pl. 1). Their geographic direction is approximately north-south. The receiving locations for 1A-56 and 1C-56 are indicated as north (N); the shooting-ship track is south in each case. Profile 1B-56 is indicated as northwest (NW) since the shot line is northwest of the receiving-ship position. All show approximately the same velocity horizons through 5.2–5.5 km/sec. Evidence for a higher velocity can be found on all three. The dashed line on 1A shows the highest velocity that can be determined, 6.7 km/sec. at 6.9 km below sea level. The lowest value possible from these data is 6.5 km/sec., 6.33 km below sea level. On profile 1B the highest determination is 6.6 km/sec., 6.4 km deep. The lowest determination possible is 6.3 km/sec., at 5.73 km depth. Profile 1C shows 5.85 km/sec. at a depth of 6.8 km. No significantly different alternative velocity can be measured.

Profile 2-56: This was unreversed over the range 38-55 seconds on Bear (east) end. The 3.84-km/sec. layer is determined on first arrivals on Atlantis end (west) only. Comparable observations were taken on Bear so that this layer must be regarded as masked there. The 4.62-km/sec. horizon is well established on both ends of the profile. The 6.39-km/sec. horizon is strongly shown on both ends. On the Atlantis end the 4.62-km/sec. arrivals became undetectable at about 17 seconds water-travel time, although they should normally have continued as the first arrival until about 25 seconds. In this interval the 6.39-km/sec. arrival was evident. The same range interval for Bear is too sparsely shot to make this effect evident. However, if this gap were due to inadequate gain or some other shortcoming in the observations arrivals of intermediate velocity might have been found. We decided on the interpretation shown, since (1) no such arrivals were observed here, and (2) no such velocities were found either on near-by 29-55 or 36-55. A very well-defined 8.04-km/sec. horizon is indicated by the unreversed Atlantis data in the range 50-80 km.

Profile 3-56: Velocities of 4.36 and 4.96 km/sec are determinable in the refraction data. Although data were recorded beyond the range indicated in the 4.96-km/sec. region, the records are so poor that no higher velocities can be determined.

III. *Outer Continental Slope and Ridge Area—Plate 2C*

Profiles 31-55 to 35-55, and 37-55 to 39-55; 4-56 to 8-56

(a) Atlantis 213—Bear 113
Atlantis 223—Bear 140

On profile 37-55 there is refraction evidence for the 1.83-km/sec. horizon. On all other stations in this general region, reflection evidence has been used for the 1.83-km/sec. velocity.

Profiles 31-55 and 32-55 are more like oceanic structure than are the stations to the north and east. There is strong second-arrival refraction evidence on Bear (north) end of 32-55 for 2.06 km/sec velocity. A few second arrivals on Atlantis (south) end indicate the same velocity but are not adequate to establish it. Profile 31-55 shows weak arrivals

licating a velocity in the region of 1.89 km/sec.,
t these data are not adequate for deriving pre-
e values. Velocities of 6.70 km/sec. (31-55) and
5 km/sec. (32-55) are relatively well determined.
profile 31-55 6.70 km/sec. overlies 7.85 km/sec.
ofile 32-55 shows 7.34 km/sec. as its highest
ocity, which is equivalent in depth (10–11 km)
the 7.5 km/sec. layer found on adjacent profiles.

Profile 33-55: There is evidence here for a 2.44-
/sec. layer above one of 5.67 km/sec. which
pears only on Atlantis (northwest) but has
n assumed present across the profile and proba-
masked on Bear by the 8.1-km/sec. layer which
s not show on Atlantis.

Profile 34-55: There is fair evidence for layers
2.2 km/sec. and 2.96 km/sec., followed by 5.20
/sec. and a higher-velocity layer of 6.33 km/sec.
e 7.36-km/sec. layer is observed on Bear
utheast) but is not apparent on Atlantis
rthwest).

Profile 35-55: There is fair evidence for 2.17-km/
and 2.57-km/sec. layers above 5.24 km/sec.
e Bear (east) travel-time curve for the 5.24
/sec. is sigmoid with a maximum excursion of
proximately 0.04 sec. The Atlantis (west)
vel-time plot indicates horizons of 6.69 km/sec.
d 7.20 km/sec. Bear records show 6.69 km/sec.
akly. Weak evidence for 7.20 km/sec. on Bear
enabled computation of the thickness on this
of the profile. Also, a few arrivals occurring
later events on the refraction trace indicate the
sible presence of 8-km/sec. velocity. Since this
pears as a first arrival at the very end of the
vel-time plot, possibly a longer profile would
ve established the presence of this horizon.

Profile 37-55: Velocity lines 2.77, 3.89, and 6.1
/sec. are shown. A velocity of 7.42 km/sec. is
l founded on good evidence from Atlantis
st), and although it appears on the Bear travel-
e plot in a region of rather poor records, it can
identified there.

Profile 38-55: This profile has second-arrival evi-
ce for a layer of 2.38 km/sec. velocity, over-
g one of 3.98 km/sec. The 6.36-km/sec. layer
vell supported by arrivals on Bear (southwest)
is weak on the Atlantis (northeast) travel-
e plot. The 7.73-km/sec. layer is well estab-
ed on Bear, but there is scatter of about 0.05
on the Atlantis travel-time plot.

Profile 39-55: There is good second-arrival evi-
ce, on Bear (south), for a 2.64-km/sec. horizon.
et of widely spaced (because of shot spacing)
ond and third arrivals on Atlantis (north)
es uncertain indications of this velocity. The
-km/sec. layer is based on first arrivals on the
ar end of the profile, but there is only second-
val evidence on Atlantis, mainly because of
of shots in the critical range. The 6.45- and 7.12-km/sec. layers are evident on the two ends of the profiles. The 7.95-km/sec. horizon occurs only on Bear, at the end of the profile, and is indicated as very deep (21 km). A computation that assumes the presence of this horizon at the Atlantis end gives a tentative depth of 20 km.

(b) Atlantis 223—Bear 140 (Profiles 4-56 to 8-56)

Profile 4-56: Reflection data indicate the 1.68-km/sec. velocity. The 2.43-km/sec. has strong refraction arrivals on both ends of the profile. We have assumed a masked 3.75-km/sec. velocity, indicated by dashed lines on the travel-time plot, from good evidence for such a layer on adjacent profiles. The higher velocities, 4.46, 6.7, and 7.63 km/sec., are very well established by Bear (northeast) data but are less evident on Atlantis (southwest), showing some scatter because of low recording gain and slow paper speed throughout the station. The 7.63-km/sec. horizon does not appear on Atlantis.

Profile 5-56: This profile was reversed but was located over such complicated structure that it could not be so computed. Hence the data have been interpreted and computed as two unreversed profiles. The 1.83-km/sec. layer has been assumed present on both ends. The 2.26-km/sec. (east) and 2.24-km/sec. (west) horizons are measured on second-arrival evidence. Apparent velocities of 5.37 and 7.16 km/sec. are measured on the east end, with indicated fault in the 7.16-km/sec. layer. On the west the apparent deeper velocities are 3.94, 6.51, 7.31, and 8.60 km/sec.

Profile 6-56: This is a reversed profile which has similar velocity lines for first arrivals. However, two low-velocity horizons (apparent velocity 2.20 and 2.78 km/sec.) were measured by refraction data on the Atlantis (east) end but only from reflection data on the Bear (west) end (Table 4). The resulting apparent velocities agree well. However, we lack proper data for computing velocities, slopes, and thicknesses for these layers. Hence we have preferred to treat the two ends separately as unreversed profiles. The 7.55-km/sec. line on the west end shows a well-defined fault displacement.

Profile 7-56: All the velocities shown on the travel-time plot are well established.

Profile 8-56: The 2.35-km/sec. horizon is established by second arrivals on both Bear (south) and Atlantis (north), and by good sub-bottom reflections on Bear. The 3.71-km/sec. layer occurs on Atlantis as first arrivals in the range 9–10 sec. There are no refraction arrivals in the range on Bear, but the layer has been assumed to exist across the station area from Atlantis data and evidence on adjacent profiles. The 6.24-, 7.10-, and 8.43-km/sec. horizons are well determined on both ends.

Contribution No. 974

Särtryck ur Tellus nr 2, 1959

The Moving Flame Experiment

By MELVIN E. STERN, Woods Hole Oceanographic Institution*

(Manuscript received May 13, 1958)

Abstract

When a flame is rotated around the outside bottom rim of a cylindrical pan of water initially at rest, D. Fultz has observed that the fluid acquires a net vertical component of angular momentum opposite to the rotation of the heat source. We have repeated this experiment in a cylindrical annulus in order to restrict the radial motions and have found that the same phenomenon occurs. Using a simple model based on the latter experiment we investigate the mechanism by which a fluid can acquire and maintain this momentum, considering that friction is the only force which can exert a net torque about the vertical.

The effects of the heat source are replaced by a forced temperature field which has sinusoidal variations in the circumferential direction and which rotates about the vertical axis at a constant rate. The correlation between vertical and horizontal velocity components in the equilibrium state has been computed from the linearized two-dimensional vorticity equation. It is shown that when the viscosity is small or when the speed of the heat source is large there is a convergence of horizontal momentum towards the center of the channel which is balanced by the viscous stress of the induced mean motion. The total momentum of the fluid is computed from the conservation principle and is found to vary inversely as the square root of the molecular viscosity and inversely as the 5/2 power of the speed of the heat source.

. Introduction

In a recent unpublished report FULTZ (1956) escribes an experiment in which a flame is otated around the outside bottom rim of a ylindrical vessel filled with water. The exeriment was stimulated by a question posed y Lord Kelvin in 1892 as to whether or ot the fluid would acquire a net spin about vertical axis as was originally suggested by IALLEY (1686). Fultz concludes that "... alhough no quantitative measurements have een made in the interior [of the fluid] it is ractically certain that in the course of estabshing the motion from rest the total absolute ngular momentum of the fluid increases in ie anti-flame sense. Thus the mechanisms involved must give rise to net torques during the establishment phase." We have reproduced this qualitative experiment using a central core to confine the motion to a cylindrical annulus whose radial width was small enough to be completely covered by the bunsen flame and large compared to the vertical depth (2 cm) of the water. In this manner we were able to reduce the radial convection which was present in the previously cited experiment and to determine whether the same phenomenon would occur in a flow which was approximately two-dimensional. When the flame was rotated at 4 r.p.m. at a mean radius of 15 cm we generally observed that the dust particles in the water performed small horizontal oscillations along a concentric circle in response to the alternating solenoidal field induced by the rotating heat source. However, the mean position of the

---

* This work was performed under the auspices of the ffice of Naval Research and is Contribution No. 74) from the Woods Hole Oceanographic Institution.

particles changed slowly with a rotation which was opposite to that of the flame. Marked deviations from this flow pattern were also observed, from an impulsive motion of the particles, to a regular rotary motion with imperceptible oscillatory motion, to no net motion when the heating reached a stage where very intense vertical convection occurred. However, by observing the net displacement of paper markers placed on the surface and from permanganate tracers in the interior we have concluded that an average anti-flame rotation does exist in this geometry, whose order of magnitude was 0.1 % to 1.0 % of the rotation rate of the heat source, up to the point where boiling-like motions occur. This qualitative experiment encourages us to look at simple two-dimensional models in order to explain the following question. Considering that friction is the only force which can exert a net torque about the vertical axis, how can the fluid acquire and maintain a net angular momentum, and what determines its direction?

II. The Theoretical Model

The rectangular channel shown in Fig. 1 represents an approximation to the geometry of a cylindrical annulus of large mean radius. The x-axis corresponds to the circumferential distance in the circular annulus, and by requiring that the motions be periodic in x we shall achieve a correspondence in the lateral boundary conditions. The width of the channel in the y-direction, corresponding to the radial width of the annulus, is taken to be large compared with the vertical depth H. In addition we consider a distribution of heat sources and sinks which moves in the $-x$-direction with uniform speed U, and which forces a density distribution which is a sinusoidal function of x and time t, but which is independent of y and z. The average horizontal momentum of the fluid in the equilibrium state will be determined, and this will correspond to the vertical component of angular momentum in the cylindrical geometry. Regarding the assumed forced density distribution it should be mentioned that in the experiments the temperature field does have variations of static stability and moreover cannot be divorced from the convective motions. However, the thermodynamics are secondary to the question at hand, since we should like to know how any thermal field can produce a net motion of the liquid perpendicular to the force of gravity. The model chosen is perhaps the simplest one to elucidate this phenomenon, and it does have a superficial resemblance to the differential temperature field produced by a moving flame.

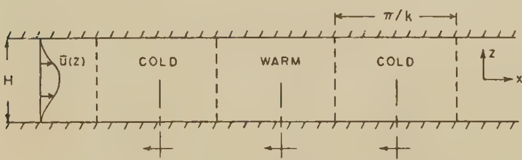

Fig. 1. Schematic diagram of the theoretical model. The hypothesized heat sources and sinks move with speed U producing a neutrally stable temperature or density perturbation (ϱ'). The sinusoidal variations of density with x and time induce a mean velocity in the fluid whose equilibrium profile $\bar{u}(z)$ is to be computed.

If the Navier-Stokes equations are accepted, then the only way in which an average horizontal motion can be maintained in Fig. 1 is through a transport of momentum by the vertical (w')and horizontal (u') velocity perturbations which are produced by the alternating solenoidal field. In the equilibrium state, which will be considered first, the vertical flux of horizontal momentum

$$\nu \frac{d\bar{u}(z)}{dz} - \overline{w'u'} \tag{1}$$

must be constant, where ν is the viscosity and the single bar indicates an average value over a horizontal plane or over one wavelength. In this approximate statement of the momentum principle, as well as in what follows, we have used the Boussinesq approximation and neglected density variations except for the buoyancy force. Since $\bar{u}$ and $\overline{w'u'}$ are zero at the top and bottom of the channel, a vertical integration of (1), denoted by a second bar, gives the value of the constant as $-\overline{\overline{w'u'}}$. Consequently the total momentum of the fluid is proportional to

$$\bar{\bar{u}} = \frac{1}{H\nu}\int_{-H/2}^{+H/2} dz \int_{-H/2}^{z} \left(\overline{w'u'} - \overline{\overline{w'u'}}\right) dz_1 \tag{2}$$

. Computation of the Correlation

The correlation between w' and u' will be termined from the vorticity and continuity uations. Denoting the $-y$ component of rticity by $\eta = \frac{\partial w'}{\partial x} - \frac{\partial u}{\partial z}$ these become:

$$\frac{d\eta}{dt} = -\frac{g}{\varrho_0}\frac{\partial \varrho'}{\partial x} + \nu \nabla^2 \eta \qquad (3)$$

$$\frac{\partial u'}{\partial x} + \frac{\partial w'}{\partial z} = 0$$

t the forced density perturbation ϱ' be presented by the real part of $\Delta\varrho\, e^{ik(x+Ut)}$, here $\Delta\varrho$ is the amplitude and k the wave umber. Then the vertical velocity may be presented by $w'(x, z, t) = w(z)\, e^{ik(x+Ut)}$, if, e assume a linear response. Although the ablishment of a net momentum is a non-ear effect, it is assumed that the correlation tween the velocity components is insignif- ntly modified by the mean flow it induces, d that this quantity may be computed from e linearized hydrodynamic equations. This ill be a valid approximation if, as was the se in the experiments, the induced mean otion and the velocity perturbations are all compared to U. The range of validity ay be inferred from the final results. The rizontal velocity perturbation as computed om the continuity equation is

$$u'(x, z, t) = \frac{i}{k}\frac{dw(z)}{dz}\, e^{ik(x+Ut)} \qquad (4)$$

d consequently the vertical transport of omentum is

$$\overline{w'u'} = \frac{k}{2\pi}\int_0^{2\pi k} dx \;\; Re\, w(z) e^{ik(x+Ut)}.$$

$$\cdot\; Re \frac{i}{k}\frac{dw}{dz}\, e^{ik(x+Ut)} \qquad (5)$$

$$\overline{w'u'} = \frac{1}{2k}\;\; Im w(z) \frac{dw^{\star}}{dz} \qquad (5)$$

here *Re* denotes "real part", *Im* denotes maginary part" and $w^{\star}(z)$ is the complex njugate of $w(z)$.

When $\nabla^2 w' = \frac{\partial \eta}{\partial x}$ is substituted into the linearized vorticity equation the following expression for the vertical velocity is obtained:

$$\left(\frac{\partial}{\partial t} - \nu\nabla^2\right)\nabla^2 w' = -\frac{g}{\varrho_0}\frac{\partial^2 \varrho'}{\partial x^2} = \frac{g}{\varrho_0}k^2 \Delta\,\varrho e^{ik(x+Ut)} \qquad (6)$$

If the depth of the fluid is small compared with the horizontal scale of the motion ($k/\pi \ll H^{-1}$) this reduces to the ordinary differential equation

$$\left(ikU - \nu\frac{d^2}{dz^2}\right)\frac{d^2}{dz^2} w(z) = \frac{g\Delta\varrho}{\varrho_0}k^2 \qquad (7)$$

and we shall confine the discussion to this limiting case. Introducing the abbreviations

$$z = H\zeta \quad R = kUH^2\nu^{-1} \quad \alpha = i^{1/2}R^{1/2}$$

$$w(z) = \frac{g\Delta\varrho}{\varrho_0}k^2 H^4 \nu^{-1} f(\zeta) \qquad (8)$$

into eq. (7) we obtain the following equation and boundary conditions for $f(\zeta)$:

$$\frac{d^2}{d\zeta^2}\left(iR - \frac{d^2}{d\zeta^2}\right) f(\zeta) = 1 \qquad (9)$$

$$f(-1/2) = f(1/2) = f'(-1/2) = f'(1/2) = 0 \qquad (10)$$

The solution of (9), (10) is

$$2iRf(\zeta) = \zeta^2 - 1/4 + \frac{\sinh\alpha}{\alpha(\cosh\alpha - 1)} - \frac{\cosh\alpha\zeta}{\alpha\sinh\alpha/2} \qquad (11)$$

Substituting this in (5) there results

$$\overline{w'u'} = \frac{1}{8R^2kH}\left(\frac{g\Delta\varrho}{\varrho_0}\;\frac{k^2H^4}{\nu}\right)^2 Im\phi(z) \qquad (12)$$

where

$$\phi(\zeta) = \left[\zeta^2 - 1/4 + \frac{\sinh\alpha}{\alpha(\cosh\alpha - 1)} - \frac{\cosh\alpha\zeta}{\alpha\sinh\alpha/2}\right] \cdot \left[2\zeta - \frac{\sinh\alpha^{\star}\zeta}{\sinh\alpha^{\star}/2}\right] \qquad (13)$$

---

llus XI (1959), 2

Since $\phi(-\zeta) = -\phi(\zeta)$ then $\overline{\overline{w'u'}} = 0$ and (2) becomes

$$\bar{u} = \frac{H}{\nu}\int_{-1/2}^{+1/2} d\zeta \int_{-1/2}^{\zeta} \overline{w'u'}\, d\zeta_1$$

$$\bar{\bar{u}} = -\frac{2}{8R^2 k\nu}\left(\frac{g\Delta\varrho}{\varrho_0}\,\frac{k^2H^4}{\nu}\right)^2 Im\int_0^{1/2}\zeta\phi(\zeta)d\zeta \qquad (14)$$

It may be noted that the anti-symmetric form of $\phi(\zeta)$ implies that the net stress on the bottom and top surfaces are not only equal to each other but are also zero. The sign of the total momentum of the fluid depends upon the integral in (14), and although this may be evaluated exactly in terms of elementary functions it will be sufficient for our purposes to indicate the qualitative behavior and the quantitative results in two limiting cases. When the viscosity is very large, or when R is small compared to unity, an expansion of $\phi(\zeta)$ in ascending powers of α leads to the result

$$Im\int_0^{1/2}\zeta\phi(\zeta)d\zeta = 2\times 10^{-6}R^3 + \ldots.$$

The case which is of greater interest to us is when R is much larger than unity. When we make the approximation $|e^{\alpha}| \gg 1$ the integral in (14) may be expanded in a power series in α^{-1}, which leads to the following result:

$$Im\int_0^{1/2}\zeta\phi(\zeta)d\zeta = -\frac{1}{12\sqrt{2}}R^{-1/2} + \frac{3}{4}R^{-1} + \ldots \qquad (15)$$

The significant point to note is the change in sign of the integral, and the consequent reversal of the total momentum (14) as R increases from zero to values which are much greater than unity. By setting the right hand side of (15) equal to zero we estimate that this change occurs when $R = kH\dfrac{UH}{\nu}$ is of the order of 10^2. For values of R which are much larger than this (and when $kH \ll \pi$). The average $+x$ momentum of the fluid as obtained from (14) and (15) is

$$\frac{u}{U} = \frac{1}{48\sqrt{2}}R^{1/2}\left(\frac{gh}{U^2}\,\frac{\Delta\varrho}{\varrho_0}\right)^2 \qquad (16)$$

IV. Discussion

The quadratic dependency of the mean field (16) upon the buoyancy force is quite expected in view of the linear variation of the velocity perturbations with this force. However, the quantity R, which represents the ratio of inertial and viscous forces and may be thought of as the characteristic Reynolds number, is of primary importance for the qualitative features of the flow. When the relative velocity of the density field and the ambient fluid is large so that $R \gg 10^2$ the fluid acquires a net motion opposite to that of the density field. The form of the velocity profile for this regime may also be obtained from (13) and we find that $Im\,\phi(\zeta) \rightarrow -2^{-1/2}R^{-1/2}\zeta$ so that $\overline{w'u'}$ is proportional to $-\zeta$ for $|\zeta| < {}^1/_2$. Therefore the mean velocity profile is parabolic except for the boundary regions where $\bar{u}'(\zeta) = 0$. Consequently in the equilibrium state both the top and bottom surfaces exert no net stress on the fluid, while in the interior there is an upward transport of momentum ($\overline{w'u'} > 0$) below the central level ($\zeta = 0$) and a downward transport of momentum above $\zeta = 0$, both of which are balanced by the viscous stress of the mean motion. It is noted that the transport is proportional to the square root of the viscosity while the total momentum varies as $\nu^{-1/2}$. In an ideal fluid without viscosity there would be no mean motion since there would be zero correlation between w' and u', whereas in a real fluid with very small viscosity the mean motion would be very large.

Although the transient process has not been studied quantitatively the mechanism by which the liquid acquires the net momentum seems reasonably clear. Suppose the thermal field is slowly imposed on a fluid initially at rest. We infer from the conclusions of the preceding paragraph that for large Reynolds numbers the slowly varying velocity perturbations will be such as to produce a convergence of horizontal momentum towards the center of the channel. Since there is initially no mean field to balance this, the $+x$ component of momentum will increase at the center of the channel at the expense of the fluid near the boundaries which will tend to move in the opposite direction. In so doing the fluid will exert a net stress on both boundaries in the

direction, thereby increasing the total
c momentum of the fluid as it comes to
ilibrium.

view of the fact that the phenomenon
ussed here was used by Halley as an ex-
ation of the atmosphere's general circula-
, it is of some interest to estimate the
gnitude of the angular momentum pro-
ed by the westward progression of the
relative to the earth. Consider a 1 km
th which is alternatively heated and cooled
1° C once a day, and assume that the induced
izontal motion is in a zonal direction on a
ude circle of radius 2×10^8 cm. Using the
molecular viscosity of air we find that R must be less than $3 \times 10^{+6}$ and that the angular momentum which is induced in the earth's atmosphere by the diurnal heating of the sun corresponds to an eastward moving current whose order of magnitude is less than one centimeter per second.

REFERENCE

FULTZ, D., 1956: Studies in Experimental Hydrodynamics (I) *Final Report*, Hydrodynamics Lab. University of Chicago, B37—B40.

HALLEY, E., 1686: An historical account of the trade winds and monsoons, etc. *Phil. Trans. Roy Soc. Lon.*, **16**, pp. 153—158.

PRINTED IN SWEDEN
ESSELTE, STHLM 59

Contribution No. 975

Reprinted from LIMNOLOGY AND OCEANOGRAPHY
Vol. 4, No 2, April, 1959
Printed in U.S.A.

The Use of Conversion Factors for the Determination of the Concentration of Nutrients in Culture Media[1]

Although artificial and enriched culture media have been used for many years, there apparently has been no attempt to standardize the method of reporting the concentration of nutrients in media. The most realistic method of reporting the concentration of elements or compounds is in terms of molar units. However, this unit has not been generally employed in the field of culture study, although oceanographers routinely use the microgram atom unit. Generally, a particular unit of concentration is used by an investigator. It is, though, difficult to translate rapidly from units given by other investigators into terms of one's own experience. It would be desirable to have a table available permitting easy and rapid conversion.

The concentration of nutrients in culture media is most commonly expressed in one of three general ways. The concentration may be expressed in terms of molar units, or as the weight of the element, or of the compound. Concentrations expressed in molar units are easily interconvertible to gram equivalent units. On a weight basis, the concentration may be given as parts per million, milligrams per liter, per cent, milligrams per cent, etc. All of these units are interconvertible, but the difficulty arises in rapidly converting from a concentration of a particular element to the concentration of a compound in which the element is delivered, or vice versa.

Two tables are presented which may be used for rapid conversion into any of the common units desired. In Table 1 an attempt has been made to list the compounds, and the various hydrated forms, generally used as inorganic sources of major elements in culture media. The microelements most commonly added to culture media are listed in Table 2, but only the most hydrated compounds are presented. By using these tables, it is possible to rapidly convert from milligrams of a particular element to milligrams of the compound in which the element is delivered by multiplying the conversion factor times the weight of the element. Conversely, if the weight of the compound is known, the weight of the element can be determined by dividing the factor into the weight of the compound. Factors are also presented in the tables for converting from the weight of the compound to the number of micromoles per milligram of compound. If the weight of the compound in milligrams is known, the factor times the weight gives the number of micromoles of the compound. The number of micromoles of an element in a compound is the same as the number of the micromoles of the com-

TABLE 1. *Conversion factors for converting from milligrams of a major element to milligrams of a compound, and from milligrams of a compound to micromoles of a compound*

	N	P	K	Na	Ca	Mg	Cl	S	Si	Micromoles/ milligram of compound
$Na_2HPO_4 \cdot 2H_2O$		5.75		3.87						5.62
$Na_2HPO_4 \cdot 7H_2O$		8.67		5.83						3.73
$Na_2HPO_4 \cdot 12H_2O$		11.56		7.79						2.79
$NaH_2PO_4 \cdot H_2O$		4.46		6.00						7.25
$Na_2SiO_3 \cdot 9H_2O$				6.18					10.15	3.52
$NaNO_3$	6.07			3.70						11.76
Na_2SO_4				3.09				4.43		7.04
$NaCl$				2.54			1.65			17.11
NH_4NO_3	2.86									12.49
NH_4Cl	3.82						1.51			18.69
$CaCl_2 \cdot 2H_2O$					3.67		2.07			6.80
$CaCl_2 \cdot 6H_2O$					5.47		3.09			4.56
$Ca(NO_3)_2 \cdot 4H_2O$	8.42				5.89					4.23
$MgCl_2 \cdot 6H_2O$						8.36	2.87			4.92
$MgSO_4 \cdot 7H_2O$						10.14		7.69		4.06
KCl			1.91				2.10			13.41
KNO_3	7.22		2.59							9.89
K_2HPO_4		5.62	2.23							5.74
KH_2PO_4		4.39	3.48							7.35

---

[1] Contribution No. 975 from the Woods Hole Oceanographic Institution.

pound, or the number of microcoles times the number of atoms of a particular element in the compound.

It is hoped that these tables will be an aid to investigators. It is also entered as a plea for standardization of chemical units reported for culture media. It would be desirable that the molar unit, which has been used for decades in physiology, be adopted as the standard unit of concentration. Inasmuch as it is the number of reactive units and not the weight of these units which is important, molar concentrations are much more informative. For example, ratios of calcium/magnesium and nitrogen/phosphorus are frequently expressed in the literature on a weight basis. In this form, these data are not so meaningful as molar units, as it is the number of atoms rather than the weight of these elements which should be considered. By using molar concentrations, it is also possible to rapidly evaluate and prepare isotonic solutions and media.

TABLE 2 *Conversion factors for converting from milligrams of a micrcelement to milligrams of a compound, and from milligrams of a compound to micromoles of a compound*

	B	Co	Cu	Fe	Mn	Mo	Zn	Micromoles/ milligram of compound
H_3BO_3	5.72							16.17
$CoCl_2 \cdot 6H_2O$		4.04						4.20
$CoSO_4 \cdot 7H_2O$		4.77						3.56
$CuCl_2 \cdot 2H_2O$			2.68					5.87
$CuSO_4 \cdot 5H_2O$			3.93					4.00
$FeCl_3 \cdot 6H_2O$				4.84				3.70
$Fe_2(SO_4)_3 \cdot 9H_2O$				10.06				1.78
$MnCl_2 \cdot 4H_2O$					3.60			5.05
$MnSO_4 \cdot 4H_2O$					4.06			4.48
$H_2MoO_4 \cdot H_2O$						1.88		5.56
$Na_2MoO_4 \cdot 2H_2O$						2.52		4.13
$ZnCl_2$							2.08	7.34
$ZnSO_4 \cdot 7H_2O$							4.40	3.48

There are certain instances though when it may be more advantageous to present concentrations on a mass basis rather than on a molar basis. For example, in comparing total dissolved material in natural waters, or in comparing experiments on the fertilization of lakes with culture media, the data are more appropriately handled on a mass basis. However, from a physiological standpoint, the advantages of the molar system are much more applicable.

JACK MCLACHLAN[2]
GUY C. MACLEOD[3]
Woods Hole Oceanographic Institution
Woods Hole, Massachusetts

---

[2] Public Health Service Research Fellow of the National Institutes of Health.

[3] Supported by a grant from the National Science Foundation (G-2510). Present address: Biological Laboratories, Harvard University, Cambridge, Massachusetts.

Contribution No. 980

Reprinted from Limnology and Oceanography
Vol. IV, No. 4, October, 1959
Printed in U.S.A.

Spectrographic Analyses of Marine Plankton[1]

G. D. Nicholls[2]

Cabot Spectrographic Laboratories, M.I.T., Mass.

Herbert Curl, Jr., and V. T. Bowen

Woods Hole Oceanographic Institution, Woods Hole, Mass.

ABSTRACT

The results of spectrographic analyses of ten species of zooplankton are presented. The methods used are described in detail. The elements determined quantitatively were boron, molybdenum, vanadium, nickel, cobalt, titanium, chromium, lead, tin, and copper. Manganese, cesium, rubidium, barium, strontium, and silver were detected in some or all of the specimens. Antimony, germanium, gallium, gold, and arsenic were sought for but not found. Cadmium was just detectable in only one species, the squid *Ommastrephes* (*Illex*) *illecebrosa*. The analytical results support the view that boron is actively concentrated or excluded by some marine animals. There is evidence that sedimentation of pteropod shells could be a major pathway for the removal of vanadium and lead from sea water. Lead was greatly enriched in *Centropages*. Nickel and cobalt showed random variations with respect to one another.

The elemental composition of marine organisms has interested chemists and biologists for a variety of reasons since before the nineteenth century, and an imposing amount of data has been accumulated. Most of the analyses obtained up to 1944, and some more recent, have been summarized and discussed by Vinogradov (1953). Unfortunately for those engaged in study of ecological or geochemical relationships in the oceans, or for those who wish to use such information to supplement physical oceanographic investigations, it appears that very few appropriate data exist. Not merely have few analyses been performed on species found in the marine plankton which represents, in spite of small individual dimensions, by far the major part of the biomass in the sea, but those few analyses which are available have often been made on specimens of uncertain provenance, and with methods of uncertain accuracy. We need a large number of analyses on simultaneously collected members of food chains, such collections being made often enough and from sufficiently varied localities, to permit comparative interpretation. Modern quantitative spectrographic techniques are capable of the required accuracy and precision when carefully controlled. They are the only techniques readily available that yield data, for large numbers of elements, on the small samples usually convenient for the marine biologist to collect in species purity high enough to permit the most complete interpretation.

The advent of atomic weapons testing has led to increased interest in the inorganic composition of marine organisms. Many marine plankters accumulate a variety of elements which may or may not have obvious biological significance. Some of these elements have radioactive isotopes which could eventually find their way into marine products of commerce, either directly or via food chains. Along these pathways the elements can be either concentrated or diluted depending upon the organisms involved.

In the most general sense, the presence of ence of a particular element in proto- sm has a "reason" behind it, and detec- ı or lack of detection, particularly when y sensitive techniques are employed, mits us to construct hypotheses either ut the chemical behavior of the organisms ıbout their environment.

---

[1] Contribution No. 980 from the Woods Hole Oceanographic Institution, Woods Hole, Massachusetts. The work was supported partly by the Atomic Energy Commission (AEC contract AT (30-1)-1918) and the National Science Foundation.

[2] The analytical program was carried out in the Cabot Spectrographic Laboratory of the Department of Geology and Geophysics, M.I.T., during the tenure of a Robert Blair Fellowship of the London County Council and a Fellowship of the School for Advanced Study, M.I.T. Present address: Dept. of Geology. University of Manchester, Manchester, England.

he observations given in this paper are a t of a program instituted to study plank- ecology on the continental shelf of the theastern United States (Ketchum *et al.*, 7). This program is yielding data from ıonthly samplings at the same series of 22 ions, on the standing crop, rate of phy- lankton carbon fixation, and species ıposition of both phytoplankton and plankton communities. It appeared to that data on the composition, for both ıor and minor elements, of as many as sible of the major plankton species would mit interesting geochemical interpreta- ıs. This report of our first series of lyses is intended to emphasize the ıcticality of moderately precise analyses spectrochemical methods on very small ıples, and the interest of the results so ained.

t is a pleasure to acknowledge the assist- e of Mrs. Doris Sutton in preparing the ıdard salt mixtures used.

METHODS

Collecting

he majority of the collections were con- ted by towing a ¾-meter plankton net ipped with #2 nylon bolting cloth. The end consisted of a brass cup with monel metal screening and a rubber-stoppered outlet. All metal parts were coated with epoxyresin lacquer to prevent contamination of the sample. Tows were made at night when the deep scattering layer was near the surface, or when a just previous tow had revealed the presence of a desirable population. Large scyphozoans, salps, and ctenophores were collected with a dip net.

Collections were sorted, when necessary, but an effort was made to catch initially clean, pure species material. Each sample was drained on #2 bolting cloth and placed in a large porcelain crucible which had been cleaned with *aqua regia*. A few drops of 40 per cent solution of reagent-grade formaldehyde was stirred into each sample, and the crucible was then suspended over silica gel for preliminary drying on shipboard.

In the laboratory drying was continued *in vacuo* over silica gel. The samples were finally ashed to constant weight in a muffle furnace at 450°C to avoid loss of volatile components. Representative specimens of the species to be analyzed were prepared to obtain wet, dry, and ash weights.

The station locations for all the cruises have been described (Ryther and Yentsch 1958).

Data concerning the conditions and location of each collection are given in Table 1. It may be remarked that *Ommastrephes*, a squid, is by no means planktonic. However, it is included for the sake of comparison with other molluscs that are planktonic, and also because it was observed feeding extensively upon *Euphausia krohnii.*

TABLE 1. *Collection data for plankton samples analyzed spectrographically*

	Date	Time	Station	Collection
hausia krohnii Brandt	15 Jan. '57	2400	C	Surface tow
öe cucumis Fabricius	15 Jan. '57	2400	C	Surface tow
tropages typicus (Lilljeborg) & *ımatus* Kroyer	17 Jan. '57	1800	A	Surface tow
itta elegans Verrill	14 Feb. '57	0230	C	Surface tow
anus finmarchicus (Gunnerus)	22 Mar. '57	—	E	Surface tow
pa fusiformis Cuvier	24 Mar. '57	—	M	Surface tow
anus finmarchicus (Gunnerus) lus neritic phytoplankton	24 Mar. '57	0230	M	Surface tow
ıacina retroversa Fleming	29 Apr. '57	—	B	Surface tow
ınea capillata Eschschotty	29 Apr. '57	—	B	Dip net
one limacina (Phipps)	29 Apr. '57	—	B	Surface tow
mastrephes illecebrosa (Lesueur)	2 May '57	0001	H	Dip net

Analysis

A semi-quantitative total emission spectrographic procedure was used for the determination of the trace element contents of the ashed specimens.

A standard base, of composition 600 mg $CaCO_3$, 20 mg $MgCO_3$, 200 mg Na_2CO_3, 30 mg K_2CO_3, 65.5 mg H_2SiO_3, 100 mg Al_2O_3, was prepared. To this base varying amounts of compounds of a number of elements were added to give standards with a range of trace element contents from 5 to 500 ppm for most of the elements sought. For Ti the range was 10–500 ppm. Standards and ashed samples subsequently received identical treatment.

Two different arcing procedures were used, one for the relatively involatile elements B, Ti, V, Cr, Mo, Co, Ni, and the other for the volatile elements Pb, Sn, Cu, Cd.

For the involatile element determination the samples and standards were mixed with carbon powder in the ratio 1 part by weight sample (or standard) to 2 parts by weight carbon. Approximately 15 mg (actual weight recorded) of each carbon-sample or standard mix was loaded into a cylindrical cavity, 1.4 mm diameter and 7.1 mm deep, cut in the end of a carbon rod of diameter 3.2 mm. This loaded rod was made the anode of a DC arc, with a pointed carbon rod of diameter 4.2 mm forming the cathode. The arc was struck at 3 amp, and after 10 sec the current was raised to 6 amp and held there until the anode charge had been completely consumed (normally requiring 1 to 1½ minutes).

For the determination of the volatile elements a cooler arc is desirable. To achieve this, graphite electrodes were used, and the samples (and standards) were mixed with NaCl instead of carbon, 1 part by weight NaCl being added to 1 part by weight sample or standard. The dimensions of the graphite electrodes were the same as those of the carbon electrodes described above. Ten mg of sample-NaCl mix were loaded, the exact weight taken being recorded. The DC arc was struck at 3 amp, and after 1 minute the current was raised to 6 amp for a further 20 seconds, after which the arc was quenched. Preliminary examination had disclosed that emission of the volatile elements was complete in this time.

During all arcings an 8-stepped sector was interposed in the light beam before it entered a Hilger Fully Automatic Large Quartz and Glass Spectrograph. For the involatile elements a slit width of 0.30 mm was used, and for the volatile elements one of 0.45 mm. Spectra from the sample-carbon burns were recorded on Eastman Kodak 103-0 plates, those from sample-NaCl burns on Eastman Kodak 103a-0 plates. The plates were processed according to maker's instructions.

The lines used were:

B	2497.73 Å	V	3185.40 Å
Pb	2833.07 Å	Ti	3199.92 Å
Sn	2839.99 Å and 3175.02 Å	Cu	3247.54 Å and 3273.96 Å
Ni	3012.00 Å and 3414.76 Å	Co	3453.51 Å
Mo	3170.35 Å	Cr	4254.35 Å

Intensity measurements were made on each step of each line using a Hilger Hand-operated Microphotometer, and corrections were applied for background intensity. From the data obtained from the standards, working curves of log line intensity versus log concentration were constructed for several steps of each analysis line. From one arcing of an unknown sample the determination of line intensity in more than one step allowed more than one plot on the series of working curves. Such multiple plotting reduces the possibility of reporting aberrant results arising through local plate damage or inhomogeneity through error in a single measurement, and indicates the extent of error due to photographic recording (individual values range up to ±10 per cent of mean value).

Where possible, replicate arcings were made, thus permitting an estimate of error due to variations in arcing conditions. In most cases this error exceeded that due to the use of photographic recording. An attempt to reduce the error was made by recalculating all intensities to a given weight of sample or standard in the electrode (4.5 mg in the same carbon burns, 5.0 mg in the sample-NaCl burns) on the assumption that the slope of the working curve had the theoretical value of 45°. This was not otably successful and is not recommended future work. Subsequent determinations the slopes of the working curves indicated at they were frequently rather less than °, and this may help to explain the un-tisfactory results of the correction pro-dure.

The amount of some samples, *e.g. Clione*, s too small to permit multiple arcing, and e values for these samples (noted in the ble by an asterisk) are thus somewhat less liable than the others.

The working curves based on standards ly extended up to 500 ppm. All values gher than this have been obtained by trapolation and are thus less reliable the gher they are above this value.

Analysis for V has given some trouble, e only satisfactory standard available ing that of 50 ppm. The working curve this case was constructed by drawing the eoretical 45° line through carefully repro-ced values on the satisfactory standard. nsidering the range of sample values, this is unlikely to have introduced any large error—it may possibly have introduced a tendency for recorded values above 50 ppm to be slightly low and those below 50 ppm to be slightly high. Subject to these reservations, the errors involved are estimated where multiple arcings were possible, to amount in sum to ±30 per cent for boron and to ±15 per cent for the other elements reported.

At the time of making these analyses, suitable standards were not available for manganese, cesium, rubidium, barium, strontium, or silver. Lines of these elements do, however, appear in the spectrograms of some or all specimens. Standards are being prepared, and these values will be available for a subsequent report.

RESULTS

The analytical results are set out in Table 2 as parts per million of element in the ashed sample. For each specimen the per cent ash in the dry material (110°C) and the per cent dry weight of the fresh sample

TABLE 2. *Elements in plankton samples as parts per million of ash*

	Dry (% Fresh)	Ash % Dry	Ppm in Ash									
			B	Mo	V	Ni	Co	Ti	Cr	Pb	Sn	Cu
elenterata												
yanea capillata	4.6	63.0	100	3	5	<1	3	3	<1	6	4	13
enophora												
eröe cucumis	4.7	70.3	115*	3*	8*	<1*	<1*	<1*	<1*	6*	7*	700*
llusca Pteropoda												
imacina retroversa	18.7	64.2	50	8	85	2	20	5	<1	200	<1	30
lione limacina	9.0	33.3	90*	<1*	16*	4*	30*	<1*		65*	20*	70*
llusca Cephalopoda												
mmastrephes illicebrosa	22.7	7.7	420	4	4	<1	3	6	<1	5	3	2700
thropoda Copepoda												
entropages typicus & hamatus	15.8	22.8	160	10	16	55	4	3	260	1300	50	600
anus finmarchicus	10.2	17.6	760*	12*	21*	165*	3*	10*		575	<1	1350
anus finmarchicus ith ∼ 50% neritic phytoplankton	12.2	36.3	325*	36*	54*	70*	80*	70*		75	90	300
thropoda Euphausiacea												
uphausia krohnii	20.3	18.6	440	17	45	6	5	9	<1	20	<1	600
aetognatha												
agitta elegans	10.6	21.6	130	3	13	480	110*	3	<1	300	20	1100
nicata												
alpa fusiformis	4.0	77.1	50	<1	7	60	<1	1	<1	3	8	500
Salt	35.1		131[1]	0.4[2]	0.07[2, 3]	0.06[2]	0.007[3, 4]	0.20[2]	0.05[2]	0.11[1, 5]	0.09[4]	0.03[6, 7]

*—values based on a single arcing.

[1]—values taken from Kalle 1945.

[2]—values taken from Black and Mitchell 1952.

[3]—values taken from Ishibashi 1953.

[4]—value taken from Noddack and Noddack 1939.

[5]—value taken from Boury 1938.

[6]—value taken from Chow and Thompson 1952.

[7]—value taken from Morita 1953.

TABLE 3. *Spectrographic lines and estimated limits of sensitivity of analyses for elements sought but not found*

Spectra are from arcings for volatile elements.

Element	Wavelength of line Å	Limit of sensitivity ppm
As	2780.2	200
Au	2675.9	30
Ga	2934.6	3
Ge	2651.8	5
Sb	2877.9	100

are also presented. In addition to the ten elements shown in Table 2, antimony, germanium, gallium, gold, and arsenic were sought in each specimen, but not found. The estimated limits of sensitivity for these elements, with the methods used, are shown in Table 3. Cadmium was looked for despite the high (500 ppm) limiting sensitivity available. In the squid, *Ommastrephes*, cadmium was just detectable, whereas in all other specimens it was below the limit of detectability. The situation with respect to manganese, strontium, barium, silver, cesium, and rubidium has been discussed above in the section on methods.

For comparison we also present a compilation of the concentrations of the pertinent elements in sea salt, recalculated from sea water analyses of various authors, as listed. All values were normalized to 35.0‰ salinity, and calculated to ppm dry salt, taking Kalle's value of 35.141 g salt in 1000 g sea water of that salinity.

DISCUSSION

As we have stated above, few analyses of zooplankton are available. Those that can be cited offer some interesting comparisons.

Cyanea capillata was analyzed, also spectrographically, by the Noddacks (1939) for many of the same elements that we report. The two sets of analyses, as parts per million dry weight, are shown in Table 4.

The lack of correspondence between the two sets of values may reflect the fact that our specimens were caught well offshore, while theirs were from a landlocked fiord. It seems, however, quite as likely that organisms of very low ash-to-fresh-weight ratio, as coelenterates and ctenophores, exhibit a composition strongly reflecting that of recent food organisms. This point will require more observation. It is perhaps of interest that, with the exception of copper, our analyses for *Cyanea* and for *Beröe* agree quite closely. Unless we postulate for *Cyanea* an exceptionally slow regulation of Ti and of Sn, we do not know of any food organisms that might be responsible for such high values of these elements as were found by the Noddacks.

Calanus finmarchicus has been examined for element content by several workers, quoted by Vinogradov (1953). Our values (Table 5) indicate considerably greater enrichment of boron, nickel, and copper. Percentage-wise the nickel concentration is outstanding.

Although some assumptions have to be made about the composition of the phytoplankton contaminants, the analyses (Table 2) on *Calanus* plus 50 per cent phytoplankton, provide some support for the high nickel figure. Since the phytoplankton is unlikely to have been free of boron, lead, or copper, the values for the mixed sample may be taken to indicate that this *Calanus* population was lower in these elements, than was the pure. This is not surprising in view of Vinogradov's emphasis on the variability of total ash content of *Calanus* collections. With the exception of boron the general correspondence of values between *Calanus* and *Centropages* is quite good.

Ommastrephes has not previously been analyzed for any of the elements cited above, but our values show good correspondence with those cited (Vinogradov) for *Loligo:*

TABLE 4. *Comparison of analyses of Cyanea*

	Element ppm dry wt.								
	Mo	V	Ni	Co	Ti	Cr	Pb	Sn	Cu
Noddacks' value	2	5	30	7.1	6	1.3	27	32	68
Our value	1.9	3.1	0.6	1.9	1.9	0.6	3.8	2.5	8.2

TABLE 5. *Comparison of analyses of Calanus*

	Element ppm dry wt.					
	B	Mo	V	Ni	Ti	Cu
ogradov's alues	71.6	0.6*	0.4*	0.12	6.4	present
values	134	2.1	3.7	29	1.7	238

* Values for *Carcinus maenas* (a benthic malacostracan, but
most closely related organism for which analyses could be
ıd).

ı, 200 ppm vs. 158; Mo, 0.3 vs. 0.3; and
0.3 vs. 0.4. As might have been ex-
cted, although the squids were caught
ıen actively feeding on *Euphausia*; there
no striking correspondence of predator
d food composition. No analyses for
dmium are reported for cephalopods, but
ebb (1937) reported 10 to 400 ppm of ash
a variety of marine molluscs. It is thus
o soon to say whether the high Cd of our
nmastrephes is a general molluscan char-
ter or the result of secondary concentra-
n of the relatively high Cd of fish—one
the squid's major foods.

Intercomparison of the various specimens
Table 2 also yields some interesting
ints. Even though Webb (1937) had
ported for marine molluscs a range of
ron contents from 100 to 700 ppm of ash,
nogradov (1953) postulated that boron,
ing a major ion of sea water and not of
ophysiological importance, could be used
an indicator of sea water equilibration.
is clear that our analyses are consistent
th the range reported by Webb, and
pport the view that some marine animals
tively concentrate this element, while
hers like *Limacina*, *Clione*, and *Salpa* must
rtially exclude it.

For molybdenum our uniformly rather
gh values for crustaceans are interesting,
ough not surprising in view of the indica-
n that the phytoplankton mixed with one
lanus sample, was really quite rich in this
ement. There appears to be no evidence
r such a connection of Mo and Cu as is
ported for mammals (Marston 1952).

In the case of the two pteropods it is
mpting to base comparisons on the pres-
nce of a shell in *Limacina* (highly phos-
atic shell, according to Vinogradov and our own determinations) and the absence of any shell in *Clione*. Should this be a reasonable basis for comparison, Mo, V, Pb, and possibly Ti are indicated as strongly enriched in the pteropod shell, V and Pb so much so that sedimentation in this way might be estimated to be a major pathway of removal of these elements from the sea.

The random variation of nickel and cobalt with respect to each other is quite striking. No support appears for the sort of phylogenetically regular Ni:Co ratios that were postulated by Bertrand and Macheboeuf (1925). Both pteropods and the squid agree in being exceptions to Vinogradov's generalization that in Mollusca nickel is found more frequently than cobalt and in larger quantities. Reasonable assumptions about ash weight:dry weight ratios, applied to the nickel analyses reported by Laevastu and Thompson (1956) for several mixed plankton hauls, indicate adequate agreement between our crustacean data and theirs. Very possibly, nickel accumulation will prove to be typical of copepods. The enormous values for Ni and Co for *Sagitta* interest us considerably. It should, however, be noted that because of its higher total ash content, *Limacina* proves to concentrate Co on a fresh weight basis, to the same extent that *Sagitta* does. This illustrates a pitfall of working from ash or dry weight concentrations only.

The very wide range of concentrations of lead is striking. It is interesting to note that Vinogradov had suspected a reported value of 25 ppm (dry) in lobster, as improbably high. Our value of 1300 ppm (ash) for *Centropages* presents some problems of physiological interpretation. We hope that parallel data for silver, and analyses of phytoplankton blooms for both elements, will help to clear up this.

We believe the high values for Ti and Sn in the *Calanus*-plus-phytoplankton sample are likely to represent silt particle collection in a rather turbid coastal water. It is, however, clear that considerable amounts of these, often called bio-inert, elements are commonly retained by phytophages, and even by such secondary predators as *Cyanea* or *Ommastrephes*. Their cycles in the sea will surely prove to have considerable contribution from biological processes.

The relatively few analyses herein presented clearly demonstrate the need for many more. For subsequent geochemical applications it is essential that a variety of elements should be sought in the same organism and this requirement suggests a spectrographic method of analysis. In this exploratory work a rapid, semi-quantitative method was used. The results obtained indicate that internal standardization techniques with greater analytical precision would certainly prove worth while, and we intend to adopt them in our future work. Most generalizations that might have been indicated by previous studies prove not to hold, and the picture of the diversity of chemical behavior among the members of plankton communities is most striking. Certainly the safest generalization promises to be that for any given chemical element there will eventually be found at least one plankton species capable of spectacularly concentrating it.

REFERENCES

Bertrand, G., and M. Macheboeuf. 1925. Sur la presence du nickel et du cobalt chez les animaux. Compt. Rend. Acad. Sci., Paris, **180:** 1380.

Black, W. A. P., and R. L. Mitchell. 1952. Trace elements in the common brown algae and in sea water. J. Mar. Biol. Ass. U. K., **30:** 575–584.

Boury, M. 1938. Le plomb dans le milieu marine. Rev. Trav. Office des Peches Maritimes, **11:** 157–166.

Chow, T. J., and T. G. Thompson. 1952. Determination and distribution of copper in sea water. I. The spectrophotometric determination of copper in sea water. J. Mar. Res. **11:** 124–138.

Ishibashi, M. 1953. Studies on minute elements in sea water. Rec. Oceanogr. Works, Japan n.s., **1:** 88–92.

Kalle, K. 1945. Der Stoffhaushalt des Meeres. In: Probleme der Kosmischen Physik., **23:** xii + 263 pp.

Ketchum, B. H., V. T. Bowen, and J. H. Ryther. 1957. Biological and chemical studies of coastal plankton populations. Unpublished, Woods Hole Oceanographic Inst., Ref. 57-18, 18 pp.

Laevastu, T., and T. G. Thompson. 1956. The determination and occurrence of nickel in sea water, marine organisms and sediments. J. Cons. Intern. Explor. Mer, **21:** 125–143.

Marston, H. R. 1952. Cobalt, copper and molybdenum in the nutrition of animals and plants. Physiol. Rev., **32:** 66–121.

Morita, Y. 1953. Copper and zinc in Pacific waters. Rec. Oceanogr. Works, Japan, n.s., **1:** 49–51.

Noddack, I., and W. Noddack. 1939. Der Haufigkeiten der Schwermetalle in Meerestieren. Arkiv f. Zool., **32A:** 1–35.

Ryther, J. H., and C. S. Yentsch. 1958. Primary productivity of continental shelf waters off New York. Limnol. Oceanogr., **3:** 327–335.

Vinogradov, A. P. 1953. The elementary chemical composition of marine organisms. Sears Found. Mar. Res., Memoir **2,** xiv + 647 pp.

Webb, D. A. 1937. Spectrographic analyses of marine invertebrates with special reference to the chemical composition of their environment. Sci. Proc. Roy. Dublin Soc., **21:** 505–539.

Contribution No. 982

Reprinted from **ANALYTICAL CHEMISTRY**, Vol. 31, Page 44, January 1959

Copyright 1958 by the American Chemical Society and reprinted by permission of the copyright owner

Radiochemical Separation of Fission Products from Large Volumes of Sea Water

Strontium, Cesium, Cerium, and Promethium

T. T. SUGIHARA, H. I. JAMES, and E. J. TROIANELLO
Department of Chemistry, Clark University, Worcester, Mass.
V. T. BOWEN
Woods Hole Oceanographic Institution, Woods Hole, Mass.

CONTRIBUTION NO. 982

▶ The amount of long-lived fission products from nuclear weapons detonations deposited on the surface of the Atlantic Ocean can be estimated from terrestrial measurements. A study of their concentrations can be used to estimate horizontal and vertical transport in the ocean. Chemical methods were used to isolate 28-year strontium-90, 30-year cesium-137, 280-day cerium-144, and 2.4-year promethium-147 from as much as 200 liters of sea water. Strontium separation involves precipitation of mixed strontium-calcium carbonates directly and in the presence of (ethylenedinitrilo)tetraacetate ion, precipitation of strontium nitrate, scavenging with ferric hydroxide–barium chromate, and conversion to strontium carbonate. Strontium-90 activity is measured by separating and counting the daughter yttrium-90 activity. Cesium is coprecipitated with dipotassium sodium cobaltinitrite, separated as cesium silicotungstate, converted to the perchlorate, and freed of trace potassium and rubidium by ion exchange. Rare earths are removed by initial coprecipitation on ferric hydroxide. Uranium, protactinium, and thorium are removed by ion exchange; radium and lead are scavenged with barium sulfate. The cerium fraction is obtained in pure form by separation as cerium(IV); promethium, by cation exchange.

Fission products have been deposited on the surface of the Atlantic Ocean as a consequence of nuclear weapons detonations (*13*). If the concentration of certain nuclides is measured in ocean waters as a function of depth and location, it should be possible to estimate horizontal and vertical transport in the ocean. Geochemical considerations suggested the study of 28-year strontium-90, 30-year cesium-137, 280-day cerium-144, and 2.4-year promethium-147 from the wide spectrum of fission products. The amount of strontium-90 activity expected in Atlantic waters can be estimated from terrestrial measurements of this nuclide (*13*). If a low level counter is used that can detect 1 disintegration per minute (d.p.m.) with reasonable accuracy, it is calculated that from 50 to 200 liters of sea water must be processed to obtain detectable amounts of strontium-90. Preliminary measurements of strontium-90 in North Atlantic surface waters (*1*) indicate that this is correct. The concentration of the other nuclides should be of the same order of magnitude as that of strontium-90.

Because large volumes of sea water are difficult to obtain and transport, all of these nuclides must be separated from the same water sample. No existing radiochemical procedures could be readily adapted for use in these separations because of the very large volumes required and the many interfering ions that sea water contains. There are two prerequisites for a successful procedure. There must be a relatively fast and simple method to remove the nuclide of interest from the bulk of the sea water and because the amount of activity to be detected is very small, the nuclide isolated must be subjected to very extensive radiochemical purification.

The following procedures are suitable with sea water volumes as large as 200 liters. However, the specific amounts of reagents used are given for a 100-liter sample. Wherever possible, polyethylene containers have been used to minimize problems of contamination and adsorption.

EXPERIMENTAL

The sea water concentrations of elements of interest to these separations are listed in Table I. Cesium (carrier added) is readily carried on dipotassium sodium cobaltinitrite and the rare earths can be coprecipitated on ferric hydroxide. However, no method has been devised that removes strontium without also removing calcium and in this procedure, strontium and calcium are precipitated together.

PROCEDURE

Transfer the 100-liter sea water sample to a 30-gallon polyethylene drum. Add concentrated hydrochloric acid to pH 2. (All reagents are analytical reagent grade.) Store on board ship under these conditions.

In the shore laboratory, add the following carriers: 3.80 grams of strontium chloride hexahydrate (1.25 grams as strontium), 12.7 mg. of cesium chloride (10.0 mg. as cesium), and 2.4 grams of ferric chloride hexahydrate (0.50 gram as iron). Mix well.

Add slowly, while stirring by a stream of nitrogen gas (Matheson Co., Inc., East Rutherford, N. J.), solid sodium hydroxide to about pH 7, and then about 1.2 kg. of sodium carbonate. Continue stirring 4 to 5 hours. Let the precipitate settle overnight and check the supernate for complete precipitation with 5% sodium carbonate solution. Siphon off the supernate which constitutes the cesium fraction. (It is not practical to filter at this point because of the very large amount of precipitate; the cesium loss in this step is 10 to 15%.) Add concentrated hydrochloric acid to the supernate to pH 2.

Dissolve the precipitate, which consists of calcium carbonate, strontium carbonate, some magnesium hydroxide, and ferric hydroxide in a minimum volume of concentrated hydrochloric acid (about 500 ml. will be required). Add concentrated ammonium hydroxide until the precipitation of ferric hydroxide is complete. Filter on 24-cm. Whatman No. 54 paper in a porcelain No. 5 Büchner funnel. The filtrate constitutes the strontium fraction.

Dissolve the precipitate with a minimum of concentrated hydrochloric acid and filter off any remaining residue. This residue usually consists of relatively large organisms and other non-acid-soluble materials. Reprecipitate ferric hydroxide from the filtrate and filter. Add the filtrate from the latter step to the strontium fraction.

DISCUSSION

A series of preliminary experiments was carried out to determine the amount of ferric hydroxide necessary to carry cerous ion quantitatively from sea water. Carrier-free cerium-144 was used as a tracer. Twenty milligrams of ferric ion are sufficient for 100 liters of sea water. The much larger amount used here (500 mg.) was chosen because it was desirable to coprecipitate antimony also. The antimony method and results will be reported elsewhere.

STRONTIUM AND YTTRIUM

The relatively high strontium concentration in sea water makes it impossible to count strontium-90 directly because of the very low specific activity. However, it is easy to isolate and count the 64-hour yttrium-90 daughter as a thin sample. The chemical separation of strontium is complicated by the very much higher calcium concentration and the very close similarity between strontium and calcium.

Reagents. Distilled hydrochloric acid, distilled in an all-glass still, collected in polyethylene, and diluted with redistilled water.

Redistilled water, distilled from all-glass still and stored in polyethylene.

Ammonium hydroxide, carbonate-free, about 1*M*, prepared by bubbling ammonia gas (Matheson Co., Inc.) into redistilled water, stored in polyethylene.

Ammonium carbonate, analytical reagent grade, saturated solution in water, and solution containing 1 gram per 1000 grams of water (0.1%).

Ammonium chloride solution, 1 gram of analytical reagent grade per 1000 grams of redistilled water (0.1%).

Ferric chloride solution, purified, prepared by dissolving 1 gram of analytical reagent grade iron wire in 25 ml. of 3*M* distilled hydrochloric acid, adding carbonate-free ammonium hydroxide to pH 4, removing ferric hydroxide by centrifuging, oxidizing remaining ferrous ion with 30% hydrogen peroxide, and acidifying with distilled hydrochloric acid to pH 1, final volume about 30 ml.

Nitric acid, concentrated, 70 grams as nitric acid per 100 grams solution (70%); 35%, prepared by dilution; and fuming (90%); all reagent grade.

Versene solution, tetrasodium (ethylenedinitrilo)tetraacetate, 34%, commercial grade (Dow Chemical Co., Framingham, Mass.).

Table I. Concentration of Certain Elements in Sea Water

Element	Concentration,[a] Mg./Kg.	Reference
Sodium	10.6×10^3	(*24*)
Potassium	380	(*24*)
Rubidium	0.1–0.2	(*7, 19, 24*)
Cesium	5×10^{-4} – 3×10^{-3}	(*7, 19, 24*)
Calcium	400	(*24*)
Strontium	9.0–9.1	(*3, 6, 18*)
Cerium	4×10^{-4}	(*24*)
Lanthanum	3×10^{-4}	(*24*)

[a] For sea water of chlorinity 19.00 parts per thousand.

Procedure. Adjust the pH of the strontium fraction to about 7. Add 940 ml. of 34% Versene solution and mix thoroughly. Precipitate mixed carbonates with 450 grams of sodium carbonate. Stir 2 hours, let settle, and siphon off supernate. (Filtration is not necessary at this point; less than 5% of the mother liquor remains after siphoning.) Add 10 liters of water and a minimum of concentrated hydrochloric acid to dissolve the precipitate. Transfer to a 19-liter polyethylene beaker and reprecipitate the carbonates in the presence of Versene solution as above with 200 grams of sodium carbonate. Filter with suction on 24-cm. Whatman 54 filter paper in a Büchner funnel (No. 5). Dry the precipitate at 105° C. and transfer to a 4-liter glass beaker.

Dissolve the precipitate in a measured minimum volume of 35% nitric acid. For each milliliter of 35% nitric acid used, add 4 ml. of 70% nitric acid and 5 ml. of 90% nitric acid. Mix well, chill in ice bath, and filter with suction on a medium-porosity glass filter. Do not wash.

Dissolve in water and bring volume to 500 ml. Add 10 mg. of barium ion as carrier. Add concentrated ammonium hydroxide to pH 7 to 8 (phenol red) and add 2 ml. of 0.5*M* sodium chromate. Filter through Whatman 41 paper and discard the precipitate. Precipitate strontium carbonate from the filtrate with 25 grams of sodium carbonate, filter on a medium-porosity glass filter, and dry at 105°. Transfer the precipitate to a 1-liter beaker. Dissolve in 15 ml. of 35% nitric acid, add 60 ml. of 70% nitric acid, and 75 ml. of 90% nitric acid. Chill in ice bath. Filter on a glass filter. Suck the precipitate dry, but do not wash. Dissolve in 150 ml. of redistilled water and transfer to a polyethylene beaker.

Add 10 mg. each of iron(III) and barium carriers; adjust pH to about 7 with concentrated ammonium hydroxide. Add 1 ml. of 0.5*M* sodium chromate and filter (polyethylene funnel) through Whatman 41 paper into a 1-liter polyethylene beaker. Discard precipitate. To filtrate add saturated ammonium carbonate solution to precipitate strontium carbonate. Filter on glass filter. Wash with 0.1% ammonium carbonate solution, dry 8 to 10 hours at 110°, and weigh.

Let the strontium carbonate sample stand for about 15 days to allow yttrium-90 to grow into equilibrium with its parent. In a polyethylene beaker, dissolve the strontium carbonate by adding a minimum volume of distilled 3*M* hydrochloric acid. Boil for a few minutes.

Add 2 mg. of purified iron(III) carrier and precipitate ferric hydroxide with carbonate-free ammonium hydroxide. Filter with suction on a 24-mm. Millipore RA filter (Millipore Filter Corp., Watertown, Mass.) supported by a glass filter plate. Use a second Millipore filter in series to filter the air before it passes through the sample-containing filter. Add 2 to 3 ml. of distilled 3*M* hydrochloric acid to filtrate and store in a polyethylene bottle. Wash the precipitate 5 times with 0.1% ammonium chloride in redistilled water. Dry at 110° for 15 minutes. Mount on a split Bakelite sample cylinder (*1*) and count.

After a 15-day interval, repeat the above step to obtain a second yttrium fraction.

Remove a known aliquot of the strontium-containing solution (60 to 90 mg. of strontium is a convenient size). Add appropriate volumes of 70% nitric acid and 90% nitric acid such that the final volume is about 60 ml. and the nitric acid concentration is about 75%. Cool in an ice bath. Filter the strontium nitrate on a glass filter. Suck dry but do not wash. Dissolve the strontium nitrate in 20 ml. of water and add saturated ammonium carbonate solution to precipitate strontium carbonate. Filter on a glass filter. Wash with 0.1% ammonium carbonate solution. Dry 1 to 2 hours at 110° and weigh. Use this weight and the aliquot size to compute the chemical yield of strontium, taking into account the amount of stable strontium originally present in the sea water. The chlorinity of each sea water sample is routinely measured. Because the ratio of concentrations of strontium to chloride is a constant (*3, 6, 18*), the amount of stable strontium present in the water is readily calculated.

RESULTS AND DISCUSSION

The chemical yield of strontium following this procedure is about 70%. In some early experiments, lower yields were obtained. This was due to excessive use of (ethylenedinitrilo)-tetraacetate (EDTA). Because the calcium-EDTA stability constant is about 100 times greater than that of strontium-EDTA (*14*), the presence of EDTA reduces the amount of calcium carbonate precipitate formed, but the strontium is hardly affected as long as the number of moles of EDTA present is somewhat less than that of calcium. However, this method of partial calcium-strontium separation cannot be used unless the strontium-calcium weight ratio is at least 1 to 20. This explains the amount of strontium carrier used.

Under the conditions used for the initial precipitation of calcium and strontium carbonates, some of the magnesium also precipitates, mostly as the hydroxide, although the carbonate is no doubt also present. In subsequent steps of the calcium-strontium separation, the magnesium contamination of the strontium fraction is reduced to a negligible amount.

The precipitation of strontium nitrate in this procedure is done with 76% nitric acid. Sunderman and Meinke (*22*) have shown that the precipitation of strontium is not quantitative with nitric acid of a concentration less than 70%. They have shown also that calcium will increasingly be carried on the strontium nitrate as the nitric acid concentration is increased. At the end of the step in which strontium carbonate is precipitated after scavenging with ferric hydroxide–barium chromate, the calcium contamination was found to be in the range from 5 to 15%. The procedure used in the last step is based on auxiliary experiments in which, under the conditions specified, the strontium recovery was quantitative over a wide range of calcium concentrations (up to a 1 to 1 weight ratio of calcium to strontium).

Because the amount of radioactivity to be measured is small, of the order 1 d.p.m., it is necessary to be very careful about contamination. A blank sample of 50 liters of distilled water was processed using the same reagents in the same amounts as used in a sample. Less than 0.1 count per minute (c.p.m.) of activity was observed and there was no evidence for a half life similar to 64-hour yttrium-90. At this level of detection, short-lived airborne activities seriously interfere with early counting data. The Millipore filter in series ahead of the sample filter reduces this problem to negligible proportions.

CESIUM

The initial separation of 10 mg. of cesium from the very large amount of sodium in 100 liters of sea water was readily accomplished by coprecipitation with dipotassium sodium cobaltinitrite. Contaminating potassium-40 and rubidium-87 were removed by an ion exchange procedure.

Reagents. Silicotungstic acid solution, 1 gram of analytical reagent grade per milliliter of solution (approximately 0.3*M*).

Anion exchange resin Dowex-1 × 8, 100 to 200 mesh (Dow Chemical Co., Midland, Mich.). Resin washed in batch form with 1*M*, 0.01*M*, and 2*M* hydrochloric acid; washed in column form with 1*M* hydrochloric acid, and finally with water, column 1.0 cm. in diameter by 20 cm.

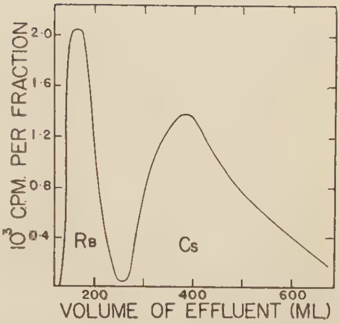

Figure 1. Elution curve for separation of rubidium and cesium on Duolite C-3

H$^+$ form, 150 to 200 mesh, 1 cm. diameter time 10 cm., flow rate 1.0 ml. per minute, eluent 0.30*M* hydrochloric acid

Carrier-free rubidium-86 and 10 mg. of cesium carrier plus tracer cesium-134 were adsorbed on column

Three-milliliter fractions counted on well scintillation counter

Cation exchange resin, Duolite C-3 (Chemical Process Co., 901 Spring St., Redwood City, Calif.). The commercially available material is a very coarse-mesh resin. It should be ground in a ball or rod mill and sieved to 150 to 200 mesh and used in hydrogen form. Resin is washed with 3*M* hydrochloric acid, water, 3*M* sodium hydroxide, water, 3*M* hydrochloric acid, water, and finally equilibrated with 0.30*M* hydrochloric acid, column 1.0 cm. in diameter by 10 cm.

Procedure. While stirring with a stream of nitrogen gas, slowly add 250 grams of sodium cobaltinitrite to the cesium fraction. Continue stirring for several hours. Let stand 36 to 40 hours or until supernate is clear. Siphon to remove supernate.

Filter the precipitate on 15-cm. Whatman 42 paper in a Büchner funnel and wash with sufficient 0.01*M* hydrochloric acid to transfer the precipitate to the filter. Dissolve the precipitate in a minimum volume of hot 6*M* hydrochloric acid (about 500 ml.). Add 15 ml. of silicotungstic acid solution and digest at 90° for 1 hour. Let stand for an additional 4 or 5 hours. The cesium silicotungstate precipitate forms very slowly. Filter on a fine-porosity glass filter. Wash the precipitate with 6*M* hydrochloric acid. Transfer the precipitate with a minimum volume of water to a 100-ml. glass beaker. Heat to boiling and add the minimum number of sodium hydroxide pellets required to dissolve the silicotungstate. Cool to room temperature. Pass the solution through the Dowex-1 column. Wash the column with 0.001*M* sodium hydroxide. Collect the first 30 ml. of effluent which contains chiefly cesium chloride and sodium chloride. The anions from the decomposition of the silicotungstate remain on the column. Regeneration of the column is not feasible. Fresh resin should be used for each cesium sample. Precipitate cesium perchlorate from the effluent as given by Elkin in Kleinberg's compilation (*10*).

Dissolve the cesium perchlorate (containing some potassium and rubidium) in a minimum amount of 0.30*M* hydrochloric acid. Adsorb on the Duolite C-3 column. Elute with 0.30*M* hydrochloric acid at a flow rate of 1.0 ml. per minute, disregarding the first 250 ml. of effluent. Rubidium and lighter alkali metals should be in this fraction. Change the eluent to 3.0*M* hydrochloric acid and collect the next 100 ml. of effluent. This should contain the cesium fraction substantially free of potassium and rubidium. Precipitate cesium perchlorate as in the step above, and transfer to a tared paper filter disk. Use air filtered through a Millipore filter as in the strontium procedure. Dry at 110° for 15 minutes, cool, and weigh. Use this weight to compute the chemical yield. Mount the sample in a manner analogous to the yttrium-90 sample and count.

RESULTS AND DISCUSSION

The chemical yield of cesium in this procedure has been about 60%. The initial step of coprecipitation of cesium with the mixed potassium sodium cobaltinitrite is remarkably quantitative for cesium under conditions in which potassium recovery is much less than quantitative. Kahn, Smith, and Straub (*8*) have found cesium recovery in the coprecipitation step to be 97% when 20 mg. of cesium were separated from 1 liter of river waters of varying potassium concentration.

In a well known radiochemical separation of cesium from fission products (*10*), cesium silicotungstate is precipitated and dissolved in sodium hydroxide. On acidification, silica and tungstic oxide are precipitated and removed. In this latter step, preliminary experiments using cesium tracer show that the bulky silica and tungstic oxide precipitate removes as much as 30% of the cesium. In the recommended procedure, the anion exchange step removes silicate, tungstate, and hydroxide ions without affecting the cesium recovery.

Niday's ion exchange method (*17*) for separating rubidium and cesium has been adapted here. Other workers have shown (*9*, *16*, *17*) that rapid and simple separation of cesium from other alkali-metal ions is best done on a phenol-sulfonic type of cation exchanger. Duolite C-3 is such a resin. A typical elution curve obtained in the cation exchange separation of rubidium and cesium on Duolite C-3 is shown in Figure 1. In this experiment, carrier-free rubidium-86 (less than 0.1 mg. as rubidium) and 10 mg. of cesium ion plus tracer cesium-134 were adsorbed on the column and eluted with 0.30*M* hydrochloric acid. Three - milliliter fractions were collected and counted on a well scinitillation counter. In many preliminary experiments the position of the rubidium band was found to be reproducible. Because potassium is expected to elute before rubidium, the cesium fraction should be free of contamination due to potassium and rubidium.

When a 20-mg. sample of the cesium chloride used in the carrier solution was counted, a contaminating activity of about 1 c.p.m. was observed. The contamination could be due to potassium-40, rubidium-87, or both. When the carrier solution was run through the ion exchange step, the resultant cesium fraction showed less than 0.05 c.p.m. A complete reagent blank on distilled water indicates less than 0.05 c.p.m. in the cesium sample.

CERIUM AND PROMETHIUM

The initial removal of radiocerium and promethium is very simply accomplished by coprecipitation on ferric hydroxide. The major concern was to work out a method in which the contamination due to uranium, thorium, and daughter radioactivities could be eliminated from the cerium and promethium fractions. A combination of scavenging precipitations and ion exchange successfully produced uncontaminated cerium and promethium fractions.

Reagents. Carrier solutions (each 10 mg. of rare earth per ml.); 12.28 grams of ceric oxide per liter in 0.1*M* hydrochloric acid, 11.66 grams of neodymium oxide per liter in 0.1*M* hydrochloric acid, 11.60 grams of samarium oxide per liter in 0.1*M* hydrochloric acid (rare earth oxides from Lindsay Chemical Co., Chicago, Ill.).

Lactic acid solution, analytical reagent grade, 0.75*M*, prepared by dilution of concentrated (85%) reagent, ammonium hydroxide added to pH 3.32 ± 0.02.

Anion exchange resin Dowex-1 × 8, 50 to 100 mesh (Dow Chemical Co., Midland, Mich.). Resin pretreated with 12*M* hydrochloric acid, water, 6*M* sodium hydroxide, and water. Equilibrated with 12*M* hydrochloric acid for the separation of rare earths from uranium and protactinium, column 0.5 cm. in diameter by 12 cm. Equilibrated with 7.5*M* nitric acid for separation of rare earths from thorium, column 1.0 cm. in diameter by 7 cm.

Cation exchange resin Dowex-50 × 12, colloidal mesh (Microchemical Specialties Co., Berkeley, Calif.). Resin pretreated with water, 3*M* hydrochloric acid, water, a solution of citric acid (5 grams of acid dihydrate in 95 grams of water) to which ammonium hydroxide was added to pH 7, and water, finally equilibrated with 0.75*M* lactate solution of pH 3.32. Column dimensions 1 cm. in diameter by 35 cm., elution at room temperature.

Cation exchange resin Dowex-50 × 12, 100 to 200 mesh (Dow Chemical Co., Midland, Mich.). Resin pretreated with 3*M* hydrochloric acid, water, 3*M* sodium hydroxide, water, 3*M* hydrochloric acid, water, 3*M* ammonium chloride, water.

Procedure. Dissolve the ferric hydroxide containing the rare earth fraction in a minimum amount of warm 6*M* hydrochloric acid. Add 10 mg. each of neodymium, samarium, and cerium(III) as chlorides. Precipitate the mixed hydroxides with concentrated ammonium hydroxide. Centrifuge and wash twice with dilute ammonium hydroxide. Dissolve the precipitate in about 10 ml. of concentrated hydrochloric acid and dilute to 30 ml. with water. Add 1.5 ml. of 49% hydrofluoric acid and digest in hot water for about 10 minutes. Centrifuge and wash the rare earth–fluoride precipitate with 10 ml. of 2*M* hydrochloric acid containing 0.5 ml. of 49% hydrofluoric acid. In this step, iron should remain in solution. Add 1 ml. of a saturated boric acid solution and 1 ml. of concentrated hydrochloric acid to the fluoride precipitate and heat gently until it is dissolved. Precipitate the rare earth hydroxides with concentrated ammonium hydroxide. Centrifuge and wash twice with dilute ammonium hydroxide.

Dissolve the hydroxide precipitate in 2 ml. of concentrated hydrochloric acid. Pass the solution through the anion exchange column equilibrated with 12*M* hydrochloric acid. The flow rate is not critical. Wash the column with four 2-ml. portions of concentrated hydrochloric acid. Collect the effluent in a Lusteroid centrifuge tube (Lusteroid Container Co., Inc.). In the ion-exchange step, uranium(VI) and protactinium(V) should be left on the column (*11*), while the rare earths are unaffected. With the tube in an ice bath, add 5 ml. of water, and then slowly add concentrated ammonium hydroxide to precipitate the rare earth hydroxides. Centrifuge and wash twice with dilute ammonium hydroxide. Dissolve the precipitate in a minimum amount of 6*M* hydrochloric acid. Add bromothymol blue indicator and concentrated ammonium hydroxide dropwise until the solution is yellow (pH ∼ 6).

Add 5 ml. of 0.01*M* sulfuric acid. Place the tube in a water bath and heat nearly to boiling. Add slowly while stirring, 2 ml. of a barium chloride solution containing 3 mg. of barium per milliliter. Digest near the boiling point for 30 minutes and cool in an ice bath for 5 minutes. Centrifuge and discard the barium sulfate precipitate. Repeat the barium sulfate scavenging operation two additional times. This step should remove radium isotopes, lead-210, and some thorium.

To the supernate from the above step add concentrated ammonium hydroxide to precipitate the rare earth hydroxides. Centrifuge and wash twice with dilute ammonium hydroxide. Dissolve the precipitate in 2 ml. of 7.5*M* nitric acid and pass through the anion exchanger equilibrated with 7.5*M* nitric acid. The flow rate should not exceed 0.2 ml. per minute. Elute with 7.5M nitric acid until 25 ml. of effluent have been obtained. Thorium is retained on the column in this step (*2*, *4*).

To the effluent from the above step, add 20 ml. of 0.35M iodic acid and 2 ml. of 2M sodium bromate. Ceric iodate precipitate should form while samarium and neodymium stay in solution. Digest at room temperature for about 10 minutes and then place in ice bath for about 10 minutes. Centrifuge and save both the precipitate and the supernate. Wash the ceric iodate precipitate with a solution containing 2 parts by volume of 0.35M iodic acid to 1 part concentrated nitric acid. Dissolve the precipitate in 2 ml. of concentrated hydrochloric acid. Add hydroxylamine hydrochloride while stirring until the solution, originally somewhat yellow [due probably to some cerium(IV) and decomposition products of IO_3^-], becomes water-white. Transfer to a Lusteroid centrifuge tube. Precipitate cerous hydroxide with concentrated ammonium hydroxide, centrifuge, and wash as before. Dissolve in a minimum amount of dilute hydrochloric acid and dilute to about 20 ml. Add bromothymol blue indicator. Add dilute ammonium hydroxide to pH 8 to 9 (slightly blue). Add 15 ml. of a saturated oxalic acid solution and digest on a hot water bath for 20 minutes. After cooling, centrifuge, and wash the cerous oxalate precipitate with water. Transfer the precipitate with water to a medium-porosity porcelain crucible. Filter with suction. Ignite at about 700° to ceric oxide. Slurry the oxide with a minimum amount of redistilled water and transfer to a tared Millipore RA filter, 24-mm. in diameter. Dry at 110° for 15 minutes, cool, and weigh. Compute the chemical yield from this weight. Mount on a sample cylinder as with the yttrium-90 sample and count.

To the supernate from the ceric iodate precipitation of the above step add a few milligrams of cerium(III) carrier and a few drops of 2M sodium bromate. Centrifuge and discard the ceric iodate precipitate. Transfer about one half of the supernate to a centrifuge tube and slowly add concentrated ammonium hydroxide while the tube is in an ice bath. When hydroxide formation appears complete, centrifuge, and discard the supernate. Add the remaining solution to this tube and again precipitate the hydroxides. Centrifuge and wash with dilute ammonium hydroxide. Dissolve the precipitate in a minimum amount of dilute hydrochloric acid, transfer to a small beaker, add about 1 gram of Dowex-50 × 12 (100 to 200 mesh, NH_4^+ form). Heat at about 90° for 2 to 3 minutes. Transfer the resin and solution phase to a cation exchange column (Dowex-50 × 12, colloidal mesh). Remove the excess solution above the resin. Elute at room temperature with 0.75M lactate, pH adjusted to 3.32 ± 0.02 with ammonium hydroxide, at a flow rate of 0.15 to 0.20 ml. per minute (*25*). Collect the first 80 ml. of effluent in one batch. Thereafter collect 10-ml. portions until a positive oxalate test is obtained, signalling the start of the samarium fraction. In the oxalate test, add an equal volume of saturated oxalic acid solution to the effluent fraction and digest on a steam bath for a few minutes. Collect the next 20 ml. in one batch. Collect 2-ml. portions until a negative oxalate test is obtained, indicating the end of the samarium fraction. Combine the samarium fractions and save for last step.

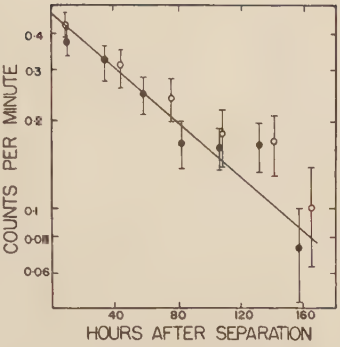

Figure 2. Decay curve for yttrium fraction

○ Separated Sept. 13, 1957
● Separated Nov. 30, 1957
— 64-hour half life. Strontium sample from South Atlantic surface water

Collect the next 50 ml. of effluent in one batch, then 2-ml. portions, until a positive oxalate test is obtained (start of neodymium band). Combine those 2-ml. portions giving a negative test with the 50-ml. portion; the total volume constitutes the promethium fraction. Collect the succeeding 40 ml. of effluent, then 10-ml. portions, until a negative oxalate test is obtained. Combine the 40-ml. neodymium fraction and the subsequent fractions containing oxalate precipitates and save for last step.

Add about 5 mg. of neodymium carrier to the promethium fraction and precipitate neodymium oxalate in a manner similar to cerous oxalate. Ignite the oxalate to neodymium oxide. Weigh and mount neodymium oxide as was done with ceric oxide. The chemical recoveries of samarium and neodymium are measured either by precipitation as the oxalate and weighing as the decahydrate or by titration with EDTA using naphthylazoxine indicator (*5*).

RESULTS AND DISCUSSION

A method frequently used to separate cerium from a fission-product mixture is to precipitate zirconium phosphate repeatedly to scavenge thorium, followed by oxidation of cerium to the ceric state, and precipitation of ceric iodate. Trace amounts of thorium are not quantitatively scavenged by zirconium phosphate. Hence an anion exchange separation of thorium in 7.5M nitric acid (*2*, *4*) was introduced.

In some preliminary experiments using carrier-free thorium-234 as a tracer, the thorium-234 activity in the effluent was not measurable after two cycles through the anion column. In these experiments about 30,000 c.p.m. of thorium-234 (as measured on an end-window Geiger counter, uncorrected for coincidence loss) were taken, and after one ion exchange cycle, about 5 c.p.m. were found in the effluent. The decontamination factor in one cycle then is of the order of magnitude of 10^4. Two cycles should be more than enough to decontaminate the sample with respect to thorium.

The ion exchange method for the separation of promethium is based on one developed for the separation of yttrium and the light rare earths in deuteron fission of uranium (*20*). The position of the samarium, promethium, and neodymium bands is reproducible (*25*). However, with a different batch of resin, a slightly different pH or lactate concentration, the detailed procedure may have to be adjusted slightly for optimum collection of the promethium band. The total time required to elute through the neodymium fraction is about 25 hours. About 275 ml. of eluent are required. If the temperature were raised or if gradient elution, continuous or stepwise, were introduced, the time required could probably be reduced. These changes have not been considered necessary, however, because the elution proceeds in a routine way, unattended for the most part. If coarser mesh resin or a shorter column is used, the promethium separation is not entirely satisfactory.

Reagent blanks were run on distilled water, using the same amounts of reagents as were used in the rare earth procedure. Less than 0.05 c.p.m. of activity has been found in the cerium and promethium fractions. In an experiment designed to test decontamination with respect to thorium, about 7 × 10^4 d.p.m. of thorium-234 were added to distilled water and less than 0.1 c.p.m. was found in the cerium and promethium fractions.

Chemical yields of cerium have been about 50% and of promethium about 70%. The chemical yield of promethium is taken to be the mean of the measured samarium and neodymium yields.

COUNTING METHODS

The beta counter used was a thin-wall, cylindrical flow Geiger counter, $^5/_8$ inch in diameter by $2^1/_2$ inches, of a type that has been described (*21*). The counting mixture used was 99.05% helium and 0.95% isobutane at one atmosphere pressure. When shielded by seven inches of iron and a ring of 13 anti-coincidence counters, $1^3/_4$ × 22 inches, the background rate has been 0.22 c.p.m. and very steady. The counter, shield, electronics, and counting method are similar to those described by Martell (*15*). Counting corrections to convert observed rates to disintegration rates were made using the method of Libby and coworkers (*12, 20, 23*).

The identification of strontium-90 is easy because of the characteristic 64-hour half life of the daughter nuclide yttrium-90. Minor contamination appearing as a long-lived tail in a decay curve can easily be resolved, as long as the initial activity of yttrium-90 is at least ten times the contribution of contamination. Figure 2 shows a typical decay curve for yttrium fractions separated from the strontium sample on two different occasions. Because of the relatively low counting rates and rapid decay, no attempts have been made to measure the absorption curve of the yttrium-90 beta ray.

Because the half lives of cesium-137, cerium-144, the promethium-147 are all very long compared to the usual time of counting, decay is not conveniently observed. Identification of these species must depend on beta absorption curves and certainty regarding the contribution of contamination. In Figures 3 and 4 are shown absorption curves obtained for a cerium fraction and for a promethium fraction. Polyethylene or Mylar absorbers were used because they are easily obtained in uncontaminated form. The observed half-thicknesses for cerium-144 (4.7 mg. per sq. cm.), praseodymium-144 (150 mg. per sq. cm.), and promethium-147 (4.0 mg. per sq. cm.) are consistent with those expected (*12*) for the beta rays of these nuclides. The reagent blanks indicate that the contribution of long-lived contamination will be substantially zero. The soft beta ray of promethium-147 (220 kev.) requires that thin samples be used to reduce self-absorption. This is readily controlled by adding an appropriately small amount of neodymium carrier to the promethium fraction taken off the ion exchange column.

COUNTING RESULTS

Some preliminary results obtained for strontium-90 concentrations in North Atlantic surface waters have been reported elsewhere (*1*). Values ranged from 0.06 to 0.3 d.p.m. per liter. A few results obtained for the rare earths show that the cerium-144 concentrations in North Atlantic surface waters (as of March 1958) is less than that of strontium-90 in some samples and greater in others. The ratio of activities, cerium-144 to promethium-147, is in the range from 1.5 to 3.5. The variation probably is related to the age of the fission products. Comparison of the rare earth data with those of strontium-90 is difficult because of uncertainty in the zero time for the decay correction. No cesium samples from surface waters have been counted.

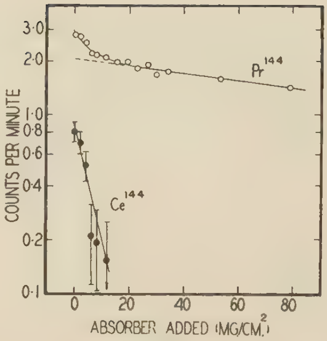

Figure 3. Absorption curve on cerium fraction

○ Observed points (counting error less than diameter of circles)
● Obtained by subtracting hard component from observed data

Polyethylene absorbers used. Straight lines correspond to half-thickness of 150 mg. per sq. cm. (praseodymium-144) and 4.7 mg. per sq. cm. (cerium-144)

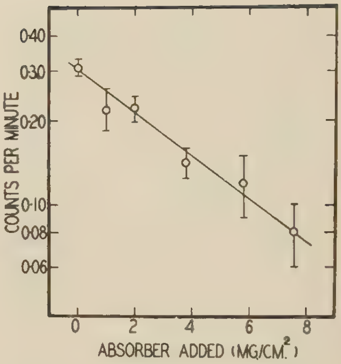

Figure 4. Absorption curve on promethium fraction

Mylar and polyethylene absorbers used. Straight line corresponds to half-thickness of 4.0 mg. per sq. cm.

CONCLUSION

Chemical methods for the isolation of radiochemically pure strontium, cesium, cerium, and promethium samples from 100 liters of sea water have been described. Chemical yields are routinely in the range from 50 to 80%. The blank correction for contamination is negligible in all fractions. Because of the very small amounts of activity involved, counting is done on a small flow Geiger counter of background 0.22 c.p.m.

ACKNOWLEDGMENT

The authors are indebted to H. L. Caron and J. Roesmer, Clark University, for assistance in the chemical separations and in some of the counting, and to Sybil A. Campbell, Woods Hole Oceanographic Institution, for assistance in chemical separations and in clarifying some details of the strontium procedure.

LITERATURE CITED

(1) Bowen, V. T., Sugihara, T. T., *Proc. Natl. Acad. Sci. U. S.* **43**, 576 (1957).
(2) Carswell, D. J., *J. Inorg. & Nuclear Chem.* **3**, 384 (1957).
(3) Chow, T. J., Thompson, T. G., Anal. Chem. **27**, 18 (1955).
(4) Danon, J., *J. Am. Chem. Soc.* **78**, 5953 (1956); *J. Inorg. & Nuclear Chem.* **5**, 237 (1958).
(5) Fritz, J. S., Lane, W. J., Bystroff, A. S., Anal. Chem. **29**, 821 (1957).
(6) Hummel, R. W., Smales, A. A., *Analyst* **81**, 110 (1956).
(7) Ishibashi, Masayoshi, Hara, Tadashi, *Records Oceanog. Works Japan* **2**, 45 (1955).
(8) Kahn, Bernd, Smith, D. K., Straub, C. P., Anal. Chem. **29**, 1210 (1957).
(9) Kayas, G., *J. chim. phys.* **47**, 408 (1950).
(10) Kleinberg, Jacob, Los Alamos Rept. **LA-1721** (1954).
(11) Kraus, Kurt, Moore, George, Nelson, Frederick, *J. Am. Chem. Soc.* **78**, 2692 (1956).
(12) Libby, W. F., *Phys. Rev.* **103**, 1900 (1956); Anal. Chem. **29**, 1566 (1957).
(13) Libby, W. F., *Proc. Natl. Acad. Sci. U. S.* **42**, 365 (1956); **43**, 758 (1957).
(14) Martell, A. E., Calvin, M., "Chemistry of Metal Chelate Compounds," p. 537, Prentice-Hall, New York, 1952.
(15) Martell, E. A., U. S. Atomic Energy Commission, Rept. **AECU-3262** (1956).
(16) Miller, H. S., Kline, G. E., *J. Am. Chem. Soc.* **73**, 2741 (1951).
(17) Niday, J. B., *Phys. Rev.* **98**, 42 (1955).
(18) Odum, H. T., *Science* **114**, 211 (1951).
(19) Smales, A. A., Salmon, L., *Analyst* **80**, 37 (1955).
(20) Sugihara, T. T., Drevinsky, P. J., Troianello, E. J., Alexander, J. M., *Phys. Rev.* **108**, 1264 (1957).
(21) Sugihara, T. T., Wolfgang, R. L., Libby, W. F., *Rev. Sci. Instr.* **24**, 511 (1953).
(22) Sunderman, D. N., Meinke, W. W., Anal. Chem. **29**, 1578 (1957).
(23) Suttle, A. D., Jr., Libby, W. F., *Ibid.*, **27**, 921 (1955).
(24) Sverdrup, H. U., Johnson, M. W., Fleming, R. H., "The Oceans," p. 176, Prentice-Hall, New York, 1942.
(25) Troianello, E. J., James, H. I., Sugihara, T. T., U. S. Atomic Energy Commission, Rept. **NYO-7756** (1958).

Received for review May 14, 1958. Accepted October 9, 1958. Work supported at Clark University in part by U. S. Atomic Energy Commission under contract AT(30-1)-1930 and at Woods Hole Oceanographic Institution by Office of Naval Research under contract Nonr-1238(00), and by U. S. Atomic Energy Commission under contract AT(30-1)-1918. Contribution 982 from Woods Hole Oceanographic Institution.

Contribution No. 984

Relative Significance of the Net Phytoplankton and Nanoplankton in the Waters of Vineyard Sound[1]

By

Charles S. Yentsch and **John H. Ryther**
Woods Hole Oceanographic Institution

I. Introduction

Phytoplankton ecologists divide phytoplankton into two major groups based on cell size. To the portion of the population which will pass through the pores of a fine plankton net the term nanoplankton has been applied (LOHMANN, 1903), while the portion of the population retained by the net is termed net phytoplankton. BIRGE and JUDAY (1922) were probably the first workers to assay quantitatively the biomass of these two proportions. They found that the quantity of net phytoplankton showed pronounced seasonal trends while that of the nanoplankton did not. In making quantitative estimates of the standing crop some workers have claimed that net collections are representative (BURKHOLDER, 1933; HARVEY *et al.*, 1935); however, it is apparent from the work of RILEY (1941), HARVEY (1950), WOOD and DAVIS (1956), and STEEMANN NIELSEN (1938, 1957) that a great majority of phytoplankton in most regions of the oceans pass through the fine net.

In this paper we are comparing chlorophyll, photosynthesis, and cell numbers in the net- and nanoplankton in the waters of Vineyard Sound. Our observations cover the period March to the end of July, 1956. We have attempted to assay the importance of the micro-flagellates in the phytoplankton and wherever possible have compared Vineyard Sound data to values found by other workers in different regions of the oceans.

II. Methods

Surface water samples were collected from Vineyard Sound in volumes of 6–20 l by a plastic bucket and poured through a silk No. 25 plankton net (aperture size: 0·065 mm). Care was taken not to clog the net. This plankton sample was then washed into a known volume of filtered sea water from which equal aliquots of the sample were taken for chlorophyll analysis, photosynthesis measurements, and cell counting. Similar analyses were made on the unfiltered

---

[1] Contribution No. 984 from the Woods Hole Oceanographic Institution, Woods Hole, Mass. This was supported by research grants from the National Science Foundation.

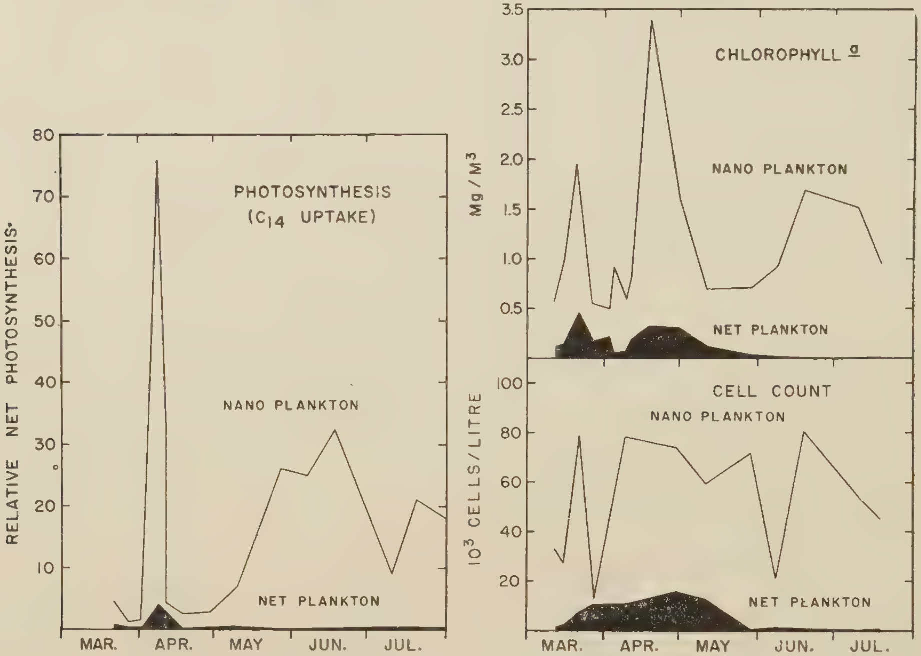

Figure 1. Chlorophyll, photosynthesis, and cell numbers in the net- and nanoplankton in Vineyard Sound, March–July 1956.

raw water collected at the same time. The method of chlorophyll analysis has been described by Richards with Thompson (1952) and modified for use with a millipore filter by Creitz and Richards (1956). Photosynthesis measurements were made by adding 1 ml of $C^{14}O_3''$ to clear and dark glass stoppered bottles to which aliquots of the plankton samples were added. The bottles were suspended in surface waters from a floating dock between the hours of 0900–1500 after which the samples were millipore filtered and the filters counted according to Steemann Nielsen (1952). Photosynthesis corrected for dark uptake is expressed in relative units. Cell counts were made on 1 ml aliquots of the net sample in a Sedgwick-Rafter counting chamber under 100× and 400× magnification. Cell counts were made on a *raw* water sample concentrate obtained by adding 10 ml of neutral formalin to a 500 ml sample and allowing the organisms to settle.

The differences between values of chlorophyll, photosynthesis, and cell number in the *raw* water samples and those obtained from samples collected by the fine net are expressed in this paper as characteristics of the nanoplankton.

III. Results

A. Seasonal sequence

In Figure 1 we have compared net phytoplankton to nanoplankton in terms of the quantity of chlorophyll, cell numbers, and photosynthesis. During the period of observation the net plankton, on the average, comprised 8% of the total chlorophyll, 9% of total cell numbers, and 2% of the photosynthesis. A

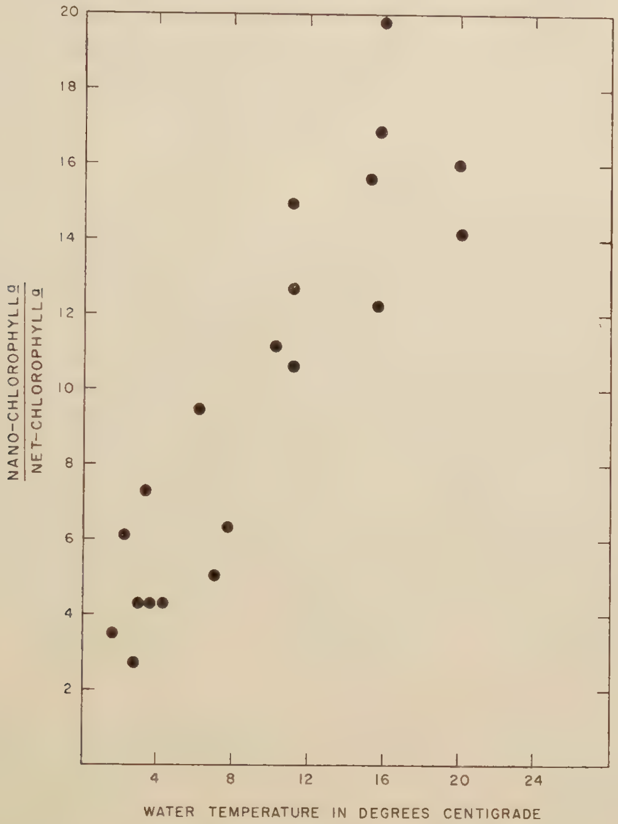

Figure 2. Comparison of mean monthly water temperature on the proportion of net- to nanoplankton chlorophyll.

marked seasonal trend was observed in net plankton chlorophyll, cell number, and photosynthesis. Chlorophyll and cell numbers were highest during March, April, and May while photosynthesis was highest in April. The cell numbers in the nanoplankton exhibited no uniform seasonal trend. However, chlorophyll quantities exhibited three major peaks, one in the middle of March, the other two at the end of April and mid-June. The highest concentration of chlorophyll occurred in April and coincided with the maximum photosynthetic activity. This was also the case in the June peak.

The considerable variability in the biomass of net plankton pointed out by RILEY (1941) and others is confirmed by our observations. In Vineyard Sound the ratio between the largest and smallest standing crop of net plankton chlorophyll is 25:1. The same ratio in the nanoplankton chlorophyll is only 6·8:1.

The proportion of the two components of the population, as shown by the ratio of the nanoplankton chlorophyll: net plankton chlorophyll was closely related to the mean monthly water temperature (Fig. 2). During our observations water temperatures covered the range of 2°–21°C. The catching efficiency of the fine net as shown by the ratio of nano- to net plankton chlorophyll varied from 3–20. Hence the proportion of nanoplankton in the total population increased seven fold between March and July. The observed correspondence with temperature does not infer that temperature *per se* is responsible for the decreased cell size, which may be influenced by other factors such as light or nutrients.

B. Composition of net- and nanoplankton

The numbers retained by the net when compared with direct counts indicate that even the larger diatoms are not completely collected by fine nets. Species such as *Rhizosolenia styliformis*, *Nitzschia delicatissima*, and *N. seriata* whose over-all cell size is large and whose length greatly exceeds their width could be expected to be retained by chance 50% of the time in the fine net. Likewise, spinous species such as *Chaetoceros* could also have a high retention coefficient. General morphological types such as these were caught at times by the fine net in numbers half as large as the numbers in the settled volume (Fig. 3). Some of the larger genera, *Coscinodiscus*, *Peridinum*, and *Ceratium* were frequently caught with 100% efficiency by the net. Yet the inefficiency of the fine net is shown by the number of different genera whose individuals were never caught by the net, and the large number of genera of which the nets caught less than 10% of the population indicated by the direct count. Examples of these are the genera, *Navicula*, *Thalassiosira*, *Licmophora*, *Gyrosigma*, *Pleurosigma*, *Leptocylindrus*, *Nitzschia closterium*, and the summer form of *Skeletonema*.

C. Chlorophyll content of net- and nanoplankton samples

In all cell counts made on whole water samples marine flagellates such as *Carteria*, or *Dunaliella*, and small dinoflagellates of the genus *Gymnodinium* comprised no more than 2% of the total cell numbers. Therefore, the main constituents of the nanoplankton were diatoms which were not retained by the fine net. If formalin preservation or discrimination difficulties caused large counting errors by omission, the values for cellular chlorophyll in the portion of the population not retained by the net would be unusually large. This does not, however, appear to be the case. In Figure 4 we have compared the cellular

Table 1

Chlorophyll content of different species of phytoplankton

Organisms	Chlorophyll *a* in a single cell (mg)	One mg1) count
Greater than 10 microns		
*Rhizosolenia alata*2)	$1{\cdot}8\times10^{-8}$	56×10^{4}
– *Shrubsolei*2)	$1{\cdot}6\times10^{-8}$	62×10^{4}
*Ditylum Brightwellii*2)	$1{\cdot}7\times10^{-8}$	59×10^{4}
Skeletonema costatum	$2{\cdot}8\times10^{-9}$	35×10^{7}
Phaeodactylum tricornutum	$2{\cdot}0\times10^{-10}$	50×10^{8}
Less than 10 microns		
Dunaliella euchlora	$6{\cdot}0\times10^{-10}$	16×10^{8}
Carteria sp.	$5{\cdot}8\times10^{-10}$	17×10^{8}
Isochrysis galbana	$7{\cdot}5\times10^{-11}$	13×10^{9}
Nannochloris atomus	$3{\cdot}0\times10^{-11}$	32×10^{9}

---

1) Number necessary to comprise one mg of chlorophyll.

2) FLEMING (1940).

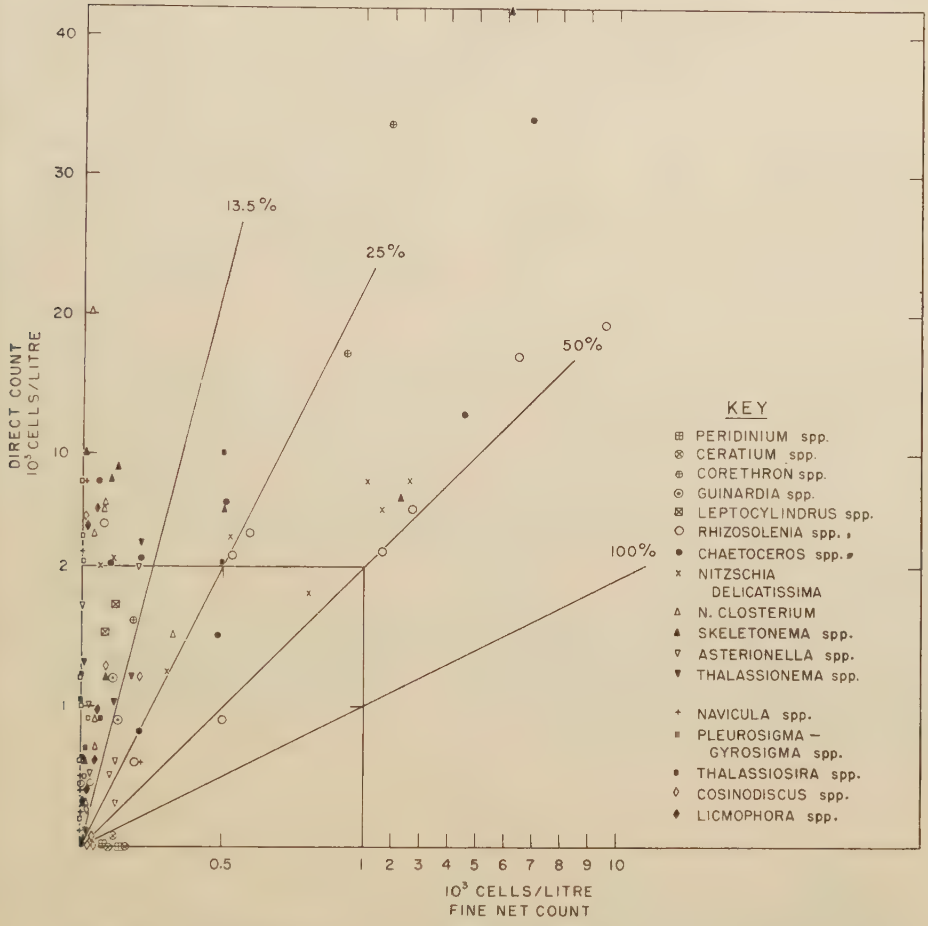

Figure 3. Net retention ratios of major diatom genera sampled in Vineyard Sound, March–July 1956. The two distinct morphological types in the genus *Nitzschia* are separated by species.

chlorophyll content of net plankton and nanoplankton samples. The chlorophyll per cell values for the net samples are representative, almost exclusively, of diatoms because of their larger size. The scatter of the nanoplankton points appears to be no greater than could be expected from analysis of the cell contents of different diatom sizes. Moreover, the points group well around the line which corresponds to $1{\cdot}6 \times 10^{-8}$ mg chlorophyll *a*/cell. This is near the average chlorophyll content of the genus *Rhizosolenia* (see Table 1), which again emphasizes that a major proportion of the chlorophyll in the waters of Vineyard Sound is contained in diatoms, and the nanoplankton is largely diatoms which pass through the fine net. It is perhaps surprising that diatoms within a wide range of cell size have roughly the same amount of chlorophyll. These analyses confirm the visual observation that chloroplasts occupy a proportionately larger fraction of the cell contents of smaller diatoms. Unfortunately little information is available on the cellular chlorophyll content of

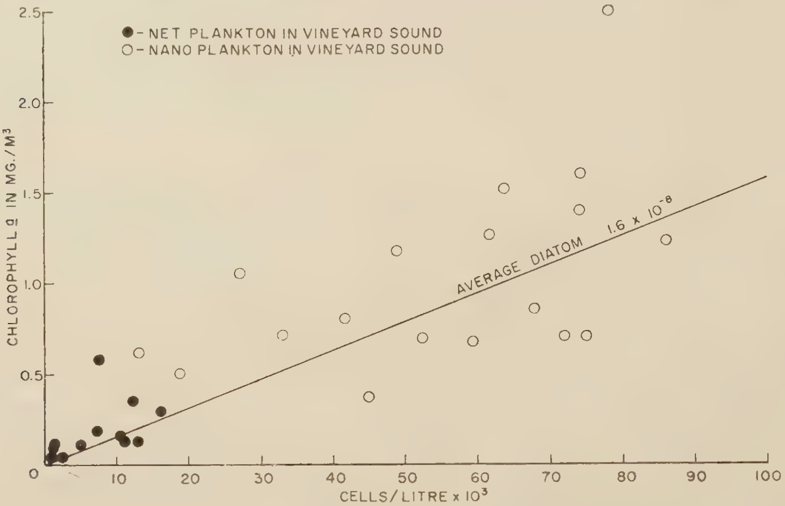

Figure 4. Chlorophyll cell number ratios, Vineyard Sound, March–July 1956.

different species of diatoms. In Table 1 we have compared the cell contents of some diatoms and flagellates. The large differences in cell volumes are apparent when one considers that a diatom such as *Rhizosolenia alata* contains 1000 times more chlorophyll *a* than a cell such as *Nannochloris*. Some of the larger flagellates (*Carteria*, *Dunaliella*) do, however, have chlorophyll contents as large as some of the smaller diatoms.

Discussion

In Table 2 data from various sources compare the percentage of total phytoplankton biomass that can be caught by a net in the various areas sampled. Large percentages of the total phytoplankton biomass may be retained by fine nets in Arctic waters (Digby, 1953) as opposed to net retention values given by Riley (1939) and Wood and Davis (1956) for water of lower latitudes. Observations made in more temperate regions where the temperature range is large (Harvey, 1950; Riley, 1941; and this paper) tend to include the extreme net plankton percentages of northern and southern regions. This latitudinal distinction is probably valid for natural marine communities where little influences from land are present such as Vineyard Sound. In an estuary, however, the percentage of phytoplankton retained by a fine net might be much lower due to the prevalence of smaller forms.

Some workers have suggested that the bulk of the organic production in parts of the oceans may be due to the activities of autotrophic flagellates rather than diatoms (Atkins, 1945; Knight-Jones and Walne, 1951). Due to the small volume of these cells the numbers necessary to contribute a sizable quantity of chlorophyll are large. For example, Knight-Jones and Walne (1951) report counts of 50,000 cells of *Chromulina pusilla* per litre in the North Sea. Using the chlorophyll per cell value shown in Table 1 for *Nannochloris*, which is comparable in size to *Chromulina*, the total quantity of chlorophyll

Table 2

The percentage of phytoplankton biomass caught by a No. 25 plankton net in different regions of the oceans

Location	Latitude	% of the total	Author
Scoresby Sound, East Greenland .	70°N	66	DIGBY (1953)
Off Plymouth, England..........	50°N	10–26	HARVEY (1950)
Long Island Sound	41°N	9–56	RILEY (1941)
Vineyard Sound	41°N	2–47	
New South Wales, Australia	33°S	3–4	WOOD and DAVIS (1956)
Tortugas	24°N	1	RILEY (1939)

in the *C. pusilla* populations would be 10^{-3} mg/m³ or 1/1000 the average chlorophyll content in nearshore marine waters (RYTHER and YENTSCH, 1958). The counts given by the English workers for *C. pusilla* in rivers and estuaries are much higher and should cause a visible green turbidity which is seldom observed in natural marine conditions. RILEY's (1957) data show a range in diatom numbers in the poor waters of the Sargasso Sea of 2,000–58,000 cells/litre. Assuming that the average cellular chlorophyll content of these cells is $1{\cdot}6 \times 10^{-8}$ mg (Table 1), the range of chlorophyll contributed by diatoms alone would be 0·03 — 0·9 mg/m³, which is generally the range observed in this open ocean region. Others have claimed that the importance of the micro-flagellates in the total phytoplankton biomass has been overestimated (BALLANTINE, 1953). CUSHING (1955) states that in most of the oceans diatom numbers are six times higher than flagellates which in terms of chlorophyll would allow the diatom contribution to be 100–1000 times the flagellate contribution. Thus it would appear unlikely that micro-flagellate populations could ever comprise a significant proportion of the bulk of organic production in the oceans.

Summary

Chlorophyll content, photosynthesis, and cell numbers have been compared in the net- and nanoplankton in Vineyard Sound waters. The net portion comprised a small percentage of the total population and exhibited marked seasonal trends while the nanoplankton did not. The composition of the net phytoplankton was exclusively diatoms which because of size or shape were retained by the net. The nanoplankton was comprised almost exclusively of smaller diatoms, or diatoms whose shape was not suitable for net retention.

References

ATKINS, W. R. G., 1945. "Autotrophic flagellates as the major constituent of the oceanic phytoplankton". Nature, Lond., **156**: 446.

BALLANTINE, D., 1953. "Comparison of the different methods of estimating nanoplankton". J. Mar. Biol. Assoc. U. K., **32**: 129–47.

BIRGE, E. A. and JUDAY, C., 1922. "The inland lakes of Wisconsin. The plankton. Part I. Its quantity and chemical composition". Wis. Geol. Nat. Hist. Surv., Bull., **64**: 1–222.

BURKHOLDER, P. R., 1933. "A study of the phytoplankton of Frenchman's Bay and Penobscot Bay, Maine". Int. Rev. d. ges. Hydrobiol. Hydrogr., **28**: 262–84.

CREITZ, G. I., & RICHARDS, F. A., 1955. "The estimation and characterization of plankton populations by pigment analysis. III. A note on the use of 'millipore' membrane filters in the estimation of plankton pigments". J. Mar. Res., **14**: 211–16.

CUSHING, D. H., 1955. "Production and pelagic fishery". Fish. Invest. Lond., Ser. 2, **18** (7).

DIGBY, P. S. B., 1953. "Plankton production in Scoresby Sound, East Greenland". J. Animal Ecol., **22**: 289–322.

FLEMING, R. H., 1940. "Composition of plankton and units for reporting populations and production". Proc. 6th Pac. Sci. Congr., **3**: 535–40.

HARVEY, H. W., COOPER, L. H. N., LEBOUR, M. V., & RUSSELL, F. S., 1935. "Plankton production and its control". J. Mar. Biol. Assoc. U.K., **20**: 407–41.

HARVEY, H. W., 1950. "Production of living matter in the sea off Plymouth". J. Mar. Biol. Assoc. U.K., **29**: 97–137.

KNIGHT-JONES, E. W., & WALNE, P. R., 1951. "*Chromulina pusilla* Butcher, a dominant member of the ultraplankton". Nature, Lond., **167**: 4450.

LOHMANN, H. 1903. "Neue Untersuchungen über den Reichtum des Meeres an Plankton und über die Brauchbarkeit der verschiedenen Fangmethoden". Komm. Wissensch. Untersuch. d. Deutschen Meere in Kiel und d. Biologischen Anstalt auf Helgoland, Wiss. Meeresunters., N.F., Abt. Kiel, **7**: 1–86.

RICHARDS, F. A., with THOMPSON, T. G., 1952. "The estimation and characterization of plankton populations by pigment analysis. II. A spectrophotometric method for the estimation of plankton pigments". J. Mar. Res., **11**: 156–72.

RILEY, G. A., 1939. "Plankton studies. II. The western North Atlantic, May–June". J. Mar. Res., **2**: 145–62.

RILEY, G. A., 1941. "Plankton studies. III. Long Island Sound". Bull. Bingham Oceanogr. Coll., **7** (3): 1–93.

RILEY, G. A., 1957. "Phytoplankton of the north central Sargasso Sea". Limnol. Oceanogr., **2**: 252–70.

RYTHER, J. H., & YENTSCH, C. S., 1958. "Primary production of continental shelf waters off New York". Limnol. & Oceanogr., **3**: 327–35.

STEEMANN NIELSEN, E., 1938. "Über die Anwendung von Netzfängen bei quantitativen Phytoplanktonuntersuchungen". J. Cons. int. Explor. Mer, **13**: 197–205.

STEEMANN NIELSEN, E., 1952. "The use of radioactive carbon (C^{14}) for measuring organic production in the sea". J. Cons. int. Explor. Mer, **18**: 117–40.

STEEMANN NIELSEN, E., & AABYE JENSEN, E., 1957. "Primary oceanic production, the autotrophic production of organic matter in the oceans". Galathea Rep., **1**: 50–125.

WOOD, E. J. F., & DAVIS, P. S., 1956. "Importance of smaller phytoplankton elements". Nature, Lond., **177**: 438.

Contribution No. 985

Reprinted without change of pagination from the
Journal of Fluid Mechanics, *volume* 5, *part* 3, *pp.* 401–435, 1959

Cellular convection with finite amplitude in a rotating fluid

By G. VERONIS
Woods Hole Oceanographic Institution, Woods Hole, Massachusetts

(Received 3 July 1958)

When a rotating layer of fluid is heated uniformly from below and cooled from above, the onset of instability is inhibited by the rotation. The first part of this paper treats the stability problem as it was considered by Chandrasekhar (1953), but with particular emphasis on the physical interpretation of the results. It is shown that the time-dependent (overstable) motions occur because they can reduce the stabilizing effect of rotation. It is also shown that the boundary of a steady convection cell is distorted by the rotation in such a way that the wavelength of the cell measured along the distorted boundary is equal to the wavelength of the non-rotating cell. This conservation of cellular wavelength is traced to the constancy of horizontal vorticity in the rotating and non-rotating systems. In the finite-amplitude investigation the analysis, which is pivoted about the linear stability problem, indicates that the fluid can become unstable to finite-amplitude disturbances before it becomes unstable to infinitesimal perturbations. The finite-amplitude motions generate a non-linear vorticity which tends to counteract the vorticity generated by the imposed constraint of rotation. Under experimental conditions the two fluids, mercury and air, which are considered in this paper, will not exhibit this finite amplitude instability. However, a fluid with a sufficiently small Prandtl number will become unstable to finite-amplitude perturbations. The special role of viscosity as an energy releasing mechanism in this problem and in the Orr-Sommerfeld problem suggests that the occurrence of a finite-amplitude instability depends on this dual role of viscosity (i.e. as an energy releasing mechanism as well as the more familiar dissipative mechanism). The relative stability criterion developed by Malkus & Veronis (1958) is used to determine the preferred type of cellular motions which can occur in the fluid. This preferred motion is a function of the Prandtl number and the Taylor number. In the case of air it is shown that overstable square cells become preferred in finite amplitude, even though steady convective motions occur at a lower Rayleigh number.

Introduction

The columnar structure in figure 1 represents the manner in which the boundary of a hexagonal convection cell in a fluid is distorted by an imposed uniform rotation of the entire system. The distortion plays an important role in the determination of the finite amplitude effects in the convecting fluid. We shall study this geometry of cellular convection as part of a more general investigation into the nature of cellular convection in a rotating fluid.

The constraint of rotation is, of course, only one of a large number of externally imposed constraints to which a fluid may be subjected. Yet a detailed knowledge of the constraining effect of rotation and of the finite-amplitude behaviour of the rotating fluid may provide an insight into the mechanism of a broad class of problems in which the system is constrained externally.

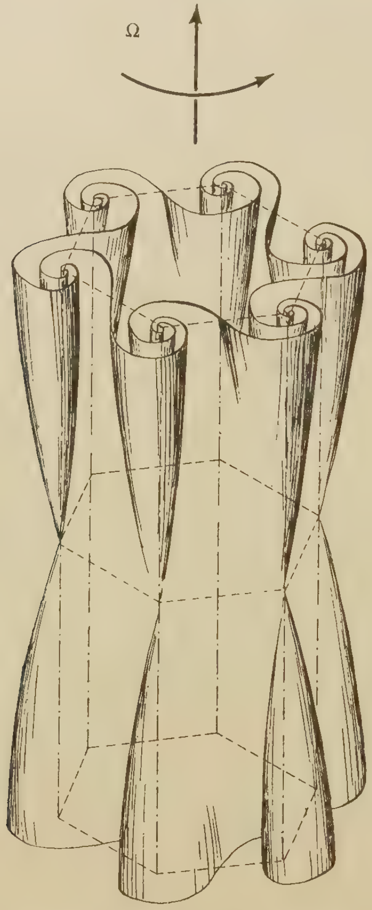

FIGURE 1. A perspective sketch of a hexagonal convection cell as it is distorted by an imposed rotation of the fluid.

As a starting-point for this discussion, we have available several previous studies. The stability problem has been investigated theoretically by Chandrasekhar (1953) and by Nakagawa & Frenzen (1955) (hereafter these papers will be referred to as II and III respectively), and experimentally by Nakagawa & Frenzen (1955) and by Fultz & Nakagawa (1955). Finite amplitude cellular convection in a non-rotating fluid has been considered by Malkus & Veronis (1958) (hereafter referred to as I). The questions which we may hope to answer in this paper may be posed more clearly in the light of these investigations.

When a horizontally infinite layer of fluid is heated uniformly from below and cooled from above, the system is stable to infinitesimal disturbances for values of the Rayleigh number λ below a critical value λ_0. Here, $\lambda = \alpha g \beta_m d^4/\kappa\nu$, where g is the gravitational acceleration; α, ν and κ are respectively the coefficients of expansion, kinematic viscosity and thermometric diffusivity of the fluid; d is the depth of the fluid; and $\beta_m = (T_H - T_C)/d$, where T_H and T_C are respectively the temperatures at the bottom and top surfaces of the layer. When $\lambda \geqslant \lambda_0$, the fluid is unstable and convective motions occur leading to a distortion of the mean (horizontally averaged) temperature field. Experimentally, convection is observed to set in as a fairly regular cellular pattern in the horizontal.

The specific value of λ_0 depends on the boundary conditions. In the non-rotating system, λ_0 is constant for a particular set of boundary conditions. In the rotating fluid, the specific value of the critical Rayleigh number depends on the value of the Taylor number $\mathscr{T}^2 = 4\Omega^2 d^4/\nu^2$ (where Ω is the uniform angular velocity of the system) and on the value of the Prandtl number $\sigma\,(\equiv \nu/\kappa)$. The general effect of the rotation is to increase λ_0 and to decrease the horizontal scale of the cells. For large, but experimentally realizable, values of $\mathscr{T}^2$, the value of λ_0 may be as high as 10^5 times the critical Rayleigh number corresponding to the non-rotating system. It has been noted both experimentally and theoretically (cf. II and III) that for a range of values of the parameters σ and $\mathscr{T}^2$, instability can arise as a time-periodic motion. In the greater part of the range, this so-called 'overstability' occurs before steady convective instability.

A number of interesting questions arise from the study of the stability problem. Although the horizontal scale of the cells diminishes with rotation, what similarities exist between the motions of the constrained and unconstrained systems? What physical mechanism causes overstability to occur and to be preferred to steady convective instability? Is it possible that the initial instability occurs as convection, but that overstability can enter and become the preferred state of motion in finite amplitude? Is the reverse possible?

As we have noted, the constraining effect of rotation manifests itself principally by making the system more stable, i.e. by increasing the value of λ_0. That the rotating system will behave differently from the non-rotating fluid in finite amplitude is indicated by the fact that viscosity plays a dual role here. In addition to its more familiar role of dissipating the kinetic energy of the fluid, the viscosity serves also as the energy releasing mechanism. The fluid particles are constrained by the rotation to move in the direction of the rotation vector $\mathbf{\Omega}$. Only through the presence of viscosity do they find a means for achieving cross-isobar flow through which potential energy is released. This dual role of viscosity as a function of rotation is no more evident than it is in the fact that (cf. II) for sufficiently high rotation rates, a fluid confined by rigid boundaries becomes unstable for a value of λ_0 lower than the λ_0 corresponding to a fluid confined by free boundaries where viscous effects are smaller. In the non-rotating case, the free boundary conditions have always led to lower λ_0.

As a further guide to the finite amplitude study we turn to the analysis of finite amplitude convection in the non-rotating system (I).

After the fluid has become unstable, the convective motions lead to a distortion of the mean temperature profile. When the Prandtl number is large, the amount of heat which is transported vertically by convection is determined principally by this distortion of the mean temperature field. For $\sigma < 1$, the self-distortion of the cellular structure plays an important role in the determination of the vertical heat transport. Since the constraint of rotation adds to the distortion of the cellular structure, we can anticipate that in the present study the self-distortion of the cell will be more important in determining the heat transport.

All close-packed cellular patterns (rectangles, hexagons, triangles and two-dimensional rolls) are mathematically possible in finite amplitude. A relative stability criterion was developed in I to determine which of the many possible steady solutions will actually be realized. When the system has vertical symmetry and free boundaries, square cells are the preferred pattern for $\sigma > 0{\cdot}8$, and limiting rectangles (one side becomes infinitely long) for $\sigma \leqslant 0{\cdot}8$. When a vertical asymmetry is present (e.g. free upper boundary, rigid lower boundary), hexagonal cells are preferred when λ exceeds λ_0 by a small amount.

The qualitative results relating to symmetrical and asymmetrical systems ought not to be altered by the presence of rotation. However, is the preferred cellular pattern for a symmetric system a function of the rotation rate? What effect has overstability on the geometrical pattern of the flow?

More general questions are the following. What is the mechanism through which the constraint manifests itself in the flow? Does the fluid organize itself so as to minimize the effects of the externally imposed constraint? Indeed, is it possible for the fluid to generate its own 'constraint' to offset the imposed one?

1. Equations and boundary conditions

This problem is one of a large class of convection problems in which the Boussinesq (1903) approximation may be applied. The density is considered to be constant everywhere in the equations except in the buoyant force term. The equations for the local conservation of heat, momentum and mass are then

$$\frac{\partial \tilde{T}}{\partial t} - \kappa \nabla^2 \tilde{T} = -\mathbf{v}.\nabla \tilde{T}, \tag{1.1}$$

$$\frac{\partial \mathbf{v}}{\partial t} + \mathbf{v}.\nabla\mathbf{v} + 2\Omega\mathbf{k}\times\mathbf{v} = -\frac{1}{\rho_m}\nabla p + \gamma\tilde{T}\mathbf{k} + \nu\nabla^2\mathbf{v}, \tag{1.2}$$

$$\nabla.\mathbf{v} = 0, \tag{1.3}$$

where the equation of state

$$\rho = \rho_m(1-\alpha\tilde{T}) \tag{1.4}$$

has been used in the buoyancy term. In these equations $\tilde{T}$ is the deviation of the temperature from its mean value, ρ_m is the mean density of fluid, $\mathbf{v}$ is the three-dimensional velocity field (u, v, w) in the directions (x, y, z) respectively, t is the time, $\mathbf{k}$ is the unit vector in the vertical (z) direction, ∇^2 is the three-dimensional Laplacean operator, $p = \tilde{p} - gz$, where $\tilde{p}$ is the pressure, $\gamma = \alpha g$, and the remaining terms have been defined in the introduction.

We consider an ensemble of systems with the given fixed boundary conditions. These systems will have arbitrary phases in time and horizontal space. An ensemble average denotes an average over these arbitrary phases, and, consequently, $\tilde{T}$ can be subdivided into a portion which is a function only of the vertical co-ordinate and a fluctuation which is a function of x, y, z and t.

Let

$$\tilde{T} = T(z) + T(x,y,z,t), \tag{1.5}$$

where $T(z)$ denotes the ensemble-average temperature. Thus, letting a bar over a quantity denote the ensemble-average, we have

$$\overline{\tilde{T}} = T(z), \quad \overline{T(x,y,z,t)} = 0.$$

The substitution of (1.5) into (1.1) yields

$$\frac{\partial T}{\partial t} - \kappa \frac{\partial^2 T(z)}{\partial z^2} - \kappa \nabla^2 T = \beta w - \mathbf{v} \, . \, \nabla T, \tag{1.6}$$

where $\beta = -\partial T(z)/\partial z$ is the negative vertical gradient of mean temperature. By taking an ensemble-average of (1.6), one gets

$$-\kappa \frac{\partial^2 T(z)}{\partial z^2} = -\frac{\partial}{\partial z} (\overline{wT}), \tag{1.7}$$

which can be integrated once to yield

$$\kappa \beta + \overline{wT} = H, \tag{1.8}$$

where H is the vertical heat flux in the fluid and is constant for an ensemble of systems with given fixed boundary conditions. Thus, taking a vertical average $\left(= \frac{1}{d} \int_0^d H \, dz \right)$ yields

$$\kappa \beta_m + \{wT\}_m = H, \tag{1.9}$$

where $\{ \ \}_m$ denotes both an ensemble and a vertical average.

From (1.8) and (1.9), we have

$$\frac{\beta}{\beta_m} = 1 + \frac{\{wT\}_m - \overline{wT}}{\kappa \beta_m}. \tag{1.10}$$

Equation (1.10) provides a means for determining the distortion of the mean temperature field from the values of the fluctuation quantities w and T.

Substituting (1.7) into (1.6) and making use of (1.10), we have

$$\frac{\partial T}{\partial t} - \kappa \nabla^2 T - \beta_m w = \frac{\{wT\}_m - \overline{wT}}{\kappa} - h, \tag{1.11}$$

where $h = \mathbf{v} \, . \, \nabla T - \partial(\overline{wT})/\partial z$ represents the zero-average heat advection terms.

The pressure p (relative to hydrostatic pressure) can be eliminated from (1.2) to yield

$$\frac{\partial}{\partial t} \nabla^2 w + 2\Omega \frac{\partial \zeta}{\partial z} - \gamma \nabla_1^2 T = \nu \nabla^4 w + L, \tag{1.12}$$

where $$L = \frac{\partial}{\partial z}\left[\frac{\partial}{\partial x}(\mathbf{v} \, . \, \nabla u) + \frac{\partial}{\partial y}(\mathbf{v} \, . \, \nabla v)\right] - \nabla_1^2(\mathbf{v} \, . \, \nabla w). \quad \nabla_1^2 = \frac{\partial^2}{\partial x^2} + \frac{\partial^2}{\partial y^2};$$

and $\zeta = \partial v/\partial x - \partial u/\partial y$ is the vertical component of vorticity. From the first two equations of (1.2), an additional relation between ζ and w can be derived:

$$\frac{\partial \zeta}{\partial t} - \nu \nabla^2 \zeta - 2\Omega \frac{\partial w}{\partial z} = -Z, \tag{1.13}$$

where $Z = \frac{\partial}{\partial x}(\mathbf{v} \, . \, \nabla v) - \frac{\partial}{\partial y}(\mathbf{v} \, . \, \nabla u)$. The terms L and Z appearing in (1.12) and (1.13) are both zero-average non-linear terms.

Because the subsequent analysis will be based on an expansion of each of the variables, it is convenient to work with the equations in dimensionless form. Thus, letting $\mathbf{v} = \nu\mathbf{v}'/d$, $\mathbf{r} = d\mathbf{r}'$, $\nabla = d^{-1}\nabla'$, $T = \kappa\nu T'/\gamma d^3$, $t = d^2\tau/\kappa$, $\sigma = \nu/\kappa$, one has

$$\left(\frac{\partial}{\partial\tau} - \nabla^2\right) T - \sigma\lambda w = \sigma^2[\{wT\}_m - \overline{wT}]\, w - \sigma h, \tag{1.11 bis}$$

$$\left(\frac{1}{\sigma}\frac{\partial}{\partial\tau} - \nabla^2\right) \nabla^2 w + \mathscr{T}\frac{\partial\zeta}{\partial z} - \frac{1}{\sigma}\nabla_1^2 T = L, \tag{1.12 bis}$$

$$\left(\frac{1}{\sigma}\frac{\partial}{\partial\tau} - \nabla^2\right) \zeta - \mathscr{T}\frac{\partial w}{\partial z} = -Z, \tag{1.13 bis}$$

where the primes have been dropped from the variables. *Throughout the remainder of the work, unprimed quantities will denote dimensionless variables unless otherwise noted.* In these equations $\mathscr{T} = 2\Omega d^2/\nu$ is the square root of the Taylor number.

The analysis will be pivoted about the linear stability solution and it is therefore convenient to eliminate all but one of the variables in the linear operators. Elimination of T and ζ from the left-hand sides of (1.11), (1.12) and (1.13) gives

$$\begin{aligned}\left(\frac{1}{\sigma}\frac{\partial}{\partial\tau} - \nabla^2\right)^2 \left(\frac{\partial}{\partial\tau} - \nabla^2\right) \nabla^2 w + \mathscr{T}^2\left(\frac{\partial}{\partial\tau} - \nabla^2\right)\frac{\partial^2 w}{\partial z^2} - \left(\frac{1}{\sigma}\frac{\partial}{\partial\tau} - \nabla^2\right)\lambda\nabla_1^2 w \\ = \sigma\left(\frac{1}{\sigma}\frac{\partial}{\partial\tau} - \nabla^2\right)[\{wT\}_m - \overline{wT}]\,\nabla_1^2 w \\ + \mathscr{T}\left(\frac{\partial}{\partial\tau} - \nabla^2\right)\frac{\partial Z}{\partial z} - \left(\frac{1}{\sigma}\frac{\partial}{\partial\tau} - \nabla^2\right)\nabla_1^2 h + \left(\frac{\partial}{\partial\tau} - \nabla^2\right)\left(\frac{1}{\sigma}\frac{\partial}{\partial\tau} - \nabla^2\right) L.\end{aligned} \tag{1.14}$$

Equations (1.3), (1.11), (1.13) and (1.14) are the basic equations of our analysis. A perturbation method similar to that employed in I is used to derive approximate solutions.

Let

$$\left.\begin{aligned} w &= \epsilon w_0 + \epsilon^2 w_1 + \epsilon^3 w_2 + \epsilon^4 w_3 + \dots, \\ T &= \epsilon T_0 + \epsilon^2 T_1 + \epsilon^3 T_2 + \epsilon^4 T_3 + \dots, \\ u &= \epsilon u_0 + \epsilon^2 u_1 + \epsilon^3 u_2 + \epsilon^4 u_3 + \dots, \\ v &= \epsilon v_0 + \epsilon^2 v_1 + \epsilon^3 v_2 + \epsilon^4 v_3 + \dots. \end{aligned}\right\} \tag{1.15}$$

The parameter ϵ must be identified with the amplitude. Since the value of λ determines the amplitude, a relation between λ and ϵ must also be deduced. As in I, λ is also expanded in terms of ϵ: thus

$$\lambda = \lambda_0 + \epsilon\lambda_1 + \epsilon^2\lambda_2 + \epsilon^3\lambda_3 + \epsilon^4\lambda_4 + \dots, \tag{1.16}$$

where the λ_i are to be determined.

If the expansions (1.15) and (1.16) are introduced into equations (1.3), (1.11), (1.13) and (1.14), and if the coefficients of each order of ϵ are equated, a series of equations is derived involving the variables w_i, T_i, u_i and v_i. We shall postpone writing the resulting relations explicitly until we come to the specific sections on finite-amplitude steady convection and finite-amplitude overstability.

An additional equation, which we shall find useful, results from multiplying (1.2) by $\mathbf{v}$ and averaging. This yields in non-dimensional form

$$\sigma\{\mathbf{v}\,.\,\nabla^2\mathbf{v}\}_m + \{wT\}_m = \frac{\partial}{\partial\tau}\{\tfrac{1}{2}\mathbf{v}\,.\,\mathbf{v}\}_m. \tag{1.17}$$

Equation (1.17) asserts that the rate of change of kinetic energy is equal to the rate of release of potential energy minus the rate of viscous dissipation of kinetic energy (the first term on the left is negative definite). In our problems the right-hand side will vanish.

Boundary conditions

If the boundary at the top or the bottom surface is considered 'free', the conditions on the velocities are

$$w = 0, \quad \frac{\partial v}{\partial z} = \frac{\partial u}{\partial z} = \frac{\partial^2 w}{\partial z^2} = 0 \tag{1.18}$$

at the boundary. At rigid boundaries, the conditions are

$$w = 0, \quad u = v = \frac{\partial w}{\partial z} = 0. \tag{1.19}$$

In the present investigation both boundaries are considered 'free'. Although this is an idealization, nevertheless it permits one to determine most of the qualitative features of the flow. The rigid boundary conditions lead to such a formidable computational problem (cf. I) that the present method of solution is practically useless.

Thermally, the boundaries are considered perfect conductors. For air or water, most metal boundaries will by comparison be nearly perfect conductors. For a fluid such as mercury, silver or copper boundaries approximate the ideal boundary material. Hence, at the bounding surfaces, we take

$$T = 0. \tag{1.20}$$

If we evaluate the basic equations (1.11) and (1.12) at a free boundary where $T = 0$, then (1.12) becomes

$$\frac{\partial^4 w}{\partial z^4} = 0. \tag{1.21}$$

2. Stability problem

The equations for the stability problem can be determined either by substituting the expansions (1.15) and (1.16) in equations (1.3), (1.11), (1.13) and (1.14), and then taking only the first-order terms in ϵ, or alternatively by simply neglecting all the non-linear terms in the equations. In either case, the equations are

$$\left(\frac{\partial}{\partial \tau} - \nabla^2\right) T_0 - \sigma\lambda_0 w_0 = 0, \tag{2.1a}$$

$$\left(\frac{1}{\sigma}\frac{\partial}{\partial \tau} - \nabla^2\right) \zeta_0 - \mathscr{T}\frac{\partial w_0}{\partial z} = 0, \tag{2.1b}$$

$$\left(\frac{1}{\sigma}\frac{\partial}{\partial \tau} - \nabla^2\right)^2 \left(\frac{\partial}{\partial \tau} - \nabla^2\right) \nabla^2 w_0 + \mathscr{T}^2\left(\frac{\partial}{\partial \tau} - \nabla^2\right)\frac{\partial^2 w_0}{\partial z^2} - \left(\frac{1}{\sigma}\frac{\partial}{\partial \tau} - \nabla^2\right)\lambda_0 \nabla_1^2 w_0 = 0, \tag{2.1c}$$

$$\frac{\partial u_0}{\partial x} + \frac{\partial v_0}{\partial y} + \frac{\partial w_0}{\partial z} = 0, \tag{2.1d}$$

where the subscript zero has been included in order to identify the variables with the stability problem.

Experimentally, convection is seen to occur as a close-packed cellular regime. This indicates that a useful analytical approach to the stability problem is to assume separability of horizontal and vertical dependence and to assume a periodic horizontal structure. These two simplifications are written as

$$w_0 = e^{p_0\tau} f(x,y)\, g(z), \quad \nabla_1^2 f(x,y) = -\alpha^2\pi^2 f(x,y), \tag{2.2}$$

where α is the effective horizontal wave number and the time dependence is chosen as $e^{p_0\tau}$ as is customary in linear stability theory.

The stability problem can now be solved immediately (cf. II) since the free boundary conditions on w_0 are satisfied by $g(z) = \sin n\pi z$. If

$$w_0 = e^{p_0\tau} f(x,y) \sin n\pi z \tag{2.3}$$

is substituted into (2.1*c*), it is found that

$$(\alpha^2+n^2)\,[p_0+\pi^2(\alpha^2+n^2)]\,[p_0/\sigma+\pi^2(\alpha^2+n^2)]^2+\mathscr{T}^2 n^2[p_0+\pi^2(\alpha^2+n^2)] \\ -\alpha^2\lambda_0[p_0/\sigma+\pi^2(\alpha^2+n^2)] = 0,$$

hence, on rearrangement,

$$p_0^3+(2\sigma+1)\,\pi^2(\alpha^2+n^2)\,p_0^2+[\pi^4(\alpha^2+n^2)^2\,(\sigma^2+2\sigma)+(\mathscr{T}^2 n^2\sigma-\alpha^2\lambda_0)\,\sigma/(\alpha^2+n^2)]\,p_0 \\ +\sigma^2\pi^6(\alpha^2+n^2)^3+\sigma^2\pi^2(\mathscr{T}^2 n^2-\alpha^2\lambda_0) = 0. \tag{2.4}$$

A. *Steady convective instability*

If p_0 is real, marginal instability occurs when $p_0 = 0$, i.e. when

$$\frac{\lambda_0}{\pi^4} = \frac{(\alpha^2+n^2)^3+\mathscr{T}_1^2 n^2}{\alpha^2}, \tag{2.5}$$

where $\mathscr{T}_1^2 = \mathscr{T}^2/\pi^4$. From

$$\frac{\partial\lambda_0}{\partial\alpha^2} = 2\alpha^6+3\alpha^4 n^2-n^6-\mathscr{T}_1^2 n^2 = 0, \tag{2.6}$$

we can find that value of α^2, as a function of $\mathscr{T}_1^2$ and n^2, which minimizes λ_0/π^4.

We note immediately from (2.6) and (2.5) that $\lambda_0/\pi^4 \to 3(\frac{1}{2}\mathscr{T}_1^2 n^2)^{\frac{2}{3}}$ and $\alpha^2 \to (\frac{1}{2}\mathscr{T}_1^2 n^2)^{\frac{1}{3}}$ as $\mathscr{T}_1^2 \to \infty$. Thus, as the Taylor number increases, λ_0 increases and the cellular diameter decreases. It is evident also that λ_0/π^4 attains its minimum value when $n = 1$ (neglecting the trivial case $n = 0$ when there is no motion). A curve of λ_0/π^4 *vs* $\mathscr{T}_1^2$ is plotted in figure 5.

Since $\mathscr{T}_1^2$ is inversely proportional to the square of the viscosity, the asymptotic expression, $\lambda_0/\pi^4 \to 3(\frac{1}{2}\mathscr{T}_1^2 n^2)^{\frac{2}{3}}$ asserts that both the critical Rayleigh number and the actual critical temperature difference $T_H - T_C$ decreases with increasing viscosity. This destabilizing effect of viscosity plays an important role in the finite-amplitude behaviour of the fluid, and we shall refer to it again later.

The motions associated with the point of instability depend on the particular cellular pattern which is postulated. These motions will be presented here in some detail because a knowledge of them provides some insight into the finite-amplitude behaviour of the fluid.

B. *Geometry of the fluid motion*

The possible horizontal patterns for close-packed cells are limited to two-dimensional rolls, hexagons, triangles and rectangles. Though the first of these cannot occur in an experimental investigation, it represents the simplest type of motion and will be discussed first.

Rolls. Let w_0 be independent of the y-co-ordinate. The solution (2.2) which satisfies the symmetry condition $\partial w_0/\partial x = 0$ at the walls of the cell is

$$w_0 = 2\cos\pi\alpha x \sin\pi z, \tag{2.7}$$

where, for reasons which will appear later, w_0 has been normalized, i.e. $\{w_0^2\}_m = 1$. (The normalization does not affect the present discussion.)

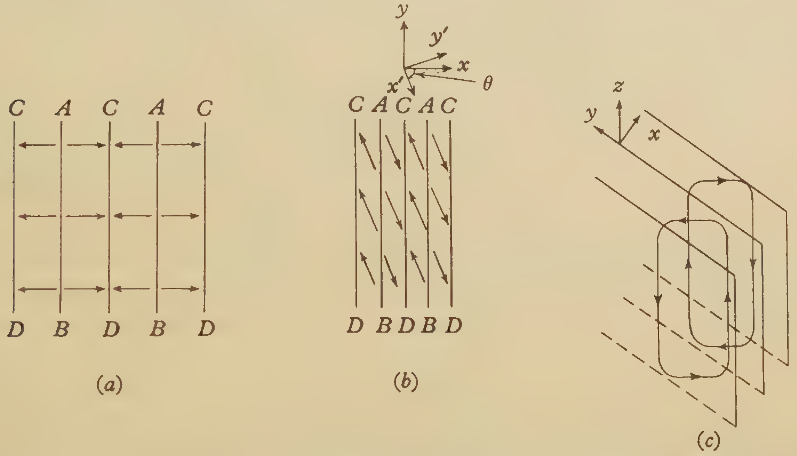

(*a*) (*b*) (*c*)

FIGURE 2. (*a*) A top view of two-dimensional rolls in a non-rotating fluid. The arrows indicate the direction of motion of the fluid. (*b*) The same in a system rotating counter-clockwise. (*c*) A perspective view of fluid particle motions in a role when the fluid is rotated.

From equations (2.1), the temperature T_0 and the velocity components u_0, v_0 are

$$T_0 = \frac{2\sigma\lambda_0}{\pi^2(\alpha^2+1)}\cos\pi\alpha x\sin\pi z, \quad u_0 = -\frac{2}{\alpha}\sin\pi\alpha x\cos\pi z,$$

$$v_0 = \frac{2\mathscr{T}_1}{\alpha(\alpha^2+1)}\sin\pi\alpha x\cos\pi z. \tag{2.8}$$

When $\mathscr{T}_1 = 0$, we have $v_0 = 0$ and the fluid motion is in the x-direction only. In figure 2*a* a view of the top of a non-rotating fluid layer is shown. The fluid has maximum upward velocity along lines AB and maximum downward velocity along lines CD.

When the system is rotated, the coriolis force introduces a velocity component parallel to the isobars (isotherms in this case), i.e. in the y-direction. Therefore, the streamlines are oriented at an oblique angle to the y-axis (figure 2*b*).

The wave-number α of the cell is a function of $\mathscr{T}_1^2$ as given by (2.6). The wave number corresponding to the oblique cell, i.e. in the direction of the orientation of the cell, can be computed from (2.8). Let θ be the angle from the x-axis to the streamline path as indicated in figure 2b. Then

$$\theta = \tan^{-1}\left(\frac{v_0}{u_0}\right) = -\tan^{-1}\left(\frac{\mathscr{T}_1}{\alpha^2+1}\right). \tag{2.9}$$

The square of the wave-number of the oblique cell is given by

$$\alpha^2\cos^2\theta = \frac{\alpha^2(\alpha^2+1)^2}{\mathscr{T}_1^2+(\alpha^2+1)^2}. \tag{2.10}$$

With (2.6), this expression reduces to

$$\alpha^2\cos^2\theta = \alpha^2(1/2\alpha^2) = \tfrac{1}{2}. \tag{2.11}$$

In other words, although the wavelength of the cell decreases with rotation, the wavelength of the cell measured in the direction of the orientation of the cell is the same as in the non-rotating case.

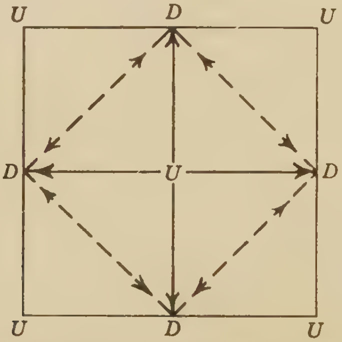

FIGURE 3a. A top view of square cells in a non-rotating fluid. Points marked U are points of maximum upward velocity; those marked D are points of maximum downward velocity. The region within the dotted lines would be seen as a cell in an experiment.

Square cells. From the analysis of the non-rotating system we anticipate that square cells will be the preferred form for a system with vertical symmetry. Paralleling the argument for rolls, we can write

$$\left.\begin{aligned} w_0 &= 2\sqrt{2}\cos\frac{\pi\alpha x}{\sqrt{2}}\cos\frac{\pi\alpha y}{\sqrt{2}}\sin\pi z, \quad T_0 = \frac{\sigma\lambda_0}{\pi^2(\alpha^2+1)}w_0, \\ u_0 &= -\left[\frac{2\mathscr{T}_1}{\alpha(\alpha^2+1)}\cos\frac{\pi\alpha x}{\sqrt{2}}\sin\frac{\pi\alpha y}{\sqrt{2}}+\frac{2}{\alpha}\sin\frac{\pi\alpha x}{\sqrt{2}}\cos\frac{\pi\alpha y}{\sqrt{2}}\right]\cos\pi z, \\ v_0 &= \left[-\frac{2}{\alpha}\cos\frac{\pi\alpha x}{\sqrt{2}}\sin\frac{\pi\alpha y}{\sqrt{2}}+\frac{2\mathscr{T}_1}{\alpha(\alpha^2+1)}\sin\frac{\pi\alpha x}{\sqrt{2}}\cos\frac{\pi\alpha y}{\sqrt{2}}\right]\cos\pi z. \end{aligned}\right\} \tag{2.12}$$

When $\mathscr{T}_1 = 0$, both the horizontal and the vertical motions form a square pattern. A top view of the fluid is illustrated in figure 3a, where U and D define points of maximum upward and downward motions respectively. The cell is shown with fluid rising in the centre, but the pattern can equally as well be displaced by a half wavelength in the x- or y-direction to yield a cell with sinking at the centre. In actuality the region within the dotted lines is what one would see as a cell in an experiment.

When $\mathscr{T}_1 > 0$, the coriolis force causes the fluid to turn as it moves toward or from the centre so that part of the flow is parallel to the isobars. The spiral curves in figure 3*b* correspond to the straight lines shown in figure 3*a*. As the spiral crosses the x- and y-axes, it coincides with the inverse logarithmic spiral $r = \alpha^{-1}\exp\{\mathscr{T}_1\theta/(\alpha^2+1)\}$ (in polar co-ordinates r, θ), but the regions intermediate to the axes, it deviates from the logarithmic spiral. (The actual spiral is not equiangular, i.e. it does not cross all radial lines with the same angle at each traversal. The logarithmic spiral was used to construct the figure and to compute the half wavelength along the path.) By computing the length of the spiral, one can derive expression (2.11) for the horizontal 'wave-number' along the spiral. The wavelength measured along the distorted cellular boundary is again equal to that of the non-rotating case.

Figure 3*c* is a perspective sketch of a complete trajectory of a particle which travels from the centre of the cell to the edge and back again. The particle spirals upward and clockwise (for counterclockwise Ω) from the centre of the cell, crosses to the corner near the top of the cell and spirals downward and counterclockwise. Halfway down it reverses its direction of rotation, spirals downward and clockwise crosses back toward the middle of the cell, and begins a counterclockwise upward motion toward the centre.

The reversal of rotation as a particle crosses the middle plane is due to the fact that at this point the horizontal divergence of the fluid changes sign. As the fluid moves outward, it is deflected to the right by the coriolis force and spirals in a clockwise manner. Converging fluid spirals counterclockwise when deflected to the right.

The square cell shown in the diagram corresponds to the basic geometry of the vertical velocity. The actual cell is distorted by the rotation and is not reproduced here.

Hexagonal cells. The preferred pattern for the vertical velocity is the hexagonal pattern when the boundary conditions provide a vertical asymmetry. Since most experimental observations of cells are made when the upper surface is free, hexagonal cells will ordinarily occur.

The discussion parallels that for square cells. The analytical form as proposed by Christopherson (1940) is

$$w_0 = \frac{2}{\sqrt{3}}\left\{2\cos\frac{2\pi x}{\sqrt{3}L}\cos\frac{2\pi y}{3L} + \cos\frac{4\pi y}{3L}\right\}\sin\pi z, \tag{2.13a}$$

where $L = 4/(3\alpha)$ is the length of one side of the regular hexagon. The remaining variables have the form

$$\left.\begin{aligned} T_0 &= \frac{\sigma\lambda_0}{\pi^2(\alpha^2+1)}\,w_0, \\ u_0 &= -\left[\frac{3L}{2}\sin\frac{2\pi x}{\sqrt{3}L}\cos\frac{2\pi y}{3L} + \frac{\sqrt{3}L\mathscr{T}_1}{2(\alpha^2+1)}\left(\cos\frac{2\pi x}{\sqrt{3}L}\sin\frac{2\pi y}{3L} + \sin\frac{4\pi y}{3L}\right)\right]\cos\pi z, \\ v_0 &= \left[\frac{3L\mathscr{T}_1}{2(\alpha^2+1)}\sin\frac{2\pi x}{\sqrt{3}L}\cos\frac{2\pi y}{3L} - \frac{\sqrt{3}L}{2}\left(\cos\frac{2\pi x}{\sqrt{3}L}\sin\frac{2\pi y}{3L} + \sin\frac{4\pi y}{3L}\right)\right]\cos\pi z. \end{aligned}\right\} \tag{2.13b}$$

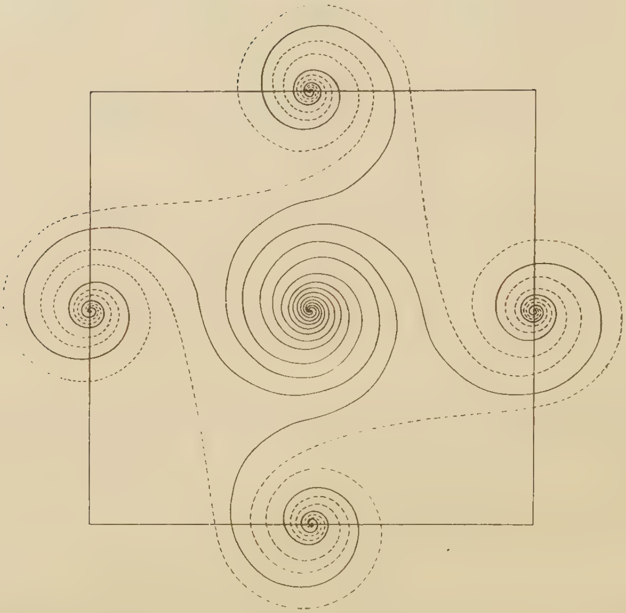

FIGURE 3*b*. A square cell in a rotating fluid. The particle motions from the centre outward follow the spiral curves. The dashed curves form the boundary of the square cell.

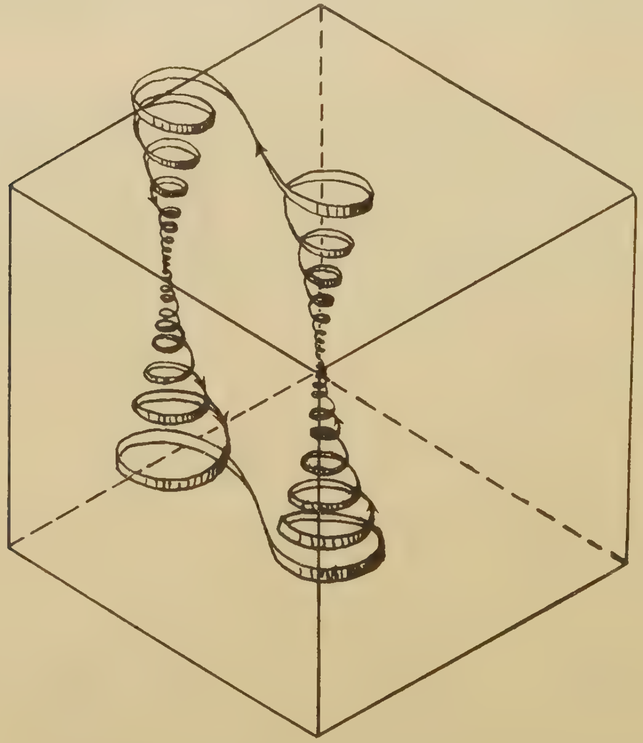

FIGURE 3*c*. A perspective sketch of a fluid particle motion in the square cell.

Figure 4*a* illustrates the particle motion at the top of a non-rotating-cell. Figure 4*b* is a top view of a rotating cell and of the six adjacent cells. The dashed spirals form the upper boundary of the centre cell. Each centre is surrounded by six corners and each corner receives fluid from the three adjacent centres.

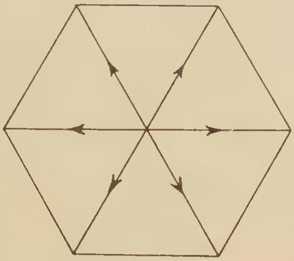

FIGURE 4*a*. Top view of a non-rotating hexagonal cell. The fluid rises in the centre and spreads outward to the six corners where it descends.

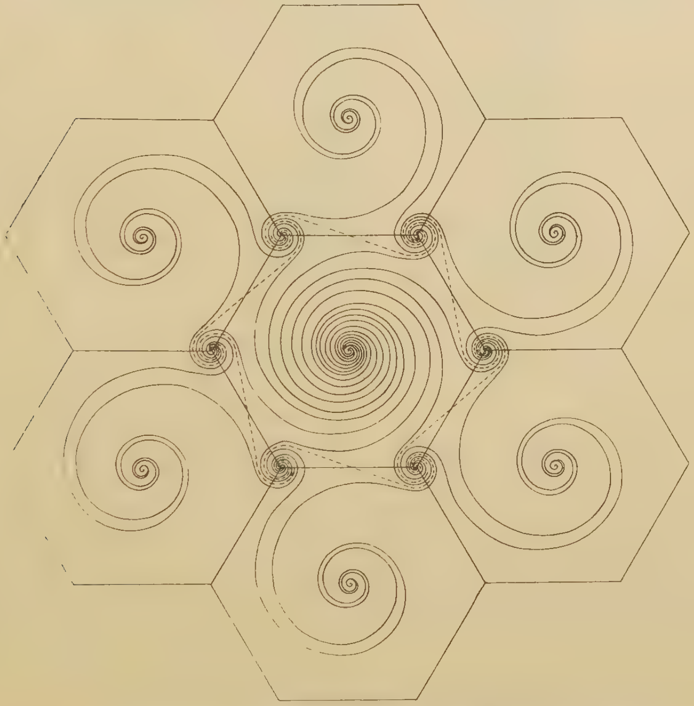

FIGURE 4*b*. A top view of seven rotating hexagonal cells. The fluid particles follow spiral paths from the centre toward the corners. The dashed lines form the boundaries of the centre cell.

A perspective sketch of a fluid particle path in three dimensions is shown in figure 4*c*. Figure 1 illustrates the manner in which the cell is distorted by the rotation.

The effective wave-number of the non-rotating cell is again equal to the wave-number measured along the spiral curve.

The three cases discussed here indicate that the wave-number measured along the curved path is invariant. It is clear that such an invariance must be intimately coupled with a physical property of the fluid which is unaffected by the imposed constraint. The one property of the fluid which is not affected by a rotation about a vertical axis is the horizontal vorticity. We shall show here how the constancy of horizontal vorticity preserves the wave-number measured in the direction of flow for the simplest type of motion, viz. that of rolls.

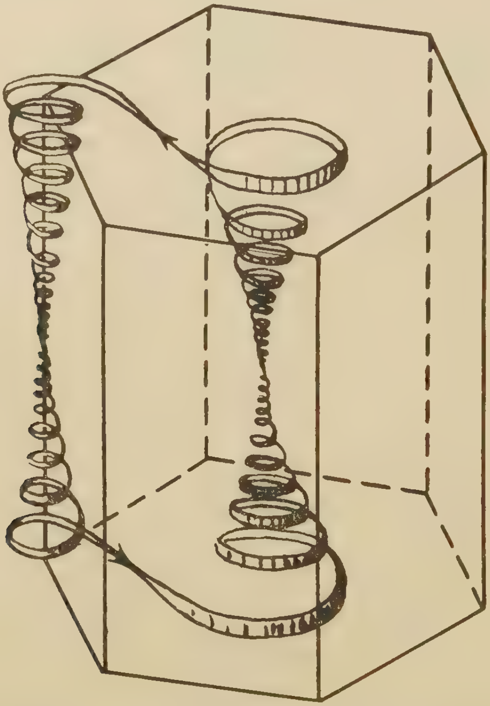

FIGURE 4c. A perspective sketch of a fluid particle path which passes through the centre of the cell.

Consider a rotation of the horizontal co-ordinates so that the x'-direction is measured along the direction of flow (figure 2b). Then the horizontal vorticity about the y-axis is given by $\partial u'/\partial z - \partial w/\partial x'$, where the primes correspond to a measure of the quantities along the new axes. Since the horizontal vorticity is constant, we have

$$\left\{\left(\frac{\partial u'}{\partial z}-\frac{\partial w}{\partial x'}\right)^2\right\}_m = \left\{\left(\frac{\partial u}{\partial z}-\frac{\partial w}{\partial x}\right)^2\right\}_m = \text{const.}, \tag{2.14}$$

where the middle expression corresponds to the non-rotating system, i.e. when x' is parallel to x. From the equation of continuity, we have

$$\frac{\partial u'}{\partial x'}+\frac{\partial w}{\partial z} = 0, \quad \frac{\partial u}{\partial x}+\frac{\partial w}{\partial z} = 0. \tag{2.15}$$

Since w is normalized and since the z-distance is fixed, equation (2.15) yields a relation between the wave-number measured in the x (or x') direction and the amplitude of u (or u'). From (2.14) we then note that the wave-number must be the same in the two systems. When the vertical velocity is normalized the amplitudes of the horizontal velocities are equal.

C. *Overstability*

Though p_0 must be real in the non-rotating system, p_0 may be complex when $\mathscr{T}^2 > 0$. The coefficients of (2.4) are real; therefore, in general p_0 will have one real and two complex conjugate roots. These can be written in the form

$$(p_0 - p')(p_0 - p_r - ip_i)(p_0 - p_r + ip_i) = 0,$$

or
$$p_0^3 - (p' + 2p_r)p_0^2 + (2p_r p' + p_i^2 + p_r^2)p_0 - p'(p_i^2 + p_r^2) = 0,$$

where p', p_i and p_r are real.

For marginal stability $p_r = 0$, and

$$p_0^3 - p'p_0^2 + p_i^2 p_0 - p'p_i^2 = 0. \tag{2.16}$$

Hence, for marginal stability, the product of the coefficients of p_0^2 and p_0 must equal the coefficient of p_0^0. By (2.4) this condition becomes

$$\frac{\lambda_0}{\pi^4} = 2(\sigma+1)\left[\frac{(\alpha^2+n^2)^3 + \dfrac{\sigma^2}{(\sigma+1)^2}n^2\mathscr{T}_1^2}{\alpha^2}\right], \tag{2.17}$$

which has a minimum when $\partial\lambda_0/\partial\alpha^2 = 0$, i.e. when

$$2\alpha^6 + 3\alpha^4 n^2 = n^6 + \frac{\sigma^2}{(\sigma+1)^2}n^2\mathscr{T}_1^2. \tag{2.18}$$

Thus $\alpha^2 \to 2^{-\frac{1}{3}}[\sigma n\mathscr{T}_1/(\sigma+1)]^{\frac{2}{3}}$ and $\lambda_0/\pi^4 \to 2^{\frac{1}{3}}3(\sigma+1)[\sigma n\mathscr{T}_1/(\sigma+1)]^{\frac{2}{3}}$ as $\mathscr{T}_1^2 \to \infty$. (The above results do not obtain for $\sigma = 0$, but this case is physically uninteresting and will not be considered.)

The remainder of the discussion will be confined to the lowest eigenvalue, i.e. to the case $n = 1$.

When p_0 is imaginary, the coefficient of p_0 in (2.16) is real and positive. From (2.4), we find that

$$p_i^2 = \pi^4(\alpha^2+1)^2(\sigma^2+2\sigma) + \frac{\sigma}{\alpha^2+1}(\mathscr{T}^2\sigma - \alpha^2\lambda_0) \geqslant 0,$$

or, using (2.17), that

$$p_i^2 = -\sigma^2\pi^4(\alpha^2+1)^2 + \frac{\mathscr{T}^2\sigma^2(1-\sigma)}{(\alpha^2+1)(1+\sigma)} \geqslant 0. \tag{2.19}$$

Therefore, a necessary condition for overstability is

$$\mathscr{T}_1^2 \geqslant \frac{\sigma+1}{-\sigma+1}(\alpha^2+1)^3. \tag{2.20}$$

Eliminating $\mathscr{T}_1^2$ from (2.18) and the equality of (2.20), we can find the value of α^2 at which overstability can just occur, i.e. when $p_i = 0$. This value satisfies

$$(2-3\sigma^2)\alpha^2 + 3(1-2\sigma^2)\alpha^4 - 3\sigma^2\alpha^2 - 1 = 0. \tag{2.21}$$

When $\sigma = \sqrt{\frac{2}{3}}$, $\alpha^2 = \infty$. Therefore $\sigma = \sqrt{\frac{2}{3}}$ represents the (upper) limiting value of the Prandtl number for which overstability can occur.*

Equation (2.17) together with (2.18) determines the minimum value of λ_0 for each pair of values of $\mathscr{T}_1^2$ and σ. The curves in figure 5 show the dependence of λ_0/π^4 on $\mathscr{T}_1^2$ for a number of values of σ. The curve C corresponds to steady convective instability.

It is possible, of course, that the fluid may become unstable in a steady convective manner and that overstability may occur in finite amplitude or that overstability may occur first and convection be preferred in finite amplitude. Figure 6 shows three divided regions in the $(\sigma, \mathscr{T}_1^2)$-plane. In region A overstability cannot arise because (2.20) cannot be satisfied. In region B convection occurs first but overstability may be the preferred state in finite amplitude.

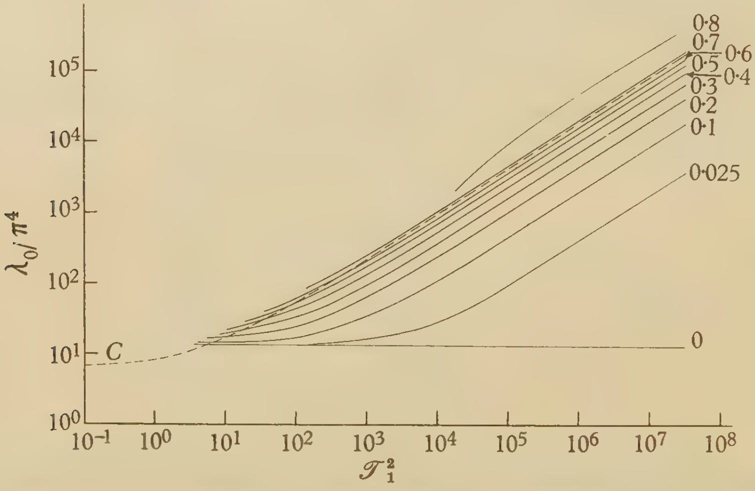

FIGURE 5. The λ_0/π^4 *vs* $\mathscr{T}_1^2$ relations for marginal stability. The dashed curve corresponds to steady convective instability. The solid curves correspond to instability in the form of time-periodic motions. The numbers on the curves are the values of the Prandtl numbers.

The curve between regions B and C marks the points at which overstability and convection occur simultaneously. The system will become overstable to infinitesimal disturbances when σ and $\mathscr{T}_1^2$ have values in the region C. Here, however, convection may come in at finite amplitude.

Why can overstability occur in the rotating systems and not when $\mathscr{T} = 0$? To answer this question we shall look into the energetics of the fluid.

For the two-dimensional case the solution to (2.1 c) is

$$w_0 = 2\sqrt{2}\cos p_0\tau \cos \pi\alpha x \sin \pi z, \tag{2.22}$$

where p_0^2 is equal to p_i^2 in (2.19). The remaining variables T_0, u_0, v_0 can be determined from equations (2.1) and are listed in §4. If these expressions are substituted into the power integral expression (1.17) (with the right-hand side equal to zero), and if we use (2.19) for p_0^2, we have

---

* Nakagawa & Frenzen (III) show in figure 7 the value of λ_0 for overstability (R_c^* in their notation) in water ($\sigma \doteqdot 6$). That overstability cannot occur for $\sigma \geqslant \sqrt{\frac{2}{3}}$ is clear from the above argument. In addition, they derive the value $\lambda_0 = 2(\sigma+1)\,\alpha^{-2}\,(\alpha^2+1)^3$ when $\mathscr{T}_1^2 = 0$. However, condition (2.20) is violated so that this result is also incorrect.

$$\frac{\lambda_0/\pi^4}{(1+\sigma)\left[(\alpha^2+1)^2+\dfrac{\sigma^2}{(\sigma+1)^2}\dfrac{\mathscr{T}_1^2}{(\alpha^2+1)}\right]}=2\frac{\alpha^2}{\alpha^2+1}, \tag{2.23}$$

where the left-hand side represents the rate of release of potential energy, $\{wT\}_m$, and the right-hand side the rate of dissipation of kinetic energy $\{\mathbf{v}.\nabla^2\mathbf{v}\}_m$. Equation (2.23) is equivalent to (2.17). Therefore the eigenvalue equation is a statement that a balance of the rate of viscous dissipation and the rate of release of potential energy is achieved by the fluid at the point of instability. The equivalent expression for the steady case is given by (2.5).

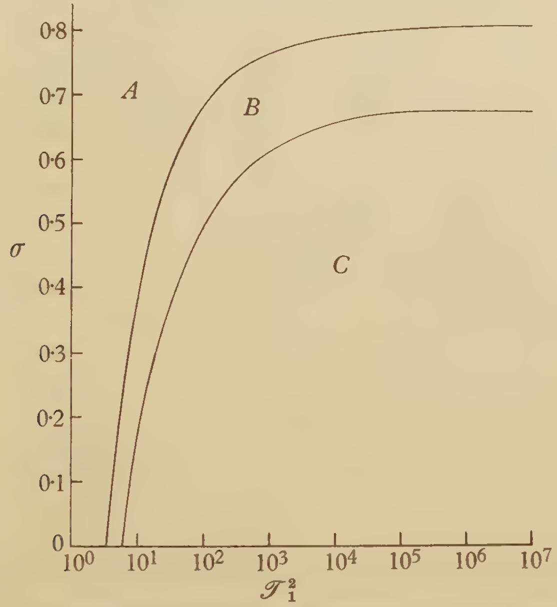

FIGURE 6. The $(\sigma, \mathscr{T}_1^2)$-plane is divided into three regions which are significant in the stability problem. In A instability occurs as steady convection. In B steady convective instability occurs first but overstability is possible for higher λ_0. In C overstability occurs before steady convection.

For fixed values of the convective heat transport, $\{wT\}_m$, and the rate of dissipation of kinetic energy, a decrease of σ in the overstable case reduces the effect of the external constraint $\mathscr{T}^2$. To compensate for the reduction of σ it is necessary that λ_0 be decreased. In the steady system the energy balance at the point of instability is unaltered by a change of σ. Therefore, in the overstable case, it is possible for the value of the Rayleigh number to be smaller than the value corresponding to the steady regime because the effect of the constraint is small when the Prandtl number is small.

From the stability problem, we have derived information concerning the onset of steady convective instability and of overstability. However, the amplitude of the motions for a given value of λ, the energetics of the fluid, the preferred motions for a given set of external parameters, and still other features are unknowns which can be determined only in a finite-amplitude study. Therefore, we shall now go on to a study of finite-amplitude steady convection.

3. Finite-amplitude steady convection

The equations which govern steady convection are given by (1.3), (1.11), (1.13) and (1.14) with $\partial/\partial\tau \equiv 0$. Thus, the following equations are obtained by collecting terms in ϵ, ϵ^2 and ϵ^3 respectively: equations corresponding to ϵ^4, etc., can be found in the same way:

$$\left.\begin{aligned}\mathscr{L}w_0 &\equiv \left[\nabla^6+\mathscr{T}^2\frac{\partial^2}{\partial z^2}-\lambda_0\nabla_1^2\right]w_0 = 0.\\ \mathscr{L}w_1 &= \lambda_1\nabla_1^2 w_0-\nabla^2 L_{00}+\mathscr{T}\frac{\partial Z_{00}}{\partial z}-\nabla_1^2 h_{00},\\ \mathscr{L}w_2 &= \lambda_2\nabla_1^2 w_0+\lambda_1\nabla_1^2 w_1-\nabla^2(L_{01}+L_{10})+\mathscr{T}\frac{\partial}{\partial z}(Z_{01}+Z_{10})\\ &\qquad -\nabla_1^2(h_{01}+h_{10})+\sigma[\{w_0T_0\}_m-\overline{w_0T_0}]\,\nabla_1^2 w_0;\end{aligned}\right\} \tag{3.1}$$

$$\left.\begin{aligned}-\nabla^2 T_0 &= \sigma\lambda_0 w_0,\\ -\nabla^2 T_1 &= \sigma\lambda_0 w_1+\sigma\lambda_1 w_0-\sigma h_{00},\\ -\nabla^2 T_2 &= \sigma\lambda_0 w_2+\sigma\lambda_1 w_1+\sigma\lambda_2 w_0+\sigma^2[\{w_0T_0\}_m-\overline{w_0T_0}]\,w_0-\sigma(h_{01}+h_{10});\end{aligned}\right\} \tag{3.2}$$

$$\left.\begin{aligned}-\nabla^2\zeta_0 &= \mathscr{T}\frac{\partial w_0}{\partial z},\\ -\nabla^2\zeta_1 &= \mathscr{T}\frac{\partial w_1}{\partial z}-Z_{00},\\ -\nabla^2\zeta_2 &= \mathscr{T}\frac{\partial w_2}{\partial z}-(Z_{01}+Z_{10});\end{aligned}\right\} \tag{3.3}$$

$$\frac{\partial u_i}{\partial x}+\frac{\partial v_i}{\partial y}+\frac{\partial w_i}{\partial z} = 0 \quad (i = 0, 1, 2, \ldots). \tag{3.4}$$

Here the subscripts i, j correspond to the order of the variables to be substituted into each expression: e.g. $h_{ij} = \mathbf{v}_i\,.\,\nabla T_j-\dfrac{\partial}{\partial z}(\overline{w_i T_j})$.

The method of solution is the same as the method used in the non-rotating problem (I). A brief outline of the method is given below.*

The form of w_0 can be determined by inspection from (3.1). Expressions for T_0, u_0 and v_0 are derived from the normalized expression for w_0 by means of equations (3.2), (3.3) and (3.4). The right-hand side of the second equation of (3.1) can then be computed directly since it is composed of zero-order functions only. However, two difficulties appear at this point. The inhomogeneous term in the w_1 equation will, in general, contain terms of the form of w_0 as well as the unknown parameter λ_1. In solving for the particular solution for w_1, one will obtain secular terms in addition to terms which are spatially periodic. In addition, the homogeneous solution of w_1 will contain the form of w_0 with an arbitrary amplitude.

* *Note added in proof.* A method for treating the finite-amplitude range has also been proposed by L. P. Gor'kov (1957). His method and that of Malkus & Veronis yield the same finite-amplitude results for λ_2.

Since λ_1 multiplies a term of the form of w_0 in the inhomogeneous term, we can evaluate λ_1 to cancel the remaining amplitudes of w_0. Secular terms are thereby eliminated and the assumed periodicity of the solution is maintained. Furthermore, by specifying that ϵ be the total amplitude of that part of w which contains w_0, we can write $\{ww_0\}_m = \epsilon$ or $\{w_i w_0\}_m = 0$ for $i > 0$, i.e. the homogeneous part of w_i $(i > 0)$ which has the form of w_0 has zero amplitude. The system of equations can now be solved for the w_i, T_i, u_i, v_i and λ_i. We shall apply the method first to determine an approximate finite-amplitude solution for the two-dimensional rolls. Though this case is unrealistic, it is the only case which, with a reasonable amount of effort, can be carried beyond the second approximation. Because the roll is not truly descriptive of the actual physical system, we shall discuss certain qualitative features of this case only. Later, in the analysis for the square cell, additional observable features of the flow will be presented.

(*a*) *Rolls*

The solution to the stability problem is given by equations (2.7) and (2.8). This is

$$\left.\begin{aligned} w_0 &= 2\cos\pi\alpha x\sin\pi z, & T_0 &= \frac{2\sigma\lambda_0}{\pi^2(\alpha^2+1)}\cos\pi\alpha x\sin\pi z,\\ u_0 &= -\frac{2}{\alpha}\sin\pi\alpha x\cos\pi z, & v_0 &= \frac{2\mathscr{T}_1}{\alpha(\alpha^2+1)}\sin\pi\alpha x\cos\pi z,\end{aligned}\right\} \tag{3.5}$$

where the value of α corresponding to a given value of $\mathscr{T}_1$ is given by (2.6), and λ_0 is given by (2.5)

The inhomogeneous term for w_1 can be evaluated directly; thus

$$Z_{00} = \frac{\partial}{\partial x}(\mathbf{v}_0 . \nabla v_0) - \frac{\partial}{\partial y}(\mathbf{v}_0 . \nabla u_0) = -\frac{4\mathscr{T}}{\alpha^2+1}\cos 2\pi\alpha x,$$

$$L_{00} = \frac{\partial}{\partial z}\left[\frac{\partial}{\partial x}(\mathbf{v}_0 . \nabla u_0) + \frac{\partial}{\partial y}(\mathbf{v}_0 . \nabla v_0)\right] - \nabla_1^2(\mathbf{v}_0 . \nabla w_0) = 0,$$

$$h_{00} = \mathbf{v}_0 . \nabla T_0 - \frac{\partial}{\partial z}(\overline{w_0 T_0}) = 0.$$

Therefore, $\mathscr{L}w_1 = -\pi^2\alpha^2\lambda_1 w_0$.

Now λ_1 is evaluated so as to cancel the form of w_0 from the right-hand side. Since the only term containing the form of w_0 is $\lambda_1\nabla_1^2 w_0$, it is necessary that $\lambda_1 = 0$. Thus,

$$\lambda_1 = 0, \quad w_1 = 0, \quad T_1 = 0, \quad u_1 = 0. \tag{3.6}$$

The second equation of (3.3) gives

$$v_1 = \frac{\mathscr{T}_1}{2\pi\alpha^3(\alpha^2+1)}\sin 2\pi\alpha x. \tag{3.7}$$

To solve for w_2, we note that $L_{01} = L_{10} = h_{01} = h_{10} = Z_{10} = 0$, and

$$\mathscr{T}\frac{\partial Z_{01}}{\partial z} = \frac{\mathscr{T}^2}{\alpha^2(\alpha^2+1)}[3\cos 3\pi\alpha x - \cos\pi\alpha x]\sin\pi z,$$

$$\sigma[\{w_0 T_0\}_m - \overline{w_0 T_0}]\,\nabla_1^2 w_0 = -\frac{\alpha^2\sigma^2\lambda_0}{\alpha^2+1}\cos\pi\alpha x(\sin 3\pi z - \sin\pi z),$$

$$\lambda_2\nabla_1^2 w_0 = -2\pi^2\alpha^2\lambda_2\cos\pi\alpha x\sin\pi z.$$

Thus, $$\mathscr{L}w_2 = \left[-2\pi^2\alpha^2\lambda_2 + \frac{\alpha^2\sigma^2\lambda_0}{\alpha^2+1} - \frac{\mathscr{T}^2}{\alpha^2(\alpha^2+1)}\right]\cos\pi\alpha x\sin\pi z + \frac{3\mathscr{T}^2}{\alpha^2(\alpha^2+1)}\cos 3\pi\alpha x\sin\pi z - \frac{\alpha^2\sigma^2\lambda_0}{\alpha^2+1}\cos\pi\alpha x\sin 3\pi z. \quad (3.8)$$

The first term on the right-hand side has the form of w_0 and must vanish. Hence,

$$\lambda_2 = \frac{\sigma^2\lambda_0}{2\pi^2(\alpha^2+1)} - \frac{\mathscr{T}^2}{2\pi^2\alpha^4(\alpha^2+1)}. \quad (3.9)$$

The evaluation of λ_2 provides the first finite-amplitude result. From the expression (1.9) for the heat transport, we can write

$$\frac{H}{\kappa\beta_m} = 1 + \frac{\sigma}{\lambda}\{wT\}_m, \quad (3.10)$$

where w and T are non-dimensional. Expanding w and T as in (1.15), we have

$$\{wT\}_m = \epsilon^2[\{w_0T_0\}_m + \epsilon\{w_0T_1 + w_1T_0\}_m + \epsilon^2\{w_0T_2 + w_1T_1 + w_2T_0\}_m + \epsilon^3\{w_0T_3 + w_1T_2 + w_2T_1 + w_3T_0\}_m + \epsilon^4\{w_0T_4 + w_1T_3 + w_2T_2 + w_3T_1 + w_4T_0\}_m + \dots]. \quad (3.11)$$

Therefore, to the ϵ^2 approximation for the convective heat transport, we get

$$\frac{\sigma}{\lambda}\{wT\}_m = \frac{\sigma}{\lambda}\epsilon^2\{w_0T_0\}_m. \quad (3.12)$$

To the same approximation (1.16) becomes

$$\epsilon^2 = \frac{\lambda-\lambda_0}{\lambda_2}. \quad (3.13)$$

Hence, $$\frac{\sigma}{\lambda}\{wT\}_m = \frac{\sigma}{\lambda_2}\left(1-\frac{\lambda_0}{\lambda}\right)\{w_0T_0\}_m = \frac{\sigma^2\lambda_0}{\pi^2(\alpha^2+1)\lambda_2}\left(1-\frac{\lambda_0}{\lambda}\right). \quad (3.14)$$

We can see from (3.14) that to the ϵ^2 approximation the convective heat transport varies inversely as λ_2. Table 1 contains values of the convective heat transport $\sigma\{wT\}_m/(\lambda-\lambda_0)$ of rolls for various values of σ and $\mathscr{T}_1^2$. The range of σ is restricted to the values for which overstability can also occur. Not that λ_2 and therefore $\sigma\{wT\}_m/(\lambda-\lambda_0)$ are negative for small Prandtl numbers and positive for larger values. In most of the range where λ_2 is negative overstability will occur before steady convection. However, for sufficiently low rotation rates, overstability cannot arise and the flow will be steady.

Since $\epsilon^2 > 0$, it is clear from (3.13) that negative λ_2 implies that $\lambda < \lambda_0$. According to this analysis, which is pivoted about the linear stability problem, the system will behave as follows. As λ increases toward λ_0, heat is transported by pure conduction (figure 7). When $\lambda = \lambda_0$ convection will occur but now λ can be decreased below λ_0 and convection will be maintained. According to the ϵ^2 approximation, one could decrease λ indefinitely and convection would continue; therefore, one must go to a higher approximation to determine when the curve begins to turn up again.

	$\mathscr{T}_1^2$					
σ	0·1	0·5	1	5	10	10^2
0·025	−0·0239	−0·00702	−0·00487	−0·00377	−0·00406	−0·00724
0·1	−0·569	−0·117	−0·0808	−0·0619	−0·0671	−0·122
0·2	−6·01	−0·562	−0·365	−0·274	−0·0299	−0·600
0·3	4·87	−1·94	−1·07	−0·735	−0·827	−2·16
0·4	2·99	−14·36	−3·24	−1·81	−2·17	−24·2
0·5	2·54	7·39	−63·0	−5·60	−8·68	6·51
0·6	2·34	4·06	7·10	40·1	13·7	3·85
0·687	2·25	3·26	4·41	6·77	5·75	3·16
0·7	2·23	3·19	4·23	6·56	5·37	3·09
0·8	2·18	2·80	3·37	4·40	3·86	2·74

	$\mathscr{T}_1^2$					
σ	10^3	10^4	10^5	10^6	10^7	10^8
0·025	−0·0150	−0·0326	−0·0715	−0·168	−0·382	−1·06
0·1	−0·270	−0·690	−2·47	11·2	3·28	2·44
0·2	−1·82	77·6	3·66	2·55	2·21	2·09
0·3	29·6	3·53	2·50	2·23	2·09	2·04
0·4	4·20	2·64	2·25	2·14	2·05	2·02
0·5	3·01	2·37	2·16	2·10	2·03	2·01+
0·6	2·60	2·25	2·11	2·07	2·02	2·01−
0·687	2·43	2·18	2·09	2·04	2·01+	2·01−
0·7	2·41	2·16	2·08	2·03	2·01	2·01−
0·8	2·29	2·14	2·06	2·02	2·01−	2·00+

TABLE 1. Values of $\dfrac{\sigma\{wT\}_m}{\lambda-\lambda_0} = \dfrac{\sigma^2\lambda_0}{\pi^2(\alpha^2+1)\lambda_2}$ for rolls.

Experimentally, one would not observe the sequence of events described above. If a finite-amplitude perturbation were present, the system would become unstable at λ_U (figure 7), and the motions would grow very quickly from C to A, i.e. until the fluid transported the amount of heat corresponding to point A. A further increase in λ would be needed to increase H. On the other hand, if no finite-amplitude disturbance were present, instability would occur at λ_0, but the motions would grow very rapidly with $\lambda = \lambda_0$ until the heat transport corresponded to point B. If the system were allowed to 'run down', i.e. if λ were decreased from a value above λ_0, then the system would always follow the path $BACO$.

The onset of instability as a finite-amplitude disturbance in the rotating system marks a definite point of departure from the results of the non-rotating system. In the latter case, convective heat transport is possible only for values of $\lambda > \lambda_0$. Why does the rotating system respond so differently in finite amplitude? What is the mechanism for the occurrence of finite amplitude instability?

The answers to these questions can be found in equation (1.14). For the steady convective case, we have

$$\nabla^6 w + \mathscr{T}^2 \frac{\partial^2 w}{\partial z^2} - \lambda \nabla_1^2 w = \sigma[\{wT\}_m - \overline{wT}]\, \nabla_1^2 w + \mathscr{T} \frac{\partial Z}{\partial z} - \nabla_1^2 h - \nabla^2 L. \quad (3.15)$$

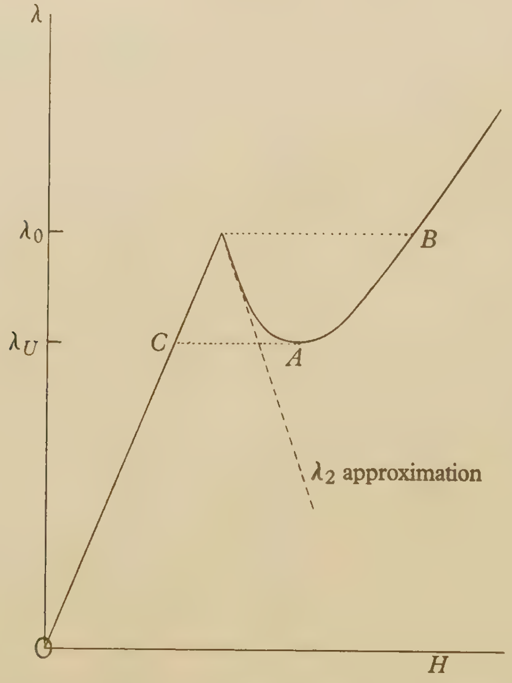

FIGURE 7. The λ *vs* H curve when λ_2 is negative.

The term $$Z = \frac{\partial}{\partial x}(\mathbf{v}\,.\,\nabla v) - \frac{\partial}{\partial y}(\mathbf{v}\,.\,\nabla u)$$

can be written in the form

$$Z = \mathbf{v}_1\,.\,\nabla_1 \zeta - \boldsymbol{\omega}_1\,.\,\nabla_1 w = \nabla_1\,.\,[\mathbf{v}_1 \zeta - \boldsymbol{\omega}_1 w], \quad (3.16)$$

where the subscript 1 corresponds to the horizontal vectors and $\boldsymbol{\omega}_1$ is the horizontal vorticity vector. If the term $\mathscr{T}(\partial Z/\partial z)$ is taken to the left-hand side of the equation (3.15), the second term can be written (with the aid of (1.3))

$$\mathscr{T} \frac{\partial}{\partial z} \nabla_1 \cdot \{\mathbf{v}_1 \mathscr{T} - \mathbf{v}_1 \zeta + \boldsymbol{\omega}_1 w\}. \quad (3.17)$$

The individual terms within the brackets correspond respectively to the horizontal transport of imposed vertical vorticity, the horizontal transport of local vertical vorticity, and the vertical transport of horizontal vorticity. In finite amplitude, therefore, the fluid can generate a local vorticity whose net effect is to decrease the role of the constraining first term in (3.17). When the viscosity is large, the generation of local vorticity is accompanied by strong viscous dissipation so that the non-linear terms will stabilize the system.

It is important to note that the possibility of a finite-amplitude instability is brought about by interactions of the zero-average non-linear terms which do not contribute *per se* to the distortion of the mean temperature profile. These terms play an increasingly important role as the Prandtl number diminishes. In the non-rotating system, the heat transport curve of a fluid with small Prandtl number breaks away from the conduction line with a slope one-third greater than that of pure conduction, whereas when the Prandtl number is large the slope of the heat transport curve is twice the conduction slope. When an external constraint is present, the heat convected by the fluid varies as a function of the constraint.

When λ_2 is positive, heat is transported by convection only when λ is increased beyond λ_0. We shall discuss this case in some detail in a subsection on square cells.

When $\lambda_2 < 0$, it is necessary to consider the next approximation in order to find the point at which the λ *vs* H curve turns upward. We can feel fairly confident that the ϵ^2 approximation is valid only in a very limited range, otherwise the λ, H curve would cross the H axis, i.e. the fluid would transport a finite amount of heat in the absence of a temperature gradient.

λ_4 *for rolls.* Because of the vertical symmetry, $\lambda_i = 0$ for odd i. Hence, it is necessary to go to the ϵ^4 approximation to determine the higher-order effect on the heat transport.

The equations governing the ϵ^4 approximation can be determined from equation (3.15) and from the expansions (1.15) and (1.16). The results only will be listed here:

$$\left.\begin{aligned} w_2 &= w_{20}\cos\pi\alpha x\sin 3\pi z + w_{21}\cos 3\pi\alpha x\sin\pi z,\\ T_2 &= \frac{\sigma\lambda_0 w_{20}+\sigma^2 N_0}{\pi^2(\alpha^2+9)}\cos\pi\alpha x\sin 3\pi z + \frac{\sigma\lambda_0 w_{21}}{\pi^2(9\alpha^2+1)}\cos 3\pi\alpha x\sin\pi z\\ &\qquad - \frac{\sigma\mathscr{T}_1^2}{\alpha^4(\alpha^2+1)^2}\cos\pi\alpha x\sin\pi z; \end{aligned}\right\} \tag{3.18}$$

$$\left.\begin{aligned} \lambda_3 &= 0,\\ \lambda_4 &= -\frac{\sigma^2}{4}\left[\frac{\mathscr{T}_1^2}{\alpha^4(\alpha^2+1)^2} + \frac{\sigma^2 N_0}{\alpha^2+9}\left(\frac{\alpha^2\lambda_0/\pi^4}{A}+1\right)\right]\\ &\qquad - \frac{\sigma^4 N_0^2\alpha^2}{2A} + \frac{\mathscr{T}_1^2}{4\alpha^6(\alpha^2+1)}\left[\frac{1}{9\alpha^2+1}\left(1-\frac{\mathscr{T}_1^2}{B}\right)+\frac{1}{\alpha^2+1}\right], \end{aligned}\right\} \tag{3.19}$$

where $$w_{20} = \frac{\sigma\alpha^2 N_0}{\pi^4 A}, \quad w_{21} = -\frac{3\mathscr{T}_1^2}{\pi^2\alpha^2(\alpha^2+1)\,B}, \quad N_0 = \frac{\lambda_0}{\pi^2(\alpha^2+1)},$$

$$A = (\alpha^2+9)^3 + 9\mathscr{T}_1^2 - \alpha^2\frac{\lambda_0}{\pi^4}, \quad B = (9\alpha^2+1)^3 + \mathscr{T}_1^2 - 9\alpha^2\frac{\lambda_0}{\pi^4}$$

Values of λ_4 for mercury ($\sigma = 0{\cdot}025$) and air ($\sigma = 0{\cdot}687$) are given in table 2.

We can now determine the range of validity of the ϵ^2 approximation. To the ϵ^4 approximation, (1.16) becomes

$$\epsilon^2 = -\frac{\lambda_2 + \sqrt{[\lambda_2^2 + 4\lambda_4(\lambda - \lambda_0)]}}{2\lambda_4}, \tag{3.20}$$

where the positive sign in front of the radical has been chosen so that $\epsilon^2 \to 0$ as $\lambda \to \lambda_0$. Only when $\lambda_2^2 > |4\lambda_4(\lambda - \lambda_0)|$ is the ϵ^2 approximation valid. From the values of λ_2 and λ_4 for air, $\lambda - \lambda_0 = -\frac{1}{4}\lambda_2^2/\lambda_4$ when $\lambda - \lambda_0 \doteqdot \lambda_0$ in the range $0 \leqslant \mathscr{T}_1^2 \leqslant 0{\cdot}1$. As $\mathscr{T}_1^2$ increases, the limiting value of $\lambda - \lambda_0$ decreases to $0{\cdot}03\lambda_0$ at $\mathscr{T}_1^2 \doteqdot 10$ and then asymptotically approaches $0{\cdot}16\lambda_0$. For mercury the value of $\lambda - \lambda_0$ beyond which the λ_4 approximation is no longer valid is λ_0 when $\mathscr{T}_1^2 = 0$, decreases to $0{\cdot}005\lambda_0$ when $\mathscr{T}_1^2 = 0{\cdot}5$, rises to $0{\cdot}14\lambda_0$ when $\mathscr{T}_1^2 = 10^4$ and then steadily decreases to $0{\cdot}09\lambda_0$ at $\mathscr{T}_1^2 = 10^8$. Therefore, the ϵ^4 approximation is valid for a rather limited range of λ. The λ_2 curve describes the system accurately in a slightly smaller range of λ.

$\mathscr{T}_1^2$	λ_4 (air)	λ_4 (mercury)	$\mathscr{T}_1^2$	λ_4 (air)	λ_4 (mercury)
0·1	0·0495	0·0971	10^3	−0·164	$0{\cdot}956 \times 10^{-2}$
0·5	0·168	0·286	10^4	−0·203	$0{\cdot}195 \times 10^{-2}$
1	0·230	0·354	10^5	−0·229	$0{\cdot}410 \times 10^{-3}$
5	0·122	0·277	10^6	−0·245	$0{\cdot}797 \times 10^{-4}$
10	0·042	0·196	10^7	−0·253	$0{\cdot}168 \times 10^{-5}$
10^2	−0·101	0·0499	10^8	−0·257	$0{\cdot}280 \times 10^{-5}$

TABLE 2. λ_4 for rolls.

In the non-rotating system (I), the ϵ^2 approximation for rolls is accurate for $\lambda - \lambda_0 \leqslant \lambda_0$. The more limited range of validity of λ_2 for air in the rotating problem can be traced to the stability problem itself. The system becomes unstable to a disturbance with the form of the second mode, i.e. $\sin 2\pi z$, at a relatively smaller value of λ. It was shown in § 2 that $(\lambda_0)_{n=2}/(\lambda_0)_{n=1} \to (16)^{\frac{1}{3}} = 2{\cdot}52$ as $\mathscr{T}_1^2 \to \infty$, whereas in the non-rotating system the ratio equals 16. Since the finite-amplitude solution is based on the linear stability problem, it can describe the system only in the range in which the fluid is not unstable to other disturbances. This range is ten times smaller in the rotating case (for large $\mathscr{T}_1^2$); therefore the corresponding approximation is accurate in an equally limited range. This reasoning does not apply to mercury where λ_2 is negative. In this case, the range of validity of the second-order approximation must be limited for the reason mentioned earlier. Nor can we apply the above reasoning to account for the extremely small range of validity of the ϵ^2 approximation for air when $\mathscr{T}_1^2 \doteqdot 10$. As we shall see later, the fluid behaves quite differently for these smaller values of $\mathscr{T}_1^2$ than it does either for zero rotation or for higher rotation rates.

From the expressions for the heat transport (3.10) and (3.11), we have to fourth order

$$\frac{H}{\kappa\beta_m} = 1 + \frac{\sigma\epsilon^2}{\lambda}[\{w_0T_0\}_m + \epsilon^2\{w_0T_2\}_m], \tag{3.21}$$

where the remaining terms in (3.11) vanish. Therefore,

$$\frac{H}{\kappa\beta_m} = 1+\frac{\sigma\epsilon^2}{\lambda}\left[\frac{\sigma\lambda_0}{\pi^2(\alpha^2+1)}-\frac{\sigma\mathscr{T}_1^2}{2\alpha^4(\alpha^2+1)}\epsilon^2\right]. \tag{3.22}$$

For mercury, $\lambda_2 < 0$ and $\lambda_4 > 0$. Therefore, from (3.20), we note that the amplitude ϵ^2 increases as a result of the higher approximation. H increases with ϵ^2 so that the net effect of λ_4 is to turn the λ *vs* H curve (figure 7) toward the right, i.e. toward point A. In order to determine the actual behaviour of the system as the λ *vs* H curve is turned upward again, it would be necessary to consider the next approximation.

The most important result which we have obtained from this study of finite-amplitude convection for rolls is that fluids with a sufficiently small Prandtl number can become unstable to a finite-amplitude disturbance at a lower value of λ than λ_0. The non-linear vorticity generated by the finite-amplitude motions enables the fluid to reduce the effect of the external constraint and thereby become unstable at lower values of the external parameters.

(*b*) λ_2 *for rectangular cells*

Using the method outlined earlier, we can determine λ_2 for the rectangular cell. The detailed analysis is rather tedious and lengthy, so that only the results will be given.

The stability solution is

$$\left.\begin{aligned}
w_0 &= 2\sqrt{2}\cos\pi lx\cos\pi my\sin\pi z, \quad T_0 = 2\sqrt{2}\,\sigma N_0\cos\pi lx\cos\pi my\sin\pi z,\\
u_0 &= -\left[\frac{2\sqrt{2}\,m\mathscr{T}_1}{\alpha^2(\alpha^2+1)}\cos\pi lx\sin\pi my+\frac{2\sqrt{2}\,l}{\alpha^2}\sin\pi lx\cos\pi my\right]\cos\pi z,\\
v_0 &= \left[\frac{2\sqrt{2}\,l\mathscr{T}_1}{\alpha^2(\alpha^2+1)}\sin\pi lx\cos\pi my-\frac{2\sqrt{2}\,m}{\alpha^2}\cos\pi lx\sin\pi my\right]\cos\pi z,
\end{aligned}\right\} \tag{3.23}$$

where $2\sqrt{2}$ is the normalization constant for w_0, $N_0 = \dfrac{\lambda_0}{\pi^2(\alpha^2+1)}$ and $l^2+m^2 = \alpha^2$. Equations (2.5) and (2.6) again determine λ_0 and α^2 as functions of $\mathscr{T}_1$. The first-order functions are

$$\left.\begin{aligned}
w_1 &= [a_1(l_1 m)\cos 2\pi lx+a_2(l,m)\cos 2\pi my]\sin 2\pi z,\\
T_1 &= [b_1(l_1 m)\cos 2\pi lx+b_2(l,m)\cos 2\pi my]\sin 2\pi z,\\
v_1 &= \left[\frac{\alpha_1\mathscr{T}_1}{4l(l^2+1)}\sin 2\pi lx-\frac{a_2}{m}\sin 2\pi my\right]\cos 2\pi z+\frac{\mathscr{T}_1}{2\pi l\alpha^2(\alpha^2+1)}\sin 2\pi lx\\
&\quad +\frac{l\mathscr{T}_1}{2\pi\alpha^4(\alpha^2+1)}\sin 2\pi lx\cos 2\pi my,\\
u_1 &= -\left[\frac{a_1}{l}\sin 2\pi lx+\frac{a_2\mathscr{T}_1}{4m(m^2+1)}\sin 2\pi my\right]\cos 2\pi z\\
&\quad -\frac{\mathscr{T}_1}{2\pi m\alpha^2(\alpha^2+1)}\sin 2\pi my-\frac{m\mathscr{T}_1}{2\pi\alpha^4(\alpha^2+1)}\cos 2\pi lx\sin 2\pi my,
\end{aligned}\right\} \tag{3.24}$$

where
$$\lambda_1 = 0,$$

$$a_1(l,m) = \frac{\dfrac{8\pi^3 l^2 m^2 \sigma N_0}{\alpha^2} + \dfrac{32\pi^5 l^2 m^2 (l^2+1)}{\alpha^4}\left[\alpha^2+1+\dfrac{\mathscr{T}_1^2}{(\alpha^2+1)^2}\right]}{-4\pi^6[16(l^2+1)^3+\mathscr{T}_1^2 - l^2\lambda_0/\pi^4]},$$

$$b_1(l,m) = \sigma\frac{\lambda_0 a_1 - 2\pi\sigma N_0 m^2/\alpha^2}{4\pi^2(l^2+1)},$$

$$a_2(l,m) = \alpha_1(m,l), \quad b_2(l,m) = b_1(m,l).$$

From these zero- and first-order functions and from (3.1), an expression for λ_2 can be obtained:

$$\lambda_2 = \frac{\sigma^2 N_0}{2} - \frac{\pi}{2\alpha^2}(m^2 b_1 + l^2 b_2) + \frac{\pi^3}{2\alpha^4}(m^2 a_1 + l^2 a_2)\left[\frac{\mathscr{T}_1^2}{\alpha^2+1} - (\alpha^2+1)^2\right]$$
$$+\frac{\mathscr{T}_1^2\pi^3}{2\alpha^4}\left[\frac{l^2 a_2}{m^2+1} + \frac{m^2 a_1}{l^2+1} + \frac{3}{2\pi(\alpha^2+1)}\right]. \quad (3.25)$$

As a function of the parameters σ, $\mathscr{T}_1$ and the ratio l/m, expression (3.25) for λ_2 has a triply infinite set of values. We shall restrict our attention here to the values of $\mathscr{T}_1^2$ which were considered in the subsection on rolls. Furthermore, we shall consider only two values of σ, those corresponding to mercury ($\sigma = 0{\cdot}025$) and air ($\sigma = 0{\cdot}687$). The ratio l/m cannot be chosen arbitrarily, of course, for it is a parameter whose value is determined by the physics of the system. In order to decide which of the infinite number of values of l/m is chosen by the fluid we turn now to the relative stability criterion which was developed in I.

The relative stability criterion is the answer to the following question. If all of the mathematically possible solutions of a statistically steady physical system are known, which of the solutions is stable to disturbances which have the form of any of the other solutions? When all of the solutions are orthogonal to each other (as in the present case), the criterion takes a particularly simple form. The fluid chooses that solution which has the maximum value of $\{\beta^2\}_m$. From (1.10) in non-dimensional form, $\{\beta^2\}_m$ can be written

$$1+\frac{\sigma^2}{\lambda^2}\{[\{wT\}_m - \overline{wT}]^2\}_m. \quad (3.26)$$

To the ϵ^2 approximation, (3.26) is equal to

$$1+\frac{\sigma^2\epsilon^4}{\lambda^2}\{[\{w_0 T_0\}_m - \overline{w_0 T_0}]^2\}_m = 1+\frac{\sigma^4 N_0^2 \epsilon^4}{2\lambda^2} = 1+\frac{\sigma^4 N_0^2(\lambda-\lambda_0)^2}{2\lambda^2\lambda_2^2}, \quad (3.27)$$

where (3.13) was used to derive the last equality. Since N_0 is not a function of l/m, the solution with maximum $\{\beta^2\}_m$ at a given value of λ is the solution with minimum λ_2 or maximum heat transport.

For this problem λ_2 as given by (3.25) has a minimum at* $l/m = \infty$ for small $\mathscr{T}_1^2$ and at* $l/m = 1$ for large $\mathscr{T}_1^2$. The value of $\mathscr{T}_1^2$ at which the preferred shape crosses over from $l/m = \infty$ to $l/m = 1$ depends upon the Prandtl number. Values of the convective heat transport for air and mercury are given in table 3 for square cells and for limiting rectangles.

---

* When $l/m = \infty$, the cellular geometry is that of limiting rectangles, i.e. the cells take the form of rolls in the limit. When $l/m = 1$, the cells are square.

A result which is immediately evident upon comparing tables 1 and 3 is that the value of the heat transport for limiting rectangles differs markedly from the value for rolls. This difference was found also in the non-rotating case. Again the only conclusion which we can draw from these results is that one must use the limiting rectangle in the description of the two-dimensional case. Though neither the roll nor the limiting rectangle can satisfy lateral experimental boundary conditions, nevertheless the limiting rectangle can approximate long thin rectangular cells.

	Air		Mercury	
$\mathscr{T}_1^2$	Square	LR	Square	LR
0·1	1·15	1·20	0·00623	0·0155
0·5	0·971	0·961	0·00340	0·00455
1	0·900	0·862	0·00275	0·00322
5	0·896	0·782	0·00262	0·00244
10	0·983	0·807	0·00329	0·00270
10^2	1·49	1·02	0·0126	0·00481
10^3	1·95	1·11	−0·0448	0·00993
10^4	2·06	1·23	−0·0361	0·0209
10^5	2·05	1·29	−0·0587	0·0445
10^6	2·03	1·31	−0·118	0·0924
10^7	2·02	1·32	−0·249	0·184
10^8	2·01	1·33	−0·608	0·342

TABLE 3. Convective heat transport $(\sigma\{wT\}_m)/(\lambda-\lambda_0)$ for steady square cells and limiting rectangles.

An additional fact which emerges from a comparison of tables 1 and 3 is that for air the heat transport of squares exactly coincides with that of rolls when $\mathscr{T}_1^2$ is large. Whether this is a chance coincidence or has some deeper significance has not been determined. Clearly the physical factors which enter into the determination of λ_2 are quite different in the two cases.

A definite qualitative difference between the two-dimensional and three-dimensional cases is illustrated by the heat transport for mercury. For rolls a finite-amplitude instability can occur throughout the range of $\mathscr{T}_1^2$ considered, whereas limiting rectangles will not become unstable to finite-amplitude perturbations.

We may note from table 3 that steady convective instability in mercury will set in the form of limiting rectangles for the range $0 \leqslant \mathscr{T}_1^2 \leqslant 3$. For higher values of $\mathscr{T}_1^2$, convection occurs in the form of square cells. Since overstability can occur (though at a higher Rayleigh number) when $\mathscr{T}_1^2 \doteq 4$, further discussion about the expected nature of convection must be postponed until the finite-amplitude effects of overstability are presented.

One can predict the cellular structure of air over a much larger range of $\mathscr{T}_1^2$. It is evident from table 3 that limiting rectangles will be preferred only when $\mathscr{T}_1^2 < 0\cdot5$. Since overstability cannot set in until $\mathscr{T}_1^2 \doteq 108$, convection will take place in the form of steady square cells in the range $0\cdot5 \leqslant \mathscr{T}_1^2 \leqslant 108$.

It should be noted also that the very small amplitude of heat convection in mercury indicates that the heat transport curve in the *H vs* λ graph starts off practically tangent to the conduction line when instability occurs.

In air the convective heat transport is much larger than it is in mercury. An interesting property for air exhibited by table 3 is that the convective heat transport for both the limiting rectangle and the square approach asymptotic values for large $\mathscr{T}_1^2$. The asymptotic value for square cells is equal to the value for rolls. Furthermore, the non-rotating roll has precisely the same value $(\sigma\{wT\}_m/(\lambda-\lambda_0) = 2)$ for all fluids. The value of the heat transport for limiting rectangles at large $\mathscr{T}_1^2$, approaches the same value $\frac{4}{3}$ as it has in the non-rotating system.

The results for large $\mathscr{T}_1^2$ must be reconsidered in the light of finite-amplitude overstable motions. However, for small values of the Taylor number ($\leqslant 10^2$ for air, $\leqslant 10$ for mercury) it ought to be possible to check the above results experimentally. For instance, one ought to be able to see whether the limiting rectangle is actually the preferred cellular shape in air at very low rotation rates. The slope of the heat transport *vs* λ curve ought to be much steeper for low rotation rates than it is for zero rotation. Finally, the λ_4 values for rolls in air are positive when $\mathscr{T}_1^2$ is small. If this result bears even a qualitative significance to the realizable square or limiting rectangle, it would mean that for small $\mathscr{T}_1^2$ the heat transport is smaller than the value given by the λ_2 approximation.

To summarize the results of this section, we have found that in a fluid with a small Prandtl number it is possible that a finite-amplitude instability can occur before the fluid becomes unstable to infinitesimal perturbations. In this case, the finite-amplitude motions partially cancel the effect of the imposed constraint. For realizable cellular patterns in mercury this finite-amplitude instability will occur only in the range where overstability occurs first. It is, therefore, necessary to look into finite-amplitude overstable motions to determine whether the fluid can indeed be unstable to finite-amplitude disturbances.

4. Finite-amplitude overstable motions

In the analysis of these motions, the method of solution outlined in the previous section is inadequate. The difficulty which arises in the present case can be demonstrated by the following argument.

Let $w_0 = \cos p_0\tau f(x,y)\, g(z)$ be the solution to (2.1*c*). Then u_0, v_0 and T_0 can be determined from the remaining equations of (2.1). The inhomogeneous terms of the equations for w_1, w_2, etc., contain products of the lower-order functions, and the individual inhomogeneous terms are operated on by operators such as $(\partial/\partial\tau)-\nabla^2$. As a result, terms of the type $\sin p_0\tau f(x,y)\, g(z)$ may appear as forcing terms but they do not contribute to the evaluation of the λ_i since they are orthogonal to the basic solution. Therefore, they remain as inhomogeneous terms and will give rise to secular terms in w_1, w_2, etc., because they satisfy the basic homogeneous equation. One cannot avoid the difficulty by introducing an arbitrary phase since the same difficulty arises regardless of the phase of the basic solution, i.e. out of phase components are always generated.

The present difficulty is not unique to the overstable problem. Indeed, one can conceive of examples in the steady problem in which the same problem arises. For example, in the basic roll solution, $w_0 = \cos\pi\alpha x g(z)$, there are instances when a generated inhomogeneous term has the form $\sin\pi\alpha x g(z)$. In the examples of the previous section these 'resonant' terms always cancelled identically. However, it is possible that in some problems this fortuitous cancellation will not occur.

To reduce the equations to a soluble sequence once again we add an additional expansion. Specifically, let

$$\tau = t/p, \tag{4.1}$$

so that $\dfrac{\partial}{\partial \tau} = \dfrac{\partial}{\partial t}\dfrac{\partial t}{\partial \tau} = p\dfrac{\partial}{\partial t}$. We now expand p in powers of ϵ as

$$p = p_0 + \epsilon p_1 + \epsilon^2 p_2 + \dots, \tag{4.2}$$

where the p_i are to be determined.

If we add (4.1) and (4.2) to the expansions (1.15) and (1.16), the equations (1.11), (1.13) and (1.14) take the form (where we give only the ϵ^1 terms (a) and ϵ^2 terms (b))

$$\mathscr{L}w_0 \equiv \left[\left(\frac{p_0}{\sigma}\frac{\partial}{\partial t} - \nabla^2\right)^2 \left(p_0\frac{\partial}{\partial t} - \nabla^2\right)\nabla^2 + \mathscr{T}^2\left(p_0\frac{\partial}{\partial t} - \nabla^2\right)\frac{\partial^2}{\partial z^2} - \lambda_0\left(\frac{p_0}{\sigma}\frac{\partial}{\partial t} - \nabla^2\right)\nabla_1^2\right] w_0 = 0, \tag{4.3a}$$

$$\begin{aligned}\mathscr{L}w_1 = -\Big\{p_1\left[\frac{3p_0^2}{\sigma^2}\frac{\partial^3}{\partial t^3} - 2p_0\left(\frac{1}{\sigma^2} + \frac{2}{\sigma}\right)\frac{\partial^2}{\partial t^2}\nabla^2 + \left(1 + \frac{2}{\sigma}\right)\frac{\partial}{\partial t}\nabla^4\right]\nabla^2 + p_1\frac{\partial}{\partial t}\left(\mathscr{T}^2\frac{\partial^2}{\partial z^2} - \frac{\lambda_0}{\sigma}\nabla_1^2\right) \\ - \lambda_1\left(\frac{p_0}{\sigma}\frac{\partial}{\partial t} - \nabla^2\right)\nabla_1^2\Big\} w_0 + \mathscr{T}\left(p_0\frac{\partial}{\partial t} - \nabla^2\right)\frac{\partial Z_{00}}{\partial z} - \left(\frac{p_0}{\sigma}\frac{\partial}{\partial t} - \nabla^2\right)\nabla_1^2 h_{00} \\ + \left(p_0\frac{\partial}{\partial t} - \nabla^2\right)\left(\frac{p_0}{\sigma}\frac{\partial}{\partial t} - \nabla^2\right)L_{00};\end{aligned} \tag{4.3b}$$

$$\left(\frac{p_0}{\sigma}\frac{\partial}{\partial t} - \nabla^2\right)\zeta_0 = \mathscr{T}\frac{\partial w_0}{\partial z}, \tag{4.4a}$$

$$\left(\frac{p_0}{\sigma}\frac{\partial}{\partial t} - \nabla^2\right)\zeta_1 = \mathscr{T}\frac{\partial w_1}{\partial z} - \frac{p_1}{\sigma}\frac{\partial \zeta_0}{\partial t} - Z_{00}; \tag{4.4b}$$

etc.

$$\left(p_0\frac{\partial}{\partial t} - \nabla^2\right)T_0 = \sigma\lambda_0 w_0, \tag{4.5a}$$

$$\left(p_0\frac{\partial}{\partial t} - \nabla^2\right)T_1 = \sigma\lambda_0 w_1 - p_1\frac{\partial T_0}{\partial t} + \sigma\lambda_1 w_0 - \sigma h_{00}; \tag{4.5b}$$

etc.

The continuity equation has the form (3.4).

One can now proceed in the same manner as in the steady case. However, both sets of undetermined coefficients p_i and λ_i are used to eliminate the resonant terms whose forms are $\cos tf(x,y)\,g(z)$ and $\sin tf(x,y)\,g(z)$. Using this method we find that the frequency p of the overstable oscillation changes with amplitude. It is clear that if out-of-phase resonant terms had been generated in the steady case, one would have had to expand α in powers of ϵ, i.e. the basic spatial wave number would have been a direct function of amplitude also.

The algebra involved in the solution of the overstable case is so extremely tedious and lengthy that only the solution to the stability problem and the method of procedure will be outlined here. The expressions for w_1, T_1, etc., and for λ_2, p_2 will not be written explicitly.

For the general rectangle, the solution of the stability problem is*

$$\left.\begin{aligned}
w_0 &= 4\cos t\cos\pi lx\cos\pi my\sin\pi z,\\
T_0 &= \frac{4\pi^2\sigma\lambda_0/\pi^4}{p_0^2/\pi^4+(\alpha^2+1)^2}[(\alpha^2+1)\cos t+p_0/\pi^2\sin t]\cos\pi lx\cos\pi my\sin\pi z,\\
u_0 &= -4\left\{\frac{l}{\alpha^2}\cos t\sin\pi lx\cos\pi my\right.\\
&\qquad\left.+\frac{m}{\alpha^2}\mathscr{T}_1\frac{[\sigma^2(\alpha^2+1)\cos t+\sigma(p_0/\pi^2)\sin t]}{p_0^2/\pi^4+\sigma^2(\alpha^2+1)^2}\cos\pi lx\sin\pi my\right\}\cos\pi z,\\
v_0 &= 4\left\{\frac{l}{\alpha^2}\mathscr{T}_1\frac{\sigma^2(\alpha^2+1)\cos t+\sigma(p_0/\pi^2)\sin t}{p_0^2/\pi^4+\sigma^2(\alpha^2+1)^2}\sin\pi lx\cos\pi my\right.\\
&\qquad\left.-\frac{m}{\alpha^2}\cos t\cos\pi lx\sin\pi my\right\}\cos\pi z.
\end{aligned}\right\}\qquad(4.6)$$

The inhomogeneous term in (4.3b) can be determined as a function of p_1, λ_1 and the remaining (known) parameters of the problem. We now have an expression with non-resonant forcing terms plus terms of the type

$$[(ap_1+b\lambda_1+c)\cos t+(dp_1+e\lambda_1+f)\sin t]\cos\pi lx\cos\pi my\sin\pi z.$$

The coefficients a, b, c, d, e and f are functions of previously determined parameters. One evaluates p_1 and λ_1 so that the coefficients of the resonant term vanish. It is then possible to go on and determine the higher order λ_i and p_i in the same manner.

As in the steady case, λ_1 vanishes and $p_1\equiv 0$ here. Therefore, we must consider ϵ^2 terms to determine the first finite-amplitude effects. This evaluation was carried out for the case of the general rectangle and numerical results were computed for square cells and limiting rectangles in air and mercury. The results for the convection heat transport (as given by the ϵ^2 approximation (3.14)) for overstability are shown in table 4.

A comparison of the values of the convective heat transport for air in tables 3 and 4 indicates that heat is convected in air by steady cellular motions for $\mathscr{T}_1^2<10^6$. However, for $\mathscr{T}_1^2\geqslant 10^6$, overstable oscillations with a cellular pattern of squares will become the preferred motion *in finite amplitude* even though instability occurs as steady convection. The preference for overstability is very slight, and experimentally one may expect either type of motion to occur. The sequence of preferred finite-amplitude motions in air is: steady convective limiting rectangles for $\mathscr{T}_1^2 < 0{\cdot}5$, steady convective squares for $0{\cdot}5 \leqslant \mathscr{T}_1^2 < 10^6$, and overstable square cells for $\mathscr{T}_1^2 \geqslant 10^6$.

---

* We can, of course, include arbitrary phases in the horizontal co-ordinate dependence and in the time dependence. However, no loss of generality is involved in writing the solution as given by (4.6). The ensemble average is now an average over the horizontal space and time periods, i.e. $\frac{1}{8\pi lm}\int_{-l}^{l}\int_{-m}^{m}\int_{0}^{2\pi}\{\ \}\,dx\,dy\,dt.$

The cross-over from steady convection to overstability in mercury takes place at lower values of $\mathscr{T}_1^2$ and is indeed much more definite. As we noted earlier, steady limiting rectangles occur for $\mathscr{T}_1^2 < 3$ and the system changes over to steady square cells when $\mathscr{T}_1^2 \geqslant 3$. Overstable square cells are preferred when $\mathscr{T}_1^2 \doteqdot 4{\cdot}5$ and remain as the preferred motion until $\mathscr{T}_1^2 \doteqdot 20$. However, at this point overstable limiting rectangles come in and are preferred to squares until $\mathscr{T}_1^2 \doteqdot 7 \times 10^3$, when overstable square cells become preferred again. These results are summarized in figure 8. It should be noted that the preference for square cells over limiting rectangles at large Taylor numbers is based on a very small

	Mercury		Air	
$\mathscr{T}_1^2$	Square	LR	Square	LR
5	0·00416	0·0016	—	—
10	0·00431	0·00303	—	—
10^2	0·0136	0·0207	—	—
10^3	0·0394	0·0444	1·14	1·31
10^4	0·0733	0·0728	1·66	1·55
10^5	0·107	0·105	1·95	1·59
10^6	0·128	0·126	2·07	1·60
10^7	0·138	0·136	2·13	1·61
10^8	0·146	0·144	2·16	1·62

TABLE 4. Convective heat transport for overstable square cells and limiting rectangles.

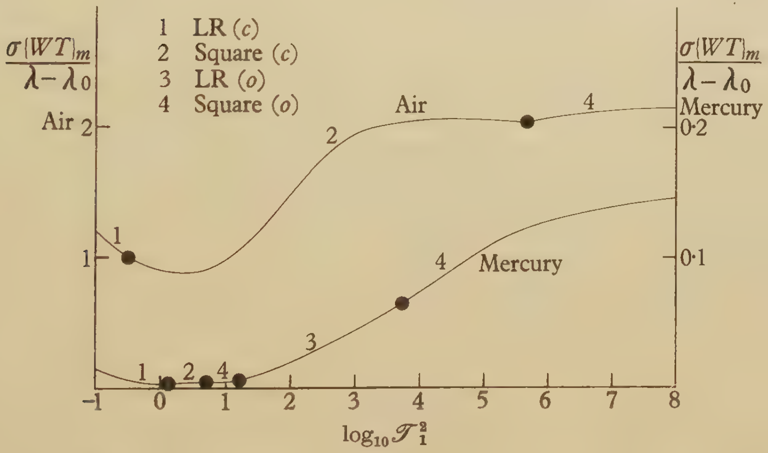

FIGURE 8. The convective heat transport values for air and mercury as functions of $\mathscr{T}_1^2$. The numbers on the portions of the curves lying between the dots mark the type of convective motions which occur in the specified ranges of $\mathscr{T}_1^2$. (*c*) corresponds to steady convective motions, (*o*) to overstable motions.

difference in heat transport (1 to 2 %). It may therefore be very difficult to obtain any recognizable stable pattern unless one were to make the determination at larger λ where higher order effects may conceivably solidify the preference.

The convective heat transport for mercury is a small fraction of the conductive heat transport throughout the range of $\mathscr{T}_1^2$ considered, and one may expect the H *vs* λ curve for $\lambda \geqslant \lambda_0$ to be practically tangent to the conduction line until higher order effects become important. In air the heat transport curve breaks away quite sharply after instability and has about twice the slope of the pure conduction line.

	Mercury		Air	
$\mathscr{T}_1^2$	Square	LR	Square	LR
5	11·3	0·735	—	—
10	2·30	1·80	—	—
10^2	0·332	1·18	—	—
10^3	$6{\cdot}28 \times 10^{-2}$	0·263	$-2{\cdot}14$	1·33
10^4	$5{\cdot}46 \times 10^{-3}$	$6{\cdot}03 \times 10^{-2}$	$-1{\cdot}16$	0·466
10^5	$-2{\cdot}48 \times 10^{-3}$	$2{\cdot}13 \times 10^{-2}$	$-0{\cdot}558$	0·160
10^6	$-1{\cdot}93 \times 10^{-3}$	$8{\cdot}61 \times 10^{-3}$	$-0{\cdot}292$	0·0616
10^7	$-9{\cdot}91 \times 10^{-4}$	$4{\cdot}20 \times 10^{-3}$	$-0{\cdot}138$	0·0260
10^8	$-5{\cdot}80 \times 10^{-4}$	$1{\cdot}80 \times 10^{-3}$	$-0{\cdot}0645$	0·0115

TABLE 5. The coefficient $p_2\lambda_0/p_0\lambda_2$ for mercury and air.

One of the most important results in the finite-amplitude study of overstable convection is that neither mercury nor air become unstable to finite-amplitude perturbations. Since the overstable oscillations in mercury take place at a much lower value of λ_0 than does steady convective instability, the fact that the latter can become unstable to finite-amplitude perturbations will not be observed experimentally.

The finite-amplitude effects on the frequency of the oscillation can be determined by (4.2) which, to the ϵ^2 approximation, has the form

$$\frac{p}{\pi^2} = \frac{p_0}{\pi^2} + \frac{\epsilon^2}{\pi^2} p_2. \tag{4.7}$$

Using (3.13), equation (4.7) can be written

$$\frac{p}{\pi^2} = \frac{p_0}{\pi^2}\left\{1 + \frac{p_2\lambda_0}{p_0\lambda_2}\left(\frac{\lambda}{\lambda_0} - 1\right)\right\}. \tag{4.8}$$

The coefficient $p_2\lambda_0/p_0\lambda_2$ is shown in table 5 for air and mercury. When the change in the frequency is negative, the correction decreases the convective heat transport (since λ_2 is a function of p_2). One of the most surprising features exhibited by the change in the frequency is the magnitude of effect on the heat transport even when the change in the frequency is extremely small, as it is for higher rotation rates in mercury. Indeed, the value of λ_2 in mercury without the

p_2 correction is negative for $10^4 \leqslant \mathscr{T}_1^2 \leqslant 10^7$. The change in frequency causes λ_2 to become positive, and the system is stable to finite-amplitude perturbations. Thus, the non-linear change in frequency effectively stabilizes the system in this part of the range. Where p_2 is positive, the non-linear change in frequency makes the system less stable.

5. Summary and conclusions

The most important conclusion in the stability investigation is that overstability occurs because the fluid is thereby able to reduce the constraint of the imposed rotation. A second conclusion of considerable interest is that in steady convective instability the wavelength of the cell measured along the boundary (as it is distorted by the rotation) is equal to the wavelength of the non-rotating cell. Other results (which are explicitly or implicitly contained in Chandrasekhar's original investigation (1953)) are that overstability cannot occur in a fluid with a Prandtl number greater than $\sqrt{\frac{2}{3}}$ because the rate of dissipation of kinetic energy always exceeds the rate of release of potential energy for larger σ, and that overstability cannot occur for sufficiently low rotation rates because the tendency of the fluid to undo the external constraint is more than offset by the increased dissipation due to the time-dependent motions.

For a range of the external parameters it is possible for the fluid, through finite-amplitude growth, to decrease the effect of the external constraint by generating a motion to counteract the effects of the imposed constraint. In cases where this happens, the fluid may become unstable to finite-amplitude disturbances before it becomes unstable to infinitesimal perturbations. Neither air nor mercury, the two fluids considered here, will exhibit this finite-amplitude behaviour under laboratory conditions.

More particular results in the finite-amplitude study are as follows. As the rotation rate is increased, the preferred cellular pattern for convection in air changes from steady limiting rectangles to steady squares to overstable squares (overstable square cells are preferred in finite amplitude even though the fluid first becomes unstable to steady convective motions). In mercury the sequence of preferred cellular shapes changes with increasing Taylor numbers from steady limiting rectangles, to steady squares, to overstable squares, to overstable limiting rectangles, and finally, when $\mathscr{T}_1^2 \doteqdot 10^6$, to overstable squares again. The heat convected by mercury after instability is only a small fraction of the conducted heat, and consequently the H *vs* λ curve will not show the very sharp breaks which are exhibited in the non-rotating system. In air the convective heat transport is at least as large as the conductive transport for all rotation rates, and the H *vs* λ curve will show a sharp break at the point of instability.

The frequency of the oscillations in overstable motions is a direct function of the amplitude. The change in frequency is too small to be noticeable in mercury when $\mathscr{T}_1^2 > 50$. However, even when small, the change in frequency has a marked effect on the heat transport.

According to the present investigation the fluid reacts to the imposed constraint by generating internal motions which counteract the external constraint. This result hints rather strongly that in general, when a fluid is subjected to external constraints, it may generate motions which tend to offset the constraint.* In particular, in an electrically conducting fluid it is possible that a magnetic disturbance will grow so as to offset even further the constraint of the imposed rotation. In such a case the preferred convective state would be one with a self-generated magnetic field.

An additional suggested result with fairly broad application is the reason for the possible occurrence of a finite-amplitude instability. In other problems, such as shear flow in a channel, a finite amplitude instability can also occur (Meksyn & Stuart 1951). The one feature which these problems have in common is the dual role of viscosity mentioned in the introduction. Viscosity acts as an energy-releasing mechanism as well as a dissipative mechanism. Since finite-amplitude growth is invariably accompanied by increased viscous dissipation, one would not expect a finite-amplitude instability to occur unless the fluid were able to release even more potential energy. The fact that viscosity can fulfil the role as the energy-releasing mechanism suggests that this dual role of viscosity is essential to finite-amplitude instability.

It is interesting to note that the information concerning the appearance of a finite-amplitude instability is a consequence of an investigation which is pivoted about the linear stability problem. Application of the method described here to other problems, such as shear flow in a channel, may yield important results concerning the possible occurrence of finite-amplitude instability. One still feels, however, that the tools which we possess for treating finite-amplitude problems are woefully inadequate and that a more direct approach to non-linear stability problems should be sought.

A note should be added about an alternative, integral, technique for determining finite-amplitude effects. The method employed by Stuart (1958) and discussed in I is based on the power integral which can be derived by multiplying (1.11) by T and averaging. If quantities with the form of the stability solution are substituted into the power integral, one can then deduce the amplitude of w or T as a function of the external parameter λ. However, in the present problem this type of evaluation would yield results which are misleading because the principal effects in the determination of amplitude are those which result from the zero-average non-linear terms. These terms do not appear in the power integral.

Finally, what are the possible applications of these results to the fields of geophysics and astrophysics? (*a*) The formal technique described here together with the relative stability criterion provides a means for determining the preferred finite-amplitude configuration of any statistically steady system with a solved stability problem. The principal limitation of the method lies in the formidable computations which may be required to carry out the analysis. (*b*) The very important role of viscosity as the energy releasing mechanism in a gyroscopically constrained system indicates that one ought to exercise some care in using such approximations as that of geostrophic flow in discussing the energetics of the fluid. (*c*) The ability of a fluid to react to externally imposed conditions may lead to a fuller understanding of the mechanistic behaviour of large-scale systems such as the atmosphere or the ocean.

---

* The first finite-amplitude result (λ_2) for rolls was computed for an electrically conducting fluid subjected to heating from below and cooling from above and with an imposed magnetic field. As Chandrasekhar (1952) has shown, the imposed magnetic field acts as a constraint on the system in much the same manner as does the rotation. In the finite-amplitude computation, λ_2 is negative for a restricted range of the parameter η/κ, where η is the magnetic diffusivity. The range lies within the range of values of η/κ within which overstability can occur. Therefore, the possibility of finite amplitude instability exists also for this case, although it cannot occur in experiments realizable in the laboratory. The parametric values correspond to those which can exist in stellar atmospheres as Chandrasekhar has shown.

A number of the ideas which are presented in this paper were a direct result of discussions with W. V. R. Malkus, and I wish to acknowledge his many valuable suggestions. The work was performed under the auspices of the Office of Naval Research and is Contribution no. 985 from the Woods Hole Oceanographic Institution.

REFERENCES

Boussinesq, J. 1903 *Theorie Analytique de la Chaleur*, **2**, 172. Paris: Gauthier-Villars.

Chandrasekhar, S. 1952 On the inhibition of convection by a magnetic field. *Phil. Mag.* (7), **43**, 501.

Chandrasekhar, S. 1953 The instability of a layer of fluid heated below and subject to coriolis forces. *Proc. Roy. Soc.* A, **217**, 306.

Christopherson, D. G. 1940 *Quart. J. Math.* **11**, 63.

Fultz, D. & Nakagawa, Y. 1955 *Proc. Roy. Soc.* A, **231**, 198.

Gor'kov, L. P. 1957 *J. Exptl. Theor. Phys.* (*U.S.S.R.*), **33**, 402.

Malkus, W. V. R. & Veronis, G. 1958 Finite amplitude cellular convection. *J. Fluid Mech.* **4**, 225.

Meksyn, D. & Stuart, J. T. 1951 *Proc. Roy. Soc.* A, **208**, 517.

Nakagawa, Y. & Frenzen, P. 1955 A theoretical and experimental study of cellular convection in rotating fluids. *Tellus*, **7**, 1.

Stuart, J. T. 1958 On the non-linear mechanics of hydrodynamic stability. *J. Fluid Mech.* **4**, 1.

PRINTED IN GREAT BRITAIN AT THE UNIVERSITY PRESS, CAMBRIDGE
(BROOKE CRUTCHLEY, UNIVERSITY PRINTER)

Contribution No. 987

THE MODELING OF FLUID FLOW ON A PLANETARY SCALE*

ALAN J. FALLER AND WILLIAM S. VON ARX

Woods Hole Oceanographic Institution

INTRODUCTION

When we speak of fluid flow on a planetary scale, we have in mind those large-scale circulations in which the rotation of the reference frame, relative to which the flow is observed, plays a dominant role in the dynamics of the circulation. This is certainly the case for the atmosphere and for the ocean circulation.

Planetary circulations need not be confined to fluid motion on the scale of our earth, however. Other systems in rotation may have similar circulations. if the physical boundary conditions, the fluid properties, and the external or internal sources of energy are in the proper ratios, one to another. It is on this basis that models of the atmospheric and oceanic circulations have been attempted in the laboratory and with rather surprising success considering the lack of similarity of certain non-dimensional parameters which are considered of basic importance in other (restricted) fields of inquiry.

Planetary hydrodynamic experiments can play two different roles: one as a method for guiding theoretical studies by fundamental experiments and as a means of verification of simplified theoretical predictions; and the other to simplify and reconstruct natural processes in miniature. Although we may all agree that the theoretical role is more productive in the long run, the history of atmospheric- and ocean-model research suggests that if rather bold (and perhaps naive) attempts had not been made at first to duplicate nature, the more fundamental studies might not yet have been initiated. Indeed, the general weight of considered opinion has definitely been against such experiments because of the impossibility of modeling the Reynolds number (in particular) and because of the obvious disparity of a model's dimensions in relation to the prototype and of geometrical difficulties encountered in reducing the spherical shape of the earth to a form suitable for laboratory study. It will be apparent in the following discussion how the initial attempts at ocean models, designed to duplicate a part of nature, have stimulated theoretical developments. These have led to more simplified experiments which have gone hand in hand with theory and eventually lent and hence to the theoretical prediction of a previously unknown ocean circulation.

---

*Contribution No. 987 of the Woods Hole Oceanographic Institution.

To appreciate the manner in which rotating coordinate systems may alter the character of fluid circulations, it is useful to consider the rotational effects from two points of view. Qualitatively we may consider the nature of the Coriolis force and show that the rotation must indeed have considerable influence on the relative motion of free particles. But it is not a simple matter to judge qualitatively all the effects of rotation on fluid systems without introducing rotation into the equations of motion.

From the qualitative point of view we may see how a particle moving inertially with respect to the rotating earth, and confined to the earth by gravity, always curves to the right in the northern hemisphere in such a manner that it appears to be subject to a horizontal force at right angles to its velocity vector. The magnitude of this apparent force, the Coriolis force, is directly proportional to the velocity. For a particle moving in the north-south plane such motion toward the right is a manifestation of the conservation of absolute angular momentum $\Omega^2 R$ = constant, in which Ω is the particle's absolute angular velocity and R is its radius from the axis of rotation. Thus if R decreases, as is the case for northward motion on the earth, Ω must increase and a component of motion toward the east is apparent. Relative motion toward the west occurs where the opposite is true, as for southward motion, where R increases and Ω decreases. Curvature to the right for a particle moving in the east-west plane is not ordinarily explained, but the apparent force to the right is readily seen to be due to an excess or deficiency of centrifugal force due to rotation about the earth's axis. The apparent centrifugal force on a particle rotating with the earth is normally balanced by a slight northward component of the geocentric gravitational force due to the earth's ellipticity, but if the particle moves toward the east it is moving faster than the earth and the excess centrifugal force causes a southward (outward) motion, while motion toward the west results in a deficiency of centrifugal force and northward acceleration occurs.

Writing the Navier-Stokes equation for flow relative to a rotating coordinate system is equivalent to inclusion of a single additional term dependent upon rotation, the Coriolis acceleration. Thus, if **c** is the relative velocity, the Navier-Stokes equation in vector notation becomes

$$\frac{d\mathbf{c}}{dt} + 2\Omega\times\mathbf{c} = -\rho\nabla p + \mathbf{g} + \mathbf{F} \qquad (1)$$

where Ω is the angular velocity vector of the coordinate system, ρ the fluid density, ∇p the gradient of pressure, **g** the acceleration due to gravity, and

F the effect of viscosity. The various terms may be simply identified as:

$$\begin{matrix}\text{inertial} \\ \text{term}\end{matrix} + \begin{matrix}\text{Coriolis} \\ \text{term}\end{matrix} = \begin{matrix}\text{pressure} \\ \text{gradient} \\ \text{term}\end{matrix} + \begin{matrix}\text{gravitational} \\ \text{term}\end{matrix} + \begin{matrix}\text{frictional} \\ \text{term}\end{matrix}$$

This basic equation has been expanded and approximated in many forms for studies of the oceanic and atmospheric circulations, and the derived equation for the vertical component of vorticity is the basis of most numerical weather forecasting techniques. In the most common approximations the inertial terms are neglected as being generally small and only steady state inviscid flow is considered, hence the equation for horizontal flow becomes the "geostrophic" equation

$$(2\Omega\times\mathbf{c})_H = -\rho\nabla_H p \quad \text{or} \quad c = \frac{1}{2\Omega\sin\phi}\,\rho\nabla_H p \tag{2}$$

where ϕ is latitude and the generally small vertical motions have been neglected in the right hand expression. Thus the geostrophic current is normal to the horizontal component of the pressure gradient. It is observed that Eq. (2) is fairly well satisfied in the atmosphere and is a good approximation to the circulation in the oceans. The subject of geostrophic flow and deviations from this state is exhaustively treated, both experimentally and theoretically, in the meteorological literature and will be discussed here only in so far as it is important to the later development of this subject.

GENERAL PLANETARY MODELING TECHNIQUES

The important consideration here is the relative significance of the various terms in the equation just discussed. If planetary circulations are essentially geostrophic. a representative model must be built and operated in such a way that the viscous forces and the relative accelerations are small compared to the Coriolis and pressure gradient terms. Let us consider the inertia term first: Inasmuch as the terms in the expansion of $d\mathbf{c}/dt$ vary as the square of velocities (e.g., as v^2/r) whereas the Coriolis term varies linearly with particle speed, a necessary condition for quasi-geostrophic flow is a slow relative circulation. The ratio of the inertial terms to the Coriolis terms is of the form $(v^2/r)/\Omega v = v/r\Omega = \mathbf{R}_o$, called the Rossby number. From the preceding argument, $\mathbf{R}_o$ is an inverse measure of the extent to which the flow is geostrophic. that is, it indicates directly the degree of unbalance between the pressure gradient and the Coriolis force. Very small values of $\mathbf{R}_o$ imply small inertial terms and highly geostrophic flow.

The arguments above have not considered the effects of viscosity, and it is quite clear that for a highly viscous fluid the criterion cited would break down. On the other hand, the large-scale circulations of the oceans and the atmosphere away from the relatively thin boundary layers are characterized by large Reynolds numbers **R**, which implies that the viscous forces are generally small in comparison with the inertial forces and do not cause appreciable departures from geostrophy. Therefore, to a first approximation, it is sufficient that the Reynolds numbers for these models be very large.

The Froude number **F** is a third independent non-dimensional parameter that may be obtained from the equation of motion, but this can be dismissed by a plausibility argument as not important for modeling the gross planetary flow. Since hydrostatic balance is generally assumed where vertical accelerations are small, gravity waves do not appear as possible solutions to the equations and **F** is not a relevant parameter. Thus the primary modeling criteria are (1) equivalent values of $\mathbf{R}_0$ and (2) sufficiently large values of **R**.

This discussion of non-dimensional numbers is only cursory, and nothing has been said concerning thermodynamic processes or the boundary conditions. By ignoring these aspects of the problem we implicitly assume that with (1) a rotating system, (2) a fluid of low viscosity, and (3) an analogous distribution of energy sources and sinks it is possible to generate circulations having appropriate Rossby numbers. It is important to note that in models of this type the relative velocities are a result of the total conditions of the experiment and are not determined independently. Therefore, it is perhaps more useful to consider the basic requirement as prescribing small relative kinetic energy, since it is often possible to control the rate of generation of kinetic energy through a suitable choice of the imposed energy sources.

In modeling planetary circulations it is also necessary to introduce geometric distortions as, for example, the almost inevitable vertical exaggeration and the use of plane models to represent the spherical earth. The first of these distortions is required to enable the viscous boundary layer at the bottom or top of the fluid to occupy only a small fraction of the total depth. For a rotating system it can be shown [1] that the boundary layer thickness is very much affected by rotation as well as by viscosity and is given by $z = \pi\sqrt{\nu/\Omega}$, in which ν is the kinematic viscosity. It follows that the ratio of the depth of the boundary layer to the total depth of fluid is

$$\frac{z}{Z} = \pi\sqrt{\frac{\nu}{\Omega Z^2}} = \pi\sqrt{\frac{\mathbf{R}_0}{\mathbf{R}}}$$

if the vertical dimension of the model is used in $\mathbf{R}_0$ and **R**. This new non-dimensional parameter, which specifies the relative depth of the viscous bounday layer has been called the Ekman number $\mathbf{E}_k$ by Lettau (personal communication). It should be noted that Fultz [2] has defined $\frac{\mathbf{R}_o}{\mathbf{R}} \approx \mathbf{E}_k^2$ as the "Rotation Reynolds number" and many others have used the Taylor number $\mathbf{T} \approx \mathbf{E}_k^4$.

The use of plane or paraboloidal, rather than spherical, models is required in all model circulations where density variations occur, so that equipotential surfaces will coincide with the "horizontal" surfaces of the models. At the low rotation rates and for the small dimensions which are generally convenient in the laboratory, the equipotential surfaces are nearly plane. The spherical shape is generally restricted to models employing uniform fluids where (if a fluid is totally enclosed) the orientation of the equipotential surfaces is of no consequence. In such cases viscous boundary layers are produced on both upper and lower surfaces, which adds a complication different from most geophysical situations.

The use of a plane model introduces an important dynamic dissimilarity in addition to the more obvious geometrical distortion of a sphere. On the spherical earth the direction of the rotation vector changes with respect to the horizontal direction, or, as it is more frequently thought of in geophysics, the normal (vertical) component of the Coriolis parameter ($2\Omega \sin \phi$) is a function of latitude. Thus from Eq. (2) the geostrophic flow for a given pressure gradient is a function of latitude on the earth but this is not so in a plane model where the vertical component of the rotation is 2Ω at all points. The curvature of the spherical prototype enters also into consideration of the changes of the relative vorticity of parcels of fluid which move meridionally, but it will be shown in the ensuing discussion how this effect may be simulated in a particular class of experiments.

Despite these and other awkward modeling problems, laboratory flows similar to the major wind systems and large scale ocean currents can be produced. The requirements are: (1) a fluid of low viscosity (relative to the dimension of the model) and (2) generating forces which have the same approximate geometrical arrangements and are of the proper strength to produce a circulation with an appropriate Rossby number. A major difference between atmospheric and oceanic systems is the absence or presence of meridional barriers (the continents), and we may list a third primary requirement (3) the general boundary conditions.

We will now survey briefly some recent work with atmospheric models to illustrate the manner in which these planetary modeling criteria are applied. Following this, ocean models will be discussed to illustrate the sequence of their development and eventual contribution to a modern theory of the ocean circulation.

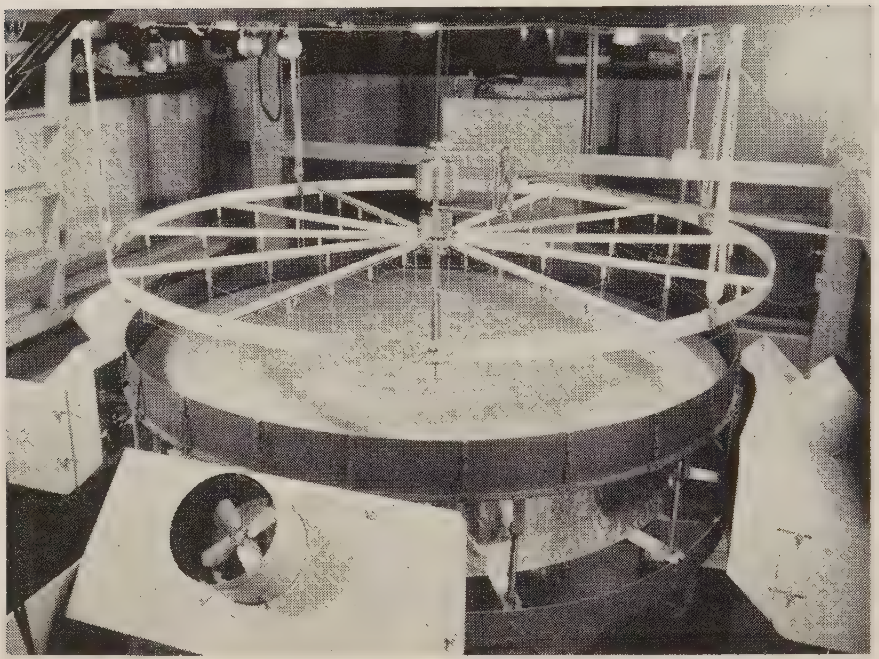

FIG. 1. ROTATING TANK FOR MODELS OF ATMOSPHERIC CIRCULATION.

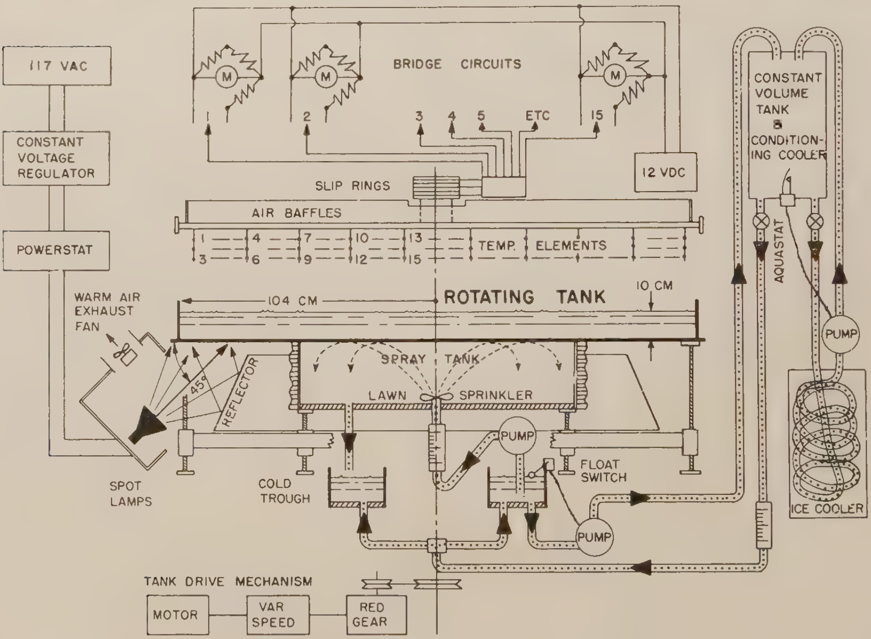
117 VAC
CONSTANT VOLTAGE REGULATOR
POWERSTAT
BRIDGE CIRCUITS
M
1
2
3
4
5
ETC
15
12 VDC
SLIP RINGS
AIR BAFFLES
1 3 4 6 7 9 10 12 13 15
TEMP. ELEMENTS
CONSTANT VOLUME TANK & CONDITIONING COOLER
AQUASTAT
PUMP
ICE COOLER
WARM AIR EXHAUST FAN
104 CM
ROTATING TANK
10 CM
45°
REFLECTOR
SPRAY TANK
LAWN SPRINKLER
PUMP
FLOAT SWITCH
SPOT LAMPS
COLD TROUGH
PUMP
TANK DRIVE MECHANISM
MOTOR
VAR SPEED
RED GEAR

FIG. 2. DIAGRAM OF APPARATUS SHOWN IN FIG. 1.

AN ATMOSPHERIC MODEL

Figure 1, an oblique photograph, and Fig. 2, a schematic diagram, illustrate the principal features of an atmospheric model which has been set up at the Woods Hole Oceanographic Institution. The tank consists of a copper plate $\frac{1}{4}$ in. thick and 7 ft. in diameter surrounded by a brass rim 6 in. high. This tank is supported by several leveling screws around the rim and by a cold-source tank beneath the center. Heat is provided near the rim by illuminating the blackened bottom with incandescent spot lamps, and cooling near the center is accomplished by spraying water of constant temperature against the under side of the plate. The aluminum frame, shown suspended, normally rests on the rim and rotates with the tank. This frame supports a glass cover, to eliminate undesirable energy exchange between the free surface and the environment, and also carries a number of resistance-wire elements, for measuring the zonally-averaged temperatures. The temperatures are recorded by photographing a panel of meters coupled to the resistance wires through a stack of slip rings.

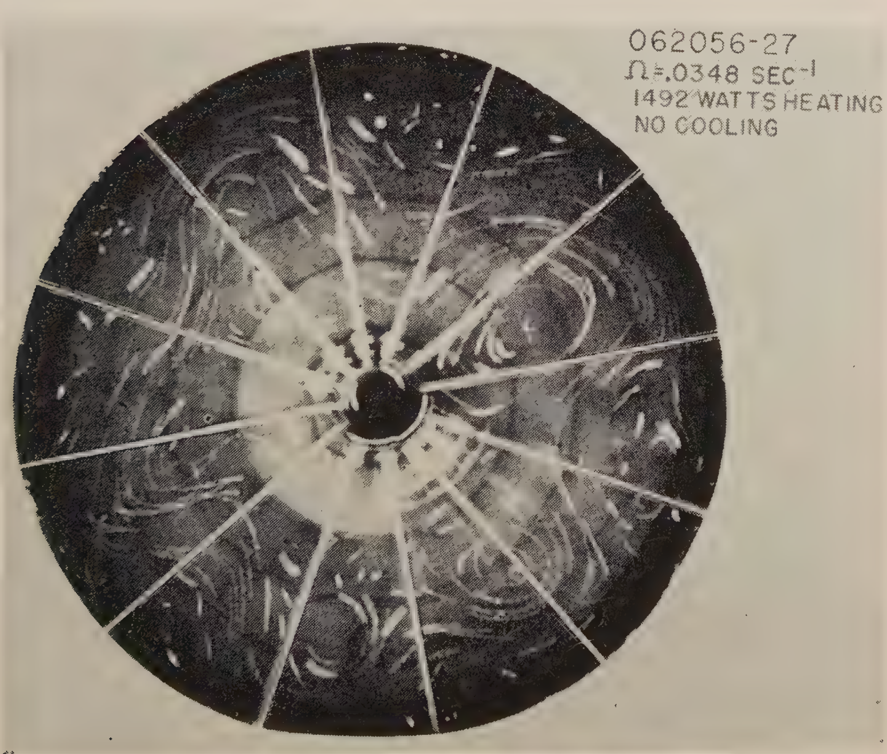

FIG. 3. THIRTY-SECOND STREAK PHOTOGRAPH ILLUSTRATING TYPICAL CIRCULATION ON FREE SURFACE OF ATMOSPHERIC MODEL.

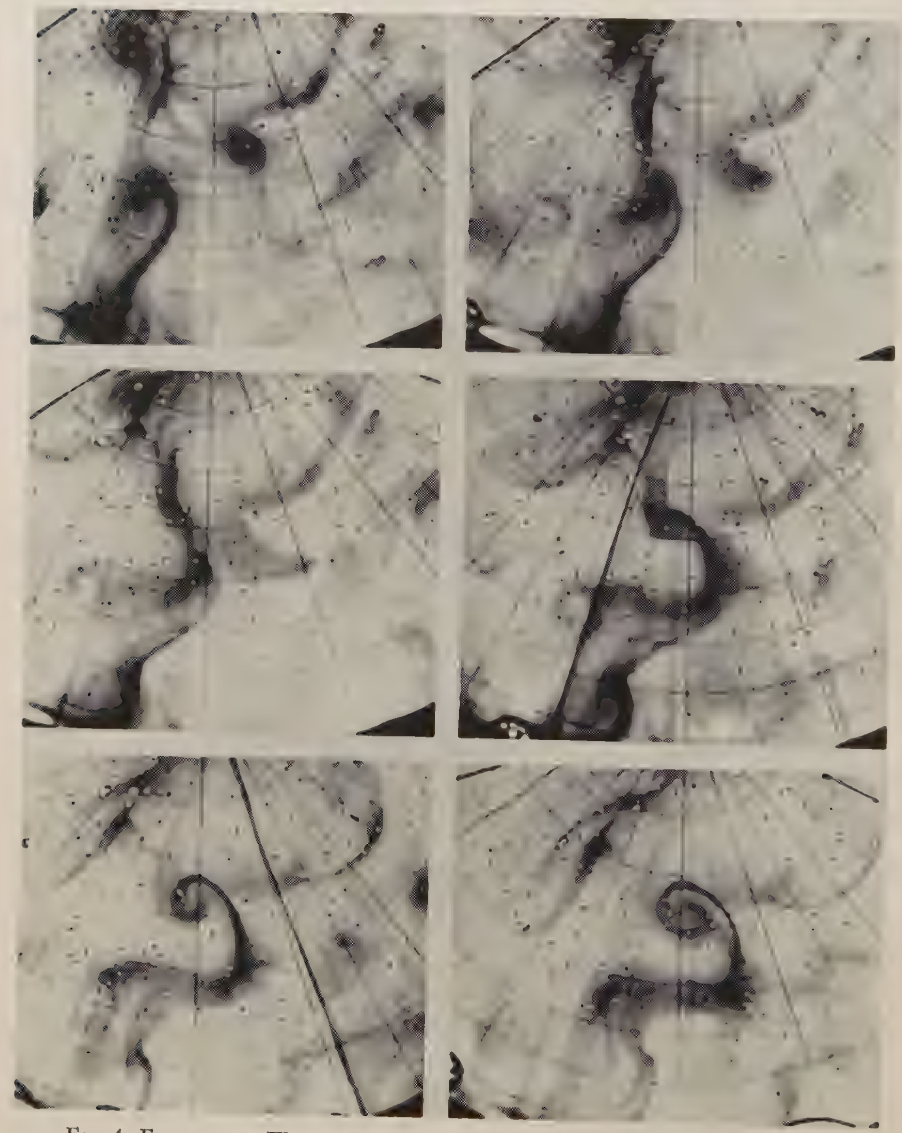

FIG. 4. FRONTS AND WAVE CYCLONES NEAR BOTTOM OF ATMOSPHERIC MODEL. ILLUSTRATED BY POTASSIUM PERMANGANATE DYE. (READ FROM TOP LEFT TO TOP RIGHT TO CENTER LEFT, ETC.)

The free surface circulation is readily observed in streak photographs of floating paper particles. With the proper combination of heating rate and rotation rate a pattern of water motion is obtained similar to that at the tropopause level of the atmosphere. Figure 3 is a streak photograph showing the displacements of paper discs during a 30-second exposure, with a heating rate of 1500 watts, and a rotation rate $\Omega = 0.035$ radians per second. In this instance the depth of fluid was 10 cm and the cold source was not used; so that the fluid warmed at a constant and uniform rate. The five-wave pattern is rather similar to conditions found in the northern hemisphere, and the band of maximum velocities is of the same nature as the jet-stream circulation which flows from west to east in a meandering pattern.

Qualitative information concerning the nature of the interior circulation is generally obtained through the use of dye tracers. Potassium permanganate crystals have indicated the presence of fronts and wave cyclones in an experimental arrangement similar to that above [3], where the plumes from the dissolving crystals indicated the flow at the bottom of the fluid and the eventual concentration of dye (after about 10 revolutions) defined the regions of low-level convergence. An example of a circulation pattern analogous to the atmosphere is that shown in Fig. 4 which illustrates a sequence of events in a sector of the model. The time interval between photographs is one revolution and the sequence proceeds from left to right and from top to bottom. The development of two waves may be seen on the principal front. The one in the center of the field of view reached occlusion rapidly while the cyclone near the bottom developed more slowly. Moving cold fronts, other than those in the principal frontal system, can be seen in the upper left and upper right portion of each photograph.

More detailed studies of these models have revealed important areas of dissimilarity which require further investigation. For instance the curvature of the earth has a marked influence on the propagation rate of the planetary waves of the atmosphere but since a similar situation is not physically possible in the plane model the waves move approximately with the mean zonal flow. Studies of the generation and dissipation of kinetic energy reveal that the time constant for kinetic energy decay is of the order of one rotation in the model compared to estimates of 20 days (rotations) for the atmosphere. To explain this we may note that although the Reynolds number in the model was so great that viscosity did not interfere with geostrophic flow, the large difference in **R** can account for the excessive rate of dissipation of kinetic energy of the model. Since to a first approximation the rate of dissipation of energy may be regarded as proportional to the kinetic energy itself, it appears that an equality of Rossby numbers could only have been achieved with a relatively large rate of generation of kinetic energy. As was pointed out in the earlier discussion, the experiments and theory to date have not specifically considered modeling the boundary conditions but have relied upon our ability to obtain an equality of Rossby numbers by empirical means.

A more detailed discussion of related work is available in the final report [2] of the Hydrodynamics Laboratory of the University of Chicago, which contains many reprints and a very complete historical bibliography.

OCEANOGRAPHIC MODELS

Probably the first model built to represent the large-scale ocean circulation was that made by Lassareff who was interested in the consequences

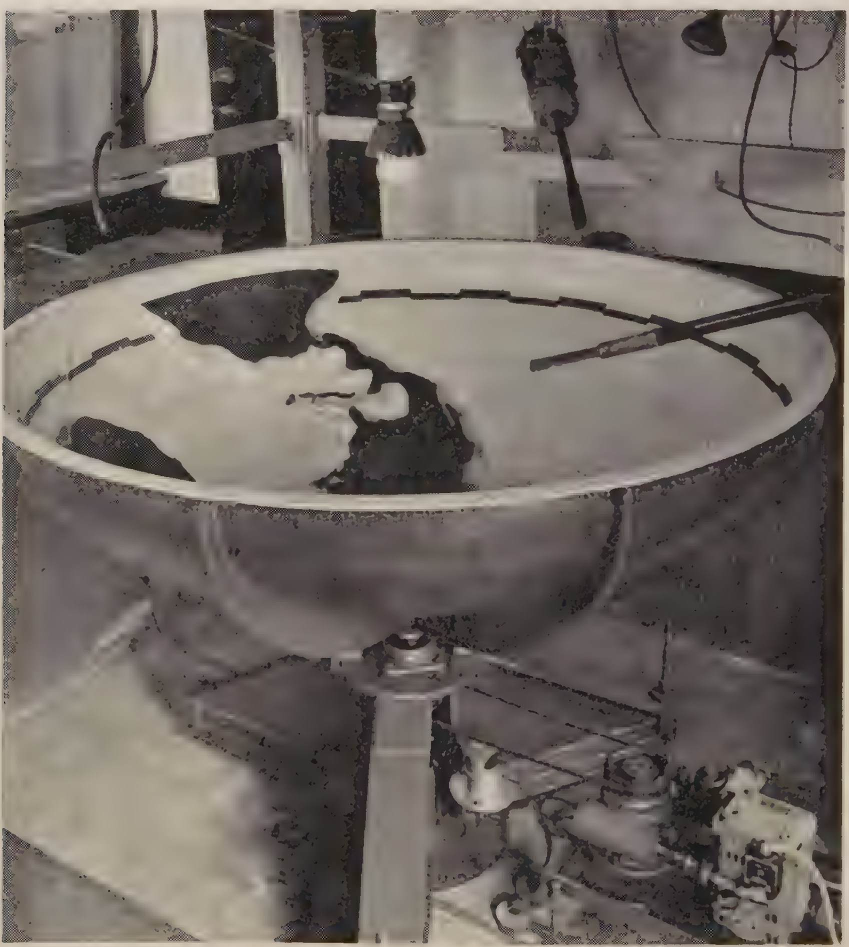

FIG. 5. PARABOLOIDAL OCEAN MODEL WITH VACUUM-CLEANER BLOWERS.

of continental distributions different from those of the present day. His experiments were performed in a stationary system so that neither the effect of rotation nor the combined effects of rotation and the curvature of the earth were present. On the basis of recent theories of the ocean circulation by Sverdrup [5], Stommel [6], and Munk [7], Arx constructed [8] a rotating model of the wind-driven ocean circulation. In essence the theories explained the swift flow of ocean water along the western boundary of the oceans as a consequence of the change in the vertical component of the relative vorticity of fluid parcels moved meridionally over the curved surface of the rotating earth. To simulate the spherical nature of the earth, in so far as practicable in a laboratory model with a free upper boundary, experiments were first conducted in rotating paraboloids. The details of construction of the continental boundaries and an explanation of the operation of the model are given in an earlier publication [8] and a photograph of the experimental arrangement is shown in Fig. 5. The circulation was generated by wind stress; an appropriate distribution of trade winds and westerlies being arranged through a combination of the relative motion of air in the laboratory and the drafts of additional blowers.

The rotation rate (and therefore the time scale) first used was the value of Ω at which there was a constant vertical depth between the free surface and the bottom boundary. These experiments showed almost at once that the swiftly flowing currents at the western boundaries of the oceans, such as the Gulf Stream and the Kuroshio, could only be obtained when the rotation rate was somewhat higher than the equilibrium value, that is when the depth of water at the equator (the rim) was somewhat deeper than at the pole (the axis). This effect was explained qualitatively by Rossby (personal communication) who argued that the curvature of the paraboloid simulated only in part the spherical shape of the earth and the variable depth introduced a divergence with radial motion of fluid which induced the necessary added change of relative vorticity to simulate that for a full hemisphere. These arguments may be more readily understood with reference to the equation of motion as follows:

Disregarding friction for the present and taking the curl of Eq. (1) we obtain the equation for the rate of change of the total vorticity

$$\frac{d\mathbf{q}_a}{dt}+\mathbf{q}_a(\nabla\cdot\mathbf{V}) = -\nabla\rho\times\nabla p+(\mathbf{q}_a\cdot\nabla)\mathbf{V} \qquad (3)$$

where $\mathbf{q}_a$ is the total absolute vorticity. If we consider only the vertical component of Eq. (3), we have, using Cartesian coordinates for simplicity,

$$\frac{d}{dt}(\zeta+f_1) = -(\zeta+f_1)(\nabla_2 \cdot V) - \left(\frac{\partial\rho}{\partial x}\frac{\partial p}{\partial y} - \frac{\partial\rho}{\partial y}\frac{\partial p}{\partial x}\right) + \xi\frac{\partial w}{\partial x} + (\eta+f_2)\frac{\partial w}{\partial y} \tag{4}$$

in which ξ, η, and ζ are the components of relative vorticity in the x (eastward), y (northward) and z (vertical) directions, respectively, and $f_1 = 2\Omega \sin \phi$ and $f_2 = 2\Omega \cos \phi$ are the components of the planetary vorticity in the z and x directions, respectively. The various groups of terms in Eq. (4) may be identified as

Change of absolute vertical vorticity = Divergence effect + Solenoid effect + Tilting effects

Since we are mainly concerned here with a uniform fluid the solenoid effects vanish, and since vertical velocities are generally very small, we may omit the tilting terms. Further, the planetary vorticity f_1 is a function of latitude alone so that we may write

$$\frac{d\zeta}{dt} = -(\zeta+f_1)(\nabla_2 \cdot V) - \frac{\partial\phi}{\partial f_1}\frac{dt}{d\phi} \tag{5}$$

Thus we note that, apart from viscous processes, changes in the vertical component of the relative vorticity of a uniform fluid occur by meridional motion $d\phi/dt$ and by horizontal divergence. The effect of a radial increase depth is such as to produce horizontal divergence of the proper sign to augment the insufficient planetary vorticity change of the paraboloid. By carrying this argument to its logical limit it was predicted [9] that, if a plane model were constructed, the planetary vorticity would be constant ($f_1 = 2\Omega$), and the divergence associated with a radial increase in depth could be used alone to simulate the variation of the Coriolis parameter with latitude. Following Rossby's [10] notation, this is often called the β-effect. The first parabolic model employed the gnomonic projection as an approximation to the proper distribution of latitude circles on the paraboloid. Subsequently the theory provided a simple mathematical law for the projection of latitudes on flat-bottomed tanks; namely

$$r'_\phi = \frac{r_\phi}{R} = \left(\frac{e^{1-\sin\phi} - 1}{e-1}\right)^{1/2}$$

in which R is the radius of the equator ($\phi = 0$), and r_ϕ is the radius of the latitude ϕ. This equation is valid only for a plane model with a rotation rate such that $D_R/D_0 = e$; where D_R is the depth at the equator and D_0 is the depth at the center. On the basis of these criteria plane models were constructed [11] for both the Northern and Southern Hemispheres. Figure 6 shows one of these models.

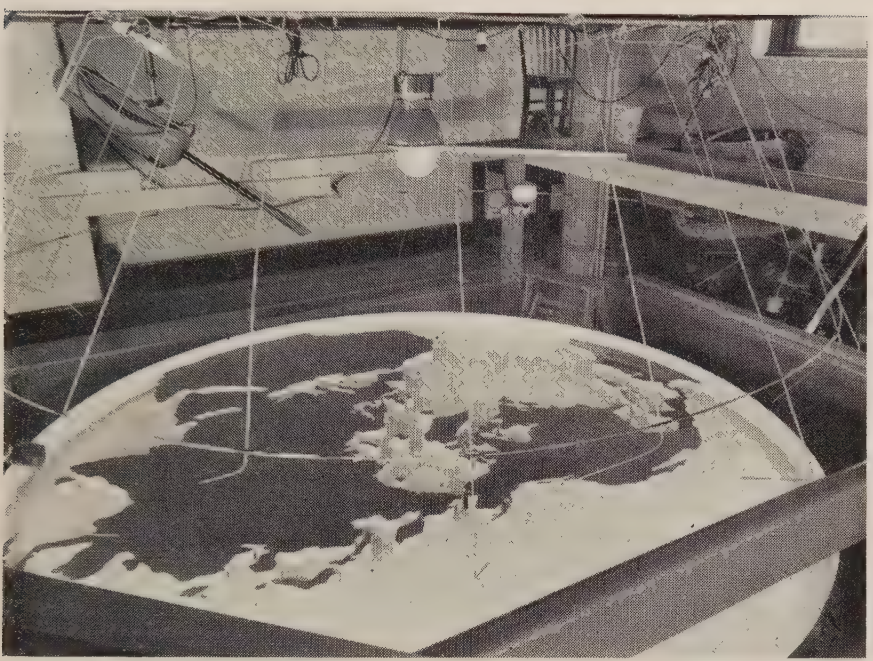

FIG. 6. PLANE OCEAN MODEL—CONTINENTS CUT FROM SPONGE RUBBER.

It hardly need be said that the favorable outcome of these experiments has lent considerable support to the hypothesis that the primary driving force for the surface circulation of the ocean is the wind stress; for the simple model, with a uniform fluid and excited only by the action of the wind, can be made to reproduce the major surface currents of the ocean with surprising fidelity. In nature these circulations are known to be intimately connected with density gradients due to temperature and salinity variations, and one cannot conclude on the basis of these experiments that thermo-haline processes are of minor importance. For example, the currents of the deep ocean well below the main thermocline layer have a rather different circulation pattern and appear to derive their energy primarily from the density structure.

In reviewing the historical literature of theories of the ocean circulation, Stommel [12] noticed a deep-rooted similarity between various studies. In particular the theories developed by Hough [13] and Goldsbrough [14], which attempted to interpret the effects of evaporation and precipitation as energy sources for the ocean circulations, were found to be similar to the theories involving wind stress. This is because the action of a wind stress on the surface of a rotating fluid is confined to a relatively thin layer [1] and the net transport of mass in this layer is 90° to the right of the wind stress. The effect of the average wind is to skim off the surface layer and to produce convergences and divergences of mass in much the same pattern as the sources and sinks of mass accompanying evaporation and precipitation over the earth.

These similarities taken together with other plausible physical mechanisms, such as the necessity of rapidly flowing western boundary currents to satisfy continuity of mass in the oceans as a whole, become possible on the earth only because of the β-effect. This effect can be simulated in the plane model by a suitably chosen radial variation of depth. Another important consideration is the latitudinal variation implicit in the geostrophic equation. From Eq. (2) it can be shown that the mass transport between any two isobars becomes greater with approach toward the equator and smaller with approach toward the pole. This is to say, that meridional geostrophic currents develop divergence due to the curvature of the earth. Fortunately, the radial variation of depth also stimulates this phenomenon. Thus the elements essential to test Stommel's theory of the ocean circulation were present in the most simplified wind-driven model, and new experiments were proposed with more rigorously controlled sources and sinks of mass in place of wind stress and with simplified boundary conditions.

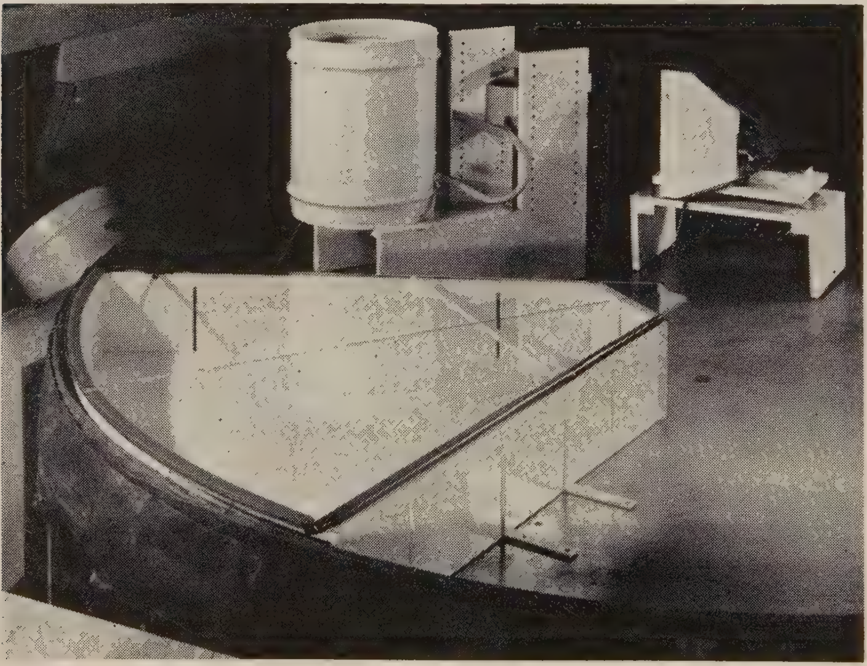

FIG. 7. IDEALIZED OCEAN BASIN OF 60 DEGREES WIDTH WITH PROVISIONS FOR CONTROLLED SOURCES AND SINKS OF MASS.

Without attempting to provide more detail at this time one can see in the following photographs some of the rather surprising circulations which have been found in the simplified model. (For the mathematical development and a more complete physical description see [15].) Figure 7 illustrates the experimental apparatus, a 60° sector of the tank used for the atmospheric models. The sides of the enclosed sector were provided with slots for the introduction or extraction of mass. In certain other instances it was preferable to use a small glass tube to introduce the colored source water at some point in the interior. The remaining equipment on the rotating table is a pump and a constant-level tank for controlling the slow and steady flow of the source water. The rate of inflow was adjusted to 120 cc per minute to obtain a Rossby number of the order of 0.001 in the western boundary current, a value appropriate for the Gulf Stream system. Other conditions were $R = 100$ cm, and $\Omega = 1.0$ radian per second; the mean depth was 8 cm, and the depth at the rim was twice that at the center.

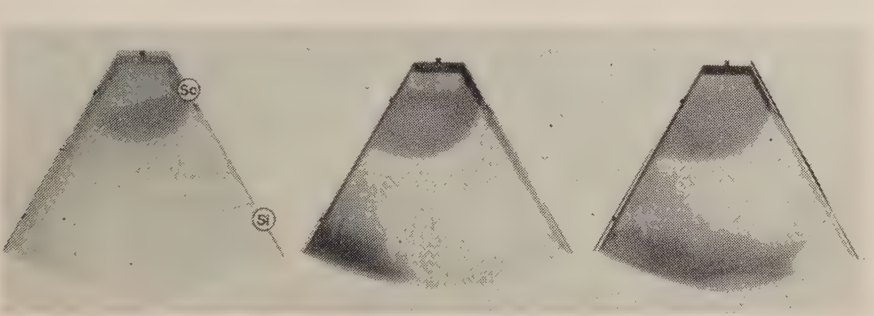

FIG. 8. PHOTOGRAPHS AT 20, 80, AND 220 MINUTES AFTER INTRODUCTION OF DYE, SHOWING FLOW FROM SOURCE (SO) TO SINK (SI).

Figure 8 illustrates the resultant circulation with the source in the eastern boundary near the pole and with the sink in the same wall near the rim.

Because of the dominant constraints of rotation and the radial-variation of depth, the flow took the peculiar course directly across the tank to the western boundary, down the western boundary to the "latitude" of the sink, and across to the eastern boundary where the sink was located. Disregarding secondary frictional circulations, radial flow in the interior is not permitted by the theory except in circumstances where a source or sink of mass exists. A case of this kind is shown in Fig. 9 where the source was situated at the apex of the sector and all exits were closed to permit the mean level of water in the tank to rise slowly. This rise of the mean water depth is equivalent to a distributed sink and according to the physical hypotheses the flow in the interior had to be radially inward. To accommodate this constraint and to provide continuity, the source water flowed down the western boundary

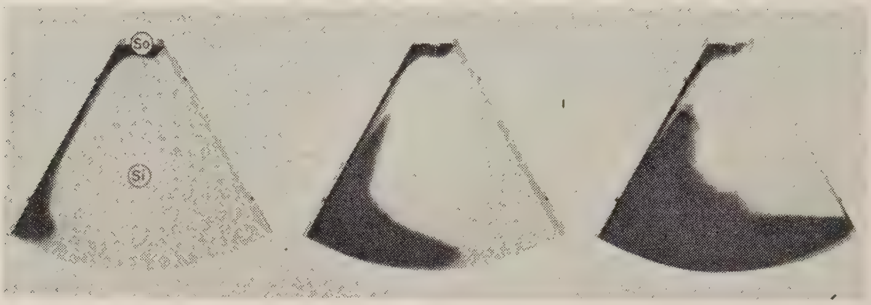

Fig. 9. Photographs at 20, 60, and 80 Minutes with Source at Apex and no External Sink.

and spread radially across the rim before filling the tank.

In Fig. 10 the source of mass was in the southwest corner and the sink was at the pole. There were no interior sources or sinks and thus no radial motion was permitted except at the western boundary where a narrow boundary current was observed. Such a current is somewhat similar to the Gulf Stream circulation.

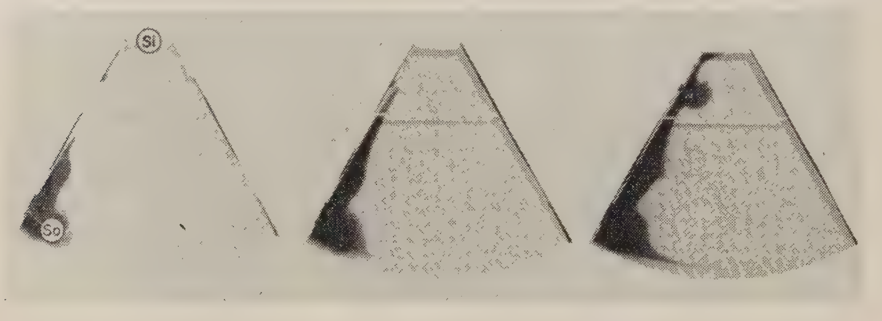

Fig. 10. Photographs at 5, 10, and 20 Minutes with Dye Injected Through Vertical Glass Tube in Southwest Corner of Tank and Sink at Apex.

Finally, in the previous case the sink at the apex was closed (Fig. 11); consequently the water level rose and a uniformly distributed sink developed. Northward motion occurred in the interior and a southward flowing boundary current was required to maintain continuity.

It is important to note that these circulations were predicted on the basis of relatively simple physical notions *before* the experiments were actually performed, and they therefore constitute a highly satisfactory vertification of the theory. There is every reason to believe that these same principles apply to the ocean circulation and may be used to construct a picture of the gross circulation pattern as Stommel has done [12], assuming certain sources and

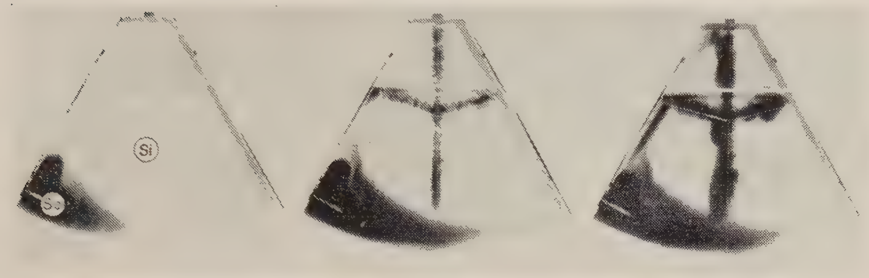

FIG. 11. PHOTOGRAPHS AT 15, 32, AND 35 MINUTES WITH CONDITIONS AS IN FIG. 10 EXCEPT WITHOUT EXTERNAL SINK AT APEX. POTASSIUM PERMANGANATE DYE FROM CRYSTALS INTRODUCED THROUGH SLITS IN GLASS COVER SHOWS SOUTHWARD-FLOWING WESTERN-BOUNDARY CURRENT.

sinks of mass. Further, if the geometrical configurations of the model are sufficiently close to those of nature, one can draw analogies between the two situations and regard them as examples of model and prototype in the more usual sense.

CONCLUSIONS

The wind driven model embodies the most realistic distribution of continental boundaries, and of sources and sinks of mass produced by Ekman layer convergence, and, therefore, has resulted in the most realistic approximation of natural ocean circulation patterns. The more simple model, on the other hand, is more readily amenable to mathematical description and is somewhat more versatile. For example, the physical situation of Fig. 9 may be regarded as an idealized model of the deep ocean circulation where a source of mass is present in the polar regions of the Atlantic ocean due to the sinking of cold saline water. To a first approximation we believe that this water eventually rises more or less uniformly over the remainder of the ocean—a uniformly distributed sink. The model verifies the theoretical anticipation that there would be a southward flowing western boundary current beneath the more obvious Gulf Stream. This circulation was subsequently observed in nature by a joint British-American expedition. Ingeniously contrived floats having neutral buoyancy at a level deep beneath the rapidly flowing Gulf Stream were tracked by ship for several days to obtain conclusive evidence of this circulation [16].

In some branches of fluid mechanics it is practical to construct laboratory models, which are both geometrically similar and satisfy the pertinent non-dimensional modeling criteria, to produce circulations which may be directly interpreted in terms of the prototype. This is far from the case for models on the planetary scale where geometrical distortions are unavoidable and other difficulties occur in abundance. In the present stage of development the relationship of model to prototype must be made more through theoretical interpretation than through direct comparisons with nature.

The development of oceanographic models, initially undertaken on rudimentary physical bases, has contributed to the development of sound physical concepts. These concepts have been fed back into simplified models which in turn have served both to verify concepts and promote their application to theoretical studies of full scale geophysical processes.

REFERENCES

1. Ekman, V. W., "On the Influence of the Earth's Rotation on Ocean Currents," *Arkiv. f. Matematik. Astronomi, och Fysik* 2 (11), 1905.
2. Fultz, D., "Studies in Experimental Hydrodynamics Applied to Large-Scale Meteorological Phenomena," *Final Report (in 2 parts), Contract AF 19(122)-160,* University of Chicago, 1956.
3. Faller, A. J., "A Demonstration of Fronts and Frontal Waves in Atmospheric Models," *J. Meteor.*, 13 (1), 1956.
4. Lasareff, P., "Sur une méthode permettant de démontrer la dependence des courants océaniques des vents alizes et sur le rôle des courants océaniques dans le changement du climat aux époques géologiques," *Gerlands Beitr. Geophys.*, 21, 1929.
5. Sverdrup, H. U., "Wind-Driven Currents in a Baroclinic Ocean; with Application to the Equatorial Currents of the Eastern Pacific," *Proceedings, Nat. Acad. Sci.* 33, 1947.
6. Stommel, H., "The Westward Intensification of Wind-Driven Ocean Currents," *Transactions, A.G.U.*, 29, 1948.
7. Munk, W. H., "On the Wind-Driven Ocean Circulation," *J. Meteor.* 7, 1950.
8. Arx, W. S. von, "A Laboratory Study of the Wind-Driven Ocean Circulation," *Tellus* 4, 1952.
9. Faller, A. J., and Arx, W. S. von, "The Variation of the Coriolis Parameter and its Simulation in Models of the Ocean Circulation," Woods Hole Oceanographic Institution, (Unpublished manuscript), 1955.
10. Rossby, C.-G., "Relation Between Variations in the Intensity of the Zonal Circulation of the Atmosphere and the Displacements of the Semi-Permanent Centres of Action," *J. Marine Res.* 2, 1939.
11. Arx, W. S. von, "An Experimental Study of the Dependence of the Primary Ocean Circulation on the Mean Zonal Wind Field," Doctoral Dissertation, Massachusetts Institute of Technology, 1955.
12. Stommel, H., "A Survey of Ocean Current Theory," *Deep-Sea Res.*, 4, 1957.
13. Hough, S. S., "On the Application of Harmonic Analysis to the Dynamical Theory of the Tides. Part I: On Laplace's 'Oscillations of the First Species,' and on the Dynamics of Ocean Currents," *Philosophical Transactions,* Vol. 189, 1897.
14. Goldsbrough, G. R., "Ocean Currents Produced by Evaporation and Precipitation," *Proceedings, Royal Society,* A, Vol. 141, 1933.
15. Stommel, H., Arons, A. B., and Faller, A. J., "Some Examples of Stationary Planetary Flow Patterns in Bounded Basins," *Tellus,* 10 (2), 1958.
16. Stommel, H., "The Circulation of the Abyss," *Scientific American*, 1958.

DISCUSSION

Wallis Hamilton asked why, since gravity appeared unimportant in this type of model, the modeling should not be done between spherical surfaces. The speaker replied that gravity should not be considered unimportant, except insofar as modeling the Froude number is concerned because of the absence of vertical accelerations or gravity waves, but that it is important in atmospheric models which deal with density differences. Experiments have been performed between spherical shells but the stress on the outer surface must be considered, and there is no simple way of generating circulation comparable to blowing air over the free surface to provide controlled stresses on it. In any case, the spherical shape would not contribute much to the experiment.

James Dailey commented that the experiments described by the speaker involve phenomena similar to friction between a stationary and a rotating disk with oil between them. Disk experiments have been performed at MIT using oils. The secondary motion and the expression for the Ackerman boundary layer thickness are the same that the rotating-disk boundary-layer theory brings out. He inquired if the speaker had looked into that literature or made any comparisons with flow between disks. The speaker said that he had not but that the same phenomenon is an explanation of the so-called "tea cup" effect. When water is stirred in a cup there must be flow toward the rim while the flow is being accelerated and this occurs primarily in the boundary layer at the bottom where the viscous effects cause the outward flow. Then as the flow slows down, there is an inward flow in the bottom boundary layer essentially because of viscosity.

Chesley Posey inquired about duplication of known patterns or discovery of unknown patterns in the field of atmospheric circulation. The speaker replied that the modeling is not sufficiently exact to discover any new patterns because the atmosphere has been fairly well explored. Some experiments were done and the patterns noted but nobody recognized them for what they were. Had their significance been recognized the jet stream circulation would have been known about much sooner and without so many upper-air observations. Although there have been no predictions made as a result of experiments with atmospheric circulation, the experiments have helped greatly in the theoretical analysis of the equations of motion as applied to atmospheric phenomena.

Wallis Hamilton commented on the fact that the equation presented was for a laminar boundary layer which does not seem right for atmospheric flow although it might be correct in the oceans. The speaker said that this was an important point. The basis for the modeling is the fact that in the atmosphere there is a large eddy coefficient and in the model there is a molecular coefficient of viscosity. Only if a comparison is made between the eddy coefficient and the molecular coefficient can one obtain a boundary layer of the same relative thickness. In the atmosphere the boundary layer is on the order of 500 to 1500 feet thick. This is about one-tenth the significant thickness of the atmosphere. It is modeled by making the depth of the viscous boundary layer about one centimeter in a total depth of ten centimeters. Similarly in the ocean circulation, at the rotation rates used in the model, the depth of the boundary layer will be one millimeter to three millimeters and this approximately models the thickness of the boundary layer in the ocean.

James Dailey supplemented his previous comment with the statement that the secondary motion in rotating machinery, in general, is related to this, and that the similarity goes beyond simple disk-friction applications.

Contribution No. 988

[Reprinted from *The Geographical Review*, Vol. XLIX, No. 2, April, 1959]

ORIGIN OF THE SEA ISLANDS OF THE SOUTHEASTERN UNITED STATES*

JOHN M. ZEIGLER

THE coast of South Carolina and Georgia is characterized by a chain of islands parallel to the mainland and separated from it by salt marshes; passes or sounds between the islands lie approximately opposite the mouths of coastal rivers. This sea-island coast was of special interest to the participants of photographic flights carried out in 1953, 1956, 1957, and 1958 as part of coastal geographic studies conducted by the Woods Hole Oceanographic Institution and sponsored by the Office of Naval Research, Geography Branch.[1] On these flights motion pictures were taken of the east coast of the United States. Many of the islands were examined from the air much more closely than the shore line itself, and the writer's curiosity led him later to make two trips by land into the sea-island area to examine features that had been seen from the air. Field work was not detailed, but coverage extended from Winyah Bay, S. C., to the Florida boundary. The films, of course, were available for restudy of the features seen in the field.

Nature of the Sea-Island Coast

It is evident that two generations of rivers drain the coastal plain and form the sounds that separate the islands (Fig. 1): (1) pre-Wisconsin rivers, which cross the coastal plain and form part of the drainage of the Piedmont (for example, the Santee, the Edisto, the Savannah, the Ogeechee, the Altamaha, and the Satilla); and (2) post-Wisconsin rivers (such as the Medway, the Newport, and the Turtle), which terminate at or near the foot of the Wisconsin-age Pamlico scarp.[2]

**Contribution No. 988 from the Woods Hole Oceanographic Institution.* The writer is grateful to the Geography Branch of the Office of Naval Research for supporting coastal photographic flights that made it possible to see the entire sea-island coast several times. The ideas set forth in this paper more or less grew out of observations made during those flights. Dr. Robert A. Ragotzkie, director of the University of Georgia Marine Institute at Sapelo Island, encouraged the writer to examine his earlier ideas more closely and report them to the Marsh Conference held at Sapelo Island, March, 1958, and sponsored jointly by the National Science Foundation and the Marine Institute. The writer also wishes to thank Professors Donald C. Scott and Wilbur Duncan of the University of Georgia for many helpful suggestions. Encouragement from, and discussions with, Professor J. A. Steers of the University of Cambridge are gratefully acknowledged, as is criticism of the manuscript by Professors Alfred C. Redfield, Sherwood D. Tuttle, and Wilbur Duncan.

[1] See J. M. Zeigler and F. C. Ronne: Time-Lapse Photography—An Aid to Studies of the Shoreline, *Research Reviews,* Office of Naval Research, Washington, D. C., April, 1957, pp. 1–6.

[2] These relationships can be seen on Plate 19 of F. S. MacNeil: Pleistocene Shore Lines in Florida and Georgia, *U. S. Geol. Survey Professional Paper 221–F,* 1950.

➤ DR. ZEIGLER is a research associate in marine geology at the Woods Hole Oceanographic Institution.

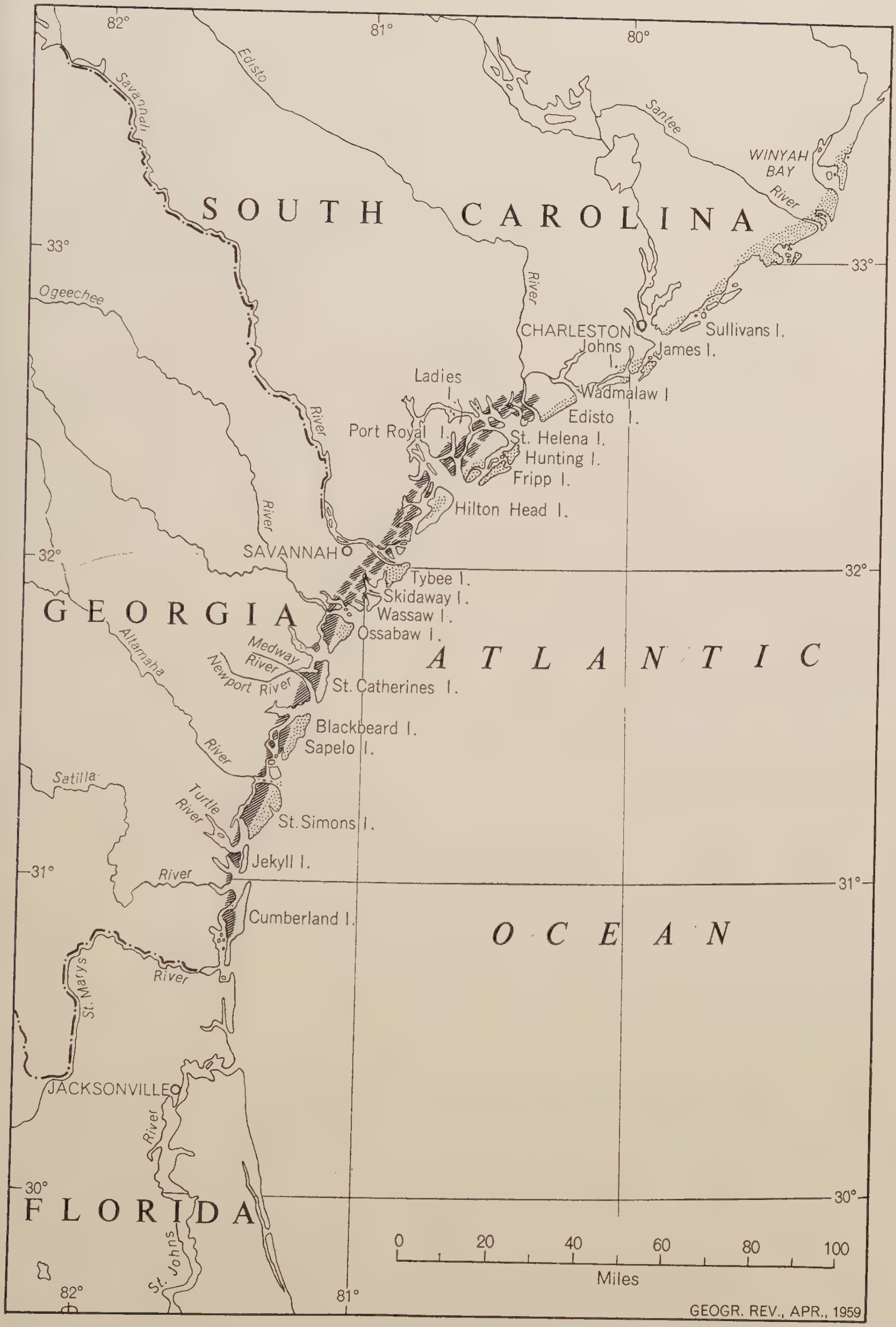
82°
81°
80°
Edisto
Savannah
Santee
WINYAH BAY
River
SOUTH CAROLINA
33°
Ogeechee
River
CHARLESTON
Sullivans I.
Johns I.
James I.
Ladies I.
Wadmalaw I
Edisto I.
Port Royal I.
St. Helena I.
Hunting I.
Fripp I.
River
Hilton Head I.
River
SAVANNAH
32°
Tybee I.
Skidaway I.
Wassaw I.
Ossabaw I.
GEORGIA
Altamaha
Medway River
Newport River
ATLANTIC
St. Catherines I.
Blackbeard I.
Sapelo I.
River
Satilla
Turtle River
St. Simons I.
Jekyll I.
31°
River
Cumberland I.
OCEAN
St. Marys
River
JACKSONVILLE
River
30°
FLORIDA
St. Johns
0
20
40
60
80
100
Miles
82°
81°
GEOGR. REV., APR., 1959

Fig. 1—Sea-island coast of Georgia and South Carolina, showing marsh types and locations. Ruled pattern indicates marsh areas localized by a zone of less resistant sediments. Dotted pattern shows location of marshes behind constructional features—beach ridges and beach ridge islands.

The sea-island coast is not uniform throughout its length either in appearance or in origin. South of the Edisto River in South Carolina it is composed of sea islands separated by sounds. North of the Edisto it is characterized by vast marshes, narrow beach-ridge islands, and fewer rivers. The location and pattern of the marshes also change from one end of the sea-island coast to the other. A well-defined band of marshes 2½ to 3 miles wide, developed in a long, narrow valley, extends continuously for 100 miles between Cumberland Island on the south and Skidaway Island on the north. The origin of the valley is the main concern of this paper.

Northward from Wassaw Island, Ga., the valley changes gradually into a zone of marshes and scattered, ragged-edge islands, both large and small (Fig. 1). This zone of marshes and islands terminates at Edisto Island; however, several large rivers that flow parallel to the coast line extend the marshes along a series of waterways to a point just north of Charleston. Above Charleston the coast is the marsh and beach-ridge island complex mentioned above.

Fenneman identifies a part of the Coastal Plain province of the southeastern United States as the "Sea Island section" and describes it as "young to mature terraced coastal plain with submerged border."[3] Following Veatch,[4] he suggests[5] that the islands of the coast of Georgia and South Carolina are parts of the Pamlico terrace,[6] "isolated by a slight submergence." The passageways between the islands were cut by streams during post-Pamlico emergence and were enlarged by tidal scour after postglacial submergence.

Flint[7] observed that many of the streams on the coastal plain flow parallel to the modern coast line in areas where the elevation is not more than 100 feet. He felt that the drainage pattern of the eastern part of the coastal plain was determined in part by the irregularities of an emerging sea floor. Before emergence numerous bars had been built on the sea floor, and these later controlled the drainage on the emerged coastal plain.

---

[3] N. M. Fenneman: [Map of] Physical Divisions of the United States, 1:7,000,000 (U. S. Geological Survey, 1946; reprinted 1949), reference in legend.

[4] Otto Veatch and L. W. Stephenson: Preliminary Report on the Geology of the Coastal Plain of Georgia, *Georgia Geol. Survey Bull. No. 26,* 1911, pp. 37–38.

[5] N. M. Fenneman: Physiography of Eastern United States (New York and London, 1938), p. 44.

[6] According to Cooke (C. W. Cooke: Correlation of Coastal Terraces, *Journ. of Geol.,* Vol. 38, 1930, pp. 577–589; reference on p. 578), the Pamlico terrace was named for North Carolina by Stephenson (L. W. Stephenson: The Quaternary Formations, *in* The Coastal Plain of North Carolina [by W. B. Clark and others], *North Carolina Geol. and Econ. Survey,* Vol. 3, 1912, pp. 266–290; reference on p. 286).

[7] R. F. Flint: Pleistocene Features of the Atlantic Coastal Plain, *Amer. Journ. of Sci.,* Vol. 238, 1940, pp. 757–787; reference on pp. 772–773.

The "bedrock" of the coastal area of Georgia and South Carolina is usually considered to be Quaternary sediments (Pleistocene and Recent). These deposits, for the most part relatively thin, also blanket the older formations.[8] Cooke[9] named these blanketing sediments Pamlico, as making up the terrace of the same name. The Pamlico formation as defined is a thin body of marine silt, clay, and sand containing a marine fauna that lived when temperatures were slightly higher than those of today. It was presumably deposited during the Sangamon interglacial. Its surface is a well-preserved sea-floor plain that rises gently landward from the present shore line to an elevation of about 25 feet, where it ends at the Suffolk strand line.[10] Everywhere within the area under discussion the Pleistocene sediments are less than 150 feet thick and dip seaward at less than 100 feet per mile.[11] However, stratigraphic succession is extremely difficult to determine because outcrops are infrequent and inaccessible.

Davis[12] long ago developed a genetic terminology for the erosional development of a coastal plain. Such a region is ideally of low elevation and is composed of sedimentary strata that have a gentle seaward dip. During the development of a drainage system, subsequent tributaries to the master consequent streams may erode headward along the outcrops of less resistant beds. This action produces a rectangular drainage pattern with the subsequent streams flowing in the strike valleys. The interfluves produced between these subsequent streams are elongate ridges called "cuestas." The southern part of the Atlantic Coastal Plain is underlain along the shore by relatively unconsolidated marine strata of Pleistocene age that dip seaward at less than 1°.[13]

EROSION REMNANT ISLANDS

There seem to be three different types of islands along the Georgia-South Carolina coast: erosion remnant islands, marsh islands, and beach-ridge

---

[8] A 2001-foot well at Charleston penetrated 75 feet of Pleistocene sediments described as dark-gray, finely arenaceous and micaceous clay, very coarse quartz sand, and shells and shell fragments. Below the Pleistocene were about two feet of Pliocene greenish phosphatic pebbles, and below that to 220 feet the Cooper marl of the uppermost Eocene or the Oligocene, composed of sandy and argillaceous limestone and nodules of phosphatic sandstone (L. W. Stephenson: A Deep Well at Charleston, South Carolina, *U. S. Geol. Survey Professional Paper 90–H*, 1914).

[9] *Op. cit.* [see footnote 6 above].

[10] R. F. Flint: Glacial and Pleistocene Geology (New York and London, 1957), pp. 266 and 363.

[11] H. G. Richards: Subsurface Stratigraphy of Atlantic Coastal Plain between New Jersey and Georgia, *Bull. Amer. Assn. of Petroleum Geologists*, Vol. 29, 1945, pp. 885–955; reference on p. 945.

[12] W. M. Davis: The Drainage of Cuestas, *Proc. Geologists' Assn.*, Vol. 16, 1899, pp. 75–93. See also O. D. von Engeln: Geomorphology (New York, 1942), pp. 106–132.

[13] Richards, *op. cit.* [see footnote 11 above], pp. 940 and 945.

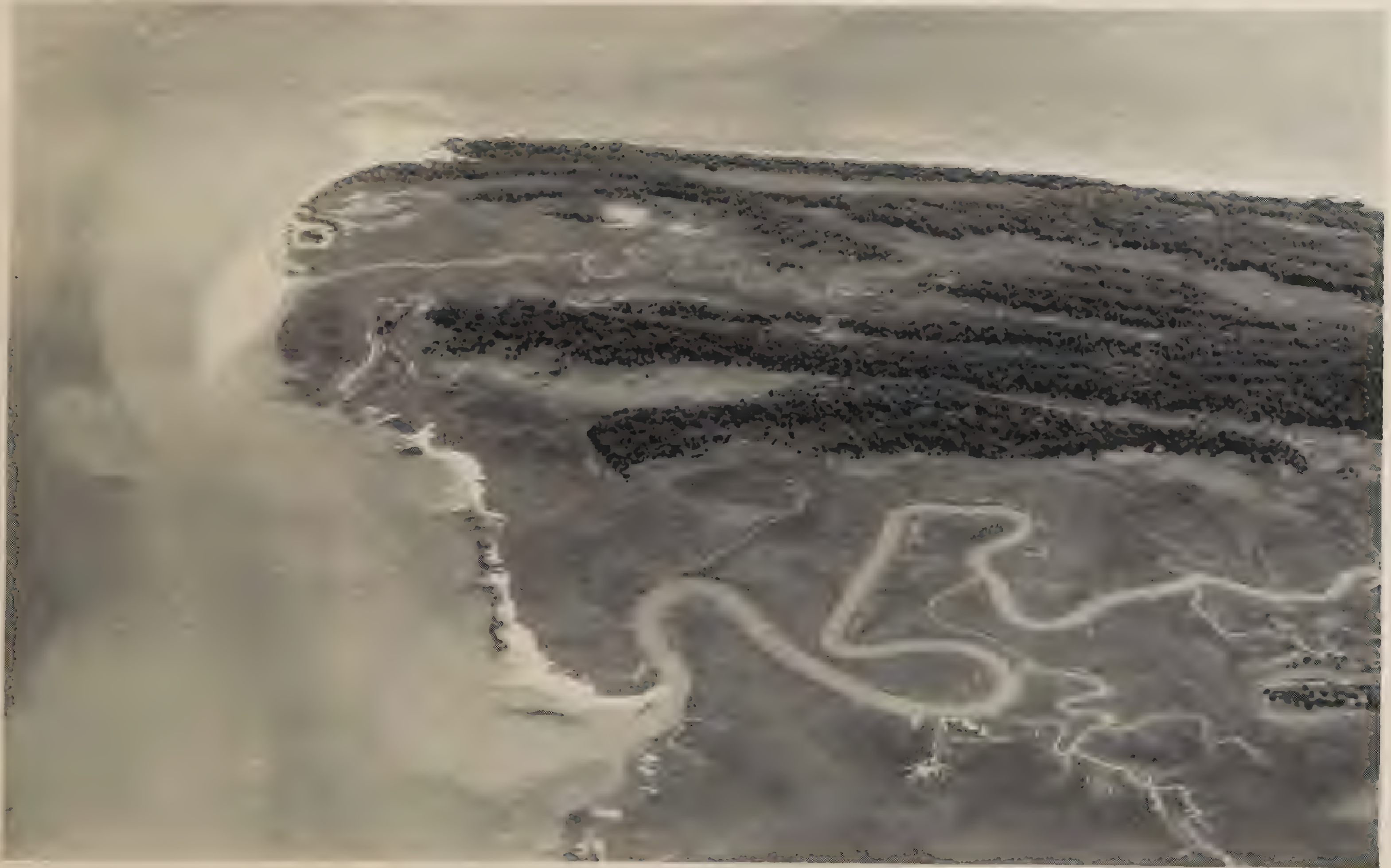

FIG. 2—The north end of Wassaw Island, a typical beach-ridge island, looking east.

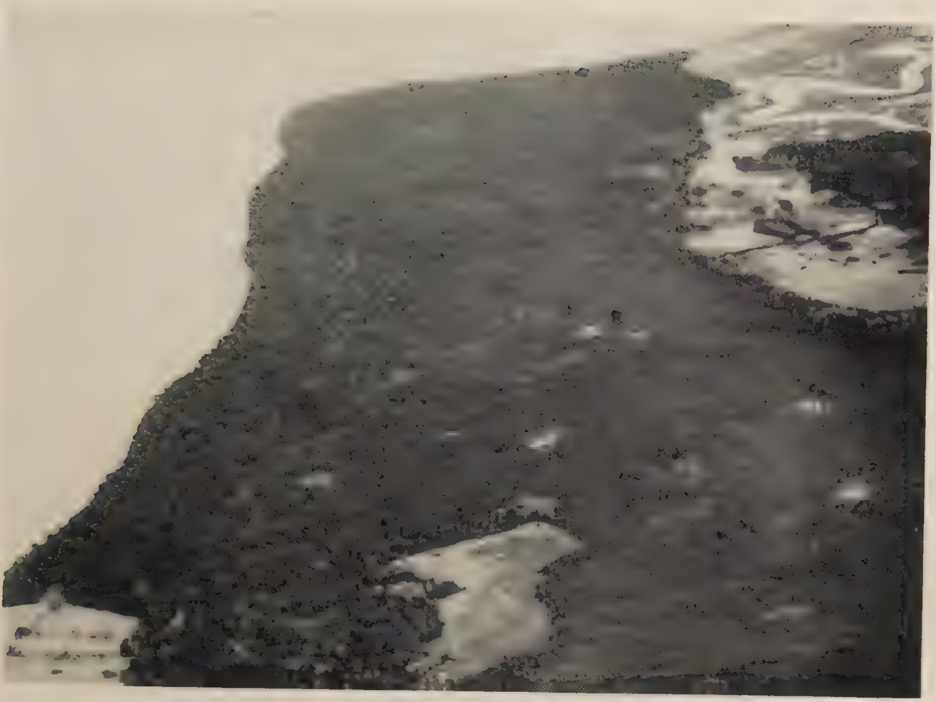

FIG. 3—View south over Sapelo Island—an erosion remnant island.

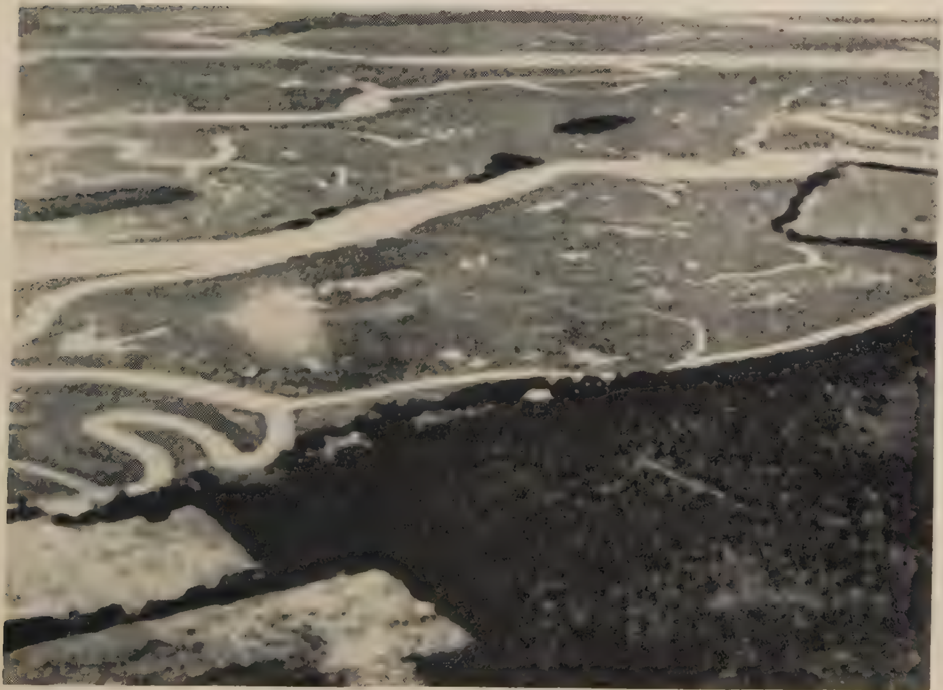

FIG. 4—Typical marsh islands, lying behind Sapelo Island.

islands. In general, the erosion remnant islands are sand-covered and irregular in outline (Fig. 3), the marsh islands are lower and are formed of detritus intermixed with vegetation (Fig. 4), and the beach-ridge islands have a characteristic topography of subparallel and arcuate ridges (Fig. 2). If the three types are present in the same area, they always occur in the same relative position to one another.

Erosion remnant islands are found from Charleston south to Florida (Figs. 5–7). The northern group, including Edisto, Port Royal, and Wadmalaw Islands, have conspicuously reticulate outlines and remind one of scattered pieces of a jigsaw puzzle. The southern group—for example, Cumberland and Sapelo Islands—are simpler in outline. The characteristic irregularity of the outline is apparently caused by the variable resistance of the sediments to erosion by streams. Erosion of the edges is primarily by marsh streams except along the sides facing the open coast. The pattern of the present topography is not uniform, and the resulting remnants have ragged edges. It is the writer's contention that the long, narrow, marsh-filled valley between the Florida border and Skidaway Island, described above, was eroded in a less resistant member of the coastal-plain sediments, which changes character northward, becoming not greatly different from the surrounding sediments, and finally disappears (Fig. 1). When it does, the zone of marshes and remnant islands also disappears. This explanation supports the thesis that many of the sea islands originated by the drowning of cuestas. Other criteria supporting erosional origin are types of sediment, types of bedding, and topographic form. If a fragment of the mainland was isolated by erosion, one would expect the island to have a similar lithology. Moreover, one would expect to be able to see the difference between typical coastal-plain sediments and the sediments making up beach ridges or barrier islands. In this part of the coastal plain the sediments are mostly sands and clayey or limy sands with scattered pockets of clay.[14] The beach ridges on this part of the Atlantic seaboard are made up of well-sorted fine sands.

The writer examined outcrops on some of the large islands—Sullivans, James, Johns, Wadmalaw, St. Helena, Hilton Head, Port Royal, Ladies, Sapelo, and Anastasia (south of the sea-island area in Florida)—and also visited scores of smaller islands; the results of his investigations are significant. Clay deposits were found on several of the remnant islands, and evidence for clay was found on others. There is a reddish clay deposit on Sapelo north of Marsh

---

[14] L. W. Stephenson: Major Marine Transgressions and Regressions and Structural Features of the Gulf Coastal Plain, *Amer. Journ. of Sci.*, Ser. 5, Vol. 16, 1928, pp. 281–298; Veatch and Stephenson, *loc. cit.* [see footnote 4 above]; and Richards, *op. cit.* [see footnote 11 above], pp. 919 and 922.

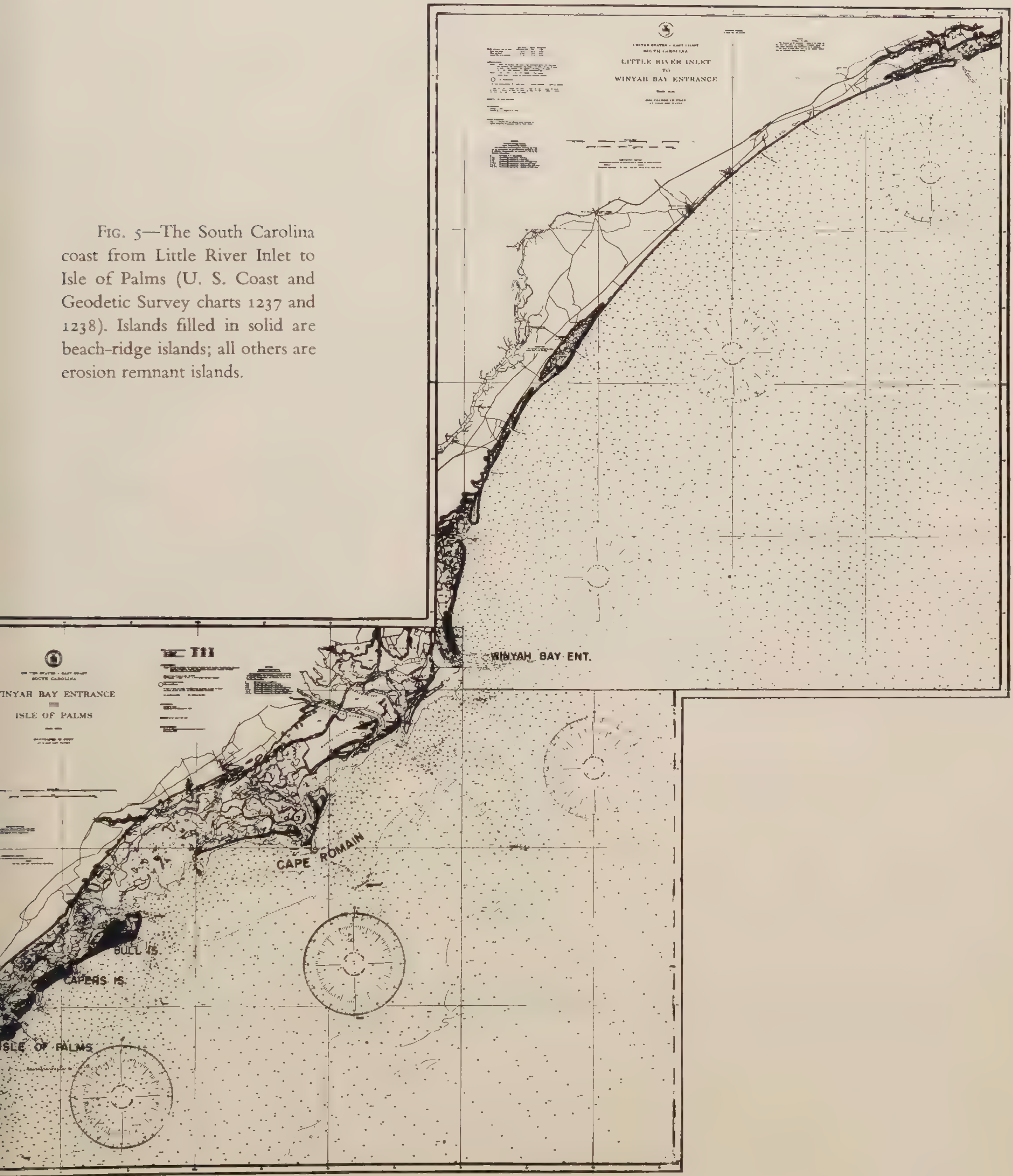
SOUTH CAROLINA
LITTLE RIVER INLET
TO
WINYAH BAY ENTRANCE
SOUTH CAROLINA
INYAH BAY ENTRANCE
ISLE OF PALMS
WINYAH BAY ENT.
CAPE ROMAIN
BULL IS.
CAPERS IS.
SLE OF PALMS

FIG. 5—The South Carolina coast from Little River Inlet to Isle of Palms (U. S. Coast and Geodetic Survey charts 1237 and 1238). Islands filled in solid are beach-ridge islands; all others are erosion remnant islands.

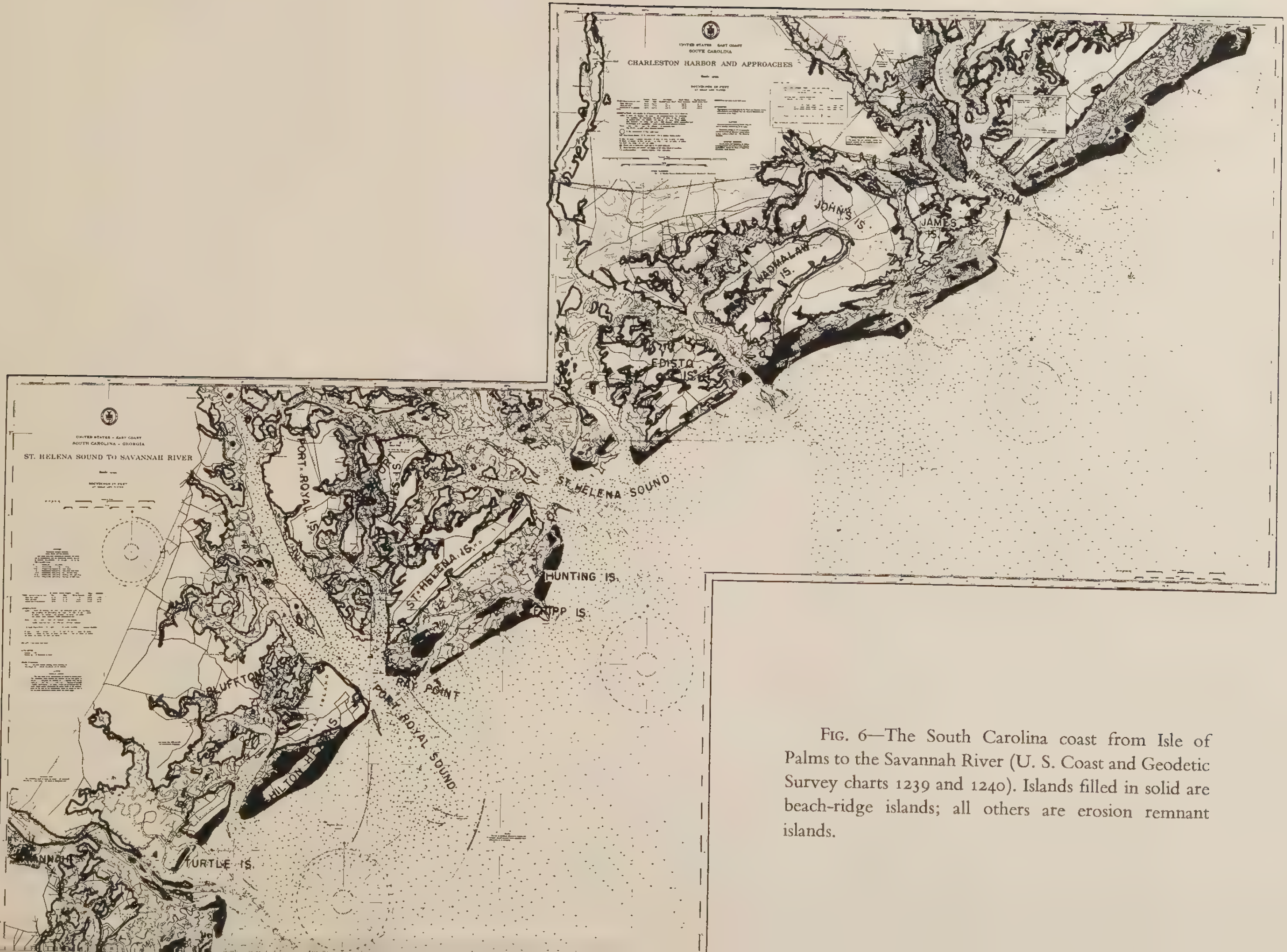
UNITED STATES - EAST COAST
SOUTH CAROLINA
CHARLESTON HARBOR AND APPROACHES
UNITED STATES - EAST COAST
SOUTH CAROLINA - GEORGIA
ST. HELENA SOUND TO SAVANNAH RIVER
CHARLESTON
JAMES IS.
JOHN'S IS.
WADMALAW IS.
EDISTO IS.
ST. HELENA SOUND
HUNTING IS.
FRIPP IS.
ST. HELENA IS.
PORT ROYAL IS.
RAY POINT
PORT ROYAL SOUND
BLUFFTON
HILTON HEAD IS.
TURTLE IS.

FIG. 6—The South Carolina coast from Isle of Palms to the Savannah River (U. S. Coast and Geodetic Survey charts 1239 and 1240). Islands filled in solid are beach-ridge islands; all others are erosion remnant islands.

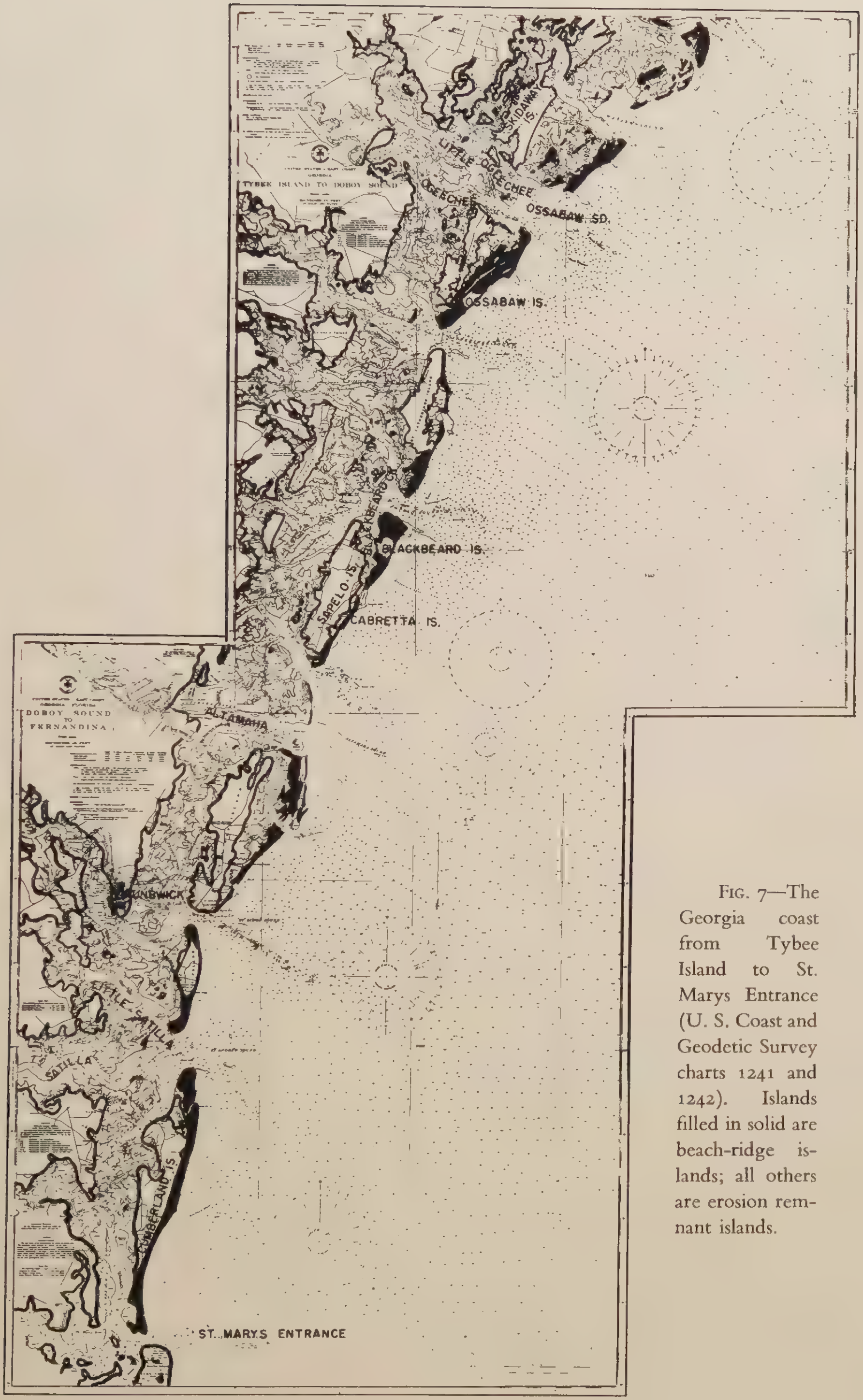
SKIDAWAY IS.
LITTLE OGEECHEE
OGEECHEE
OSSABAW SD.
TYBEE ISLAND TO DOBOY SOUND
OSSABAW IS.
BLACKBEARD IS.
SAPELO IS.
CABRETTA IS.
DOBOY SOUND TO FERNANDINA
ALTAMAHA
BRUNSWICK
LITTLE SATILLA
SATILLA
CUMBERLAND IS.
ST. MARYS ENTRANCE

FIG. 7—The Georgia coast from Tybee Island to St. Marys Entrance (U. S. Coast and Geodetic Survey charts 1241 and 1242). Islands filled in solid are beach-ridge islands; all others are erosion remnant islands.

Landing. Extensive clay deposits, interbedded with fine tan-colored sand, crop out at the Bears Bluff Laboratory on Wadmalaw Island, and bricks are made today from a large clay deposit on Johns Island. No clay was found on Port Royal Island, but a brickyard creek was noted there. None of the deposits were exposed enough to indicate the total extent or the origin of the clay. The presence of clay, which would be unlikely on sand bars or barrier islands, indicates that the larger islands are indeed similar lithologically to the mainland.

A comparison shows differences in bedding between dunes, beach-ridge areas, and erosional remnants of coastal-plain formations. An excellent area for comparison is Raccoon Bluffs on Sapelo Island. Here Blackbeard Creek has cut into evenly bedded, fossiliferous sands, but on the other side of the creek one can see beautiful cross-bedded sands on Blackbeard Island, a beach-ridge island. Uniform bedding is also visible at Bears Bluff on Wadmalaw Island, an erosion remnant island. It is difficult to find bedding of any kind in many exposures which are sand from top to bottom, but at no place did the writer find cross-bedding on either large islands or small except those which were topographically obviously beach ridges. The presence of regular, even bedding is taken to mean that the cores of many of the sea islands are erosion remnants and not constructional marine features.

The different appearance of the erosion remnant islands from beach-ridge islands as seen from the air first attracted the writer's attention. The topography of the erosion remnant islands in no way resembles beach-ridge or barrier-beach topography. Even though the surface cover of the islands is sand, ancient dune topography is absent. The surficial appearance is like that of the mainland, even to the presence of a few small Carolina bays on Sapelo Island. Of course, there is no reason why the erosion remnant islands should not have superimposed marine features dating from the time when sea level fell from a level above them. Pleistocene bars and beaches have been recognized on much of the coastal plain of Georgia and South Carolina.[15]

Suggestions of old bars were seen from the air on Johns Island and Wadmalaw Island and questionably on Hilton Head Island, but these were not examined on the ground. It is certain that they are not beach ridges, nor have they trapped flooded areas behind them; they are still at much higher elevations than the bluffs bordering the marsh on Wadmalaw and Johns Islands. Linear features could, of course, aid the drainage to establish a trellis pattern. If this is the case in Georgia, the linear features themselves were also cut away when the long valley was formed.

---

[15] Flint, Pleistocene Features of the Atlantic Coastal Plain [see footnote 7 above]; and MacNeil, *op. cit.* [see footnote 2 above].

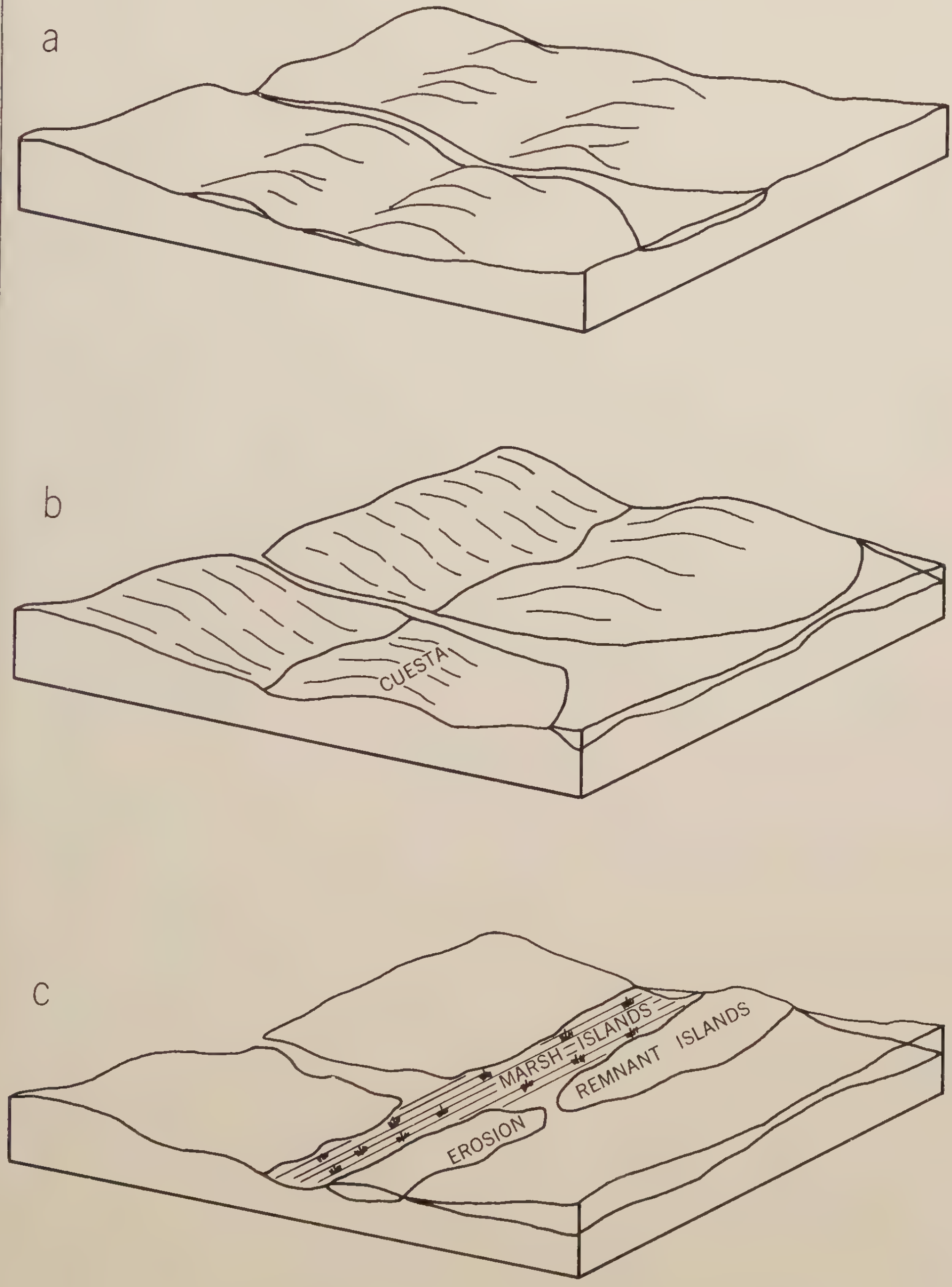
a
b
CUESTA
c
MARSH ISLANDS
REMNANT ISLANDS
EROSION

GEOGR. REV., APR., 1959

FIG. 8—Physiographic history of marsh islands and erosion remnant islands: (a) consequent stream cutting across the coastal plain at time of low sea level; (b) development of subsequent tributaries producing strike valleys and cuestas; (c) formation of erosion remnant islands by drowning; the marsh islands are now located in the position of the subsequent streams, while the cuesta tops remain as erosion remnant islands.

The sea covered coastal Georgia and South Carolina during the last interglacial period (Sangamon). As the Wisconsin glaciers advanced, sea level dropped and various marine features were left behind on the land (spits, sand bars, wave-cut scarps, and the like). Marine features were probably present all the way across the now submerged continental shelf to the Wisconsin shore line, 150 feet below the present sea level.[16] At the time of lowest sea level the present-day erosion remnant islands were part of the divides between the watersheds of rivers that drained the emerged portion of the coastal plain (Fig. 8a). Part of the developing drainage system followed the edge of a stratum of less resistant sediments roughly parallel to the present-day coast, and a valley that extended from Cumberland Island on the south to Skidaway Island on the north was cut into this less resistant stratum, and it truncated the main divides (Fig. 8b). As the subsequent valleys became flooded by the rising sea, sediments accumulated and marshes could and did develop on them between the mainland and the sea islands (Fig. 8c). The less resistant stratum is presumed to change its lithologic character northward until it gradually becomes no different from the surrounding sediments, its differential resistance to erosion decreases and becomes less uniform, and the resulting valley becomes less regular and finally is not found north of Edisto Island.

Marsh Islands

Marsh islands consist of various plants, mostly *Spartina* sp., growing on clay, silt, and peat. The general argument is that the marsh vegetation begins to grow on sand or mud flats exposed at low tide. Silt and clay are trapped by the stems and roots of the plants, and the level of the marsh is raised. Furthermore, the level will continue to rise as sea level rises. The rate of growth of the marsh vegetation does not exceed the rate at which sea level rises, because *Spartina* can flourish only in environments that are flooded by sea water from time to time; therefore the *Spartina* marshes are not built much above the average sea level. This summary of the formation of marsh islands is highly simplified; many complicating factors must be considered if one works with a specific marsh island, but in general the Carolina-Georgia marshes evolved in this manner.

The marsh islands form where marsh vegetation can survive, as in a bay or on a protected mud flat. Great marshes are forming in some of the drowned river valleys—for example, the Ogeechee—of this coastal area. One does not expect vigorous marsh growth on the beaches exposed to the open sea on the Georgia–South Carolina coast.

---

[16] Flint, Glacial and Pleistocene Geology [see footnote 10 above].

BEACH-RIDGE ISLANDS

Beach-ridge islands are unmistakable from the air (Fig. 2). They all show clear-cut lineation of ridges and swales, often accentuated by different vegetation on the ridges from that in the swales. They are formed entirely of well-sorted sand, predominantly quartz. The islands may be single long, thin strips or groups of parallel strips protruding through the marsh, or they may be sizable islands of ridges and swales facing the open sea, in which case marsh has grown up on the protected side.

The beach ridges of this part of the coast have several ages. Some are forming at present, such as those on the south end of Cabretta Island or on the south end of St. Catherines Island (Fig. 7), two older beach-ridge islands. Some formed during Wisconsin time as sea level dropped, and, of course, many are post-Wisconsin, formed during the subsequent rise in sea level.

There is some disagreement concerning the origin of beach ridges. A summary of the leading theories was given by Johnson.[17] The present writer believes that beach ridges indicate abundance of sand for transport. They are constructional features and indicate a net gain in elevation to the beach or coast on which they are built. When they are built at the tip of a pre-existing spit or island, as is often the case, they provide a lee or quiet area behind them where marshes can develop. The great marshes between Charleston and Winyah Bay developed in the lee of beach-ridge islands.

Beach-ridge islands are found along the entire coastal area under study; they are particularly well developed seaward of St. Helena Island, S. C., which is an erosion remnant island. An area of marsh 3½ miles wide has developed between St. Helena Island and the beach-ridge islands of Hunting, Fripp, and Ray Point. Many island groups show this complex structure of beach-ridge islands facing the sea, marshes behind them, and, finally, closest to the mainland, an erosion remnant island. Sapelo Island is bordered on the east by a marsh that developed behind the beach-ridge islands of Blackbeard and Cabretta (Fig. 7). St. Simons, Ossabaw, Skidaway, Hilton Head, Johns, and James Islands also show this complexity. To what extent the older erosion remnant islands influenced beach-ridge development seaward of them is not known, but if these erosion remnant islands represent fragments of higher land, divides between rivers, then the divides themselves extended farther seaward and would have represented shoal areas in the sea. Submarine contours showing the seaward extent of divides are well illustrated off Winyah Bay, Cape Romain, and Bull Bay, northeast of Charleston (Fig. 5). The shoals would have been places where wave energy was focused by wave refraction and thus increased the tendency for erosion. Erosion means removal of sand, and unless the sea is able to carry away the eroded sediment offshore, it must be transported by littoral drift alongshore. Since erosion would have been most intense on the submarine extensions of the divides, the eroded sand would indeed represent an excess of sediment near the edge of the divides. Wave attack would have tended to focus on headlands at a time of falling sea level (Wisconsin) just as it does on headlands today, but destruction of the headlands would have been delayed because even as they were being destroyed the sea dropped, and emerging contours would tend to keep the shoal areas emerging. Consequently, the retreating sea would have been continually piling up excess sediment, most likely to the sides of the shoals or headlands.

---

[17] D. W. Johnson: Shore Processes and Shoreline Development (New York and London, 1919), pp. 297–299.

With the rise of sea level after the Wisconsin, the beach-ridge areas were modified. We do not know how far seaward they may have extended. They have all been destroyed except those which now face the sea. In general, the central coasts of the islands erode, and the ends of the islands grow as new material from the center is added at the ends.

The Silver Bluff shore line, so called by Cooke,[18] roughly coincides with the western edge of a marsh-filled former valley. Its scarp stands about eight feet above sea level and is well developed on the mainland west of Ossabaw Island. It can be followed with little difficulty along most of the Georgia and South Carolina coast, even though it has been considerably dissected by river meanders in most places. MacNeil[19] thinks the scarp was cut on the landward side of a sound during the climatic optimum, 4000–6000 years ago, when sea level was presumably higher than it is now. It should be clear that the existence of a Silver Bluff shore line does not explain the formation of the valley which became flooded to form the sound in the first place.

Erosional Control

We seek, then, some control that will explain a long, narrow valley. If the control could also explain why the valley ends as it does, this would contribute additional strength to the argument. Of the choices available for this erosional control, the writer chooses stratigraphic control as the most likely. It is in no way unusual for coastal-plain formations to be lenslike in aspect, nor is it unexpected for coastal-plain sediments to change lithologic character. Detailed lithologic descriptions of this coastal area are scarce, partly because outcrops that expose more than 20 or 30 feet of surface deposits are rare and partly because much field work remains to be done.

---

[18] C. W. Cooke: Geology of Florida, *Florida Geol. Survey Geol. Bull. No. 29,* 1945, p. 248.

[19] *Op. cit.* [see footnote 2 above], pp. 100 and 104.

Structural control would also explain a narrow valley, but the coastal plain is not in a geologic province where one would expect large-scale block faulting since the Wisconsin. Thus the process of elimination supports the theory indicated by the sedimentary data and physiographic observations that the long, narrow valley between Cumberland Island and Skidaway Island owes its origin to erosion of a less resistant sedimentary unit. For if the valley is not structural, it must have been formed either by erosion or by trapping behind constructional marine features such as beach-ridge islands or barrier islands. Although many of the marshes north of the valley originated by trapping behind beach-ridge islands, the valley behind erosion remnant islands could not have had such an origin.

Contribution No. 989

Reprinted from THE JOURNAL OF EXPERIMENTAL BIOLOGY,
Vol. 36, No. 2, pp. 227–252, June 1959.
[*All rights reserved*] PRINTED IN GREAT BRITAIN

IONIC REGULATION IN THE BROWN TROUT (*SALMO TRUTTA* L.)

By MALCOLM S. GORDON*
Department of Zoology, Yale University, and Woods Hole Oceanographic Institution†

(*Received* 11 *July* 1958)

INTRODUCTION

Studies of osmotic and ionic regulation in aquatic organisms may be divided into three major categories:

1. Descriptions of the overall patterns of osmotic and ionic regulation in the internal fluids of the organism when the organism is subjected to various physiologically or experimentally interesting osmotic and ionic stresses. Variations due to sex, time of year, temperature, age and size of organism, etc. should be considered in such descriptions.
2. Studies of the various pathways for movement of water, inorganic ions and other osmotically active substances into and out of the internal fluids of the organism. Such studies may be kinetic, biochemical, pharmacological, etc., and should include any internal movements of ions between the tissues and the internal fluids.
3. Studies of the mechanisms resulting in internal integration of the action of the various pathways (hormones and the central nervous system).

Teleost fishes have been studied to some extent in each of these ways, but a great deal more remains to be learned. Recent reviews of various aspects of the work that has been done are those of Beadle (1957), Black (1957), Fontaine (1954, 1956), Hoar (1953), Hoar, Black & Black (1951), Pickford & Atz (1957), D. C. W. Smith (1956) and von Buddenbrock (1956).

The euryhaline teleosts are of particular interest on account of their ability to survive in environments varying widely in salinity. The adult stages of several such forms have been investigated in some detail, though with greatly varying degrees of completeness.

Fairly complete Category 1 studies investigating the total osmotic pressure and chloride concentration of serum have been carried out on eels (*Anguilla spp.*: Duval, 1925; Boucher-Firly, 1935; Callamand, 1943; Koch, 1949; Fontaine & Koch, 1950, for summary), on the Atlantic salmon (*Salmo salar*: Benditt, Morrison & Irving, 1941; Fontaine, Callamand & Vibert, 1950), on the three-spined stickleback (*Gasterosteus aculeatus*: Gueylard, 1924; Heuts, 1942, 1945; Koch and Heuts, 1942, 1943), and on the ten-spined stickleback (*Pungitius pungitius*: Heuts, 1943).

Much less complete studies of osmotic pressure and/or chloride have been carried out on a number of other forms. Most of this work consists simply of measurements of blood concentration in groups of fish acclimatized to fresh water and to salt water, no attention having been given to temperature, season, etc. The forms investigated include brown trout (*Salmo trutta*: Dekhuyzen, 1905; Parry, 1958), rainbow trout (*Salmo gairdneri*: Busnel, 1942; Parry, 1958), chinook salmon (*Oncorhynchus tchawytscha*: Greene, 1904, 1926), various Japanese salmonids (*Oncorhynchus spp.* and *Salvelinus spp.*: Kubo, 1953), Arctic char (*Salvelinus alpinus*: Gordon, 1957), shad (? *Alosa sp.*: Fontaine, 1930) and killifish (*Fundulus heteroclitus*: Burden, 1956; Garrard, 1935).

---

* Present address: Department of Zoology, University of California, Los Angeles 24, California.

† Contribution number 989 from the Woods Hole Oceanographic Institution.

Eels and Atlantic salmon are the only forms for which any significant amount of information is available on sodium, potassium and phosphorus concentrations in serum—and the data are very sparse even for these. Sodium and potassium were studied in the eel by Drilhon (1943), phosphorus by Fontaine & Firly (1932), Boucher-Firly (1935) and Ichikawa (1955). Sodium in the Atlantic salmon was studied by Fontaine, Callamand & Vibert (1950).

Some additional information available for the brown trout includes: studies of survival in hypertonic environments (D.C.W. Smith, 1956; Parry, 1958); values for the concentrations of most of the major inorganic ions in the serum of trout in fresh water in summer (Phillips & Brockway, 1958); and values for sodium and potassium in the serum of trout in fresh water in winter (Spalding, in Jones, 1956).

Many fewer Category 2 studies have been carried out on fishes, much less on euryhaline forms. Most of the work which has been done is thoroughly discussed in the reviews listed above and elsewhere. It should be noted, however, that with the exception of the somewhat fragmentary work of Mullins (1950) on *Gasterosteus* no work has been done on estimations of ion flux rates along the various pathways, or on the detailed mechanism of salinity adaptations, using modern methods.

A further omission, from the older literature as well as the new, has been a consideration of the possible significance for regulation of blood concentrations of internal ion movements between various tissues, especially the muscles, and the blood. The only references to this topic known to me are in the very partial studies of Drilhon (1937) and Callamand, Fontaine, Olivereau & Raffy (1951) on the eel. Drilhon suggests, and the data of Callamand *et al.* seem to lend some support to her suggestion that the muscles of the eel act as a reservoir of salts when the fish is in salt water.

The reader is referred to the reviews listed above for summaries of the Category 3 work carried out on euryhaline fishes.

The present paper falls into both Categories 1 and 2. The form studied was the brown trout (*Salmo trutta* L.), a euryhaline salmonid fish which is often anadromous. Information on the differences between sea-run and strictly fresh-water brown trout is given by Gordon (1959).

The main purpose of the work was to establish in some detail the overall pattern of normal variation (and the changes occurring in this pattern following osmotic stresses similar to those which would be encountered during migration to the sea) of the quantitatively most important inorganic constituents of the blood and muscles of brown trout. With this end in view, sexually mature brown trout within a limited size range were acclimatized for varying periods of time to fresh water and to half- and to full-strength sea water. Such acclimatization experiments were repeated three times during the course of a year at one temperature, and once at a different temperature. Blood and muscle samples were taken from groups of fish at various times during the acclimatization process. These were analysed for the following components:

Serum: freezing-point depression, ° C. (Δ); chloride, m-equiv./l. (Cl_s); sodium, m-equiv./l. (Na_s); potassium, m-equiv./l. (K_s); and total phosphorus, mg./l. (P).

Muscles: total solids, g./kg. wet weight; chloride, m-equiv./kg. wet weight (Cl_m); sodium, m-equiv./kg. wet weight (Na_m); and potassium, m-equiv./kg. wet weight (K_m).

The results of this overall (Category 1) survey will be presented first, consideration being given to the effects of season and temperature. The implications of these results will then be considered under the following headings: water and ion movements between the muscles and the blood (a test of Drilhon's (1937) ion store hypothesis—Category 2), and ecological implications.

MATERIAL AND METHODS

Animals

Sexually mature brown trout 18–24 cm. in standard length were obtained from two hatcheries in the states of Connecticut and Massachusetts respectively, the majority coming from the Massachusetts hatchery. All handling necessary was done as gently as possible, usually by means of smooth linen nets. The fish were transported from the hatcheries to the laboratory in 20-gal. galvanized iron garbage cans painted on the inside with black asphaltum varnish. Considerable mortality occurred in preliminary experiments using unpainted cans.* The fish were not fed for several days prior to, and during, the experiments. In order to prevent them from fighting the fish were maintained separately in smaller enclosures within the large tanks used.

Hatchery water temperatures varied seasonally from about 2° to 24° C. Experimental series involving temperatures significantly different from these hatchery temperatures were preceded by a gradual thermal acclimatization of the fish over 12–24 hr. The fish were maintained in aerated hatchery water during this period.

Experimental design

All experimental series followed the same pattern. Control fish were sampled (i) directly from aerated fresh water in the hatchery tanks, (ii) in the laboratory after having undergone the same thermal acclimatization as the experimentals (zero time controls), and (iii) at intervals during the experimental period. They were handled and otherwise treated as experimentals. Experimental fish were transferred from fresh water (salinity < 0·2‰) directly to aerated running half-strength sea water (salinity 15 ± 2‰) or to aerated running full-strength sea water (salinity 31·5 ± 0·5‰). Groups of fish were sampled at intervals up to ten days following transfer. In the 20° C. series, where direct transfer to full sea water proved fatal to all fish within 15–30 hr., fish acclimatized to half sea water for 10 days were further transferred to full sea water and samples were taken up to 10 days following the second transfer. The work of Boucher-Firly (1935) on *Anguilla*, that of Gordon (1959) and Parry (1958) on *Salmo trutta*, and the present results indicate that ten days is enough time for at least all major changes in internal concentrations to have taken place.

---

* Unpainted galvanized tubs were used by Gordon (1957) for handling Arctic char at Churchill, Manitoba. It seems likely that much of the mortality encountered in that work was due to this cause.

Experimental series were designed to demonstrate (i) seasonal effects, if any, at constant temperature, and (ii) temperature effects within one season. One preliminary experiment was done using fish from the Connecticut hatchery, but all other experiments were done with Massachusetts fish. Experiments with Massachusetts fish were as follows:

1. Seasonal effects at constant temperature (20 ± 2° C.):

(*a*) controls; half and full sea-water transfers in the breeding season (September–November). (*b*) controls; half and full sea-water transfers in winter and spring (February–April). (*c*) controls; half and full sea-water transfers in summer (June–August).

2. Temperature effects within one season (winter—a few data from the breeding season were also obtained):

(*a*) controls and full sea-water transfers at 10 ± 2° C. (*b*) controls; half and full sea-water transfers at 20 ± 2° C. (Exp. 1 (*b*)).

Details of the experimental protocols are given in Table 1.

The preliminary experiment using Connecticut fish included fresh-water controls and transfers to seven-eighths sea water (salinity 28‰) at 10° C. in February. Its principal purpose was to test technique and it was continued for only three days.

Complete series of serum and muscle analyses were done on all fish in Exps. 1 (*a*), (*b*), 2 (*a*), (*b*), in the fresh-water controls in 1 (*c*) and in the preliminary experiment. Determinations of muscle solids only were done on the half and full sea-water transfers in 1 (*c*).

Photoperiod was uncontrolled in all experiments, but the fish were obtained from outdoor tanks at the hatchery in which they had been exposed to the seasonal variations in light.

Analytical techniques

Blood samples. 1·0–2·0 ml. of whole blood were usually easily obtained by heart puncture with a 1 ml. tuberculin syringe and a fine (no. 22) needle. In cases where difficulties were encountered, samples were taken with the same syringe from the caudal artery and vein dorsal to the anterior edge of the insertion of the anal fin. Grafflin (1935) and Forster (1953) have shown that samples obtained in these two

Table 1. *Protocols of experiments with Massachusetts fish*

(August 1956 to August 1957.)

Starting date	Hatchery water temp. (° C.)	No. of fish	Samples obtained (state of acclimatization, no. of fish in sample)
1 (*a*) Breeding season series—20 ± 3° C.			
4. ix. 56	16	20	20 in ½ SW: 2 hr. 2; 4 hr. 2; 8 hr. 2; 12 hr. 2; 24 hr. 4; 48 hr. 2; 72 hr. 3. 3 dead.
20. ix. 56	11	22	14 in ½ SW: 8 hr. 2; 48 hr. 4; 240 hr. 7. 1 dead. 8 in FW: 72 hr. 4; 240 hr. 3. 1 dead.
2. x. 56	12	26	6 in FW: 0 hr. 6. 20 in SW: 2 hr. 2; 4 hr. 2; 8 hr. 2; 12 hr. 2; 24–30 hr. 9. 3 dead.
8. x. 56	12	12	9 in ½ SW. 7 survivors after 240 hr. to SW: 12 hr. 2; 48 hr. 5. 3 in SW: 3 hr. 1; 18 hr. 1. 1 dead.
10. x. 56	11	6	Hatchery controls—6.
24. x. 56	13	9	9 in ½ SW. 9 survivors after 240 hr. to SW: 130 hr. 2; 240 hr. 6. 1 dead.
1 (*b*) Winter and spring series—20 ± 2° C.			
18. ii. 57	3	15	15 in FW: 0 hr. 6; 72 hr. 6. 3 dead.
26. ii. 57	8	9	9 in SW: 8 hr. 4. 5 dead.
4. iii. 57	4	18	18 in SW: 16 hr. 3; 21–27 hr. 6. 9 dead.
8. iii. 57	6	18	18 in ½ SW: 8 hr. 4; 16 hr. 4; 24 hr. 6. 4 dead.
11. iii. 57	4	16	7 in FW: 7 dead. 9 in ½ SW: 72 hr. 6. 3 dead.
18. iii. 57	8	18	9 in FW: 240 hr. 1. 8 dead. 9 in ½ SW: 240 hr. 5. 4 dead.
28. iii. 57	9	18	9 in FW: 9 dead. 9 in ½ SW: 5 survivors after 240 hr. to SW: 240 hr. 1. 4 dead.
29. iii. 57	10	6	Hatchery controls—6.
1 (*c*) Summer series—20 ± 2° C.			
17. viii. 56	18	6	Hatchery controls—6.
27. v. 57	16	9	9 in ½ SW. 7 survivors after 240 hr. to SW: 240 hr. 3. 4 dead.
5. vi. 57	16	9	9 in ½ SW: 240 hr. 5. 4 others to SW: 4 dead.
21. vi. 57	20	9	9 in ½ SW. 9 survivors after 240 hr. to SW: 9 dead.
25. vi. 57	20	5	Hatchery controls—5.
23. vii. 57	21	10	5 in ½ SW: 24–29 hr. 5. 5 in SW: 5 dead.
5. viii. 57	24	5	5 in SW: 12–16 hr. 5.
2 (*a*) Winter series—10 ± 2° C.			
11. ii. 57	3	24	6 in FW: 0 hr. 6. 18 in SW: 18 hr. 4; 24 hr. 6; 52 hr. 4 (dying); 72 hr. 4.
13. ii. 57	2	9	9 in SW: 8 hr. 4; 72 hr. 2; 240 hr. 1. 2 dead.
18. ii. 57	3	8	8 in SW: 240 hr. 1. 7 dead.
26. iii. 57	9	12	12 in FW: 72 hr. 6; 240 hr. 6.

ways do not differ significantly with respect to the concentrations being considered here.

Initially, approximately 0·2 mg. of the sodium salt of heparin was added to each sample to prevent clotting. Since this was generally ineffective, most of the samples (> 95 %) were simply allowed to clot. No significant differences were found with respect to the quantities studied between duplicate series of heparinized and unheparinized samples.

The samples were placed in centrifuge tubes, the clots and corpuscles were centrifuged down, and the clear serum was pipetted off. The serum samples were placed in acid-cleaned vials, stoppered tightly with paraffined corks, and frozen until analysed. Variable amounts of haemolysis occurred in different samples. This will be discussed further below (p. 233).

Muscle samples. Four samples of 150–350 mg. wet weight (usually 200–250 mg.) were excised from the dorsal muscle mass of each fish on the left side somewhat below the dorsal fin. Care was taken to remove all skin and adhering scales. Total muscle solids were determined by placing these samples on tared aluminium pans, weighing them wet, then re-weighing them after 24 hr. in an oven at 105° C. (samples from other parts of single fish gave identical results). It will be seen that there were only small seasonal variations in this total concentration, and for this reason possible fluctuations in fat content are considered insignificant. The dried muscle samples were stored in stoppered Pyrex test tubes (cleaned with acid and detergent) until analysed. Agreement between quadruplicate determinations of total solids was ±2 g./kg. about the mean.

Chemical methods (only Pyrex glassware used throughout). Serum Δ was determined on approximately 1 mm.^{3} of serum by the method of Kinne (1952), somewhat modified by Werntz (1957). Precision was ±0·02° C.

All other analyses were carried out on aliquots of serum or dried muscle samples digested at 100° C. for about 30 min. in 0·5–1·0 ml. concentrated nitric acid plus 0·5–1·0 ml. 30% hydrogen peroxide (both Analytical Reagent grade). A drop of caprylic alcohol was added to each muscle sample to prevent foaming; serum samples that foamed were treated similarly. Appropriate standards (both pure and additions to samples) and blanks were run. Duplicate analyses were made for each substance in each tissue of each fish. The deviation of the two observations from their mean value was recorded for many hundreds of such duplicates, and the average deviation is given below as the figure for precision of each analytical method used. Unless noted otherwise serum concentrations are expressed as per litre, muscle concentrations as per kilogram wet weight.

Chloride. Analyses were made by Volhard titration using the method of Van Slyke (1923) as modified by H. W. Smith (1930). Heilbrunn & Hamilton (1942) and Shenk (1954) have criticized this technique as applied to muscle analyses. The data presented by these authors indicate that, for muscle samples, the Van Slyke technique gives incorrect figures for total muscle chloride. However, figures given by Conway (1935, 1957) and others for inorganic muscle chloride, determined in a variety of well-tested ways (including some very similar to that used by Heilbrunn and Hamilton), agree quite well with those obtained by the Van Slyke technique. Primarily for this reason the modified Van Slyke procedure has been used throughout the present work. Serum samples were 0·100 ml., muscle samples were two of the dried pieces described above. Precision for serum analyses was +2–3 m-equiv./l., for muscle analyses ±1 m-equiv./kg.

The chloride space (assuming all muscle chloride is extracellular) has been used as an estimate of extracellular volume in the muscles throughout this work. This is known to be somewhat in error, but many studies (cf. Conway, 1957) have shown that this approximation generally results in an error in the volume calculated (compared to inulin space) of only 5–10% in the muscles of cold-blooded animals. The alternative method of calculating the extracellular volume by assuming a Donnan equilibrium across the fibre membranes (Boyle & Conway, 1941; Conway, 1957) gives significantly lower (by 40%) values than the chloride space in the present material. This would be a matter for concern if it were not for the relatively poor precision of this latter method, also for the evidence that has recently been accumulating that the basic assumption may be unjustified—at least in frog muscle (Shaw, Simon & Johnstone, 1956; Shaw, Simon, Johnstone & Holman, 1956; Simon, Shaw, Bennett & Muller, 1957; Stephenson, 1957). No estimate has been made of the blood space within the muscles.

Sodium. Analyses were made at 589 mμ with a Beckman DU quartz spectrophotometer with a flame photometer attachment using an oxygen-acetylene flame. Addition standards showed that no corrections of concentrations determined were needed to compensate for flame background changes due to the influence of the nitric acid or other materials present in the serum samples (compare Berry, Chappell & Barnes, 1946; Parks, Johnson & Lykken, 1948). A correction of −10% for muscle concentrations was indicated by similar standards, however. All figures presented here contain this correction. Excess phosphate (as ammonium hydrogen phosphate) was added to all samples for flame photometry to avoid possible variable effects of low phosphorus concentrations on sodium emission such as were found by Ramsay, Brown & Falloon (1953) (Margoshes & Vallee, 1956, however, found no such effects). Serum samples were 0·200 ml., digested, then diluted quantitatively with glass-distilled water 125 times; muscle samples were aliquots of quantitative dilutions of the nitric acid and peroxide digests of the two dried samples not used for the chloride analyses. Precision for serum analyses was ± 1–2 m-equiv./l., for muscle analyses ± 0·6 m-equiv./kg.

Potassium. Analyses were made at 771 mμ by flame photometer on the same samples as used for sodium. Precision for serum analyses was ± 0·06 m-equiv./l., for muscle samples ± 2 m-equiv./kg. Again, addition standards indicated no correction was needed for serum concentrations determined, but a correction of +5% was necessary for muscle concentrations. All figures presented here contain this correction.

Phosphorus. Analyses were made on aliquots of the quantitative dilutions of the serum samples used for flame photometry. The method of Chen, Toribara & Warner (1956), with ascorbic acid as the reducing agent, was used. Precision was ± 5 mg./l.

Effects of haemolysis

The variable amount of haemolysis occurring in serum samples was mentioned above. It would be expected that rupture of some red corpuscles would influence serum potassium and phosphorus concentrations. One might expect that higher potassium and phosphorus concentrations in any one group of fish would be correlated with greater amounts of haemolysis. A general correlation of this sort did exist, but moderate degrees of haemolysis had no significant influence on these concentrations. All values for these concentrations in strongly haemolysed samples (these constituted less than 2% of all samples) have been excluded from the figures here presented.

RESULTS

Sexual and seasonal effects

Two general points need consideration before beginning a detailed survey of the results obtained for the specific concentrations studied. These are the questions of sexual differences and seasonal effects.

No consistent sexually correlated differences have been found for any of the concentrations studied in the present work. Comparisons between values for all concentrations studied in all males and all females in both series of experiments between September and April showed no differences statistically significant at the 5% level by '*t*' test. Breeding and non-breeding males and females considered separately also showed no differences. In all the following, therefore, the sexes will be considered together.

No seasonal differences in survival of experimental fish that could not be attributed to one or more of a number of extraneous influences were noted between September and April. A decrease in survival of fish gradually acclimatized to full sea water at 20° C. was noted during the summer, however. This may have been real (see p. 244).

P_s (Table 7) and Na_m (Table 5) were the only quantities measured showing consistent statistically significant seasonal variations between September and April. Excepting these two quantities, therefore, the results of both the breeding-season and the winter–spring series of experiments at 20° C. will be considered together. The seasonal variations in P_s and Na_m will be discussed in later sections.

This absence of seasonal variation was only apparent during the period September to April. The markedly different situation existing during the summer will be described below (p. 241).

Experiments at 20° C., September to April

Survival

Table 1 shows that great variations occurred in the mortality due to other than experimental causes in different groups of fish within any one experimental series, as well as between experimental series. As stated above, this was due to many extraneous factors. Allowing for the uncertainty due to these factors, it is probably still accurate to say that trout acclimatized to half-strength sea water, or to half-strength and then to full-strength sea water at 20° C. between September and April survived in the laboratory about as well as did fresh-water controls.

Serum concentrations

Fig. 1 shows the pattern of changes in Δ following isothermal transfers to fresh water, half sea water and full sea water (both directly from fresh water and after ten days' acclimatization to half sea water) at 20° C. between September and April. Cl_s and Na_s varied in almost identical fashions.

The numerical data from these experiments are summarized in Tables 2–4. Zero time controls are separated from other controls in these tables and all following tables. Zero time fish had apparently not completely recovered from the effects of handling, thermal acclimatization, etc. (cf. P, p. 238).

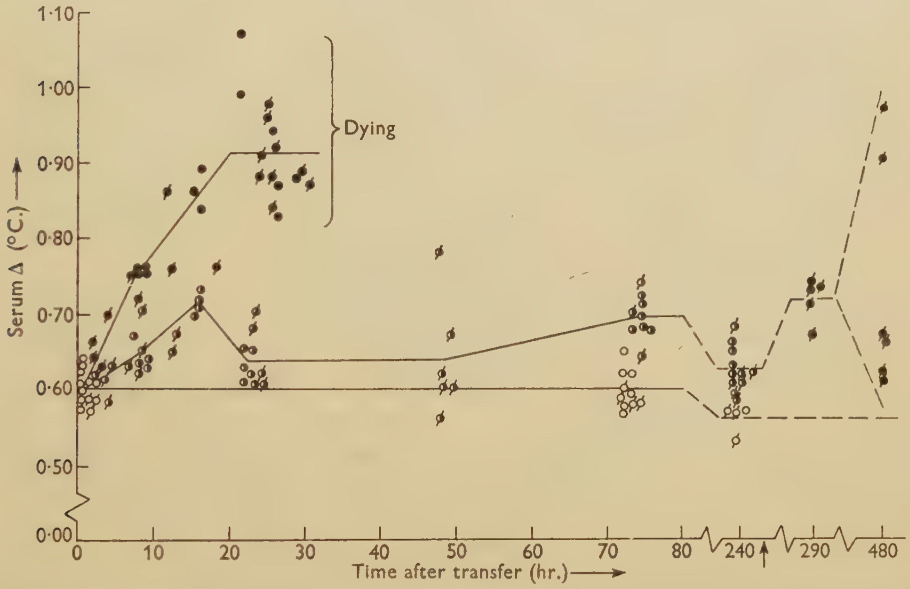

Fig. 1. Time course of changes in serum Δ in Massachusetts hatchery fish following transfers from fresh water to half-strength and to full-strength sea water at 20° C. between September and April. Open circles (○) are fresh-water controls, half-black circles (◑) half sea-water transfers, black circles (●) full sea-water transfers. Symbols with diagonal marks (e.g. ∅) represent fish sampled during the breeding season. The arrow at 240 hr. indicates transfer from half to full sea water. Ruled lines join the means for the various groups. Unless noted otherwise, the symbols used in the other figures have similar meanings.

In the control fish maintained in fresh water Δ = 0·59° C. and no significant changes occurred (240 hr. controls are insignificantly different from 72 hr. controls at the 1% level by '*t*' test). The shock of handling the fish, and also their being starved for the experimental period, therefore had no effect on their overall osmoregulatory abilities assessed in this way.

In the first few hours following transfer from fresh water to half-strength and to full-strength sea water Δ increased almost linearly with time, the rates of increase varying approximately in proportion to the initial concentration gradients established between the fishes' blood and their external environments.

In half sea water the concentration continued to increase for 10–15 hr., after which period it became more or less stabilized at a new, higher level, Δ = 0·69° C. after 72 hr.

Table 2. *Changes in serum Δ and total muscle solids following application of osmotic stresses*

(September–April.)

State of acclimatization	Serum Δ (° C.) [$\bar{x}$ ± S.E. (N)]	Muscle solids (g./kg.) [$\bar{x}$ ± S.E. (N)]
	20° C. experiments	
FW, 0 hr.	0·604 ± 0·005 (12)	210·2 ± 1·2 (12)
FW, 72–240 hr.	0·587 ± 0·008 (14)	209·7 ± 2·3 (14)
½ SW, 16 hr.	0·715 ± 0·006 (4)	233·2 ± 4·3 (4)
½ SW, 24 hr.	0·637 ± 0·010 (10)	232·0 ± 2·7 (25)
½ SW, 48 hr.	0·638 ± 0·032 (6)	
½ SW, 72 hr.	0·693 ± 0·010 (9)	
½ SW, 240 hr.	0·625 ± 0·008 (11)	210·1 ± 2·0 (12)
SW, 21–30 hr.	0·914 ± 0·016 (15)	279·7 ± 2·7 (15)
½ SW, 240 hr., SW, 47 hr.	0·716 ± 0·013 (5)	239·2 ± 7·5 (5)
½ SW, 240 hr., SW, 240 hr.	0·738 ± 0·064 (6)	225·1 ± 7·1 (7)
	10° C. experiments	
Hatchery controls	0·563 ± 0·003 (12)	205·2 ± 2·0 (12)
FW, 0 hr.	0·582 ± 0·010 (6)	207·3 ± 4·8 (6)
FW, 72–240 hr.	0·555 ± 0·006 (11)	201·8 ± 3·5 (12)
SW, 24–72 hr.	0·747 ± 0·013 (12)	252·2 ± 4·5 (12)
SW, 240 hr.	0·62, 0·81 (2)	217, 233 (2)

Table 3. *Changes in serum and muscle chloride following application of osmotic stresses*

(September–April.)

State of acclimatization	Cl$_s$ (m-equiv./l.) [$\bar{x}$ ± S.E. (N)]	Cl$_m$ (m-equiv./kg.) [$\bar{x}$ ± S.E. (N)]	Cl$_m$/Cl$_s$ × 10^3
	20° C. experiments		
FW, 0 hr.	129·2 ± 1·3 (12)*	8·2 ± 0·3 (12)	64 (59–68)†
FW, 72–240 hr.	140·5 ± 1·1 (14)*	9·6 ± 0·6 (14)	68 (60–77)
½ SW, 24 hr.	153·5 ± 3·1 (10)	10·7 ± 0·9 (10)	70 (58–82)
½ SW, 72 hr.	164·7 ± 2·9 (9)	9·6 ± 0·6 (9)	58 (51–66)
½ SW, 240 hr.	148·2 ± 2·3 (12)	9·3 ± 0·5 (12)	63 (56–70)
SW, 21–30 hr.	203·6 ± 3·3 (15)	14·0 ± 1·1 (15)	69 (58–80)
½ SW, 240 hr., SW, 47 hr.	170·4 ± 1·6 (5)	13·4 ± 1·0 (5)	79 (67–91)
½ SW, 240 hr., SW, 240 hr.	179·1 ± 11·5 (7)	12·5 ± 1·5 (6)	71 (54–88)
	10° C. experiments		
Hatchery controls	130·0 ± 1·3 (12)	7·8 ± 0·5 (12)	62 (52–72)
FW, 0 hr.	131·3 ± 1·2 (6)	7·5 ± 0·5 (6)	57 (50–65)
FW, 72–240 hr.	128·3 ± 1·2 (11)	8·8 ± 1·5 (6)	69 (45–92)
SW, 24 hr.	171·9 ± 3·2 (12)	10·2 ± 0·6 (6)	60 (52–66)
SW, 72 hr.		8·7 ± 0·7 (6)	50 (42–59)
SW, 240 hr.	146, 189 (2)	9, 17 (2)	62, 90

* The difference in means between these two groups of controls is due to a lag in the response of the fish to temperature change. Temperature of the hatchery water at the times these experiments were carried out was near 10° C. (See Material and Methods section.)

† Approximate 95 % confidence interval. (See p. 241.)

Table 4. *Changes in serum sodium following application of osmotic stresses*

(September–April.)

State of acclimatization	Na$_s$ (m-equiv./l.) [$\bar{x}$ ± s.e. (N)]
20° C. experiments	
FW, 0 hr.	148·1 ± 1·7 (12)
FW, 72–240 hr.	149·3 ± 1·4 (13)
½ SW, 24 hr.	165·4 ± 1·9 (10)
½ SW, 72 hr.	179·0 ± 2·3 (9)
½ SW, 240 hr.	162·1 ± 2·8 (12)
SW, 21–30 hr.	231·1 ± 4·7 (15)
½ SW, 240 hr., SW, 47 hr.	182·6 ± 1·7 (5)
½ SW, 240 hr., SW, 240 hr.	194·0 ± 15·2 (6)
10° C. experiments	
Hatchery controls	146·9 ± 1·8 (12)
FW, 0 hr.	147·5 ± 1·7 (6)
FW, 72–240 hr.	145·4 ± 1·1 (12)
SW, 24–72 hr.	188·8 ± 4·5 (12)
SW, 240 hr.	154, 190 (2)

Table 5. *Changes in total sodium in the muscles following application of osmotic stresses*

(September–April.)

State of acclimatization	Na$_m$ (m-equiv./kg.) [$\bar{x}$ ± s.e. (N)]
20° C. experiments—breeding season	
FW, 0 hr.	14·4 ± 1·4 (6)
FW, 72–240 hr.	18·8 ± 1·2 (7)
½ SW, 24 hr.	16·0 ± 1·4 (4)
½ SW, 72 hr.	13·6 ± 1·6 (3)
½ SW, 240 hr.	17·9 ± 0·8 (7)
SW, 21–30 hr.	26·6 ± 1·7 (9)
½ SW, 240 hr., SW, 47 hr.	19·6 ± 1·6 (5)
½ SW, 240 hr., SW, 240 hr.	13·6 ± 1·7 (6)
20° C. experiments—spring	
FW, 0 hr.	8·2 ± 0·2 (6)
FW, 72–240 hr.	12·0 ± 1·3 (7)
½ SW, 24 hr.	10·7 ± 1·1 (6)
½ SW, 72 hr.	12·1 ± 0·6 (6)
½ SW, 240 hr.	9·7 ± 0·8 (5)
SW, 21–30 hr.	25·0 ± 1·9 (6)
10° C. experiments—spring unless noted	
Hatchery controls	7·9 ± 0·3 (6)
Hatchery controls, breeding season	11·2 ± 0·8 (6)
FW, 0 hr.	9·0 ± 0·5 (6)
FW, 72 hr.	8·6 ± 2·0 (6)
SW, 24 hr.	13·4 ± 1·0 (6)
SW, 72 hr.	11·6 ± 0·9 (6)
SW, 240 hr.	9·4, 17·1 (2)

In full sea water the concentration continued to increase for approximately 20 hr., after which period it may well have begun to level off at about $\Delta = 0{\cdot}91°$ C., some 56 % above the fresh-water level. The fish did not survive long enough for this to be certain, however. Many were already dead after 24 hr. and all were at least moribund after about 30 hr.

The fish in half sea water survived with relatively little mortality for ten days. After this period they had all made some return toward their original fresh-water concentrations, though they still averaged 6 % above controls (difference statistically significant at the 1 % level). Such acclimatized fish transferred to full sea water again increased in concentration, but only to $\Delta = 0{\cdot}72°$ C., which is about the same value as that reached after transfer from fresh water to half sea water. As far as their ability to regulate blood concentration was concerned, full sea water had essentially become half sea water for these fish.

Ten days in full sea water were now survived with comparatively little difficulty, though the fish often became very emaciated and some died, apparently of starvation and tank injuries. After 10 days in full sea water the relative uniformity of response demonstrated to previous stresses was no longer present. Variability for serum concentration increased by a factor of 4–6. Serum concentrations equal to those found in dying fish 24 hr. after direct transfer from fresh water to full sea water were now encountered in seemingly healthy fish. Other healthy fish had returned all the way to their original fresh-water concentration levels. The significance of these observations for the present work is discussed below (p. 247).

The patterns shown by Cl_s and Na_s were, as noted above, the same as that for Δ. Assuming unit activity for the ions, chloride contributed a quite constant 40–45 % of the Δ of the blood, sodium 45–49 %. These relations are shown in Fig. 2, in which Cl_s and Na_s are plotted against Δ. The regression lines for these relations, calculated by the method of least squares, are included in Fig. 2. The equations for these lines are: $Cl_s = 211{\cdot}9\,\Delta + 13{\cdot}4$; $Na_s = 234{\cdot}6\,\Delta + 14{\cdot}7$ (using absolute values for Δ). The slopes of the lines are statistically insignificantly different from one another ($P = 0{\cdot}4$, by '*t*' test). Correlation coefficients for the two sets of data are: Cl_s, Δ: 0·654; Na_s, Δ: 0·704.

Changes in K_s and P following the various transfers were small and virtually all statistically insignificant (Tables 6 and 7). Such variations as did occur were only generally related to the other concentration changes already described. K_s on the average was regulated very well on a low level.

Within the separate experimental series P remained essentially constant. The only variation encountered which appears biologically significant is the seasonal one (see p. 245).

For brief periods following handling or some other sort of shock P often increased somewhat. This effect is illustrated in Table 7 by the higher and more variable phosphorus concentrations found in all groups of zero time controls as compared with controls which had been kept for some time under constant environmental conditions.

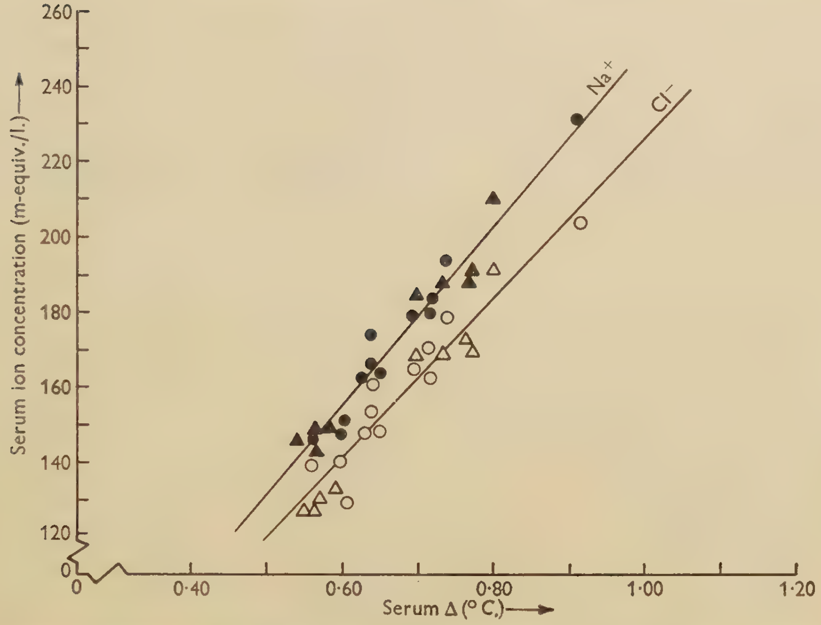

Fig. 2. Relations between Cl_s and Na_s and Δ. For clarity the only points plotted are those representing the mean values for these quantities in the variously acclimatized groups of fish. The straight lines are regression curves calculated from the original data on individual fish using the method of least squares. The equations for these curves are:

$$Cl_s = 211{\cdot}9\,\Delta + 13{\cdot}4$$

$$Na_s = 234{\cdot}6\,\Delta + 14{\cdot}7$$

Chloride concentrations are represented by open symbols, sodium concentrations by solid symbols. Triangles represent experiments at 10° C., circles those at 20° C. Only fish sampled between September and April are included.

Muscle concentrations

The patterns developed for all muscle concentrations were very similar to that described for Δ. The data are presented in Tables 2, 3, 5 and 6. Fig. 3 shows the degree of correlation between muscle total solids and Δ.

There were several quantitative differences in comparison with serum concentrations. The differences which seem worthy of mention are:

(1) The 1- to 3-day stabilization level in half sea water was only 11 % above fresh-water control (18 % for serum concentration after three days), and concentration after 20 hr. in full sea water was only 33 % above control (56 % for serum concentration).

(2) There was a complete return to fresh-water control level after ten days in half sea water (serum concentration still 6 % above control at this time).

(3) There were no significant increases in Cl_m above fresh-water control in fish transferred to half sea water. The means are identical with control from 72 hr. onwards in half sea water on.

(4) Na_m showed a significant seasonal variation; Na_s did not.

Table 6. *Changes in serum and muscle potassium following application of osmotic stresses*

(September–April.)

State of acclimatization	K_s (m-equiv./l.) [$\bar{x}$ ± S.E. (N)]	K_m (m-equiv./kg.) [$\bar{x}$ ± S.E. (N)]
20° C. experiments		
FW, 0 hr.	4·2 ± 0·6 (9)	142·6 ± 1·2 (12)
FW, 72–240 hr.	5·1 ± 0·5 (13)	142·5 ± 1·7 (14)
½ SW, 24 hr.	4·2 ± 0·7 (9)	153·7 ± 1·5 (25)
½ SW, 72 hr.	5·3 ± 0·8 (9)	
½ SW, 240 hr.	3·8 ± 0·7 (11)	141·8 ± 1·0 (12)
SW, 21–30 hr.	6·8 ± 0·6 (11)	180·8 ± 1·2 (15)
½ SW, 240 hr., SW, 47 hr.	12·4 ± 3·2 (5)	157·6 ± 2·2 (5)
½ SW, 240 hr., SW, 240 hr.	4·0 ± 0·4 (6)	151·7 ± 6·2 (6)
10° C. experiments		
Hatchery controls	2·4 ± 0·3 (12)	138·2 ± 1·4 (12)
FW, 0 hr.	1·6 ± 0·5 (6)	137·2 ± 1·2 (6)
FW, 72–240 hr.	2·8 ± 0·5 (11)	136·8 ± 2·5 (6)
SW, 24–72 hr.	6·3 ± 0·8 (11)	156·4 ± 2·3 (12)
SW, 240 hr.	4·3, 5·2 (2)	132, 156 (2)

Table 7. *Changes in serum total phosphorus following application of osmotic stresses*

(September–April.)

State of acclimatization	P (mg./l.) [$\bar{x}$ ± S.E. (N)]
20° C. experiments—breeding season	
FW, 0 hr.	120 ± 11 (4)
FW, 72–240 hr.	70 ± 4 (7)
½ SW, 24–72 hr.	72 ± 3 (13)
½ SW, 240 hr.	101 ± 9 (7)
SW, 21–30 hr.	128 ± 23 (6)
½ SW, 240 hr., SW, 47 hr.	159 ± 38 (5)
½ SW, 240 hr., SW, 240 hr.	100 ± 12 (6)
20° C. experiments—spring	
FW, 0 hr.	131 ± 11 (5)
FW, 72–240 hr.	110 ± 7 (6)
½ SW, 24–72 hr.	116 ± 7 (12)
½ SW, 240 hr.	120 ± 2 (4)
SW, 21–30 hr.	178 ± 32 (5)
10° C. experiments—spring unless noted	
Hatchery controls	118 ± 2 (6)
Hatchery controls, breeding season	81 ± 4 (6)
FW, 0 hr.	150 ± 14 (6)
FW, 72–240 hr.	109 ± 8 (11)
SW, 24–72 hr.	150 ± 12 (12)
SW, 240 hr.	95, 40 (2)

A final point is that the data on Cl_s and Cl_m considered together indicate that the volume of extracellular fluid in the muscles is quite independent of the state of salinity acclimatization of the fish. Assuming that all muscle chloride is extracellular, the ratio Cl_m/Cl_s (cf. last column in Table 3) provides an estimate of this quantity. There are no statistically significant variations in this ratio (the figures in parentheses in the last column of Table 3 are approximate 95 % confidence intervals for the ratios listed, calculated from mean $Cl_m \pm 2$ S.E.).

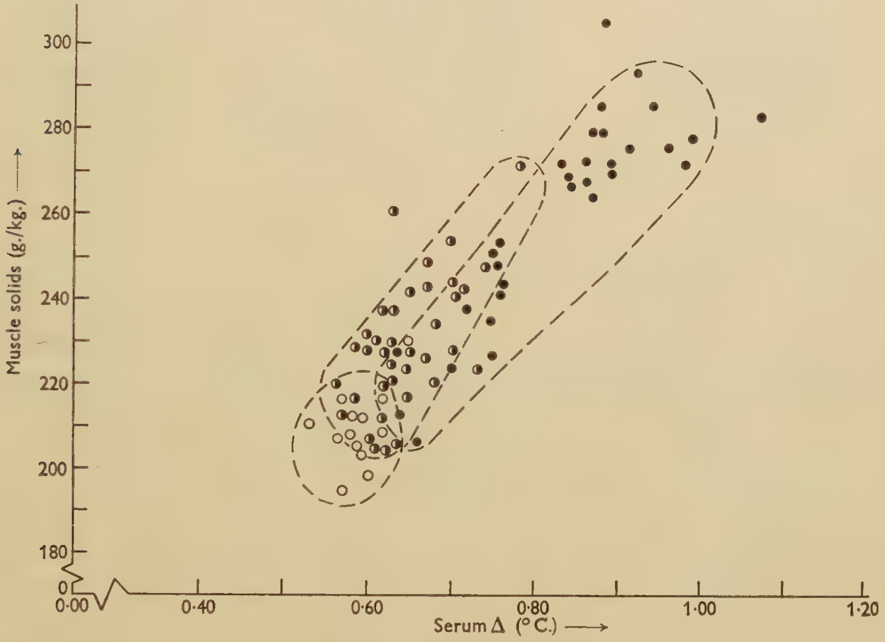

Fig. 3. Relations between muscle solids concentration and serum Δ in Massachusetts fish transferred from fresh water to half-strength and to full-strength sea water at 20° C. between September and April. Dashed lines roughly indicate boundaries of groups.

Experiments at 20° C., *June to August*

The experiments carried out at 20° C. between June and August were not as complete as those between September and April, but they serve to show that the brown trout in summer is a very different fish, at least with regard to osmotic and ionic regulatory abilities, from the brown trout at other times of year.

Two groups of fresh-water (hatchery) controls were sampled in late June and mid-August. These two series were insignificantly different from one another with respect to Cl_s and total muscle solids (the only analyses done on the June series). The August fish showed significant changes in all serum and muscle concentrations that were invariant between September and April—see Table 8.

The data on variations in total muscle solids following acclimatizations to half-strength and to full-strength sea water during the summer were as follows (figures are means ± 1 S.E.): Fresh water: 217·5 ± 2·8 (N = 11); half sea water, 24–29 hr.:

Table 8. *Seasonal variability in fresh-water control fish*

(20 ± 2° C.)

Concentration	September–April [$\bar{x}$ ± S.E. (N)]	August [$\bar{x}$ ± S.E. (N)]
Δ (° C.)	0·587 ± 0·008 (14)	0·553 ± 0·009 (6)
Cl_s (m-equiv./l.)	140·5 ± 1·1 (14)	123·2 ± 2·0 (6)
Na_s (m-equiv./l.)	149·3 ± 1·4 (13)	142·2 ± 2·7 (6)
K_s (m-equiv./l.)	5·1 ± 0·5 (13)	3·5 ± 0·3 (6)
P (mg./l.)	70 (Sept.); 110 (April)	165 ± 10 (6)
Muscle solids (g./kg.)	209·7 ± 2·3 (14)	217·2 ± 3·0 (6)
Cl_m (m-equiv./kg.)	9·6 ± 0·6 (14)	11·3 ± 0·9 (6)
Na_m (m-equiv./kg.)	18·8 (Sept.); 12·0 (April)	10·1 ± 0·6 (6)
K_m (m-equiv./kg.)	142·5 ± 1·7 (14)	129·3 ± 1·5 (6)

259·4 ± 4·7 (N = 5); half sea water, 240 hr.: 234·4 ± 5·3 (N = 5); sea water, 12–16 hr.: 297·0 ± 3·2 (N = 5); half sea water, 240 hr., sea water, 240 hr.: 238·0 ± 7·0 (N = 3).

Comparison of these data with Table 2 shows that in all states of acclimatization brown trout in summer were more concentrated (by 7–32 g./kg.) than brown trout during the rest of the year. It can also be seen that summer fish were much poorer regulators than fish during the rest of the year. Long-term acclimatizations to half, or to half and then to full, sea water did not result in as complete returns toward fresh-water levels as occurred between September and April. Furthermore, fish transferred from fresh water to full sea water survived for only about 12–16 hr. (compared to 20–30 hr. during the rest of the year), and became more concentrated. It appears that the brown trout decreases markedly in osmoregulatory ability in the months prior to, but seemingly not during, the breeding season.

Experiments at 10° C., *February*

A lowering of the temperature by 10° C. resulted in a marked improvement in the resistance of brown trout to sudden osmotic stresses. As regards survival, all fish were able to survive direct transfer from fresh water to full sea water for at least 2 days. About one-fifth of the number so transferred and not used at earlier times were able to survive this transition indefinitely (at least for 10 days).

The general pattern of concentration changes at 10° C. was similar to that occurring at 20° C., but with quantitative differences. The fresh-water controls showed the same lack of effect of handling and starvation noted for the 20° C. experiments (all differences in means insignificant at the 1 % level), but Δ and Cl_s were 5 % lower than in fish kept at 20° C. (difference statistically significant at the 1 % level). K_s in fresh water was about 2 m-equiv./l. lower at 10° C. than at 20° C. (also significant at the 1 % level).

The stabilization level reached by Δ after one day in full sea water was 35 % above fresh-water control (compared to 56 % at 20° C.). Total muscle solids were only 20 % above control at the same time (compared to 33 % at 20° C.). The two living fish sampled after 10 days in full sea water were almost as different from one another as the most extreme fish in the group which had spent 10 days in full sea water at 20° C.

The pattern shown by Δ is presented in Fig. 4. The average curve for the full sea water transfers at 20° C. is included in this figure for reference.

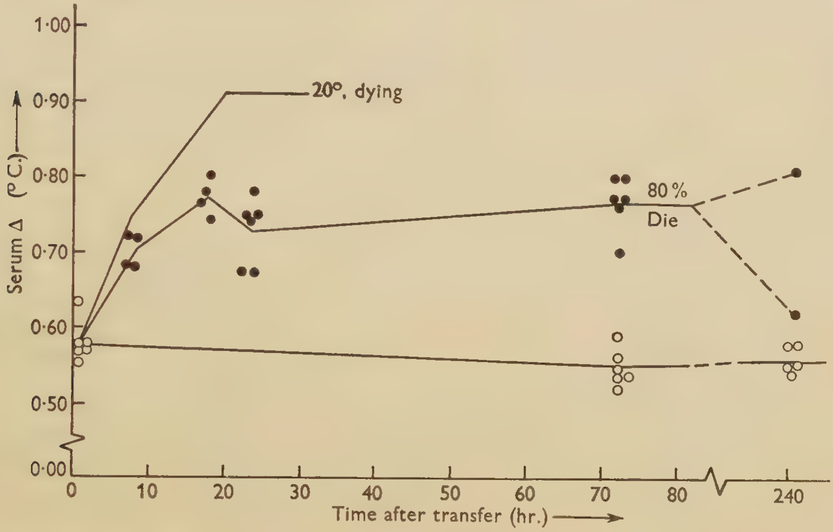

Fig. 4. Time course of changes in serum Δ in Massachusetts hatchery fish following transfers from fresh water to full-strength sea water at 10° C. in February.

The preliminary experiment using fish from the Connecticut hatchery was also done at 10° C. in February. Transfers were from fresh water to sea water of only 28‰ salinity. The general pattern of concentration changes that occurred was the same as for the Massachusetts fish, but blood concentrations in fresh water were significantly higher (Δ = 0·615 ± 0·015° C. (N = 4)), rates of increase of internal concentration following transfer were somewhat lower (they were fish in the same size range), and 1- to 3-day stabilization levels were higher (Δ = 0·794 ± 0·019° C. (N = 12)) even though the external concentration was lower.

The overall pattern of regulation of total serum concentration in Massachusetts *Salmo trutta* between September and April is summarized in the classic form of a plot of total internal *v.* total external concentration in Fig. 5. The variability of the fish acclimatized to full sea water gradually and for a long period at 20° C. (perhaps also at 10° C.) was probably an experimental artefact.

DISCUSSION

The data described above permit a description of osmotic and ionic regulation in the brown trout that is, in some ways, more detailed than for any other fish.

Seasonal effects

Seasonal changes, especially the onset of the breeding season, may or may not be associated with changes in the relation between internal and external media.

In female eels (Fontaine & Koch, 1950, for summary) overall osmoregulatory ability is apparently little affected at this period. Sticklebacks (*Gasterosteus* and *Pungitius*), however, show less osmotic regulation and are less euryhaline (Heuts, 1942, 1943, 1945; Koch & Heuts, 1942, 1943). The seasonal pattern in the brown trout is somewhat different.

D. C. W. Smith (1956) studied seasonal changes in tolerance of brown trout to artificially increased salinities (increased by addition of sodium chloride) above a previously determined 'physiological maximum' (only 24‰!). Results in two successive years differed by over 100% in absolute values, but showed more or less consistent patterns of seasonal differences. Salinity tolerance was lowest during the summer, went through a peak, was low again from October to December (the breeding season), then went through a broad peak during the spring.

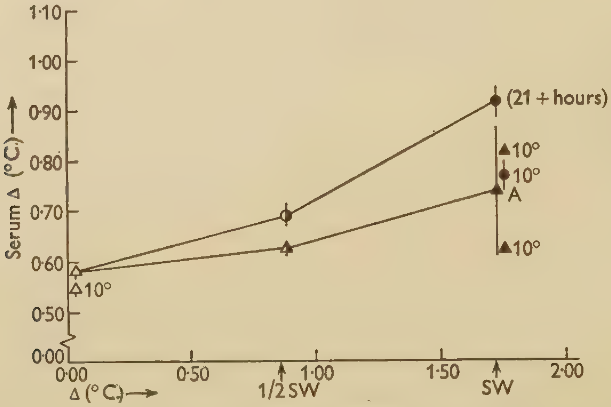

Fig. 5. Relations between freezing-point depressions of serum and external environment in Massachusetts hatchery fish acclimatized to half-strength and to full-strength sea water for varying periods at 20° C. and 10° C. Triangles indicate long-term acclimatizations (240 or more hours), circles short-term acclimatizations (72 hours unless noted otherwise). *A* means acclimatized to half-strength sea water for 240 hours first. 10° C. points are noted as such. The two 10° C. triangles in full-strength sea water are for individual fish. All other symbols indicate means for groups ± two standard errors.

The results here reported agree with Smith's as regards the summer decrease in viability, and show in addition that actual decreases in regulatory abilities are involved; the breeding season, however, was not associated with any changes in these abilities. The only changes correlated with this latter period were in serum phosphorus and total muscle sodium concentrations. Survival and regulatory abilities were seemingly constant over the entire period from autumn to spring.

Reasons for this rather odd pattern of changes in regulatory abilities are not readily apparent. Two environmental correlations which might have affected endocrine functions in some way seem possible, however:

(1) Regulatory abilities may be influenced by photoperiod. The experimental series between September and April were carried out during those parts of the year with nights longer than days. The reverse was true for the summer series.

(2) Regulatory abilities may be influenced by the long-term thermal history of the fish. The September to April series involved fish acclimatized for periods of weeks to hatchery water temperatures in the range 2–14° C. The summer series involved fish acclimatized to temperatures of 18–24° C.

The seasonal changes in muscle sodium are unaccounted for. Serum phosphorus was the only other concentration studied which varied significantly seasonally outside the summer. Its variations are probably due to various seasonal metabolic changes (Ichikawa, 1955; Laskowski, 1936).

Serum phosphorus concentrations during the breeding season were 20–50 mg./l. below the levels measured between February and April and about 90 mg./l. below summer levels. The figures given by Laskowski (1936) for one brown trout during the breeding season and one brown trout outside the breeding season show the opposite effect—breeding is approximately twice non-breeding. The reason for this discrepancy is unknown.

The fact that brown trout in fresh water in summer have different serum ion concentrations from brown trout in fresh water in winter is probably the major reason for the discrepancies existing between serum sodium and potassium concentrations reported for this species by Spalding (in Jones, 1956) and by Phillips & Brockway (1958). Spalding obtained her samples during the winter, Phillips & Brockway obtained theirs during the summer

Water and ion movements between muscles and blood

(*a*) *Water movements*

Studies of total muscle concentration (g. solids/kg. muscle wet weight or Δ of expressed tissue fluid) indicate that this quantity usually varies in a similar fashion to total blood concentration—the muscles are in some sort of osmotic equilibrium with the blood (in salmonids: Busnel, 1942; Greene, 1926; *Anguilla*: Callamand, 1943; Drilhon, 1937, 1943, Koch, 1949; Callamand *et al.* (1951), also working with eels, did not find such parallelism). This is probably true in the brown trout as well. The plot of total muscle concentration against serum Δ for the present experiments at 20° C. shown in Fig. 3 is not incompatible with the view that the muscles are in osmotic equilibrium with the blood (whether or not isotonic is another question—cf. Brodsky, Appleboom, Dennis, Rehm, Miley & Diamond, 1957).

A plot of total muscle concentration *v.* serum Δ for fish transferred to full sea water at 10° C. and 20° C. shows the same relation.

The fact that most of the changes in total muscle solids are due to changes in intracellular water content may also be demonstrated.

Table 3 shows that the extracellular volume in the muscles is small and constant. Changes in water content of the muscles occurred under some conditions which varied from 20–70 g./kg. (Table 2). With constant extracellular volume, this water could have come from no place but the fibres. Even if the statistically insignificant fluctuations in chloride space indicated in Table 3 are real they are insufficient to account for the total water-content changes which occurred.

The data of Callamand *et al.* (1951) on muscle chloride concentrations in hypophysectomized and intact female eels transferred from fresh water to full sea water indicate that a similar situation exists in *Anguilla*.

(*b*) *Ion movements*

A consideration of all the data obtained on ion concentrations in serum and muscle permits a critical test of Drilhon's (1937) hypothesis that the muscles of a fish can act as storage sites for ions.

We have seen that extracellular volume in the muscles of the brown trout is small and quite constant, at least between September and April. Serum sodium and potassium concentrations for these same fish are known, also total muscle sodium and potassium concentrations. Combining these data with those on total muscle solids (hence total muscle water), intracellular concentrations of these two ions can be calculated from the equation:

$$[A]_i = \frac{A_t - [A]_s\, V_e}{V_t - V_e}.$$

$[A]_i$ = intracellular concentration of ion species A (m-equiv./kg. intracellular water). A_t = total quantity of A (m-equiv.) in 1 kg. of wet muscle. $[A]_s$ = serum concentration of A (use m-equiv./l. as approximation to m-equiv./kg. water). V_t = total weight of water (kg.) in 1 kg. of wet muscle. V_e = weight of extracellular water (kg.), assumed to be present as serum, in 1 kg. of wet muscle.

The results of such calculations for muscle sodium in variously acclimatized brown trout are presented in Table 9. Comparable data for potassium may be taken directly from Table 6, since the extracellular space is small and serum potassium concentrations are low. The muscle sodium data will be considered first.

It should be pointed out that indistinct end-points in the muscle chloride analyses resulted in low precision for the extracellular volume estimations. Small changes in calculated extracellular volume produce large changes in intracellular sodium concentration. By reason of these analytical errors the amount of sodium calculated to be present extracellularly sometimes exceeds the amount of sodium measured in the muscle. Such cases are listed in Table 9 as having zero intracellular sodium. It seems probable that their true intracellular sodium concentrations were low.

Approximate 90% confidence intervals for intracellular sodium concentrations are given in parentheses after the mean values in Table 9. These intervals were calculated in the same manner as the means, but using the following figures. Upper bound: Mean total muscle sodium + 2 S.E., extracellular volume from mean muscle chloride − 2 S.E. Lower bound: Mean total muscle sodium − 2 S.E., extracellular volume from mean muscle chloride + 2 S.E.

Despite the uncertainty just mentioned, the calculated intracellular sodium concentrations bring up several items of interest.

The major point is that, with the exception of fish transferred directly from fresh water to full sea water at 20° C., both during and outside the breeding season,

Table 9. *Changes in intracellular sodium in the muscles following application of osmotic stresses*

(September–April.)

State of acclimatization	Na_i (m-equiv./kg. cell water)
20° C. experiments—breeding season	
FW, 0 hr.	6·7 (2–12)*
FW, 72–240 hr.	12·1 (7–17)
½ SW, 24 hr.	6·4 (0–13)
½ SW, 72 hr.	4·5 (0–11)
½ SW, 240 hr.	10·6 (7–14)
SW, 21–30 hr.	16·3 (7–25)
½ SW, 240 hr.–SW, 47 hr.	6·0 (0–15)
½ SW, 240 hr.–SW, 240 hr.	0 (0–8)
20° C. experiments—spring	
FW, 0 hr.	0 (0)
FW, 72–240 hr.	2·6 (0–8)
½ SW, 24 hr.	0 (0–5)
½ SW, 72 hr.	2·4 (0–6)
½ SW, 240 hr.	0 (0–3)
SW, 21–30 hr.	14·0 (4–24)
10° C. experiments—spring unless noted	
Hatchery controls	0 (0–1)
Hatchery controls, breeding season	2·9 (0–7)
FW, 0 hr.	0·8 (0–4)
FW, 72 hr.	0 (0–8)
SW, 24 hr.	3·0 (0–8)
SW, 72 hr.	3·0 (0–8)
SW, 240 hr.	0, 0

* Approximate 90 % confidence interval. (See p. 246.)

intracellular sodium concentrations during each experimental series were fairly constant. This argues that little, if any, sodium invaded the fibres even during the periods when they were considerably dehydrated and serum concentrations were high. If anything, the fibres excreted sodium during periods of dehydration. Thus, the muscles of the brown trout almost certainly did not act as storage sites for sodium during or after adjustments to non-fatal osmotic stresses.

The data on fish acclimatized to full sea water at 20° C. bring up a point which may bear on the question of why some fish are euryhaline, others not. Many of the fish transferred directly from fresh water to full sea water showed considerable increases in intracellular sodium, these changes being clearest outside the breeding season. But fish acclimatized to half sea water first, while in some cases having serum concentrations as high as those in the direct transfers, seemingly were able to maintain low intracellular sodium concentrations. Perhaps this apparent increase in the ability of acclimatized fish to prevent the invasion of their muscle fibres by large amounts of sodium is one of the factors which enabled them to survive blood concentrations equal to those associated with mortality in the direct transfers.

Stenohaline fishes seem to be unable to keep sodium out of their muscle fibres, even with long-term acclimatizations (Kaplanski & Boldirewa, 1933; Drilhon, 1937). Steinbach (1954) and others (cf. Glynn, 1957, p. 296) have pointed out the inhibitory effects which low concentrations of sodium have on various enzyme systems important in muscle metabolism. It is tempting to speculate that differences in ability to prevent sodium invasion of muscle fibres are a determining factor in the degree of euryhalinity shown by fishes, and that the mechanism of the effect is that discussed by Steinbach.

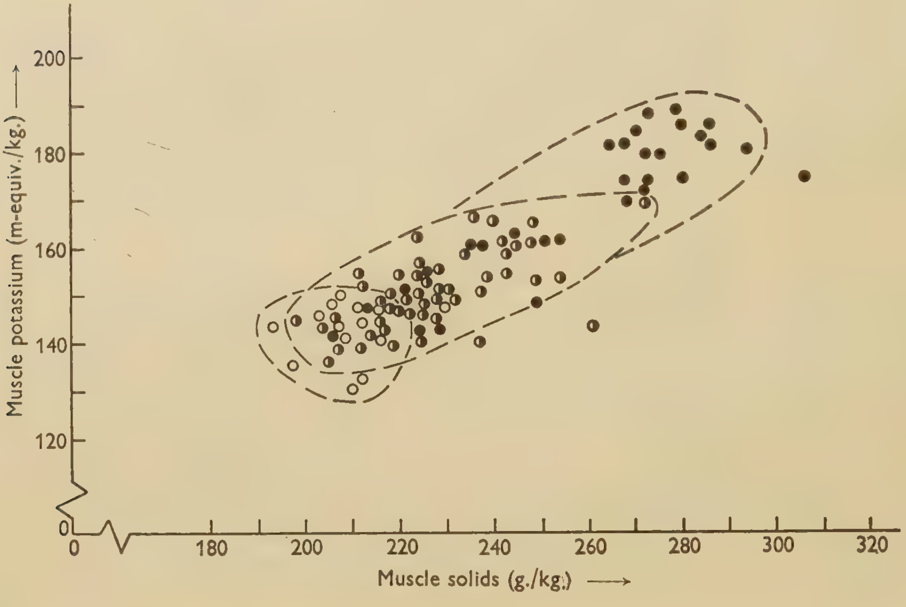

Fig. 6. Relations between muscle potassium, K_m, and muscle solids concentration in Massachusetts hatchery fish transferred from fresh water to half-strength and to full-strength sea water at 20° C. between September and April. Dashed lines roughly indicate boundaries of the three groups.

That temperature, as well as acclimatization time, may be significant in keeping sodium out of muscle fibres is illustrated by the fish transferred directly from fresh water to full sea water at 10° C. and 20° C. in the spring. The 20° C. fish, as noted, considerably increased their intracellular sodium concentrations—the 10° C. fish seemingly did not. Serum concentrations at 10° C. never reached the high levels noted at 20° C., which in itself may explain the greater survival noted at 10° C. However, the difference in behaviour of muscle sodium concentration may also have been significant.

The potassium data indicate that the muscles did not act as reservoirs for this ion, either. Small differences in large quantities are involved here, however, so it is difficult to be certain. The close correlation existing between muscle potassium and total muscle concentrations is shown in Fig. 6.

Ecological implications

Gordon (1959) has shown that responses of Scottish brown and sea trout to osmotic stresses are similar to those described for Massachusetts fish in the present paper. The many generations of genetic isolation that separate European and American populations of *Salmo trutta* have resulted in only quantitative differences in osmotic and ionic regulatory mechanisms.

In the same regard it is interesting that serum Na:Cl ratios in all groups of American fish are in the range 1·06–1·13, which is the range found in Scottish fresh water *S. trutta*. Scottish sea trout have serum Na:Cl ratios in the range 1·18–1·28. Perhaps this indicates that at least the great majority of the ancestors of present-day American *S. trutta* were brown trout, only a few, if any, having been sea trout.

Finally, the experiment at 10° C. seems to present an interesting possibility for explaining a zoogeographic problem in the distribution of the anadromous habit in at least some fishes. Brook trout (*Salvelinus fontinalis*), lake whitefish (*Coregonus clupeaformis*), various ciscoes (*Coregonus* (*Leucichthys*) *spp.*), and many other fishes are commonly anadromous in the far northern parts of their ranges (e.g. Hudson Bay) but seldom or never so near their more southern limits (Walters, 1955; Wohlschlag, 1957). Assuming that these fish make their transitions from fresh water to salt water fairly rapidly, one might postulate that, at the higher temperatures encountered in the southern parts of their ranges, they are unable to maintain their blood and muscle concentrations on a level compatible with survival. At lower temperatures in the more northerly parts of their ranges they can maintain lower blood and muscle concentrations and thus survive.

There would seem to be considerable adaptive advantage in going to sea, primarily from the standpoint of increased food supply. Some counter-selection is therefore probably operating to prevent such behaviour in the southern parts of the ranges of these fish. Perhaps the temperature effect on short-term levels of regulation of blood and muscle concentrations is part of this counter-selection.

SUMMARY

1. The osmotic and ionic regulatory abilities of adults of the euryhaline brown trout (*Salmo trutta*) have been studied in experiments roughly duplicating the stresses of migration from fresh water to the sea. Brown trout will survive indefinitely in full sea water if acclimatized to it at rates inversely related to the temperature.

2. Blood serum samples have been analysed for Na, K, Cl, total P and Δ; muscle samples for Na, K, Cl and total solids. Changes in the concentrations of these constituents following transfers from fresh water to 50% and 100% sea water have been studied. Transfers were made throughout the year and at temperatures of 10° C. and 20° C.

3. Following transfers to 50% sea water at 20° C. blood concentrations rose

significantly above fresh-water levels, but returned very nearly to these levels after about a week. Transfer from 50% sea water to 100% sea water at 20° C. caused the same sequence of changes. Transfer to 100% sea water at 20° C. was fatal, and associated with very high serum concentrations. Many fish survived transfer to 100% sea water at 10° C., however, and showed evidence of internal concentrations returning to fresh-water levels after 10 days. The brown trout is strongly homoiosmotic on a long-term basis.

4. Both survival and regulatory ability were lower during the summer. There were also seasonal variations in the blood and muscle concentrations of fish in a given state of acclimatization.

5. Muscle concentration changes closely paralleled blood changes. Extracellular volume remained constant, so muscle concentration changes were attributable to changes in intracellular water. The muscles did not act as storage sites for sodium and potassium.

These studies have been supported by National Science Foundation predoctoral fellowships for 1954–1957, a Fulbright Fellowship to the United Kingdom in 1957–1958 and a grant from the Higgins Fluid Research Fund, Yale University. This paper is a portion of a dissertation presented to the faculty of the Graduate School of Yale University in candidacy for the degree of Doctor of Philosophy. (Contribution number 989 from the Woods Hole Oceanographic Institution.)

The aid and advice of many people have been gratefully accepted in the course of this work. I would like to express my appreciation to them all, especially the following: Drs E. J. Boell, T. H. Waterman, G. E. Pickford and L. M. Passano, members of my Ph.D. dissertation committee at Yale University; Drs C. O'D. Iselin, B. H. Ketchum and A. C. Redfield, for permitting use of the excellent facilities of the Woods Hole Oceanographic Institution; MM. J. Galligan and D. Moss, Connecticut State Board of Fisheries and Game, MM. R. Bitzer and J. Macomber, Massachusetts State Division of Fisheries and Game, and Mr H. Robbins, Robbins Fish Hatchery, Wareham, Mass., for supplying fish; Drs C. M. Breder, Jr, D. Merriman, J. A. Ramsay, J. Ryther and H. Werntz, and Miss P. Rasquin, for helpful advice and discussion. Miss C. Luhrs very kindly typed the first draft of the manuscript.

REFERENCES

BEADLE, L. C. (1957). Comparative physiology: Osmotic and ionic regulation in aquatic animals. *Ann. Rev. Physiol.* **19**, 329–58.

BENDITT, E., MORRISON, P. & IRVING, L. (1941). The blood of the Atlantic salmon during migration. *Biol. Bull., Woods Hole*, **80**, 429–40.

BERRY, J. W., CHAPPELL, D. G. & BARNES, R. B. (1946). Improved method of flame photometry. *Industr. Engng Chem. (Anal. Ed.)*, **18**, 19–24.

BLACK, V. S. (1957). Excretion and osmoregulation. In *The Physiology of Fishes* (ed. Brown), vol. 1, 163–205.

BOUCHER-FIRLY, S. (1935). Recherches biochimiques sur les téléostéens apodes (Anguille, Congre, Murène). *Ann. Inst. Océanogr. Monaco*, **15**, 217–327.

BOYLE, P. J. & CONWAY, E. J. (1941). Potassium accumulation in muscle and associated changes. *J. Physiol.* **100**, 1–63.

BRODSKY, W. A., APPLEBOOM, J. W., DENNIS, W. H., REHM, W. S., MILEY, J. F. & DIAMOND, I. (1956). The freezing point depression of mammalian tissues in relation to the question of osmotic activity of cell fluid. *J. Gen. Physiol.* **40**, 183–99.

BURDEN, C. E. (1956). The failure of hypophysectomized *Fundulus heteroclitus* to survive in fresh water. *Biol. Bull., Woods Hole*, **110**, 8–28.

BUSNEL, R. G. (1942). Recherches de physiologie appliquées à la pisciculture: à propos de la migration de la truite arc-en-ciel. *Bull. Français Pêche et Pisciculture*, **15**, no. 127, 45–65.

CALLAMAND, O. (1943). L'Anguille Européenne (*Anguilla anguilla* L.). Les bases physiologiques de sa migration. *Ann. Inst. Océanogr. Monaco*, **21**, 361–440.

CALLAMAND, O., FONTAINE, M., OLIVEREAU, M. and RAFFY, A. (1951). Hypophyse et osmorégulation chez les poissons. *Bull. Inst. Océanogr., Monaco*, no. 984, 1–7.

CHEN, P. S., JR, TORIBARA, T. Y. & WARNER, H. (1956). Microdetermination of phosphorus. *Anal. Chem.* **28**, 1756–7.

CONWAY, E. J. (1935). An absorption apparatus for the micro-determination of certain volatile substances. III. The micro-determination of chloride, with application to blood, urine and tissues. *Biochem. J.* **29**, 2221–35.

CONWAY, E. J. (1957). Nature and significance of concentration relations of potassium and sodium ions in skeletal muscle. *Physiol. Rev.* **37**, 84–132.

DEKHUYZEN, M. C. (1905). Sur la pression osmotique dans le sang et dans l'urine des poissons. *Arch. néerl. Sci.* **10**, 121–36.

DRILHON, A. (1937). Étude des échanges minéraux chez les poissons homéiosmotiques. *C.R. Acad. Sci. Paris*, **204**, 1502–3.

DRILHON, A. (1943). Métaux alcalins et alcalino-terreux chez les téléostéens apodes. *C.R. Soc. Biol. Paris*, **137**, 300–2.

DUVAL, M. (1925). Recherches sur le milieu intérieur des animaux aquatiques. Modifications sous l'influence du milieu extérieur. *Ann. Inst. Océanogr. Monaco*, **2**, 233–407.

FONTAINE, M. (1930). Modifications du milieu intérieur des poissons potamotoques au cours de la reproduction. *C.R. Acad. Sci. Paris*, **191**, 736–7.

FONTAINE, M. (1954). Du déterminisme physiologique des migrations. *Biol. Rev.* **29**, 390–418.

FONTAINE, M. (1956). The hormonal control of water and salt-electrolyte metabolism in fish. *Mem. Endocrin.* no. 5, 69–82.

FONTAINE, M., CALLAMAND, O. & VIBERT, R. (1950). La physiologie du saumon. *Ann. Sta. Cent. Hydrobiol. App.* **3**, 15–26.

FONTAINE, M. & FIRLY, S. (1932). Influence des changements de salinité sur la teneur en phosphore minéral du sérum des poissons. *C.R. Soc. Biol. Paris*, **109**, 1271–3.

FONTAINE, M. & KOCH, H. J. (1950). Les variations d'euryhalinité et d'osmorégulation chez les poissons. *J. Physiol. Path. Gén.*, **42**, 287–318.

FORSTER, R. P. (1953). A comparative study of renal function in marine teleosts. *J. Cell. Comp. Physiol.* **42**, 487–509.

GARRARD, B. M. (1935). The osmotic pressure of the blood of *Fundulus* living in salt water and in fresh water. *J. Physiol.* **85**, 6*P*.

GLYNN, I. M. (1957). The ionic permeability of the red cell membrane. *Progr. Biophys.* **8**, 241–307.

GORDON, M. S. (1957). Observations on osmoregulation in the Arctic char (*Salvelinus alpinus* L.). *Biol. Bull., Woods Hole*, **112**, 28–33.

GORDON, M. S. (1959). Osmotic and ionic regulation in Scottish brown and sea trout (*Salmo trutta* L.). *J. Exp. Biol.* (in the Press).

GRAFFLIN, A. L. (1935). Chloride and total osmotic pressure in the blood of marine teleosts. *Biol. Bull., Woods Hole*, **69**, 245–58.

GREENE, C. W. (1904). Physiological studies of the chinook salmon. *Bull. U.S. Bur. Fish.* **24**, 429–56.

GREENE, C. W. (1926). The physiology of the spawning migration. *Physiol. Rev.* **6**, 201–41.

GUEYLARD, F. (1924). De l'adaptation aux changements de salinité. Recherches biologiques et physico-chimiques sur l'Épinoche (*Gasterosteus leiurus* Cuv. et Val.). *Arch. Phys. biol.* **3**, 79–197.

HEILBRUNN, L. V. & HAMILTON, P. G. (1942). The presence of chloride in muscle fibers. *Physiol. Zoöl.* **15**, 363–74.

HEUTS, M. J. (1942). Chloride excretie bij *Gasterosteus aculeatus* L. *Ann. Soc. zool. Belg.* **73**, 69–72.

HEUTS, M. J. (1943). La régulation osmotique chez l'épinochette (*Pygosteus pungitius* L.). *Ann. Soc. zoöl. Belg.* **74**, 99–105.

HEUTS, M. J. (1945). La régulation minérale en fonction de la température chez *Gasterosteus aculeatus*. Son importance au point de vue de la zoogéographie de l'espèce. *Ann. Soc. zool. Belg.* **76**, 88–99.

HOAR, W. S. (1953). Control and timing of fish migration. *Biol. Rev.* **28**, 437–52.

HOAR, W. S., BLACK, V. S. & BLACK, E. C. (1951). Some aspects of the physiology of fish. *Publ. Ontario Fish. Res. Lab.* **71**. *Univ. Toronto Biol. Ser.* no. 59, 1–111.

ICHIKAWA, R. (1955). Seasonal difference in the amount of inorganic phosphorus in blood serum of fishes. *Rec. Oceanogr. Works, Japan*, **2**, 113–16.

JONES, I. C. (1956). The role of the adrenal cortex in the control of water and salt-electrolyte metabolism in vertebrates. *Mem. Endocrin.* no. 5, 102–20.

KAPLANSKI, S. & BOLDIREWA, N. (1933). Über den Mineralstoffgehalt des Muskelgewebes von Süsswasserfischen bei gesteigertes Konzentration der Mineralsalze im Wasser. *Biochem. Z.* **265**, 422–5.

KINNE, O. (1952). Ein neues Gerät zur Bestimmung der Gefrierpunktserniedrigung kleiner Flüssigkeitsmengen. *Veröff. Inst. Meeresforsch. Bremerhaven*, **1**, 47–51.

KOCH, H. J. (1949). Quelques caractéristiques osmotiques de l'Anguille femelle jaune et argentée. *Arch. int. Physiol.* **57**, 125–32.

KOCH, H. J. & HEUTS, M. J. (1942). Influence de l'hormone thyroïdienne sur la régulation osmotique chez *Gasterosteus aculeatus* L. forme *gymnurus* Cuv. *Ann. Soc. zool. Belg.* **73**, 165–72.

KOCH, H. J. & HEUTS, M. J. (1943). Régulation osmotique, cycle sexuel et migration de reproduction chez les épinoches. *Arch. int. Physiol.* **53**, 253–66.

KUBO, T. (1953). On the blood of salmonid fishes of Japan during migration. I. Freezing point of blood. *Bull. Fac. Fish. Hokkaido Univ.* **4**, 138–48 (in Japanese, with English summary).

LASKOWSKI, M. (1936). Über das Vorkommen des Serumvitellins im Blute der Wirbeltiere. *Biochem. Z.* **284**, 318–21.

MARGOSHES, M. & VALLEE, B. L. (1956). Instrumentation and principles of flame spectrometry. Effect of extraneous ions in simultaneous determination of five elements. *Anal. Chem.* **28**, 180–4.

MULLINS, L. J. (1950). Osmotic regulation in fish as studied with radio-isotopes. *Acta physiol. scand.* **21**, 303–14.

PARKS, T. S., JOHNSON, H. O. & LYKKEN, L. (1948). Errors in the use of a model 18 Perkin–Elmer flame photometer for the determination of alkali metals. Interferences of common metals, acids and solvents. *Anal. Chem.* **20**, 822–5.

PARRY, G. (1958). Size and osmoregulation in salmonoid fishes. *Nature, Lond.*, **181**, 1218–19.

PHILLIPS, A. M., JR, & BROCKWAY, D. R. (1958). The inorganic composition of brown trout blood. *Progr. Fish Cult.* **20**, 58–61.

PICKFORD, G. E. & ATZ, J. W. (1957). *The Physiology of the Pituitary Gland of Fishes*, 613 pp. *N.Y. Zool. Soc.*

RAMSAY, J. A., BROWN, R. H. J. & FALLOON, S. W. H. W. (1953). Simultaneous determination of sodium and potassium in small volumes of fluid by flame photometry. *J. Exp. Biol.* **30**, 1–17.

SHAW, F. H., SIMON, S. E. & JOHNSTONE, B. M. (1956). The non-correlation of bioelectric potentials with ionic gradients. *J. Gen. Physiol.* **40**, 1–17.

SHAW, F. H., SIMON, S. E., JOHNSTONE, M. B. & HOLMAN, M. E. (1956). The effect of changes of environment on the electrical and ionic pattern of muscle. *J. Gen. Physiol.* **40**, 263–88.

SHENK, W. D. (1954). Tissue chloride. *Arch. Biochem. Biophys.* **49**, 138–48.

SIMON, S. E., SHAW, F. H., BENNETT, S. & MULLER, M. (1957). The relationship between sodium, potassium and chloride in amphibian muscle. *J. Gen. Physiol.* **40**, 753–77.

SMITH, D. C. W. (1956). The role of the endocrine organs in the salinity tolerance of trout. *Mem. Endocrin.* no. 5, 83–101.

SMITH, H. W. (1930). The absorption and excretion of water and salts by marine teleosts. *Amer. J. Physiol.* **93**, 480–505.

STEINBACH, H. B. (1954). The regulation of sodium and potassium in muscle fibers. *Symp. Soc. Exp. Biol.* **8**, 438–52.

STEPHENSON, W. K. (1957). Membrane potential changes and ion movements in the frog sartorius muscle. *J. Cell. Comp. Physiol.* **50**, 105–28.

VAN SLYKE, D. D. (1923). The determination of chlorides in blood and tissues. *J. Biol. Chem.* **58**, 523–9.

VON BUDDENBROCK, W. (1956). *Vergleichende Physiologie. III. Ernährung, Wasserhaushalt und Mineralhaushalt der Tiere*, 677 pp. Basel: Birkhauser.

WALTERS, V. (1955). Fishes of western Arctic America and eastern Arctic Siberia. Taxonomy and zoogeography. *Bull. Amer. Mus. Nat. Hist.* **106**, 255–368.

WERNTZ, H. O. (1957). Osmotic adaptations of species of *Gammarus* to changes in the external concentration. Unpublished Ph.D. thesis, Yale University.

WOHLSCHLAG, D. E. (1957). Differences in metabolic rates of migratory and resident freshwater forms of an arctic whitefish. *Ecology*, **38**, 502–10.

Contribution No. 992

JOURNAL OF GEOPHYSICAL RESEARCH VOLUME 64, No. 3 MARCH, 1959

Climatic Stability of Eighteen Degree Water at Bermuda*

ELIZABETH SCHROEDER AND HENRY STOMMEL
Woods Hole Oceanographic Institution
Woods Hole, Massachusetts

DAVID MENZEL AND WILLIAM SUTCLIFFE, JR.
Bermuda Biological Station
St. George's West, Bermuda

Abstract—Temperature soundings in the ocean off Bermuda are available for 85 years. All records show the water mass just beneath the surface to be remarkably constant in temperature and salinity. Oxygen measurements indicate that this water is in convective contact with the atmosphere each winter. More detailed and frequent measurements made by the ship *Panulirus* are here presented for the first time, substantiating this remarkable and puzzling climatic stability of near-surface water in the northwestern Sargasso Sea.

Introduction—Recently there has been an increasing interest in all phenomena which are suggestive of climatic change in the oceans. For example, in June 1958, at a conference held at Rancho Santa Fe under the auspices of the Scripps Institution of Oceanography, various forms of evidence were presented which suggest that there have been significant changes of surface temperature (amounting to several degrees) over vast areas of the North Pacific.

Since little subsurface data from midocean is available to determine how much these temperature fluctuations are limited in depth, it is of interest to present some evidence based on mid-Atlantic hydrographic stations near Bermuda, which exhibits a remarkable climatic stability of waters just below the surface. We have for this purpose several *Challenger* stations (no salinity) made near Bermuda in 1873; two stations from the 1920's; and during the 1930's a fair number of *Atlantis* and *Culver* stations (1932, 10; 1933, 1; 1937, 7; 1938, 13; 1939, 9). During the war years there are none, but afterwards various ships passing Bermuda occasionally made acceptable stations near Bermuda (1949, 4; 1950, 1; 1951, 1), and in 1954 the Bermuda Biological Station vessel Panulirus began a systematic series of hydrographic stations within sight of the island, so that we now can construct a reasonably accurate picture of the seasonal variations of properties over several years in succession.

The feature upon which we wish to focus attention is the body of water between the depths of 150 meters and 450 meters with a range in temperature of from 17°C to 19°C and a salinity of about 36.50 ± .10 ppm with an inflection point in the temperature sounding at about 18°C; for convenience we shall call it *18° Water* although actually its temperature is spread over a finite interval. Immediately below the 18° Water lies the main thermocline; above it lies a shallow surface thermocline subject to wide seasonal variation. The 18° Water is not strictly homogeneous; it has a gravitational stability, and this stability varies from time to time. It is not confined to the vicinity of Bermuda but occurs over most of the Sargasso Sea, an area of about 4 times 10^6 km^2. Toward its southern (about 20°N) and eastern (about 40°W) limits the 18° Water becomes much thinner than at Bermuda, but its characteristic inflection point in the vertical temperature distribution and its temperature-salinity (T-S) relation remain constant. To the north and west, the 18° Water is bounded by the Gulf Stream. Everywhere it looks like a more or less 'homogeneous' layer sandwiched between the shallow surface thermocline and the deeper main thermocline.

At the latitude of Bermuda, and to the north, winter cooling actually wipes away the shallow surface thermocline so that this layer of 18° Water is exposed to the action of surface-cooling and salinity-changing mechanisms associated with each winter's storms, and to renewal of dissolved oxygen by gas exchange across the sea surface. In southern latitudes of the Sargasso

---

* Contribution No. 992 from the Woods Hole Oceanographic Institution. Contribution No. 242 from the Bermuda Biological Station.

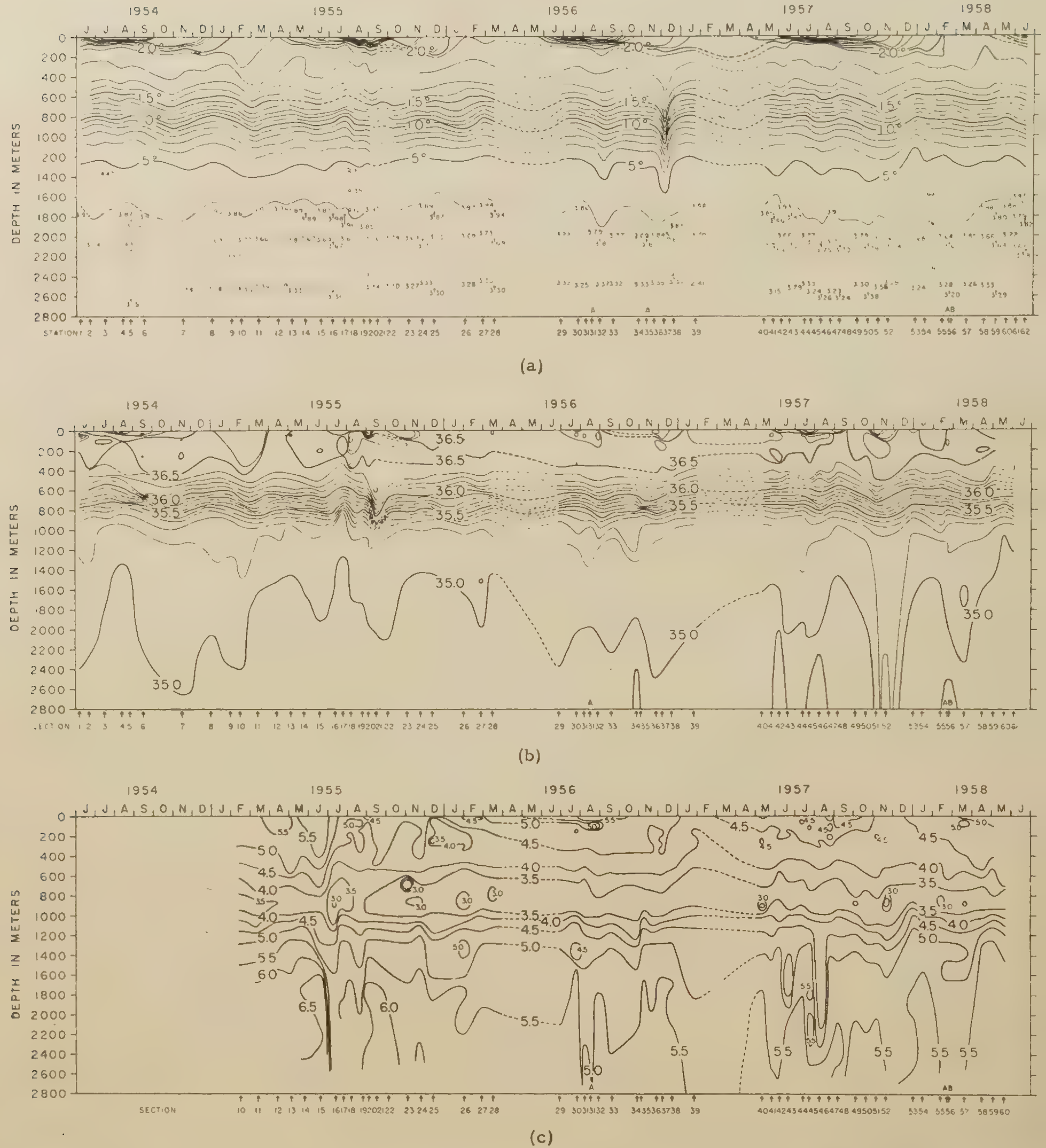

FIG. 1—The vertical distribution of various properties of the deep ocean at Bermuda, as a function of time; (a) temperature in degrees Centigrade; (b) salinity, in parts per mille; (c) dissolved oxygen, in milliliters per liter

Sea the shallow surface does not vary so much seasonally, and never disappears even in winter. Thus in these latitudes the 18° Water never is in direct contact with the atmosphere, and we must envisage it as coming from the north as a slow southward current beneath the surface thermocline. However, in this study no attempt is made to describe the geographic distribution of the 18° Water; discussion will be confined to the 18° Water at Bermuda.

The Panulirus data, 1954–1958—The most complete and homogeneous series of hydrographic data for the vicinity of Bermuda is the *Panulirus* series made from 1954 to 1958 by various members of the Bermuda Biological Station. The depths of various contours of equal

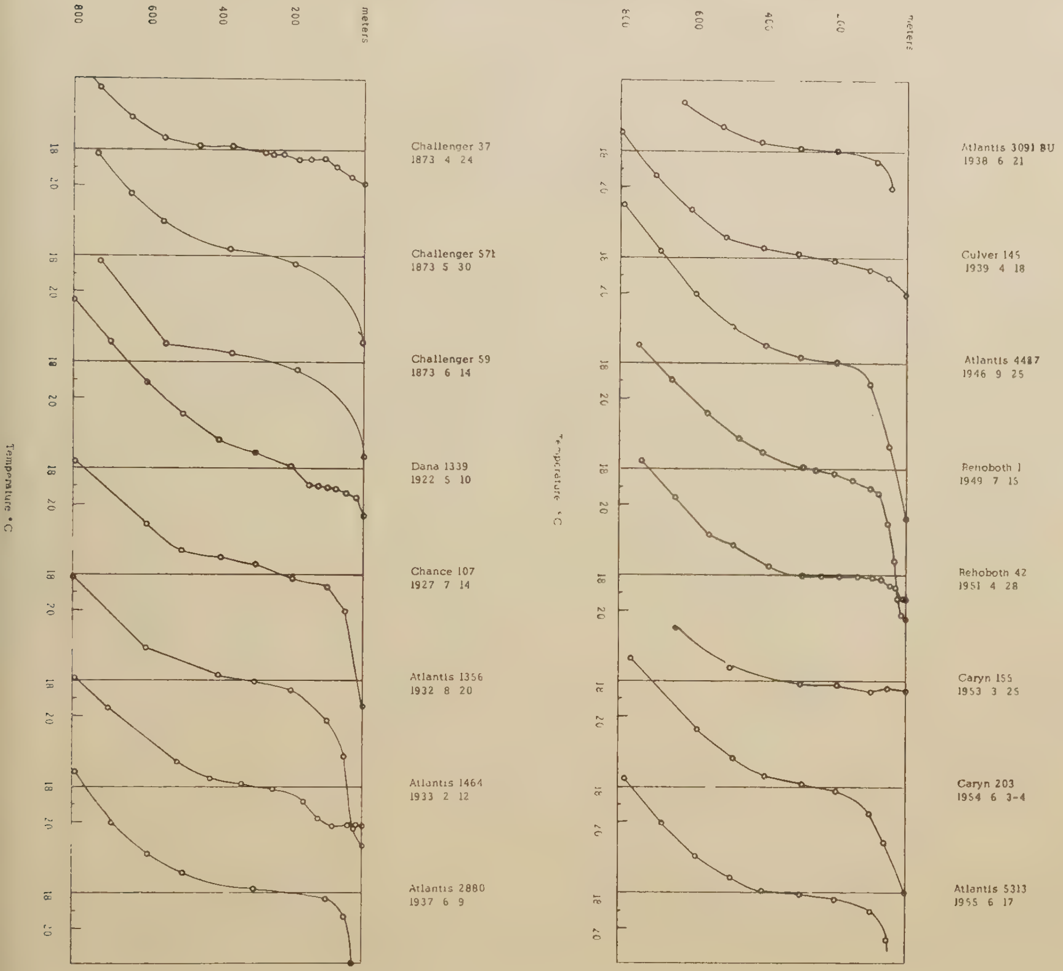

(a) (b)

Fig. 2 (a) and (b)—Detail of the temperature structure of the upper 800 meters of water at Bermuda as shown by selected stations made in the late spring of a number of years

temperature, salinity, and dissolved oxygen, plotted as a function of time, are shown in Figure 1. In the upper 150 meters there is a marked development of a seasonal thermocline. Below it there is a mass of more homogeneous water where the isotherms are less crowded vertically; this is the 18° Water. Beneath 450 meters the main thermocline begins. From station to station these isotherms move up and down as much as 100 meters. Evidence from the thermometric cable at Bermuda [*Haurwitz* and others, 1959] suggests that these vertical displacements are mostly the result of sampling errors introduced by short-period internal wave motions.

During each winter the top 150 meters is cooled off and approaches convective equilibrium with the 18° Water down to a depth of about 400 meters; therefore something like one third of the 18° Water is reformed each year. In view of the fact that each winter is variable and different from others, and that a large geographical area (32°–36°N; 40°–73°W) is involved in the cooling, it is truly remarkable that following each year's overturn the water between 150 and 450 meters (the 18° Water) remains so constant in its properties.

Long-term stability of the 18° Water—The *Panulirus* data extend over only four years. How variable is this 18° Water over longer periods? In the past the sampling has not been frequent enough to allow construction of seasonal profiles such as those in Figure 1. We can compare individual soundings made over an 85-year period, starting with the *Challenger* station in 1873. Samples (made in late spring) are shown in Figure 2. The interesting point here is that the inflection point in the temperature-depth curve for the period of observation is always at 18°C (within a few tenths of a degree).

Salinity of the 18° Water—It is interesting to enquire whether the 18° Water, which from year to year is in intimate contact with the surface, can possibly maintain a constant T-S relationship. The temperature and salinity data for every available (114) hydrographic station in the Bermuda area were plotted on graph paper and smooth curves drawn through points. The salinity was read off the curve at the depth where the temperature curve was exactly 18°C, and it was found that for a period of 36 years the salinity of the 18° Water has been 36.50 ± .02 ppm probable error; that is, it has remained constant within *titration error*. This is really quite surprising in view of the fact that in the fall and early winter, the surface waters near Bermuda have inhomogeneities of salinity of as much as 0.80 ppm over a span of a few miles. Yet a month or so later, when cooling and convection with the 18° Water begins, the salinity somehow returns to 36.50 ± .02 ppm. How is it possible that it does not vary more from year to year?

Renewal and overturn at Bermuda—In view of the fact that the data during the overturn period is rather scanty, one wonders whether there really is convective mixing of the 18° Water right to the surface at Bermuda. The temperature soundings seem marginal; thus even the near homogeneity of *Panulirus* station 57 is not complete homogeneity; and one may ask does vertical mixing of surface water into the 18° Water really occur or does it only seem to occur? The oxygen data from *Panulirus* stations show an unambiguous renewal of oxygen in 18° Water extending to considerable depths, varying from year to year, but always present.

Summary—In summary the following features at Bermuda are revealed: The inflection point in the temperature sounding between the surface thermocline and the deeper main thermocline has always been at 18°C within a few tenths of a degree during the past 85 years, according to all available data; and the salinity at 18° is remarkably uniform—within the titration error. On the other hand, the oxygen renewal each year is quite variable in the 18° Water. Since wintertime surface temperatures, salinities, and oxygen contents are all quite variable, it is puzzling to account for the fact that the 18° Water is so stable climatically.

To what extent some of the phenomena observed are produced by advection from higher latitudes we have no way of knowing; there is no systematic set of hydrographic data comparable to the *Panulirus* data from any other area near Bermuda.

Acknowledgment—In undertaking this study we have had the advantage of many discussions with F. C. Fuglister and L. V. Worthington, to both of whom the 18° Water has been a subject of interest for years. In studying the new *Panulirus* data it occurred to us that finally we had enough material to present a definite case for the amazing climatic stability of the 18° Water at Bermuda, and that this was the time to bring it to the attention of oceanographers interested in climatic change. Part of this work was supported by an AEC contract AT (30-1) -2078 with the Bermuda Biological Station, and part by an ONR contract Nonr 2196 (00) with the Woods Hole Oceanographic Institution.

REFERENCES

HAURWITZ, B., H. STOMMEL, W. H. MUNK, The thermal unrest in the sea, Rossby Memorial Volume, in press, 1959.

(Manuscript received September 8, 1958; revised January 8, 1959.)

Contribution No. 993

THE GROWTH OF UNICELLULAR ALGAE IN ARTIFICIAL AND ENRICHED SEA WATER MEDIA[1]

JACK MCLACHLAN[2]

Abstract

The growth of pure cultures of *Dunaliella euchlora* strains WHOI-1 and WHOI-2, *Platymonas subcordiformis*, *Phaeodactylum tricornutum*, *Chlorella vulgaris*, and *Cyclotella meneghiniana* was compared in two enriched sea water media and two artificial marine media. Three general patterns of growth were observed; the green flagellates grew the same in all media, *Phaeodactylum* and *Chlorella* grew more slowly in the artificial media, and *Cyclotella* did not grow in the artificial medium without organic supplements. The addition of vitamin B_{12} to the artificial medium promoted good growth of *Cyclotella*, and of the species studied this alga was the only auxotroph. Growth in the enriched sea water medium was not affected by a precipitate, but removal of the precipitate markedly affected the rate of growth and the total number of cells obtainable.

Introduction

Although unicellular marine algae have been grown in culture for many years, very little is known of the nutrient requirements of these organisms. In most studies, the diatom *Phaeodactylum tricornutum* (*Nitzschia closterium* f. *minutissima*) has been used as the experimental organism, although this alga is apparently not a normal component of the plankton (10), and most of the other organisms in culture are also "laboratory plankters."

Enriched sea water has been employed as a basal medium in most studies, though it has often been difficult to achieve consistent results (13). This inconsistency has been partly overcome by the use of "aged" sea water (17, 18), although this procedure has not been entirely successful (5). The formation of precipitates has presented another difficulty. By carefully adding nutrients to sea water after it has been autoclaved, cooled, and allowed to come to equilibrium with the carbon dioxide of the air, precipitates can often be avoided (17). This procedure is, however, tedious and increases the chances of introducing contaminants into the culture.

In a few investigations, artificial media have been used (e.g. 2, 15), but in none of these studies has the growth obtained in artificial media been compared with that in enriched sea water. However, Lewin (12) obtained comparable growth of a thallose green alga in enriched sea water and in an artificial medium. Provasoli *et al.* (13) recently listed a variety of artificial marine media, but did not indicate the range of organisms it was possible to grow in these media, nor did they give quantitative data on relative growth rates. It was the purpose of this study to compare the growth of several organisms in enriched sea water and in an artificial medium.

---

[1] Manuscript received September 22, 1958.
Contribution No. 993 from the Woods Hole Oceanographic Institution, Woods Hole, Massachusetts, U.S.A.

[2] Public Health Service Research Fellow of the National Institutes of Health.

Materials and Methods

In this study four media were used, of which two were synthetic and two were based on natural sea water. The synthetic media consisted of modifications of the ASP medium of Provasoli *et al.* (13). These four media were: (1) modified ASP medium (Table I), (2) modified ASP medium plus 5 ml soil extract per liter, (3) enriched sea water, (4) enriched sea water plus 5 ml soil extract per liter. The artificial media had an initial pH of about 6.5, and that of the sea water media was about 8.0. The water used in the ASP media was prepared according to the procedure of Provasoli and Pintner (14), and the soil extract according to that of Gross (6). The sea water media were enriched by the addition of potassium nitrate, potassium monohydrogen phosphate, sodium silicate, and micronutrients, with the exception of iron, in the concentrations employed in the ASP medium. Iron was added as ferric citrate stabilized with an equal amount of citric acid (by weight) at a concentration of 9.0 micromoles. A relatively high concentration of iron was used as Goldberg (4) found that 80 to 90% of the iron added in this form was adsorbed to the walls of the culture vessel within 1 day.

TABLE I

Composition of the modified ASP medium†

Compound	Concentration in micromoles
NaCl	410×10^3
$MgSO_4.7H_2O$	24×10^3
$MgCl_2.6H_2O$	22×10^3
$CaCl_2.2H_2O$	10×10^3
KNO_3	1000
K_2HPO_4	100
$Na_2SiO_3.9H_2O$	100
$FeCl_3.6H_2O$	1.5
H_3BO_3	185
$MnCl_2.4H_2O$	7.0
$ZnCl_2$	0.8
$CoCl_2.6H_2O$	0.02
$CuCl_2.2H_2O$	0.0002
Na_2EDTA*	30

*Sodium ethylenediaminetetraacetate.

†The modified ASP medium differs from the original ASP medium in the omission of the vitamin mix 8, B_{12}, and KCl (*c*. 8000 micromoles).

Pure cultures of the following organisms were used: *Phaeodactylum tricornutum* Bohlin, *Cyclotella meneghiniana* Kützing, *Chlorella vulgaris* (?) Beijerinck, *Platymonas subcordiformis* (Wille) Hazen, and *Dunaliella euchlora* Lerche strains WHOI-1 and WHOI-2. *Cyclotella* and *Phaeodactylum* (10) are diatoms; the others are chlorophycean algae. Stock cultures were maintained in the ASP medium without the addition of soil extract with the exception of *Cyclotella* which was cultured in enriched sea water. The absence of contaminant bacteria was established by the procedure of Spencer (16).

The cultures were grown in 125-ml Erlenmeyer flasks containing 50 ml of medium at a temperature of 16° C. A light intensity of approximately

3000 meter-candles was provided by 40-watt fluorescent lights. The flasks were not shaken or aerated. Growth rates were determined by periodic harvests by cell counts, using a Levy hemocytometer. Eight replicates of the cell counts were made, and the weighted standard error of the mean was 5.0. The results are plotted using the expression $\log_2 N_t/N_0$, where N_0 represents the initial concentration of cells and N_t the concentration at the time of harvest. An increase of one unit on the ordinate corresponds to one division of the population.

Results and Discussion

The results show three general patterns of growth. In the two strains of *Dunaliella euchlora* (Fig. 1) and *Platymonas subcordiformis* (Fig. 2), the growth rates in all four media were similar. However, the growth rates of the two strains of *D. euchlora* were quite different. Strain WHOI-1 grew almost twice as rapidly as strain WHOI-2, though morphologically these two strains are indistinguishable. Moreover, WHOI-2 tended to adhere to the surface of the culture vessels, and to settle out of suspension after active growth had ceased, whereas WHOI-1 remained evenly suspended throughout the medium. There was no indication that any of these organisms are auxotrophic. Gibor (3) likewise found *D. viridis*, *D. salina*, and *Platymonas* sp. to require no growth factors, and Droop (1) stated that *Dunaliella* spp. did not require vitamin B_{12}.

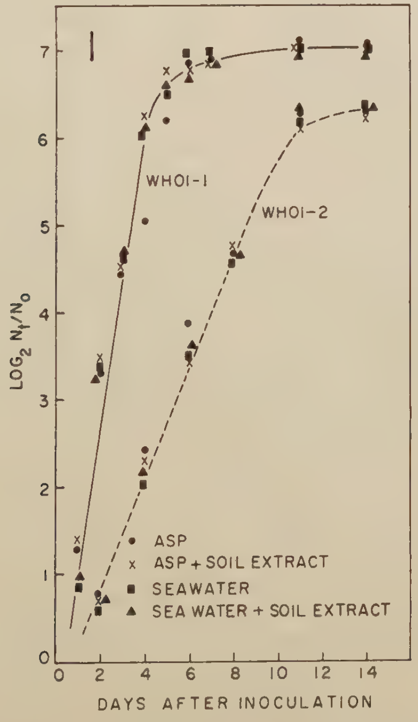

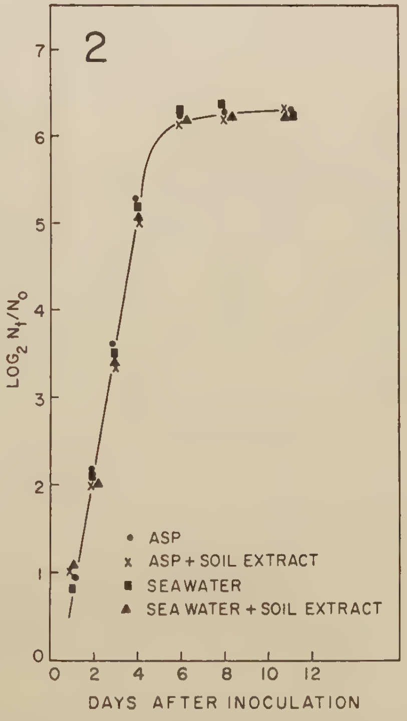

FIG. 1. The growth of *Dunaliella euchlora* strains WHOI-1 and WHOI-2 in the four media.

FIG. 2. The growth of *Platymonas subcordiformis* in the four media.

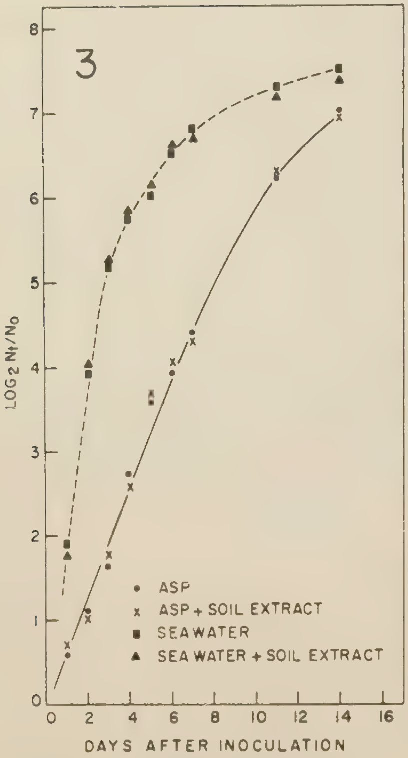

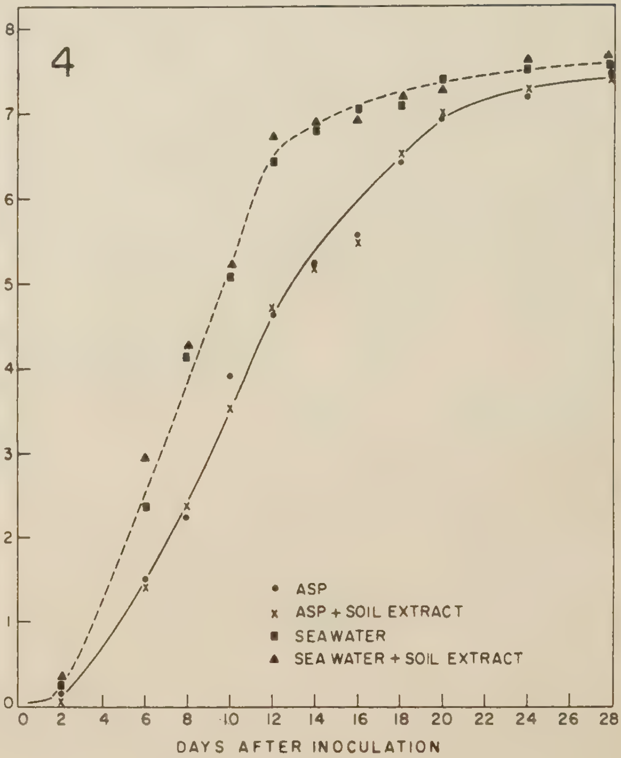

FIG. 3. The growth of *Phaeodactylum tricornutum* in the four media.
FIG. 4. The growth of *Chlorella vulgaris* in the four media.

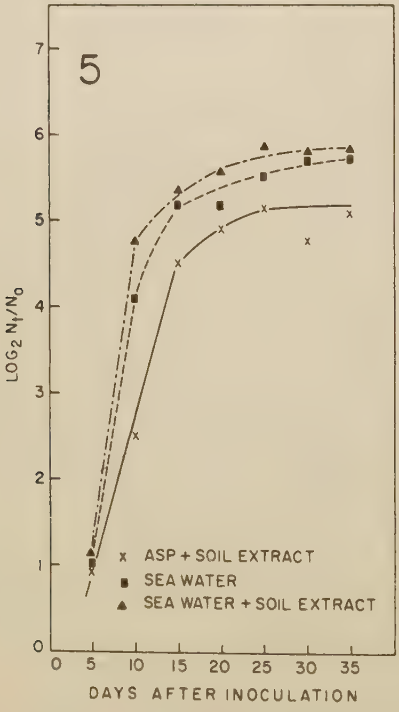

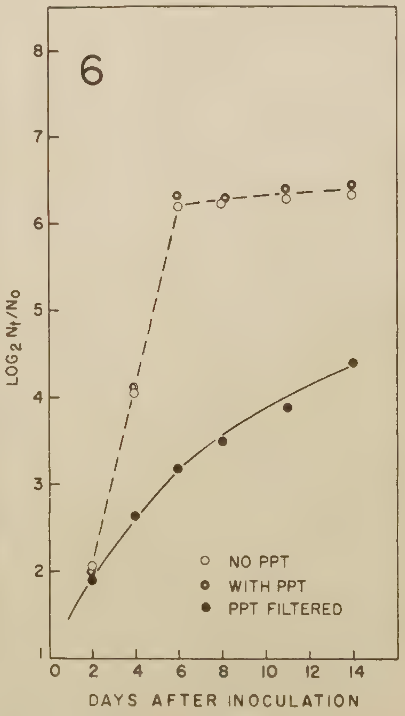

FIG. 5. The growth of *Cyclotella meneghiniana* in the four media.
FIG. 6. The growth of *Dunaliella euchlora* WHOI-1 in the enriched sea water medium without precipitate, with a precipitate, and with the precipitate removed.

Phaeodactylum tricornutum (Fig. 3) and *Chlorella vulgaris* (Fig. 4) both showed a lag phase when cultured in the artificial media, though terminal growth in all series was approximately the same, and soil extract did not prove to be stimulatory. The retardation of growth in the synthetic media may have been due to the low initial pH, but insufficient data preclude any conclusions as to pH effects.

Cyclotella meneghiniana (Fig. 5) grew well in the enriched sea water series and rather more slowly in the ASP – soil extract medium. Here, too, the low initial pH may possibly account for the slower growth in the ASP – soil extract medium. In the ASP medium without soil extract there was no growth. The lack of growth in this medium indicated a possible vitamin requirement. Dr. J. C. Lewin recently completed a vitamin-requirement survey of a number of diatoms. As *Cyclotella meneghiniana* was found to require vitamin B_{12},* it has now proved possible to obtain satisfactory growth of this alga in the ASP medium supplemented with 0.20 μg per liter of vitamin B_{12}. These results demonstrated either that vitamin B_{12} was originally present in the sea water used, or that during the "aging" process, bacterial activities resulted in its accumulation in the water.

It was also found possible to grow *Nannochloris atomus*, *Melosira* sp., and *Skeletonema costatum*, which was contaminated, satisfactorily in the ASP medium without soil extract.

Provasoli *et al.* (13) indicated that the principal objection to most marine media hitherto employed was that they tended to form precipitates. In their work the ASP medium, adjusted to an initial pH of about 7.5, occasionally formed a precipitate after autoclaving. However, this difficulty was not experienced in the present study, possibly because of the lower initial pH.

An experiment was performed to determine if precipitates in the sea water medium affect growth. In one series, nutrients were added aseptically to the medium after it had been autoclaved and cooled; no precipitate was formed. A second series was autoclaved with the nutrients, and a precipitate was formed. The medium from half the flasks in this series was filtered through a VC (100 mμ) "Millipore" filter, and both sets of flasks were re-autoclaved and all series inoculated with *Dunaliella euchlora* WHOI-1. The results (Fig. 6) show that the removal of the precipitate reduced both the rate of growth and the final number of cells. It is evident from this experiment that there is a rapid resolution of salts from the initially formed precipitate, or at least enough so that the rate of growth is not affected. It would also appear that precipitates are not really objectionable; however, as has been pointed out (13), it is difficult to reproduce the same kind of precipitate and, in consequence, to repeat the results of an experiment. Also, if growth is to be measured by optical density or packed cell volume, the objection to precipitates is obvious.

The artificial media used in this study was formulated to resemble sea water with a salinity, based on the weight of the salts, of 35‰. Using data

*Lewin, J. C. Personal communication.

presented by Harvey (7), a comparison of the conservative elements in sea water, with a similar salinity, is presented in Table II. The artificial medium had a slightly lower molarity than sea water and a reduced potassium concentration. Since no carbonate was added, this medium had a relatively low pH and was poorly buffered.

TABLE II

A comparison of the concentration (in micromoles) of the conservative elements in sea water and in the ASP medium

Element	Sea water	ASP
Sodium	482,628	410,000
Potassium	9,976	1,200
Magnesium	54,690	46,000
Calcium	10,479	10,000
Chloride	558,360	442,000
Sulphur (as sulphate)	28,695	24,000

NOTE: The Mg/Ca ratio in sea water is 5.22 and in the ASP medium 4.60, and the monovalent cation/divalent cation ratio in sea water is 7.56 and in the ASP medium 7.34.

In the sea, the ratio of nitrogen to phosphorus is about 20:1, though the total concentration of these elements varies (9), and analyses have shown that the ratio of these elements in phytoplankton is also about 20:1 (7). Since, in the present study, nitrogen and phosphorus were added at a ratio of 10:1, the media contained relatively too much phosphorus. By reducing the concentration of phosphorus and establishing a N/P ratio of 20:1, neither the growth rate nor the total population was affected.* McLachlan and Yentsch,* using *Dunaliella euchlora* WHOI-1, found that at the end of the log phase of growth, all the nitrogen added to the ASP medium had been organically incorporated. Therefore, the limiting factor to growth in the media used appeared to be nitrogen. Ryther (15) stated that certain green algae grew better at a N/P ratio of 5:1 than at a ratio of 15:1, but this does not seem to be true of *D. euchlora* WHOI-1.* Ryther found, however, that a change in the N/P ratio did not affect the growth of *Phaeodactylum.*

Silicate was always added to the medium, though it was only necessary for the diatom *Cyclotella.* Apparently enough silicate goes into solution from the glass vessels to satisfy the requirements of *Phaeodactylum* (11, 17).

Harvey's data (7) show that the concentration of carbon in sea water is approximately 2000 micromoles, though not all of this element is available for metabolic purposes. Since the average C/N ratio in phytoplankton is about 7.5/1 (8), at least an additional 5000 micromoles of carbon would be needed to metabolize all the available nitrogen in the enriched sea water media. As nitrogen has been found to be the limiting factor in these media, a considerable amount of carbon had to enter the medium by diffusion. Spencer (17) stated that the rate of diffusion of carbon dioxide into a sea water medium was sufficiently slow to cause the supply of carbon to become limiting. On the other hand, Provasoli *et al.* (13) claim that carbon dioxide is avidly absorbed at pH 8.0 to 8.4, and thus provides a means of supplying carbon without the necessity of shaking or bubbling. The data presented in these experiments tend to support the latter view as the growth rate of *D. euchlora* was not affected until the supply of nitrogen in the medium had become exhausted. It is assumed that the rate of growth of the other species was also arrested by a limitation of the nitrogen supply. Therefore, carbon does not seem to be a limiting factor under the conditions employed in this study.

---

*McLachlan, J. and Yentsch, C. Unpublished.

This study has demonstrated that some marine phytoplankters can be successfully grown in chemically defined media without precipitates. This is of considerable advantage since sea water is a complex and variable medium and not readily available inland. The results of this study also indicate that it would be possible to grow successfully a wide variety of marine organisms in an artificial solution such as the ASP medium.

Acknowledgments

The author wishes to thank Dr. E. M. Hulburt and Dr. R. A. Lewin for identifying the organisms used in this study. Dr. B. H. Ketchum, Dr. R. A. Lewin, and Dr. J. H. Ryther have read the manuscript and offered valuable suggestions.

References

1. Droop, M. R. Auxotrophy and organic compounds in the nutrition of marine phytoplankton. J. Gen. Microbiol. **16**, 286–293 (1957).
2. Droop, M. R. A pelagic marine diatom-requiring cobalamin. J. Marine Biol. Assoc. United Kingdom, **34**, 229–231 (1955).
3. Gibor, A. The culture of brine algae. Biol. Bull. **111**, 223–229 (1956).
4. Goldberg, E. D. Iron assimulation by marine diatoms. Biol. Bull. **102**, 243–248 (1952).
5. Goldberg, E. D., Walker, T. J., and Whisenand, A. Phosphate utilization by diatoms. Biol. Bull. **101**, 274–284 (1951).
6. Gross, F. Notes on the culture of some marine plankton organisms. J. Marine Biol. Assoc. United Kingdom, **21**, 753–768 (1937).
7. Harvey, H. W. The chemistry and fertility of sea waters. Cambridge University Press, Cambridge. 1957.
8. Ketchum, B. H. Mineral nutrition of phytoplankton. Ann. Rev. Plant Physiol. **5**, 55–74 (1954).
9. Ketchum, B. H. The absorption of phosphate and nitrate by illuminated cultures of *Nitzschia closterium*. Am. J. Botany, **26**, 399–407 (1939).
10. Lewin, J. C. The taxonomic position of *Phaeodactylum tricornutum*. J. Gen. Microbiol. **18**, 427–432 (1958).
11. Lewin, J. C., Lewin, R. A., and Philpott, D. E. Observations on *Phaeodactylum tricornutum*. J. Gen. Microbiol. **18**, 418–426 (1958).
12. Lewin, R. A. Culture of *Prasiola stipitata* Suhr. Can. J. Botany, **33**, 5–10 (1955).
13. Provasoli, L., McLaughlin, J. J. A., and Droop, M. R. The development of artificial media for marine algae. Arch. Mikrobiol. **25**, 392–428 (1957).
14. Provasoli, L. and Pintner, I. J. Ecological implications of *in vitro* nutritional requirements of algal flagellates. Ann. N.Y. Acad. Sci. **56**, 839–851 (1953).
15. Ryther, J. H. The ecology of the phytoplankton blooms of Moriches Bay and Great South Bay, Long Island, New York. Biol. Bull. **106**, 198–209 (1954).
16. Spencer, C. P. On the use of antibiotics for isolating bacteria-free cultures of marine phytoplankton organisms. J. Marine Biol. Assoc. United Kingdom, **31**, 97–106 (1952).
17. Spencer, C. P. Studies on the cultures of a marine diatom. J. Marine Biol. Assoc. United Kingdom, **33**, 265–290 (1954).
18. Sweeney, B. M. *Gymnodinium splendens*, a marine dinoflagellate requiring vitamin B_{12}. Am. J. Botany, **41**, 821–824 (1954).

Contribution No. 995

Reprinted from LIMNOLOGY AND OCEANOGRAPHY
Vol. IV, No. 4, October, 1959
Printed in U.S.A.

The Hydrography of Barnstable Harbor, Massachusetts[1]

JOHN C. AYERS

Department of Zoology and Great Lakes Research Institute, University of Michigan; and Woods Hole Oceanographic Institution

ABSTRACT

Barnstable Harbor, on the north shore of Cape Cod, Massachusetts, originated from the growth of an offshore barrier bar across an indentation of the coastline. In common with many other East Coast tidal embayments of similar origin it has: 1) low runoff, carried by a few small streams, which together with direct rainfall and groundwater seepage provides a total freshwater acquisition that is small compared to the tidal prism volume; 2) essentially marine internal aquatic environments; and 3) extensive salt marshes drained by tidal creek systems. The hydrography of the harbor is largely determined by the internal arrangement of its shoals and channels. The shoals and channels act as dams and weirs, distorting the tides until they approximate those found in typical river estuaries. The tidal distortion results in a time asymmetry of the maximum currents which in turn produces a net up-harbor transport of sediments, despite the fact that the ebb currents are of the greater velocity. The hydrography of the harbor in spring, summer, and fall is described. Parameters discussed include salinity, temperature, transparency, water masses, tidal currents, sediment analyses, the salinity relations of intertidal flats, and some aspects of the annual temperature regime.

INTRODUCTION

Barnstable Harbor is located on the north shore of Cape Cod in Massachusetts. The harbor consists of an indentation of the original post-glacial coastline which has been nearly cut off by an offshore barrier bar. This type of origin is common to many of the tidal embayments of the East Coast. Their similarity in origin has endowed these embayments with certain "family" characteristics, and knowledge of one becomes (in varying degree) knowledge of all.

Among the "family" characteristics of this type of tidal embayment may be listed: low runoff which is carried by a few small streams and which, with direct rainfall and ground-water seepage, provides a total freshwater acquisition that is small compared to the quantity of tidal salt water entering and leaving the embayment; internal aquatic environments are essentially marine in character; and salt marshes drained by tidal creek systems border the open water. Barnstable Harbor exhibits these family characteristics.

The author acknowledges, with thanks, financial support received from the Division of Marine Fisheries, Massachusetts Department of Conservation, during the field phases of this study. Thanks are also tendered to Dr. A. C. Redfield for reading the manuscript, and to Harry J. Turner and Charles F. Powers for assistance in the field work.

Financial assistance for publication has been given by a grant from the Horace H. Rackham School of Graduate Studies of the University of Michigan.

PHYSIOGRAPHY

The harbor lies in an area of glacial till on the north side of the Sandwich Moraine left by the Wisconsin glaciation. The soil of the upland is primarily sand and sandy loam with scattered glacial boulders. The glacial till varies in depth from five to more than thirty feet and overlies disturbed glaciofluvial sand and gravel. In the region of the harbor the sandy till is separated from the disturbed sand and gravel by a layer of hard-packed grey till locally called "hardpan." Johnson (1925) and Mather *et al.* (1942) review the geology of the area.

The harbor is bordered on the southwest,

---

[1] Contribution No. 995 from the Woods Hole Oceanographic Institution.

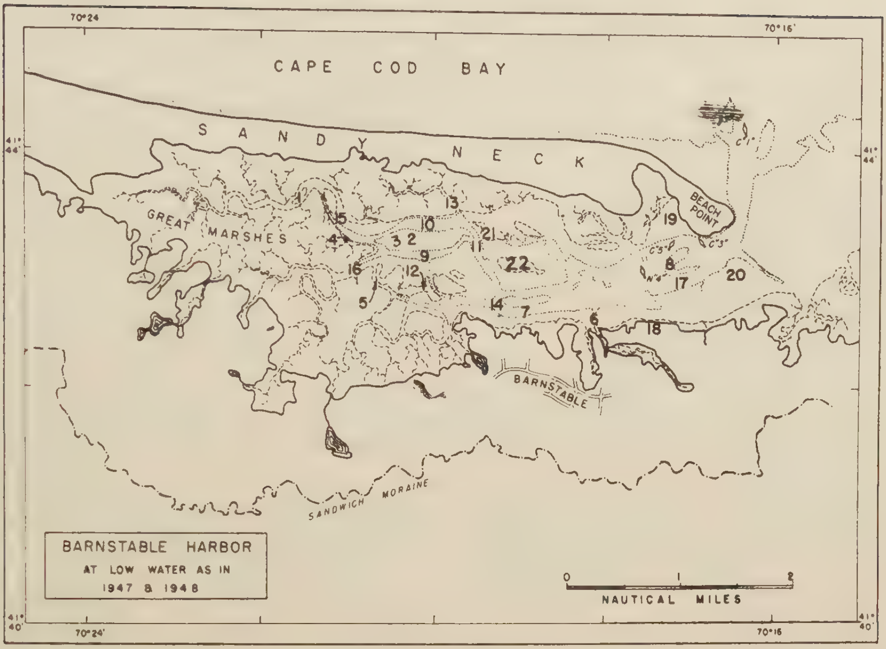

FIG. 1. Barnstable Harbor at low water as in 1947 and 1948. Dotted lines represent the junction of intertidal flats with open water; dashed lines represent the seaward edges of the salt-marsh; and a bold line indicates the meeting of salt-marsh and upland. The numbers refer to features named in Table 4.

west, and northwest by a salt marsh of considerably greater area than the harbor itself. Five major tidal creeks drain the marsh. Each tidal creek branches elaborately, and the main channels extend to the outer edge of the marsh where they receive small freshwater streams. Thirteen streams in total descend from the Sandwich Moraine and contribute to the harbor during each ebb tide about 0.3 million cubic feet of freshwater from a 22.8 square-mile watershed (Ayers 1956, p. 33).

On the north the harbor is bordered by a range of sand dunes which constitutes the barrier bar and is called Sandy Neck; this terminates in a broad sand spit at Beach Point (Fig. 1). Most of the dunes in this range are shifting, except in scattered areas where pitch pine, scrub oak, and dune grass have stabilized the sand. A continuous ocean beach lies along the north side of Sandy Neck.

Most of the harbor's inlet is occupied by intertidal sand flats. A channel cuts through these flats, but it widens and shoals offshore and terminates in a typical harbor bar at a depth of about five feet at mean low water.

At low water, shoals inside the inlet are exposed and reduce the navigable area to narrow channels. Early in the flood tide these shoals become submerged and allow water to enter through a much larger cross-section. The shoals produce a distortion of the tide which is discussed later as the "weir effect."

Numerous bars and shoals, extensive intertidal flats, and salt-grass covered islands standing two to five feet above the flats are the primary physiographic features within the harbor. In the inner parts of the harbor the intertidal flats rise about a foot above low water level. Flats rising two feet or more above the average level (three feet above low water) support the salt-grass *Spartina alterniflora* and are low (new) grassy islands.

The well-established marsh at the head of the harbor often presents cliff-like edges rising several feet above the level of the flats. Older portions of the marsh, farther back from the open water, appear to be about six inches higher than those adjacent to the harbor.

About 60 per cent of the total harbor

TABLE 1. *Mechanical analyses of surface soils from various parts of the harbor and marsh*
Organic content determined as loss on ignition. Data of Harry J. Turner, Woods Hole Oceanographic Institution.

Location	% of sample passing through sieves of				Median diameter of particles, mm	Organic content, %
	20 mesh	48 mesh	100 mesh	200 mesh		
Channel-bar east of Wicks Is. (S)	98.3	80.3	18.5	0.6	0.20	3.2
WHOI flat (south side) (SM)	99.4	99.4	82.8	22.4	0.10	1.2
WHOI flat (center) (MS)	98.9	97.5	88.1	14.9	0.10	0.85
Howes' old flat (S)	99.8	97.8	77.8	6.3	0.12	0.60
Bung-hole flat (SM)	97.7	96.6	88.0	24.3	0.09	1.05
Gull Creek flat (SM)	98.7	94.1	69.4	20.0	0.12	1.3
Wicks Island (SS)	97.8	94.1	82.2	46.8	0.07	4.6
Marsh opposite Wicks Is. (SS)	98.2	96.5	85.2	35.1	0.09	3.0

20 mesh = 0.833 mm; 48 mesh = 0.295 mm; 100 mesh = 0.147 mm; 200 mesh = 0.074 mm; MS = muddy sand; SM = sandy mud; SS = sandy silt; S = sand.

bottom is exposed at low water. The western end of the harbor becomes almost completely exposed, the remaining water being confined to narrow channels which are extensions of the main tidal creeks.

The bottom is primarily fine muddy sand, though clean coarse sand occurs in the harbor mouth, and mud or sandy mud is dominant in the tidal creeks. Bottom samples from various parts of the harbor show a considerable variation in their contents of fine sediments (Table 1, column 5; see Table 4 and Fig. 1 for sampling locations). The greatest proportions of fines occur in the stabilized surface soils of the marshes and grassy islands. Moderate proportions are present in the surfaces of the somewhat less stable intertidal flats. Shifting flats of clean sand near the harbor mouth may be expected to contain the smallest proportions of fine sediments.

The harbor is shallow in all its parts above the mouth of Maraspin Creek (Table 4 and Fig. 1), and winds produce strong wave action. Local, usually temporary, silting-up and scouring occur in all parts of the harbor. Changes in the shallow inner end of the harbor consist chiefly of meanderings of the channels back and forth across the intertidal flats. There are indications (described below) that the head of the harbor, at least, is gradually filling in.

HYDROGRAPHY

The harbor ranges in depth from 8 to 30 feet at high water. The shallowness and the large tide range result in extreme volume changes during each tidal cycle The harbor volume changes from about 1000 × 10^6 cubic feet at high water to about 71 × 10^6 cubic feet at low water, the intertidal volume or tidal prism being about 93 per cent of the high-water volume. The large tidal exchange rather quickly carries to sea the small freshwater acquisition. About five tidal cycles are required to remove from the harbor a volume of freshwater equal to the quantity of freshwater accumulated in the harbor at a given high tide (Ayers 1956, pp. 32–33).

The Tides

The mean tide range at Beach Point is 9.5 feet; the range at spring tides is 11.0 feet (U. S. Coast & Geodetic Survey Tide Tables). Because shoals inside the harbor hamper the ebb current and produce an elevated low-water level, there is a reduction in tide range between the inlet and the head of the harbor. Neap tides do not inundate the salt marsh, while spring tides cover it to depths up to 1.5 feet.

As is common in small harbors along this coast, high and low waters occur at nearly the same time in all parts of the harbor, and maximum tidal currents occur near mid-tide. Preliminary tide-guage observations indicate, as first approximations, that the interval between high waters at Beach Point and the head of the harbor is about 0.5 hour, and that the interval between low waters at these points is about 0.9 hour.

TABLE 2. *Durations of ebb and flood tides in various parts of the harbor*
Head of the harbor begins with innermost weir.

Position	Date	Duration of flood, Hrs.–Min.	Duration of ebb, Hrs.–Min.	Remarks
Can 1	17–VI–48	6–15	6–15	Normal tidal cycle
				Major weirs at this level, 6 in. rise needed to stop ebb
Nun 4	27–X–47	5–45	5–45	
Main Channel at mouth of Maraspin Cr.	21–X–47	6–25	6–15	
	17–VI–48	5–45	7–0	
Yacht Club Channel	2–VI–48	5–45	6–35	Minor weir, 3 in. needed to stop ebb
	22–X–47	5–50	6–50	
			6–30	
	28–VIII–52	5–30	7–18	
Jct. North Channel with Phillis Is. Channel	8–VI–48	6–10	7–0	Minor weir, ca 3 in. needed to stop ebb (estimated)
	17–VI–48	5–20	7–10	
Midway, S of WHOI flat	22–X–47	5–45	7–0	
	20–X–47	5–5	6–40	
	17–IX–47	4–45	7–30	
		5–5		
	21–X–47	5–25	7–0	
			6–50	
Mouth of Scorton Cr.	2–VI–48	5–35	7–10	Net elevation of low water level: ca 1 foot
	17–VI–48	5–40	7–25	

Head of harbor average: Flood 5.5 hrs.; ebb 7.1 hrs.

The durations of flood and ebb in the upper harbor are about 5.5 and 7.1 hours, respectively (Table 2).

The weir effect

Shortening of flood and prolongation of ebb is typical of the tidal wave in shoal water (Doodson and Warburg 1941), but in Barnstable this effect is exaggerated by the shoals in the harbor.

At low water Horseshoe Shoal and the flats along shore beside it act as a dam with two weirs. The two weirs are narrow channels through which the tidal currents must pass during the hours when the shoal and adjacent flats are exposed. The pronounced reduction in cross-section at this point hinders and prolongs the outflow of the ebb tide and allows a head of water to develop above the weirs. The weirs retain this head until the waters outside the harbor have passed through their low water stage and begun their flood-tide rise.

The time used in overcoming the head of water above the weirs is the period during which the weakest flood current would flow into a harbor of more usual physiography. When the head is exceeded and the flood current begins to flow through the weirs, it soon reaches a velocity close to its maximum (Fig. 2).

Temporary tide staffs have shown that the tide outside the harbor rises about six inches before the ebb current ceases to flow out through the weirs at Horseshoe Shoal. This rise is sufficient to submerge a major part of Horseshoe Shoal and adjacent flats. The shoal and flats become completely submerged soon after the flood current begins to run in through the weirs.

Lesser weirs exist at Yacht Club Channel, where tide staffs have shown that the water rises about three inches before the ebb current stops. At the points where Midway and North Channel enter Phillis Island Channel, visual estimates suggest a further three-inch rise before the ebb ceases. The weirs result not only in distortion of the flood and ebb durations but also in an elevation of low water level along the length of the harbor (Table 2).

Figure 2 shows the surface current velocities observed during a tidal cycle in Yacht Club Channel and over the crest of an inter-

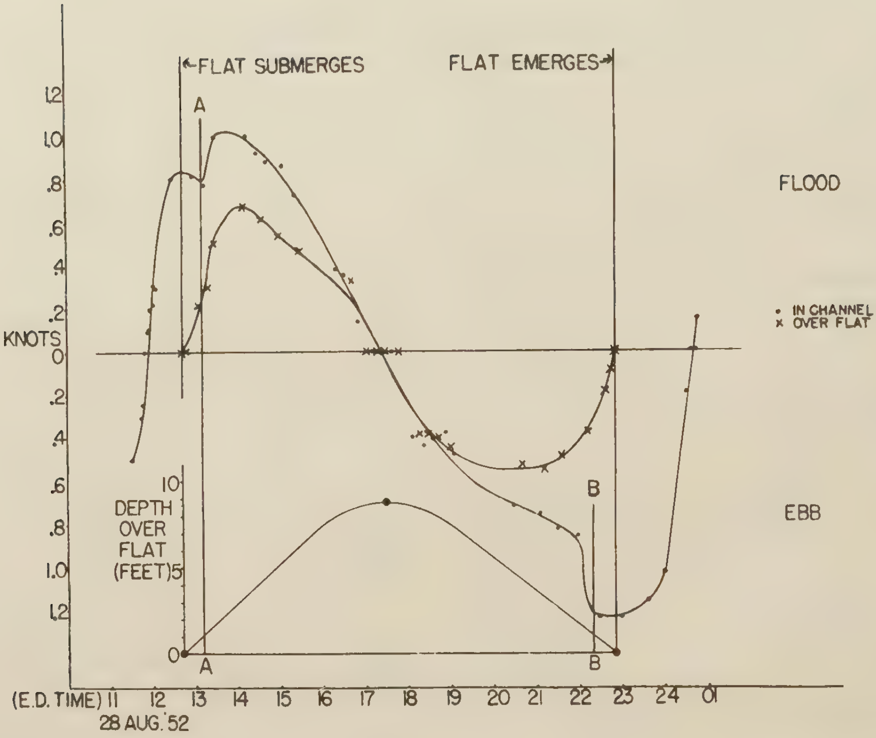

Fig. 2. Tidal current velocities in Yacht Club Channel and over the intertidal flat immediately north of that channel. 28 August 1952.

tidal flat immediately north of that channel. The very rapid increase of current velocity in the channel during early flood was interrupted by a plateau in velocity, beginning just before the adjacent flats became submerged and ending when the flats were about a foot under water (line AA). After the flats were overflowed the flood velocity in the channel quickly rose to its maximum of 1.03 knots, at the end of the second hour of flood, then declined steadily until the end of flood 3.5 hours later. The flood current over the flat attained its maximum velocity of 0.67 knot at the same time as did that in the channel and also went to zero at 5.5 hours of the flood tide, 4.7 hours after the flat's submergence.

During the first hour of ebb no velocity difference between the currents in the channel and over the flat was discernible. After 1.25 hours of ebb the current velocity over the flat became less than that in the channel. Ebb current over the flat attained its maximum velocity of 0.53 knot at the end of the third hour of ebb, after which it decreased steadily until the flat emerged after 5.5 hours of ebb. The current in the channel increased steadily to about 0.9 knot at 4.6 hours of the ebb when the water over the flat was about one foot deep (line BB); between that time and 5.1 hours of ebb (when there was about six inches of water over the flat) the channel current increased to 1.23 knots. It attained its maximum of 1.25 knots at 5.5 hours of the ebb when the flat emerged, then decreased to 1.03 knots at 6.6 hours, and went to zero at 7.3 hours of the ebb.

The data indicate that the ebb current experiences effective confinement to channels at a time when there is still about a foot of water over the flats. Prior to this time the freer drainage in the open channel tends to lower its water level and water from over the flat, retarded by friction with the flat, flows obliquely into the channel. The friction-slowed water entering the channel requires acceleration from the channel current and causes a temporary decrease in the acceleration of the channel current (see Fig. 2 between 19 and 22 hours). By the time only a foot of water remains over the flat the quantity of friction-slowed water leaving the flat has become insignificant, and its retarding effect on the velocity of the channel current disappears (Fig. 2 between 22 and 23 hours).

A condition at least superficially similar to the above occurs during submergence of the flat on the flood tide. From just before the flat submerges until it is covered by about a foot of water the velocity of flood remains nearly constant. In this case the retarding effect of friction-slowed water that crosses the flat and the increasing cross-sectional area available as the flat becomes submerged both act to reduce current velocity in the channel. The flood velocity at this period is increasing, and the two retardant effects produce only a velocity plateau. The plateau disappears when the harbor's full cross-section becomes available for flow and when the quantity of water slowed by friction of the flat becomes insignificant in the total volume flowing (Fig. 2 between 12 and 14 hours).

Effects of tidal currents on bottom physiography

Maximum velocity of the flood current occurs near mid-flood when the intertidal flats are submerged and the cross-sectional area of the harbor is large. The flood current attains maximum surface velocities of 50 to 80 cm/sec. These correspond to average velocities of 37.5 to 60 cm/sec. (Sverdrup *et al.* 1942, p. 568) through the harbor's cross-section. These average velocities are ample (Sverdrup *et al.* 1942, Fig. 251) to erode sands of particle sizes 0.06 to 3.0 mm and to transport silt particles of 0.005 to 0.01 mm toward the head of the harbor. The flood current thus is capable of moving sediments up-harbor. Plankton nets towed at the times of maximum current capture large quantities of sediment.

Sediments carried up-harbor by the flood tide settle out at slack high water. Those settling into the channels are swept seaward during the ebb. Those sinking onto the flats are subjected, during the ebb, to currents less than those that brought them there (Fig. 2). The fact that the ebb currents over the flats are nearly zero when the ebb reaches its maximum in the channels indicates that some of the sediments dropped on the flats at slack high water are able to remain on the flats. That such is taking place is indicated by the formation of new (low) *Spartina*-covered islands on the intertidal flats, by local tradition that the upper harbor (at least) is shoaling, and by the fact that the flats contain more fine sediments than do the channels (compare row 1 with rows 2–6, Table 1). Once salt-grasses are established, mechanical trapping and plant decomposition products further increase the proportion of fines in the island and marsh soils.

Maximum ebb velocity in the harbor occurs after the intertidal flats are bared sufficiently to confine the current to the channels (Fig. 2). The maximum erosive effect of the ebb current is thus limited to the channels, which it keeps open. Apparently for this reason submerged bars protruding into the channels become recurved toward the harbor mouth. Also, this is probably the reason that the intertidal flats have their long axes lengthwise of the harbor. Horseshoe Shoal just inside the inlet apparently has a central portion that does not shift, though its arms point seaward as do the other flats of the harbor.

The effect of the asymmetry of the maximum currents on sediment transport is augmented by flotation. On calm days the flood tide overflowing the flats floats off many dry particles of sediment on the water's surface film. These particles are carried up-harbor until turbulence breaks the surface film and allows them to sink.

By these means the currents achieve a net movement of sediments toward the head of the harbor, even though the ebb current is stronger than the flood.

Water types

Two parent water types, and a mixture of the two, are present in the harbor and the creeks tributary to it. They are: Cape Cod Bay Water, found at the mouth of the harbor; freshwater, entering at the periphery of the marsh; and Mixed Water, in the creeks and head of the harbor. Each type migrates back and forth under the influence of the tide.

At all stages of the tide, except in spring freshet conditions, Cape Cod Bay Water can be found along Beach Point below the weirs at Horseshoe Shoal. It is clear, greenish in color, and of salinity 31.50 to 32.50‰. The freshwater entering the creeks is typical swamp water. It is brown in color but free of silt. Its salinity near the limit of tidal influence ranges from 1.00 to 1.18‰.

The upper harbor and major portions of the tidal creeks are occupied at all stages of the tide by Mixed Water with characteristics between those of the main two types. This water is greenish-brown in color, is definitely turbid, and its salinity ranges from about 1.00‰ near the heads of the creeks to about 31.50‰ in the head of the harbor.

Tidal movements of water types

On the flood tide Cape Cod Bay Water moves into the harbor and by high water is found up-harbor to points beyond Sand

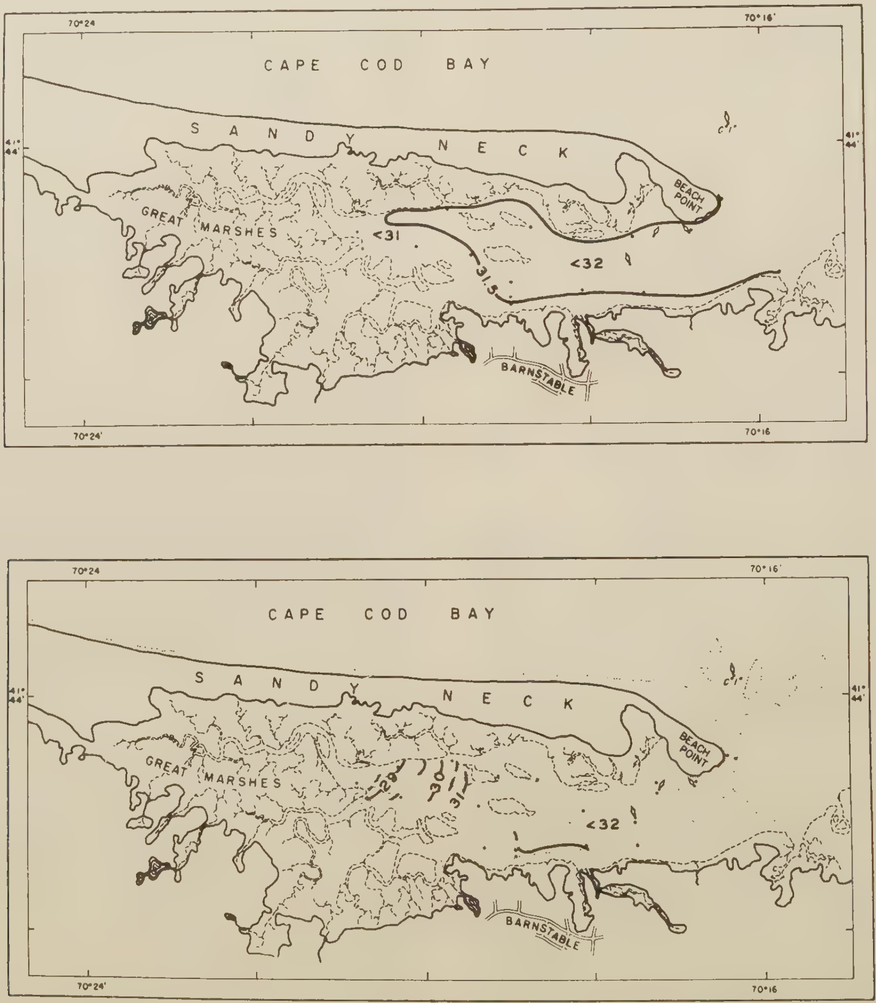
70°24'
70°16'
CAPE COD BAY
SANDY NECK
41° 44'
GREAT MARSHES
BEACH POINT
<31
31.5
<32
BARNSTABLE
70°24'
70°16'
CAPE COD BAY
SANDY NECK
41° 44'
GREAT MARSHES
BEACH POINT
32
31
<32
BARNSTABLE

FIG. 3. Distribution of surface salinity (‰) in summer. 25 and 29 August 1947. *Above*: at high water. *Below*: at low water.

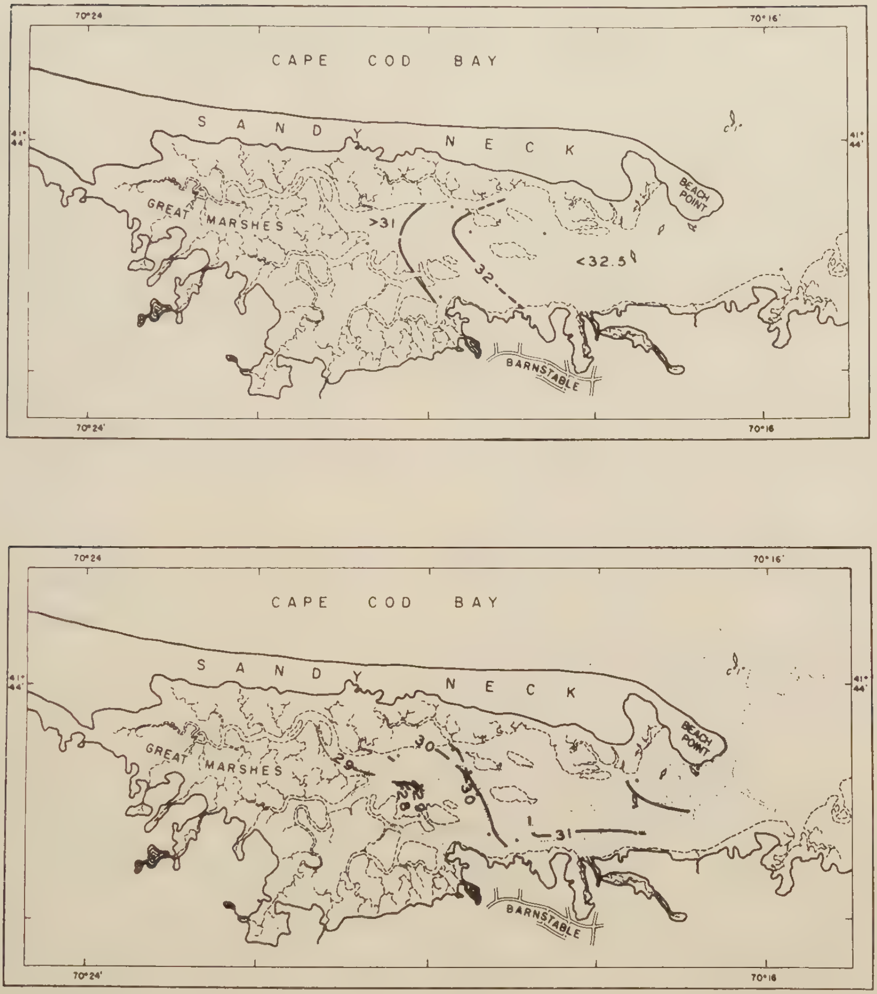
70°24'
70°16'
CAPE COD BAY
SANDY NECK
41°44'
GREAT MARSHES
>31
32
<32.5
BEACH POINT
BARNSTABLE
70°24'
70°16'
41°44'
CAPE COD BAY
SANDY NECK
41°44'
GREAT MARSHES
29
30
28
30
31
BEACH POINT
BARNSTABLE
70°24'
70°16'

FIG. 4. Distribution of surface salinity (‰) in fall. 17 November 1947. *Above*: at high water. *Below*: at low water.

Island and Wells Creek. The advance and retreat of the tide cause extensive horizontal migration of the water and result in horizontal mixing. At full high water only a small amount of the Mixed Water remains in the upper harbor near the mouths of the creeks, while the tidal creeks are filled by it. By late ebb the column of high salinity water has retreated down the harbor, and the Mixed Water has followed it. At low tide, Cape Cod Bay Water is present only between the inlet and Horseshoe Shoal. During freshets it is forced out of the harbor. The horizontal distributions of salinity in summer and fall are shown in Figures 3 and 4. Figure 5 is the salinity distribution during spring freshet.

Above the mouth of Maraspin Creek very small vertical salinity gradients are occasionally found at high water and at low water. At other times no salinity gradient is present.

The salinity relations of intertidal flats

During the advance and retreat of the tide, water moving along the shores of the harbor is outrun by that in the middle of the channels. As a result, intertidal flats along the shores are subjected to less salinity

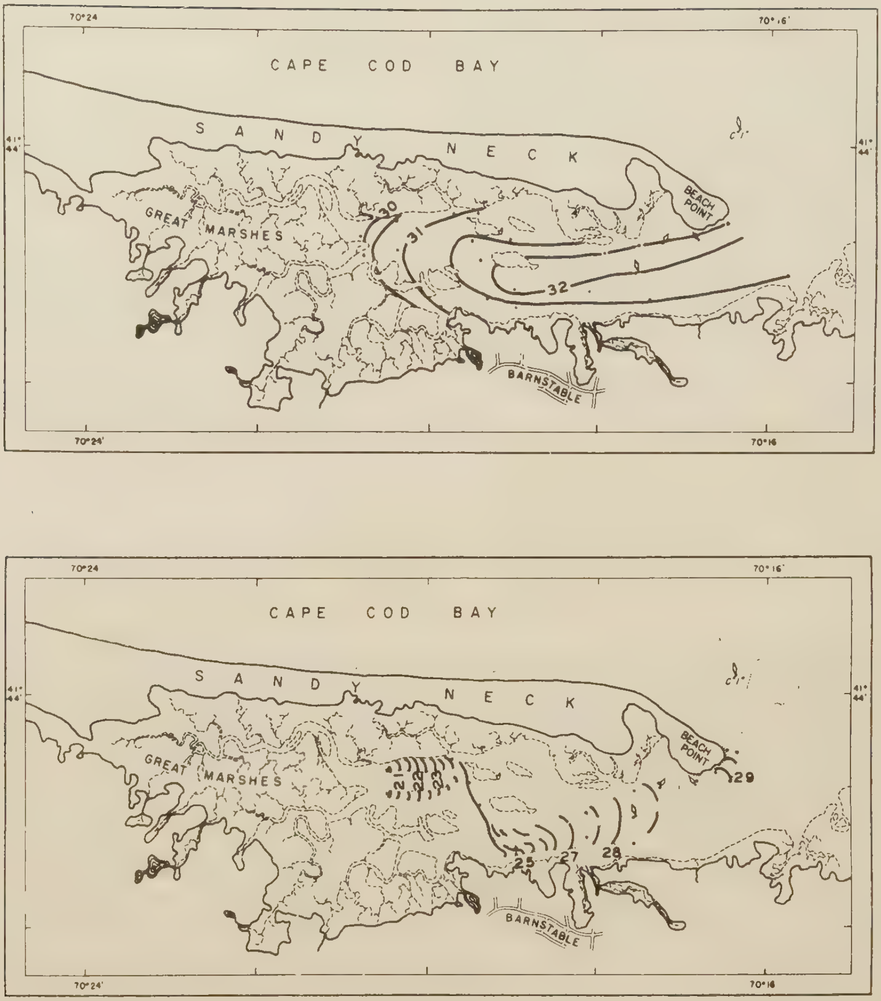
70°24
70°16'
CAPE COD BAY
SANDY NECK
GREAT MARSHES
BEACH POINT
BARNSTABLE
41°44'
30
31
32
70°24'
70°16
70°24
70°16'
CAPE COD BAY
SANDY NECK
GREAT MARSHES
BEACH POINT
BARNSTABLE
41°44'
29
25
27
28
70°24'
70°16

FIG. 5. Distribution of surface salinity (‰) during spring freshet. 12 and 16 April 1948. *Above*: at high water. *Below*: at low water.

TABLE 3. *Salinity ranges in various parts of Barnstable Harbor*
Spring freshet conditions are starred.

Location	Salinity range, ‰	Position in harbor
Beside WHOI flat	20.46*–31.40	Head of harbor
Off Sand Island	29.63 –31.73	Near head of harbor
Phillis Island Channel	24.51*–31.89	Near middle of harbor
Off Maraspin Creek mouth	27.38*–31.71	Below middle of harbor
Off Cobb's Village	28.49*–31.62	South shore near inlet
The Cove	28.62*–31.67	North shore near inlet
Beside Yarmouthport flat	31.38 –32.14	South shore, at inlet

TABLE 4. *Orientation table*

The numbers in Figure 1, and the station letters in the B and D parts of Figures 7 through 10, indicate the following locations.

1. Wicks Island
2. Experimental area of Woods Hole Oceanographic Institution
3. Howes' flat
4. Bung-hole flat
5. Gull Island flat
6. Maraspin Creek
7. Yacht Club Channel
8. Horseshoe Shoal
9. Midway Channel
10. North Channel
11. Phillis Island Channel
12. Sand Island
13. Wells Creek
14. Scudders Lane Landing
15. Scorton Creek
16. Spring Creek
17. Fisherman's Gut
18. Cobb's Village
19. The Cove
20. Yarmouthport flats
21. Big Thatcher Island
22. Phillis Island

A. Buoy "C 1"
B. Buoy "C 3"
C. Buoy "C 5"
D. Buoy "N 4"
E. Main channel, off Maraspin Creek
F. "14" in Figure 1
G. Main channel, west of Phillis Island
H. North Channel, off mouth of Wells Creek
I. "15" of Figure 1
J. Buoy "C 3"
K. "7" of Figure 1
L. Midway, south of the W. H. O. I. flat
M. "16" of Figure 1
N. North edge of Beach Point, west side of channel
O. "9" in Figure 1
P. North edge of Beach Point, east side of channel
Q. "11" in Figure 1
R. North Channel, north of W. H. O. I. flat
S. "17" in Figure 1

variation during a tidal cycle than are flats in the center of the harbor. Similar conditions have been observed in the Tees (Alexander *et al.* 1935) and in the Tamar (Milne 1938).

Although flats along the axis of the harbor are subject to more salinity variation than those along the shore, they are not subject to the whole salinity range of that part of the harbor. At low tide the least saline water encircles them, but does not cover them. It is pushed up-harbor before the flats are overflowed by the flood tide, and the flats have emerged before this water returns again during the late ebb. In the same fashion, tidal pools on the higher grassy islands are of greater salinity than those on lower islands. Increased evaporation during their longer periods out of water may also contribute to their increased salinity.

The distance of a flat from the mouth of the harbor determines which water types bathe it. Most of the flats are submerged only during the more saline two-thirds of the normal salinity range obtaining in that part of the harbor.

Table 3 gives the salinity ranges of the water in various parts of the harbor. All of the salinities observed have been used; they include conditions of drouth, of spring freshet, and of all stages of the tide. In those parts of Table 3 which include freshet values, the normal variation in salinity is approximately the most saline one-quarter of the range indicated.

Temperature distribution

Water temperatures in the harbor do not reflect the origin or composition of the water, for they depend upon the previous association of the water with the harbor. Water which has ascended furthest into the harbor is the warmest or coolest depending upon the season. In spring and summer, water passing up the harbor is warmed; in fall and winter it is cooled. The temperature of the water in any part of the harbor at low tide reflects (by its degree of heating or cooling relative to the Cape Cod Bay Water at Beach Point) the previous high-tide position of that water in the harbor.

Water remaining in the harbor at low tide is essentially isothermal from surface to bottom. The tortuous nature of the channels, irregularities on the channel bottoms, and the high velocity of the late ebb current produce thorough mixing.

During early flood the channels overflow; in spring and summer the overflowing water absorbs heat which the flats have

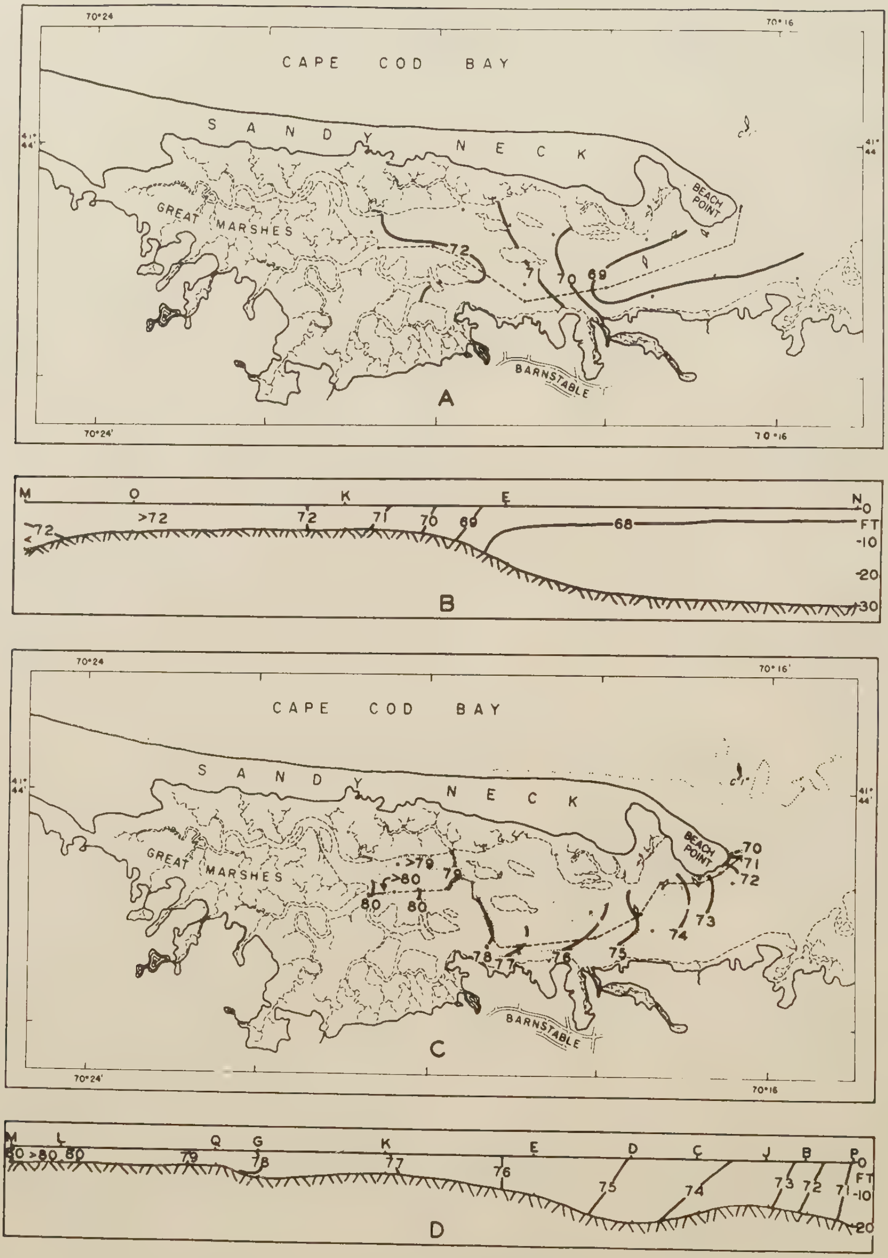
70°24
70°16
CAPE COD BAY
SANDY NECK
GREAT MARSHES
BEACH POINT
BARNSTABLE
41°44'
72
71
70
69
A
M
O
K
E
N
>72
72
71
70
69
68
0
FT
-10
-20
-30
B
>79
>80
79
80
80
70
71
72
73
74
75
76
77
78
C
M
L
Q
G
K
E
D
C
J
B
P
80
>80
80
79
78
77
76
75
74
73
72
71
0
FT
-10
-20
D

FIG. 6. Horizontal and vertical distributions of temperature (°F) in summer. 25 and 29 August 1947. Heavy dashed lines in A and C show the positions of vertical sections B and D. Station letters in B and D are as listed in Table 4. A and B at high water; C and D at low water.

acquired during their exposure to the sun and air. After the flats become submerged, the water is still shallow enough for sunlight to reach bottom throughout most of the flood tide period. During this time continued warming of the bottom by the sun and continued transfer of heat from bottom to water are both probable.

A similar warming occurs during ebb when water over the flats becomes shallow and

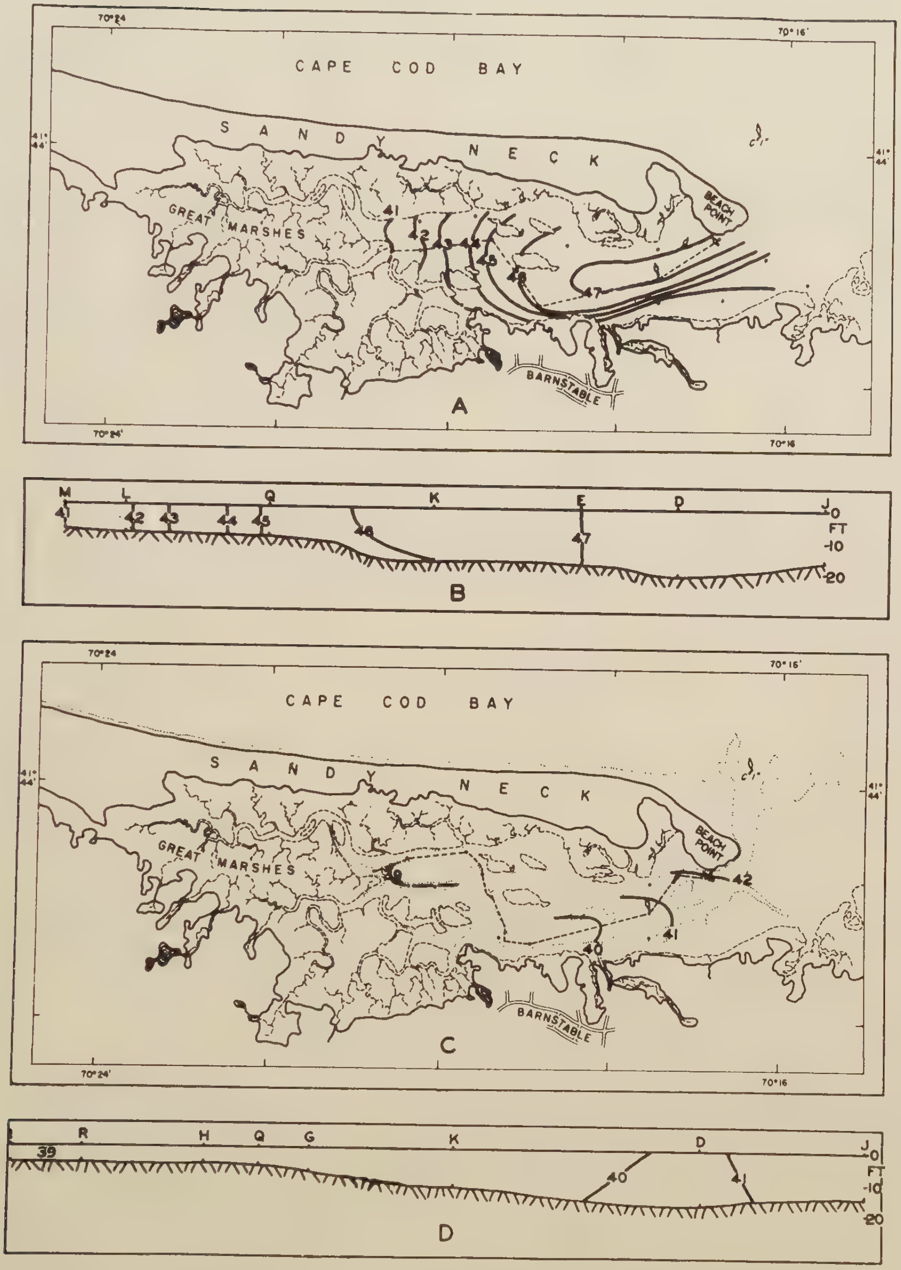
70°24'
70°16'
41°44'
CAPE COD BAY
SANDY NECK
GREAT MARSHES
BEACH POINT
BARNSTABLE
41
42
43
44
45
46
47
A
M
L
Q
K
E
D
J
0
FT
-10
-20
B
40
41
42
C
R
H
G
39
D

FIG. 7. Horizontal and vertical distributions of temperature (°F) in fall. 17 November 947. Heavy dashed lines in A and C indicate the positions of vertical sections B and D. Station leters in B and D are listed in Table 4. A and B at high water; C and D at low water.

ecedes from the flats. The warming taking lace during the ebb tide is more readily oted than that during the flood, for by ow tide the warmed waters have accumuated in the channels.

In surveys made at high water during the spring and summer the subsurface water is occasionally observed to be warmer than the surface. This water appears to be unstable and the condition temporary. In

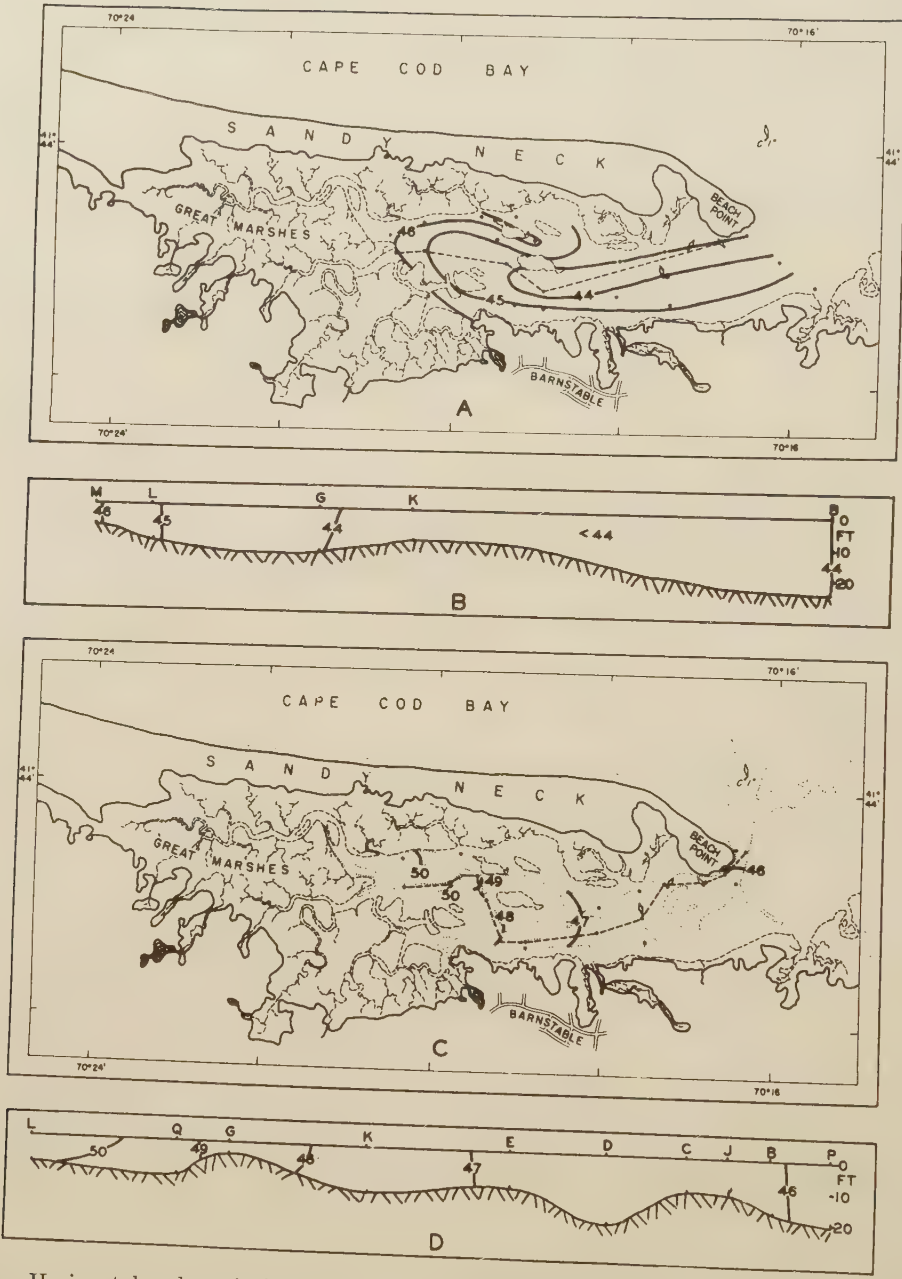
70°24
70°16'
CAPE COD BAY
SANDY NECK
GREAT MARSHES
BEACH POINT
BARNSTABLE
41°44'
48
45
44
A
70°24'
70°16
M
L
G
K
B
46
45
44
<44
44
0
FT
10
20
B
70°24
70°16'
CAPE COD BAY
SANDY NECK
GREAT MARSHES
BEACH POINT
BARNSTABLE
41°44'
50
49
50
48
47
46
C
70°24'
70°16
L
Q
G
K
E
D
C
J
B
P
50
49
48
47
46
0
FT
-10
-20
D

FIG. 8. Horizontal and vertical distributions of temperature (°F) during spring freshet. 12 and 16 April 1948. Heavy dashed lines in A and C indicate the positions of the vertical sections B and D. Station letters in B and D are listed in Table 4. A and B at high water; C and D at low water.

practically all cases this occurs in water shallow enough for sunlight to penetrate to bottom.

Figures 6, 7, and 8 show temperature distributions in summer, fall, and spring.

The transition periods

Twice a year the harbor goes through a transition period when its temperature approaches that of Cape Cod Bay. One of these periods occurs in late March or early

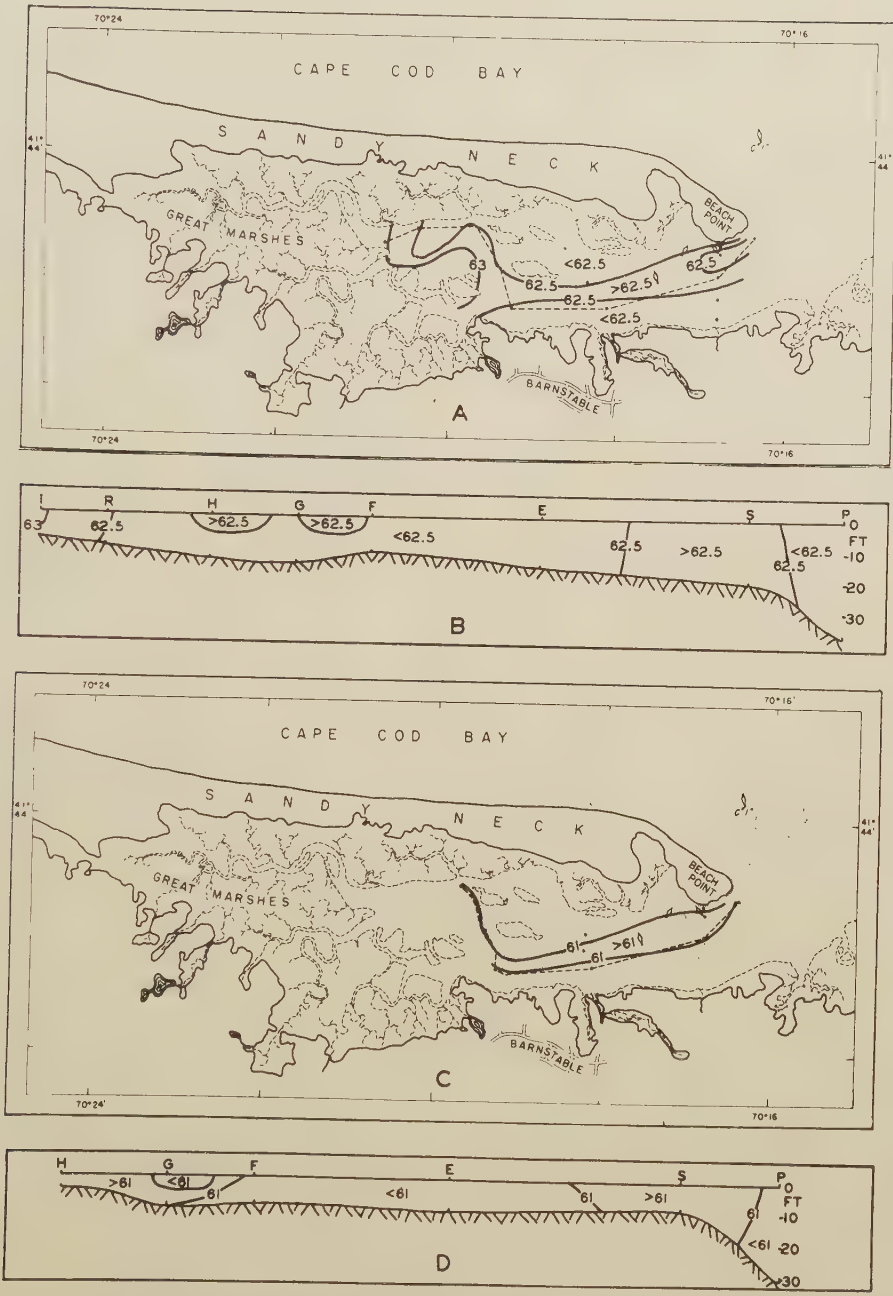
70°24
70°16
CAPE COD BAY
SANDY NECK
41° 44'
GREAT MARSHES
BEACH POINT
63
<62.5
62.5
>62.5
62.5
<62.5
62.5
BARNSTABLE
A
I
R
H
G
F
E
S
P
63
62.5
>62.5
>62.5
<62.5
62.5
>62.5
<62.5
62.5
0
FT
-10
-20
-30
B
CAPE COD BAY
SANDY NECK
GREAT MARSHES
BEACH POINT
61
>61
61
BARNSTABLE
C
H
G
F
E
S
P
>61
<61
61
<61
61
>61
61
<61
0
FT
-10
20
30
D

FIG. 9. Horizontal and vertical distributions of temperature (°F) during the fall transition period. 3 September 1948. Heavy dashed lines in A and C show the positions of the vertical sections. Station etters in B and D are listed in Table 4. A and B at high water; C and D at low water.

pril when the harbor's rather rapid spring arming overtakes the slower warming of ape Cod Bay. The other occurs when the arbor's rather rapid autumn cooling overtakes the slower cooling of Cape Cod Bay. At these times high-water and low-water temperatures become very nearly alike. In 1948 the fall transition took place during the latter part of September; Figure 9 presents surveys made on September 23rd.

Transparency

In summer, light penetrates to different depths in various parts of the harbor. Transparencies by white Secchi disc range from 6.5 feet in the Mixed Water at the head of the harbor to more than 13 feet in the Cape Cod Bay Water at Beach Point.

The decrease in transparency toward the head of the harbor is a reflection of the increasing amounts of plankton and suspended sediments which occur there.

REFERENCES

ALEXANDER, W. B., B. A. SOUTHGATE, AND R. BASSINDALE. 1931. Survey of the river Tees. Part II. The estuary—chemical and biological. Dept. Scient. Industr. Res. Water Pollution Res. Tech. Paper No. 2. His Majesty's Stationery Office, London. 22 pp.

AYERS, J. C. 1956. Population dynamics of the marine clam, *Mya arenaria*. Limnol. Oceanogr., **1** (1): 26–34.

DOODSON, A. T., AND H. D. WARBURG. 1941. Admiralty manual of tides. His Majesty's Stationery Office, London. 270 pp.

JOHNSON, D. W. 1925. The New England-Acadian shoreline. Wiley, New York. 608 pp.

MATHER, K. F., R. P. GOLDTHWAIT, AND L. R. THEISMEYER. 1942. Pleistocene geology of western Cape Cod, Massachusetts. Bull. Geol. Soc. Amer., **53** (8): 1127–1174.

MILNE, A. 1938. The ecology of the Tamar estuary. III. Salinity and temperature conditions in the lower estuary. J. Mar. Biol. Ass. U. K., **22** (2): 529–542.

SVERDRUP, H. U., M. W. JOHNSON, AND R. H. FLEMING. 1942. The oceans. Prentice-Hall, New York. 1087 pp.

U. S. Coast and Geodetic Survey. 1947–1949. Tide Tables, Atlantic coast of North America (for the years indicated).

Contribution No. 996

REPRINTED FROM THE JOURNAL OF EXPERIMENTAL BIOLOGY,
VOL. 36, NO. 2, pp. 369–376, JUNE 1959.
[*All rights reserved*] PRINTED IN GREAT BRITAIN

THE RESPONSES OF SNAILS TO POLARIZED LIGHT*†

BY EDWARD R. BAYLOR
Woods Hole Oceanographic Institution, Woods Hole, Mass.

(*Received* 21 *November* 1958)

The purpose of this paper is to call attention to the use of extra-ocular polarization analysis in the polarized light behaviour of a snail and to suggest that an extra-ocular polarization analyser could be employed by a number of organisms reported to orient to polarized light. Behaviour responses to polarized light have been reported for a number of arthropods: Verkhovskaya (1940), von Frisch (1949), Pardi & Papi (1953), Kerz (1950), Wellington, Sullivan & Green (1951), Wellington (1953, 1955), Stevens, Fingerman & Brown (1953), Baylor & Smith (1953, 1957*a*, *b*), and Vowles (1954*a*, *b*). The behaviour responses of a marine snail, *Littorina littorea*, to polarized light have been reported by Burdon-Jones & Charles (1958). The diversity of dioptric systems suggests that more than one mechanism of polarization analysis may be involved or that some ubiquitous polarizing analyser not directly associated with the dioptric system may exist.

Intra-ocular polarizing analysers suggested so far depend on the existence of 'Polaroid'-like (dichroic) structures as proposed by Autrum & Stumpf (1950); or they depend on a single reflexion-refraction at the air-corneal interface at the polarizing angle according to Stevens *et al.* (1953); or they depend on two separate double reflexion-refraction events at the corneal surface as suggested by Baylor & Smith (1953).

One extra-ocular polarizing analyser suggested by Baylor & Smith (1957*b*) for the honey bee proposes a non-uniform distribution of intensities in the pattern of light reflected from a substratum illuminated by polarized light. Vertical parallel rays of polarized light illuminating a substratum give rise to reflexions with minimum intensities in a direction parallel to the plane of polarization and maximum intensities perpendicular to the plane of polarization. But vertical parallel rays of non-polarized light illuminating a substratum give rise to reflexions of uniform intensities in all directions. In the escape reaction of the bee, orientation to polarized light occurs only if the bee is permitted to see the substratum and it occurs whether or not the bee is permitted to see the overhead source of polarized light illuminating the substratum. It remains to be seen whether the communication dances of bees described by von Frisch are mediated by extra-ocular polarization analysis or by some intra-ocular device. Indeed, in view of the non-uniform distribution of intensities reflected from appropriate substrata illuminated by polarized light it is possible that any positive phototaxis or even a light-directed klinokinesis can appear to be an ability to discriminate the plane of polarization.

---

* Contribution no. 996 from the Woods Hole Oceanographic Institution.
† Aided by a grant from National Institutes of Health.

Additionally, two other extra-ocular polarizing analysers may be available to organisms orienting to polarized light under water. Clay particles, yeast, bacteria, or phytoplankton suspended in water scatter light with greater intensity at right angles to the plane of polarization thereby providing an asymmetric intensity stimulus. The importance of using carefully filtered water for polarized light experiments is obvious. Compounds such as toluidine blue, tryptophane, riboflavine, and chlorophyll A fluoresce strongly. When these compounds are excited by polarized light fluorescence is emitted perpendicular to the plane of polarization. Such asymmetric fields of intensity produce orientation to polarized light in snails on non-analysing substrata.

METHODS AND RESULTS

The marine snail, *Nassa obsoleta*, employed in these experiments possesses a simple positive phototaxis like that of *Littorina littorea*. Both bearing and distance travelled are easily measured and provide an adequate description of the behaviour.

We did the following experiments to test whether *Nassa obsoleta* has a polarizing analyser in the eye or utilizes the pattern of intensity gradients reflected from the substratum. The snails were allowed to crawl on a substratum of black 'Lucite' illuminated by a vertical beam of light which also projected a Cartesian co-ordinate grid upon the substratum. The lines of the grid were extremely thin and did not interfere with the behaviour to be measured. Each time the snail crossed a line the event was counted. Thus the pathway of the animal is measured as the sum of all the X vectors and the sum of all the Y vectors. If orientation is random, the path lengths in the X and Y directions should be approximately equal to each other. In control experiments the light source was non-polarized. In experiments with polarized light the plane of polarization was used alternatively parallel to the X axis and to the Y axis so as to obviate any inherent bias in the system. The polished black 'Lucite' substratum showed no differential reflected intensity in non-polarized light but showed a slight differential reflected intensity in polarized light.

The results of control experiments using non-polarized light on black 'Lucite' show random orientation. In Fig. 1 the path lengths in the X and Y directions are plotted against each other. The points are distributed on both sides of the diagonal line which indicates randomness of orientation.

In contrast, results of experiments using polarized light on polished black 'Lucite' show definite orientation perpendicular to the plane of polarization. In Fig. 2, the path length perpendicular to the plate of polarization is plotted against the path length parallel to the plane of polarization. With few exceptions all the points lie above the diagonal.

In order to determine whether the organism could respond to substratum reflectivity, scratched 'Lucite' was used. The scratches on the black 'Lucite' were all parallel and threw the surface into tiny ridges and valleys. Non-polarized light striking the sides of the ridges is reflected predominantly at right angles to the direction of the scratches. Polarized light vibrating parallel to the direction of the scratches is well reflected at right angles but poorly reflected parallel to the direction of the scratches. Polarized light vibrating perpendicular to the direction of the scratches is poorly reflected perpendicular to the direction of the scratches, but is even more poorly reflected in the direction of the scratches.

Regardless of the plane of polarization of light the snails uniformly oriented perpendicular to the scratches. The data in Fig. 3 show that orientation was most pronounced when the plane of polarization was parallel to the scratches.

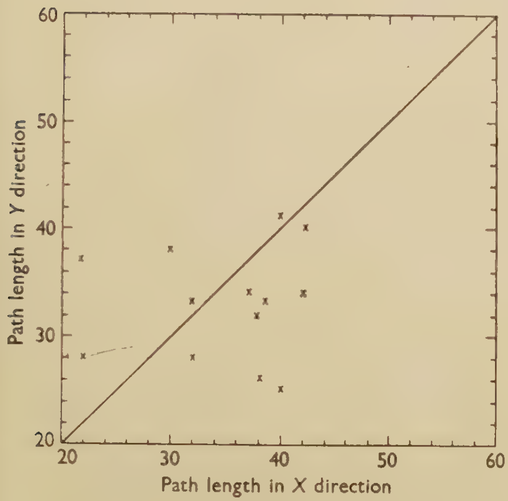

Fig. 1

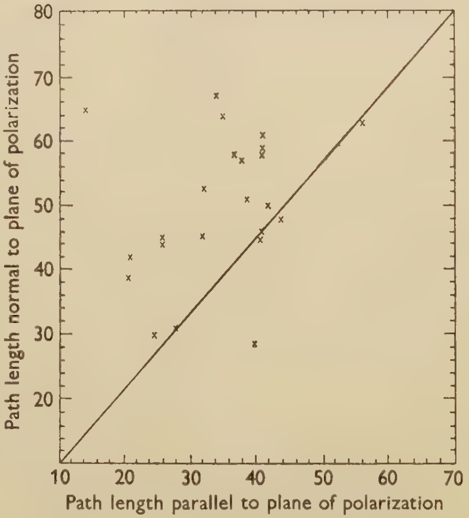

Fig. 2

Fig. 1. Orientation to non-polarized light by snails crawling on polished black 'Lucite'. Path lengths of the snails were measured and plotted on a Cartesian co-ordinate grid. When points fall equally on both sides of the diagonal line orientation is random.

Fig. 2. Orientation to polarized light by snails crawling on polished black 'Lucite'. The diagonal line represents random orientation. Orientation is predominantly at right angles to the plane of polarization.

To eliminate the possibility of snails seeing the overhead source of polarized light we attached black 'umbrellas' to the shell. The 'umbrella' was a circle of 'Scotch' photographic masking tape 10 to 20 mm. in diameter completely shading the tentacles bearing the eyes. A small area of the shell was scraped clean for attachment of the 'umbrella'. It is important that the attached 'umbrella' does not seriously alter the centre of gravity of the snail.

Snails carrying black 'umbrellas' in polarized light on polished black 'Lucite' oriented perpendicular to the plane of polarization although they could not see the incident radiation. The data from Fig. 4 show that this response was obtained in all but three experiments.

To eliminate the possibility of snails seeing the substratum and to assure their seeing only the overhead source of polarized light we caused them to crawl upside down underneath a plate of clear glass. The plate of glass was 25 mm. above the substratum. The snails carried their 'umbrellas' beneath them. It was necessary

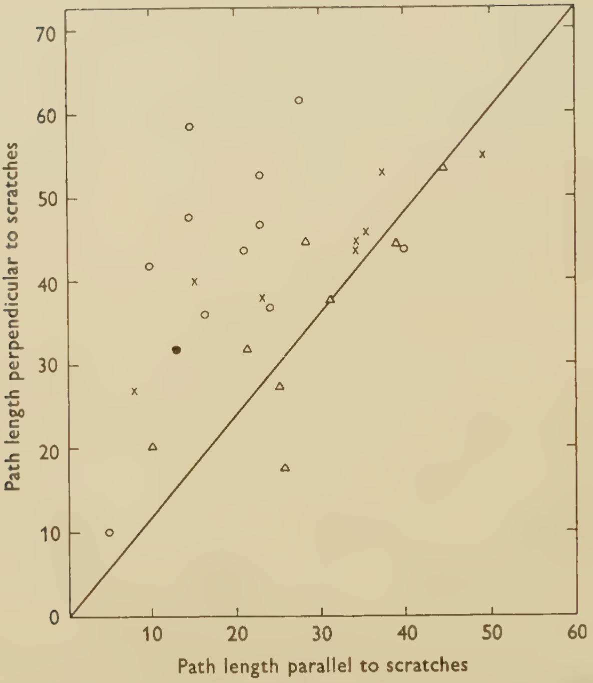

Fig. 3. Orientation of snails on scratched black 'Lucite'. Orientation to polarized light appears maximal when the plane of polarization is parallel to the scratches on the substratum. This combination of plane of polarization and direction of scratches produces maximum reflected intensity perpendicular to the scratches. The triangles are the path length in non-polarized light. Circles are path length when the plane of polarization is parallel to the scratches. Crosses are path lengths when the plane of polarization is perpendicular to the scratches.

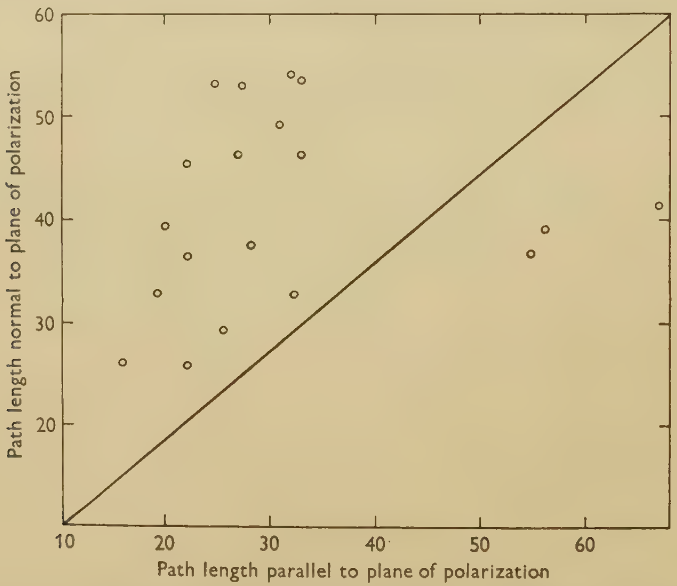

Fig. 4. Orientation to polarized light by snails carrying black 'umbrellas' while crawling upright on polished black 'Lucite'.

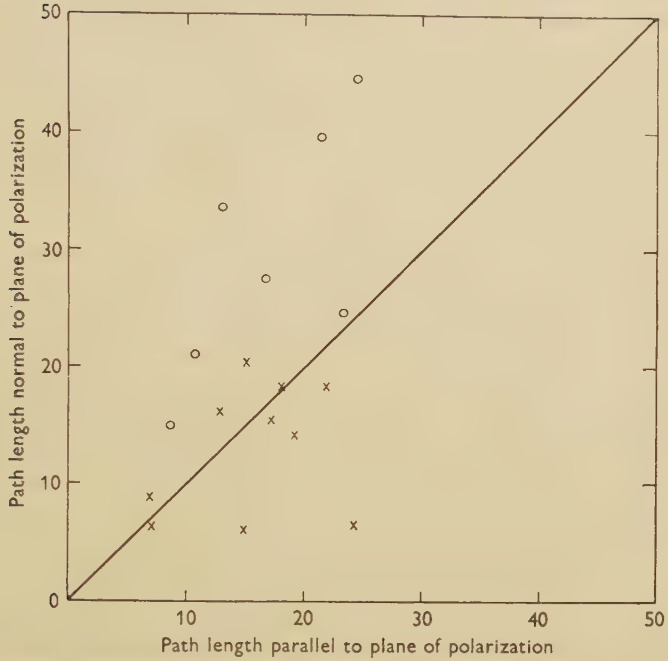

Fig. 5. Orientation to polarized light by snails crawling upside down with and without 'umbrellas' beneath them. Crosses show path lengths of snails with 'umbrellas' beneath them permitting no view of the polished black 'Lucite' substratum underneath but permitting a direct view of the polarized light source above. Circles show path lengths of snails without 'umbrellas' beneath them, permitting a view of both the substratum underneath and the polarized light source above. Orientation to polarized light appears best in snails permitted to see the substratum.

to attach a small float to prevent the snail from falling off the glass plate. No orientation was apparent in these experiments, shown in Fig. 5, although the overhead source of polarized light is fully visible to the snails. Control snails, in polarized light, crawling upside down and without 'umbrellas' orient almost as well as the snails crawling upright.

DISCUSSION

The conclusion from these experiments is that *Nassa obsoleta* under polarized light with all spurious reflexions reduced to a minimum is oriented by the intensity of substratum reflexions and not by a polarizing analyser within the eye. Also it follows from these experiments that the mere exhibition of an oriented response to polarized light does not inevitably imply the possession of a polarizing analyser within the eye.

An organism using extra-ocular polarization analysis orients to asymmetric directions of intensity or patterns of intensity which arise by: (1) preferential reflexion from the substratum; or by (2) preferential scatter from suspended particles such as yeast, algae, bacteria, clay, etc.; or by (3) preferential emission of fluorescence perpendicular to the plane of polarization of the exciting light in compounds like chlorophyll *a*, riboflavin, and chlorophyll degradation products.

So far extra-ocular polarization analysis appears to be principally a laboratory phenomenon. Its use by animals in the natural habitat is probably limited to situations where the sun but not all the sky is obscured from view, as for example in the shadow of a cliff, under trees, or in other conditions obscuring the sun. As a rule the normal intensity of light in the terrestrial environment is so much greater than the reflected intensity from polarized light that extra-ocular polarization analysis is not anticipated.

Three different mechanisms have been proposed as possible intra-ocular polarizing analysers. Autrum & Stumpf (1950) have suggested that the rhabdomeres of the honey bee are dichroic like 'Polaroid' and that they constitute more efficient receptors of polarized light than of non-polarized light. Stephens *et al.* (1953) have proposed that in accordance with the Fresnel laws a single reflexion-refraction at the corneal surface of the *Drosophila* eye serves as a polarization analyser. Baylor & Smith (1953) independently advanced a reflexion-refraction mechanism for the cladoceran and acarinid eye which involves a somewhat unusual light path having two reflexions and refractions.

The Autrum & Stumpf (1950) hypothesis of intra-ocular polarization analysis is intuitively appealing and suggests a model which is consistent with the experimental observations of von Frisch (1950) on the communication dances of bees. But actual proof of the model as a valid analogue to the eye is lacking. Menzer & Stockhammer (1951) reported birefringence of bee rhabdomeres, but they used fixed material for their observations. Using unfixed material, de Vries *et al.* (1953) finds that the birefringence, if it exists, of the bee rhabdomere is less than 1 %. The principal experimental evidence advanced by Autrum & Stumpf (1950) in favour of their model was a contention that the insect compound eye is a more efficient receptor of polarized light. This contention was based on a slightly greater magnitude electroretinogram voltage associated with polarized light stimulation than with non-polarized light stimulation. They employed a 50 % neutral density filter to give non-polarized light of the same intensity as polarized light. Thus the increased electroretinogram voltage with polarized light in their experiments can be anticipated from the fact that most 'Polaroids' are not good neutral density filters. On the contrary, depending on the conditions of manufacture, they leak at one end of the visible spectrum or at both ends. When a light source is viewed through such polaroids crossed exactly at 90 degrees to each other the light source appears blue, red, or purple. Baylor & Kennedy (1958) using better intensity and wavelength control failed to corroborate the results of Autrum & Stumpf (1950) and adduced other evidence against a dichroic model of the bee eye. Further, extra-ocular polarization analysis has been demonstrated in the escape reaction of the honey bee by Baylor & Smith (1957*b*). Their findings, which are consistent with the experimental observations of von Frisch (1950), suggests that the communication dances of the bee are 'cued' by extra-ocular polarization analysis. Although their interpretation remains to be proved, it provides a more parsimonious explanation of von Frisch's observations than the Autrum & Stumpf model.

It is quite feasible for such organisms as *Cladocera*, having both an intra-ocular polarizing analyser and apositive phototaxis, to utilize both intra- and extra-ocular polarization analysis simultaneously. It is not clear at this time how much substratum reflexion contributes to the polarized light responses of *Cladocera* but the polarized light response persists when substratum reflexions, fluorescence, and suspended particle scatter are eliminated.

In addition to substratum reflexion, *Cladocera* utilize the asymmetric intensity of scattered light found when a suspension of yeast or algae is illuminated by polarized light. Similarly, the asymmetric intensity of fluorescence of riboflavin, toluidine blue, chlorophyll degradation products, etc., excited by polarized light appears to enhance the response of daphnids.

There is no good evidence available at this time for cladoceran orientation to the polarized light of the sky.

It is unfortunate that some papers in the literature strongly imply that because there is a response to polarized light, it therefore must have evolutionary adaptive value as a navigational aid. Any timidity in pressing this classical fallacy of teleology is understandable. The invocation of polarized light as a navigational aid is probably unnecessary because usually when the sky is strongly polarized the sun is visible and inference of solar azimuth by polarized light becomes redundant. Pre-sunrise and post-sunset skies may constitute important exceptions and although both starlight and 'Gegenschein' are polarized there is as yet no necessity to invoke the polarization of either as an explanation of animal behaviour.

In concluding this discussion it seems worth while to suggest that most instances of polarized light response reported in the literature should be re-examined to determine whether they are 'cued' by intra-ocular or extra-ocular polarization analysis.

SUMMARY

1. Experiments were performed to test whether the polarized light responses of the marine snail, *Nassa obsoleta*, are mediated by a polarizing analyser within the eye or by the pattern of intensities reflected from the substratum.

2. Snails able to see only the substratum orient at right angles to the plane of vibration of vertically incident polarized light.

3. Snails unable to see the substratum but able to see the overhead source of polarized light fail to orient to the polarized light.

4. Implications regarding the rare occurrence of intra-ocular polarizing analysers and the improbability of extensive animal use of polarized light as a navigational aid are discussed.

REFERENCES

AUTRUM, H. & STUMPF, H. (1950). Das Bienenauge als Analysator für polarisiertes Licht. *Z. Naturf.* **5*b***, 118–112.

BAYLOR, E. R. & SMITH, F. E. (1953). The orientation of *Cladocera* to polarized light. *Amer. Nat.* **87**, 97–101.

BAYLOR, E. R. & SMITH, F. E. (1957*a*). Diurnal migration of plankton crustaceans. *Recent Advances in Invertebrate Physiology*, 21–36. University of Oregon Press.

BAYLOR, E. R. & SMITH, F. E. (1957*b*). Bees and polarized light. *Symposium on Pattern Recognition* 1957 (ed. W. P. Tanner, Jr). Ann Arbor, Michigan: Project Michigan Press.

BAYLOR, E. R. & KENNEDY, D. (1958). Evidence against a polarizing analyzer in the bee eye (in the Press).

BURDON-JONES, C. & CHARLES, G. H. (1958). Light reactions of littoral gastropods. *Nature, Lond.*, **81**, 129–31.

DE VRIES, H. L., SPOOR, A. & JIELOF, R. (1953). Properties of the eye with respect to polarized light. *Physica*, **19**, 419–32.

FRISCH, K. VON (1949). Die Polarisation des Himmelslichtes als orientierender Faktor bei den Tänzen der Bienen. *Experientia*, **5**, 142–8.

FRISCH, K. VON (1950). Die Sonne als Kompass im Leben der Bienen. *Experientia*, **6**, 210–21.

KERZ, M. (1950). Wahrnehmung polarisierten Lichtes durch *Eupagurus*. *Experentia*, **6**, 427.

MENZER, G. & STOCKHAMMER, K. (1951). Zur Polarisationsoptik der Facettenaugen von Insekten. *Naturwissenschaften*, **38**, 190.

PARDI, L. & PAPI, F. (1953). Richerche sull'orientatamento di *Talitrus saltator* (Montagu) (Crustacea—Amphipoda). II. *Z. vergl. Physiol.* **35**, 490–518.

STEPHENS, GROVER C., FINGERMAN, M., & BROWN, F. A. (1953). The orientation of Drosophila to plane polarized light. *Ann. Ent. Soc. Amer.* **46**, 75–83.

VERKHOVSKAYA, I. (1940). L'influence de la lumière polarisée sur la phototaxis de quelques organismes. *Bull. Soc. Nat. Moscou* (Sect. Biol.), **49**, 101–13.

VOWLES, D. M. (1954*a*). The orientation of ants. I. The substitution of stimuli. *J. Exp. Biol.* **31**, 341–54.

VOWLES, D. M. (1954*b*). The orientation of ants. II. Orientation to light, gravity, and polarized light. *J. Exp. Biol.* **31**, 356–75.

WELLINGTON, W. G., SULLIVAN, C. R. & GREEN, G. W. (1951). Polarized light and body temperature level as orientation factors in the light reactions of some hymenopterous and lepidopterous larvae. *Canad. J. Zool.* **29**, 339–51.

WELLINGTON, W. G. (1953). Motor responses evoked by the dorsal ocelli of Sarcophaga aldrichi Parker, and the orientation of the fly to plane polarized light. *Nature, Lond.*, **172**, 1177.

WELLINGTON, W. G. (1955). Solar heat and plane polarized light versus the light compass reaction in the orientation of insects on the ground. *Ann. Ent. Soc. Amer.* **48**, 67–76.

Contribution No. 997

Reprinted from

PHYSIOLOGIA PLANTARUM, VOL. 12. 1959

The Sensitivity of Several Algae to Ultraviolet Radiation of 2537 Å

By

G. C. McLeod [1] and Jack McLachlan [2]

Woods Hole Oceanographic Institution, Woods Hole, Massachusetts

Contribution no. 997
(Received November 15, 1958)

Introduction

Numerous workers have shown that algae, in common with other organisms, may be killed or mutated by ultraviolet radiations. There have been relatively few studies, however, on the comparative sensitivity of unicellular algae to ultraviolet radiations. In a recent paper, Holt, Brooks, and Arnold (1951) showed that Scenedesmus spp. and Chlorella pyrenoidosa had widely different sensitivities to ultraviolet radiation of 2537 Å. The experiments in this study extend these observations to several marine and fresh water algal species at different stages in their growth cycle.

Materials and Methods

Cultures of fresh water and marine algae were used in this study. The fresh water green species used were *Chlorella vulgaris, Scenedesmus quadricauda, Ankistrodesmus falcatus,* and the yellow-green alga *Botryococcus braunii.* The marine species included the greens, *Chlorella* sp., *Platymonas subcordiformis, Dunaliella euchlora* WHOI-1, and the diatoms *Phaeodactylum tricornutum,* and *Skeletonema costatum.* Natural marine populations were collected with a number 20 plankton net from Woods Hole Harbor.

---

[1] Present address: Biological Laboratories, Harvard University, Cambridge, Massachusetts

[2] Public Health Service Research Fellow of the National Institutes of Health.

Fresh-water algal cultures were grown in Rodhe's VIII medium (1948), and the marine species in a modification (McLachlan 1959) of the ASP medium of Provasoli *et al.* (1957). Illumination was provided by fluorescent lights, and the cultures were grown at an intensity of approximately 6,000 meter-candles at 16°C. Culture vessels were 125 ml. Erlenmeyer flasks containing 50 ml. of medium.

Growth was measured by cell counts using a Levy heamocytometer. The results are expressed as the $\log_2 N_t/N_0$, where N_0 is the initial cell concentration and N_t the cell concentration at time t. Photosynthesis was measured by the uptake of $C^{14}O_3=$ according to the procedure of Steemann Nielsen (1952), and pigment analyses were made spectrophotometrically (Yentsch 1957).

A stirred suspension of cells was irradiated in a rectangular lucite chamber (20 ml. volume) with quartz end windows. The chamber was placed eight millimeters from a Westinghouse germicidial lamp (No. 794-H) which emitted nearly monochromatic 2537 Å. The intensity at the end window of the chamber determined with an Eppley thermopile connected to a galvanometer was approximately 136 microwatts per square centimeter. Controls were irradiated in pyrex vessels, which do not transmit 2537 Å, to check for any loss of activity not attributable to the ultraviolet radiation.

To control the absorption of incident energy during growh, suspensions were adjusted to the same cell density prior to irradiation. The cells were then irradiated for one hour with 2537 Å (with a total intensity of eight millijoules per square centimeter). Then the irradiated and control cells were "tagged" with carbon 14, and placed under 6,000 meter-candles of illumination at 16°C for one hour. At the end of this time the suspensions were filtered, dried, and the photosynthetic capacity determined by the amount of radioactivity. The pigments were determined spectrophotometrically. The data are expressed as the relationship between the carbon 14 uptake after irradiation (R_0) relative to the carbon 14 uptake of the non-irradiated suspensions (R).

Results

A histogram, Figure 1, shows the relative sensitivities of several algae to 2537 Å. The species fall into three groups. Diatoms and the natural populations, which were predominantly diatoms, are most sensitive. *Scenedesmus*

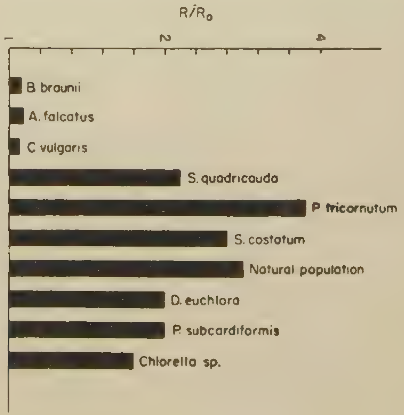

Figure 1. *Sensitivity of different algal species to 2537 Å.*

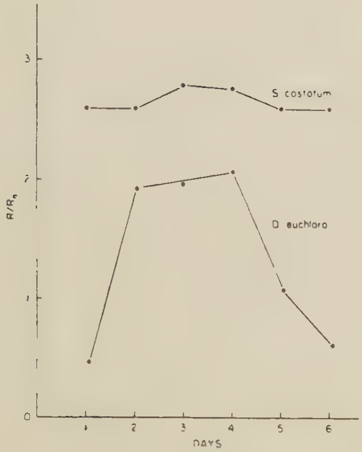

Figure 2.

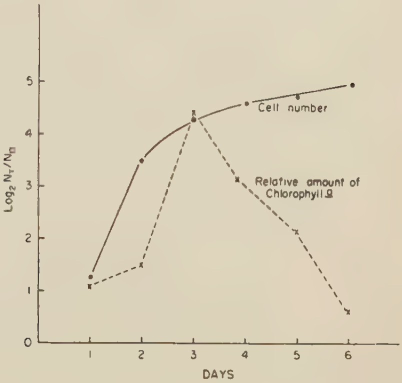

Figure 3.

Figure 2. *Relative sensitivity of photosynthesis* (R_0/R) *of Dunaliella euchlora and Skeletonema costatum to 2537 Å.*

Figure 3. *A comparison of the growth of cells and the change of the chlorophyll a content to 2537 Å in Dunaliella euchlora.*

quadricauda and the marine green algae were not as sensitive as the diatoms, but were more sensitive than the other fresh water species.

The comparative sensitivity of the algae at different stages in the growth cycle is illustrated for *Skeletonema costatum* and *Dunaliella euchlora* in Figure 2. There is a relatively low sensitivity during the lag phase of growth, followed by a marked increase during the logarithmic phase of growth. The maximum sensitivity is reached at the end of the logarithmic phase, and as the stationary phase progresses there is a gradual decline to the initial level.

Figure 3 also shows that there is a concomitant change in the pigment concentration of *Dunaliella euchlora* during the growth cycle that parallels the impairment of photosynthesis by 2537 Å. This same phenomenon occurred in the other species.

Discussion

It has recently been suggested (Clayton *et al.* 1958) that the carotenoid pigments act as a screen or block to ultraviolet radiation, and that ultraviolet damage is incurred in cells with a low carotenoid content. Diatoms, however, with a relatively high carotenoid content, are more sensitive to 2537 Å than the green algae. Since fucoxanthin efficiently transfers the energy to chlorophyll *a* (Duysens 1952), this implies that the carotenoid screen is only effective if these pigments are not closely associated with the photosynthetic mechanism.

The present results show that algae have widely different sensitivities to 2537 Å radiation. The form of the curve after radiation depends on the stage of growth of the culture. Similar results have been obtained by other workers with bacterial species subjected to ionizing radiations (Stapleton 1952). Since irradiated cells are able to perform most if not all of the normal metabolic functions, these results suggest a specific inhibition. The correct interpretation, however, must rest on a better knowledge of the effect of age, nutritional status, and other environmental factors on the sensitivity of cells exposed to ultraviolet radiation.

Summary

The comparative sensitivity of several algae, during growth, to 2537 Å is as follows: (1) a low sensitivity during the lag phase of growth, followed by an increase during the logarithmic phase of growth, and (2) a decline in sensitivity during the stationary phase of growth. There is a concomitant change in pigment content which parallels the impairment of photosynthesis by 2537 Å.

Appreciation is extended to Dr. B. H. Ketchum and Dr. J. H. Ryther for a critical reading of the manuscript. Supported in part by a grant (G 2510) from the National Science Foundation.

References

Clayton, R. K., Bryan, W. C. & Frederick, A. C.: Some effects of ultraviolet on respiration in purple bacteria. — Arch. Mikrobiol. 29: 213. 1958.

Duysens, L. N. M.: The transfer of excitation energy in photosynthesis. — Thesis. Utrecht. 1952.

Holt, A. S., Brooks, I. A. & Arnold, W. A.: Some effects of 2537 Å on green algae and chlorophyll preparations. — Jour. Gen. Physiol. 34: 627. 1951.

McLachlan, J.: The growth of unicellular algae in artificial and enriched sea water media. — Can. Jour. Microbiol. 5: 9. 1959.

Provasoli, L., McLaughlin, J. J. A. & Droop, M. R.: The development of artificial media for marine algae. — Arch. Mikrobiol. 25: 392. 1957.

Rodhe, W.: Environmental requirements of fresh water plankton algae. — Symb. Bot. Ups. 10: 1. 1948.

Stapelton, G. E.: Variations in the radio-sensitivity of Escherichia coli during the growth cycle. — Ph. D. Thesis, Univ. Tenn. 1952.

Steemann Nielsen, E.: The use of radio-active carbon (C^{14}) for measuring organic production in the sea. — Jour. du Cons. 18: 117. 1952.

Yentsch, C. S.: A non-extractive method for the quantitative estimation of chlorophyll in algal cultures. — Nature 179: 1302. 1957.

Contribution No. 999

Reprinted from "Physics and Chemistry of the Earth, Vol. 3."
PERGAMON PRESS
LONDON • NEW YORK • PARIS • LOS ANGELES

Printed in Great Britain by Pitman Press, Bath

2

GEOPHYSICAL INVESTIGATIONS IN THE EASTERN CARIBBEAN: SUMMARY OF 1955 AND 1956 CRUISES

By C. B. Officer, J. I. Ewing, J. F. Hennion, D. G. Harkrider and D. E. Miller

INTRODUCTION AND ACKNOWLEDGEMENTS

During the past several years there has been a number of investigations of crustal structure beneath oceanic areas through the use of seismic refraction techniques. These investigations have led to an increased knowledge of the composition and structure of the geologic strata and crust underlying such areas as the ocean basins themselves, oceanic islands and their immediate vicinity, mid-ocean mountain ranges, continental margins, basins of interior seas, and island arcs and deep sea trenches. This paper is concerned with an intensive examination of an island arc and deep sea trench and its associated interior basin.

The area covered is shown in Fig. 1 and 2. Briefly the geography is as follows. To the east and north-east is the Atlantic basin. To the west is the interior Venezuelan basin. The depths of water in the Venezuelan basin, around 2500 fathoms, are nearly as great as those in the Atlantic basin. Between the two are the Lesser and Greater Antilles island arc, the Puerto Rico trench, and the Barbados ridge. The island arc of the Lesser Antilles extends out from South America and curves around to the north-west. It is continued to the west by the Greater Antilles of which the island of Puerto Rico and the eastern tip of Hispaniola are shown in Figs. 1 and 2.* Exterior to the island arc is the Barbados ridge. It is a continuation of the Venezuelan geosyncline of north-eastern Venezuela and Trinidad. It also curves around to the north-west and gradually disappears as a topographic feature north-east of the island of Guadalupe. Its axis lies between that of the Antilles island arc and the Puerto Rico trench. The Puerto Rico trench parallels the island arc. It is deepest north of Puerto Rico and curves around to the south-east at diminishing depth. These are the major geographic features. Of smaller size is the Aves swell, a broad swell interior to the island arc. The area between the Aves swell and the Lesser Antilles is referred to as the Grenada trough. The area between the Lesser Antilles and the Barbados ridge is referred to as the Tobago trough.

The locations of the seismic refraction profiles have been shown on Fig. 1. The first set was made during the spring of 1955 and the second during the summer of 1956. The 1955 work was conducted from the research vessels *Atlantis* and *Caryn* and the 1956 work from the research vessels *Atlantis* and

---

* The bathymetry for Figs. 1 and 2 came primarily from U.S. Navy Hydrographic Office chart 5487.

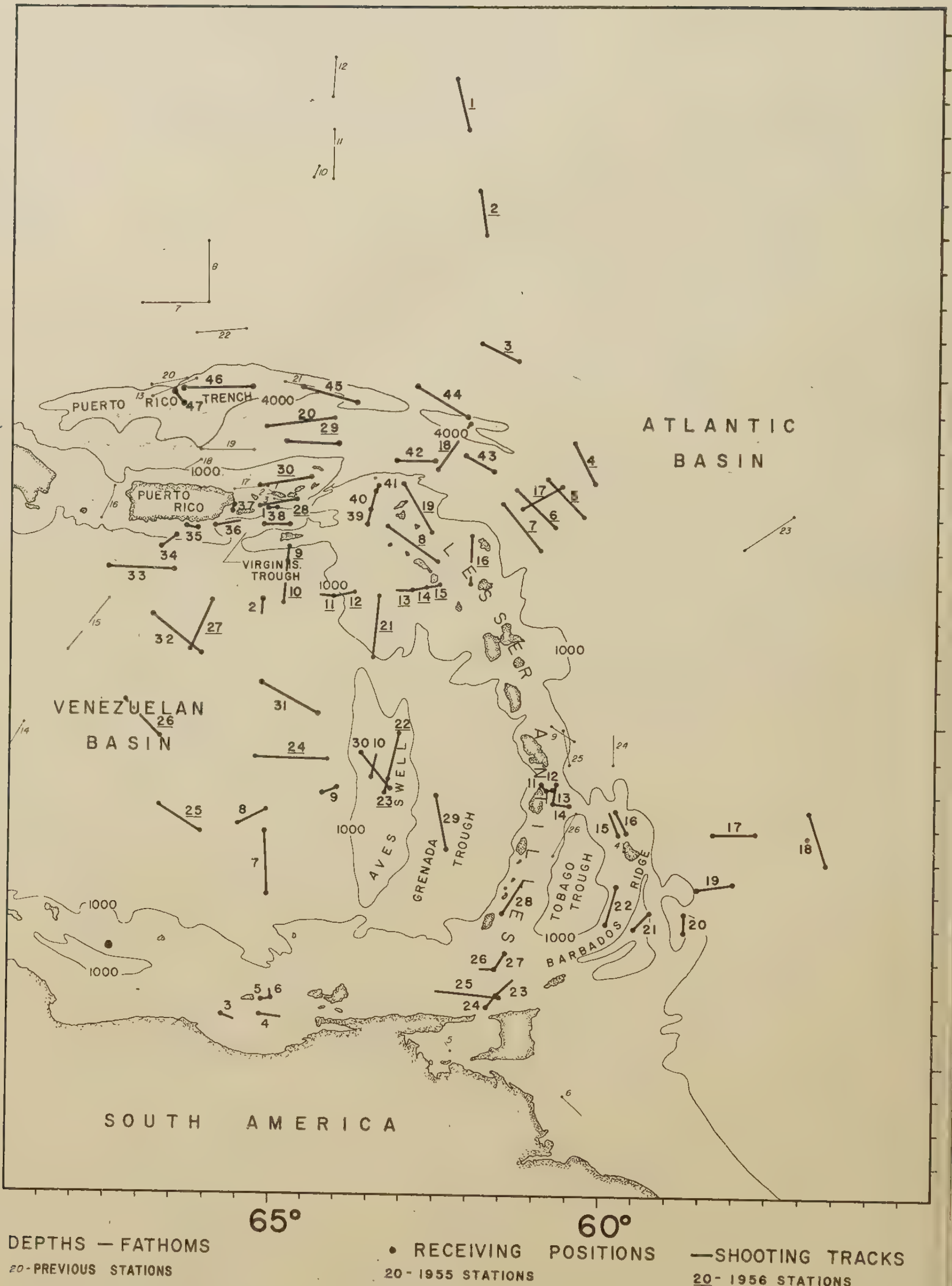
ATLANTIC BASIN
PUERTO RICO TRENCH
PUERTO RICO
VIRGIN IS. TROUGH
VENEZUELAN BASIN
AVES SWELL
GRENADA TROUGH
TOBAGO TROUGH
BARBADOS RIDGE
LESSER ANTILLES
SOUTH AMERICA
1000
4000
65°
60°
DEPTHS — FATHOMS
20 - PREVIOUS STATIONS
• RECEIVING POSITIONS
20 - 1955 STATIONS
—SHOOTING TRACKS
20 - 1956 STATIONS

Fig. 1. Geographic map of Eastern Caribbean with seismic refraction stations.

Bear, all of the Woods Hole Oceanographic Institution. A great deal of the success of both cruises was due to the fine co-operation of captains W. S. Bray, E. J. Mysona and A. Karlson and the crews of the *Atlantis*, *Bear*, and *Caryn* respectively. The scientific equipment for both cruises came from the Woods Hole Oceanographic Institution and the Lamont Geological Observatory, Columbia University. The scientific personnel engaged in one or more phases of the 1955 cruise were A. Bradshaw, W. Dunkle, G. Duys, R. S. Edwards, J. Hahn, H. R. Johnson, W. Moss, C. B. Officer, D. Owen, F. Richards, M. Rutstein, J. Ryther and R. Vaccaro, Woods Hole Oceanographic Institution; J. I. Ewing, Lamont Geological Observatory; W. Hudson, Western Electric Co.; and S. Wardani, Scripps Institute of Oceanography. The scientific personnel engaged in the 1956 cruise were J. I. Ewing and J. F. Hennion, Lamont Geological Observatory; R. S. Edwards, Woods Hole Oceanographic Institution; C. B. Officer, Rice Institute; J. W. Berg, University of Utah; J. Rose, University of Wisconsin; and W. L. Clarke, D. A. Fahlquist, G. Fermi, T. Gifft, D. Lum, and R. P. von Herzen, and L. J. Barnes, D. G. Harkrider, T. W. Lawhorn, M. Loughridge, D. E. Miller and J. J. Sisler, students at Harvard University, Massachusetts Institute of Technology, Princeton University, Cornell University, University of Utah, Scripps Institute of Oceanography, and Rice Institute respectively. These investigations were supported through contracts Nonr 1367, Nonr 2116, Nonr 2129, NObsr 43270, NObsr 43355, and NObsr 64547 with the U.S. Navy and through the Associates Fund of the Woods Hole Oceanographic Institution. The explosives were supplied by the Bureau of Ordnance, U.S. Navy. Drs. J. B. Hersey and C. O. D. Iselin of the Woods Hole Oceanographic Institution and Prof. M. Ewing of Lamont Geological Observatory were helpful in making these expeditions possible. One or more of the five authors of this paper analysed each profile; the conclusions are those primarily of the first three authors. Two papers have been published previously on the results of the 1955 cruise, OFFICER *et al.* (1957) and EWING *et al.* (1957).

A number of other seismic refraction profiles have been made throughout this area. Their locations have been included for reference in Fig. 1. Previous to this investigation there were three profiles around the island of St. Thomas (1–3), one near Barbados (4), and two near the Orinoco delta (5–6) by WORZEL and EWING (1948). HERSEY *et al.* (1952) have two profiles north of the Puerto Rico trench (7–8). TOLSTOY *et al.* (1953) have one profile near Martinique (9) and one profile north of the Puerto Rico trench (10). EWING *et al.* (1954) have two profiles north of the Puerto Rico trench (11–12). HERSEY (unpublished) has one profile in the Puerto Rico trench (13) and SUTTON and M. EWING (unpublished) have nine profiles across the Venezuelan basin and in the Puerto Rico trench (14–22); the results of these profiles have been reported in EWING and WORZEL (1954) and EWING and HEEZEN (1955). J. I. Ewing has four profiles east of the Lesser Antilles (23–26); the results of these profiles have been reported in EWING *et al.* (1957). In addition there are about seventy profiles now being prepared for publication at Lamont Geological Observatory by M. Ewing, J. L. Worzel, J. Nafe, J. Ewing, G. Sutton, J. F. Hennion, J. Antoine, and W. Ludwig. These consist primarily of a line of stations from Trinidad to Curaçao to Cuba, a line from Hispaniola to Panama, a line from the Columbia basin to the Yucatan basin, a line in the Cayman trough, and a line from Cuba eastward into the Puerto Rico trench.

INSTRUMENTATION AND FIELD TECHNIQUES

The instrumentation for these cruises was much the same as that for other marine seismic refraction cruises with some small changes and improvements. For brevity, only the instrumentation on the *Bear* will be described here. It allowed simultaneous recording of information for seismic reflection and underwater sound transmission studies as well as the primary seismic refraction information. On both cruises both ships were equipped to record and to shoot.

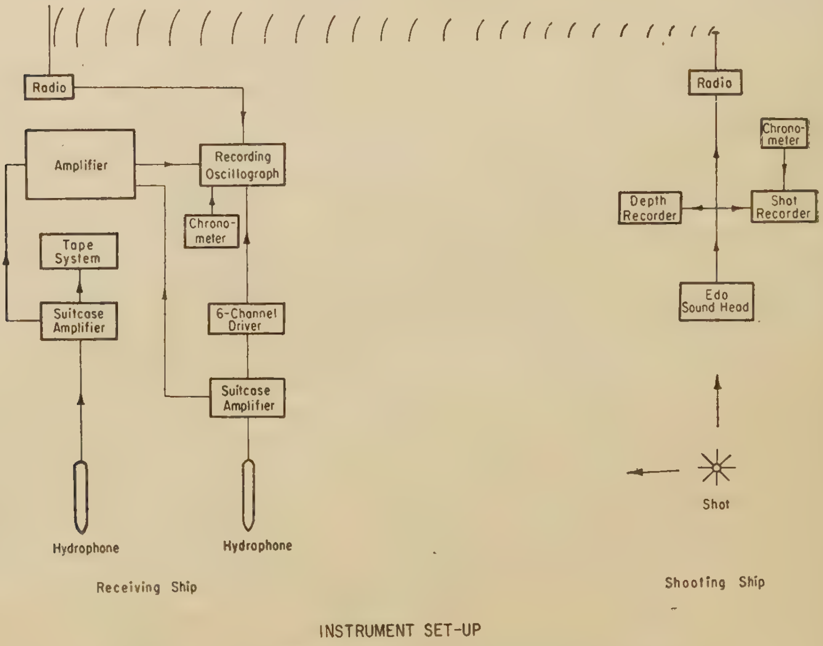
Radio
Amplifier
Recording Oscillograph
Chrono-meter
Tape System
Suitcase Amplifier
6-Channel Driver
Suitcase Amplifier
Hydrophone
Hydrophone
Receiving Ship
Radio
Chrono-meter
Depth Recorder
Shot Recorder
Edo Sound Head
Shot
Shooting Ship
INSTRUMENT SET-UP

Fig. 3. Block diagram of receiving and shooting equipment.

A block diagram of the receiving equipment is shown in Fig. 3. The detectors were Brush Development Co. type AX58 hydrophones. These hydrophones utilize two Rochelle salt piezoelectric crystals which are immersed in castor oil to give proper acoustic impedance matching to the ocean. The crystal terminals were connected to a cathode follower preamplifier in the hydrophone case to present a low impedance to the hydrophone cable. The receiving amplifier was an accurately calibrated, wide band, large dynamic range amplifier, referred to as a "suitcase" amplifier in Fig. 3. Each "suitcase" amplifier consisted of two separate amplifier channels. The output from one channel of each amplifier went to a Houston Technical Laboratories 7000-B amplifier system, consisting of twenty-four amplifiers with interstage filtering, twelve for each hydrophone. Various band pass filters from 5 to 500 c/s and various dynamic ranges were used on these amplifiers. These outputs then went to a Houston Technical Laboratories recording oscillograph, consisting of twenty-eight galvanometers whose movements were recorded by reflected light on a moving photograph paper. The output from the second channel of one amplifier went to a dual channel Magnecorder magnetic tape recorder, recording two dynamic levels. No filtering was used. This information was primarily for later seismic reflection and underwater sound transmission analyses. The primary seismic refraction information was contained on the oscillograph records. The output from the second channel of the second amplifier went to a six channel amplifier. Each channel in this amplifier had various interstage filters from 1000 to 10,000 c/s. The resulting signals were rectified and went to the recording oscillograph. These channels were used for the proper recording and identification of the direct sound wave, propagated in the surface isothermal sound channel. This arrival is used for range determination. The various channels of the Houston Technical Laboratories amplifiers were used for proper recording of the refraction arrivals from the strata underlying the ocean floor. In addition to the above the signal from a break circuit chronometer and the signal of the instant of detonation (transmitted by radio from the shooting ship) were recorded on the oscillograph record through separate galvanometers.

A block diagram of the shooting equipment is also shown in Fig. 3. The instant of shot detonation was detected by the echo sounder receiving system, consisting of an Edo Corp. transducer and amplifier. This signal was simultaneously transmitted by radio to the receiving ship and recorded on the shooting ship on a single channel Sanborn Co. direct writing oscillograph. The signal from a break circuit chronometer was superimposed on this latter record.

For receiving operation various techniques have been developed to provide quiet listening conditions. Generally the refraction arrivals were low amplitude, low frequency (5–40 c/s) signals; and it was necessary to have the hydrophone noise level down to the ambient noise level of the ocean for clear recording of these signals. For this purpose all the ship's engines and other machinery were off during the reception of refraction arrivals. Electrical energy was supplied by the ship's batteries. Occasionally other ship noises such as that caused by ballast shifting during the ship's roll or rudder movements would cause noise in the frequency range of interest and would require special precautionary measures. Other objectionable noise may be caused by improper suspension of the hydrophone in the water. If the hydrophone were lowered directly on its cable, the variation in the tension on the cable during the roll of the ship would be transmitted directly to the hydrophone and cause excessive noise. If a surface float were placed along the cable with a long bight to the ship, no noise would be caused by the roll of the ship; but surface wave motion would be transmitted directly to the hydrophone and cause excessive noise. The technique which has been used successfully almost since the first deep water refraction profile by the Lamont Geological Observatory and Woods Hole Oceanographic Institution groups and is, as with many marine geophysical techniques, due primarily to M. Ewing consists of the following. Five or six floats are placed along the hydrophone cable at increasing distances from 10 to 60 ft out from the hydrophone so that with about 200–300 ft of cable out the system has a slight positive buoyancy. Before the expected reception of the refraction arrival sufficient cable is paid out so that the system has a slight negative buoyancy. If arranged properly, the hydrophone sinks at a slow rate of about 20 ft/min. During the reception of the refraction arrival the system is then at depth and free from surface motion. This technique does indeed reach the ambient noise background of the ocean in the frequency range of interest. A period of about 1–2 min of ambient level can be obtained, sufficient for reception of the information of interest. The importance of this technique cannot be overstated; it is the most important single factor in the success of a long range seismic refraction profile in deep water. Two separate hydrophones were always used to increase the chances of clear reception of the refraction arrivals. In water depths shallower than about twenty fathoms the receiving ship was anchored, and the hydrophones were lowered to the bottom without floats.

The shooting schedule and charge sizes were determined by the receiving ship. The charge sizes varied from $\frac{1}{2}$ to 300 lb of TNT. All charges were detonated by a blasting cap from a length of safety fuse, and all charges were detonated at a sufficient depth so that their gas bubble did not break the surface with consequent loss of low frequency energy to the atmosphere. The instant of detonation was received on the echo sounder transducer and transmitted by radio to the receiving ship for the zero time on its oscillograph record. In addition the shooting ship made a recording of the instant of detonation and the first reflection from the bottom on a direct writing recorder. In case the receiving ship missed recording the instant of detonation but did record the radio transmission of the first bottom reflection, the zero time could be recovered from the shooting ship's record. In case the receiving ship missed or did not receive either the instant of detonation or the first bottom reflection, the zero time could be recovered from the shooting ship's record and the relative rate of the shooting and receiving ships' chronometers determined from other shots in which both had a recording of the instant of detonation. These precautions were important, for it goes without saying that a refraction seismogram without a zero time is of little value.

In addition to the above the shooting ship kept a record of the charge size detonated, the absolute time of the instant of detonation, and the length of time that the charge was in the water before detonation. Further the shooting ship made a continuous recording of the water depth with an Edo Corp. echo sounder and a Woods Hole Oceanographic Institution precision depth recorder, designed by Knott and Hersey (1956). The receiving ship also made an echo sounder record, between shots, of the bottom over which it was drifting. The depths of the receiving hydrophones were determined from a separate depth (pressure) sensing element on the hydrophones. Both ships made frequent bathythermograph lowerings to provide a record of ocean temperature vs. depth from the ocean surface down to a depth of 900 ft; this information is used to compute the velocity of propagation of the direct water wave.

A typical long range, reversed refraction profile of 40 nautical miles or greater took the better part of one day to complete. At the beginning of a profile one ship was hove to for receiving while the second ship then proceeded away from the first on a prescribed course firing shots scheduled by the receiving ship. Each refraction seismogram was developed and read immediately following its reception on the receiving ship, and a running travel time plot was kept of the refraction events from these recordings. Changes in charge size and shooting schedule were made as dictated by these records and the travel time plot. The end of the shooting run was also determined by the receiving ship, generally from the results of its travel time plot. At this point the shooting ship stopped and prepared to receive. The first ship then got under way on the same course as that followed by the second ship and fired shots to reverse the profile. Generally the drift of the two ships was nearly the same so that the course followed by the second ship was a true course for the first ship. Occasionally the drift of the two ships while receiving would be different, and a correction in the shooting track would be necessary during the shooting of the reverse profile. The distance between the two ships for any shot was determined from the travel time of the direct sound through the surface sound channel from the shot to the receiving ship's hydrophones. The absolute position of the profile was obtained from the ship's navigation as determined by the ship's officers through celestial fixes and lines of position, sights on islands where possible, and Loran fixes or lines of position where possible. The profile locations shown in Fig. 1 are the average from the two ships' tracks; this average track is generally valid within 2–3 miles. The drift of each ship while receiving was generally between 2–5 miles.

REFRACTION EQUATIONS, RAY PATHS, AND REDUCTION OF DATA

Several seismic arrivals are detected by the hydrophones. These may be divided conveniently into three groups as illustrated in Fig. 4, namely the direct wave (D), the bottom and sub-bottom reflections (Bn), and the refraction arrivals (G). The direct wave is propagated in the surface isothermal sound channel. Throughout this cruise, as is often the case, there is a mixed water layer of constant temperature and salinity down to a depth of 50–100 ft. The sound velocity in this isothermal layer increases slightly with depth (pressure) forming a sound channel with the ocean surface. A portion of the energy from the shot is trapped in this sound channel and propagates directly to the receiving hydrophone. As might be expected the sound channel propagation is frequently dependent; generally frequencies above about 1000 c/s are propagated well. The travel time of D multiplied by the sound velocity in the surface sound channel gives the range between the shot and the receiving hydrophone. This is an accurate range determination, valid to within 5 ft in 1 nautical mile. It is the method of range determination for the abscissa of the refraction travel time plots. The sound velocity in the surface channel is dependent primarily on temperature; it is determined from the bathythermograms and experimental tables of sound velocity in the ocean (MATTHEWS, 1939). The bottom reflection arrivals (Bn) have followed those ray paths which involve one or more reflections from the ocean bottom. Their frequency spectrum is broad, and generally they are the largest amplitude arrivals. These arrivals are not of primary concern to us here and will not be discussed further. At times the bottom reflection is followed immediately by sub-bottom reflections from horizons as deep as 3000 ft beneath the ocean floor. The refraction arrivals (G) enter the higher velocity refracting layer at the critical angle and are propagated parallel to the boundary, reradiating back into the upper medium at the critical angle. There will be a refraction arrival for each higher velocity layer. A refraction arrival is not detected at the receiving hydrophone until the range corresponding to the offset distance of its critical angle ray has been passed. The refraction arrival from a given layer will always arrive sooner than the corresponding reflection from the top of that layer. The refraction arrivals generally have small amplitudes and low frequencies (5–40 c/s). From Fig. 4 it should be clear that the travel time plots of the bottom reflections for a constant velocity ocean and a horizontal bottom are hyperbolæ. It should also be clear that the travel time plots of

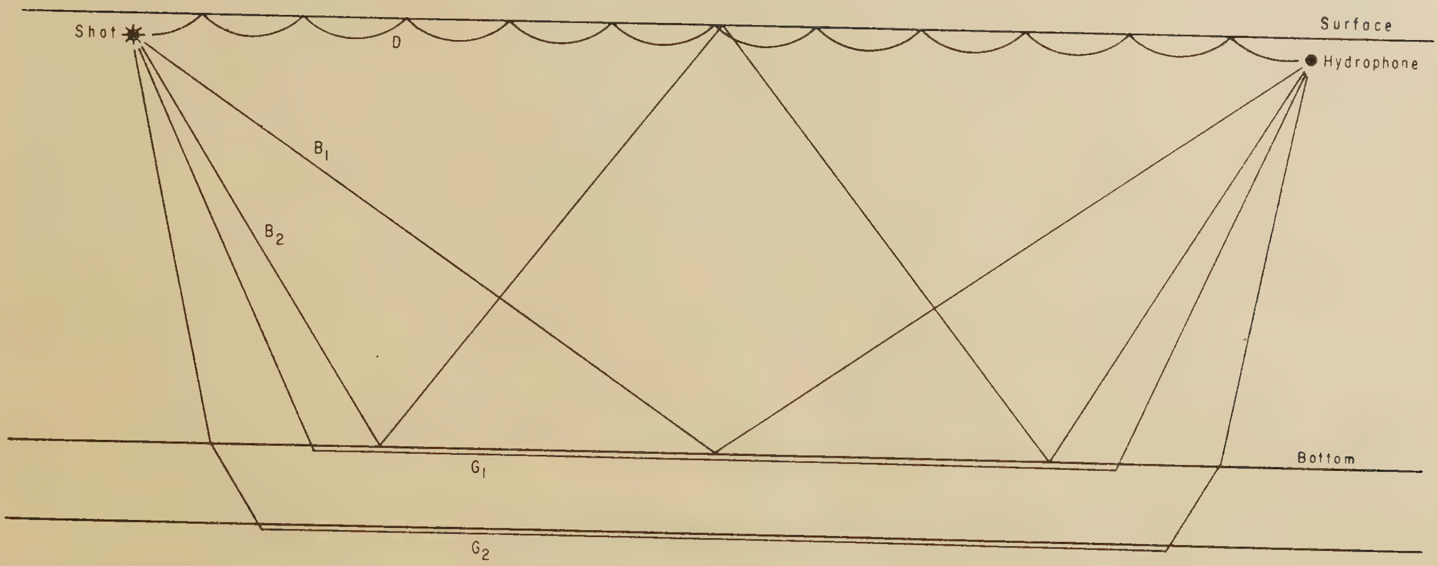
Shot
D
Surface
Hydrophone
B$_1$
B$_2$
Bottom
G$_1$
G$_2$

Fig. 4. Ray diagram of *D*, *B* and *G*.

the refraction arrivals for planar refracting surfaces are straight lines. For a more comprehensive discussion of these various points reference may be made to OFFICER (1958).

An abbreviated derivation taken from EWING *et al.* (1937) of the time–distance relations of the refraction lines is given below. It is of interest to us to describe these lines by their inverse slopes and their time intercepts, the problem then being to convert these two parameters into the depth, inclination, and seismic velocity of the given refractor. The inverse slope of a given refraction line determines the apparent velocity in the layer through which the sound arrivals were propagated. From Fig. 5 the measured apparent velocity for any refraction line is related to the incident angle of the refracted ray and the velocity of the medium underlying the detectors by

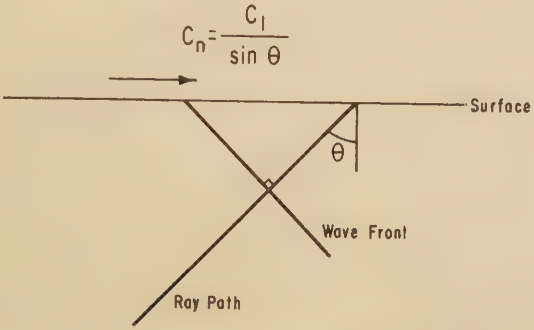
$C_n = \frac{C_1}{\sin\theta}$
Surface
θ
Wave Front
Ray Path

Fig. 5. Apparent velocity along a horizontal.

$$c_n = \frac{c_1}{\sin\theta} \tag{1}$$

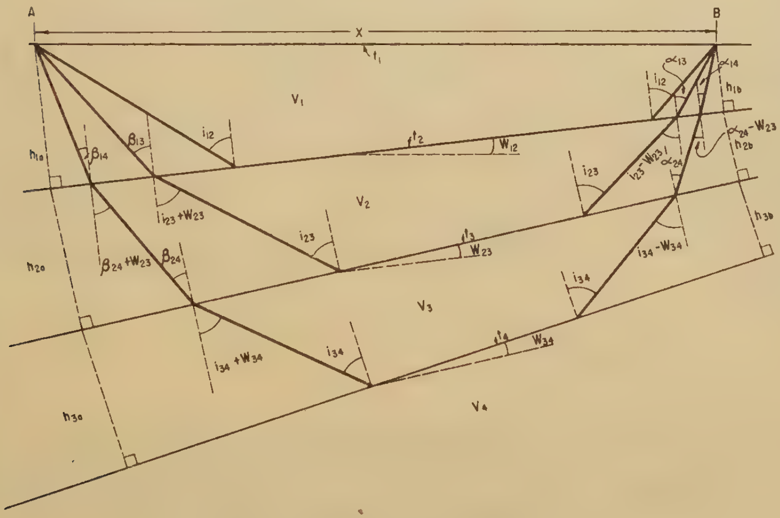
A
B
X
t_1
V_1
i_{12}
β_{13}
β_{14}
h_{1a}
t_2
W_{12}
V_2
$i_{23}+W_{23}$
i_{23}
t_3
W_{23}
h_{2a}
$\beta_{24}+W_{23}$
β_{24}
V_3
$i_{34}+W_{34}$
i_{34}
t_4
W_{34}
V_4
h_{3a}
α_{13}
α_{14}
i_{12}
h_{1b}
$\alpha_{24}-W_{23}$
h_{2b}
$i_{23}-W_{23}$
α_{24}
i_{23}
h_{3b}
$i_{34}-W_{34}$
i_{34}

Fig. 6. Refraction ray paths.

From (1) and Snell's law we will then have for the refraction paths of the reversed profile of Fig. 6

$$\left.\begin{array}{lcl}
\dfrac{c_1}{c_{2a}} = \sin(i_{12} - \omega_{12}) & & \dfrac{c_1}{c_{2b}} = \sin(i_{12} + \omega_{12}) \\
 & \dfrac{c_1}{c_2} = \sin i_{12} & \\
\dfrac{c_1}{c_{3a}} = \sin(\alpha_{13} - \omega_{12}) & & \dfrac{c_1}{c_{3b}} = \sin(\beta_{13} + \omega_{12}) \\
\dfrac{c_1}{c_2} = \dfrac{\sin\alpha_{13}}{\sin(i_{23} - \omega_{23})} & & \dfrac{c_1}{c_2} = \dfrac{\sin\beta_{13}}{\sin(i_{23} + \omega_{23})} \\
 & \dfrac{c_2}{c_3} = \sin i_{23} & \\
\dfrac{c_1}{c_{4a}} = \sin(\alpha_{14} - \omega_{12}) & & \dfrac{c_1}{c_{4b}} = \sin(\beta_{14} + \omega_{12}) \\
\dfrac{c_1}{c_2} = \dfrac{\sin\alpha_{14}}{\sin(\alpha_{24} - \omega_{23})} & & \dfrac{c_1}{c_2} = \dfrac{\sin\beta_{14}}{\sin(\beta_{24} + \omega_{23})} \\
\dfrac{c_2}{c_3} = \dfrac{\sin\alpha_{24}}{\sin(i_{34} - \omega_{34})} & & \dfrac{c_2}{c_3} = \dfrac{\sin\beta_{24}}{\sin(i_{34} + \omega_{34})} \\
 & \dfrac{c_3}{c_4} = \sin i_{34} &
\end{array}\right\} \tag{2}$$

where c_1 is the average sound velocity in the water, c_n the true seismic velocities of the refractors, c_{na} and c_{nb} the measured apparent velocities from the refraction lines for the receiving stations A and B, $\omega_{n-1,n}$ the inclinations of the given refractors with respect to the next overlying refractor, $i_{n-1,n}$ the critical angles for the given refractors, and $\alpha_{m,n}$ and $\beta_{m,n}$ the intermediate angles as defined in Fig. 6. The true velocities and inclinations of the respective layers can be calculated stepwise from equations (2). From the first set, knowing c_1, c_{2a}, and c_{2b} the angle ω_{12} and velocity c_2 can be determined. From the second set, knowing c_1, c_2, c_{3a}, c_{3b}, and ω_{12}, the angle ω_{23} and the velocity c_3 can be determined and so on for succeeding layers. The equations for the intercept times can be obtained from the following consideration. The intercept times are the times extrapolated back from the measured refraction line to zero range. The extrapolated ray paths would be those shown in Fig. 7. The times along these paths would be the sum of the times along the inclined paths out from A minus the time along the path parallel to the refraction horizon. For each refraction path this will be

$$\begin{aligned}
t_{2a} &= \frac{2h_{1a}}{c_1}\cos i_{12} \\
t_{3a} &= \frac{2h_{2a}}{c_2}\cos i_{23} + \frac{h_{1a}}{c_1}(\cos\alpha_{13} + \cos\beta_{13}) \\
t_{4a} &= \frac{2h_{3a}}{c_3}\cos i_{34} + \frac{h_{2a}}{c_2}(\cos\alpha_{24} + \cos\beta_{24}) + \frac{h_{1a}}{c_1}(\cos\alpha_{14} + \cos\beta_{14})
\end{aligned} \tag{3}$$

The times t_{na} are the measured intercept times at A and the thicknesses $h_{n-1,a}$ are as defined in Fig. 7. From equations (3) the thicknesses $h_{n-1,a}$ may be calculated stepwise. From the first equation h_{1a} can be determined. From the second equation knowing h_{1a}, h_{2a} can be determined and so on. A similar set of equations exist for point B for the calculations of h_{1b}, h_{2b}, . . . The average sound velocity of the ocean, c_1, is a time average not a straight velocity average.

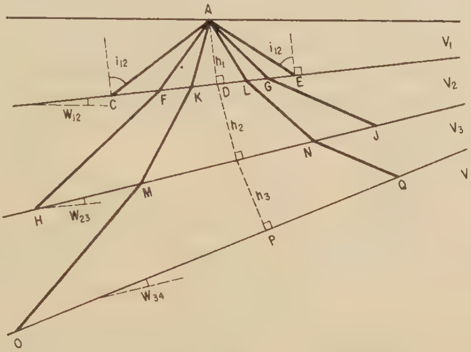

Fig. 7. Fictitious time intercept ray paths.

It is that velocity which when multiplied by half the bottom reflection time will give the true depth of water, or

$$c_1 = \frac{H}{\int_0^H \{dh/c(h)\}}$$

where H is the depth of water. Fortunately the velocity c_1 is a sufficiently slowly varying function that an average velocity may be defined over various depth ranges and areas of the ocean from the several measurements of temperature and salinity at depth. Tables of such values are available (MATTHEWS, 1939).

In principle the reading of the D and G arrivals from the refraction seismograms is straightforward; the beginning of each arrival is picked. In practice, however, as with most seismic records, the reading of the records is the most critical part of the reduction of the data. In general the D arrival offers no problems; it has a sharp, distinct beginning, easy to recognize and to read. The G arrivals are usually easy to recognize; the difficulty occurs in picking their beginnings. Some start abruptly and offer no problem. Others, however, have an emergent beginning; and care must be taken in reading them. Further, at the longer ranges the amplitudes of the refraction arrivals are generally small, offering in some cases difficulties in reading their beginnings from the associated noise background.

In reading the records emphasis is on the beginning of the first refraction arrival. As shown in Fig. 12, the first refraction arrival progresses from one refraction line to the next (representing successively deeper layers) with succeeding range so that a detailed shot schedule will usually allow a good determination of each line from first arrivals. Later refraction arrivals after the first are picked when they can be recognized and followed from one record to the next; the difficulty there is in picking the beginning of these later arrivals out of the wave train from the preceding refraction arrival. The appearance of the various arrivals is shown in Fig. 8 where one low frequency trace from each record at profile 26 *N* was duplicated and spaced according to shot distance to demonstrate the correlation of the different phases.

A number of corrections must be made to the *D* and *G* arrivals read from the seismograms before the final travel time plots can be made. These are the shot instant correction, surface of reference correction, and topographic correction. The first correction applies to all readings, the later two to only the *G* readings. The shot instant correction is simply the interval of time it took the sound to travel from the shot point to the echo sounder transducer on the shooting ship.

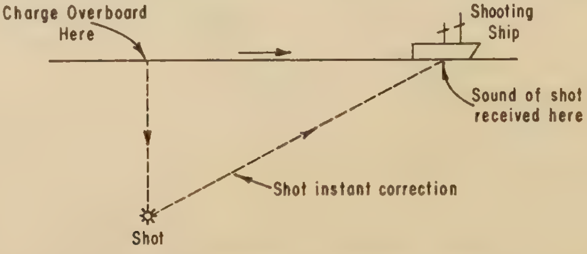

Fig. 9. Ray diagram for shot instant correction.

It is the correction to the instant of detonation from the zero of time used on the seismograms. From Fig. 9 it is simply

$$\Delta t_{si} = \frac{\{(V_{ss}\Delta T_{os})^2 + (\Delta d_s)^2\}^{\frac{1}{2}}}{c_0} \tag{4}$$

where V_{ss} is speed of the shooting ship, T_{os} the time interval that the charge was in the water before detonation, and Δd_s the depth of the shot. V_{ss} is determined sufficiently accurately from the slope of a plot of uncorrected *D* vs. the absolute time of the instant of detonation. Every explosion at moderate depths in the ocean will have one or more bubble pulses. The bubble pulses are simply the oscillations of the gas bubble and appear on the records as second shots. The time interval between the instant of detonation and the first bubble is dependent on the charge size, kind, and depth (pressure). The relation between this interval and the depth at which the charge has been detonated has been determined empirically for various size TNT charges (EWING *et al.*, 1946). The quantity Δd_s was determined from such an empirical plot. An alternative method in deep water for the deeper shots was to measure the time interval between the first bottom reflection and the arrival immediately following which had been reflected once from the ocean surface above the shot and then from the bottom; the shot depth is then simply one-half this time interval multiplied by the sound velocity. The surface of reference correction is made to refer all data to the same reference surface for calculations. This surface is taken as the ocean surface. From Fig. 10 this is the time interval between the two wave-fronts shown, or

$$\Delta t_{sr} = \frac{\Delta d_s}{c_0} \cos\left(\sin^{-1}\frac{c_1}{c_{na}}\right) + \frac{\Delta d_H}{c_0} \cos\left(\sin^{-1}\frac{c_1}{c_{nb}}\right) \tag{5}$$

for the *A* portion of a reversed profile where Δd_H is the depth of the receiving hydrophone. For this correction the use of the apparent velocities from the uncorrected travel time plot is sufficiently accurate. The depth Δd_H is small, less than 100 ft, so that only in the most exceptional case will the use of c_{na} for c_{nb} in the second term of (5) cause a measurable difference. The topographic correction is the correction for variations in arrival times due to variations in the bottom topography. The refraction equations derived above were for planar refracting surface. Variations in the thickness of any of the layers above the particular refractor will cause deviations of the plotted points away from the assumed straight lines. It is desirable to remove the deviations due to bottom topography before making the final travel time plot. The net effect of changes in bottom topography, as shown in Fig. 11, may be considered to be changes in the intercept times of the theoretical refraction line. For a change in the bottom topography of Δd_T which is caused by a layer of seismic velocity c_x the topographic correction will be

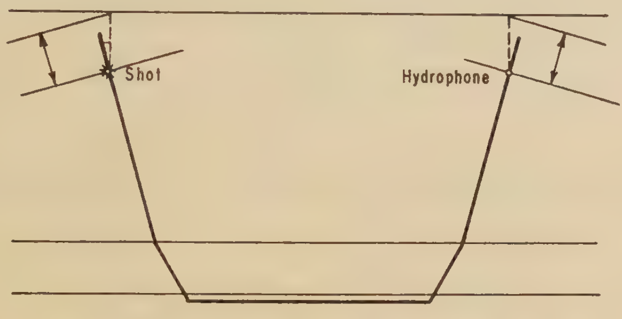

Fig. 10. Ray diagram for surface of reference correction.

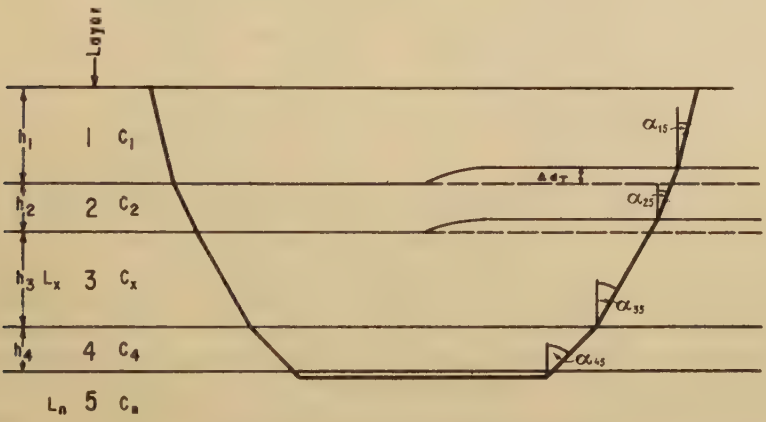

Fig. 11. Ray diagram for topographic correction.

$$\Delta t_T = \frac{\Delta d_T}{c_1}\cos\left(\sin^{-1}\frac{c_1}{c_{na}}\right) - \frac{\Delta d_T}{c_x}\cos\left(\sin^{-1}\frac{c_x}{c_{na}}\right) \tag{6}$$

for the *A* portion of a profile. The velocity c_x is generally taken as the first hig velocity refractor beneath the bottom. This is an assumption, but reasonabl changes in the velocity c_x away from this value will generally cause a negligibl error. The quantity Δd_T is measured above or below a mean bottom base line either inclined or horizontal, as determined from the shooting ship's ech sounder record. The quantity Δd_T is not measured directly beneath the sho point but at the offset distance, *R*, given by

$$R = H \tan\left(\sin^{-1}\frac{c_1}{c_{na}}\right) \quad (7$$

The corrected *G* and *D* arrivals are plotted to give the final travel time plo and are fitted with the appropriate refraction lines. This fitting is not done by

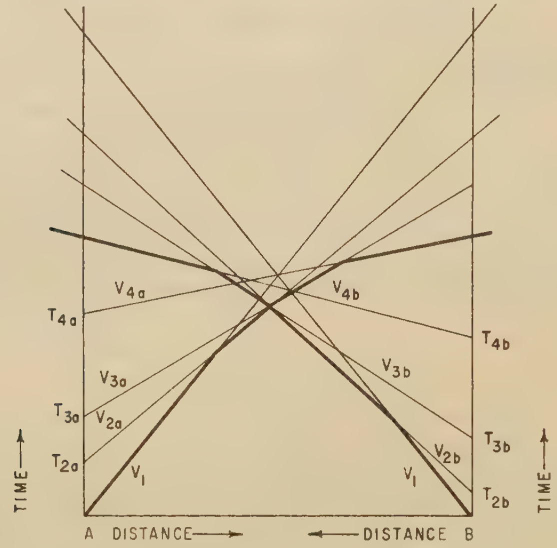

Fig. 12. Sketch of normal refraction travel time graphs.

least squares or other such means but by a qualitative weighting of each poin on the line. It is almost always true that a fit to the data by a small number o well defined lines is as good a fit as can be made. The points usually follow on line and then diverge to a second line; it is seldom that one would prefer to fit group of arrivals by a curve. Such straight line travel time plots are caused b discontinuous or rapid changes in the seismic velocity as a function of depth a contrasted to a continual gradual change in velocity. On reversed profiles th two corresponding refraction lines from the *A* and *B* receiving locations give unique determination of the depth, inclination, and seismic velocity of th particular refracting layer. However, on the longer profiles presented her the arrivals from the shallow refractors do not cover the same portion of th refracting horizon on both the *A* and *B* portions. The inclination of such a laye may change between the two portions, and a unique solution cannot be obtainec This may be partially resolved by the agreement of the reverse points, i.e., th travel time at the reverse distance, of the two corresponding lines. The deepe layers generally give good reverses. On unreversed profiles or unreversed lines of a reversed profile an assumption must be made for the inclination of the refracting horizon in order to carry out the calculations for velocity and depth. The refraction line sequence for a normal reversed profile will be as sketched in Fig. 12. Over some portion of each refraction line below the bottom the refraction arrival will appear as the first arrival on the refraction seismograms. With a sufficiently detailed shot schedule each line can be well determined from the first arrivals. On some profiles, however, the refraction line for a layer at great depth may not appear as a first arrival, as shown in Fig. 13; such a layer is referred to as being masked. The presence of such a line can generally not be determined from the seismograms; its identification can only be given from the measurement of second arrivals. It is judged that there is a masked layer on three of the longer 1956 profiles in the vicinity of the Puerto Rico trench. The first refraction line on most of the deep-water profiles of both cruises did not correspond to a refraction through the material immediately beneath the ocean bottom but to a higher velocity refractor at greater depth. In such cases it is necessary to assume a seismic velocity for the unconsolidated sedimentary material above the first refractor. Since the thickness of this undetermined sedimentary material is generally thin, possible variations in the assumed velocity from the true velocity cause little error in the calculations of the depths of the deeper horizons. For most of the deep water profiles this velocity was taken from a relation for sedimentary velocity vs. depth determined from an analysis of the sub-bottom reflection profiles from these Caribbean profiles.

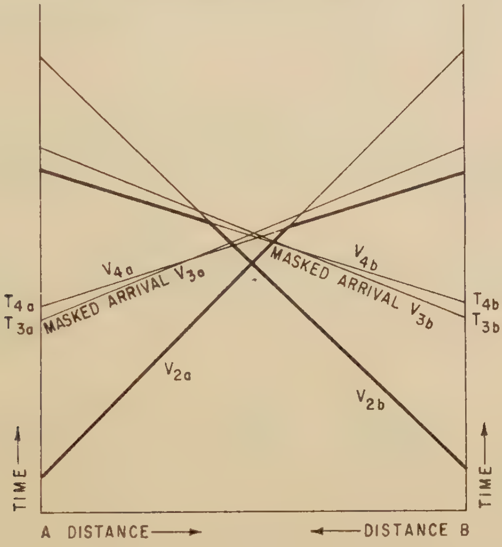

Fig. 13. Sketch of masked layer refraction travel time graph.

GEOPHYSICAL RESULTS

The geophysical results are presented in Fig. 2 and in Table 1. Each figure of Fig. 2 contains the corrected travel time plot with the plotted points for each

Table 1. Measured Seismic Velocities and Thicknesses

Profile 1		
T_W	V_W V_E	T_E
0·03	1·53	0·03
0·04	1·97	0·41
	2·56	

Profile 2	
T_N	V_N
4·21	1·51
1·54	(2·14)
	(3·80)

Profile 3	
T_W	V_W
1·36	1·50
1·37	[2·32]
	(4·48)

Profile 4	
T_W	V_W
0·95	1·50
3·13	(2·32)
	(5·27)

Profile 5		
T_W	V_W V_E	T_E
0·08	1·53	0·08
0·07	1·67	0·36
1·04	2·17	1·52
	5·72	

Profile 6	
T_S	V_S
0·08	1·53
0·46	(1·84)
1·09	(2·19)
	(5·96)

Profile 7		
T_S	V_S V_N	T_N
4·22	1·51	3·50
3·10	⟨2·67⟩	3·54
6·74	5·84	4·43
	7·38	

Profile 8		
T_W	V_W V_E	T_E
3·94	1·51	3·67
	1·72	
2·14	⟨2·38⟩	2·35
2·85	4·82	2·27
	6·85	

Profile 9		
T_W	V_W V_E	T_E
3·21	1·50	3·06
	1·78	
0·90	⟨1·75⟩	0·31
1·45	2·83	1·60
2·25	4·06	2·90
	6·68	

Profile 10	
T_S	V_S
1·28	1·50
0·70	[1·80]
0·60	[3·40]
1·61	(4·90)
	(6·20)

Profile 11		
T_N	V_N V_S	T_S
0·08	1·54	0·08
0·05	1·76	0·13
0·96	2·68	0·77
0·41	3·44	0·88
0·62	4·40	2·49
	6·31	

Profile 12		
T_W	V_W V_E	T_E
0·09	1·52	0·95
0·11	1·71	0·61
0·67	2·39	0·18
0·85	3·25	1·25
2·56	4·29	1·51
	5·97	

Profile 13		
T_N	V_N V_S	T_S
1·10	1·50	0·82
1·30	[1·70]	1·30
3·48	4·33	2·96
	5·30	

Profile 14		
T_W	V_W V_E	T_E
0·82	1·50	1·54
1·31	[1·70]	1·48
2·63	4·19	3·20
	5·35	

Profile 15	
T_S	V_S
0·73	1·50
0·78	(1·81)
2·18	(2·50)
	(3·38)

⟨ ⟩—sedimentary velocity from refl. prof. ( )—unreversed velocity. [ ]—assumed velocity.
All depths in kilometres and all velocities in kilometres per second.

Profile 16

T_S	V_S	V_N	T_N
1·09	1·50		0·37
0·27	[1·72]		0·38
0·51	2·22		2·00
3·32	3·21		5·20
	4·27		

Profile 17

T_W	V_N	V_E	T_E
2·85	1·50		4·07
0·54	[1·70]		1·20
6·21	2·58		2·62
6·79	6·74		5·79
	8·32		

Profile 18

T_N	V_N	V_S	T_S
5·05	1·51		4·84
0·25	[1·70]		0·10
1·98	2·23		3·13
6·29	6·68		4·94
	8·13		

Profile 19

T_E	V_E	V_W	T_W
2·37	1·50		2·01
	[1·70]		
2·38	1·91		0·67
2·87	2·41		5·37
3·10	4·31		3·92
	(6·77)		

Profile 20

T_N	V_N	V_S	T_S
1·27	1·50		2·10
1·63	[1·70]		0·87
4·00	[2·00]		—
2·23	(2·95)		2·23
	3·70		

Profile 21

T_N	V_N	V_S	T_S
2·19	1·50		2·19
0·35	[1·70]		0·51
3·13	1·93		1·66
4·70	3·81		3·39
	5·31		

Profile 22

T_N	V_N	V_S	T_S
1·10	1·50		1·23
1·07	[1·70]		0·32
2·56	3·97		2·82
	4·91		

Profile 23

T_S	V_S
0·14	1·50
	[1·66]
1·08	(2·01)
2·51	(2·71)
0·34	(3·68)
2·19	(5·10)
	(6·83)

Profile 24

T_N	V_N	V_S	T_S
0·14	1·52		0·10
	[1·66]		
1·08	1·93		0·90
2·51	2·75		0·37
0·34	3·43		1·74
2·19	4·80		3·03
	6·38		

Profile 25

T_E	V_E
0·13	1·52
	[1·70]
1·37	(2·01)
2·95	(2·93)
2·18	(5·20)
	(6·47)

Profile 26

T_E	V_E
0·16	1·51
	(1·64)
1·26	(2·03)
2·35	(2·57)
	(4·33)

Profile 27

T_S	V_S	V_N	T_N
0·16	1·51		0·68
	1·64		
1·26	2·03		1·66
2·35	2·57		1·93
	4·33		

Profile 28

T_S	V_S
0·04	1·51
0·06	[1·70]
1·34	(2·33)
3·05	(4·00)
	(6·40)

Profile 29

T_S	V_S	V_N	T_N
2·93	1·50		2·93
	(2·01)		
2·81	⟨2·52⟩		1·60
2·55	(3·76)		1·80
2·24	(5·28)		1·39
7·85	6·22		6·40
	7·41		

Profile 30

T_S	V_S	V_N	T_N
1·30	1·50		1·48
0·78	⟨1·84⟩		0·00
1·53	3·66		1·57
2·58	4·42		3·63
3·05	6·15		2·71
	6·69		

⟨ ⟩—sedimentary velocity from refl. prof. ( )—unreversed velocity. [ ]—assumed velocity.
All depths in kilometres and all velocities in kilometres per second.

Table 1. Measured Seismic Velocities and Thicknesses—continued

Profile 31		
T_E	V_E V_W	T_W
3·44	1·50	4·28
	1·82	
0·82	⟨1·79⟩	1·29
1·06	(2·79)	1·00
3·57	4·22	1·06
2·29	6·41	3·87
7·10	7·13	4·31
	8·31	

Profile 32		
T_E	V_E V_W	T_W
4·45	1·51	4·45
1·07	⟨1·93⟩	0·80
0·97	3·84	2·38
8·34	6·71	6·88
	8·04	

Profile 33		
T_E	V_E V_W	T_W
5·02	1·51	5·02
	(2·05)	
—	⟨1·71⟩	0·41
2·19	(3·15)	2·83
3·27	5·12	1·21
2·95	6·92	9·00
	7·78	

Profile 34		
T_S	V_S V_N	T_N
3·28	1·50	1·59
	(1·95)	
0·82	⟨1·84⟩	0·50
5·36	3·75	0·76
	4·79	

Profile 35		
T_W	V_W V_E	T_E
0·02	1·53	0·02
0·75	1·95	0·37
	5·23	

Profile 36	
T_W	V_W
1·88	1·50
	(1·97)
0·87	⟨1·93⟩
1·16	(4·94)
4·99	(5.63)
	(7·98)

Profile 37		
T_S	V_S V_N	T_N
0·01	1·53	0·01
0·25	[1·96]	0·09
	5·00	

Profile 38		
T_W	V_W V_E	T_E
4·34	1·51	4·34
0·65	⟨1·65⟩	0·01
1·73	3·07	2·57
4·09	5·77	1·63
	7·33	

Profile 39		
T_S	V_S V_N	T_N
1·35	1·50	1·04
0·91	(1·92)	0·48
1·86	2·95	0·97
	5·37	

Profile 40		
T_S	V_S V_N	T_N
1·09	1·50	0·82
0·40	[1·70]	0·46
1·02	(2·92)	0·60
	5·70	

Profile 41		
T_S	V_S V_N	T_N
0·82	1·50	0·71
0·46	[1·70]	0·52
0·60	2·34	0·63
	5·24	

Profile 42		
T_W	V_W V_E	T_E
5·94	1·52	5·94
	(2·36)	
2·29	⟨2·55⟩	2·96
	5·86	

Profile 43		
T_W	V_W V_E	T_E
6·31	1·52	5·95
0·25	⟨1·77⟩	0·96
2·09	3·49	1·31
	5·45	

Profile 44		
T_E	V_E V_W	T_W
6·17	1·52	6·17
0·66	⟨1·70⟩	0·17
0·24	4·51	2·46
6·91	6·62	2·90
	7·85	

Profile 45		
T_E	V_E V_W	T_W
6·81	1·53	6·81
2·84	⟨2·50⟩	0·00
0·00	4·28	1·61
1·97	5·50	1·01
4·77	6·24	6·70
	8·05	

⟨ ⟩ sedimentary velocity from refl. prof. ( ) unmeasured velocity. [ ] assumed velocity

1955 and 1956 Profiles

<table>
<tr><th colspan="4">Profile 46</th></tr>
<tr><th>T_E</th><th>V_E</th><th>V_W</th><th>T_W</th></tr>
<tr><td>7·87</td><td colspan="2">1·53</td><td>8·15</td></tr>
<tr><td>2·45</td><td colspan="2">3·38</td><td>2·12</td></tr>
<tr><td>7·97</td><td colspan="2">6·33</td><td>7·12</td></tr>
<tr><td></td><td colspan="2">7·94</td><td></td></tr>
</table>

<table>
<tr><th colspan="4">Profile 47</th></tr>
<tr><th>T_N</th><th>V_N</th><th>V_S</th><th>T_S</th></tr>
<tr><td>8·38</td><td colspan="2">1·53</td><td>8·38</td></tr>
<tr><td>0·21</td><td colspan="2">⟨1·94⟩</td><td>1·37</td></tr>
<tr><td>1·41</td><td colspan="2">4·70</td><td>1·65</td></tr>
<tr><td></td><td colspan="2">7·13</td><td></td></tr>
</table>

<table>
<tr><th colspan="4">Profile 1</th></tr>
<tr><th>T_N</th><th>V_N</th><th>V_S</th><th>T_S</th></tr>
<tr><td>5·87</td><td colspan="2">1·52</td><td>5·87</td></tr>
<tr><td>0·48</td><td>⟨1·75⟩</td><td></td><td>—</td></tr>
<tr><td></td><td></td><td>(4·22)</td><td>1·48</td></tr>
<tr><td>5·80</td><td colspan="2">6·87</td><td>7·11</td></tr>
<tr><td></td><td colspan="2">8·21</td><td></td></tr>
</table>

<table>
<tr><th colspan="4">Profile 2</th></tr>
<tr><th>T_N</th><th>V_N</th><th>V_S</th><th>T_S</th></tr>
<tr><td>5·86</td><td colspan="2">1·52</td><td>5·74</td></tr>
<tr><td>0·58</td><td colspan="2">⟨1·77⟩</td><td>0·39</td></tr>
<tr><td>1·25</td><td colspan="2">5·96</td><td>1·70</td></tr>
<tr><td>3·92</td><td colspan="2">6·93</td><td>4·00</td></tr>
<tr><td></td><td colspan="2">7·96</td><td></td></tr>
</table>

<table>
<tr><th colspan="4">Profile 3</th></tr>
<tr><th>T_W</th><th>V_W</th><th>V_E</th><th>T_E</th></tr>
<tr><td>5·49</td><td colspan="2">1·51</td><td>5·49</td></tr>
<tr><td>0·36</td><td colspan="2">⟨1·73⟩</td><td>0·50</td></tr>
<tr><td>3·01</td><td colspan="2">5·70</td><td>1·67</td></tr>
<tr><td>4·94</td><td colspan="2">7·11</td><td>3·31</td></tr>
<tr><td></td><td colspan="2">8·44</td><td></td></tr>
</table>

<table>
<tr><th colspan="4">Profile 4</th></tr>
<tr><th>T_N</th><th>V_N</th><th>V_S</th><th>T_S</th></tr>
<tr><td>5·91</td><td colspan="2">1·52</td><td>6·14</td></tr>
<tr><td>0·51</td><td colspan="2">⟨1·81⟩</td><td>0·60</td></tr>
<tr><td>1·97</td><td colspan="2">5·66</td><td>2·90</td></tr>
<tr><td>6·31</td><td colspan="2">6·92</td><td>4·33</td></tr>
<tr><td></td><td colspan="2">8·36</td><td></td></tr>
</table>

<table>
<tr><th colspan="4">Profile 5</th></tr>
<tr><th>T_S</th><th>V_S</th><th>V_N</th><th>T_N</th></tr>
<tr><td>6·41</td><td colspan="2">1·52</td><td>6·41</td></tr>
<tr><td>2·55</td><td colspan="2">⟨2·38⟩</td><td>1·95</td></tr>
<tr><td>1·03</td><td colspan="2">5·44</td><td>4·03</td></tr>
<tr><td>4·94</td><td colspan="2">6·98</td><td>5·09</td></tr>
<tr><td></td><td colspan="2">8·64</td><td></td></tr>
</table>

<table>
<tr><th colspan="4">Profile 6</th></tr>
<tr><th>T_S</th><th>V_S</th><th>V_N</th><th>T_N</th></tr>
<tr><td>5·58</td><td colspan="2">1·52</td><td>5·58</td></tr>
<tr><td>0·25</td><td colspan="2">⟨1·58⟩</td><td>0·08</td></tr>
<tr><td>1·21</td><td colspan="2">2·56</td><td>1·34</td></tr>
<tr><td>4·10</td><td colspan="2">3·52</td><td>2·51</td></tr>
<tr><td>2·32</td><td colspan="2">4·75</td><td>4·34</td></tr>
<tr><td>4·66</td><td colspan="2">[6·62]</td><td>6·39</td></tr>
<tr><td></td><td colspan="2">8·35</td><td></td></tr>
</table>

<table>
<tr><th colspan="4">Profile 7</th></tr>
<tr><th>T_S</th><th>V_S</th><th>V_N</th><th>T_N</th></tr>
<tr><td>4·78</td><td colspan="2">1·51</td><td>4·78</td></tr>
<tr><td>3·44</td><td colspan="2">⟨2·46⟩</td><td>1·02</td></tr>
<tr><td></td><td colspan="2">5·27</td><td>(1·89)</td></tr>
<tr><td></td><td></td><td>(6·06)</td><td></td></tr>
</table>

<table>
<tr><th colspan="4">Profile 8</th></tr>
<tr><th>T_E</th><th>V_E</th><th>V_W</th><th>T_W</th></tr>
<tr><td>0·66</td><td colspan="2">1·54</td><td>0·66</td></tr>
<tr><td>1·08</td><td colspan="2">1·97</td><td>1·09</td></tr>
<tr><td>1·95</td><td colspan="2">3·80</td><td>1·22</td></tr>
<tr><td>3·16</td><td colspan="2">5·19</td><td>2·19</td></tr>
<tr><td></td><td colspan="2">6·26</td><td></td></tr>
</table>

<table>
<tr><th colspan="4">Profile 9</th></tr>
<tr><th>T_N</th><th>V_N</th><th>V_S</th><th>T_S</th></tr>
<tr><td>1·68</td><td colspan="2">1·54</td><td>4·22</td></tr>
<tr><td>1·18</td><td colspan="2">[2·04]</td><td>0·90</td></tr>
<tr><td>0·48</td><td colspan="2">2·94</td><td>1·27</td></tr>
<tr><td>0·64</td><td colspan="2">3·73</td><td>2·18</td></tr>
<tr><td>6·07</td><td colspan="2">5·06</td><td>0·14</td></tr>
<tr><td></td><td colspan="2">[5·99]</td><td></td></tr>
</table>

<table>
<tr><th colspan="4">Profile 10</th></tr>
<tr><th>T_N</th><th>V_N</th><th>V_S</th><th>T_S</th></tr>
<tr><td>4·22</td><td colspan="2">1·54</td><td>4·22</td></tr>
<tr><td>0·74</td><td colspan="2">2·04</td><td>1·37</td></tr>
<tr><td>1·57</td><td>(3·14)</td><td></td><td>0</td></tr>
<tr><td>1·80</td><td colspan="2">3·97</td><td>0·63</td></tr>
<tr><td>9·53</td><td colspan="2">6·13</td><td>4·11</td></tr>
<tr><td></td><td colspan="2">7·58</td><td></td></tr>
</table>

<table>
<tr><th colspan="4">Profile 11</th></tr>
<tr><th>T_W</th><th>V_W</th><th>V_E</th><th>T_E</th></tr>
<tr><td></td><td colspan="2">1·54</td><td>2·09</td></tr>
<tr><td></td><td></td><td>(1·82)</td><td>0·22</td></tr>
<tr><td></td><td></td><td>(2·30)</td><td>1·09</td></tr>
<tr><td></td><td></td><td>(3·75)</td><td>1·56</td></tr>
<tr><td></td><td></td><td>(6·04)</td><td></td></tr>
</table>

<table>
<tr><th colspan="4">Profile 12</th></tr>
<tr><th>T_W</th><th>V_W</th><th>V_E</th><th>T_E</th></tr>
<tr><td>2·09</td><td colspan="2">1·54</td><td>1·34</td></tr>
<tr><td>—</td><td></td><td>[1·70]</td><td>0·30</td></tr>
<tr><td>0·22</td><td colspan="2">1·82</td><td>0·65</td></tr>
<tr><td>1·09</td><td colspan="2">2·30</td><td>0·21</td></tr>
<tr><td>1·56</td><td colspan="2">3·75</td><td>1·72</td></tr>
<tr><td></td><td colspan="2">6·04</td><td></td></tr>
</table>

<table>
<tr><th colspan="4">Profile 13</th></tr>
<tr><th>T_W</th><th>V_W</th><th>V_E</th><th>T_E</th></tr>
<tr><td>0·91</td><td colspan="2">1·54</td><td>1·28</td></tr>
<tr><td>0·63</td><td></td><td>[1·72]</td><td>0·71</td></tr>
<tr><td>1·56</td><td></td><td>(2·45)</td><td>0·71</td></tr>
<tr><td>1·03</td><td></td><td>(3·98)</td><td>2·48</td></tr>
<tr><td></td><td></td><td>(5·42)</td><td></td></tr>
</table>

⟨ ⟩—sedimentary velocity from refl. prof. ( )—unreversed velocity. [ ]—assumed velocity.
All depths in kilometres and all velocities in kilometres per second.

Table 1. Measured Seismic Velocities and Thicknesses—continued

1955 *and* 1956 *Profiles*

Profile *14*				Profile *15*				Profile *16*				Profile *17*				Profile *18*			
T_W	V_W	V_E	T_E	T_W	V_W	V_E	T_E	T_N	V_N	V_S	T_S	T_N	V_N	V_S	T_S	T_N	V_N	V_S	T_S
1·28	1·54		0·70	0·70	1·54		0·70	0·04	1·54		0·04	6·46	1·52		5·30	7·83	1·53		5·41
0·71	1·72		0·44	0·38	[1·72]		0·05	0·19	(2·08)		0·10	0·15	⟨1·68⟩		0·61	0·26	⟨1·64⟩		0·15
0·71	2·45		0·91	1·33	2·68		0·98	0·35	2·72		0·97	1·46	(2·04)		—	—		(3·48)	2·02
2·50	3·98		1·95	1·40	3·66		1·08	1·60	4·78		3·88	—		(3·85)	4·91	5·94	4·62		11·87
	5·41				5·23				6·23			5·55	5·48		6·70	3·67	[6·68]		4·18
												6·35	6·76		3·46		8·30		
													8·42						

Profile *19*				Profile *20*				Profile *21*				Profile *22*				Profile *23*			
T_N	V_N	V_S	T_S	T_E	V_E	V_W	T_W	T_N	V_N	V_S	T_S	T_N	V_N	V_S	T_S	T_N	V_N	V_S	T_S
0·06	1·54		0·06	6·02	1·52		6·02	1·21	1·54		1·94	1·74	1·54		1·41	1·41	1·54		1·22
0		(2·00)	0·38	0·04	⟨1·58⟩		0·18	1·04		(1·66)	0·83	0·73	1·67		0·62	0·67	1·65		0·77
0·63	(2·86)		0	2·63	3·66		2·17	1·12	2·61		1·38	2·51	3·23		1·30	0·96	2·90		0·88
1·41	3·83		1·61	10·05	5·55		9·18	3·78	5·44		1·76	0·87		(4·98)	2·77		4·70		
2·57	5·64		5·31	3·43	[6·79]		3·94	4·13	5·95		2·75		6·24						
	6·49				8·43				6·52										

⟨ ⟩—sedimentary velocity from refl. prof. ( )—unreversed velocity. [ ]—assumed velocity.
All depths in kilometres and all velocities in kilometres per second.

Table 1. *Measured Seismic Velocities and Thicknesses—continued*

1955 *and* 1956 *Profiles*

<table>
<tr><th colspan="4">Profile 24</th><th colspan="4">Profile 25</th><th colspan="4">Profile 26</th></tr>
<tr><th>T_E</th><th>V_E</th><th>V_W</th><th>T_W</th><th>T_E</th><th>V_E</th><th>V_W</th><th>T_W</th><th>T_N</th><th>V_N</th><th>V_S</th><th>T_S</th></tr>
<tr><td>3·41</td><td colspan="2">1·54</td><td>4·41</td><td>4·92</td><td colspan="2">1·54</td><td>5·02</td><td>4·95</td><td colspan="2">1·54</td><td>4·95</td></tr>
<tr><td>0·49</td><td colspan="2">1·70</td><td>0·37</td><td>0·63</td><td colspan="2">[1·70]</td><td>0·91</td><td>0·75</td><td colspan="2">1·73</td><td>1·45</td></tr>
<tr><td>0·40</td><td>(2·35)</td><td></td><td>0·60</td><td>0·03</td><td colspan="2">2·05</td><td>0·14</td><td>4·25</td><td colspan="2">5·99</td><td>1·77</td></tr>
<tr><td>1·93</td><td>(3·21)</td><td></td><td>0·74</td><td>1·99</td><td></td><td>(2·73)</td><td>1·63</td><td>5·08</td><td colspan="2">7·21</td><td>4·55</td></tr>
<tr><td>1·94</td><td>(4·95)</td><td></td><td>1·10</td><td>2·11</td><td colspan="2">6·23</td><td>2·16</td><td></td><td colspan="2">8·20</td><td></td></tr>
<tr><td>5·32</td><td colspan="2">6·15</td><td>5·10</td><td>2·95</td><td colspan="2">7·63</td><td>3·05</td><td></td><td colspan="2"></td><td></td></tr>
<tr><td>4·51</td><td colspan="2">7·36</td><td>5·75</td><td></td><td colspan="2">8·23</td><td></td><td></td><td colspan="2"></td><td></td></tr>
<tr><td></td><td colspan="2">8·08</td><td></td><td></td><td colspan="2"></td><td></td><td></td><td colspan="2"></td><td></td></tr>
</table>

<table>
<tr><th colspan="4">Profile 27</th><th colspan="4">Profile 28</th><th colspan="4">Profile 29</th><th colspan="4">Profile 30</th></tr>
<tr><th>T_N</th><th>V_N</th><th>V_S</th><th>T_S</th><th>T_E</th><th>V_E</th><th>V_W</th><th>T_W</th><th>T_E</th><th>V_E</th><th>V_W</th><th>T_W</th><th>T_E</th><th>V_E</th><th>V_W</th><th>T_W</th></tr>
<tr><td>4·46</td><td colspan="2">1·54</td><td>4·46</td><td>0·03</td><td colspan="2">1·54</td><td>0·03</td><td>3·67</td><td colspan="2">1·51</td><td>3·67</td><td>0·04</td><td colspan="2">1·54</td><td>0·05</td></tr>
<tr><td>0·84</td><td colspan="2">[1·80]</td><td>0·42</td><td>0·10</td><td colspan="2">1·89</td><td>0·17</td><td>0·79</td><td colspan="2">⟨1·91⟩</td><td>0·77</td><td>0·15</td><td colspan="2">1·98</td><td>0·29</td></tr>
<tr><td>1·28</td><td colspan="2">3·32</td><td>1·74</td><td>0·17</td><td colspan="2">2·90</td><td>0·51</td><td>2·64</td><td colspan="2">4·96</td><td>1·65</td><td>0·72</td><td colspan="2">2·85</td><td>1·03</td></tr>
<tr><td>2·76</td><td colspan="2">6·51</td><td>2·93</td><td>5·74</td><td colspan="2">5·71</td><td>4·15</td><td>8·30</td><td colspan="2">6·05</td><td>3·93</td><td>0·89</td><td colspan="2">4·55</td><td>3·86</td></tr>
<tr><td>5·75</td><td colspan="2">7·11</td><td>5·50</td><td></td><td colspan="2">6·61</td><td></td><td></td><td colspan="2">7·03</td><td></td><td>11·60</td><td colspan="2">5·75</td><td>5·37</td></tr>
<tr><td></td><td colspan="2">7·92</td><td></td><td></td><td colspan="2"></td><td></td><td></td><td colspan="2"></td><td></td><td></td><td colspan="2">6·98</td><td></td></tr>
</table>

⟨ ⟩—sedimentary velocity from refl. prof. ( )—unreversed velocity. [ ]—assumed velocity.
All depths in kilometres and all velocities in kilometres per second.

shot and the fitted refraction lines from which the calculations were made, the bottom topography for each shooting ship track, and the computed seismic section. Table 1 is a tabulation of the computed thicknesses and velocities for each layer. Along each refraction line in each of the figures its equation has been written in the form

$$G = \frac{D}{4{\cdot}56} + 1{\cdot}23 \qquad (8)$$

The dependent variable is the G travel time and the independent variable the D travel time. The number, 4·56, is the inverse slope with respect to D; the apparent velocity c_{na} is this number multiplied by c_0. The number, 1·23, is the time intercept t_{na}. The 1955 results presented by OFFICER *et al.* (1957) did not have topographic corrections; these profiles have been reanalysed here and some changes in the results do occur. In particular the long range Venezuelan basin profiles 31, 32, and 33 are now interpreted as having an additional deeper horizon whose velocity is slightly higher than that of the deepest horizon in the previous interpretation. The pertinent features of each of the profiles is discussed below. Their locations are given in Fig. 1 and the measured seismic velocities and thicknesses are given in Table 1.

1, 2, 3, 4. All these profiles are short and unreversed. They provide little information.

5, 6. Require no comment.

7. The drift of the *Atlantis* at the northern end of the profile was considerably greater than that for the *Caryn* at the southern end. The reverse shooting track of the *Caryn* was not true. The profile was long but was not heavily shot. No velocity above 7·38 km/sec was determined; this is probably due to the sparsity of points on the travel time graph rather than the absence of higher velocities at the depths corresponding to the distance of coverage of this profile.

8, 9. These were short reversed profiles. All velocities are well determined, but the profiles are not long enough to detect the mantle.

10. This is an unreversed profile. The true velocities used in the calculations were chosen to agree with nearby profiles 30, *22*, and *23*.

11, 12. The quality of the *Caryn* records in these profiles is sub-normal, particularly in part of profile 11, but owing to the mutual support obtained by having the profiles end-to-end, the results should be reasonably reliable.

13, 14. These profiles are well shot and have the control furnished by end-to-end reversed profiles, but there is still enough scatter of the points to make the interpretation somewhat uncertain in detail. For example, the reverse points in profile 14 fail to agree by almost 0·4 sec. This discrepancy can be attributed to an excessive delay between shooting the two halves of the profile producing a large offset in the two shooting tracks.

There is evidence from reflection data of a higher velocity sediment layer approximately 0·5 km below the ocean floor. This could be the 2·2–2·8 km/sec layer found in the neighbouring profiles and is assumed in Section 8, Fig. 21. Because of the scattering of the points in these profiles, the velocity in the deepest layer may not be determined accurately. Comparison with profile 26 (previous profiles) and profiles 11 and 12 suggest that either the velocity determination is substantially low or else the 5·3 km/sec layer is thin.

15. This profile has well determined lines but is unreversed and gives only apparent velocities.

16. Most of the lines on the travel time graph are reasonably well determined and reverse satisfactorily, although the scattering of the points, particularly on the high velocity lines, indicates a considerable amount of relief in the deeper interfaces.

17. This profile measures the thick sedimentary section on the eastern flank of the Barbados ridge and shows the westward dip of the high-velocity layers. Possibly some of the 4–5 km/sec material found in the Barbados ridge is present at the west end of this profile. Although it was not seen as a refractor it could be masked by the great thickness of low velocity material.

18. This profile, as presented by EWING *et al.* (1957), did not properly take into account the effects of the topographic rise at the south end and has been recomputed for this paper. The first computation showed more dip in the deep interface. The results here, although showing considerably more sedimentary material, are typical of ocean basin profiles. The lines, G_s, are determined by transformed shear waves.

19. The interpretation of this profile was complicated, and the results given by it are very uncertain. Although no arrivals could be picked in the *Caryn* records to fit the G_5 line, it was assumed that they were too weak to be seen. Any alternate structural interpretation which would fit the data and even approximately satisfy the conditions for a reversed profile, requires a very large fault or flexure near one end of the profile (west side down relative to the east side).

20. This profile shows a very large fault or steep flexure near the north end. An alternate interpretation might be considered wherein it would be assumed that the last three points in the Atlantis profile and all the points in the *Caryn* profile came from multiply refracted arrivals. It is very improbable, however, that all the first arrivals in the *Caryn* records could have been missed, since there was normal sensitivity and no unusual noise.

21. Although the upper layers in this profile are satisfactorily determined, the velocity in the deepest one is not. On the basis of two very weak records (points not plotted) between the last two in the *Caryn* profile, there is some possibility of increasing the velocity in the deepest layer by a small amount, thereby slightly increasing the depth to that layer at the south end.

22. This is a long profile, but the shots at the greater distances were not large enough to penetrate to the deeper layers. The scatter of points indicates a rather large amount of relief in the layers. Perhaps complexity in the layering, as well as, or rather than great thickness prevented the detection of arrivals from deeper layers. The dashed lines G_4 were drawn to compute the minimum depth to a velocity of 6·5 km/sec, assuming that the longest recorded shots were large enough to penetrate to the required depth but that the range was not sufficient to give a first arrival from such a layer. The computed minimum depth is 12 km, but there is not much significance attached to it in such a complicated area as this.

23, 24. This end-to-end pair consists of one unreversed and one reversed profile. The layer thicknesses at the north end of 23 were computed on the assumption that the velocity in each layer does not change appreciably between the two profiles. The high point on the end of the G_6 line probably represents a downward flexure or fault in the 6·4 km/sec layer. This layer was not detected at profiles 26 and 27, a few miles further north, presumably because of its great depth, and it is unfortunate that profile 23 was not longer to provide more confirmation of this depth.

25. This is a long unreversed profile shot approximately parallel to the northern coast of Trinidad and Venezuela. The layer thicknesses were computed on the assumption that there was no component of dip in the direction of the profile.

26, 27. The most significant feature of these profiles is their failure to detect the 6·0–6·5 km/sec crustal layer, which is found at a depth of 4–6 km near Grenada and Trinidad. Minimum depth computations for profile 27, which is relatively long and heavily shot, give a depth of at least 12 km to this layer. This is the evidence on which the synclinal feature shown in Section 9 was based.

28. This unreversed profile was shot along the Lesser Antilles arc between Grenada and St. Vincent. Although only apparent velocities were measured, probably these are not seriously effected by slope since the shot line is approximately parallel to the structure of the arc. The section for this profile does not show the structure indicated by the offset in the G_3 line at about 27 sec of D time. This effect can be accounted for by either an elevation (north relative to south) of the 6·4 km/sec layer or an elevation of both the 4·0 and the 6·4 km/sec layers. In the former case, an elevation of 3 km is required, which would bring the top of the 6·4 layer approximately to the level of the top of the 4·0 layer as it appears in the section. The latter case requires the elevation of both the lower layers approximately 1·5 km, which would raise the 4·0 km/sec layer to about water depth, i.e. there would be a negligible thickness of the lower-velocity materials at the north end of the profile.

29. The *Atlantis* segment of this reversed profile gave a good determination of all the velocity layers. The *Caryn* reverse was not completed and only gave a reversed profile for the two highest velocity lines.

30. Requires no comment.

31. A reinterpretation of this profile was made. The topographic corrections made a considerable change in the higher velocity lines, showing an additional line with velocity 8·31 km/sec. The solution given here is more compatible within itself and is more in agreement with nearby profiles than the solution given previously by OFFICER *et al.* (1957).

32. A reinterpretation of this profile, particularly of the arrivals determining the highest velocity line, indicated that the highest velocity could be drawn with a higher velocity, 8·04 km/sec, than that given previously. The arrivals at the longer ranges, necessary for a good determination of this line, were weak; their beginnings could not be determined accurately.

33. A reinterpretation of this profile, including topographic corrections, made a considerable change in the velocity and configuration of the higher velocity layers. The arrivals on the highest velocity line were weak; the line is not well determined.

34. The topographic slope is steep. The profile is short, but the underlying configuration is well determined. There is a considerable difference in the apparent velocities of the two sides of the reverse.

35, 37. Require no comments.

36. This is a well determined unreversed profile. The highest velocity line probably does not represent a true seismic velocity. A change in the assumed

lope, needed for velocity calculation, would give a lower velocity than that hown in Table 1.

38. The lines are well determined. A masked arrival line, given in the previous nterpretation, was not included here.

39, 40, 41. These form three end-to-end, reversed profiles. Only one high elocity line was determined. The profiles give a good determination of the hange in configuration of this surface along the surveyed line.

42. Corrections for the large change in topography across the profile provided early straight lines. Only one velocity line was measured.

43. Similar to 42 only one velocity line was determined. This was a long rofile; and only the first high velocity line, near the ocean bottom was measured. These two profiles are approximately over the negative gravity anomaly minimum, where the 5·5–5·8 km/sec layer is presumed to be thickest.

44. This is a well determined profile in the northern portion of the Puerto Rico trench. Topographic corrections removed most of the scatter of the observed oints from the determined lines.

45. This is a well determined profile. The displacement of the velocity lines n both halves of the reversed profile is interpreted as a fault as shown.

46. Requires no comment.

47. This profile was shot normal to the axis of the trench. The large change n topography caused complications in the interpretation. The profile was hort, but large charges, 300 lb of TNT, had to be used for the more distant oints in order to get readable refraction seismograms. This is to be compared vith 25 lb of TNT for the same distance on profile 46.

1. The topography from both ships shows an abrupt peak about $\frac{1}{2}$ km high. This is formed by the 4·22 km/sec material. The last point on each line falls vell above the highest velocity line.

2. The effect due to the change in topography on the *Bear* shooting track was emoved by a topographic correction. The points define well determined lines.

3. The effects due to the change in topography on both shooting tracks was emoved by a topographic correction. The points define well determined lines.

4, *5*. Require no comment.

6. The overlying materials with velocities 2·56, 3·52 and 4·75 km/sec are hick under this profile. The dashed lines are the masked or nearly masked elocity lines for the crustal refraction arrival. It has been included in the depth alculation.

7. This is a poor profile. The arrivals are weak and do not give well defined ines.

8. Topographic corrections were applied assuming the bottom to be level at 60 fathoms and all interfaces parallel. The residuals indicate that there is a onsiderable amount of relief in one or more of the deeper layers. The structure ection was drawn to correspond to the assumed structure. Actually all interaces on the west end are deeper by the amount of increased water depth.

9, *10*. Topographic corrections were applied for a level base line at 2240 athoms for profile *10* and to a sloping base line paralleling the topography in rofile *9*. All interfaces are actually about 0·8 km. higher than shown at the orth end of the section. The accuracy is probably not high in profile *9* due to he steep slope. The lines have been drawn to give the best fit of the points, as vell as to produce a satisfactory agreement with profile *10*. The velocity in the

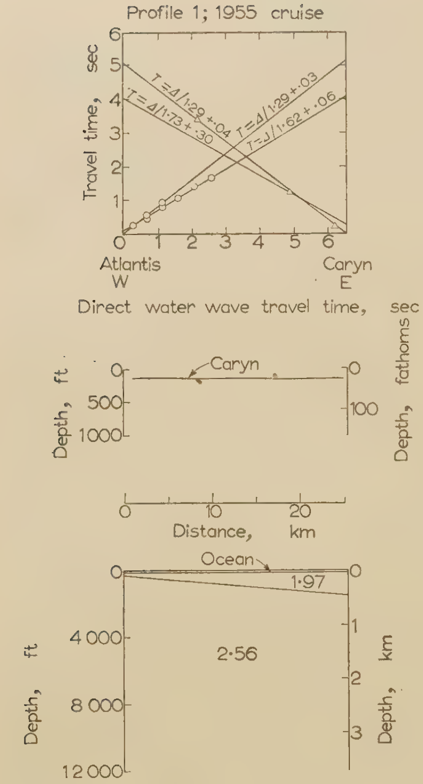
Profile 1; 1955 cruise
Travel time, sec
0
1
2
3
4
5
6
T=Δ/1·29+·04
T=Δ/1·73+·30
T=Δ/1·29+·03
T=Δ/1·62+·06
Atlantis
W
Caryn
E
Direct water wave travel time, sec
Depth, ft
0
500
1000
Caryn
Depth, fathoms
0
100
0
10
20
Distance, km
Ocean
1·97
2·56
Depth, ft
0
4 000
8 000
12 000
Depth, km
0
1
2
3

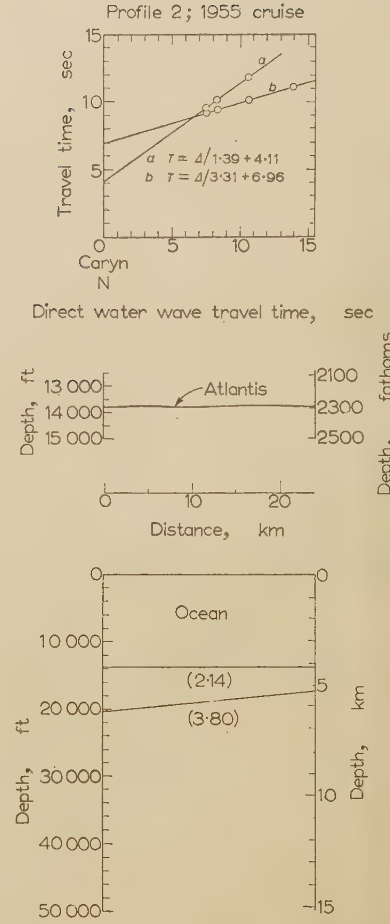
Profile 2; 1955 cruise
Travel time, sec
0
5
10
15
a
b
a T = Δ/1·39 + 4·11
b T = Δ/3·31 + 6·96
Caryn
N
Direct water wave travel time, sec
Depth, ft
13 000
14 000
15 000
Atlantis
2100
2300
2500
Depth, fathoms
0
10
20
Distance, km
Ocean
(2·14)
(3·80)
Depth, ft
0
10 000
20 000
30 000
40 000
50 000
Depth, km
0
5
10
15

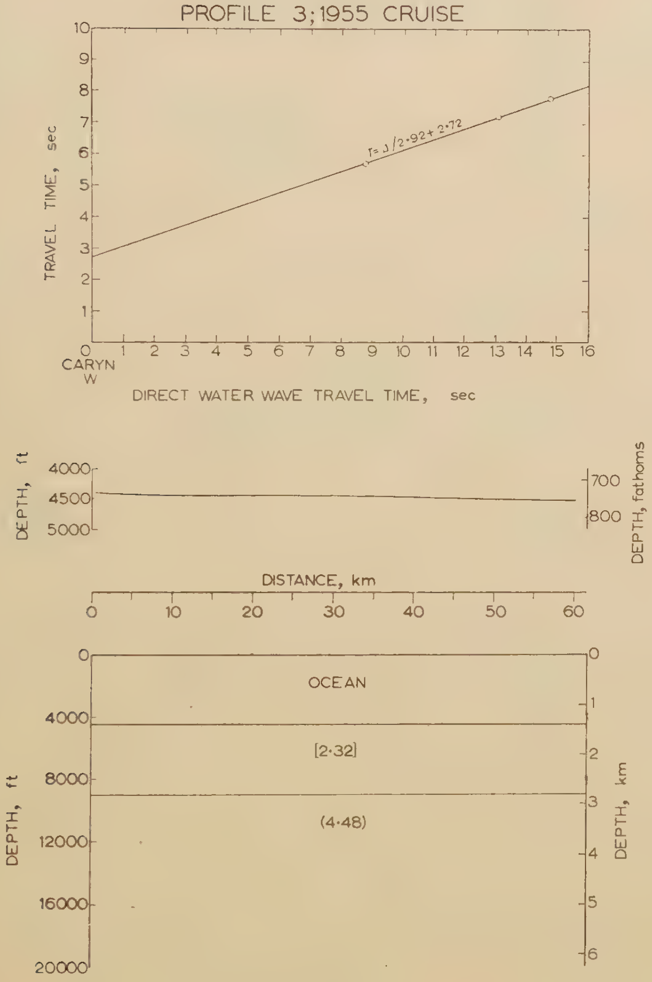
PROFILE 3;1955 CRUISE
TRAVEL TIME, sec
10
9
8
7
6
5
4
3
2
1
0
1
2
3
4
5
6
7
8
9
10
11
12
13
14
15
16
CARYN
W
T= Δ/2·92+ 2·72
DIRECT WATER WAVE TRAVEL TIME, sec
DEPTH, ft
4000
4500
5000
700
800
DEPTH, fathoms
DISTANCE, km
0
10
20
30
40
50
60
DEPTH, ft
0
4000
8000
12000
16000
20000
OCEAN
[2·32]
(4·48)
DEPTH, km
0
1
2
3
4
5
6

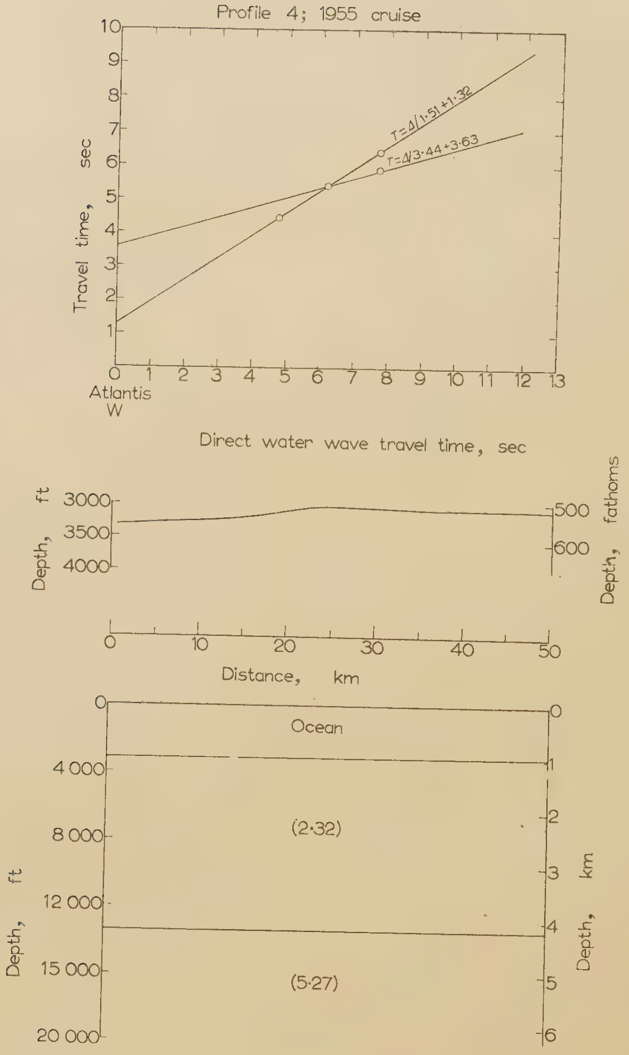
Profile 4; 1955 cruise
Travel time, sec
T=Δ/1·51+1·32
T=Δ/3·44+3·63
Atlantis W
Direct water wave travel time, sec
Depth, ft
3000
3500
4000
500
600
Depth, fathoms
Distance, km
Ocean
(2·32)
(5·27)
4 000
8 000
12 000
15 000
20 000
Depth, km

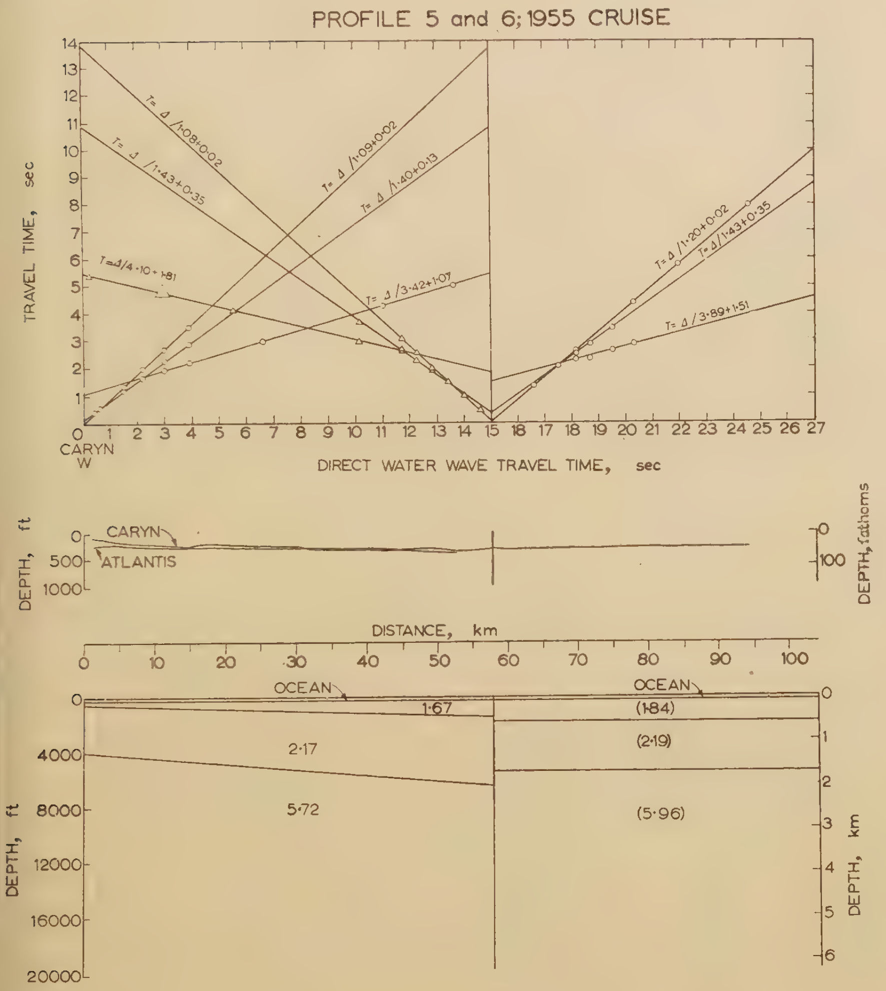

PROFILE 5 and 6; 1955 CRUISE

PROFILE 7; 1955 CRUISE

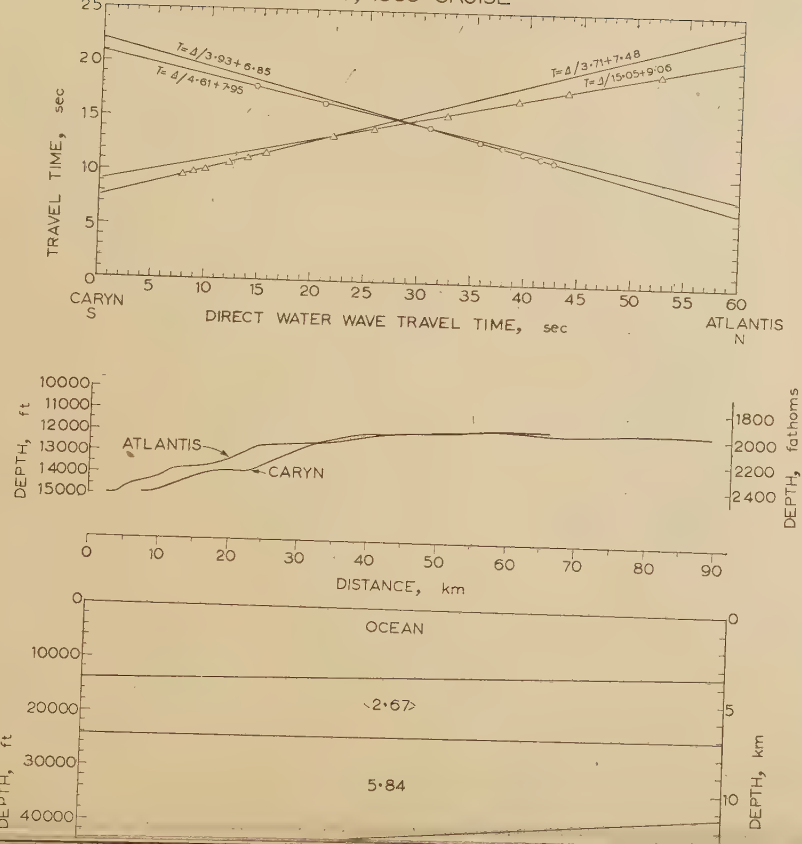

PROFILE 8; 1955 CRUISE

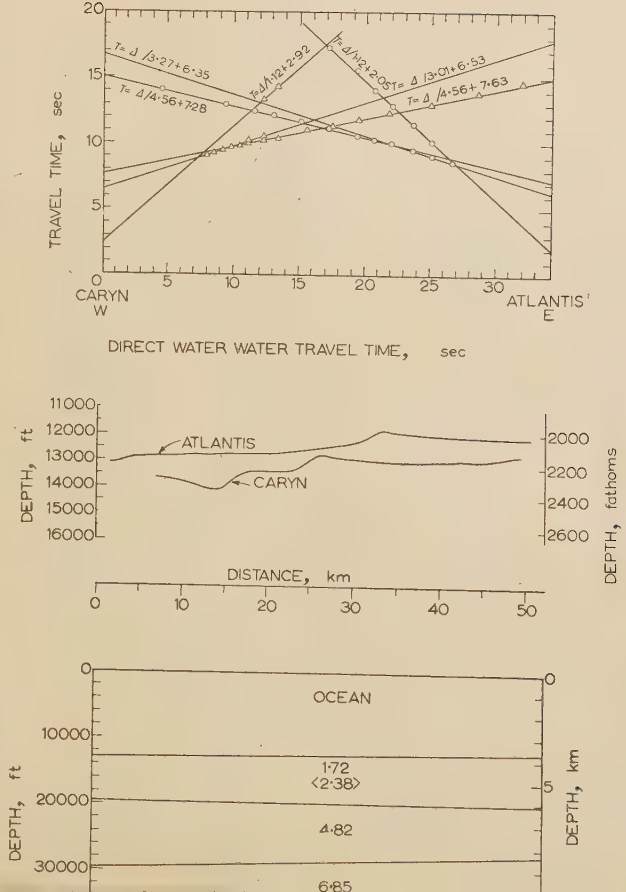

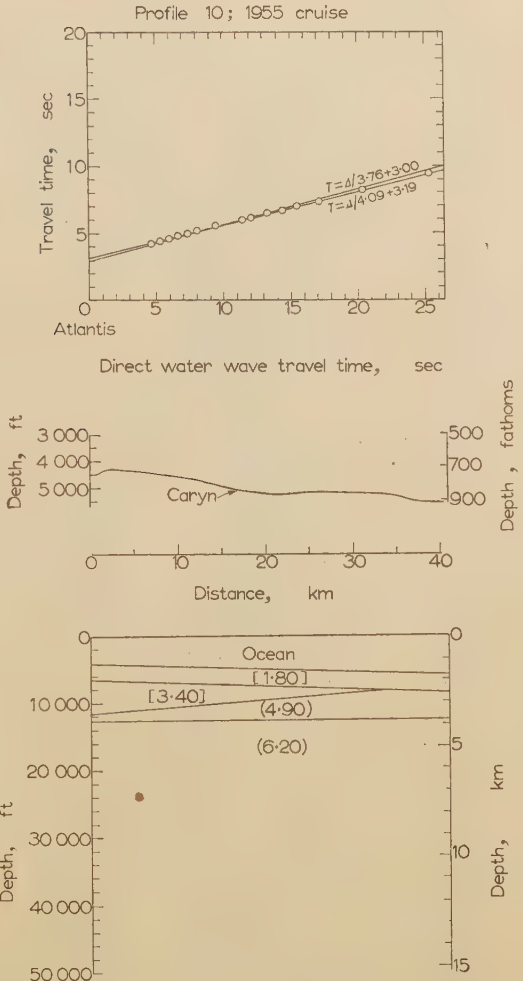
Profile 10; 1955 cruise
Travel time, sec
20
15
10
5
0
T=Δ/3·76+3·00
T=Δ/4·09+3·19
5
10
15
20
25
Atlantis
Direct water wave travel time, sec
Depth, ft
3 000
4 000
5 000
Caryn
500
700
900
Depth, fathoms
0
10
20
30
40
Distance, km
0
Ocean
[1·80]
[3·40]
(4·90)
(6·20)
10 000
20 000
30 000
40 000
50 000
Depth, ft
0
5
10
15
Depth, km

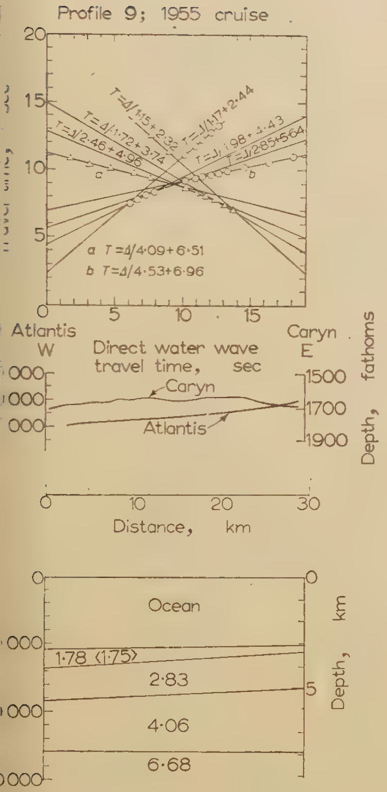
Profile 9; 1955 cruise
20
15
10
5
T=Δ/1·15+2·32
T=Δ/1·72+3·74
T=Δ/2·46+4·96
T=Δ/1·17+2·44
T=Δ/1·98+4·43
T=Δ/2·85+5·64
c
b
a T=Δ/4·09+6·51
b T=Δ/4·53+6·96
0
5
10
15
Atlantis
W
Direct water wave travel time, sec
Caryn
E
000
000
000
Caryn
Atlantis
1500
1700
1900
Depth, fathoms
0
10
20
30
Distance, km
0
Ocean
000
1·78 ⟨1·75⟩
2·83
000
4·06
000
6·68
0
5
Depth, km

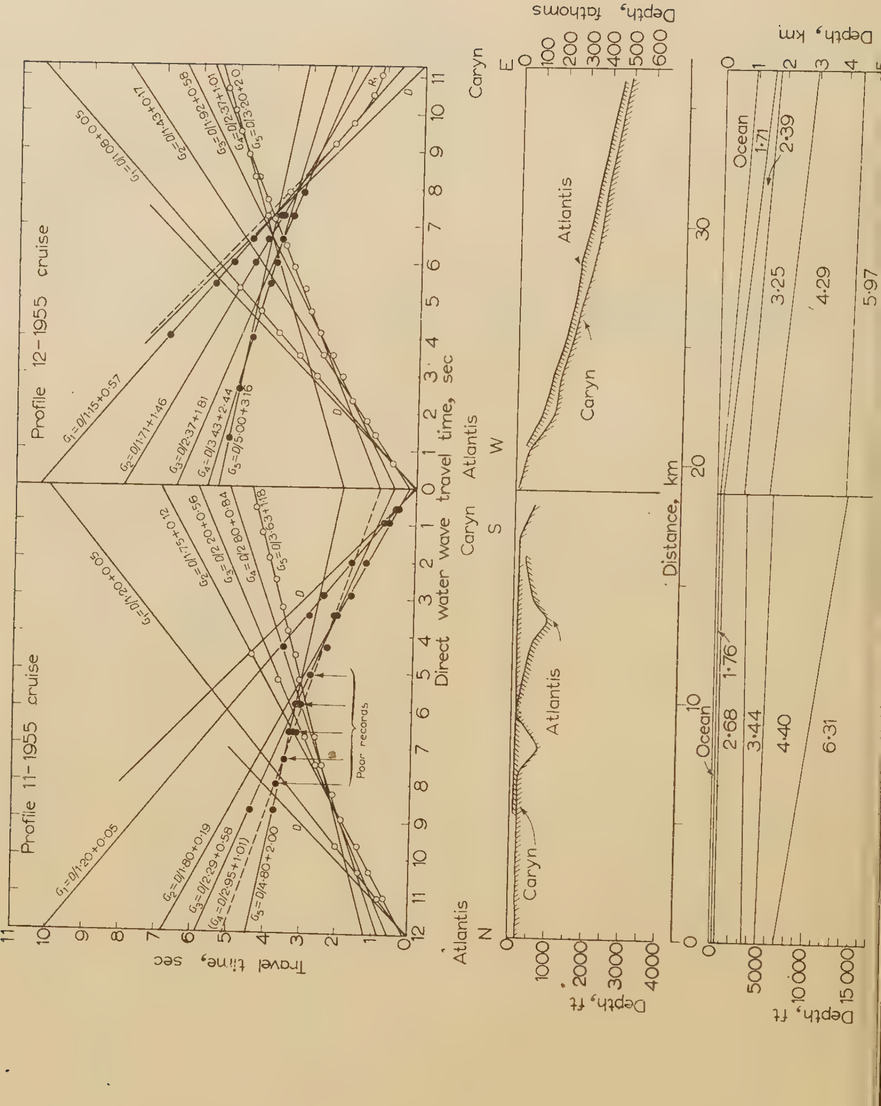
Profile 11-1955 cruise
Profile 12-1955 cruise
Travel time, sec
Direct water wave travel time, sec
G1=0/1·20+0·05
G2=0/1·80+0·19
G3=0/2·29+0·58
(G4=0/2·95+1·01)
G5=0/4·80+2·00
G1=0/1·20+0·05
G2=0/1·75+0·12
G2=0/2·20+0·56
G3=0/2·80+0·84
G4=0/2·80+0·84
G5=0/3·63+1·18
G1=0/1·15+0·57
G2=0/1·71+1·46
G3=0/2·37+1·81
G4=0/3·43+2·44
G5=0/5·00+3·16
G1=0/1·08+0·05
G2=0/1·43+0·17
G2=0/1·43+0·58
G3=0/1·92+1·01
G4=0/2·37+1·01
G5=0/3·20+2·0
Poor records
D
R1
Atlantis
N
Caryn
S
Caryn
Atlantis
W
Caryn
E
Caryn
Atlantis
Atlantis
Caryn
Depth, ft
Depth, fathoms
Distance, km
Depth, ft
Depth, km
Ocean
1·76
2·68
3·44
4·40
6·31
Ocean
1·71
2·39
3·25
4·29
5·97

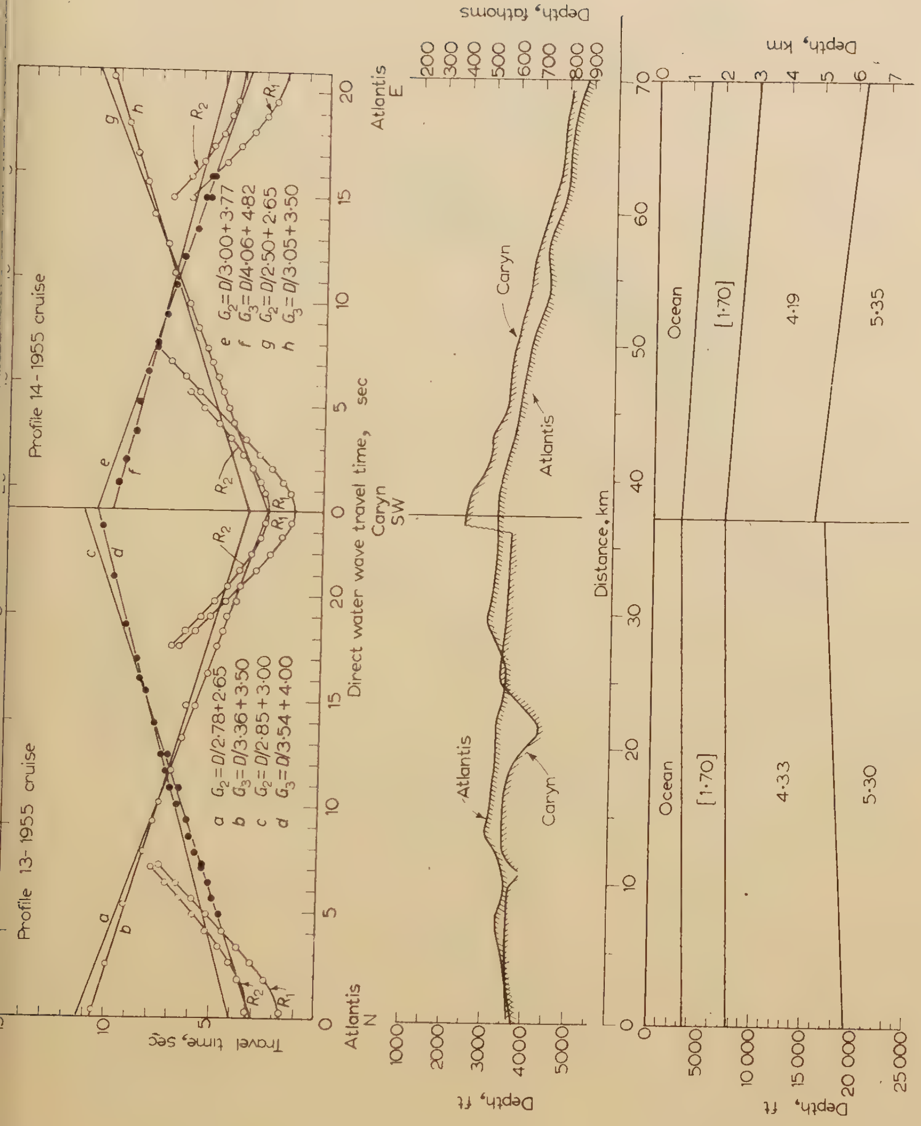
Profile 13 - 1955 cruise
Profile 14 - 1955 cruise
a $G_2 = D/2{\cdot}78 + 2{\cdot}65$
b $G_3 = D/3{\cdot}36 + 3{\cdot}50$
c $G_2 = D/2{\cdot}85 + 3{\cdot}00$
d $G_3 = D/3{\cdot}54 + 4{\cdot}00$
e $G_2 = D/3{\cdot}00 + 3{\cdot}77$
f $G_3 = D/4{\cdot}06 + 4{\cdot}82$
g $G_2 = D/2{\cdot}50 + 2{\cdot}65$
h $G_3 = D/3{\cdot}05 + 3{\cdot}50$
R_1
R_2
Travel time, sec
Direct water wave travel time, sec
Atlantis N
Caryn SW
Atlantis E
Atlantis
Caryn
Depth, ft
Depth, fathoms
Distance, km
Depth, km
Ocean
[1·70]
4·33
5·30
4·19
5·35
0
5
10
15
20
1000
2000
3000
4000
5000
200
300
400
500
600
700
800
900
30
40
50
60
70
10 000
15 000
20 000
25 000
1
2
3
4
6
7

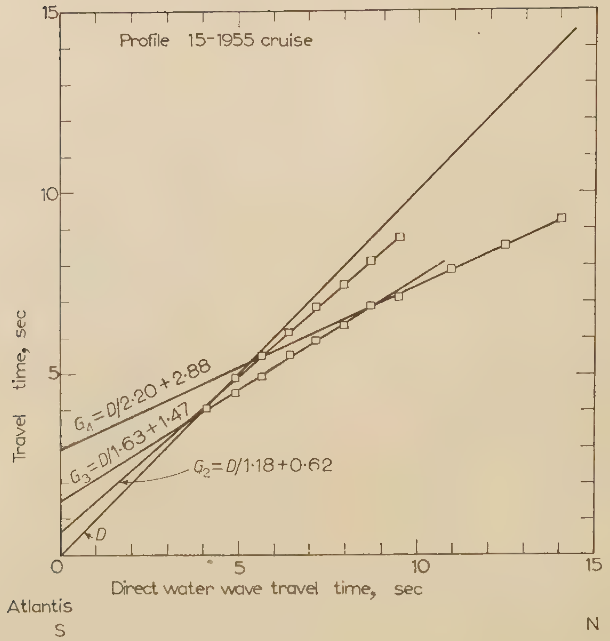
Profile 15-1955 cruise
G4=D/2·20+2·88
G3=D/1·63+1·47
G2=D/1·18+0·62
D
Travel time, sec
Direct water wave travel time, sec
0
5
10
15
Atlantis
S
N

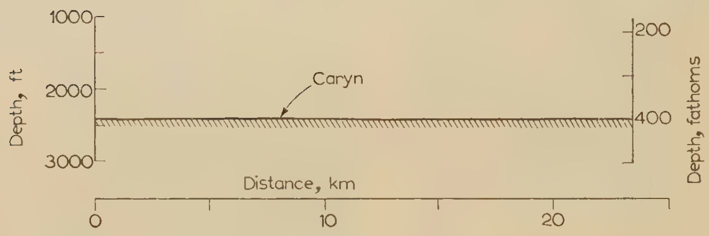
Caryn
Depth, ft
1000
2000
3000
Depth, fathoms
200
400
Distance, km
0
10
20

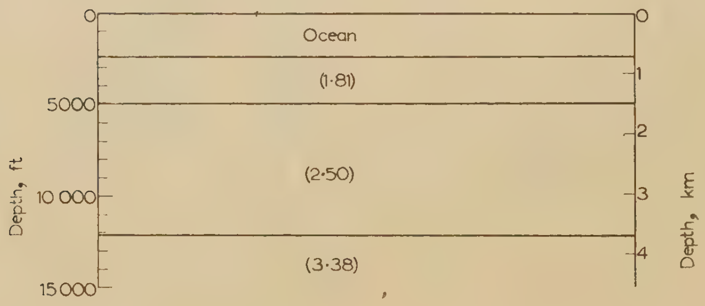
Ocean
(1·81)
(2·50)
(3·38)
Depth, ft
0
5000
10 000
15 000
Depth, km
0
1
2
3
4

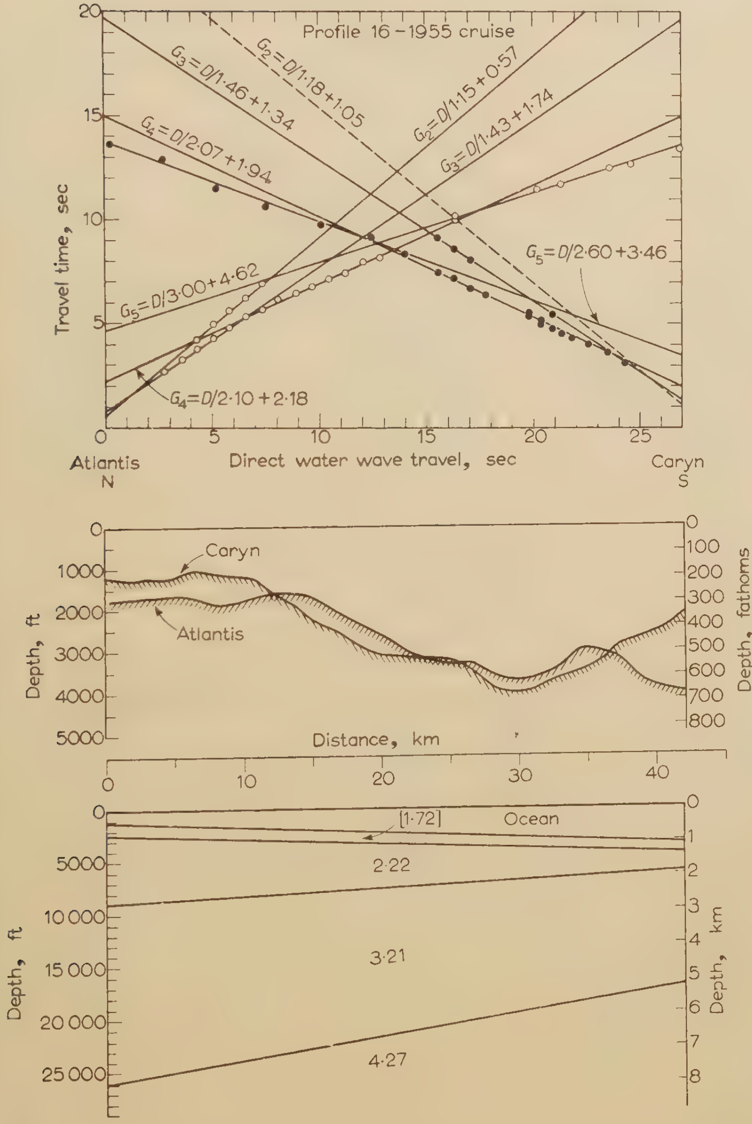
Profile 16 – 1955 cruise
$G_2=D/1{\cdot}18+1{\cdot}05$
$G_3=D/1{\cdot}46+1{\cdot}34$
$G_4=D/2{\cdot}07+1{\cdot}94$
$G_2=D/1{\cdot}15+0{\cdot}57$
$G_3=D/1{\cdot}43+1{\cdot}74$
$G_5=D/2{\cdot}60+3{\cdot}46$
$G_5=D/3{\cdot}00+4{\cdot}62$
$G_4=D/2{\cdot}10+2{\cdot}18$
Travel time, sec
20
15
10
5
0
5
10
15
20
25
Atlantis
N
Direct water wave travel, sec
Caryn
S
Caryn
Atlantis
Depth, ft
0
1000
2000
3000
4000
5000
Depth, fathoms
0
100
200
300
400
500
600
700
800
Distance, km
0
10
20
30
40
[1·72]
Ocean
2·22
3·21
4·27
Depth, ft
0
5000
10 000
15 000
20 000
25 000
Depth, km
0
1
2
3
4
5
6
7
8

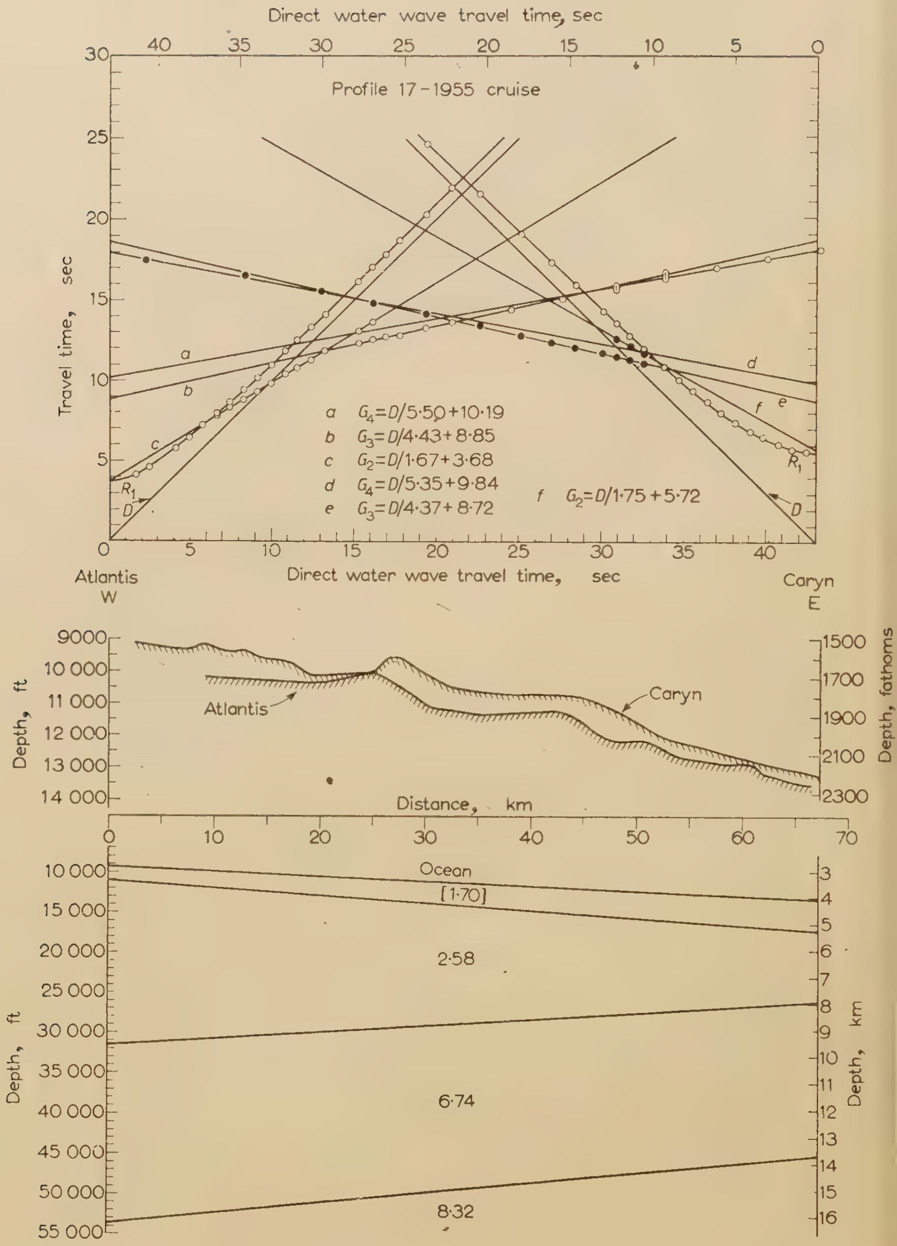
Direct water wave travel time, sec
Profile 17–1955 cruise
Travel time, sec
a G4=D/5·50+10·19
b G3=D/4·43+8·85
c G2=D/1·67+3·68
d G4=D/5·35+9·84
e G3=D/4·37+8·72
f G2=D/1·75+5·72
R1
D
Direct water wave travel time, sec
Atlantis W
Caryn E
Depth, ft
Depth, fathoms
Atlantis
Caryn
Distance, km
Ocean
[1·70]
2·58
6·74
8·32
Depth, ft
Depth, km

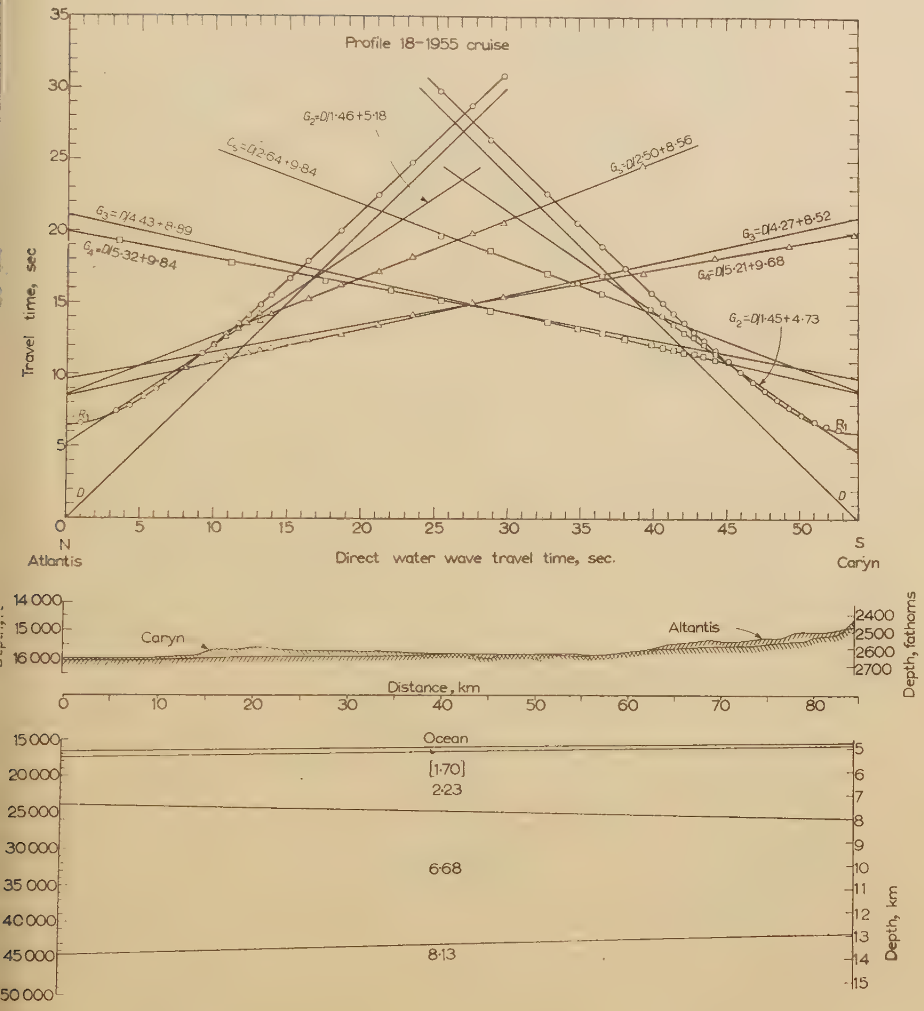
Profile 18–1955 cruise
Travel time, sec
35
30
25
20
15
10
5
0
$G_2=D/1{\cdot}46+5{\cdot}18$
$C_5=D/2{\cdot}64+9{\cdot}84$
$G_5=D/2{\cdot}50+8{\cdot}56$
$G_3=D/4{\cdot}43+8{\cdot}89$
$G_4=D/5{\cdot}32+9{\cdot}84$
$G_3=D/4{\cdot}27+8{\cdot}52$
$G_4=D/5{\cdot}21+9{\cdot}68$
$G_2=D/1{\cdot}45+4{\cdot}73$
R_1
R_1
D
D
0 5 10 15 20 25 30 35 40 45 50
N
Atlantis
Direct water wave travel time, sec.
S
Caryn
14 000
15 000
16 000
Caryn
Altantis
2400
2500
2600
2700
Depth, fathoms
Distance, km
0 10 20 30 40 50 60 70 80
15 000
20 000
25 000
30 000
35 000
40 000
45 000
50 000
Ocean
[1·70]
2·23
6·68
8·13
5
6
7
8
9
10
11
12
13
14
15
Depth, km

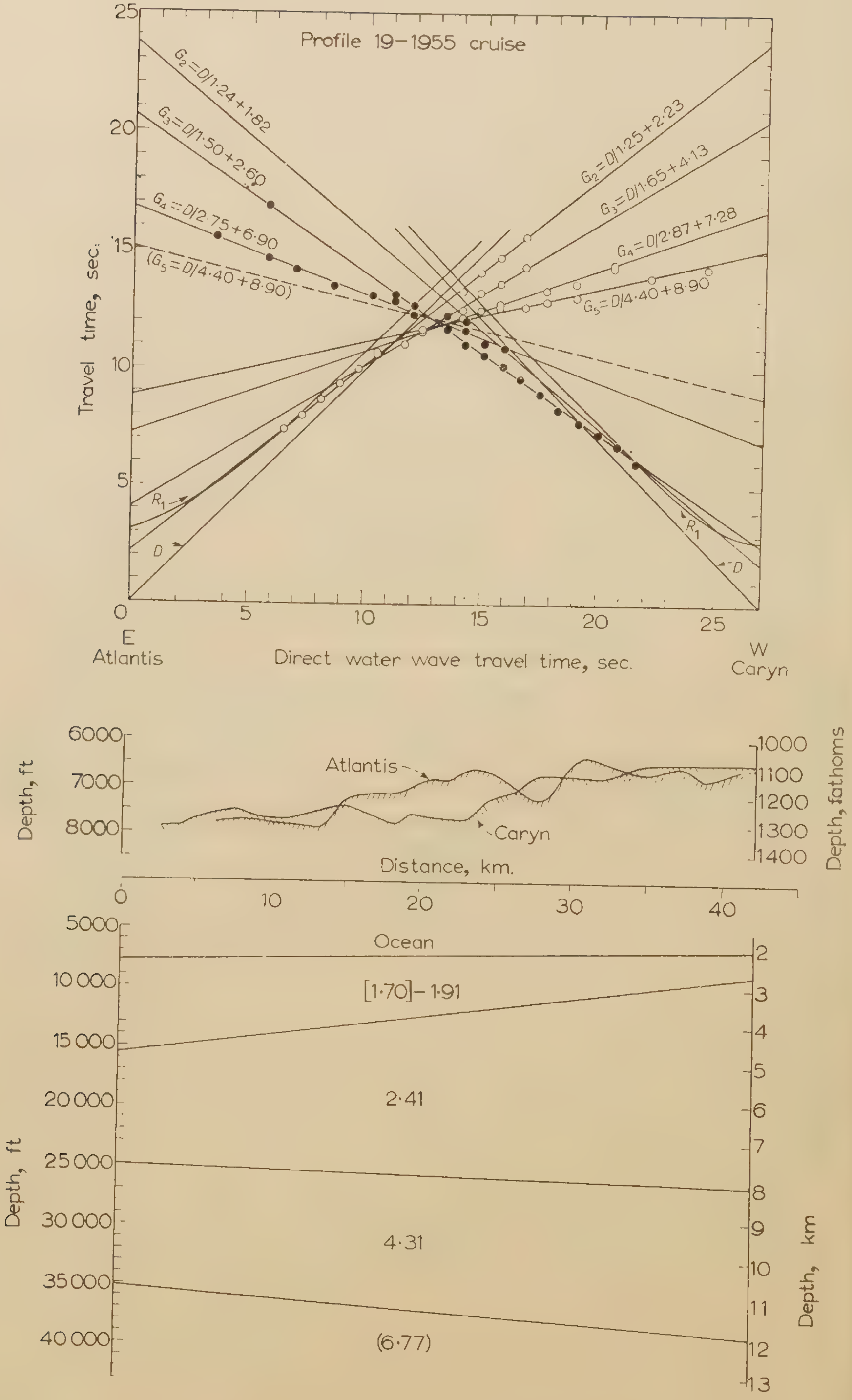
Profile 19—1955 cruise
$G_2 = D/1{\cdot}24 + 1{\cdot}82$
$G_3 = D/1{\cdot}50 + 2{\cdot}60$
$G_4 = D/2{\cdot}75 + 6{\cdot}90$
$(G_5 = D/4{\cdot}40 + 8{\cdot}90)$
$G_2 = D/1{\cdot}25 + 2{\cdot}23$
$G_3 = D/1{\cdot}65 + 4{\cdot}13$
$G_4 = D/2{\cdot}87 + 7{\cdot}28$
$G_5 = D/4{\cdot}40 + 8{\cdot}90$
R_1
D
Travel time, sec.
0
5
10
15
20
25
Direct water wave travel time, sec.
E
Atlantis
W
Caryn
Depth, ft
6000
7000
8000
Atlantis
Caryn
1000
1100
1200
1300
1400
Depth, fathoms
Distance, km.
0
10
20
30
40
5000
10 000
15 000
20 000
25 000
30 000
35 000
40 000
Depth, ft
Ocean
[1·70]– 1·91
2·41
4·31
(6·77)
2
3
4
5
6
7
8
9
10
11
12
13
Depth, km

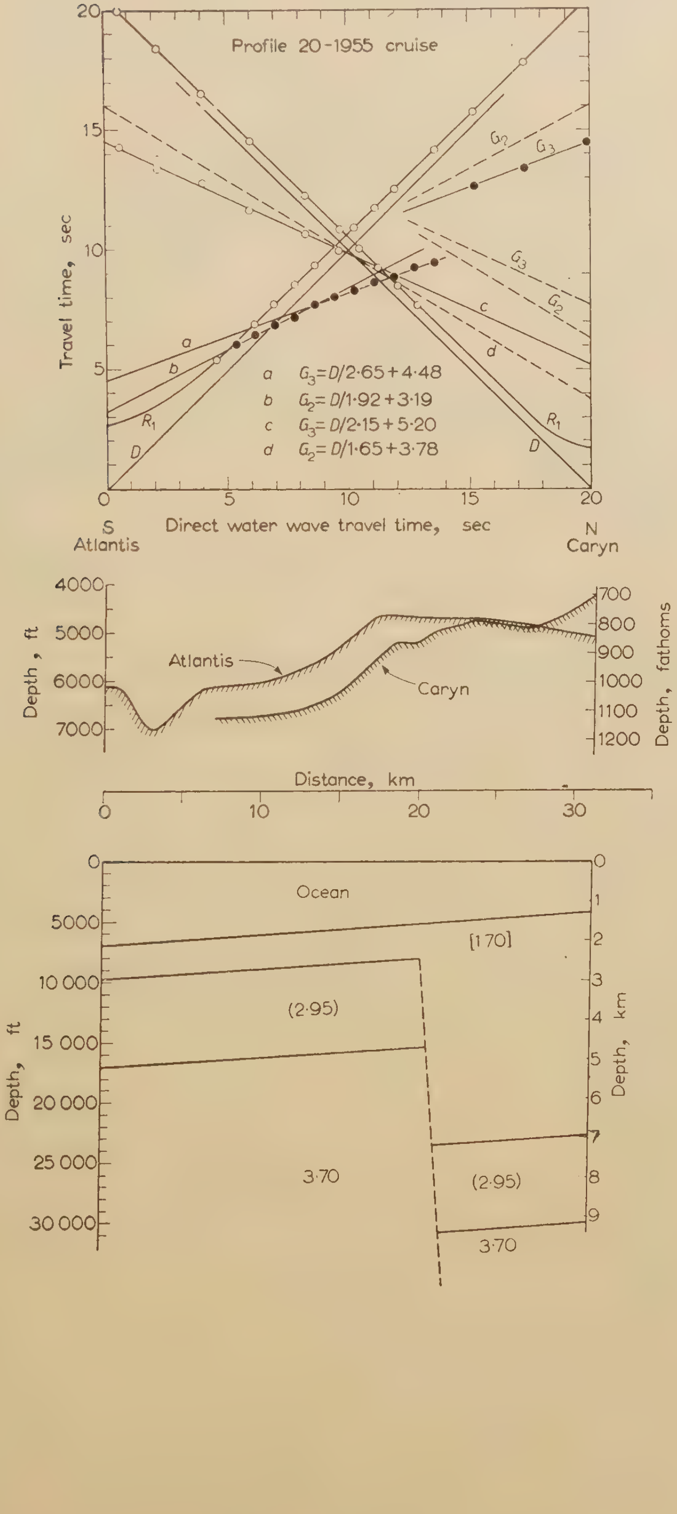
Profile 20-1955 cruise
Travel time, sec
Direct water wave travel time, sec
S
Atlantis
N
Caryn
a $G_3=D/2{\cdot}65+4{\cdot}48$
b $G_2=D/1{\cdot}92+3{\cdot}19$
c $G_3=D/2{\cdot}15+5{\cdot}20$
d $G_2=D/1{\cdot}65+3{\cdot}78$
R_1
D
G_2
G_3
Depth, ft
Depth, fathoms
Atlantis
Caryn
Distance, km
Ocean
[1.70]
(2·95)
3·70
(2·95)
3·70
Depth, ft
Depth, km

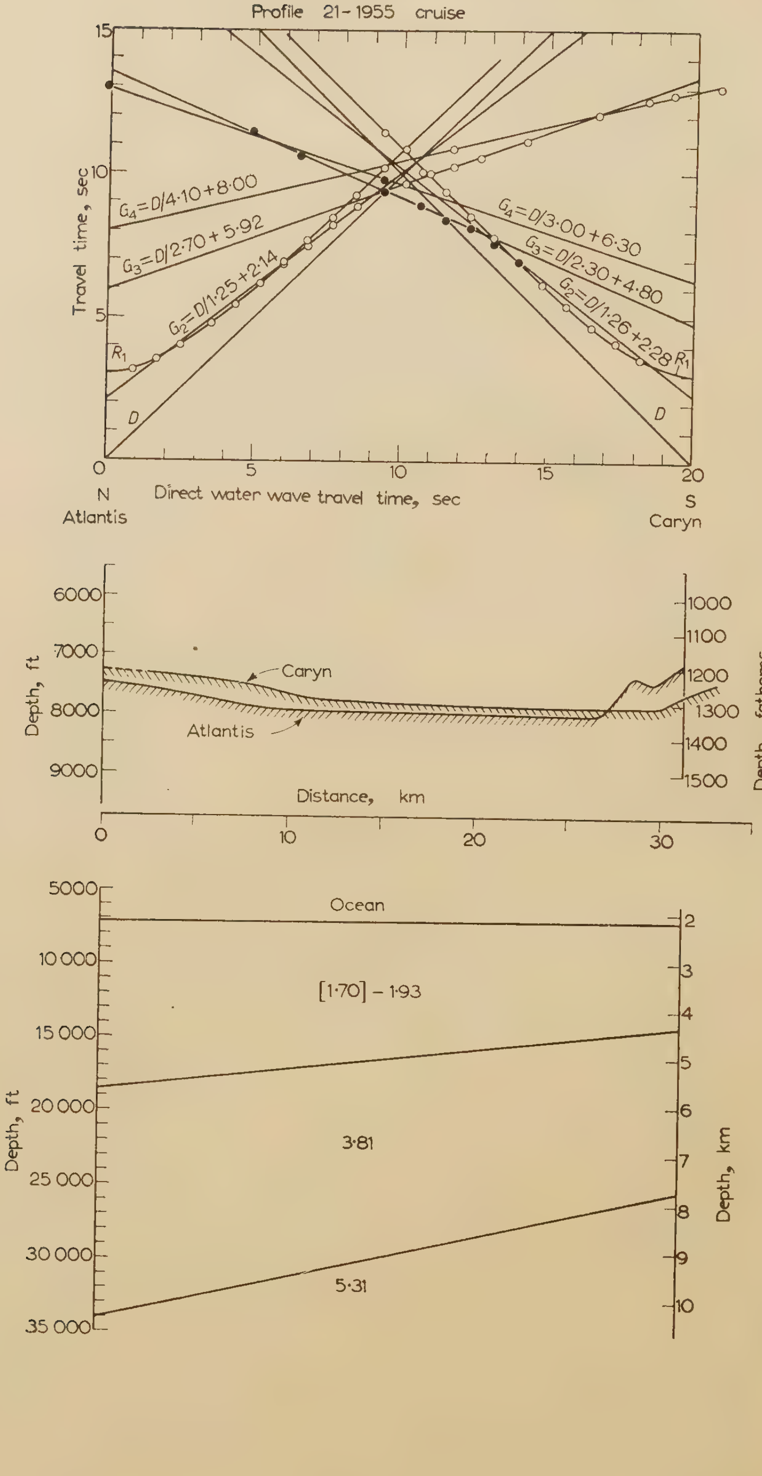
Profile 21-1955 cruise
Travel time, sec
15
10
5
0
5
10
15
20
G4=D/4·10+8·00
G3=D/2·70+5·92
G2=D/1·25+2·14
R1
D
G4=D/3·00+6·30
G3=D/2·30+4·80
G2=D/1·26+2·28
R1
D
N
Atlantis
Direct water wave travel time, sec
S
Caryn
Depth, ft
6000
7000
8000
9000
Caryn
Atlantis
1000
1100
1200
1300
1400
1500
Depth, fathoms
Distance, km
0
10
20
30
Depth, ft
5000
10 000
15 000
20 000
25 000
30 000
35 000
Ocean
[1·70] – 1·93
3·81
5·31
2
3
4
5
6
7
8
9
10
Depth, km

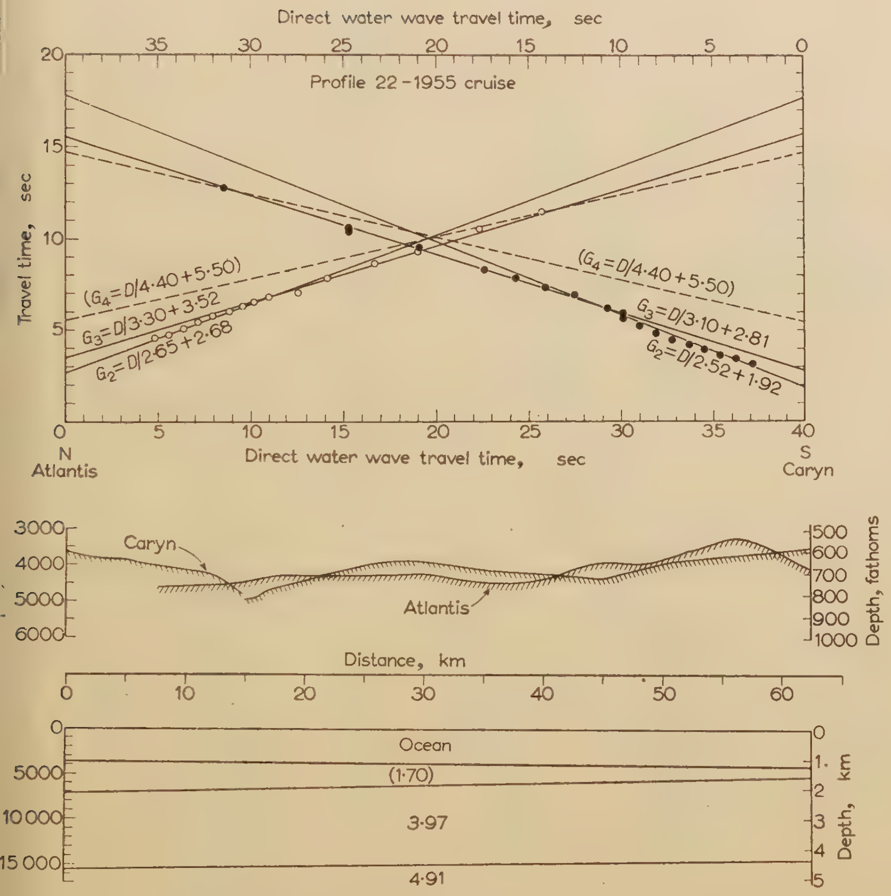
Direct water wave travel time, sec
35
30
25
20
15
10
5
0
Profile 22–1955 cruise
20
15
10
5
0
Travel time, sec
$(G_4 = D/4{\cdot}40 + 5{\cdot}50)$
$G_3 = D/3{\cdot}30 + 3{\cdot}52$
$G_2 = D/2{\cdot}65 + 2{\cdot}68$
$(G_4 = D/4{\cdot}40 + 5{\cdot}50)$
$G_3 = D/3{\cdot}10 + 2{\cdot}81$
$G_2 = D/2{\cdot}52 + 1{\cdot}92$
0
5
10
15
20
25
30
35
40
N
Atlantis
Direct water wave travel time, sec
S
Caryn
3000
4000
5000
6000
Caryn
Atlantis
500
600
700
800
900
1000
Depth, fathoms
Distance, km
0
10
20
30
40
50
60
0
5000
10 000
15 000
Ocean
(1·70)
3·97
4·91
0
1.
2
3
4
5
Depth, km

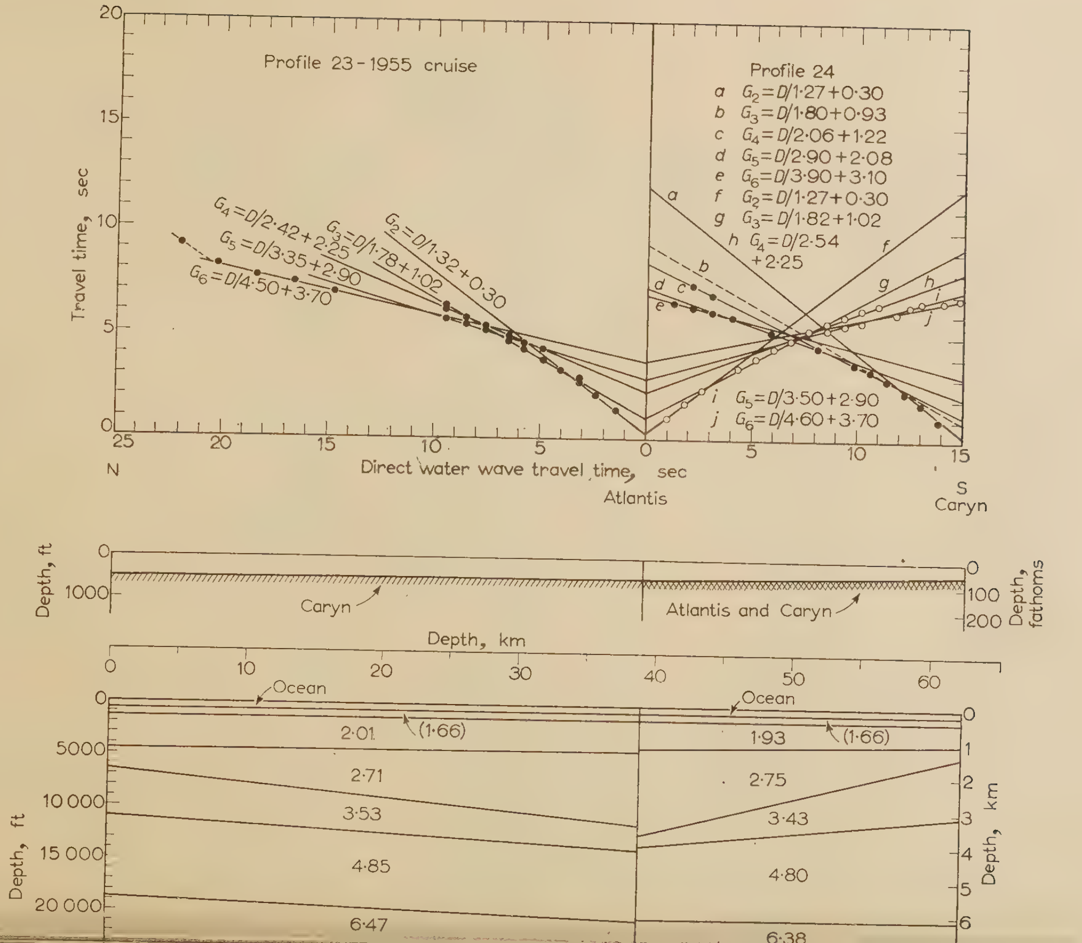
Profile 23 - 1955 cruise
Profile 24
a $G_2=D/1{\cdot}27+0{\cdot}30$
b $G_3=D/1{\cdot}80+0{\cdot}93$
c $G_4=D/2{\cdot}06+1{\cdot}22$
d $G_5=D/2{\cdot}90+2{\cdot}08$
e $G_6=D/3{\cdot}90+3{\cdot}10$
f $G_2=D/1{\cdot}27+0{\cdot}30$
g $G_3=D/1{\cdot}82+1{\cdot}02$
h $G_4=D/2{\cdot}54+2{\cdot}25$
i $G_5=D/3{\cdot}50+2{\cdot}90$
j $G_6=D/4{\cdot}60+3{\cdot}70$
$G_2=D/1{\cdot}32+0{\cdot}30$
$G_3=D/1{\cdot}78+1{\cdot}02$
$G_4=D/2{\cdot}42+2{\cdot}25$
$G_5=D/3{\cdot}35+2{\cdot}90$
$G_6=D/4{\cdot}50+3{\cdot}70$
Travel time, sec
20
15
10
5
0
25
20
15
10
5
0
5
10
15
N
Direct water wave travel time, sec
Atlantis
S
Caryn
Depth, ft
0
1000
Caryn
Atlantis and Caryn
0
100
200
Depth, fathoms
Depth, km
0
10
20
30
40
50
60
Ocean
Ocean
2·01
(1·66)
1·93
(1·66)
2·71
2·75
3·53
3·43
4·85
4·80
6·47
6·38
Depth, ft
0
5000
10 000
15 000
20 000
Depth, km
0
1
2
3
4
5
6

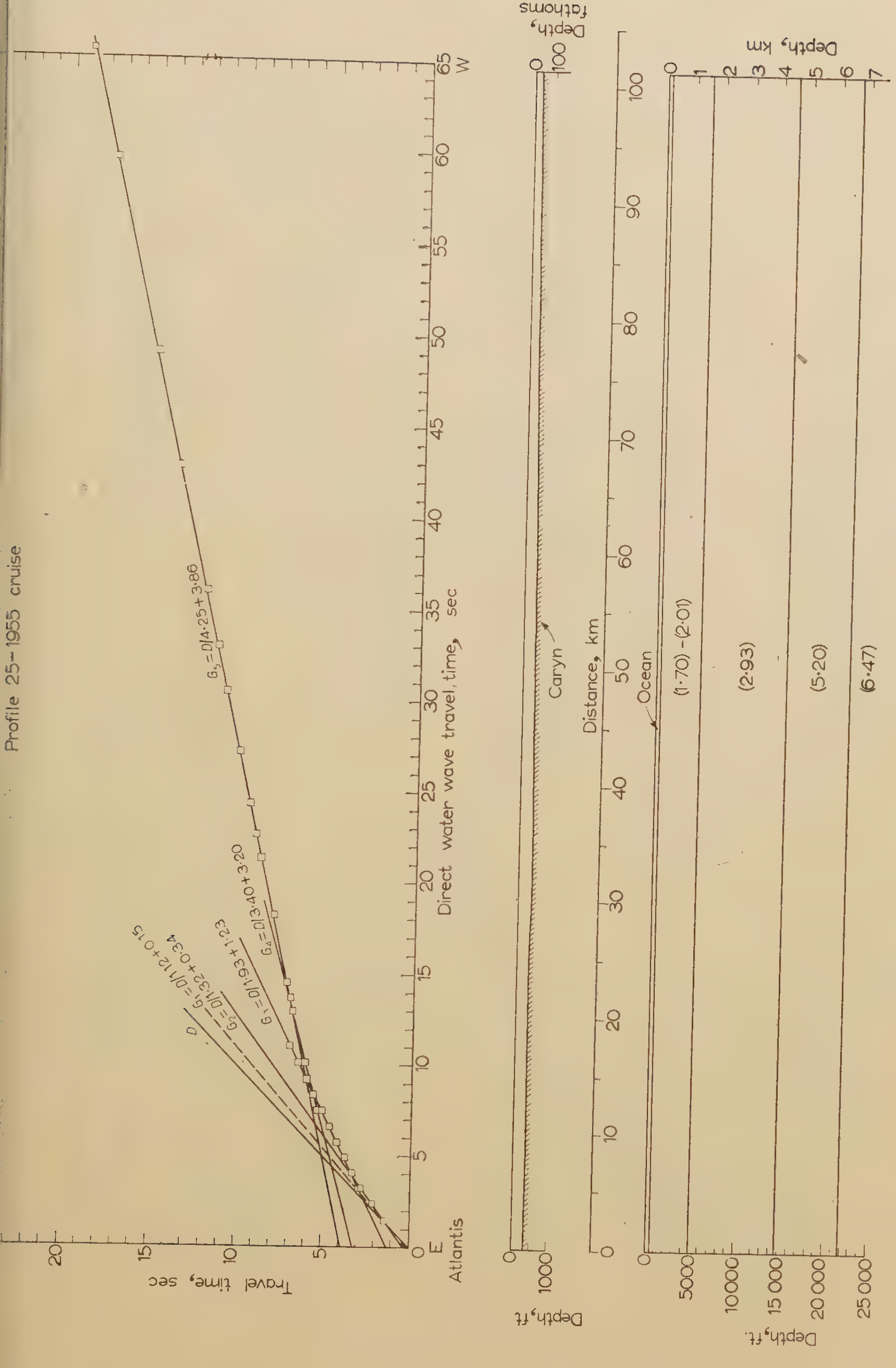
Profile 25-1955 cruise
Travel time, sec
0
5
10
15
20
Direct water wave travel time, sec
0
5
10
15
20
25
30
35
40
45
50
55
60
65
E
W
Atlantis
D
G₁ = D/1·12+0·15
G₂ = D/1·32+0·34
G₃ = D/1·93+1·23
G₄ = D/3·40+3·20
G₅ = D/4·25+3·86
Depth, ft
0
1000
Depth, fathoms
0
100
Caryn
Distance, km
0
10
20
30
40
50
60
70
80
90
100
Ocean
(1·70)-(2·01)
(2·93)
(5·20)
(6·47)
Depth, km
0
1
2
3
4
5
6
7
Depth, ft.
0
5000
10000
15 000
20 000
25 000

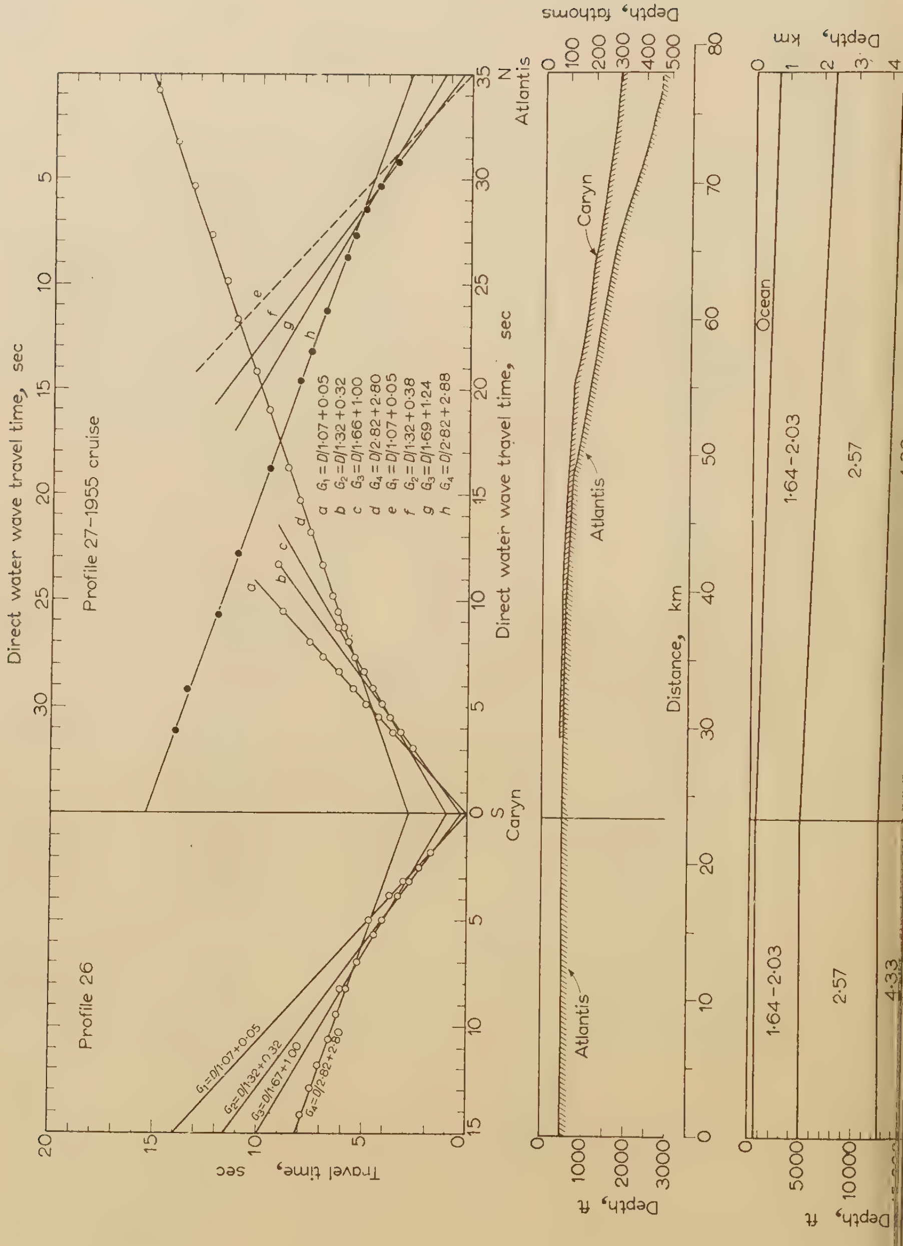

Direct water wave travel time, sec
Profile 27–1955 cruise
Profile 26
Travel time, sec
Direct water wave travel time, sec
Caryn
S
N
Atlantis
$G_1 = D/1{\cdot}07 + 0{\cdot}05$
$G_2 = D/1{\cdot}32 + 0{\cdot}32$
$G_3 = D/1{\cdot}67 + 1{\cdot}00$
$G_4 = D/2{\cdot}82 + 2{\cdot}80$
a $G_1 = D/1{\cdot}07 + 0{\cdot}05$
b $G_2 = D/1{\cdot}32 + 0{\cdot}32$
c $G_3 = D/1{\cdot}66 + 1{\cdot}00$
d $G_4 = D/2{\cdot}82 + 2{\cdot}80$
e $G_1 = D/1{\cdot}07 + 0{\cdot}05$
f $G_2 = D/1{\cdot}32 + 0{\cdot}38$
g $G_3 = D/1{\cdot}69 + 1{\cdot}24$
h $G_4 = D/2{\cdot}82 + 2{\cdot}88$
a
b
c
d
e
f
g
h
Depth, ft
Depth, fathoms
Caryn
Atlantis
Atlantis
Distance, km
Depth, km
Depth, ft
Ocean
1·64–2·03
2·57
1·64–2·03
2·57
4·33

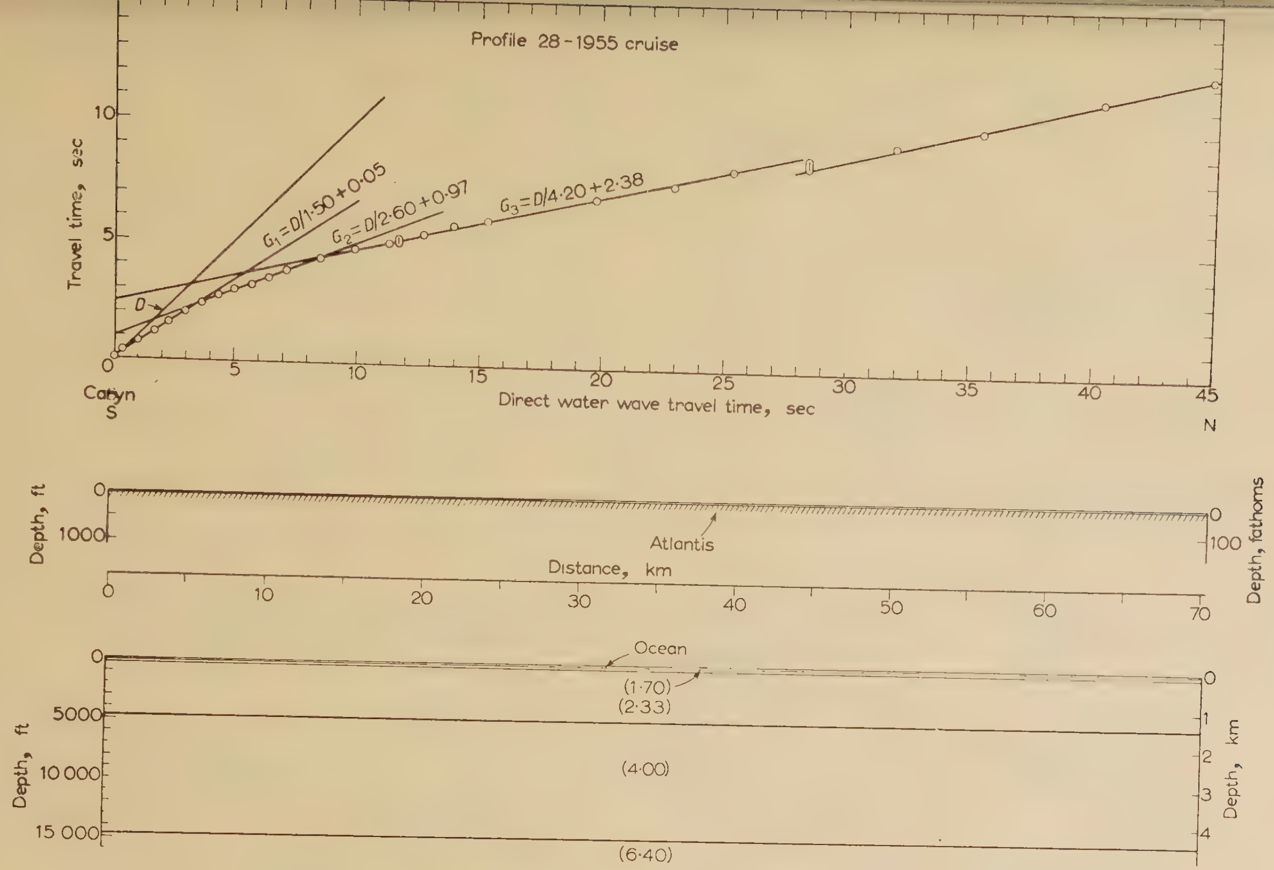
Profile 28-1955 cruise
Travel time, sec
0
5
10
$G_1=D/1{\cdot}50+0{\cdot}05$
$G_2=D/2{\cdot}60+0{\cdot}97$
$G_3=D/4{\cdot}20+2{\cdot}38$
D
Catyn
S
N
Direct water wave travel time, sec
0
5
10
15
20
25
30
35
40
45
Depth, ft
0
1000
Atlantis
Depth, fathoms
0
100
Distance, km
0
10
20
30
40
50
60
70
Ocean
(1·70)
(2·33)
(4·00)
(6·40)
Depth, ft
0
5000
10 000
15 000
Depth, km
0
1
2
3
4

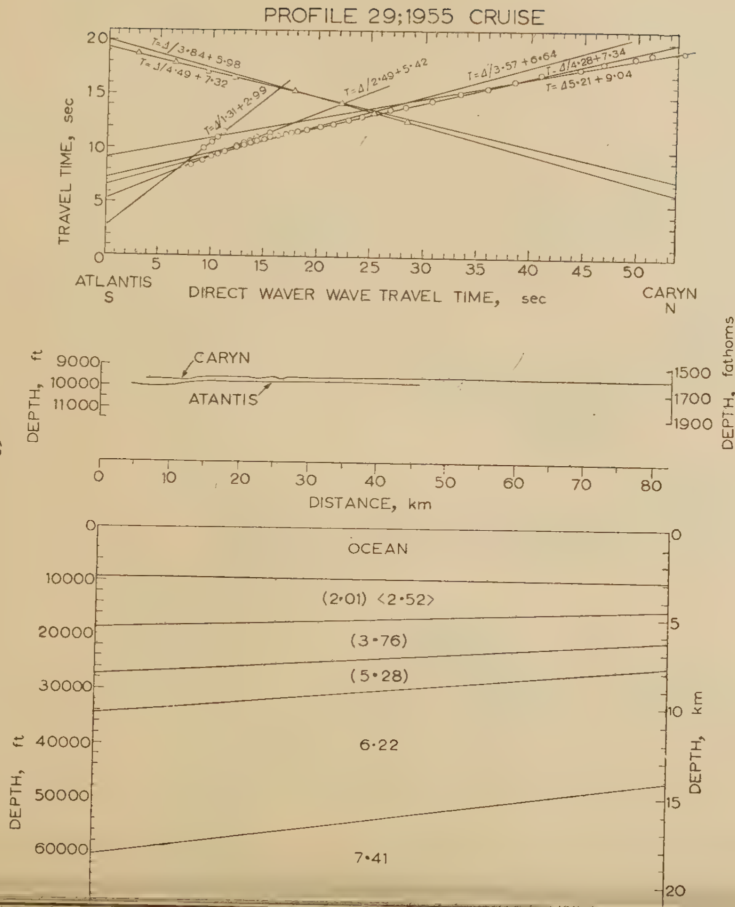
PROFILE 29;1955 CRUISE
T=Δ/3·84+5·98
T=Δ/4·49+7·32
T=Δ/1·31+2·99
T=Δ/2·49+5·42
T=Δ/3·57+6·64
T=Δ/4·28+7·34
T=Δ5·21+9·04
TRAVEL TIME, sec
ATLANTIS S
DIRECT WAVER WAVE TRAVEL TIME, sec
CARYN N
CARYN
ATANTIS
DEPTH, ft
DEPTH, fathoms
DISTANCE, km
OCEAN
(2·01) <2·52>
(3·76)
(5·28)
6·22
7·41
DEPTH, ft
DEPTH, km

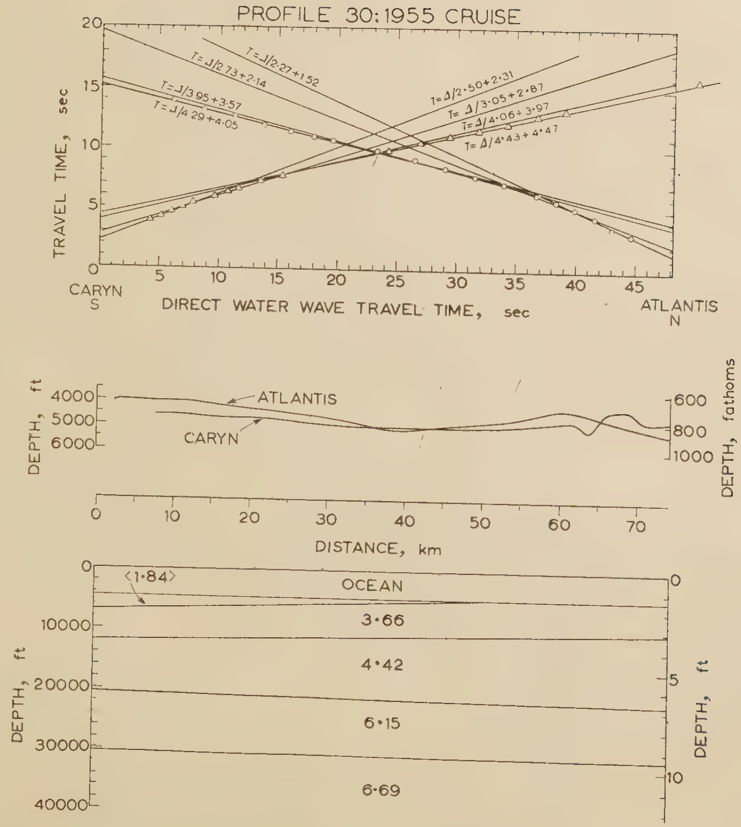
PROFILE 30:1955 CRUISE
T=Δ/2·27+1·52
T=Δ/2·73+2·14
T=Δ/3·95+3·57
T=Δ/4·29+4·05
T=Δ/2·50+2·31
T=Δ/3·05+2·87
T=Δ/4·06+3·97
T=Δ/4·43+4·47
TRAVEL TIME, sec
CARYN S
DIRECT WATER WAVE TRAVEL TIME, sec
ATLANTIS N
ATLANTIS
CARYN
DEPTH, ft
DEPTH, fathoms
DISTANCE, km
<1·84>
OCEAN
3·66
4·42
6·15
6·69
DEPTH, ft
DEPTH, ft

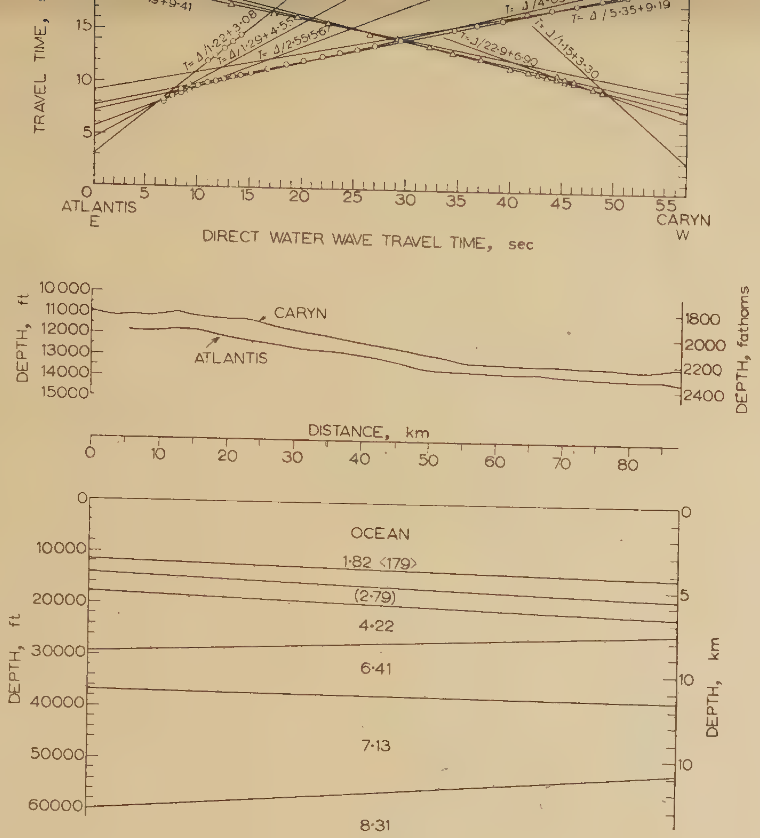
+9·41
T= Δ/1·22+3·08
T= Δ/1·29+4·55
T= Δ/2·55+5·67
T= Δ/4·
T= Δ/5·35+9·19
T= Δ/22·9+6·90
T= Δ/1·15+3·30
TRAVEL TIME,
15
10
5
0
ATLANTIS
E
5
10
15
20
25
30
35
40
45
50
55
CARYN
W
DIRECT WATER WAVE TRAVEL TIME, sec
DEPTH, ft
10000
11000
12000
13000
14000
15000
CARYN
ATLANTIS
1800
2000
2200
2400
DEPTH, fathoms
DISTANCE, km
0
10
20
30
40
50
60
70
80
DEPTH, ft
0
10000
20000
30000
40000
50000
60000
OCEAN
1·82 ‹179›
(2·79)
4·22
6·41
7·13
8·31
0
5
10
10
DEPTH, km

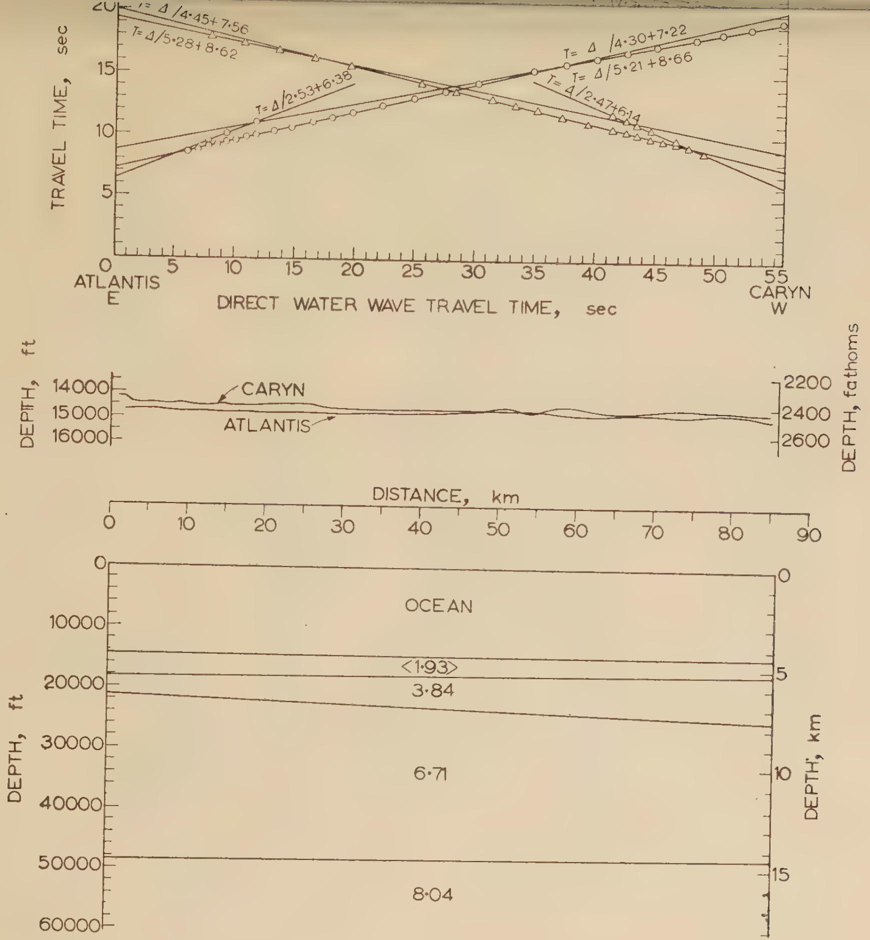
T= Δ/4·45+7·56
T= Δ/5·28+8·62
T= Δ/2·53+6·38
T= Δ/4·30+7·22
T= Δ/5·21+8·66
T= Δ/2·47+6·14
TRAVEL TIME, sec
20
15
10
5
0
ATLANTIS
E
5
10
15
20
25
30
35
40
45
50
55
CARYN
W
DIRECT WATER WAVE TRAVEL TIME, sec
DEPTH, ft
14000
15000
16000
CARYN
ATLANTIS
2200
2400
2600
DEPTH, fathoms
DISTANCE, km
0
10
20
30
40
50
60
70
80
90
DEPTH, ft
0
10000
20000
30000
40000
50000
60000
OCEAN
‹1·93›
3·84
6·71
8·04
0
5
10
15
DEPTH, km

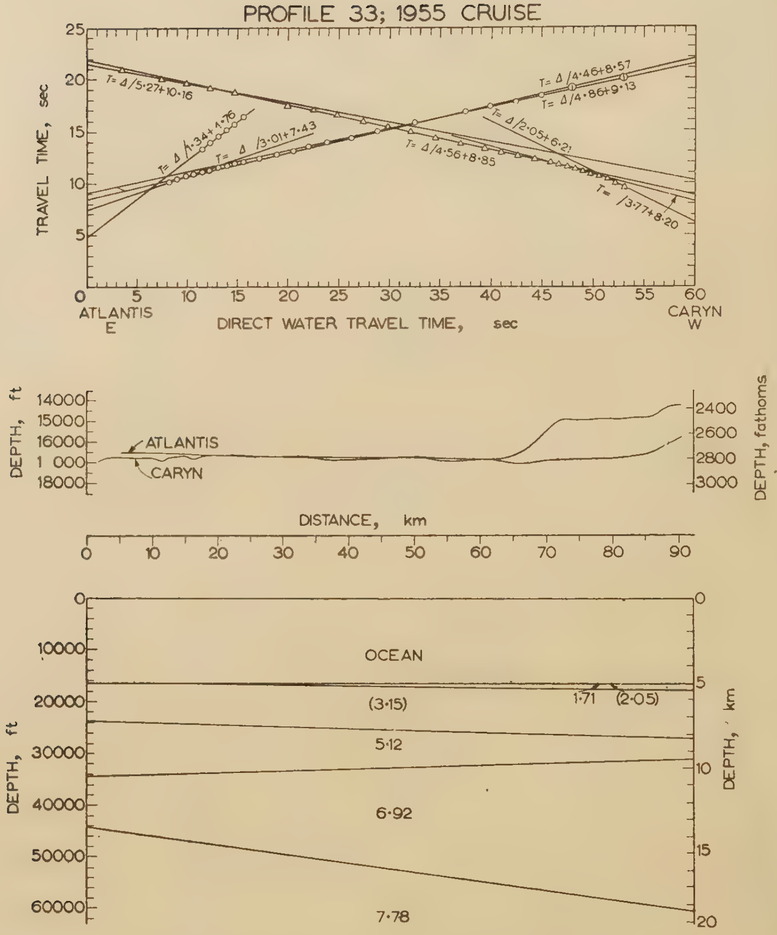
PROFILE 33; 1955 CRUISE
TRAVEL TIME, sec
25
20
15
10
5
0
5
10
15
20
25
30
35
40
45
50
55
60
ATLANTIS
E
DIRECT WATER TRAVEL TIME, sec
CARYN
W
T= Δ/5·27+10·16
T= Δ /1·34+4·76
T= Δ /3·01+7·43
T= Δ/4·56+8·85
T= Δ /4·46+8·57
T= Δ/4·86+9·13
T= Δ/2·05+6·21
T= /3·77+8·20
DEPTH, ft
14000
15000
16000
1 000
18000
ATLANTIS
CARYN
2400
2600
2800
3000
DEPTH, fathoms
DISTANCE, km
0
10
20
30
40
50
60
70
80
90
0
10000
20000
30000
40000
50000
60000
DEPTH, ft
OCEAN
(3·15)
1·71
(2·05)
5·12
6·92
7·78
0
5
10
15
20
DEPTH, km

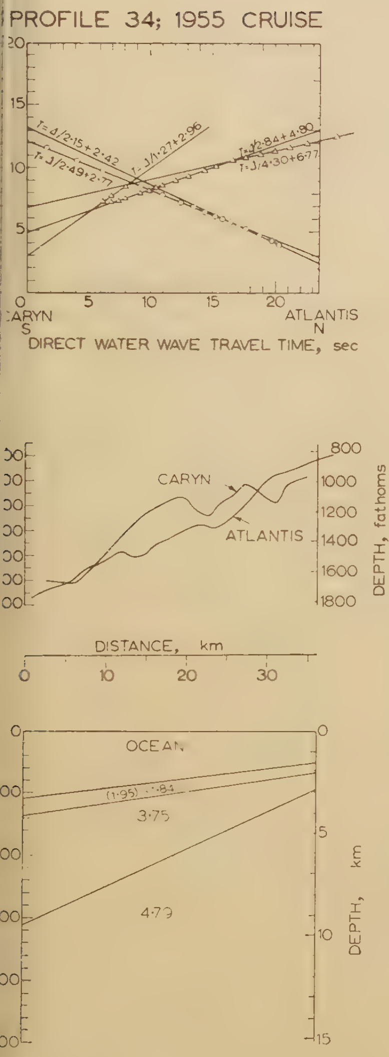
PROFILE 34; 1955 CRUISE
20
15
10
5
T=Δ/2·15+2·42
T=Δ/2·49+2·77
T=Δ/1·27+2·96
T=Δ/2·84+4·90
T=Δ/4·30+6·77
0 5 10 15 20
CARYN S
ATLANTIS N
DIRECT WATER WAVE TRAVEL TIME, sec
CARYN
ATLANTIS
800
1000
1200
1400
1600
1800
DEPTH, fathoms
DISTANCE, km
0 10 20 30
OCEAN
(1·95)
·84
3·75
4·79
0
5
10
15
DEPTH, km

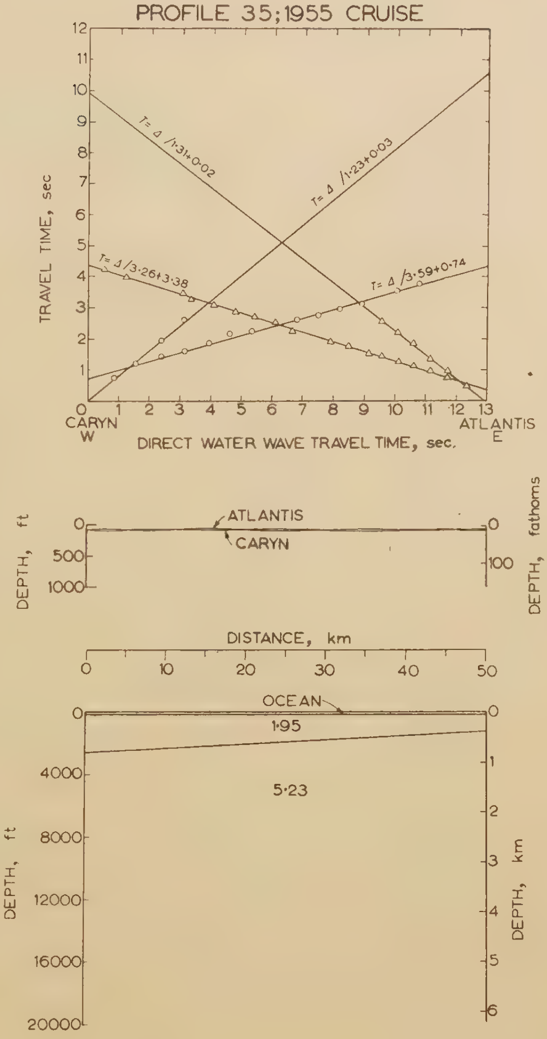
PROFILE 35; 1955 CRUISE
12
11
10
9
8
7
6
5
4
3
2
1
TRAVEL TIME, sec
T=Δ/1·31+0·02
T=Δ/1·23+0·03
T=Δ/3·26+3·38
T=Δ/3·59+0·74
0 1 2 3 4 5 6 7 8 9 10 11 12 13
CARYN W
ATLANTIS E
DIRECT WATER WAVE TRAVEL TIME, sec.
ATLANTIS
CARYN
0
500
1000
DEPTH, ft
0
100
DEPTH, fathoms
DISTANCE, km
0 10 20 30 40 50
OCEAN
1·95
5·23
0
4000
8000
12000
16000
20000
DEPTH, ft
0
1
2
3
4
5
6
DEPTH, km

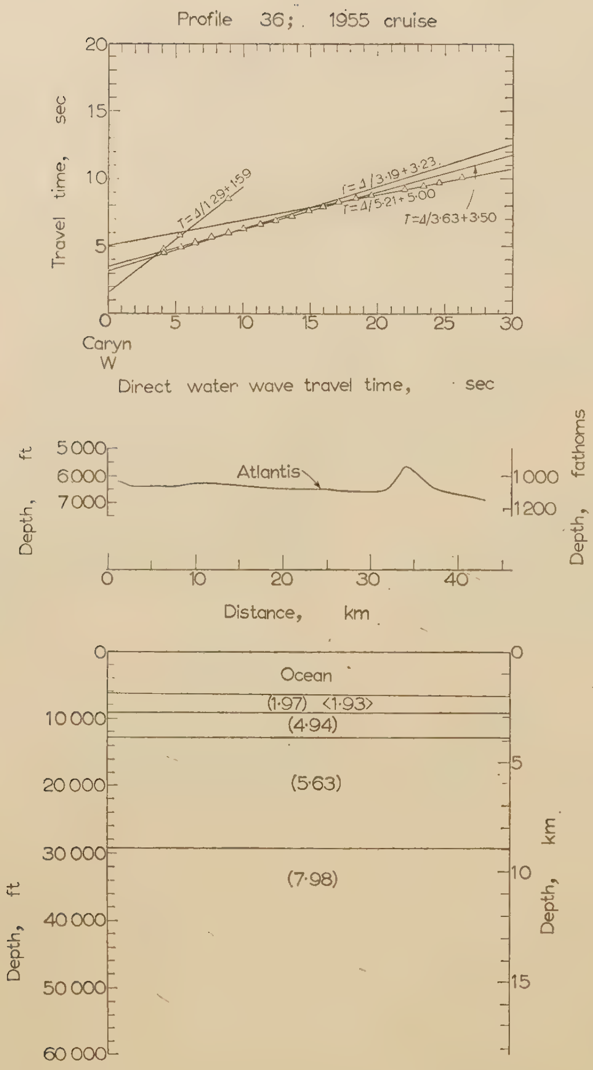
Profile 36; 1955 cruise
Travel time, sec
20
15
10
5
0
T=Δ/1·29+1·59
T=Δ/3·19+3·23
T=Δ/5·21+5·00
T=Δ/3·63+3·50
0 5 10 15 20 25 30
Caryn
W
Direct water wave travel time, sec
Depth, ft
5000
6000
7000
Atlantis
1000
1200
Depth, fathoms
0 10 20 30 40
Distance, km
0
10 000
20 000
30 000
40 000
50 000
60 000
Ocean
(1·97) ‹1·93›
(4·94)
(5·63)
(7·98)
0
5
10
15
Depth, km

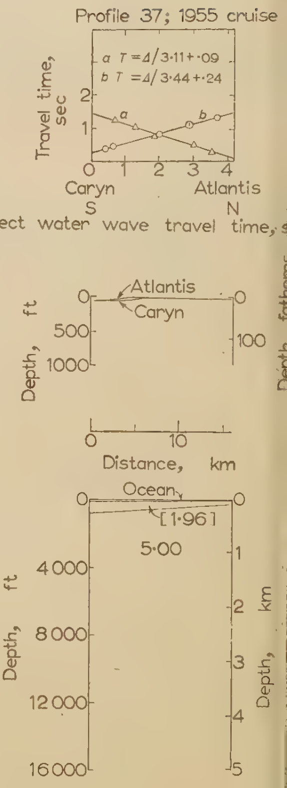
Profile 37; 1955 cruise
a T=Δ/3·11+·09
b T=Δ/3·44+·24
Travel time, sec
2
1
a
b
0 1 2 3 4
Caryn
S
Atlantis
N
Direct water wave travel time,
Atlantis
Caryn
Depth, ft
0
500
1000
0
100
0 10
Distance, km
Ocean
[1·96]
5·00
0
4000
8000
12 000
16 000
0
1
2
3
4
5
Depth, km

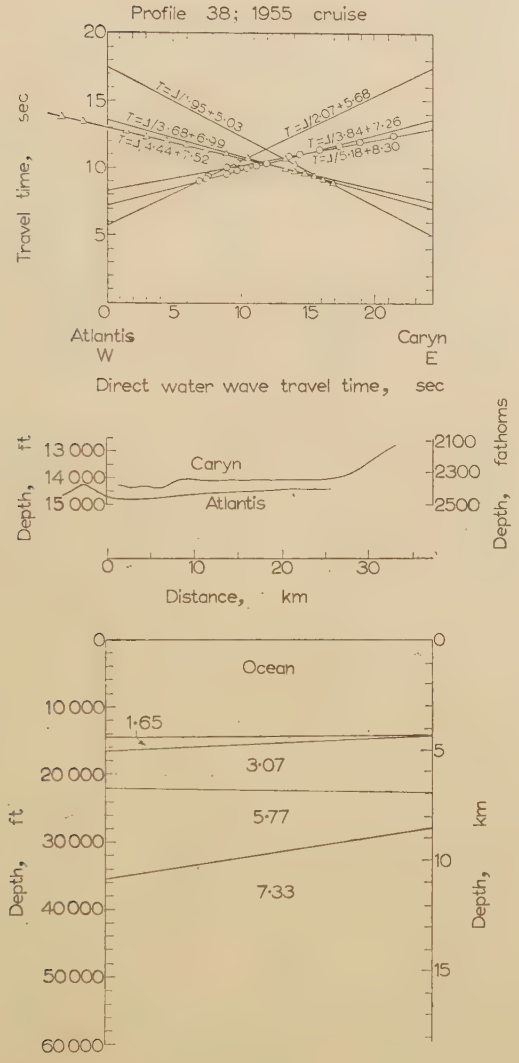
Profile 38; 1955 cruise

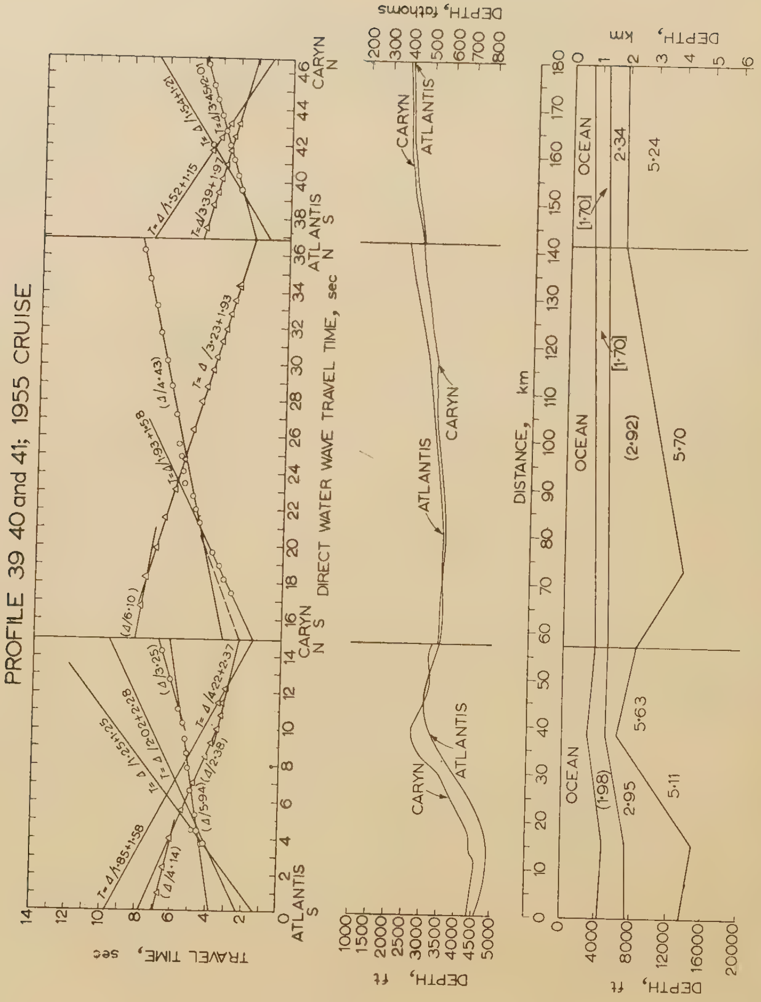
PROFILE 39 40 and 41; 1955 CRUISE

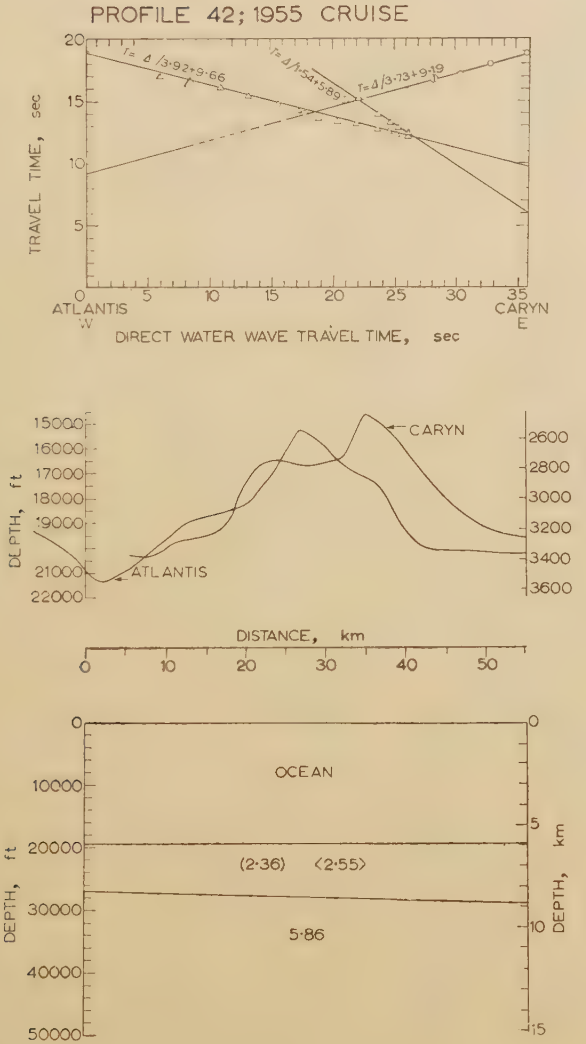
PROFILE 42; 1955 CRUISE
T= Δ /3·92+9·66
T= Δ/1·54+5·89
T=Δ/3·73+9·19
TRAVEL TIME, sec
20
15
10
5
0
5
10
15
20
25
30
35
ATLANTIS
W
CARYN
E
DIRECT WATER WAVE TRAVEL TIME, sec
CARYN
ATLANTIS
DEPTH, ft
15000
16000
17000
18000
19000
21000
22000
DEPTH, fathoms
2600
2800
3000
3200
3400
3600
DISTANCE, km
0
10
20
30
40
50
OCEAN
(2·36)
⟨2·55⟩
5·86
DEPTH, ft
0
10000
20000
30000
40000
50000
DEPTH, km
0
5
10
15

PROFILE 43; 1955 CRUISE

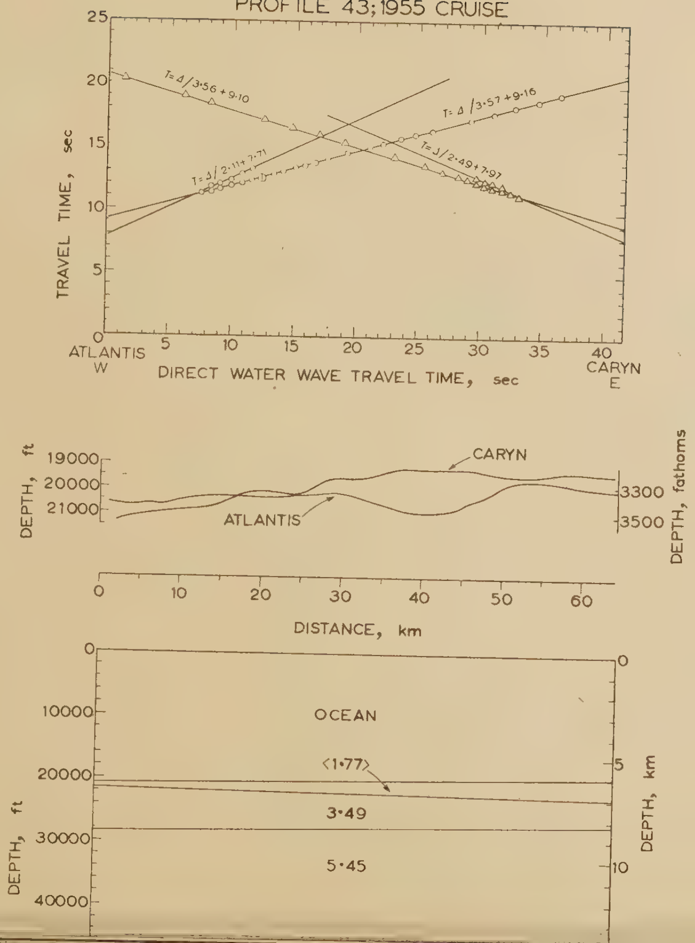

PROFILE 44; 1955 CRUISE

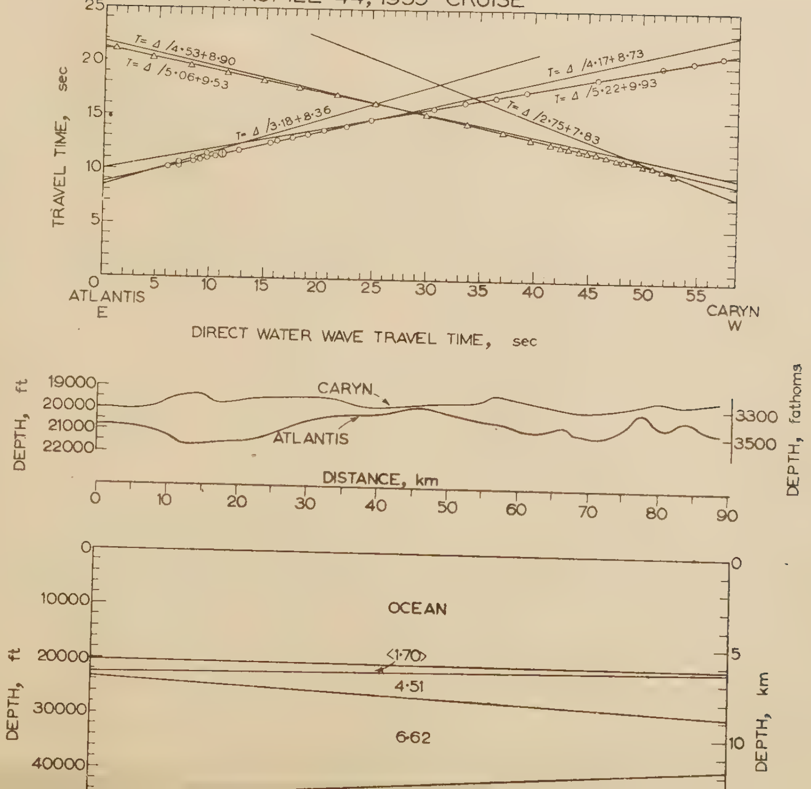

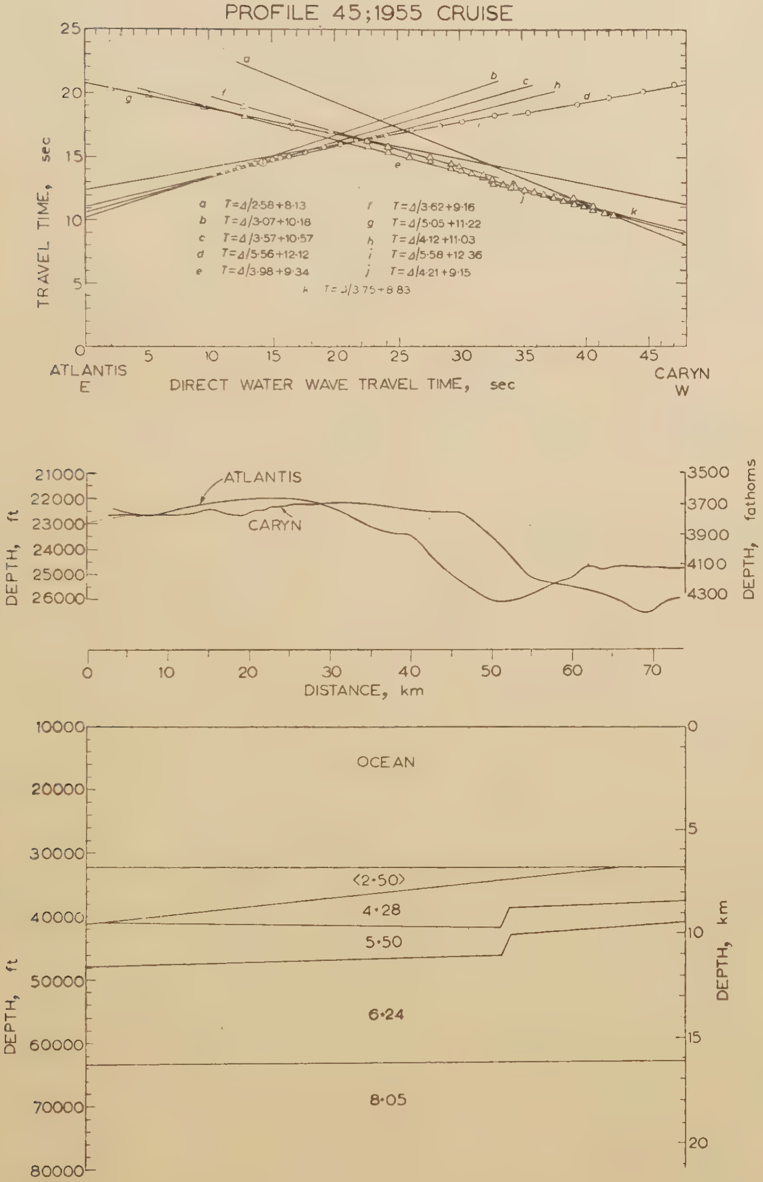
PROFILE 45;1955 CRUISE
TRAVEL TIME, sec
25
20
15
10
5
0
a
b
c
h
d
f
g
e
i
j
k
a T=Δ/2·58+8·13
b T=Δ/3·07+10·18
c T=Δ/3·57+10·57
d T=Δ/5·56+12·12
e T=Δ/3·98+9·34
f T=Δ/3·62+9·16
g T=Δ/5·05+11·22
h T=Δ/4·12+11·03
i T=Δ/5·58+12 36
j T=Δ/4·21+9·15
k T=Δ/3 75+8 83
5
10
15
20
25
30
35
40
45
ATLANTIS
E
DIRECT WATER WAVE TRAVEL TIME, sec
CARYN
W
DEPTH, ft
21000
22000
23000
24000
25000
26000
ATLANTIS
CARYN
3500
3700
3900
4100
4300
DEPTH, fathoms
0
10
20
30
40
50
60
70
DISTANCE, km
DEPTH, ft
10000
20000
30000
40000
50000
60000
70000
80000
OCEAN
⟨2·50⟩
4·28
5·50
6·24
8·05
0
5
10
15
20
DEPTH, km

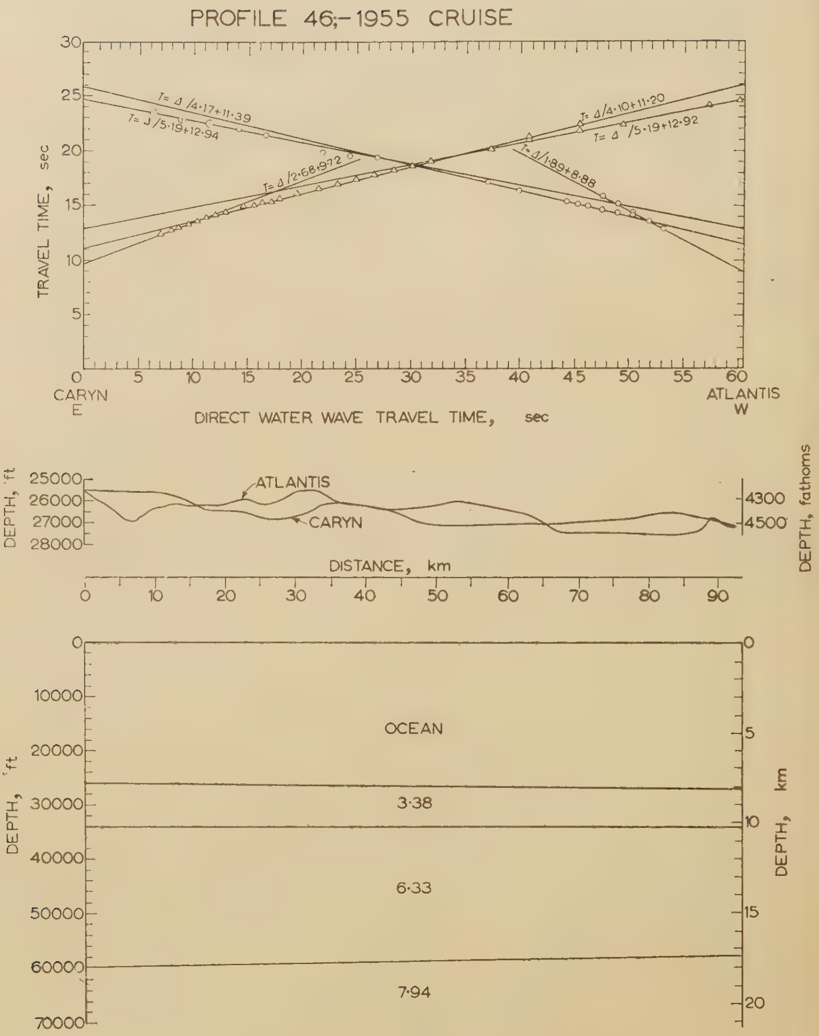
PROFILE 46;-1955 CRUISE
TRAVEL TIME, sec
30
25
20
15
10
5
T= Δ /4·17+11·39
T= Δ /5·19+12·94
T= Δ /2·68+9·72
T= Δ/4·10+11·20
T= Δ /5·19+12·92
T= Δ/1·89+8·88
0
5
10
15
20
25
30
35
40
45
50
55
60
CARYN
E
ATLANTIS
W
DIRECT WATER WAVE TRAVEL TIME, sec
DEPTH, ft
25000
26000
27000
28000
ATLANTIS
CARYN
4300
4500
DEPTH, fathoms
DISTANCE, km
0
10
20
30
40
50
60
70
80
90
DEPTH, ft
0
10000
20000
30000
40000
50000
60000
70000
OCEAN
3·38
6·33
7·94
0
5
10
15
20
DEPTH, km

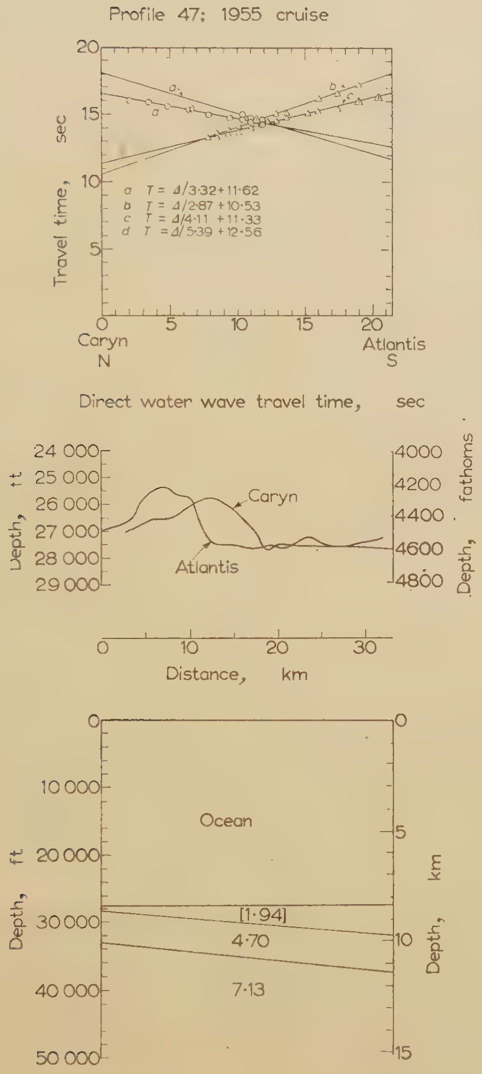
Profile 47; 1955 cruise
20
15
10
5
Travel time, sec
a T = Δ/3·32+11·62
b T = Δ/2·87 +10·53
c T = Δ/4·11 +11·33
d T = Δ/5·39 +12·56
a
b
c
0
5
10
15
20
Caryn
N
Atlantis
S
Direct water wave travel time, sec
24 000
25 000
26 000
27 000
28 000
29 000
Depth, ft
4000
4200
4400
4600
4800
Depth, fathoms
Caryn
Atlantis
0
10
20
30
Distance, km
0
10 000
20 000
30 000
40 000
50 000
Depth, ft
0
5
10
15
Depth, km
Ocean
[1·94]
4·70
7·13

deepest layer in *9* could be made to agree more closely with the 6·13 km/se layer in *10* by assuming a steeper northward dip.

11, *12*. Topographic corrections were applied assuming a sloping base lin from 1420 fathoms at the west end of *11* to 720 fathoms at the east end of *12* These profiles were greatly complicated by a strong westerly drift whic apparently offset the shooting tracks by 10–15 km. This undoubtably reduce the accuracy of the results appreciably, and the section shows, at best, only th general structural configuration.

13, *14*, 15. Topographic corrections were applied for sloping base line which approximate the topography in profiles *13* and *14*. A level base line at depth of 700 fathoms was assumed for profile *15*. The computations accordin to this assumption produced the section partially represented by the dashe lines. The re-adjustment of the interfaces (solid lines) show the actual structure In these profiles some complications and uncertainties were introduced by drift of approximately 7 km in the direction of the shot lines. This is clearl shown by the offset in the two fathograms.

16. Topographic corrections were applied for a level base line 18 fathom deep. The two fathograms differ somewhat here because the *Bear*'s shootin run was approximately 1 km east of *Atlantis*. After topographic correction were made there were still high points in the region of the topographic low i both sets of records. The structure shown in the section accounts for thes points and is suggested by the observed topography. The section does not sho the depression in the two upper layers.

17. The bottom topography is irregular along this profile but the refractio lines are well determined. The overlying materials with velocities 2·04, 3·85 and 5·48 km/sec are thick under this profile. The crustal arrival is well define by a first arrival refraction line on one-half of the profile. It appears as a maske refraction line on the other half.

18. The bottom topography is irregular along this profile. The crustal refraction line is again masked. As on profiles *6* and *17* it has been included in th calculations. The other refraction lines are well determined.

19. Topographic corrections were applied for a level base line 30 fathom deep. These corrections removed the effects of the depression near the *Atlanti* receiving position, indicating that approximately the same relief is present i the deeper interfaces.

20. The crustal refraction is masked but has been included in the calculations The mantle refraction line is defined, but its velocity is not well determined.

21. Topographic corrections were applied for a base line which slopes fro 670 fathoms in the north to 1060 fathoms in the south. The topography assumed to be approximately duplicated in the deeper interfaces, is not show in the section.

22, *23*. Require no comment.

24. Topographic corrections were applied for a sloping base line from 182 fathoms at the east end to 2340 fathoms at the west. A westerly drift cause the deviation in the two echo sounder records. The second, third and fourt layers were not detected in the *Atlantis* records but were assumed to be maske The fourth layer (4·95 km/sec) was almost masked at the east end; but there i additional evidence for its presence since a similar velocity was measured a profiles 9, 10, 30, 31, *22* and *23*.

25. The base line for topographic corrections for this profile slopes from a pth of 2700 fathoms at the east end to 2780 fathoms at the west. The deter-nation of three high-velocity layers here may be questionable. A reasonably od fit of the data may be achieved with two lines representing velocities of out 6·4 and 7·8 km/sec. However, the three-layer interpretation which is own gives a slightly better fit and is in better agreement with the other data the area.

26. Topographic corrections were applied for a level base line at 2720 fathoms. e three high-velocity layers were well determined here by both compressional d transformed shear waves. The *Atlantis* records in particular contain an usually strong set of shear wave arrivals. These are shown in Fig. 8, which a tracing of one low frequency trace from each record, spaced according to ot distance. The shear wave arrivals are labelled G_s.

27. Topographic corrections were made for an assumed level base line at 50 fathoms depth. The three high-velocity lines are reasonably well determined, t it is possible that a somewhat different interpretation might be made. There little doubt that the 6·5 km/sec velocity is correct, and it also seems certain at the highest velocity is near 7·9 km/sec; but it is difficult to determine sitively whether there is a separate intermediate layer or a gradual change tween the 6·5 and 7·9 km/sec layers.

28. Requires no comment.

29. There is considerable change in topography along this profile, but the es were well determined. The mantle was not detected.

30. Requires no comment.

STRUCTURE CROSS-SECTIONS

e geophysical results have been summarized in a number of structure cross-ctions. Their locations are shown in Fig. 2. We consider these cross-sections convenient pictorial manner in which to present the results. Most of the atures on them are quite clear and need little or no comment. Some of the ore striking results are mentioned and discussed below.

ction 1

Section 1, shown in Fig. 14, begins near the middle of the Venezuelan basin d crosses the northern end of the Aves swell, the inner volcanic arc of the sser Antilles near Nevis, the outer arc between Antigua and Barbuda, the uth-eastern end of the Puerto Rico trench, and ends about 140 miles north-east Barbuda. The section is about 500 miles long and includes the data from teen profiles. With a few exceptions the measured velocities can be separated o general groups represented by the five layers in the cross-section.

The entire crustal section was measured at profiles *26* and *27* in the Venezuelan sin and at profiles *4*, *5*, *6*, and *17* in the Atlantic basin outside the island arc. the other profiles the mantle was not reached, although most of them asured the section down to the high velocity crustal layer. The velocities nd for this layer vary between 6·0 and 7·6 km/sec, with most of the varia-ity coming in the Caribbean and island arc profiles. In general, in the inter-tation of the travel time data for the Venezuelan basin profiles, the best fit achieved with two lines representing the crustal material: one for a velocity

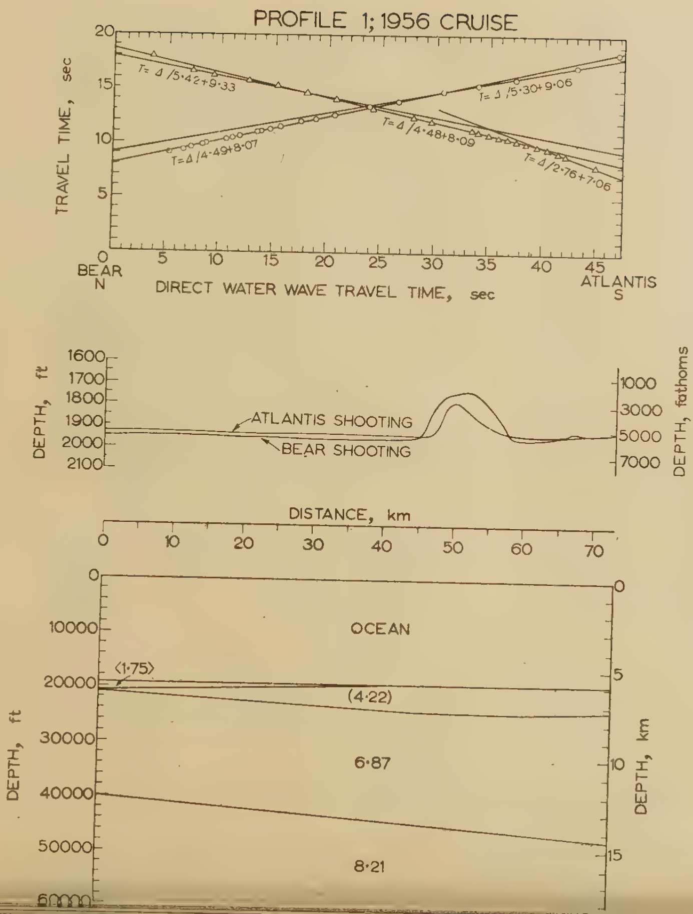
PROFILE 1; 1956 CRUISE
TRAVEL TIME, sec
DIRECT WATER WAVE TRAVEL TIME, sec
BEAR N
ATLANTIS S
T= Δ /5·42+9·33
T= Δ /5·30+9·06
T=Δ /4·49+8·07
T=Δ /4·48+8·09
T=Δ /2·76+7·06
DEPTH, ft
DEPTH, fathoms
ATLANTIS SHOOTING
BEAR SHOOTING
DISTANCE, km
DEPTH, km
OCEAN
⟨1·75⟩
(4·22)
6·87
8·21

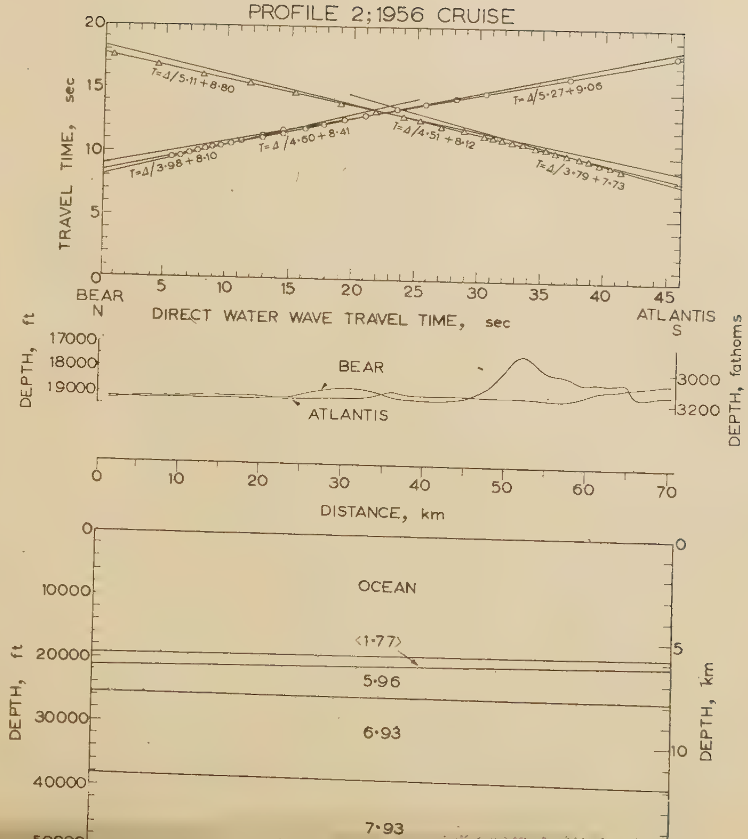
PROFILE 2; 1956 CRUISE
TRAVEL TIME, sec
DIRECT WATER WAVE TRAVEL TIME, sec
BEAR N
ATLANTIS S
T=Δ/5·11+8·80
T=Δ/5·27+9·06
T=Δ/3·98+8·10
T=Δ /4·60+8·41
T=Δ/4·51+8·12
T=Δ/3·79+7·73
DEPTH, ft
DEPTH, fathoms
BEAR
ATLANTIS
DISTANCE, km
DEPTH, km
OCEAN
⟨1·77⟩
5·96
6·93
7·93

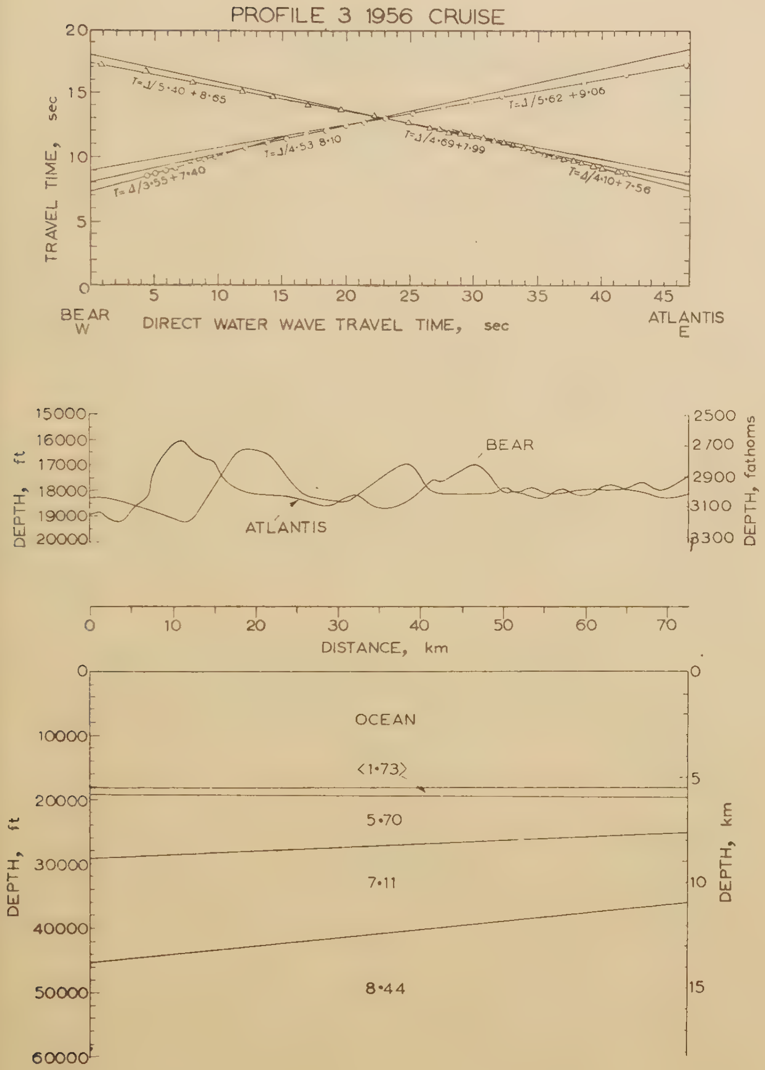
PROFILE 3 1956 CRUISE
TRAVEL TIME, sec
20
15
10
5
0
5
10
15
20
25
30
35
40
45
T=Δ/5·40 + 8·65
T=Δ/5·62 +9·06
T=Δ/4·53 8·10
T=Δ/4·69+7·99
T=Δ/3·55+7·40
T=Δ/4·10+7·56
BEAR W
DIRECT WATER WAVE TRAVEL TIME, sec
ATLANTIS E
DEPTH, ft
15000
16000
17000
18000
19000
20000
BEAR
ATLANTIS
2500
2700
2900
3100
3300
DEPTH, fathoms
0
10
20
30
40
50
60
70
DISTANCE, km
DEPTH, ft
0
10000
20000
30000
40000
50000
60000
OCEAN
<1·73>
5·70
7·11
8·44
0
5
10
15
DEPTH, km

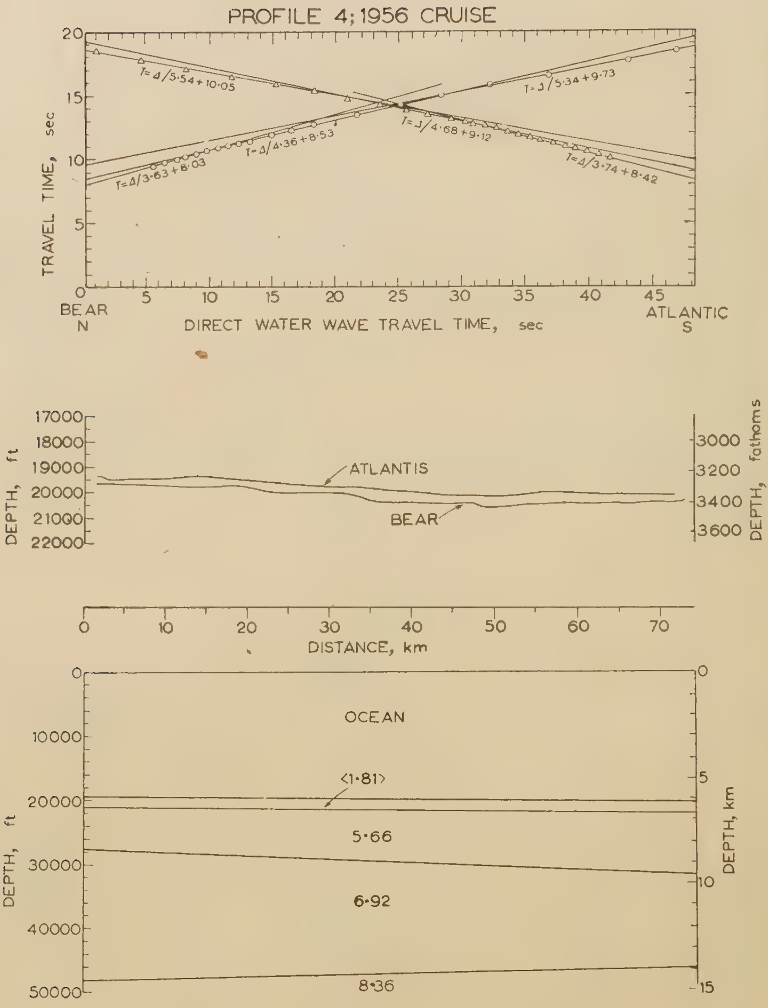
PROFILE 4; 1956 CRUISE
TRAVEL TIME, sec
0
5
10
15
20
T=Δ/5·54+10·05
T=Δ/5·34+9·73
T=Δ/4·36+8·53
T=Δ/3·63+8·03
T=Δ/4·68+9·12
T=Δ/3·74+8·42
BEAR
N
5
10
15
20
25
30
35
40
45
ATLANTIC
S
DIRECT WATER WAVE TRAVEL TIME, sec
DEPTH, ft
17000
18000
19000
20000
21000
22000
ATLANTIS
BEAR
3000
3200
3400
3600
DEPTH, fathoms
0
10
20
30
40
50
60
70
DISTANCE, km
DEPTH, ft
0
10000
20000
30000
40000
50000
OCEAN
⟨1·81⟩
5·66
6·92
8·36
0
5
10
15
DEPTH, km

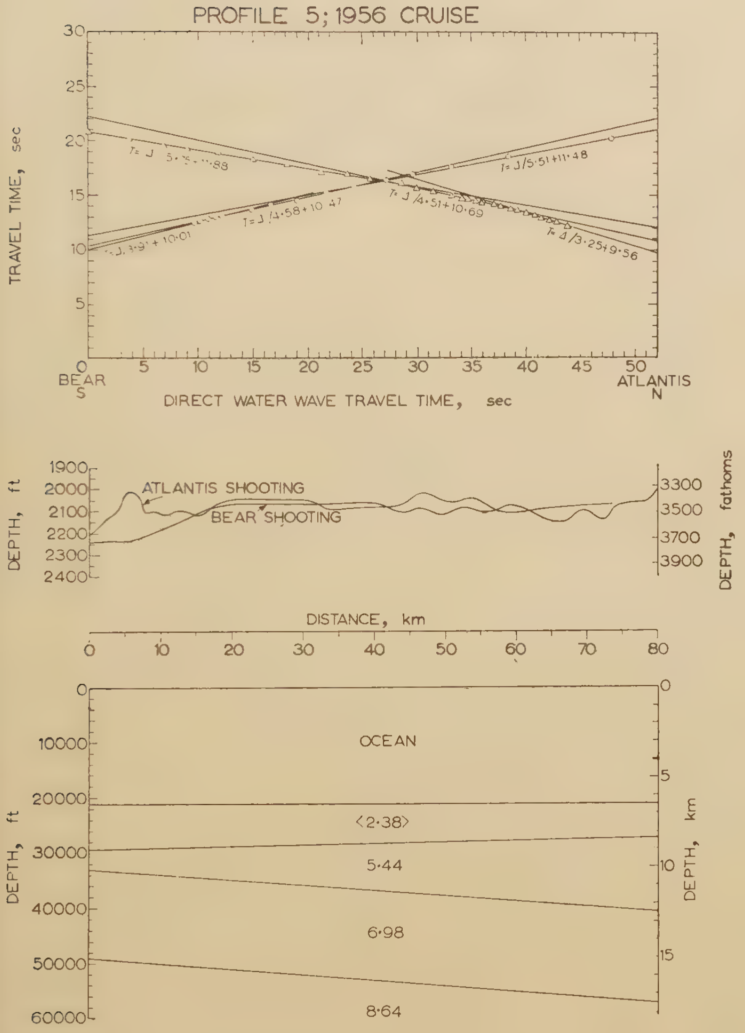
PROFILE 5; 1956 CRUISE
TRAVEL TIME, sec
30
25
20
15
10
5
0
T= J/5·5 + 11·88
T= J/5·51+11·48
T= J/4·58+10·47
T= J/4·51+10·69
J/3·9 + 10·01
T= Δ/3·25+9·56
5
10
15
20
25
30
35
40
45
50
BEAR
S
ATLANTIS
N
DIRECT WATER WAVE TRAVEL TIME, sec
DEPTH, ft
1900
2000
2100
2200
2300
2400
ATLANTIS SHOOTING
BEAR SHOOTING
3300
3500
3700
3900
DEPTH, fathoms
DISTANCE, km
0
10
20
30
40
50
60
70
80
DEPTH, ft
0
10000
20000
30000
40000
50000
60000
OCEAN
⟨2·38⟩
5·44
6·98
8·64
0
5
10
15
DEPTH, km

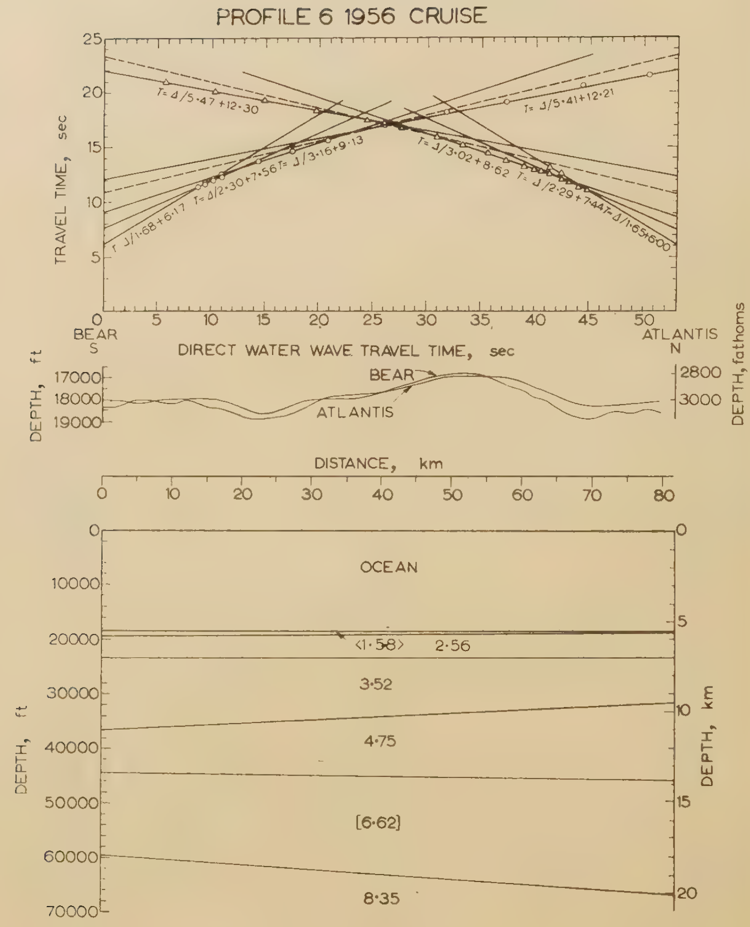
PROFILE 6 1956 CRUISE
TRAVEL TIME, sec
25
20
15
10
5
T= Δ/5·47+12·30
T= Δ/5·41+12·21
T= Δ/1·68+6·17
T= Δ/2·30+7·56
T= Δ/3·16+9·13
T= Δ/3·02+8·62
T= Δ/2·29+7·44
T= Δ/1·65+6·00
0 5 10 15 20 25 30 35 40 45 50
BEAR
S
DIRECT WATER WAVE TRAVEL TIME, sec
ATLANTIS
N
DEPTH, ft
17000
18000
19000
BEAR
ATLANTIS
2800
3000
DEPTH, fathoms
DISTANCE, km
0 10 20 30 40 50 60 70 80
DEPTH, ft
0
10000
20000
30000
40000
50000
60000
70000
OCEAN
<1·58>
2·56
3·52
4·75
[6·62]
8·35
DEPTH, km
0
5
10
15
20

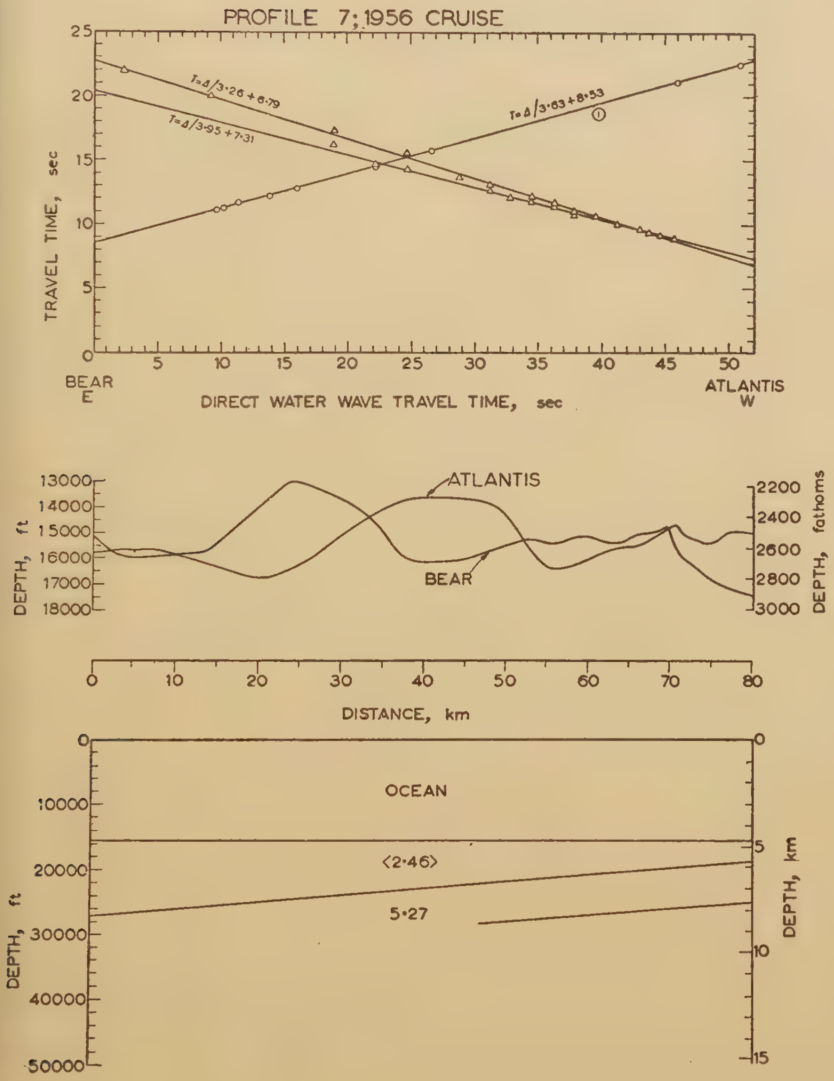
PROFILE 7; 1956 CRUISE
TRAVEL TIME, sec
25
20
15
10
5
0
5
10
15
20
25
30
35
40
45
50
BEAR
E
DIRECT WATER WAVE TRAVEL TIME, sec
ATLANTIS
W
T=Δ/3·26+6·79
T=Δ/3·95+7·31
T=Δ/3·63+8·53
①
DEPTH, ft
13000
14000
15000
16000
17000
18000
ATLANTIS
BEAR
2200
2400
2600
2800
3000
DEPTH, fathoms
0
10
20
30
40
50
60
70
80
DISTANCE, km
0
10000
20000
30000
40000
50000
DEPTH, ft
OCEAN
<2·46>
5·27
0
5
10
15
DEPTH, km

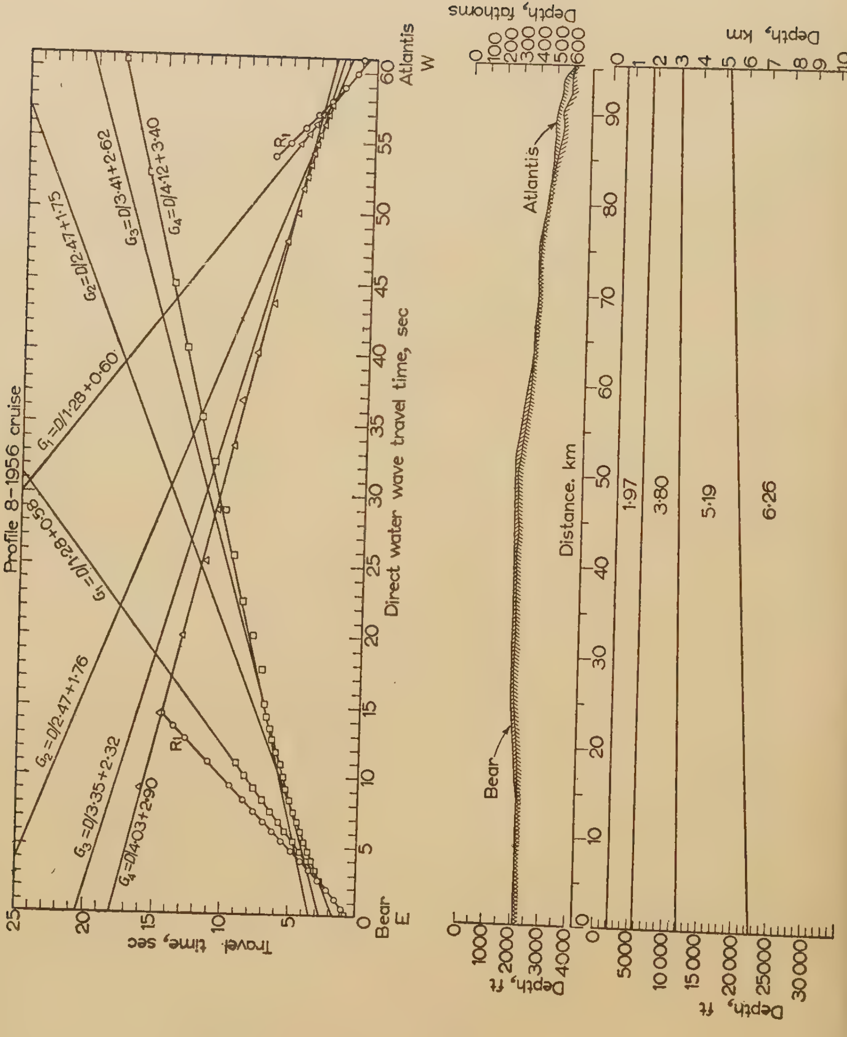
Profile 8-1956 cruise
Travel time, sec
Direct water wave travel time, sec
Bear
E
Atlantis
W
$G_1=D/1{\cdot}28+0{\cdot}58$
$G_1=D/1{\cdot}28+0{\cdot}60$
$G_2=D/2{\cdot}47+1{\cdot}76$
$G_2=D/2{\cdot}47+1{\cdot}75$
$G_3=D/3{\cdot}35+2{\cdot}32$
$G_3=D/3{\cdot}41+2{\cdot}62$
$G_4=D/4{\cdot}03+2{\cdot}90$
$G_4=D/4{\cdot}12+3{\cdot}40$
R_1
R_1
0
5
10
15
20
25
30
35
40
45
50
55
60
Depth, ft
Depth, fathoms
Bear
Atlantis
Distance, km
Depth, km
1·97
3·80
5·19
6·26

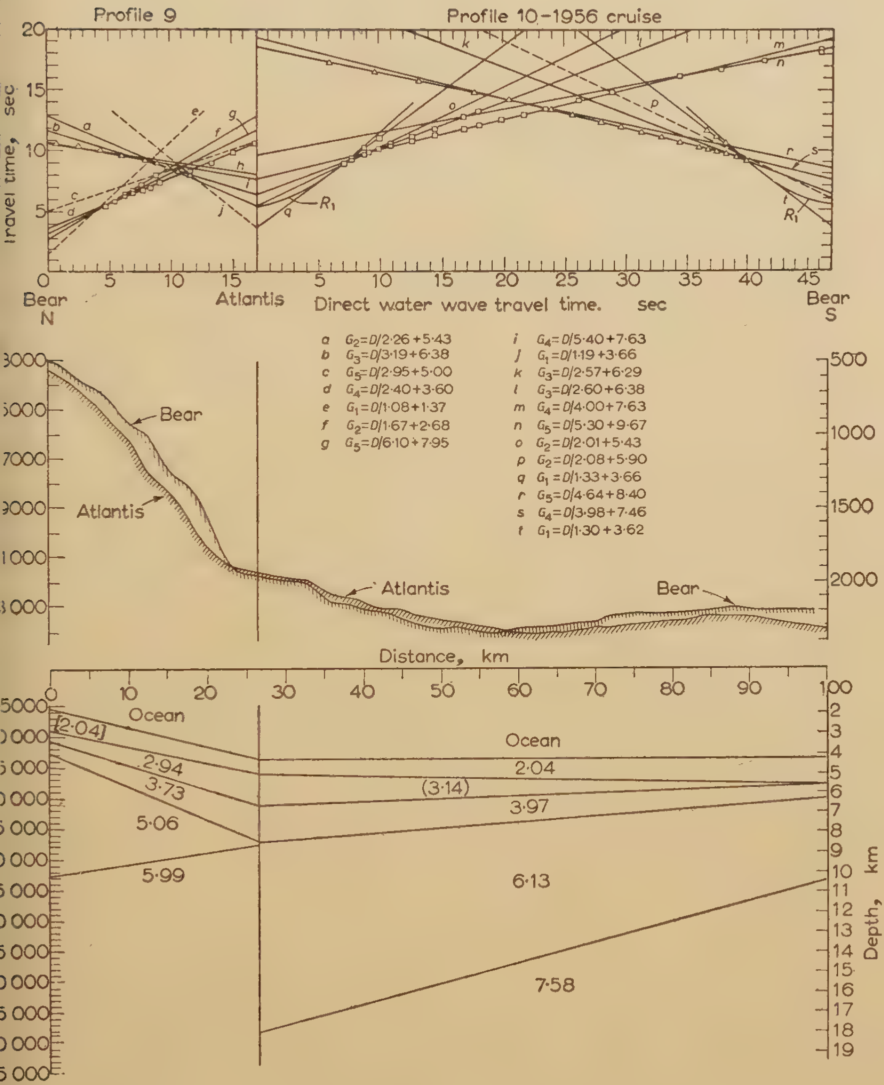

Profile 9
Profile 10–1956 cruise
Travel time, sec
20
15
10
5
0
5
10
15
Bear N
Atlantis
5
10
15
20
25
30
35
40
45
Direct water wave travel time. sec
Bear S
a b c d e f g h i j k l m n o p q r s t
R_1
a $G_2=D/2{\cdot}26+5{\cdot}43$
b $G_3=D/3{\cdot}19+6{\cdot}38$
c $G_5=D/2{\cdot}95+5{\cdot}00$
d $G_4=D/2{\cdot}40+3{\cdot}60$
e $G_1=D/1{\cdot}08+1{\cdot}37$
f $G_2=D/1{\cdot}67+2{\cdot}68$
g $G_5=D/6{\cdot}10+7{\cdot}95$
i $G_4=D/5{\cdot}40+7{\cdot}63$
j $G_1=D/1{\cdot}19+3{\cdot}66$
k $G_3=D/2{\cdot}57+6{\cdot}29$
l $G_3=D/2{\cdot}60+6{\cdot}38$
m $G_4=D/4{\cdot}00+7{\cdot}63$
n $G_5=D/5{\cdot}30+9{\cdot}67$
o $G_2=D/2{\cdot}01+5{\cdot}43$
p $G_2=D/2{\cdot}08+5{\cdot}90$
q $G_1=D/1{\cdot}33+3{\cdot}66$
r $G_5=D/4{\cdot}64+8{\cdot}40$
s $G_4=D/3{\cdot}98+7{\cdot}46$
t $G_1=D/1{\cdot}30+3{\cdot}62$
3000
5000
7000
9000
1000
3000
Bear
Atlantis
Atlantis
Bear
500
1000
1500
2000
Depth, fathoms
Distance, km
0
10
20
30
40
50
60
70
80
90
100
5000
0000
5000
0000
5000
0000
5000
0000
5000
0000
5000
0000
5000
Ocean
[2·04]
2·94
3·73
5·06
5·99
Ocean
2·04
(3·14)
3·97
6·13
7·58
2
3
4
5
6
7
8
9
10
11
12
13
14
15
16
17
18
19
Depth, km

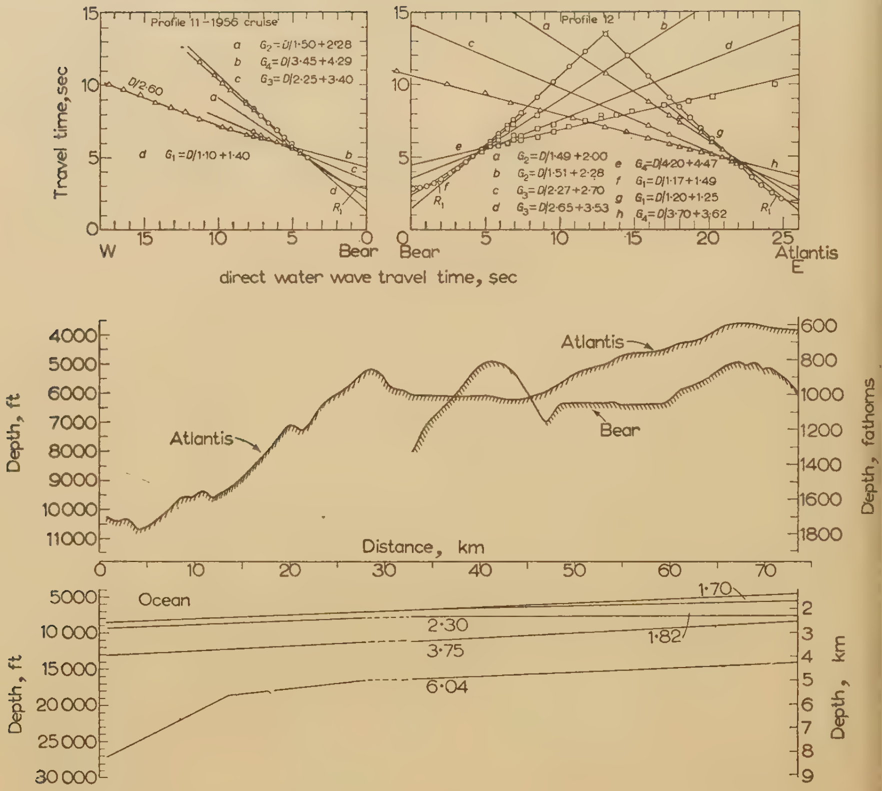
Profile 11 – 1956 cruise
a G2 = D/1·50 + 2·28
b G4 = D/3·45 + 4·29
c G3 = D/2·25 + 3·40
d G1 = D/1·10 + 1·40
D/2·60
R1
Travel time, sec
15
10
5
0
W
Bear
Profile 12
a G2 = D/1·49 + 2·00
b G2 = D/1·51 + 2·28
c G3 = D/2·27 + 2·70
d G3 = D/2·65 + 3·53
e G4 = D/4·20 + 4·47
f G1 = D/1·17 + 1·49
g G1 = D/1·20 + 1·25
h G4 = D/3·70 + 3·62
Atlantis
E
direct water wave travel time, sec
Depth, ft
4000
5000
6000
7000
8000
9000
10000
11000
Atlantis
Bear
Depth, fathoms
600
800
1000
1200
1400
1600
1800
Distance, km
0
10
20
30
40
50
60
70
Ocean
5000
10 000
15 000
20 000
25 000
30 000
1·70
2·30
1·82
3·75
6·04
Depth, km
2
3
4
5
6
7
8
9

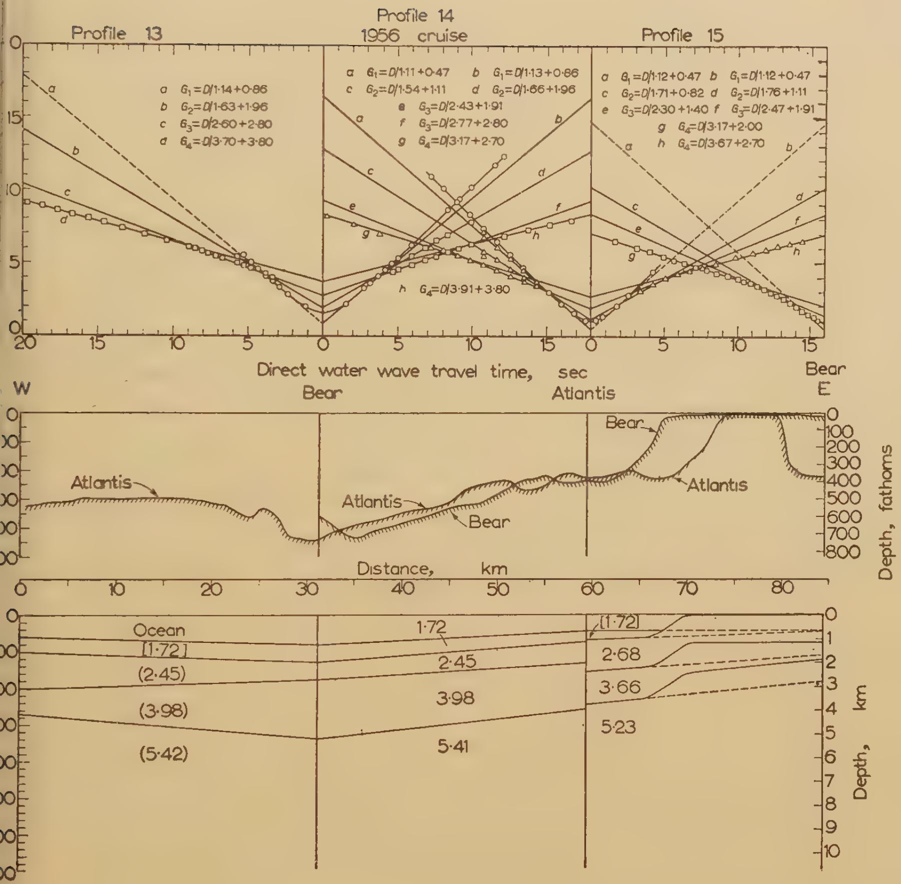
Profile 13
Profile 14
1956 cruise
Profile 15
a G₁=D/1·14+0·86
b G₂=D/1·63+1·96
c G₃=D/2·60+2·80
d G₄=D/3·70+3·80
a G₁=D/1·11+0·47
b G₁=D/1·13+0·86
c G₂=D/1·54+1·11
d G₂=D/1·66+1·96
e G₃=D/2·43+1·91
f G₃=D/2·77+2·80
g G₄=D/3·17+2·70
h G₄=D/3·91+3·80
a G₁=D/1·12+0·47
b G₁=D/1·12+0·47
c G₂=D/1·71+0·82
d G₂=D/1·76+1·11
e G₃=D/2·30+1·40
f G₃=D/2·47+1·91
g G₄=D/3·17+2·00
h G₄=D/3·67+2·70
0
15
10
5
0
20
15
10
5
0
5
10
15
0
5
10
15
Direct water wave travel time, sec
W
Bear
Atlantis
Bear
E
Atlantis
Atlantis
Bear
Bear
Atlantis
0
100
200
300
400
500
600
700
800
Depth, fathoms
Distance, km
0
10
20
30
40
50
60
70
80
Ocean
[1·72]
(2·45)
(3·98)
(5·42)
1·72
2·45
3·98
5·41
[1·72]
2·68
3·66
5·23
0
1
2
3
4
5
6
7
8
9
10
Depth, km

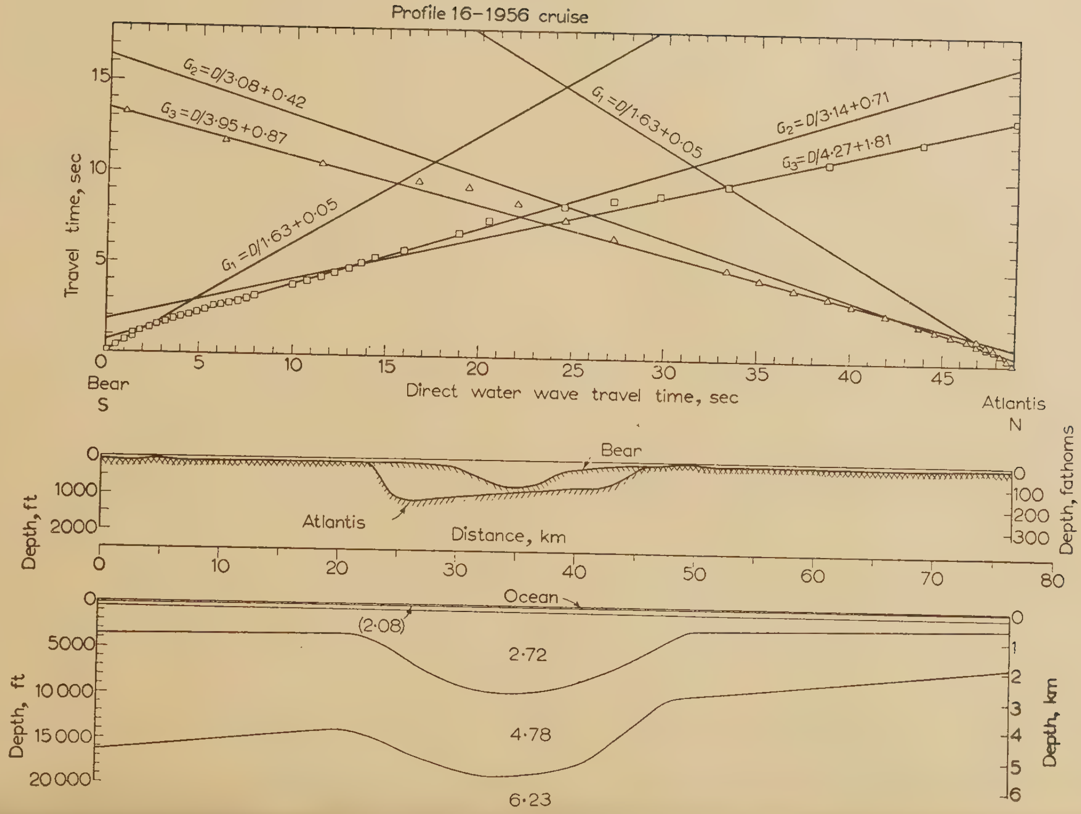
Profile 16–1956 cruise
$G_2=D/3{\cdot}08+0{\cdot}42$
$G_3=D/3{\cdot}95+0{\cdot}87$
$G_1=D/1{\cdot}63+0{\cdot}05$
$G_1=D/1{\cdot}63+0{\cdot}05$
$G_2=D/3{\cdot}14+0{\cdot}71$
$G_3=D/4{\cdot}27+1{\cdot}81$
Travel time, sec
15
10
5
0
5
10
15
20
25
30
35
40
45
Bear
S
Direct water wave travel time, sec
Atlantis
N
Bear
Atlantis
Depth, ft
0
1000
2000
Depth, fathoms
0
100
200
300
Distance, km
0
10
20
30
40
50
60
70
80
Ocean
(2·08)
2·72
4·78
6·23
Depth, ft
0
5000
10 000
15 000
20 000
Depth, km
0
1
2
3
4
5
6

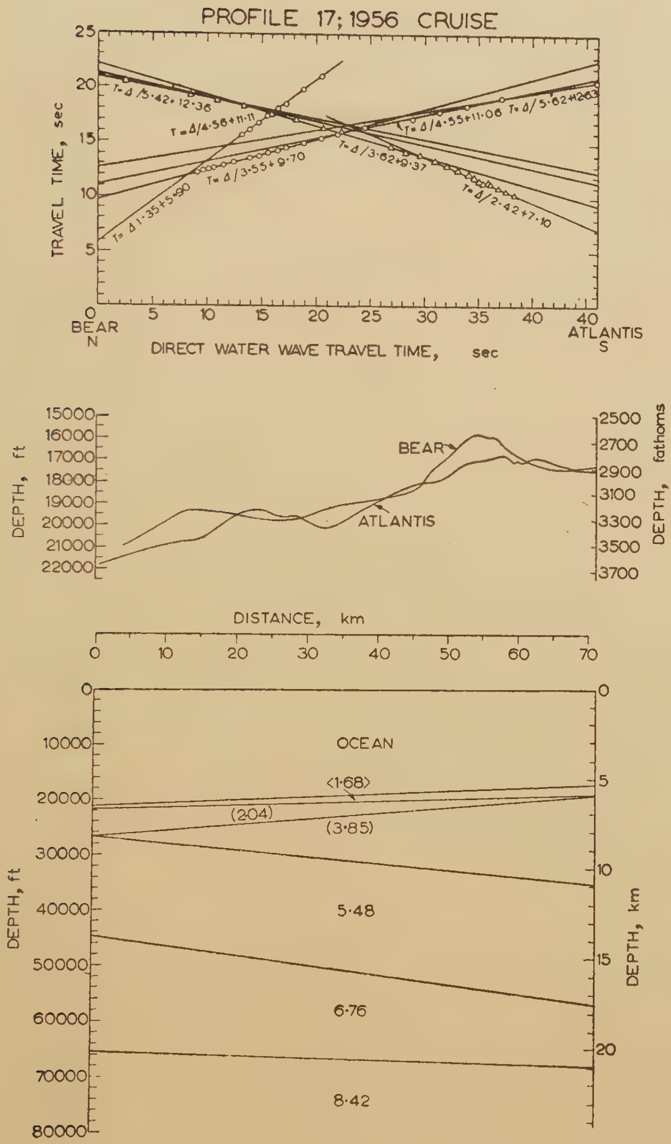
PROFILE 17; 1956 CRUISE
TRAVEL TIME, sec
25
20
15
10
5
0
T= Δ/5·42+12·36
T=Δ/4·56+11·11
T= Δ/3·55+9·70
T= Δ1·35+5·90
T= Δ/4·55+11·06
T= Δ/5·62+12·63
T= Δ/3·62+9·37
T= Δ/2·42+7·10
BEAR
N
5
10
15
20
25
30
35
40
40
ATLANTIS
S
DIRECT WATER WAVE TRAVEL TIME, sec
DEPTH, ft
15000
16000
17000
18000
19000
20000
21000
22000
BEAR
ATLANTIS
2500
2700
2900
3100
3300
3500
3700
DEPTH, fathoms
DISTANCE, km
0
10
20
30
40
50
60
70
DEPTH, ft
0
10000
20000
30000
40000
50000
60000
70000
80000
OCEAN
<1·68>
(2·04)
(3·85)
5·48
6·76
8·42
0
5
10
15
20
DEPTH, km

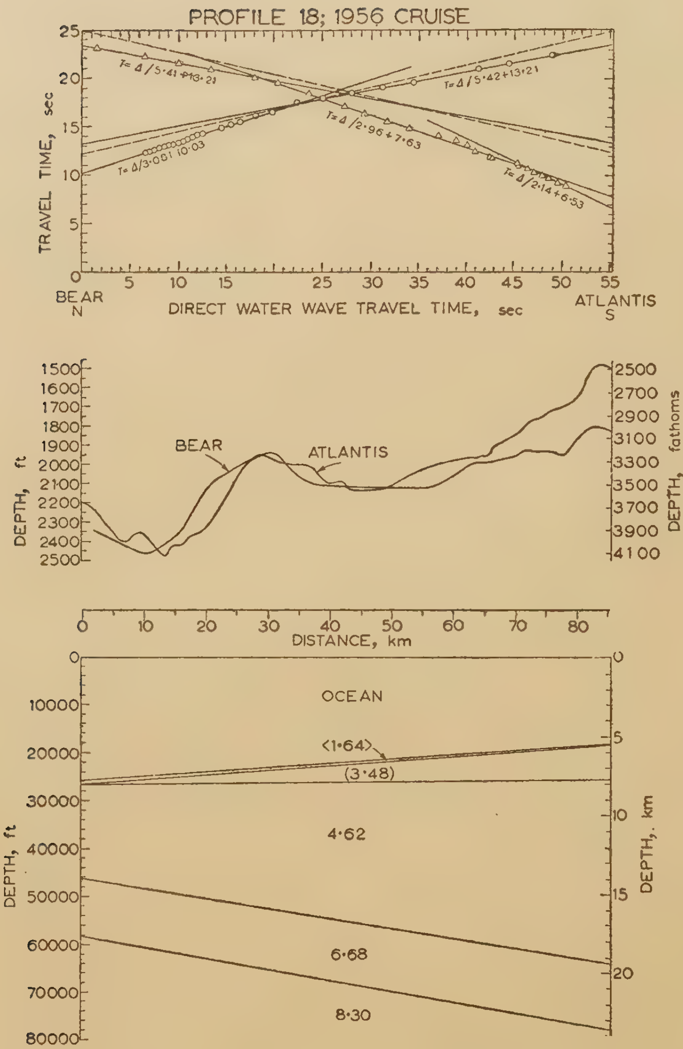
PROFILE 18; 1956 CRUISE
TRAVEL TIME, sec
25
20
15
10
5
0
T= Δ/5·41 +13·21
T= Δ/5·42+13·21
T= Δ/2·96+7·63
T= Δ/3·081 10·03
T= Δ/2·14+6·53
5
10
15
25
30
35
40
45
50
55
BEAR
N
DIRECT WATER WAVE TRAVEL TIME, sec
ATLANTIS
S
DEPTH, ft
1500
1600
1700
1800
1900
2000
2100
2200
2300
2400
2500
BEAR
ATLANTIS
2500
2700
2900
3100
3300
3500
3700
3900
4100
DEPTH, fathoms
0
10
20
30
40
50
60
70
80
DISTANCE, km
0
10000
20000
30000
40000
50000
60000
70000
80000
DEPTH, ft
OCEAN
<1·64>
(3·48)
4·62
6·68
8·30
0
5
10
15
20
DEPTH, km

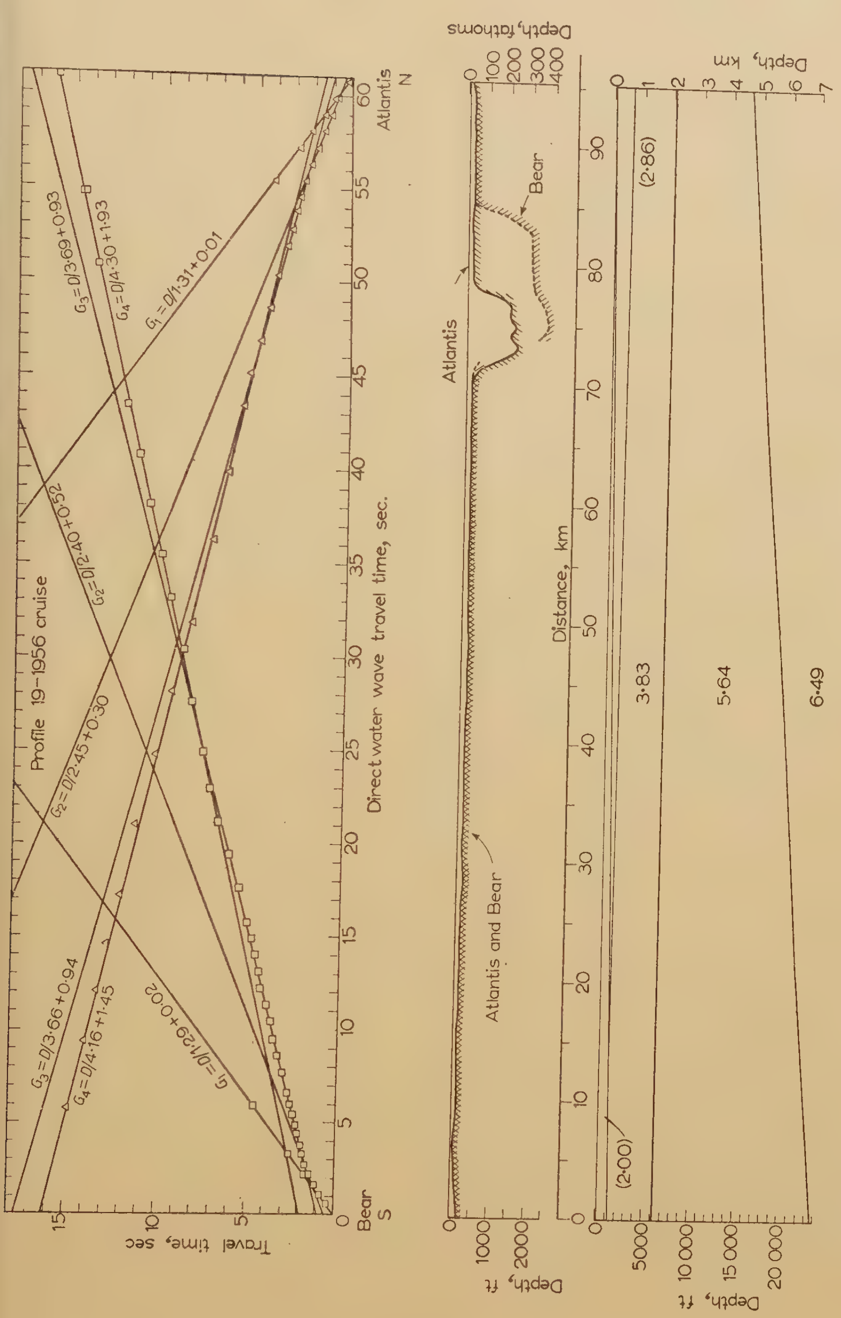
Profile 19-1956 cruise
$G_3=D/3{\cdot}69+0{\cdot}93$
$G_4=D/4{\cdot}30+1{\cdot}93$
$G_1=D/1{\cdot}31+0{\cdot}01$
$G_2=D/2{\cdot}40+0{\cdot}52$
$G_2=D/2{\cdot}45+0{\cdot}30$
$G_3=D/3{\cdot}66+0{\cdot}94$
$G_4=D/4{\cdot}16+1{\cdot}45$
$G_1=D/1{\cdot}29+0{\cdot}02$
Travel time, sec
0
5
10
15
20
25
30
35
40
45
50
55
60
Direct water wave travel time, sec.
Bear
S
Atlantis
N
Atlantis
Bear
Atlantis and Bear
Depth, fathoms
100
200
300
400
Depth, ft
1000
2000
Distance, km
10
20
30
40
50
60
70
80
90
Depth, km
1
2
3
4
5
6
7
(2·86)
(2·00)
3·83
5·64
6·49
5000
10 000
15 000
20 000

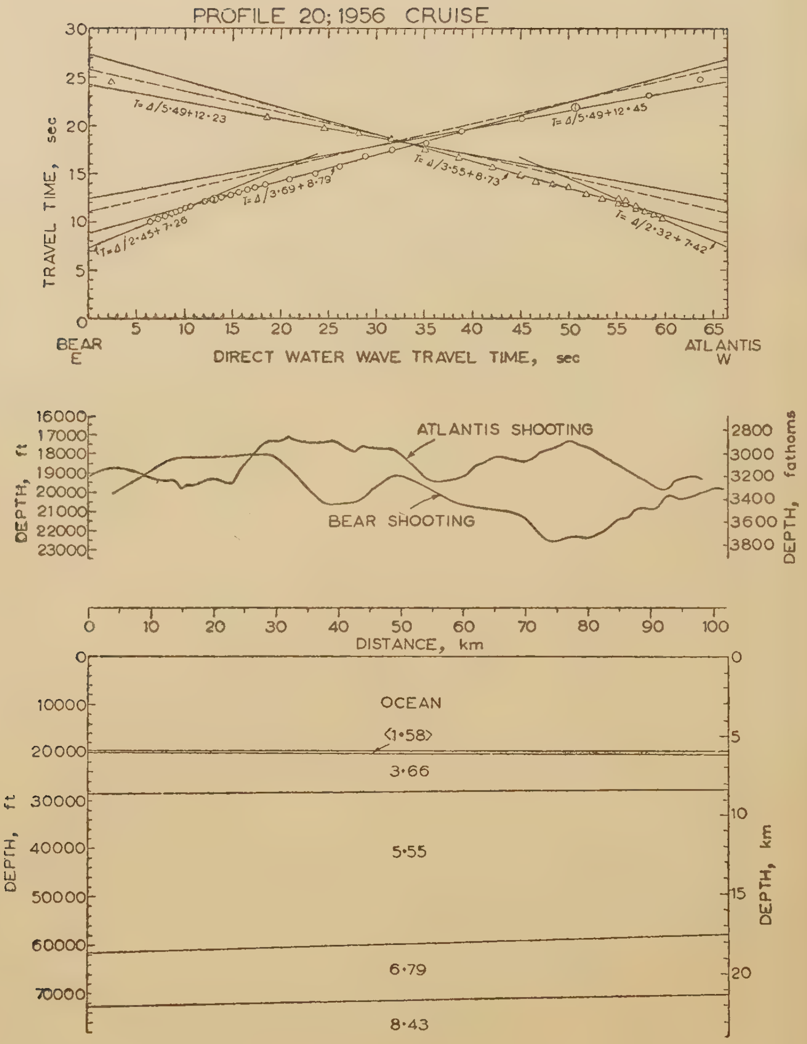
PROFILE 20; 1956 CRUISE
TRAVEL TIME, sec
T= Δ/5·49+12·23
T= Δ/5·49+12·45
T= Δ/3·55+8·73
T= Δ/3·69+8·73
T=Δ/2·45+7·26
T= Δ/2·32+7·42
BEAR E
ATLANTIS W
DIRECT WATER WAVE TRAVEL TIME, sec
DEPTH, ft
DEPTH, fathoms
ATLANTIS SHOOTING
BEAR SHOOTING
DISTANCE, km
OCEAN
<1·58>
3·66
5·55
6·79
8·43
DEPTH, km

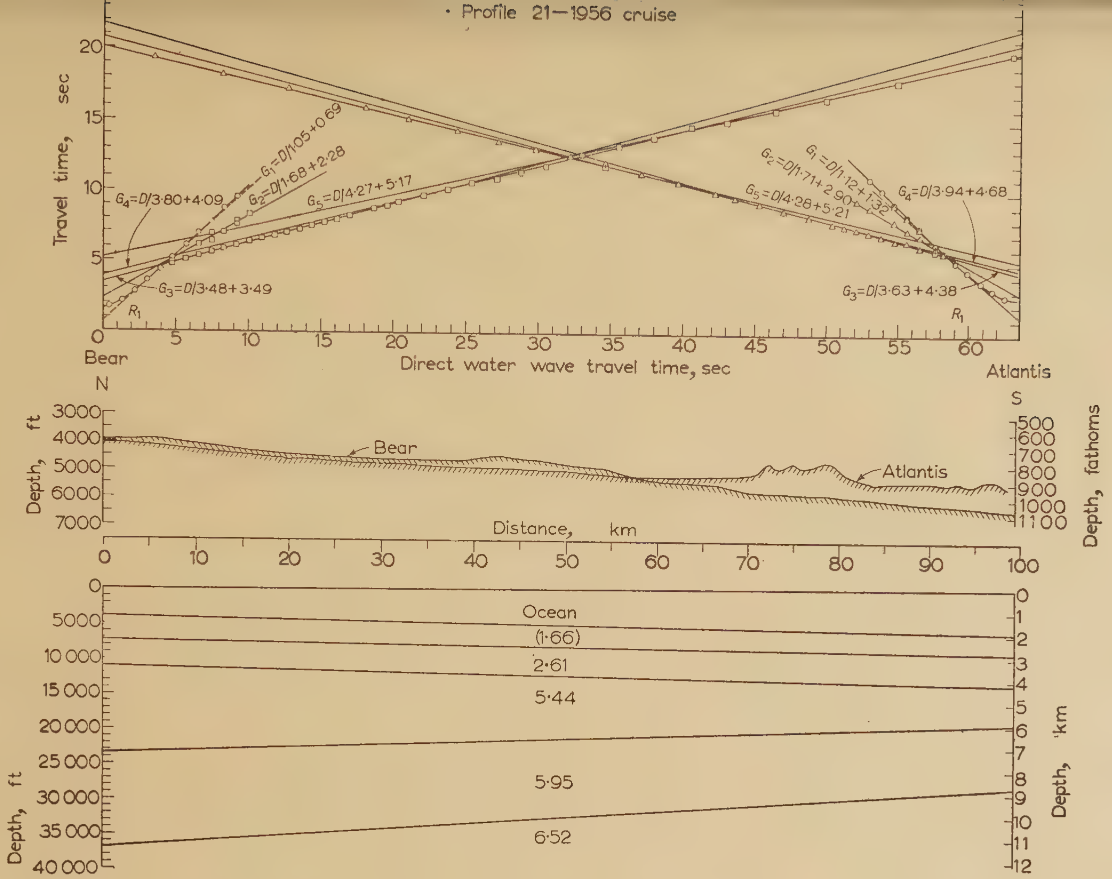

· Profile 21—1956 cruise

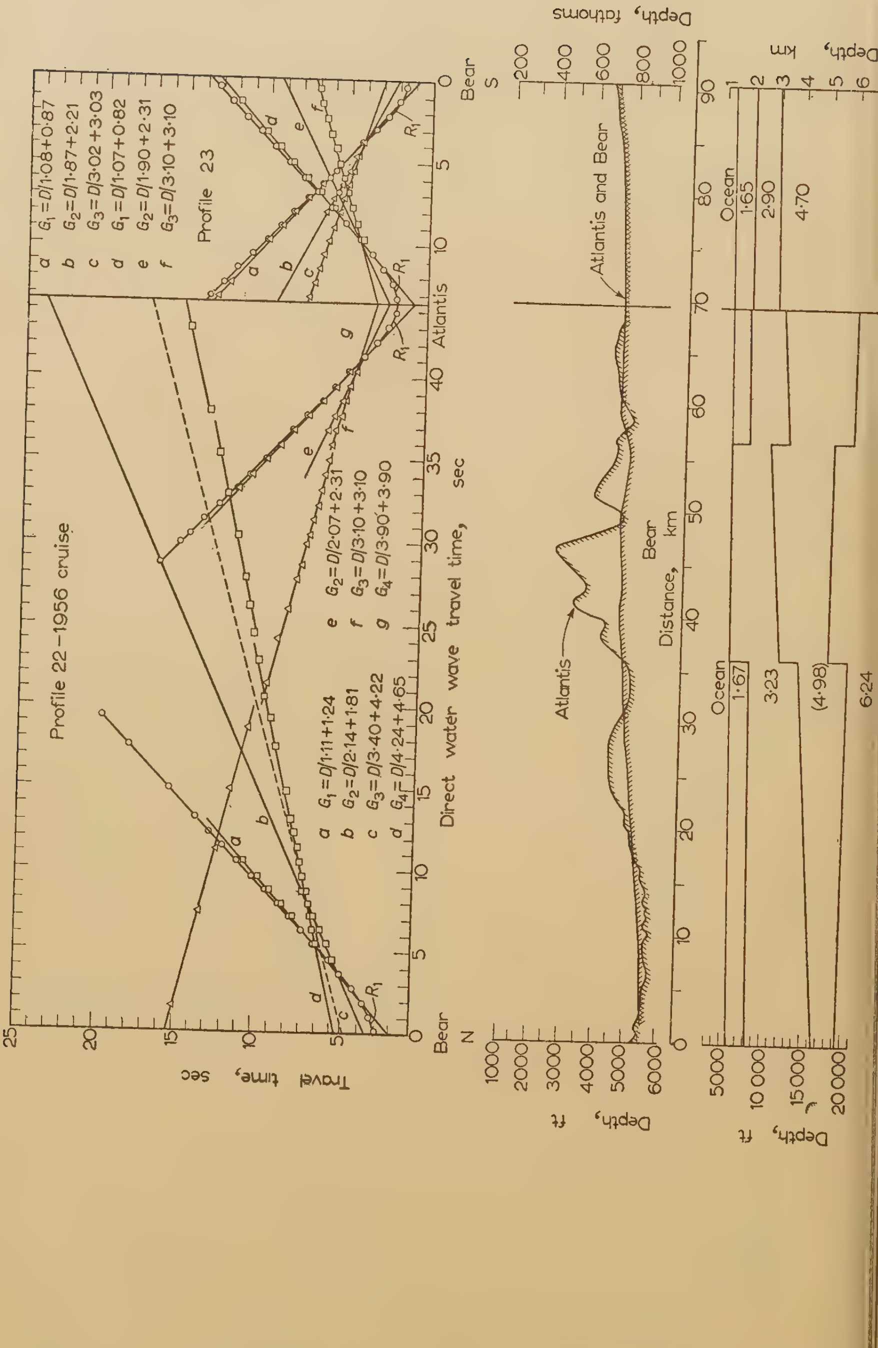

Profile 22—1956 cruise
a G1=D/1·11+1·24
b G2=D/2·14+1·81
c G3=D/3·40+4·22
d G4=D/4·24+4·65
e G2=D/2·07+2·31
f G3=D/3·10+3·10
g G4=D/3·90+3·90
Profile 23
a G1=D/1·08+0·87
b G2=D/1·87+2·21
c G3=D/3·02+3·03
d G1=D/1·07+0·82
e G2=D/1·90+2·31
f G3=D/3·10+3·10
R1
Travel time, sec
0
5
10
15
20
25
Direct water wave travel time, sec
Bear N
Atlantis
Bear S
Depth, ft
1000
2000
3000
4000
5000
6000
Depth, fathoms
200
400
600
800
1000
Atlantis
Atlantis and Bear
Bear
Distance, km
0
10
20
30
40
50
60
70
80
90
Ocean
1·67
3·23
(4·98)
6·24
Ocean
1·65
2·90
4·70
Depth, ft
5000
10 000
15 000
20 000
Depth, km
1
2
3
4
5
6

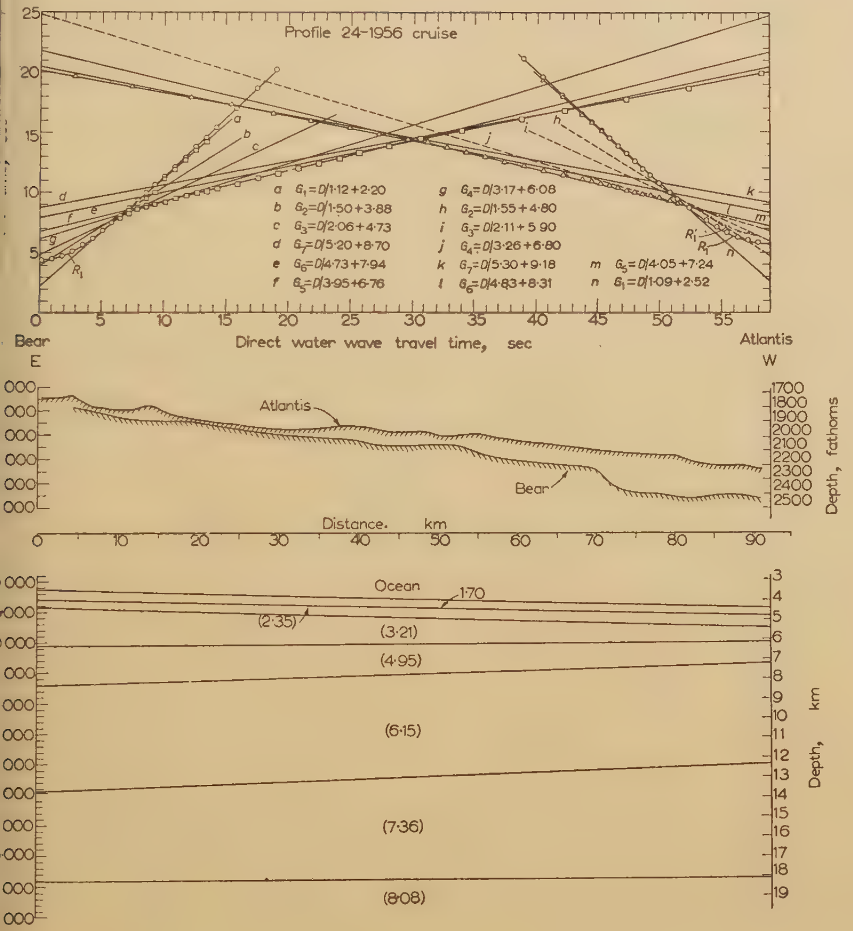
Profile 24-1956 cruise
a $G_1=D/1{\cdot}12+2{\cdot}20$
b $G_2=D/1{\cdot}50+3{\cdot}88$
c $G_3=D/2{\cdot}06+4{\cdot}73$
d $G_7=D/5{\cdot}20+8{\cdot}70$
e $G_6=D/4{\cdot}73+7{\cdot}94$
f $G_5=D/3{\cdot}95+6{\cdot}76$
g $G_4=D/3{\cdot}17+6{\cdot}08$
h $G_2=D/1{\cdot}55+4{\cdot}80$
i $G_3=D/2{\cdot}11+5\ 90$
j $G_4=D/3{\cdot}26+6{\cdot}80$
k $G_7=D/5{\cdot}30+9{\cdot}18$
l $G_6=D/4{\cdot}83+8{\cdot}31$
m $G_5=D/4{\cdot}05+7{\cdot}24$
n $G_1=D/1{\cdot}09+2{\cdot}52$
R_1
R_1'
25
20
15
10
5
0
5
10
15
20
25
30
35
40
45
50
55
Direct water wave travel time, sec
Bear
E
Atlantis
W
Atlantis
Bear
1700
1800
1900
2000
2100
2200
2300
2400
2500
Depth, fathoms
Distance. km
0
10
20
30
40
50
60
70
80
90
Ocean
1·70
(2·35)
(3·21)
(4·95)
(6·15)
(7·36)
(8·08)
3
4
5
6
7
8
9
10
11
12
13
14
15
16
17
18
19
Depth, km

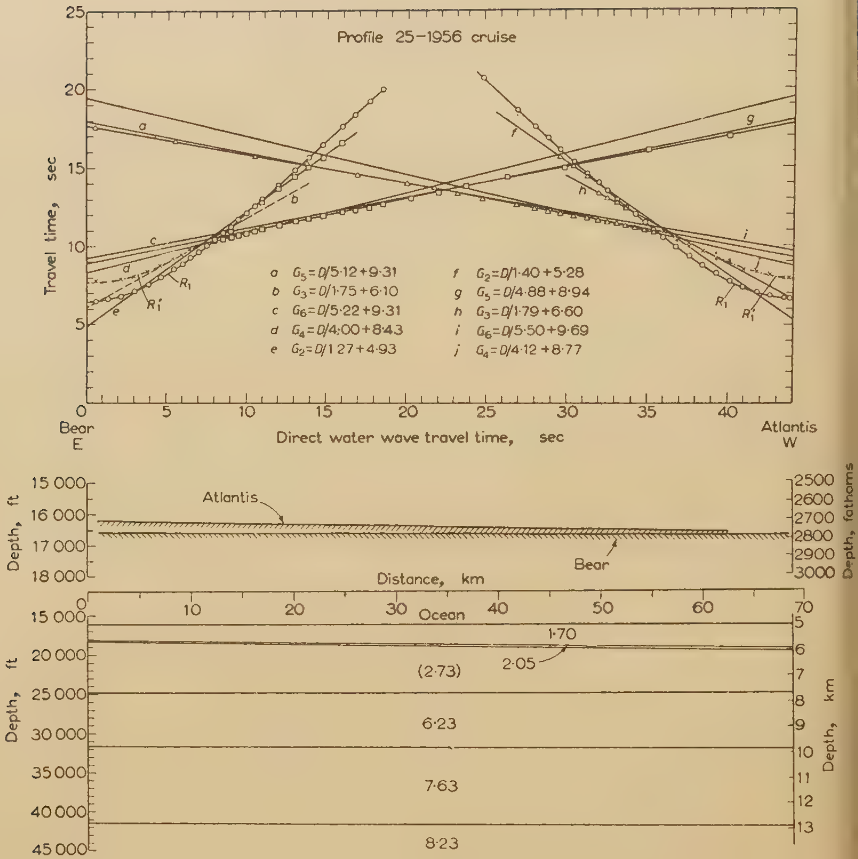
Profile 25–1956 cruise
Travel time, sec
25
20
15
10
5
0
5
10
15
20
25
30
35
40
Bear
E
Atlantis
W
Direct water wave travel time, sec
a
b
c
d
e
f
g
h
i
j
R1
R1'
a G5=D/5·12+9·31
b G3=D/1·75+6·10
c G6=D/5·22+9·31
d G4=D/4:00+8·43
e G2=D/1 27+4·93
f G2=D/1·40+5·28
g G5=D/4·88+8·94
h G3=D/1·79+6·60
i G6=D/5·50+9·69
j G4=D/4·12+8·77
Depth, ft
15 000
16 000
17 000
18 000
Atlantis
Bear
Depth, fathoms
2500
2600
2700
2800
2900
3000
Distance, km
0
10
20
30
40
50
60
70
Ocean
1·70
2·05
(2·73)
6·23
7·63
8·23
Depth, ft
15 000
20 000
25 000
30 000
35 000
40 000
45 000
Depth, km
5
6
7
8
9
10
11
12
13

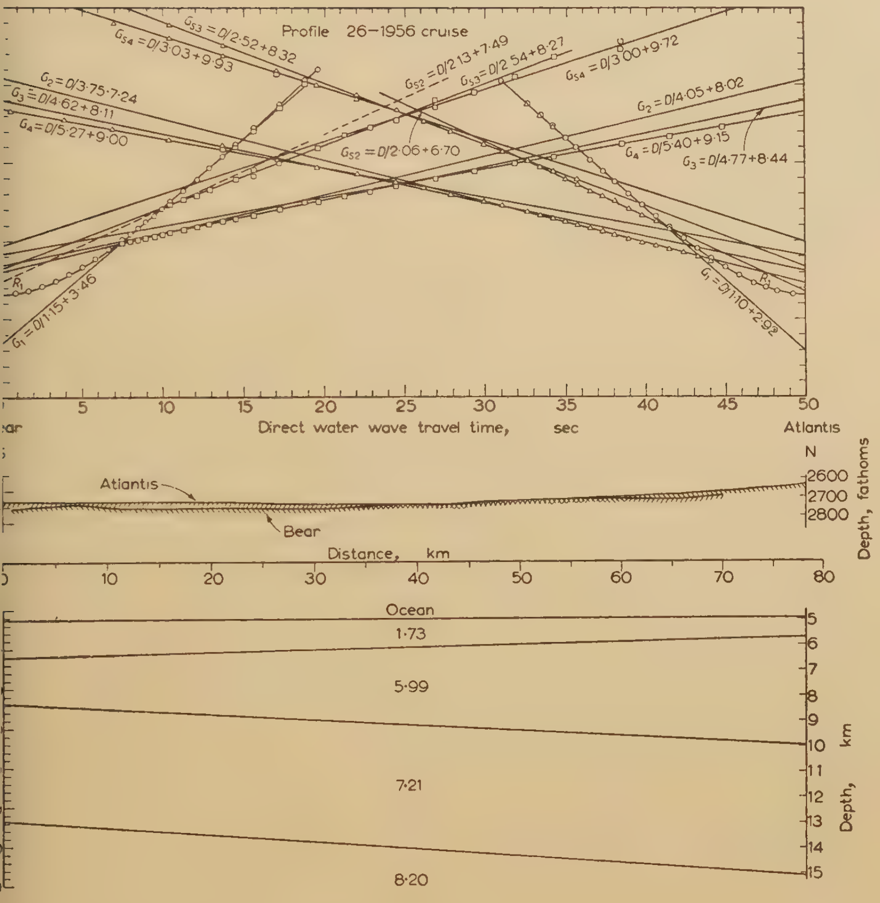
Profile 26—1956 cruise
$G_{S3}=D/2{\cdot}52+8{\cdot}32$
$G_{S4}=D/3{\cdot}03+9{\cdot}93$
$G_2=D/3{\cdot}75{\cdot}7{\cdot}24$
$G_3=D/4{\cdot}62+8{\cdot}11$
$G_4=D/5{\cdot}27+9{\cdot}00$
$G_{S2}=D/2{\cdot}13+7{\cdot}49$
$G_{S3}=D/2{\cdot}54+8{\cdot}27$
$G_{S4}=D/3{\cdot}00+9{\cdot}72$
$G_2=D/4{\cdot}05+8{\cdot}02$
$G_{S2}=D/2{\cdot}06+6{\cdot}70$
$G_4=D/5{\cdot}40+9{\cdot}15$
$G_3=D/4{\cdot}77+8{\cdot}44$
R_1
$G_1=D/1{\cdot}15+3{\cdot}46$
$G_1=D/1{\cdot}10+2{\cdot}92$
R_1
5
10
15
20
25
30
35
40
45
50
ear
Direct water wave travel time, sec
Atlantis
N
Atlantis
Bear
2600
2700
2800
Depth, fathoms
Distance, km
10
20
30
40
50
60
70
80
Ocean
1·73
5·99
7·21
8·20
5
6
7
8
9
10
11
12
13
14
15
Depth, km

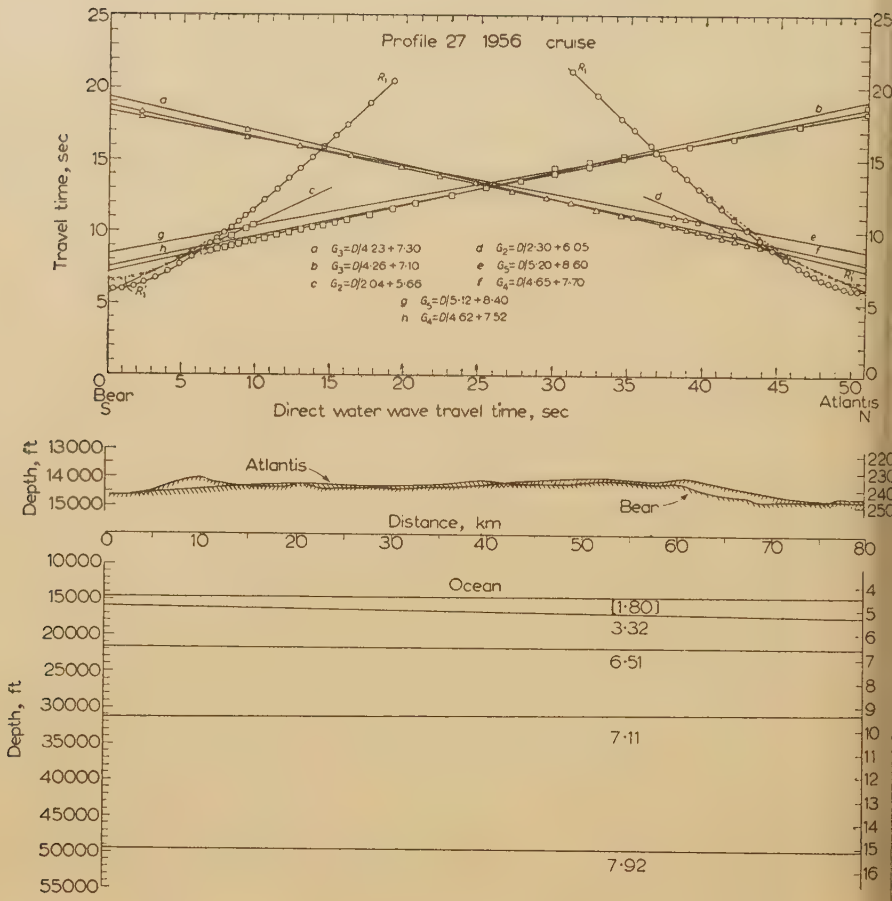
Profile 27 1956 cruise
Travel time, sec
Direct water wave travel time, sec
Bear S
Atlantis N
R_1
R_1'
a $G_3=D/4\ 23+7{\cdot}30$
b $G_3=D/4{\cdot}26+7{\cdot}10$
c $G_2=D/2\ 04+5{\cdot}66$
d $G_2=D/2{\cdot}30+6\ 05$
e $G_5=D/5{\cdot}20+8\ 60$
f $G_4=D/4{\cdot}65+7{\cdot}70$
g $G_5=D/5{\cdot}12+8{\cdot}40$
h $G_4=D/4\ 62+7\ 52$
0 5 10 15 20 25 30 35 40 45 50
0 5 10 15 20 25
Depth, ft
13000 14 000 15000
Atlantis
Bear
Distance, km
0 10 20 30 40 50 60 70 80
Ocean
[1·80]
3·32
6·51
7·11
7·92
10000 15000 20000 25000 30000 35000 40000 45000 50000 55000
4 5 6 7 8 9 10 11 12 13 14 15 16

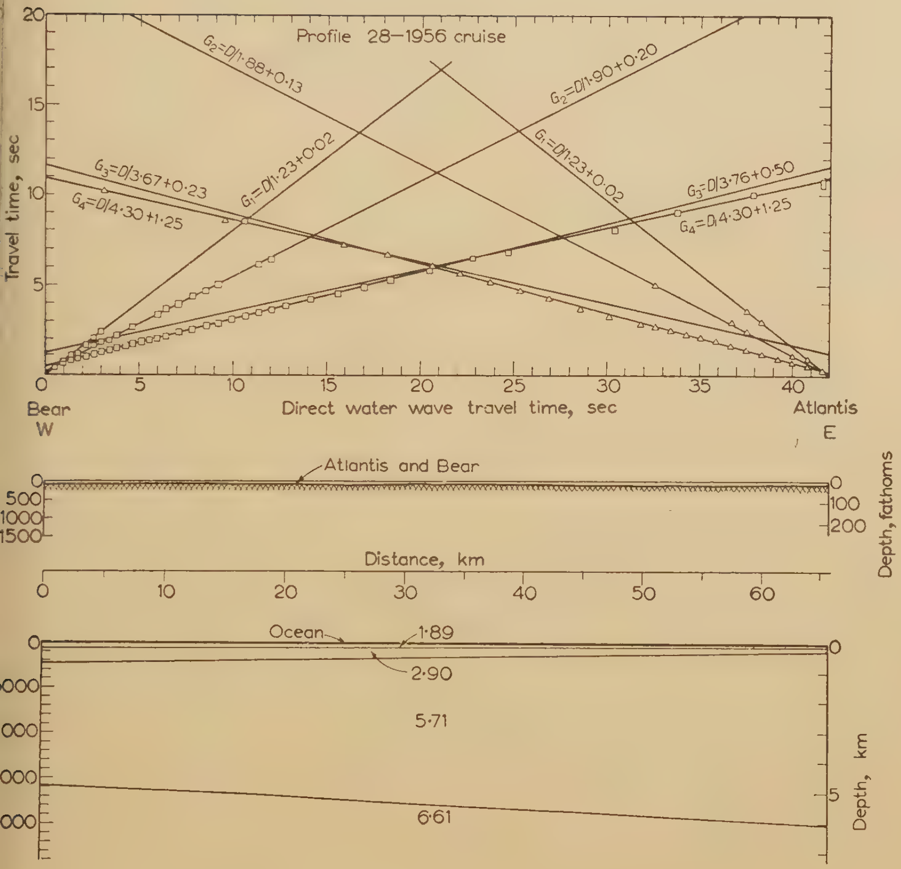
Profile 28—1956 cruise
Travel time, sec
Direct water wave travel time, sec
Bear
W
Atlantis
E
$G_2=D/1{\cdot}88+0{\cdot}13$
$G_1=D/1{\cdot}23+0{\cdot}02$
$G_3=D/3{\cdot}67+0{\cdot}23$
$G_4=D/4{\cdot}30+1{\cdot}25$
$G_2=D/1{\cdot}90+0{\cdot}20$
$G_1=D/1{\cdot}23+0{\cdot}02$
$G_3=D/3{\cdot}76+0{\cdot}50$
$G_4=D/4{\cdot}30+1{\cdot}25$
0
5
10
15
20
25
30
35
40
Atlantis and Bear
Depth, fathoms
0
500
1000
1500
100
200
Distance, km
0
10
20
30
40
50
60
Ocean
1·89
2·90
5·71
6·61
Depth, km
5
000
000
000
000

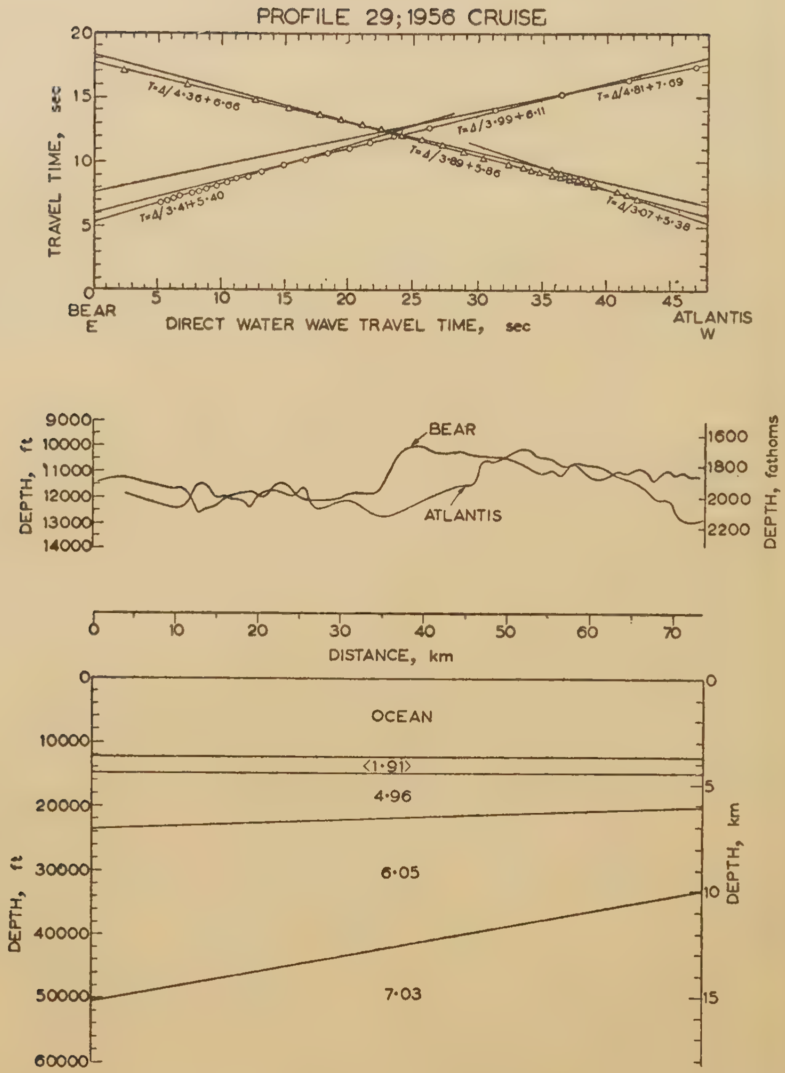
PROFILE 29; 1956 CRUISE
TRAVEL TIME, sec
20
15
10
5
0
T=Δ/4·36+6·66
T=Δ/4·81+7·69
T=Δ/3·99+6·11
T=Δ/3·89+5·86
T=Δ/3·41+5·40
T=Δ/3·07+5·38
5
10
15
20
25
30
35
40
45
BEAR
E
DIRECT WATER WAVE TRAVEL TIME, sec
ATLANTIS
W
DEPTH, ft
9000
10000
11000
12000
13000
14000
BEAR
ATLANTIS
1600
1800
2000
2200
DEPTH, fathoms
0
10
20
30
40
50
60
70
DISTANCE, km
0
10000
20000
30000
40000
50000
60000
DEPTH, ft
OCEAN
<1·91>
4·96
6·05
7·03
0
5
10
15
DEPTH, km

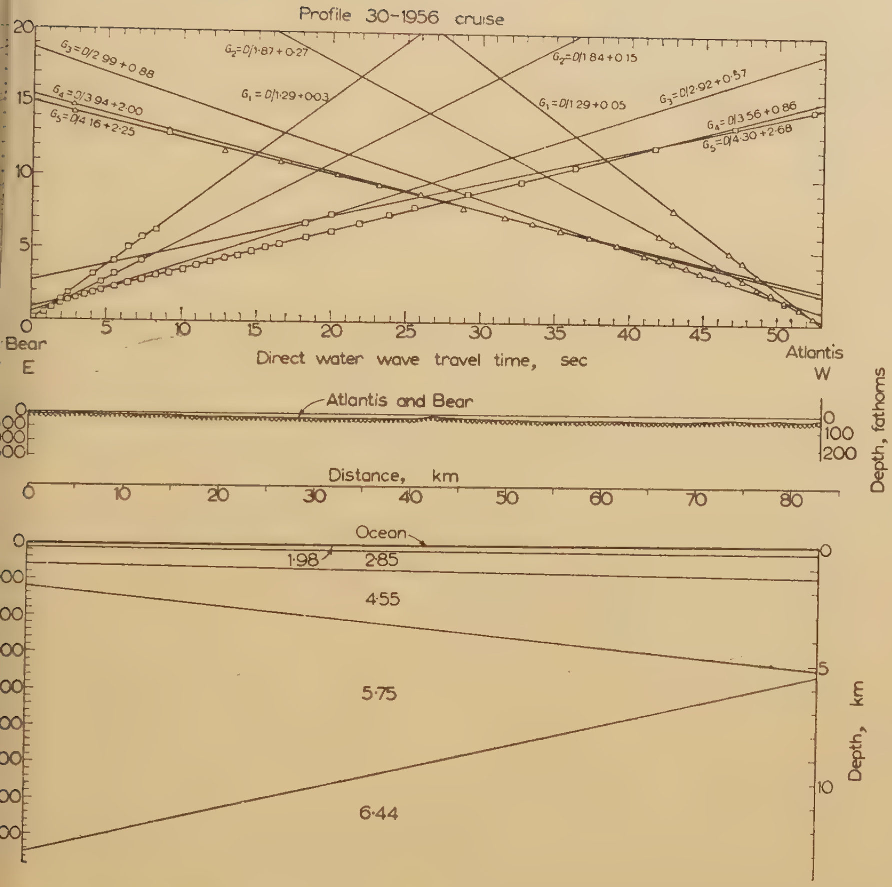
Profile 30–1956 cruise
$G_3 = D/2{\cdot}99 + 0{\cdot}88$
$G_2 = D/1{\cdot}87 + 0{\cdot}27$
$G_1 = D/1{\cdot}29 + 0{\cdot}03$
$G_4 = D/3{\cdot}94 + 2{\cdot}00$
$G_5 = D/4{\cdot}16 + 2{\cdot}25$
$G_2 = D/1{\cdot}84 + 0{\cdot}15$
$G_1 = D/1{\cdot}29 + 0{\cdot}05$
$G_3 = D/2{\cdot}92 + 0{\cdot}57$
$G_4 = D/3{\cdot}56 + 0{\cdot}86$
$G_5 = D/4{\cdot}30 + 2{\cdot}68$
20
15
10
5
0
5
10
15
20
25
30
35
40
45
50
Bear
E
Direct water wave travel time, sec
Atlantis
W
Atlantis and Bear
0
100
200
Depth, fathoms
Distance, km
0
10
20
30
40
50
60
70
80
Ocean
1·98
2·85
4·55
5·75
6·44
0
5
10
Depth, km

on the order of 6·0–6·5 km/sec and one for a velocity of 7·0–7·5 km/sec. This is not entirely consistent, however; and it is usually difficult to tell whether the velocity change from the top to the bottom of the layer is continuous or discontinuous. The Atlantic basin profiles are satisfactorily fit with a single crustal line.

This section shows the contrast in structure going from the interior basin of the Caribbean across the arc to the Atlantic basin. Probably the most noticeable change is between the greatly thickened crust under the Aves swell and the island arc and the comparatively thin crust under the Puerto Rico trench. Also the sharp change in depth to the high velocity crustal layer between Barbuda and profile *6* is striking. The southwestward dip of the high velocity layers here, although possibly interpretable in some other way, strongly suggests an overthrust of the Caribbean crust onto the oceanic crust. The depression of the higher velocity, denser layers provides an explanation of the negative gravity anomaly belt whose axis is approximately coincident with profile *7*.

The material constituting the upper layers in this section is difficult to identify specifically from seismic velocity alone. In general the profiles have not been located to allow a tie-in with detailed land geology; but from the work of the several investigators listed in the references, we have a general knowledge of the variety of sedimentary, metamorphic, volcanic, and igneous rocks present. It has been the primary aim of these seismic investigations to study the broader, more general features of island arc structure; hence we will not attempt to identify each layer as a specific geologic bed, such being considered somewhat speculative from the existing data. The upper layer (stipples) has velocities which are associated with unconsolidated and with slightly lithified sediments. The next two deeper layers (diagonals and hachures) have velocities characteristic of many sedimentary, igneous, and metamorphic rocks, the lower velocities being more characteristic of sedimentary and volcanic rocks and the higher velocities of igneous and metamorphic rocks. The high velocity crustal layers (checks) have been most often identified as basic igneous in composition. In the present case it seems quite possible that the upper part, which tends to lower velocities, may be more acidic than normal oceanic crustal composition. The deepest layer (verticals), with a velocity of about 8 km/sec or higher, is identified as the mantle. The mantle material is considered to be ultrabasic in composition.

In general, on nearby profiles, the hachured layer correlates with the igneous basement complex of the islands. The diagonalled layer correlates with the volcanic, detrital sedimentary, and reef limestone rocks. The stippled layer correlates with the sediment.

There is a discrepancy in the results of profiles *5* and *6* and profile *17*, possibly due to the difference in the direction of the shooting but more likely due to navigation. In this area the depths are changing rapidly and a relatively small error in navigation could produce the disagreement. The structure section has been drawn using the average values from these profiles.

Section 2

Section 2, shown in Fig. 15, begins on the Aves swell and continues north along its axis, crosses the inner volcanic arc of the Lesser Antilles at St. Eustatius and outer arc at St. Barthelemy, and continues across the Puerto Rico trench out to e Atlantic basin. The section is about 700 miles long and includes the data om thirteen profiles.

As is valid for the other sections, the seismic velocities and their associated vering can be separated conveniently into the five groups shown. The vertical es designate mantle material. The checks designate crustal material. The chures designate material with seismic velocities somewhat lower than those rmally associated with the suboceanic crust; the velocities are characteristic many metamorphic and igneous intrusive rocks. The diagonals designate a oup whose velocities are characteristic of many sedimentary and volcanic cks. The stipples designate unconsolidated and partially lithified sediments.

The mantle was reached only on profiles *1*, *2*, *3*, 44, and *18* in the Atlantic sin and Puerto Rico trench. None of the Lesser Antilles or Aves swell stations easured the Mohorovicic discontinuity. As with Section 1, there is a conicuous difference between the crust of the Lesser Antilles and that of the tlantic basin and Puerto Rico trench. The crust in the latter area is fairly niform with a thickness of 4–5 km and a velocity of 6·6–7·1 km/sec. Beneath e Lesser Antilles and Aves swell the crust is considerably thicker and more riable in configuration and velocity composition. Two crustal layers are bserved. The upper crustal layer has a lower seismic velocity than that norally associated with an oceanic crust, suggestive of a somewhat more acidic mposition.

The abrupt change in the deep structure across the slope from the Lesser ntilles to the Puerto Rico trench is conspicuous on this section. The thickened nd lower velocity crustal section of the Caribbean suggests that the primary echanism in its development has been the introduction of a differentiate of ghter material from deep in the mantle into the upper mantle and crustal yers. The abrupt change in configuration at the edge of the Caribbean suggests at a second mechanism of importance has been an overthrusting along a major acture zone of the island arc portion of the Caribbean onto the Puerto Rico ench portion of the Atlantic. The force for such a deformation is presumed be a horizontal compression, probably associated with the introduction of the fferentiate material in the Caribbean. The geometry and elementary mechanics r such a configuration have been given by Gunn (1947).

ection 3

Section 3, shown in Fig. 16, begins on the north coast of Venezuela, crosses e Cariaco trough and the westward extension of the Lesser Antilles north of outh America, crosses the Los Rocques trench and continues along the Veneelan basin near its boundary with the Aves swell, crosses the Greater Antilles and arc at the St. Croix ridge, Virgin Island trough, Island of St. Thomas, and elf north of St. Thomas, and continues across the Puerto Rico trench out to the tlantic basin. The section is about 750 miles long and includes the data from ghteen profiles.

The mantle was reached on profiles *24*, 31, 32, and *27* in the Caribbean and profiles *20* and 45 in the Atlantic. The depth to the Mohorovicic discontinuity erages 17 km in the Caribbean and 12 km in the Atlantic. The Caribbean ction shows, as before, a thick crust variable in configuration and velocity mposition as compared with the Atlantic basin crust.

The island arc portion, here across the Greater Antilles, is different from that shown on the section across the Lesser Antilles. From the seismic velocities it is difficult, if not impossible, to distinguish the upper crustal portion from the next overlying layer (hachures). On Section 2 the velocity of this layer averages 5·4 km/sec; here the velocity is 5·8 km/sec. The underlying crustal velocities are also higher than those on the adjacent Lesser Antilles sections. From surface geology the Greater Antilles are presumed to be older than the Lesser Antilles; their geologic development has taken place over a longer period of time than that of the Lesser Antilles. From this it is suggested that these measured velocity differences, higher velocities under the Greater Antilles than those at corresponding depth under the Lesser Antilles, could have occurred and would be an expected result of later stage intrusion and metamorphism

It should be noted, also, that the change in the deep structure across the slope from the island arc to the trench is not as great here as it is in Sections 1 and 2 across the Lesser Antilles. There is more similarity here between the configuration underlying the northern and southern slopes from the island arc than on the other sections.

Section 4

Section 4, shown in Fig. 17, begins near the middle of the Venezuelan basin and crosses the Aves swell, Grenada trough, Lesser Antilles arc, Tobago trough, Barbados ridge and ends in the western edge of the Guiana basin about 200 miles east of Barbados. This section is 720 miles long and includes the data from fifteen profiles. With a few exceptions the measured velocities can be separated into general groups represented by the five layers in the cross-section.

The entire crustal section was measured at profiles *24* and *26* in the Venezuelan basin and profiles 17 and 18 in the Guiana basin. The mantle was not detectable by any of the other profiles along this section, presumably because it was at too great a depth. The high velocity crustal rocks vary in velocity between 6·0 and 7·4 km/sec. This layer has a wider range of velocities and is thicker in the Caribbean than in the Atlantic. The high velocity crust is thickest and reaches its highest elevation under the Aves swell and the Lesser Antilles arc. Its upper surface is deepest underneath the Barbados ridge. Although it was not detected under the central portion of the ridge, this layer, by extrapolation and by minimum depth computations, appears to be at least 13–14 km deep. Thus the configuration of the high velocity crustal layer and the mantle in this section is much like that in Sections 1, 2, and 4 which cross the Puerto Rico trench. However, the down-thrust or down buckle under the Barbados ridge is much broader than that under the Puerto Rico trench and has a greater sedimentary fill, presumably owing to its proximity to the continent and a good source of sedimentary material. The structure of the Barbados ridge is significantly different from the ridges forming the Aves swell and the Lesser Antilles. The Barbados ridge is composed of the intermediate velocity, derived materials which themselves lie in the trough of the down buckled high velocity layers. The Barbados ridge and the thick sequence of derived material are coincident with the negative anomaly axis (local isostatic or Bouguer). The thick sequence of derived material provides the explanation for the negative anomaly axis. It is surmised that the ridge itself was formed as a result of readjustment of stresses in the crust and mantle toward a more local isostatic equilibrium.

The overlying material, comprising the three upper layers, has velocities rying from 1·7 to 5·4 km/sec. There is considerable difficulty in correlating ese layers throughout the section, understandably so since many volcanic, etamorphic, igneous intrusive, and sedimentary rocks could be included in is velocity range and are probably present in the area. For example, in one ace a velocity of 4 km/sec. may represent limestone, and in another it may present volcanic or metamorphic rock. The greatest thickness of these aterials is in the Barbados ridge, where up to 10 km, and possibly much more, found. In general the profiles on the Barbados ridge are more complicated an usual, with strong dips, faults, and folds. The upper layers (stippled) are obably sedimentary. The large thickness in the Tobago trough and east of e Barbados ridge suggests that the Orinoco river and perhaps the rivers of e Guianas have been major sources of these sediments.

ection 5

Section 5, Fig. 18, crosses the northern end of the Lesser Antilles. To the uth of the section is Saba bank. To the northwest is Sombrero, part of the e outer and older line of limestone-capped volcanoes. This line extends down om Sombrero to Anguilla, St. Martin, Barbuda, Antigua, Grande Terre, and arie Galente. To the south-east of the central portion of the section are Saba d St. Kitts, part of the inner and younger line of volcanoes. This line extends own from Saba and St. Kitts to Montserrat, Guadaloupe, Dominica, Mar-nique, St. Lucia, St. Vincent, the Grenadine islands, and Grenada. The ructure cross section shows the subsurface extension of the Saba–St. Kitts dge. This extension is indicated in the surface topography but is more pro-ounced across the buried ridge itself.

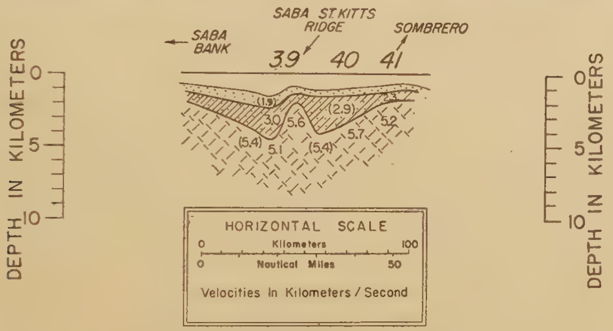

Fig. 18

ection 6

Section 6, Fig. 19, crosses the southern slope of Puerto Rico. A rather large ickness of sedimentary rock (diagonals and stipples) is measured above the gh velocity, crystalline basement (hachures) under the slope. This thick diment correlates with coastal plain sediments of Miocene and Oligocene age the south coast of Puerto Rico; the basement correlates with the folded retaceous shales and igneous basement complex of Puerto Rico. This entire quence of sedimentary rock, 12,000–14,000 ft thick, is then presumed to be of rtiary age. This type of sedimentary development does exist for many other

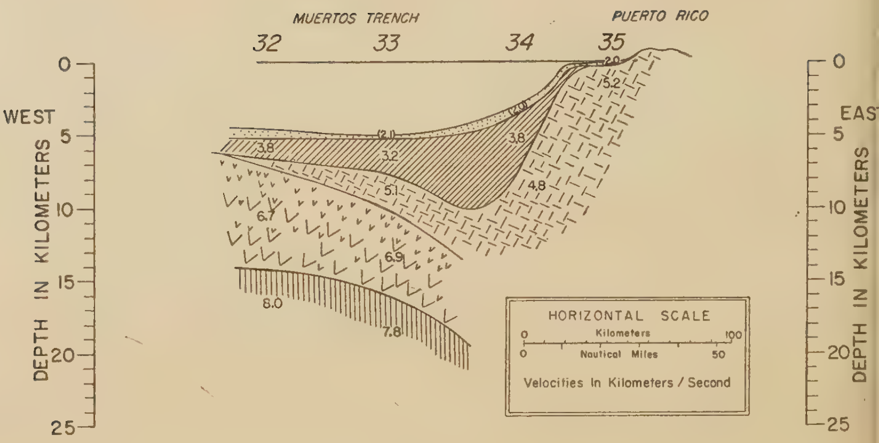
MUERTOS TRENCH
PUERTO RICO
32
33
34
35
WEST
EAST
DEPTH IN KILOMETERS
0
5
10
15
20
25
2.0
5.2
(2.1)
3.8
3.2
3.8
5.1
4.8
6.7
6.9
8.0
7.8
HORIZONTAL SCALE
Kilometers
0
100
Nautical Miles
0
50
Velocities In Kilometers / Second

Fig. 19

localities where the adjacent land mass has remained high; it seems likely tha this process is one of the more important ones in the continued outward growt of the land-mass areas.

Section 7

This section, shown in Fig. 20, runs south-east from St. Lucia along the ridg which forms the northern boundary of the Tobago trough. Correlation of th

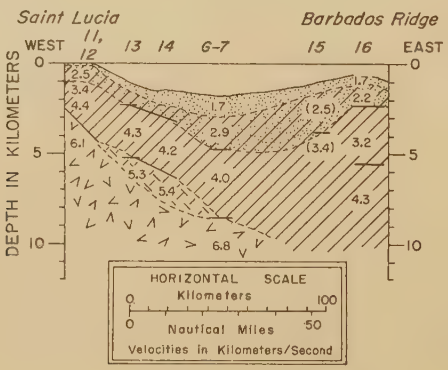
Saint Lucia
Barbados Ridge
WEST
11, 12
13
14
6-7
15
16
EAST
DEPTH IN KILOMETERS
0
5
10
2.5
3.4
4.4
1.7
1.7
2.2
(2.5)
4.3
2.9
6.1
4.2
(3.4)
3.2
5.3
5.4
4.0
4.3
6.8
HORIZONTAL SCALE
Kilometers
0
100
Nautical Miles
0
50
Velocities in Kilometers/Second

Fig. 20

deeper layers is uncertain, and the reader may prefer a different interpretatio from the one shown here. The highest velocity measured was 6·0–6·3 km/se at profiles 11 and 12 very near St. Lucia. The shot lines at these profiles wer relatively short and probably do not give an accurate determination of th velocity in the deepest layer. If the velocities were somewhat lower, they migh be correlated with the 5·3 km/sec layer found in profiles 13 and 14, in which th 6 km/sec material would be deeper than has been shown. However, the fac that the highest velocity at profiles 11 and 12, although poorly determinec does appear to be 6 km/sec or higher and the fact that no 5·3 km/sec layer wa

nd at profiles G7 (26, previous stations) or 28 gave preference to the interpre-
ion we have shown in Fig. 20.

ction 8

Section 8, Fig. 21, runs north–south between Trinidad and Grenada utilizing
data from six profiles. The large syncline shown in the middle of the section
not positively determined, but there is good evidence that the high velocity
er is much deeper there than at either end. Profile 27, located about midway

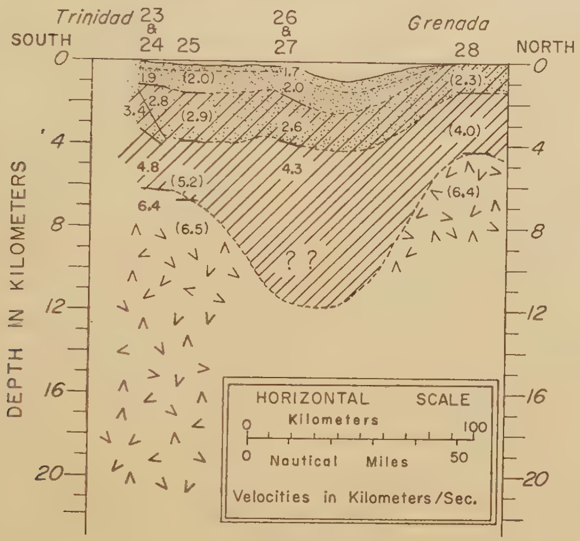
Trinidad
Grenada
SOUTH
NORTH
23 & 24
25
26 & 27
28
0
4
8
12
16
20
DEPTH IN KILOMETERS
1.9
(2.0)
1.7
2.0
(2.3)
2.8
3.4
(2.9)
2.6
(4.0)
4.8
4.3
(5.2)
6.4
(6.4)
(6.5)
? ?
HORIZONTAL SCALE
Kilometers
0
100
0 Nautical Miles 50
Velocities in Kilometers/Sec.

Fig. 21

ong the section, was heavily shot; and no velocity higher than 4·3 km/sec was
termined by first arrivals, even by the longest shots which were at a range of
out 30 miles. Second arrivals give some indication of a 6·4 km/sec layer at a
pth of about 12 km, but the evidence is not good enough to warrant drawing
lines on the travel time graph. However, the failure of the travel time graph
show a break from the 4·3 km/sec layer means that the depth to a high
locity crustal layer must be on the order of that shown. To the right (north)
this section the higher velocity layers rise under the Lesser Antilles arc. To
left (south) they rise similarly under northern Trinidad. The synclinal or
wndropped area between is possibly a branch of the main downbuckle under
Barbados ridge.

Near Trinidad the 2·3–2·9 km/sec sedimentary layer almost pinches out on
ofile 24, as both the 3·4 km/sec layer and the 4·8–5·2 km/sec layers slope up
her sharply southward. These upward sloping layers are probably the northern
nk of the Northern Coast range of Trinidad and Venezuela. An alternate
erpretation of profiles 23 and 24 is possible which could combine the thickness
w constituted by the 3·4 km/sec layer and the 2·7 km/sec layer into a single
er with a velocity of about 2·9 km/sec. In either case the depth to the high
ocity crustal layer is about the same.

Profile 25 was long and heavily shot, producing strong arrivals through th 6·5 km/sec layer out to a range of 100 km. From this the minimum depth t the mantle was computed to be 21 km, a reasonable depth near the edge of continent.

CONCLUSIONS ON THE ORIGIN AND DEVELOPMENT OF THE EASTERN CARIBBEAN

Except for the Cayman trough in the northwestern part, the deepest wate found inside the island arc of the Caribbean is in the Venezuelan basin. A broad area, approximately between latitudes 12° and 17° north and longitude 66° and 70° west, is deeper than 2500 fathoms; and in some places the depth i greater than 2900 fathoms. In view of the fact that the water depth is nearl as great as that in ocean basins, it was expected that the measurements woul show the crustal structure to be similar to oceanic. The average oceanic structur is 5 km of water, 1 km of low velocity sediments, and 5 km of crustal rock (velocity about 6·5 km/sec) overlying the mantle (velocity about 8·1 km/sec) e.g. Officer *et al.* (1952), M. Ewing *et al.* (1954), Katz and M. Ewing (1956) Raitt (1956), and J. I. Ewing and M. Ewing (in press).

Indeed, the structure, particularly in the deepest part, was found to be simila to oceanic structure; however there were significant differences. In particular the high velocity crustal rock is not included in a single layer with the sam velocity throughout as in an oceanic section, but instead is constituted such tha the lower part has an appreciably higher velocity than the upper part. It i difficult to say whether the crust is composed of two distinct layers, implyin two types of material, or whether there is a velocity gradient which, due to scatte in the travel time graph, is interpreted as a discontinuous change in velocit rather than a continuous change. In addition, the crustal materials are thicke in general than the normal oceanic crust and thicken appreciably out from th central portion of the basin. Further, the lower velocity materials (1·7–5·5 km sec) overlying the crust are thicker here than in the Atlantic basin.

At stations *24*, *25*, *26*, and 32 a velocity was measured which can positively b associated with the mantle. At these stations the velocity is greater tha 8 km/sec. At stations *27* and 33 the velocity below the deep discontinuit is 7·8–7·9 km/sec, which can probably be associated with the mantle; but th slightly lower than normal velocity suggests that contamination, differentiatio or some other process has altered the normal mantle material. The deviatio from a standard oceanic structure is even more pronounced at stations 7, *10* and 29. At these stations, which are in shallower water around the edge of th basin, the highest velocity measured is between 7·0 and 7·6 km/sec. Since al of the profiles discussed here were of about the same length, there is no doub that the depth to mantle velocity is appreciably less in the deeper areas of th basin than around the edges, as might be expected from isostatic considerations

In the elevated regions, such as the Aves swell, the depth to mantle by extrapolation is on the order of 20–25 km. Along the island arc the depth is probabl

---

* At many of the stations in the Pacific reported by Raitt, an additional layer with velocit about 5 km/sec is found. The reason that this layer is not generally found on *Atlantis* station may be that it is masked by a greater thickness of sediment. It is observed, however, o Atlantic basin profiles *1*, *2*, and *3*, as shown in cross-section 2.

r that found under the continental coastal plains. Ewing and Worzel
54) have computed a depth of 20 km under Puerto Rico from gravity and
smic measurements. The velocities in the various layers of these elevated
ions cover a wide range. Aside from the low velocity sediments, the layers
ge in velocity from 3–4 km/sec in the upper part to about 6·5 km/sec deeper
the crust. In view of the results from the other stations there is a strong
elihood that at the deeper levels the intermediate velocities 7·0–7·6 km/sec
uld be found between the material which is primarily crustal and that which
primarily mantle.

In previous papers dealing with the Caribbean (Officer *et al.*, 1957; Ewing
al., 1957), it has been pointed out that the Venezuelan basin structure differs
m typical oceanic structure in having a thicker crust, a wider range in crustal
ocities, and a lower velocity beneath the deepest discontinuity. It was inter-
eted that the Caribbean was formerly an oceanic area which has been altered,
roughout geologic time. It was surmised that this alteration had occurred
ncipally through the introduction of material from depth in the mantle. The
w results can be interpreted similarly. The results at stations *25* and *26*
owing that the mantle is only slightly deeper than under the ocean basins
ves little possibility that the Caribbean could have been created by the
undering of a segment of a continent. If this area was formerly a continent, it
ust have been uplifted 25–30 km, eroded down to sea-level, then submerged
out 5–6 km, and overlain by up to 2·5 km of sediments. On the other hand,
it is allowed that the structure was originally oceanic, the main requirements
e the addition of large amounts of crustal material, particularly along the
and arc and on the Aves swell. It is considered that this would produce the
served effects, namely a thicker crust, a wider range in crustal velocities (both
gher and lower than average oceanic crustal velocity), a more gradual change
om crustal to mantle velocity, and a greater thickness of derived materials
erlying the crust.

As mentioned earlier, a major difference in an oceanic section and a Caribbean
ction is that in the former there appears to be an abrupt change in velocity
om about 6·5 to 8·1 km/sec at the crust-mantle boundary, whereas in the latter
usually find material whose velocity is 7·1–7·7 km/sec between the mantle
d the 6·5 km/sec crustal material. In addition, the average Caribbean crust is
cker and usually has lower velocities in the upper part than does the oceanic
ust.

If it were simply a question of explaining the presence of an intermediate
locity material between the mantle and crust, a possible approach might be to
sume that the Mohorovicic discontinuity is the level about which the pressure
d temperature effects produce a change of state in a material whose chemical
nstitution is about the same above and below. Under these circumstances in
active region like the Caribbean, a relatively thick section of intermediate
mposition material might have been created. Another possible process for the
rmation of this intermediate velocity material is the partial serpentinization
peridotite as suggested by Hess (1954). However, neither of these processes
itself would explain the other observed features. From the earlier work in
Caribbean it was suggested (Officer *et al.*, 1957), (Ewing *et al.*, 1957) that
entire area has been extensively intruded by a differentiate migrating upward
m deep in the mantle, and that the raised portions—island arcs and submarine

ridges—were the areas where most of the material reached the surface, and f
ther that the deep sea-trench was the result of the expanded Caribbean cr
having been overthrust onto the oceanic crust. This overthrust has depres
the high velocity layers on the oceanic side of the arc creating the deep
trench and the associated negative anomaly belt. These views still seem to
the most logical ones in the light of the additional data provided by the 1
cruise. In particular, the stations outside the island arc give even more convinc
evidence than the earlier work that the high velocity crustal layer and the ma
dip steeply underneath the arc (Figs. 14, 15 and 16). The additional measu
ments on the island arc and on the Aves swell show in more detail the grea
thickened crustal section, the velocity increasing with depth in the section, a
the presence throughout these areas of much material with velocities charact
istic of extrusive and intrusive igneous rock. All of these features are conside
to be evidence in favour of the hypothesis that the primary mechanism in
formation of the eastern Caribbean, and presumably other such features, l
been the introduction into the upper mantle and crustal layers of a differenti
of lighter material rising from depth in the mantle.

In formulating the ideas presented here we have found among others
following references particularly useful, Bucher (1950), Gunn (1936, 19
1947, 1949), Hess (1938), Lawson (1932), Poldervaart (1955), Stille (195
Tilley (1950) and Waters (1955). Descriptions of the pertinent geology of
Antilles are given in Butterlin (1956), Christman (1953), Davis (192
Maxwell (1948), Meyerhoff (1933), Schuchert (1935), and Woodri
(1954).

REFERENCES

Bucher W. (1950) Megatectonics and geophysics. *Trans. Amer. Geophys. Un.* **31,** 495–5

Butterlin J. (1956) *La Constitution Géologique et la Structure des Antilles.* Centre Natio
de la Recherches Scientifiques, Paris.

Christman R. A. (1953) Geology of St. Bartholomew, St. Martin and Anguilla, Lesser Antil
Bull. Geol. Soc. Amer. **64,** 65–96.

Davis W. M. (1926) *The Lesser Antilles.* Amer. Geogr. Soc. Publ. No. 2.

Ewing J. I. and Ewing M. Seismic refraction measurements in the Atlantic ocean bas
in the Mediterranean sea, on the Mid-Atlantic ridge, and in the Norwegian sea. *B*
Geol. Soc. Am. (in press).

Ewing J. I., Officer C. B., Johnson H. R. and Edwards R. S. (1957) Geophysical inve
gations in the Eastern Caribbean–Trinidad shelf, Tobago trough, Barbados ridge, Atla
Ocean. *Bull. Geol. Soc. Amer.* **68,** 897–912.

Ewing M., Crary A. P. and Rutherford H. M. (1937) Geophysical investigations in
emerged and submerged Atlantic Coastal Plain: Part I, Methods and results. *Bull. G*
Soc. Amer. **48,** 753–802.

Ewing M. and Heezen B. C. (1955) Puerto Rico trench topographic and geophysical d
in Crust of the Earth (Edited by Poldevaart A.). pp. 255–267. *Geol. Soc. Amer. Spe*
Paper 62.

Ewing M., Sutton G. H., and Officer C. B. (1954) Seismic refraction measurements in
Atlantic Ocean: Part VI. Typical deep stations; North America basin. *Bull. Seismol. S*
Amer. **44,** 21–38.

Ewing M., Woolard G. P., Vine A. C. and Worzel J. L. (1946) Recent results in subma
geophysics. *Bull. Geol. Soc. Amer.* **57,** 909–934.

Ewing M. and Worzel J. L. (1954) Gravity anomalies and structure of the West Indies. Pa
Bull. Geol. Soc. Amer. **65,** 165–173.

Gunn R. (1936) On the origin of the continents and their motion. *J. Franklin Inst.* 2
475–492.

ɴ R. (1937) A quantitative study of mountain building on an unsymmetrical earth. *J.*
nklin Inst. **224,** 19–53.

ɴ R. (1947) Quantitative aspects of juxtaposed ocean deeps, mountain chains, and
canic ranges. *Geophysics* **12,** 238–255.

ɴ R. (1949) Isostasy extended. *J. Geology* **57,** 263–279.

ey J. B., Officer C. B., Johnson H. R. and Bergstrom S. (1952) Seismic refraction
servations north of the Brownson deep. *Bull. Seismol. Soc. Amer.* **42,** 291–306.

H. H. (1938) Gravity anomalies and island arc structure with particular reference to the
st Indies. *Proc. Amer. Phil. Soc.* **79,** 71–96.

H. H. (1954) Geological hypotheses and the earth's crust under the oceans. *Proc. Roy.*
. A **222,** 341–348.

S. and Ewing M. (1956) Seismic-refraction measurements in the Atlantic Ocean. Part
I. Atlantic Ocean basin west of Bermuda. *Bull. Geol. Soc. Amer.* **67,** 475–510.

t S. T. and Hersey J. B. (1956) Interpretation of high-resolution echo-sounding tech-
ues and their use in bathymetry, marine geophysics, and biology. *Deep-Sea Res.* **4,** 36–44.

son A. C. (1932) Insular arcs, foredeeps, and geosynclinal seas of the Asiatic coast. *Bull.*
ol. Soc. Amer. **43,** 353–381.

thews D. J. (1939) *Tables of the Velocity of Sound in pure Water and Sea Water for use in*
ho-sounding and Echo-ranging. British Hydrographic Department *H.D.* 282.

well J. C. (1948) Geology of Tobago. *Bull. Geol. Soc. Amer.* **59,** 801–854.

rhoff H. A. (1933) *Geology of Puerto Rico.* University of Puerto Rico Monograph *B.*

cer C. B. (1958) *Introduction to the Theory of Sound Transmission.* McGraw-Hill, New
rk.

cer C. B., Ewing M. and Wuenschel P. C. (1952) Seismic refraction measurements in the
lantic Ocean: Part IV. Bermuda, Bermuda rise, and Nares basin. *Bull. Geol. Soc.*
ner. **63,** 777–808.

cer C. B., Ewing J. I., Edwards R. S. and Johnson H. R. (1957) Geophysical investiga-
ns in the eastern Caribbean: Venezuelan basin, Antilles island arc, and Puerto Rico
nch. *Bull. Geol. Soc. Amer.* **68,** 359–378.

ervaart A. (1955) Chemistry of the earth's crust, in Crust of the Earth (Edited by
ldervaart A.) pp. 119–144. *Geol Soc. Amer. Special Paper* 62.

t R. W. (1956) Seismic-refraction studies of the Pacific Ocean basin: Part I. Crustal
ckness of the Central Equatorial Pacific. *Bull. Geol. Soc. Amer.* **67,** 1623–1640.

chert C. (1935) *Historical geology of the Antillean-Caribbean region.* John Wiley, New
rk.

A. (1940) Paleogene of Barbados and its bearing on history and structure of Antillean-
ribbean region. *Bull Amer. Ass. Petrol. Geol.* **24,** 1548–1610.

le H. (1955) Recent deformations of the earth's crust in the light of those of earlier epochs,
Crust of the Earth (Edited by Poldervaart A.) pp. 171–191. *Geol. Soc. Amer. Special*
per 62.

ey C. E. (1950) Some aspects of magmatic evolution: *Quart. J. Geol. Soc. Lond.* **106,** 37–61.

toy I., Edwards R. S., and Ewing M. (1953) Seismic refraction measurements in the
lantic Ocean: Part III. *Bull. Seismol. Soc. Amer.* **43,** 35–48.

chman C. T. (1935) Geology and fossils of Carriacou, West Indies. *Geol. Mag.* **72,** 529–555.

ers A. C. (1955) Volcanic rocks and the tectonic cycle, in Crust of the Earth (Edited by
ldervaart A.) pp. 703–722. *Geol. Soc. Amer. Special Paper* 62.

dring W. P. (1954) Caribbean land and sea through the ages. *Bull. Geol. Soc. Amer.* **65,**
9–732.

zel J. L. and Ewing M. (1948) Explosion sounds in shallow water, in Propagation of
und in the Oceans (Edited by Ewing M., Worzel J. L. and Pekeris C. L.) pp. 1–53.
ol. Soc. Amer. Memoir 27.

ds Hole Oceanographic Institution Contribution No. 999.
ont Geological Observatory Contribution No. 314.

Contribution No. 1002

THE NAUTILUS

Vol. 72 APRIL, 1959 No. 4

INFESTATION OF PECTEN IRRADIANS BY POLYDORA[1]

By HARRY J. TURNER, JR., AND JAMES E. HANKS

A heavy infestation of the spionid polychaete, *Polydora ciliata,* in bay scallops, *Pecten irradians,* in Fairhaven, Massachusetts, is of interest because there appears to be only one previous report of such an occurrence in the literature. In addition the infestation was associated with unusually high mortalities of the scallops and may have been a contributing factor.

The bay scallop, *Pecten irradians,* is of considerable importance to the fall and winter economy of a number of coastal communities in southern Massachusetts. The principal sources of employment in these communities are involved with the summer tourist trade. Consequently the inhabitants depend heavily on fishing and shellfishing during the off seasons to augment their incomes. The scallop crop, which may reach a value of $100,000 or more, is so important that failure of a single generation of scallops can bring about a considerable strain on community welfare budgets. Consequently any factor that may adversely affect the bay scallop population is justifiably viewed with alarm.

At the opening of the scallop season in October, 1958, the shellfish officer of Fairhaven, Massachusetts, discovered that the fishermen were getting an unusually large number of empty scallop shells in their dredges. In addition adductor muscles (the only portion marketed) in the living scallops appeared to be of poor quality. A number of specimens were sent to the authors for study.

Every specimen examined contained the calcified blisters characteristic of *Polydora* along the inside edge of both shells, each associated with a second blister containing fine mud overlain with a thin layer of conchiolin. In addition, many specimens contained one or more large mud blisters around and under the adductor muscle. Worms removed from the blisters were identified as *Polydora ciliata* by Dr. Marian Pettibone, of the University

---

[1] Contributions number 1002 from the Woods Hole Oceanographic Institution.

Särtryck ur Tellus nr 3, 1959

THE OCEANIC THERMOCLINE

Authors' Foreword to the Two Following Papers on the Oceanic Thermocline

Each of the two following papers attempts to provide a theoretical framework for explaining the oceanic thermocline, and the associated thermohaline circulation of the ocean. They were developed independently, and then the authors exchanged copies of their papers. As they stand, the two theories are not compatible; but the results of each are similar in certain respects, and apparently resemble the actual ocean insofar as we actually know it. Because of the basic differences in the two theories we have decided not to try to combine them into a single paper, but to publish them together in the same number of this journal, so that they should both appear in the literature simultaneously, and so that the marked contrasts in the basic formulation should be immediately evident to the reader.

Allan Robinson, Henry Stommel, Pierre Welander

The Oceanic Thermocline and the Associated Thermohaline Circulation[1]

By ALLAN ROBINSON[2] and HENRY STOMMEL

Woods Hole Oceanographic Institution, Woods Hole, Massachusetts

(Manuscript received November 15, 1958)

Abstract

A study is made of the thermal structure of an ocean which is dynamically geostrophic, bounded by an eastern coast, and driven by an imposed surface temperature distribution and wind-stress. The heat equation contains vertical diffusion in the form of a virtual eddy mixing parameter and non-linear terms of vertical and north-south advection. Comparison of the results with the North Atlantic shows an agreement with the observed temperature distribution in the thermocline region, including the deepening of isotherms in mid-latitudes. The value of the vertical component of velocity at the bottom of the thermocline is predicted, and a numerical value for the eddy-conductivity obtained.

Introduction

Ninety years ago the question of whether e wind-stresses or thermally produced differ- ices of density are the predominant cause oceanic circulation was a subject of public debate.[3] Since that time, this central issue of physical oceanography has been treated with more caution, and is only indirectly alluded to in present-day textbooks. That the vertical integral of mass transport of the ocean can probably be attributed to the wind-stress acting upon the surface was established by Sverdrup in 1947. This important concept, and its further elaboration in the hands of Munk (1950), Hidaka (1950), and others, are described in a survey article by Stommel (1957). Computation of a vertical integral, however, gives no idea of the distribution of a property in the vertical, whereas the geostrophic calculation of currents from observed hydrographic station data gives only the vertical distribution of the velocity vector, but not its integral. Moreover, the vertical integration completely cancels the contribution of the thermohaline circulation. Consequently, there was a tendency, starting in 1950, to minimize the possible role of the thermohaline circulation.

---

[1] Contribution No. 1003 from the Woods Hole ceanographic Institution.

[2] Present address, Dept. of Physics, Harvard Univer- y. Part of the material presented here has been included a doctoral thesis presented to the Dept. of Physics, arvard University.

[3] The exchange of letters in NATURE during the 1870's between W. B. Carpenter and James Croll shows how futile simple verbal arguments can be in discussing such issues. The reader with a morbid interest in fallacious verbal theories may find it entertaining to look over the work of the English eccentric William Leighton Jordan, "The Ocean, its tides and currents and their causes", Longman's Green and Co., London, 1873.

The first attempts to formulate a model containing an active thermal-convective process were

(1) an important Russian paper by P. S. Lineykin (1955)
(2) an unpublished doctoral dissertation by Fofonoff (1954)
(3) chapter XI in a book on the Gulf Stream, written in 1954—5 by Stommel (published in 1958).

Studies (1) and (2) had no meridional boundary —the key feature of the Sverdrup wind-driven model—and so were not directly applicable to actual oceanic basins. Study (3) treated only the horizontal patterns of flow that would ensue in a meridionally bounded basin on the assumption of a fixed vertical mass flux at mid-depth, and did not treat the important vertical heat flux portion of the problem.

Later, Veronis and Stommel (1957) and Lineykin (1957) were able to modify study (1) so that the important influence of the variation of the Coriolis parameter with latitude could be incorporated; and obtained expressions for the depth of the thermocline which seemed more related to reality. On the basis of these models Stommel (1958) indicated how they might be applied to give a rather detailed picture of the patterns of flow in the thermohaline circulation of the world-ocean. Nevertheless, as explained in the survey article (Stommel, 1957) neither of these models imitates the actual oceanic density distribution very closely; hence it was desirable to construct a theoretical model of the oceanic thermohaline circulation with an eastern wall to inhibit zon
flow, driven by a meridional temperatu
gradient fixed at the surface, and witho
using the totally unrealistic large vertic
temperature gradient imposed by both Line
kin and Veronis and Stommel on the mod
mentioned above for the sake of lineariz
tion of the convection equation.

The present paper is an attempt to constru
such a model, and we believe it is a substanti
improvement upon previous studies. Howeve
it contains—as they also do—a parametr
treatment of the mixing processes embodie
in an "eddy thermometric conductivity" paran
eter $\varkappa$. This parameter is assumed to be un
form and constant over the entire ocean bas
—in contradistinction to other studies whi
attribute the oceanic thermocline essentially
variations in $\varkappa$ (for example, Defant, 193
Munk and Andersen, 1948). Thus we envisa
the ocean as being slowly and evenly stirr
by some physical process which we cann
specify, and the necessity for so doing is
measure of how far short we are of actual
being able at present of giving a comple
physical account of the thermal convecti
circulation of the ocean.

2. Formulation

We consider an ocean thermally driven
an imposed north-south temperature distr
bution on the surface. The constraint of rotatic
is represented by a Coriolis parameter varyin
linearly with latitude. The ocean is taken
be infinitely deep and bounded only by
east coast. We inquire into the non-linear
coupled temperature and velocity fields
the steady state.

Let (x, y, z) represent the east-west, nort
south, and vertical respectively, with $(u, v,$
the corresponding velocity components. T
origin is fixed in the east coast at mid-latitude
The region of interest is $x < 0$, $y_1 < y <$
$z < 0$. The fluid system to be considered
defined explicitly by the following assum
tions.

The equation of state of the fluid vari
linearly with temperature only. Furthermo
the coefficient of thermal expansion, α, is co
sidered zero except when coupled with
the acceleration of gravity. In the equations
motion we neglect all viscous and inert

ms, balancing by the pressure gradient the ıvitational force in the vertical and the oriolis accelerations in the horizontal. In nmary we use purely geostrophic dynamics gether with the Boussinesq approximation. e equations of motion and of mass con- uity take the form

$$f\varrho_0 v - \frac{\partial p}{\partial x} = 0 \qquad (1)$$

$$f\varrho_0 u + \frac{\partial p}{\partial y} = 0 \qquad (2)$$

$$g(\varrho_0)(1 - \alpha T) + \frac{\partial p}{\partial z} = 0 \qquad (3)$$

$$\frac{\partial u}{\partial x} + \frac{\partial v}{\partial y} + \frac{\partial w}{\partial z} = 0 \qquad (4)$$

ere $f = f_0 + \beta y$, the Coriolis parameter, ϱ_0 the mean density, p the pressure, and T temperature.

In the heat equation we assume a balance tween diffusion in the vertical by a constant dy-conductivity $\varkappa$, and vertical and north- th advections,

$$\varkappa \frac{\partial^2 T}{\partial z^2} - w\frac{\partial T}{\partial z} - v\frac{\partial T}{\partial y} = 0 \qquad (5)$$

e choice of $\varkappa$ will be discussed later. The glect of $u\frac{\partial T}{\partial x}$ can be justified only in terms boundary conditions and anticipated results. e z boundary conditions on the temperature ll be to specify T as a function of y only at $= 0$, and to require that T approach a constant, o, asymptotically as $z \to -\infty$. The horizontal locities, both of the same order of magnitude, ll be largest at the surface and go to zero mptotically. Thus, near the surface, u, v, and - have their largest values while $\frac{\partial T}{\partial x}$ is speci- d as zero. Clearly $v\frac{\partial T}{\partial y}$ will dominate over $\frac{T}{x}$. The inclusion of a western boundary uld, of course, change the above considera- ns locally.

The fields of primary interest are T and w; two equations in these alone can be obtained. By cross-differentiation of (1) and (2) and use of (4), we obtain

$$\beta v - f\frac{\partial w}{\partial z} = 0 \qquad (6)$$

Cross-differentiation of (1) and (3) yields

$$f\frac{\partial v}{\partial z} - \alpha g\frac{\partial T}{\partial x} = 0 \qquad (7)$$

Inserting v from (6) into (5) and (7) yields the desired equations,

$$\varkappa \frac{\partial^2 T}{\partial z^2} - w\frac{\partial T}{\partial z} - \frac{f}{\beta}\frac{\partial w}{\partial z}\frac{\partial T}{\partial y} = 0 \qquad (8)$$

and

$$\frac{\partial^2 w}{\partial z^2} - \left(\frac{\alpha\beta g}{f^2}\right)\frac{\partial T}{\partial x} = 0 \qquad (9)$$

The boundary conditions imposed at $z = 0$ are $T = T_0 + T_1 y$, and $w = 0$; as $z \to -\infty$, $T \to 0$, and w remains finite, i.e. $w \to w_\infty(x, y)$. The boundary condition at $x = 0$ is taken, for mathematical convenience, as $T = 0$. This assures no flow through the plane $x = 0$, but is otherwise physically unrealistic. However, in no real fluid or ocean would the above equations describe the region near such a boundary; therefore our detailed results very near the coast will not be valid. Anticipating carrying the y-dependence parametrically, we reserve discussion of this boundary condition.

3. The Similarity Transformation

T and w are specified at $z = 0$ and approach arbitrarily close to their asymptotic values along some curve $z = f(x)$. In related problems it is often found that at a given x_0 the approach of the fields to their asymptotic values depends only on the ratio of the actual depth to the value $f(x_0)$, of the curve at this point (GOLDSTEIN, 1938). The formal analogy to these boundary layer problems occurs because only vertical mixing is allowed, so that only higher order derivatives with respect to z are present. Formally, we seek separated solutions of the form $T = G(x)\vartheta(\xi)$, $w = H(x)\omega(\xi)$, where $\xi = zF(x)$, and all functions are tacitly functions of y. This transformation is also convenient for satisfying the z boundary conditions, e.g., at $z=0$, $\xi=0$ and T becomes a function of x. In the following a prime denotes differentiation with respect to ξ, and a subscript y, differentiation with respect to y.

Taking x and z derivatives in terms of x and ξ, and inserting these in (8) and (9), we obtain

$$\varkappa F\vartheta'' - H\left[\omega\vartheta' - \left(\frac{f}{\beta}\right)\omega'\vartheta_y\right] = 0 \quad (10)$$

$$HF^2\omega'' - \left(\frac{\alpha\beta g}{f^2}\right)\left[G'\vartheta + \frac{GF'}{F}\xi\vartheta'\right] = 0 \quad (11)$$

The condition for separability of (10) in x and ξ is merely that H be a constant times F; this constant can be absorbed into ω, so we require $F=H$. For equation (11) to separate all three terms must have the same x-dependence. The second and third terms require that G'/G be a constant times F'/F, or that G be an arbitrary power of F. The first and second terms then require that F be some power of $x+c$ where c is a constant.

In summary, under the general transformation

$$\xi = z(x+c)^k, \quad T = (x+c)^{3k+1}\vartheta(\xi),$$
$$w = (x+c)^k\omega(\xi)$$

(8) and (9) take the form

$$\varkappa\vartheta'' - \omega\vartheta' - \left(\frac{f}{p}\right)\omega'\vartheta_y = 0 \quad (12)$$

$$\omega'' - \left(\frac{\alpha\beta g}{f^2}\right)\left[(3k+1)\vartheta + k\xi\vartheta'\right] = 0 \quad (13)$$

The constants k and c are determined by the particular boundary conditions. To make the surface temperature independent of x, we choose $k=-\frac{1}{3}$. The choice of $c=0$ gives $\xi = zx^{-1/3}$; $\xi\to\infty$ for both $z\to-\infty$ and $x\to 0$, and the east coast temperature will automatically correspond to the bottom temperature.

4. Order of Magnitude Considerations

Equations (12) and (13) are still too complicated to be solved exactly. However, from them we can determine certain gross properti
of the temperature and velocity fields: the
general structure, the asymptotic value of
and the scale of ξ within which all asymptot
values are essentially obtained. Moreover,
would not be much more meaningful
have the details of the exact solutions becau
the mathematical model which we are using
itself not detailed, and also because the resul
are to be compared with the averaged observ
tions of the real ocean.

In seeking unknown orders of magnitud
it is convenient to introduce known magn
tudes in terms of slightly different parameter
Let $\eta = 10^8 y$, $\gamma(y) = \frac{f(y)}{\beta}\cdot 10^{-8}$, and $\varepsilon(y) = \frac{\alpha\beta g}{3f^2(y)}$
η and γ are of order unity while ε is of orde
10^{-6}. We expect $\varkappa$ also to be order unity. T
determine how ε affects the amplitude of
and scale of ξ we write $\zeta = \varepsilon^a\xi$ and $W = \varepsilon^{-b}$
We assume that the scale of ζ and amplitude
W are of order unity, and further that ϑ an
W are smooth functions of ζ, i.e. the functio
and all their derivatives are also of order unit

Under these assumptions, (12) and (1
become, with a prime now denoting diffe
entiation with respect to ζ

$$\varepsilon^{2a}\varkappa\vartheta'' - \varepsilon^{a+b}W\vartheta' - \varepsilon^{a+b}\gamma W'\vartheta_\eta = 0 \quad (1$$

$$\varepsilon^{2a+b}W'' + \varepsilon\zeta\vartheta' = 0 \quad (1$$

Requiring that the dynamical equation (1
always retain both terms gives $2a+b=1$.
the heat equation (14), we notice that bo
advections are necessarily the same order
magnitude. Insisting that vertical eddy-diffusi
be comparable to the advections yields $a=b=$
The parameter ε now disappears from (1
and (15), which now contain only terms
roughly unit magnitude. From the similari
transformation we have obtained the depen
ence of the asymptotic value of w and t
scale depth on x, from the above conside
tions the order of magnitude and major pa
of the y dependence of these quantities.

5. Parametric Linearization and Solution

The mathematical difficulties remaining a
inherent in the two nonlinear terms of (1
To obtain approximate results, we shall repla

se actual terms by linear terms, a technique iich has found frequent use in convection oblems (LEWIS and CARRIER, 1949). In the t term of (14) we allow for convection th an average temperature gradient instead the actual ϑ_η. In the next to the last term allow for convection by an average ver- al velocity instead of the actual W. The erages are not to be taken over the full range ζ, but only from the surface to a depth L at iich asymptotic values are obtained arbitra- y closely. For convenience we define L plicitly as the depth at which the fields have proached to within e^{-2} of their asymptotic lues.

At this point the difficulty arises that the erage values of ϑ_η and W are unknown. owever, we do know that ϑ_η ranges from T_1 the surface to essentially zero at the depth L. e therefore crudely take $T_1/2$ as the average , although the true average will vary in γ ith the shape of ϑ. However, we have abso- tely no information about W. Therefore, e shall allow the unknown average value of to enter the equations and parameterize e solutions. Then, consistently taking the erage of the parameterized solution actually otained will yield an algebraic equation in e average W. Finally, the solution of the gebraic equations, in terms of the external rameters, is inserted back into the solutions r ϑ and W.

Replacing (14) and rewriting (15), the final iear set of equations is

$$\varkappa\vartheta'' - \varphi\vartheta' - \gamma\frac{T_1}{2}W' = 0 \qquad (16)$$

$$W'' + \zeta\vartheta' = 0 \qquad (17)$$

here

$$\varphi = \frac{1}{L}\int_0^L W(\zeta)\,d\zeta \qquad (18)$$

defining equation for L in terms of φ and e external parameters will be immediately ailable from the solutions of (16) and (17).

Exact solutions of (16) and (17) for ϑ and have been found. These solutions consist exponentials times Airy functions of purely mplex argument, containing φ in an involved anner. The solution ϑ and W have the sired properties, i.e. they can satisfy all the oundary conditions. It would be possible but tedious to calculate φ from the exact solutions. At this point, with the knowledge of the exact solutions, and with the lack of real meaning of the detailed form of the solutions W and ϑ, we again proceed approximately.

The quantities of primary interest are the depth L and the value of W_∞. To find these properties of the solutions, we shall use forms for W and ϑ which exactly satisfy the boundary conditions and exactly satisfy the first integrals of the differential equations, i.e. have the exact average properties. Most simply, we take

$$\vartheta = \vartheta_0 e^{-\frac{2}{L}\zeta} \qquad (19)$$

$$W = W_\infty\left(1 - e^{-\frac{2}{L}\zeta}\right) \qquad (20)$$

Multiplying (16) and (17) by $d\zeta$, integrating from zero to infinity,

$$-\varkappa\vartheta'(0) + \varphi\vartheta_0 - \frac{\gamma T_1}{2}W_\infty = 0 \qquad (21)$$

$$W'(0) + \int_0^\infty \vartheta\,d\zeta = 0 \qquad (22)$$

In (21) and (22) the derivatives and integral can be substituted from the forms (19) and (20). From (20) we also have simply $\varphi = \frac{W_\infty}{2}$.

Solving the algebraic equations, we obtain

$$\left.\begin{aligned} L &= 2\left\{(2\varkappa)\left[\vartheta_0 - T_1\gamma\right]^{-1}\right\}^{\frac{1}{3}} \\ &= 2\left\{(2\varkappa)\left[T_0 + \frac{T_1\times 10^{-8}f_0}{\beta}\right]^{-1}\right\}^{\frac{1}{3}} \end{aligned}\right\} \qquad (23)$$

which is independent of γ, and

$$W_\infty = -\vartheta_0 L^2/4 \qquad (24)$$

The above results could of course be improved by taking higher moments of eq. (16) and (17) and introducing additional constants into the forms (19) and (20).

The approximate forms for the temperature and vertical velocity are

$$T = \vartheta_0(\gamma)\exp$$

$$\left\{-\left[\frac{1}{2\varkappa}\frac{\alpha\beta g}{3f^2(\gamma)}\left(T_0 + \frac{T_1 f_0}{\beta}\times 10^{-8}\right)\frac{1}{x}\right]^{\frac{1}{3}}z\right\} \qquad (25)$$

$$w = \vartheta_0(\gamma)\left[\frac{\alpha\beta g}{3f^2(\gamma)}\left(\frac{2\varkappa}{T_0 + \frac{T_1 f_0}{\beta}\times 10^{-8}}\right)^2 \frac{1}{x}\right]^{\frac{1}{3}} \cdot$$
$$\cdot\,(1 - \exp\{\ \}) \qquad (26)$$

6. Finite depth

It is apparent that in mid-latitudes the thermocline is so shallow that it occupies only a small fraction of the actual ocean depth, and that the assumption of infinite depth is justified in making the calculations of ϑ and W in the thermocline region itself. James Crease showed us in private correspondence concerning an earlier form of the thermocline model that this was likely to be the case. But the real ocean in fact has a bottom, and if this bottom were flat the vertical component of velocity W must vanish there. Thus we regard the quantity W_∞ as being a measure of the vertical velocity just beneath the thermocline (that is, at infinity so far as the thermal boundary layer is concerned). The form of the similarity transformation does not permit us to fix the bottom at z = constant; instead, it is necessary to put the bottom at $\zeta = \zeta_b$ where $\zeta_b \gg L$, a very mild compromise. Evidently we can still use the form of solution for temperature given by equation (19) and need modify equation (20) only as follows

$$W = W_\infty\left(1 - \zeta/\zeta_b - e^{-\frac{2}{L}\zeta}\right) \qquad (20')$$

where the quantities $e^{-\frac{2}{L}\zeta_b}$ are so small at $\zeta = \zeta_b$ that they are truly negligible ($\sim e^{-10}$) and we can assert that these solutions very closely satisfy the boundary conditions $W = 0$, $\vartheta = 0$ at the bottom $\zeta = \zeta_b$. In the region of the thermocline the quantity $1 - \zeta/\zeta_b$ is so nearly unity that the formal results given in equations (21) and (22) and (23) are not changed except that in (21) the term $\frac{-\gamma T_1}{2} W_\infty$ will vanish altogether unless we restrict this approximate form of ϑ_η, $T_1/2$ to depths shallower than $\zeta = L$, and set it equal to zero for $\zeta > L$. This is quite reasonable to do under the circumstances. Thus the computation of L and φ is not affected by the presence of a bottom at a depth of several times the depth of the thermocline and the temperature field is essentially unaffected throughout the ocean. The only modificatio of the vertical distribution of the vertical component of velocity W is that instead of approaching a constant asymptotic value W_∞ a great depths it approaches a maximum valu just beneath the thermocline, which we fin convenient to call W_∞ nevertheless becau this is still infinite depth so far as the thermocline depth is concerned, and then vari linearly from this maximum just under th thermocline to zero at the bottom. Howeve so far as horizontal components of velocit below the thermocline are concerned, th presence of a finite depth has a major effec it gives them a finite amplitude (in the case o infinite depth they vanish beneath the thermocline). They are calculated from equatio (6) the terms of which no longer tend to zer under the thermocline.

The depth of no meridional motion is a the depth at which $v = 0$ or at $W' = 0$, hence a $\zeta = \frac{L}{2}\ln\frac{2\zeta_b}{L}$. Since throughout most of th oceans in mid-latitudes $2\zeta_b/L \geq 5$, the depth o no meridional motion (or reference level fo "dynamic calculations") is $\geq L$, or quit distinctly at the bottom of the thermoclin In the absence of wind-stress at the surface, V must vanish at both top and bottom of th ocean, so that the vertically integrated valu of v, by equation (6) must vanish. This i consistent with Sverdrup's earlier wind-drive model. The thermohaline circulation is entirel an internal mode and does not contribute t vertical integrals of horizontal velocity components—but it is important in trying t understand the oceanic circulation just th same.

7. Inclusion of wind-stress

The dynamical equations (1) and (2) ar non-viscous. For the wind stress to work upo the ocean it is necessary to allow viscosit to play a role somewhere, and this has generall been done by a boundary-layer analysis of th form of Ekman. Experience suggests that th Ekman viscous boundary layer is confined t an upper one hundred meters in the ocea At any point in the ocean the total verticall integrated mass transport in the Ekman laye is to the right (in Northern hemisphere) of th direction of the applied wind-stress, τ, and c gnitude τ/f. Since both τ and f vary as func- 1s of position over the ocean, the mass 1sport of the Ekman layer also varies from ce to place. If we form the horizontal ergence of the Ekman layer, we find that implies by equation (4) a vertical compo- 1t of velocity at the bottom of the Ekman er of an amount

$$w_e = -\frac{\partial}{\partial y}\left(\frac{\tau_x}{f}\right) + \frac{\partial}{\partial x}\left(\frac{\tau_y}{f}\right) \tag{27}$$

regions of divergence of the Ekman layer, vertical velocity is directed upward, and need merely adopt this value instead of value $W = 0$ in forming the function given equation (20). In regions where the vertical nponent of velocity beneath the Ekman er is downward—as in the centers of the d-latitude oceanic current gyres—the ver- 1l velocity actually must pass through zero a function of depth before it reaches the ward directed value W_∞ just beneath the rmocline. Since, in forming the parameter we take a vertical average of W it would be ppropriate to try to treat this case by ceeding as before.

The two cases are treated separately:

se I: $w_e < 0$, $W_e > 0$ (the Ekman layer is ergent; z is positive upward, ζ is positive wnward). The forms of the solution (19) d (20) are rewritten as follows

$$\vartheta = \vartheta_0 e^{-\frac{2}{L}\zeta} \tag{19''}$$

$$W = W_\infty\left(1 - ae^{-\frac{2}{L}\zeta}\right) \tag{20''}$$

$$\zeta = 0, \quad W = W_\infty(1 - a) = W_e \tag{28}$$

1ce $a < 1$. The definition of φ is now

$$\varphi = \frac{1}{L}\int_0^L W(\zeta)\,d\zeta = W_\infty\left(1 - \frac{a}{2}\right) \tag{18''}$$

e first integrals are now of the form

$$-\varkappa\vartheta'(0) + \varphi\vartheta_0 + \frac{\gamma T_1}{2}(W_e - W_\infty) = 0 \tag{21''}$$

$$W'(0) + \int_0^\infty \vartheta d\zeta = 0 \tag{22''}$$

and with the indicated substitutions the following relations obtain

$$\frac{2\varkappa}{L}\vartheta_0 + W_\infty\left(1 - \frac{a}{2}\right)\vartheta_0 + \frac{\gamma T_1}{2}(W_e - W_\infty) = 0$$

$$\frac{2aW_\infty}{L} + \frac{L}{2}\vartheta_0 = 0$$

The definition of a is given by (28).

In these equations $\varkappa$, r, T_1, W_e, ϑ_0 are regarded as known, the quantities a, L, W_∞ are to be found. In this case the value of L is given by the cubic

$$\frac{L^3}{8}(\vartheta_0 - \gamma T_1) - LW_e = 2\varkappa \tag{23''}$$

instead of the simple cube root (23). Once having obtained this we find

$$W_\infty = W_e - \frac{L^2\vartheta_0}{4} \tag{24''}$$

Case 2: $w_e < 0$, $W_e > 0$ (the Ekman layer is convergent). Here there is a reversal of the vertical component of velocity, W, with depth, and therefore we must divide the ocean into two layers: one from $\zeta = 0$ where $W = W_e$ to $\zeta = h$ where $W = 0$; and the other from $\zeta = h$ to $\zeta = \infty$ where $W = W_\infty$ which we treat exactly as before. For our purposes, if we define the unknown temperature at h as ϑ_1 we can write the temperature and vertical velocity in the lower layer as:

$$\vartheta = \vartheta_1 e^{-\frac{2}{L}(\zeta - h)} \tag{19'''}$$

$$W = W_\infty\left(1 - e^{-\frac{2}{L}(\zeta - h)}\right) \tag{20''}$$

The quantity h is also unknown, of course, however, we can write the quantities L and W_∞ in terms of ϑ_1 by equations (23) and (24). The only change here is that we can probably drop the advective term γT_1 in the expression for L, because we will incorporate the meridional advection mostly in the upper layer. As we have already seen, this term does not play a major quantitative role in the results. If the upper layer is not very thick a very rough approximation of the vertical velocity is given by a linear relation (see numerical computations, STOMMEL (1956)).

$$W \simeq W_e(1 - \zeta/h) \qquad (29)$$

The average of W from $\zeta=0$ to $\zeta=h$ is obviously $W_e/2$ and the vertical derivative W_e/h; moreover the approximate form of $\partial T/\partial y$ in the upper layer is T_1, so that we now can insert these approximations in the non-linear temperature equation and obtain (we can obtain a more accurate form for W later by solving the dynamical equation (22))

$$\varkappa\vartheta'' - \frac{W_e}{2}\vartheta' = -\gamma\frac{W_e}{h}T_1 \qquad (30)$$

The solution of this equation is of the form

$$\vartheta = C_1 e^{\frac{W_e\zeta}{2\varkappa}} + C_0 + 2\gamma T_1\left(\frac{\zeta}{h}\right) \qquad (31)$$

where C_1 and C_0 are constants of integration. The temperature must be equal to ϑ_0 at $\zeta=0$ and to ϑ_1 at $\zeta=h$; therefore

$$C_1 + C_0 = \vartheta_0 \qquad (32)$$

$$C_1 e^{\frac{hW_e}{2\varkappa}} + C_0 = \vartheta_1 - 2\gamma T_1 \qquad (33)$$

Also, the temperature gradients at $\zeta=h$ must equal each other in both layers

$$C_1 e^{\frac{hW_e}{2\varkappa}} + \frac{2\gamma T_1}{h} = -\vartheta_1\frac{2}{L} \qquad (34)$$

and so must the vertical derivative of the vertical velocity component:

$$-\frac{W_e}{h} = \frac{2W_\infty}{L} \qquad (35)$$

Eliminating the constants of integration, C_0 and C_1 and also W_∞, we obtain three equations in which there are three unknowns h, L, and ϑ_1:

$$\left(1 - e^{\frac{-hW}{2\varkappa}}\right)\frac{2\varkappa}{W_e}\left(-\frac{2\gamma T_1}{h} - \frac{2\vartheta_1}{L}\right) + {}$$
$$+ \vartheta_0 + 2\gamma T_1 - \vartheta_1 = 0 \qquad (36)$$

$$\frac{W_e}{h} = \frac{L\vartheta_1}{2} \qquad (37)$$

$$L = 2(2\varkappa/\vartheta_1)^{\frac{1}{2}} \qquad (38)$$

One of these is, unfortunately, transcendental so that a general solution cannot be obtained, but different methods will be appropriate fo different values of the parameters, involved Rather than delving into a lot of algebra, w would like to point out that when dealing with the application of these ideas to the ocean, we do not really know $\varkappa$ to begin with. Instead we form an estimate of h, L and ϑ_1, from the shape of the vertical temperature sounding. We obtain a rough estimate o W_e from charts of wind-transport of the surface layers, and then we do not use equation (36), (37), (38) in the same way. Equation (38) is used to obtain an estimate of $\varkappa$: and equations (36) and (37) can be used as consistency check on the applicability of the model to the ocean. We know all the quantitie that go into them, and they ought to be satisfied if the theory is applicable. We can then use equation (35) to calculate the vertical velocity just beneath the thermocline, W_∞ A further point: because of the nature of the similarity transformation, it is not easy to introduce vertical velocity at the surface, w_e with an arbitrary x dependence: in fact we are restricted to w_e distributions of the form $x^{-1/3}$.

8. Application to a real ocean basin

The fact that the field of density calculated from equation (25) superficially resemble that naturally occurring in the ocean is demonstrated in figures 1 and 2. Figure 1 is a dimensionless perspective diagram of the solution (25) with an imposed surface temperature distribution of the form

$$\vartheta_0(y) = 20°\text{C} - 25°\text{C}\times y' \qquad L_y = 10^8\ \text{cm}$$

where we have introduced the non-dimensiona lengths x', y' by the relations $x=L_x x'$, $y=L_y y'$, $z=Dz'$. L_x and L_y are dimensiona constants defining the scales of the phenomenon, and chosen so as to make the number x', y' be in a range near unity. Thus the actual formula used in constructing the diagram was

$$T = (20 - 2.5\eta)\exp\left\{-H\frac{z'}{x'^{\frac{1}{3}}}\right\}$$

$$L_x = 5\times10^8\ \text{cm}$$
$$D = 10^5\ \text{cm}$$

where

$$H = \left[\frac{\alpha\beta g}{6\varkappa f^2}(20 + 12.5)\frac{D^3}{L_x}\right]^{\frac{1}{3}}$$

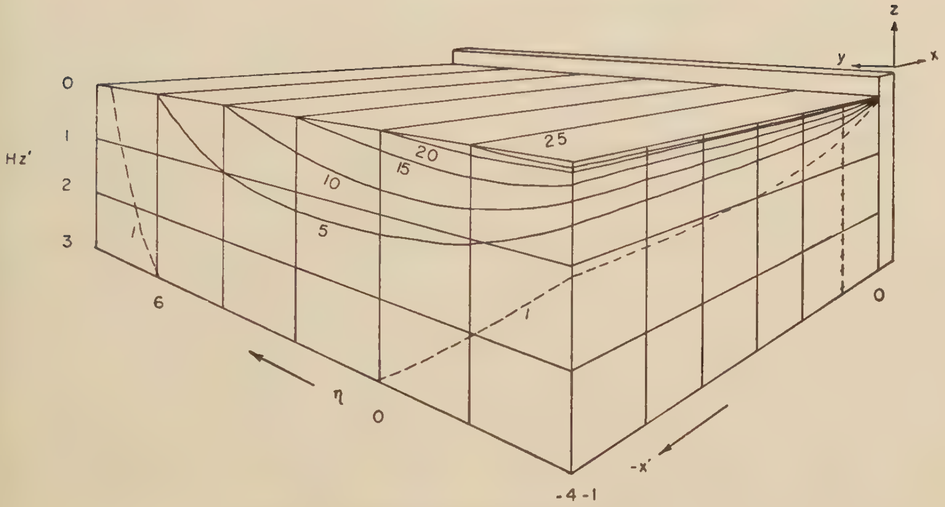

Fig. 1. Theoretical temperature field (see text).

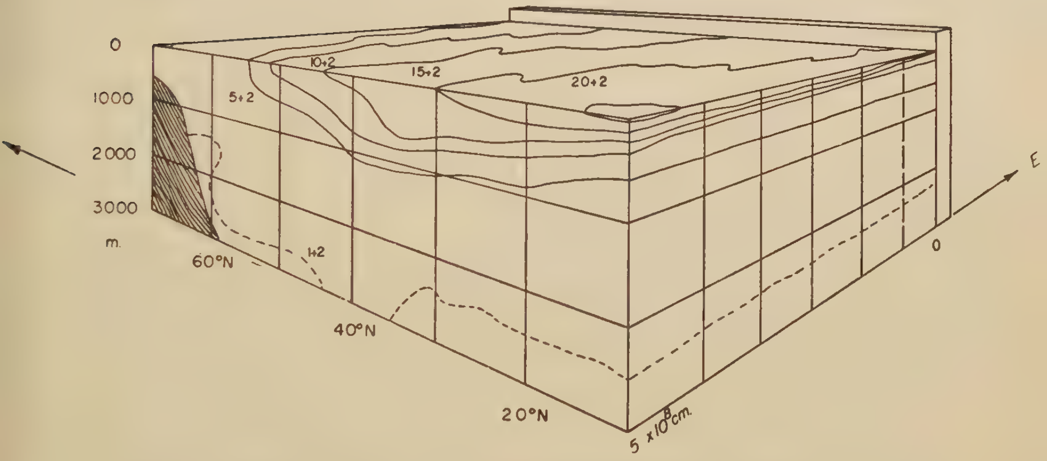

Fig. 2. Schematic temperature field observed in the North Atlantic Ocean.

e data for the North Atlantic Ocean is etched roughly in figure 2. This diagram is sed upon (i) the longitudinal profile of nperature on the western side of the Atlantic esented in Wüst's (1936) monograph on oceanic stratosphere, (ii) Böhnnecke's 36) chart of the North Atlantic surface nperature for the month of March, and (iii) 1957 CRAWFORD section at 8° North lati- le. The deep temperature of the Atlantic is C, not 0° C, so in comparing isotherms, write the 17° C isotherm in figure 2 as $15+2$, and compare it with the 15° isotherm in figure 1. Certain similarities of the two figures are, of course, forced, for example we have chosen the surface temperature distribution in figure 1 to correspond roughly with that of figure 2. Also the vertical scale of figure 1 was drawn to look like that of figure 2, but actually matching determines the parameter $\varkappa$. Even allowing for the forced elements of similarity in the picture, the remaining portions correspond surprisingly well. Of particular interest is the fact that the isothermal surfaces are deepest in mid-latitudes—a fact which hitherto has been attributed to the surface convergence of wind-driven surface layers. Here of course, in figure 1, there is no wind acting; whereas, in the real ocean diagram, figure 2, we must be on the lookout for the effect of the wind which actually does act on the North Atlantic.

Before attempting to account for the effect of the wind, first we calculate various quantities such as the parameter $\varkappa$ and the vertical component of velocity by fitting the two figures 1 and 2 as they stand. Thus the real Atlantic Ocean is roughly 5,000 km wide and 10,000 km long, and taking $L_x = 5{,}000$ km, $L_y = 10{,}000$ km makes the horizontal scales of the two figures agree. Setting $= 10^{-4}\ \text{sec}^{-1}$, $T_0 = 20°$, $T_1 = -2.5 \cdot 10^{-8}\ °\text{C/cm}$, $\beta = 2 \cdot 10^{-13}\ \text{cm}^{-1}\ \text{sec}^{-1}$, $\alpha = 2 \times 10^{-4}/°\text{C}$, $g =$ $= 10^3$ cm/sec. To fit the vertical scales we want the value Hz′ equal to 1 to correspond to the depth 1,000 meters at $y' = 0$ and $x' = -1$, and we obtain the value of the parameter $\varkappa$:

$$\varkappa = 10\ \text{cm}^2/\text{sec}$$

The vertical velocity at the bottom of the main thermocline may be written in terms of the thermocline thickness z_t defined as the depth at which the temperature is e^{-1} of the surface temperature locally. This useful relation is obtained by elimination of $\varkappa/\left(T_0 + \frac{T_1 f}{\beta}\right)$ between equations (25) and (26).

$$w(\infty) = (T_0 + T_1 y)\,\frac{\alpha\beta g}{3 f^2(y) x}\, z_t^2$$

If the thermocline thickness were 1,000 meters (as it appears at first glance to be at $y' = 0$, $x' = -1$) the sub-thermocline vertical velocity is

$$w(\infty) = 53 \times 10^{-5}\ \text{cm sec}^{-1}$$

The expression for the vertical velocity in terms of thermocline thickness is interesting because it does not involve the parameter $\varkappa$ explicitly. It is very similar to the expression used by STOMMEL (1958) in an analysis of the abyssal circulation, but using the much more primitive model of VERONIS and STOMMEL (1957). We believe that both these values, of $\varkappa$ and $w(\infty)$ are an order of magnitude too high. The reason is that we are comparing a model in figure 1 with no winds, to a schemati representation of the real North Atlanti Ocean which does suffer being acted upon b winds. In mid-latitudes Montgomery (1936 has computed that there ought to be a convergent Ekman layer at the surface, directl beneath which there is a vertical component o velocity downwards, $w_e = -5 \times 10^{-5}$ cm sec^{-} We expect therefore that part of the warn water layer in the upper portions of figure really must correspond to the wind-drive layer of thickness h, and that below this laye the proper thermohaline regime begins. Th thickness of thermocline which we used befor was too big. It included both h and z_t. A muc better idea of the rate of exponential deca of temperature in the main thermocline $a\ x' =$ $= 1$, $y' = 0$ can be obtained from curve NA in figure 3.

Let us proceed by first writing the quantitie L, h, and W_e in terms of the original coordinates. This is advisable because the dimension of these quantities are rather odd

$$\frac{L}{2} = (\varepsilon/x)^{\frac{1}{3}} z_t$$

$$h = (\varepsilon/x)^{\frac{1}{3}} z_h$$

$$W_e = (x/\varepsilon)^{\frac{1}{3}} w_e$$

where z_t is the "thickness" of the thermocline estimated by the shape of the temperatur curve well below the inflection point a $\partial^2\vartheta/\partial\zeta^2 = 0$ in the temperature curve, and z is the "depth" of the wind-driven layer whicl we identify in figure 3, for example, as th depth of the inflection point. The temperatur at the inflection point is defined as ϑ_1. The information we obtain from the North Atlantic curve in figure 3 is as follows

$$z_t \cong -3.5 \times 10^8\ \text{cm}$$

$$z_h \cong -9.0 \times 10^4\ \text{cm}$$

$$\vartheta_1 \cong 10°\ \text{C}$$

These estimates are for a geographical positio corresponding to

$$x = -5 \times 10^8\ \text{cm}$$
$$y = 0$$

at which

$$\varepsilon \cong 10^{-6}\ (°\text{C sec})^{-1}$$

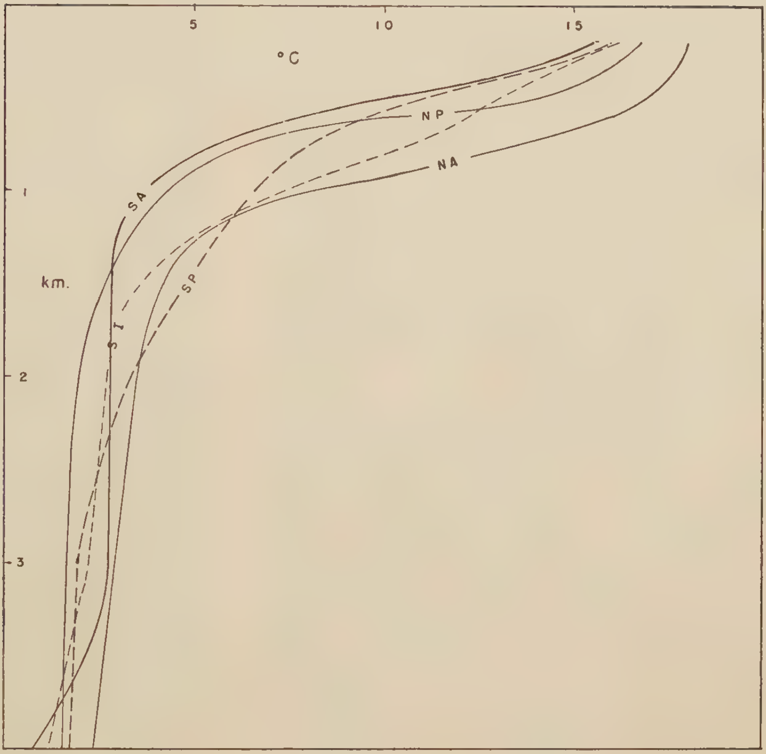

3. Temperature vs Depth mid-latitudes in western ;ions of various oceans. = North, S = South, A = lantic, I = Indian, P = Pacific.

d from Montgomery's wind-transport arts

$$w_e \cong -5 \times 10^{-5} \text{ cm sec}^{-1}$$

ie quantities for other ocean basins are newhat different. Using these quantities we mpute

$= 0.44$ cm$^{2/3}$ (sec °C)$^{-1/3}$;

$$W_e = 4.0 \text{ cm}^{4/3} \text{ sec}^{-2/3} \text{°C}^{1/3}$$

$= 0.72$ cm$^{2/3}$ (sec °C)$^{-1/3}$; $\vartheta_1 = 10°$ C

cording to the formulation in section 7, se 2, these quantities are not all independent. e need only specify two, and the others are nputable. However, there is a degree of certainty in identifying any one of these antities from oceanographic data, so it is pful to list them all, and then using the ations (36) and (37) inquiring whether they mutually consistent. Thus, from equation) we have the remarkable relation

$$\vartheta_1 = \frac{W_e 2}{Lh}$$

Inserting the values of W_e, h and $L/2$ we obtain $\vartheta_1 = 12.6$ °C which is not very different from the rough estimate $\vartheta_1 = 10°$ C obtained by inspection of figure 3. The above relation is indeed a rather fascinating one, because the applied surface temperature does not appear directly in it. We now calculate $\varkappa$ and W_∞ from the equations (38) and (35) and obtain

$$\varkappa = 0.85 \text{ cm}^2/\text{sec}$$
$$W_\infty = -2.5 \text{ cm}^{4/3} \text{ sec}^{-2/3} \text{ °C}^{1/3}$$

Thus the actual upwelling velocity beneath the thermocline obtained from by transformation to the original coordinates is

$$w_\infty = 3.1 \times 10^{-5} \text{ cm sec}^{-1}.$$

We believe that the order of magnitude of the mixing parameter $\varkappa$ and the deep upwelling velocity w_∞ computed from the North Atlantic temperature distribution in this manner is much more in accord with the estimates of the magnitude of mixing processes and of the deep-ocean transports, than the numbers obtained neglecting the wind. Thus in applying these ideas to the actual ocean it is essential to

---

is XI (1959), 3

include the wind stress in the model. The two causes of oceanic circulation (wind-stress and thermohaline process) are connected in a basically non-linear fashion and cannot be super-posed as additive solutions. Fofonoff has already pointed this out for a zonal ocean. Of course, in this model, vertical integrals of the transports depend on wind-stress alone—as has now been known for twelve years.

The reader can now substitute the various constants into the expression for the temperature in the upper layer and see that it affords a reasonable approximation to the form of that actually observed.

The state of affairs in the North Atlantic Ocean is not markedly different from that in other oceans. The vertical distribution of temperature at 30° latitude near the western sides (but east of the western boundary currents) of other meridionally bounded oceanic basins is shown in figure 3. (NA, North Atlantic; SA, South Atlantic; S. I., South Indian; NP, North Pacific; SP, South Pacific.) Actually the thermocline in the North Atlantic is somewhat anomalously deep compared to those in other oceans, but the shape of the main thermoclines themselves are very similar: i.e. the value of z_t is about the same. The fact that the Pacific is twice as wide as the Atlantic is of no consequence because width of the ocean appears only as a cube root factor. Some of the complications in the temperature curves shown in figure 3 are due to salinity effects on the density field—but these are details which at the present stage of the theory do not merit immediate consideration.

The model shown in figure 1 exhibits a number of general features which ought to be mentioned. First, the warm water in mid ocean does not tend to move toward the poles —but flows with an equatorward meridional component. At low latitudes it turns west (since it cannot cross the equator, according to equation (6)) where presumably it forms a western boundary current when it encounters the western boundary of the ocean. The western boundary current is a higher-order dynamical regime which can occur under fairly general conditions of stratification, so there is no reason to doubt that the thermal circulation can be "closed" on the western side by such a boundary current—although we have not attempted a formal demonstration for this particular mod-
el. Everywhere in deep water there is a sl
upward component of velocity. The way
which the solution for a single basin can
connected together with solutions for ot
basins to form a scheme descriptive of
general circulation of the world ocean
already been pointed out by STOMMEL (195

9. Comments on the parametric treatmen of mixing, the quantity $\varkappa$

The inclusion of an eddy-conductivity,
is a parametric way of including small sc
vertical mixing processes into the theoreti
model. Although this is a very common thi
to encounter in the earlier oceanographi
literature, it is a technique which present-d
oceanographers are very reluctant to employ
except as a last resort. It means that we simp
do not know anything about the physics
the mixing process. Despite our ignorance
the cause of mixing or the mechanism, we
have some idea, as we will show below, of t
order of magnitude of the mixing. We take
by these other considerations, to be of or
of magnitude unity (c.g.s.), or five hundr
times the molecular diffusion coefficient. T
assumption has important consequences
how the model is to be set up, as was sho
in equation (14). If $\varkappa$ were much greater th
unity, equation (14) would become $\vartheta''=$
yielding a linear form for ϑ which would ha
no thermocline-like character. If $\varkappa$ were mu
less than unity equation (14) would becom
$W\vartheta' - \gamma W'\vartheta_\eta = 0$, which describes a pur
advective process. This equation, together w
(15), has been solved by the method outlin
in the beginning of section 4. The soluti
exhibits something like a thermocline, but
dependence on latitude does not agree w
observations. Therefore, the choice for $\varkappa$
order unity seems necessary. In the results
note that only the cube root of $\varkappa$ appears
the depth L, so that $\varkappa$ may vary by an ord
of magnitude without changing the resu
significantly.

In the calculations we have taken $\varkappa$ to b
constant. A more valid $\varkappa$ would probably
general be a function of depth. Were t
the case, the first term of the heat equati
(16) would be replaced by $[\varkappa(\xi)\vartheta'(\xi)]'$.
the resulting calculation, the first term of (
would be replaced by $\varkappa(0)\vartheta'(0)$, and $\varkappa$
would replace $\varkappa$ in all the results. This mea

: within the validity of the above calcula- ıs the form of $\varkappa$ is not critical. If more ments of equations (16) were taken, inte- l properties of $\varkappa(\xi)$ would enter.

:he mean distribution of many oceanic iables like salinity, oxygen, carbon-14, etc., st depend to a large extent on the same an velocity field and parametric mixing as se which determine the mean thermal field. : the most part these properties have no portant dynamical effect—except, of course, nity which can play a dominant role, but in tropical areas usually plays a definitely ondary role in determining the density tribution. Therefore these properties are in a se tracers whose distribution depends upon thermal circulation and the parametric xing, but which does not in turn effect m. Thus they provide a means for testing r model of the oceanic circulation for inter- consistency. In order to make such a test does not seem likely that very small scale periments, or transitory phenomena will be ry convincing because we are so completely norant about the nature of the mixing process at we do not even know its scale or spectrum, how uniformly it acts in time. Under the cumstances we prefer to employ tracer phe- mena whose horizontal and vertical and ne scales are all comparable to those of the eanic thermocline itself; and we want these cers to be located quite close to or within thermocline. We offer two examples from Atlantic. In both cases salinity is the tracer.

Case 1: The first case is the layer of Antarctic ermediate Water in the South Atlantic ean. At Meteor Profile VII in the eastern lf of the ocean, between Stations 177 and ɔ, the salinity minimum lies at a depth of ɔ meters, where the temperature is about C, thus lying immediately beneath the main rmocline. The thickness of the layer is tween 500 meters and 1,000 meters—depend- upon how it is defined. The salinity in minimum here is about 0.2 ‰ lower than t 200 meters above and below the minimum $s/\partial z^2 \cong 10^{-9}$ ‰ cm^{-2}). The salinity gradient the east direction is small ($\partial s/\partial x \cong 0$) as mpared to that in the northward direction $/\partial y \cong 7 \times 10^{-10}$ ‰ cm^{-1}). Wüst (1956) has de dynamical calculations of the velocity tween stations 177—180 at 700 meters and ds a mean northward velocity of as little as $v = 0.2$ cm sec^{-1}. The mixing parameter computed from this situation is 0.14 cm^2 sec^{-1} [$\varkappa \cong (v \partial s/\partial x)/(\partial^2 s/\partial z^2)$]. According to our theory there ought to be an upward velocity of about 2×10^{-4} cm sec^{-1} at this level, so that we might expect the level of the minimum to slope upward toward the north with a slope of about 10^{-4}, which indeed it does.

Case 2: The second case to be discussed is a layer of maximum salinity which covers much of the southern North Atlantic in the area of the North Equatorial Current, and passes westward through the entire Caribbean, during which passage the intensity of the maximum decreases by about 0.3 ‰ ($\partial s/\partial x \cong +0.20 \times 10^{-8}$ ‰ cm^{-1}). Upon entering the Caribbean this layer is at a level of 125 meters and upon leaving through the Yucatan Channel it is 200 meters deep. The mean westward velocity of this layer of water is about 3 cm sec^{-1} ($u = -3.0$ cm sec.$^{-1}$) and its salinity maximum is about 0.6 ‰ greater than the salinity 100 meters above or below it ($\partial^2 s/\partial z^2 = 1.2 \times 10^{-8}$ ‰ cm^{-2}); thus one computes $\varkappa = 0.5$ cm^2 sec^{-1}, again a value more or less consistent with the requirements of our model. This saline layer originates at the surface in the subtropical surface salinity maximum, and sinks downward as it flows southward and westward. The layer is at a temperature of 20° C, hence it lies near to the top of the thermocline—and the vertical velocity should be downward here: this latter is in accord with the downward slope of the layer as it traverses the Caribbean (slope of 5×10^{-5}).

10. The Abyssal Circulation

As the reader can judge, this model of the thermohaline circulation implies many definite quantitative things about the circulation of the deep waters of the ocean. For example, we should be able to derive the total amplitude of the deep circulation of the ocean by integrating the deep upwelling velocity over the whole water-covered globe (in spherical coordinates instead of the beta-plane). In this way we should be able to predict the average age of the deep waters, a topic of current interest to geochemists, and a subject of much present day experimental enquiry, and sea-going activity. This further extension of the ideas here presented is treated in a separate paper by A. B. Arons and Henry Stommel which is being prepared for publication after this one.

REFERENCES

Defant, A., 1936: Entstehung und Erhaltung der troposphärischen Sprungschicht. *Zeit. f. Geoph.* **12**, 7/8 pp. 281—286.

Fofonoff, N., 1954: A steady flow in a frictionless homogeneous ocean. *J. Marine Res.* **13**, pp. 254—262.

Goldstein, S. (Editor), 1938: *Modern Developments in Fluid Dynamics.* Oxford University Press, p. 133 ff.

Hidaka, K., 1950: Drift currents in an enclosed ocean. *Tokyo Univ., Geophys. Notes* **3** (23), pp. 1—23.

Lewis, J. A. and Carrier, G. F., 1949: Some remarks on the flat plate boundary layer. *Quart. Applied Math.* **7** p. 228.

Lineykin, P. S., 1955: On the determination of the thickness of the baroclinic layer in the sea. *Dokl. Akad. Nauk USSR* **101**, pp. 461—464.

— 1957: On the dynamics of the baroclinic layer in the ocean. *Dokl. Akad. Nauk USSR* **117**, pp. 971—974.

Munk, W. H., and Anderson, E. R., 1948: Notes on a theory of the thermocline. *J. Marine Res.* **7**, pp. 276—295.

Munk, W. H., 1950: On the wind-driven ocean circu lation. *J. Met.* **7**, pp. 79—93.

Stommel, H., 1956: On the determination of the dept of no meridional motion. *Deep-Sea Res.* **3**, pp. 273- 278.

— 1957: A survey of ocean current theory. *Deep-Se Res.* **4**, pp. 149—184.

— 1958: *The Gulf Stream.* Univ. Cal. Press and Camb Univ. Press.

— 1958: The Abyssal Circulation. *Deep-Sea Res.* **5**, pp 80—82.

Veronis, G., 1956: Partition of energy between geo strophic and non-geostrophic oceanic motions. *Deep Sea Res.* **3**, pp. 157—177.

Veronis, G., and Stommel, H., 1956: The action variable wind stresses on a stratified ocean. *J. Marin Res.* **15**, pp. 43—75.

PRINTED IN SWEDEN
ESSELTE, STHLM 59

Contribution No. 1004

Deep-Sea Research, 1959, Vol. 5, pp. 312 to 314. Pergamon Press Ltd., London. Printed in Great Britain

SHORTER COMMUNICATION

Amplification of transient response of the ocean to storms by the effect of bottom topography

(*Received* 13 *November* 1958)

VERONIS and STOMMEL (1956) showed that the ocean responds barotrophically to short-period large-cale fluctuations in the winds. Since motions in such a case extend all the way to the bottom it is atural to enquire whether irregularities in the topography of the bottom might modify the nature f the transient response; but VERONIS and STOMMEL did not consider this question.

The actual ocean bottom is very complicated in form. We do not propose to try to approximate his complexity in the following analysis. Also, it seems certain that irregularity of the bottom nhances the baroclinic mode's response (CHARNEY, 1957), but we consider here merely a barotropic nodel.

It is well known that in a homogeneous model the β-effect can be approximated by introducing slope of the bottom upward in the y-direction. The equations which we will use are

$$\frac{\partial u}{\partial t} - fv = -g\frac{\partial \zeta}{\partial x} \tag{1}$$

$$\frac{\partial v}{\partial t} + fu = -g\frac{\partial \zeta}{\partial y} \tag{2}$$

$$\frac{\partial \zeta}{\partial t} + \frac{\partial}{\partial x}(hu) + \frac{\partial}{\partial y}(hv) = S(x, y, t) \tag{3}$$

where u and v are velocity components, ζ is the displacement of the free surface, f the Coriolis parameter, and $S(x, y, t)$ a driving agency – in this case explicitly a variable mass source : for example recipitation. There is no problem in making this mass source absorb the effects of other current roducing mechanisms such as normal pressure, wind-stress, etc. (see STOMMEL, 1957). The quantity is the variable depth of the ocean.

Assuming that the function S is of the form $S(x, y)\,e^{i\sigma t}$ we can eliminate u and v from the above quations and obtain

$$\left\{-\sigma g\left(h\nabla^2 + \frac{\partial h}{\partial y}\frac{\partial}{\partial y} + \frac{\partial h}{\partial x}\frac{\partial}{\partial x}\right) + igfJ(h,\ ) + \sigma(f^2 - \sigma^2)\right\}\zeta = (f^2 - \sigma^2)\,S(x, y) \tag{4}$$

where the factor $\rho^{i\sigma t}$ has been removed from ζ,

The depth h may be written as

$$h = H(1 - \delta y + \epsilon\, b(x, y)) \tag{5}$$

his form is convenient because it separates the scale depth H from the small gentle slope δH (which e introduce to simulate the β-effect) and the bottom irregularity $H\epsilon\, b(x, y)$ where ϵ is a perturbation arameter which we define as the fraction of the total depth occupied by the submarine topography, nd $b(x, y)$ is the functional form of the bottom topography with an amplitude of unity. This ubstitution makes equation (4) a linear partial differential equation in ζ with *non-constant* coefficients. we regard ϵ as a small perturbation number ($\epsilon \ll 1$) and assert that the solution is of the form $= \zeta_0 + \epsilon\zeta_1 + \ldots$ we obtain the following equation

$$(L + \epsilon B)(\zeta_0 + \epsilon \zeta_1 + \ldots) = (f^2 - \sigma^2) S(x, y) \tag{6}$$

where L is the linear operator

$$L = \left\{ - \sigma g H \left[(1 - \delta y) \nabla^2 - \delta \frac{\partial}{\partial y} \right] + i g f H \delta \frac{\partial}{\partial x} + \sigma (f^2 - \sigma^2) \right\} \tag{7}$$

and the non-constant coefficients are contained in the operator B

$$B = \left\{ - \sigma g H \left[b \nabla^2 + \frac{\partial b}{\partial y} \frac{\partial}{\partial y} + \frac{\partial b}{\partial x} \frac{\partial}{\partial x} \right] + i g f H J(b, \ ) \right\} \tag{8}$$

To zero order, we therefore have the equation

$$L \zeta_0 = (f^2 - \sigma^2) S(x, y) \tag{9}$$

If $S(x, y)$ is taken to be of the form $S_0 e^{i(\mu x + \nu y}$ the solution of (9) is

$$\zeta_0 = a_1 e^{i(\mu x + \nu y)}$$

$$a_0 = \frac{S_0 (1 - s^2)}{f \{ s \lambda^2 \mu^2 + \nu^2 + i \delta \nu) - \lambda^2 \delta \mu + s (1 - s^2) \}} \tag{10}$$

$$\lambda^2 = \frac{gH}{f^2} \qquad s = \frac{\sigma}{f}.$$

This expression contains the effect of the large scale gentle slope $- \delta H$; and if $s \ll 1$ we are dealing with quasi-geostrophic motion of essentially the same kind as the planetary (Rossby, second kind) waves deduced by VERONIS and STOMMEL (1956, equation 4.3).

The first order perturbation effect of the bottom topography on ζ is given by the following equation equation with constant coefficients

$$L \zeta_1 = - B \zeta_0 \tag{11}$$

Consider a cellular form for the bottom topography : $b(x, y) = e^{i(mx + ny)}$. In this case the solution of equation (11) is

$$\zeta_1 = a_1 e^{i[(\mu + m)x + (\nu + n)y]}$$

$$a_1 = \frac{- s [\mu^2 + \nu^2 + n\nu + m\mu] - i m \nu + i n \mu}{s [(\mu + m)^2 + (\nu + u)^2 - i \delta (\nu + n)] - \delta (\mu + m) + \frac{s}{\lambda^2} (1 - s^2)} \times a_0 \tag{12}$$

Since we imagine that the scale of the bottom topography is smaller than the scale of the moving wind systems we must regard at least one of the quantities m and n as being larger than either μ or ν. The perturbation method works only for ranges of parameters where $\epsilon \zeta_1 / \zeta_0 \ll 1$, or $\epsilon a_1 / a_0 \ll 1$. On the other hand, the ratio A of the velocities produced by the bottom topographic perturbation to those produced on the flat-bottom model is of the form

$$A = \frac{\epsilon a_1}{a_0} \left(\frac{m + n}{\mu + \nu} \right)$$

and can be considerably greater than unity without violating the conditions of the perturbation method. The quantity A may be called an amplification factor because it expresses the degree to which bottom topography can produce small scale geostrophic motions with greater amplitude than the planetary geostrophic motions of the scale of the wind-system.

By addition of elementary solutions (12) with various combinations of signs for μ, ν, m, n, σ, it is possible to construct solutions for all kinds of progressive and standing storm shapes and for submarine mountains with various configurations of crests. By Fourier superposition more elaborate forms can be obtained, but if the motive is comparison with transient current observed in nature, this model does not merit such elaboration. We are content merely to obtain an order of magnitude indication of whether the perturbation method works for the range of scales, etc., of interest, and roughly what the amplification of velocities is likely to be. Therefore we will restrict our attention to a definite range of scales and frequencies.

Consider a mid-latitude region where $f = 10^{-4}$ sec^{-1} and the mean depth H is 4×10^5 cm. The slope δ corresponding to the equivalent β-effect is 10^{-9} cm^{-1}. Gravity is 10^3 cm sec^{-2} thus $\lambda^2 = 4 \times 10^{16}$ cm^2.

The dimensions of storms are in the neighbourhood of 3000 km wavelength both east-west and north-south. Therefore we take $\mu = \nu = 2 \times 10^{-8}$ cm^{-1}. We restrict the range of frequencies to 3 to 30 days ($2 \times 10^{-2} < s < 2 \times 10^{-1}$). Furthermore we consider mountains on the bottom with a range of wavelengths from 6 to 600 km (10^{-5} cm$^{-1} \geqslant m$ or $n \geqslant 10^{17}$ cm^{-1}). Within this range the value of the ratio of amplitude of the vertical displacement is

$$\left|\frac{\epsilon a_1}{a_0}\right| = \frac{2i\mu}{sn}\epsilon$$

where we can interchange μ and ν or m and n. If the quantity should exceed, say, 0·2, the perturbation analysis would not be applicable, but this does not happen in the range under consideration. The amplification factor A for the velocities is

$$A \cong \left|\frac{\epsilon a_1}{a_0}\right| \left(\frac{m+n}{\mu+\nu}\right) \cong \frac{2i}{s}\epsilon$$

in the range under consideration. It is noteworthy that there is no strong effect of the wave-length of the mountains on the amplification factor. The only resonance frequency introduced by the bottom is at approximately $s = \delta/m$ from equation (12) and this is well outside the range of parameters under consideration. Low frequencies are favoured.

Dr. JOHN C. SWALLOW's measurements of transient currents off Portugal in May-June 1958 are compatible with this result. Take $\epsilon = 0{\cdot}20$, and the wavelength of the low topographic elements as 60 km (m and $n = 10^{-6}$ cm^{-1}). If the moving wind system occurs at bi-weekly intervals ($s = 0{\cdot}05$), the amplification factor is 8, hence the velocities of the small scale geostrophic motions associated with the bottom topography are of an order of magnitude greater than those with the scale of the moving wind-system; an estimate of the latter from Figure 2 of VERONIS and STOMMEL gives deep layer velocities of about 0·1 cm sec^{-1} so that we could expect geostrophic eddies of 60 km scale with velocities of around 1·6 cm sec^{-1}, and a frequency of once every two weeks. Shorter periods are not proportionately amplified. One concludes therefore that the irregularity of the bottom topography which actually occurs in the ocean is of dominant important in fixing the scale and amplitude of the transient barotrophic motions induced by storms.

Woods Hole Oceanographic Institution ALLAN ROBINSON
Woods Hole Mass., U.S.A. HENRY STOMMEL

Contribution from Woods Hole Oceanographic Institution No. 1004.

REFERENCES

CHARNEY J. G. (1955) The generation of ocean currents by wind. *J. Mar. Res.* **14** (4) : 477-498.
STOMMEL H. (1957) A survey of ocean current theory. *Deep-Sea Res.* **4**, 149-184.
VERONIS G. and STOMMEL H. (1956) The action of variable wind stresses on a stratified ocean. *J. Mar. Res.* **15** (1) : 43-75.
SWALLOW J. C. (1958) Private communication.

Printed in Great Britain by The Salisbury Press Ltd., Publicity House, Wilton Road, Salisbury, Wilts. (15667)

Contribution No. 1006

Second United Nations
International Conference
on the Peaceful Uses of
Atomic Energy

P/176 Sweden

On the Use of Tritium as a Tracer for Water in Nature

By B. Bolin*

In a series of recent papers Libby and his co-workers and Craig have investigated the amount of tritium in natural waters.[1–5] At an early stage it was clear that tritium would be of great value as a tracer for water and the more recent investigations have clearly demonstrated the potentialities of this technique. Interesting deductions have been made concerning the ocean circulation and the hydrological cycle over the American continent. These considerations have been made using measurements from the time before man-made tritium was introduced by the thermonuclear test explosions begun in 1954 as giving the distribution of natural tritium formed by cosmic-ray bombardment of the atmosphere and by direct accretion from the sun, but also by interpreting the variations of tritium observed since 1954 as being essentially due to thermonuclear bomb-explosions. Today an appreciable amount of tritium in nature originates from this latter source. The interpretation of the data therefore has become more difficult but additional information may be obtained if the data are treated properly.

For any use of tritium as a tracer it is necessary, however, to have as clear a picture as possible of the naturally occurring tritium. Unfortunately, very few measurements were made before significant amounts of man-made tritium were released and the measurements are very unevenly distributed over the world and often not representative for an investigation of average global conditions. We may use our knowledge about the turnover and motion of the atmosphere and the ocean from other kinds of measurements to fit the existing measurements of tritium into a logical pattern. C^{14} measurements in the ocean and Sr^{90} and Cs^{137} measurements in the stratosphere have been particularly useful for this purpose. Deductions of this kind have been made in the papers quoted above and a few additional aspects of this problem will be discussed here.

The water cycle over the North American continent has been studied in more detail by Begemann and Libby[3] using bomb tritium. They have estimated the amount of ground water in the Mississippi valley as well as the average storage time and they also compute the amounts of rain of oceanic and continental origin in this area. Their interesting results depend, however, critically on a number of assumptions made and we shall discuss some of these in this paper.

THE EXCHANGE OF TRITIUM BETWEEN A FREELY-FALLING WATER DROP AND ITS ENVIRONMENT

Before beginning a discussion about the global distribution of tritium and its exchange between reservoirs in nature we shall analyze in a little more detail the microphysical processes at work in evaporation and condensation.

Natural tritium is brought into the troposphere from aloft and is carried downwards by turbulent processes and by falling precipitation. We would therefore expect a decreasing amount of tritium in the atmosphere proceeding downwards. Falling raindrops will therefore gradually come into less tritium-rich air and because of the steady exchange of molecules between the drops and the vapour in the environment, an adjustment of the tritium amount in the drop to the new conditions will occur. The speed of this adjustment will depend upon the size of the drop and upon the humidity and temperature conditions in the air. It is of primary importance for the following discussion to know more precisely how rapidly this process takes place.

Before entering the discussion it should be pointed out that the concentration of tritium found in nature is often only a few tritium units, T.U. (1 T.U. means 1 T atom/10^{18} H atoms). In such a case a drop of 1 mm radius contains a few hundred or a thousand T atoms, but in cloud droplets and drizzle droplets often there is not a single T atom present. In water vapour the characteristic tritium concentration is a few atoms/cm^3. In the following analysis the microphysical concepts used, such as concentration, gradients, should be looked upon as probabilities and the deductions do not apply to individual droplets; we obtain average conditions for a large number of drops. This is quite sufficient since in the following we shall only be concerned with the large exchange processes occurring in nature.

Kinzer and Gunn[6] have analyzed the evaporation from falling water drops both theoretically and experimentally. The exchange of tritium is quite analogous. A few important differences exist, however. The saturation pressure of HTO is about 15% lower than that of H_2O at atmospheric temperatures because of the difference in the weight of the molecules (Price[7]). Furthermore with regard to the small amounts of tritium present, the exchange of tritium between the drop and its environment will not influence the heat transfer and thus the temperature of the drop. The heat transfer is instead controlled by the evaporation and condensation of ordinary water and direct turbulent exchange. Finally, if the transfer HTO relative to H_2O is not proportional to the tritium concentration, a tritium transfer inside the drop must occur. For very small drops molecular diffusion is sufficient to maintain an approximate constant tritium concentration inside the drop; for larger drops the motion of the drop relative to the surrounding air will set up internal motions that very rapidly (in the matter of seconds) will equalize any inhomogeneous distribution of tritium. We shall therefore assume in the following that the tritium concentration at the surface of the drop is the same as in the interior.

---

* International Meteorological Institute, Stockholm, and Woods Hole Oceanographic Institution, Woods Hole, Mass. Contribution No. 1006 from the Woods Hole Oceanographic Institution.

Proceeding in a way analogous to Kinzer and Gunn we can derive the following expression for the change of tritium concentration in a drop under the influence of surroundings containing no tritium:

$$\frac{1}{M_s}\frac{dM_s}{dt} = \frac{3}{a^2} D \frac{s_a}{s_d}\left(1 + \frac{F\,\mathrm{Re}^{\frac{1}{2}}}{(4\pi\rho D/\eta)^{\frac{1}{2}}}\right). \tag{1}$$

Here $M_s^{-1}dM_s/dt$ is the relative change of tritium concentration in the drop with radius a. s denotes the amount of tritium per unit volume with subscript d indicating conditions in the drop and a in the air at the surface of the drop. F gives the effect of ventilation and is thus dependent upon the motion of the drop as is the Reynolds number, Re. ρ is the air density, D the molecular diffusivity of the air and η its viscosity. s_a depends upon the temperature of the drop and is therefore determined by the evaporation or condensation of ordinary water. We shall here compute the rate of exchange of tritium, when no net transfer of ordinary water vapour occurs and thus the radius of the drop remains constant. Its temperature may in this case be taken as that of the environment.

We next compare the rate given by (1) with the rates of evaporation experimentally found by Kinzer and Gunn[6] for a drop falling through dry air. It is given theoretically by

$$\frac{1}{M}\frac{dM}{dt} = -\frac{3}{a^2} D\rho_v \left(1 + \frac{F\,\mathrm{Re}^{\frac{1}{2}}}{(4\pi\rho D/\eta)^{\frac{1}{2}}}\right). \tag{2}$$

ρ_v is the water-vapour density at the surface of the drop. From (1) and (2) we obtain

$$\frac{1}{M_s}\frac{dM_s}{dt} = \frac{s_a}{s_d\rho_v}\frac{1}{M}\frac{dM}{dt}. \tag{3}$$

Now if f denotes the fractionation factor, i.e., the ratio of the saturation pressure of HTO and H_2O, we have

$$s_a/s_d = f(\rho_v)_0, \tag{4}$$

and we finally obtain:

$$\frac{1}{M_s}\frac{dM_s}{dt} = f\frac{(\rho_v)_0}{\rho_v}\frac{1}{M}\frac{dM}{dt} = c_1\frac{1}{M}\frac{dM}{dt}. \tag{5}$$

$(\rho_v)_0$ is the water-vapour density at the drop surface when no net condensation or evaporation occurs, while ρ_v is the corresponding value when a falling drop is evaporating in dry air. Putting $f = 0.75$ and evaluating $(\rho_v)_0$ and ρ_v at an environmental temperature of +10°C and sea-level pressure we obtain $c_1 = 1.63$. The adjustment time, $M_s^{-1}dM_s/dt$, i.e., the time required for decreasing the tritium amount in a drop to $1/e$ of its original value, is obtained using Kinzer and Gunn's values for $M^{-1}dM/dt$ and is given in Table 1 as a function of the size of the drop. The two last columns of Table 1 give the terminal velocity for the various drops according to Gunn and Kinzer[8] and the distance, d, thus travelled by the drop in the time of adjustment given by column 2.

Table 1. The Adjustment Time for Tritium in a Drop and the Distance, d, Travelled in This Time

Radius a, cm	$[M_s^{-1}dM_s/dt]^{-1}$, *sec*	*Terminal velocity v, m/sec*	*d, m*
0.005	3.3	0.27	0.9
0.010	7.1	0.72	5.1
0.025	33	2.1	69
0.050	93	4.0	370
0.075	165	5.4	890
0.10	245	6.5	1600
0.15	365	8.1	3000
0.20	435	8.8	3800

In the above computation it was assumed that the drop remains of the same size while falling. In view of Eq. (5) one finds that the values for the adjustment time given here mean an overestimate when the net flux of HTO and H_2O is in the same direction and an underestimate if the contrary is true. The errors are not likely to exceed 50% and are usually much less.

We can thus conclude that the tritium content of rain gives a description of the tritium content of the water vapour at quite different levels in the atmosphere depending upon whether the raindrops are small or large. Making use of measurements by Blanchard[9] showing that the median volume diameter in rain is a function of rain intensity, we find that a light rain of an intensity of 0.1–1.0 mm/hr reflects the tritium present in the water vapour in the lowest 100 m of the atmosphere, a moderate rain of about 5 mm/hr is indicative of conditions up to about 300–600 m, while only the heavy rains with intensities of more than 10 mm/hr give information of the tritium amounts present at 1 or 2 km elevation. It should be remarked, however, that when precipitation falls during a longer period of time, the tritium content of the air through which the drops fall, of course, is also influenced significantly by the exchange of water vapour with the drops. The lower parts of the atmosphere may gradually be enriched in tritium if the tritium concentration is high aloft and vice versa if it is low.

In view of this discussion it would be of great interest to study the tritium concentration at the beginning and at the end of a rainstorm. Only two such cases have been published (von Buttlar and Libby[2]). In one case the tritium concentration was the same at the beginning and the end, 19.9 and 20.0 T.U. respectively; in the other case it increased from 7.3 to 13.5 T.U. General conclusions cannot, of course, be drawn from only two cases.

In this connection it is also interesting to compare the tritium concentration found in snow and rain in the winter. In the former case no appreciable adjustment of the tritium concentration to new environments can occur because the exchange of molecules inside the snowflakes is insignificant. The tritium concentration in snow should therefore show the concentration at the level of formation of the precipitation. During the period 20 November–15 March in the two winters 1952–53 and 1953–54 samples from 14 rainstorms and 10 samples of snow or snow mixed with rain have been collected in Chicago and analyzed for tritium content. The mean values for the tritium concentrations and standard deviations from them are respectively 8.4±5.2 T.U. and 16.3±7.9 T.U. A significant test shows that the probability is only about 10% that these two samples belong to the same population. Interpreted as an effect of the abovementioned process a difference of the tritium concentration at about 2 km elevation and close to the earth's surface should be at least about 8 T.U.

It is also of some interest to notice that the data collected in Chicago show no significant difference between winter and summer if only the rains are considered in the cold season. Thirteen rains analyzed during the time 15 April–30 September 1953 had an average concentration of 8.1 T.U. compared with 8.4 T.U. for the winter rains as mentioned previously.

THE TURBULENT EXCHANGE OF TRITIUM IN THE ATMOSPHERE

From the analysis in the previous section we have obtained some ideas of the interchange of tritium between drops and the surrounding air. When falling, these drops carry tritium to the surface of the earth. It will, however, be obvious from the following discussion that a considerable turbulent transfer also must occur. Because of the low concentrations found in the oceans and the relatively high values of tritium present at higher elevations in the atmosphere a vertical gradient exists. It is therefore of considerable interest to study in more detail the relation between the vertical distribution of tritium and the associated turbulent transfer. To do this we shall make use of our knowledge about turbulence in the atmosphere as reflected in the distribution of water vapour over the ocean and evaporation. The investigation by Sverdrup[10] will be particularly useful for this purpose.

We shall first restrict ourselves to the lowest 50–100 m of the atmosphere, within which we may assume the turbulent transfer to be approximately independent of height. The exchange in this layer is quite sensitive to the character of the underlaying surface, i.e., whether it is smooth or rough. Sverdrup's investigation shows quite conclusively that the best agreement with the actually observed evaporation from the ocean is obtained by considering the ocean surface as rough. We will follow Sverdrup and assume a roughness parameter $z_0 = 0.6$ cm. In spite of having a rough surface there seems to exist a thin boundary layer (depth, δ) immediately above the water surface, through which the transport of water vapour and thus also tritium takes place through diffusion. When considering a tritium transfer into the ocean which is proportionally larger than the transfer of ordinary water, or as is usually the case in reality, in the opposite direction to it, some mechanism must also exist whereby tritium is brought through a corresponding boundary layer in the water sufficiently far down into the ocean for turbulence to be effective for the further downward transfer. The concentration of tritium in water (per unit volume) is about 10^5 times that of water vapour in air. On the other hand the coefficient of diffusion is about 10^4 times less in water than in air. Thus the gradient in a boundary layer in the water need only be about $\frac{1}{10}$ of that in the air to maintain the same transfer if diffusion plays the dominating rôle. Probably the diffusion layer is thinner in water than in air, but since we know very little about actual conditions, we shall assume for the following rough estimates that the average tritium concentration in the mixed layer of the ocean also is representative for the sea surface. For a given difference in tritium concentration between the sea and the free atmosphere we overestimate the transfer by such an assumption.

Let κ denote the coefficient of diffusion for HTO vapour through air and F_s the flux of tritium, which is assumed to be independent of height. For the boundary layer just above the water surface we then obtain

$$F_s = \frac{\kappa}{\delta}(s_w - s_\delta), \tag{6}$$

where w refers to the ocean surface and δ to the upper boundary of the diffusion layer.

Above the boundary layer the turbulent transfer is active. Following standard procedures we shall assume that the eddy diffusivity, K, is a linear function of height

$$K = k_0 u^*(z + z_0), \tag{7}$$

where k_0 is a constant $= 0.38$, u^* the friction velocity defined by $u^* = (\tau/\rho)^{\frac{1}{2}}$, τ being the stress and ρ the air density. The turbulent transfer of tritium is now given by

$$F_s = -K\frac{\partial s}{\partial z}. \tag{8}$$

Combination of Eqs. (6), (7) and (8) finally yields

$$s - s_w = -F_s\left[\frac{\delta}{\kappa} + \frac{1}{k_0 u^*}\ln\frac{z + z_0}{z_0 + \delta}\right]. \tag{9}$$

To obtain the tritium concentration expressed in T.U. we also need to know the humidity distribution in this layer. For the following estimates we shall assume that the specific humidity (q) is constant with height. If a decrease by a certain percentage actually exists, as is usually the case in nature (Sverdrup[10]), obviously a corresponding increase in the difference of the tritium concentration is present. Again it means if anything an overestimate of the transfer for a given difference in the tritium concentration. δ and u^* are functions of the wind speed as well as the static stability of the atmosphere. We shall here choose values principally in agreement with those published by Sverdrup and based upon measurements by Montgomery. Assuming a transfer $F_s = -1$ atom/cm^2 sec and putting $\kappa = 0.22$ cm^2 sec^{-1} with due regard to HTO being heavier than H_2O we obtain values for the difference in tritium concentration at 50 m and at the sea surface that are given in Table 2.

Table 2. Difference in Tritium Concentration at 50 m Height and at Sea Level for a Transfer of 1 atom cm² sec

u, *m/sec*	*u**, *cm/sec*	δ, *cm*	$s_{50} - s_w$, *expressed in T.U.*		
			$q = 5\times10^{-3}$	$q = 10\times10^{-3}$	$q = 20\times10^{-3}$
2	10	0.3	8.3	4.1	2.1
4	20	0.2	4.8	2.4	1.2
7	35	0.1	3.1	1.6	0.8

It is clear from Sverdrup's treatment, as well as the presentation above, that we do not know in detail the processes responsible for the vertical exchange. It is a fact, however, that Sverdrup's equations give very reasonable values for the average global evaporation using measurements of the vertical gradient of water vapour above the oceans. The relation between the transfer and vertical distribution of tritium therefore probably is of about the same accuracy.

We can now make certain estimates of the natural production of tritium in the troposphere. This has recently been discussed by Craig[5] using considerations similar to those developed for radiocarbon (Craig[11]).

The exchange of tritium in the ocean may be considered to a first approximation as a direct exchange process between two well-mixed reservoirs, the top one being the relatively warm water masses above the thermocline and the bottom layer representing the deep ocean below. Assuming the depth of the mixed layer to be about 75 m, making use of the approximate residence time (100–500 years) in the deep sea as deduced from radiocarbon data and finally taking due regard of the proportions of land and sea on the earth, Craig finds that the tritium flux into the sea (in number of atoms cm^{-2} sec^{-1}) is 5.4 to 1.7 times the tritium concentration in the mixed layer (in T.U.). Relatively few measurements of the concentration in the ocean exist from the time before bomb tests began. Furthermore the concentrations found are generally very low and thus the values obtained are rather inaccurate. The first measurements reported by von Buttlar and Libby[2] gave values well below 1 T.U., while Begemann and Libby[3] in their recent study take an average value of 1 T.U. as a characteristic value before March 1954. As will be seen below, there are several factors that indicate that this is too large a value. With a turnover time for the deep sea of 500 years it would mean a downward flux of 1.7 atoms/cm^{-2} sec^{-1} through the atmosphere and for 1000 years the corresponding value would be 1.2 atoms cm^{-2} sec^{-1}.

The yearly evaporation from the ocean amounts to about 0.9 m meaning an upward flux of 0.15 tritium atoms cm^{-2} sec^{-1} with the assumption of 1 T.U. in the ocean and a fractionation factor of 0.75. 0.8 m of rain falls each year over the ocean and about 0.1 m of water is brought back to the sea by rivers. The tritium concentration in oceanic rains varies from 0.5 T.U. on Hawaii to values between 2 and 3 T.U. in the Atlantic. Accepting an average value of 2 T.U. and a concentration of 5 T.U. for river water (von Buttlar and Libby[2]) gives a flux of 0.44 atoms cm^2 sec^{-1} back to the sea. A net flux into the ocean of about 0.3 atoms cm^{-2} sec^{-1} is thus maintained by the water cycle in nature. A total flux of 1.7 atoms cm^{-2} sec^{-1} and even 1.2 atoms cm^{-2} sec^{-1} would thus mean that turbulence is by far the most important mechanism for the vertical exchange in the atmosphere. The previous results indicate that in such a case the tritium concentration at 50 m elevation would have to be at least 1 T.U. and most likely 2–3 T.U. higher than in the ocean. Considering that the bulk of the precipitation falls with moderate or large intensity, the tritium concentration a few hundred meters up in the atmosphere can hardly be much greater than the average tritium concentration in oceanic rains. In low latitudes the concentrations in rain are from 0.5 to 1.7 T.U., thus indicating a difference in the tritium concentration over the lowest hundred meters of 0–1 T.U. and a turbulent transfer appreciably smaller than 1 atom cm^{-2} sec^{-1}. In middle latitudes the concentrations found in rain are larger but most likely less than 3 T.U., as indicated not only by rains collected over the ocean but also from analysis of river water in western Europe where the oceanic influence is great. In view of the lower values of q when going further north and the fact that a continued increase of tritium upwards must exist above the logarithmic layer to maintain a downward turbulent transfer, it seems rather unlikely that even in these latitudes the turbulent flux is larger than 1.0 atom/cm^{-2} sec^{-1}. As will be seen in the following section, continuity considerations over the American Continent seem to indicate a total flux from the stratosphere or production in the troposphere of less than about 1 atom cm^{-2} sec^{-1}, which thus would agree quite well with the general results obtained here. Considering the large area of the earth as being in low latitudes, it seems therefore quite clear that the average flux from aloft into the troposphere or production within it for the earth as a whole is less than, rather than greater than, 1 atom cm^{-2} sec^{-1}. The data and the discussion above seem also to support tentatively the idea of a larger flux into the troposphere in middle latitudes than further south equator-wards, similar to what has been found for Sr^{90} (Bolin[12] and Stewart[13]).

THE TRITIUM BUDGET OF LAKES AND THE SOIL

We next direct our attention to the exchange of tritium between different reservoirs in continental areas. By considering the observed variations of tritium in rain, lakes and rivers after the hydrogen bomb explosion in March 1954 one can deduce some interesting relations (Begemann and Libby[3]). Begemann and Libby used the observed increase of tritium in a number of lakes and the top layer of the ocean to estimate the total deposition of tritium that resulted from the bomb tests and obtained a value of 2×10^9 atoms cm^{-2}. They admit that large errors are inherent in this estimate. Particularly important is, however, our previous results that a considerable amount of tritium may be brought into the ocean, and thus also most likely into lakes, by direct molecular exchange at the water surface. Such a transfer is particularly large if the water body is deep so that the specific activity of the water is kept at a low level by vertical mixing even if large amounts of tritium are transferred. In view of this, it is of interest to make an independent estimate of the amount of tritium brought down by rain.

Regular measurements of the amount of tritium in rain in Chicago were conducted in the spring, summer and fall of 1954. About 40% of the total amount of rainfall was thus analyzed. There are appreciable variations from one rain to another, but the over-all variation with high values between 300 and 400 T.U. in the spring and early summer, decreasing to about 30 T.U. during the summer and fall, is quite well established. By interpolating the tritium amounts in the rains not analyzed we calculate the total deposition of tritium by rain in the Chicago area to be about 1.0×10^9 tritium atoms cm^{-2}. This is considerably less than the 1.9×10^9 as obtained for the deposition over Lake Michigan by studying the observed tritium change in the lake (Begemann and Libby[3]). The scatter of the individual measurements does not appear large enough to explain this discrepancy. Let us instead assume that the difference is due to direct molecular exchange and estimate how large a fraction of the total deposition over the lake may then be due to this direct exchange. It is then obviously necessary to consider the run-off from the drainage area into the lake in a similar way as done by Begemann and Libby, and for this purpose we need some information about the exchange of water between the atmosphere and the soil.

Most of the rain falling over land is quickly absorbed in the upper parts of the soil. A comparatively small amount is carried to the lakes, rivers and finally to the ocean by surface run-off. The water in the soil slowly moves downward towards the ground water table, but obviously only a small part reaches it since large amounts are used by vegetation in their production of organic matter. Thus considerable amounts of the water is in this way brought back to the atmosphere. It is generally accepted that most of the evapo-transpiration is due to transpiration of plants and also evaporation directly from the soil, while evaporation from exposed ground water is small, as only small areas are covered by open ground water bodies. Estimates of the run-off from continents show that only $\frac{1}{3}$ or $\frac{1}{4}$ of the precipitation finds its way into the main body of ground water, to the rivers and finally to the sea.

The amount of water stored in the upper parts of the soil varies considerably and may amount to 20 or 30 cm. No significant mixing can possibly occur between this soil moisture and the ground water and thus the tritium content of the soil moisture to a first approximation will be about the same as the average tritium content of the rain during the last few months. Appreciable amounts of tritium must therefore be brought back to the atmosphere by evaporation and may come down as rain a second time somewhere else. This was mentioned briefly by von Buttlar and Libby[2] and partly considered by Begemann and Libby.[3]

As a result of evaporation from the ground a relatively high concentration of tritium will be maintained at low levels in the atmosphere, while this is not the case over the ocean, where tritium is steadily removed by the ocean surface. We therefore should expect a rapid direct molecular transfer when continental air moves out over a lake with a relatively low tritium content. In the case of a large lake like Lake Michigan the tritium in the lowest layers of the atmosphere is soon removed and a considerably slower transfer occurs which is essentially controlled by the turbulent transfer from aloft. The air spends, on the other hand, a relatively short time over a small lake, new air masses are constantly moving out over the lake and large amounts of tritium may be transferred into the lake. Let us denote by α the ratio between the amount of tritium transferred into the lake by direct molecular exchange and the corresponding amount being brought down by precipitation. We let E be the amount deposited by precipitation, γ be the fractional run-off, S_d and S_l the size of the drainage area and the lake respectively, Δs the observed change of the tritium concentration in the lake and h the average depth of the lake. Thus

$$E\left(1+\alpha+\gamma\frac{S_d}{S_l}\right)=\Delta s h. \tag{10}$$

For Lake Michigan, $\gamma = 0.46$, and we shall assume the same value for two other lakes in the United States for which tritium data are available: Lake Tahoe and Crater Lake. This may be unrealistic, particularly for Crater Lake, but the exact value is of relatively little importance as will be seen in the following. Using other pertinent data as given by Begemann and Libby[3] we obtain the values for α given in Table 3. According to this the major part of the tritium found in these lakes is transferred by turbulence and not by precipitation. The values are of course rather uncertain in view of, for example, the assumption that the fallout by rain is the same at all these places and the fractional run-off does not vary, but the general trend of a small α for a large lake and vice versa is undoubtedly correct.

We next ask ourselves if the tritium amounts thus transferred can be provided from the air passing over the lake. We may assume that most of the increase occurred during the six months following the first increase of tritium in the rain in Chicago. During this time the average concentration in rain may be put at 200 T.U. Owing to the effect of fractionation at condensation we may assume the tritium condensation in water vapour to be $s = 150$ T.U. Let us assume that a wind of average velocity v blows across the lake and that the specific humidity of the air is q. We then compute how large a fraction, σ, of the tritium present in the lowest 1 km of the air that passes over the lake during the time τ must be transferred into the lake in order to account for the values obtained for α:

$$\sigma = \frac{c_2 \alpha E S_l^{\frac{1}{2}}}{q \rho s v \tau l}. \tag{11}$$

Here c_2 is a constant, $c_2 = 1.5\times10^{-5}$ if s is expressed in T.U. Putting $q = 8\times10^{-2}$, $\rho = 1.2\times10^{-3}$ g cm^{-3}, $v = 3$ m sec^{-1}, $l = 10^5$ cm and $\tau = 1.6\times10^7$ sec we obtain the values given in the last column of Table 3. In this computation it has furthermore been assumed that the extension of the lake perpendicular to the average wind velocity may be put equal to the square root of the area of the water body, which at least in the case of Lake Michigan is an underestimate. A more detailed discussion of the various values is of course not justifiable in view of the large number of assumptions made. We notice, however, that σ is larger for Lake Michigan than for the other lakes, which is to be expected, since an air column spends considerably longer time over a large than over a small lake. We conclude thus that it is meteorologically reasonable that the direct molecular exchange is of major importance for the tritium budget of a lake and due regard must be taken of this process when trying to estimate the deposition by precipitation through budget considerations.

There are measurements also from Zürichsee in Switzerland, which show a much smaller increase of tritium (Begemann and Libby[3]). It is, however, clear from measurements of tritium in rain over Europe in the spring and summer of 1954 that the concentration was considerably lower than over the USA. Furthermore the drainage area of the lake is comparatively large and the average depth small and a sizable fraction of the tritium brought into the lake therefore leaves it within six months. A direct comparison with the three lakes in the United States is thus not possible.

Table 3. An Estimate of the Relative Importance of Direct Molecular Exchange for the Tritium Budget of a Lake

(Cf. Begemann and Libby[3] and text)

	S_l, km^2	S_d, km^2	h, m	Δs, atoms per cm$^3\times10^5$	α	σ
Lake Michigan	57,100	110,000	93	3.8	1.5	0.68
Lake Tahoe	492	3,800	191	4.7	4.4	0.19
Crater Lake	49	15	490	4.0	18	0.24

The fact that evaporation from the soil is of importance for the tritium budget of the atmosphere over land must be considered in estimating the storage time of tritium in the atmosphere. Begemann and Libby[3] arrived at a residence time of 40 days using the fallout of bomb tritium. This is considerably longer than the residence time of tropospheric moisture obtained from rainfall data. The difference is explained as being due to the comparatively slow descent of moisture from the stratosphere into the troposphere. The authors do not attempt to explain the fact that the tritium content in rain remained fairly constant for about 3 months after the explosions occurred. A more detailed discussion of the troposphere-soil system and its environment is here necessary.

Obviously it is not only a change in the flux into the troposphere from aloft (F_T) which is of importance but also the flux from the upper part of the soil into the ground water reservoir ($F_G s_b$, where F_G is the flux of water and s_b the tritium concentration of the soil moisture (T.U.)) and the exchange of air of continental and oceanic origin since tritium is removed much more rapidly from the atmosphere over the ocean than over the continents. Let us assume that the oceanic air coming in over the continent carries X (g sec^{-1}) of water with an average tritium concentration of s_X (T.U.) while in the same way y (g/sec) of water leaves the continental area via the air and then has a tritium concentration s_a (T.U.). We denote the amounts of water present in the air over land and in the soil by aA and by bA respectively, where A is the area of the continent. Finally we assume first-order exchange processes between the atmosphere and the soil and consider these two reservoirs as well-mixed for our purpose. The exchange coefficient atmosphere-soil is k_a and the coefficient for the exchange in the opposite direction k_b. It should be noted that the exchange described by k_a involves a condensation process in the clouds explaining the occurrence of a factor f^{-1}. We then obtain (Fig. 1)

$$\begin{aligned} &\frac{d}{dt}(as_a) - \frac{x}{A}s_x + \frac{y}{A}s_y - fk_b bs_b + k_a as_a - F_T &= 0, \\ &\frac{d}{dt}(bs_b) \qquad\qquad + fk_b bs_b - k_a as_a + F_G s_b &= 0. \end{aligned} \tag{12}$$

From continuity considerations of water we similarly have

$$\begin{aligned} &\frac{da}{dt} - \frac{x}{A} + \frac{y}{A} - k_b b + k_a a &= 0, \\ &\frac{db}{dt} \qquad\qquad + k_b b - k_a a + F_G &= 0. \end{aligned} \tag{13}$$

Considering first the steady state conditions, we obtain by elimination of $k_b b$ from the second equation in (12) and (13) an expression for s_b

$$s_b = s_a \Big/ \left(f + \frac{(1-f)F_G}{k_a a} \right) = c_3 s_a. \qquad (14)$$

We may here assume that k_a is essentially determined by the amount of rainfall and neglect the possible transfer through direct molecular exchange. The open water bodies over which this could be of importance constitute a small area of the continent. Under all circumstances we thereby obtain an upper limit for c_3. Putting $1/k_a = 10$ days, $a = 3$ cm, $F_G = 0.04$ cm day^{-1} and $f = 0.75$ yields $c_3 = 1.7$. The value of c_3 is insensitive to the values chosen and may therefore be accepted as rather accurate. *In the steady state the soil moisture has about* 70% *higher tritium content than atmospheric moisture owing essentially to the fractionation effect.* There exists to my knowledge no measurements that could verify this general result.

With the aid of the first Equation (12) we may now determine the F_T necessary to maintain the tritium concentration in precipitation over land and in the soil at a considerably higher level than in the atmosphere over the ocean,

$$F_T = \left[\frac{y}{A} + F_G \Big/ \left(f + \frac{(1-f)F_G}{k_a a} \right) \right] s_a - \frac{x}{A} s_x. \qquad (15)$$

According to Benton and Estoque[14] x and y are of the order of magnitude 4×10^{11} g sec^{-1} and $A = 1.6 \times 10^{17}$ cm^2. With the values used previously we find that the second term within the bracket is relatively important ($\approx$35% of the first one). This means physically that to a first approximation there is a balance between the horizontal exchange of tritium between land and sea on the one hand and the flux of tritium from aloft on the other and that the tritium finding its way into the ground water reservoir is of less importance. This picture differs from that presented by Begemann and Libby.[3] It is due essentially to the shielding effect of the soil, which was not considered by them.

Introducing first the values for s_a and s_x found before March 1954, $s_a = 6$ T.U., $s_x = 2.5$ T.U. (Begemann and Libby[3]), and using the average values for x and y as given by Benton and Estoque, $x = 4.3 \times 10^{11}$ g sec^{-1}, $y = 3.6$ g sec^{-1}, which are in agreement with the daily run-off of 0.04 cm/day used for F_G, we obtain $F_T = 0.8$ atoms cm^{-2} sec^{-1}, about 30% less than the value obtained by Begemann and Libby. It should be remarked here that this may be a slight underestimate, since the values for x and y probably are somewhat too low. The transport of any characteristic property such as water vapour or tritium is a turbulent process. The values for x and y represent, however, the net inflow and outflow, which have been computed after averaging in time (for three months) and along a coastline of considerable extension. It is difficult to estimate the errors introduced without detailed considerations about the variability of the wind and humidity around the continent. Benton and Estoque's computations show, however, that only ¼ or ⅓ of the total transport of water over the continent is due to large-scale turbulence while the remaining part is carried by the mean westerly flow. This may be taken as an indication that the x and y used here are not underestimated. In view of the discussion in this and the preceding section we may summarize our results to say that *the flux of naturally formed tritium into the troposphere and production within it is* 0.9 ± 0.2 *atoms sec*$^{-1}$ *cm*$^{-2}$.

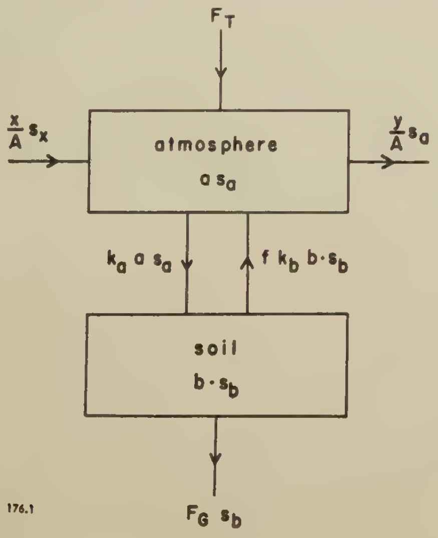

Figure 1

From October 1954 and for about nine months a new equilibrium was established with a characteristic tritium concentration in rain of about $s_a/f = 21$ T.U. (with due regard taken of the fractionation at the condensation process). No measurements are available from oceanic areas during this time, but in view of the rapid exchange between the atmosphere and the sea the values most likely were only slightly higher than before the Castle tests. Putting $s_x = 3$–6 T.U. gives $F_T = 3.1$–2.5 atoms cm^{-2} sec^{-1}. Thus even one year after the explosions occurred in the Pacific, bomb tritium seemed to come down into the troposphere from aloft. This indicates that a considerable part of the water thrown up into the stratosphere at the bomb explosion evaporated from the droplets and ice crystals formed and did not precipitate into the troposphere as suggested by Begemann and Libby. The exchange of water vapour between the stratosphere and the troposphere is then, of course, as slow as found for Sr^{90} with an estimated half-life of the order of 10 years (Libby[15]). Accepting this half-life of the tritium in vapour form in the stratosphere and putting $F_T = 2.5$ atoms cm^2 sec^{-1} yields an estimate of about 0.5×10^9 T atoms cm^{-2} present is the stratosphere in the fall of 1954 because of the bomb tests. Thus only about ⅔ of the tritium introduced into the atmosphere fell out in the first six months.

Finally, we shall discuss the decrease of tritium in the atmosphere that occurred in the summer of 1954 using Eqs. (12) and (13). During the summer the continent is a donor of water and very little of the precipitation that falls ever reaches the ground water reservoir. We shall therefore assume $F_G = 0$. The value for $(x-y)$ given by Benton and Estoque for the summer means a net loss of water from the system-atmosphere-soil of about 1 cm per month. This fact must be taken into consideration and we put

$$\frac{1}{a}\frac{da}{dt}=\frac{1}{b}\frac{db}{dt}. \tag{16}$$

We shall furthermore assume

$$\frac{1}{s_a}\frac{ds_a}{dt}=\frac{1}{s_b}\frac{ds_b}{dt}=-\lambda, \tag{17}$$

where λ is the observed decrease of the tritium concentration for the period concerned. This implies that the adjustment time of tritium content in the soil and the atmosphere above is short compared with the gradual decrease during the whole summer as reflected in the tritium concentration in rain. Eliminating da/dt, db/dt and k_b from Eq. (12) we obtain

$$\begin{aligned}&\left(\frac{ax+by}{Aa(a+b)}+k_a-\lambda\right)s_a-f\left(k_a-\frac{b(x-y)}{aA(a+b)}\right)s_b\\&=\frac{F_T}{a}+\frac{x}{aA}s_x,\\&-\frac{a}{b}k_as_a+\left[fk_a\frac{a}{b}+\frac{(1-f)(x-y)}{A(a+b)}\right]s_b=0.\end{aligned} \tag{18}$$

Eliminating s_b between these two equations the only remaining unknown variable is b. If assuming that

$x = 4.3\times10^{11}$ g sec^{-1} (Ref. 14),
$y = 4.9\times10^{11}$ g sec^{-1} (Ref. 14),
$k_a a = 0.3$ cm day^{-1},
$\lambda^{-1} = 40$ days (according to Begemann and Libby[3]),
$f = 0.75$,
$A = 1.6\times10^{17}$ cm^2,

we obtain $b = 3$–4 cm for values of $a = 2$–4 cm, $F_T = 0$–5 atoms cm^{-2} sec^{-1}, $s_a = 100$–400 T.U. and $s_x/s_a = 0$–0.05, which all are quite extreme limits, possibly with the exception of F_T (*cf.* below). It is easily seen that an upper limit for b is obtained by putting $F_T = 0$. A good approximation is obtained in this case by putting $da/dt = db/dt = 0$. We then have

$$\frac{1}{b}=\frac{\lambda}{fk_aa}\left[1+\frac{k_aa}{\dfrac{y}{A}-\lambda a-\dfrac{x}{A}\dfrac{s_x}{s_a}-\dfrac{F_T}{s_a}}\right]. \tag{19}$$

In conclusion we may say that *the amount of water in the soil of the American Continent in direct communication with the atmosphere essentially through vegetation was equal to or less than* 4 *cm in the summer of* 1954.

We may finally ask: What is the maximum flux from aloft compatible with the decrease of tritium observed in the summer of 1954? Putting $b = 0$, which means that all precipitation is very soon returned to the atmosphere through evaporation, assuming furthermore that $s_x \ll s_a$, we obtain

$$F_T < (y/A - a\lambda)s_a = 0.12s_a, \tag{20}$$

where $x = 4.3\times10^{11}$ g/sec and s_a is given in T.U.

It is clear from the discussion in this section that the presence of moist soil is of great importance for a discussion of the tritium exchange over a continent. In several respects it has a shielding effect in that most of the tritium that is brought down by precipitation is returned to the atmosphere and the exchange between the ground water reservoir and the atmosphere is considerably reduced. For a more detailed study of the exchange between the soil and the ground water reservoir reference is made to Eriksson.[16]

ACKNOWLEDGEMENTS

The author is greatly indebted to Drs. Gustaf Arrhenius and Erik Eriksson for many interesting discussions of the ideas presented in this article. Thanks are also due to Dr. F. Begemann for pointing out an inconsistency in Eq. (12) as originally formulated and a few other remarks.

REFERENCES

1. S. Kaufmann and W. F. Libby, *The Natural Distribution of Tritium*, Phys. Rev., *93*, 1337–1344 (1954).
2. H. von Buttlar and W. F. Libby, *Natural Distribution of Cosmic-ray Produced Tritium II*, J. Inorg. Nuclear Chem., *1*, 75–91 (1955).
3. F. Begemann and W. F. Libby, *Continental Water Balance, Ground Water Inventory and Storage Times, Surface Ocean Mixing Rates and World-wide Water Circulation Patterns from Cosmic-ray and Bomb Tritium*, Geochim. et Cosmichim. Acta, *12*, 277–296 (1957).
4. H. Craig, *Isotopic Tracer Techniques for Measurement of Physical Processes in the Sea and Atmosphere*, Final report National Academy of Science Committee on Effects of Atomic Radiation on Oceanography, Washington (1956).
5. H. Craig, *Distribution, Production Rate and Possible Solar Origin of Natural Tritium*, Phys. Rev., *105*, 1125–1127 (1957).
6. G. D. Kinzer and R. Gunn, *The Evaporation, Temperature and Thermal Relaxation Time of Freely Falling Water Drops*, J. Meteorol., *8*, 71–83 (1951).
7. A. H. Price, *Vapour Pressure of Tritiated Water*, Nature, 181, 262 (1958).
8. R. Gunn and G. D. Kinzer, *The Terminal Velocity of Fall for Water Droplets in Stagnant Air*, J. Meteorol., *6*, 243–248 (1949).
9. D. C. Blanchard, *Raindrop Size-distribution in Hawaiian Rains*, J. Meteorol., *10*, 457–473 (1953).
10. H. U. Sverdrup, *On the Evaporation from the Oceans*, J. Marine Research, *1*, 3–14 (1937).
11. H. Craig, *The Natural Distribution of Radiocarbon and the Exchange Time of Carbon Dioxide between Atmosphere and Sea*, Tellus, *9*, 1–17 (1957).
12. B. Bolin, *Vertical Distribution of Radioactivity in the Atmosphere*, Ann. Int. Geophys. Yr., *5* (in press, 1958).
13. N. G. Stewart, *On the Atmospheric Distribution and Deposition of Radioactive Dust from Nuclear Test Explosions*, Presented at UGGI meeting in Toronto 1957.
14. G. S. Benton and M. A. Estoque, *Water Transfer Over the North American Continent*, J. Meteorol., *11*, 462–477 (1954).
15. W. F. Libby, *Radioactive Strontium Fall-out*, Science *42*, 365–390 (1956).
16. E. Eriksson, *The Circulation of Some Atmospheric Constituents in the Sea*, to be published in the Rossby Memorial Volume (1958).

Contribution No. 1008

Reprinted from
BULLETIN OF MARINE SCIENCE
OF THE GULF AND CARIBBEAN
Vol. 9, No. 2, pp. 222, 223
JUNE, 1959

FLORIDA STRAITS TRANSPORTS: JUNE 1956 - JULY 1958[1]

HENRY STOMMEL
Woods Hole Oceanographic Institution
Woods Hole, Massachusetts

The data presented here are continuations of those presented in an earlier number of this journal (Vol 7, No. 3, pp. 252-254), and are subject to the same explanations, qualifications, and are in the same units. The chief point of interest is the rather high set of numbers in June and July of 1958. As explained in the earlier report, there may be something specious about the interpretation of these measured voltages in terms of transport so that I hope these numbers will be accepted with caution by other investigators.

TABLE 1

24-HOUR AVERAGES OF FLORIDA STRAITS TRANSPORTS IN MILLIONS OF CUBIC METERS PER SECOND.

1956		
June	10	25.6
	24	(26.4) very noisy
	30	23.2
July	1	22.9
	7	22.4
	8	21.4
	14	23.4
	15	23.4
	21	23.0
	28	23.7
	29	24.2
Aug.	4	25.0
	5	24.8
	11	24.9
	12	26.5
	18	24.4
	19	23.7
	25	20.8
	26	21.5
Sept.	1	24.5
	2	22.9
	9	26.5
	15	25.6
	22	32.1
	23	32.8
	29	30.2
	30	29.0
Oct.	6	28.8
	7	28.9
	13	20.0
	14	18.6
	20	22.5
	21	24.3
	27	20.5
	26*	23.7
	27*	21.3
Nov.	3	19.6
	4	17.5
	11	21.3
	17	29.7
	18	31.2
	24	25.0
	25	26.4
Dec.	2	24.3
	9	26.6
	15	32.3
	16	32.1
	22	28.1
	23	28.8
	29	27.6
	30	26.6

---

[1] Contribution No. 1008 of the Woods Hole Oceanographic Institution. This work was done under contract with the Office of Naval Research: N6onr-27701.

TABLE 1 (Continued)

1957		
Jan.	5	30.6
	6	32.0
	12	29.5
	13	28.3
	19	22.3
	20	22.1
	26	23.9
	27	23.8
Feb.	2	22.6
	3	21.4
	9	21.5
	10	21.5
	16	21.9
	17	20.6
	24	23.1
Mar.	3	29.8
	9	27.3
	15	25.6
	16	25.7
	22	24.0
	23	24.5
Apr.	14	23.9
	20	20.9
	21	21.3
June	1	27.0
	2	28.5
	8	29.6
	9	30.4
	15	32.4
	16	33.7
	22	30.4
	23	30.0
	29	29.2
July	13	24.7
	20	31.4
	27	31.8
Aug.	3	26.8
	10	22.4
	17	24.9
Aug.	24	20.9
	31	30.3
Sept.	7	34.1
	21	26.1
Oct.	12	24.6
	19	21.8
	26	24.6
Nov.	2	21.1
	23	26.3
	30	23.9
Dec.	7	19.3
	14	20.2
	28	30.8
1958		
Feb.	16	28.9
Mar.	2	29.7
	8	27.2
Apr.	5	29.6
	6	28.6
June	1	35.5
	8	33.3
	14	38.1
	15	38.2
	21	38.2
	22	38.9
	29	43.0
July	5	41.2
	6	42.6
	19	49.6
	20	54.2

Contribution No. 1010

Reprinted from BIOLOGICAL BULLETIN, Vol. 116, No. 3, pp. 461–471, June, 1959
Printed in U. S. A.

OBSERVATIONS ON THE GROWTH OF DUNALIELLA EUCHLORA IN CULTURE[1]

JACK McLACHLAN[2] AND CHARLES S. YENTSCH

Woods Hole Oceanographic Institution, Woods Hole, Mass.

Under natural conditions, an intimate, but poorly understood relationship exists between bacteria and phytoplankton. Some investigators have claimed that phytoplankton produce a substance which is inhibitory to the growth of bacteria (Steemann Nielsen, 1955a, 1955b; Steemann Nielsen and Jensen, 1957). Contrariwise, the results of Waksman *et al.* (1937) suggest a harmonious relationship between algae and bacteria.

In experimental work, the use of bacteria-free cultures is customary. It has not always been possible to obtain bacteria-free cultures, and the assumption has been that the growth of the alga would have not been altered if axenic cultures had been used (*cf.* Goldberg *et al.,* 1951; Kain and Fogg, 1958). This assumption seems correct when using media with no organic additions (McLachlan, unpublished). However, little is known of the effects of bacteria on the growth of algae in cultures containing organic supplements.

In the present investigation, growth of the green flagellate *Dunaliella euchlora* WHOI-1 in pure culture and contaminated cultures containing organic enrichments was studied. Growth was estimated by cell numbers and chlorophyll *a* synthesis. The production of algal and bacterial inhibitors was also investigated.

MATERIALS AND METHODS

A pure culture of *Dunaliella euchlora* Lerche strain WHOI-1 (McLachlan, 1959) was used in this study. The alga was grown in a modification of the ASP medium of Provasoli *et al.* (1957); the composition of this medium is presented in Table I. In some of the experiments, the ASP medium was enriched with organic material by the addition of beef extract (0.3 g./l.) and bactopeptone (0.5 g./l.). At 16% nitrogen, this corresponds to an addition of about 9.1 mM of organic nitrogen, or nine times as much as is available in the basic medium. The cultures were incubated at 16° C. under 3,000 meter-candles of illumination provided by 40-watt fluorescent lights. Growth of the alga was determined by cell counts made in duplicate with a total of eight replicate counts using a Levy hemocytometer, and is expressed as $\log_2 N_t/N_o$ where N_o is the concentration of cells at inoculation and N_t the concentration at time t.

Chlorophyll *a* was measured spectrophotometrically in acetone extractions according to the Richards with Thompson method (1952) as modified for use with the millipore membrane filter procedure of Creitz and Richards (1955). The con-

---

[1] Contribution no. 1010 from the Woods Hole Oceanographic Institution. This investigation was supported, in part, by a grant from the National Science Foundation.

[2] Public Health Service Research Fellow of the National Institutes of Health.

TABLE I

Composition of the modified ASP medium

NaCl	410 mM	$FeCl_3 \cdot 6H_2O$	1.5 μM
$MgSO_4 \cdot 7H_2O$	24 mM	H_3BO_3	185.0 μM
$MgCl_2 \cdot 6H_2O$	22 mM	$MnCl_2 \cdot 4H_2O$	7.0 μM
$CaCl_2 \cdot 2H_2O$	10 mM	$ZnCl_2$	0.8 μM
KNO_3	1 mM	$CoCl_2 \cdot 6H_2O$	0.02 μM
K_2HPO_4	100 μM	$CuCl_2 \cdot 2H_2O$	0.0002 μM
$Na_2SiO_3 \cdot 9H_2O$	100 μM	Na_2EDTA	30.0 μM

centration of chlorophyll *a* was determined using the nomographs of Duxbury and Yentsch (1956), and the organic nitrogen content of the cells was estimated by the procedure of Yentsch and Vaccaro (1958).

RESULTS

1. *Growth in contaminated beef extract-peptone cultures.* To determine the effect of bacterial contamination on the growth of *Dunaliella euchlora,* the alga was inoculated into autoclaved and unautoclaved ASP medium, and autoclaved and

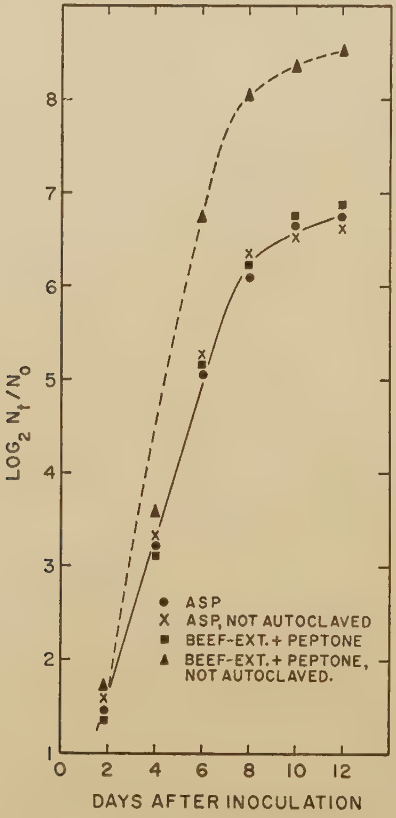

FIGURE 1. Growth of the alga in contaminated and non-contaminated ASP medium and contaminated and non-contaminated ASP medium containing beef extract and peptone.

unautoclaved ASP cultures containing beef extract and peptone. In the unautoclaved cultures with organic enrichments, approximately 2.5 times as many cells were obtained as in the other cultures (Fig. 1). The growth rate and the final number of cells in the other treatments were approximately the same. From these results it can be seen that the addition of beef extract and peptone *per se* did not increase the growth of the alga, but bacterial breakdown of these materials was of considerable benefit.

The unautoclaved cultures with organic additions became very dense, and after twelve days of growth contained approximately three times as much chlorophyll *a* per cell as the autoclaved enriched culture (Table II). Using the method of Yentsch and Vaccaro (1958), it was found that in the enriched contaminated cultures about 10 mM per liter of organic nitrogen was incorporated into the algal cells, or approximately 0.91×10^{-6} μM of nitrogen per cell. In contrast, the non-contaminated enriched culture contained about 0.9 mM per liter of organic nitrogen as algal cellular material, or approximately 0.23×10^{-6} μM of nitrogen per cell. The chlorophyll content of the two cultures containing only inorganic additions was not determined, but other estimates have indicated that at the end of exponential growth, all of the added nitrate-nitrogen is organically incorporated. This suggests

TABLE II

The size of the population of Dunaliella euchlora, *and the chlorophyll* a *content after growth in media treated as discussed in the text*

Experiment	Treatment	Days of growth	No. cells/ml. $\times 10^4$	Mg Chl^a/cell $\times 10^{-9}$
Beef extract-peptone no. 1	Enriched and contaminated	12	1,089	2.24
	Enriched, not contaminated	12	397	0.74
	ASP-autoclaved	12	384	—
	ASP-not autoclaved	12	370	—
Nitrate-nitrogen	1.0 mM	14	444	0.41
	2.0 mM	14	868	0.40
	5.0 mM	14	839	0.44
	8.0 mM	14	716	0.39
	10.0 mM	14	617	0.51
Beef extract-peptone no. 2	−3	15	320	0.81
	0	15	634	0.66
	+2	15	924	0.47
	+4	15	1,631	0.60
	+7	15	1,198	1.11
	+11	15	792	0.68
	Control	15	497	0.79
Dunaliella filtrate	ASP	11	504	0.44
	Autoclaved filtrate	11	527	0.93
	Unautoclaved filtrate	11	491	1.27
Bacteria filtrate	ASP	12	477	0.43
	Filtrate	12	958	0.80

that in the non-contaminated beef extract peptone culture all of the incorporated organic nitrogen had been obtained from the added nitrate-nitrogen, and not from the organic material.

2. *Growth in various concentrations of nitrate-nitrogen.* To determine if the number of cells and the amount of chlorophyll *a* obtained in the contaminated beef extract-peptone cultures could be obtained by the addition of inorganic nitrogen, sodium nitrate was added at the following concentrations: 1.0 (ASP level), 2.0, 5.0, 8.0 and 10.0 mM. The ASP concentration of potassium was maintained by the addition of potassium chloride, and the phosphorus concentration was maintained at 100 μM in all cultures. The two highest concentrations of nitrogen slightly inhibited the growth of the alga (Fig. 2), but the total number of cells in all cultures exceeded that of the 1.0 mM culture after fourteen days of growth. The maximum density of cells developed in the 2.0 and 5.0 mM cultures had a final cell count of almost twice that of the 1.0 mM culture (Table II), although the initial growth rates of these three cultures were approximately the same.

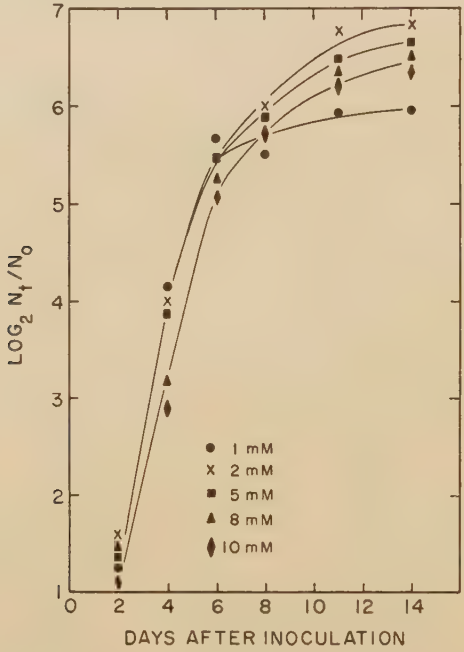

FIGURE 2. Growth of the alga in various concentrations of nitrate-nitrogen.

Pigment analysis showed that the chlorophyll *a* content of the cells in all cultures was about the same (Table II). The total number of cells obtained in the cultures containing 2.0 and 5.0 mM of nitrate-nitrogen approached that obtained in the contaminated beef extract-peptone culture of the previous experiment, but the amount of chlorophyll *a* was considerably less. Since the maximum amount of chlorophyll synthesized in these cultures was considerably less than was found in the contaminated culture containing beef extract and peptone, it may be concluded that available nitrogen alone is not the limiting factor. Perhaps release of other nutrients in beef extract and peptone by bacterial activity or direct utilization of organic breakdown products by the alga also stimulated chlorophyll synthesis.

3. *Growth in beef extract-peptone cultures with periodic addition of bacteria.* To determine the effects of organic breakdown products on the growth of the alga at different phases of growth, a mixed culture of marine bacteria was obtained from the surface waters of Woods Hole Harbor, and uniform inocula were added periodically to cultures of *Dunaliella* containing beef extract and peptone. The original bacterial inoculum was collected using a sterile container so only bacteria present in the surface water were introduced into culture. The bacteria were grown in the ASP medium with the addition of beef extract and peptone under the same conditions as the algal cultures. Before the bacterial cultures were used in the experimental work, they were carried through a number of transfers in order to obtain a uniform population.

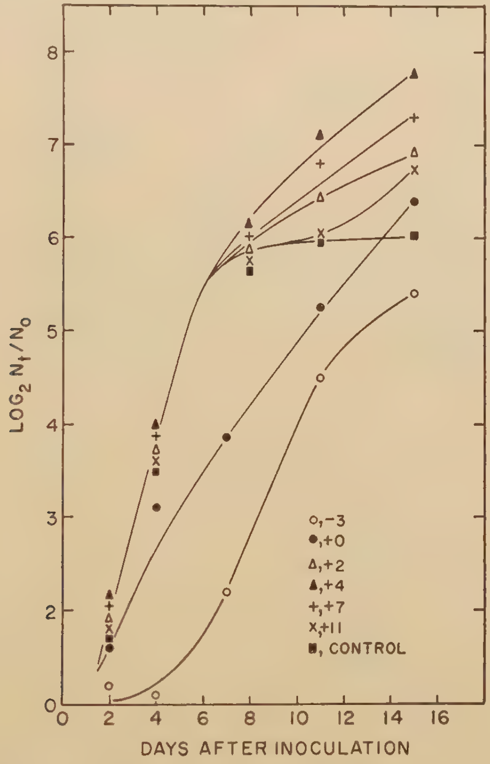

FIGURE 3. Growth of the alga in the ASP medium containing beef extract and peptone to which bacteria were added periodically.

Beef extract and peptone were added to the ASP medium and inoculated periodically with 1 ml. of the bacterial culture. In all cases the bacteria inocula were from three-day-old cultures when introduced into the experimental flasks. Inoculation

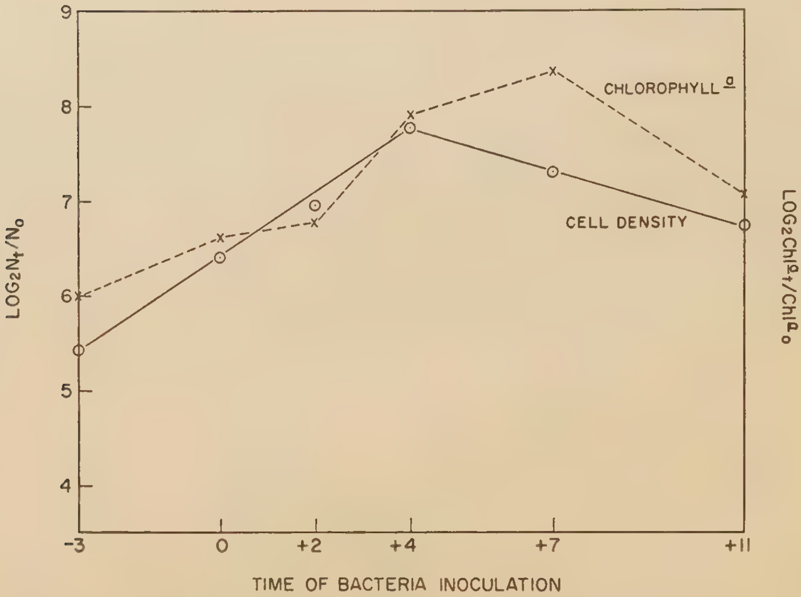

FIGURE 4. A comparison of algal cell density and chlorophyll *a* in cultures to which bacteria were added periodically.

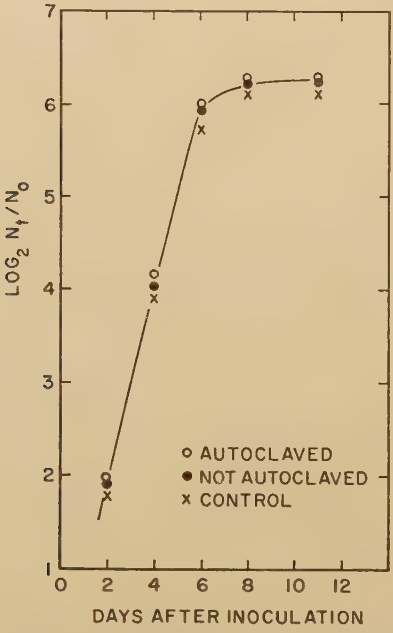

FIGURE 5. Growth of the alga in autoclaved and non-autoclaved algal filtrate.

took place at the following times: three days before inoculation with the alga, at the same time as the alga, two days, four days, seven days, and eleven days after inoculation with the alga.

Bacteria introduced three days before and at the time of inoculation with *Dunaliella* inhibited the growth of the alga (Fig. 3). In all cultures, except the one inoculated with bacteria three days before the alga, growth after fifteen days exceeded that of the control. In Figure 4 cell density and chlorophyll *a* after fifteen days of growth are presented. The greatest number of cells occurred in the culture which was inoculated with bacteria four days after the alga, and those cultures which were inoculated with bacteria prior to this time showed less growth. Less growth was also obtained in the cultures which had been inoculated with bacteria seven and eleven days after inoculation with the alga. However, the cells in the culture inoculated with bacteria seven days after the alga contained more chlorophyll *a* than the other cultures after fifteen days of growth (Table II). These results show that growth of the alga was directly related to the time at which the bacteria were added. Under the conditions of this experiment, chlorophyll *a* synthesis preceded cell division (Fig. 4). The highest concentration of chlorophyll per cell, however, was not as great as that obtained in the previous beef extract-peptone experiment.

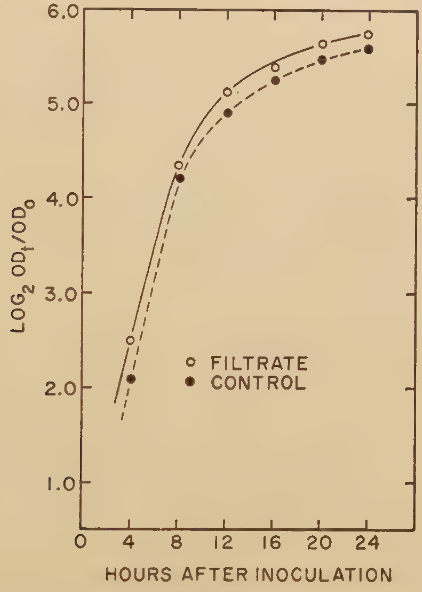

Figure 6. Growth of Woods Hole Harbor bacteria in the algal filtrate containing beef extract and peptone.

4. *Growth of the alga in the algal filtrate.* To determine if auto-inhibitors are produced by *Dunaliella euchlora,* growth of the alga in the ASP medium was compared with growth in the filtrate of a *Dunaliella* culture which had reached maximum density. Part of the filtrate was autoclaved and the other part was not

autoclaved as there has been a suggestion of heat-labile inhibitors (Lefèvre *et al.*, 1952). Nitrogen, phosphorus, and iron were added to all cultures at ASP concentrations. Growth in all cultures was identical as shown by the data in Figure 5. The chlorophyll *a* content per cell was greater in the filtrate cultures than in the control whether or not the filtrate had been autoclaved (Table II). This indicates that the filtrate contained something which enhanced chlorophyll synthesis, but did not promote cell division.

5. *Growth of the bacteria in the algal filtrate.* To determine if *Dunaliella* filtrate would inhibit the growth of bacteria, a filtrate was obtained from a five-day culture of the alga. Beef extract and peptone were added to the filtrate and to the control ASP medium, and inoculated with the previously isolated Woods Hole Harbor bacteria. Growth of the bacteria was measured by optical density at 750 mμ using a Beckman model DU spectrophotometer, and is expressed as $\log_2 OD_t/OD_0$. The growth of the bacteria was approximately the same in the filtrate as in the enriched ASP medium with no suggestion of a bacteriostatic substance produced by the alga (Fig. 6).

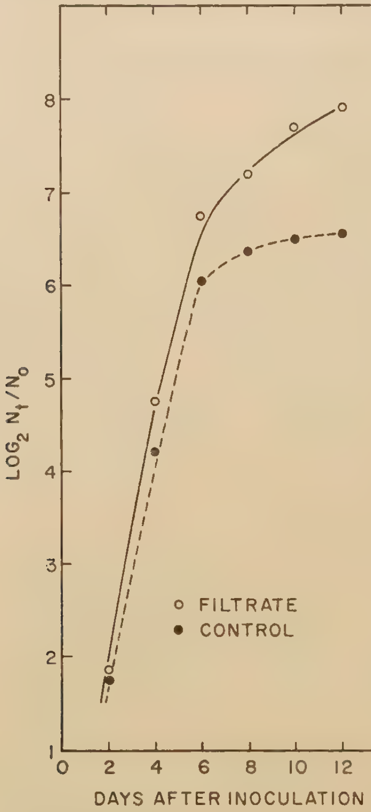

FIGURE 7. Growth of the alga in the Woods Hole Harbor bacteria filtrate.

6. *Growth of the alga in the bacterial filtrate.* To determine the effects of the bacterial filtrate on the growth of *Dunaliella,* a culture of the Woods Hole Harbor bacteria was grown in the ASP medium containing beef extract and peptone. After three days of growth, the culture was passed through a HA millipore filter resulting in a clear filtrate which was autoclaved and inoculated with the alga. There was a considerable increase in the maximum cell density in the filtrate culture as compared with the control (Fig. 7). The inhibition noted in the previous beef extract-peptone experiment where the bacteria had been added to the culture three days before the alga did not occur in this experiment. This suggests that the inhibitory substance is volatile or heat-labile. Pigment analysis also showed the cells in the filtrate culture contained considerably more chlorophyll *a* than those in the control culture (Table II).

Discussion

The addition of beef extract and peptone to bacteria-free cultures of *Dunaliella euchlora* did not stimulate the growth of the alga. In the presence of bacteria, however, a considerable increase in the algal population, as determined by cell counts and chlorophyll analysis, was observed. This increase presumably resulted from the bacterial hydrolysis of the added organic material. The organic additions were not entirely inert to algal metabolism as the amount of chlorophyll *a* per cell in the uncontaminated cultures always exceeded that obtained with only the addition of inorganic salts.

The large amount of synthesis of chlorophyll *a* suggested that the alga was able to utilize nitrogenous breakdown products of the peptone and beef extract. A large fraction of the utilizable nitrogen from the beef extract and peptone was probably present as ammonia, nitrite, or simple organic compounds since the conversion of these to nitrate-nitrogen by marine bacteria is a slow process (Harvey, 1955; Sverdrup *et al.,* 1942). Harvey (1940) and Gibor (1956) observed that several species of *Dunaliella* were able to utilize some amino acids as nitrogen sources. There are also numerous reports of other autotrophic algae capable of utilizing organic nitrogen compounds (Fogg, 1953; Ryther, 1954). In addition, Huzisige *et al.* (1957) found that *Euglena* synthesized chlorophyll more rapidly when provided with casein hydrolysate than when provided with inorganic nitrogen compounds.

Growth of the alga in cultures containing organic additions was inhibited if bacteria were introduced before the alga began to grow. However, no inhibition of the alga was observed in the bacterial filtrate which had been autoclaved. This suggests a volatile or heat-labile inhibitor. Inhibition could have resulted from ammonia which is known to be toxic at low concentrations (Fogg, 1953; Myers, 1951). Any ammonia present in the bacterial filtrate would have been lost during autoclaving, and the inhibition noted in the second beef extract-peptone experiment may have been due to toxic concentrations of ammonia.

In the cultures which developed a heavy suspension of cells and chlorophyll, light and probably carbon dioxide may have been limiting, but organic carbon could have been utilized by the alga. Organic carbon could have been incorporated by the alga simultaneously with the utilization of organic nitrogen (Fogg, 1953; Krauss, 1958), or as separate compounds. If the alga is capable of heterotrophic growth, light would not necessarily be a limiting factor. It seems probable that the very dense cultures obtained in this study may have been due in part to heterotrophic growth.

It was not possible in this study to demonstrate that *Dunaliella* inhibited the growth of bacteria, nor was there any indication of auto-inhibitors produced by the alga. The production of antibiotics by algae may not be a general phenomenon.

The authors wish to express their grateful appreciation to Dr. Bostwick H. Ketchum for his many helpful suggestions in preparing the manuscript.

SUMMARY

1. Bacteria added to cultures of *Dunaliella euchlora* in the presence of nitrogenous organic matter stimulated the growth of the alga, and enhanced the synthesis of chlorophyll *a*.

2. It was not possible to obtain comparable concentrations of chlorophyll *a* by the addition of nitrate-nitrogen, although a comparable number of cells could be obtained.

3. If the bacteria obtained a "head-start" in the enriched cultures, growth of the alga was inhibited. This inhibition could be overcome by autoclaving the filtrate from the bacteria cultures.

4. Growth of the bacteria was not inhibited in the algal filtrate, nor was the growth of the alga inhibited in the algal filtrate.

LITERATURE CITED

CREITZ, G. I., AND F. A. RICHARDS, 1955. The estimation and characterization of plankton populations by pigment analysis. III. A note on the use of "millipore" membrane filters in the estimation of plankton pigments. *J. Mar. Res.*, **14**: 211–216.

DUXBURY, A. C., AND C. S. YENTSCH, 1956. Plankton pigment nomographs. *J. Mar. Res.*, **15**: 92–101.

FOGG, G. E., 1953. The Metabolism of Algae. Methuen and Co., Ltd., London.

GIBOR, A., 1956. The culture of brine algae. *Biol. Bull.*, **111**: 223–229.

GOLDBERG, E. D., T. WALKER AND A. WHISENAND, 1951. Phosphate utilization by diatoms. *Biol. Bull.*, **101**: 274–284.

HARVEY, H. W., 1955. The Chemistry and Fertility of Sea Waters. Cambridge University Press, Cambridge.

HARVEY, H. W., 1940. Nitrogen and phosphorus required for the growth of phytoplankton. *J. Mar. Biol. Assoc.*, **24**: 115–123.

HUZISIGE, H., T. TERADA, M. NISHIMURA AND T. UEMURA, 1957. Effect of amino acids and streptomycin on the chlorophyll formation in *Euglena*. *Biol. J. Okayama Univ.*, **3**: 209–222.

KAIN, J. M., AND G. E. FOGG, 1958. Studies on the growth of marine phytoplankton. I. *Asterionella japonica* Gran. *J. Mar. Biol. Assoc.*, **37**: 397–413.

KRAUSS, R. W., 1958. Physiology of fresh-water algae. *Ann. Rev. Plant Physiol.*, **9**: 207–244.

LEFÈVRE, M., H. JAKOB AND M. NISBET, 1952. Auto. et Hétéroantagonisme chez les Algues d'eau douce. *Ann. de la Stat. Cent. d'Hydrob.*, **4**: 5–198.

McLACHLAN, J., 1959. The growth of unicellular algae in artificial and enriched sea water media. *Canad. J. Microbiol.*, **5**: 9–15.

MYERS, J., 1951. Physiology of the algae. *Ann. Rev. Microbiol.*, **5**: 157–180.

PROVASOLI, L., J. J. A. McLAUGHLIN AND M. R. DROOP, 1957. The development of artificial media for marine algae. *Arch. Mikrobiol.*, **25**: 392–428.

RICHARDS, F. A., WITH T. G. THOMPSON, 1952. The estimation and characterization of plankton populations by pigment analysis. II. A spectrophotometric method for the estimation of plankton pigments. *J. Mar. Res.*, **11**: 156–172.

RYTHER, J. H., 1954. The ecology of the phytoplankton blooms of Moriches Bay and Great South Bay, Long Island, New York. *Biol. Bull.*, **106**: 198–209.

STEEMANN NIELSEN, E., 1955a. An effect of antibiotics produced by plankton algae. *Nature*, **176**: 553.

STEEMANN NIELSEN, E., 1955b. The production of antibiotics by plankton algae and its effect upon bacterial activities in the sea. *Pap. Marine Biol. Oceanogr., Deep-Sea Res. Suppl.*, **3**: 281–286.

STEEMANN NIELSEN E., 1958. Experimental methods for measuring organic production in the sea. *Rapp. Proc. Verb. Cons. Internat. Explor. Mer.*, **144**: 38–46.

STEEMANN NIELSEN, E., AND E. A. JENSEN, 1957. Primary oceanic production. *Galathea Report*, **1**: 49–136.

SVERDRUP, H. U., M. W. JOHNSON AND R. H. FLEMING, 1942. The Oceans, Their Physics, Chemistry and General Biology. Prentice-Hall, Inc., N. Y.

WAKSMAN, S. A., J. L. STOKES AND M. R. BUTLER, 1937. Relation of bacteria to diatoms in sea water. *J. Mar. Biol. Assoc.*, **22**: 359–373.

YENTSCH, C. S., AND R. F. VACCARO, 1958. Phytoplankton nitrogen in the oceans. *Limnol. Oceanogr.*, **3**: 443–448.

Contribution No. 1011

Reprinted from SCIENCE, May 22, 1959, Vol. 129, No. 3360, pages 1428–1429.

Metabolically Induced Precipitation of Trace Elements from Sea Water

Abstract. The presence of organic material in some manganese-rich nodules suggests that the nodules are of biological origin. This suggestion leads to the proposal that in sea water, heavy metals get protection from hydrolysis by organic complexing; parts of these complexes become metabolized, the remaining parts then precipitate. These processes would explain a number of interesting observations.

Two recent detailed papers (*1*, *2*) discuss from the physicochemical standpoint the genesis of the commonly found (*3*) manganese-rich deposits on the sea floor. Adequate consideration has never been given, however, to the possibility that these deposits stem from biological processes.

I have recently been examining some typical manganese-rich nodules from the Blake Plateau (collected in August 1957 at latitude 30° 51′N, longitude 78° 27′W in about 400 fathoms) and have succeeded in finding in them a fraction of a percent of organic material. A crushed and ground nodule, when rinsed with distilled water (*p*H 7), yields a bright yellow solution with *p*H about 4. If this solution is acidified, the color is eliminated. Ethyl acetate extracts from this colorless solution a fraction which can be recovered, by extraction into a weakly ammoniacal solution, and which then becomes yellow. Paper chromatography of this solution reveals at least three components. Extraction of the nodule with 7*N* NH_4OH yields further organic material which can be charred by heating it in an open dish. Some material having free amino groups has been detected with Ninhydrin. A further organic fraction can be extracted with 95 percent ethyl alcohol.

This organic material might have been adsorbed from sea water during the inorganic process of deposition of the trace elements, or alternatively, it could be accounted for directly if bottom-dwelling organisms are the agents by which the nodules are made. A nonphotosynthetic organism would be required for the latter interpretation, since manganese-rich deposits have been found throughout the depths of the oceans. A nonchemosynthetic organism also seems to be required by the fact that the deposits are found at all depths where adequate oxygen is available. Food would have to be derived from the several milligrams per liter of organic material that are present in sea water at most depths. The composition of this material is poorly known, but tyrosine analysis of hydrolyzed sea water assays this amino acid at a fraction of a milligram to a few milligrams per liter (*4*); many others should be present in comparable amounts. These amino acids and protein-derived compounds could serve as a valuable part of the nutrients of a great variety of organisms; if they were an important part, slow growth would be required for life on this starvation diet.

It is well known that by various types of chemical bonding, amino acids, peptides, and proteins form complex molecules with numerous metallic ions (*5*). Some of these complexes are sufficiently stable that the usual properties of the metallic ions in solution become effectively masked, and it is then impossible to treat their chemistry by the usual rules of solubility, *p*H sensitivity, and so forth, that apply to the simple inorganic ions in dilute solution. Many of these complexes are so stable that it seems quite certain that they must exist in sea water if the proper ingredients are available.

Unfortunately, not enough is yet known to predict, with assurance, the metabolic fate of such complex compounds in biological systems. We may suppose, however, if bottom-dwelling organisms feeding on these complexes in the sea water are responsible for deposition of manganese and iron hydroxide along with appreciable quantities of numerous other trace elements, that these organisms are able to metabolize the organic part of the complex molecule and reject the inorganic part. It can be imagined that by this process a concentration of inorganic ions is built up within or in the neighborhood of the living organisms. The ions, freed of their organic complexing agent which protected them from hydrolysis, then precipitate as hydroxides in the sea water. The metabolic processes of the organisms might not be able to compete successfully with all reactions involved in forming especially stable complexes, but it would seem from the variety of trace elements present in these deposits that complexes of appropriate stability are common.

From this hypothesis, a number of inferences can be drawn.

1) If manganese-rich deposits are being formed today by living biological agents, it should be possible to detect metabolic activity in fresh samples. A generation time of about 2 weeks is suggested by calculations based on the following assumptions: rate of deposition, 1 mm/1000 years; organism 1 μ thick having the same composition as *Escherichia coli*; 2 moles of amino acid used per mole of manganese deposited. Faster deposition, as advocated by Goldberg and Arrhenius (*2*), would reduce the generation time proportionally.

2) If temperature has no limiting effect on quality or quantity of nutrients, then, as in any other biological system, there should be an optimum growth temperature.

3) If the rate of growth is solely a function of the rate at which nutrients are supplied by the moving bottom currents, then it should be possible to recognize differences in abundances in areas swept by currents and in areas where the currents are known to be minimal. On a small scale, this effect might be detected by detailed examination of the geometry of individual samples.

4) If the various organic complexes that provide material for trace-element deposition have a sharp inverse dependence of their stability on temperature, then, in general, the detailed composition of the deposits should become simpler with increased temperature of formation.

5) Elements that do not form organic complexes or that already are strongly complexed inorganically will be missing from the deposits.

6) If it is correct that complex molecules are required for trace-element deposition on the sea floor, then their importance in other chemical and biological processes in the sea is to be expected.

This hypothesis affords plausible explanations for a number of well-established facts about the manganese-rich deposits of the sea floor. (i) A mechanism is provided for effecting vast concentration of a wide variety of trace elements from sea water. Fluctuations in composition reflect changes in the nutrients. (ii) The concentrated product is poorly organized crystallographically, partly because of the variety of elements in it, but more particularly because of the manner of disperse formation on a minute size-scale basis. (iii) From an analysis of the Challenger Expedition report (*6*) it is seen that the probability of finding manganese-rich deposits is high (.45) in water between 34° and 38°F and low (.076) in water that is now warmer than 38°F; no manganese nodules can be identified in the hundreds of photographs (*7*) of the Mediterranean and Red Sea floors where the temperatures are about 56° and 72°F, respectively. Such findings are consistent with the needs of an organism living on a starvation diet. Deposits of this type are thus naturally associated with an ice age. (The deposits on the Blake Plateau where the bottom temperature is now 45°F may no longer be increasing.) (iv) The presence of extensive adherent coatings of manganese-rich deposits on basic igneous rocks and their scarcity on lime, and, in nodules, the common nuclei of sharks' teeth, earbones of whales, fragments of previous nodules, and so forth, merely reflect the needs of the organisms for certain types of materials on which to attach (*8, 9*).

Note added in proof: In *Nature* (in press), J. W. Graham and S. C. Cooper give additional evidence bearing on the hypothesis of this report.

JOHN W. GRAHAM
Woods Hole Oceanographic Institution, Woods Hole, Massachusetts

References and Notes

1. E. D. Goldberg, *J. Geol.* 63, 249 (1955).
2. E. D. Goldberg and G. O. S. Arrhenius, *Geochim. et Cosmochim. Acta* 13, 153 (1958).
3. H. W. Menard and C. J. Shipek, *Nature* 182, 1156 (1958).
4. W. W. Anderson and J. E. Gehringer, *U.S. Fish Wildlife Service Spec. Sci. Rept. Fisheries No. 265* (1958).
5. F. R. N. Gurd and P. E. Wilcox, *Advances in Protein Chem.* 11, 311 (1956).
6. J. Murray and H. F. Renard, "Deep-Sea Deposits," *Challenger Expedition Rept.* (London, 1891).
7. H. E. Edgerton, J. Cousteau, D. M. Owen, J. W. Graham, unpublished results.

8. This work was supported, in part, by contract Nonr-2196 with the Office of Naval Research. It is a pleasure to acknowledge that my former colleagues at the Department of Terrestrial Magnetism of the Carnegie Institution of Washington had a strong and direct influence on this synthesis.
9. This report is contribution No. 1011 from Woods Hole Oceanographic Institution.

15 December 1958

Contribution No. 1012

SPHERICAL VORTEX THEORY OF BUBBLE-LIKE MOTION IN CUMULUS CLOUDS[1,2]

By Joseph Levine

Woods Hole Oceanographic Institution

(Original manuscript received 6 January 1959; revised manuscript received 25 April 1959)

ABSTRACT

The bubble concept is here put on a more quantitative basis by approximating the buoyant bubble in a cloud by a spherical vortex. The approximate solution of the equations of motion is made with the aid of "Hill's Spherical Vortex" as described by Lamb (1932). In the solution as presented here, two arbitrary parameters representing the aerodynamic interaction and the mass exchange of the bubble with the surrounding air are introduced. Qualitative features of the motion are independent of the parameter values.

The effects of entrainment on the motion are determined by a refined application of Stommel's method (1947, 1951) of computing entrainment. The solution of the problem, therefore, is given in terms of integrated differential equations which for given values of the arbitrary parameters, environmental potential temperature and specific humidity, and initial conditions yield the bubble velocity and potential temperature as a function of height.

Specific applications of the solution are made to bubble motions in a saturated and an unsaturated environment.

1. Introduction

Ideas concerning the nature of cumulus-cloud convection have evolved from simple stability analyses based on the state of a hypothetical parcel moved upward adiabatically to the present-day bubble concept. The present-day bubble notion is actually a more complex version of the original parcel idea in which account is taken of interaction with the environment. Thus, it appears that the evolution of thought concerning cumulus convection has made a complete circle by way of the steady-state jet concept linked with entrainment back to a bubble or modified parcel concept.

The meteorological implications of the atom-bomb theory of Taylor (1950) and the bubble theory of Davies and Taylor (1950) appear to have their beginnings in a paper by Sutton (1947). The bubble concept has been further elaborated in various papers (Scorer and Ludlam, 1953a, b; Malkus and Scorer, 1955; Scorer, 1957). In this paper, an attempt is made to put the bubble concept on a more quantitative basis so that it can be compared with the more detailed cumulus-cloud observations now being made with aircraft. The treatment of the problem here puts a greater emphasis than in earlier papers on the existence of a vortex ring within the hypothetical bubble. Then the problem is idealized sufficiently so that the steady-state solution of the inviscid-fluid-flow equations in terms of Hill's "spherical vortex" as described by Lamb (1932) may be applied approximately.

The entrainment ideas of Stommel (1947, 1951) are adapted in differential form so that the bubble's interaction with its environment is taken into account. The viscous drag on the bubble is approximated in terms of the form drag of an equivalent solid sphere and the mass exchange resulting from entrainment.

The descriptive aspect of cumulus-cloud convection in terms of the bubble concept as generally treated in the literature is largely accepted here. Briefly, the physical picture of the visible cumulus cloud may be described as a relatively large diffuse mass of liquid-water droplets slowly mixing with the environment and evaporating. The portion of the cloud in which no strong updrafts are occurring may be considered to be inactive. The inactive portion may be cooler than the environment and therefore negatively buoyant with respect to the clear environment.

The existence of bubble-like entities has been inferred from observation of time-lapse motion pictures. The inactive mass of the cloud at lower levels is characterized by fuzzy boundaries, but the towers which shoot up from the fuzzy mass appear sharply defined. The cauliflower-like appearance of cumulus-cloud tops has led to the inference that these bubbles have nearly spherical tops. The towers are considered to be bubbles which have escaped the protective environment of the fuzzy mass.

The bubble is considered to be protected from the cooling effects of evaporation while immersed in the inactive cloud. When the bubble penetrates the inac-

---

[1] The research done in this report has been carried out under U. S. Weather Bureau Contract CWB9241.

[2] Contribution No. 1012 from the Woods Hole Oceanographic Institution.

tive cloud top, it appears as a bulge or tower which rapidly loses its buoyancy in the clear air and gradually evaporates completely or becomes part of the inactive cloud mass.

The cloud base may be considered the principal source of bubbles. Turbulent motions in the subcloud layer may cause isolated bubbles of relatively warm air to start upwards through the inactive cloud mass. Although there is no theoretical justification for considering these bubbles to have a spherical leading surface as in the case of air bubbles in a liquid, the irregular shape of a bubble or parcel of buoyant air is probably most closely approximated by a sphere rather than any other regular solid figure. Therefore, in the analysis contained in this paper, the bubble is assumed to be spherical.

2. Mathematical theory

The equations of motion in the coordinate system stationary relative to the earth of a spherical bubble may be written as

$$\left.\begin{aligned} \frac{dM(W+w)}{dt} &= -\frac{M}{\rho}\frac{\partial P}{\partial z} - Mg + MF_z \\ \frac{dMu}{dt} &= -\frac{M}{\rho}\frac{\partial p}{\partial \omega} + \mathrm{MF}_\omega \end{aligned}\right\}; \quad (1)$$

the equation of motion of the air outside the bubble must then be

$$\left.\begin{aligned} \frac{dw}{dt} &= -\frac{1}{\rho_0}\frac{\partial P}{\partial z} - g + F_{0z} \\ \frac{du}{dt} &= -\frac{1}{\rho_0}\frac{\partial p}{\partial \omega} + F_{0\omega} \end{aligned}\right\}. \quad (2)$$

The variables are W, the vertical velocity of the bubble's center of mass; w, the vertical velocity relative to the center of mass inside and relative to the earth outside the bubble; u, the horizontal velocity in either frame of reference; $P = P_0 + p$, the total pressure (P_0 the hydrostatic and p the aerodynamic pressure); ρ, the density; M, the bubble mass; F_z and F_ω, the frictional force components per unit mass; z, the vertical coordinate directed upward; ω, the horizontal coordinate referred to the vertical axis of the bubble; and t, the time. The subscript 0 is used to refer to the environment. The densities ρ and ρ_0 are assumed to be different but functions of z only. Thus, the density is assumed to be discontinuous at the bubble surface.

By use of the hydrostatic equation, the equations of motion in the vertical become

$$\frac{dM(W+w)}{dt} = -\frac{M}{\rho}\frac{\partial p}{\partial z} + Mg\left(\frac{\rho_0 - \rho}{\rho}\right) + MF_z \quad (3)$$

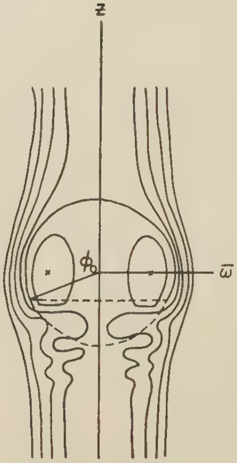

FIG. 1. Streamlines about a spherical bubble showing a qualitative picture of the wake behind it.

and

$$\frac{dw}{dt} = -\frac{1}{\rho_0}\frac{\partial p}{\partial z} + F_{0z}. \quad (4)$$

Then take the average value of equation (3) so that

$$\frac{dMW}{dt} = Mg\left(\frac{\rho_0 - \rho}{\rho}\right) + M\bar{F}_z. \quad (5$$

Now subtract equation (5) from equation (3) to obtain

$$\frac{dMw}{dt} = -\frac{M}{\rho}\frac{\partial p}{\partial z} + M(F_z - \bar{F}_z)$$

which is the equation for the interior motion of the bubble.

For the analysis of the internal motion of the bubble, $w(dM/dt)$ may be assumed small compared to $M(dw/dt)$ so that the above equation reduces to

$$\frac{dw}{dt} = -\frac{1}{\rho}\frac{\partial p}{\partial z} + F_z - \bar{F}_z. \quad (6)$$

The viscous forces in the interior of the bubble are considered negligible compared to the effects of turbulence at the surface of the bubble and in the wake behind it. The layer at the surface to an angle ϕ_0 with the z axis (see fig. 1) may be assumed to be a discontinuity in the shear as well as density, since the turbulence is very likely confined to a thin layer the thickness of which is small compared to the radius of the bubble. Below the surface represented by the dashed line in fig. 1, the average aerodynamic pressure p is assumed to drop to zero in the turbulent wake of the bubble.

Therefore, in the bubble interior above the plane $z = z_0$ the viscous force term $F_z - \bar{F}_z$ in equation (6) may be neglected. Then the stream functions for Hill's spherical vortex define the flow approximately if $\partial w/\partial t$ is small compared to $u(\partial w/\partial \omega) + w(\partial w/\partial z)$ above the plane $z = z_0$. The stream functions are given by the equations

$$\psi = -\frac{3}{4}\frac{W}{a^2}\omega^2(a^2 - r^2) \tag{7}$$

inside the bubble and

$$\psi = \tfrac{1}{2}W\omega^2\left(1 - \frac{a^3}{r^3}\right) \tag{8}$$

outside where a is the bubble radius. The corresponding velocity components are

$$\left.\begin{aligned} u &= \frac{1}{\omega}\frac{\partial\psi}{\partial z} = \frac{3}{2}\frac{W}{a^2} r^2 \sin\phi\cos\phi \\ w &= -\frac{1}{\omega}\frac{\partial\psi}{\partial\omega} = \frac{3}{2}\frac{W}{a^2}(a^2 - r^2 - r^2\sin^2\phi) \end{aligned}\right\} \tag{9}$$

inside the bubble and

$$\left.\begin{aligned} u &= \frac{3}{2}\frac{Wa^3}{r^3}\sin\phi\cos\phi \\ w &= \frac{Wa^3}{r^3}(1 - \tfrac{3}{2}\sin^2\phi) \end{aligned}\right\} \tag{10}$$

outside the bubble. Note that the stream functions and velocities as given in equations (7) to (10) are in the bubble center of mass coordinate system inside the bubble and in the earth system outside the bubble.

The corresponding aerodynamic pressure as a function of ϕ at $r = a$ the bubble surface is

$$p = \frac{9}{8}\rho_0 W^2\cos^2\phi \tag{11}$$

if the small difference of density is ignored. The resultant vertical component of force on the bubble if p drops to zero for $z < z_0$ is

$$(\text{external drag force}) = \tfrac{9}{16}\pi\rho_0 W^2 a^2(\cos^4\phi_0 - 1).$$

The corresponding drag coefficient which has been used in the literature is

$$C_D = \frac{9}{8}(1 - \cos^4\phi_0).$$

In addition, the drag due to turbulent mass exchange between the bubble and its environment may be written as

$$(\text{surface drag force}) = -\left[\left(\frac{dM}{dt}\right)_+ + \left(\frac{dM}{dt}\right)_-\right]W$$

where $(dM/dt)_+$ is the mass flux into the bubble and $(dM/dt)_-$ is the mass flux out. The total friction drag is then

$$M\vec{F}_z = -\left[\left(\frac{dM}{dt}\right)_+ + \left(\frac{dM}{dt}\right)_-\right]W - \tfrac{1}{2}C_D\pi\rho_0 W^2 a^2. \tag{12}$$

The mass fluxes $(dM/dt)_+$ and $(dM/dt)_-$ may be computed in terms of the downward mass flux through the $z = 0$ plane (bubble frame of reference);

$$(\text{downward mass flux}) = \tfrac{3}{8}\pi\rho W a^2.$$

Let

$$\left.\begin{aligned} \left(\frac{dM}{dt}\right)_- &= \tfrac{3}{8}K_1\pi\rho W a^2 \\ \text{and}\quad \left(\frac{dM}{dt}\right)_+ &= \tfrac{3}{8}K_2\pi\rho_0 W a^2 \end{aligned}\right\} \tag{13}$$

where K_1 is the fraction of the downward flux transferred out to the environment and K_2 is the fraction of the upward flux transferred in from the environment.

$$\begin{aligned} \frac{dM}{dt} = \left(\frac{dM}{dt}\right)_+ - \left(\frac{dM}{dt}\right)_- &= \frac{3}{8}\left(\frac{K_2\rho_0 - K_1\rho}{\rho}\right)\pi\rho W a^2 \\ &\simeq \tfrac{3}{8}(K_2 - K_1)\pi\rho W a^2. \end{aligned} \tag{14}$$

The physical meaning of the mixing parameters K_1 and K_2 may best be understood by considering extremes in their values. If $K_1 = K_2 = 0$, then there is no entrainment. If $K_1 = K_2 = 1$, then the bubble has a complete exchange of mass with the environment during one half a complete cycle of the bubble's average circulation. If $K_2 > K_1$, then the bubble mass is increasing. The opposite is true if $K_2 < K_1$.

Equation (5) may now be written as

$$\frac{dW}{dt} = g\frac{\theta - \theta_0}{\theta_0} - \tfrac{3}{8}(\tfrac{3}{2}K_2 + C_D)\frac{W^2}{a} \tag{15}$$

where θ is the potential temperature.

The equations for the conservation of mixing ratio x and potential temperature θ may be expressed as

$$\left.\begin{aligned} \frac{dMx}{dt} &= x_0\left(\frac{dM}{dt}\right)_+ - x\left(\frac{dM}{dt}\right)_- - M\left(\frac{dx}{dt}\right)_c \\ \frac{dM\theta}{dt} &= \theta_0\left(\frac{dM}{dt}\right)_+ - \theta\left(\frac{dM}{dt}\right)_- + M\left(\frac{d\theta}{dt}\right)_c \end{aligned}\right\} \tag{16}$$

where the subscript c represents changes due to evaporation or condensation. The following relation also holds:

$$\left(\frac{d\theta}{dt}\right)_c = \frac{L}{C_p}\left(\frac{dx}{dt}\right)_c \tag{17}$$

where L is the latent heat of vaporization of water and C_p is the specific heat of air at constant pressure.

Then, by equations (13) and (14), it follows that

$$\frac{dx}{dt} = -\frac{9}{32}K_2\frac{W}{a}\Delta x - \left(\frac{dx}{dt}\right)_c \tag{18}$$

$$\frac{d\theta}{dt} = -\frac{9}{32}K_2\frac{W}{a}\Delta\theta + \frac{L}{C_p}\left(\frac{dx}{dt}\right)_c \tag{19}$$

where $\Delta x = x - x_0$ and $\Delta\theta = \theta - \theta_0$.

Now it is desirable to have equations differentiated with respect to z or p rather than t, since θ, x, and W are observed as functions of z or p. Therefore, the following transformation of the d/dt operator is made;

$$\frac{d}{dt} = W\frac{d}{dz}.$$

Then equations (15), (18), and (19) become

$$\frac{d}{dz}W^2 = 2g\frac{\Delta\theta}{\theta_0} - G\frac{W^2}{a} \tag{15$'$}$$

$$\frac{dx}{dz} = -\frac{H}{a}\Delta x - \left(\frac{dx}{dz}\right)_c \tag{18$'$}$$

$$\frac{d\theta}{dz} = -\frac{H}{a}\Delta\theta + \frac{L}{C_p}\left(\frac{dx}{dz}\right)_c \tag{19$'$}$$

where $H = \frac{9}{32}K_2$ and $G = \frac{3}{4}(\frac{3}{2}K_2 + C_D)$.

In addition to these equations, x must be known as a function of θ and z. This can be determined at least numerically from meteorological thermodynamic charts. To do this, the following relation is written with the intention of evaluating the partial derivatives from a thermodynamic chart:

$$\frac{dx}{dz} = \alpha + \beta\frac{d\theta}{dz} \tag{20}$$

where $\alpha = -g\rho(\partial x/\partial p)_\theta$ and $\beta = (\partial x/\partial\theta)_p$. The coefficients α and β are considered to apply to a saturated atmosphere. Since the bubble and environment static pressures are the same, the bubble specific humidity may be written approximately as

$$x = x_{0s} + \beta\Delta\theta. \tag{21}$$

Then, in general, when the bubble environment is unsaturated,

$$\Delta x = x_{0s} - x_0 + \beta\Delta\theta = \Delta x_s + \beta\Delta\theta, \tag{22}$$

where x_{0s} is the saturation specific humidity of the environment and

$$\Delta x_s = x_{0s} - x_0.$$

With the aid of equations (20) and (22), both dx/dz and Δx may be eliminated from equation (18′). Then the resulting equations may be used to eliminate $(dx/dz)_c$ from equation (19′) with the result that

$$\frac{d\Delta\theta}{dz} + \frac{H}{a}\Delta\theta = -\frac{d\theta_0}{dz} - \frac{\alpha + \frac{H}{a}\Delta x_s}{\beta + \frac{C_p}{L}}. \tag{23}$$

A differential equation for a may be derived from equation (14) of the form

$$\frac{da}{dz} + \frac{a}{3}\frac{d\ln\rho_0}{dz} = \tfrac{3}{32}(K_2 - K_1). \tag{24}$$

Equations (15′), (23), and (24) are the system of equations to be integrated in order to find W, $\Delta\theta$, and a as functions of z. The integrations may be made by multiplying with appropriate integration factors. The following equations are the result:

$$a = \left(\frac{\rho_0}{\rho_{01}}\right)^{-\frac{1}{3}}\left[a_1 + \tfrac{3}{32}(K_2 - K_1)\int_0^z\left(\frac{\rho_0}{\rho_{01}}\right)^{\frac{1}{3}}dz\right], \tag{25}$$

$$\Delta\theta = e^{-\xi}\Delta\theta_1 - e^{-\xi}\int_0^z\left[\frac{d\theta_0}{dz} + \frac{\alpha + \frac{H}{a}\Delta x_s}{\beta + \frac{C_p}{L}}\right]e^{\xi}dz, \tag{26}$$

and

$$W^2 = e^{-\eta}W_1^2 + 2ge^{-\eta}\int_0^z e^{\eta}\frac{\Delta\theta}{\theta_0}dz \tag{27}$$

where

$$\xi(z) = H\int_0^z\frac{dz}{a}$$

and

$$\eta(z) = G\int_0^z\frac{dz}{a}$$

and the subscript 1 is used to signify the initial value of a variable. The initial level is taken to be at $z = 0$. For a bubble in a saturated environment, $\Delta x_s = 0$.

Equation (26) may be considerably simplified by introduction of the moist adiabatic potential temperature θ_m of the moist adiabat through the cloud-base pressure of the environment sounding which can easily be read from a thermodynamic chart. For a bubble not mixing with the environment, $K_2 = K_1 = 0$ and equation (26) therefore becomes

$$\Delta\theta = \Delta\theta_1 - \int_0^z\left[\frac{d\theta_0}{dz} + \frac{\alpha}{\beta + \frac{C_p}{L}}\right]dz = \theta_m - \theta_0$$

or

$$\frac{d\theta_m}{dz} = -\frac{\alpha}{\beta + \frac{C_p}{L}}.$$

Then equation (26) reduces to

$$\Delta\theta = e^{-\xi}\Delta\theta_1 + e^{-\xi}\int_0^z e^{\xi}\frac{d(\theta_m - \theta_0)}{dz}\,dz - He^{-\xi}\int_0^z \frac{e^{\xi}\Delta x_s dz}{a\left(\beta + \dfrac{C_p}{L}\right)}. \qquad (28)$$

Some approximate computations may be made to illustrate the behavior of $\Delta\theta$ and W in a saturated environment in the altitude interval 600 to 2000 m where undisturbed trade cumuli usually occur. For a bubble starting at 600 m (cloud base), the increase in bubble radius due to density decrease alone is only about 5 per cent. Therefore, for a discussion of undisturbed trade cumuli limited by a definite trade-wind inversion, the variation of the radius may be neglected. Also, if $K_1 = K_2 = K$ is assumed, then the effect of entrainment on bubble radius may be neglected. In addition, let $\gamma = d(\theta_m - \theta_0)/dz$ be a constant. Then, with $\Delta\theta_1 = W_1 = 0$, equations (28) and (27) assume the form

$$\Delta\theta = \frac{\gamma a}{H}(1 - e^{-Hz/a}) \qquad (29)$$

$$W^2 = \frac{2g\gamma a^2}{\bar{\theta}_0(G - H)}\left(\frac{1 - e^{-Hz/a}}{H} - \frac{1 - e^{-Gz/a}}{G}\right). \qquad (30)$$

The equations for $\Delta\theta$ and W^2 may be written in the following form for convenience in graphing and making calculations:

$$\Delta\theta = \gamma a F_1(z/a, H)$$

$$W^2 = \frac{g\gamma a^2}{\bar{\theta}_0} F_2(z/a, G, H)$$

where

$$F_1 = \frac{1}{H}(1 - e^{-Hz/a}) \qquad (H \neq 0)$$

$$F_2 = \frac{2}{G - H}\left(F_1 - \frac{1 - e^{-Gz/a}}{G}\right) \qquad (G \neq 0, H \neq 0)$$

$$F_1 = z/a \qquad (H = 0)$$

$$F_2 = \frac{2}{G^2}\left(G\frac{z}{a} - 1 + e^{-Gz/a}\right) \qquad (G \neq 0, H = 0)$$

$$F_2 = \frac{2}{H^2}\left(\mathrm{H}\frac{z}{a} - 1 + e^{-Hz/a}\right) \qquad (G = 0, H \neq 0)$$

$$F_2 = (z/a)^2 \qquad (G = H = 0).$$

Graphs of F_1 and $\sqrt{F_2}$ are given for $C_D = 9/8$, and 0 in figs. 2, 3, and 4. With the aid of these graphs, comparisons can be made with observations to see how closely observed temperatures and motions conform to theory and to arrive at reasonable values of the constants K and C_D.

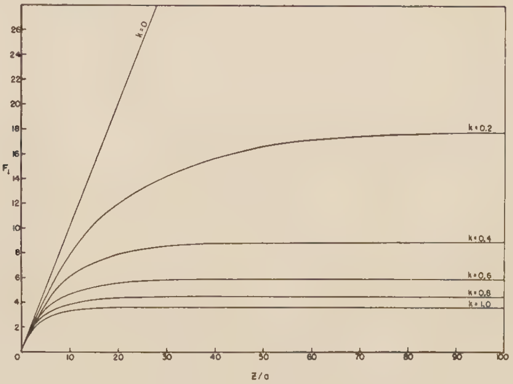

FIG. 2. F_1 as a function of z/a for various values of K.

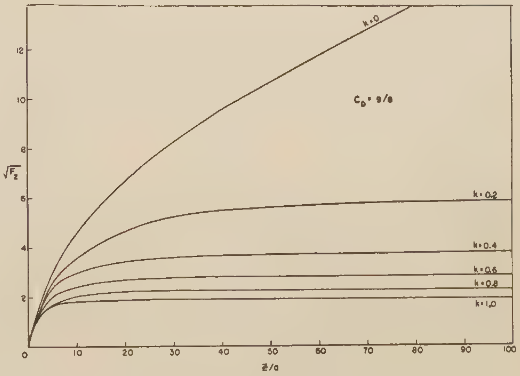

FIG. 3. $\sqrt{F_2}$ as a function of z/a for various values of K and $C_D = 9/8$.

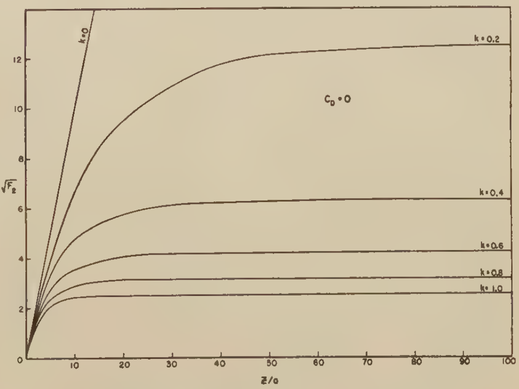

FIG. 4. $\sqrt{F_2}$ as a function of z/a for various values of K and $C_D = 0$.

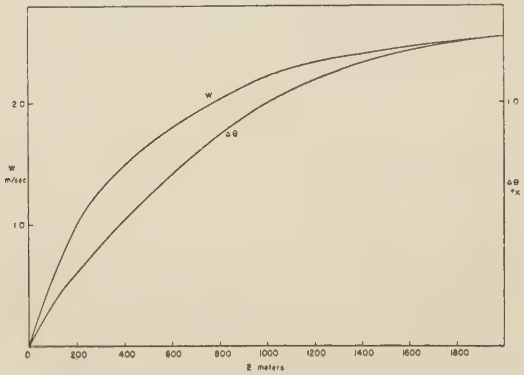

FIG. 5. W and $\Delta\theta$ as a function of z the altitude above cloud base of a bubble of radius $a = 100$ m.

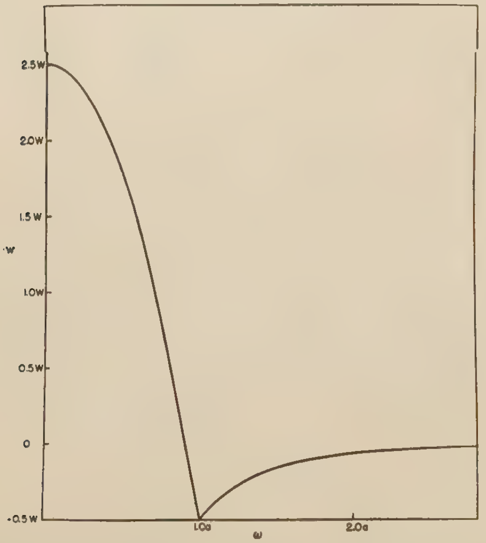

FIG. 6. Theoretical curve of vertical velocity w relative to the earth against ω along a horizontal line passing through the bubble center.

3. Numerical results for saturated bubble environment

For purposes of approximate computation, a typical well developed trade-cumulus-cloud system may be considered to have its base at 600 m and its highest tower tops at 2600 m. The coefficients of F_1 and $\sqrt{F_2}$ may be evaluated in terms of a, H, G, and γ. A typical value of $\gamma = 1.8 \times 10^{-5}\ K\ \text{cm}^{-1}$ and $\bar{\theta}_0 = 293\ K$ may be assumed. For example, if a bubble radius $a = 100$ m is assumed, then $\Delta\theta$ and W as a function of z may be found for various values of K and C_D. Plausible values of $K = 0.4$ and $C_D = 9/8$ may be assumed to illustrate hypothetical bubble behavior. The resulting curves of W and $\Delta\theta$ as functions of z are given in fig. 5.

A rough comparison of theory with observation may be made in the case of some observed updrafts. The comparisons have only order-of-magnitude significance, since the line of flight must be assumed to pass through the center of the bubble. The bubble diameter is assumed to be the distance between the two velocity minima on either side of the velocity peak. According to the theory, W is 2/5 of the peak updraft velocity if the line of flight is right through the bubble center (see fig. 6). Temperature excesses are taken with respect to the immediate environment, since wetting of the temperature element by rain or large cloud drops may cause a fictitious temperature decrease with respect to the air outside of the cloud due either to lower drop temperature or evaporation. Some typical values from data taken during field trips on 15 November 1957 and 24 February 1958 are tabulated in table 1.

TABLE 1. A comparison of observed and computed values of $\Delta\theta$ and $\frac{5}{2}W$ for several cloud updrafts.

		Observed		Computed	
z	a	$\Delta\theta$	$\frac{5}{2}W$	$\Delta\theta$	$\frac{5}{2}W$
100 m	400 m	0.6	1.5 m/sec	0.16	1.6 m/sec
100	120	0.3	0.7	0.15	1.5
100	180	0.3	0.9	0.16	1.6
1000	1000	2.0	8.8	1.6	14.3

In view of the assumed value of γ, the difficulty of measuring air temperature in a cloud, the uncertainty in position of line of flight with respect to bubble center, and the assumed values of K and C_D, the comparison of observed and computed values is encouraging.

4. Bubbles rising from cloud base to tropopause

When the trade-wind inversion usually located at 2000 m or somewhat higher is weak or absent as during the passage of a tropical disturbance, conditions are favorable for convection to occur up to the tropopause. The process may be envisioned as the building up by a rapid succession of bubbles of a saturated region about several kilometers in horizontal diameter extending up to about the 600-mb (4500-m) level. Then, finally, a bubble about one km in diameter starts at cloud base and bursts through the top of the saturated region with enough energy derived from condensation to survive the journey to the tropopause through an unsaturated environment or, possibly, an almost saturated region is developed by a succession of bubbles penetrating to greater and greater heights until finally a tower reaches the tropopause (Harrington, 1958).

It is possible to compute a, $\Delta\theta$, W exactly for a hypothetical bubble of initial radius a, and assumed values of K_1, K_2, and C_D by numerical integration of equations (25), (27), and (28). In the actual application of these equations, due to lack of any observational or theoretical indication of the values of the parameters K_1, K_2, and C_D, a detailed numerical integration is not of any greater value than a less exact easier method.

Calculations have been made on the basis of two soundings, one at San Juan which has been used by Malkus and Ronne (1954) in connection with pictures taken of cumulus clouds which nearly reached the tropopause and another at Wake Island which coincided with cumulus development observed there by Malkus and Ronne. The results of these calculations are contained in figs. 7 and 8.

The approximate computations were made in a manner such as to avoid the necessity for numerical integration. The particular soundings used lent themselves to division into three or four regions each with a constant value of γ. These regions were limited enough in range of z so that an average value of a could be taken allowing approximately for increasing radius with decreasing density as z increases. As in the above calculations for trade cumulus, $K_1 = K_2 = K$ was assumed so that no expansion of a due to entrainment was included.

The calculations were made for both a saturated and unsaturated environment. For the case of an unsaturated environment, an approximate empirical relation for

$$\gamma = \frac{\Delta x_s}{\beta + \dfrac{C_p}{L}}$$

was found of the form

$$y = y_1 e^{-\lambda z}$$

where $\lambda = 2.4 \times 10^{-6}$ cm^{-1}. The above empirical equation was fitted to the Wake Island sounding above 4500 m and also used for the San Juan sounding to demonstrate the effect of a relatively dry environment.

With the assumptions outlined above, simplified forms of equations (27) and (28) are obtained as follows:

$$\Delta\theta = A + Be^{-Hz/a} - Ce^{-\lambda z}$$

$$W^2 = A' + B'e^{-Hz/a} - C'e^{-\lambda z} - (A' + B' - C' - W_1^2)e^{-Gz/a}$$

where

$$A = \gamma a/H, \quad B = \Delta\theta_1 - \frac{\gamma a}{H} + \frac{y_1}{1 - \lambda \dfrac{a}{H}}, \quad C = \frac{y_1}{1 - \lambda \dfrac{a}{H}}$$

$$A' = 2gaA/\bar{\theta}_0 G, \quad B' = 2gaB/\bar{\theta}_0(G - H),$$
$$C' = 2gaC/\bar{\theta}_0(G - \lambda a).$$

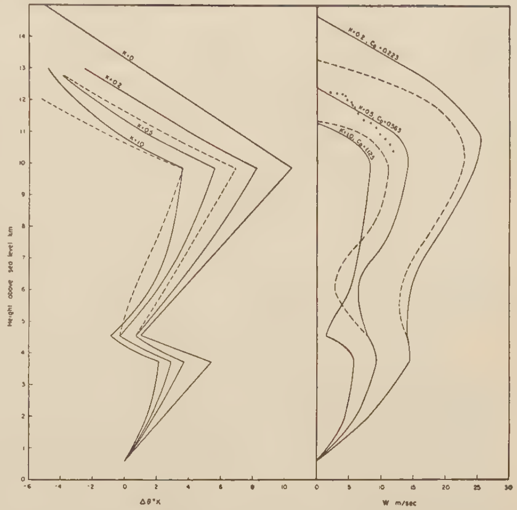

FIG. 7. Computed curves of $\Delta\theta$ and W for San Juan sounding of 1500Z, 1 April 1953. Solid lines represent results for saturated environment and dashed lines results for environment with relative humidity of 30 per cent above 4500 m. The circles represent observed values of W.

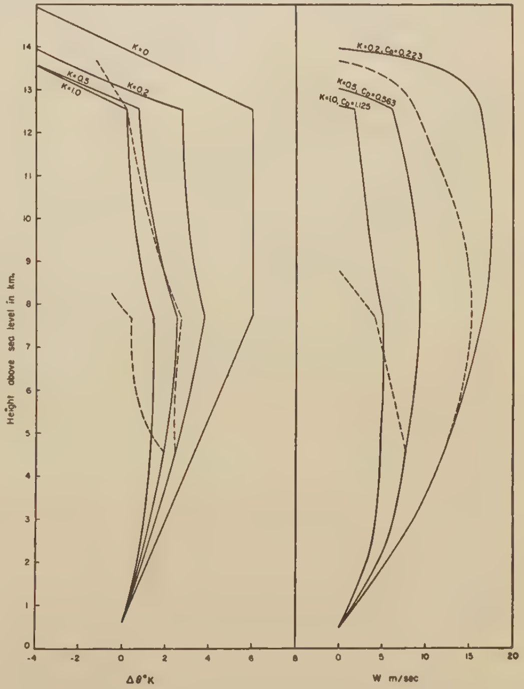

FIG. 8. Computed curves of $\Delta\theta$ and W for Wake Island sounding of 0000Z, 18 August 1957. Solid and dashed lines have same meaning as in fig. 7.

For the special case $\lambda a/H \simeq 1$,

$$\Delta\theta = A + Be^{-Hz/a} - H\gamma_1 \frac{z}{a} e^{-Hz/a}$$

$$W^2 = A' + \left(B' + \frac{H'}{G-H}\right) e^{-Hz/a} - H' \frac{z}{a} e^{-Hz/a}$$
$$- \left(A' + B' + \frac{H'}{G-H} - W_1^2\right) e^{-Gz/a}$$

where A, B, A', and B' are the constants appropriate for a saturated environment and

$$H' = 2gaHy_1/\bar{\theta}_0(G-H).$$

The results of the computations show that a hypothetical bubble starting at cloud base with a diameter of one km can certainly reach the tropopause if the environment is saturated and is conditionally unstable for a large enough height interval. Observed velocities of the tower tops as evaluated from photographs taken at Anegada (Malkus and Ronne, 1954) when superimposed on the theoretical vertical-velocity curves appear to agree best with the velocity curve corresponding to a bubble rising through a saturated environment with intermediate parameter values $K = 0.5$ and $C_D = 0.563$. However, the results are not inconsistent within the accuracy of the theory and observations with a bubble rising through a dry environment.

The analysis based on the Wake Island soundings can only be compared with observed tower heights and diameters, since the aircraft photographs taken at the time cannot be measured accurately enough and over a long enough period to determine cloud-tower-top velocities of ascent.

In general, observations of maximum cloud-top height have been found to agree quite well with the maximum height of positive buoyancy of the undilute parcel lifted from cloud base. This has led to the inference that entrainment is negligible in bubbles which reach the tropopause. According to the theory developed in this paper, the maximum height is relatively insensitive to variation in the constants G and H so that the undilute parcel method gives quite reasonable results. Therefore, approximate agreement of observed maximum tower heights with heights indicated by the undilute parcel method is not a conclusive indication that entrainment is a negligible factor in the development of cumulus-cloud towers.

The theoretical computations in general appear to show that a very stable layer (isothermal or inversion) can stop the ascent of a bubble within a distance less than a bubble radius. This merely confirms the effectiveness of a strong trade-wind inversion or the tropopause as a lid for cumulus-cloud convection.

5. Bubble penetration of stable layer between cloud and subcloud levels

In the trade-wind area, there often exists a shallow stable layer at about the 600-m level. The ease with which a bubble of unsaturated air may penetrate this stable layer may be discussed with the aid of the equations

$$\Delta\theta = E + (\Delta\theta_1 - E)e^{-Hz/a}$$

$$W^2 = E' + \left[\frac{2ga\Delta\theta_0}{\bar{\theta}_0(G-H)} - \frac{GE'}{G-H}\right] e^{-Hz/a}$$
$$- \left[E' + \frac{2ga\Delta\theta_1}{\bar{\theta}_0(G-H)} - \frac{G}{G-H} E' - W_1^2\right] e^{-Gz/a}$$

which are the solutions of (23) and (15′), respectively, for a bubble of unsaturated air. In the above equations, $E = -\epsilon a/H$ where $\epsilon = d\theta_0/dz$ for an isothermal layer at the 600-m level and $E' = 2gaE/\bar{\theta}_0 G$.

A measure of the penetrability of the stable layer by turbulent impulses in the subcloud layer may be found by asking the value of either $\Delta\theta_1$ or W_1 required for an unsaturated bubble to just barely move from the bottom to the top of the stable layer. The condition to be satisfied is $W = 0$ when z equals the thickness of the stable layer. Thus, then $\Delta\theta_1$ or W_1 may be found as functions of z and a as follows:

$$\Delta\theta_1 = E\left[1 - \frac{G-H}{G}\left(\frac{1 - e^{-Gz/a}}{e^{-Hz/a} - e^{-Gz/a}}\right)\right],$$

$$W_1^2 = E'\left[1 - e^{Gz/a} + \frac{G}{G-H}\left(e^{(G-H)z/a} - 1\right)\right].$$

Graphs of the above functions of z and a are given in figs. 9 and 10 for parameter values $K = 0.5$ and $C_D = 0.563$. From these graphs, it may be concluded that penetration of a stable layer more than 100 m thick by subcloud layer turbulent impulses is very unlikely in view of root-mean-square measurements of $\Delta\theta_1$ and W_1 obtained by Bunker (1955, 1959) near the top of the subcloud layer in the Caribbean trade-wind area. Extremes of his root-mean-square values are $\Delta\theta_1 = 0.2$C and $W_1 = 42$ cm per sec. Therefore, extreme individual values of $\Delta\theta_1 = 1.0$C and $W_1 = 2$ m per sec may be possible even though highly improbable.

6. Supplementary remarks

The comparison of the foregoing theory with observation may not at first sight appear particularly significant or conclusive because of the considerable latitude available in the choice of the parameters K and C_D. However, one should note that K is restricted

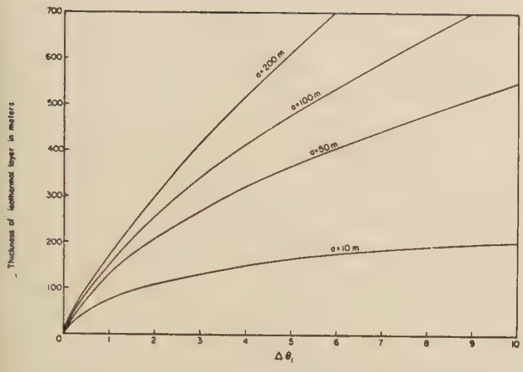

FIG. 9. $\Delta\theta_1$ required for an unsaturated bubble to just barely reach the top of an isothermal inversion layer of thickness z.

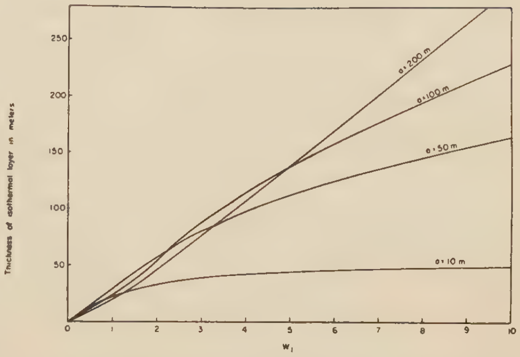

FIG. 10. W_1 required for an unsaturated bubble to just barely reach the top of an isothermal inversion layer of thickness z.

to the range 0 to 1 and C_D to the range 0 to 9/8 where $C_D = 9/8$ represents the drag if the plane $z = z_0$ passes through the center of the bubble. Thus, even qualitative agreement between the idealized bubble behavior and the actual motions observed in clouds is certainly a hopeful indication. Perhaps the range of plausible choice of K and C_D may be narrowed considerably by adaptation of Oseen's theory as described by Lamb (1932) to the problem. This, combined with a treatment of the manner in which vorticity is created in a bubble, might lead to a more significant comparison of observation and theory.

An ideal observational test of the theory would be in connection with atomic bomb tests. In the case of an atomic bomb blast, an isolated mass of hot air is created which can easily be observed by motion-picture photography. The detailed observations that have undoubtedly been made in connection with atomic bomb tests would be an excellent proving ground for the bubble theory described here and would also furnish accurate empirical values of the parameters K_1, K_2, and C_D.

The question of interaction between bubbles has been left open because of the difficulties involved in a theoretical treatment of this problem. The importance of this problem depends on how frequently bubble-like masses of air rise through a given cloud system. If bubble convection is a practically continuous process, then one must consider the interaction of individual bubbles in modifying both their internal and external behavior and even their coalescence to form larger bubbles. Further observational work is necessary to determine the importance of interaction and how closely the theoretical bubble model approximates cumulus convection.

One might possibly question the necessity or justification for assuming inviscid flow in the interior of the bubble, a spherical form for the bubble, and the ignoring of the process by which vorticity is created. Viscous effects inside the bubble or immediately outside are taken care of by the parameters K and C_D as far as the behavior of W and $\Delta\theta$ are concerned. The degree to which inviscid flow approximates motion in and ahead of the bubble is only of importance in describing the vertical-velocity profile along a horizontal line through the bubble for purposes of comparison with observed vertical velocity. Departures from inviscid flow and spherical form should show up largely in departures of observed peak velocities from $(5/2)W$ and in the occurrence of small irregularities.

From flight data made with a single airplane, no exact indication of actual bubble shape is possible, since the observed velocity and temperature profile could be just as well explained by a horizontally flattened lens-shaped or vertical plume-like structure. Differences in initial boundary conditions and bubble interactions might be responsible for quite radical departures from a spherical shape. If convection in clouds is extremely intermittent in nature, as indicated by observation, then the sphere is probably on the average the closest approximation to the shape of isolated masses of relatively warm air rising through a cloud.

The neglect of vorticity considerations appears to be the least important of the possible defects in the theory. There is no obvious physical reason why the density distribution and viscous effects might not combine in such a way as to create the vorticity distribution necessary for the theoretical or observed vertical-velocity profile to exist.

The method whereby entrainment has been introduced is actually independent of the bubble-vortex theory here presented. This method of treating entrainment could have been applied in Stommel's (1947, 1951) and Malkus' (1954) work on entrainment. In terms of the symbols of this paper, Stommel's assumptions may be stated as

$$\left(\frac{dM}{dt}\right)_- = \tfrac{3}{8}K_1\pi\rho_0 W a^2 = 0$$

and

$$\left(\frac{dM}{dt}\right)_+ = \tfrac{3}{8}K_2\pi\rho_0 W a^2 = \frac{dM}{dt}.$$

Then Stommel's $(1/M)(dM/dz)$ in terms of the theory in this paper becomes

$$\frac{1}{M}\frac{dM}{dz} = \frac{9K_2}{32a}.$$

A different approach to the dynamic problem would have the effect of modifying the numerical coefficient of K_2/a.

If any other dynamic description of cumulus-cloud convection were to be brought forth, entrainment as treated here could very easily be adapted to it.

Acknowledgments. The author is indebted to Dr. Joanne S. Malkus for her criticisms and suggestions concerning the mathematical theory of this report and its application, and to Mr. Andrew F. Bunker for obtaining observational data and for suggestions concerning the reduction of data. In addition, the thoughts of the writer were considerably clarified by discussions with Mrs. Ruth Wexler concerning her reduction of data obtained during a field trip to the Caribbean in August 1957. The author also wishes to express appreciation for the helpful comments of others too numerous to mention.

REFERENCES

Bunker, A. F., 1955: Turbulence and shearing stresses measured over the North Atlantic Ocean by an airplane-acceleration technique. *J. Meteor.*, **12**, 445–455.

——, 1959: Latent and sensible heat fluxes in air flowing southward over the North Atlantic Ocean. To be published in *J. Meteor.*

Davies, A. M., and G. I. Taylor, 1950: The mechanics of large bubbles rising through extended liquids and through liquids in tubes. *Proc. r. Soc.* (*London*), A, **200**, 375–390.

Harrington, E. L., 1958: Observations on the appearance and growth of tropical cumuli. *J. Meteor.*, **15**, 127–130.

Lamb, H., 1932: *Hydrodynamics.* Cambridge, 738 pages.

Ludlam, F. H., and P. M. Saunders, 1956: Shower formation in large cumulus. *Tellus*, **8**, 424–442.

Malkus, J. S., 1954: Some results of a trade-cumulus cloud investigation. *J. Meteor.*, **11**, 220–237.

——, and C. Ronne, 1954: On the structure of some cumulonimbus clouds which penetrated the high tropical troposphere. *Tellus*, **6**, 351–366.

——, and R. S. Scorer, 1955: The erosion of cumulus towers. *J. Meteor.*, **12**, 43–57.

Scorer, R. S., 1957: Experiments on convection of isolated masses of buoyant fluid. *J. Fluid Mechanics*, **2**, 583–594.

——, and F. H. Ludlam, 1953: Bubble theory of penetrative convection. *Quart. J. meteor. Soc.*, **79**, 94–103.

——, and F. H. Ludlam, 1953: Reviews of modern meteorology, 10: Convection in the atmosphere. *Quart. J. meteor. Soc.*, **79**, 317–341.

——, and C. Ronne, 1956: Experiments with convection bubbles. *Weather*, **11**, 151–154.

Stommel, H., 1947: Entrainment of air into a cumulus cloud. *J. Meteor.*, **4**, 91–94.

——, 1951: Entrainment of air into a cumulus cloud II. *J. Meteor.*, **8**, 127–129.

Sutton, O. G., 1947; The atom bomb as an experiment in convection. *Weather*, **2**, 105–110.

Taylor, G. I., 1950: The formation of a blast wave by a very intense explosion. *Proc. r. Soc.* (*London*), A, **201**, 159–186.

Contribution No. 1013

Reprinted from BIOLOGICAL BULLETIN, Vol. 116, No. 2, pp. 258–264, April, 1959
Printed in U. S. A.

HISTOLOGY AND METABOLISM OF FROZEN INTERTIDAL ANIMALS

JOHN KANWISHER

Woods Hole Oceanographic Institution, Woods Hole, Massachusetts

HISTOLOGY AND METABOLISM OF FROZEN INTERTIDAL ANIMALS[1]

JOHN KANWISHER

Woods Hole Oceanographic Institution, Woods Hole, Massachusetts

Many invertebrate animals are normally exposed to environmental temperatures far below the freezing point of their body fluids. Although supercooling may sometimes be a factor in survival (Salt, 1950; Ditman *et al.*, 1942; Scholander *et al.*, 1953), freezing occurs in nature among insects (Asahina *et al.*, 1954; Scholander *et al.*, 1953), shore animals (Kanwisher, 1955), and other groups (Luyet and Gehenio, 1940.) On the shore during winter, for example, freezing and thawing occurs twice a day when the animals are exposed to the cold air by the tide. Intertidal animals in the Arctic may be frozen for as long as 6 months (Kanwisher, 1955). The survival of these animals depends on their being able to have most of their body water turned to ice. It is remarkable that no injury is produced in a living system when more than half of its bulk is changed to a crystalline solid. I am reporting here some investigations on the histology and metabolism of these intertidal animals.

HISTOLOGY

In the freeze-drying histological technique, tissue is cooled very quickly with liquid nitrogen. Freezing occurs so fast that ice crystals do not have time to grow very large and cellular organization is very little disturbed. The water is removed by vacuum while the sample is kept cold. The resulting dehydrated tissue matrix is imbedded, sectioned, and stained in a conventional manner. I have used the method here to capture the situation in tissue from shore animals frozen to relatively mild natural temperatures. Comparison with material from unfrozen animals has shown the distortions caused by the freezing.

Animals were collected from the shore at Woods Hole in January and moved to a −10° cold room without thawing. Sections of tissue about 1 mm. thick were cut with a cold knife, held with cold tweezers, and plunged into a vial of isopentane suspended in a container of liquid nitrogen. The isopentane allows a faster heat transfer because it does not boil and form an insulating gas layer. The hard frozen samples were quickly transferred to the already cold dehydrating chamber and vacuum applied for 24 hours at about −45°. The dehydrated tissue was then imbedded in de-gassed paraffin already in the chamber with the vacuum still applied. Photomicrographs of 10-micron sections are shown in Figure 1. The unfrozen controls were tissue taken from identical animals that had thawed at room temperature for an hour.

---

[1] Contribution Number 1013 from the Woods Hole Oceanographic Institution. This study was aided by a contract between the Office of Naval Research and the Arctic Institute of North America.

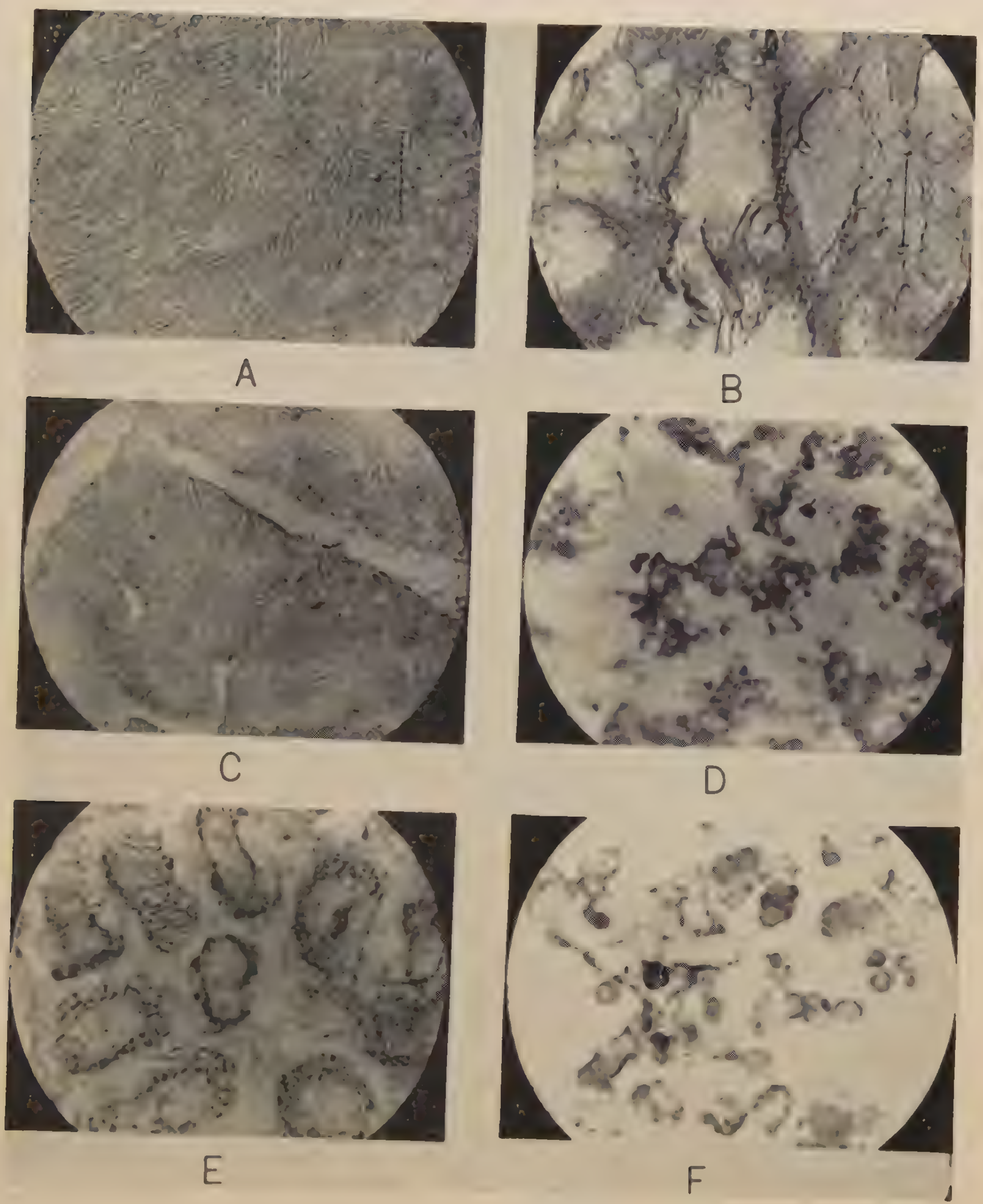

FIGURE 1. Photomicrographs of unfrozen and frozen tissue.

Figure 1, A is the unfrozen foot of the shore snail *Littorina littorea*. The purpose of the randomly arranged muscle fibers is related to the snail's type of locomotion. In the frozen tissue in Figure 1, B, the ice forms in large pockets with a resulting shrinkage and distortion of the cells.

The extreme distortions indicated in the initial results were surprising enough to warrant the following procedure. The frozen muscle slice was cut in two pieces. One was used as the frozen specimen. The other was warmed for less than a minute on the palm of my hand and then hard frozen in the liquid nitrogen. When sectioned it appeared nearly the same as tissue from an unfrozen animal. Figures 1, A and 1, B are actually sections from this run.

A transverse section of the unfrozen adductor muscle in the oyster, *Crassostrea virginicus,* is shown in Figure 1, C. The parallel muscle fibers are viewed end-on. In its frozen counterpart in Figure 1, D, the fibers are clumped into groups to make room for the intervening ice. The prominent elements that resulted are all about the same size. There may be membranes not visible in the unfrozen muscle to account for this regularity. The same regular clumping was seen in the adductor muscle of two mussels, *Modiolus modiolus* and *Mytilus edulis.*

Figure 1, E is of the eggs in the unfrozen ovary of the blue mussel *Mytilus edulis.* When frozen as in Figure 1, F, the detail is much less distinct but the eggs clearly have shrunken during the formation of the large amounts of intercellular ice. Comparable distortions were seen in other tissues from these and other species.

Metabolism of Frozen Animals

Scholander *et al.* (1953) measured respiration at freezing temperatures by following the decrease in oxygen concentration in a closed volume containing the animal. The same method has been used here. Manometric and volumetric techniques can not be used because of the volume change when water turns to ice.

The snails to be used were frozen in 20-ml. syringes in a cold bath. Only those in which the snail froze while fully extended from its shell were used. A short section of tubing on the tip of the syringe extended above the surface of the liquid and was closed with a pinch clamp. A sample of gas could be withdrawn without removing the syringe from the bath. The plunger was free to move up and replace the volume lost in sampling. Allowance was made for the decreased volume in calculating the rate of oxygen removal.

Duplicate oxygen analyses good to 0.02 per cent were made with the half-cc. analyzer of Scholander (1947). Serial samples were plotted against time and the slope was used in computing the oxygen consumption. The concentration was never allowed to go below 18 per cent in any run. Respiration was assumed to be independent of tension over this small range.

After the snails were placed in the cold bath, at least 6 hours were allowed for phase equilibration between ice and water in the tissues. Previous experience (Kanwisher, 1955) had shown that there was no appreciable increase in ice after this length of time. The syringe was then flushed with cold outside air. A series of oxygen determinations showed that such air did not vary appreciably from 20.94 per cent so this was considered the starting concentration. At intervals ranging from 2 to 120 hours samples were withdrawn with a mercury gas sampler.

Volumetric respirometers (Scholander *et al.,* 1952) were used above 0°. One ml. of sea water was included in the vial with the animals. At 0° such values were in good agreement with those made by gas analysis which is specific for oxygen. The often used and rarely proven hypothesis is thus confirmed that the volume decrease is due to oxygen being consumed.

The respiration temperature data from −10 to +30° C. are plotted in Figure 2. Between 0 and +20°, oxygen consumption shows the usual logarithmic increase with a Q_{10} of 2 to 3. Above this respiration decreases, probably due to thermal injury. Below 0° the metabolic activity drops sharply with an apparent Q_{10} of about 50.

At −10°, respiration was so low it took 6 days for the snails to consume a measureable amount of oxygen. Even in this length of time the concentration change was smaller than desired for accurate determination. This may account for the greater spread of values at this low temperature. At −15° the empty syringes gave blank values of one-third the oxygen decrease in those containing snails. This may be due to oxidation of grease used on the syringe plunger. It did not seem that this technique could be trusted on the slower rates to be expected at still lower temperatures.

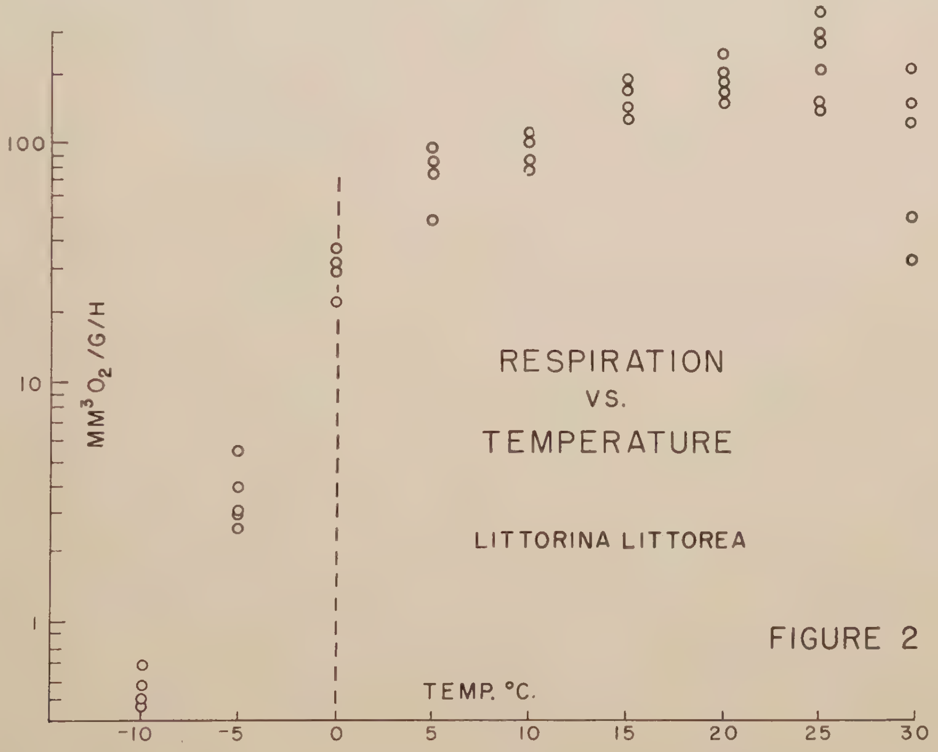

Figure 2. Variation of oxygen uptake with temperature.

Salinity Effect on Respiration

Scholander *et al.* (1953) have given several reasons why the respiratory gas exchange of a frozen animal drops so much more rapidly with temperature than it does above 0° when no ice is present. The ice may act as a diffusion barrier to the gases. The increased viscosity of the body fluids may slow the reaction rates. Finally the increased salinity may directly inhibit the animal's metabolism. No way could be devised to test the first two hypotheses. The respiratory response to increased salinity above 0° can be determined independently of any ice effects.

Higher than normal salinities were made by freezing sea water and using the brine. Dilution with fresh water gave lower than normal salinities. Freshly collected snails were placed in jars containing the different salinities for a minimum of 6 hours before being used. At very high and low values the snails withdrew into their shells. Experience had shown that the operculum blocks respiratory gas exchange so these could not be used.

For the respiration measurements single snails were placed in 20-ml. syringes filled with the desired salinity. The syringes were kept in a constant temperature bath except when sampling. One-ml. samples were removed at convenient intervals and analyzed gasometrically for oxygen by the method of Scholander *et al.* (1955).

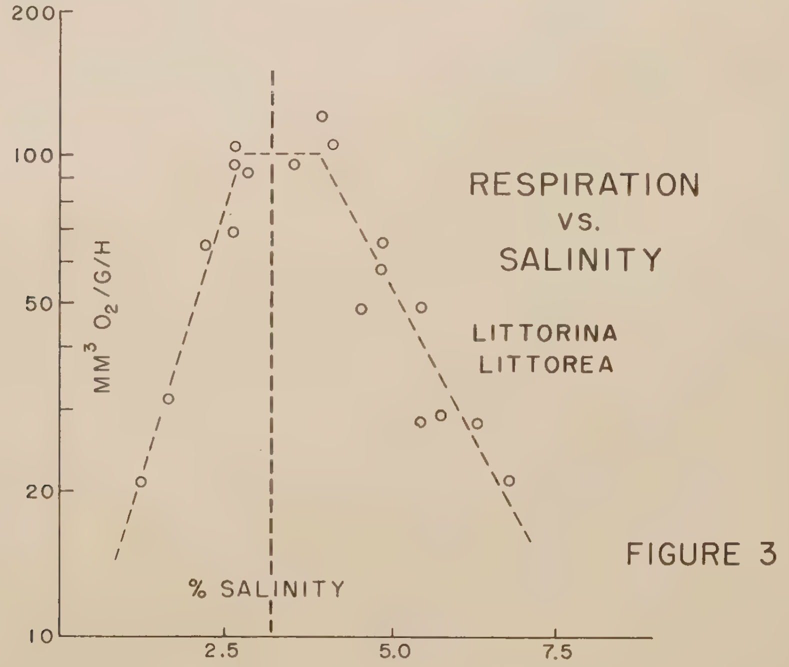

FIGURE 3. Response of oxygen uptake to different salinities.

Since this is a physical extraction of the gases it could be relied on in spite of the water sometimes becoming cloudy with waste products.

As in the low temperature gas analysis method several serial readings were used to indicate the rate of oxygen removal by the snails. Low oxygen tensions were avoided by working in the range of 2.5 to 6 mm.^{3} of oxygen per ml. The curves showed that respiration was independent of tension over this range.

The variations of oxygen consumption with changes in the external salinity are shown in Figure 3. High salinity depresses the respiration of *Littorina littorea.* This is a reversible effect since the rate increases again when the snail is returned to normal salinity. When the snails withdrew into their shells at higher salinities than shown, no oxygen consumption could be detected. They are apparently able to subsist for long periods anaerobically.

Since freezing occurs throughout the animal, the remaining body fluids in all parts of the animal are concentrated. If any effect of external salinity above 0° is to be related to freezing, it must be shown that the animal is not osmotically regulating. Increased salinity could conceivably be effective in only altering the absorption of oxygen at the surface. Tissues of snails from water of different salinities were analyzed for chlorides. By carefully cracking the shell, the animal could be removed whole. Excess water was mopped off and the weight quickly taken. The water was removed by drying for several hours in a 100° oven. The dry weight then gave the total water by difference. The dry tissue was then digested and titrated for the amount of total chlorides present. This amount was considered dispersed in all the animal water in order to calculate the concentration in the live animal. From the resulting normalities at different external salinities it was clear that internal chloride concentration was proportional to that outside the animal. Any result of externally varied salinity can reasonably be viewed as arising from a corresponding change throughout the animal.

Discussion

Chambers and Hale (1932) observed plant and animal cells freezing under the microscope. They found that ice formation inside the cellular membrane always resulted in the death of the cell. The detailed studies of Asahina and his colleagues (1954) have described the freezing process in the blood and isolated organs of insect pre-pupae and in the intact insects themselves. They also found that intra-cellular freezing is lethal to the cell or tissue. Such results are responsible for the general belief that all freezing in animals and plants takes place outside the cells.

The impressive liquid air freezing experiments of nematodes by Luyet and Gehenio (1940) have almost certainly been an instance of ice within cells. Lack of injury here has been attributed to the very rapid rate of freezing. This vitrification does not allow time enough for ice crystals to grow to a size where they can damage protoplasmic structures. It forms the basis of the histology used here. This phenomenon probably has little to do with the normal ecology of these animals in nature.

Shore animals that are exposed to freezing are in shells. This impedes heat transfer and gives ice crystals time to grow. One can readily see them in an opened animal. The tissues of such an animal are similar in texture and appearance to a frozen piece of meat. It is not surprising when one considers that water makes up three-fourths of the bulk of the animal and four-fifths or more of it may be ice. The photomicrographs presented here show the large amount of distortion necessary at the cellular scale to make room for this ice. Yet this can change back to a more or less normal appearing tissue in 30 seconds as shown in Figures 1, A and B. Siminovitch and Briggs (1949) have related frost hardiness in plants to the ability of water to migrate rapidly in and out of the cells. Unfortunately no equivalent test could be devised to apply this to shore animals.

Littorina littorea was found to remain out of its shell and behave normally in salinities of 2 to 7 per cent. It sharply decreased its metabolism in response to a salinity increase. In Figure 3, the data indicate that doubling the salinity above the optimum decreases the oxygen demand to about a third. As the salinity of the body fluids is increased by the freezing out of water, oxygen uptake must drop in the same fashion. From the freezing curves in a previous paper (Kanwisher, 1955) 70 to 80 per cent of the water in this species is frozen at −10°. This would result in a Q_{10} from the salinity of about 10. Above 0° the Q_{10} due to the usual temperature effect on reaction rates is between 2 and 3. Combining these one would expect a Q_{10} in the range of 20 to 30 below 0°. The actually observed one is closer to 50. The effect of ice as a gaseous diffusion barrier and that from the loss of water itself may account for the difference. It is felt that the present data do not warrant a more vigorous interpretation. Similar work with intertidal algae (Kanwisher, 1957) has shown that the drying effect of freezing was chiefly responsible for a similar large decrease in respiration. A three-times increase in salinity had little effect on the oxygen uptake of these plants.

Freezing in shore animals to the extent shown here is a normal occurrence twice daily in the winter with no obvious injury to the animal. This freezing hardiness is probably connected with the ability to stand the internal distortions and high salinities that result. The greatly lowered metabolism may be of adaptive significance in severe locations where shore animals are frozen into the ice for months at a time. As such it could represent a considerable saving in food reserves.

Summary

1. Histology of frozen shore animals has shown large pockets of intercellular ice with consequent shrinkage and distortion of the surrounding cells.

2. The Q_{10} drops precipitously in the region of ice formation and may be as high as 50.

3. High tissue salinity without freezing decreases oxygen uptake. Thus the salinity increase that results from freezing is responsible for a large part of the high Q_{10}.

LITERATURE CITED

Asahina, E., K. Aoki and J. Shinozaki, 1954. The freezing process of frost-hardy caterpillars. *Bul. Entomological Research,* **45**: 329–339.

Chambers, R., and H. P. Hale, 1932. The formation of ice in protoplasm. *Proc. Roy. Soc. London, Ser. B,* **110**: 336–352.

Ditman, L. P., G. B. Vogt and D. R. Smith, 1942. The relation of unfreezable water to cold hardiness in insects. *J. Economic Entomology,* **35**: 265–272.

Kanwisher, J. W., 1955. Freezing in intertidal animals. *Biol. Bull.,* **109**: 56–63.

Kanwisher, J. W., 1957. Freezing and drying in intertidal algae. *Biol. Bull.,* **113**: 275–285.

Luyet, B. J., and P. M. Gehenio, 1940. Life and Death at Low Temperatures. Biodynamica, Normandy, Missouri.

Salt, R. W., 1950. Time as a factor in the freezing of undercooled insects. *Canadian J. Res.,* **28**: sect. D: 285–291.

Scholander, P. F., 1947. Analyzer for accurate estimation of respiratory gases in one-half cubic centimeter samples. *J. Biol. Chem.,* **167**: 235–250.

Scholander, P. F., C. Lloyd Claff, J. R. Andrews and D. F. Wallach, 1952. Microvolumetric respirometry. *J. Gen. Physiol.,* **35**: 375–395.

Scholander, P. F., W. Flagg, R. J. Hock and L. Irving, 1953. Studies on the physiology of frozen plants and animals in the Arctic. *J. Cell. Comp. Physiol.,* **42**: supplement 1, 1–56.

Scholander, P. F., L. van Dam, C. L. Claff and J. W. Kanwisher, 1955. Micro-gasometric determination of dissolved oxygen and nitrogen. *Biol. Bull.,* **109**: 328–334.

Siminovitch, D., and D. R. Briggs, 1949. The chemistry of the living bark of the black locust tree in relation to frost-hardiness. *Arch. Biochem.,* **23**: 8–17.

Contribution No. 1014

Reprinted from LIMNOLOGY AND OCEANOGRAPHY
Vol. 4, No. 2, April, 1959
Printed in U.S.A.

Polarographic Oxygen Electrode[1]

JOHN KANWISHER

Woods Hole Oceanographic Institution, Woods Hole, Massachusetts

ABSTRACT

A method has been developed for the continuous monitoring of oxygen tension in solutions and gases. The oxygen is reduced at a platinum surface which is covered with a plastic membrane. The silver-silver oxide reference electrode is also included under the membrane. Drift is less than 10 per cent for a period of days, and temperature compensation is possible. A number of uses to which it has been put are described.

The intimate involvement of oxygen in nature makes its measurement a problem of recurring interest. In many investigations present techniques of oxygen determination limit the amount and type of data that can be taken. A method of continuously monitoring oxygen tension in liquids and gases will be described in this paper. It is based on the polarographic reduction of molecular oxygen at a platinum electrode. Many of the previous shortcomings of polarographic systems have been overcome. The variety of tasks to which it has been applied include the determination of biological oxygen demand in domestic sewerage, continuous flow respirometry of a variety of marine and freshwater invertebrates and fishes, determination of respiration and photosynthesis in algae, analyzing respiratory gases for oxygen, determination of oxygen tension in 1-ml samples of water and biological fluids, and vertical profiles of oxygen in fresh and salt water. Interest has been sufficient to indicate that the technique should be published separately as a research method. An explanation of how the electrode functions will be followed by a description of some of the above uses to indicate its potentialities. A more complete description of the theory and chemical behavior of the electrode will be presented elsewhere.

I. THEORY OF THE OXYGEN ELECTRODE

The present system consists of a platinum electrode held at −.8 volts to a silver-silver oxide reference electrode. Molecular oxygen is reduced at the platinum surface, and a current flows. The magnitude of this current depends upon the amount of oxygen reaching the platinum surface. Thus a bare platinum electrode in sea water makes an acceptable polarograph for a short time. The sensitivity of such an electrode decreases with time, apparently due to metals plating out on the platinum. The sensitivity cannot be regained by reversing the current. In complex biological media such as blood, red cells or other material usually collect on the surface and reduce the sensitivity by partially blocking the access of oxygen. Dropping mercury electrodes partly overcome the difficulty by continually renewing the metallic surface, but they are inconvenient and may be poisonous to living systems. Such chemical and physical factors have prevented polarographic methods of oxygen determination from being widely used.

In an effort to overcome the shortcomings of a bare platinum electrode in biological fluids, Davies and Brink (1942) covered the metal with agar and also a membrane of collodion, and Clark and colleagues (1953) later investigated a variety of other plastic films. A recent symposium has summarized the present state of the art (Federation Proceeding 1957). Interest in such systems has been mostly among biologists for application to specific problems. The present work was undertaken to develop a generally useful technique for biological and oceanographic work.

Preliminary experiments with uncovered

---

[1] Contribution No. 1014 from the Woods Hole Oceanographic Institution.

electrodes led to the conclusion that a practical platinum polarographic system must have two features. The platinum should operate in a simple medium to prevent changes in electrode sensitivity due to chemical interference, and there should also be a standardized diffusion arrangement between the platinum surface and the medium in which oxygen is being measured. Polyethylene and teflon have the necessary properties to realize both of these conditions. Molecular oxygen can diffuse through them, while at the same time they are impermeable to ions. The platinum electrode can operate behind a thin film of polyethylene in a pure solution of KOH. Under this condition its sensitivity does not change. The plastic represents a considerable but fortunately unchanging diffusion barrier.

The physical arrangement of the electrode system is shown in Figure 1. The silver-silver oxide reference electrode is concentric around the platinum. A film of polyethylene is stretched tightly over this and held by a retaining ring. The film is put on the electrode while the entire assembly is held under the surface of a solution of 0.5 N KOH. A small amount of this solution is trapped under the plastic. It forms only a very thin layer between the plastic and the platinum.

The initial reaction of the oxygen at the platinum forms OH ions.

$$4e^- + O_2 + 2H_2O \rightarrow 4OH^- \qquad (1)$$

A piece of indicator paper laid across the platinum under the plastic shows increased pH a few seconds after a current due to O_2 starts to flow. The OH ions then diffuse to the reference electrode and react with the Ag to form Ag_2O.

$$2Ag + 2OH^- \rightarrow Ag_2O + H_2O + 2e^- \qquad (2)$$

The end result is the formation of Ag_2O which appears as a dark brown or black coating on the surface of the silver. The Ag_2O then forms the half cell which makes contact with the solution to complete the circuit with the platinum electrode. Since the Ag can be made thick such an electrode system will last for many months of continuous operation.

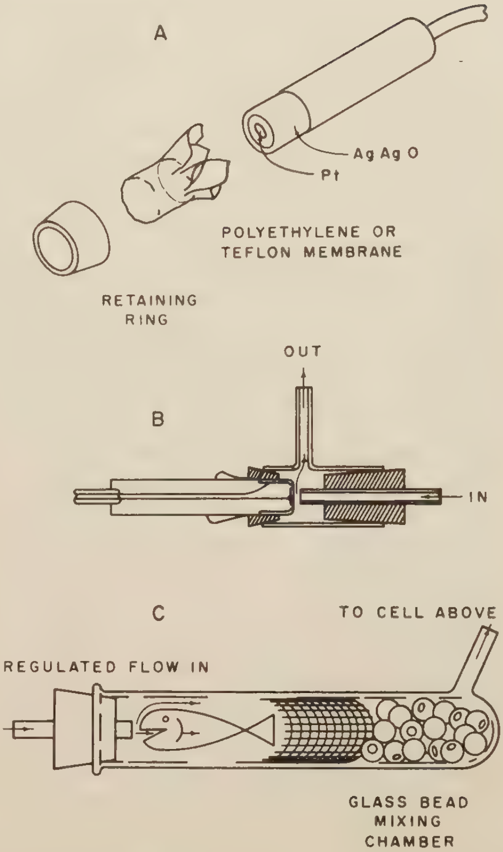

FIG. 1. *A*. Exploded view of the oxygen electrode showing how the membrane is stretched tightly over the end surface and held this way by an elastic retaining ring. *B*. Cell with which the electrode can be introduced into a stream of solution or gas. *C*. An arrangement for continuous flow respirometry of small fishes or other aquatic animals.

The diffusion situation of O_2 in the electrode is as follows. When the electrode is turned on a current passes which is the same as if a bare electrode were used, since the KOH solution has previously established oxygen tension equilibrium across the film. The current decreases in a few seconds as the small amount of oxygen in solution behind the film is consumed by the above reaction. Oxygen from the medium begins to diffuse across the film because of the gradient produced. A steady state is soon reached where the oxygen consumed at the platinum equals that diffusing across the film. With a 0.0015″ thick polyethylene film the current will now be about $\frac{1}{1000}$ as large as if the platinum were uncovered. The O_2 tension behind the film must be reduced from that outside by this factor. Thus in air-saturated water this tension is only a fraction of a mm of Hg when a steady state is reached.

If the electrode is turned off and then turned on again, the current is initially very large. Oxygen tension equilibrium has been partly reestablished across the film in the interim. If a sensitive meter is used as a current indicator, it is necessary to protect it from this initial surge of current.

The tension increment across the film is nearly equal to the value of the tension in the medium, since it has been shown that that in the KOH is very low. So little oxygen diffuses from the medium into the film the system is much less dependent upon the flow of water past the electrode. Going from an absolutely quiescent condition to vigorous stirring increases the current only 25 to 50 per cent. A very slight motion of about 1 cm/sec. brings the current nearly up to saturation. This much movement is supplied easily by random motion when an electrode is dangled on the end of a cable over the side of a boat.

The platinum electrode "sees" more than its own area of polyethylene, and diffusion takes place through this increased area. Due to this edge effect the polarographic current does not increase linearly with the area of platinum. For electrodes of less than 2 mm diameter, it is more nearly a function of the diameter. This gradually changes to an area dependence in larger electrodes as the edge area becomes a smaller fraction of the whole. Platinum electrodes from 0.2 to 2 cm in diameter have been used. There seems to be no reason why larger electrodes with correspondingly greater currents are not feasible.

Equation 1 states that the electrode reaction consumes a molecule of oxygen for every 4 electrons of current flow. If one microamp of current flows for one hour the amount of oxygen consumed is about 2×10^{-4} ml. This consideration may limit the current and thus the size of the electrode to be used in a small closed system, where the total quantity of dissolved oxygen is small.

Most of the electrode systems have been made from a length of silver tubing and a disc of platinum. These are soldered onto a cable and then cast in an epoxy plastic so that only the two desired metals are exposed. Lucite has also been used successfully as an insulating support for the electrodes.

The silver is then electrolytically coated with oxide until it is black. This eliminates a period of several hours initial equilibration. The area of the silver should be at least ten times that of the platinum for the quickest response.

The polarographic cell is an amperometric device in which the oxygen concentration rather than the voltage applied determines the current that flows. With a given oxygen concentration this current increases about 5 per cent for every degree centigrade. Unless measurements are made at the calibration temperature, they must be corrected. Automatic compensation can be effected by taking the voltage drop of the current through a thermistor with a temperature coefficient equal in magnitude and opposite in sign to the cell. The thermistor is exposed to the same temperature as the solution being measured and can conveniently be cast in the plastic electrode block. The relatively high temperature coefficient represents a combination of the effect of temperature on the diffusion and solubility of oxygen, and also the temperature kinetics of the chemical reactions involved.

A 1-cm platinum electrode covered with a 0.0015″ polyethylene film will give a current of about 20 microamperes at 25°. This can be measured directly on a meter. For smaller electrodes it is necessary to use either a galvanometer or recording potentiometer. The latter instrument can be driven from the voltage drop across a ten-turn potentiometer. With provision for offsetting the zero, the recorder can be made to cover only the range of interest.

If small changes in oxygen are to be recorded, the flow past the electrode must be constant. To accomplish this in closed bottles, magnetic stirring has been used. A large magnetron magnet turned by a synchronous motor will rotate a small magnet inside a bottle in a water bath from as far as a foot away.

Small fluctuations in cell current have been traced to small bubbles on the polyethylene. Unfortunately bubbles seem to form preferentially on plastic rather than glass. The trouble usually develops when the water being measured has been warmed up from a lower temperature, and is thereby super-saturated. For coarse work a few small bubbles do not seem to matter.

A cell for continuous flow work is shown in Figure 1B. The entering flow is directed against the area of plastic directly over the platinum. By bringing the entering tube to within 0.5 mm of the electrode surface, a flow of 5 to 10 ml/min. can produce a saturation current.

It must be kept in mind that a polarographic electrode is a diffusion-dependent device and therefore measures oxygen tension rather than content. Fresh and salt water equilibrated with the same gas mixture will give the same reading despite the salt water having less oxygen. If an instrument is to read in amount rather than in tension, it must be calibrated with a solution of the same gas solubility. Fortunately the salting out effect on gas solubility is not large. A change of 0 to 3.5 per cent salt decreases the oxygen solubility by only 20 per cent. When solutions of blood pigments are involved the oxygen content is not linearly related to tension. Reference must then be made to the loading curve of the pigment for the pH and temperature of the measurement. Since tension is the driving force of diffusion, it is sometimes a more pertinent variable than oxygen content.

The overall analytical performance of these electrodes has been investigated with a recording potentiometer and independent physical determinations of the oxygen tension (Scholander *et al.* 1955). Since these latter measurements were accurate only to 1 or 2 per cent, knowledge of the electrode is correspondingly limited. Operation of the device is as follows:

1. Current is a linear function of oxygen tension over at least the range of 0 to 1 atmosphere oxygen.
2. It is stable to a few per cent over a period of days, and changes less than 25 per cent in a period of several weeks. During the time there are no abrupt changes. Thus, standardization every few hours is sufficient.
3. Short period changes of 0.01 ml per liter in sea water can be detected. This is about 0.2 per cent of the amount in solution when equilibrated with air.
4. The electrode as described gives 90 per cent of full response in about 20 seconds, and has reached 99 per cent in 2 minutes.
5. The electrode has operated successfully in dilute acids and alkalies, sea water, and a variety of polluted waters. No chemical interference has been noted. Only gross fouling on the plastic surface appreciably reduces the current. It is insensitive to the osmotic concentration of the medium.

II. EXPERIMENTAL USES

A. Algal respiration and photosynthesis

The algal sample is placed in a bottle of sea water with a stirring magnet. An

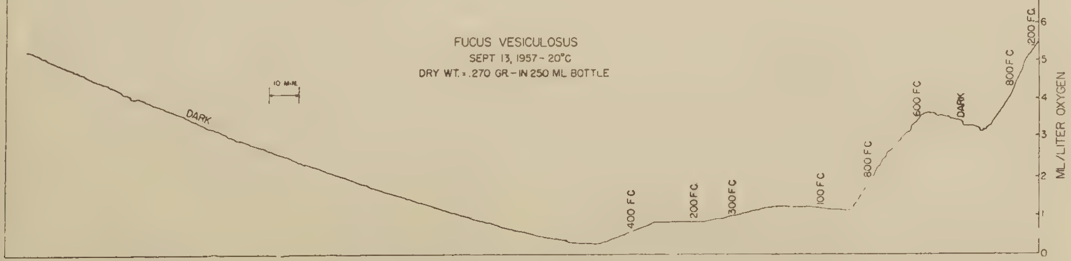

FIG. 2. Continuous time curve of oxygen in a closed bottle containing algae. The change in slope represents different rates of respiration and photosynthesis.

oxygen electrode is used as the stopper. Changes in dissolved oxygen are recorded while the alga is exposed to different light intensities in a temperature bath. The resulting curve for *Fucus vesiculosus* in Figure 2 shows an initial decrease of oxygen in the dark due to respiration. The oxygen tension dependence of respiration is shown by the decrease in slope as the oxygen content becomes smaller. This is plotted in Figure 3. The drop is probably due to diffusion limiting the supply of oxygen to the cells at the center of the relatively thick thallus. Thin species such as *Ulva* maintain a nearly constant respiratory rate to lower values of oxygen.

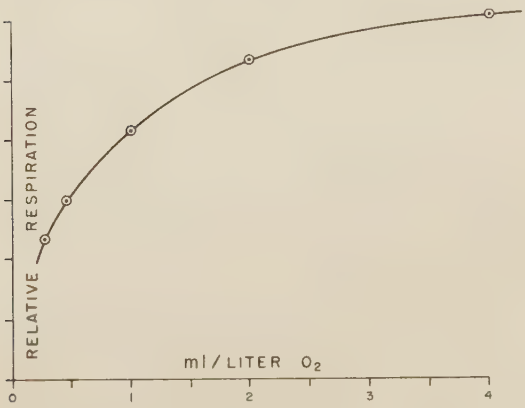

FIG. 3. Curve showing variation in respiration with oxygen tension in Figure 2.

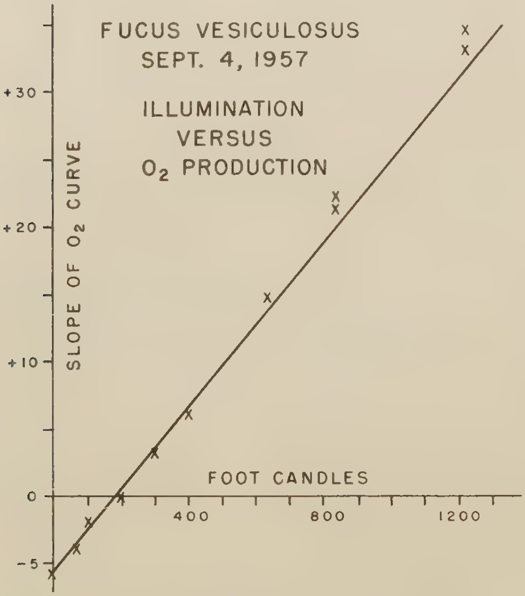

FIG. 4. Change of slope with illumination in Figure 2. This is a measure of the rate of oxygen production and therefore of photosynthesis.

The rates of oxygen production at different light levels are indicated by changes in slope from that in the dark. The slope was zero at 200 foot-candles, indicating that photosynthesis just balanced respiration. In Figure 4 it is clear that at 1200 foot-candles there was no sign of saturation. Quantum efficiency studies in the ultra violet are being done in an analogous manner with a quartz chamber.

C^{14} labelled carbon dioxide is being used to follow carbon fixation simultaneously with oxygen production during photosynthesis in unicellular algal cultures. The culture is confined in a hypodermic syringe with an electrode in the end of the plunger. With such a container serial samples can be withdrawn for counting while the oxygen in solution is continuously recorded.

B. Animal respirometry

The oxygen consumption of many invertebrates and fishes has also been measured in closed containers. If the animal is allowed to remove all the oxygen, an analogous curve relating respiration to oxygen tension can be calculated. The electrode has also been used in a continuous flow respirometer in which the water in the animal chamber is continously replaced. The animal is thus not exposed to an increasing accumulation of its own waste products. Flow rate times the increment of oxygen between ingoing and outgoing water indicates the instantaneous respiration rate. The time resolution of such a system depends on how fast the water in the animal chamber is replaced, and thus is a function of flow rate and chamber volume. If the flow rate and oxygen content of the entering water are constant, a single electrode in the water leaving the chamber will record the time course of metabolism. The method has been useful with a variety of animals ranging from a 0.5-g snail to a 30-kg shark.

An arrangement for measuring the metabolism of a fish weighing a few grams or more is shown in Figure 1C. The fish is placed in a tube small enough so that it cannot turn around. Its head faces the incoming water. Some of the water goes into the fishes mouth and through its gills. The rest passes around the fish. These are mixed in the glass beaded chamber at the end of the tube, and pass to the electrode. One can see wide excursions in the oxygen uptake when the fish is frightened by a light or a noise. A motor driven syringe has been used to deliver a toxic substance to the inflowing water. The time course and severity of its effect on oxygen consumption could be recorded.

A *Venus* clam was kept continuously in a flow respirometer for several days. As would be expected there was negligible drop in the oxygen of the water leaving the chamber when the shell was closed. Upon opening there was an abrupt decrease as the sea water enclosed in the shell mixed with that in the rest of the chamber. The drop was always the same amount and indicated that the oxygen tension must be close to zero inside the shell when it had been closed for more than 30 minutes. Even when the shell was open with the animal pumping, the instantaneous oxygen consumption varied considerably. An average would have to be taken over a considerable length of time to be an accurate measure of metabolism in such an animal.

C. *Small sample techniques*

A liquid sample in a syringe can be ejected through the cell in Figure 1B to measure its oxygen tension. A small electric motor has been conveniently used to advance the plunger at a constant rate. A single determination takes two minutes, and needs 5 to 10 ml. Frequent use of calibrating samples make it unnecessary to reach saturation velocity at the electrode surface.

It has also been possible to measure the oxygen tension in a 2-ml sample drawn into a syringe with an electrode in the plunger. A small magnetic rod has been previously placed in the syringe. Stirring for two minutes produces a maximum reading and then a gradual decline as the electrode reaction slowly consumes the dissolved oxygen. It is necessary to handle the sample quickly and with a minimum exposure to the air. A series of standards can be kept in large syringes for running before and after an unknown. Since the tension measurement does not destroy or consume the sample any additional operation can be performed on it afterwards. This technique has been convenient with human blood. After a reading part of the sample can be injected directly into a Van Slyke analyzer to measure oxygen content as opposed to oxygen tension.

D. *Field experiments*

The electrode has been used as a field instrument to obtain vertical profiles of oxygen in natural waters. Accessory temperature information is necessary to correct the readings. The electrode and a thermistor have both been operated on the same cable. Calibration just before lowering is done by immersing the electrode in a container of water that has been air-saturated by swirling for several minutes.

The hypolimnion and epilimnion clearly showed in a pond used for the local water supply. Water was being drawn from below the thermocline so that tap water was only about one-third saturated in late summer. An electrode was being used to monitor this when a fall storm produced considerable vertical mixing. The tap water oxygen content doubled in two days.

The diurnal oxygen variation in a shallow pond in mid summer was followed by an instrument supported on a pole pushed into the bottom and read by a telescope from shore. A thick plant growth covering the bottom was the main source of photosynthetic oxygen. Bubbles formed on the plants in the sunshine and were analyzed and found to be largely oxygen. The electrode read off scale when pushed in among the plants. The electrode was then hung at mid-depth and moved horizontally from shore by a string to produce a satura-

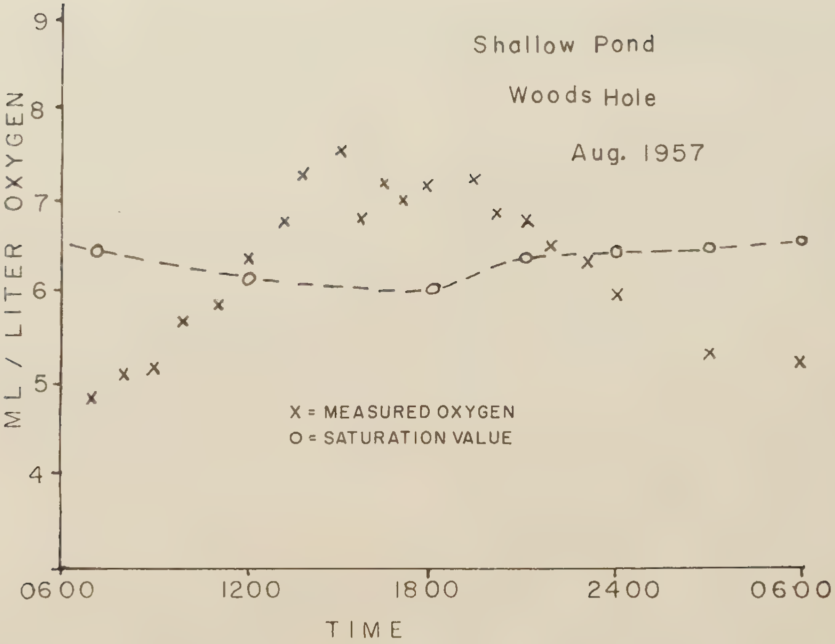

FIG. 5. Diurnal change in dissolved oxygen in a shallow pond is shown by the X's. The saturation value (small circles) changes due to temperature change.

tion current. This movement is only necessary just before taking a reading.

The record for one day in Figure 5 shows oxygen supersaturation produced photosynthetically during the day and a corresponding undersaturation from night time respiration. A strong wind in the afternoon mixed the water and unloaded some of the excess gas. The increasing concentration during the morning can be used to estimate the productivity per unit area when the entire water column is taken into consideration. The uncertain amount of atmospheric exchange makes this a poor method with strong winds.

On one instance a submersible pump was used to deliver a constant stream of water from depths up to 100 feet in the ocean. An electrode was inserted in the line on deck and the pump was gradually lowered. Winkler samples taken at the same time showed that the electrode agreed within 3 per cent. Such an arrangement is only useful to moderate depths in still water. An arrangement for recording in situ with a lowered instrument is being planned.

III. CONCLUSION

Some possible uses of the polarographic oxygen electrode have been explored in the experiments described. Others will be reported in separate publications. As a laboratory instrument the electrode will indicate oxygen tension to 1 or 2 per cent. Because of its marked temperature sensitivity no effort has been made to equal this in field experiments. There seems to be no reason why such accuracy cannot be realized if attention is paid to such factors as flow past the electrode and temperature of the water. The measurement is no more difficult or involved to perform than that of pH.

The development of the electrode has been done in cooperation with Dr. Dayton Carritt of the Chesapeake Bay Institute. He will report more fully on its chemical functioning and on additional uses.

The electrode will be made commercially by the Jarrell-Ash Company, Newtonville, Massachusetts.

REFERENCES

Davies, P. W., and F. Brink. 1942. Microelectrodes for measuring local oxygen tension in animal tissues. Rev. Sci. Instr., **13:** 524–533.

Clark, L. C., R. Wolf, D. Granger, and A. Taylor. 1953. Continuous recording of blood oxygen tensions by polarography. J. Appl. Physiol., **6:** 189–193.

Symposium on tissue oxygen tension. 1957. Fed. Proc., Fed. Am. Soc. Exp. Biol., **16:** 665–703.

Scholander, P. F., L. Van Dam, C. Lloyd Claff, and J. W. Kanwisher. 1955. Micro gasometric determination of dissolved oxygen and nitrogen. Biol. Bull., **109:** 328–324.

Contribution No. 1015

Deep-Sea Research, 1959, Vol. 5, pp. 297 to 305. Pergamon Press Ltd., London. Printed in Great Britain

The 18° water in the Sargasso Sea

L. V. WORTHINGTON

(*Received 5 January 1959*)

Abstract—The surface waters of the northern Sargasso Sea cool to a temperature of about 18°C each winter, forming an isothermal layer more than 350 m deep. This layer is also isohaline at 36·5‰. Much water with these characteristics is converged in this area and flows off to the south at the 300 m level. The excess of " 18° water " formed each winter immediately south of the Gulf Stream can be clearly detected throughout the Sargasso Sea, at least as far south as the 20th parallel North. Some of the implications of this are discussed.

INTRODUCTION

It has long been known that in the northern Sargasso Sea a deep, well mixed layer is found during the winter months (ISELIN, 1936). This layer reaches its greatest depth (about 400 m) in early March when the whole water column above that depth is nearly isothermal and isohaline. Below this depth is found the main thermocline, which lies between 500 and 1200 m.

During the spring and summer a seasonal thermocline develops but the identity of the winter surface layer is never entirely destroyed : it persists throughout the year as a nearly isothermal/isohaline layer between the bottom of the seasonal thermocline and the top of the main thermocline until it is renewed at the end of the following winter. Even in late autumn there is still a pronounced inflexion at the 300 m level and at no time is the thickness of the nearly isothermal layer less than about 250 m in the northern (N of 32°N) Sargasso Sea. The temperature and salinity of this layer are remarkably constant. At the inflexion point which always occurs close to 300 m depth, the temperature is 17·9° ± 0·3°C and the salinity 36·50‰ ± 0·10‰. For convenience water of these characteristics can be called " 18° water."

The 18° water is of more than usual interest because it is found in super-abundance far to the south of its area of formation, in places where the winter surface temperature minimum is far higher than 18°, and there is no possibility of its having been formed locally. Consequently excessive amounts of this water must be formed in the late winter in the area immediately south of the Gulf Stream, converge and spread out over the main thermocline (which represents an impenetrable density layer) in a manner reminiscent of bottom water formation in high latitudes. If the Sargasso Sea were only 400 m deep oceanographers would have no difficulty in describing what had occurred ; it would be clear that bottom water had been formed at the northern end of the sea in late winter and had flowed off to the south along the bottom. In view of the current interest in the problems of bottom water formation this 18° water assumes a special importance in that it might be possible by means of rapid and systematic measurements during one winter to estimate quantitively the various cooling effects necessary to converge and sink large amounts of surface water.

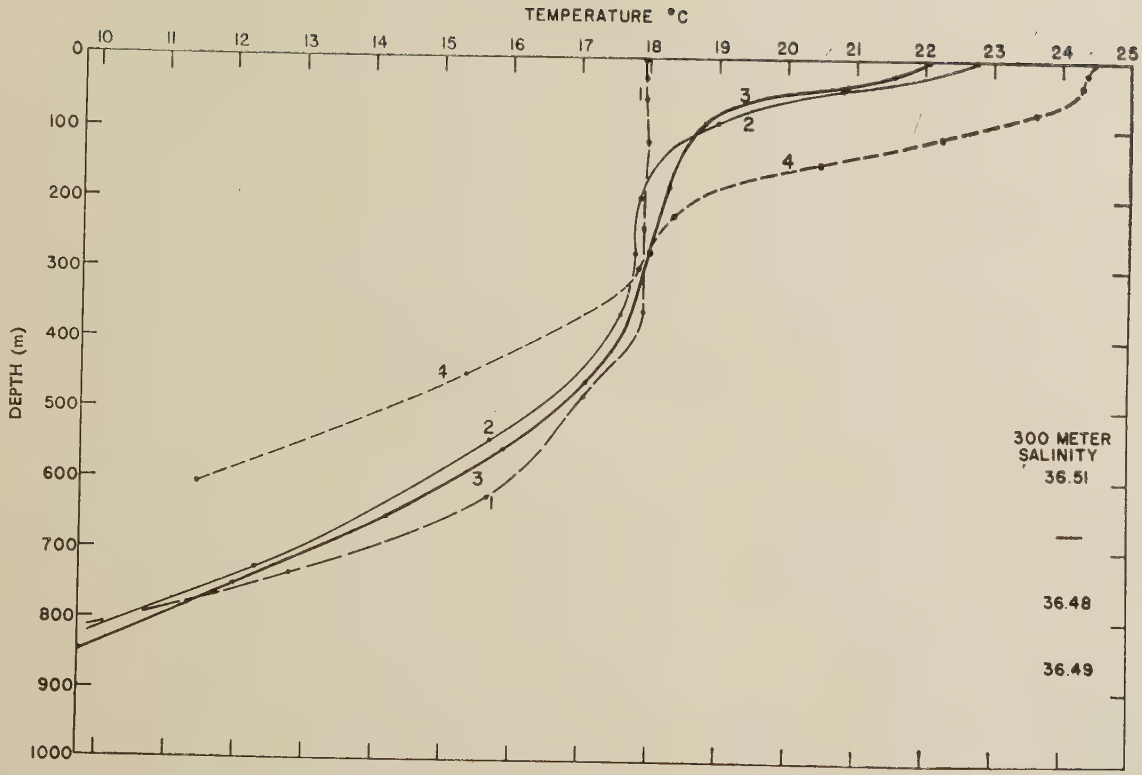

Fig. 1. Temperature-depth curves in the Sargasso Sea.

1 *Atlantis* 1153, 28 Feb. 1932 34° 02′ N 54° 05′ W
2 *Challenger* 53, 26 May, 1873 36° 30′ N 63° 40′ W
3 *Atlantis* 5306, 11 June, 1955 34° 53′ N 70° 16′ W
4 *Atlantis* 1483, 4 March, 1933 21° 46′ N 62° 48′ W.

THE FORMATION OF THE 18°C WATER

The northern limit of 18° water is the Gulf Stream which transports surface water of 20°C or warmer at all seasons and whose surface salinity is 36·1‰ (ISELIN, 1936, 1940). The southern limit can be approximately delimited by means of BÖHNECKE's (1936) atlas, which shows winter minimum surface temperatures of 19° in lat. 33°. It is thus unlikely that any 18° water is formed to the south of Bermuda, at lat. 32°. The western limit of the formative area is again the Gulf Stream and the eastern limit, though ill-defined, is in the neighbourhood of 45°, or approximately over the Mid-Atlantic Ridge.

The formation of this water has been observed on three occasions ; at one station in the eastern portion (Table 1, Fig. 1) of the formative area and at two consecutive stations in the western portion.

Table 1

Atlantis 1153, 34° 02′N 54° 05′W, 28 *February* 1932

Depth	*Temp.* °C	*Sal.* ‰	0_2 *ml/l*
0	17·94	36·55*	5·08
30	17·92	36·51	5·02
61	17·92	36·50	4·97
122	17·96	36·50	5·05
183	17·91	36·50	5·00
242	17·91	36·51	5·00
363	17·90	36·51	5·01
484	17·04	36·35	4·53
628	15·65	36·08	4·19

On the eastern portion, the water is for all normal purposes isothermal, isohaline and of equal oxygen down to 363 m (Table 1). The two stations in the western portion of the area (*Atlantis* 4170, 34° 17′N 69° 26′W, 3 March 1941 and *Atlantis* 4171, 35° 18′N 68° 24′W, 4 March 1941) were both isothermal at 17·84°C (± 0·04°C), the former to a depth of at least 284 m and the latter to at least 297 m.† Both were isohaline at 36·50‰ ± 0·02‰ to these depths.

These are the only hydrographic stations which show deep, winter mixing of 18° water but there are vast numbers of bathythermograms from the whole length of the northern Sargasso Sea which show isothermal water at about 18° to at least 450 ft (137 m) and a lesser number to at least 900 ft (274 m) in late winter. These slides cannot be used for an adequate study of yearly variations in the supply of 18° water because, unfortunately, 274 m is about 100 m short of the bottom of the mixed layer.

Examples of vertical temperature curves from various points in the Sargasso Sea are shown in Fig. 1. Curve 1 is from the late winter station which has been tabulated above, illustrating the 18° water at its time of formation. Curves 2 and 3 are from the northern Sargasso Sea in spring, showing the extent of the seasonal temperature gradient at that season. *Challenger* station 53 (Curve 2) was included to show the remarkable consistency of the temperature at the inflexion in point of time. Curve 4 is from the southern Sargasso Sea where the 18° water is barely detectible. The 300 m temperature and salinity at this station (17·86°C, 36·49‰) remain the same as in the northern Sargasso Sea.

---

* The salinity value is probably high because a bucket was used instead of a Nansen bottle.

† The bottles on all these stations were spaced at about 100 m intervals so the isothermal layer was almost certainly deeper in each case.

THE DISTRIBUTION OF THE 18° WATER

WYVILLE-THOMSON (1877, pp. 286, 287) was the first to remark on the overabundance of 18° water which he encountered at *Challenger* station 28, in lat. 24° 39′ long. 65° 25′. He was sufficiently impressed by its anomalous appearance at the station that he took an extra series of measurements to confirm its existence. *Challenger's* sections from New York to Bermuda to St. Thomas are reproduced for historical interest and because they illustrate the southward penetration of this water very clearly (Fig. 2).

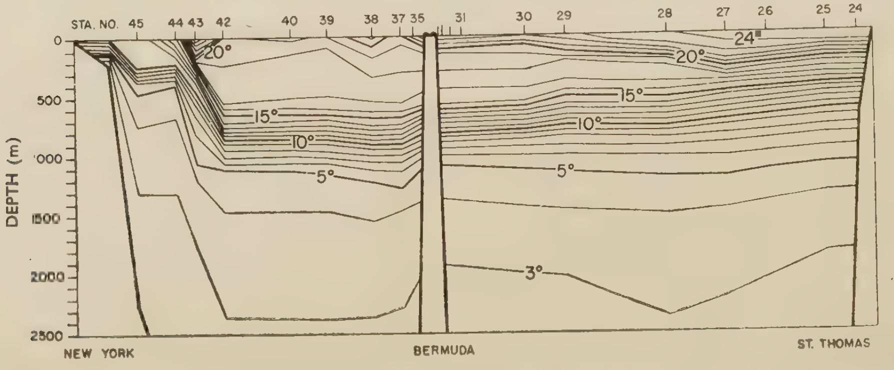

Fig. 2. *Challenger* Sections, 1873. St. Thomas to Bermuda, Bermuda to New York. Reproduced from WYVILLE-THOMSON (1877).

Water of northern Sargasso origin is found at the 300 m level throughout the Sargasso Sea. It can be recognized by either its temperature (usually a fraction of a degree below 18°) or by its salinity which lies close to 36·50‰. A chart of salinity at 300 m has been prepared from station data in the files at Woods Hole (Fig. 3). The black squares delimit the area in which 18° water is found. The eastern boundary is the least well-defined but east of lat. 40° no further water of north Sargasso origin is encountered. A surprising amount enters the Caribbean Sea, presumably through the Windward Passage, but while the squares in question are marked black they are borderline cases very close to 36·40‰. The high salinity values near 24°N 70°W are probably erroneous. The stations in question were made by the author in January 1947 : no postwar salinity data from Woods Hole can be relied upon until April of that year.

Further error would have been introduced if many of the U.S. Hydrographic Office stations had not been eliminated, since their salinity values appear to have had a higher scatter than was acceptable for this work. For evidence of this a histogram of salinity variation in the Bermuda area is reproduced through the courtesy of F. C. Fuglister (Fig. 4). The standard deviation from the mean T/S curve for Hydrographic Office data is ± 0·08‰ to ± 0·09‰ while all other sources up to 1954 yield a standard deviation of ± 0·03‰. Apart from these exceptions this 300 m salinity chart represents a good physical description of the extent of the Sargasso Sea.

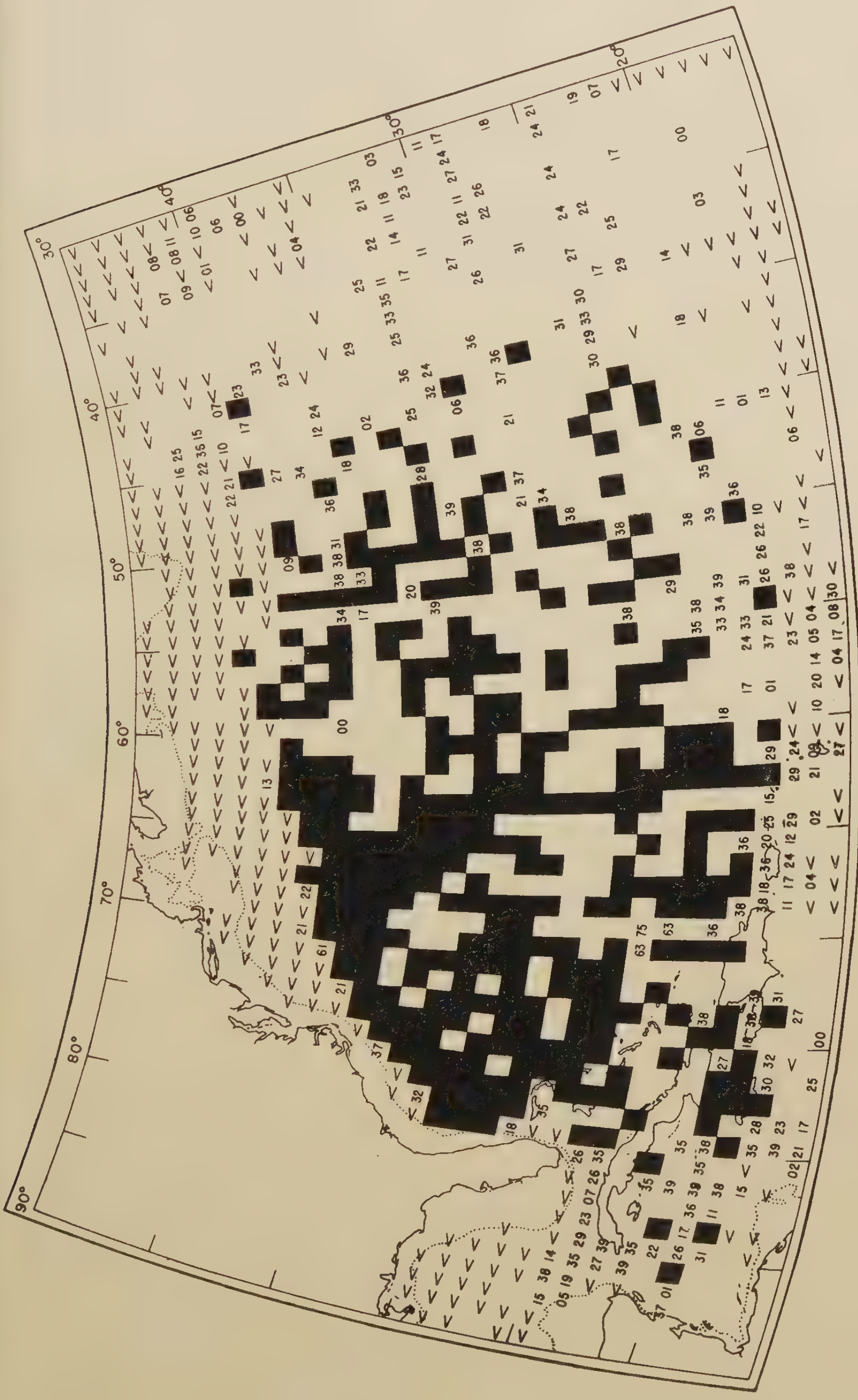
30°
40°
50°
60°
70°
80°
90°
40°
30°
20°

Fig. 3. Salinity at 300 m.
Black squares – 36·40‰ to 36·60‰ only
Numbered squares – 36·00‰ to 36·39‰ and 36·61‰ to 36·99‰
< for values below 36·00‰.

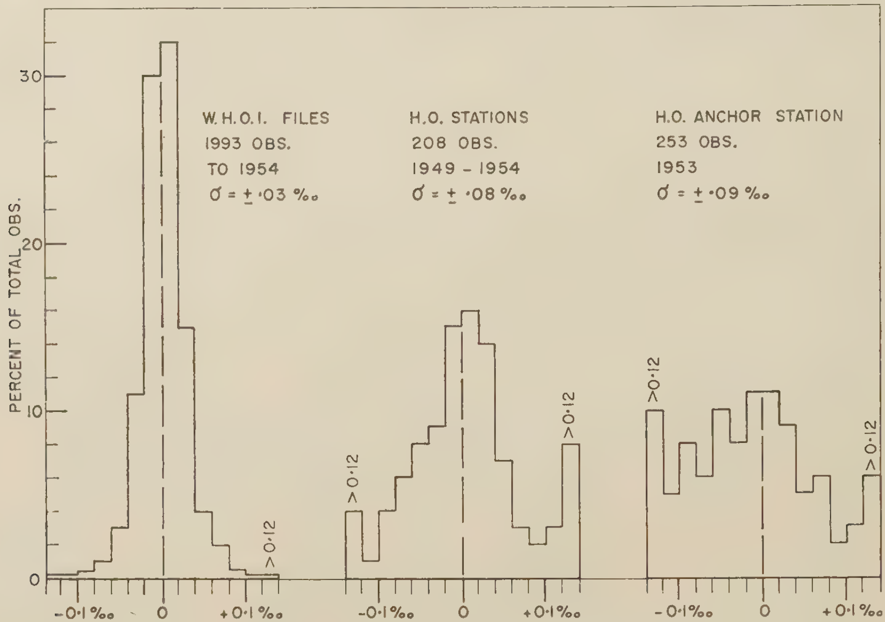

Fig. 4. Salinity variation about a mean curve for $T = \leqslant 18$°C in the Bermuda area (29° to 34°N, 60° to 69°W).

THE OXYGEN CYCLE

It can be seen from the temperature, salinity and oxygen values (Table 1) that the 18° water, during its formation in late winter, is a layer of homogeneous water which is overturned constantly. During the remainder of the year, after thermal stability has developed this water has no further access to the sea surface and its oxygen diminishes slowly due to biological demand.

Rakestraw and Carritt (1948) made a study of the seasonal variations in the chemistry of sea-water at three stations on the Montauk-Bermuda section, which were repeatedly occupied during 1937-1938. Their oxygen values at 300 m at station " C " which lies within the area of formation (op. cit. Fig. 5) were as follows :

		ml/l	*Putative Age*
December	1937	4·55	9 months
April	1938	4·95	1 month
July	1938	4·75	4 months
September	1938	4.45	6 months

This suggests that the biological consumption of oxygen is of the order of 0·5 ml/l/year in the core of the 18° water.

Further south in the Sargasso Sea the 18° water is characterized by an inflexion in the oxygen curve, or, more frequently by a reversal of the downward oxygen trend at 300 m. At station 1483 (curve 4, Fig. 2) the oxygen at 225 m was 4·63 ml/l and at 301 m, 4·75 ml/l. Reversals of this nature, while small, are almost always found south of 33°N to about 20°N in the Sargasso Sea. Of 172 recent stations which lie in an area between 33°N and 20°N and between 50°W and the Florida Current, 117 show a reversal of the oxygen curve at or near 300 m. Forty-seven show an inflexion of the curve at that depth and in only 8 is the influence of the 18° water not perceptible in the oxygen curve. The latter almost without exception lie in the extreme southern border of the area. These reversals which are not found elsewhere in the North Atlantic suggest that the water at 300 m is of more recent origin than that immediately above it. Since this higher oxygen layer is maintained despite a biological demand of 0·5 ml/l/year it should follow that the convergence of 18° water is active during most winters.

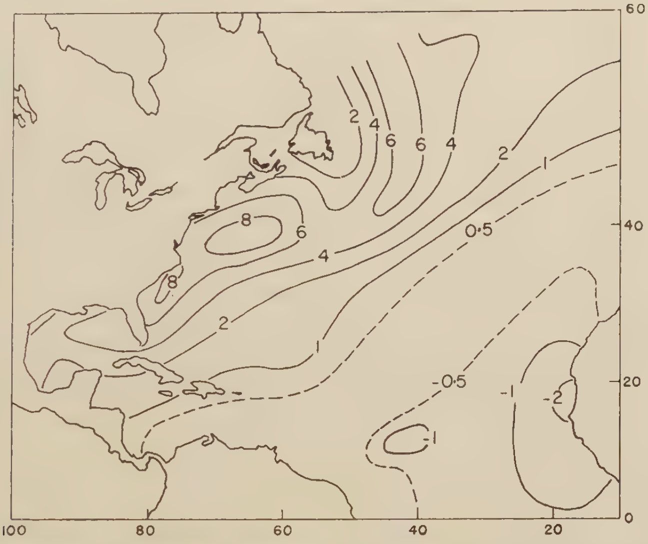

Fig. 5. Mean temperature difference (Fahrenheit) between sea-surface and air. December, January and February. From " Atlas of Climatic Charts of the Oceans." U.S. Weather Bureau No. 1247, 1938.

DISCUSSION

The 18° water in the Sargasso Sea is formed by a convergence which appears to be active at the end of nearly every winter. The convergence is caused by the extreme difference between water and air temperatures in winter (Fig. 5) producing the water type $T = 18°$, $S = 36{\cdot}5‰$ in excess quantity. This water then flows southward along the density surface for $\sigma t = 26{\cdot}4$, or thereabouts. It is difficult to suggest why the 18° isotherm is favoured ; one might have expected that in an extremely cold winter, water in the region south of the Gulf Stream might be cooled to 17°C but this has never been observed and one must judge on the basis of existing measurements that anomalously cold winters merely produce a larger volume of water of the same type.

The salinity value of 36·5‰ is easier to understand since the convergence must draw on the surface waters to the south for its supply of water. These waters according to Böhnecke's (1936) atlas are close to that value. The Gulf Stream can be safely eliminated as a source since its surface temperature is too high and its surface salinity too low at all times of year to reach $\sigma t = 26{\cdot}4$.

The volume of 18° water can be roughly estimated by considering it as a wedge. The base of the wedge which represents the northern boundary of 18° water is 250 m thick and 2000 km long (east to west). The wedge tapers to its apex about 1500 km south of the northern boundary. The volume of water in the wedge is thus 375,000 km^3.

Probably all of this water is not renewed at the end of each winter but if it were, the amount of water turned over would be immense. If it is assumed that the renewal takes place in about 11·6 days (roughly a million seconds) the turnover would average 375 million m^3/sec during that period. If only 20 per cent were renewed, which seems conservative, the turnover would be 75 million m^3/sec, or roughly the equivalent of the Gulf Stream's transport (ISELIN, 1940). The average southward velocity necessary to effect this transport (in the latter case) is 15 cm/sec which is well within the scope of modern current measuring devices.

The importance of 18° water to the study of general circulation is that it provides a simple example of the way the thermocline structure of the oceans is affected by the atmosphere at the sea surface. At present the different shapes assumed by the thermocline are only dimly understood. The influence of the late winter weather conditions south of the Gulf can be felt as far south as the Caribbean Sea (Fig. 3). If the Geostrophic Equation is to be believed these conditions must have considerable influence on the volume transport of the upper layers of the Gulf Stream.

There is good evidence that the same sort of convergence occurs south-east of Japan, south of the Kuroshio where similar winter weather conditions prevail. Here, however, the water at the inflexion is characterized by a temperature of about 16·5° (and a salinity of 34·75‰ at a depth of 250 m*). In both oceans there is a strong thermocline beneath the isothermal layer formed by the winter convergence. If we assume that these permanent thermoclines represent the bottom, the waters above resemble a small scale thermal model of the world oceans.

A parallel can be drawn, for example, between the shallow waters of the Sargasso Sea and the North Atlantic as a whole, if we consider the 18° water in the former case to be analogous to the North Atlantic Deep Water in the latter. In both cases it is important to realize that the largest quantities of water converged come very close to being a single water type : in the upper 400 m of the Sargasso Sea the water type is $T = 18°$, $S = 36{\cdot}5‰$; in the Atlantic as a whole the water type is potential temperature $= 2°C$, $S = 34{\cdot}9‰$.

MONTGOMERY (1958) has presented diagrams of potential temperature versus salinity for the Atlantic Ocean (and the world ocean) in which the volume of water for each 0·5°C increment of potential temperature and each 0·1‰ of salinity has been estimated. By far the largest node in his Atlantic Diagram (op. cit. Fig. 3) is between 1·5°C and 4°C and 34·8‰ to 35·0‰ which represents North Atlantic Deep Water. This node comprises 40 per cent of the entire volume of the North and South Atlantic, exclusive of adjacent seas.

The principal weakness in the analogy between the two water types is that new 18° water is abundantly available for convergence at the end of each winter in the northern Sargasso Sea while no appreciable quantity of water resembling $T = 2°C$, $S = 34{\cdot}9‰$ can be found within 2000 m of the surface in the North Atlantic at the present time. The conclusion (WORTHINGTON, 1954) that North Atlantic Deep Water is no longer being produced in bulk is strengthened by this comparison. However, it is clearly necessary to make a more careful investigation of the formative areas of both water types in late winter in order to assess the climatic conditions which must prevail if large quantities of water are to be converged.

---

* A particularly fine example was provided by the Japanese Research Ship *Kosyu's* section " A " in August 1936 ; Hydrographic Bulletin, Special Number, No. 8. Maritime Safety Agency, Tokyo, Japan, p. 83.

Woods Hole Oceanographic Institution
Woods Hole, Massachusetts

Contribution No. 1015 *from the Woods Hole Oceanographic Institution. This research was sponsored by the Office of Naval Research under contract Nonr*-2196.

REFERENCES

Böhnecke Günther (1936) Atlas zu : Temperatur, Salzgehalt und Dichte an der Oberfläche des Atlantischen Ozeans. Deutsche Atlantische Expedition METEOR 1925-1927, *Wiss. Erg., Bd.* V, Berlin.

Iselin C. O'D. (1936) A study of the circulation of the western North Atlantic. *Pap. Phys. Oceanogr. Meteor.* **4**, 1-101.

Iselin C. O'D. (1940) Preliminary report on long-period variations in the transport of the Gulf Stream system. *Pap. Phys. Oceanogr. Meteor.* **8** 1-40.

Montgomery R. B. (1958) Water characteristics of Atlantic Ocean and of world ocean. *Deep-Sea Res.* **5**, 134-148.

Rakestraw N. W. and Carritt D. E. (1948) Some seasonal chemical changes in the open ocean. *J. Mar. Res.* **7** 362-369.

Thomson C. Wyville (1877) The voyage of the *Challenger*. *The Atlantic*. Macmillan London, Vol. 1, 1-424.

Worthington L. V. (1954) A preliminary note on the time scale in North Atlantic circulation. *Deep-Sea Res.* **1** 244-250.

Printed n Great Britain by The Salisbury Press Ltd., Publicity House, Wilton Road, Salisbury, Wilts. (15664)

Contribution No. 1016

Reprinted from SCIENCE, September 11, 1959, Vol. 130, No. 3376, pages 602–608.

Potential Productivity of the Sea

Organic production by marine plankton algae is comparable to agricultural yields on land.

John H. Ryther

Under ideal conditions for photosynthesis and growth, what is the maximum potential rate of production of organic matter in the sea? Is this potential ever realized, or even approached? How does the sea compare with the land in this respect? These questions may be approached empirically with some measure of success but, aside from the time and effort required by this method, one can never be certain how close to the optimum a given environment may be and, hence, to what extent the biotic potential is realized.

However, we do know with some degree of certainty the maximum photosynthetic efficiency of plants under carefully controlled laboratory conditions; and there is a considerable literature concerning the effects of various environmental conditions on photosynthesis, respiration, and growth, particularly with respect to the unicellular algae. From such information it should be possible to estimate photosynthetic efficiencies and, for given amounts of solar radiation, organic production under natural conditions. This indirect and theoretical approach cannot be expected to provide exact values, but it does furnish a supplement to the empirically derived data which may help substantiate our concepts both of the environmental physiology of the plankton algae and the level of organic production in the sea.

An attempt has been made to use this joint approach for the marine environment in the following discussion. The only variable considered is light, and the assumption is made that virtually all of the light which enters the water (and remains) is absorbed by plants. Such situations are closely approximated in plankton blooms, dense stands of benthic algae, eelgrass, and other plants. For the rest, it is assumed that temperature, nutrients, and other factors are optimal, or at least as favorable as occur under ideal culture conditions. Given these conditions, I have attempted to calculate the organic yields which might be expected within the range of solar radiation incident to most of the earth. These data are then compared with maximal and mean observed values in the marine environment and elsewhere, and an attempt is made to explain discrepancies.

The calculations which appear below are based, for the most part, upon experimentally derived relationships between unicellular algae and the environment, and are therefore applicable only to this group. This must be kept in mind when, later in the discussion, comparisons are drawn between the theoretical yields and observed values

---

The author is on the staff of the Woods Hole Oceanographic Institution, Woods Hole, Mass. This article is based on a paper presented by the author at the AAAS meeting in Washington, D.C., December 1958.

of production by larger aquatic and terrestrial plants.

The values for the efficiency of photosynthesis under natural conditions are based on the utilization of the visible portion of the solar spectrum only (400 to 700 mμ), or roughly half of the total incident radiation. In converting these efficiencies to organic yields, it is assumed that the heat of combustion of the dry plant material is 5.5 kcal per gram, which closely approximates values for unicellular algae reported by Krogh and Berg (*1*), Ketchum and Redfield (*2*), Kok (*3*), Aach (*4*), Wassink *et al.* (*5*), and others.

Reflection and Backscattering

Of the sunlight which strikes the surface of the ocean, a certain fraction is reflected from its surface and never enters the water. The remainder penetrates to depths which depend upon the concentration of absorbing and scattering particles or dissolved colored substances. While scattering may be as important as absorption in the vertical attenuation of the light, it makes little difference as far as the biological utilization of the radiation is concerned, since the scattered light is eventually absorbed, with the exception of a small fraction which is backscattered up out of the water. The combined reflected and backscattered light is lost to the aquatic system; the rest remains in the water, where, under the ideal conditions postulated, it is absorbed entirely by plants.

The fraction of the incident radiation which is reflected and backscattered has been studied by Powell and Clarke (*6*), Utterback and Jorgenson (*7*), and Hulburt (*8*). The two factors have been treated separately, but they may be considered together here. Their combined effect is rather small, ranging from about 3 to 6 percent, depending somewhat upon who made the measurements and the conditions under which the measurements were made. The highest values were observed when the sky was overcast. Sea states, ranging from flat calm to whitecap conditions, made surprisingly little difference. Reflection and backscattering were also found by Hulburt to be independent of the sun's angle, despite the fact that reflection increases greatly with the angle (from the zenith) of the incident light, particularly at angles above 60°. The explanation for this apparent contradiction lies in the fact that as the sun approaches the horizon, indirect sky light becomes increasingly important, and it eventually exceeds the intensities of the sun itself.

Hulburt's data also indicate that backscattering is not greatly influenced by the amount of particulate matter in the water, since his values in the clear Gulf Stream did not differ appreciably from those made in the turbid waters of Chesapeake Bay.

For the calculations which are made here, it is considered that an average of 5 percent of the incident radiation is lost through the combined effects of reflection and backscattering.

Photosynthesis and the Visible Spectrum

We first consider the efficiency of photosynthesis in sunlight at levels below the saturation intensity. Within this range, photosynthesis is directly proportional to the light intensity (or very nearly so), and the efficiency is therefore constant.

Despite the vast numbers of studies of quantum yield (that is, photosynthetic efficiency) in the literature, few data are available for the entire visible spectrum. Figure 1*A* shows two such series of measurements, one with the green alga *Chlorella* (Emerson and Lewis, *9*), the other with the diatom *Navicula*

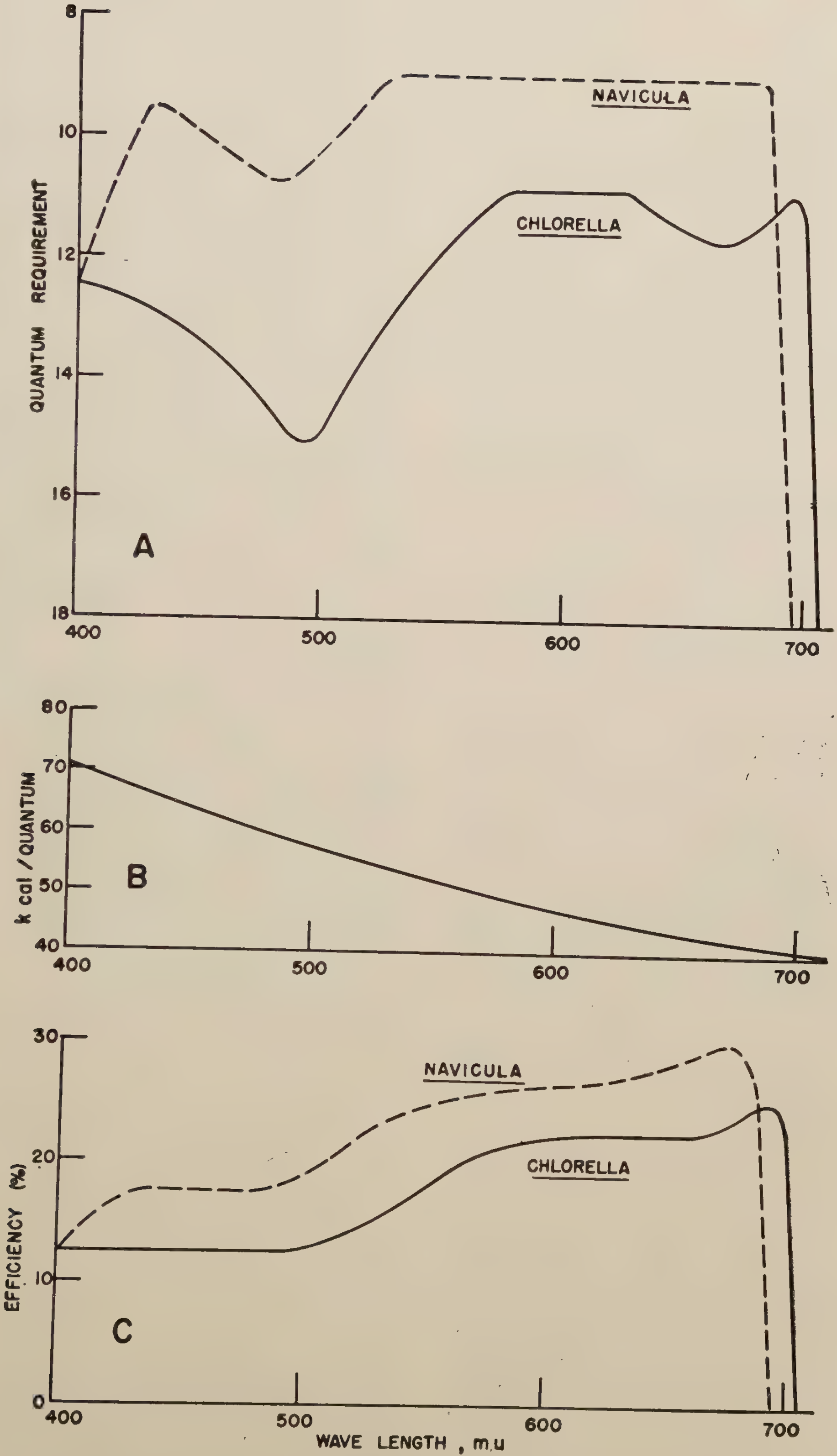

Fig. 1. (*A*) Quantum requirement of photosynthesis as a function of wavelength of light for *Chlorella* [after Emerson and Lewis, *9*] and for *Navicula* [after Tanada, *10*]. (*B*) Energy per mole quantum of light as a function of wavelength. (*C*) Efficiency of photosynthesis as a function of wavelength, calculated from (*A*) and (*B*).

minima (Tanada, *10*). The ordinate is expressed as quantum requirement (the number of quanta required to reduce 1 mole of CO_2) rather than a reciprocal, quantum yield (moles of CO_2 reduced per quantum) as shown originally by the authors. Although the two organisms have strikingly different pigment complements, the curves are surprisingly similar, with minimal requirements in the red and yellow parts of the spectrum, maximal in the blue-green. *Navicula* appears to be somewhat more efficient than *Chlorella,* but the differences may not be significant.

Figure 1*B* illustrates the fact that the energy per quantum between 400 and 700 mμ decreases from a maximum of 71 kcal per mole quanta of blue light to 41 cal per mole quanta of red light. The heat of combustion of one reduced mole of CO_2 (reduced to CH_2O) is 112 kcal. A quantum requirement of 10 therefore represents an efficiency of $112/(41 \times 10) = 27.3$ percent in red light and $112/(71 \times 10) = 15.7$ percent in blue light. Figure 1*C* shows the efficiencies of *Chlorella* and *Navicula* throughout the visible solar spectrum.

The spectral distribution of daylight varies with solar altitude and with the water vapor, carbon dioxide, and dust content of the atmosphere. Figure 2 shows the spectral distribution of daylight under average atmospheric conditions and with an air mass of 2 (solar angle = 30° from zenith) as given by Moon (*11*).

If the curves in Fig. 1*C* are averaged and the mean efficiency for the entire visible spectrum is calculated, weighing the mean for the average spectral distribution of sunlight as given in Fig. 2, this value turns out to be 18.4 percent. Taking into consideration a 5-percent reflection and backscattering loss, the efficiency of photosynthetic utilization of visible sunlight *below saturation intensity* incident to the water surface is 17.5 percent.

In extremely turbid waters and in those containing organic stains (the "yellow substance" described by Kalle, *12*), blue and green light may be selectively absorbed, resulting in somewhat higher efficiencies in the utilization of the light penetrating to greater depths. On the other hand, in normal, clear oceanic water the red light is selectively absorbed by the water and blue-green light penetrates to the greatest depths, where it is used still less effectively than the average incident daylight considered above. These modifications are not considered in this article, since we are dealing with an idealized situation in which all of the light entering the water is absorbed by plants.

Intensity Effect

Above the saturation point, photosynthesis does not increase in proportion to light intensity, but remains constant or, at high intensities, is actually depressed, owing to photooxidation or other inhibitory processes.

Figure 3*A* shows a curve of photosynthesis by marine plankton algae as a function of light intensity, from Ryther (*13*). This is a mean curve of experiments with cultures of 14 species of organisms, preconditioned to a variety of different light regimes. Photosynthesis was measured by C^{14} uptake under solar radiation during the 4-hour period (10 A.M. to 2 P.M.) when the intensity is nearly constant and maximum. Graded intensities were obtained with neutral density filters. Almost identical curves were obtained by Steemann Nielsen and Jensen (*14*) for natural plankton populations.

Photosynthetic efficiencies remain constant, or nearly so, up to the saturation point, but then decline sharply at higher intensities. This decrease is illustrated by the difference between the actual photosynthesis curve in Fig. 3*A* and the dotted

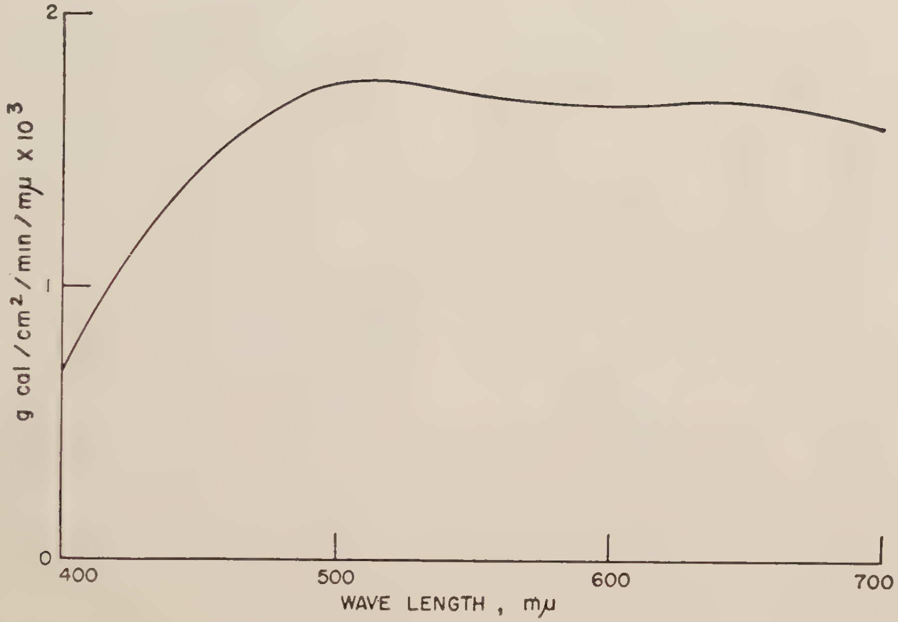

Fig. 2. The spectral distribution of daylight under average atmospheric conditions with air mass equal to 2. [After Moon, *11*]

line, which is an extrapolation of the linear portion of the solid curve and represents photosynthesis if the efficiency remained constant. Figure 3*B* shows relative efficiencies as a function of light intensity, obtained from the ratio between the solid and dotted lines in Fig. 3*A*.

Using the data in Fig. 3*A*, Ryther (*13*) has calculated relative photosynthesis throughout the day and at various depths within the euphotic (illuminated) zone of the ocean for days with different values for total incident radiation. Several curves were thereby produced showing values for total daily photosynthesis at several depths within the euphotic zone relative to the hourly rate of photosynthesis at light saturation.

On extremely dull days, when the intensity never reaches the saturation region, photosynthesis is directly proportional to light intensity at all depths, and the curve of photosynthesis with depth shows an exponential decrease from the surface, as does that of light. On bright, sunny days, intensities at the surface exceed saturation and normally produce inhibition (which occurs at ⅓ or less the intensity of full sunlight). On such days, photosynthesis at the surface is less than that at intermediate depths. In all cases, photosynthesis at depths where the surface light is reduced to 10 percent or less is directly proportional to intensity, and in this region it decreases exponentially, following the light curve.

By extrapolating the lower, exponential portion of the photosynthesis curve to the surface, one may create a hypothetical curve of photosynthesis if the latter maintained the same efficiency at all depths. The ratio of the actual photosynthesis curve to this hypothetical exponential curve will then show the reduction in efficiency caused by light intensities above saturation in the upper waters. This has been done in Fig. 4 for a series of photosynthesis curves on days of varying incident radiation. Since photosynthesis at the various depths is a function of light intensity and not of depth per se, the units on the ordinate of Fig. 4 are natural logarithms of I_0/I and thus represent the depths to which given fractions of the incident radiation penetrate. The curve for the day with lowest radiation (20 gcal/cm² day) is exponential all the way to the surface, indicating that on such a day there is no reduction in photosynthetic efficiency from the effects of light intensity. On days of progressively higher light intensity, the photosynthesis curve departs more and more from the exponential curve illustrating the increasing reduction in efficiency.

If it is assumed that the maximum efficiency (with no intensity effect) is 17.5 percent, as calculated in the previous section, Fig. 5 shows the cumulative intensity effect with efficiencies plotted as a function of total daily incident radiation. The points were obtained from Fig. 4 from the ratio of the actual photosynthesis curves for each value of radiation to the exponential curve of maximum (17.5 percent efficiency. It may be seen that efficiencies decrease from 17.5 percent at low intensities to 6.5 percent on a day when 600 g cal/cm² reaches the earth's surface. It is noteworthy that the efficiency curve does not decrease in a regular way with increasing intensities, but that the rate of decrease becomes less at higher intensities. This is due to the fact that higher values of daily radiation are caused not only by higher intensities of sunlight but to an even greater extent by longer days including more hours of low intensity light.

We are now ready to calculate photosynthesis for different values of incident radiation from the efficiency curve shown in Fig. 5. This is done by multiplying the efficiency by one-half the appropriate values of radiation (that portion of the solar spectrum available for photosynthesis). This gives the amount of energy fixed in photosynthesis. Dividing this by 5.5 (the heat of combustion of a gram of average plant material, as discussed in the first section) we obtain a value which represents grams of organic matter produced per day beneath a square meter of water surface, provided that all the light entering this 1-meter-square column of water is effectively absorbed by plants. These values, shown as the upper broken line in Fig. 5, are equivalent to "real photosynthesis" or "gross production." They are hypothetical in the sense that they cannot be observed as a yield, since the plants must draw upon this organic matter to satisfy their own metabolic requirements. We must therefore subtract an amount of organic matter equivalent to the plants' respiration in order to calculate the amount of material available for harvest, the so-called "net production."

Respiratory Loss

Under conditions of active growth, photosynthesis at light saturation is some 10 to 20 times as great as dark respiration (see Ryther, *15*). Higher values have been reported, but it seems doubtful that they could represent steady-state conditions in natural populations. If we take a ratio of 15:1 as average for $P:R$ (photosynthesis: respiration) at optimal light, it is obvious that over a 24-hour period, half of which is dark, and within an entire plant community, of which many of the plants are in suboptimal light at all times, respiration must account for a much greater fraction of photosynthesis.

In calculating the ratio $P:R$ in natural communities, the oversimplified assumption will be made that respiration remains constant and independent of light and photosynthesis. While the literature pertaining to this subject is contradictory and in a state of great confusion (see, for example, Rabinowitch, *16*), there is mounting evidence that respiration and photosynthesis are not wholly independent processes. However, since there is no good quantitative formulation of a relationship between them which may be incorporated into our calculations, it must be neglected here.

As mentioned above, the data from Fig. 3*A* together with light intensity values for a group of days with varying total incident radiation have been used to calculate photosynthesis as a function of radiation. (See Ryther, *13,* for a full description of these calculations). The values given by this treatment represent photosynthesis per day beneath a square

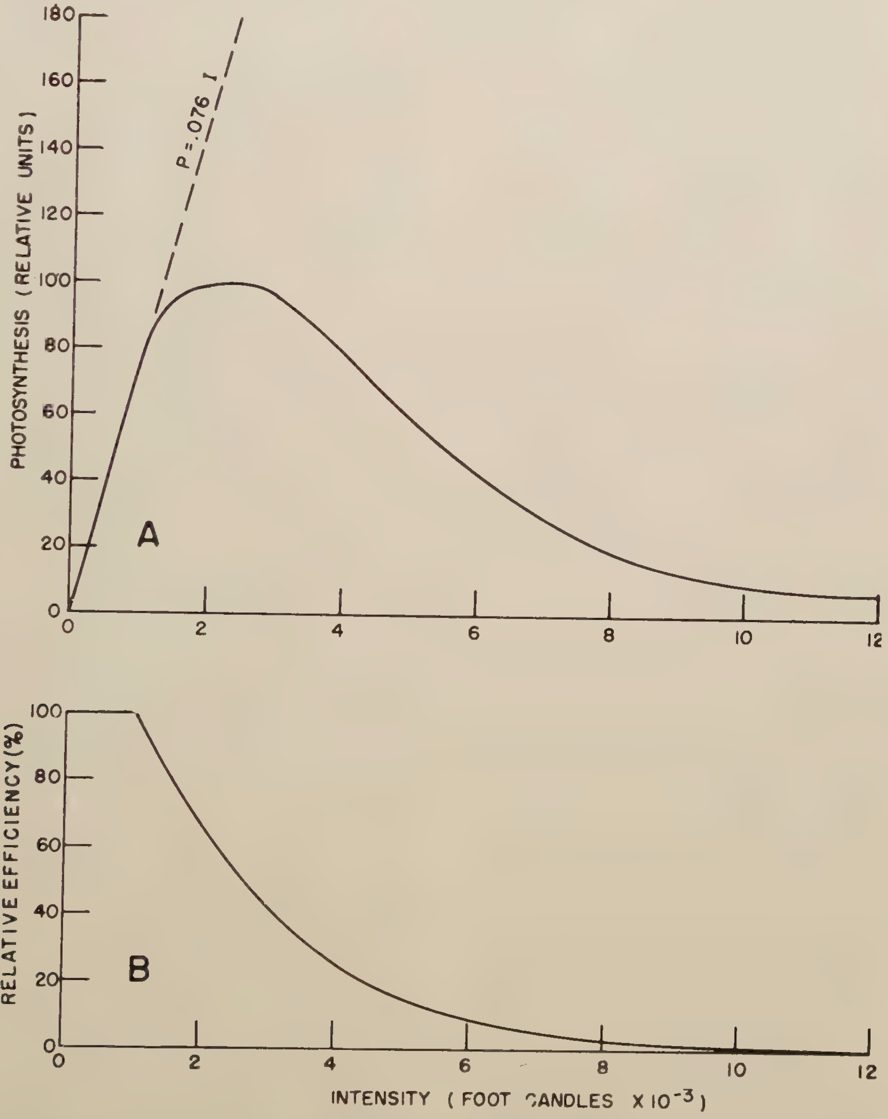

Fig. 3. (*A*) Photosynthesis of marine phytoplankton as a function of light intensity [after Ryther, *13*]. Broken line is the extrapolation of the linear portion of the solid line representing hypothetical sustained maximum photosynthetic efficiency. (*B*) Efficiency of photosynthesis as a function of light intensity, calculated from *A*.

meter of surface relative to the value for photosynthesis per cubic meter per hour at light saturation. For example, a value of 100 would mean that daily photosynthesis beneath a 1-meter-square water column is 100 times as great as photosynthesis within a 1-cubic-meter aliquot of that water column for 1 hour at optimal light intensity (assuming that the plant population is evenly distributed within this water column).

Since respiration is 1/15 photosynthesis at light saturation and is also stipulated to be constant with respect to light, depth, and time of day, we may calculate total daily respiration in the same relative units as photosynthesis. The curves of photosynthesis and respiration as functions of radiation are shown in Fig. 6. They cross at 100 g cal/cm^2 × day, which may be considered the daily compensation level for an entire plant community. The value $(R/P) \times 100$ is the percentage of respiratory loss and is shown as the lower broken line in Fig. 6. It ranges from 100 percent at radiation values of 100 g cal/cm^2 day or less to 28 percent on extremely bright, long days.

Net Production

Returning to Fig. 5, gross production may be reduced by the respiratory loss (Fig. 6), giving the curve of net production, which begins at 100 g cal/cm^2 day and reaches a value of 25 g/m^2 day under radiation of 600 g cal/m^2 day (the lower broken line in Fig. 5).

Although the annual range of daily incident radiation is extremely wide, even for a given latitude, this short-term variability is probably not very significant in affecting the general level of organic production of a given area. If one examines the tables compiled by Kimball (*17*) showing mean monthly radiation for different latitudes, it appears that over 80 percent of the data (including all latitudes and seasons) fall within a range of 200 to 400 g cal/cm^2 day. Thus, over most of the earth for most of the year a potential production of organic matter of some 10 to 20 g/m^2 day may be expected, while for shorter periods of fine summer weather, a net production of 25 g/m^2 day or slightly more may occur.

Comparison of Theoretical and Observed Production Rates

We may now compare the production rates which were calculated in the preceding sections with some values which have been observed empirically. Since the former are based on hypothetical situations in which all light entering the water is absorbed by plants, the observational data, to be comparable, must be restricted to natural environments in which these conditions are at least closely approximated (for example, in dense plankton blooms, thick stands of benthic algae and rooted plants). In addition to these maximal values, the theoretical potential may be contrasted with average oceanic productivity rates.

We may also extend this comparison to the terrestrial environment, including some of the better agricultural yields, bearing in mind, however, that the physiology and hence, perhaps, the biotic potential of land plants may differ significantly from those of algae.

Finally, we may include the yields of *Chlorella* grown in outdoor mass culture, drawing here upon the excellent, continuing studies of H. Tamiya and his collaborators. These are of particular interest, since the conditions of these experiments were as optimal as possible and since the physiology of *Chlorella* is identical or closely similar to that of the organisms upon which our calculations are based. Thus the *Chlorella* yields will serve as a check for the theoretical production rates.

Table 1. Gross and net organic production of various natural and cultivated systems in grams dry weight produced per square meter per day.

System	Gross	Net
A. Theoretical potential		
Average radiation (200 to 400 g cal/cm² day)	23–32	8–19
Maximum radiation (750 g cal/cm² day)	38	27
B. Mass outdoor Chlorella *culture* (*26*)		
Mean		12.4
Maximum		28.0
C. Land (*maximum for entire growing seasons*) (*18*)		
Sugar cane		18.4
Rice		9.1
Wheat		4.6
Spartina marsh		9.0
Pine forest (best growing years)		6.0
Tall prairie		3.0
Short prairie		0.5
Desert		0.2
D. Marine (*maxima for single days*)		
Coral reef (*27*)	24	(9.6)
Turtle grass flat (*28*)	20.5	(11.3)
Polluted estuary (*29*)	11.0	(8.0)
Grand Banks (Apr.) (*30*)	10.8	(6.5)
Walvis Bay (*23*)	7.6	
Continental Shelf (May) (*19*)	6.1	(3.7)
Sargasso Sea (Apr.) (*31*)	4.0	(2.8)
E. Marine (*annual average*)		
Long Island Sound (*32*)	2.1	0.9
Continental Shelf (*19*)	0.74	(0.40)
Sargasso Sea (*31*)	0.88	0.40

It is important, in making these comparisons, to keep in mind the distinction between gross and net production as defined above. Some of the data refer to true photosynthesis measurements (gross production) while others, such as the *Chlorella* experiments and the agricultural yields, are based on the actual harvest of organic matter (net production). In those cases in which only gross production values are available and where radiation data are given, net production has been obtained from Figure 5 and is shown in parentheses.

The theoretical production potential for average and maximal radiation, and the observational data for both marine and terrestrial environments, are given in Table 1. In each case the original source is given, except for the land values, where reference is made to the recent compilation by Odum (*18*). The various methods by which the values were obtained will not be discussed here except in the case of the unpublished data, in which gross production was calculated from chlorophyll and light, according to the method of Ryther and Yentsch (*19*) and net production was measured by the C^{14} method, uncorrected for respiration as this method is interpreted by Ryther (*20*). Where gross production (photosynthesis) was originally reported as oxygen evolution, this has been converted to carbon assimilation, using an assimilatory quotient

$$\left(\Delta\frac{+O_2}{-CO_2}\right)$$

of 1.25 (see Ryther, *20*). Carbon uptake, in turn, has been converted to total organic production by assuming that the latter is 50 percent carbon by weight.

The maximal values for the marine environment represent the seven highest such values known to me. In addition to these, data are given for three regions (one inshore, one coastal, and one offshore) which have been studied over long enough periods of time to justify the calculation of annual means.

Discussion

The mean yield of *Chlorella* obtained by the Japanese workers is almost identical to the mean theoretical production for days of average radiation (12.4 versus 13.5 g/m² day). These yields of *Chlorella* were produced only during the warmer part of the year, presumably owing to the poor growth of *Chlorella* at low temperatures. The highest yields of *Chlorella* (up to 28 g/m² day) were, according to Tamiya, "obtained on fair days in the warmer months." This maximum is approximately the same as the theoretical net production for days of maximum radiation. Thus, the *Chlorella* yields agree very well with the theoretical productive potential of the sea.

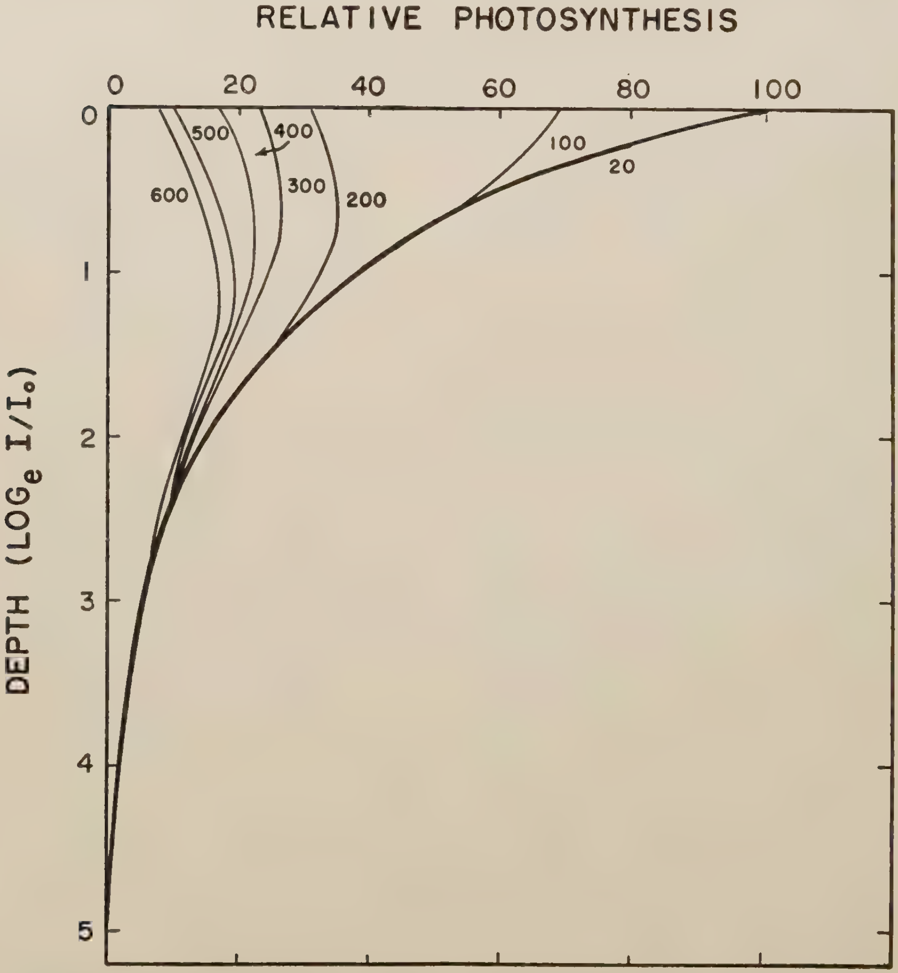

Fig. 4. Relative photosynthesis as a function of water depth for days of different incident radiation. Numbers beside curves show gram calories per square centimeter per day.

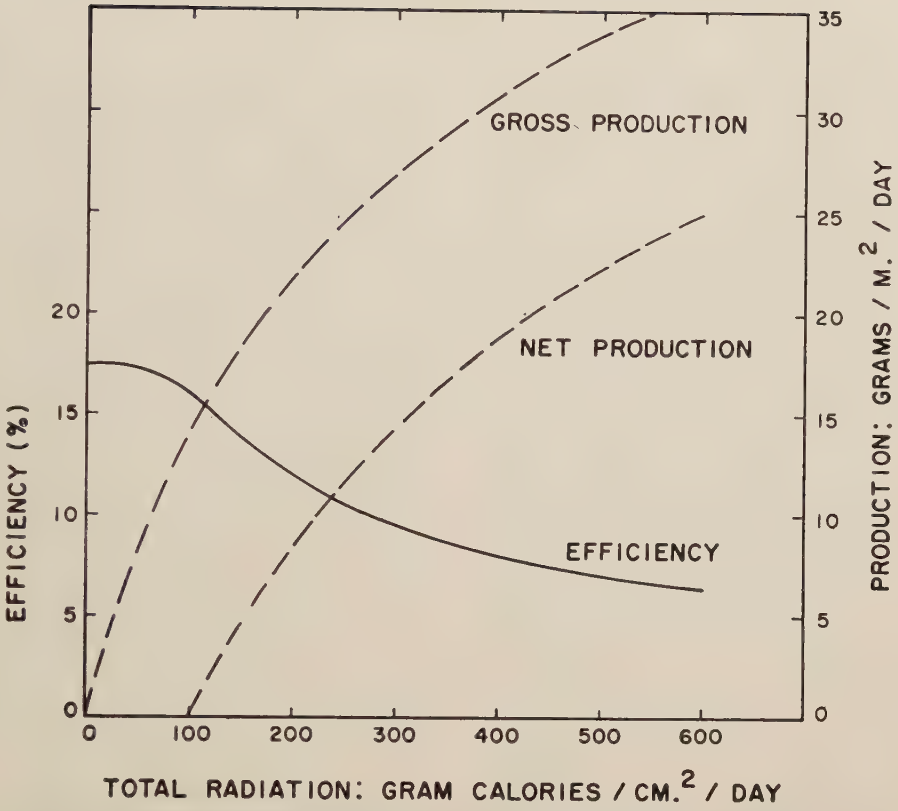

Fig. 5. Photosynthetic efficiency and theoretical maximum potential gross and net production as a function of incident radiation.

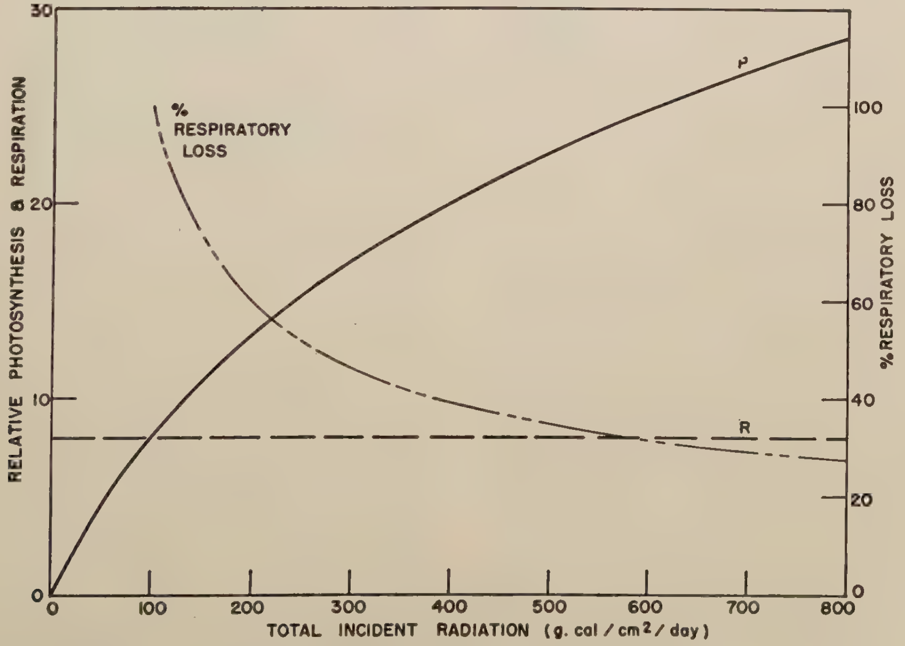

Fig. 6. Relative photosynthesis, respiration, and percentage of respiratory loss as a function of incident radiation.

The land values for net production quoted from Odum's tables range from 18.4 g/m² day for the highest yields of sugar cane to 0.2 g/m² day for deserts. The best agricultural yields are generally of the same order of magnitude as the theoretical net production of the sea, as are the values for the salt marsh and the pine forest (during its years of best growth). Uncultivated grasslands range from 3.0 for tall prairie to 0.2 for desert conditions. Because of the extreme contrasts among terrestrial environments, mean values for the land as a whole are difficult to determine and would have little meaning. It is interesting, however, that Schroeder's estimate (*21*) of the annual production of all the land is equivalent to a mean daily production of 0.55 g/m², roughly the same as the value given in Table 1 for short prairie grass.

With regard to the marine data, it is perhaps surprising that net production rates differ by less than a factor of 2 in such diverse environments as a coral reef, a turtle grass flat, a polluted creek, and the Grand Banks. This alone would indicate that production in each case is limited by the same basic factor, the photosynthetic potential of the plants, and indeed these and the other high values in *D* in Table 1 all closely approach the theoretical potential.

Seasonal studies have been made of three marine areas, Long Island Sound, the continental shelf off New York, and the Sargasso Sea off Bermuda. In each case temporary rates of production were observed during the spring flowering which approached the theoretical maximum, but the annual means were more than an order of magnitude lower (*E* in Table 1). True, these regions do not, throughout the year, satisfy the postulated conditions necessary to obtain this maximum, namely, that all light entering the water be absorbed by plants. For example, in his Long Island Sound studies, Riley (*22*) found that no more than one-third of the incident radiation was utilized by plants, the remainder presumably being absorbed by nonliving particulate and dissolved materials. Using Riley's techniques, I estimated that only 25 to 40 percent of the light penetrating the continental shelf waters was absorbed by the phytoplankton. This alone, however, is insufficient to account for the discrepancy between observed and potential production rates. In the clear waters of the Sargasso Sea only 10 to 20 percent of the light is absorbed by the phytoplankton during most of the year. But there is little if any other particulate matter present; the remainder of the light is absorbed by the water itself. This is not a cause but an effect of low production. The underlying reason for low production rates here and in most parts of the ocean is the limitation of essential nutrients in the upper, euphotic layers and the inadequacy of vertical mixing processes in bringing deep, nutrient-rich water to the surface.

With the exception of the three planktonic communities which have been discussed, the seasonal cycles of marine production are largely unknown and can only be surmised. Probably high levels may be maintained throughout the year in benthic populations such as the coral reef, the turtle grass flats (see *D* in Table 1) and in thick beds of seaweeds, provided that seasonal temperature extremes do not impair growth. While the concentrations of nutrients in the surrounding waters may be very low, the fact that they are continually being replenished as the water moves over the plants probably prevents their ever being limiting. Plankton organisms, on the other hand, suspended as they are in their milieu, can probably never maintain high production rates in a given parcel of water, for their growth rapidly exhausts the nutrients from their surrounding environment and any mixing process which enriches the water must, at the same time, dilute the organisms.

However, high plankton production may be sustained in a given geographic area (a polluted estuary, a region of permanent upwelling of deep water, and so forth), which is continually replenished with enriched water. In these situations, the productive capacity of the sea may be sustained for long periods, perhaps permanently.

For most of the ocean, as stated above, no such mechanism for nutrient replenishment is available. The combined meteorological and hydrographic conditions which produce the typical spring flowering of the phytoplankton over much of the oceans have been adequately described elsewhere and need not be discussed here. Suffice it to say that, in the oceans as a whole, as seasonal studies have demonstrated, high production approaching the theoretical maximum under optimal conditions is restricted to periods of a few days or, at most, weeks, per year.

Steemann Nielsen (*23*) has recently estimated the net production of the entire hydrosphere as 1.2 to 1.5×10^{10} tons of carbon per year, roughly one-tenth the earlier estimates made by Riley (*24*) and others, and about comparable to Schroeder's figure (*21*) for the land. Our production estimates are somewhat higher than those of Steemann Nielsen, the annual mean net production of organic matter for the Sargasso Sea (0.40 g/m^2 day) being about 6 times as great as his value for the same area, and twice his average for the oceans as a whole. This discrepancy appears to be largely due to the fact that Steemann Nielsen's values are based on single observations which probably seldom included seasonal maxima. His observations in the Sargasso Sea, for example, were made in June and did not differ greatly from our June values, which were the seasonal minima. If the Sargasso Sea is one of the less fertile parts of the ocean, as is generally believed, then our data would indicate that the seas are more than twice as productive as the land (*25*).

References and Notes

1. A. Krogh and K. Berg, *Intern. Rev. ges. Hydrobiol. Hydrog.* 25, 205 (1931).
2. B. H. Ketchum and A. C. Redfield, *J. Cellular Comp. Physiol.* 33, 281 (1949).
3. B. Kok, *Acta Botan. Neerl.* 1, 445 (1952).
4. H. G. Aach, *Arch. Mikrobiol.* 17, 213 (1952).
5. E. C. Wassink, B. Kok, J. L. P. van Oorschot, "The efficiency of light-energy conversion in *Chlorella* cultures as compared with higher plants," in "Algal Culture from Laboratory to Pilot Plant," *Carnegie Inst. Wash. Publ. No. 600* (1953), pp. 55–62.
6. W. M. Powell and G. L. Clarke, *J. Opt. Soc. Am.* 26, 111 (1936).
7. C. L. Utterback and W. Jorgensen, *ibid.* 26, 257 (1936).
8. E. O. Hulburt, *ibid.* 35, 698 (1945).
9. R. Emerson and C. M. Lewis, *Am. J. Botany* 30, 165 (1943).
10. T. Tanada, *ibid.* 39, 276 (1951).
11. P. Moon, *J. Franklin Inst.* 230, 583 (1940).
12. K. Kalle, *Ann. Hydrog. mar. Meteor.* 66, 1 (1938).
13. J. H. Ryther *et al., Biol. Bull.* 115, 257 (1958).
14. E. Steemann Nielsen and E. A. Jensen, *Galathea Repts.* 1, 49 (1957).
15. J. H. Ryther, *Deep-Sea Research* 2, 134 (1954).
16. E. I. Rabinowitch, *Photosynthesis and Related Processes* (Interscience, New York, 1956), vol. 2, part 2, pp. 1925–1939.
17. H. H. Kimball, *Monthly Weather Rev.* 56, 393 (1928).
18. E. P. Odum, *Fundamentals of Ecology* (Saunders, Philadelphia, ed. 2, 1959).
19. J. H. Ryther and C. S. Yentsch, *Limnol. Oceanog.* 2, 281 (1957).
20. ———, *ibid.* 1, 72 (1956).
21. H. Schroeder, *Naturwissenschaften* 7, 8 (1919).
22. G. A. Riley, *Bull. Bingham Oceanog. Coll.* 15, 15 (1956).
23. E. Steemann Nielsen, *J. conseil, Conseil permanent intern. exploration mer* 19, 309 (1954).
24. G. A. Riley, *Bull. Bingham Oceanog. Coll.* 7, 1 (1941).
25. This paper is contribution No. 1016 of the Woods Hole Oceanographic Institution. The work was supported in part by research grant G-3234 from the National Science Foundation and under contract AT (30-1)-1918 with the Atomic Energy Commission.
26. H. Tamiya, *Ann. Rev. Plant Physiol.* 8, 309 (1957).
27. H. T. Odum and E. P. Odum, *Ecol. Monographs* 25, 291 (1955).
28. H. T. Odum, *Limnol. Oceanog.* 2, 85 (1957).
29. J. H. Ryther *et al., Biol. Bull.* 115, 257 (1958).
30. J. H. Ryther and C. S. Yentsch, unpublished data.
31. J. H. Ryther and D. W. Menzel, unpublished data.
32. G. A. Riley, *Bull. Bingham Oceanog. Coll.* 15, 324 (1956).

Contribution No. 1017

(*Reprinted from Nature, Vol.* 183, *pp.* 1050–1051, *April* 11, 1959)

Biological Origin of Manganese-rich Deposits of the Sea Floor

RECENTLY, one of us has advanced arguments[1] in support of the idea that manganese-rich deposits of the sea floor may result from the metabolic activity of a bottom-dwelling organism that derives its nutrients from organic complexes in the water. We present here some new evidence that is relevant to that concept.

On December 18, 1958, at lat. 34° 48′ N., long. 60° 30′ W., in 5,139 m. of water, Mr. L. V. Worthington on *Chain* Cruise No. 2 retrieved about 50 gm. of light tan mud and preserved it for us in borate-buffered (*p*H 8) formalin. The present bottom temperature at this site is 2·3° C. The finer fractions of this material were removed by suspension in water and decantation, and it was possible to isolate a few mgm. of a relatively coarse fraction, which, for the most part, consists of the vacant tests of agglutinated arenaceous (? *Rhabdammina* sp.) and of calcareous Foraminifera. It is of particular interest that almost all the former are coated inside and out with a dark brown or black, earthy or shiny veneer which, by one-dimensional paper chromatography, is seen to be markedly similar in composition to manganese-rich nodules from the Blake plateau, that is, containing appreciable quantities of nickel, cobalt and copper as well as abundant manganese and iron. Treatment with 6 *N* hydrochloric acid removes the dark coating and leaves the Foraminifera tests intact, thus demonstrating that the manganese-rich material was formed as a surface deposit, and not through the capture of pre-existing manganese-rich particles by the living Foraminifera. All manganese-rich particles in this sample apparently were formed by deposition on agglutinated Foraminifera the natural surfaces of which seem to be studded with detrital quartz grains ; no comparable manganese-rich deposits are visible on calcareous tests or on isolated sand grains. That the uncoated agglutinated Foraminifera have on their surfaces some protein-rich material is suggested by their adsorption of rose bengal dye[2], and by their reaction with ninhydrin.

To us, these observations support the argument that manganese-rich deposits of the sea floor originate through biological rather than inorganic processes. It would seem that the protein-rich exudate of these agglutinated Foraminifera has provided a favourable substrate which promoted the growth of a colony of organisms that are capable of extracting trace elements from sea water. Siliceous detrital grains on the sea floor, that were lacking in the protein-rich coating, were not such biologically attractive sites, nor were the calcareous tests of other associated Foraminifera.

We are now making preparations for a careful search for the organism which, we expect, is responsible for this type of deposition of trace elements from sea water.

This work was supported, in part, by Contract *Nonr*-2196 with the Office of Naval Research, U.S. Navy.

JOHN W. GRAHAM
SUSAN C. COOPER

Woods Hole Oceanographic Institution*,
Woods Hole, Massachusetts.

Feb. 27.

---

* Contribution No. 1017.

[1] Graham, John W., *Science* (in the press).

[2] Walton, W. R., *Cushman Found. for Foram. Res.*, 3, 56 (1952).

Printed in Great Britain by Fisher, Knight & Co., Ltd., St. Albans.

Contribution No. 1019

Reprinted from LIMNOLOGY AND OCEANOGRAPHY
Vol. IV, No. 2, April, 1959
Printed in U.S.A.

Quantitative Records of the Luminescent Flashing of Oceanic Animals at Great Depths[1]

GEORGE L. CLARKE AND CHARLES J. HUBBARD

Harvard University and Woods Hole Oceanographic Institution

ABSTRACT

The bathyphotometer described previously and capable of responding to illumination as low as 10^{-7} μw/cm^2 has been modified in respect to circuit, housing, and cable, so that measurements of underwater light could be undertaken at greater depths. Graphical records were obtained of the intensity, duration, and frequency of flashes of luminescent animals at stations in the slope water SE of New York at depths as great as 3750 m (about 2⅓ miles). During the night flashes were recorded from 50 m downward and reached their greatest frequency of over 160 per minute at 100 m, with a secondary maximum of about 90 flashes per minute at 900 m. During the day flashes appeared above the background light penetrating from the surface beginning at about 400 m and increased in frequency with depth to over 110 per minute at 900 m. The brightest flashes were more than 100,000 times the dark level of the instrument. Flashes ranged from less than 0.2 sec to more than 1 sec in duration, with light from overlapping flashes lasting sometimes for more than 10 sec. Tests with animals in the laboratory indicated that the flashes recorded at sea originated within 10 m of the photometer. The nature of the vertical distribution of animal populations, as suggested by the variation in flashing, is compared with information derived from other types of observation. The brightness and varied pattern of bioluminescence is discussed in relation to the ecology of the deep sea.

INTRODUCTION

The development of the bathyphotometer containing a photomultiplier tube, described by Clarke and Wertheim (1956), made possible the extension of measurements of light in the sea to depths at which the intensity is reduced to 10^{-7} μw/cm^2 or to about 10^{-12} of full sunlight. In very clear water off the Atlantic coast, the penetration of daylight was measured to depths of about 600 m under conditions of bright sun. In the strata just above this during the middle of the day, and at all levels at night, flashes of luminescent animals were detected, and qualitative records of their occurrences were obtained (Clarke and Backus 1956). Similar luminescent flashing has been reported in Pacific waters by Boden and Kampa (1957).

Further extensions of this work immediately suggested themselves. It was desired to record quantitatively the intensity, frequency, and wave-form of the luminescent flashes that had been observed and to determine what the nature of the bioluminescence might be at still greater depths. To meet these objectives it was necessary to redesign the bathyphotometer and to provide a stronger housing with a greater length of cable. The measurements to be described extend to depths as great as 3750 m, or about 2⅓ miles, and were made in the slope water southeast of New York during the summers of 1956 and 1957.

The authors are indebted to C. V. MacCoy R. C. Stross, C. Olson, J. O. Gates, D. B. Clarke, and C. J. George for assistance in the observations at sea and in the laboratory, and to L. R. Breslau for the operation of the bathyphotometer in 1957. We wish to thank J. B. Buck and J. F. Case for information and material in relation to the firefly studies. We are indebted to W. S. Richardson and E. N. Harvey for valuable suggestions, and to J. B. Hersey for providing sonic measurements and other facilities on the cutter YAMACRAW. The investigation was supported by funds from Research Grant G-3838 of the National Science Foundation and Contract Nonr 1720(00) (NR-083-116) with the Office of Naval Research and the Bureau of Aeronautics.

---

[1] Contribution No. 1019 from the Woods Hole Oceanographic Institution.

DESCRIPTION OF MODIFIED BATHYPHOTOMETER

Design considerations

It was desired that the instrument be capable of recording a wide range of light intensity using a fixed recorder sensitivity, and that moderate to low light levels produced by strong and weak luminescent flashes be measured with the same accuracy. These requirements imply a logarithmic-type response to light intensity that would give the same percentage accuracy at all light levels.

The photometer needed to have fast transient response in order to delineate

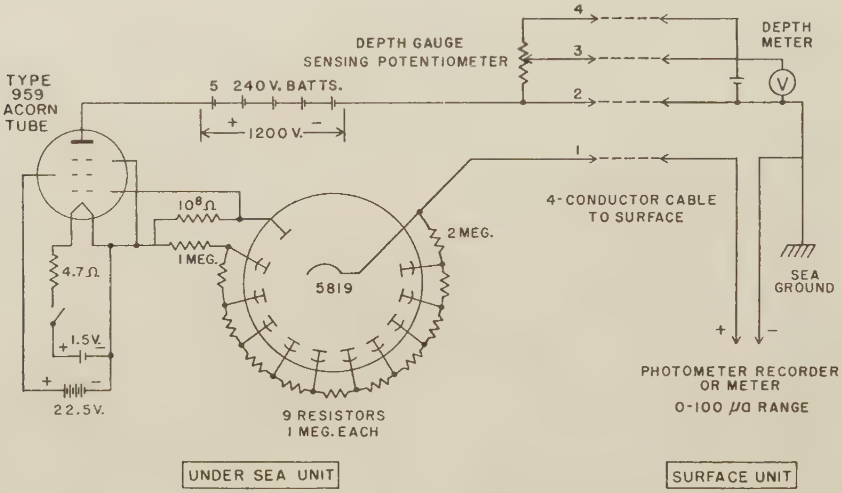
4
3
2
1
DEPTH GAUGE
SENSING POTENTIOMETER
DEPTH METER
V
TYPE 959 ACORN TUBE
5 240 V. BATTS.
+ 1200 V. −
$10^8\Omega$
1 MEG.
2 MEG.
5819
4-CONDUCTOR CABLE TO SURFACE
SEA GROUND
4.7Ω
1.5V.
+
22.5V.
+ −
9 RESISTORS
1 MEG. EACH
+ −
PHOTOMETER RECORDER OR METER
0-100 μa RANGE
UNDER SEA UNIT
SURFACE UNIT

Fig. 1. Circuit for the bathyphotometer.

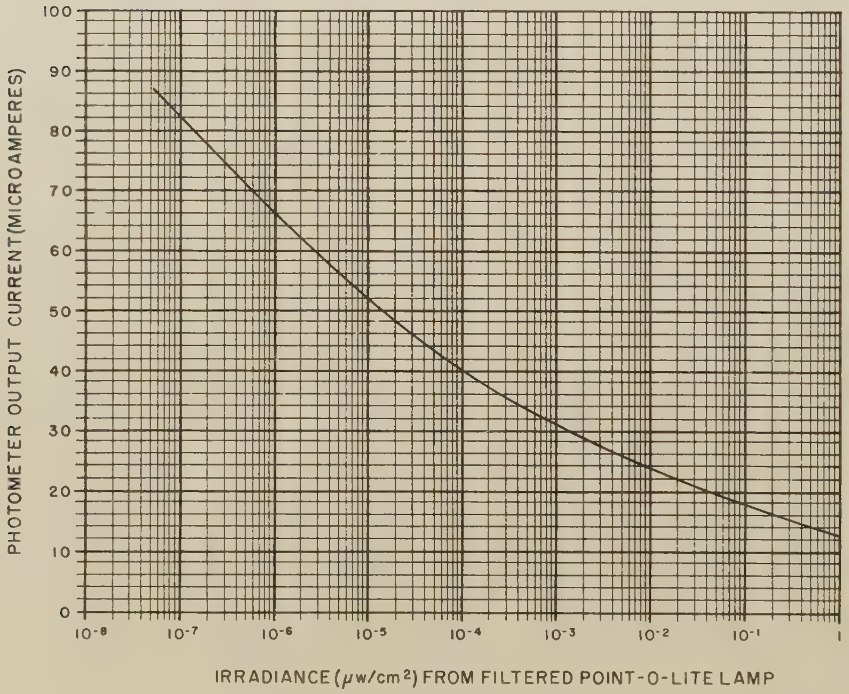

Fig. 2. Calibration curve of the bathyphotometer.

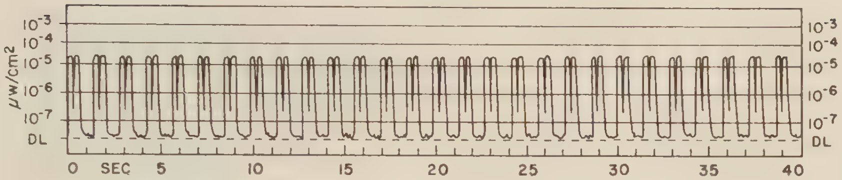

FIG. 3. Transient response test. Section of record from Sanborn Recorder during exposure of bathyphotometer to interrupted light source.

accurately the wave form of light flashes the duration of which may be of the order of 0.1 second. A similar requirement is imposed on the transient response of the recorder. A system with a rise-time much longer than 0.1 second would integrate the bioluminescent flashes, giving an erroneous value of the peak intensity.

The instrument was suspended on a long, multiconductor cable which necessarily resulted in a large electrical capacity between leads. In order to maintain the fast transient response the cable had to be terminated by a low impedance. The additional possibility of inter-conductor electrical leakage dictated that no appreciable amount of voltage, other than the photometer output signal, be present on leads in the cable. All batteries had therefore to be contained in the underwater unit.

Circuit employed

A photomultiplier tube has the property that the applied voltage necessary to maintain a fixed anode current varies logarithmically as the illumination changes. For a typical phototube (RCA type 5819), whose anode current is fixed at .01 μa, the total irradiance range of 10^{-7} to 10 μw/cm^2 implies a voltage variation of from 1150 v to 100 v. A vacuum tube in series with the high voltage supply can be used to maintain the anode current at the desired fixed value, the control grid voltage being derived from the phototube anode current by means of a high resistance in series with the anode lead. A determination of the resulting applied voltage yields the intensity of the light to be measured. Such a circuit was first used by Sweet (1946), in whose circuit the control tube was a large transmitting power tube.

The choice of the control tube to be employed in the present bathyphotometer was difficult, as the tube had to be capable of cutting off over 1,000 volts, and yet be small physically and present very little drain to the filament battery. In addition, the tube could draw only negligible grid current (less than 10^{-9} amperes) so that the grid would not divert any of the small phototube anode current. It was fortunate that a tube was found that satisfied these exceedingly stringent requirements. The type 959 "acorn" pentode was employed, which has the additional feature that the leads emerge at widely spaced points on the glass bulb, thereby reducing the problem of current leakage around the tube. Mr. J. M. Snodgrass (private communication) has independently arrived at the same choice for the control tube in a similar photometer circuit.

The complete circuit employed is shown in Figure 1. Inasmuch, as the bleeder current is uniquely related to the bleeder voltage, and hence to the light intensity, it can be passed directly to the surface via the long suspending cable. This presents a very large output impedance, eliminating any effect due to the resistance in the cable. The range of currents encountered runs from 0 to 100 μa. In the present measurements the cable was terminated at the surface by a 2,500 ohm resistor, and the voltage across this resistor was fed into a Sanborn high-speed recorder-amplifier.

The undersea circuitry was placed with the photomultiplier tube in a stainless steel cylinder one meter long with internal diameter of 7 cm and external diameter of 8.9 cm. One end cap contained a hole 5.1 cm in diameter into which the phototube fitted. The photo-emissive surface was therefore flush with the outside surface of the end cap. This was covered with a tempered glass plate 3.8 cm thick and 7.6 cm in diameter. Pressure tight seals were provided by neoprene O-rings.

Calibration

Due to the geometry employed the photometer obeys a Lambert's law of collection over a solid angle of approximately π stearadians centered on the axis of the phototube. The instrument therefore measures irradiance within this angle, under the assumption that all the incident light falls in a wavelength region where the spectral response of the phototube is constant. This is approximately satisfied for the 5819 phototube by sunlight in the ocean at depths below one-hundred meters (Clarke and Wertheim 1956, Fig. 4) and is also satisfied by much of the bioluminescent emission of marine organisms thus far studied (Harvey 1952, Boden and Kampa 1957, and Kampa and Boden 1957).

The instrument was calibrated by the procedure described by Clarke and Wertheim, using a "point-O-lite" bulb in combination with Corning blue-green filter No. 4303. The incident calibration energy thus falls in the constant region of the phototube characteristic. The calibration curve is shown in Figure 2, in which the cable current is plotted against the incident energy flux. It must be stressed that this calibration is valid only for incident light that falls in the wavelength band (approx. 400–500 mμ) over which the photomultiplier tube has constant spectral sensitivity.

The transient response of the instrument was carefully measured with a pulsed light source, and was found satisfactory. The response time at the leading edge of the pulse was faster than 0.02 second; the decay time of the photometer was approximately 0.2 second at the trailing edge. A section of the record is reproduced in Figure 3. The light source was a rotary chopper with two unsymmetrically placed holes.

The pressure case also contained a depth-sensing element, consisting of a commercial pressure-actuated potentiometer (Bourns Model 304) that covered the range from 0 to 352 kg/cm^2 (5,000 lbs/in^2), equivalent to a depth in sea water of 3340 m. The potentiometer was energized by a 1.5 v battery on deck, via one lead of the suspending cable. The output voltage, uniquely related to the depth, was recorded on an adjacent channel of the Sanborn recorder.

The suspending cable used in 1956 was designated as U. S. Signal Corps "Spiral 4," and contained four insulated conductors surrounded by a steel braid, the latter furnishing a breaking strength of about 360 kg. In 1957 a change to an "Amergraph" cable, (Am. Steel & Wire Co., type 4HO) with an outside diameter of 4.8 mm and a breaking strength of 1225 kg enabled us to reach much greater depths. The cable contained four insulated copper conductors wrapped with two counterwound layers of steel armor coated with rust-resisting "Amertex." The cable was lowered from a winch equipped with slip rings, so that measurements could be performed while raising or lowering the instrument. A more complete description of the bathyphotometer as used in the present investigation is given by Hubbard (1956).

OBSERVATIONS AT SEA

Procedure

Measurements in 1956 and 1957 were made in the slope water and near the edge of the Gulf Stream at distances of 150 to 300 miles southeast of New York in the same general region as in 1955 (Fig. 4). The observations of July 17, 18, and September 6, 1956, made from the Research Vessel CARYN, were all located at the same position with a bottom depth of 2170 m. Other stations were occupied on August 11, 1957 (depth 3540 m), and on September 15, 1957 (depth 3750 m), working from the Coast Guard Cutter YAMACRAW.

In our previous observations the bathyphotometer was lowered in the upright position so that its window, provided with a diffusing disc, received light from the hemisphere above it. The transparency of the water was calculated from the intensity of light penetrating from the sea surface (Clarke and Wertheim 1956). In the study of the relation of light intensity to the vertical migration of deep-sea animals and in the previous records of luminescent flashing,

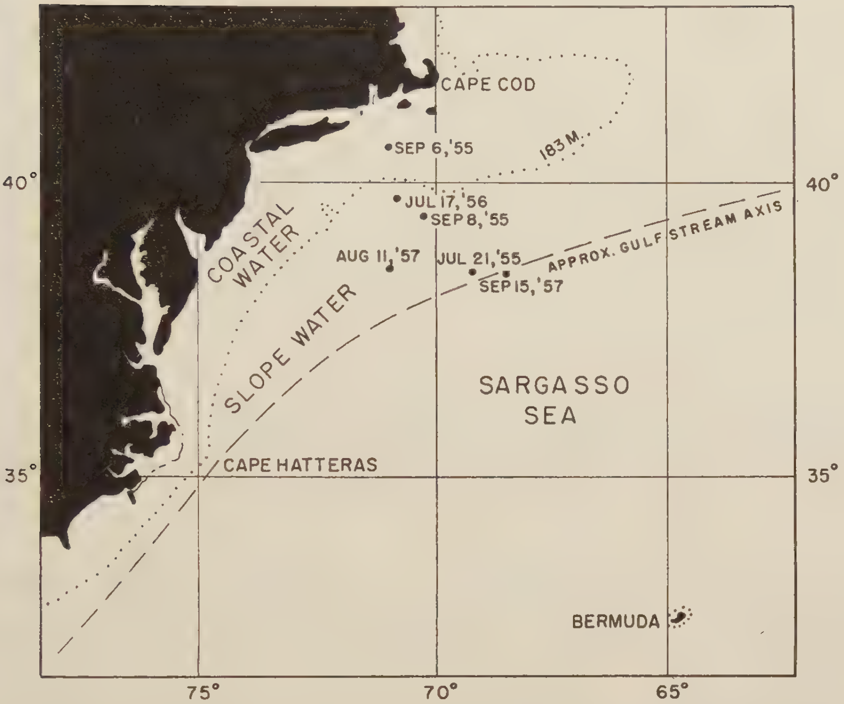

FIG. 4. Location of stations. July 17, 18, and September 6, 1956: lat 39° 39′ N, long 70° 51′ W. August 11, 1957: lat 38° 29′ N, long 71° 00′ W. September 15, 1957: lat 38° 27′ N, long 68° 33′ W.

the bathyphotometer had been employed in the same way (Clarke and Backus 1956). In the present study it was desired to measure luminescent flashes at as wide a range of depths as possible with the minimum of interference from light penetrating from the surface. For this reason the bathyphotometer was hung in the reverse position so that its clear glass window was exposed to light from below. Since in the present investigation interest was centered on the less intense portion of the light range, the protective hood and diffusing disc previously used for measurements of sunlight near the surface were not employed. The geometry of the window was such that the photometer received light from a 90° cone centered on the axis of the instrument.

For observations during the daytime the bathyphotometer, in the inverted position, was lowered to about 300 m before measurements were begun, since at shallower levels flashes would be undetectible against the background illumination from the surface. Comparison with measurements made with an upright photometer in water of similar transparency (Clarke and Wertheim 1956, Fig. 8) shows that the intensity of the upward passing light was about 1% of the downward passing light at 300 m. During the night time measurements could be made from about 50 m on down. As the bathyphotometer was lowered to greater depths, the cable winch was at first stopped for periods of several minutes while records of the illumination were made. When it was observed that the records taken while reeling in or out were not detectibly different from those taken with the winch stationary, the photometer was raised or lowered continuously at speeds up to 20 m per minute. The Sanborn recorder provided a continuous graphical record of the changes in illumination and in depth.

Day and night measurements at same station

During the daytime series of measurements of July 17, 1956, a continuous record of the light intensity from 320 m to 1,600 m was obtained. Sample sections of this

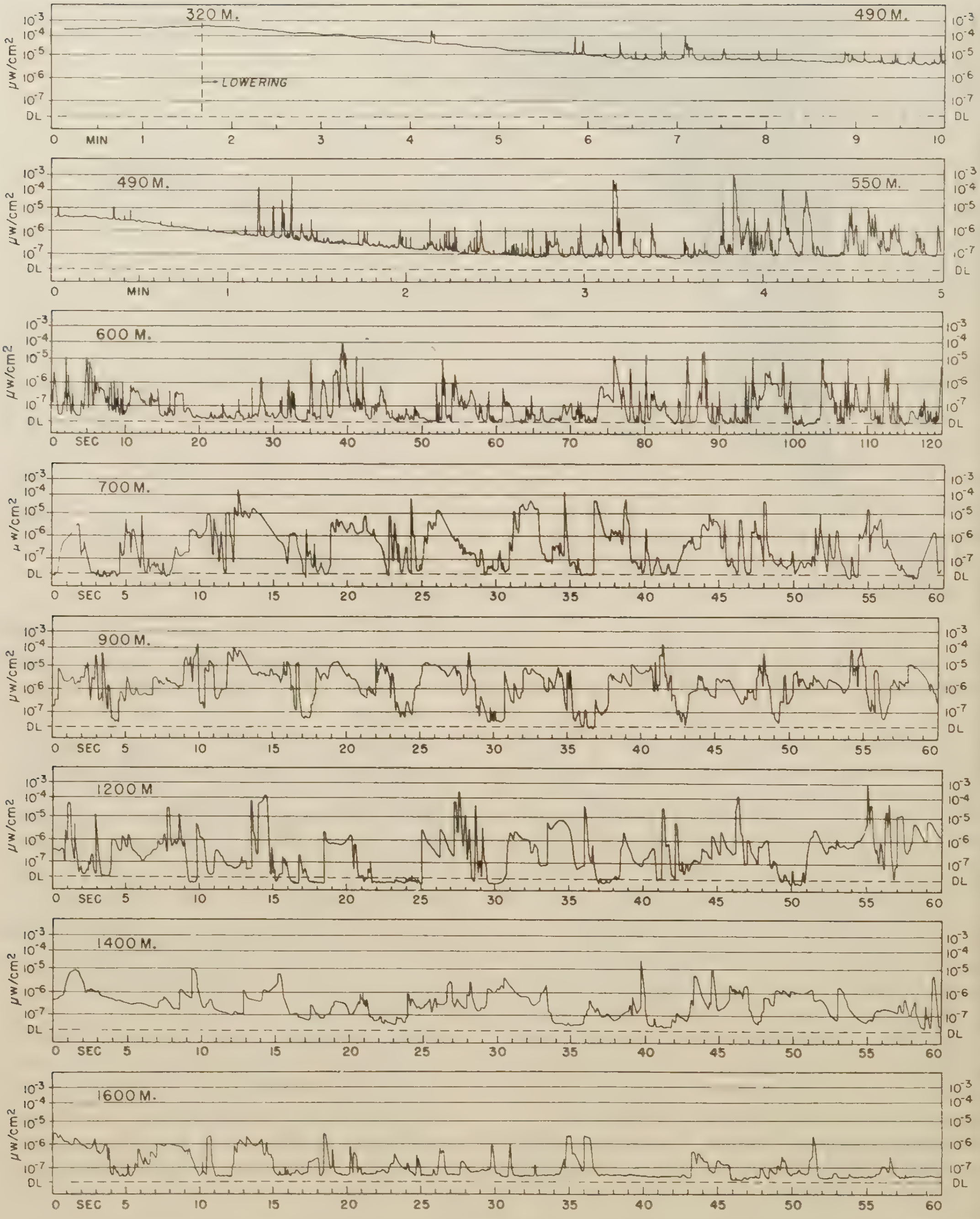

FIG. 5. Sections of record for July 17, 1956, 1008 to 1133 hrs EST showing light received on inverted photometer at indicated depths. Bottom depth 2170 m. DL = "dark level" response of the instrument.

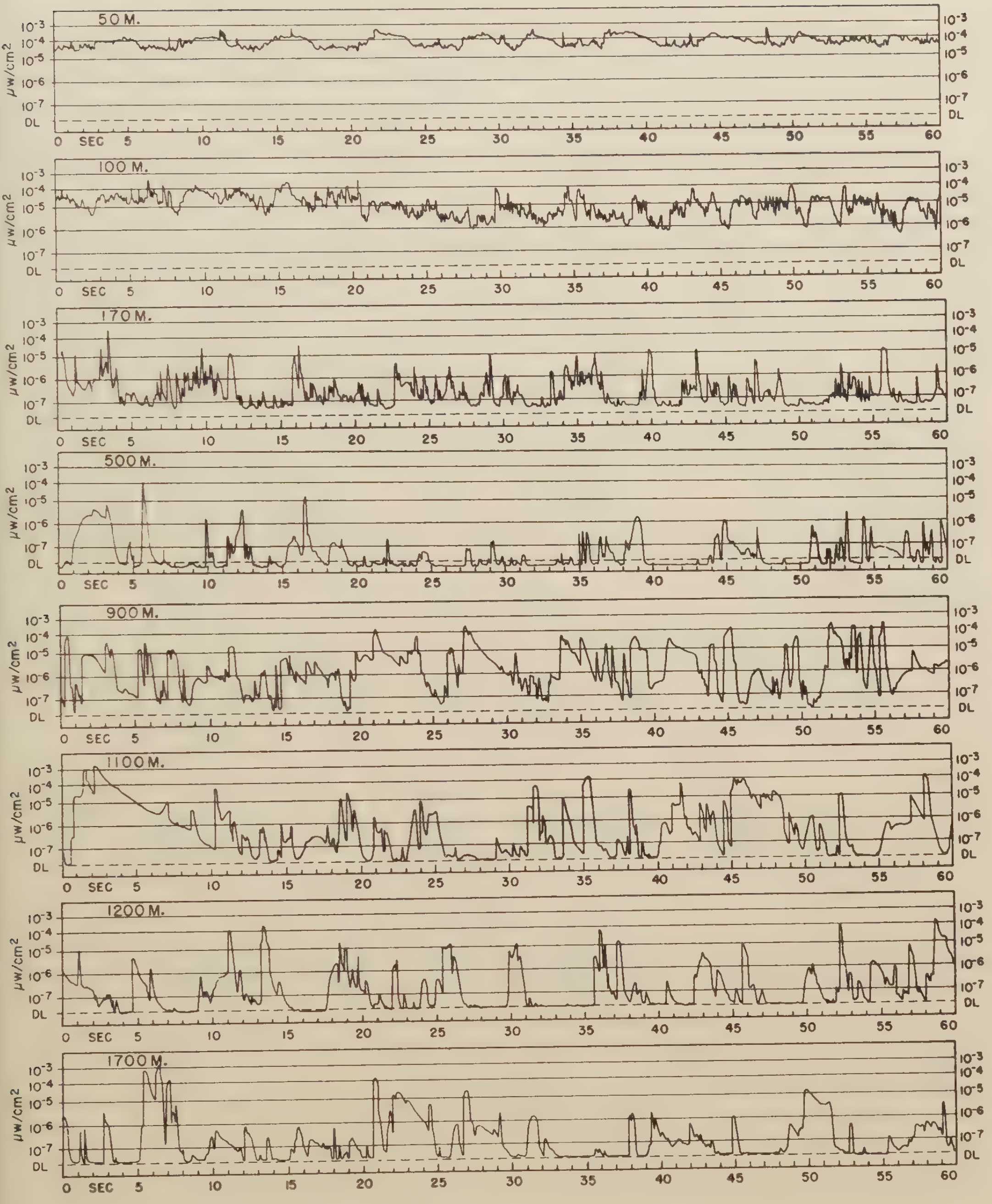

Fig. 6. Sections of record for July 18, 1956, 0000 to 0202 hrs EST. Bottom depth 2170 m.

record are reproduced photographically in Figure 5. At a depth of 320 m the intensity of the upward passing light was about 4 × 10^{-4} μw/cm^2 (as shown at left hand end of upper strip). As the photometer was lowered, the concomitant reduction in the intensity of the scattered light received from the surface is shown as the trace moves to the right, and in the following sections of the record. The sudden, short increases in light beginning at depths reached a few minutes after lowering began are interpreted

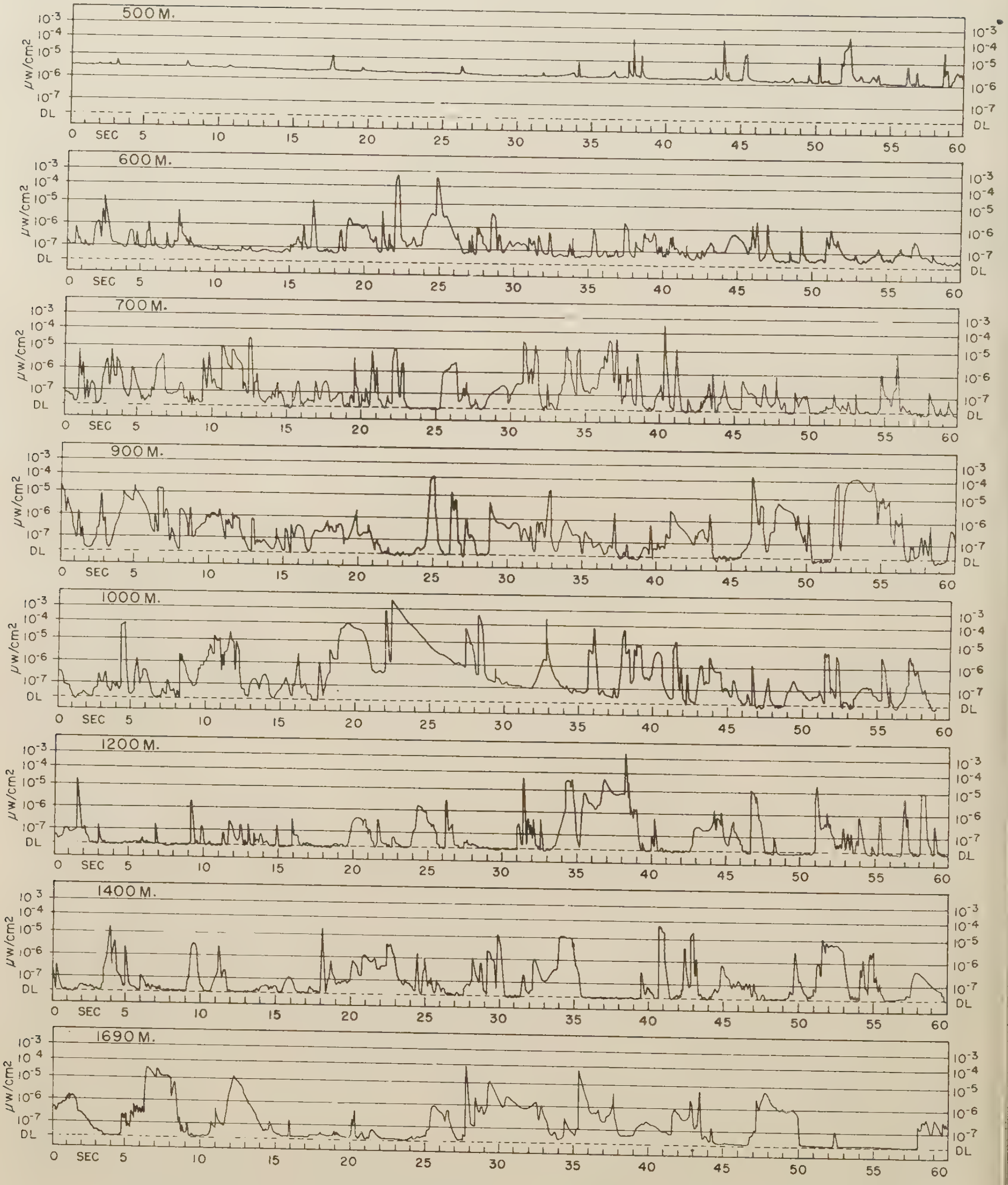

Fig. 7. Sections of record for September 6, 1956, 1000 to 1050 hrs EST. Bottom depth 2170 m.

as flashes from luminescent animals occurring at undetermined distances from the photometer within its conical field of view. At a depth of 490 m the background light had an intensity of about 4 × 10^{-6} μw with flashes ranging between 10^{-4} and 10^{-5} μw. As the photometer approached 500 m, a group of 4 or 5 flashes was encountered one of which reached an intensity of 10^{-3} μw. At 550 m background illumination was reduced to 10^{-7} μw, and at 620 m it had diminished to less than a fifth of this, or a value approaching the "dark level" response of the instrument and hence the

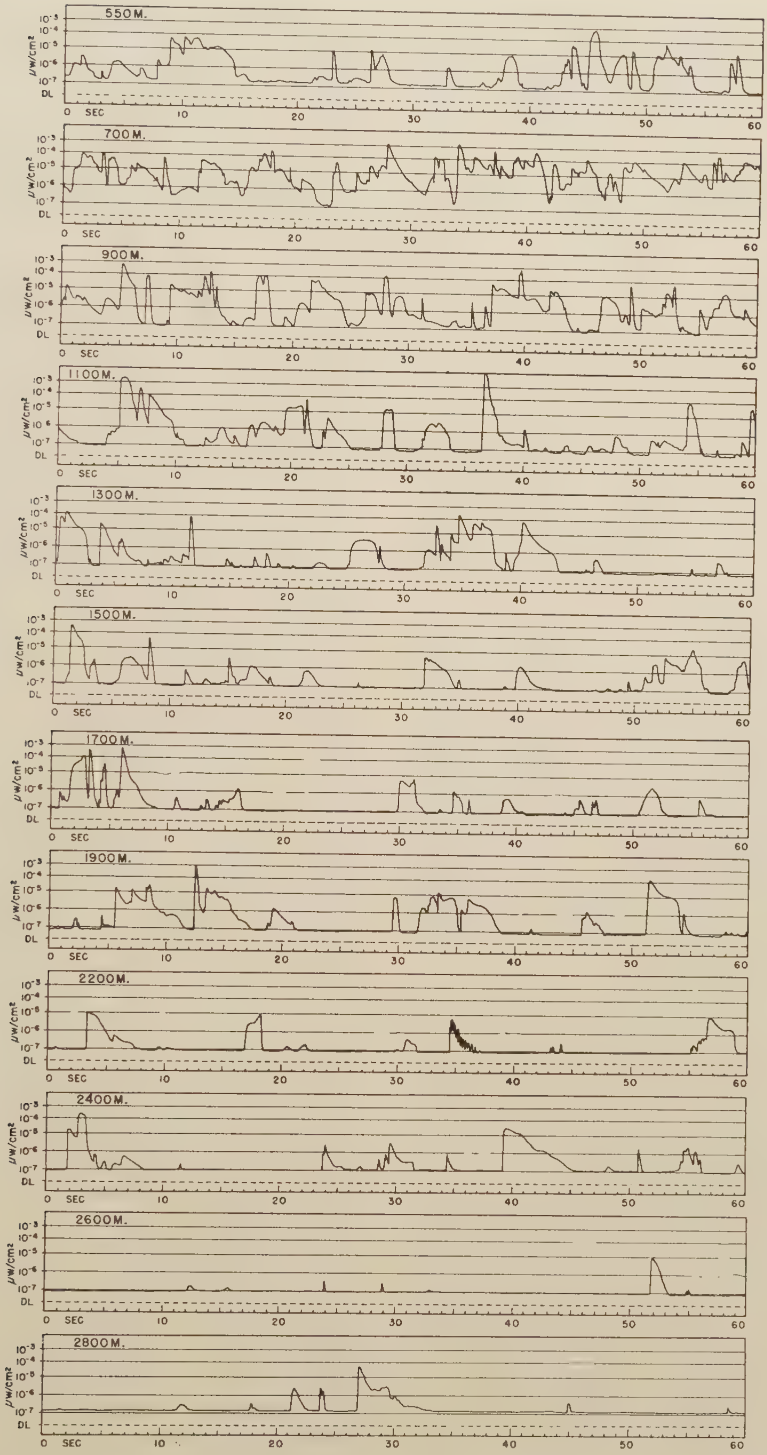

FIG. 8. Sections of record for August 11, 1957, 1750 to 1935 hrs EST. Bottom depth 3540 m.

TABLE 1. *Depth distribution of flashes in daytime*

July 17, 1956; 150 miles SE of New York

Depth (Meters)	Time EST	Number flashes per minute				Total
		10^{-2} to 10^{-4} μw/cm²	10^{-4} to 10^{-5} μw/cm²	10^{-5} to 10^{-6} μw/cm²	10^{-6} to 10^{-7} μw/cm²	
490	1008	0	7	—	—	7
550	1015	3	6	18	—	27
600	1021	1	6	21	39	67
600	1022	1	8	13	38	60
700	1028	2	13	45	36	96
800	1038	3	21	36	44	104
900	1044	3	25	73	17	118
1000	1050	4	19	41	30	94
1100	1056	3	14	46	33	96
1200	1103	4	15	28	37	80
1300	1108	2	21	41	21	85
1400	1117	0	3	24	39	66
1500	1121	0	0	21	42	63
1600	1133	0	0	16	38	54

approximate lower limit of measurement. As the background illumination fell below 10^{-5} μw, and later below 10^{-6} μw, an increasing number of flashes appeared on the record. Flashes were found in abundance at every level from their first appearance to the maximum depth attained. A scrutiny of the entire record, of which the excerpts reproduced here are only a small part, reveals the fact that at no level below 500 m were there periods of more than a few seconds without flashing.

Changes in the frequency, intensity, and duration of the flashes at the various levels may be observed from the graphical record and also from Table 1 in which actual counts of the number of flashes per minute for four magnitudes of intensity are presented. The brightest flashes—between 10^{-3} and 10^{-4} μw in intensity—occurred between 1 and 4 times per minute at all levels except at 490 m and below 1,300 m. Flashes reaching the next lower order of magnitude were more frequent, and flashes less intense than 10^{-5} μw occurred still more abundantly. The total number of flashes of all magnitudes reached a maximum of 118 per minute at 900 m and dropped off to 54 per minute at 1,600 m. There was a noticeable lack of larger flashes at 1,400 m and below, with longer intervals between flashes. The duration of flashes varied from about 0.2 sec, which is the shortest which could be reliably traced by the Sanborn recorder, to single flashes or combinations of overlapping flashes, lasting for five seconds or more. The apparent rhythm in the flashing with a period of about six seconds, seen in certain parts of the record, is probably due to the roll of the ship. The resulting periodic movement of the supporting cable may have produced turbulence or caused the photometer to strike luminescent animals near the window of the instrument and thus stimulated them to give extra or prolonged flashes. It might be argued that all or most of the flashes recorded were the result of mechanical stimulation by the moving photometer. However, the fact that sections of the record with no apparent periodicity show many flashes indicates that at least much of the flashing is spontaneously induced by the animals themselves.

During the night following the foregoing series of measurements and at the same station a continuous record of light was made from 50 m to 1,700 m. Sample sections obtained between 0000 and 0200 hrs on July 18, 1956, are presented in Figure 6, and a summary of the frequency distribution of flash size at representative depths is given in Table 2. The background intensity of scattered light received by the inverted photometer at a depth of 50 m at midnight with no moon and partly cloudy sky was about 8×10^{-5} μw. Many flashes slightly brighter than this were recorded together with a periodic oscillation of the background or of the intensity of flashing. This rhythm, with a period of about 6 sec, was again probably due to the roll of the ship causing a mechanical stimulation of the luminescent animals or possibly a slight tilting of the photometer which might thus have received more light from the sky. The record shows much less indication of periodicity at greater depths. Because of the fluctuating level of background light no precise count of the number of flashes at 50 m can be made especially for intensities lower than 10^{-4} μw. However, no reason suggests itself to suppose that the flashes in the record rising to intensities above 10^{-4}

TABLE 2. *Depth distribution of flashes at night*

July 18, 1956; 150 miles SE of New York

Depth (Meters)	Time (EST)	Number of flashes per minute				Total
		10^{-3} to 10^{-4} μw/cm²	10^{-4} to 10^{-5} μw/cm²	10^{-5} to 10^{-6} μw/cm²	10^{-6} to 10^{-7} μw/cm²	
50	0000	23	—	—	—	23
100	0002	6	88	72	—	166
170	0004	1	11	45	78	135
330	0100	1	3	8	24	36
400	0103	0	1	12	20	33
500	0108	1	2	9	29	41
600	0111	0	5	8	35	48
700	0115	1	3	16	40	60
800	0120	4	16	32	34	86
900	0124	8	27	33	25	93
1000	0127	6	19	28	39	92
1100	0131	4	16	23	27	70
1200	0138	0	4	10	20	34
1300	0148	1	5	10	35	51
1400	0151	0	6	19	38	63
1500	0154	0	6	13	29	48
1600	0159	3	5	14	26	48
1700	0202	4	4	15	37	60

μw were produced by anything other than the flashes of animals. The number of flashes of this magnitude is much greater than at any other level and thus indicates at this depth that either the number of animals producing the brightest flashes was larger or that the animals present flashed more frequently.

At 100 m the total of 166 flashes recorded in one minute was the largest number observed at any level. Of these the flashes between 10^{-4} and 10^{-5} μw were the most numerous, but almost as many ranged between 10^{-5} and 10^{-6} μw. At 170 m the background light had dropped below 10^{-7} μw. Of the 135 flashes observed in one minute the majority ranged between 10^{-6} and 10^{-7} μw. From this depth downward the largest number of flashes at each level (with one exception) were in this weakest intensity category, with smaller numbers in successively brighter ranges of intensity. Below 170 m the total number of flashes per minute dropped off sharply and then increased to a secondary maximum at 900 m with considerably lower numbers from this level down to 1,700 m.

From 600 m down at each level the total number of flashes was less at night than during the day, suggesting that many luminescent animals may have migrated from depths below 600 m to the upper levels during the evening. Presumably a large number of the animals producing such an abundance of flashing at 100 m and at 170 m migrated to levels deeper than 500 m during the day, but it is possible that many of them remained in the upper layers. If they continued to flash during the day, their luminescence could not have been detected because of the high level of the ambient light. More probably the flashing of any animals near the surface would be inhibited by the high illumination.

At 500 m and below many periods of prolonged luminescence were recorded due either to sustained light emission from one animal or to the overlapping of flashes of several animals. In the first part of the record at 1,100 m the emitted light exceeded 10^{-3} μw, or almost 100,000 times the intensity represented by the dark level, and the light remained above the baseline for more than 13 seconds. At 900 m the light was almost continuously above the dark level, with the illumination dropping below 10^{-7} μw only occasionally and usually for less than a second. This situation may be contrasted to the conditions at 500 m and 1,100 m. At no depth did the illumination remain at or below the dark level for more than four or five seconds at a time; periods of one to four seconds without flashes occurred at 500 m but chiefly at depths below 900 m.

A third series of measurements, made at the same station on September 6, 1956, extended from 500 m to 1,690 m, and sections of the record are reproduced in Figure 7. The illumination received by the inverted photometer at 500 m was about 3 × 10^{-6} μw, or about the same intensity as reported for that depth during the measurements of July 17. Flashes above the ambient light level were encountered at strata just below 500 m and became increasingly abundant at depths greater than 600 m. A maximum in the frequency of flashing was again encountered at 900 m.

Deeper observations

The modifications of the photometer described above made possible the exploration of bioluminescent flashing at still greater depths in 1957. Representative sections of the record from 550 to 2800 m made in the late afternoon of August 11 are presented in Figure 8. During this series the dark level of the instrument was somewhat higher than for previous measurements and occurred at about 10^{-7} μw/cm^2. At 550 m a moderate amount of bioluminescent activity was recorded but with intervals of 5 sec or so with little or no flashing. A maximum of luminescence was encountered between 700 and 900 m, and in this stratum the overlapping flashes maintained the illumination well above the dark level for more than a half a minute at a time. At greater depths flashing was less frequent, but at least a few flashes of high intensity were found at every level down to 2000 m. Below this depth luminescent activity became progressively curtailed with periods of more than 20 sec during which no flash was recorded. However, a few flashes with intensities greater than 10^{-5} μw/cm^2 were observed at 2800 m, or about 1.7 miles beneath the surface. At 2200 m a curious pattern of luminescent discharge was recorded in which the light rose abruptly to an intensity of about 100 times the dark level and then dropped off in a cascade of peaks of decreasing size. Future investigation may show that certain types of animals can be identified by the pattern of their flashing.

An even deeper series of measurements was carried out with the same instrument by Mr. Lloyd Breslau during the night of Sept. 15–16, 1957. Excerpts of the record (Fig. 9) give a synoptic view of the light conditions for the entire depth from 100 to 3750 m, or about 2.3 miles. The record shows a profound variation in the frequency, intensity, and duration of flashing at various levels. Primary and secondary maxima in luminescent activity occurred at 200 m and 900 m in similar fashion to previous night records. At a depth of 100 m the general level of background light was about 10 times the dark level of the instrument. Flashing was frequent, but the majority of flashes were weaker than 10^{-5} μw. At 200 m more flashes were recorded, with a considerable number brighter than 10^{-4} μw and a few brighter than 10^{-3} μw. The frequency of flashing was so high that the light did not remain steady for more than half a second at a time. The number of flashing animals was very much less at 300 m and 500 m, but the flashing rate began to increase again at 600 m, reached a peak at 900 m, and continued high to about 1000 m. Although the flashes were fewer at this depth than at 200 m, they were more sustained, so that the illumination was well above the dark level of the instrument for periods of ten seconds or more. Below 1300 m luminescence gradually diminished, but many of the individual discharges were as intense as at shallower depths. At 2700 m a few bright flashes occurred within each one-minute period. At greater depths, however, the flashes were weaker and fewer than one per minute. As the photometer approached the bottom at 3750 m, there was no indication of an increase in the amount in luminescent activity.

Laboratory observations

In the foregoing observations at sea the flashes recorded may have been produced by animals of either large or small size at a variety of distances from the receiving window of the photometer. In order to ascertain the appearance on our record of the trace of a known animal's flash at a known distance, recordings were made in the laboratory of luminescent discharges of the ctenophore, *Mnemiopsis leidyi*, which occurs in Woods Hole waters during August, and of the common firefly, *Photuris pennsylvanica*.

One specimen of *Mnemiopsis* was placed in a square-sided glass vessel of sea water and set in a light-tight black box into one end of which the head of the photometer was inserted in a fashion similar to that described by Clarke and Backus (1956). A record of flashes, sections of which are shown in Figure 10, was made with the same photometer sensitivity and the same speed of recording as in the observations at sea.

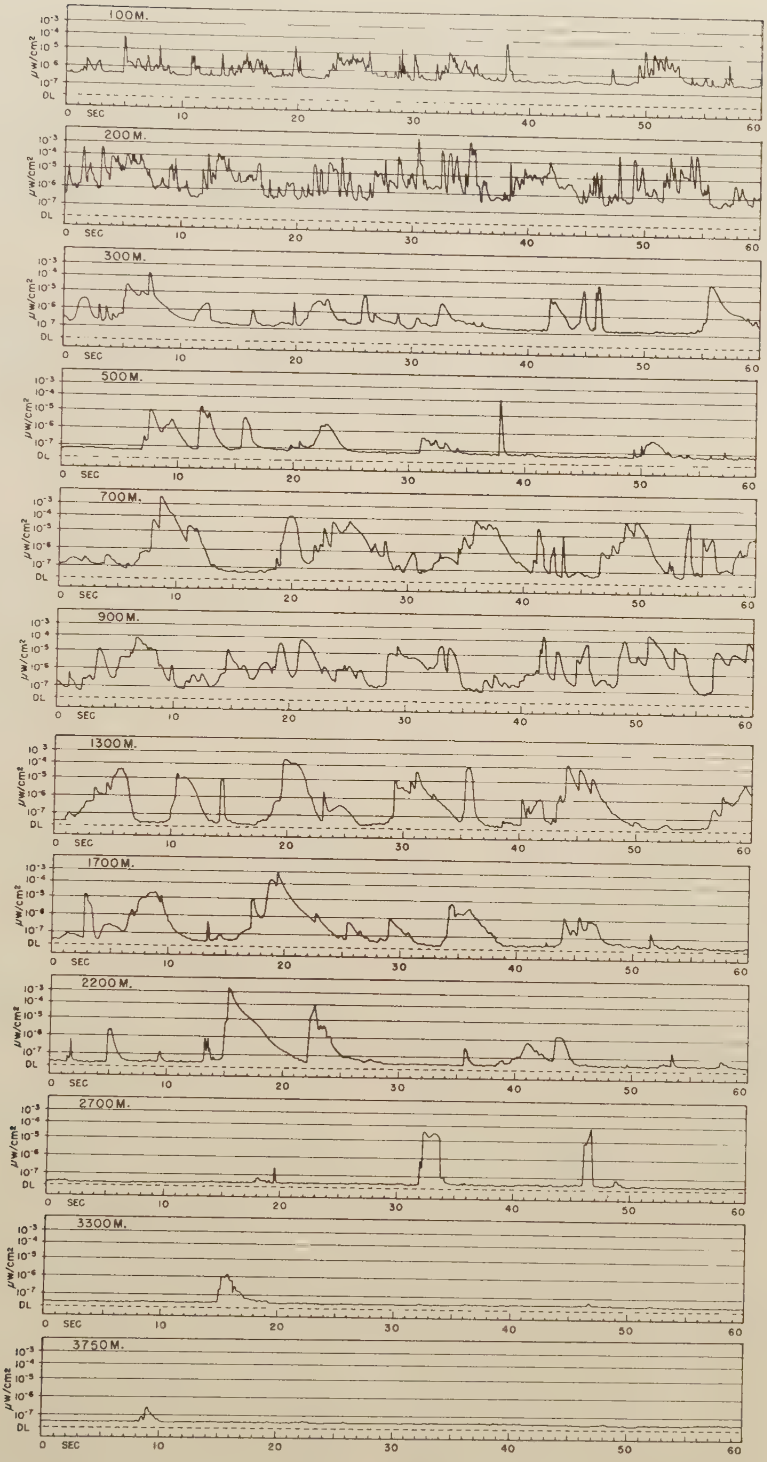

FIG. 9. Sections of record for September 15–16, 1957, 2300 to 0100 hrs EST. Bottom depth 3750 m.

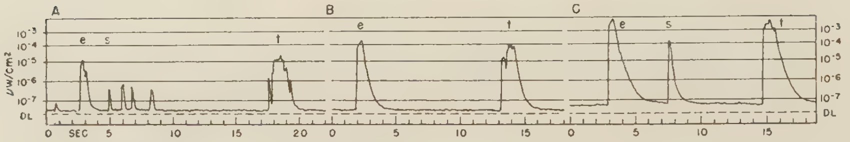

FIG. 10. Flashes produced by a 55-mm specimen of ctenophore, *Mnemiopsis leidyi*, in the laboratory on August 1, 1957, at distances from the photometer of (A) 80 cm, (B) 37 cm, and (C) 1 cm. Luminescence resulted from (*e*) electrical stimulation, (*t*) mechanical stimulation, and (*s*) spontaneous activity.

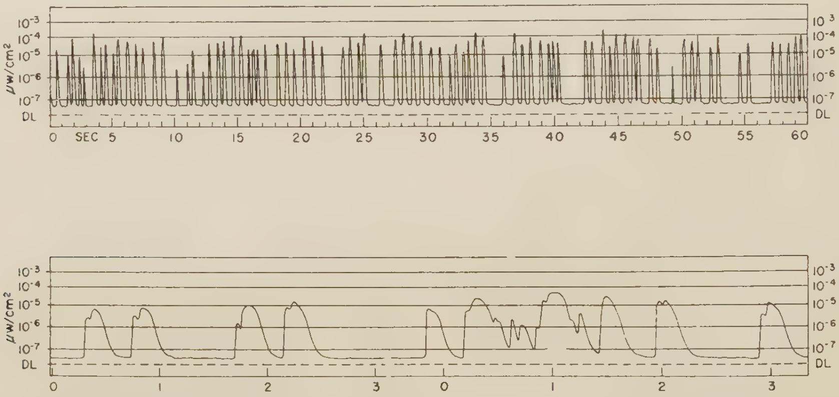

FIG. 11. Spontaneous flashes of firefly, *Photuris pennsylvanica* recorded in the laboratory on July 17, 1957, at 37 cm from photometer at regular speed (upper) and at increased speed (lower) of the recorder.

Tracings were obtained of light flashes with the animal at distances of 80 cm, 37 cm, and 1 cm from the photometer during spontaneous luminescence as well as following electrical and mechanical stimulation. The discharges were greater following artificial stimulation; in some instances the response was unimodal and in some it was irregular. Generally, the light flash reached its peak of intensity within a small fraction of a second and then died away over the ensuing few seconds. The form of light discharge is thus similar to many records obtained at sea.

The firefly was placed in a glass vial and held by a plug of cotton against the glass with its ventral surface toward the photometer at a distance of 37 cm. The flashing was spontaneous and fairly regular with an average period of slightly less than one second (82 flashes per minute) although there were some longer and shorter intervals. Sections of the record at the previously used speed, and at a much higher speed, are presented in Figure 11. The bimodal nature of many of the flashes is probably due to a slight overlap in the discharge of the two photophores of the firefly.

DISCUSSION

The foregoing measurements together with those of Boden and Kampa (1957) and Kampa and Boden (1957) represent a first step in the quantitative investigation of luminescence in the deep sea. The present records reveal the nature of the changes in frequency, intensity, and duration of flashing under the circumstances of observation at the depths and locations sampled. It is obvious that luminescence may differ greatly from place to place, and more information is desired about certain aspects of the measurements before general conclusions can be reached. For example, with the existing arrangement of the apparatus neither the exact position of the flashing animal relative to the photometer nor the extent to which mechanical agitation may affect the amount of luminescence is known.

Observations in a variety of other localities and further refinements of the procedure are planned.

As an additional extension of the investigation an instrument known as the luminescence camera has been designed and constructed by Breslau and Edgerton (1958, 1959) for the purpose of identifying the principal flashing animals in various strata by causing them to take their own photographs. The instrument consists of a photomultiplier detector arranged to pick up light from a cone of water outside its receiving window, an electronic flash which, when discharged, illuminates this cone, and a camera in a water-tight case which is focused upon the same volume of water. When any luminescent animal moves into the sensitive cone, its flash triggers the device with the result that the electronic flash is set off, and the camera takes a picture of the animal. The device is designed to operate at depths down to 6000 m, and it may be used in conjunction with the bathyphotometer. Photographs already obtained in the upper layers indicate that a large number of flashers are extremely small animals, although many euphausiids, ctenophores, medusae, and siphonophores have been photographed. The camera is now being employed at greater depths, and the results will be reported as soon as opportunity permits.

Certain information in regard to the effect of the distance of the animals from the photometer may be deduced from the laboratory experiments. The electrical stimulation of *Mnemiopsis* in the laboratory produced an illumination of about 10^{-5} μw/cm^2 at the photometer window at a distance of 80 cm; at 37 cm the flash was 10x brighter, and at 1 cm it was about 700x brighter than at 80 cm. If the animal's luminous discharge is treated as a point source and the inverse square law applied, we find that at 800 cm the light intensity would have been reduced to 1 per cent of its value at 80 cm, or to a value approximately 10x the dark level of the instrument. At sea the light emitted would be further reduced by adsorption and scattering by the water through which it passed, but the additional reduction would amount to only about 40 per cent for passage through 8 m of clear ocean water. The measured intensity of flashes received from points not on the axis of the instrument would be reduced by $\cos^2 \theta$, but for the extreme measurable angle of 45° the reduction would be only one half. We may conclude, therefore, that luminescent flashes of any animal equal in magnitude to the largest recorded in the laboratory for *Mnemiopsis* could have been detected by the bathyphotometer in the sea at distances up to 8 m or slightly more.

Very little is known about the absolute magnitude of the luminescent flashes of oceanic animals under natural conditions, and relatively few laboratory studies have been conducted (Harvey 1952). It seems probable, however, that few deep sea animals produce flashes that are very much brighter than *Mnemiopsis*. If this be true, we may conclude that the bathyphotometer does not record flashes to any important extent from animals farther away than 10 m, and that it does provide a reliable index of the population of the brightest flashers within this distance. The smallest signals on the tracing may be due to flashes from the brightest animals at extreme range or at oblique angles, or to weak flashes near the photometer window. During laboratory observations when water from Woods Hole harbor was placed in a small, square-sided glass vessel close to the window of the bathyphotometer, individual flashes of protozoans such as *Tintinnopsis* were recorded. Thus certain of the light impulses detected in the sea may be from relatively minute animals which have flashed spontaneously or which have been stimulated by striking the photometer window. On any occasion when large numbers of small luminescent forms are present, a strong movement of the photometer, due for example to the roll of the ship, would be expected to result in a volley of discharges. Many flashes may overlap to produce a seemingly continuous glow, such as the familiar "burning water" seen at the sea surface due to breaking waves or to an object moving through the water.

The differences in the frequency and

nature of light flashes at different depths may be considered in relation to the vertical distribution of the pelagic fauna. General summaries of the changes in the kinds and abundance of animals with increasing depths in the open sea are presented by Marshall (1954) and Hardy (1956). Direct observations from the bathyscaph in the Mediterranean and off the Atlantic coast have been reported by Bernard (1955), Furnestin (1955), Trégouboff (1956), Pérès and Picard (1956), Pérès, Picard, and Ruivo (1957), Piccard and Dietz (1957), and Dietz (1959). These investigators found distinct strata of abundance and of scarcity at various levels from the surface to depths of several thousand meters. For the most part their observations in deep water were made with the underwater search lights of the bathyscaph turned on but occasional periods with the lights off provided some information on the occurrence of bioluminescence. Off the coast of Portugal Pérès, Picard, and Ruivo (1957) observed that the plankton which was rich near the surface diminished to a minimum at about 300–400 m. From 400 m to 800 m the plankton again became rather rich and then diminished to another minimum between 1,100 and 1,400 m. Piccard and Dietz (1957) state: "Particularly during the 1956 dives to 1100, 2000, and 3700 m the bathyscaph traversed zones between 500 to 800 m where the density of life appeared to be remarkable. Hundreds of tunicates could be seen at one time, mainly salpa ($\frac{1}{2}$ − 1 cm long) which flashed with an almost white luminescence. At times there seemed to be about ten dozen salpa per cubic meter of water. . . . With the lights extinguished in deep water a small point of bioluminescence is seen every few seconds."

Several series of quantitative plankton hauls were made by Leavitt (1938) in the deep water southeast of New York, in the same general region as the present investigation. Using closing nets towed at levels 200 m apart from 200 m to 3000 m. Leavitt found major peaks in the size of the total catches at depths of 200 m and 800 m and a minor peak at 1600 m. At his Station 2216, located 110 miles SE of our July 17–18, 1957 station, the percentages of fish, copepods, euphausiids, decapods, chaetognaths, salps, and coelenterates taken in each stratum were determined. Each of these taxonomic groups showed a sharp maximum at 800 m and some showed secondary peaks of abundance at 200 m and 1600 m. Numbers were very small for all groups at 400 m, from 1000 to 1400 m, and below 2000 m. It is of great interest to note that a general correspondence exists between the pattern of the vertical distribution of all animals taken in Leavitt's plankton nets and our records of the vertical changes in luminescence, even though at least some of the animals caught in the earlier study were presumably not luminescent. Since Leavitt did not sample the 900 m level, his maximum at 800 m may very likely represent the same population as that which produced the peak at 900 m in our records of light flashes. Our maximum at 900 m occurred during both day and night observations; our maximum in the upper 100 or 200 m could be observed only during the night.

None of the maxima in abundance discussed above correspond with the level of the deep scattering layers in this region as detected by the usual echo-sounder recorders. During the previous year's investigation a single scattering layer was found at about 400 m during the middle of the day, and one of two scattering layers was followed up to about 50 m in the evening after which echoes from it merged with the near-surface reverberation (Clarke and Backus 1956). During the day and during twilight hours the scattering layers were found at levels where the ambient daylight would obscure the weaker flashes, and in the present study no increase in the abundance of flashes brighter than the background was detected in the water strata occupied by the scattering layer animals.

Any correspondence between the total abundance of pelagic animals, the amount of luminescence, and the occurrence of sound scatterers is of interest, but instances of non-conformity are not to be regarded as surprising. Large aggregations of animals may exist without luminescent forms necessarily being among them. A strong sonic scattering layer may be produced by a group of animals of a type that reflect sound effectively but which are not as numerous as animals at another depth which are poor sound scatterers. However, light is probably so important in controlling the vertical distribution and the activity of many, if not most, pelagic animals that a definite relation between the illumination from the surface, the abundance of animals, and the occurrence of luminescence might be expected. The present measurements indicate a significant increase in luminescent flashing in the neighborhood of 900 m. This is probably just below the depth at which light from the surface affects animal activity.

The minimum illumination in the central part of the visible spectrum under which shallow-water fishes can see small objects is probably 10^{-10} of sunlight (Clarke 1936). The human eye has approximately the same threshold. If deep-sea fishes can see equally well in the blue region of the spectrum, minimum light for their vision would exist at a depth of about 600 m in water as transparent as this part of the ocean (Clarke and Wertheim 1956). Observers in the bathyscaph could detect daylight when looking horizontally and could see light reflected from objects in the water at depths down to about 600 m (Dietz 1959). If a deep-sea fish had eyes 100 times more sensitive than man's, it could see objects 120 m deeper, or at a total depth of about 720 m, since daylight is reduced by a factor of 10 for each depth increase of 60 m in clear ocean water (Clarke and Wertheim 1956). Animals looking toward the surface could presumably detect the difference between day and night at somewhat greater depths, provided that bioluminescence did not interfere. The studies of Denton and Warren (1957) indicate that the eyes of certain deep-sea fishes are 60–120 times more sensitive to a large field of daylight than the human eye. In any situation in which bioluminescence is as strong as that received by our photometer at every depth investigated, the visual detection of small objects illuminated by biological light would be easily possible. In the water layers above the ultimate maximum for daylight detection, deep-sea animals can presumably perceive differences in light received from the surface during periods of no nearby luminescent discharge, and perhaps can distinguish qualitatively at all times between background daylight and bioluminescence from localized sources.

Certain animals have been found to carry out diurnal vertical migrations, presumably in response to changes in submarine daylight, at depths of 800 m or possibly slightly greater (Waterman *et al.* 1939). A depth of about 900 m to 1000 m would appear to be the shallowest level in clear water at which day and night changes in illumination would be below the threshold of perception and at which daylight would never be sufficiently strong for the inhabitants to be seen by their predators or by their prey. For these or related reasons a large population may have come to occupy this stratum. The fact that a high degree of luminescence has been observed to characterize the animals at this depth might appear to be contradictory to the foregoing suggestion, but the flashing might have developed as counter-measures of defense, recognition, or the luring of prey. The findings of other investigators, cited above, suggest that a concentration of pelagic animals at about 900 m may be of widespread occurrence.

Whether or not any validity will be found in the foregoing speculations, the present investigation has shown that bioluminescence may provide detectible illumination at depths at least as great as 3750 m. Although further exploration will be required before generalities can be established, the variation in frequency, intensity, and duration of the flashes here reported indicate the presence of very different populations at various depths. The brightness and varied pattern of the bioluminescence observed suggest that the phenomenon is probably of even greater significance in the ecology of the deep sea than previously supposed.

REFERENCES

Bernard, F. 1955. Densité du plancton vu au large de Toulon depuis le Bathyscaphe FNRS-

3. Bull. Inst. Océanogr. Monaco, No. 1063. 16 pp.

Boden, B. P., and E. M. Kampa. 1957. Records of bioluminescence in the ocean. Pacific Science, **11**: 229–235.

Breslau, L. R., and H. E. Edgerton. 1958. The luminescence camera. Woods Hole Oceanographic Institution. Unpublished manuscript. Ref. No. 58-14.

Breslau, L. R., and H. E. Edgerton. 1959. The luminescence camera. J. Biol. Photogr. Assoc. (in press).

Clarke, G. L. 1936. On the depth at which fish can see. Ecology, **17**: 452–456.

Clarke, G. L., and R. H. Backus. 1956. Measurements of light penetration in relation to vertical migration and records of luminescence of deep sea animals. Deep-Sea Res., **4**: 1–14.

Clarke, G. L., and G. K. Wertheim. 1956. Measurements of illumination at great depths and at night in the Atlantic Ocean by means of a new bathyphotometer. Deep-Sea Res., **3**: 189–205.

Denton, E. J., and F. J. Warren. 1957. The photosensitive pigments in the retinae of deep-sea fish. J. Mar. Biol. Ass. U. K., **36**: 651–662.

Dietz, R. S. 1959. 1100-meter dive in the bathyscaph TRIESTE. Limnol. Oceanogr., **4**: 94–101.

Furnestin, J. 1955. Une plongée en Bathyscaphe. Rev. Trav. Inst. Pêche Marit., **19**(4): 435–442.

Hardy, A. C. 1956. The open sea. Collins, London. 335 pp.

Harvey, E. N. 1952. Bioluminescence. New York, Academic Press. 632 pp.

Hubbard, C. J. 1956. A wide range, high-speed bathyphotometer. Woods Hole Oceanogr. Inst., unpublished manuscript Ref. No. 56–68.

Kampa, E. M., and B. P. Boden. 1957. Light generation in a sonic-scattering layer. Deep-Sea Res., **4**(2): 73–92.

Leavitt, B. B. 1938. The quantitative vertical distribution of macrozooplankton in the Atlantic Ocean Basin. Biol. Bull., **74**: 376–394.

Marshall, N. B. 1954. Aspects of deep sea biology. Philosophical Library, Inc., N. Y. 380 pp.

Pérès, J. M., and J. Piccard. 1956. Nouvelles observations biologiques effectivées avec le Bathyscaphe F. N.R.S. III et considérations sur le système aphotique de la Méditerranée. Bull. Inst. Océanogr. Monaco, No. 1075. 10 pp.

Pérès, J. M., J. Piccard, and M. Ruivo. 1957. Résultats de la campagne de recherches du Bathyscaphe F.N.R.S. III. Bull. Inst. Océanogr. Monaco, No. 1092. 29 pp.

Piccard, J., and R. S. Dietz. 1957. Oceanographic observations by the bathyscaph *Trieste* (1953–1956). Deep-Sea Res., **4**: 221–229.

Sweet, M. H. 1946. Logarithmic photometer. Electronics, **19**: 106–109.

Trégouboff, G. 1956. Prospection biologique sous-marine dans la region de Villefranche-sur-Mer en Juin 1956. Bull. Inst. Océanogr. Monaco, No. 1085. 24 pp.

Waterman, T. H., R. F. Nunnemacher, F. A. Chace, Jr., and G. L. Clarke. 1939. Diurnal vertical migration of deep water plankton. Biol. Bull., **76**: 256–279.

Contribution No. 1020

BULLETIN OF
MATHEMATICAL BIOPHYSICS
VOLUME 21, 1959

A NOTE ON THE TRANSIENT STAGE OF THE RANDOM DISPERSAL OF LOGISTIC POPULATIONS*

RICHARD BARAKAT**
WOODS HOLE OCEANOGRAPHIC INSTITUTION,
WOODS HOLE, MASSACHUSETTS

The transient stage of the random dispersal of logistic populations is investigated, using a Sturm-Liouville series leading to an infinite system of non-linear integral equations. These equations are then solved via a successive approximation scheme. R. A. Fisher's (steady-state) velocity of advance paradox is discussed. An illustrative example is worked to the second order of approximation.

Introduction. The random dispersal of populations of living organisms subject to a logistic growth rate is a natural extension of the Lotka-Volterra theory to include space dependence, as well as time dependence, of the population density function. Unfortunately, the introduction of a logistic growth rate leads to a formidable non-linear partial differential equation describing the biological situation. There are two ways to avoid the difficulties of solving the time-dependent equation. The first method merely neglects the time dependence of the density function by assuming that a steady state exists; the analogous genetic problem was first treated in this manner in a classic paper by R. A. Fisher (1937). In this paper, Fisher was led to a paradox concerning the indeterminacy of the velocity of the "wave of advance of advantageous genes" because his analysis neglects the initial conditions. Similarly, J. G. Skellam (1951), treating the steady-state ecological problem, encountered the same difficulty. The steady-state problem is really anomalous because we are making a statement about the biological system that holds for all time. The Lotka-Volterra biological mechanics, however, is involved only with the predictive description of the system from specified initial conditions.

---

*Contribution No. 1020 of the Woods Hole Oceanographic Institution.

**Present address: Physical Research Laboratory, Itek Corporation, Boston 15, Massachusetts.

The second method retains the time dependence but involves a perturbation scheme designed to linearize the equation by considering a biological state near equilibrium. This scheme is also unsatisfactory, since it is valid for only very small time intervals.

Finally, we are led to consider the equation without any simplifying assumptions. To the author's knowledge, the only investigation of the transient case has been by H. D. Landahl (1957), who used an interesting approximation technique. The transient-state analysis can also be attacked by utilizing a Sturm-Liouville series leading to an infinite system of non-linear integral equations. In this manner, we treat the problem as an initial-value one and pass to the steady state by letting the time become infinite. Using this technique, we can resolve the indeterminacy of the velocity by taking the initial conditions into account in the analysis. Although we can prove that there is some unique velocity, it is not necessarily equal to Fisher's minimum velocity of the "wave of advance." The further advantage of this method lies in its constructional value; we can solve the resulting nonlinear system of integral equations to any desired degree of accuracy in the space-time domain.

Method of solution. In what follows, we restrict ourselves to the one-dimensional case; extension to the two-dimensional case is immediate, and we do not consider it in this paper.

The usual one-dimensional equation describing the random dispersal of a logistic problem is given by

$$\frac{\partial\psi}{\partial t} - a^2 \frac{\partial^2\psi}{\partial x^2} = \gamma\psi(1-\psi), \tag{1}$$

where $\psi(x_1 t)$ = population density, a^2 = diffusion constant, and γ = logistic growth coefficient. This equation is derived under the assumption that the dispersion is normal. If, however, non-normal dispersion were to take place, then our fundamental equation (1) would take the form

$$\frac{\partial\psi}{\partial t} - \sum_{n=1}^{\infty} (-1)^n \frac{K_n}{n!} \frac{\partial^n \psi}{\partial x^n} = \gamma\psi(1-\psi), \tag{2}$$

where K_n is the nth cumulant of the non-normal distribution considered. When normal dispersion occurs, then (2) degenerates to (1).

Equation (1) is not the most general description of the normal process, for we can consider the diffusion and logistic coefficients as being functions of distance instead of being merely constants. The basic equation then is

$$\frac{\partial\psi}{\partial t} - \frac{\partial}{\partial x}\left[\rho(x)\frac{\partial\psi}{\partial x}\right] = \gamma(x)\,\psi(1-\psi). \tag{3}$$

Equation (3) is a non-linear partial differential equation of parabolic type, the non-linearity being due to the presence of the function $\gamma(x)\,\psi(1-\psi)$. It is possible to solve equation (3) (under fairly mild restrictions) using a Fourier method (Sundaram, 1939), which consists of converting the partial differential equation into an infinite system of non-linear equations. This infinite equation system is then solved by using the method of successive approximations; in this manner we account for both boundary and initial conditions explicitly.

Let $\rho(x)$ (distance-dependent diffusion function) be a positive bounded continuous function with bounded first and second derivatives:

$$0 \leq \rho(x) \leq M, \quad |\rho'(x)| \leq M, \quad |\rho''(x)| \leq M. \tag{4}$$

We try to determine a solution of equation (3) which is regular in the domain

$$0 \leq x \leq \pi, \; 0 \leq t \leq \infty, \tag{5}$$

and which will satisfy the initial condition

$$\psi(x, 0) = \psi_0(x) \ (0 \leq x \leq \pi) \tag{6}$$

and the boundary conditions

$$\psi(0,t) = \psi(\pi,t) = 0 \quad (t \geq 0). \tag{7}$$

(Without any great change in the argument we can consider other boundary conditions; we merely use the specific boundary conditions to illustrate the method.)

We write the solution of (3) as an infinite series of eigenfunctions

$$\psi(x, t) \sim \sum_{n=1}^{\infty} U_n(t)\, \phi_n(x), \tag{8}$$

where the $\phi_n(x)$'s are the complete ortho-normal eigenfunctions of the Sturm-Liouville differential equation (in $0 \leq x \leq \pi$),

$$\frac{d}{dx}\left[\rho(x)\, \frac{d\phi}{dx}\right] + \lambda\phi = 0, \tag{9}$$

with the boundary conditions,

$$\phi(0) = \phi(\pi) = 0. \tag{10}$$

Denote by λ_n the eigenvalue corresponding to $\phi_n(x)$. We can prove that the eigenvalues λ_n are non-negative for the boundary conditions (10):

$$\lambda = \lambda \int_0^{\pi} [\phi(x)]^2\, dx = \int_0^{\pi} \rho\, \phi'^2\, dx, \tag{11}$$

where the first term vanishes and the integral is positive (except when ϕ is a constant).

The initial-value function can be written

$$\psi_0(x) \sim \sum_{n=1}^{\infty} C_n \, \phi_n(x), \tag{12}$$

where $C_n = U_n(0)$. Finally, we *assume* the expansion of

$$f(x, t, \psi) = \gamma(x) \, \psi(1-\psi) \tag{13}$$

in a series of $\phi_n(x)$. As Sundaram has remarked, a necessary condition that $f(x, t, \psi)$ satisfy the boundary conditions (7) is that

$$f(0, t, 0) = f(\pi, t, \psi) = 0. \tag{14}$$

Now let f have the expansion

$$\begin{gathered} f(x, t, \psi) \sim \sum_{n=1}^{\infty} F_n(t) \, \phi_n(x), \\ F_n(t) = \int_0^{\pi} \gamma(x) \, \psi(1-\psi) \, \phi_n \, dx. \end{gathered} \tag{15}$$

Our problem reduces to the determination of the coefficients $U_n(t)$ such that (3) and (6) can be satisfied. Substituting (8) in (3) and equating the Fourier coefficients $\phi_n(x)$ on both sides, we find that $U_n(t)$ must satisfy the non-linear differential equation system:

$$\begin{gathered} \frac{dU_n}{dt} + \lambda_n U_n = F_n(t), \\ U_n(0) = C_n \quad (n = 1, 2, \ldots). \end{gathered} \tag{16}$$

(We could throw this into matrix form and consider the topology of the system, but this will not be done.) Equation (16) is equivalent to the non-linear integral equation system:

$$U_n(t) = C_n e^{-\lambda_n t} + \int_0^t e^{-\lambda_n (t-s)} F_n \,[s, U_1(s), \ldots]\, ds. \tag{17}$$

Sundaram (1937) has shown that this system can be solved uniquely by the method of successive approximations, provided that we impose the condition that

$$\sum_{n=1}^{\infty} \lambda_n C_n < \infty; \tag{18}$$

in fact, it can be shown that the convergence of this series shows that $\psi'(x)$ exists and is integrable L^2. These conditions upon the initial-value function $\psi_0(x)$ are not severe but do exclude certain functions which do not die out rapidly enough at infinity and yet are of possible ecological interest.

If we use the successive approximation scheme,

$$\begin{aligned} &U_n^{(0)}(t) = 0, \\ &U_n^{(m)}(t) = C_n e^{-\lambda_n t} + \int_0^t e^{-\lambda_n (t-s)} F_n \,[s,\, U_1^{(1)}(s), \ldots]\, ds, \end{aligned} \tag{19}$$

we can prove that

$$\lim_{m \to \infty} U_n^{(m)}(t) = U_n(t) \tag{20}$$

will exist for all t in any finite interval and all m.

Velocity of the wave of advance. The solutions of equation (3) must be non-negative functions, seeing that they represent population densities. Under this restriction of positive-definite solution and assuming that a steady state exists, R. A. Fisher (1937) showed that progressive waves are possible with any velocity greater than, or equal to, a certain minimum velocity determined by both the diffusion and the logistic growth coefficients where these coefficients are now taken as constants. (In the remainder of this paper we restrict ourselves to constant diffusion and logistic growth coefficients, not so much for mathematical reasons as for ecological reasons. We do not know enough about these coefficients at present to warrant the added mathematical complexity of their space dependency.)

If we restrict the logistic growth coefficient γ to be greater than zero (growth problem), then we can show (Fisher, 1937; Kendall, 1948) that the only possible velocities of propagation are

$$|v| \geq 2a\gamma^{\frac{1}{2}}.$$

The minimum velocity $2a\gamma^{\frac{1}{2}}$ will be termed v_c. This velocity of propagation of the wave of advance is independent of the initial conditions and indeterminate because there is no one definite velocity of propagation but a multiplicity of possible velocities. If we take cognizance of the initial conditions, we should be able to show that there is only one possible velocity of propagation. As M. G. Kendall has remarked, "... the conclusion would be that the velocity of advance ultimately has the minimum value v_0, whenever the initial distribution of mutant genes is strictly local in character." The rate at which the derivative of the initial distribution approaches zero as x approaches infinity is the critical factor determining the ultimate velocity of propagation of the wave of advance.

In the previous section we saw that our basic equation can be solved *uniquely*, provided that $\psi_0'(x)$ exists and is L^2 integrable Suppose that there were more than one velocity possible, then we would have a corresponding number of possible solutions to the dispersion-growth equation. If we assume that the specified conditions hold, then our uniqueness condition asserts that there is a contradiction; hence there is only one possible velocity. This velocity is time-dependent during the transient state but should approach a constant value as time passes (steady state). We are still faced with the question as to whether this wave front will be set up; again, with our uniqueness theorem holding, we can assert that there is some unique wave front in the steady state. This steady-state velocity should correspond to v_0, but the author has not been able to prove this as a general statement. The stability of this wave front has already been shown by Skellam. If the initial-value function were such as not to be subsumed under our stated conditions, then we have no assurance that the velocity is v_0 but may well differ from it (see Kendall, 1948, for a discussion of the analogous linear problem). Intuitively we can see what is happening by looking at (17). The λ_n's are always positive, but, unless we have a bound on the order of the Fourier coefficients C_n, we cannot assert that in the passage to the steady state the inhomogeneous term containing the initial values is insignificant.

In this respect one has to reduce drastically the generalities by constructing concrete examples. In a paper in preparation, the Sturm-Liouville method is being applied to a number of interesting ecological situations. Unfortunately, a considerable body of manipulation is necessary for quantitative results; however, for purposes of illustration we demonstrate the essentials of the method by only going to the second order of approximation.

Illustrative example. We consider the case of a favorable habitat flanked by extremely unfavorable conditions at 0 and π. Then we have to solve equation (1) subject to the boundary conditions

$$\psi(0, t) = \psi(\pi, t) = 0 \quad (t \geq 0). \tag{21}$$

Let the initial-value function be a sine function:

$$\psi_0(x) = \frac{1}{\sqrt{\pi}} \sin x. \tag{22}$$

The diffusion and logistic growth coefficients are set equal to unity to simplify the arithmetic.

The normalized eigenfunctions $\phi_n(x)$ which satisfy the conditions $\phi(0) = \phi(\pi) = 0$ are

$$\phi_n(x) = \frac{1}{\sqrt{\pi}} \sin nx \quad (n = 1, 2, \ldots). \tag{23}$$

The expansion of $\psi(x, t)$ is

$$\psi(x,t) \sim \frac{1}{\sqrt{\pi}} \sum_{n=1}^{\infty} U_n(t) \sin nx, \tag{24}$$

as in (15).

Now to expand $f(x, t, \psi) = \psi^2 - \psi$,

$$f(x,t,\psi) \sim \frac{1}{\sqrt{\pi}} \sum_{n=1}^{\infty} F_n(t) \sin nx, \tag{25}$$

where

$$F_n(t) = \frac{2}{\pi} \int_0^{\pi} (\psi^2 - \psi) \sin nx \, dx. \tag{26}$$

Substituting for the series (24) for ψ, we obtain

$$F_n(t) = -\frac{U_n(t)}{\sqrt{\pi}} + \frac{1}{\pi^3} \sum_{l=1}^{\infty} \sum_{m=1}^{\infty} Q(l,m,n) \, U_l(t) \, U_m(t); \tag{27}$$

here

$$Q(l,m,n) = \int_0^{\pi} \sin lx \sin mx \sin nx \, dx. \tag{28}$$

Our infinite system of non-linear integral equations (17) now is

$$U_n(t) = \delta_{n1} e^{-nt} + \frac{e^{-nt}}{\sqrt{\pi}} \int_0^t e^{ns}\, U_n(s)\, \mathrm{ds} -$$

$$\frac{1}{\pi^3} \int_0^t e^{-n(t-s)} \sum_{l,m=1}^{\infty} Q(l,m,n)\, U_l(s)\, U_m(s)\, ds. \quad (29)$$

We solve this infinite system by truncating to only the first three $U_n(t)$. The truncated system is to be solved by successive approximations. Letting

$$U_n^{(0)}(t) = 0, \quad n = 1,2,3, \quad (30)$$

then the first approximations are, from (19),

$$\begin{aligned} U_1^{(1)}(t) &= e^{-t}, \\ U_2^{(1)}(t) &= U_3^{(1)}(t) = 0. \end{aligned} \quad (31)$$

The second approximation $U_n^{(2)}(t)$ is obtained from

$$U_n^{(2)}(t) = \delta_{n1} e^{-nt} + \int_0^t e^{-n(t-s)} \frac{U_n^{(1)}(s)}{\sqrt{\pi}}\, ds -$$

$$\frac{1}{\pi^3} \int_0^t e^{-n(t-s)} \sum_{l,m=1}^{3} Q(l,m,n)\, U_l^{(1)}(s)\, U_m^{(1)}(s)\, ds. \quad (32)$$

Carrying out the indicated operations, we have

$$U_1^{(2)}(t) = e^{-t}(1 + \pi^{-\frac{1}{2}} t),$$

$$U_2^{(2)}(t) = 0, \tag{33}$$

$$U_3^{(2)}(t) = \frac{4}{15\pi^3}(e^{-2t} - e^{-3t}).$$

Thus to the second order of approximation; from (24), we get

$$\psi^2(x,t) = \frac{1}{\sqrt{\pi}}\left[e^{-t}\left(1 + \frac{1}{\sqrt{\pi}}\right)\sin x + \frac{4}{15\pi^3}(e^{-2t} - e^{-3t})\sin 3x\right]. \tag{34}$$

This approximation is good for only small values of t. Note that, when $t = 0$, $\psi^{(2)}(x, 0) = \psi(x, 0)$. Now $\psi^2(x, t)$ is a decreasing function of the time (for fixed x); this can be interpreted as stating that dispersion is the dominating factor for small t. The reason is simple enough: the outflow due to diffusion just balances the linear growth term, leaving the negative quadratic term $\psi^2(x,t)$.

LITERATURE

Fisher, R. A. 1937. "The Wave of Advance of Advantageous Genes." *Ann. Eugenics, London* 7, 335–69.

Kendall, M. G. 1948. "A Form of Wave Propagation Associated with the Equation of Heat Conduction." *Proc. Camb. Phil. Soc.*, 44, 591–93.

Landahl, H. D. 1957. "Population Growth under the Influence of Random Dispersal." *Bull. Math. Biophysics*, 19, 171–86.

Skellam, J. G. 1951. "Random Dispersal in Theoretical Populations." *Biometrika*, 38, 196–218.

Sundaram, S. M. 1939. "On Non-Linear Partial Differential Equations of the Parabolic Type." *Proc. Ind. Acad. Sci.*, 9A, 479–94.

RECEIVED 12-9-58

Contribution No. 1021

Reprinted for private circulation from
THE ASTROPHYSICAL JOURNAL
Vol. 130, No. 1, July 1959
Copyright 1959 by the University of Chicago
PRINTED IN U.S.A.

MAGNETOCONVECTION IN A VISCOUS FLUID OF INFINITE ELECTRICAL CONDUCTIVITY

W. V. R. Malkus
Woods Hole Oceanographic Institution, Woods Hole, Massachusetts
Received November 23, 1958; revised March 23, 1959

ABSTRACT

A determination is made of the stable magnetic fields associated with steady-state convection in a fluid with no electrical resistance. The viscosity and thermal diffusivity which determine the amplitude of the fields are retained in the analysis. It is found that the most stable magnetic field is that one which alters the advection of momentum in a manner that minimizes the constraints on the convection. For the non-rotating fluid with small Prandtl number, the stable state is one of detailed local equipartition of magnetic and kinetic energy. For the rotating fluid the stable state can be one of vastly greater magnetic energy than kinetic energy. In speculating on the applicability of these results to astrophysical convection, it is suggested that the stable "magnetostrophic" fields are by far the largest part of the observed fields.

This is a study of the non-linear interaction of magnetic and motion fields in an electrically conductive fluid. Only those situations will be discussed in which no external magnetic fields are imposed on the fluid system. The more formal part of this work is restricted to the determination of the stable magnetic fields of a steady-state motion when the fluid has no electrical resistance. The convective motions which act as an energy source for the magnetic field are controlled by viscous and thermal diffusion. These diffusive terms in the dynamic and heat equations will be retained so that a steady state can be achieved.

A recent paper on finite-amplitude cellular convection (Malkus and Veronis 1958; hereinafter referred to as "Paper I") describes a method to determine solutions of the dynamic equations in a limited range of the parameters beyond a point of convective instability. It was found that there were an infinite number of formal steady-state solutions to this non-linear problem, differing in plan form and amplitude. A "relative stability" criterion was deduced which selected the realizable motions from these solutions. These techniques will be applied in this paper to select an optimum magnetoconvective field from a limited set of solutions to the magnetic equations.

Two types of limiting magnetoconvection will be studied. The first of these is the simple Rayleigh-like convection in a layer of fluid heated from below. In the initial finite-amplitude motion after instability, the non-linear momentum transfer plays only a stabilizing role. We shall find that the most stable magnetic field is one which opposes this momentum transfer, permitting an optimum rate of release of potential energy. When the Prandtl number is small, this opposition leads to a local equipartition of magnetic and kinetic energy.

A second type of magnetoconvection to be studied is convection in a rotating system. Chandrasekhar (1953) has solved the stability problem, and Veronis (1959; hereinafter referred to as "Paper II") has found the initial finite-amplitude fields of motion and temperature. Here we shall find that the most stable magnetic field can have a vastly greater magnetic than kinetic energy density. The reasons for this relate again to the role played by the non-linear momentum transfer. In Paper II it was shown that momentum transfer can reduce the constraints imposed by rotation, hence increasing the rate of release of potential energy. The preferred magnetic field optimizes this destabilizing momentum transfer process.

Solutions for the flow in a medium of finite electrical conductivity have not been attempted in this paper. Yet, to maintain the magnetic fields found here, the loss of magnetic energy by electrical dissipation must be balanced by a transfer from the kinetic energy of the field of motion (the generator problem). In turn, the field of motion will maintain its transferable kinetic energy only if the presence of the magnetic field produces forces that assist in the release of potential energy. It is hoped that this study of the role of the magnetic field in releasing potential energy will contribute to continuing work (Bullard 1954; Backus and Chandrasekhar, 1956; Herzenberg, 1958) on the generator problem.

The preceding formal problems differ in kind from the problems of stability which arise when an external magnetic field is imposed on the fluid system (e.g., Chandrasekhar 1956*b*). Perhaps the most significant difference is that the imposed magnetic fields are, in general, stabilizing, i.e., they inhibit the release of potential energy, while the "self-generated" magnetic fields are realized because they reduce the constraints on the fluid motion. The role of the electrical conductivity also differs in these two situations. The restraint on motion caused by the imposed magnetic fields becomes smaller as the conductivity decreases, while a decrease in conductivity would reduce the amplitude of the optimum magnetic fields found here.

This work treats only two of a large class of similar problems and, perhaps, will suggest to the reader other non-linear studies with radiative heat sources, with different dissipative mechanisms, or in shearing flows rather than in convection.

The applicability of these findings to geomagnetism, solar convection, and interstellar turbulence is explored in Section V.

I. FORMULATION OF A TRACTABLE PROBLEM

The dynamic equations to be used are those of Boussinesq (1903) and are applicable when the fluctuations of density of the fluid medium are a small fraction of the mean density. These equations are

$$\left(\frac{\partial}{\partial t}-\nu\nabla^2\right)\boldsymbol{v}=-\frac{1}{\rho}\nabla\bar{P}-2\Omega\times\boldsymbol{v}-\boldsymbol{v}\cdot\nabla\boldsymbol{v}+\frac{\mu}{4\pi\rho}(\nabla\times\boldsymbol{H})\times\boldsymbol{H}+\gamma T\boldsymbol{k}, \tag{1.1}$$

$$\left(\frac{\partial}{\partial t}-\kappa\nabla^2\right)T=-\boldsymbol{v}\cdot\nabla T, \tag{1.2}$$

$$\nabla\cdot\boldsymbol{v}=0\,, \tag{1.3}$$

where $\boldsymbol{v}$ is the vector velocity; ρ is the average density; $\bar{P}=P-gz$, where P is the pressure and g is the acceleration of gravity; Ω is an imposed uniform rotation; μ is the magnetic permeability; $\boldsymbol{H}$ is the magnetic field; $\gamma=\alpha g$, where α is the linear coefficient of expansion of the fluid, $\boldsymbol{k}$ is a unit vector in the vertical direction; T is the departure from the average temperature; ν is the kinematic viscosity; and κ is the thermometric conductivity. The electromagnetic equations necessary to the discussion are

$$\left(\frac{\partial}{\partial t}-\eta\nabla^2\right)\boldsymbol{H}=\nabla\times\boldsymbol{v}\times\boldsymbol{H}=\boldsymbol{H}\cdot\nabla\boldsymbol{v}-\boldsymbol{v}\cdot\nabla\boldsymbol{H}, \tag{1.4}$$

$$\nabla\cdot\boldsymbol{H}=0, \tag{1.5}$$

where the magnetic diffusivity $\eta=(4\pi\mu\sigma')^{-1}$ and σ' is the electrical conductivity.

Both convective motions to be considered are in a fluid contained between two horizontal surfaces separated by a distance d (z is measured upward from the lower surface). The boundaries are assumed to be perfect heat conductors held at constant temperature, with the lower boundary at the higher temperature. The dynamic boundaries are assumed to be "free" and support no stress. The electrical boundaries are also assumed to be perfect conductors. Hence

$$T=W=\frac{\partial^2 W}{\partial z^2}=H_z=\frac{\partial^2 H_z}{\partial z^2}=0$$

at both boundaries, where W is the vertical component of the velocity, T is the fluctuation about the horizontally averaged temperature, and H_z is the vertical component of the magnetic field. In this simple case $\boldsymbol{H}$ and $\boldsymbol{v}$ satisfy the same boundary conditions.

One notes that any exact solution to equations (1.1)–(1.5) is also an exact solution if the sign of $\boldsymbol{H}$ is reversed. Hence no preferred sign for $\boldsymbol{H}$ can be deduced from these equations.

It can be seen from equation (1.4) that if the velocity field can generate a magnetic field, it will first do so at some critical value of the magnetic Reynolds number R_m, where $R_m \equiv |V|l/\eta$, where $|V|$ is a representative amplitude of the velocity and l is a representative scale. As the electrical conductivity approaches infinity, η will approach zero, and R_m will become arbitrarily larger than the critical R_m. In this limit the balance in equation (1.4) is between the advective terms and the time variations of $\boldsymbol{H}$. However, the fields of convection that we shall discuss are independent of time. Then equation (1.4) requires that

$$\nabla \times \boldsymbol{v} \times \boldsymbol{H} = \boldsymbol{H} \cdot \nabla \boldsymbol{v} - \boldsymbol{v} \cdot \nabla \boldsymbol{H} = 0 \, . \tag{1.6}$$

That solution of equation (1.6) which permits the electric field to vanish everywhere in this infinitely conducting medium is

$$\boldsymbol{H} = c\boldsymbol{v} \tag{1.7}$$

where c is a scalar field. The restriction on c is, from equations (1.3) and (1.5),

$$\boldsymbol{v} \cdot \nabla c = 0 \tag{1.8}$$

and, from (1.6) that $\partial c/\partial z = 0$ at the boundaries. Equation (1.8) requires that c be a constant along any streamline.

The infinite class of solutions (1.7) can now be incorporated into the dynamic equations (1.1). Noting that

$$(\nabla \times \boldsymbol{H}) \times \boldsymbol{H} = -\tfrac{1}{2}\nabla(\boldsymbol{H} \cdot \boldsymbol{H}) + \boldsymbol{H} \cdot \nabla \boldsymbol{H}$$

and

$$\boldsymbol{v} \cdot \nabla c\boldsymbol{v} = c\boldsymbol{v} \cdot \nabla \boldsymbol{v} \, ,$$

we may write equation (1.1) thus:

$$\left(\frac{\partial}{\partial t} - \nu\nabla^2\right)\boldsymbol{v} + \frac{1}{\rho}\nabla\bar{P}' + 2\Omega \times \boldsymbol{v} - \gamma T\boldsymbol{k} = -\left(1 - \frac{\mu c^2}{4\pi\rho}\right)\boldsymbol{v} \cdot \nabla \boldsymbol{v} \, , \tag{1.9}$$

where

$$\bar{P}' = \bar{P} + \frac{\mu H^2}{8\pi} = \bar{P} + \left(\frac{\mu c^2}{8\pi}\right) v^2 \, .$$

From equation (1.9) one sees that the role of the limiting class of magnetic solutions (1.7) is to reduce the normal advection of momentum. It is also of significance that

$$\left[\boldsymbol{v} \cdot \left(1 - \frac{\mu}{4\pi\rho} c^2\right) \boldsymbol{v} \cdot \nabla \boldsymbol{v}\right]_m = 0 , \tag{1.10}$$

where the subscript m indicates an average over the entire field of motion. The vanishing of equation (1.10) means that the mean momentum advection due to both the velocity and the magnetic field does not contribute to the release of potential energy. (If σ' were finite, eq. [1.10] would make a positive-definite contribution to the dissipation of energy.)

Equations (1.2), (1.3), and (1.9) are five equations in five unknowns, $\boldsymbol{v}$, T, and P and the arbitrary function c. Our problem is to determine what choice of c leads to a stable field of motion.

For very small temperature differences between the bottom and top of the fluid layer the only solution to equations (1.2), (1.3), and (1.9) is the state of pure thermal conduction. However, at some value of the parameter $R \equiv \gamma d^3 \Delta T/\kappa\nu$, called the "Rayleigh number," the thermal field becomes unstable to infinitesimal disturbances. This critical value of R depends upon Ω, increasing as Ω increases. Since the magnetic field enters equation (1.2) as a quadratic term (c^2), it is clear that it will not influence the critical value of R for the growth of an infinitesimal disturbance. However, it is possible that a finite-amplitude disturbance, involving the magnetic field, can be unstable at a value of R less than its critical value for infinitesimal disturbance. We shall investigate this possibility in Section IV. In any event, the solutions involving the magnetic field must be non-linear solutions, and the determination of the realizable magnetic fields involves a stability analysis of these non-linear solutions.

The complexity of this task is reduced by restricting the magnetic fields considered to those for which c is a constant. The problem then is to determine the most stable value for c in the range $-\infty \leq c \leq +\infty$. It is possible that more stable limiting magnetic fields exist in which the value of c varies from streamline to streamline. Though this more general problem is not dealt with here, it will be easier to face in the light of solutions for the restricted values of c.

Before describing the technique used to generate finite-amplitude solutions of equations (1.2), (1.3), and (1.9) for a given c, the problem of the "relative stability" of solutions will be discussed.

II. THE RELATIVE STABILITY OF SOLUTIONS

To be observable, a steady-state solution to the basic equations must be stable against all the disturbances associated with the experiment. Unfortunately, the problem of the stability of a known solution, $\boldsymbol{v}$, $\boldsymbol{H}$, and T, is so difficult that it has been resolved only in the simplest cases. In addition, the soluble stability problems treat only the limiting case of "infinitesimal disturbances," neglecting any non-linear effects of the physically real "small disturbances."

However, when there are several solutions to the basic equations for the same boundary conditions, the realizability of one or more of these solutions can often be established by a method used in Paper I. It is assumed, first, that the complete set of steady and statistically steady solutions is known. Then any observable solution is contained in this set. The stability of one of these solutions is assured only when all possible disturbances have been considered, but instability can be proved by finding a single example. Hence, if it can be shown by example that all but one of the solutions are unstable, then the remaining solution must be the stable one. If all but a few solutions are unstable to a restricted class of disturbances, then either these few solutions can be realized separately, or a broader class of disturbances must be considered to remove the remaining indeterminacy.

The method used in Paper I was based on the assertion that a solution is unstable if the mean-square value of a disturbance increases in the first instant after it is imposed on the solution. To support this assertion, we note that whatever the disturbance may do in a later instant, it will have caused a finite distortion of the solution by its initial growth. As one extreme, the disturbance may decay after this initial growth, but it will reoccur aperiodically because of the random background fluctuations. Since an average finite distortion of the solution will result, this solution is not realized. (In this extreme example "solution" plus distortion must be one of the other solutions in our complete list of solutions.)

The class of initial disturbances of a solution which are considered are those disturbances which have the form of other solutions. Hence we seek the "relative stability" of the solutions.

An answer to the relative stability question will be sought by using the complete equations (1.1)–(1.5), $\eta \neq 0$, and then specialized to the case of infinite electrical conductivity.

The equations satisfied by an arbitrary disturbance $\boldsymbol{v}'$, $\boldsymbol{H}'$, and T' to a solution $\boldsymbol{v}$, $\boldsymbol{H}$, and T of equations (1.1)–(1.5) are

$$\left(\frac{\partial}{\partial t} - \nu\nabla^2\right)\boldsymbol{v}' = \frac{-1}{\rho}\nabla\bar{P}' - 2\Omega\times\boldsymbol{v}' - \boldsymbol{v}\cdot\nabla\boldsymbol{v}' - \boldsymbol{v}'\cdot\nabla\boldsymbol{v} - \boldsymbol{v}'\cdot\nabla\boldsymbol{v}' + \gamma T'\boldsymbol{k}$$
$$+\frac{\mu}{4\pi\rho}\left(\nabla\times\boldsymbol{H}'\right)\times\boldsymbol{H} + \frac{\mu}{4\pi\rho}(\nabla\times\boldsymbol{H})\times\boldsymbol{H}' + \frac{\mu}{4\pi\rho}(\nabla\times\boldsymbol{H}')\times\boldsymbol{H}', \tag{2.1}$$

$$\left(\frac{\partial}{\partial t} - \kappa\nabla^2\right)T' = -\boldsymbol{v}\cdot\nabla T' - \boldsymbol{v}'\cdot\nabla T - \boldsymbol{v}'\cdot\nabla T', \tag{2.2}$$

$$\nabla\cdot\boldsymbol{v}' = 0\,, \tag{2.3}$$

$$\left(\frac{\partial}{\partial t} - \eta\nabla^2\right)\boldsymbol{H}' = \nabla\times\boldsymbol{v}'\times\boldsymbol{H} + \nabla\times\boldsymbol{v}\times\boldsymbol{H}' + \nabla\times\boldsymbol{v}'\times\boldsymbol{H}', \tag{2.4}$$

$$\nabla\cdot\boldsymbol{H}' = 0\,. \tag{2.5}$$

From these, one constructs the integrals for the total energy of the disturbance and for the mean-square fluctuations of the internal energy:

$$\frac{1}{2}\frac{\partial}{\partial t}\left(\boldsymbol{v}'\cdot\boldsymbol{v}' + \frac{\mu}{4\pi\rho}\boldsymbol{H}'\cdot\boldsymbol{H}'\right)_m = \nu\,(\boldsymbol{v}'\cdot\nabla^2\boldsymbol{v}')_m + \frac{\eta\mu}{4\pi\rho}(\boldsymbol{H}'\cdot\nabla^2\boldsymbol{H}') + \gamma\,(W'T')_m$$
$$+\left[\left(\frac{\mu}{4\pi\rho}\boldsymbol{H}'\cdot\boldsymbol{H}' - \boldsymbol{v}'\cdot\boldsymbol{v}'\right)\cdot\nabla\boldsymbol{v}\right]_m + \frac{\mu}{4\pi\rho}\left[(\boldsymbol{v}'\cdot\boldsymbol{H}' - \boldsymbol{H}'\cdot\boldsymbol{v}')\cdot\nabla\boldsymbol{H}\right]_m, \tag{2.6}$$

$$\frac{1}{2}\frac{\partial}{\partial t}(T'^2)_m = \kappa\,(T'\cdot\nabla^2T')_m + (W'T'\beta)_m - (T'\,\boldsymbol{v}'\cdot\nabla T)_m, \tag{2.7}$$

where the subscript m denotes an average over the whole fluid system and W' is the vertical component of $\boldsymbol{v}'$. Here T has been written $T = \langle T\rangle + T$ and $\beta = -\partial\langle T\rangle/\partial z$, where the broken brackets denote an average over a horizontal plane. (All integrals of the form $[S\boldsymbol{v}\cdot\nabla S]_m$ vanish, as they represent conservative advections.) If $\boldsymbol{v}$, $\boldsymbol{H}$, T is unstable to the disturbance $\boldsymbol{v}'$, $\boldsymbol{H}'$, T', the right-hand side of equations (2.6) and (2.7) will be positive.

The class of disturbances is now restricted to those which have the initial form of steady or statistically steady solutions of the basic equations. That is,

$$\boldsymbol{v}' = A\,\boldsymbol{v}_1\,, \qquad \boldsymbol{H}' = A\boldsymbol{H}_1\,, \qquad T' = bT_1\,, \tag{2.8}$$

where A and B are arbitrary amplitudes and $\boldsymbol{v}_1$, $\boldsymbol{H}_1$, and T_1 are correct solutions. Then, from equations (2.6) and (2.7), the initial changes in A and B are determined by

$$\frac{\partial A}{\partial t} = -I_{11}A + I_{12}B,$$
$$\frac{\partial B}{\partial t} = I_{21}A - I_{22}B, \tag{2.9}$$

where the numbers I_{ij} are

$$
\begin{aligned}
I_{11} &= \frac{[-\nu(\boldsymbol{v}_1\cdot\nabla^2\boldsymbol{v}_1)_m - (\eta\mu/4\pi\rho)(\boldsymbol{H}_1\cdot\nabla^2\boldsymbol{H}_1)_m - f_v]}{[v_1^2 + (\mu/4\pi\rho)(H_1^2)]}, \\
I_{12} &= \frac{[\gamma(W_1T_1)_m + f]_H}{[v_1^2 + (\mu/4\pi\rho)\,H_1^2)]}, \\
I_{21} &= \frac{[(W_1T_1\beta)_m + f_T]}{(T_1^2)_m}, \qquad I_{22} = \frac{[-\kappa(T_1\nabla^2T_1)_m]}{(T_1^2)_m}, \\
f_v &= \left[\left(\frac{\mu}{4\pi\rho}\boldsymbol{H}_1\cdot\boldsymbol{H}_1 - \boldsymbol{v}_1\cdot\boldsymbol{v}_1\right)\cdot\nabla\boldsymbol{v}\right]_m, \\
f_H &= \frac{\mu}{4\pi\rho}[(\boldsymbol{v}_1\cdot\boldsymbol{H}_1 - \boldsymbol{H}_1\cdot\boldsymbol{v}_1)\cdot\nabla\boldsymbol{H}]_m, \qquad f_T = -(T_1\boldsymbol{v}_1\cdot\nabla T)_m.
\end{aligned}
\tag{2.10}
$$

In order to be able to find an A and B so that both $\partial A^2/\partial t$ and $\partial B^2/\partial t$ will be positive, it is necessary that

$$I_{12}I_{21} - I_{11}I_{22} > 0 \tag{2.11}$$

when I_{22} and I_{12} are greater than zero. If this condition (2.11) is fulfilled, one is assured that $\boldsymbol{v}$, $\boldsymbol{H}$, T will be initially unstable to a disturbance of the form $\boldsymbol{v}_1$, $\boldsymbol{H}_1$, T_1.

To interpret this instability requirement, we first make use of several integral properties of the solution $\boldsymbol{v}_1$, $\boldsymbol{H}_1$, T_1. From the basic equations (1.1)–(1.5), we obtain

$$
\begin{aligned}
-\nu(\boldsymbol{v}_1\cdot\nabla^2\boldsymbol{v}_1)_m &= \gamma(W_1T_1)_m + \frac{\mu}{4\pi\rho}(\boldsymbol{v}_1\cdot\boldsymbol{H}_1\cdot\nabla\boldsymbol{H}_1)_m, \\
-\kappa(T_1\nabla^2T_1)_m &= (W_1T_1\beta_1)_m, \\
-\eta(\boldsymbol{H}_1\cdot\nabla^2\boldsymbol{H}_1)_m &= (\boldsymbol{H}_1\cdot\boldsymbol{H}_1\cdot\nabla\boldsymbol{v}_1)_m,
\end{aligned}
\tag{2.12}
$$

where one notes that the left-hand intregrals, hence also the right-hand integrals, are positive-definite. Then equation (2.11) may be written

$$[\gamma(W_1T_1)_m + f_H]\cdot[(W_1T_1\beta)_m + f_T] - [(W_1T_1\beta_1)_m]\cdot[\gamma(W_1T_1)_m - f_v] > 0\,. \tag{2.13}$$

Also f_v, f_H, and f_T may be reduced to double-product integrals for

$$
\begin{aligned}
-f_v &= \left[\boldsymbol{v}\cdot\left(\frac{\mu}{4\pi\rho}\boldsymbol{H}_1\cdot\nabla\boldsymbol{H}_1 - \boldsymbol{v}_1\cdot\nabla\boldsymbol{v}_1\right)\right]_m \\
&= \left[\boldsymbol{v}\cdot\left(\frac{\partial\boldsymbol{v}_1}{\partial t} - \nu\nabla^2\boldsymbol{v}_1 + \frac{1}{\rho}\nabla\bar{P}_1' + 2\Omega\times\boldsymbol{v}_1 + \gamma T_1\boldsymbol{k}\right)\right]_m, \\
-\frac{4\pi\rho}{\mu}f_H &= [\boldsymbol{H}\cdot(\boldsymbol{H}_1\cdot\nabla\boldsymbol{v}_1 - \boldsymbol{v}_1\cdot\nabla\boldsymbol{H}_1)]_m = \left[\boldsymbol{H}\cdot\left(\frac{\partial\boldsymbol{H}_1}{\partial t} - \eta\nabla^2\boldsymbol{H}_1\right)\right]_m, \\
-f_T &= [T(\boldsymbol{v}_1\cdot\nabla T_1)]_m = \left[T\left(\frac{\partial T_1}{\partial t} - \kappa\nabla^2T_1 - \gamma W_1\beta_1\right)\right]_m.
\end{aligned}
\tag{2.14}
$$

In order to use inequality (2.13) in the general case, it would be necessary to evaluate not only integrals involving a single solution, such as $\gamma(W_1T_1\beta_1)_m$, but also interaction integrals such as f_T. However, if the field $\boldsymbol{v}_1$, $\boldsymbol{H}_1$, T_1 is statistically independent of $\boldsymbol{v}$, $\boldsymbol{H}$, T (e.g., two different turbulent solutions), then only the interaction integral $\gamma(W_1T_1\beta)_m$ can have a non-zero value. In this special case, condition (2.13) reduces to

$$[W_1T_1(\beta-\beta_1)]_m > 0 . \tag{2.15}$$

Since $(\kappa\beta + \langle WT\rangle)$ is independent of z for each solution, inequality (2.15) may be written

$$(\beta_1^2 - \beta\beta_1)_m > 0 . \tag{2.16}$$

From formula (2.16) it is seen that $(\beta_1^2)_m > (\beta^2)_m$ is a *sufficient* condition for instability, for applying Schwarz's inequality $(\beta_1^2)_m^2 > (\beta^2)_m \cdot (\beta_1^2)_m \geq (\beta\beta_1)_m^2$.

Now we may invert our instability argument and find that a *necessary* condition for the stability of a solution is that

$$(\beta^2)_m \geqslant (\beta_i^2)_m , \tag{2.17}$$

where the index i ranges over all solutions, i.e., the stable solution has a greater mean-squared gradient than any other solution.

The set of finite-amplitude solutions we have proposed to generate are not necessarily statistically independent. However, when $\eta = 0$, $\boldsymbol{H} = c\boldsymbol{v}$ and $\boldsymbol{H}_1 = c_1\boldsymbol{v}_1$; then $f_H = 0$ and

$$f_v = \left(\frac{\mu}{4\pi\rho}\, c_1^2 - 1\right) \cdot (\boldsymbol{v}_1 \cdot \boldsymbol{v}_1 \cdot \nabla \boldsymbol{v})_m .$$

Condition (2.13) now becomes

$$[W_1T_1(\beta-\beta_1)]_m + f_T + f_v \frac{(W_1T_1\beta_1)_m}{\gamma(W_1T_1)_m} > 0 . \qquad \text{(2.18}$$

We shall find that this f_v and f_T are zero for the finite-amplitude solutions generated by the iterative method of the following section. When this is so, inequality (2.18) reduces to the simply relative stability condition (2.17).

III. GENERATION OF FINITE-AMPLITUDE SOLUTIONS

The detailed technique for the determination of finite-amplitude solutions of equations like (1.2), (1.3), and (1.9) is described in Papers I and II. An outline suited to the present purpose is given here.

Cross-differentiation of the five equations (1.2), (1.3), and (1.9) permits the construction of one non-linear equation which contains linear terms in the vertical velocity, W, only. Auxiliary non-linear equations connect W to U and V, the x- and y-components of velocity, and to T and P. The method of solution consists of expanding W and the other variables in a form

$$W = \epsilon W_0 + \epsilon^2 W_1 + \epsilon^3 W_2 + \ldots , \tag{3.1}$$

where ϵ is a constant parameter, and requiring that (3.1) satisfy the complete equations of motion for all values of ϵ less than some maximum ϵ. For the resulting set of linear inhomogeneous equations to constitute a soluble iterative sequence, it is first necessary to identify ϵ with the amplitude of W_0,

$$\epsilon \equiv (W_0W)_m , \tag{3.2}$$

and hence, from (3.1), assuring that W_0 is orthogonal to all W_i. A second requirement for solvability is that the inhomogeneous terms do not produce a secular response in the particular integrals. To see how this can be assured, we turn to the non-dimensionalized form of the W equation, in which

$$v \equiv \frac{\kappa}{d} v', \qquad T = \frac{\nu\kappa}{\gamma d^3} T', \qquad (x, y, z) \equiv d(x', y', z'), \qquad t \equiv \frac{d^2}{\kappa} t'; \tag{3.3}$$

and the primes have then been suppressed. This is

$$\begin{aligned}\left[\left(\frac{\partial}{\partial t} - \nabla^2\right)\left(\frac{1}{\sigma}\frac{\partial}{\partial t} - \nabla^2\right)^2 \nabla^2 + \tau^2 \left(\frac{\partial}{\partial t} - \nabla^2\right)\frac{\partial^2}{\partial z^2} - R\left(\frac{1}{\sigma}\frac{\partial}{\partial t} - \nabla^2\right)\nabla_1^2\right] W \\ = \left(\frac{1}{\sigma}\frac{\partial}{\partial t} - \nabla^2\right)\left[(\langle WT\rangle)_m - \langle WT\rangle\right] \nabla_1^2 W + \frac{\tau}{\sigma_c}\left(\frac{\partial}{\partial t} - \nabla^2\right)\frac{\partial Z}{\partial z} \\ - \left(\frac{1}{\sigma}\frac{\partial}{\partial t} - \nabla^2\right)\nabla_1^2 h + \frac{1}{\sigma_c}\left(\frac{1}{\sigma}\frac{\partial}{\partial t} - \nabla^2\right)\left(\frac{\partial}{\partial t} - \nabla^2\right) L,\end{aligned} \tag{3.4}$$

where the Prandtl number,

$$\sigma = \frac{\nu}{\kappa}, \qquad \sigma_c = \frac{\sigma}{[1 - (\mu/4\pi\rho)\, c^2]},$$

the Taylor number $\tau = 2\Omega d^2/\nu$, and the Rayleigh number $R = \gamma\beta_m d^4/\nu\kappa$. The right-hand side of equation (3.4) contains the non-linear terms

$$\begin{aligned} Z &= \frac{\partial}{\partial x}(v \cdot \nabla V) - \frac{\partial}{\partial y}(v \cdot \Delta U), \\ h &= v \cdot \nabla T - \frac{\partial}{\partial z}\langle WT\rangle, \\ L &= \frac{\partial}{\partial z}\left[\frac{\partial}{\partial x}(v \cdot \nabla U) + \frac{\partial}{\partial y}(v \cdot \nabla V)\right] - \nabla_1^2 (v \cdot \nabla W). \end{aligned} \tag{3.5}$$

If equation (3.4) is multiplied from the left by W and averaged over the entire system, a relation between τ, R, σ, c, and integrals of W, U, V, and T results. Using (3.1), this relation may be written

$$\begin{aligned} R = R_0(\tau, W_0, T_0) + \epsilon R_1(c, \sigma, \tau, v_0 T_0, v_1 T_1) \\ + \epsilon^2 R_2(c, \sigma, \tau, v_0 T_0, v_1 T_1, v_2 T_2) + \ldots, \end{aligned} \tag{3.6}$$

where the numbers R_i are integrals of the indicated fields. In the expansion of equation (3.4) in an ϵ sequence determined by equations (3.1) and (3.6), the $R_i (i > 0)$ can be chosen to remove those parts of the inhomogeneous terms which would cause a secular response. This choice for the R_i both assures solvability and provides an explicit relation, (3.6), between the amplitude of the motion and the physical parameters of the problem.

In the following we will restrict attention to steady convection. Then the ϵ sequence of equations from (3.4) is

$$\begin{aligned} &\left[\nabla^6 - \tau^2 \frac{\partial^2}{\partial z^2} + R_0 \nabla_1^2\right] W_0 \equiv \mathfrak{L} W_0 = 0, \\ &\mathfrak{L} W_1 = -R_1 \nabla_1^2 W_0 - \frac{\tau}{\sigma_c} \frac{\partial Z_{00}}{\partial z} + \nabla_1^2 h_{00} + \frac{1}{\sigma_c} \nabla^2 L_{00}, \\ &\mathfrak{L} W_2 = -R_1 \nabla_1^2 W_1 - R_2 \nabla_1^2 W_0 - [(W_0 T_0)_m - \langle W_0 T_0 \rangle] \nabla_1^2 W_0 \\ &\qquad - \frac{\tau}{\sigma_c} \frac{\partial}{\partial z} (Z_{01} + Z_{10}) + \nabla_1^2 (h_{01} + h_{10}) + \frac{1}{\sigma_c} \nabla^2 (L_{01} + L_{10}). \end{aligned} \tag{3.7}$$

The subscripts on the non-linear terms indicate the orders of v_i and T_i which they contain. The first of equations (3.7) is the linear stability problem solved by Chandrasekhar (1953). Here $R_0(\tau)$ is the eigen-value of the (normalized) eigenfunction W_0. The second of equations (3.7) can be solved if

$$R_1 = \frac{-\tau/\sigma_c \, [W_0 (\partial/\partial z) Z_{00}]_m + (W_0 \nabla_1^2 h_{00})_m + 1/\sigma_c \, (W_0 \nabla^2 L_{00})_m}{(W_0 \nabla_1^2 W_0)_m}, \tag{3.8}$$

for this determination of R_1 removes any contribution from the inhomogeneous terms which could cause a secular response in the particular integral. In a similar fashion,

$$\begin{aligned} R_2 (W_0 \nabla_1^2 W_0)_m = &-R_1 (W_0 \nabla_1^2 W_1)_m - \{W_0 [(W_0 T_0)_m - \langle W_0 T_0 \rangle] \nabla_1^2 W_0\}_m \\ &- \frac{\tau}{\sigma_c} \left[W_0 \frac{\partial}{\partial z} (Z_{01} + Z_{10})\right]_m + [W_0 \nabla_1^2 (h_{01} + h_{10})]_m + \frac{1}{\sigma_c} [W_0 \nabla^2 (L_{01} + L_{10})]_m . \end{aligned} \tag{3.9}$$

If R_1 does not vanish, it determines the first finite-amplitude effects after the point of instability. However, when the top and bottom boundary conditions are identical, it was found in Paper I that R_1 always vanishes (as is suggested by the symmetry). Then, from equations (3.6) and (3.9), the first finite-amplitude effects are

$$\epsilon^2 = \frac{R - R_0}{R_2}, \qquad \langle WT \rangle = \epsilon^2 (\langle W_0 T_0 \rangle) . \tag{3.10}$$

Equation (3.10) asserts that the amplitude of the motion depends upon both the initial form of the disturbance, W_0, T_0, and the first distortion of this form, W_1, T_1. However, the form of the motion depends on W_0 and T_0 only and is not a function of σ or c.

Equation (3.10) provides as many solutions for the initial finite-amplitude motion as there are solutions W_0, T_0 to the stability problem. In addition, for each of these solutions there is a singly infinite number of values of c, each affecting the amplitude ϵ^2 and corresponding to a different solution for the magnetic field. To determine which of these many solutions can be realized, we apply the relative stability criterion.

One first notes that f_V and f_T in equations (2.14) vanish when comparing the stability of two solutions with the same form W_0, T_0 but different c. Second, f_V and f_T vanish when comparing simple periodic solutions which are orthogonal. Since all different eigen-solutions of equation (3.7) are orthogonal (having different horizontal plan forms), then the appropriate relative stability criterion to establish the realized motions from equations (3.10) is equation (2.17). Indeed, equation (2.17) may be further simplified, for

$$R^2 \left[\frac{(\beta^2)_m}{\beta^2_m} - 1\right] = (\langle WT^2 \rangle)_m - (\langle WT \rangle)^2_m \equiv (\langle WT \rangle)^2_m \mathfrak{F}, \tag{3.11}$$

where the ratio $\mathfrak{F}$ depends upon the vertical form of $\langle WT \rangle$ only. Hence a maximum value of $(\beta^2)_m$ is achieved at maximum heat transport, $(\langle WT \rangle)_m$, for motions with the same $\mathfrak{F}$. Therefore, the preferred value of c associated with any W_0 and T_0 will be that c which make ϵ^2 a maximum or, from (3.10), that c which makes R_2 a minimum.

Fortunately, c enters equations (3.7) only in connection with the Prandtl number σ, producing the "effective" Prandtl number, σ_c. Hence the solutions of equations (3.7) and the value of R_2 may be taken from Papers I and II with σ_c substituted for σ.

In the absence of rotation, the preferred convective motion for the boundary conditions (1.6) was found in Paper I to have a square horizontal plan form for all $\sigma_c > 1$ (or $\sigma_c < -\frac{5}{8}$). The eigen-solution for this problem is

$$W_0 = 2\sqrt{2} \cos \pi \frac{a}{\sqrt{2}} x \cos \pi \frac{a}{\sqrt{2}} y \sin \pi z \qquad (3.12$$

and

$$R_0 = \frac{\pi^4 (1+a^2)^3}{a^2} .$$

The solution to the second of equations (3.7) from (3.1) to (3.6) of Paper I is

$$W_1 = C_a (\cos \sqrt{2} \pi a x + \cos \sqrt{2} \pi a y) \sin 2\pi z , \qquad (3.13$$

where

$$C_a = \frac{-\pi^3 (1+a^2)^2 [1 + 4\sigma_c^{-1} (1 + a^2/2) / (1+a^2)]}{32\pi^4 (1 + a^2/2)^3 - a^2 R_0} .$$

From these solutions and the auxiliary equations for T, U, and V one constructs R_2 (eq. [3.11] of Paper I), which is

$$R_2 = \frac{N_0}{2} \left[1 + \frac{8X^2}{(1+a^2)(32X^3 - 1)} \left(1 + \frac{1}{4X^2 \sigma_c} + \frac{1}{2X\sigma_c^2} \right) \right] , \qquad (3.14)$$

where

$$X \equiv \frac{1 + a^2/2}{1+a^2} \quad \text{and} \quad N_0 \equiv \frac{\pi_2 (1+a^2)^2}{a^2} .$$

When the fluid is rotating, the initial convective instability can occur both as a steady motion or as a time-dependent "overstable" motion. However, Chandrasekhar (1953) established that the "overstable" motion cannot occur if the Prandtl number is greater than $\sqrt{\frac{2}{3}}$. At first, we shall restrict our attention to $\sigma > \sqrt{\frac{2}{3}}$, in order to assure steady motions. It will be found that this restriction may be removed in the finite-amplitude motions when R_2 is dominated by the optimum σ_c.

The "square" cellular convection in a rotating system has the same W_0 as the non-rotating case, i.e., equation (3.12). However, the rotation imposes severe constraints on the horizontal motions, and these are (Paper II, eq. [3.12])

$$U_0 = -\left[\frac{2\tau}{a(1+a^2)} \cos \pi \frac{a}{\sqrt{2}} x \sin \pi \frac{a}{\sqrt{2}} + \frac{2}{a} \sin \pi \frac{a}{\sqrt{2}} x \cos \pi \frac{a}{\sqrt{2}} y \right] \cos \pi z ,$$

$$(3.15$$

$$V_0 = \left[-\frac{2}{a} \cos \pi \frac{a}{\sqrt{2}} x \sin \pi \frac{a}{2} y + \frac{2\tau}{a(1+a^2)} \sin \pi \frac{a}{\sqrt{2}} x \cos \pi \frac{a}{\sqrt{2}} y \right] \cos \pi z .$$

A perspective sketch of the motion of a fluid particle in the rotating system is reproduced from Paper II in Figure 1. This is the extreme path in the "square" cell for a counter-clockwise Ω. Besides illuminating solution (3.15), Figure 1 will assist interpretation of results found later in this text.

The constraint imposed by rotation causes the lowest critical Rayleigh number for marginal stability to be larger than in the non-rotating case. From the work of Chandrasekhar (1953) this eigen-value is

$$R_0 = \frac{\pi^4 (1+\alpha^2)^3 + \tau^2}{\alpha^2}, \tag{3.16}$$

and from equation (3.25) of Paper II,

$$R_2 = \frac{N_0}{2}(1+\tau_0^2)\left(A + \frac{B}{\sigma_c} + \frac{C}{\sigma_c^2}\right), \tag{3.17}$$

where

$$A = 1 + \frac{16X^3 + \tau_0^2}{2X(1+\alpha^2)(32X^3 - 1 + \tau_0^2)}$$

$$B = \frac{2X - \tau_0^2}{X(1+\alpha^2)(32X^3 - 1 + \tau_0^2)},$$

$$C = \frac{3}{2}\,\frac{1}{\alpha^2}\,\frac{\tau_0^2}{1+\tau_0^2} + \frac{4X\,[1 - \tau_0^2(1 + 1/X)]}{(1+\alpha^2)(32X^3 - 1 + \tau_0^2)},$$

$$\tau_0^2 \equiv \frac{\tau^2}{\pi^4(1+\alpha^2)^3} \text{ with } X \text{ and } N_0 \text{ as in equations (3.14)}.$$

Equations (3.14) and the more general (3.17) provide the functional dependence of amplitude on c. Minimization of these expressions with respect to the "effective" Prandtl number, σ_c, will determine the most stable magnetic fields associated with these

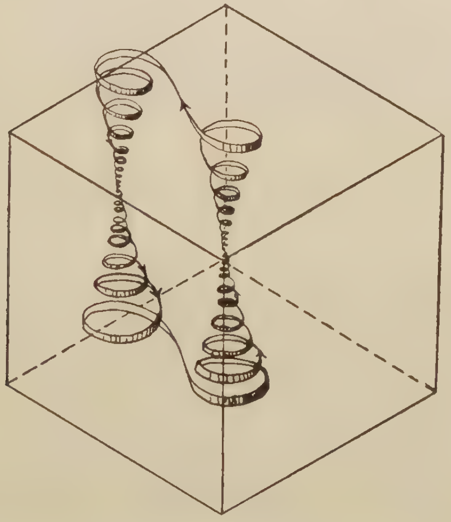

FIG. 1.—The extreme particle trajectory in "square" cellular convection constrained by rotation about the vertical axis.

convective motions. This minimization and its interpretation are undertaken in the following section.

IV. THE OPTIMUM MAGNETIC FIELDS

The initial cellular motion occurs for values of R in excess of the minimum value for R_0. In the non-rotating case, this minimum $R_0 = \frac{27}{4}\pi^4$ when the horizontal wave number $\alpha^2 = \frac{1}{2}$, from equations (3.12). For this α^2 the value of σ_c which minimizes R_2 of equations (3.14) is

$$\sigma_c = \frac{\sigma}{[1 - (\mu/4\pi\rho)\, c^2]} = -4X = -\tfrac{10}{3} \tag{4.1}$$

or

$$\frac{\mu}{4\pi\rho}\, c^2 = 1 + \tfrac{3}{10}\,\sigma\,.$$

The stable magnetic field then has an energy density

$$\frac{\mu H^2}{8\pi} = (1 + \tfrac{3}{10}\,\sigma)\,\frac{\rho}{2}\, v^2 \tag{4.2}$$

from equation (1.9). For $\sigma > 0$ the advection of momentum by this magnetic field more than cancels the normal advection by the velocity. For $\sigma \sim 0$ equation (4.2) leads to an equipartition of magnetic and kinetic energy as the preferred state. However, this is not a statistical equipartition but a detailed local equipartition resulting from the detailed balance of the two advections of momentum.

Chandrasekhar (1956*a*) has established that this equipartition solution, $\boldsymbol{v} = \pm \boldsymbol{H}(\mu/4\pi\rho)^{1/2}$, is stable in an incompressible inviscid fluid of infinite electrical conductivity. Here we find that the inclusion of both viscous and thermal conductive effects alters this conclusion only when σ is large.

The determination of the optimum magnetic field in the rotating fluid is considerably more involved than in the non-rotating case. From equations (3.16) the lowest R_0 occurs when

$$3\,(1+\alpha^2)^2 = \frac{(1+\alpha^2)^3 + \tau^2/\pi^4}{\alpha^2} = \frac{R_0}{\pi^4}\,. \tag{4.3}$$

This is a cubic in $\alpha^2 = \alpha^2(\tau^2)$. Rather than solve this cubic, we shall express R_2 of equations (3.17) in terms of α^2, treating it as the independent variable rather than τ^2. The correct α^2 and R_0 for any τ^2 can then be found from equation (4.3). Hence, from equations (3.17) and (4.3), we obtain

$$R_2 = \tfrac{3}{2}\,\pi^2\,(1+\alpha^2)\left(A + \frac{B}{\sigma_c} + \frac{C}{\sigma_c^2}\right),$$

where

$$\begin{aligned} A &= \frac{1 + [16X^3 - 1 + 3\alpha^2/(1+\alpha^2)]}{2X\,(1+\alpha^2)\,[32X^3 + 3\alpha^2/(1+\alpha^2) - 2]}\,, \\ B &= \frac{2X + 1 - 3\alpha^2/(1+\alpha^2)}{X\,(1+\alpha^2)\,[32X^3 + 3\alpha^2/(1+\alpha^2) - 2]}\,, \end{aligned} \tag{4.4}$$

and

$$C = \left\{\frac{3}{2}\,\frac{1}{\alpha^2}\left(1 - \frac{1+\alpha^2}{3\alpha^2}\right) + \frac{4X\{1 + [1 - 3\alpha^2/(1+\alpha^2)][1 + (1/X)]\}}{1 + \alpha^2\,[32X^3 + 3\alpha^2/(1+\alpha^2) - 2]}\right\}.$$

The "independent" variable α^2 ranges from $\alpha^2 = \frac{1}{2}$ for $\tau^2 = 0$ to $\alpha^2 = +\infty$ for $\tau^2 = \infty$ from equation (4.3).

The value of σ_c which minimizes R_2 of equations (4.4) is

$$\sigma_c = \frac{-2C}{B} \text{ if } C > 0, \text{ and } \sigma_c = 0 \text{ for } C < 0\,. \tag{4.5}$$

Inspection of equations (4.4) establishes that C becomes negative for an α^2 between 5 and 6 ($C = 0$ at $\alpha^2 = 5.22$ from a graph of the function). In addition, B changes sign at $\alpha^2 = 3$. Hence conditions (4.5) must be interpreted cautiously. Then, where $C > 0$,

$$\frac{\mu}{4\pi\rho}\, c^2 = 1 + \sigma\frac{B}{2C}; \tag{4.6}$$

but, since c^2 cannot be negative, $c^2 = 0$ in that range of α^2 bounded at a lower α^2 determined from $-B/2C = 1/\sigma$ and an upper α^2 determined from $C = 0$. For an $\alpha^2 > 5.22$,

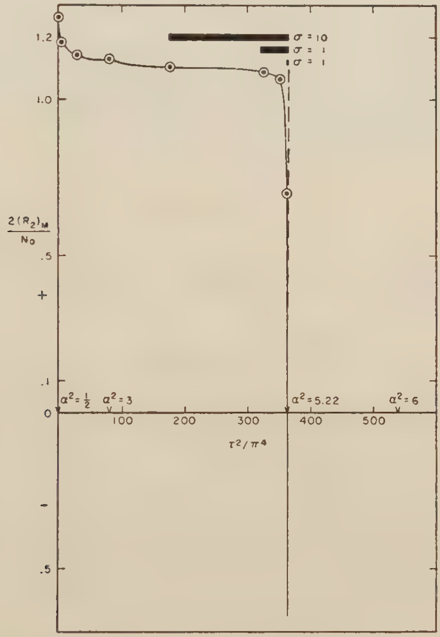

FIG. 2.—The optimum R_2 as a function τ^2/π^4

the minimum $R_2 = -\infty$ corresponding to $c^2 = +\infty$. Figure 2 is a graph of the minimum R_2 versus τ^2/π^4. The range of α^2 in which the preferred magnetic field is zero is indicated on the graph by heavy bars labeled with the appropraite values of σ.

The most suggestive result of these computations for rotating convection is that, for $\tau^2/\pi^4 > 365$, R_2 is negative, and the magnetic energy is infinitely larger than the kinetic energy. In the non-magnetic study, Paper II, a similar negative R_2 could arise with special choices for σ, τ, and plan form. The interpretation there is also applicable here. It was shown that when R_2 becomes negative, a finite amplitude disturbance could occur at a lower Rayleigh number than the critical Rayleigh number for an infinitesimal disturbance. How much lower this finite disturbance would first appear depends upon the next higher approximation (R_4) in the iterative sequence. The process which permits a negative R_2 is the reduction of the initial constraint of rotation by the advection of momentum. That is, the fluid evolves a finite-amplitude field of motion in which the release of potential energy increases more than the dissipation. In this magnetic convection the preferred magnetic field optimizes this effect. Of course, the magnetic field could, at best, completely remove the constraint of rotation; hence it will not be infinite. Without venturing into the complexity of the next higher (R_4) approximation, we can estimate the limiting value of the magnetic field which would cancel most of the rotational constraint, permitting less "inhibited" thermal convection.

From equations (1.1) and (1.7) we seek a rough balance of the rotation and magnetic terms so that

$$-2\Omega\times \boldsymbol{v}+\frac{\mu c^2}{4\pi\rho}(\nabla\times \boldsymbol{v})\times \boldsymbol{v}\simeq 0\,. \tag{4.7}$$

Of course, such a balance is possible only if ($\nabla \times \boldsymbol{v}$) has the vector direction of Ω. Figure 1 provides assurance that ($\nabla \times \boldsymbol{v}$) is almost entirely in the vertical for large τ^2 in the initial convective motion, but, unfortunately, ($\nabla \times \boldsymbol{v}$) has one sign over half the fluid and the opposite sign over the other half. It is here that we can first visualize the role of the finite-amplitude distortions of the initial convection. They produce asymmetries in the rising and descending spirals which permit the major vertical convection of heat to occur in those spirals where Ω and ($\nabla \times \boldsymbol{v}$) have the same sign. In these important parts of the motion, the balance,[1]

$$\frac{\mu c^2}{4\pi\rho}\nabla\times \boldsymbol{v}\simeq 2\Omega\,, \tag{4.8}$$

will provide an estimate of the optimum magnetic field in terms of $\boldsymbol{v}$.

From equation (1.7) this is

$$\frac{\mu H^2}{8\pi}\sim\left(\tfrac{1}{2}\rho\,|\,\boldsymbol{v}\,|\,\Omega d\right), \tag{4.9}$$

where d is a characteristic dimension of the motion. Of course, it is not suggested that the discussion leading to conditions (4.8) and (4.9) is an adequate substitute for further analysis by the formal iterative method.

In summary of this section, it has been found that the preferred magnetic field in initial non-rotating convection has an energy density comparable to the kinetic energy density. In contrast, the initial convection in a rotating system can be a finite-amplitude instability in which the magnetic energy density is vastly greater than the kinetic energy density.

V. SPECULATIONS CONCERNING ASTROPHYSICAL CONVECTION

The generalization of the preceding work appears to be that magnetic fields are the preferred (stable) companions of convection in conducting fluids because they are able to reduce the external and internal constraints on such motion.

In non-rotating systems the constraint removed by the magnetic field is the advection of momentum. This prevents shearing instability, for momentum advection is the direct energy source for such instability. In other words, the optimum magnetic field can prevent the evolution of an "eddy" viscosity which would decelerate the flow. It is an interesting consequence of a disappearance of the net momentum advection that the usual picture of a Kolmogoroff decay spectrum would be drastically altered. Only the heat advection, $\boldsymbol{v}\cdot\nabla T$, would remain to produce non-linear interaction between the various scale of motion.

[1] Bullard (1954) has noted that the estimated magnitude of motions and magnetic fields in the earth's interior require a balance like condition (4.8). Here we have suggested why such a balance should occur.

In rotating systems the constraint imposed by the rotation can be reduced by the great increase in momentum advection due to the preferred magnetic field. Here the mechanism permitted to the fluid is the production of an opposing vorticity about the lines of rotation. Energy-releasing motions relative to this finite-amplitude vortex "see" less of the restricting external rotation. The arguments at the end of the preceding section suggest that a system is effectively "a rotating system" when $\Omega d > v$, where Ωd is the characteristic imposed rotation velocity and v is the internal convection velocity.

Since most geophysical and astrophysical motions have their origin in buoyancy forces and since most of these are convections in electrically conductive fluids, it seems desirable to explore the applicability of the preceding remarks to the real world. However, an apparently basic difference between natural flows and the steady-state motions studied here is that the former are time-dependent "turbulent" motions. To make any comparison between the steady state and turbulent regimes, we must estimate the contribution of the time-dependent terms in the basic equations.

To do this it is of value to make use of the important discovery made long ago in the study of large-scale meteorological and oceanographic motions. This discovery was that the instantaneous large-scale flow in rotating systems was very nearly at right angles to the large-scale pressure gradient in all but the most unusual circumstances. From equation (1.1) one can see that this is possible only if the viscous term, the non-linear term, and the time term contribute negligibly to the dynamics. Meteorological computations based on the assumption that these terms are unimportant in the description of the gross dynamics are called "geostrophic" approximations. Further, it is found that meteorological flows which depart from ideal geostrophic motion can be rationalized by including only the non-linear term, either as a "cyclostrophic" term, v^2/γ, or, as a "Reynolds stress" parameterizing the small-scale momentum advection.

No attempt will be made here to determine why the balance of forces in geophysical flows appears so independent of the local time rate of change of the velocity. Rather, an analogous assumption is made concerning the role of the time term in the magnetic equations. It is proposed that equation (1.6) be termed the "magnetostrophic" approximation, and it is plausible that if the "geostrophic" approximation works well in geophysical flows, then the "magnetostrophic" approximation will work even better in astrophysical flows, for the latter approximation does not neglect the non-linear terms.

Then, if astrophysical flows are "magnetostrophic" or "quasi-magnetostrophic," we have a basis for applying the findings of the paper to natural fluid systems. In certain astrophysical convections the results of work on non-magnetic turbulent convection (Malkus 1954) might provide one with the values of the velocities needed to determine the accompanying optimum magnetic fields. However, that will not be attempted here. What we will do is to accept the observed velocities as given, estimate the corresponding optimum magnetic fields from equations (4.2) and (4.9), and compare these results with the observed or estimated fields.

Characteristic velocities for convection in the solar photosphere are reported by Allen (1949) as approximately 2.5 km/sec. This velocity is much greater than the characteristic dimensions of the motions times the angular velocity of the sun. Hence the optimum magnetic field is determined from equation (4.2). In addition, the effective Prandtl number is much less than unity in most astrophysical situations, for the heat flux is dominated by radiation. Therefore, local equipartition of magnetic and kinetic energy will be the optimum state in the photosphere. For a density at the top of the photosphere of 10^{-7} gm/cc, the equipartition magnetic field would be 280 gauss. By chance, equipartition of magnetic and kinetic energies at a density of 10^{-7} gm/cc is such that the "Zeeman broadening" of the spectral lines used to determine the velocity would be comparable to the Doppler broadening (Zeeman broadening would dominate at greater densities). Because of this, it may be that Allen's velocities and therefore the magnetic field found here are too large by a factor of $\sqrt{2}$. Evidence for fields of 10^2–10^3 gauss is found in eruptions from the photospheric layer. There is as yet, however, no observational proof of equipartition in solar convection.

Characteristic velocities in nearby interstellar matter are estimated as 10–100 km/sec. The estimated densities are 10^{-24} gm/cc. From equation (4.2) the optimum magnetic fields would range from 3×10^{-6} to 3×10^{-5} gauss. The existence of fields of these strengths is suggested by the polarization of light from distant stars.

Characteristic velocities in the core of the earth measured from the westward drift of surface anomalies in the magnetic field are reported by Bullard as approximately 0.04 cm/sec. As this is very small compared to the rotational velocity in the core, the optimum magnetic field must be determined from equation (4.9). For a density of approximately 10 gm/cc and a characteristic dimension of the motions in the core as its radius, 3.5×10^3 km, equation (4.9) leads to a magnetic field of 350 gauss. (This is a magnetic energy density 10^6 greater than the kinetic energy density.) This large field cannot be directly observed. However, the core has a finite electrical conductivity; Powell (1953) estimates that $\eta \leq 10^5$ cm²/sec; and one can expect that complete "magnetostrophy" would not be achieved.[2] A measure of the quasi-steady non-magnetostrophic component of the magnetic field is easily obtained from the basic magnetic equation (1.4). If one writes equation (1.4) as

$$\eta \nabla^2 (\boldsymbol{H} + \boldsymbol{H}_d) = \nabla \times \boldsymbol{v} \times (\boldsymbol{H} + \boldsymbol{H}_d) , \tag{5.1}$$

where $\boldsymbol{H} = c\boldsymbol{v}$ and $\boldsymbol{H}_d$ is a small non-magnetostrophic component at right angles to $\boldsymbol{H}$, then

$$-\eta c \nabla^2 \boldsymbol{v} = \eta c \nabla \times \nabla \times \boldsymbol{v} \simeq \nabla \times \boldsymbol{v} \times \boldsymbol{H}_d . \tag{5.2}$$

Hence, from equations (4.2) and (4.8), we obtain

$$| \boldsymbol{H}_d | \simeq \frac{8\pi \rho \eta \Omega}{\mu | \boldsymbol{H} |} \leqslant 5 \text{ gauss}, \tag{5.3}$$

using $\eta \leq 10^5$ cm²/sec and the previous estimate $\boldsymbol{H} = 350$ gauss. If the motions in the core spiral along the lines of rotation as does the convective motion in Figure 1, then $\boldsymbol{H}_d$ is an estimate of the external dipole strength at the surface of the core. The corresponding dipole strength at the surface of the earth is close to the observed value, so close that one must expect a fortuitous element in the reasoning.

VI. CONCLUDING REMARKS

The numerical results of this last section are neither particularly new nor should they be called "theoretical predictions." Rather, they have been presented to suggest that the role played by the optimum magnetic fields in the formal steady-state problem may be the role played by the magnetic fields in astrophysical and geophysical convection. If this is so, it would justify a more complete exploration of the stable magnetic fields in Rayleigh-like convection. In particular, the higher-order terms in the iterative analysis determining the finite-amplitude motions would deserve attention.

---

[2] Indeed the energy dissipation of the fluid motions in the core must be almost entirely due to electrical heating. Therefore, the observed convective velocities will be principally determined by η and not by the Rayleigh number. Independent of the dissipative mechanism, however, a change in the magnetic field from its optimum value will increase the constraints on the convection and reduce the rate of release of potential energy. It should be recalled that this optimum magnetic field can be approached only if the magnetic Reynolds number is much greater than its critical value for instability. If the η of the core were several orders of magnitude larger, this would not be the case (and the earth would have no magnetic field).

The author wishes to thank Dr. George Veronis for his many valuable comments on the magnetoconvection problem. This work was performed under the auspices of the Office of Naval Research and is Contribution No. (1021) from the Woods Hole Oceanographic Institution.

REFERENCES

Allen, C. W. 1949, *M.N.*, **109**, 343.
Backus, G. E., and Chandrasekhar, S. 1956, *Proc. N.A.S.*, **42**, No. 3, 105.
Boussinesq, J. 1903, *Théorie analytique de chaleur*, **2**, 172 (Paris: Gauthier-Villars).
Bullard, E., and Gellman, H. 1954. *Phil. Trans. R. Soc. London*, **247**, 213.
Chandrasekhar, S. 1953, *Proc. R. Soc. London, A*, **217**, 306.
———. 1956*a*. *Proc. N.A.S.*, **42**, 273.
———. 1956*b*, *Proc. R. Soc. London, A*, **237**, 476.
Herzenberg, A. 1958, *Phil. Trans. R. Soc. London*, **250**, 543.
Malkus, W. V. R. 1954, *Proc. R. Soc. London, A*, **225**, 196.
Malkus, W. V. R., and Veronis, G. 1958, *J. Fluid Mech.*, **4**, 225.
Powell, R. W. 1953, *Phil. Mag.*, **44**, 772.
Veronis, G. 1959, *J. Fluid Mech.*, **5**, 401.

Contribution No. 1022

Reprinted from The Journal of the Acoustical Society of America, Vol. 31, No. 7, 1038–1039, July, 1959
Copyright, 1959 by the Acoustical Society of America.
Printed in U. S. A.

Transistorized Velocimeter for Measuring the Speed of Sound in the Sea*

E. Tschiegg, *National Bureau of Standards, Washington 25, D. C.*
and
Earl E. Hays, *Woods Hole Oceanographic Institution*
Woods Hole, Massachusetts
(Received April 8, 1959)

IRECT measurements on the speed of sound in the sea, for depths ranging from the surface to about 1000 fathoms, been made recently by the Woods Hole Oceanographic Institution. The instrument used to make these measurements was designed and built by the National Bureau of Standards. It is transistorized version of the "sing around" velocimeter described in a recent paper.[1] Briefly, the velocimeter is essentially an ultrasonic delay line which synchronizes a relaxation oscillator. The repetition frequency is controlled by the transit time in the water for a pulse traveling between two transducers. The transit time in turn depends on the speed of sound. High stability and sensitivity are feasible in the system permitting absolute measurement of speed to be made with an uncertainty of less than 1 ft/sec. Readings taken in the field are reproducible to within about 0.5 ft/sec, which includes battery aging and temperature effects on the circuit elements. The circuit and battery compartment are housed inside a stainless steel case about 3 in. in diam and 14 in. long. Figure 1 shows the sound path in detail. The case and transducer mounts are pressure-tested for leaks and mechanical failure up to 16 000 lb/sq in., corresponding to a maximum depth of about 6000 fathoms. The circuit diagram and function of each stage are shown in Fig. 2.

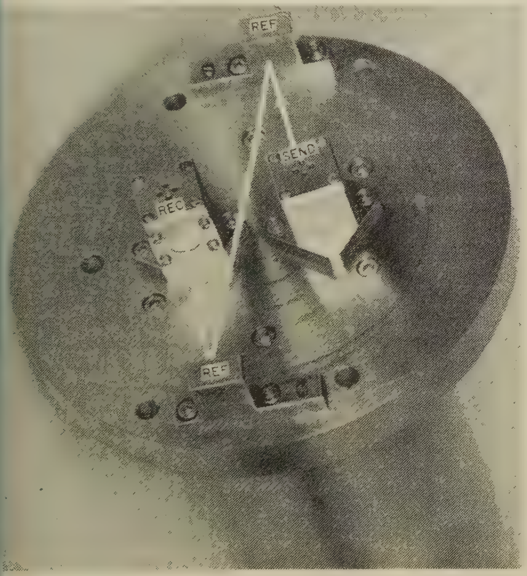
REF
SEND
REC
REF
Fig. 1. Sound path with protective plate removed. Effective path length is about 21 cm.

Approximately 20 lowerings were made in the Mediterranean, North Atlantic, and the Tongue of the Ocean before the instrument was lost at sea. The accompanying graph shows the sound velocity as measured by the instrument in one of the Tongue of the Ocean lowerings. Points are plotted for raising and lowering to demonstrate the lack of hysteresis. A sound source attached to the velocimeter emitted pulses that were detected on the ship; the depth of the instrument was determined from the time difference between a directly received pulse; and the pulse returned via bottom reflection. The depth of the water was determined by echo sounding.

The data were collected on a recording counter which printed out every 2 sec the frequency measured during a period of 1 sec. The depth information was recorded on a Woods Hole Precision Graphic Recorder, with time correlation between the two instruments.

Lowering at a rate of a fathom per second was quite feasible but of course this speed tends to eliminate detail in the velocity structure.

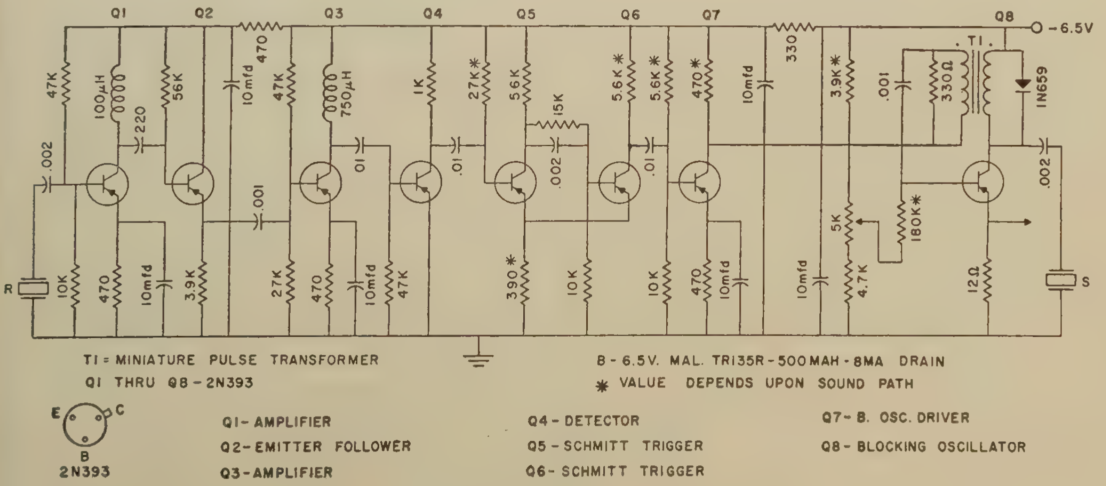
Q1
Q2
Q3
Q4
Q5
Q6
Q7
Q8
-6.5V
47K
100μH
220
56K
10mfd
470
47K
750μH
.01
1K
27K*
.01
56K
15K
.002
5.6K*
5.6K*
.01
470*
10mfd
330
3.9K*
.001
330Ω
T1
1N659
.002
.002
.001
R
10K
470
10mfd
3.9K
27K
470
10mfd
47K
390*
10K
10K
470
10mfd
10mfd
5K
4.7K
180K*
12Ω
S
T1 = MINIATURE PULSE TRANSFORMER
Q1 THRU Q8 - 2N393
B - 6.5V. MAL. TR135R - 500 MAH - 8MA DRAIN
* VALUE DEPENDS UPON SOUND PATH
E
C
B
2N393
Q1 - AMPLIFIER
Q2 - EMITTER FOLLOWER
Q3 - AMPLIFIER
Q4 - DETECTOR
Q5 - SCHMITT TRIGGER
Q6 - SCHMITT TRIGGER
Q7 - B. OSC. DRIVER
Q8 - BLOCKING OSCILLATOR
Fig. 2. Velocimeter circuit diagram.

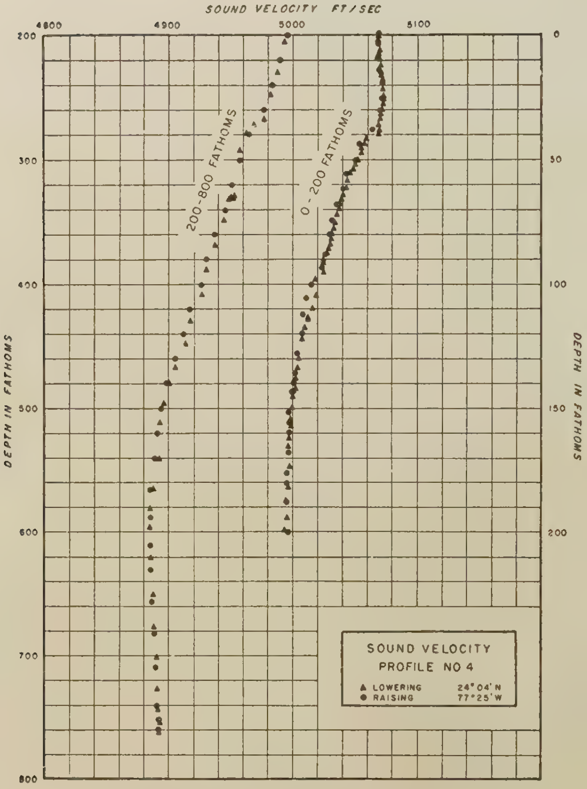

FIG. 3. Speed of sound *vs* depth as measured near the Bahama Islands. October 1958.

Calibration tests after a three month cruise showed velocity measurements made with the instrument to be still correct within 1 part in 10 000. The only maintenance required was flushing of the transducers with fresh water after immersion and an occasional battery change.

---

* Contribution No. 1022 from the Woods Hole Oceanographic Institution. This work supported by the Office of Naval Research under Contract No. Na-onr-23-58.

[1] M. Greenspan and C. E. Tschiegg, Rev. Sci. Instr. 28, 897 (1957).

Contribution No. 1024

PALYNOLOGICAL STUDIES OF THE BARNSTABLE MARSH, CAPE COD, MASSACHUSETTS

At the annual meeting of the Ecological Society of America in Boston in December, 1953, Patrick Butler presented a paper under the above title. Owing to his accidental and untimely death in Alaska during the following summer Butler's study of the Barnstable Marsh was not completed, though he had already amassed a large body of data on the palynological and sedimentary history of this area of eastern Massachusetts. Fortunately he had prepared an abstract of the results obtained from analysis of the pollen and spores in one of the

Reprinted from *Ecology*, Vol. 40, No. 4, October, 1959

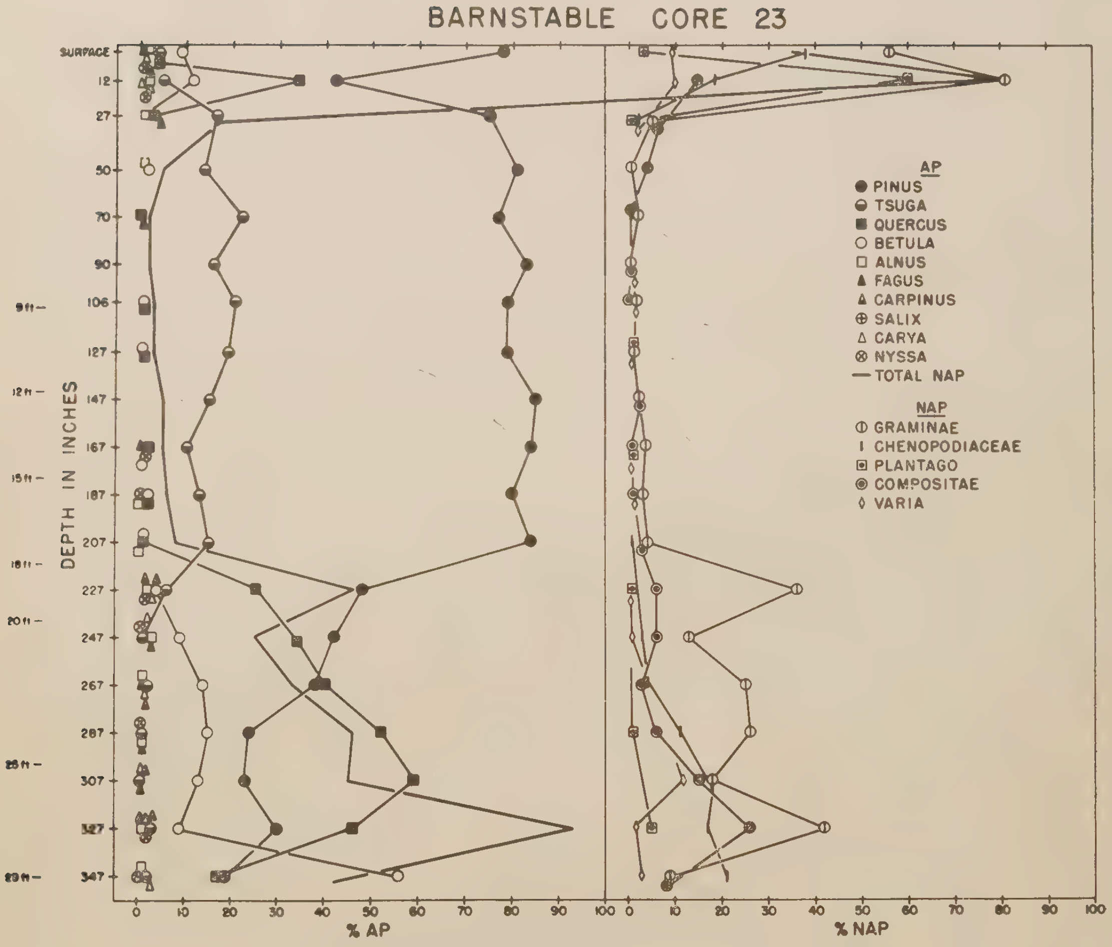

Fig. 1. Pollen diagrams from the Barnstable Marsh.

most significant and complete of his many cores. Discusion of his detailed study of this core (Barnstable core #23) comprised the substance of Butler's paper at the Boston meeting and the basis for his paleoecological interpretations of the vegetational history of the Barnstable Marsh. Subsequently A. C. Redfield relocated the site of this core, which was the deepest found in his transects of the marsh and extended approximately 347 in. from the surface, and secured samples of peat from four critical horizons. The samples were processed and the C^{14} activity measured by Meyer Rubin of the U. S. Geological Survey. Since the age determinations add significantly to the limited precise information available on the climate, vegetational change and rate of sea level changes during the past 5,000 years on the Massachusetts coast, Butler's abstract, pollen diagram, and the chronological data are presented herewith.

Abstract

(January 19, 1954)—The Woods Hole Oceanographic Institute has for the past two summers supported the field work of a study of the Great Marshes in Barnstable on Cape Cod. The purpose of the study is to find any changes in climate and sea level during the recent past in southeastern New England. It is hoped that this study will elucidate the age and developmental history of the marsh.

Last summer ten complete peat cores were taken at selected points across the widest part of the marsh. The pollen analysis of the deepest of these has been completed. The peat at this point is 29 feet deep.

The results (Figure 1) indicate that the marsh began to be formed at the end of the postglacial warm, moist period, which is usually said to have ended about 5,000 years ago. The warm, dry period which followed is reflected in the increase of oak, hickory and birch pollen. These genera dominate the pollen content of the peat from near the bottom of the core to about nineteen feet from the surface. Here, the pollen of these genera gradually give way to pine and hemlock. This indicates a return to cooler, more moist conditions which have lasted nearly to the present. A local increase in grass pollen and ash, hickory and birch near the top probably reflects the influence of white man on the vegetation over the past three hundred years.

Since the grasses forming the peat can grow only at rather restricted levels below mean high water, the implication is that there has been a gradual rise in sea level at least over the last 5,000 years. If the sea level has risen 29 feet in five thousand years, the average rate of rise along this part of the North Atlantic coast has therefore been about 6 or 7 in. per century.

Chronological Data and Conclusions

The site of Butler's core #23 was located at a point approximately 900 feet bearing 56° 50′ true from the intersection of U. S. Route 6 and the railroad, a short distance east of the West Barnstable Railroad Station. Table I gives the pertinent data on 4 samples of peat secured at this point. The peat samples were 2 in. in diameter and 6 in. in length and were taken from the indicated mean depth below the surface of the marsh, which in this area is a few in. above mean high water. The plant cover in the vicinity is dominated by *Spartina patens* (Ait.) Muhl.

TABLE I. Age and physical characteristics of Barnstable Marsh peat within increasing depth

Mean depth	C^{14} Age	USGS Lab. No.	Loss on drying	Loss on ingition	Ash	Character of peat
inches	yrs. BP		%	%	%	
21......	400± 100	W-677	72.6	6.3	21.2	fibrous
33......	770± 100	W-675	78.5	7.7	13.7	soft fibrous
207......	1880± 100	W-678	85.8	4.0	10.2	very soft fibrous
327......	5480± 120	W-676	54.1	4.7	41.2	firm fibrous

Although Butler's abstract presents only a bare minimum of his interpretation of the pollen profile, he added much detail to this in his oral presentation at the Boston meeting. Regrettably none of this exists in written form. Attention should be drawn, however, to several features of the pollen diagram which are of special interest, particularly in view of the currently established C^{14} dates.

The sample from 327 in., dated 5480 ± 100 yrs B.P. (Before Present), confirms Butler's estimate of the age of the lower portion of the core. His interpretation that this material, marked by a parallelism in the rise and fall in the percentage of oak and non-arboreal pollen, was produced at the end of the postglacial warm period is in close agreement with that of Johnson et al. (1942, 1949) made from studies of the Boylston Street Fish Weir in which evidence that the climate 5,000 years ago was somewhat warmer than at present, was drawn from a wide range of evidence.

The sample from 207 in., dated 1880 ± 100 yrs B.P., coincides with the horizon at which pine and hemlock became dominant, which Butler considered to indicate a return to cooler, moister conditions than at present. Because of the very soft character of the peat at this horizon coring was difficult and contamination of the sample by younger material may have caused the age to be undervalued.

The striking changes between 27 and 12 in. shown by the vast increase in non-arboreal pollen associated with increase in oak and decrease in pine seem assuredly to be assignable to European colonial influence in deforesting the New England coastal region, as Butler intimated. His inference is nicely supported by the radio-carbon date of 400 ± 100 years at the 21 ± 3 in. level. It should also be noted that the decline of non-arboreal pollen, increase in pine and decrease in oak between the 12 in. level and the surface conform consistently with phenomena which were induced by cultural changes in eastern New England during the middle and later 19th century, viz.: the abandonment of farms and the return of forest conditions over formerly cleared and cultivated areas. With exception of certain major urban centers this trend continues to the present.

The deepest highly organic sample, taken from 327 in. (approx. 27 feet), was immediately underlain by a deposit of compact pale blue-gray clay-like material exhibiting a loss on ignition of 2%. The thickness of this deposit is unknown. In gross physical character it is similar to the subsoil of nearby uplands. The sample at 327 in. appears to represent the earliest accumulation of a true peat at this position in the basin of the encroaching marsh and cannot have undergone appreciable vertical displacement as a result of compaction of the underlying sediments. In view of the fact that the entire peat column, from the present surface to the 327 in. level is comprised of salt marsh peat it is evident that a slowly progressing marine influence has been responsible for the aggradation of the entire body of the marsh peat. The age of the peat at the lowest level (approx. 5,500 years), therefore, indicates aggradation of a mean rate of 6 in. per century. This mean value almost precisely confirms Butler's estimate based largely on palynological considerations.

In connection with the complex problem of geologically recent sea level change on the New England coast this study of the Barnstable Marsh provides a very interesting and significant corollary to the postglacial sequence exposed in deep excavations in the city of Boston (Johnson et al., 1949). In the sedimentary complex exposed in the Back Bay area of Boston there is an estuarine sequence superimposed on a thin peaty horizon. The peat shows transition from fresh water forest swamps to salt marsh. The whole complex lies on the subaerially eroded surface of a late-glacial marine (?) clay. The stratigraphic sequence deduced from the paleobotanical evidence shows that the swamp forest was drowned by rising water, followed by development of a reed swamp (*Phragmites*) which in turn was suddenly terminated by a marine invasion followed by transitory thin salt marsh deposits (*Spartina*). The fresh water peat is at a depth of 25 ± 1 feet below the present mean tidal level (29 ± 1 feet below mean high water, and thus corresponding closely to the deepest Barnstable Core). The age of this peat, at the level immediately below the marine invasion, is 5,700 ± 750 years, indicating a mean rate of rise of sea level of a slightly less than 6 in. per century. This value is remarkably consistent with the evidence from the Barnstable Marsh, which lies about 60 miles to the southeast of the Boston basin. These values fall in line with radiocarbon measurements on peat and shell material from the coasts of Holland, Texas and Louisiana recently reviewed by Shepard and Suess (1956).

It should be emphasized that neither from the Barnstable Marsh studies nor from the Boylston Street Fish Weir data is it possible to distinguish whether submergence has resulted from crustal down warping or from eustatic rise of sea level.

REFERENCES

Johnson, F. et al. 1942. The Boylston Street Fish Weir. Papers of the Robert S. Peabody Foundation for Archaeology. Vol. 2.

Johnson, F. et al. 1949. The Boyston Street Fish Weir II. Papers of the Robert S. Peabody Foundation for Archaeology. Vol. 4, No. 1, p. 60.

Shepard, F. P. and Suess, H. E. 1956. Rate of post glacial rise of sea level. Science 123: 1082-1083.

PATRICK BUTLER[1]

---

[1] Formerly Graduate Student in the Faculty of Arts and Sciences, Department of Biology, Harvard University. This manuscript, prepared by Elso E. Barghoorn and Alfred C. Redfield, Harvard University, is contribution No. 1024 from the Woods Hole Oceanographic Institution.

Contribution No. 1025

REPRINTED FROM THE ATMOSPHERE AND THE SEA IN MOTION
THE ROSSBY MEMORIAL VOLUME
THE ROCKEFELLER INSTITUTE PRESS AND OXFORD UNIVERSITY PRESS 1959

DISTRIBUTION OF MATTER IN THE SEA AND ATMOSPHERE

Changes in the Carbon Dioxide Content of the Atmosphere and Sea due to Fossil Fuel Combustion[1]

By BERT BOLIN and ERIK ERIKSSON

International Meteorological Institute in Stockholm

Abstract

The dissociation equilibrium of carbon dioxide in the sea is discussed with particular emphasis on the buffering effect of sea water, when changes of the partial pressure of CO_2 in the gas phase take place. The results are used in a study of the changes of the carbon dioxide content of the atmosphere and the sea that occur as a result of release of CO_2 to the atmosphere by fossil fuel combustion. It is shown that the steady state considerations given by previous authors hereby are considerably modified. Thus an increase of the CO_2 content of the atmosphere of about 10% as reported by Callendar may be compatible with a Süess effect of only a few percent. Because of the small buffering effect of the sea it seems likely that the biosphere on land may play a more important role for the changes actually occurring in the atmosphere due to release of CO_2 by combustion than previously believed. This problem warrants further investigation, but already the present treatment indicates that an appreciable increase of the amount of CO_2 in the atmosphere may have occurred since last century. This increase will continue and should be detectable with present techniques for measuring CO_2 in the atmosphere within a few years in areas with little or no local pollution due to fossil fuel combustion as in the Antarctica or on Hawaii.

1. Introduction

Fossil fuel combustion has added considerable amounts of carbon dioxide to the atmosphere during the last 100 years. In view of the great importance of CO_2 in the atmosphere for maintaining a radiational balance between the earth and space it is of great interest to know whether this output of CO_2 has caused a significant increase of the total content of carbon dioxide in the atmosphere or whether most of it has been transferred into the oceans. Some twenty years ago CALLENDAR (1938) could show that most likely a noticeable increase of the CO_2 in the atmosphere had occurred and he has recently (CALLENDAR, 1958) indicated that this increase in 1955—56 amounted to about 10 % as compared with an output due to combustion of about 14 % of the total amount of CO_2 present in the atmosphere (cf. REVELLE and SÜESS, 1957). His conclusions have recently been supported by BRAY (1959) in a detailed statistical investigation. However, by studying the C^{14} distribution in the atmosphere and the sea and its variation in the atmosphere during the last 100 years as revealed by the ratio C^{14}/C^{12} in wood one has been able to show that the exchange time between the atmosphere and the ocean is about 5 years (CRAIG, 1957, 1958; REVELLE and SÜESS, 1957; ARNOLD and ANDERSON, 1957; RAFTER and FERGUSSON, 1958). It has then been concluded (REVELLE and SÜESS, l.c.) that most of the CO_2 due to combustion has been transferred into the ocean and that a net increase of CO_2 in the atmosphere of only a few percent has actually occurred. Callendar's deduction has therefore been rejected particularly since the CO_2 measurements from the 19th century are indeed very uncertain.

---

[1] The research reported in this paper was partly sponsored by the Office of Naval Research through the Woods Hole Oceanographic Institution. Contribution No. 1025 from the Woods Hole Oceanographic Institution.

Towards the end of their paper Revelle and Süess point out, however, that the sea has a buffer mechanism acting in such a way that a 10 % increase of the CO_2-content of the atmosphere need merely be balanced by an increase of about 1 % of the total CO_2 content in sea water to reach a new equilibrium. The crude model of the sea they used assuming it to be one well-mixed reservoir of CO_2, did not permit them to study the effect of this process more in detail.

The low buffering capacity of the sea mentioned by Revelle and Süess is due to a change in the dissociation equilibrium between CO_2 and H_2CO_3 on one hand and HCO_3 and CO_3 ions on the other. An addition of CO_2 to the water will change the pH and thereby decrease the dissociation resulting in a larger portion of CO_2 and H_2CO_3 molecules. Since the pressure of CO_2 in the gas phase being in equilibrium with CO_2 dissolved in water is proportional to the number of CO_2 and H_2CO_3 molecules in the water, an increase of the partial pressure occurs which is much larger (about 12.5 times) than the increase of the *total content* of CO_2 in the water. The change of this equilibrium in the sea is almost instantaneous. However, in course of its circulation the ocean water gets in contact with solid $CaCO_3$ on the bottom of the sea whereby a change towards another equilibrium takes place. This latter process is extremely slow and may be disregarded when discussing changes due to fossil fuel combustion. It will, however, be indicated in section 2 how this equilibrium is of major interest when being concerned with processes with a time scale of several thousand years.

In discussing the consequences of such a shift in the dissociation equilibrium with respect to the exchange of CO_2 between the atmosphere and the sea and within the sea it is not sufficient to treat the ocean as one well-mixed reservoir. We shall instead first follow a suggestion by Craig (1957) and divide the ocean in two layers. The upper reservoir, in direct contact with the atmosphere, is the part of the ocean located above the thermocline and constitutes about 1/50 of the total sea. This part of the ocean is well mixed due to wind action and convection. The remaining part of the ocean, the deep sea, is also taken as a well-mixed water body in direct exchange with the mixed layer above. Certainly this latter assumption is a poor approximation to actual conditions but will, as we shall see, give internally consistant results. In the first instance we shall neglect the effect of living matter on the earth but some general remarks about the exchange of CO_2 between vegetation and the atmosphere will be given towards the end of the paper.

It is obvious that an addition of CO_2 to the atmosphere will only slightly change the CO_2 content of the sea but appreciably effect the CO_2 content of the atmosphere. It is possible to deduce a relation between the exchange coefficient for transfer from the atmosphere to the sea and the corresponding coefficient for the exchange between the deep sea and the mixed layer. It turns out that a 10 % increase of the CO_2 content of the atmosphere as a result of a total output due to combustion amounting to 13 % of the total CO_2 content of the atmosphere would result for a residence time of water in the deep sea of around 500 years. Only a considerably more rapid turn over of the ocean model yields appreciably lower values, while the rate of exchange between the atmosphere and the sea is much less important.

The change in the dissociation equilibrium in water resulting from a transfer of CO_2 to the sea also effects the C^{14} distribution in the three reservoirs and Revelle's and Süess' (1957) considerations in this matter are thereby appreciably changed. It is clear that a large percentage change of the CO_2 in the atmosphere and a comparatively small percentage change in the sea will yield a C^{14}/C^{12} ratio in the sea which is considerably greater than that of the atmosphere. The distribution of C^{14} between these two reservoirs is therefore not in equilibrium any longer. A transfer of C^{14} from the sea to the atmosphere will result. A more detailed study of this secondary effect reveals that

a) the steady state considerations of CO_2 exchange between the atmosphere and the sea as given by Craig (1957, 1958) are somewhat modified and a likely residence time for CO_2 in the atmosphere is 5 years.

b) the Süess effect would be 3—5 % depending on the rate of overturning of the sea.

In view of the observed values of the Süess-effect being around 3 % in 1954 (before the hydrogen bomb tests) (cf. Broecker and Walton, 1959; de Vries, 1958) the values obtained in this analysis are somewhat too large if using a value for the residence of water in the deep sea of 500 years. One possible explanation of this discrepancy would be the neglect of the exchange of CO_2 between the atmosphere and the biosphere. The main difficulty met when trying to incorporate this effect is, that we actually do not know whether a net increase of the amount of CO_2 present in vegetation may have occurred due to a transfer from the atmosphere or whether the direct influences from man's activities have had an effect in the opposite direction. It is clear, however, that even if no net transfer of CO_2 from the atmosphere into living or dead matter on land has occurred these exchange processes will modify the estimate of the "Süess effect" obtained by merely considering the atmosphere and the sea.

2. The CO_2-system in the sea

The different components of CO_2 present in the sea are CO_2, H_2CO_3, HCO_3^- and CO_3^{-2}. As CO_2 is difficult to distinguish from H_2CO_3 it is customary to express the sum of these species as CO_2. The sea is also in contact with ample amounts of solid $CaCO_3$ which should be considered in equilibrium being attained over several "turnover times" of the sea itself. Another important item in the system is the carbonate alkalinity, denoted here by A which is the sum of those cations which balance the charges of HCO_3^- and CO_3^{-2}. The following average values for the concentrations of the different components will be used here:

C_{CO_2} $=0.0133$ mmol × 1^{-1} (sum of CO_2 and H_2CO_3)
$C_{HCO_3^-}=1.90$ mmol × 1^{-1}
$C_{CO_3^{-2}}=0.235$ mmol × 1^{-1}

The sum of all these species is denoted by ΣC_{CO_2} and becomes 2.148 mmol × 1^{-1}. A is given in mval × 1^{-1} and becomes, $A=C_{HCO_3^-}+2\ C_{CO_3^{-2}}=$ $=2.37$ mval × 1^{-1}. Now the following relationships can be derived, namely

$$\sum C_{CO_2}=\left(1+\frac{K_1}{C_{H^+}}+\frac{K_1K_2}{C_{H^+}^2}\right)C_{CO_2} \qquad (1)$$

$$A=\left(\frac{K_1}{C_{H^+}}+\frac{2K_1K_2}{C_{H^+}^2}\right)C_{CO_2} \qquad (2)$$

where K_1 and K_2 are the first and second dissociation constants of H_2CO_3 in sea water and C_{H^+} is the hydrogen ion concentration. It is convenient to have the average values of the fractions within the brackets. They are

$$\frac{K_1}{C_{H^+}}=143 \qquad \frac{K_1K_2}{C_{H^+}^2}=18$$

As to calcium carbonate, its solubility product L_p can be written

$$C_{Ca^{+2}}\cdot C_{CO_3^{-2}}=L_p$$

or more conveniently

$$C_{Ca^{+2}}=L_p\frac{C_{H^+}^2}{K_1K_2}\frac{1}{C_{CO_2}} \qquad (3)$$

and in sea water $C_{Ca^{2+}}=10$ mmol × 1^{-1}.

Finally we have for the equilibrium between the atmospheric CO_2 and that in sea water

$$P_{CO_2}=\frac{1}{\alpha}C_{CO_2} \qquad (4)$$

where α is a proportionality constant and P_{CO_2} is the partial pressure of CO_2 in the atmosphere.

The constants K_1, K_2, L_p and α are only functions of temperature and salinity and will be regarded as constants in the following. We may therefore consider relations between small variations in P_{CO_2}, C_{CO_2}, ΣC_{CO_2}, A, C_{H^+} and $C_{Ca^{2+}}$. Using the variational method applied on equations (1) to (4) one obtains

$$\frac{\delta\Sigma C_{CO_2}}{\Sigma C_{CO_2}}=\frac{\delta C_{CO_2}}{C_{CO_2}}+ \\ +\frac{\frac{\partial}{\partial C_{H^+}}\left(1+\frac{K_1}{C_{H^+}}+\frac{K_1K_2}{C_{H^+}^2}\right)}{1+\frac{K_1}{C_{H^+}}+\frac{K_1K_2}{C_{H^+}^2}}\delta C_{H^+} \qquad (5)$$

$$\frac{\delta A}{A}=\frac{\delta C_{CO_2}}{C_{CO_2}}+\frac{\frac{\partial}{\partial C_{H^+}}\left(\frac{K_1}{C_{H^+}}+\frac{2K_1K_2}{C_{H^+}^2}\right)}{\frac{K_1}{C_{H^+}}+\frac{2K_1K_2}{C_{H^+}^2}}\delta C_{H^+} \qquad (6)$$

$$\frac{\delta C_{Ca^{+2}}}{C_{Ca^{+2}}}=\frac{2\,\delta C_{H^+}}{C_{H^+}}-\frac{\delta C_{CO_2}}{C_{CO_2}} \qquad (7)$$

$$\frac{\delta P_{CO_2}}{P_{CO_2}}=\frac{\delta C_{CO_2}}{C_{CO_2}} \qquad (8)$$

First we see that if P_{CO_2} varies and the hydrogen ion concentration were kept constant, the relative changes would be the same in the sea as in the atmosphere. As the total amount of CO_2 in the sea is about 50 times that in the air, practically all excess CO_2 delivered to the atmosphere would be taken up by the sea when equilibrium has been established. One cannot, however, assume that pH is uninfluenced by changes in the ΣC_{CO_2} of the sea. We may see if any condition can be imposed upon the alkalinity. Obviously this should be kept constant if we consider changes that take place over a relatively short time interval, less than the "turnover time" of the sea, because A is really the concentration of cations that balance the charges of HCO_3^- and CO_3^{-2}. If $CaCO_3$ is excluded the sum of these charges must remain constant. And then we see that any change in the P_{CO_2} will also change C_{H^+}. From eq. (5), (6) and (8) we get by putting $\delta A = 0$

$$\frac{\delta P_{CO_2}}{P_{CO_2}} = \frac{\delta C_{CO_2}}{C_{CO_2}} = 12.5\,\frac{\delta \Sigma C_{CO_2}}{\Sigma C_{CO_2}} \qquad (9)$$

using the numerical values listed earlier. This tells us that 1 percent change in the total CO_2 concentration in the sea would require 12.5 percent change in the atmospheric CO_2 to maintain equilibrium. If we consider only the "mixed layer" of the oceans, i.e. the surface layer which contains about as much CO_2 as the atmosphere less than 10 percent of the excess fossil CO_2 in the atmosphere should have been taken up by the mixed layer. It is therefore obvious that the mixed layer acts as a bottleneck in the transport of fossil CO_2 into the deep sea (cf. the following section).

It may be of interest also to consider the effect of the $CaCO_3$ on the bottom of the oceans; the effect this may have for the final equilibrium which is attained after a long time. Then alkalinity will change by $\delta A = 2\ \delta C_{Ca^{+2}}$ and with this condition using the whole system of equations and $C_{Ca^{+2}} = 10$ mmol × 1^{-1},

$$\frac{\delta P_{CO_2}}{P_{CO_2}} = \frac{\delta C_{CO_2}}{C_{CO_2}} = 2.36\,\frac{\delta \Sigma C_{CO_2}}{\Sigma C_{CO_2}} \qquad (10)$$

which shows that the sea, given enough time, has an appreciable buffer capacity for atmospheric CO_2. However, in the case of eq. (10) part of the change of total CO_2 comes from dissolution or precipitation of $CaCO_3$ and this has obviously to be subtracted if we want to know how much of the excess of atmospheric CO_2 the sea ultimately can consume. The amount that dissolves or precipitates is obviously equal to $\delta C_{Ca^{+2}}$ and becomes

$$\delta C_{Ca^{+2}} = 0.444\,\frac{\delta C_{CO_2}}{C_{CO_2}}$$

Expressed as a part of the total CO_2 it becomes

$$\frac{\delta C_{Ca^{+2}}}{\Sigma C_{CO_2}} = 0.206\,\frac{\delta C_{CO_2}}{C_{CO_2}} \qquad (11)$$

Now, rewriting (9) we find

$$\frac{\delta \Sigma C_{CO_2}}{\Sigma C_{CO_2}} = 0.424\,\frac{\delta C_{CO_2}}{C_{CO_2}}$$

The part of the increase in total CO_2 that has come from the atmosphere is therefore

$$\Delta\,\frac{\delta \Sigma C_{CO_2}}{\Sigma C_{CO_2}} = \frac{\delta \Sigma C_{CO_2}}{\Sigma C_{CO_2}} \quad \frac{\delta C_{Ca^{+2}}}{\Sigma C_{CO_2}} = 0.238\,\frac{\delta C_{CO_2}}{C_{CO_2}} \qquad (12)$$

or

$$\frac{\delta P_{CO_2}}{P_{CO_2}} = \frac{\delta C_{CO_2}}{C_{CO_2}} = 4.20\,\Delta\left(\frac{\delta \Sigma C_{CO_2}}{\Sigma C_{CO_2}}\right) \qquad (13)$$

Thus, in equilibrium one percent increase in ΣC_{CO_2} obtained from the atmosphere would occur for a 4.2 percent increase in the atmospheric partial pressure of CO_2. In other words, any excess CO_2 put into the atmosphere will ultimately be distributed so that about $^{11}/_{12}$ of it goes into the sea (again assuming the sea contains 50 times more CO_2 than the atmosphere) while about $^{1}/_{12}$ remains in the atmosphere. Of the part that goes into the sea, 87 percent has taken part in the reaction

$$CaCO_3\,(s) + H_2CO_3\,(aq) = Ca^{+2} + 2\,HCO_3^{-1}$$

The rest has been used to lower the pH of sea water by the reaction

$$H_2CO_3\,(aq) \rightarrow H^+ + HCO_3^-$$

If the turnover time of the sea is of the order of 1,000 years, several thousands of years would be required to reach equilibrium with the $CaCO_3$ at the bottom of the sea.

It should finally be noted that, in case atmospheric CO_2 was withdrawn by some process, this would result in precipitation of $CaCO_3$ in the sea.

3. The exchange of inactive carbon between the atmosphere and the sea

In order to see more clearly the effect of the shift in the dissociation equilibrium in the sea we shall first disregard the role played by the biosphere and merely consider the atmosphere and the sea, the latter composed of two reservoirs. The top one, the mixed layer, is confined to the layer above the thermocline and the lower one, the deep sea, consists of the remainder of the sea. Both these reservoirs as well as the atmosphere are considered to be well-mixed and the exchange between them takes place through first order exchange processes. Introduce the following notations:

N_i = the total amount of C^{12} and C^{13} in reservoir i in a state of equilibrium as before 1850.

N_i = the total amount of C^{14} in reservoir i in a state of equilibrium as before 1850.

N_i' = the amount of C^{12} and C^{13} in reservoir i present in the form of CO_2 or non-dissociated H_2CO_3 (only for the ocean) in a state of equilibrium as before 1850.

$N_i^{*\prime}$ = the amount of C^{14} in reservoir i present in the form of CO_2 or non-dissociated H_2CO_3 (only for the ocean) in a state of equilibrium as before 1850.

$n_i, n_i^*, n_i', n_i^{*\prime}$ indicate the deviations from the equilibrium values given above.

k_{i-j} = exchange coefficient for transfer of C^{12} and C^{13} from reservoir i to reservoir j.

k_{i-j} = exchange coefficient for transfer of C^{14} from reservoir i to reservoir j.

$\tau_{i-j} = 1/k_{i-j}$

$\tau_{i-j} = 1/k_{i-j}^*$

λ = decay constant for C^{14}

$\gamma(t)$ = release of C^{12} and C^{13} due to fossil fuel combustion as a function of time t.

Q = mean production of C^{14} in the atmosphere due to cosmic rays.

The indices a, m and d refer to the atmosphere, the mixed layer and the deep sea respectively. The nomenclature is in part very similar to that used by CRAIG (1957).

Considering now first conditions for inactive carbon we obtain the following equilibria

$$\left.\begin{aligned} -k_{a-m}N_a + k_{m-a}N_m' &= 0 \\ k_{a-m}N_a - k_{m-a}N_m' - k_{m-d}N_m + k_{d-m}N_d &= 0 \\ k_{m-d}N_m - k_{d-m}N_d &= 0 \end{aligned}\right\} \tag{14}$$

Notice here particularly that the transfer from the sea to the atmosphere is put proportional to N_m' and not to the total amount of carbon in the mixed layer, N_m. On the other hand the transfer from the mixed layer to the deep sea and *vice versa* is due to the motion of water and should therefore be proportional to the total amounts of carbon present in the two reservoirs, *i.e.* N_m and N respectively. It should be pointed out here that an exchange of carbon between various strata of the ocean also occurs through the motion of organisms and the settling of dead organic material and precipitated $CaCO_3$ which is gradually being dissolved. From a recent paper by ERIKSSON (1958) it can be estimated that this is about 1/3,000 of the total amount of CO_2 in the sea per year. Naturally it is compensated by an upward flux of dissolved CO_2. This flux is small compared to the advective flux from deep water which is about the same as the horizontal transfer of atmospheric CO_2 in Eriksson's model giving a residence time of ≈ 600 years. His paper suggests anyway that the ratio between advective flux and gravitational is about 5. From (14) we now get

$$\left.\begin{aligned} k_{m-a} &= \frac{N_a}{N_m'}\, k_{a-m} = \alpha k_{a-m} \\ k_{m-d} &= \frac{N_d}{N_m}\, k_{d-m} = \beta k_{d-m} \end{aligned}\right\} \tag{15}$$

Due to combustion a deviation from this equilibrium now has occurred, which is governed by the following set of equations

$$\left.\begin{aligned} \frac{dn_a}{dt} &= -k_{a-m}n_a + k_{m-a}n_m' + \gamma(t) \\ \frac{dn_m}{dt} &= k_{a-m}n_a - k_{m-a}n_m' - k_{m-d}n_m + k_{d-m}n_d \\ \frac{dn_d}{dt} &= k_{m-d}n_m - k_{d-m}n_d \end{aligned}\right\} \tag{16}$$

In the previous section we found that the following relation exists between n_m' and n_m (cf. eq. (9))

$$n_m' = 12.5\, \frac{N_m'}{N_m}\, n_m = B_1 n_m \tag{17}$$

Introducing this expression for n_m' into (16) we obtain a system of three ordinary linear differential equations for the three dependant variables n_a, n_m and n_d. Eliminating two of the three variables we obtain

$$\frac{d^3n_i}{dt^3} + [(1+B_1\alpha)k_{a-m} + (1+\beta)k_{d-m}]\frac{d^2n_i}{dt^2} + \\ + [1 + B_1\alpha + \beta]k_{a-m}k_{d-m}\frac{dn_i}{dt} = S_i \quad (18)$$

$$i = a,\ m,\ d$$

where

$$\left.\begin{aligned} S_a &= \gamma''(t) + [B_1\alpha k_{a-m} + (1+\beta)k_{d-m}]\gamma'(t) + \\ &\qquad + B_1\alpha k_{a-m}k_{d-m}\gamma(t) \\ S_m &= k_{a-m}\gamma'(t) + k_{a-m}k_{d-m}\gamma(t) \\ S_d &= \beta k_{a-m}k_{d-m}\gamma(t) \end{aligned}\right\} \quad (19)$$

The general solution of (18) is

$$n_i = C_{1i}e^{\lambda_1 t} + C_{2i}e^{\lambda_2 t} + C_{3i}e^{\lambda_3 t} + P_i \quad (20)$$

where C_{1i}, C_{2i} and C_{3i} are integration constants, λ_1, λ_2 and λ_3 solutions to the algebraic equation

$$\lambda_3 + [(1+B_1\alpha)k_{a-m} + (1+\beta)k_{d-m}]\lambda^2 + \\ + [1 + B_1\alpha + \beta]k_{a-m}k_{d-m}\lambda = 0 \quad (21)$$

and P_i are particular solutions depending on the functions S_i. Assuming now that [CRAIG (1957)]

$$\left.\begin{aligned} N_m &= 1.2\ N_a \\ N_d &= 60\ \ N_a \end{aligned}\right\} \quad (22)$$

we obtain

$$\left.\begin{aligned} B_1\alpha &= 12.5\frac{N'_m}{N_m}\frac{N_a}{N'_m} = 10.4 \\ \beta &= \frac{N_d}{N_m} = 50 \end{aligned}\right\} \quad (23)$$

The values chosen for N_m and N_d are somewhat uncertain but as we shall see later, do not influence the results significantly. The solutions to eq. (21) then are, due regard taken to the fact that $k_{a-m} \gg k_{d-m}$ and thus $(1+B_1\alpha)\cdot k_{a-m} + (1+\beta)k_{d-m} \gg (1 + B_1\alpha + \beta)k_{a-m}k_{d-m}$ where $\gg$ denotes about two orders of magnitude

$$\left.\begin{aligned} \lambda_1 &= 0 \\ \lambda_2 &= -\frac{(1+B_1\alpha+B)k_{a-m}k_{d-m}}{(1+B_1\alpha)k_{a-m} + (1+\beta)k_{d-m}} \\ \lambda_3 &= -[(1+B_1\alpha)k_{a-m} + (1+\beta)k_{d-m}] \end{aligned}\right\} \quad (24)$$

To obtain the particular solutions we have to specify $\gamma(t)$. We shall assume that $\gamma(t)$ may be approximated by

$$\gamma(t) = \gamma_0 e^{rt} \quad (25)$$

where

$$\left.\begin{aligned} \gamma_0 &= 4.96\ N_a\ 10^{-4} \\ r &= 0.029\ \text{year}^{-1} \end{aligned}\right\} \quad (26)$$

which fits the values given by REVELLE and SÜESS (1957) for carbon production until today and also the estimated values to year 2010 with sufficient accuracy if $t = 0$ at 1880 (see table 1).

Table 1. CO$_2$ added to the atmosphere by fossil fuel combustion and a comparison with an analytical expression

Decade	Average amount added per decade (% of N_a)		Cumulative total added (% of N_a)	
	measured or estimated	$\gamma(t)$	measured or estimated (since 1860)	$\int_0^t \gamma(t)dt$ (since 1880)
1880—89	0.54	0.57	1.13	0.57
1890—99	0.79	0.77	1.92	1.34
1900—09	1.27	1.03	3.19	2.37
1910—19	1.72	1.37	4.91	3.74
1920—29	2.00	1.83	6.91	5.57
1930—39	2.11	2.47	9.02	8.04
1940—49	2.71	3.17	11.73	11.21
1950—59	3.9	4.4	15.6	15.6
1960—69	5.4	5.8	21.0	21.4
1970—79	7.5	8.0	28.5	29.4
1980—89	10.5	10.4	39.0	39.8
1990—99	14.5	13.7	53.5	53.5
2000—09	20.0	19.0	73.5	72.5

Thus we obtain

$$\left.\begin{aligned} S_a &= \gamma_0[r^2 + \{B_1\alpha k_{a-m} + (1+\beta)k_{d-m}\}r + \\ &\qquad + B_1\alpha k_{a-m}k_{d-m}]e^{rt} = \gamma_0 S_{a0}e^{rt} \\ S_m &= \gamma_0[k_{a-m}r + k_{a-m}k_{d-m}]e^{rt} = \gamma_0 S_{m0}e^{rt} \\ S_d &= \gamma_0\beta k_{a-m}k_{d-m}e^{rt} = \gamma_0 S_{d0}e^{rt} \end{aligned}\right\} \quad (27)$$

One then easily finds the particular solutions

$$P_i = \frac{\gamma_0}{r}\frac{S_{i0}}{S_{a0} + S_{m0} + S_{d0}}e^{rt} \quad (28)$$

$$i = a,\ m,\ d$$

In order to determine the three constants C_{ij} for each solution $n_i(t)$ we shall apply the initial conditions

$$\left.\begin{aligned}
& n_a = n_m = n_d = 0 \\
& \text{which yields} \\
& \frac{dn_a}{dt} = \gamma(t); \qquad \frac{dn_m}{dt} = \frac{dn_d}{dt} = 0 \\
& \frac{d^2 n_a}{dt^2} = \gamma'(t) - k_{a-m}\gamma(t) \\
& \frac{d^2 n_m}{dt^2} = k_{a-m}\gamma(t); \\
& \frac{d^2 n_d}{dt^2} = 0
\end{aligned}\quad t = 0 \right\} \tag{29}$$

These equations are obtained from the system (16) and also yield

$$n_a + n_m + n_d = \frac{\gamma_0}{r}(e^{rt} - 1) \tag{30}$$

As can easily be verified the final solutions of n_a, n_m and n_d will be independant of the exact initial conditions for $t \gg 200$ years if the values for τ_{a-m} and τ_{d-m} are of the order of 5 and 500 years respectively. It also follows that $\lambda_3 = -2$ years^{-1} and that thus the term containing exp $(\lambda_3 t)$ in (20) may be neglected for $t \gg 2$—3 years. With due regard taken to this latter fact we finally obtain

$$\left.\begin{aligned}
n_a &= \frac{\gamma_0}{r}\left[\frac{S_{a0}}{S}(e^{rt} - 1) + \right. \\
&\qquad \left. + \frac{r}{\lambda_2}\left(1 - \frac{S_{a0}}{S}\right)(e^{\lambda_2 t} - 1)\right] \\
n_m &= \frac{\gamma_0}{r}\frac{S_{m0}}{S}\left[(e^{rt} - 1) - \frac{r}{\lambda_2}(e^{\lambda_2 t} - 1)\right] \\
n_d &= \frac{\gamma_0}{r}\frac{S_{d0}}{S}\left[(e^{rt} - 1) - \frac{r}{\lambda_2}(e^{\lambda_2 t} - 1)\right] \\
S &= S_{a0} + S_{m0} + S_{d0}
\end{aligned}\right\} \tag{31}$$

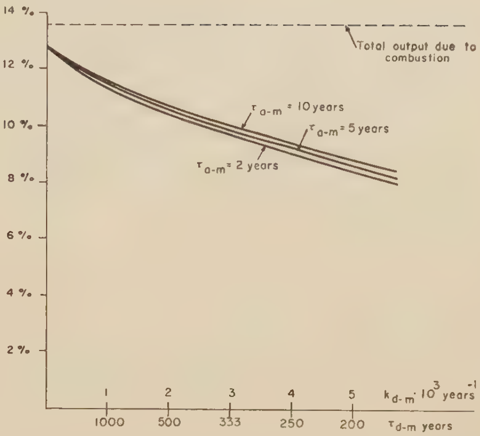

Fig. 1. Net increase of CO_2 in the atmosphere in 1954 due to release of fossil CO_2 according to UN-estimates as dependant on the rate of exchange between the atmosphere and the sea and the mixed layer and the deep sea.

From Craig's (1957, 1958) investigation of the exchange time for carbon dioxide between the atmosphere and the sea and the exchange within the sea the best estimates of τ_{a-m} and τ_{d-m} at present are $\tau_{a-m} = 5$ years and $\tau_{d-m} = 500$—1,000 years. Fergusson and Rafter (1958) give a value $\tau_{a-m} = 3$ years. Fig. 1 shows the amount to be expected in the atmosphere 1954, when the total fossil fuel combustion since the middle of the last century is estimated to have been 13.2 % of the previous content of the atmosphere, for values of τ_{a-m} and τ_{d-m} in the vicinity of those quoted above. It first of all shows that *the net increase in the atmosphere is almost independant of the precise rate of exchange between the atmosphere and the sea.* This depends on the fact that the top layer of the ocean only need to absorb a small amount of CO_2 from the atmosphere as compared to the quantities released to be in approximate balance. Its capacity is therefore too small to be of any major importance. The decisive factor is instead the rate of overturning of the deep sea. Thus even using a residence time of only 200 years for the deep sea water an 8—9 percent increase of CO_2 in the atmosphere must have taken place. For a value of $\tau_{d-m} = 500$ years an increase of the atmosphere's content of CO_2 of about 10 percent would have occurred in 1954. This value compares very favourably with the value of 10 percent given by Callendar (1958) as the total increase until 1955 deduced from a careful survey of all available measurements.

The results obtained above are, however, dependant on our assumptions of the size of the three reservoirs, i.e. N_a, N_m and N_d. Of course, the total amount of CO_2 in the atmosphere, N_a is quite well known, but the division of the sea into two layers is somewhat arbitrary. It is of some interest to see how sensitive the solution is to a variation of N_m and N_d. Instead of chosing the values given in (22) we shall assume

$$\text{a)}\left\{\begin{aligned} N_m &= 0.8\ N_a \\ N_d &= 60\ N_a \end{aligned}\right. \qquad \text{b)}\left\{\begin{aligned} N_m &= 2\ N_a \\ N_d &= 59\ N_a \end{aligned}\right\} \tag{32}$$

We then obtain the values $n_a = 10.6\,\%$ and $n_a = 10.0\,\%$ respectively as compared with $n_a = 10.3\,\%$ previously, using $\tau_{a-m} = 5$ years and $\tau_{d-m} = 500$ years. Our solution is quite insensitive to the exact division of the ocean. However, the value of the total amount of carbon dioxide in the sea ($\approx 61\ N_a$) effects the solution more, but here we quite accurately know the actual amounts as just mentioned.

4. The exchange of radio-carbon between the atmosphere and the sea

REVELLE and SÜESS (1957) assume that the exchange of radio carbon between the atmosphere and the sea takes place independantly of changes in the distribution of inactive CO_2. If this were the case the decrease of the C^{14}/C^{12} ratio in the atmosphere since 1850, the Süess effect, would be a direct measure of the increase of the inactive CO_2 during the same time, since fossil fuel contains no C^{14}. As a matter of fact, they deduce an exchange coefficient for transfer of CO_2 from the atmosphere to the sea on this basis. As was indicated in the introduction this is not correct. The change of pH in the sea will shift the dissociation equilibrium also for the carbon dioxide containing C^{14}. We may assume an equilibrium rapidly being established and have

$$\frac{N_m^{*\prime}}{N_m} = \varkappa \frac{N_m'}{N_m} \tag{33}$$

where $\varkappa$ is dependant on the fractionation. If changes of N_m and N_m' occur as discussed in the previous section, we obtain by variation the following expression for the changes in N_m and $N_m^{*\prime}$

$$\frac{n_m^{*\prime}}{N_m^{*\prime}} - \frac{n_m^*}{N_m^*} = \frac{n_m'}{N_m} - \frac{n_m}{N_m} \tag{34}$$

Making use of (17) we obtain

$$\left.\begin{aligned} n_m^{*\prime} &= \frac{n_m^*}{N_m^*} N_m' + 11.5 \frac{n_m}{N_m} N_m^{*\prime} \\ &= B_2 n_m^* + B_3 n_m \end{aligned}\right\} \tag{35}$$

We see here clearly how a change of the total amount of CO_2 in the top layer of the ocean will influence the amount of radioactive carbon in the form of CO_2 and H_2CO_3 and therefore the partial pressure, which will mean that the equilibrium with the atmosphere is disturbed. Actually the amount of C^{14} in the form of undissociated CO_2 is much more influenced by changes in the *total* amount of CO_2 present in the water than by changes of the amount of *radioactive* carbon dioxide.

Corresponding to the system of equations in (16) we have the following set describing the transfer of radioactive carbon

$$\left.\begin{aligned} \frac{dn_a^*}{dt} &= -k_{a-m}^* n_a^* + k_{m-a} n_m^{*\prime} - \lambda n_a^* \\ \frac{dn_m^*}{dt} &= k_{a-m}^* n_a^* - k_{m-a} n_m^{*\prime} - \\ &\qquad - k_{m-d} n_m^* + k_{d-m} n_d^* - \lambda n_m^* \\ \frac{dn_d^*}{dt} &= k_{m-d} n_m^* - k_{d-m} n_d^* - \lambda n_d^* \end{aligned}\right\} \tag{36}$$

Notice here that the exchange coefficients between the atmosphere and the sea are different from those used in equation (16) thereby taking into consideration the fractionation effect. Following CRAIG (1957) we have

$$\frac{k_{m-a}^*}{k_{a-m}^*} = \mu \frac{k_{m-a}}{k_{a-m}} = \mu \frac{N_a}{N_m'} \approx \frac{N_a}{N_m'} \tag{37}$$

where $\mu = 1/1.012 = 0.988$. The deviation of μ from unity will be completely irrelevant in the following discussion and we will therefore put $\mu = 1$ as indicated by the last expression in (37). We shall also put $k_{a-m}^* = k_{a-m}$ and thus neglect fractionation. For the exchange between the top layer of the ocean and the deep sea the exchange is the same as for inactive carbon with the assumption made that it is due to the motion of sea water only.

Introducing (35) into (36), taking into consideration (15) and (37) and rearranging terms we obtain

$$\left.\begin{aligned} \left(\frac{d}{dt} + k_{a-m} + \lambda\right) n_a^* - B_2 \alpha k_{a-m} n_m^* \qquad\qquad &= B_3 \alpha k_{a-m} n_m \\ - k_{a-m} n_a^* + \left(\frac{d}{dt} + B_2 \alpha k_{a-m} + \beta k_{d-m} + \lambda\right) n_m^* - k_{d-m} n_d^* &= -B_3 \alpha k_{a-m} n_m \\ - \beta k_{d-m} n_m^* + \left(\frac{d}{dt} + k_{d-m} + \lambda\right) n \quad &= 0 \end{aligned}\right\} \tag{38}$$

We find thus that the changes of n_m appear as "driving forces" for the C^{14}-system. Knowing n_m as a function of time, we may calculate the changes that will occur in the distribution of radio carbon and thus also compute the Süess effect. The problem is implicit, however, since the distribution of n_m depends on k_{a-m} and k_{d-m} as shown in the previous section and our problem is therefore to find the particular pair of values that are in agreement with observed changes in the total amount of CO$_2$ in the atmosphere *and* the changes of the C^{14}/C^{12} ratio. Eliminating n_m^* and n_d^* from the equations (38) and in doing so taking account of the fact that $k_{a-m} \gg k_{d-m} \gg \lambda$ we obtain

$$\frac{d^3 n_a^*}{dt^3} + [(B_2\alpha + 1) k_{a-m} + (\beta + 1) k_{d-m}] \frac{d^2 n_a^*}{dt^2} + (1 + \beta + B_2\alpha) k_{a-m} k_{d-m} \left(\frac{dn_a^*}{dt} - n_a^*\lambda\right) =$$

$$= B_3 \alpha k_{a-m} \left[\frac{d^2 n_m}{dt^2} + (\beta + 1) k_{d-m} \left(\frac{dn_m}{dt} + \lambda n_m\right)\right] \qquad (39)$$

Now $|n_m^{-1} dn_m/dt| \gg \lambda$ and we shall also assume that our solution n_a^* satisfies the same relation, which will be verified *a posteriori*. It means that the decay of C^{14} is unimportant for the discussion of the exchange between the atmosphere and the sea. We thus finally obtain

$$\frac{d^3 n_a^*}{dt^3} + [(B_2\alpha + 1) k_{a-m} + (\beta + 1) k_{d-m}] \frac{d^2 n_a^*}{dt^2} + (1 + \beta + B_2\alpha) k_{a-m} k_{d-m} \frac{dn_a^*}{dt} =$$

$$= B_3 \alpha k_{a-m} \left[\frac{d^2 n_m}{dt^2} + (1 + \beta) k_{d-m} \frac{dn_m}{dt}\right] \qquad (40)$$

This equation is principally the same as eq. (18) and thus possesses a solution of the character given by (20) where now λ_1^*, λ_2^* and λ_3^* are solutions of an equation similar to (24). From the three equations (38) and with due regard to the expression for dn_m/dt given by eq. (16) we obtain the initial conditions

$$n_a^* = \frac{dn_a^*}{dt} = \frac{d^2 n_a}{dt^2} = 0 \qquad (41)$$

and similar expressions for n_m^* and n_d^* if we wish to study their variations. Introducing the expression for n_m given by equation (31) and solving for n_a^* we obtain with some simplifications similar to those done previously

$$\frac{n_a^*}{N_a^*} = Q_1 \left[e^{rt} - 1 - \frac{r}{\lambda_2^*}(e^{\lambda_2^* t} - 1)\right] -$$

$$- Q_2 \left[e^{\lambda_2 t} - 1 - \frac{\lambda_2}{\lambda_2^*}(e^{\lambda_2^* t} - 1)\right] \qquad (42)$$

where

$$\left.\begin{aligned} Q_1 &= \frac{[r + (1 + \beta) k_{d-m}]\, H}{r\,[r^2 + \{(B_2\alpha + 1) k_{a-m} + (1 + \beta) k_{d-m}\}\, r + (1 + \beta + B_2\alpha) k_{a-m} k_{d-m}]} \\ Q_2 &= \frac{[(1 + \beta) k_{d-m} + \lambda_2]\, H}{\lambda_2\,[\lambda_2^2 + \{(B_2\alpha + 1) k_{a-m} + (1 + \beta) k_{d-m}\}\, \lambda_2 + (1 + \beta + B_2\alpha) k_{a-m} k_{d-m}]} \end{aligned}\right\} \qquad (43)$$

having introduced the symbol H and λ_2^* according to

$$H = B_3 \alpha \frac{\gamma_0}{r} \frac{k_{a-m}^2 (r + k_{d-m})\, r}{r^2 + [(B_1\alpha + 1) k_{a-m} + (1 + \beta) k_{d-m}]\, r + (1 + \beta + B_1\alpha) k_{a-m} k_{d-m}} \qquad (44)$$

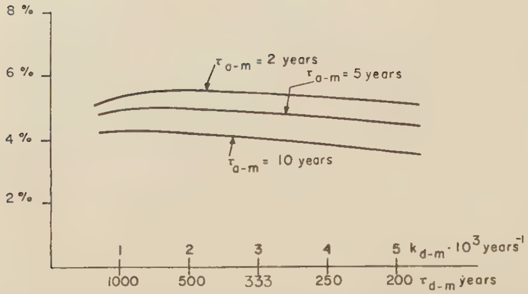

Fig. 2. The increase of C^{14} in the atmosphere in 1954 by a net transfer from the sea resulting from release of fossil CO_2 and a change of the dissociation equilibrium in the sea.

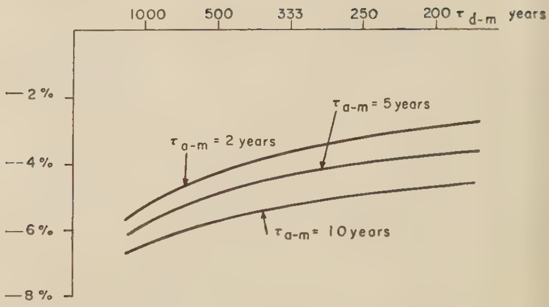

Fig. 3. The expected value of the Süess effect in 1954 for various rates of exchange between the atmosphere and the sea and within the sea.

$$\lambda_2^* = -\frac{(1+\beta+B_2\alpha)k_{a-m}k_{d-m}}{(1+B_2\alpha)k_{a-m}+(1+\beta)k_{d-m}} \tag{45}$$

Figure 2 shows the values of n_a^* in 1954 when the total output of CO_2 into the atmosphere is estimated to have been 13.2 %. A more pronounced variation with the value of $\tau_{a-m}=k_{a-m}^{-1}$ is here obtained than was the case for n_a. This is easily understandable. The slower the exchange between the atmosphere and the sea takes place the less rapid is the response of the sea to changes of the CO_2 content of the atmosphere. If $\tau_{a-m}=0$ and $\tau_{d-m}=\infty$ obviously $12.5\times\left(\frac{n_m}{n_a}\right):\left(\frac{N_m}{N_a}\right)=1$ according to equation (17). Computing n_m from (31) and inserting we obtain here

$$12.5\cdot\frac{n_m}{n_a}\cdot\frac{N_a}{N_m}=\begin{Bmatrix}0.77\\0.73\\0.69\end{Bmatrix} \text{ for } \tau_{a-m}\begin{Bmatrix}2 \text{ years}\\5 \text{ years}\\10 \text{ years}\end{Bmatrix} \tag{46}$$

which values are almost independant of the value of τ_{d-m} in the range 200—1,000 years considered here. The changes of n_m are the "driving force" for changes in the C^{14} system and again the slower the exchange between the sea and the atmosphere is, the greater the lag of the C^{14} adjustment in the atmosphere relative to the sea becomes.

The results obtained from eq. (42) are again quite independant of the exact division of the ocean into two reservoirs. Making the computations with the values of N_a and N_m given in (32) yields values of n_a^* only a few tenths of a percent different from those shown in fig. 2.

By a comparison of the results given by eq. (31) and (42) we can compute the changes of the C^{14}/C^{12} ratio in the atmosphere, the "Süess effect". The result is shown in fig. 3. It is of special interest to compare these values with actually observed values. Süess' measurements give an average value of —1.7 % which may be considered representative for about 1946 (REVELLE and SÜESS 1957). BROECKER and WALTON (1959) have found a value of —2.9% for 1938, and a lower value of —1.8% for 1954. The latter sample may, however, already have been influenced by the Castle tests in the Pacific early in 1954. Finally DE VRIES (1958) gives a value of —2.9 % for 1954. Summarizing these measurements a value of —2.5 to —3 % seems plausible for the Süess effect in 1954 before any appreciable amounts of C^{14} had been introduced into the atmosphere due to atomic bomb tests. More measurements from all over the world would, however, be desirable to determine this value more accurately. It is seen from fig. 3 that the computed value is somewhat larger particularly if the exchange between the three reservoirs is relatively slow.

CRAIG (1958) has given the value $\tau_{a-m}=5$ years as the most likely value for the exchange time between the atmosphere and the sea. It is obtained by studying the difference in the C^{14}/C^{12} ratio in the atmosphere and the sea with due regard taken to fractionation. It is furthermore assumed that the Süess effect is —1.25%, which seems to be an underestimate even if it is true that some of the values later reported perhaps are not truely representative. Chosing a value of —3 % would yield a value of about 3 years. However, due to the fact that a net transfer of CO_2 from the atmosphere to the sea occurs at present $(N_a+n_a)\,(N_m+n_m)^{-1}$ is somewhat larger than would be the case in equilibrium. On the other hand a net transfer of C^{14} takes place from the sea to the atmosphere and therefore $(N_a^*+n_a^*)\,(N_m^*+n_m^*)^{-1}$ is smaller than in equilibrium. The deviations are larger the slower the

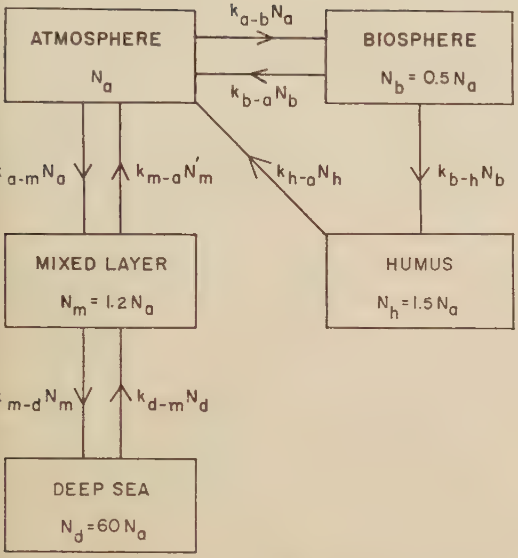

Fig. 4. Model of the CO_2 exchange between the deep sea, the mixed layer of the sea, the atmosphere, the biosphere and humus on land.

exchange between the atmosphere and the sea takes place. Thus the difference of the C^{14}/C^{12} ratio in the atmosphere and the sea (corrected for fractionation) should be larger in the equilibrium case than in the case where a net transfer occurs as indicated here.

It should be pointed out at this moment that similar deviations of the C^{13}/C^{12} ratios from the equilibrium values may occur if the net transfer of C^{13} and C^{12} are different. This is important since all C^{14} measurements are corrected for fractionation with the aid of the C^{13}/C^{12} ratio. Obviously such a procedure assumes equilibrium conditions. In the case of exchange between the atmosphere and the sea this need not be the case as we have shown above. It so happens, however, that the ratio C^{13}/C^{12} is almost the same in fossil fuel as in the atmosphere, the difference being only about 2 %. Thus no significant errors are therefore introduced in assuming equilibrium conditions.

With the model presented above one can now easily compute how large the deviations from equilibrium are which are due to the fact that a net transfer of both inactive and radioactive carbon occurs. The most likely value of the exchange time again becomes $\tau_{a-m} = 5$ years.

Measurements of C^{14} in the deep sea BROECKER (1957) and RAFTER and FERGUSSON (1958) in many cases indicate an age relative surface waters of 500 years or more and the interpretation of these values are not essentially influenced by considerations of the kind presented here. It is thus seen from fig. 3 that the computed value of the Süess effect should be around —5 % in comparison with the observed value of about —3 %. There may be many explanations for this discrepancy but first of all the accuracy of our model is not greater than it could be explained merely as due to this crudeness. Our assumption of a well-mixed deep sea is of course an unrealistic one and a more complete formulation of the problem in this respect seems very desirable. Secondly, we have completely neglected the effect of the biosphere on land. In view of the relatively small buffering effect of the sea the changes of the CO_2 (as well as $C^{14}O_2$) content of the atmosphere are here computed to be quite large. One may therefore very well expect that the biosphere also is influenced in some way (cf. ERIKSSON and WELANDER, 1956).

5. Estimates of the effect of CO_2 exchange between the atmosphere and the biosphere

The amount of carbon stored in the biosphere on land N_b is not very well known. Different estimates give values varying between 12 % (CRAIG, 1957) and about 85 % (ERIKSSON and WELANDER, 1956) of the amount present in the atmosphere. Estimates of dead organic matter, humus (N_h), also vary considerably, between values of 1.1 N_a to 1.7 N_a. For the following estimates we shall assume $N_b = 0.5\,N_a$ and $N_h = 1.5\,N_a$.

We may now extend our previous model of the CO_2-exchange in nature to the one depicted in fig. 4, which in case of equilibrium has been studied by CRAIG (1957). In complete analogy with the previous analysis we obtain in the equilibrium case

$$\left.\begin{array}{l}
-k_{a-m}N_a + k_{m-a}N'_m - k_{a-b}N_a + \\
\qquad\qquad + k_{b-a}N_b + k_{h-a}N_a = 0 \\
k_{a-b}N_a - k_{b-a}N_b - k_{b-h}N_b \qquad = 0 \\
-k_{h-a}N_h + k_{b-h}N_b \qquad\qquad = 0 \\
k_{a-m}N_a - k_{m-a}N'_m - k_{m-d}N_m + \\
\qquad\qquad + k_{d-m}N_d = 0 \\
k_{m-d}N_d - k_{d-m}N_d \qquad\qquad = 0
\end{array}\right\} \quad (47)$$

Again denoting the deviations from equilibrium due to fossil fuel combustion by n_i we obtain

$$\left.\begin{aligned}
&\frac{dn_a}{dt} + k_{a-m}n_a - k_{m-a}n'_m + k_{a-b}n_a - \\
&\qquad\qquad - k_{b-a}n_b - k_{h-a}n_h = \gamma(t) \\
&\frac{dn_b}{dt} - k_{a-b}n_a + k_{b-a}n_b + k_{b-h}n_b \qquad = 0 \\
&\frac{dn_h}{dt} + k_{h-a}n_h - k_{b-h}n_b \qquad\qquad = 0 \\
&\frac{dn_m}{dt} - k_{a-m}n_a + k_{m-a}n'_m + k_{m-d}n_m - \\
&\qquad\qquad - k_{d-m}n_d = 0 \\
&\frac{dn_d}{dt} - k_{m-d}n_m + k_{d-m}n_d \qquad\qquad = 0
\end{aligned}\right\} \quad (48)$$

It is hardly justified to carry through such a complete analysis here as presented previously in view of the fact that the assumptions made about the exchange processes between the atmosphere, biosphere and humus are more doubtful. An estimate shows, however, that $n_a \approx +7\,\%$ if we assume $\tau_{a-m} = 5$ years, $\tau_{d-m} = 500$ years, $\tau_{a-b} = 30$ years and $\tau_{b-h} = 30$ years compared with 10 % in the case of no net increased assimilation as a result of increased CO_2 content of the atmosphere.

Obviously the distribution of $C^{14}O_2$ between the various reservoirs also is influenced by an exchange with the biosphere and this would be the case even if no net increase of inactive CO_2 in the biosphere and in the humus has occurred. We can obtain a lower limit for the Süess effect if we assume an infinitely rapid adjustment of the C^{14} content between the four reservoirs, the atmosphere, the mixed layer of the sea, the biosphere and humus, i.e. the Süess effect is the same in all reservoirs and also considering that no C^{14} is supplied from the deep sea to these reservoirs. Since $N_m + N_a + N_b + N_h \approx 4\ N_a$ and since the exchange between the mixed layer and the deep sea is comparatively slow so that only a small part (0.02—$0.04\ N_a$) of the fossil CO_2 released until 1954 ($\approx 0.13\ N_a$) has found its way into the deep sea we estimate that the Süess effect should be 2—2.5 %. As pointed out previously the observed Süess effect was about —3 % in 1954 which is in very good agreement with this estimate.

6. Forecast of the CO_2 changes in the atmosphere during the remainder of the 20th century

Certainly the estimates presented above are partly quite uncertain but it is of some interest to see what they imply with regard to future changes of the CO_2-content of the atmosphere. An upper limit is obtained if neglecting the exchange with the biosphere as done in section 4. A lower limit on the other hand is determined if an infinitely rapid exchange between the atmosphere and the biosphere takes place and obviously this would be equivalent to putting N_a equal to the sum of the CO_2 found in the atmosphere, the biosphere and the humus. Introducing the values for the various residence times as given in the previous section yields a forecast in between these two extremes. Fig. 5 shows the variations to be expected until year 2000 based on an output of CO_2 into the atmosphere as given by table 1. The most likely value for n_a at that time seems to be about + 25 %, it may possibly be larger but probably not exceed 40 %. These values are considerably larger than those estimated for example by REVELLE and SÜESS (1957). The implications with regard to the radiational equilibrium of the earth in such a case may be considerable but falls outside the scope of this paper.

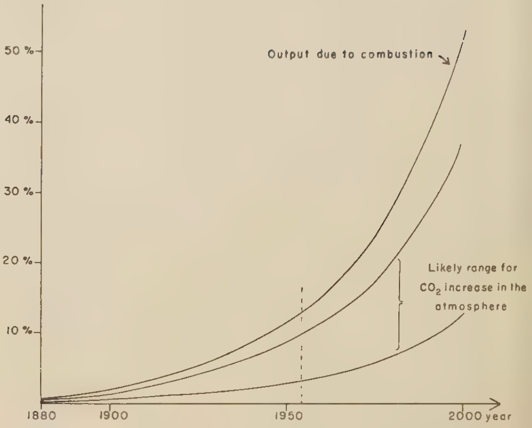

Fig. 5. Estimate of likely range for CO_2 increase in the atmosphere as a result of fossil fuel combustion according to UN estimates.

Fig. 5 also shows that the present increase of CO_2 in the atmosphere probably is 0.1—0.3 % per year. Recent measurements in regions far away from industrial areas such as Hawaii and the Antarctica (personal communication from Rakestraw) show remarkably constant values of the CO_2 content in the atmosphere throughout the year. It should therefore be possible within a few years to observe whether an increase occurs with this computed rate or not.

REFERENCES

Arnold, J. R. and Anderson, E. C., 1957: The distribution of carbon-14 in nature. *Tellus*, **9**, p. 28.

Bray, J. R., 1959: An analysis of the possible recent change in atmospheric carbon dioxide concentration. *Tellus*, **11** (in press).

Broecker, W., 1957: Application of radiocarbon to oceanography and climate chronology. *Thesis Faculty of Pure Science, Columbia Univ.*

Broecker, W. and Walton, A., 1959: The geochemistry of C14 in the fresh water system. *Geochimica et Cosmochimica Acta*, **16**, p. 15—38.

Callendar, G. S., 1938: The artificial production of carbon dioxide and its influence on temperature. *Q. J. Roy. Met. Soc.*, **64**, p. 223.

Callendar, G. S., 1958: On the amount of carbon dioxide in the atmosphere. *Tellus*, **10**, p. 243.

Craig, H., 1957: The natural distribution of radio carbon and the exchange time of carbon dioxide between atmosphere and sea. *Tellus*, **9**, p. 1.

Craig, H., 1958: A critical evaluation of radio carbon techniques for determining mixing rates in the oceans and the atmosphere. *Second United Nations International Conference for the Peaceful Uses of Atomic Energy*, Geneva (in press).

Eriksson, E., 1959: The circulation of some atmospheric constituents in the sea. *Rossby Memorial Volume.* Esselte, Stockholm, pp. 147—157.

Eriksson, E. and Welander, P., 1956: On a mathematical model of the carbon cycle in nature. *Tellus*, **8**, 155—175.

Harvey, H. W., 1955: *The chemistry and fertility of sea waters.* Cambridge University Press.

Rafter, T. A. and Fergusson, G. J., 1957: Recent increase in the C14 content of the atmosphere, biosphere and surface waters of the ocean. *N.Z. J. Science and Tech.*, B 38, p. 871.

Rafter, T. A. and Fergusson, G. J., 1958: Atmospheric radio carbon as a tracer in geophysical circulation problems. *Second United Nations International Conference on the Peaceful Uses of Atomic Energy*, Geneva (in press).

Revelle, R. and Süess, H., 1957: Carbon dioxide exchange between atmosphere and ocean and the question of an increase of atmospheric CO_2 during past decades. *Tellus*, **9**, p. 18.

(Manuscript received November 15, 1958)

Contribution No. 1026

Deep-Sea Research, 1959, Vol. 6, pp. 65 to 69. Pergamon Press Ltd., London. Printed in Great Britain

LETTER TO THE EDITORS

Enrichment experiments as a means of studying nutrients limiting to phytoplankton production

(*Received* 18 *February* 1959)

By inference from indirect evidence, it is generally agreed that nutrients limit photosynthesis in most of the oceans, particularly when the surface waters are thermally stratified. Phytoplankton growth is usually accompanied by a decrease in the concentrations of nitrate, phosphate, and silicate, and these elements sometimes reach levels during the summer which are undetectable by normal analytical procedures.

From the composition of the mineral nutrients in plankton algae relative to carbon, one may calculate from photosynthesis measurements the rate at which the nutrients must be supplied to the plants. This frequently reveals that their supply at any given time is adequate for no more than a few days growth. Unfortunately, we know little about the rate at which these materials are supplied to the surface waters by vertical mixing, and almost nothing of the rate at which they are regenerated through bacterial decomposition, animal excretion, etc. *in situ* in the surface waters. Thus conclusions concerning a dynamic process, growth, are often based entirely upon observations of a static property, the instantaneous nutrient concentrations.

Even here, however, the complete picture is usually lacking. Chemical nutrient studies accompanying biological investigations in the ocean usually include phosphate, frequently nitrate, occasionally silicate. There are a number of other elements essential to plant growth which are not major constituents of sea-water but which are seldom measured in relation to plant growth. Examples of these include iron, copper, manganese, cobalt, and the vitamins.

Furthermore, nitrate and phosphate measurements do not necessarily give the complete picture of the available nitrogen and phosphorus. In addition to nitrite and ammonia (which are sometimes measured and are usually at very low concentrations) both elements may be present as dissolved organic compounds of unknown identity in concentrations as high as or higher than the inorganic fractions. We can arrive at no conclusions regarding the biological significance of these compounds without knowing what they are. But it is not improbable that some of them may be used directly, if not preferentially, as a source of nutrients by some species of phytoplankton.

For these various reasons, then, the nutrient chemical observations normally made at sea rarely, if ever, provide sufficient information to draw qualitative or quantitative conclusions concerning the specific substances which limit phytoplankton production. We have therefore attempted to attack this problem by a more direct, experimental approach. These experiments entailed adding various nutrients to samples of surface water containing its natural phytoplankton and measuring their rate of uptake of $^{14}CO_3^{=}$ in an illuminated incubator (1500 ft candles) for 24 hours. As controls, we have employed unenriched surface water. In addition, since deep water invariably supports high levels of production when brought to the surface (i.e., in upwelling areas), we have used as a second control samples containing 1/2 surface water and 1/2 filtered deep water, doubling the observed ^{14}C uptake in these samples to make them comparable to the others which contained all surface water. The objectives in these experiments were twofold : (1) to see whether we could simulate the productive capacity of deep water by artificial enrichment and (2) to determine which of the added nutrients were critical in limiting ^{14}C uptake in the unenriched surface water.

The nutrients which were employed for these experiments are those which are used routinely in this laboratory for the culture of marine phytoplankton, but their concentrations have been adjusted to levels which for the most part are comparable to, though somewhat higher than, the maximum concentrations of these elements in sea-water. The complete medium consists of nitrate, phosphate, silicate, thiosulphate, trace metals (including iron), and vitamins, (Table 1). The experiments consisted of the two controls described above, one sample enriched with the complete medium and six

Table 1. Medium used in enrichment experiments

1. $Na\,NO_3$	50 μgA N/litre
2. $Na_2\,PHO_3\,.\,12\,H_2\,O$	5 μgA P/litre
3. $Na_2\,SiO_3\,.\,9\,H_2\,O$	50 μgA Si/litre
4. $Na_2\,S_2\,O_3\,.\,5\,H_2\,O$	8 μgA S/litre
5. Vitamin mix	
Thiamin . HC1	0·2 mg/litre
Biotin	1·0 μg/litre
B_{12}	1·0 μg/litre
6. Iron and trace metal mix	
Fe-sequestrine	1·30 mg/litre Fe
$Cu\,SO_4\,.\,5H_2\,O$	0·005 mg/litre Cu
$Zn\,SO_4\,.\,7H_2\,O$	0·010 mg/litre Zn
$Co\,Cl_2\,.\,6H_2\,O$	0·005 mg/litre Co
$Mn\,Cl_2\,.\,4H_2\,O$	0·100 mg/litre Mn
$Na_2\,Mo\,O_4\,.\,2H_2\,O$	0·005 mg/litre Mo

additional samples enriched with the same medium but each with one successive constituent omitted. At each station, then, there were 9 separate ^{14}C experiments which may be summarized as follows :

1. Surface water.
2. 1/2 surface water and 1/2 filtered deep water (results doubled).
3. Surface water and complete enrichment medium.
4. Surface water and enrichment medium with NO_3^- omitted.
5. Surface water and enrichment medium with $PO_4^{=}$ omitted.
6. Surface water and enrichment medium with $Si\,O_3^{=}$ omitted.
7. Surface water and enrichment medium with $S_2\,O_3^{=}$ omitted.
8. Surface water and enrichment medium with Fe + trace metals omitted.
9. Surface water and enrichment medium with vitamins omitted.

The dark uptake of ^{14}C was not measured in these experiments, so the absolute rates of photosynthesis could not be calculated. The strength of the ^{14}C was approximately 10 μ curies. The samples enriched with iron and trace metals developed a slight precipitate which was removed on filtration. The counts are corrected for ^{14}C adsorbed on the filters and on this precipitate by means of appropriate blank experiments with filtered, sterile water.

This preliminary report will describe the results of enrichment experiments at 13 stations occupied on a section between Montauk Pt., New York and Bermuda on the oceanographic cruise *USNS Chain II* in December, 1958. The first seven stations included that part of the section across the continental shelf and into the Gulf Stream. The remaining six stations were located in the Sargasso Sea. The deep water used for the enrichment experiments was collected from 100 m or less at Stations 1-10, from 1000 m or more at Stations 11-16.

Table 2 shows the station numbers, positions, sonic depths, depth of the wind mixed layer (from bathythermograph records), depths from which the deep samples were taken for the enrichment experiments, and the concentrations of phosphate, nitrate plus nitrite, and silicate in the surface and deep samples. Table 3 shows the results of the individual enrichment experiments with photosynthesis (^{14}C uptake) reported as a percentage relative to the maximum carbon uptake observed in each experiment. This permits results to be compared from station to station, and to be averaged.

While the results from one station to the next were somewhat variable and inconsistent, certain trends in the data are obvious. Stations 1-10 were significantly different from Stations 11-16, so these two groups have been averaged separately. For the first group (shelf, slope, and Gulf Stream), the surface water controls averaged about 75 per cent of the samples enriched with complete medium. Adding subsurface water from depths to 100 m did not increase photosynthesis of the surface water. The omission of nitrate, phosphate, thiosulphate, and vitamins produced results not appreciably different from the complete enrichment, but the omission of silicate gave results which may be

Table 2. Description of the stations and water conditions where enrichment experiments were made (chemical concentrations in μ gA/1)

Sta. No.	*Position*		*Depth* (m)			PO_4		$NO_3 + NO_2$		SiO_3	
			Bottom	*Wind mixed*	*'Deep sample'*	*Surface*	*'Deep'*	*Surface*	*'Deep'*	*Surface*	*'Deep'*
1	40° 57′N	71° 48′W	40	40	30	0·77	0·81	1·28	1·33	1·18	1·41
2	40° 43′N	71° 40′W	70	70	60	0·89	0·89	0·78	2·13	2·81	2·70
3	40° 31′N	71° 34′W	67	67	60	0·69	0·70	3·24	3·88	4·12	3·76
7	39° 36′N	70° 56′W	2248	25	100	0·51	0·92	2·19	13·2	2·35	6·23
8	38° 49′N	70° 19′W	2862	61	100	0·33	0·65	1·51	7·65	2·35	4·70
9	38° 00′N	69° 39′W	4018	76	100	0·22	0·55	0·87	4·67	2·35	2·59
10	37° 10′N	68° 30′W	4574	25	100	0·08	0·30	0·18	0·23	1·06	1·06
11	36° 25′N	68° 02′W	4850	153	4785	0·12	1·35	0·16	—	1·18	32·81
12	35° 36′N	67° 20′W	4978	67	1000	0·13	1·35	0·30	14·6	—	13·52
13	33° 11′N	65° 15′W	4744	110	1000	0·13	1·51	0·08	14·9	1·18	15·11
14	33° 03′N	64° 58′W	4830	76	1000	0·13	1·34	0·08	16·1	1·18	13·88
15	33° 58′N	65° 49′W	5075	—	1000	0·10	1·51	0·12	14·8	1·29	14·94
16	34° 48′N	66° 30′W	5133	159	1000	0·14	1·48	0·38	18·0	1·76	15·41

Table 3. *Relative uptake of* ^{14}C *(24 hours at* 1500 *ft candles illumination) of enriched and unenriched surface water samples. (Headings of columns* 5-10 *represent substances omitted from the enrichment medium in each case)*

Sta. No.	*Control*	*Deep water*	*Complete medium*	$-NO_3$	$-PO_4$	$-SiO_3$	$-S_2O_3$	*– Vitamins*	– Fe + *Trace metals*
1	79	60	100	76	91	87	92	92	77
2	68	75	89	100	87	76	96	89	64
3	67	77	82	100	91	95	85	96	62
7	100	84	99	99	96	83	98	99	—
8	84	70	94	100	99	95	89	91	63
9	30	39	93	91	91	57	100	91	91
10	49	67	87	90	100	87	70	80	43
Mean (1-10)*	72	71	98	100	99	87	95	96	71
11	30	100	95	89	98	59	86	100	39
12	50	94	83	100	87	60	83	77	43
13	8	100	58	57	80	12	57	100	32
14	16	79	100	84	80	89	25	100	39
15	12	69	100	76	46	37	96	90	14
16	26	81	85	92	100	40	67	88	51
Mean (11-16)*	26	95	94	90	89	53	74	100	39

*—to a maximum of 100 in each case.

significantly lower. However, the enrichment with everything but the iron-trace metal mixture had exactly the same effect as no enrichment at all.

In the Sargasso Sea samples, the unenriched controls assimilated only about one quarter as much ^{14}C as the samples enriched with complete medium. Again the omission of nitrate, phosphate, and vitamins did not subtract from the effectiveness of the enrichment mixture. Thiosulphate may have helped somewhat, while if silicate was left out, only about half as much photosynthesis occurred as in the complete medium. The omission of iron and trace metals again had the most pronounced effect, reducing photosynthesis almost to the level of the controls. In this group of experiments, the addition of water from 1000 m or more of depth stimulated photosynthesis to almost exactly the same extent as did the enrichment with the complete artificial medium.

The fact that enrichment with deep water did not stimulate photosynthesis at the first group of stations is not surprising, since the water in most cases was wind-mixed to approximately the same depths as that from which the samples were taken, and, therefore, the surface and ' deep ' water were essentially the same. This is borne out by the relative concentrations of nitrate, phosphate, and silicate at the two depths (see Table 2). The same criteria demonstrate the dissimilarity between the truly deep water (1000 m or more) and the surface water at Stations 11-16, and help explain the stimulatory effect of the former upon photosynthesis.

But it was the artificial enrichment experiments, particularly at the Sargasso Sea stations, that produced the most surprising results. Although the surface concentrations of nitrate and phosphate were extremely low, the addition of these elements apparently had no effect on photosynthesis. This recalls the earlier statement that the phytoplankton may be dependent upon the rate of regeneration of these elements and/or their presence as dissolved organic compounds, and more-or-less independent of their instantaneous concentrations as inorganic salts.

Rather than nitrogen and phosphorus, the nutrients limiting photosynthesis in these waters appear to be silicate and one or more components of the iron-trace metal mixture. This does not imply, of course, that if these substances were present in excess, nitrogen and phosphorus would not eventually, perhaps very quickly, become the limiting factors. It does imply, however, that they would become limiting at a higher rate of photosynthesis, which is another way of saying that the rate of primary production in the Sargasso Sea, at the time of our observations, was limited by nutrients other than nitrogen and phosphorus.

The purpose of this paper is to point out the possibilities of this approach in studying nutrient relations to photosynthesis in the sea. The results of our preliminary experiments, while suggestive, are not in themselves adequate to establish new ideas or refute conventional ones. The obvious next step is to separate and distinguish the critical elements in the iron-trace metal mixture. With this and perhaps other refinements to the technique, seasonal and regional studies of the specific nutrient elements limiting primary oceanic production may be undertaken.

Acknowledgements—The authors were assisted in the field by R. B. WILLIAMS. The chemical analyses reported in Table 2 were carried out by N. CORWIN, R. F. VACCARO and F. A. RICHARDS.

Woods Hole Oceanographic Institution J. H. RYTHER
Woods Hole, Mass. R. R. L. GUILLARD

Contribution No. 1026 *of the Woods Hole Oceanographic Institution supported by the United States Atomic Energy Commission Contract AT* (30-1)-1918 *and by the National Science Foundation.*

Printed in Great Britain by The Salisbury Press Ltd,, Publicity House, Wilton Road, Salisbury, Wilts. (18732)

Contribution No. 1027

Deep-Sea Research, 1959, Vol. 6, pp. 72 to 74. Pergamon Press Ltd., London. Printed in Great Britain

LETTER TO THE EDITORS

Absorption curves of acetone extracts of deep water particulate matter

(*Received* 1 *April* 1959)

MEASUREMENTS of light scattering in sea-water have revealed the presence of considerable quantities of particulate matter at depths far below euphotic layers. The size of this particulate matter and its effects on the attenuation of submarine illumination have been extremely controversial subjects in oceanography. Many workers have felt that these particles are of much greater size than wavelengths of light that they scatter and hence they do not selectively scatter any particular visible wavelength. CLARKE and JAMES (1939) observed that the increased attenuation of light in sea-water was caused largely by ' suspendoids ' that could be removed by fine filtration. The ' suspendoids,' according to these workers, did not selectively attenuate light. According to Lord Rayleigh if particles are small compared to the wavelength of radiation, scattering will be proportional to $\lambda/4$. This selectivity due to small size causes shorter wavelengths to be more strongly attenuated. UTTERBACK'S data (1936) indicates that the selective absorption in sea-water is due, in part, to selective scattering. KALLE (1938) and BURT (1955a, b; 1958) are also of this opinion. KALLE has also shown that sea-water at times contains water soluble pigments which are yellow in colour, and claims that these pigments are representative of some fairly stable metabolic product of phytoplankton.

On a recent summer cruise to the Sargasso Sea (CRAWFORD, No. 17) we were able to collect large quantities of water at depths of 300, 500 and 1000 m. Particulate matter from these depths was immediately concentrated by passing the water through a Millipore-type AA filter. The pore size of this filter is approximately 0·80 μ. After about 10 l. of water had passed through the filter, signs of partial clogging were apparent, and at this point the filter became perceptively coloured. Generally 20 to 25 l. of water from each sample was filtered, after which the filters were removed and stored under refrigeration in the dark. In the laboratory, the filters were extracted in 90 per cent acetone for 24 hours in a darkened refrigerator. Each extract was adjusted to a constant volume of approximately 25 cm^3 and centrifuged in a standard clinical centrifuge for 15 minutes. The absorption spectra of the greenish extracts were measured between 400 and 700 mμ at 5 mμ intervals using a Beckman DU spectrometer with a 5 cm light path.

The absorption spectra of the extracts of deep water particulate matter are characterized by strong absorption between 400 and 500 mμ (Fig. 1). When these curves are compared to absorption curves from extracts of the surface water samples the former differ markedly by either the reduction or the absence of the chlorophyll peak in the region of 665 to 670 mμ. In many respects the shape of the absorption curves of the deep samples suggests the presence of algal carotenoids ; hence one might assume that the deep water extracts are representative of phytoplankton which has spent a considerable period in the darkness. It is well known that light is necessary for the development of chlorophyll *a*, and prolonged periods of darkness generally results in a gradual diminution of this chlorophyll peak.

The ratio of peak absorbencies at 420–430 mμ to 660 -670 mμ in natural phytoplankton populations range between 2-3 ; in nitrogen-starved algal cultures this ratio may be as high as four. Absorption ratios of this type for the 0 and 300 m samples are within the natural phytoplankton range; however, the 500 and 1000 m samples have ratios greater than twenty, thus illustrating the extent to which the greater absorption of blue light occurs in these extracts. If we are to assume that particulate matter at these depths is representative of dead and decomposing phytoplankton it is quite obvious from the absorption curves that the most stable component of the pigment system are carotenoids which absorb most strongly in the blue region.

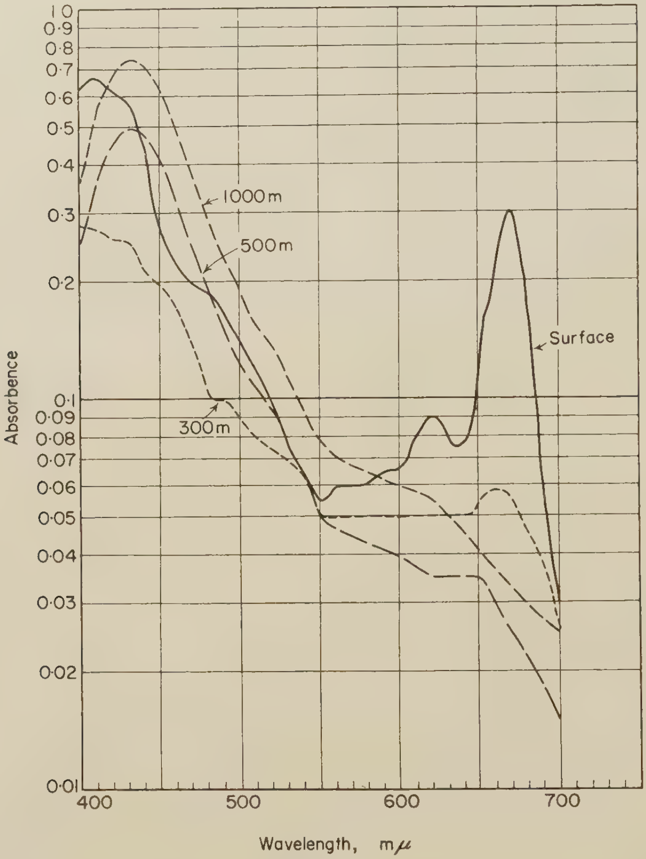

Fig. 1. Absorption curves of acetone extracts of particulate matter from the surface and three depths in the Sargasso Sea. July, 1957.

Regardless of the form of the particulate matter at these depths our observations indicate that the particles are strongly coloured. The actual size of the particles retained by the millipore filter are too large to have any selective influence on the scattering of visible light. However, the colour of these particles and their absorption of the blue light portion of the spectrum exert a selective influence on the attenuation of submarine radiation. This point appears to have been overlooked by many workers. It would appear that many of the observations of the selective attenuation of light by particulate matter may be partly, if not largely, due to absorption by coloured particles rather than being caused by Rayleigh scattering alone.

Woods Hole Oceanographic Institution C. S. Yentsch
Woods Hole, Mass. J. H. Ryther

Contribution No. 1027 *from W.H.O.I. Aided by A.E.C. Grant No. AT* (30-1)-1918.

REFERENCES

Burt W. V. (1955a) Interpretation of spectrophotometer readings on Chesapeake Bay waters. *J. Mar. Res.* **14**, 33-46.

Burt W. V. (1955b) Distribution of suspended materials in Cheasapeake Bay. *J. Mar. Res.* **14**, 47-62.

Burt W. V. (1958) Selective transmission of light in tropical Pacific. *Deep-Sea Res.* **5**, 51-61.

Clarke G. L. and James H. R. (1939) Laboratory analysis of the selective absorption of light by sea water. *J. Opt. Soc. Amer.* **29**, 43-45.

Kalle K. (1938) Zum problem der Mureswasserfarbe. *Aron. d. Hydrogr. emd Mar. Meteor,* Bd. **66**, S. 1-13.

Utterback C. L. (1936) Spectral bands of submarine solar radiation in the north Pacific and adjacent inshore waters. Conseil Perm. *Intern. p. L'Explor. de la Mer. Rapp. et Proa.-Verb.* **101**, pt. 2, No. 4.

Printed in Great Britain by The Salisbury Press Ltd., Publicity House, Wilton Road, Salisbury, Wilts. (18734)

Contribution No. 1028

Särtryck ur Tellus nr 1, 1959

Computations of the Growth by Condensation of a Populatio of Cloud Droplets

By W. MORDY, International Meteorological Institute in Stockholm[1]

(Manuscript received June 15, 1958)

Abstract

The number and size of cloud droplets formed on several condensation nucleus spectra is computed numerically. The relative humidity is treated as a dependent variable and the settling of droplets by Stokes Law is accounted for.

A model is presented for studying simultaneous variations in vertical velocity, nucleus distribution, and humidity by the use of an electronic computer. To date eight computations have been made for three types of nucleus spectra at different rates of rise. Both nucleus distribution and rate of rise produce significant differences in resulting cloud droplet distributions.

The concentration of cloud droplets computed ranges from 1 cm^{-3} to 470 cm^{-3} for vertical velocities ranging from 5 cm/sec to 100 cm/sec.

1. Introduction

In the development of a cloud the spectrum of droplet sizes is initially determined by the number and size of condensation nuclei and the rate of cooling of the air. Subsequently the spectrum is altered by turbulence, coalescence, evaporation, sedimentation, and entrainment or mixing. Still later modification may occur by the Bergeron process.

Because these later processes act to modify the *initial* distribution it is important in the study of such processes to know in some detail the character and importance of the factors which control the shape of this *initial* distribution formed by condensation.

To date one of the most complete investigations of this kind has been made by HOWELL (1949) who investigated the growth of a population of varied sized droplets in
cooled at a uniform rate. In the years followi
Howell's work Woodcock made detail
measurements of the number and size of co
densation nuclei larger than 10^{-12} g (Howel
max. size) and found them to be a very in
portant portion of the nucleus spectrum
terms of the mass of salt found in the air.

The spectra of condensation nuclei used
Howell therefore will be replaced here by ne
ones based on more recent information whi
indicates appreciable numbers of very lar
nuclei. These "giant nuclei", as they are som
times called, are in some instances large enou
at cloud base to have appreciable fall velociti
a factor for which it was not necessary
account in Howell's investigation. A n
investigation requires therefore also that t
sedimentation of droplets be considered.

Howell formulated a growth equation fo
droplet growing by condensation. It is
ordinary differential equation in which t
growth is mainly dependent on only fo

---

[1] This work has been supported by the U.S. Office of Naval Research and the Woods Hole Oceanographic nstitution. Contribution number 1028 of the Woods Hole Oceanographic Institution.

ctors, namely the radius, humidity, nucleus ze, and time. Because of the very large variaons in the growth rate of different sized conensation nuclei, and because of the "feed ack" of the water vapor consumption, by ondensation, on the humidity of the droplet nvironment, integration of this equation for a opulation of droplets becomes a laborious sk. Howell proceeded with hand computaons for three cases, believed to be characeristic of natural conditions and chosen to epresent conditions which would demonstrate ariations in the drop size spectrum. He found mong other conclusions that the "conditions nder which operation of the growth equation ost favors a broad spectrum are not adeuately clarified". This somewhat indecisive esult was due at least partly to inadequate nformation about the condensation nuclei.

With modern computer techniques and ith new observational information it now eems desirable to make a new and extended pproach to this problem.

The author presents here a mathematical odel which lends itself to an extension of owell's work by investigation of a number f additional factors which influence droplet rowth by condensation.

. The model and its behavior

Consider a column of air rising vertically. t the base of this column, air is being introuced which contains a given population of ifferent sized condensation nuclei. The smallest f these nuclei are initially at near equilibrium ith the humidity conditions in their environent. The largest nuclei because of their latively slow growth are arbitrarily assigned a ze which represents a certain lag in adapting the environment.

The air in the column rises, according to a iven function of height and time, increasing decreasing the relative humidity by adiabatic pansion or compression. The droplets grow, cording to the condensation drop growth uation, reducing the relative humidity by nsuming water vapor and adding heat to e environmental air.

The relative humidity or supersaturation creases until a level is reached where the nsumption of water vapor by the droplets d the latent heat of condensation balance e humidity changes which would result from the adiabatic cooling. At this point of balance the highest supersaturation is reached. This maximum value determines the smallest size of condensation nucleus which will exceed its critical radius according to the classical curves of KÖHLER (1926), which in a revised form are given in figure 1 showing the equilibrium radii for droplets with given nuclei at given relative humidities. Droplets which exceed this critical radius continue to grow as long as the relative humidity exceeds the equilibrium values for the droplets. Droplets which fall short of this critical radius cannot exceed the equilibrium value and will remain on the lower or stable side of the curve.

Therefore when maximum supersaturation is reached, the droplet size spectrum is divided into growing cloud droplets on the one hand and nucleus droplets nearly in equilibrium on the other.

The balance struck between the growing droplets and the humidity changes which result from cooling, is soon altered. As the radii of these droplets increase, their water consumption also increases, until they consume more water than for the balanced condition. The supersaturation is thus reduced gradually following the growth of the particles.

The largest of these droplets will settle noticably against the rising air. If the rate of settling is an appreciable portion of the vertical velocity, the concentration of these particles increases. For any given size of nuclei when the fall velocity of the particles equals the vertical velocity of the air, a high concentration of droplets may exist in a thin horizontal layer which in turn may affect the water consumption for this layer and therefore the humidity conditions. In certain cases, therefore, the maximum humidity or supersaturation is influenced by this increased population of larger drops. This process would be especially important in the lowest few meters of the cloud. Although it is not a part of the phase of the investigation reported here it should be pointed out that coalescence between droplets quite conceivably could by this mechanism exert a strong influence on subsequent droplet growth by condensation. The resulting influence would be to reduce the number of growing droplets as time passes. These fewer droplets therefore will grow faster than the preceding ones.

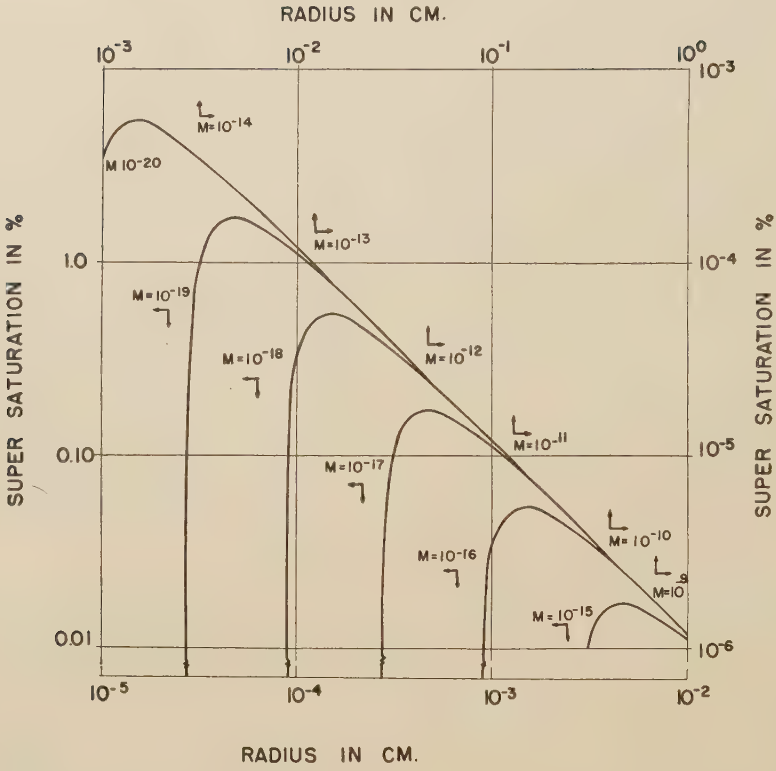

Fig. 1. Köhler type equilibrium curves for droplets formed on given nuclei sizes. Coordinates given at the left and bottom indicate humidity and radius for NaCl nucleus size M in moles indicated at left of curves while coordinates at top and right indicate values for nucleus size indicated at right of curve.

For the sake of simplicity the above remarks have referred to a steady, rising current with a fixed nucleus spectrum. In the model as it is actually used, it is possible to make the vertical velocity a function of time and height and hence better to simulate cloud conditions. The number of condensation nuclei introduced at cloud base can also be altered during the course of the computation. In fact, a variety of circumstances can be studied, i.e. vertical velocity, temperature and humidity, nuclei distribution. The results of some of these altered considerations will be given in a subsequent report.

3. The droplet growth equation

To compute the growth of a droplet in a changing environment of temperature and humidity one must know the rate of diffusion of water vapor to the droplet, and the rate of diffusion of heat away from the droplet Knowing these factors and the heat capacit of the droplet, one can determine its heat water vapor budget and hence growth.

Evaporation or condensation of the drople or droplets affects the environment which i turn affects the subsequent particle growth so no computation of droplet growth is adequate for meteorological purposes which doe not consider droplets *in relation to each othe and in relation to a changing environment.*

The growth of a droplet by diffusion ma be satisfactorily expressed by:

$$\frac{dm}{dt} = 4\pi r \frac{\varepsilon D}{RT}(e_\infty - e_r) \qquad (1$$

for a steady state case (for example, JOHNSO 1954):

where m = mass of droplet
ε = ratio of molecular weight of water vapor and air
D = water vapor diffusion coefficient
R = *the gas constant*
T abs temperature
r = droplet radius

The equilibrium vapor pressure over a droplet was derived by Kelvin (1870) and modified and revised for meteorological purposes by Köhler (1926). Equations governing the growth of droplets by condensation have been given as well by Howell (1949), Vierhout (1949), Squires (1953), Mason (1957) and others. The equations, as presented here, differ in certain details following the suggestions of McDonald (1953), Mason (1957 a), and Rooth (1957).

The expression for the equilibrium condition is:

$$e_r = e_{T_r}\left(1 + \frac{2\sigma\varepsilon}{\varrho R T r} - \frac{3iMm_\omega}{4\pi\varrho r^3}\right) =$$

$$= e_{T_r}\left(1 + \frac{A}{r} - \frac{iBM}{r^3}\right) \qquad (2)$$

$$A = \frac{2\sigma\varepsilon}{\varrho R T} \qquad B = \frac{3m_\omega}{4\pi\varrho}$$

where e_r = vapor pressure over the *droplet* surface in bars
e_{T_r} = *saturation* vapor pressure at the temp T_r in bars
σ = surface tension of water at temp T in dynes/cm²
ε = ratio mol · wt H_2O to dry air = 18/29 = .621
R = gas const $= 1.87 \times 10^6$ ergs g^{-1} $°C^{-1}$
T = temp in °K
r = droplet radius in cm
i = van 't Hoff factor (2)
M = wt in moles of condensation nucleus
m_ω = mol wt of water
ϱ = density of water g/cm³

Two terms in this expression should be pecially noted. The first is the term containing A which describes the increase of the vapor pressure over the curved surface of the droplet. The second term is the one containing B which describes the lowering of the vapor pressure by the presence of a solute, in this case assumed to be NaCl, in the droplet.

The ambient vapor pressure, (e_∞), at a distance far enough from the droplet to be unaffected by it we shall presume is the saturation vapor pressure corresponding to the dewpoint temperature of the air. The vapor pressure at the surface of the droplet, (e_r), is the vapor pressure of a droplet of salt solution with a known nucleus size and at the temperature of the *surface* of the droplet. The temperature of the droplet surface cannot be known directly in the condensation process and must be deduced from a consideration of the heat balance of the droplet in a known environment.

a) *Drop temperature*

To do this, one must have a second equation which describes the heat budget of the droplet. The diffusion of heat to or away from a droplet, analogous to equation (1), is given by:

$$\frac{dQ}{dt} = 4\pi r k (T_\infty - T_r) \qquad (3)$$

where k = thermal diffusion coefficient
$\frac{dQ}{dt}$ = the heat flux inwards through the droplet surface
T_∞ = the temperature of the environment at a sufficient distance to be unaffected by the droplet
T_r = the temperature of the droplet surface

To determine the droplet temperature we may consider that the heat gained by condensation, less the heat lost by heat diffusion, equals the change in heat stored in the droplet, i.e.

$$L\frac{dm}{dt} + \frac{dQ}{dt} = \frac{4}{3}\pi r^3 \varrho c \frac{dT_r}{dt} \qquad (4)$$

c = specific heat
ϱ = density of liquid water
L = latent heat of evaporation of water

Strictly, T_r, should be the average temperature within the droplet but it has been written here as approximated by the surface temperature. The term containing $\frac{dm}{dt}$, as taken from equation (1), is expressed in terms of the vapor pressure. The objective here is to express the drop temperature in terms of the ambient temperature and dew point. This is done by use of the Clausius-Clapeyron equation, that is

$$\frac{1}{e}\frac{\Delta e}{\Delta T} = \frac{\varepsilon JL}{RT^2}$$

or

$$e - e_0 \approx \frac{\varepsilon JLe}{RT^2}(T - T_0) \qquad (5)$$

if $\Delta e \ll e$

where J = mech. equiv. of heat,
e, e_0 = vapor pressure at T, T_0

Using equation (5) as:

$$e_{T'} - e_{T_r} = \frac{\varepsilon JLe}{RT^2}(T' - T_r)$$

where T' = dew point temperature
$e_{T'}$ = sat. vapor pressure at T'
e_{T_r} = sat. vapor pressure at T_r

and the equilibrium vapor pressure over a droplet of dilute salt solution written as:

$$e_r = e_{T_r}\left(1 + \frac{A}{r} - \frac{iBM}{r^3}\right)$$

we can write that:

$$e_{T'} - e_r = \frac{e\varepsilon JL}{RT^2}\left(T' - T_r - \frac{A^\star}{r} + \frac{iB^\star M}{r^3}\right) \quad (6)$$

where

$$A^\star = \frac{RT^2}{\varepsilon JL}A$$

$$B^\star = \frac{RT^2}{\varepsilon JL}B$$

and $\frac{e_{T_r}}{e}$ is taken ≈ 1 when multiplied by $\left(\frac{A}{r} - \frac{iBM}{r^3}\right)$

If we substitute this in equations (1) and we have then:

$$\frac{4}{3}\pi r^3 c\frac{dT_r}{dt} + 4\pi rk(T_r - T_\infty) =$$

$$= L\cdot\frac{\varepsilon D}{RT}\left[\frac{\varepsilon JLe}{RT^2}\left(T' - T_r - \frac{A^\star}{r} + \frac{iB^\star M}{r^3}\right)\right]$$

where $\varrho_\omega = 1$.

This gives us an equation from which can determine the drop temperature from ambient temperature and the dew point te perature. From (7) we write:

$$c_1\frac{dT_r}{dt} + c_2(T_r - T_\infty) =$$
$$+ c_3(T'^\star - T_r)$$

where

$$c_1 = r^2/ec$$
$$c_2 = k$$
$$c^3 = \frac{L\varepsilon D}{RT}\left[\frac{\varepsilon DLe}{RT^2}\right]$$

$$T'^\star = T' - \frac{A^\star}{r} + \frac{iB^\star M}{r^3}$$

HOWELL (1949), SQUIRES (1952) and ARC and KEITH (1954) have pointed out, howev that a complete solution to this equation unnecessary as the heat capacity of the drop may be neglected. Writing this equation

$$T_r = \frac{c_3 T'^\star + c_2 T_\infty}{c_3 + c_2} + \frac{1}{c_3 + c_2}\frac{dT_r}{dt}$$

the second term on the right side of equat (8) indicates the lag in temperature of droplet due to its heat storage. The rate can not be expected to be much larger th the rate of change of the temperature of environment $\frac{dT_\infty}{dt}$ which can easily be e mated. For drops less than 100 μ theref the lag will not exceed ± .005° C assumin lapse rate of 0.01° C/m and a vertical veloc of 3 m/sec and will be 5×10^{-6}° C for 1 droplets. This is negligible in relation to the other terms.

From equations (1), (2), (5) and (8) we can now write

$$\frac{dm}{dt} = 4\pi r \frac{\varepsilon D}{RT}(e_\infty - e_r) =$$

$$= 4\pi r \frac{\varepsilon D}{RT}(e_\infty - e_s + e_s - e_r)$$

Here we shall designate e_s to mean the saturation vapor pressure at the ambient temperature T_∞ (i.e. corresponds to the saturation mixing ratio as opposed to the actual mixing ratio).

From equation (5) we can write,

$$e_s - e_r = e_s - e_{T_r}\left(1 + \frac{A}{r} - \frac{iBM}{r^3}\right)$$

From equation (5)

$$e_s - e_{T_r} = \frac{\varepsilon JLe}{RT^2}(T_\infty - T_r)$$

From equation (8), by omitting the term containing $\frac{dT_r}{dt}$,

$$L\frac{dm}{dt} = 4\pi kr(T_\infty - T_r)$$

Combining these expressions we get

$$e_s - e_{T_r} = \frac{\varepsilon JLe}{RT^2} \cdot \frac{L}{4\pi kr}\frac{dm}{dt}$$

The growth equation then becomes

$$\frac{dm}{dt} = 4\pi r \frac{\varepsilon d}{RT}\left[e_\infty - e_s - e_{T_r}\left(\frac{A}{r} - \frac{iBM}{r^3}\right)\right] +$$

$$+ \frac{4\pi r \varepsilon D}{RT} \cdot \frac{\varepsilon JL^2 e}{kRT^2} \cdot \frac{1}{4\pi^2}\frac{dm}{dt}$$

or

$$\frac{dm}{dt} = \left(\frac{1}{1 + \frac{\varepsilon^2 JL^2 De}{kR^2T^3}}\right) 4\pi r \frac{\varepsilon D}{RT}$$

$$\left[e_\infty - e_s - e_{T_r}\left(\frac{A}{r} - \frac{iBM}{r^3}\right)\right]$$

In the last term of the expression e_{T_r} can be replaced by e_s without seriously changing the results since it is the difference between $\frac{A}{r}$ and $\frac{iBM}{r^3}$ which is the dominating quantity here. In this way the equation takes the form

$$\frac{dm}{dt} = 4\pi r \frac{\varepsilon D}{RT}\left(\frac{1}{1 + \frac{\varepsilon^2 JL^2 De}{kR^2T^3}}\right) \cdot$$

$$\cdot \left[e_\infty - e_s\left(1 + \frac{A}{r} - \frac{iBM}{r^3}\right)\right] \tag{9}$$

The term

$$\left(\frac{1}{1 + \frac{\varepsilon^2 JL^2 De}{kR^2T^3}}\right)$$

indicates the modification of the vapor pressure difference between the droplet and the environment caused by the heating associated with the droplet growth.

b) *The vapor pressure reduction due to the dissolved nucleus*

The nuclei used in the present computations are assumed to be composed of sodium chloride while the numbers of these nuclei correspond to the numbers of *sea salt* particles as measured by Woodcock (1949), Moore and Mason (1957), or in the case of the very smallest particles by Junge (1952). It is necessary therefore to compare the reduction in vapor pressure over solutions of sea salt and sodium chloride to see how well they correspond at concentrations implied by the droplet sizes involved in the computations.

The vapor pressure reduction over sea salt solutions has been investigated in some detail by Arons and Kientzler (1954). It will therefore suffice to compare the reduction in vapor pressure of NaCl as indicated in the growth equation (9), with the values they determined empirically, to establish the accuracy of the assumption made in the computation.

As computed in the growth equation, the reduction in vapor pressure due to the presence of the salt nucleus is an approximate form of

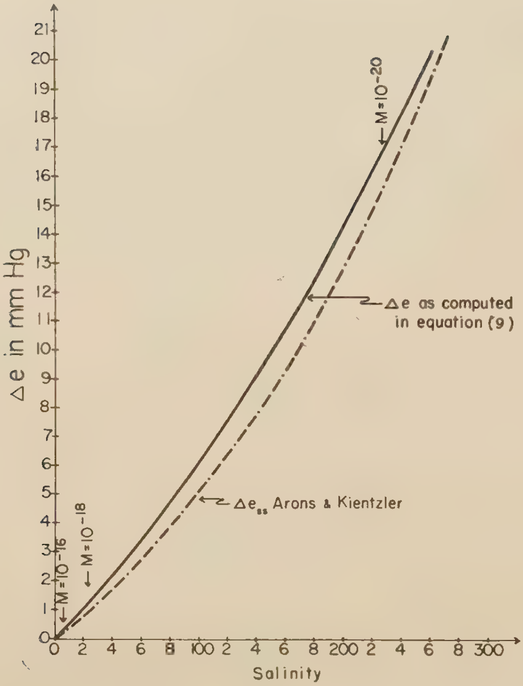

Fig. 2. The reduction of vapor pressure over sea salt solution of varying salinity (Arons and Kientzler) and over solutions of NaCl as assumed in the computations here. Concentrations found in small droplets in equilibrium with 100 % rel. hum. are indicated by arrows along the curve.

Raoult's Law as modified by the van 't Hoff factor, i.e.

$$\frac{\Delta e}{e}=\frac{im_s}{im_s+m}\approx\frac{im_s}{m}$$

or

$$\frac{\Delta e}{e}=\frac{iMm_\omega}{\frac{4}{3}\pi r^3\varrho}$$

as given in equation (9).

Therefore, if we plot Δe as computed in this approximate form to $\Delta e_{(\text{sea salt})}$ as measured by Arons and Kientzler, we can estimate the error caused by assuming a NaCl nucleus. This has been done in figure 2 for 10° C. Salinity in the case of the empirical data is computed in the usual way from the chlorinity (sal $=0.03+1.805$ cl, SVERDRUP ET AL, 1942). Salinity as *computed* was the approximate value m_s/m rather than $\frac{m_s}{m_s+m}$. The van't Hoff factor varies from 1.82 to 2.91 according to M DONALD (1953) in the range of values co sidered, but in these computations it was co sidered constant, $i=2$.

The computed values of Δe are not mo than 15 % from the empirical sea salt valu which is not a serious factor in the comput tions in view of the uncertainties concerni the exact chemical composition of the nucl Analyses of rainwater such as reported l ERIKSSON (1952) and MORDY (1953) indica that salts do not appear in rainwater in t same ratio as in sea water. Furthermore, whi the assumption that the nuclei are sea salt m be relatively safe in the case of the very lar nuclei as measured by WOODCOCK, the small particles as has been shown by JUNGE (195 and others, may consist of a variety of su stances. These smaller particles sometimes co sist of highly concentrated solutions even 100 % relative humidity due to the size of t capillarity term A/r in the growth equati (10) below.

It will later be shown that the domina factor in the initial condensation process determining the environmental humidity a therefore droplet number for a given nucle distribution, is the rate of cooling, and that consideration of this controlling factor, sm errors in the nucleus term are relatively uni portant.

c) *Ventilation*

The work of FRÖSSLING (1938) shows th the modification of this equation necessary provide for ventilation of the droplets is give by empirically determined coefficients to t diffusion equations, i.e.

$$\frac{dm}{dt}=4\pi r\frac{\varepsilon D}{RT}(e_\infty-e_r)F_1$$

$$\frac{dQ}{dt}=4\pi rk(T_\infty-T_r)F_2$$

where

$$F_1=F_1(R_e,\sigma)=1+0.276\sqrt[3]{\sigma}\sqrt{R_e}$$

$$F_2=F_2(R_e,\sigma')=1+0.276\sqrt[3]{\sigma'}\sqrt{R_e}$$

and R_e = Reynold's number.
σ = Prandtl's number.
σ' $=\nu/D$

when these ventilation coefficients are introduced in the equations above, equation (9) becomes:

$$\frac{dm}{dt} = 4\pi r \frac{\varepsilon D}{RT} F_1 \left[\frac{1}{1 + \frac{\varepsilon^2 J L^2 De}{kR^2 T^3}} \right] \cdot \qquad (10)$$

$$\cdot \left[e_\infty - e_s \left(1 - \frac{A}{r} + \frac{iBM}{r^3} \right) \right]$$

Errors due to the omission of the ventilation terms are not serious before the radius exceeds 30 microns. In the experimental measurements of droplet growth of Keith and Arons (1954), they conclude that it is not important for droplets of a radius less than 50 or 60 microns.

d) *Diffusion coefficients for small droplets*

Rooth (1957) has shown that for small droplets, $r < 5\ \mu$, the condensation coefficient of water molecules on a water surface becomes an important factor in determining the rate of droplet growth.

In the case of equilibrium

$$q_e = \beta q_c$$

where q_e = molecules escaping surface
q_c = molecules colliding with surface
β = condensation coefficient

From gas kinetics

$$q_c = \frac{e}{\left(\frac{2\pi RT}{\varepsilon}\right)^{\frac{1}{2}}} \text{ and the refore } q_e = \frac{\beta e_0}{\left(\frac{2\pi RT}{\varepsilon}\right)^{\frac{1}{2}}}$$

If the evaporation

$$q = q_e - \beta q_c$$

$$e = e_0 \left(1 - \frac{q}{\beta q_e} \right)$$

For a sphere, as in equation (1)

$$\frac{dm}{dt} = -4\pi r^2 q = 4\pi r^2 \frac{\varepsilon D}{RT} \left(\frac{e_\infty - e_r}{r} \right)$$

But

$$e_r - e_s = \frac{-q e_0}{\beta q_e} = \frac{-q}{\beta} \sqrt{\frac{2\pi RT}{\varepsilon}}$$

$$= \frac{e_\infty - e_r}{r} \cdot \frac{\varepsilon D}{RT\beta} \sqrt{\frac{2\pi RT}{\varepsilon}}$$

If we let

$$l = \frac{D}{\beta} \sqrt{\frac{2\pi\varepsilon}{RT}}$$

then

$$e_r - e_s = \frac{l}{r} (e_\infty = e_r)$$

Eliminating we get

$$\frac{dm}{dt} = 4\pi r^2 \frac{\varepsilon D}{RT} \left(\frac{e_\infty - e_0}{l + r} \right)$$

If the droplet radius is comparable to or smaller than the mean free path in the surrounding gas, then a further correction for the geometry of the collisions has to be made.

Although the values for β are difficult to determine and are therefore somewhat uncertain, using the values at hand, Rooth calculates, with $\beta = .036$ at 10° C (Alty and Mackay), that $l = 5.1\ \mu$

If we therefore apply this correction $\left(\frac{r}{r + l} \right)$ to the diffusion coefficient, we find that its values differ markedly from Langmuir's values as used by Howell and Squires.

Langmuir's (1944) corrections to the diffusion coefficients are given as:

$$\frac{1}{D'} = \frac{r}{D(r + a\lambda)} + \frac{1}{r} \sqrt{\frac{2\pi\varepsilon}{RT}}$$

D' = modified diffusion coefficient
a = Cunningham constant
λ = mean free path of water molecules in air.

In the above expression the first term is for the purpose of correcting for the geometry of capture of the molecules. The second term is the same as described by Rooth except that a has been assumed to be $a = 1$. If this expression is put in comparable form to the expressions above, we find

$$\frac{1}{D'} = \frac{1}{D} \left[\frac{r}{r + a\lambda} + \frac{\varepsilon D}{rRT} \sqrt{2\pi RT} \right]$$

$$= \frac{1}{D} \left[\frac{1}{1 + \frac{a\lambda}{r}} + \frac{\beta}{r} \right]$$

$$\text{or,} \qquad D' = D \left[\frac{r\left(1 + \frac{a\lambda}{r}\right)}{r + \beta l \left(1 + \frac{a\lambda}{r}\right)} \right]$$

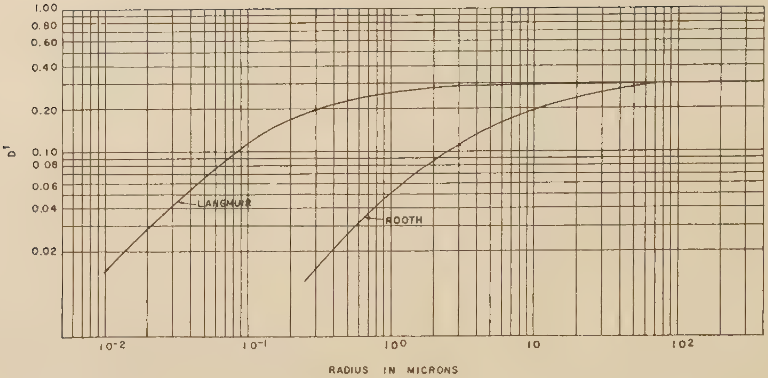

Fig. 3. A comparison of the correction to the water vapor diffusion coefficient for small droplets as used by Langmuir and Howell, and the values used here as derived by Rooth.

while Rooth's expression is:

$$D' = D\left[\frac{r}{r+l}\right]$$

It should be noted here that the term

$$\left(1+\frac{a\lambda}{r}\right)$$

is important only when $a\lambda$ is comparable to r. As

$$\lambda \approx 10^{-5}\ \text{cm} \quad \text{and} \quad a = 0.7$$

this term becomes important for droplets $< 0.1\ \mu$ but has been neglected in the present computations.

By analogy the heat diffusion coefficient is written:

$$\frac{1}{k'} = \frac{1}{k}\left[\frac{1}{1+\frac{a\lambda}{r}} + \frac{4k}{r\varrho_a c_p f}\sqrt{\frac{\varrho_v}{3e}}\right]$$

Graphs of the values of the water vapor diffusion coefficients for different values of r are given in figure 3.

e) *Final equation*

After these considerations, the droplet growth equation as used in the computation is written

$$\frac{dm}{dt} = 4\pi r^2 \varrho \frac{dr}{dt} = 4\pi\left(\frac{r^2}{r+l}\right)\frac{\varepsilon D}{RT}F_1 \cdot$$

$$\left(\frac{1}{1+\frac{\varepsilon^2 JL^2 De}{kR^2T^3}}\right)\left[e_\infty - e_s\left(1-\frac{A}{r}+\frac{iBM}{r^3}\right)\right] \text{(1}$$

The term $\frac{F_1}{F_2}$ as it occurs in the temperatu feedback term $\left[\frac{1}{1+\frac{\varepsilon^2 JL^2 De}{kR^2T^3}\left(\frac{F_1}{F_2}\right)}\right]$ is ve nearly equal to one in the particle size rang involved in the computations and has be neglected.

4. Computational procedure

Numerical computations were accomplishe by the following stepwise procedure.

1) cooling the parcel containing the dropl (i.e. reducing p),
2) computing droplet growth,
3) computing humidity and temperatu changes,
4) computing droplet settling and positio
5) introducing new droplets at the clou base,
6) repeating the process.

This is indicated in the block diagram giv in fig. 4.

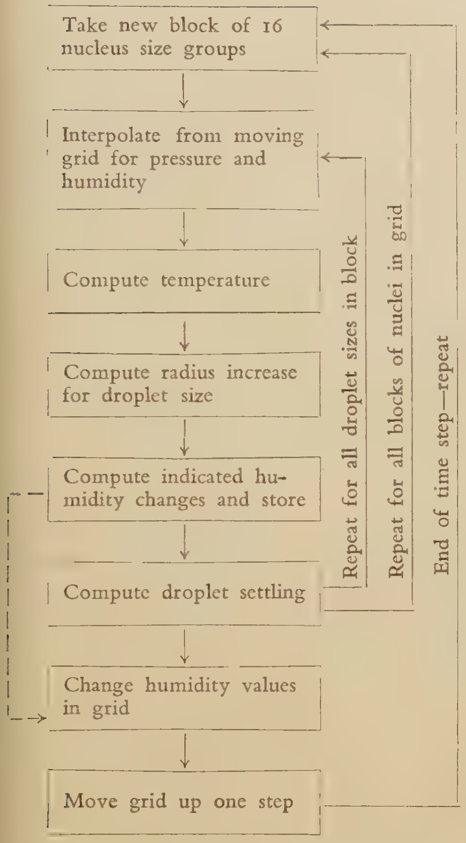
Take new block of 16 nucleus size groups
Interpolate from moving grid for pressure and humidity
Compute temperature
Compute radius increase for droplet size
Compute indicated humidity changes and store
Compute droplet settling
Change humidity values in grid
Move grid up one step
Repeat for all droplet sizes in block
Repeat for all blocks of nuclei in grid
End of time step—repeat

Fig. 4. Block diagram for computing sequence.

The position of the droplets was defined ith respect to a grid moving upward with e same speed as the vertical wind velocity. ach fourth time step a new grid level was dded at the bottom of the column. Each me step a new block of nuclei was added to e base of the column. The nucleus distri- ution was represented by this block of 16 zes (values of *M*) or groups of nuclei with e number of particles assigned to each of ese groups according to the different nucleus istributions assumed. Values of the environ- ental temperature and humidity, which ere obtained for the growth of the nuclei, ere determined by appropriate interpolation this moving grid system. Humidity and mperature corrections due to condensation ere apportioned to the immediate upper and wer grid level above and below the droplets cording to the position of the droplets tween the levels. These corrections were summed for all droplets through one time step before they were applied at each level.

a) *Temperature changes*

The temperatures of the individual air parcels were determined by interpolation from the moving grid system. Temperature changes on this grid were accomplished by computing the adiabatic change in temperature (approximated) for the increment in pressure assumed for each time step, and correcting this change by the latent heat released as indicated by the change in mixing ratio resulting from the condensation on the droplets. These changes in the mixing ratio were made by dividing the condensed water on each size group of droplets between the upper and lower grid level according to the droplets' position between the grid levels. The change in the mixing ratio at the end of each time step was the sum of all such corrections for droplets in the levels lying just above or below the grid level in question.

The adiabatic temperature change was approximated by a linear expression so that temperature changes were computed by

$$T_\infty = T_0 + K_1(p - p_0) + K_2(x - x_0)$$

where T_∞ = the temperature
p = pressure
x = mixing ratio.
The constant K_1 = the average dry adiabatic lapse rate assumed for the pressures used (≈ 0.1° C/mb).
K_2 = the latent heat of evaporation divided by the density and specific heat of the air.

Buoyancy effects due to heat changes were not considered as the air was displaced vertically according to assumed rates of rise.

b) *Droplet growth*

As indicated in sections 4 and 6, droplets were classified according to the size of their nucleus. Droplet radius and pressure level (i.e. location) were stored in the computer, the appropriate nucleus size and number being indicated by the storage cell where this information was kept. As needed for droplet growth computation, pressure, temperature and humidity were obtainable from the grid system; radius, nucleus size, and droplet height location from the stored blocks of nuclei information.

The droplet growth equation (11) in finite difference form was written simply,

$$\Delta r = \Delta t \cdot F_1 \cdot \alpha \left(\frac{1}{1 + \frac{l}{r}} \right) \cdot \left[px - \varepsilon e_s \left(1 + \frac{A}{r} - \frac{2BM}{r_3} \right) \right] \qquad (12)$$

where

$$\alpha = \frac{D}{RT} \left[\frac{1}{1 + \frac{\varepsilon^2 JL^2 De}{kR^2 T^3}} \right] \approx \alpha_0 + \frac{\partial \alpha}{\partial T} dT = \alpha_0 + \alpha_1 \Delta T$$

where $\Delta T = T_\infty - T_0$

and e_∞ was approximated from $x = \frac{\varepsilon e_\infty}{p - e_\infty} \approx \frac{\varepsilon e_\infty}{p}$

The saturation vapor pressure e_s was determined from an empirical expression derived from the saturation vapor pressure data, that is,

$$e_s = e_0 + \frac{\partial e}{\partial T} dT + \frac{\partial^2 e}{\partial T^2} dT^2 = $$
$$= e_0 + e_1 \Delta T + e_2 \Delta T^2$$

the values of e_1, and e_2 being computed from the vapor pressure tables appropriate to the initial conditions.

c) *Droplet sedimentation*

Droplet motion was assumed to be determined by Stoke's law, that is,

$$v = \omega - \frac{2 \varrho g r^2}{9 \eta} \approx \omega - kr^2$$

where ω = the vertical velocity of the air current
ϱ = density of water
g = gravitational acceleration
η = coefficient of viscosity of air

This assumption is reasonable as long as the droplets are less than 40 μ in radius (GUNN and KINZER 1949).

5. Special problems in the computation

The rate at which very small droplets re
to changes in the ambient humidity is e
tremely fast and this fact necessitates qu
short time steps and small changes in the hum
ity during the computations. However, or
the term containing the nucleus diminish
in importance, i.e. when the droplets rea
their critical radius $\left(r_c = \sqrt{\frac{3iBM}{A}} \right)$ on t
Köhler equilibrium curves fig. 1, grow
proceeds more slowly. A limitation in t
length of time step which can be taken occu
when the changes indicated in pressure, humi
ity, and temperature for a given time step a
too small for accurate representation in t
storage of the computer. Furthermore, d
to the storage capacity of the BESK comput
the length of the computations is limited
256 time steps or 64 grid levels. If very sho
time steps are chosen, computations can or
proceed for only a very short drop growth p
riod. A useful measure of this time scale is giv
by the time constant, the time it would ta
a droplet not in equilibrium with an enviro
ment of constant temperature and humidi
to decrease its deviation from equilibrium
a factor 1/2.718.

The time constant as computed is:*

$$t_0 = \frac{1}{-\frac{1}{\Delta r}\frac{d(\Delta r)}{dt}} - \approx \frac{1}{\frac{\partial}{\partial r}\left(\frac{dr}{dt}\right)} \text{ where } \Delta r = r -$$

$$\frac{\partial}{\partial r}\left(\frac{dr}{dt}\right) \approx \frac{\partial}{\partial r}\left(\frac{\alpha}{r}\right) \left[e_\infty - e_s \left(1 + \frac{A}{r} - \frac{iBM}{r^3} \right)\right.$$

$$\approx -\frac{\alpha}{r^2} \left[e_\infty - e_s \left(1 + \frac{2A}{r} - \frac{4iBM}{r^3} \right) \right]$$

$\alpha \approx$ const

At 100 % R.H., $e_\infty = e_s$ and for a nucl
droplet in equilibrium $\frac{A}{r} = \frac{iBM}{r^3}$

---

* In these expressions the corrections of the w
vapor diffusion coefficient have been omitted, t
become important when the nucleus size $M <$ 10
However for sizes smaller than this the time const
is very small and variation in the time constant du
these corrections have little significance in the pres
computations.

herefore

$$t_0 = \frac{r^5}{2\alpha iBMe_s} = \frac{(iBM)^{3/2}}{2\alpha A^{5/2} e_s} \approx 1.9 \times 10^{24}(M)^{3/2}$$

haracteristic values of t_0 are given in table 1.

able 1. Time constants for various nucleus sizes at 100 % humidity.

	10^{-12}	10^{-13}	10^{-14}	10^{-15}	10^{-16}	10^{-17} moles
	1.9×10^{6}	58×10^{3}	1.9×10^{3}	58	1.9	.058 seconds

t the critical radius on the equilibrium curves,
ig. 1, $t_0=\infty$, i.e.

$$\frac{de}{dr}=0, \quad \frac{A}{r_c^2}=\frac{3iBM}{r_c^4}, \quad e_\infty - e_s = \frac{2iBMe_s}{r^3}$$

is easily shown that the time constants
ngthen as the particles grow.

The nuclei used in the computations ranged
1 size from $M=10^{-10.2}$ to $M=10^{-19.2}$. For
he smallest nuclei therefore it was not possible
o use time steps short enough to overcome
he problem of their very rapid growth.

It was possible to circumvent this problem
y comparing the computed droplet growth
or each change in humidity with an approxi-
nate growth amount taken from its equilib-
ium value before and after the change in
umidity. If the computed growth was too
rge (i.e.8 $\Delta r > r$) then the equilibrium value
ppropriate to the environmental humidity
as substituted. It was found that this was nec-
ssary only for $M < 10^{-17}$ in the first part of
ese droplets' growth. By the time the drop-
ts reached their critical radii, their growth
as being computed by the growth equation.
his method seems quite practical since with
ch short time constants the radii of these
nall droplets can never differ appreciably
om their equilibrium radii in early stages of
rowth at *observed rates of rise in clouds*, and
ttle error in the computations can result.

Conditions chosen for study

As indicated above, the distributions exam-
ed by HOWELL (1949) were for nuclei
naller than those since found also important,
OODCOCK (1953, 1955), MOORE and MASON
957). Woodcock has related the distribution of these larger ($M=10^{-11}$) particles at cloud base level to wind velocity and measured their vertical distribution over the sea. As mentioned above the nucleus distributions for the larger particles as used in the computations were largely taken from his data. The smaller nucleus data were representative values taken from the work of Junge.

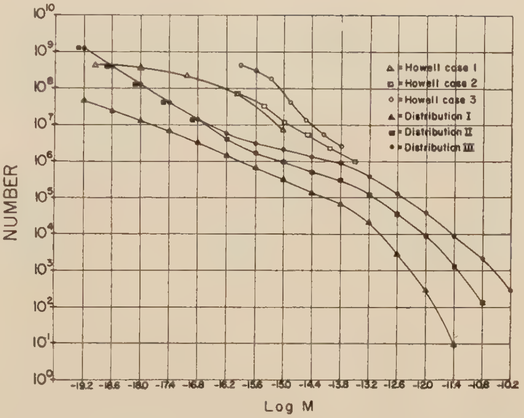

Fig. 5. The cumulative numbers of the nuclei used in the computations indicated opposite the logarithm of their weight in moles—open symbols indicate the distributions used earlier by Howell.

The distributions used in the computations together with those used by Howell are shown for comparison in figure 5. For the purpose of comparing the computations here with Howell's earlier work, computations were also made with his Case 1 and Case 3 distributions. His Case 2 could not be checked due to the assumption of a 1.5 cm/sec vertical velocity which required computing accuracy not available in the computer program as written.

The distributions given in figure 4 are designated Distribution I, II, III, corresponding to low, moderate or high concentrations of large salt particles ($M=10^{-13.8}$) as measured by Woodcock in Hawaii and elsewhere. They approximately correspond to the salt distributions which he gives as characteristic for days where the wind force was Beaufort force 1, 4, and 7 respectively.

The objective of this study was to determine the range of cloud particle sizes implied by the observed ranges in nucleus sizes and cloud vertical velocity. Comparison of these results with recent cloud droplet size data then should allow some separation of the condensation process from other processes such as turbulence, coalescence, and freezing. To do this, the range of particle numbers indicated in Woodcock's measurements characteristics of distributions for Beaufort wind force 1, force 4, and force 7, were extended arbitrarily into the Junge-Aitken range of smaller particles. These extended distributions were then assigned initial radii.

a) *The radii of nuclei at cloud base*

The largest nuclei measured by Woodcock were more than $M = 10^{-10}$ moles. Such particles require days (see table 1) to come to their equilibrium radii at 100 %. In fact their equilibrium radii are so large that it is unlikely that they would remain supported in the air at this level for a large fraction of the length of time required to reach equilibrium. The smallest nuclei ($M = 10^{-16}$), however, reach their equilibrium radii in seconds or fractions of a second. It is safe therefore to assume that for smaller sizes, the initial radii used in the computations should be their equilibrium size at the assumed *initial* relative humidity some distance below cloud base.

To determine precisely the radii of the large particles at cloud base, however, one should know the history of the individual particle, for with varied humidity in the sub-cloud layer and the probable turbulent transfer of these particles from sea surface to cloud level, each particle would arrive after a different travel time. This travel time of course is not possible to measure practically, and certain assumptions must be made concerning the level from which the particles are drawn into the cloud, the humidity and the velocity with which they are brought up. The assumption of uniform size for particles with a given larger M value is therefore probably in serious error. Initially these largest nuclei, due to their small numbers do not noticably affect the growth of the smaller particles however.

Woodcock has also measured the number of particles at various levels above the sea surface. From his data it is possible to estimate, using turbulent transfer theory, characteristic sizes of the nucleus droplets at each level. For example, from these data one obtains an estimate of $\frac{dN(M)}{dz}$, the change in number of a particular nucleus size M with increasing height Z. F a steady state

$$\frac{\partial N_m}{\partial t} = \frac{\partial}{\partial z}\left(K\frac{\partial N_m}{\partial z} + v_m N_m\right) = 0$$

where v_m = velocity of fall of the M size p ticles = cr_m^2 and K = the exchange coefficie From this we write,

$$K\frac{\partial(\log N)}{\partial z} = cr^2$$

In reality of course K varies consideral with height, wind velocity, and stability. T assumption that the vertical flux is zero is a made here, so this is admittedly a crude es mate.

If we take $\bar{K} = 10^{-5}$ cm^2/sec^{-1}, a value cor monly used over the sea at levels well above t boundary layer, and take $\frac{\partial(\log N)}{\partial z}$ fro Woodcock's measurements during proj shower (Tellus 1957), we obtain values f $r_m(z)$. The values obtained in this way re resent the radius corresponding to the avera rate of fall (cr^2) or therefore represent the ro mean square radius.

The values of r_m calculated, and r_{me} in equ librium with the relative humidity at 99 % a 100 % are given in figure 6 for comparis with the actual initial conditions chosen f study. Interestingly, the radii of the drop formed on the largest salt nuclei collect near cloud base, as estimated in this wa were smaller than expected due to unexpe edly high numbers of particles at this lev Consequently this estimate at the large e of the spectrum cannot be used. The high numbers of particles suggest that two or mo mechanisms rather than just one may important in the production of the larger pa ticles. This is to say that in addition to t surf and foam at the sea surface, the coalescen and evaporation of cloud droplets is probab important also in producing significant nu bers of the largest nuclei.

However, the values of the initial radii the rest of the droplets appear to be reasonal both in terms of:

1) the humidity gradient in the sub clo layer and

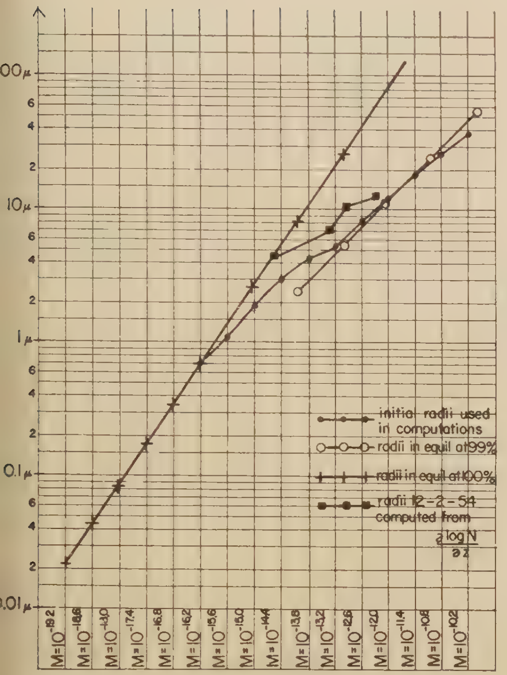

g. 6. Initial radii for nuclei droplets used in the compution. Line with (+) symbols indicates radii of droplets in equilibrium with 100 % R.H. Open circles indicate dii of large particles if in equilibrium with 99 % R.H. ack dots indicate actual radii sizes used for larger parles. Radii for smaller particles were taken from 100 % lues. Square symbols indicate radii calculated from turlence theory and based on observed decrease in number upwards from sea surface.

2) the turbulent transfer of these particles ward.

If, however, an appreciable number of *larger* t particles is produced by the coalescence d subsequent evaporation of cloud droplets, en these particles should be somewhat ger than those formed on the same size cleus *ascending* from the sea surface due to e long time constants. Such a case has not en considered here.

Radii of the droplets formed on particles $=10^{-15.6}$ and smaller were assumed to be equilibrium at 100 % relative humidity. ose droplets formed on particles $M=$ $^{-12.6}$ and larger were assigned radii approiate to equilibrium at 99 % relative humidity d those between at intermediate values as own in the figure.

b) *Vertical velocity, temperature and pressure*

A summary of the conditions for which computations have been made to date are given in table 2.

Table 2

Nucleus distribution	Vertical velocity cm/sec	T_0 °C	P_0 mb	Rel. Hum. %
1. Howell Case 1	60	0	800	100
2. Howell Case 3	30.2	0	800	100
3. Distribution I	15	10	800	100
4. Distribution I	100	10	800	100
5. Distribution II	15	10	800	100
6. Distribution II	50	10	800	100
7. Distribution II	100	10	800	100
8. Distribution III	5	10	800	100
9. Distribution III	15	10	800	100
10. Distribution III	100	10	800	100

The two Howell cases were computed with the present model to compare the differences in machine computing methods with Howell's hand computations, and as a control for accuracy. For case No. 1 the comparison was excellent (Fig. 7) considering that the exact values of the constants as well as the initial radii of the droplets selected by Howell were not precisely known. In case No. 3 (fig. 8) results were also qualitatively the same, but some discrepancies appear probably due to the fact that the initial radii used in the two computations were somewhat different.

In computing the other cases, the initial temperature (10°) and pressure (800 mb) and the initial radii selected were all the same for the purpose of comparing the cases with each other. Vertical velocities chosen ranged from 5 cm/sec to 100 cm/sec. The effects of *varying* vertical velocity *during the ascent* and of varying the nucleus distributions during the course of the computations have been left for a later study. The range of vertical velocities was chosen to demonstrate the most likely differences in the drop size spectrum which result from condensation. Due to the longer time constants for the larger particles, slower rates of rise do not allow the initial differences in radii to be overcome so readily as the more rapid rates of rise. Consequently very slow rates of rise produce the greatest differences in drop radius formed on a given pair of large nucleus sizes. Such differences represent differences in fall velocity and conse-

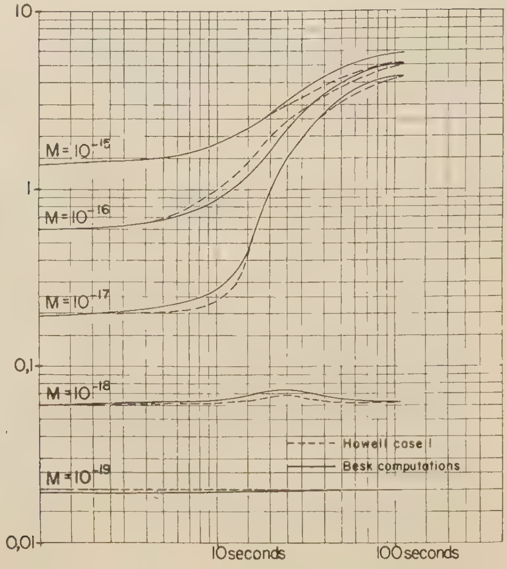

Fig. 7. A comparison of Howell's case 1 computation with computations made here with same initial conditions and nuclei distribution (ω = 60 cm/sec, T_0 = 0° C, P_0 = 800 mb).

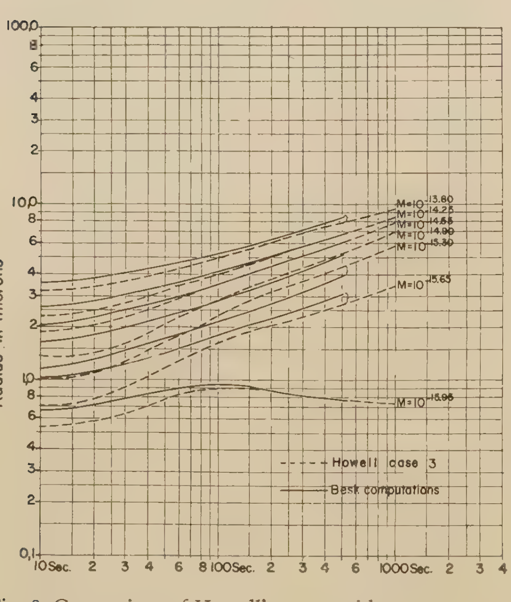

Fig. 8. Comparison of Howell's case 3 with present computations. (ω = 30.2 cm/sec, T_0 = 0° C, P_0 = 800 mb).

quently coalescence probability and thus are primary concern of this study.

Rates of rise in excess of 1 m/sec yield a more nearly uniform drop size spectrum than lower rates as will be shown in section 7 b and the interest in such computations from tl standpoint of subsequent coalescense dimi ishes accordingly.

In the process of testing the machine pr gram for the BESK computer a number errors occurred which showed that lar variation in the main coefficient of the dr growth equation (α in equation 12 f example) produced relatively small chang (comparable to doubling the vertical velocit in the results of the computations. This tantamount to saying that even if the rate growth of the individual particles as indicate by the equation is, for example, doubled, tl number and radii of the growing droplets not dramatically changed due to the fee back on the ambient humidity. For th reason, the initial pressures and temperatur were not changed during the course of tl present study.

It might have been interesting to ha varied the relative humidity (that is to st computations below cloud base) and/or t initial radii sizes, but choosing suitable a realistic conditions for such computations more difficult, since the exact nature of t nuclei present is not well known. Howeve certain experimental calculations of this natu are planned in connection with further wor

7. Some remarks on the results of the computations

With the foregoing considerations in mi we shall now look at two main aspects of t study, that is

1) the differences produced by the vario nucleus distributions and

2) the effects of different vertical velociti

The cases which have been computed, given in table 2, may be thought of in t reference as constituting a contingency ta representing several vertical velocities one coordinate, and the three nucleus dist butions on the other.

In discussing the computations it is helpf if certain classical considerations in the proc are borne closely in mind. In the initial co densation on the entire nucleus spectru condensation occurs preferentially (i.e. *dm* is larger) on the larger droplets due to the f that the radius enters the equation as a mu plying factor. This tendency is further acce

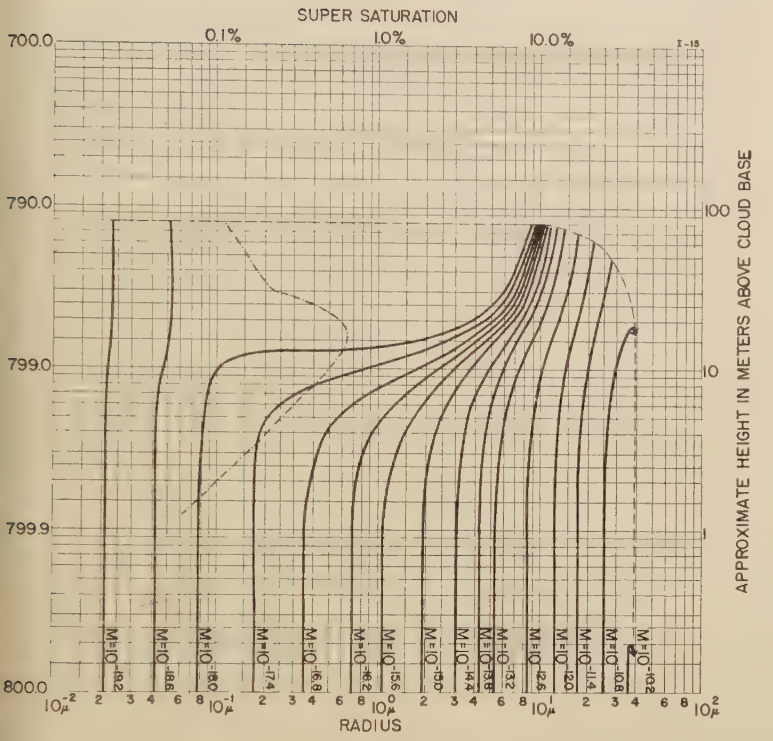

Fig. 9. Results of computation for sparse nucleus concentration, Distribution I at 15 cm/sec rate of rise. Initial radii and nucleus size are given at bottom of graph. Dashed line indicates supersaturation in % at appropriate heights, as given at top of graph.

ited if, as is the general case, these larger :oplets, due to their long time lag, are well ·low their equilibrium radii for the ambient ımidity. For a steady rate of cooling, if the ımber of these particles is sufficiently large, ey will consume water rapidly enough to :event the humidity from increasing. If not, e humidity will rise. As is well known, for ven temperatures a maximum attainable uilibrium vapor pressure value exists for ch nucleus size, corresponding to r_c in ction 5. If the ambient vapor pressure exceeds is value, no equilibrium condition is possible tween the droplet and the environment, d it must continue to grow until conditions : altered. A rise in humidity, as indicated ove, means that this maximum value will exceeded for successively smaller and smaller clei. Since these smaller nuclei are present increasingly larger numbers, the consumpn of water increases until finally the huidity no longer rises, after which the conmption of water is generally slightly faster a steady cooling rate than is needed to intain a balance, and the humidity gradually ls, approaching saturation.

In this way the number of growing droplets is determined, the smaller droplets, passing this humidity "barrier", dominating the water consumption thereafter as $N \cdot (dm/dt)$ increases for these smaller sizes (see for example fig. 22). In other words the maximum humidity is determined by the nucleus (or drop size) distribution and the cooling rate. The drop size distribution is determined largely by the maximum humidity. Hence there is a combined effect of the vertical velocity and the nucleus distribution. These are the main variables therefore to be investigated here. The other factor in these computations which can influence the above factors is the falling velocity of the droplets. This has the effect of a continual change in the drop size distribution at one level until a steady state situation is obtained. At points where some particles have a fall velocity equal to the updraft, a very high concentration of particles can develop. If this point lies in the zone of maximum humidity it can affect not only the number of large droplets but also the number of small droplets by reducing the environmental humidity.

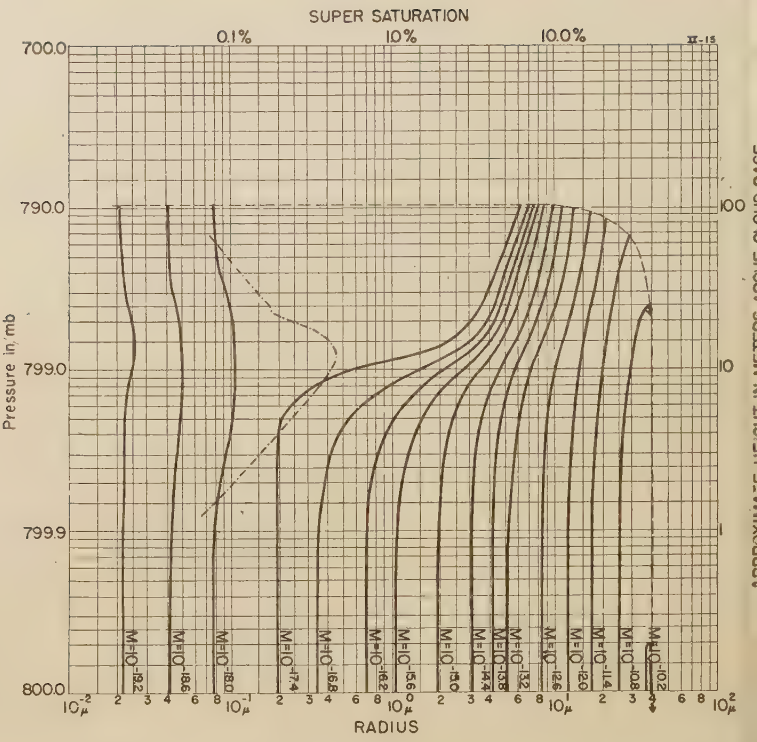

Fig. 10. Computation for a medium nucleus concentration, Distribution II at 15 cm /sec rate of rise. Data represented as in Fig. 9.

One further point is important to bear in mind. In two similar cloud droplet distributions, drops of the same radius may have formed on quite different nucleus sizes due to different initial nucleus distributions or environmental conditions. Measurements of droplet size and number in natural clouds therefore cannot determine to any fine degree the probable size of the nuclei involved during the formation of the cloud. It is possible for two quite similar cloud droplet spectra to have formed on different nucleus spectra due to higher supersaturation in one instance. Hence one is primarily concerned with comparing the cloud spectra produced and not the *radii* of the droplets formed on a *given nucleus size* in the different computations discussed below.

a) *The effect of the different nucleus spectra studied on the cloud droplet spectra*

In figures 9, 10 and 11 the results of three computations made for different nucleus distributions at approximately the same rate of rise (15—16 cm/sec) are shown. Sixteen nucleus size groups, representing the Distributions I, II and III, shown in figure 5, were use In these three figures and in the similar figur which follow, the radii of the droplets forme on the different nucleus size groups are plotte against their height above cloud base (100 humidity). Initial radii of the nuclei are th same in all cases. In the case of Distribution all but two of these sixteen nucleus sizes e ceeded their critical radii and grew to clou droplet size. In the case of Distributions and III all but three grew. The minimur nucleus to grow was $M = 10^{-17.4}$ moles f Distributions II and III and $M = 10^{-18}$ mol for Distribution I. This represents nucl which belong to the largest Aitken nucle size groups.

The total number of growing drops these three cases, however, is perhaps somewhat greater interest. In the case Distribution I approximately 1.3×10^7 growin drops were produced while for Distributio II and III only slightly more than this numbe 4.7×10^7 were produced.

If we make the same comparison for a mo rapid rate of rise, 100 cm/sec, as shown figures 12, 13 and 14, we find that the dro

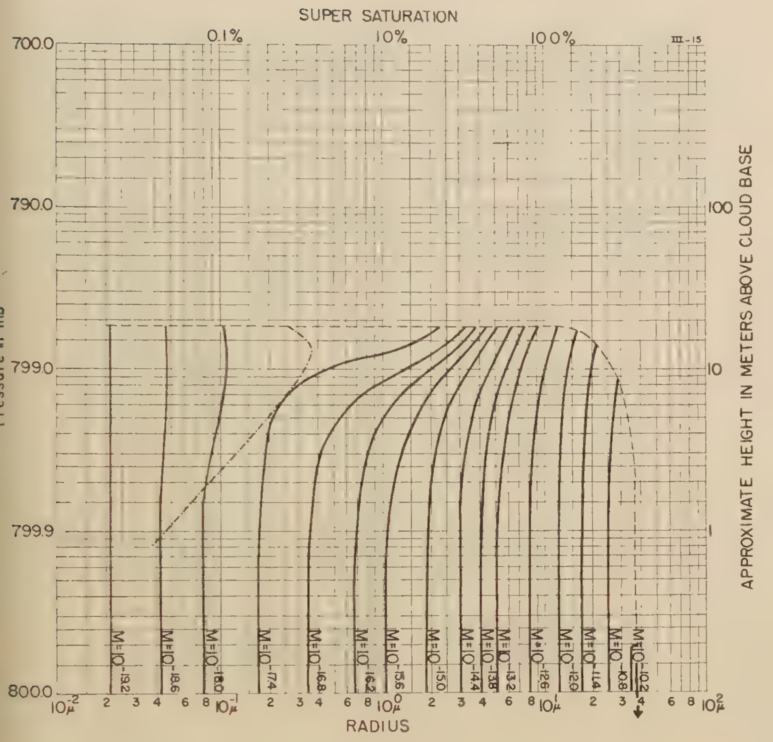

Fig. 11. Computation for dense nucleus concentration, Distribution III at 15 cm/sec. Data represented as in Fig. 9.

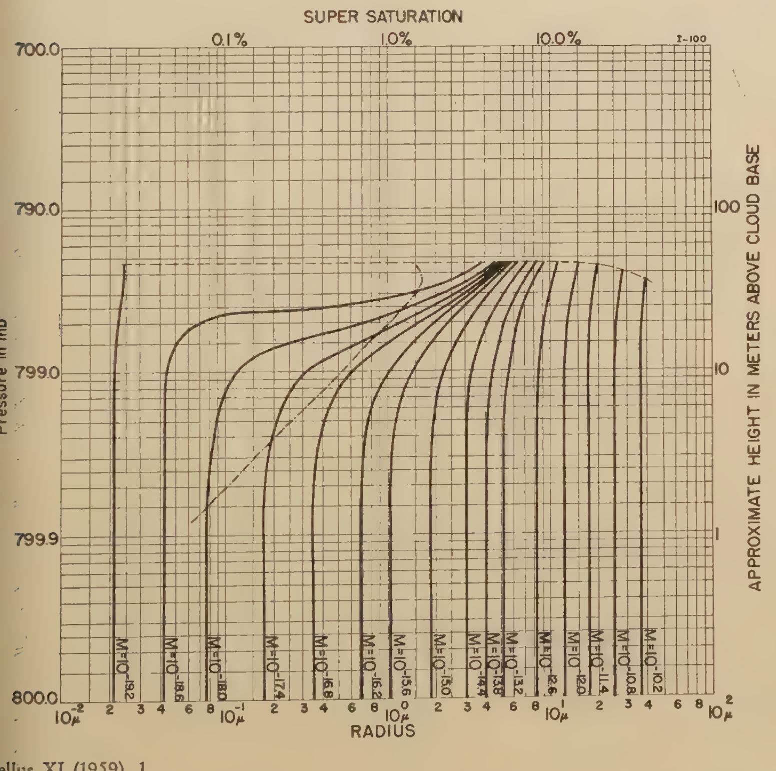

Fig. 12. Computation for sparse nucleus concentration, Distribution I at 100 cm/sec of rise. Data represented as in Fig. 9.

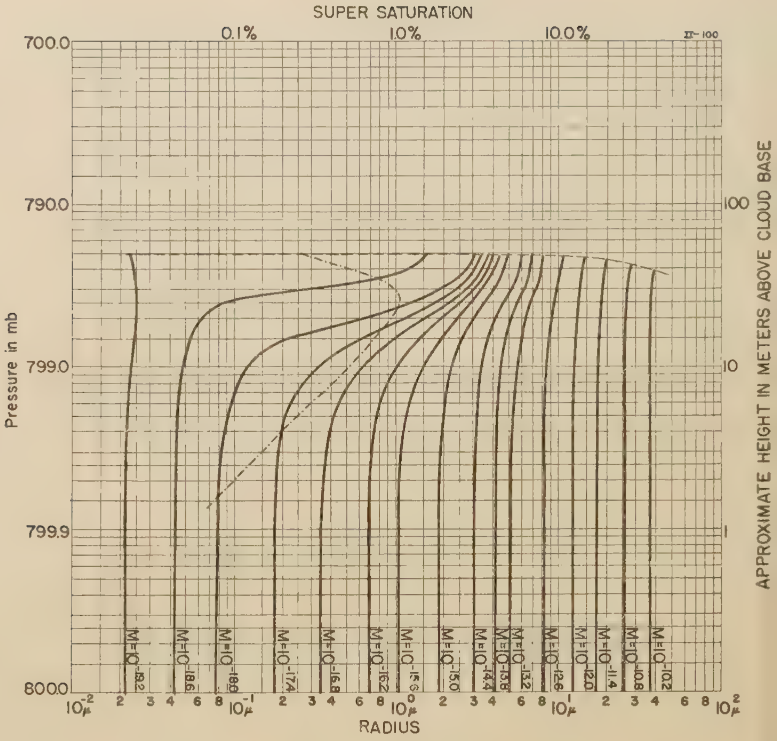

Fig. 13. Computation for medium nucleus concentration, Distribution II at 100 cm/sec rate of rise. Data represented as in Fig. 9.

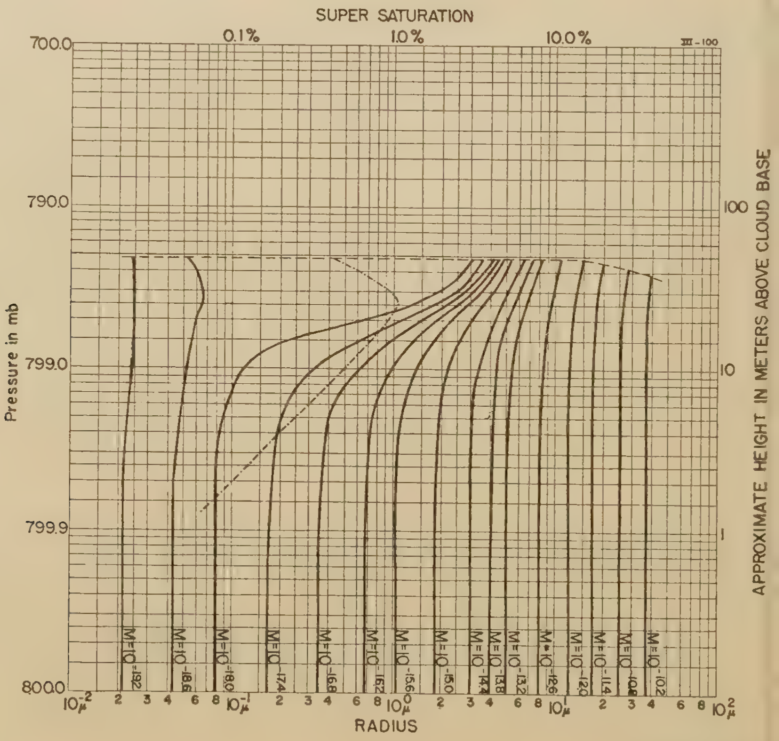

Fig. 14. Computation for dense nucleus concentration, Distribution III at 100 cm/sec rate of rise. Data represented as in Fig. 9.

umbers are altered much more dramatically. Iere Distribution I produces 2.5 × 10^7 growing loud droplets on nuclei down to $M = 10^{-18.6}$ ı size. Distribution II produces however 4.7 × 0^8 or twenty times as many growing droplets n nuclei ranging down to the same size. In ontrast Distribution III produces *fewer* growing roplets, 1.4 × 10^8, due to the fact that the rowth of the larger number of large nuclei vas sufficient to slightly lower the maximum ıpersaturation in this case.

It should be emphasized that due to the se of discrete size categories of nuclei both ıe maximum supersaturation and the number f cloud particles produced are accurate only vithin the limits marked out by two adjacent roups of nuclei. This is to say that the maximum supersaturation which would be reached a continuous representation of the spectrum vere used must lie between the critical superıturation values representing the smallest two roups *to grow*, and the critical supersaturation alue for the largest nucleus group, whose roplets *do not grow* past their critical radius. Consequently, the fact that slightly more rowing droplets were produced for Distribuon II as opposed to Distribution III in this ıtter case probably has less significance than appears to have, since the maximum superıturation reached in the two cases was so early the same, and the slight difference appened to be just sufficient to allow the ext category to grow.

This behavior should be discussed in terms f theoretical factors which are related here. he problem is in the nearly balanced adjustıent of the rate of water consumption to the ıte of cooling. Two factors are involved, ıe number of cloud droplets and their rate f growth. The water consumption is:

$$\sum_{i=1}^{j} N_i \frac{dm_i}{dt}$$

$_i$ = mass of the droplet in group i

$_i$ = number of droplets in group i

= number of actively growing groups

$= \sum_{i=1}^{j} N_i$ = number of actively growing droplets

An increase in relative humidity can increase either N or $\frac{dm}{dt}$ = depending upon the nature of the distribution, and the rate of rise. If the rate of rise is extremely slow, the largest particles, in spite of their long time lag, can keep abreast of the cooling rate and consume all the water. As the rate of rise or cooling increases so does the humidity, hence starting new groups of droplets, with shorter time lags,

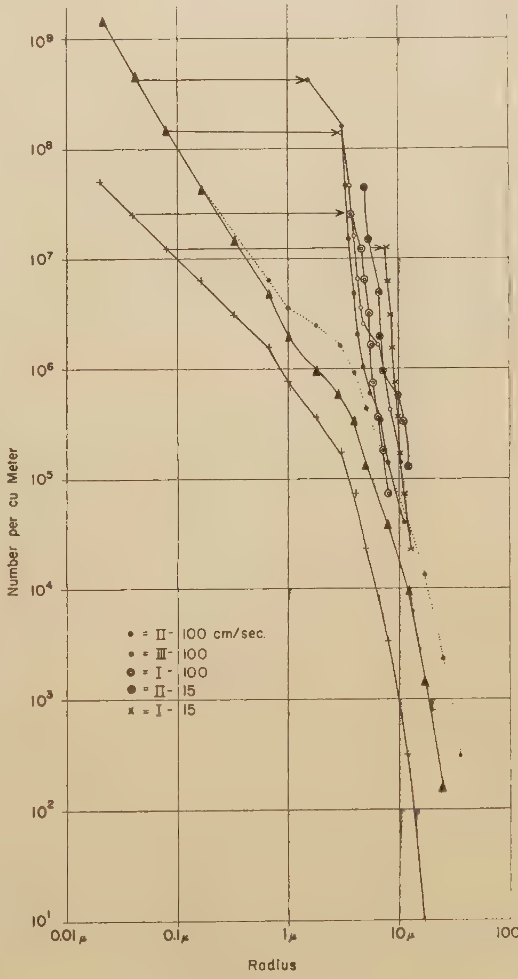

Fig. 15. A comparison of the cumulative number and radius of the droplets at 45 to 50 meters up into the cloud produced by the *three different distributions* at the *same rate of rise*. Distribution III at 15 cm/sec was computed only to 18 meters and therefore is not included. Initial radii and numbers are indicated by the curves at left side of diagram.

growing until the actively growing droplets can limit the further increase in relative humidity. This is to say that as the vertical velocity is increased the water consumption is first adjusted mainly by changes in N but with further increases the final adjustment is increasingly in terms of $\frac{dm}{dt}$ because for very small nuclei, the critical values of the supersaturation rises rapidly with decreasing r_c (see section 5). In the "dense" distribution N is the variable which is controlling. In the "sparse" distribution the adjustment takes place only when $\frac{dm}{dt}$ is large.

Therefore in the cases cited above, at a slow rate of rise (15 cm/sec), N adjusted to nearly the same value for the three distributions, while at 100 cm rate of rise the term $\frac{dm}{dt}$ became more important in the Distribution I case than for Distributions II and III. To the degree that these distributions are characteristic of natural conditions one may conclude t initial differences in nuclei distributions more manifest in cloud droplet concentratio when the vertical velocity is greater.

Another way of approaching this conclusi is to consider the *slope* of the nucleus distrib tion curves. "Dense" nucleus distribution used here refers of course to a larger numb of large, "Woodcock" nuclei while the "m dium" concentration has the same number smaller nuclei but fewer Woodcock nuclei

Distribution I ("sparse") however has few nuclei in all categories. These distributio were chosen to represent *observed* conditions a hence do not clearly demonstrate the impli differences in cloud droplet concentrati which may result from the two variabl *distribution slope* and *concentration.*

Given otherwise equal conditions a ste distribution slope will prevent the supe saturation from increasing to a large val since the *number* of growing cloud dropl adjusts more rapidly to increasing humidi

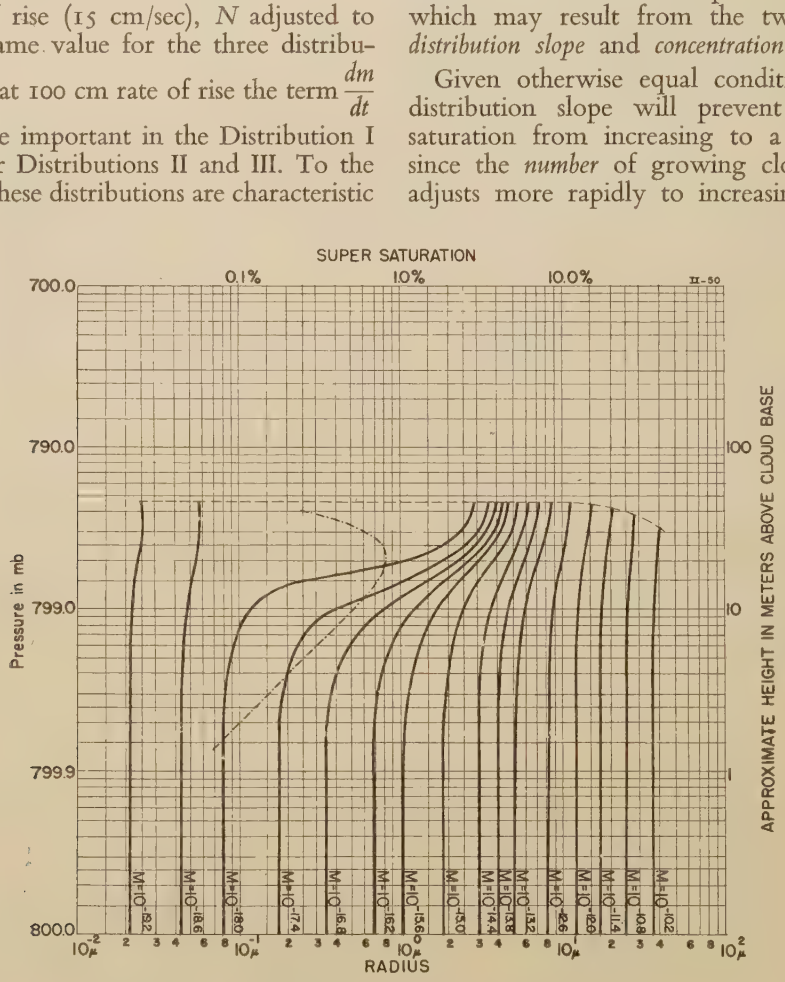

Fig. 16. Computation for medium nucleus concentration, Distribution II at 50 cm/sec rate of rise. Data represented as in Fig. 9.

nditions. If the slope is more gradual there more interaction between the growth rates the large and small droplets in the spectrum. ere much greater increases in humidity are quired to start new groups of nuclei growing stably and these increases of humidity beme increasingly retarded by greater water nsumption by the larger cloud droplets oduced by the same higher humidity contions.

In the cases discussed above, the points hich divide the nucleus spectrum from the oud droplet spectrum lie in the range $= 10^{-18.6}$ to $M = 10^{-17.6}$ In these points istributions II and III have the same slope d almost the same number while Distribuon I has a more gradual slope and a smaller ncentration.

The larger difference in number of growing oplets between Distribution I and Distribuon II at the rapid rate of rise seems to indicate at the important fact in this discussion is the *pe* of the distribution curve in the range of smallest few categories of nuclei to grow. increase in vertical velocity produces a eater change in the number of cloud droplets rmed on high slope distributions than for opposite.

These results are combined for comparison figure 15. Here the drop size spectra proced at 45 to 50 meters above cloud base are mpared for five of the six cases cited above. ie case for Distribution III at 15 cm/sec was mputed only to about 12 meters above oud base and consequently is not included. this diagram both the number and the dii of the droplets are represented as they ght be if measured in natural cloud. In dition to the number comparison made ove, it is possible here to compare the differces in radii which result from the different nditions represented. In all cases the droplets rmed on nuclei with initial radii smaller in 3 μ have nearly equal radii at distances ore than a few tens of meters above cloud se. Droplets formed on larger nuclei due to ir longer time constants (see sec. 5) continue exhibit their initial size differences for ich longer growth intervals. Consequently radii differences at the large end reflect inly the differences in the original nucleus ectrum.

b) *Some additional effects of varying vertical velocity on cloud droplet spectra*

It is also instructive to note differences in drop number and size which result from variation in the rate of cooling or vertical velocity alone. One such comparison is possible with Distribution II by referring to figures 10, 13 and 16 which show the growth of the Distribution II particles at 15, 50 and 100 cm/sec. Each increase of the vertical velocity increases

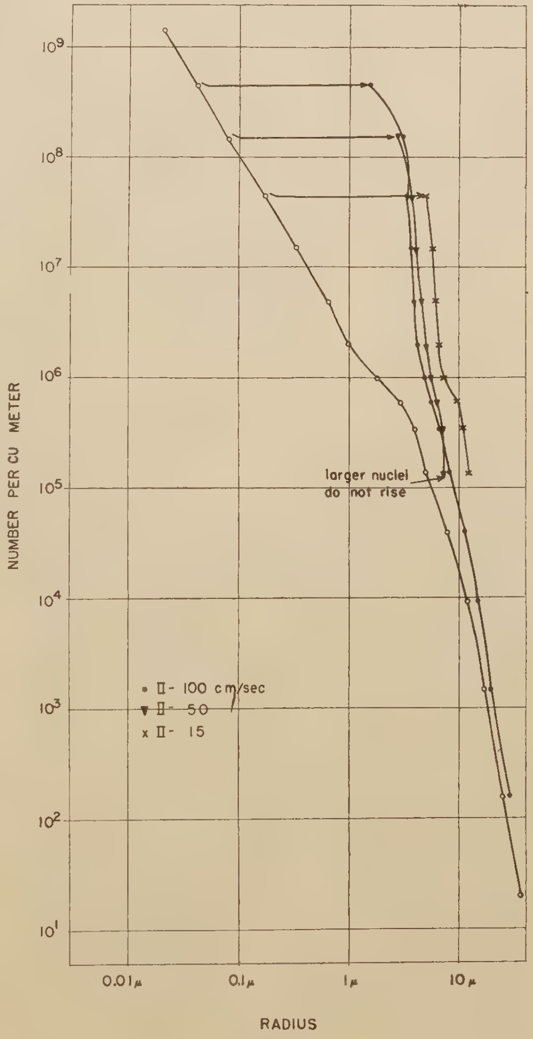

Fig. 17. A comparison of the number and radius of the droplets at 45 to 50 meters above cloud base produced by three different rates of rise (15, 50, 100 cm/sec) on the medium nucleus concentration, Distribution II. Original distribution is at left marked with open circles.

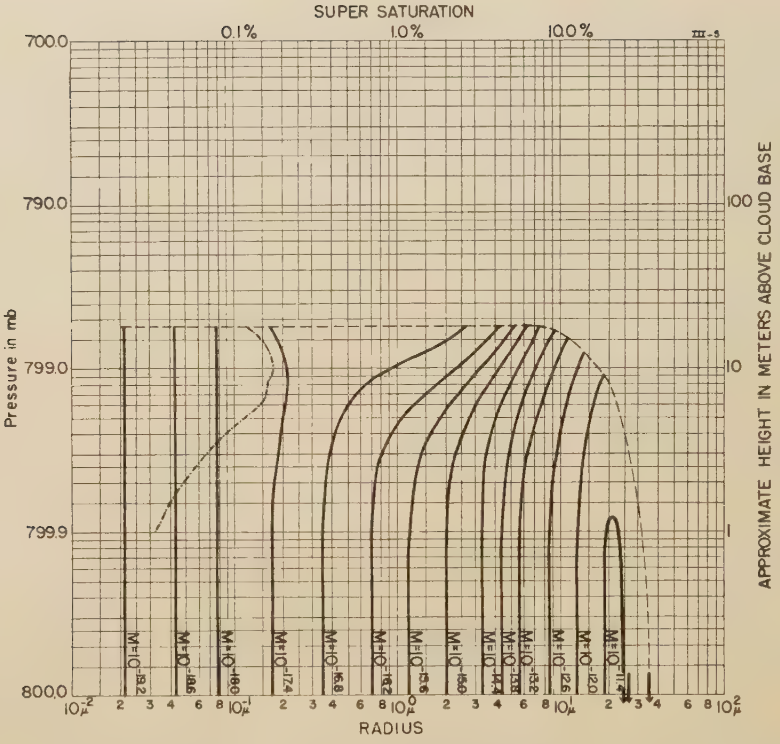

Fig. 18. Computation for a dense nucleus population. Distribution III at 5 cm/sec rate of rise. Data represented as in Fig. 9.

the number of growing particles roughly by a factor three, by including among the growing droplets one more smaller group of nuclei. This is to say that for 15 cm/sec there were 4.7×10^7 growing droplets, while at 50 cm/sec there were 1.4×10^8, and at 100 cm/sec there were 4.7×10^8 droplets. This is nearly as great a variation in number as the different distributions produced at 100 cm/sec rate of rise, that is, ten times as opposed to thirty.

In fig. 17, the cumulative cloud droplet distributions produced at 45 to 50 meters above cloud base are compared both by radius and number, as they were in figure 15. In the case of the slowest rate of rise both the minimum growing drop size and the maximum size of the droplets are larger, a condition which is believed by most investigators to be conducive to the coalescence process.

Note in figure 17 (and in figure 15) that it would be very difficult if not impossible to distinguish these drop size distributions from one another by measurements in natural conditions in terms of the size of the dropl produced. The smaller droplets are so nea the same size that the inaccuracy of measu ments and local variations in cloud wo completely mask these size differences. the large end of the spectrum the pos bility of coalescence between the droplets ru out the possibility of detecting differen between the different drop size spectra p duced. Only the *number* of cloud dropl is indicative of the conditions in which droplet spectrum first forms.

c) *Comparison of the extreme cases in the com tations*

It might be thought that a *rapid rate* of for a *sparse* nucleus population and a sl rate of rise for a dense concentration sho provide the greatest contrast in the result condensation cloud spectra. In the first of th cases the supersaturation should rise to highest possible value while the number cloud particles would be limited by the nucl pectrum. This should produce a more uni- orm spectrum since the condensed water vould be "forced" onto a smaller number of uclei. The largest nuclei, due to their longer ime constants, also lag behind more in the ase of rapid cooling which further tends to arrow the size spectrum.

In the case of a slow rise on a dense popula- ion, the size of the smallest droplets to grow ; not much larger than for the sparse distri- ution, while the slower cooling rate permits ıore of the larger nuclei to "keep up" with ıe condensation rate. In this way a broader pectrum should be formed.

With these suggestions in mind it is inter- sting to look at two such cases as computed ere. The two extreme cases computed were he case of Distribution I at 100 cm/sec shown ı fig. 12 and Distribution III at 5 cm/sec hown in fig. 18. In these cases the number of rowing cloud droplets produced was nearly he same (2×10^7 vs. 1.5×10^7) but the radii vere quite different. However, at some few 00's of meters above cloud base it is clear hat the dominant size group (smallest) will ave essentially the same radius in both in- tances and only the larger particles will differ narkedly.

These computations were not carried out o the same height above cloud base and rict comparison at the same height cannot be nade. By recourse to the type of graph used ı figures 15 and 17 though, it is possible to xtrapolate visually the cloud droplet spectrum. he smaller end becomes more and more niform in size, as the two cases plotted in g. 19 show. Here it is clearly seen how the ze spectra diverge rapidly toward larger article sizes. This is true even though the ower rate of rise used in the Distribution III ase had not carried the particles nearly so igh into the cloud when the computation was opped as in the case of the rapidly rising istribution I case. However, there is one miting or compensating effect to offset this ndency. This is the fact that if the rate of se is slow, the largest particles begin to settle ut against the rising current, tending to arrow the spectrum from the large end.

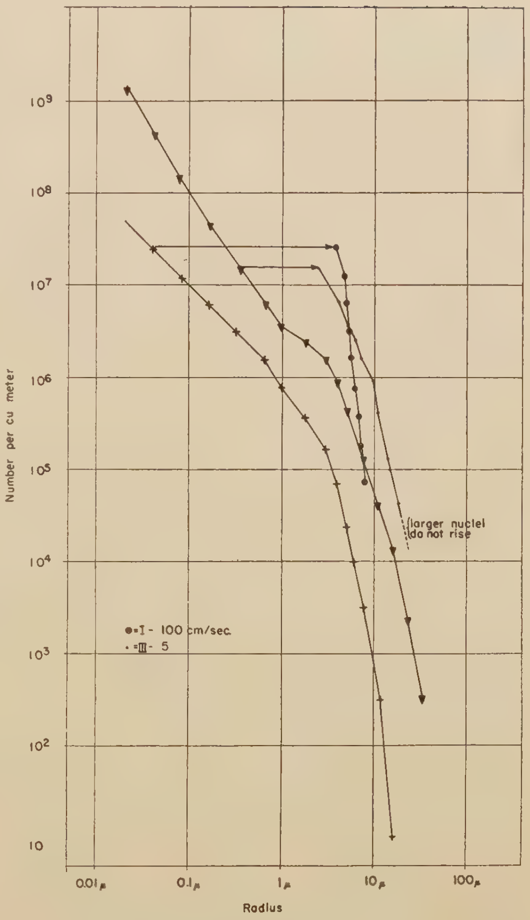

Fig. 19. Cumulative drop size distributions resulting from two extreme cases in the computations, sparse (Dist I) concentration at 100 cm/sec rate of rise and dense (Dist III) at 5 cm/sec producing more and less uniform spectra respectively.

Actually the largest differences in droplet ectra in these computations seem to come in rms of droplet number or *concentration*. These fferences occurred for quite the opposite pairs of conditions from those discussed above, namely between a sparse population with a slow rate of rise and a dense population with a rapid rate of rise. These conditions are represented here by the 15 cm/sec rate of rise for the Distribution I case and 100 cm/sec for the Distribution II (or III) case, shown in figures 9 and 13. The fact that this extreme difference occurred for the medium rather than the most dense population of particles has been discussed above in section 7a. If a somewhat more rapid rate of rise had been chosen, the denser population of Distribution III would have produced more growing droplets than Distribution II. Consequently this fact is only of minor importance.

In the two cases represented here there is a difference of thirty times in the number of particles per unit volume of cloud. This *range of particle concentration* is in agreement with cloud droplet measurements made by a number of the most recent investigators, ZAITSEV (1950), WEICKMANN and AUFM KAMPE (1953), SQUIRES (1957, 1958) etc. Except for the smallest droplets, droplet radii *all along the spectrum* in almost all cases are smaller than those observed in clouds.

d) *Deviations from the moist adiabatic lapse rate*

It is possible also to look at the total amount of water condensed at various levels above cloud base as indicated in the computations and compare it with the amount theoretically condensed according to moist adiabatic expansion. Such a comparison here is not *strictly* accurate due to the approximation used for the dry adiabatic lapse rate. Deviations due to this discrepancy however are small since the vertical distances considered are all less than 80 meters.

Such a comparison is possible by considering the curves shown in figure 20. In this figure the dashed line indicates the water which would have been condensed if the process were moist adiabatic while the curves at the left indicate the water condensed at each level for the Distribution II cases at 15, 50, and 100 cm/sec. The curves are separated until air reaches from 30 to 50 meters above cloud base while after this, condensation proceeds almost exactly along the moist adiabatic condensation line.

In figure 21 the values computed for the different distributions are compared at 15 and 100 cm/sec. The largest deviation from the moist adiabatic rate is indicated for the Distribution I case at 100 cm/sec where, unfortunately the computation was stopped before the condensation rate approached the moist adiabatic condensation line. Extrapolation of this curve however indicates that the curves join at about 80 meters.

Differences between the curves for the three distributions at 15 cm/sec are of little interest while it appears that sparse distributions at higher vertical velocities might cause deviations from the moist adiabatic lapse rate up to 100 meters or more. Such deviations coul be detected in carefully taken cloud tempera ture measurements and suggest the possibilit of roughly identifying nuclei conditions in th way.

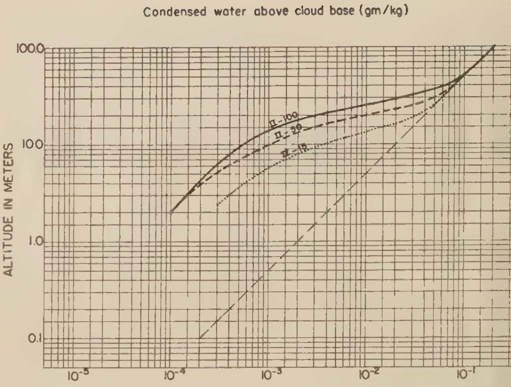

Fig. 20. Deviations of the cloud liquid water conte *comparing different rates of rise* from that computed wi the moist adiabatic assumption. The straight line indicat the cloud liquid water with moist adiabatic assumptio The curved lines show the liquid water as computed f the three different rates of ascent for Distribution II.

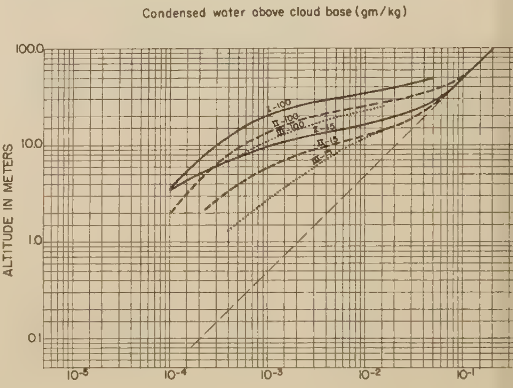

Fig. 21. Deviations of cloud liquid water from that con puted with moist adiabatic assumption *comparing the diffe ent distributions* at two rates of rise. The curved lines sho the cloud liquid water as computed in this study whi the straight line indicates that computed with the adi batic assumption.

8. Discussion

It has long been recognized that condens tion alone cannot account for the range cloud and rain droplet sizes which are found nature. In spite of this fact it must be recog nized that the condensation process provid

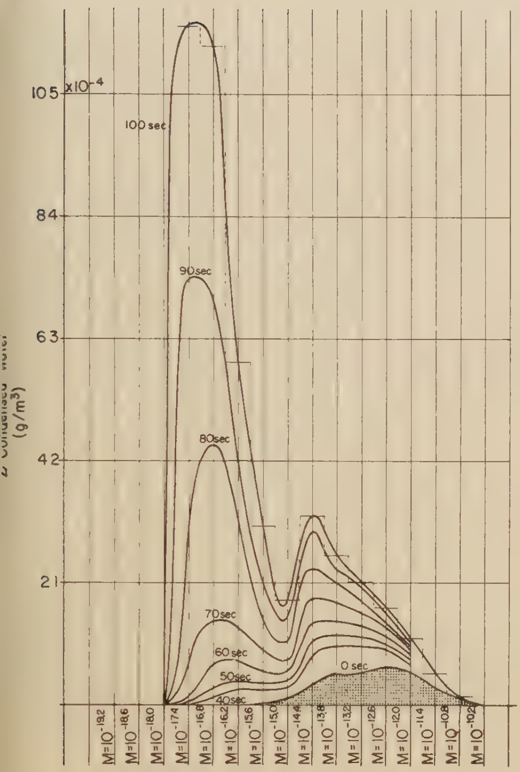

ig. 22. Graph indicates the liquid water condensed on ie different nuclei sizes in Distribution II at 15 cm/sec ite of rise at given time intervals after the beginning of ie computations. It shows how the large nuclei consume early as much water up to level of maximum super-turation (13 meters) as the smaller ones, but soon there-ter nearly all water is condensed on the smallest few nuclei size.

ie first spectrum of cloud droplets which ther processes later modify and determines ie *maximum concentration* of cloud particles. ecause of this, any theoretical discussion of ther processes, such as coalescence, drop reaking, entrainment, turbulence, freezing c., which alter the condensation produced pectrum, should be based on as complete understanding of this process as possible.

From the present computations several eneral features of the condensation process n be seen rather well. If the water which condensed on the different sized droplets graphed, as in figure 22 above, it is possible get a visual impression of the dynamics of e condensation process. In this diagram we n visualize the building up of liquid water on the Distribution II nucleus spectrum during the early stages of condensation. It can be seen that, as postulated above, the largest part of the condensed water initially goes to the largest nuclei. Gradually as the humidity continues to rise the liquid water condensed on the smaller nuclei increases until after 70 seconds the smaller droplets contain about the same total amount of water as the larger ones. Shortly thereafter, in an almost explosive way, the smallest droplets grow until they contain nearly all the cloud water.

In terms of the theoretical remarks in section 3, the initial dominance of the larger particles is due to the fact that these particles have a higher salt concentration and a larger initial radius, hence the vapor pressure lowering over the droplet is very great and the water content of the individual droplet is increased rapidly. This condition prevails for these droplets for a very long time but they are too few to play a dominant role for long as they do not consume water at a rate sufficient to keep the humidity from rising. They can, however, if sufficiently numerous, reduce the maximum humidity somewhat and thereby reduce the total drop number. Gradually then the smaller and smaller droplets begin to grow, each group consuming more water than the next larger group until the humidity no longer rises.

In fig. 22 therefore the double maximum is due to the fact that the droplets at the large end of the spectrum are growing by virtue of their *hygroscopicity*, which in some cases produces more than 1 % vapor pressure difference between the drop surface and the environment, while the smaller droplets are growing largely due to the increased humidity of the *environment*.

The effect of the different distributions of particles is illustrated by comparing fig. 22 with fig. 23 where the same type of graph is shown for Distribution III at the same rate of rise. Here the greater number of large particles increases the liquid water content in the large end of the spectrum so that for the first 100 seconds, as opposed to 70 seconds for Distribution II, it dominates the growth. This is noteworthy since the maximum humidity (see figures 10 and 11) is reached at 12 to 13 meters in both instances, illustrating how these large particles can in some instances

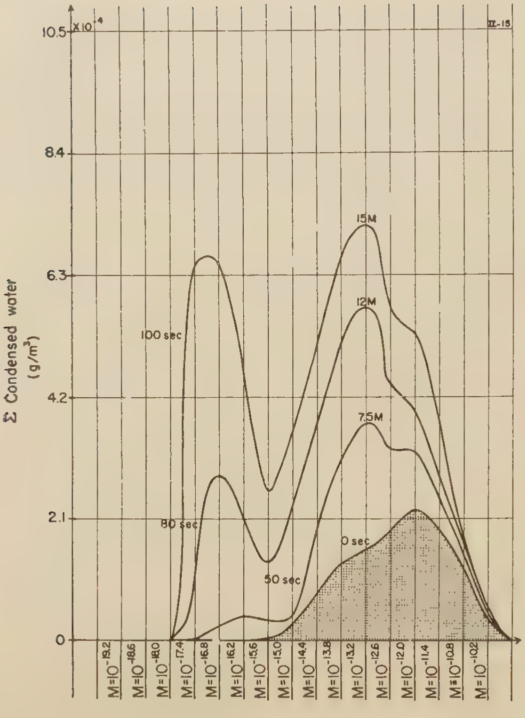

Fig. 23. Same as fig. 20 for Distribution III at 15 cm/sec showing greater effect of the largest nuclei.

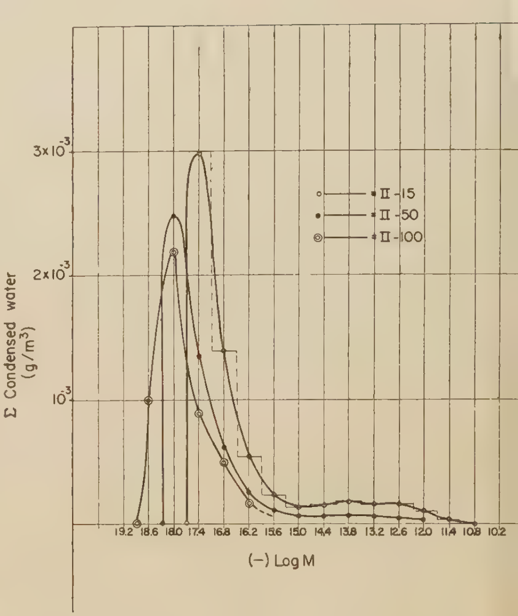

Fig. 24. Graph shows the liquid water contained in t droplets formed on the different nuclei sizes in the Distr bution II case. 45—50 meters above cloud base (100 R.H.) at 15.50, and 100 cm/sec rates of rise.

limit the maximum humidity and hence the droplet concentration.

After a period of time sufficient to carry the particles 45 to 50 meters high, nearly all cloud water is contained in the droplets formed on the smallest two or three nucleus sizes. This is shown in figures 24 and 25 which are similar to figures 22 and 23 except that the vertical scale has been shortened and the comparisons are made for 45–50 meters above cloud base. In figure 24 the effects of the three rates of rise on the Distribution II cases are compared. In fig. 25 the three distributions are compared at the same rate of rise, 100 cm/sec.

9. Summary

a) The *number* of cloud particles produced is dependent *both* on the vertical velocity and the nucleus distribution. This result is at variance with Howell's conclusion that the vertical velocity was the primary factor, and is mainly a result of the differences in the

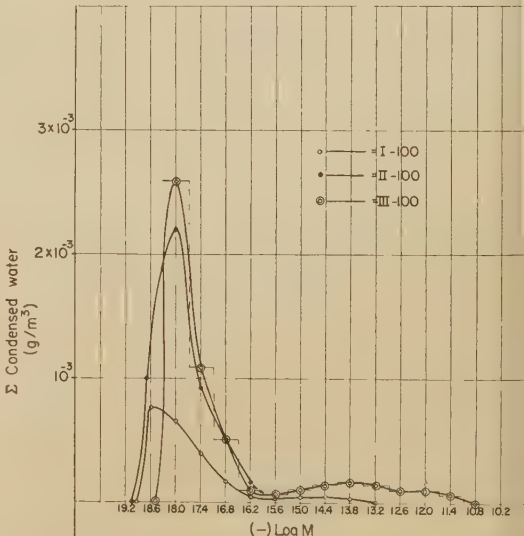

Fig. 25. Liquid water contained in the droplets formed the different nuclei sizes of the three Distributions I, and III at 10 cm rate of rise 45—50 meters above clo base.

nucleus spectra considered. The cloud particle concentrations calculated agrees with the observed range in natural clouds.

b) The *radii* of droplets found at given heights above cloud base, both by reason of differences in concentration and growth rate, may be significantly different in the different conditions studied here. Although in general, if given enough time, all growing droplets converge toward a uniform radius, the rate at which this takes place may be quite different. This is increasingly noticable as larger nuclei are considered. Presumably subsequent coalescence depends on these size differences and hence the conditions which produce them deserve considered attention.

c) The effect of drop sedimentation on condensation conditions is of importance

1) only when the vertical velocity is extremely slow (1 to 10 cm sec^{-1}),

2) there is an extremely dense nucleus distribution (such as Distribution III),

3) if there is an increase of settling droplets due to coalescence.

d) The drop size spectra indicated by these computations does not adequately describe the observed spectra in natural clouds. There are too few large droplets in the computed cases. The size and number of the smallest droplets however are in accord with observations.

e) The *relative* humidity values seldom exceed saturation by more than 1 % confirming Howell's conclusion. The depth of the layer where the lapse rate of temperature differs from the moist adiabatic may exceed 100 meters in some conditions of low nucleus concentrations.

Acknowledgement

The author is deeply indebted to Mr. Claes Rooth, Institute of Meteorology, University of Stockholm, for considerable assistance in the preparation of this study for the Besk Computer, for aid in determining the stability of the computations, and along with other members of the International Meteorological Institute for many stimulating and helpful discussions.

REFERENCES

Alty, T. and Mackay, C. A., 1935: The accommodation coefficient and the evaporation coefficient of water. *Proc. Roy. Soc.*, London, **A 199**, pp. 104—116.

Arons, A. B. and Kientzler, C. F., 1954: Vapor pressure of sea-salt solutions. *Trans. A. G. U.* **35**, pp. 722—728.

Bergeron, T., 1935: On the physics of cloud and precipitation. *Proc. 5th assembly UGGI*, Lisbon **2**, pp. 156—178.

Eriksson, E., 1952: Composition of atmospheric precipitation. *Tellus* **4**, pp. 215—232.

Eriksson, E., 1952: Composition of atmospheric precipitation. *Tellus* **4**, pp. 280—303.

Frössling, N., 1938: *Beitr. Geophys.* **52**, p. 170.

Gunn, R. and Kinzer, G. D., 1949: The terminal velocity of fall for water droplets in stagnant air. *J. of Met.* **6**, pp. 243—248.

Houghton, H. G., 1938: *Bull. Amer. Met. Soc.* **19**, p. 152.

Howell, W. E., 1949: The growth of cloud drops in uniformly cooled air. *J. of Met.* **6**, pp. 134—149.

ohnson, J. C., 1954: Physical Meteorology. *John Wiley and Sons*, New York, 210 pp.

unge, C., 1952: *Ber. Dtsch. Wetterdienst US Zone*, **35**, p. 261.

Keith, C. H. and Arons, A. B., 1954: The growth of sea-salt particles by condensation of atmospheric water vapor. *J. of Met.* **11**, pp. 173—184.

Köhler, H., 1921: Zur Kondensation des Wasserdampfe in der Atmosphäre. *Geophys. Publ.* **2**, pp. 3—15.

— 1926: Zur Thermodynamik der Kondensation an hygroskopischen Kernen und Bemerkungen über das Zusammenfliessen der Tropfen. *Medd. Met. Hydr. Anst. Stockholm* **3**:**8**.

— 1936: *Trans. Faraday Soc.* **32**, p. 1152.

— 1941: *Reg. Soc. Sci.* Uppsala, *Nova Acta*, **12**.

— 1950: On the problem of condensation in the atmosphere. *Medd.* **15**, *Nova Acta Reg. Soc. Sci. Ups.*, Uppsala, 75 pp.

Langmuir, I., 1944: Super cooled droplets in rising of cold saturated air. *General Electric Company*, Schenectady, N.Y., 150 pp.

McDonald, J. E., 1953: Erroneous cloud-physics applications of Raoult's law. *J. of Met.* **10**, pp. 68—70.

Mason, B. J., 1957: The physics of clouds. *Oxford Press*, 470 pp.

— and Ghosch, D. K., 1957: The formation of large droplets in small cumulus. *Quart. J. Roy. Met. Soc.* **83**, pp. 501—507.

Moore, D. J. and Mason, B. J., 1952: *Quart. J. Roy. Met. Soc.* **78**, p. 596.

Mordy, W. A., 1953: A note on the chemical composition of rainwater. *Tellus* **5**, pp. 470—474.

Project Shower 1957: Tellus 9, pp. 471—590.

Rooth, C., 1957: On a special aspect of the condensation process and its importance in the treatment of cloud particle growth. *Tellus* **9**, pp. 372—377.

Squires, P., 1952: The growth of cloud drops by condensation. I. General characteristics. *Austr. J. of Sci. Res.* **5**, pp. 59—86.

— 1952: The growth of cloud drops by condensation. II. The formation of large cloud drops. *Austr. J. of Sci. Res.* **5**, pp. 473—499.

— and Warner, J., 1957: Some measurements in the orographic cloud of the Island of Hawaii and in trade wind cumuli. *Tellus* **9**, pp. 475—494.

Squires, P., 1958: The microstructure and colloidal stability of warm clouds. *Tellus* **10**, pp. 256—271.

Sverdrup, H. U. et al., 1942: The oceans. *Prentice-Hall*, p. 51.

Vierhout, R. R., 1949: On the formation of drops in clouds and fog. *Mededelingen en verhandelingen van het Koninklijk Nederlands Meteorologisch Instituut, De Bilt* **125**, serie B, 20 pp.

Weickmann, H. K. and aufm Kampe, H. J., 1953: Phys- ical properties of cumulus clouds. *J. of Met.* **10**, pp 204—211.

Woodcock, A. H. and Gifford, M. M., 1949: Samplin atmospheric sea-salt nuclei over the ocean. *J. of Marin Res.* **8**, pp. 177—197.

Woodcock, A. H., 1953: Salt nuclei in marine air as function of altitude and wind force. *J. of Met.* **5**, pp 362—371.

— and Mordy, W. A., 1955: Salt nuclei, wind and dail rainfall in Hawaii. *Tellus* **7**, pp. 291—300.

Zaitsev, V. A., 1950: Liquid water content and distribution of drops in cumulus clouds. *Trudy Glavno Geofizicheskoi Observatorii*, **19** Translation: *National Research Council of Canada, Tech. Trans.* **TT-395**, 2 pp.

PRINTED IN SWEDEN
ESSELTE, STHLM 59

Contribution No. 1029

On a Criterion of Representativeness of Sea-Surface Temperature Data[1, 2]

Irving I. Schell

Tufts University and Woods Hole Oceanographic Institution

(Manuscript received 12 February 1959)

ABSTRACT

Three pairs of historical series of mean monthly sea-surface temperatures in the North Atlantic were analyzed, one pair from the tropical area, 15N to 20N, 60W to 65W, dominated by the North Equatorial Current; the second from the semitropical area, 30N to 35N, 55W to 60W, by the Gulf Stream; and the third pair from the polar area, 45N to 50N, 45W to 50W, off Newfoundland by the Labrador Current.

The results obtained show that, by successively eliminating those values based upon few observations per month, the standard deviation, σ, tends to become relatively constant and may then serve as a criterion of the representativeness of sea surface temperature data.

1. Introduction

In recent years, considerable interest has been shown in developing historical series of sea-surface temperatures. As notable examples, we must mention the work carried out over a period of years by Smed (1947 to 1953) for the area north of 50N in the North Atlantic, the series of mean monthly temperature anomalies for another portion of the North Atlantic by Riehl (1956), the series for selected areas on the route from Europe to South America by Bullig (1954), and others. Considering that the oceans intimately interact with the atmosphere and that they retain an excess of "heat" or "cold" in its surface or sub-surface layers and thereby affect the future weather, the development of comprehensive historical series of sea-surface temperatures takes on added significance.

It is very fortunate, therefore, that the number of observations regarding the oceans has grown rapidly in recent years. However, this large body of data cannot be treated simply for, despite the large number of the total, their distribution both in time and space is for the most part quite inhomogeneous. Thus, the problem of developing historical series of sea-surface temperatures requires for its solution the application of criteria which, in the face of this handicap, can lead us to a reasonable evaluation of the data and their use for studying the various unsolved problems involving ocean temperatures. Although these criteria must be essentially statistical, they cannot be divorced from meteorological and oceanographic considerations; also, since these can be expected to vary with each particular problem, our criteria must similarly vary. Therefore, because of the relatively small number of observations available for most areas, a historical series of 5-day mean temperatures will pose a greater problem than one of monthly and seasonal values. Furthermore, the problem of evaluating climatic trends where the value of an individual year need not loom large in their consideration would be less difficult than the problem of a historical series where the year-by-year conditions must be known. This report will limit itself mainly to a discussion of longer-period historical series in terms of monthly means, with special reference to "bench marks" or areas representative of relatively homogeneous or distinct ocean systems.

2. Criteria of representativeness

Among the criteria indicating the representativeness of mean monthly or other time-interval values of sea-surface temperatures, the number of observations comprising the mean, their spread within the period examined, the size of the area considered, the hour of the observation, and the relation of an observation in a given area to that in an adjacent area have all figured in attempts to develop historical series of sea-surface temperatures (Petersen, 1910; Liepe, 1911; Sandstrom, 1942; Bullig, 1954; Riehl, 1956). For example,

---

[1] Tufts University Meteorological Studies No. 3 and Contribution No. 1029 from the Woods Hole Oceanographic Institution.

[2] The research reported in this article has been made possible through support and sponsorship extended by the U. S. Weather Bureau under Contract Cwb-9011.

TABLE 1. Averages of mean monthly values of sea-surface temperature, their range, their standard deviation, σ, and standard error of the mean, $\sigma_{\bar{x}}$, based on mean monthly values with one or more ($N \geq 1$), six or more ($N \geq 6$), eleven or more ($N \geq 11$), and sixteen or more ($N \geq 16$) observations.

	Area 1 (15N to 20N, 60W to 65W)			Area 2 (30N to 35N, 55W to 60W)				Area 3 (45N to 50N, 45W to 50W)			
	January			January				April			
	$N \geq 1$	$N \geq 6$	$N \geq 11$	$N \geq 1$	$N \geq 6$	$N \geq 11$	$N \geq 16$	$N \geq 1$	$N \geq 6$	$N \geq 11$	$N \geq 16$
Mean:	78.3	78.3	78.3	68.0	67.9	68.1	68.0	40.0	38.0	37.8	37.9
No. of cases:	68	59	50	58	49	38	35	65	47	38	28
σ:	1.18	1.18	1.18	1.47	1.38	1.11	1.13	6.14	3.01	2.47	2.27
Range:	5.7	5.7	5.7	5.8	5.8	4.7	4.7	31.2	13.4	10.8	8.7
$\sigma_{\bar{x}}$:	0.14	0.15	0.17	0.19	0.20	0.18	0.19	0.76	0.44	0.40	0.43
	July			July				July			
	$N \geq 1$	$N \geq 6$	$N \geq 11$	$N \geq 1$	$N \geq 6$	$N \geq 11$	$N \geq 16$	$N \geq 1$	$N \geq 6$	$N \geq 11$	
Mean:	81.5	81.5	81.5	78.8	78.9	78.9	78.9	50.8	50.6	50.5	
No. of cases:	57	49	43	58	54	44	40	71	66	55	
σ:	0.90	0.93	0.90	1.64	1.64	1.14	1.15	3.14	2.99	2.94	
Range:	3.9	3.9	3.9	8.9	8.9	5.6	5.6	13.8	13.8	13.5	
$\sigma_{\bar{x}}$:	0.12	0.13	0.14	0.22	0.22	0.17	0.18	0.37	0.37	0.40	

consideration of the time spread of the observations would not only serve to better apportion the weight of the observations by showing over how many days within the month they were distributed but would also reduce the disproportionate weight of any large number that may have been taken on a single day. On the other hand, a value observed on a given day may be related to the value some time before or afterward with respect to the general tendency towards persistence observed in the oceans. Similarly, in some areas where conditions are rather uniform, as few as 10 observations may be deemed sufficient, while in others, where convergence or upwelling may be found or where the area in question may be under the influence of rapidly changing air masses, a much greater number would be required to obtain a representative monthly mean. Again, the practice of relating an observation in a given area to that in an adjacent area (long considered helpful in working up meteorological series) also involves some danger if the area represents more than one kind of water mass or more than one current system.

Obviously, the greater the number of observations per given unit of time, the greater their spread, and the smaller the area considered, the more representative the mean value based upon them will be. However, since the number of observations is quite small in relation to the vastness of the oceans, the area chosen for developing a historical series cannot be too small nor the time interval very short. Therefore, the plan followed here was to take a month as the unit of time and a 5 deg Marsden square as the unit of area. The areas chosen were: Area 1, with the limits 15N to 20N, 60W to 65W, representing tropical conditions and traversed by the North Atlantic Equatorial Current; Area 2: 30N to 35N, 55W to 60W, representing semitropical conditions and influenced by the Gulf Stream; and Area 3: 45N to 50N and 45W to 50W (off Newfoundland), representing polar conditions and dominated by the Labrador Current. The months chosen were January and July except in case of Area 3 where April was selected instead of January in order to register also the ice effects which reach their peak in that area during that month.

An examination of the six selected series of mean monthly temperatures shows that the number of observations in a given month varied greatly, from as many as 150 in one month to some months with only one or two observations, depending on the area and the month considered. Since the number of observations is a determining factor in the monthly mean, we considered the series on the basis of (1) all the mean monthly values, regardless of the number of observations on which a given month's value was based, (2) the means for those months having 6 or more observations per month, (3) the means for those months with 11 or more observations per month, and (4) in some instances, only the means for those months with 16 or more observations per month. The respective long-term means, ranges, standard deviations, σ, and standard error of the mean, $\sigma_{\bar{x}}$, are shown (table 1).

The standard error of the mean (the last row of table 1), fluctuated very little or none at all in cases except the April series of Area 3. This

Table 2. Mean decadal values* (midpoint to midpoint) of mean January or April, and July sea-surface temperature for western North Atlantic areas based on mean monthly values with one or more (≥ 1), six or more (≥ 6), and eleven or more (≥ 11) observations each month.

	Months:	January			July		
	No. of Observations:	≥ 1	≥ 6	≥ 11	≥ 1	≥ 6	≥ 11
	1876–1885	78.4^{6}					
	1886–1895	78.3^{9}	78.3^{9}	78.4^{8}	81.4^{7}		
Area 1:	1896–1905	78.6^{6}					
	1906–1915	77.5^{9}	77.7^{8}	77.6^{7}	81.0^{7}	81.1^{6}	
15N to 20N	1916–1925	77.4^{8}	76.9^{6}		80.8^{9}	80.8^{9}	81.0^{6}
60W to 65W	1926–1935	77.9^{10}	77.9^{10}	77.9^{10}	81.2^{10}	81.2^{10}	81.2^{10}
	1936–1945	79.4^{10}	79.2^{8}	79.1^{7}	82.4^{9}	82.3^{8}	82.3^{8}
	1946–1955	79.3^{8}	79.3^{8}	79.3^{8}	82.1^{9}	82.1^{9}	82.1^{9}
			January			July	
	1876–1885						
	1886–1895				77.6^{6}		
Area 2:	1896–1905						
	1906–1915	68.1^{9}	67.6^{7}		77.8^{9}	78.1^{8}	78.2^{6}
30N to 35N	1916–1925	67.0^{7}	67.0^{7}		77.5^{8}	77.5^{8}	78.2^{6}
55W to 60W	1926–1935	67.8^{10}	67.8^{10}	67.8^{10}	78.7^{10}	78.7^{10}	78.7^{10}
	1936–1945	68.5^{10}	68.3^{9}	68.3^{9}	79.8^{10}	79.8^{10}	79.4^{8}
	1946–1955	68.8^{10}	68.6^{9}	68.6^{9}	79.9^{10}	79.9^{9}	79.9^{9}
			April			July	
	1876–1885	40.9^{7}			51.6^{7}		
	1886–1895	39.7^{8}			51.5^{10}	51.5^{10}	50.9^{8}
Area 3:	1896–1905						
	1906–1915				49.4^{9}	49.4^{9}	49.4^{6}
45N to 50N	1916–1925	37.2^{7}	35.8^{6}		47.9^{10}	47.9^{10}	47.9^{10}
45W to 50W	1926–1935	38.2^{10}	37.7^{9}	36.8^{8}	51.1^{10}	51.1^{10}	51.1^{10}
	1936–1945	38.8^{10}	37.8^{8}	37.8^{8}	52.3^{8}	51.5^{7}	51.3^{6}
	1946–1955	38.8^{10}	38.8^{10}	38.8^{10}	52.2^{9}	52.2^{9}	52.0^{8}

* Based on 6 or more years of observations. Number of years in decade shown by exponent.

suggests that the long-term mean obtained on the basis of all the monthly values may be, in all cases but one, representative of the long-term mean as calculated from an abbreviated series. In the Area 3 April series, the standard error, ± 0.76, derived by using all the data, drops rather sharply to ± 0.40 when only the values with 6 or more observations are retained. This result favors using the mean derived from the abbreviated series instead. Table 1 also shows that the standard deviation, σ, or error of the individual monthly value is quite constant for both the January and July months in Area 1 as we go from the series based on all values to the series based on only those with 6 or more observations. Next we find that σ is appreciably (though not seriously) changed in the case of Area 2. Finally, the value of σ in Area 3 is also quite constant for July but drops sharply for that area in April. This indicates that, except for Area 3 in April and, to a lesser extent, Area 2 for both January and July, the error of an individual value is no less when derived from an abbreviated series than if all the years were used.

Although Area 3 is basically polar in character with a long-term mean April temperature of only 38 deg, it occasionally registers temperatures as high as 63 deg during that month, undoubtedly due to Gulf Stream eddies that penetrate into that area from time to time. These high values cannot be regarded as spurious, but their elimination is fully justified if, when taken alone in very small numbers, they happen to represent the monthly mean.

To indicate how much a series needs to be abbreviated in order to keep the error of the individual "observation" (in this case the mean monthly value) at a minimum, the relative constancy of the standard deviation, σ, may serve as a valid guide. When this criterion is applied to series with progressively fewer mean monthly values, by successively eliminating values with few observations, the point at which the standard deviation drops and then tends to stay constant may be the point beyond which it is unwise to discard further data. Although the standard deviation does not tell us about the actual composition and range of temperatures of a given mean monthly value, which may vary greatly from year to year though yielding the same mean, it suggests when the values which remain (after those instances having a limited number of observations have been eliminated) are closer to the true mean monthly values than before. A mean monthly value derived from few observations in a relatively large area is more likely to include a greater proportion of extreme values than a value derived from a larger number of observations.

Table 2, giving mean decadal values of mean monthly temperature (midpoint to midpoint) for each area and each month, which were obtained by eliminating values with progressively fewer observations, on the whole shows a greater uniformity of trend after the values with 5 or fewer observations have been eliminated. This is most apparent in the case of area 3 for April. The value of 40.9 deg derived for the period 1876 to 1885, which was based on mean monthly values including those with 5 or fewer observations, is larger than the value for the decade 1946 to 1955. In all the other series, the highest value occurs in the last or next to the last decade, which is in keeping with a widely noted trend shown in other data (Brown, 1952; Bullig, 1954; Smed, 1949; Schell, 1956). By using the relative constancy of the standard deviation, σ, test, a reasonably reliable method for developing historical series suitable for studying decadal or other trends seems at hand.

On the same principle, the use of the above criterion in developing mean seasonal historical year-by-year series would appear justified since the month would count less within a season than when alone.

3. Summary and conclusions

Significant progress has been made in our attempts to develop historical series of sea-surface temperatures through the application of the relative constancy of the standard deviation, σ, test. Application of the criterion appears to be successful with respect to historical series where a number of years (*e.g.*, a decade) have been combined and, we suspect, also with respect to a year-by-year historical series in which several months are taken together.

By eliminating the mean monthly values based on few observations, we have, generally speaking, eliminated a greater proportion of cases that are not representative of true mean monthly values than those that are (if all the months were kept in) and, in that way, have come closer to developing also a year-by-year historical series of mean monthly and shorter time-interval sea temperatures. For a definitive year-by-year mean monthly and other time-interval series, additional analysis involving characteristics of the individual observations would be necessary.

Acknowledgment. I am indebted to officials of the National Weather Records Center, Asheville, N. C., for the data used in this study.

REFERENCES

Brown, P. R., 1953: Climatic fluctuation in the Greenland and Norwegian Seas. *Quart. J. r. Meteor Soc.*, **79**, 272–281.

Bullig, H. J., 1954: *Atlas der Monatswerte von Wassertemperatur, Wind und Bewolkung auf dem Seeweg Europa-Südamerika.* Deutsch. Wetterd. Seewetteramt, Einzenveröf. Nr. 5. Hamburg.

Liepe, H., 1911: Temperaturschwankungen der Meeresoberfläche von Quessant bis St. Paul-Fels. *Ann. Hydrog. Mar. Meteor.* **39**, 471–485.

Petersen, H., 1910: Uperiodische Temperaturschwankungen in Golfstrom und deren Beziehung zu der Luftdruckverteilung. *Ann. Hydrog.* **38**, 397–417.

Riehl, H., 1956: *Sea surface temperatures of the North Atlantic 1887–1936.* Chicago, Univ. Chicago, multigraphed.

Sandstrom, H. W., 1942: On the relation of the surface temperature of the sea to the air temperature. *Ark. f. Mat. Astro. Fys.*, **26A**, 1–24.

Schell, I. I., 1956: Interrelations of Arctic ice with the atmosphere and the ocean in the North Atlantic-Arctic and adjacent areas. *J. Meteor.*, **13**, 46–58.

Smed, H., 1942–1945, 1946, 1947, 1948, 1949, 1950, 1951, 1952. Monthly anomalies of the surface temperature. *Cons. perm. internatl. Explor. Mer. Ann. Biol.*, **2**, 17–22; **3**, 12–24; **4**, 11–26; **5**, 10–15; **6**, 18–27; **7**, 9–13; **8**, 19–20; **9**, 16–19.

—— 1949: The increase in the sea temperature in northern waters during recent years. *Cons. perm. internatl. Explor. Mer. Rapp. Proc.-Verb.*, **125**, 21–25.

Contribution No. 1030

THE ENERGETICS OF HARBOR SEALS IN AIR AND IN WATER WITH SPECIAL CONSIDERATION OF SEASONAL CHANGES[1]

J. S. HART AND L. IRVING[2]
With the assistance of B. MACKENZIE

Abstract

The energetics of six harbor seals in air at temperatures from 25° C to −20° C and in water from 25° C to 0° C was studied in animals acclimatized to summer conditions at Woods Hole, Mass. Over the above temperature range, the temperature of skin of the back cooled from about 35° to 1° with lowering temperature of the medium. Temperatures of the flippers were less dependent upon the surroundings than those of the body skin. The dependence of metabolism upon temperature was operative below 2° C in air and below 20° C in water (the critical temperatures), but the body skin temperature at these critical temperatures was the same, viz. 21° C. Metabolism in air and in water was the same over the range of comparable skin temperatures. Body insulation was equal in air and in water at the respective critical temperatures. The insulation index of the air was approximately 20 times that of the water. Heat conductivity of living blubber to water averaged 2.5 cal/cm^2/hr/°C, which exceeded that reported for dead blubber by about 50%.

When compared with seals tested at St. Andrews during December, summer seals had a higher critical temperature, a lower body insulation index at the critical temperature, and a warmer body skin temperature for the same metabolic rate. No seasonal changes were found in thermoneutral metabolic rate, and no discernible changes in skin temperatures or in thermal gradients in the blubber.

Introduction

The phenotypic modifications of mammals following changes in climate fall into two general categories, metabolic and insulative (4). In the former, cold is met by the development of an enhanced ability to produce heat, while in the latter it is met by reducing heat loss either by greater pelage insulation or greater cooling of peripheral tissues. Natural metabolic acclimatization, which has been observed by Hart in deer mice (5), may occur in species of small body size. In animals such as the fox and porcupine with thick fur, Irving and co-workers (9) have found that there was a marked restriction of the emission of heat associated with the thicker fur during winter. Their findings complemented the observations of Scholander *et al.* (10) on the importance of fur for the low critical temperatures of arctic animals during winter, and those of Hart (3) on the greater winter pelage insulation of the larger mammals.

In "bare skinned" animals such as pigs (6), and seals (7), fur has little or no protective value and the skin surface assumes a dominant role in the loss of heat. Any modifications to suit low winter air or water temperatures must therefore be brought about either by greater heat production or by reduction

---

[1] Manuscript received April 22, 1959.

Contribution from the Division of Applied Biology, N.R.C., Ottawa. The research was aided by a grant from the National Science Foundation to the Woods Hole Oceanographic Institution where the work was carried out. W.H.O.I. Contribution No. 1030.

Issued as N.R.C. No. 5259.

[2] Present address: Arctic Health Research Center, Anchorage, Alaska.

N.R.C. No. 5259

of heat loss through greater cooling of the living peripheral tissues. The remarkable capability of seals to show surface cooling in cold environments has already been demonstrated by Irving and Hart (7). The close correlation between the degree of cooling and the metabolic response in different individuals suggested the direction for further study of seasonal changes.

In the present investigation, the results obtained on a sample of harbor seals during December 1955 are compared with those obtained on a sample of the same population during the summer of 1956. With these additional data it has been possible to give a more detailed account of the energetics of seals in air and in water than was possible during the winter of 1955.

Experimental Animals

Six harbor seals, *Phoca vitulina concolor*, captured at Boothbay Harbour, Maine, in May 1956 were shipped to Woods Hole, Mass., during July 1956. They were held in a large pound and fed frozen fish during the period of captivity from July to September. Observations on the animals were made in August and September, during which period water temperature varied from 20 to 22° C. The animals were presumably from the same population as those studied during the winter of 1955 (7). The similarity of the animals and methods of testing facilitate direct comparison of the 1955 and 1956 results.

Methods

The test methods used were identical with those reported earlier (7) except for the automatic instead of manual recording of temperature gradients. The availability of a cold room also made it possible to utilize a greater range of air temperatures than was possible in 1955. In brief, the procedure consisted in the testing of one animal per day at three or four different temperature conditions in air and in water. Surface temperatures were measured on a potentiometer indicator and tissue temperatures at various depths were recorded at 16 points in each 4 minutes by means of gradient needles (7) prepared by L. J. Peyton.

After thermal balance was obtained in approximately 1 hour, three or four 10–15 minute samples of expired air were obtained for the measurement of oxygen consumption during the second hour, as previously described (see Fig. 3).

In addition to these measurements, a few observations were made on the heat flow from the seal's surface to water of various temperatures to correlate heat flow with the observed thermal gradients measured close to the same site. For this purpose the rise of temperature of the water in a small Dewar flask held against the seal's side was measured with a calibrated thermocouple and a sensitive Leeds and Northrup d-c. amplifier. The calorimeter, which was previously calibrated by producing heat electrically, had a precision of approximately ±5%.

Results

Resting Metabolism

The metabolism of seals during the summer was dependent on environmental temperature below about 20° C in water and 2° C in air. The resting metabolism of all the seals in air and water warmer than these critical temperatures is shown in Table I together with body weights and respiratory quotients. The mean resting metabolism (18.3 ml/min/$kg^{3/4}$) did not differ significantly from that found for winter animals (Table I).

TABLE I

Average metabolism of seals at Woods Hole in air above 0° C and in water above 20° C

Seal No.	Weight, kg	O_2 consumption ml/min	O_2 consumption ml/min/$kg^{3/4}$	R.Q.	No. of tests
1	32.8	237	17.4	.76	13
2	31.7	219	16.3	.76	7
3	25.1	207	18.4	.69	7
4	24.4	217	19.8	.74	5
5	22.8	208	18.9	.71	7
6	27.4	213	18.1	.70	7
Mean summer	27.4		18.3 ± .38		
Mean winter*	33.7		19.3 ± .55		

*Excluding "runt" seal.

Owing to insufficient data in winter, it was not possible to compare the metabolic rates of summer and winter seals in air below the critical temperature but the comparisons for animals tested in water (Fig. 1) illustrate some appreciable differences. At subcritical temperatures, summer seals at Woods Hole had higher metabolic rates than winter seals at St. Andrews. The difference was reflected in a higher critical temperature in water in summer than in winter animals. In spite of the seasonal trends it may be seen that the exceptionally high metabolism of the "runt" seal tested during the winter was still greater than that found for any of the seals during the summer. The individual variability was also exemplified by summer seal No. 2 (◒), which had a much lower metabolism than any of the winter seals and which did not maintain a constant deep body temperature. The data on these exceptional seals have not been included in the subsequent results.

Skin Temperatures in Air and in Water

The data shown in Fig. 2 indicate that skin temperature on the surface of the back and on the flippers is closely dependendent on air or water temperature. In air, skin temperatures on the back fell markedly with lowering of the ambient temperature. The difference in temperature between skin and ambient increased with lowering tempearature even in the thermoneutral range (above 2° C). There were no discernible seasonal differences in skin temperatures, but insufficient data were obtained in air below the thermoneutral range for an adequate comparison.

The temperatures of the flippers in air, while following the general trend of temperatures of skin of the back, were more variable and this implies separate control of heat flow through these appendages as noted in our earlier study (7).

In water, skin surface temperatures showed a small increase above water temperatures as the latter fell from 26° to 0° C. As previously shown (7), differences in temperature between skin and water were small, the greatest

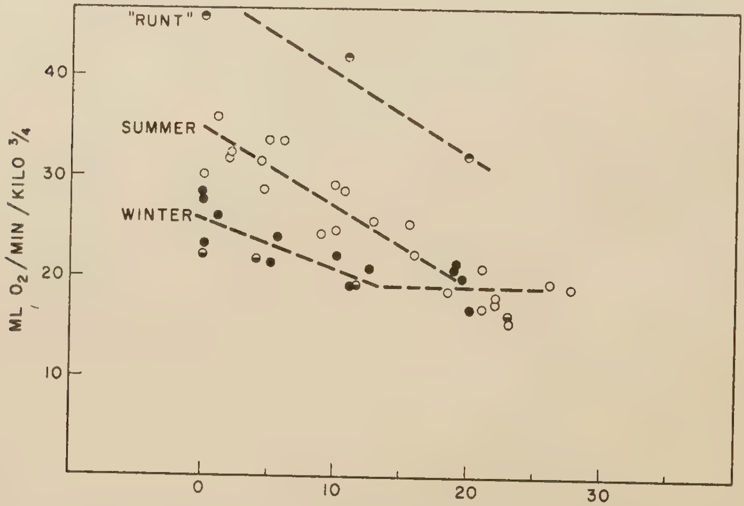

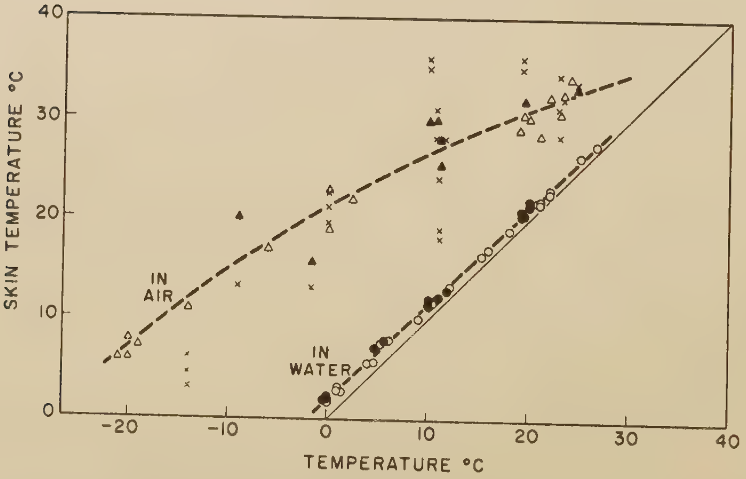

FIG. 1. Oxygen consumption of harbor seals during winter (●) and summer (○) in water. Large variation is illustrated by exceptionally high metabolism of "runt" (◓) seal (winter) and low metabolism of seal No. 2 (◒, summer).

FIG. 2. Body skin temperature of seals during winter (▲ ●) and summer (△ ○) are shown as a function of air (▲ △) and water (● ○) temperature. Each point is average of 3–5 measurements. Flipper temperatures (×) as a function of air temperature are more variable than those of body skin. Solid line indicates equality of skin and environmental temperature, broken lines indicate skin temperature trends. Difference between skin temperature and ambient is given by broken line minus solid line.

difference (2° C) occurring at 0° C. In water, no discernible seasonal differences in skin temperatures were evident but the accuracy of thermocouple measurements was probably insufficient for their detection.

Temperature Gradients and Heat Flow

Temperature gradients in the seal's tissues represent one parameter effecting heat flow which becomes meaningful when the conductivity of the tissues is known. Winter gradient curves, obtained from temperature measurements at various depths, have been previously reported (7). Figure 3 shows temperature contours for a summer seal under five different thermal conditions. The rapid attainment of thermal equilibrium within about 30 minutes indicates active regulation, which is also manifested in ice water by synchronous oscillations of 1 to 2° C in temperature of the subcutaneous tissues to a depth of 23 mm. In many such tests the flippers showed a marked tendency for independence in regulation, differing by 5 to 10° C from the temperature of the body surface.

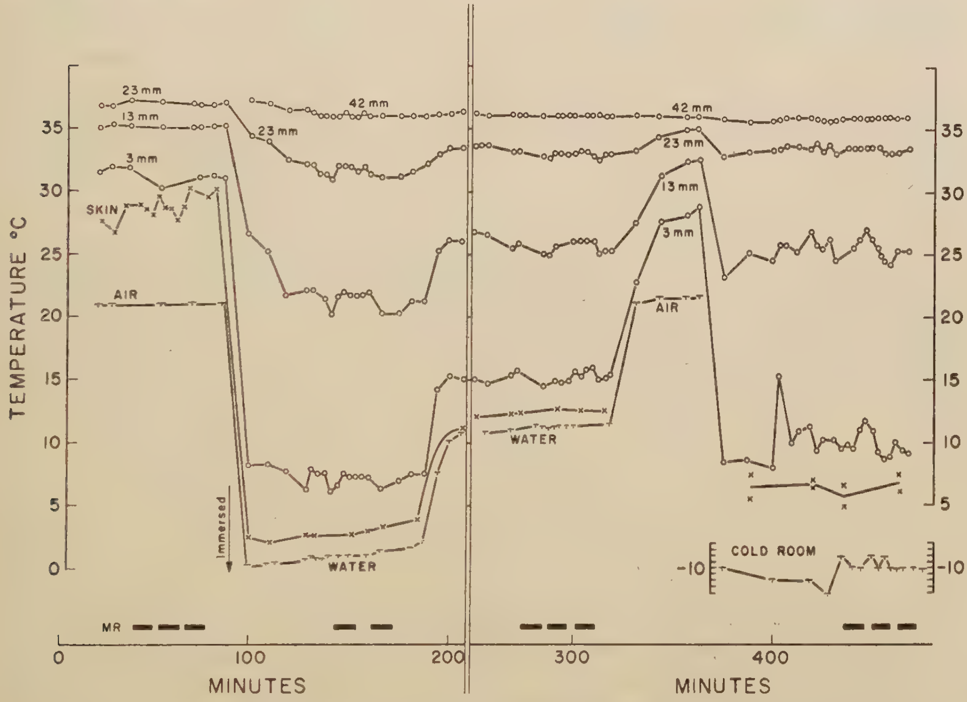

FIG. 3. Temperature measurements at various depths in a seal in air at 21° C, in water at 0–2° C, in water at 10–12° C, in air at 22° C, and in air at −10° C. Air temperatures, mean of five points within 25 cm of seal, agreeing within 1.5°. Water temperatures, mean of eight points in tank, agreeing within 0.1°. Skin temperature mean of two points on back just posterior to axilla and differing less than 0.5°. Horizontal bars marked "MR" show when gas samples taken.

In Fig. 4 are shown simultaneous records during 9 hours of two gradient needles inserted into the back 16 cm apart. The general similarity in response at the two locations and the speed of attainment of thermal balance is demonstrated. Plotting the simultaneously recorded gradients of the two positions at time 560 (Fig. 5) showed that around 5 to 20 mm in depth the two curves differed by 2° to 3° C. Owing to the shifting of the needles by 1 to 3 mm during the 9 hours of recording, the difference of 2° to 3° C represented the error to be expected when the gradient is steep. In water at 5° C (Fig. 5) the base of the blubber was 3° C cooler than the maximum recorded temperature of the deep musculature. Thus the temperature gradient is not confined to blubber and may at times involve only part of it.

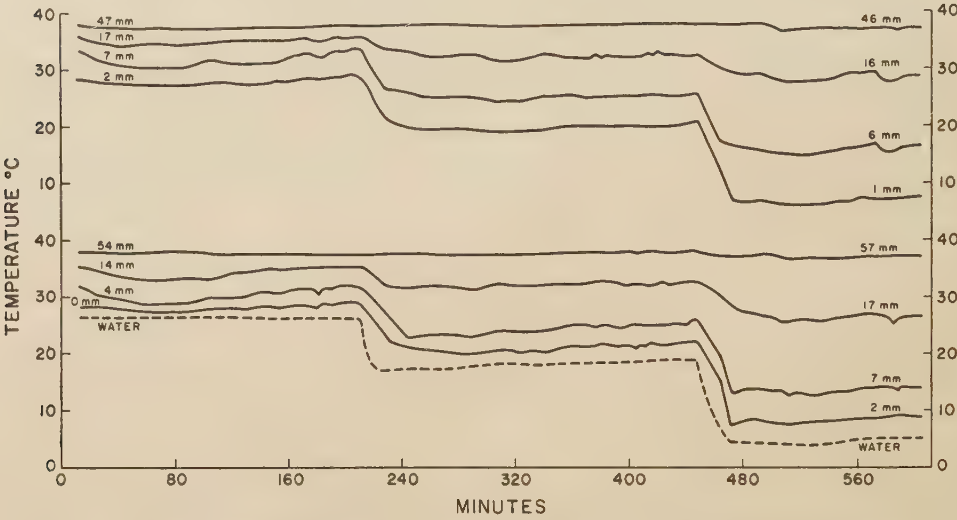

FIG. 4. Simultaneous records of temperature gradients of a seal at points separated by 16 cm on back over thorax. Upper record, point embedded in rib; lower, point intercostal.

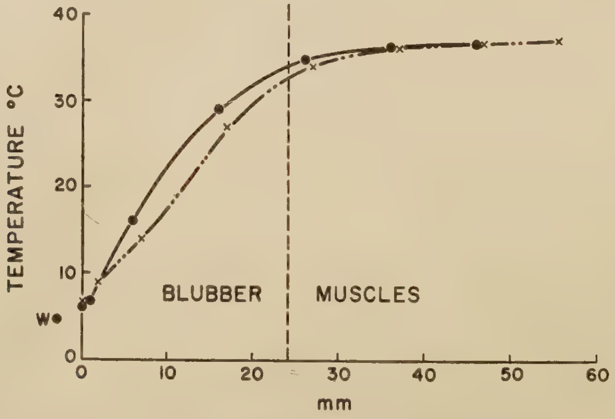

FIG. 5. Simultaneous recorded gradients from time 560 in Fig. 4.

To compare the temperature gradients during summer and winter, the temperature difference from skin to 37° C has been correlated with the depth of tissue corresponding to that difference (gradient length) shown in Fig. 6. Whether tested in air or water, summer or winter, the temperature–depth patterns were sensibly the same. The individual variability was marked and exceeded the errors in measurement.

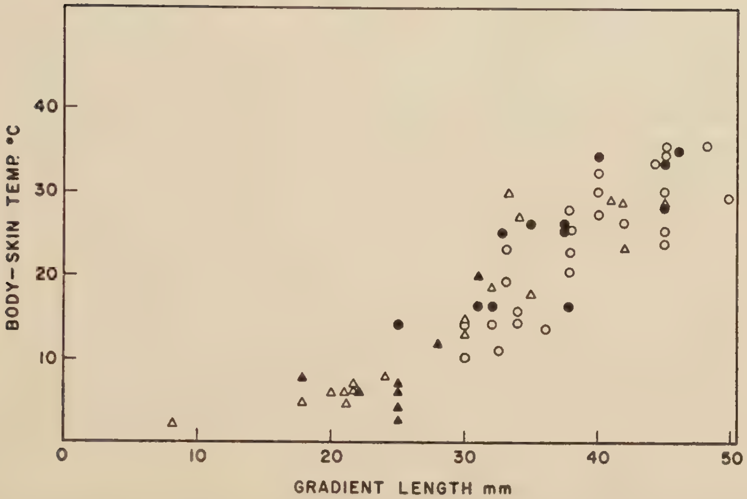

FIG. 6. Length of gradient as a function of the difference in temperature between deep body and skin surface for summer (△ ○) and winter (▲ ○) in air (▲ △) and in water (● ○)

Heat flow from the seal to water was measured on four animals at two or three temperatures (Table II). The heat flow increased with increasing gradient and decreasing temperature of the water. Conductivity values showed considerable variability between animals and temperatures. The average value of 2.5 cal/cm²/hr/°C is about 50% greater than the 1.6 cal/cm²/hr/°C measured by Scholander *et al.* (12) for dead blubber. The greater conductivity is attributable to the circulation of the living blubber.

Two seals (Nos. 1 and 3) were tested at temperatures well above the critical level (20° C). It is interesting to note that in warm water the conductivity of the blubber was not greater than that found at temperatures lower than the critical temperature.

TABLE II

Thermal characteristics of living seal blubber

Seal No.	Water temp., °C	Heat flow, cal/cm²/hr	Gradient,* °C/cm	Conductivity, cal/cm²/hr/°C
1	27.0	9.2	4.2	2.2
	18.0	15.8	7.0	2.3
	4.5	29.8	11.0	2.8
2	23.0	8.4	4.5	1.9
	11.0	12.1	6.5	1.9
3	26.0	11.2	4.0	2.8
	12.5	20.7	6.5	3.2
	2.0	31.6	9.5	3.3
6	22.0	13.9	6.0	2.3
	9.2	18.6	8.0	2.1
	0.0	29.8	11.7	2.5

*Measured in outer 10 mm of tissue.

Metabolism in Air and Water

The oxygen consumption of seals in air and water of various temperatures during the summer is shown in Fig. 7. As illustrated previously in Fig. 1, oxygen consumption began to increase in water at temperatures below 20° C and increased to nearly twice the thermoneutral rate at 0°C. In air, the oxygen consumption began to increase at temperatures just below 2° C and increased to about 50% above thermoneutral at −20° C.

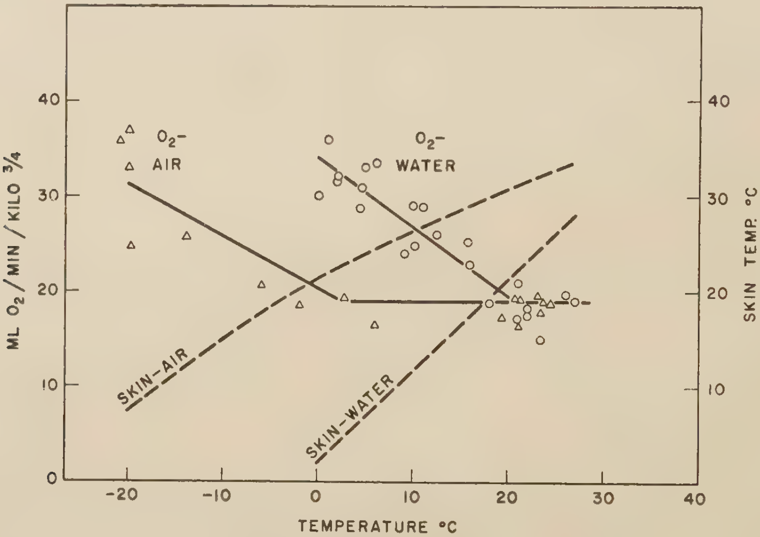

FIG. 7. Oxygen consumption of seals in air (△) and in water (○) at different temperatures during the summer. Body skin temperatures as a function of temperature of medium are also shown.

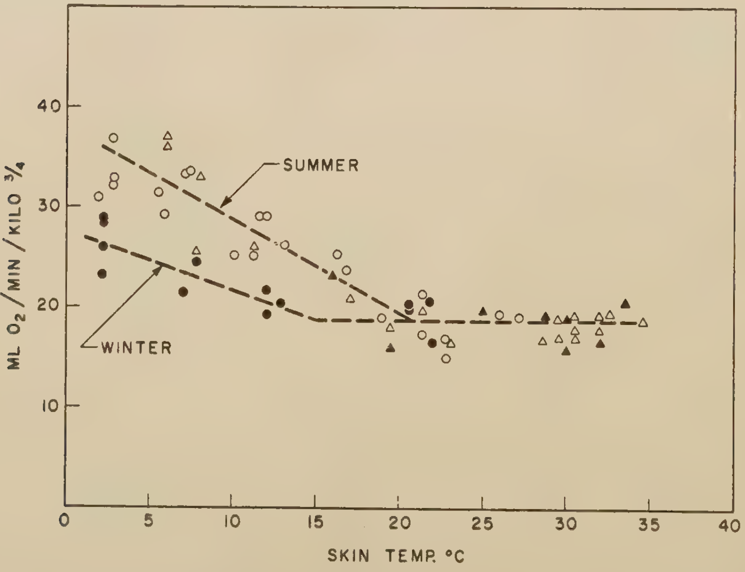

FIG. 8. Oxygen consumption as a function of body skin temperature for seals during winter and summer. Symbols same as for Fig. 2.

The broken lines in Fig. 7 give the average temperatures of skin of the back as a function of air or water temperature previously illustrated in detail in Fig. 2. A comparison of metabolism and skin temperatures brings out the fact that for a given skin temperature in air or water the metabolism is nearly the same. Thus, the critical temperature occurs at a skin temperature of approximately 21° C in water and in air. For an oxygen consumption rate of 30 ml/min/kg$^{3/4}$ the skin temperature is about 6° C in water, 8° C in air. These comparisons illustrate the general correspondence between metabolism and skin temperature in air and water.

The correspondence shown in Fig. 7 leads to the correlation between metabolism and skin temperature shown in Fig. 8, which combines results obtained both in air and in water into a composite description of seasonal changes. It is apparent that the principal differences between results obtained during the winter and those obtained during the summer is that in the latter metabolism began to increase at a higher skin temperature and was maintained at a higher level for the same skin temperature.

Insulation of Body and Medium

From the heat production, body, skin, and ambient temperatures, the insulation index (including evaporative heat loss) may be derived (Table III). Comparisons are made at the critical temperatures at which total body insulation is theoretically maximal (10). Insulation indices of body, medium, and total (body + medium) are calculated for summer and winter seals in water and for summer seals in air and in water.

The estimations show that the insulation index of the medium is some 20 times greater for air than for water but the errors in the measurements of small temperature differences in water renders the quantitative comparisons uncertain. In spite of the large difference in the cooling effects of air and water the total insulation in air is only about double that in water because the

TABLE III

Thermal properties of seals at critical temperature

(T = temperature, °C; MR = mean standard metabolism; I = insulation index)

	In water, winter	In water, summer	In air, summer
T, medium	13	20	2°
T, skin	14.5	21.0	21.0
T, body	37.0	37.0	37.0
MR, Cal/kg$^{3/4}$/min	.909	.862	.862
I, medium $= \frac{T\,(\text{skin}-\text{medium})}{MR}$	1.2	1.2	22.1
I, body $= \frac{T\,(\text{body}-\text{skin})}{MR}$	24.8	18.6	18.6
I, total $= \frac{T\,(\text{body}-\text{medium})}{MR}$	26.4	19.8	40.7

insulation index of the body is about equal in air and water at the respective critical temperatures. Finally, the insulation index of the seals' body in water appears to have been approximately 30% greater during the winter of 1955 than during the summer of 1956. The lower insulation in summer follows from the higher critical temperature and metabolic rate below the critical level observed in the seals during the summer.

Discussion

The study of the energetics of harbor seals in air and in water during winter and summer has revealed two principal new findings. The first was that increase of metabolism by cold during the summer was closely dependent upon the degree of body-skin cooling whether the medium was air or water (Fig. 7). The metabolic rates were approximately the same at comparable skin temperatures in water or in air with 20 times the cooling effect as water. It was also shown in summer that the body insulation index was the same in air or water at the critical temperature (skin temperature about 21° C). The metabolic rates could not be correlated with temperatures of the extremities, which showed a much less regular dependence on ambient temperature.

The second new finding was that, apart from two exceptional seals, the seasonal changes paralleled in direction the seasonal insulative acclimatization seen in certain land mammals with thick fur (9), i.e. the critical temperature was higher and over-all insulation was lower during the summer, and the heat production was greater over most of the temperature range. Unlike the land mammals, the seasonal change in energetics of harbor seals cannot be associated primarily with changes in insulation of the fur but with physiological adjustments in the living tissues themselves. The greater heat production at comparable cool temperatures during the summer suggests higher skin temperatures and an altered distribution of temperatures within the blubber. Yet, no seasonal differences in skin temperatures or in temperature gradients were observed, owing, presumably, to insufficient data for seals in air and to insufficient sensitivity of thermocouple measurements for seals in water. It may be appreciated that with the existing small temperature differences between skin and water (maximum 2° C), more sensitive methods would be required for the detection of seasonal changes, which might be no more than 1/2° C.

A puzzling outcome of this study was the seasonal shift in metabolic response to cold corresponding to the same skin temperature. So far as we are aware, this adjustment has not been previously reported. It is apparent that the same skin temperature corresponded to a greater heat flow in the summer than in the winter animals, and that compensatory shifts must have occurred in the avenues of heat loss. One possibility is that the temperature of the body surface was not changed, but more heat was lost from the appendages during the summer, through some modification in operation of the heat-exchanger system characteristic of aquatic mammals (11). Another possibility is that more heat was lost by evaporative cooling during the summer, but when the seal was in water this would have to be entirely from the lungs.

The seasonal changes suggested above can be regarded as extensions of the immediate compensations to changes in ambient temperature. As the body skin temperature increased, above critical temperature, heat loss from the body surface apparently decreased while heat loss through other channels (appendages and possibly evaporation) must have increased. This can be deduced from the fact that metabolism (and total heat loss) was independent of ambient temperature at skin temperatures above about 21° C (Fig. 8), yet the temperature difference between skin and ambient (and hence heat flow) decreased as the skin temperature increased above 21° C (Fig. 2). Direct measurements of heat flow from the body surface in water also suggest decreasing flow through that surface with increasing temperature in the thermoneutral zone, but the data were insufficient for final decision.

The central importance of skin temperatures in the metabolic responses of seals raises important problems concerning the stimulation of metabolism through peripheral nervous impulses. The approximate equality of metabolism in air and water at equal skin temperatures conforms with the view (1, 2) that thermogenesis is determined by peripheral impulses that are dependent on temperature in the skin. The seasonal shift in metabolic response for the same skin temperature implies a shift in nervous impulses with greater peripheral stimulation of metabolism in summer animals. It is unfortunate that integrative methods do not exist for assessing peripheral nervous stimulation, for very large species differences must exist, particularly between well-furred species with regularly warm skin and "bare skinned" species with variably cold skin.

Acknowledgment

We are grateful to L. W. Scattergood, U.S. Fisheries, Wildlife Service, Boothbay Harbor, for advising us of the steps necessary to assure the capture of seals.

References

1. Bazett, H. C. Theory of reflex controls to explain regulation of body temperature at rest and during exercise. J. Appl. Physiol. **4**, 245–262 (1951).
2. Carlson, L. D. Man in cold environment. Arctic Aeromed. Lab. Monog. 77–79 (1954).
3. Hart, J. S. Seasonal changes in insulation of the fur. Can. J. Zool. **34**, 53–57 (1956).
4. Hart, J. S. Climatic and temperature induced changes in the energetics of homeotherms. Rev. can. biol. **16**, 133–174 (1957).
5. Hart, J. S. and Heroux, O. A comparison of some seasonal and temperature changes in *Peromyscus;* cold resistance, metabolism, and pelage insulation. Can. J. Zool. **31**, 528 (1953).
6. Irving, L. Physiological insulation of swine as bare-skinned mammals. J. Appl. Physiol. **9**, 414–420 (1956).
7. Irving, L. and Hart, J. S. The metabolism and insulation of seals as bare-skinned mammals in cold water. Can. J. Zool. **35**, 497–511 (1957).
8. Irving, L. and Krog, J. Temperature of skin in the arctic as a regulator of heat. J. Appl. Physiol. **7**, 355–365 (1955).
9. Irving, L., Krog, J., and Monson, M. The metabolism of some Alaskan animals in winter and summer. Physiol. Zool. **88**, 173 (1935).
10. Scholander, P. F., Hock, R., Walters, V., Johnson, F., and Irving, L. Heat regulation in some arctic and tropical mammals and birds. Biol. Bull. **99**, 237–258 (1950).
11. Scholander, P. F. and Schevill, W. E. Countercurrent vascular heat exchange in the fins of whales. J. Appl. Physiol. **8**, 279–282 (1955).
12. Scholander, P. F., Walters, V., Hock, R., and Irving, L. Body insulation of some arctic and tropical mammals and birds. Biol. Bull. **99**, 225–236 (1950).

Contribution No. 1032

Wind-Induced Changes in the Water Column Along the East Coast of the United States*

Joseph Chase

Woods Hole Oceanographic Institution
Woods Hole, Massachusetts

Abstract—Two types of changes in the water column at certain lightships are linked to the wind pattern. In one type there is a replacement of the whole water column, whereas in the other there is a fluctuation in the thickness of the upper layer.

ntroduction—A program** of bathythermo- phic and water sampling observations at ven lightships along the east coast of the ited States was begun late in 1955. The data ıs collected provide an interesting daily rec- l of hydrographic events [*Bumpus*, 1957; *y*, 1959]. Of particular interest are parts of records from Frying Pan Shoals, Chesa- ıke, Winter Quarter, Five Fathom, Barnegat, l Ambrose lightships.

'rying Pan Shoals lightship is located about miles southwest of Cape Hatteras. The ers are spread along the coast from the uth of Chesapeake Bay to the offing of New rk (Fig. 1).

FRYING PAN SHOALS, FALL 1956

'emperature—From October 1, 1956 to the l of the year, the water column at Frying ı Shoals lightship was essentially homogene- , the temperature difference between top and tom (70 ft) being generally less than 0.5°F l the bottom salinity being generally within)‰ of the corresponding surface salinity. ottom salinity samples are taken once a week l surface samples are taken daily.) The hythermograph profile and salinity graphs 'igure 2 illustrate the general vertical homo- eity.

The surface temperature, which is thus a very good indicator for the whole column, provides a convenient means of studying the temporal changes during this season. A graph of the daily (0945 EST) surface temperatures, together with a dashed straight 'trend' line connecting its ends, is seen in Figure 3A.

At first the temperature line was close to the trend line, later (November 9 through Dec. 7) it was consistently below it, and still later (December 8 through 25) it was consistently above it. Reasons for this behavior were sought in daily 1230z weather maps. It soon appeared that temperature fluctuations were associated with air-mass movements. In general, warming occurred ahead of cold fronts (when southwesterly winds are prevalent) and cooling occurred after passages of cold fronts (when northerly winds prevail). The times of cold frontal passages are marked in the figure by arrows. (Note that the graph contains only one temperature per day and therefore does not show exactly when each temperature change began.)

The cold period from November 9 through December 7 was marked by many cold frontal passages, whereas during the subsequent warm period only three cold fronts passed the lightship. During this latter period on three occasions lasting two, six, and four days, respectively, the lightship was less than 300 miles south of a system of waves on a cold front.

The foregoing suggests the transfer of heat to the atmosphere as a mechanism for the lowering of water temperature in the wake of cold fronts, and indeed, rough calculations of heat loss yield figures of the right order of magnitude. How-

---

Contribution No. 1032 from Woods Hole anographic Institution.

* This program was instituted by the Woods le Oceanographic Institution under a contract h the U. S. Fish and Wildlife Service. The ob- vations at the lightships were made by the S. Coast Guard.

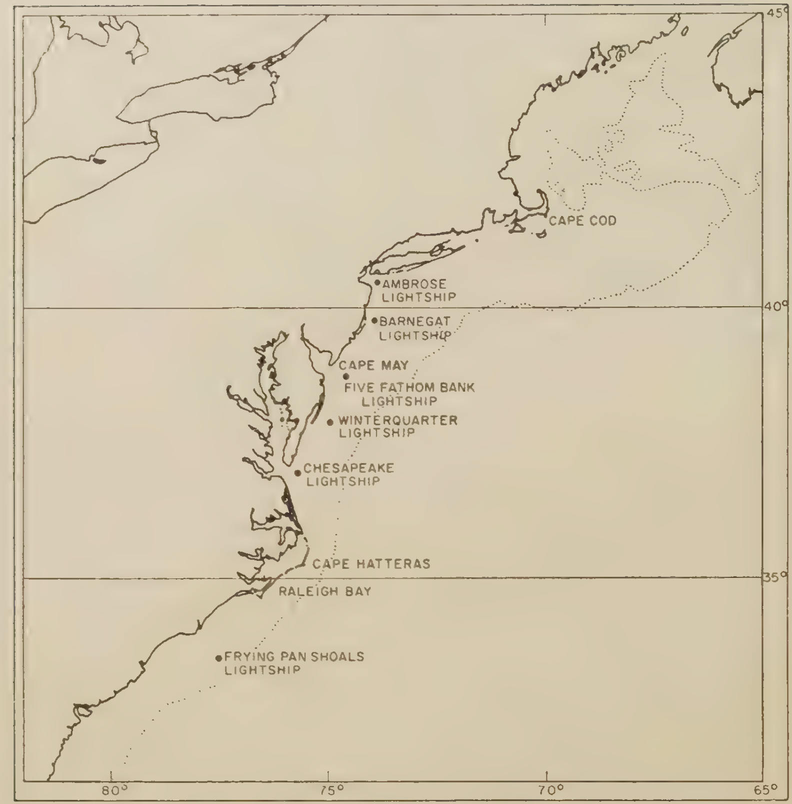
CAPE COD
AMBROSE LIGHTSHIP
BARNEGAT LIGHTSHIP
CAPE MAY
FIVE FATHOM BANK LIGHTSHIP
WINTERQUARTER LIGHTSHIP
CHESAPEAKE LIGHTSHIP
CAPE HATTERAS
RALEIGH BAY
FRYING PAN SHOALS LIGHTSHIP
45°
40°
35°
80°
75°
70°
65°

Fig. 1—East coast of the United States

ever, corresponding drops in the curve of salinity make such an explanation inadequate.

Salinity—The salinity at Frying Pan Shoals lightship is normally about 36‰ but during the period from October 6 through December 2, 1956 it ranged between 32.66‰ and 35.11‰ and averaged about 34‰ (Fig. 3B).

Water fresher than 34‰ is often found close to shore in this area. *Bumpus* [1955, p. 603] found that the amount of this 'fresh' water reflected the trends in runoff. He also found that the outflow from Pamlico Sound could account for considerable amounts of water fresher than 34‰ in Raleigh Bay. However, the amount of water available from these sources is hardly sufficient to account for the 34‰ found in the 70-ft column at the lightship.

A further and sufficient source is water from the Virginia coast which occasionally breaches the hydrographic barrier at Cape Hatteras and extends into Raleigh Bay. *Bumpus* and *Pierce* [1955, p. 96] reported such a breaching, wh occurred in January 1954 after a three-c northeast storm.

During October and the first half of Nove ber 1956, well over half of the winds recor at 0945 EST at the lightship were from north-northeast, northeast, and east-northe This is about twice the normal frequency. T chart of mean surface pressure for October 1 (Fig. 4) indicates that northeasterlies prevai as far north as New England; that is, abou degrees of latitude farther than normal.

Average surface-pressure charts of two riods of persistent northeasterly winds at lightship are seen in figures 5A and 5B. On these is for October 23 to 29, the days lead up to the regime of lower salinity, and the ot is for November 2 to 7, early in the regi Characteristic of all three charts is the ind tion of (1) northeasterly flow along the Ca lina coast and (2) a long sweep of northeast

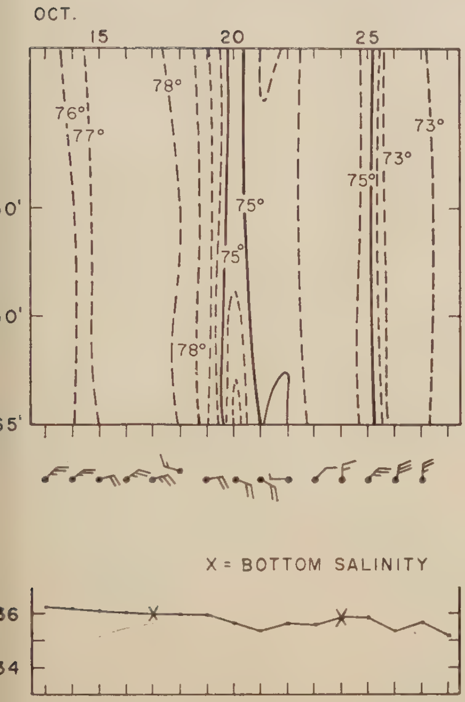

. 2—Typical bathythermograph profile and ty record at Frying Pan Shoals lightship, fall

asterly winds toward the coast between Hatteras and Cape Cod.

ese same characteristics are found in the s of the storm of January 22 to 24, 1954 6), after which *Bumpus* and *Pierce* [1955] l water from the Virginia coast in Raleigh And it was after such a pattern of isobars appeared on four successive days that two bottles released off Cape May by *Miller* 2] were found on the shores of Raleigh *Bumpus* [1955, p. 604] stated, "These are nly bottles on record to have rounded the in that direction or, for that matter, to been recorded as moving southerly in this n."

ree of Bumpus' figures show the distribu- of salinity off Cape Hatteras. During the *ross III* cruises in May 1949, the 34‰ ine was found at about the latitude of Hatteras, although during the surveys of ary and February 1950 it was found far- north. The northeast pattern described e was prevalent (though the winds were light) just prior to the May 1949 cruises but was not prevalent just before the cruises of January and February 1950.

Thus there is a consistent record of association of the northeast pattern with the movement of water southward to or past Hatteras.

A connection between characteristic (1), local northeast winds, and invasions of water from the Virginia coast into Raleigh Bay is not surprising, but the importance of characteristic (2), a long broad northeasterly or easterly flow of wind toward the coast north of Hatteras, is less obvious. However, *Miller* [1957, p. 30] showed that there was a maximum of setup* at Atlantic City under just such conditions. Presumably the effect is felt elsewhere along the coast and as far as Cape Hatteras. Possibly a pressure head thus developed contributes to the southward flow of water off the Cape. As a partial check on this concept, the surface-temperature records from Ambrose, Barnegat, Five Fathom, Winter Quarter, and Chesapeake lightships were examined. All showed a definite though slight lessening of cooling rate during late October and early November when the northeast pattern was prevalent. No greater effect would be expected, since the gradient of surface temperature between these lightships and the continental slope is very small at that time of year [*Bigelow*, 1933, Fig. 54].

The occasions when the northeast pattern was present for two or more successive days are indicated by the bars of Figure 3C. The incidence of the pattern was greater in this case than in any of the other cases studied, and it is not surprising that this corresponds to the greatest known excursion of Virginia coastal water. Four northeasterly regimes occurred in October and early November, and a fifth occurred on November 19 and 20.

The salinity at the lightship first dropped sharply after the third regime, fell still lower after the fourth, and fell again after the fifth. Superimposed on this record are the smaller drops associated with cold fronts. A possible explanation of the foregoing is that:

A. As a result of (1) northeast winds along the Carolina coast and (2) a long broad northeasterly or easterly wind flow toward the coast

---

* Or wind tide.

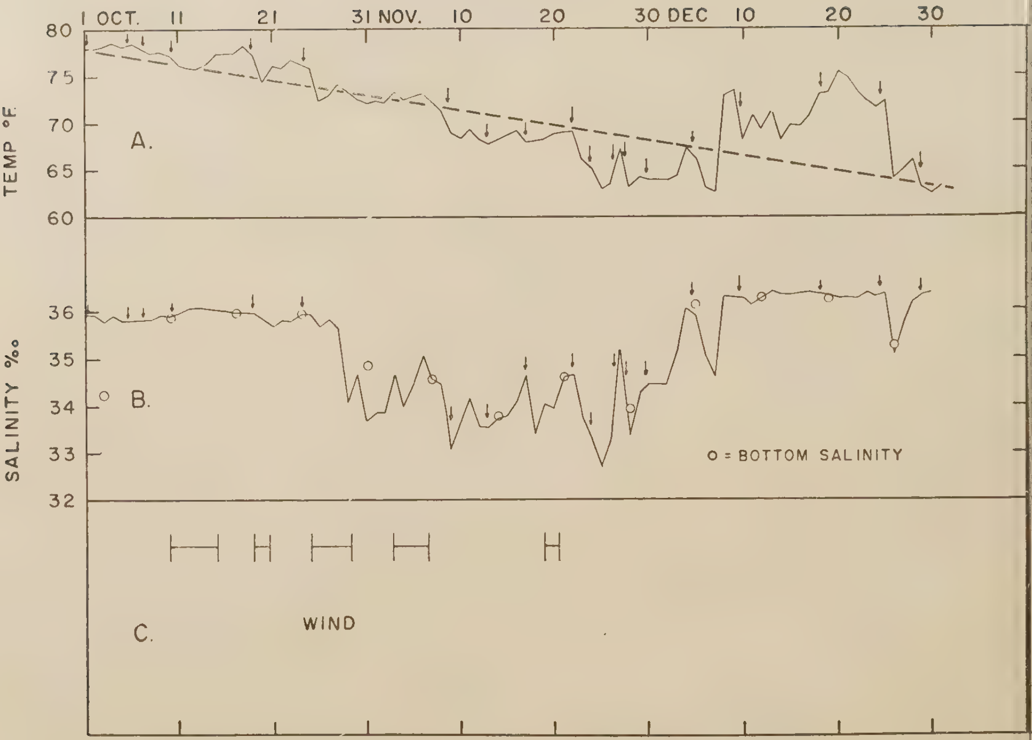

FIG. 3—(A) Daily surface temperature, Frying Pan Shoals lightship, fall 1956; (B) Daily salinity, F ing Pan Shoals lightship, fall 1956; (C) Graph of occurrence of typical northeast pattern, Frying Shoals lightship, fall 1956

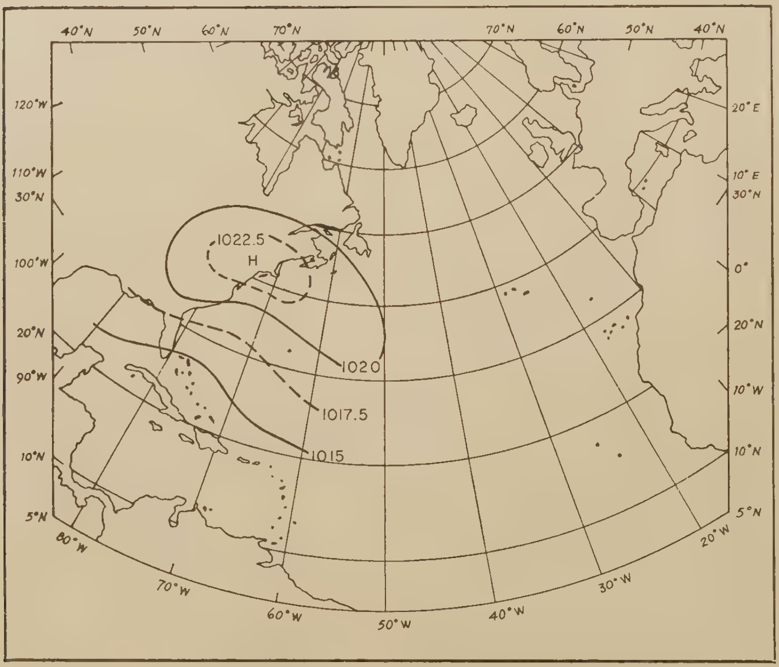
40°N
50°N
60°N
70°N
70°N
60°N
50°N
40°N
120°W
110°W
30°N
100°W
20°N
90°W
10°N
5°N
80°W
70°W
60°W
50°W
40°W
30°W
20°W
20°E
10°E
30°N
0°
20°N
10°W
10°N
5°N
1022.5
H
1020
1017.5
1015

FIG. 4—Mean surface pressure, October 1956

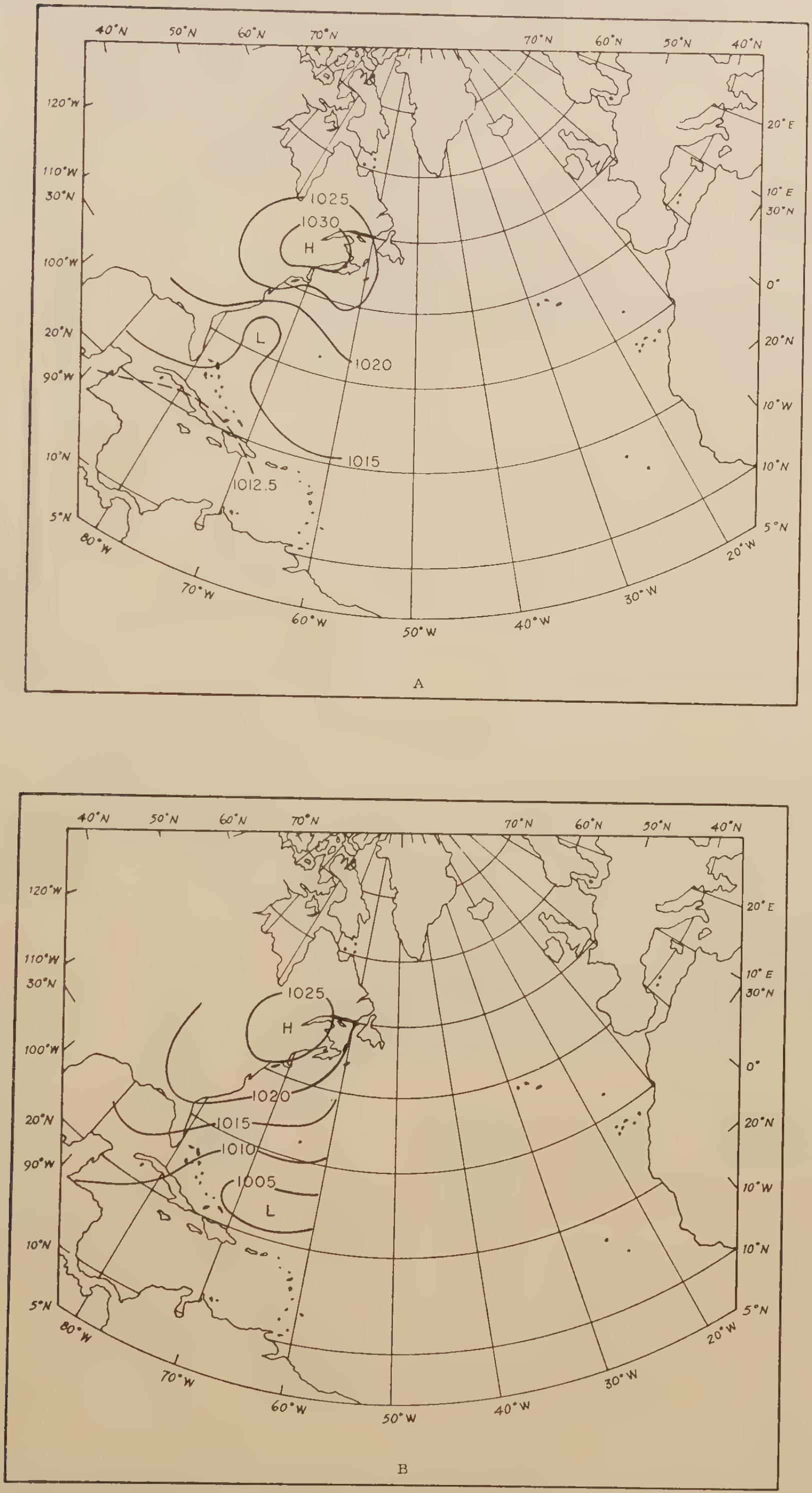
40°N
50°N
60°N
70°N
70°N
60°N
50°N
40°N
120°W
110°W
30°N
100°W
20°N
90°W
10°N
5°N
80°W
70°W
60°W
50°W
40°W
30°W
20°W
5°N
10°N
10°W
20°N
0°
30°N
10° E
20° E
1025
1030
H
L
1020
1015
1012.5
A
1025
H
1020
1015
1010
1005
L
B

5—Average surface pressure during two periods of persistent northeasterly winds at Frying Pan Shoals lightship; (A) October 23–29, 1956; (B) November 2–7, 1956

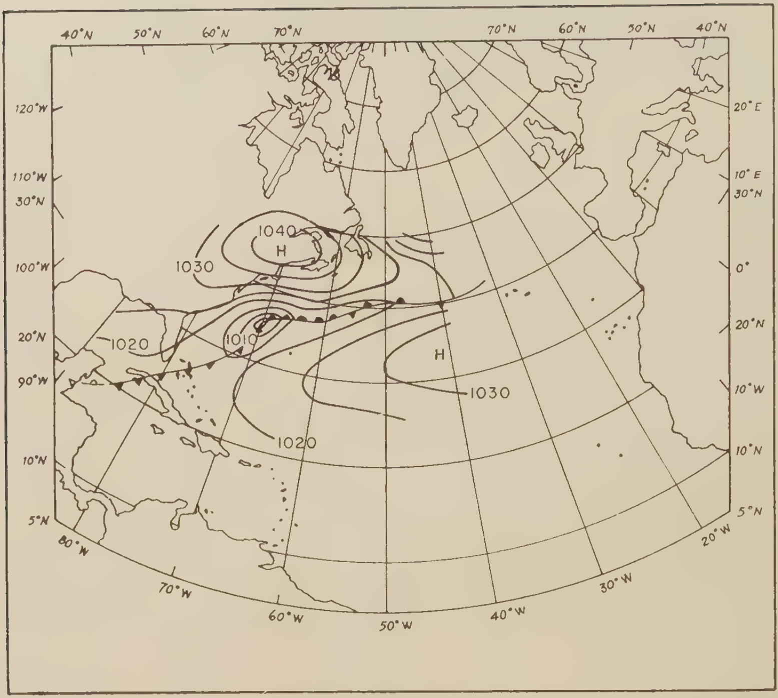
40°N
50°N
60°N
70°N
70°N
60°N
50°N
40°N
120°W
110°W
30°N
100°W
20°N
90°W
10°N
5°N
80°W
70°W
60°W
50°W
40°W
30°W
20°W
20°E
10°E
30°N
0°
20°N
10°W
10°N
5°N
1040
H
1030
1020
1010
H
1030
1020

FIG. 6—Surface pressure, January 23, 1954

between Cape Hatteras and Cape Cod, Virginia coastal water can be swept southward around Cape Hatteras. This is an extension of a theory proposed by *Bumpus* and *Pierce* [1955, p. 95].

B. When, in the fall, this pattern of northeast wind occurs with sufficient frequency and wind strength, large volumes of water from the Virginia coast can be carried as far south as Frying Pan Shoals. This results in a lowering of both temperature and salinity in the whole water column.

C. In the fall, under the action of post-cold-frontal winds, relatively cold water is blown seaward as far as Frying Pan Shoals lightship. When a large column of Virginia coastal water is in the immediate vicinity, the temperature drop tends to be large, and an appreciable drop in salinity is also observed.

From November 25 to December 8 there was an over-all upward trend in salinity toward the normal value of 36‰. This suggests a gradual mixing of the previously advected Virginia coastal water with the more saline Carolina coastal or Florida Current waters which are normally found in the area.

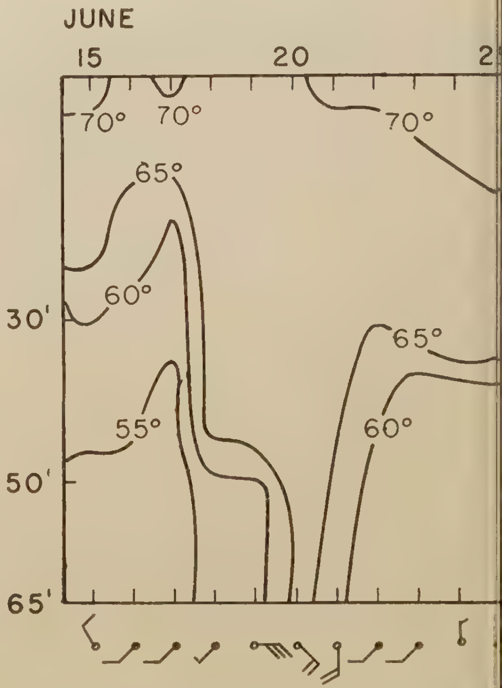

FIG. 7—Temperature profile, Chesapeake lightsh
June 15–25, 1956

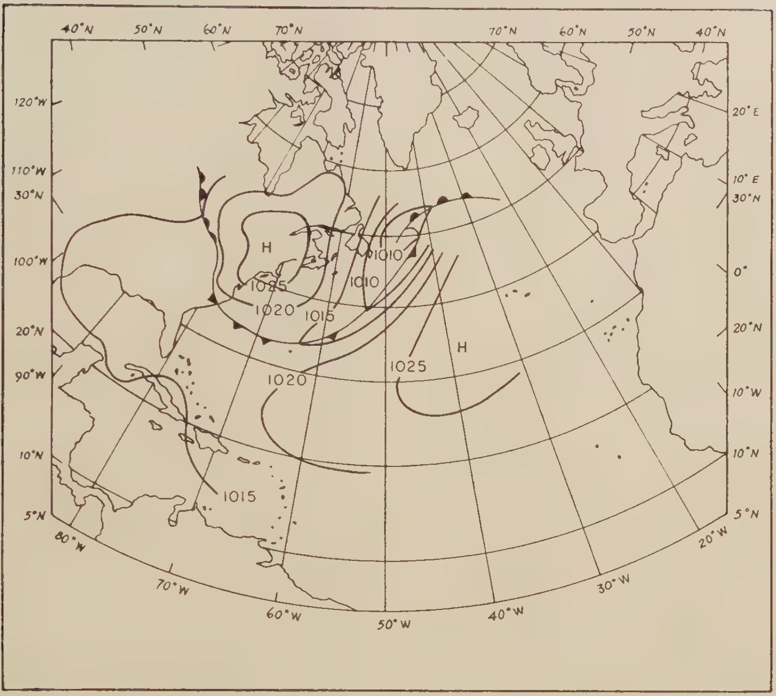

Fig. 8—Surface weather map, 0730 EST, June 19, 1956

The drop in salinity to about 35‰ on De-mber 26, after the passage of a sharp cold ont, suggests that the mixture had migrated orthward from Frying Pan Shoals but was hen pushed southward by the post-frontal inds.

hesapeake to Ambrose, June to September

The summer data from Chesapeake, Winter uarter, Five Fathom, Barnegat, and Ambrose ghtships reveal many instances when the ther-ocline rose or fell as the warm surface layer ecame thinner or thicker. Particularly dra-atic were three occasions in 1956 when at hesapeake warm water flooded the entire col-mn, driving out the cold water normally found t the bottom. These occasions were June 17 to), August 5 to 7, and August 21 to 24. Each as accompanied by an easterly wind at the ghtship and, farther offshore, a large area of ortheasterly or easterly winds. *Bumpus* [1957] oted the basic relationship in his discussion of n-day means of temperature.

The situation is analogous to that at Sambro Nova Scotia) Light Vessel as described by *Longard* and *Banks* [1952]. Whereas at Sambro a force 6 wind was needed to fill the 300-ft water column with warm water, force 4 was enough at Chesapeake (65 ft).

Figures 7, 9, and 11 are temperature profiles showing the thickening of the warm surface layer and the increase of temperature in the deeper water. The weather charts of Figures 8, 10, and 12 give the type of pressure distribution associated with the periods of warming. Each indicates that a large off-shore area was subject to northeasterly or easterly winds.

It is interesting that at a depth of 30 ft, on June 17 and 18, there was an increase of nearly 14°F (Fig. 7), even though the local wind was southwesterly; whereas on August 2 and 3 (Fig. 9), when the local winds were easterly, the temperature was virtually unchanged. These two cases indicate the importance of the winds at sea. In the former case a large area of easterlies was advancing southward from New England but had not yet reached the lightship. In the latter, although there were some easterlies off shore, they were weak, of short duration, and of small extent.

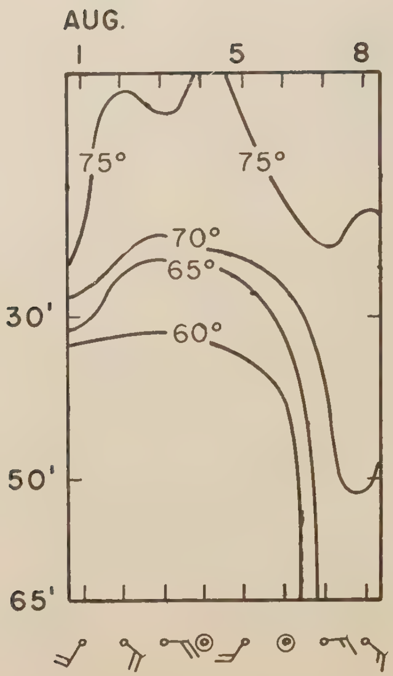

FIG. 9—Temperature profile, Chesapeake lightship, August 1–8, 1956

At Winter Quarter, Five Fathom, Barneg and Ambrose lightships, similar though not ways parallel reactions to wind occur. Dur June 17 to 20, 1956, Chesapeake showed largest reaction and Winter Quarter the seco largest. Evidently, the more northerly sh were somewhat in the lee of Cape Cod and L Island. From September 16 to 20, 1958, on other hand, the bottom temperature at *Ambr* rose 12°F while the other stations showed response. At this time *Ambrose* was in a field easterly winds on the north side of a front, the other lightships were south of the fr where the southwesterly winds evidently p vented an accumulation of surface water.

It is not always easy to find an explanation such selectivity. Possibly some of the floodi have a period of considerably less than 24 ho and thus can be missed by daily observatio The column at Winter Quarter respond markedly (11° at 50 ft) to the easterlies of A gust 2, 1956, while no response was evident the other ships.

Immediately after the flooding of June 17 20, 1956 (Fig. 7), cold water flowed back i

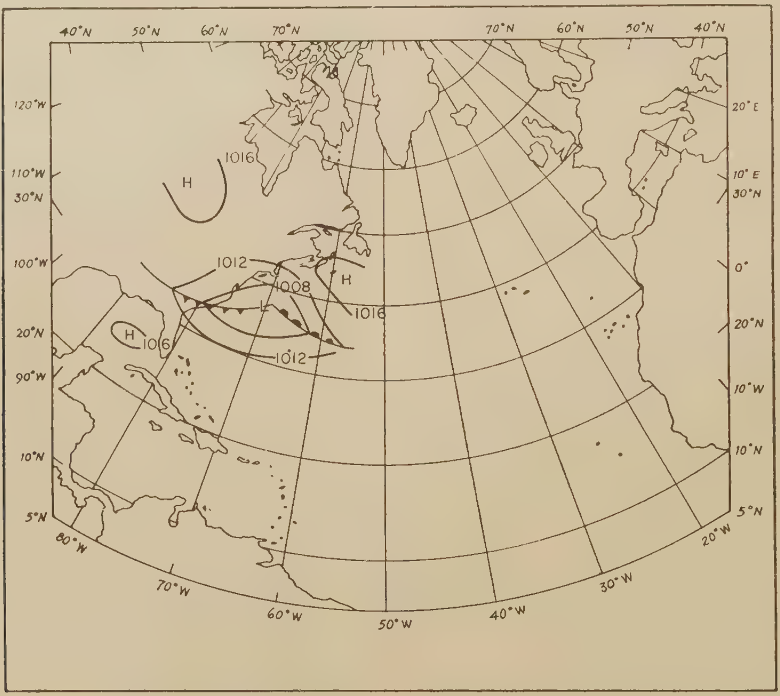
40°N
50°N
60°N
70°N
70°N
60°N
50°N
40°N
120°W
20°E
110°W
10°E
30°N
30°N
1016
H
100°W
1012
0°
1008
H
1016
20°N
H
1016
20°N
1012
90°W
10°W
10°N
10°N
5°N
5°N
80°W
20°W
70°W
30°W
60°W
40°W
50°W

FIG. 10—Surface weather map, 0130 EST, August 7, 1956

lower 25 ft of the column at Chesapeake. is return was probably helped by the south- y winds of June 21 to 23, but, since the winds ré rather light, it appears that this was, in main, a return to hydrostatic equilibrium. e cold water became much thicker in early ly after a period of stronger southwesterly nds. *Taylor* and *Steward* [1959] have re- rted similar upwelling along the east coast of rida.

It would be interesting to know the thickness the warm and the cold layers, the thermocline der equilibrium conditions, and to what ex- nt these thicknesses may change during the son. The averages probably will not reveal s, for the average wind, which is southwest- y, would tend to push surface water seaward d thus disturb the balance. Equilibrium con- ions can probably be determined most easily rough the examination of data taken in peri- s of extended calm. This is a study for some ure time when sufficient data have become ailable.

In the summers of 1957 and 1958 there were

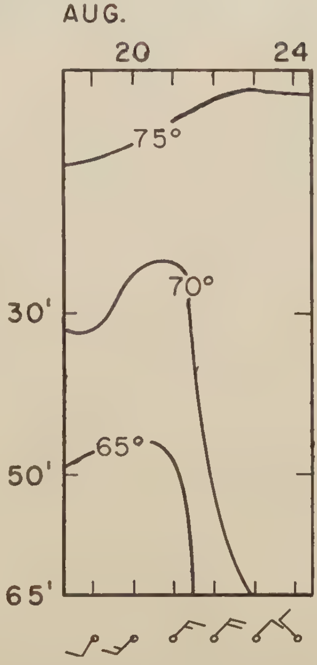

FIG. 11—Temperature profile, Chesapeake lightship, August 19–24, 1956

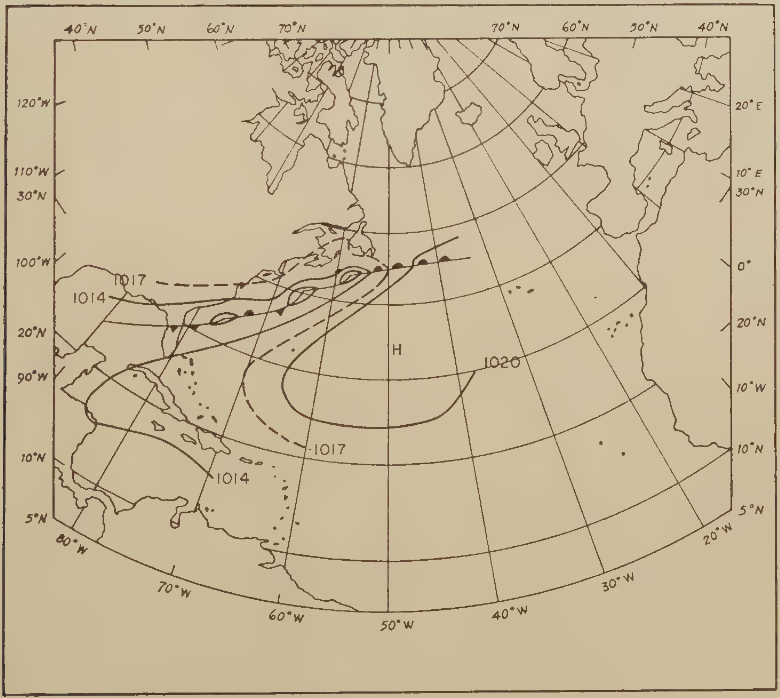
40°N
50°N
60°N
70°N
70°N
60°N
50°N
40°N
120°W
110°W
30°N
100°W
20°N
90°W
10°N
5°N
80°W
70°W
60°W
50°W
40°W
30°W
20°W
5°N
10°N
10°W
20°N
0°
30°N
10°E
20°E
1017
1014
H
1020
1017
1014

FIG. 12—Surface weather map, 0730 EST, August 22, 1956

many responses to wind like those of 1956, but none so abrupt. A gradual warming at all five stations occurred during the first three weeks of August 1957, a period when northeasterly winds far outnumbered the southwesterlies. In 1958, hurricane Daisy caused warming at all five stations as it moved northward along the coast. This hurricane caused warming in the lower part of the column at Frying Pan Shoals lightship also, although much of the time this column fails to respond to wind in the manner of the columns from Chesapeake to Ambrose.

No use has been made of the Chesapeake salinity data to indicate water movement because (1) the distribution of salinity off the mouth of Chesapeake Bay is too complicated [*Miller* 1952, Fig. 4] and (2) the data are insufficient for determining the exact times of maxima and minima.

The relationship between northeasterly or easterly wind fields and the flooding of surface waters along the Middle Atlantic coast is essentially the same as that conjectured in the section on fall conditions at Frying Pan Shoals lightship.

Acknowledgements—The writer wishes to express his appreciation to Dean Bumpus for his interest and guidance and to Raymond Wexler and G. Godfrey Day for their helpful suggestions.

This study was sponsored by the Office of Naval Research under contract Nonr 2196(00) NR 083-004.

References

Bigelow, H. B., Studies of the waters on the c
tinental shelf from Cape Cod to Chesape
Bay, I—The cycle of temperature, *Pap. Ph*
Oceanog. and Meteorol., 2(4), 1–135, 1933.

Bumpus, D. F., The circulation over the contin
tal shelf south of Cape Hatteras, *Trans. A*
Geophys. Union, 36, 601–611, 1955.

Bumpus, D. F., Oceanographic observations, 19
East Coast of the United States, *U. S. F*
Wildlife Serv. Spec. Sci. Rept., Fisheries S
233, 132 pp., 1957.

Bumpus, D. F., and E. L. Pierce, The hydrolo
and distribution of chaetognaths over the con
nental shelf off North Carolina, *Deep-Sea R*
search, Suppl., 3, 92–109, 1955.

Day, C. G., Oceanographic observations, 1957, E
Coast of the United States, *U. S. Fish. Wild*
Serv. Spec. Sci. Rept., Fisheries Ser., 282, 123 p
1959.

Longard, J. R., and R. E. Banks, Wind-induc
vertical movement of the water on an op
coast, *Trans. Am. Geophys. Union*, 33, 377–3
1952.

Miller, A. R., A pattern of surface coastal cir
lation inferred from surface salinity-temperatu
data and drift bottle recoveries, *Woods H*
Oceanogr. Inst. Tech. Rept. 52–28, unpubl. m
14 pp., 1952.

Miller, A. R., The effect of steady winds on
level at Atlantic City, *Meteorol. Monographs*,
24–31, 1957.

Taylor, C. B., and M. B. Stewart, Jr., Summ
upwelling along the east coast of Florida,
Geophys. Research, 64, 33–40, 1959.

(Manuscript received April 13, 1959.)

Contribution No. 1036

JOURNAL OF SEDIMENTARY PETROLOGY, VOL. 29, NO. 4, PP. 513–539
FIG. 1, DECEMBER, 1959

MINERALOGY AND PETROGRAPHY OF MARINE BOTTOM SEDIMENT SAMPLES OFF THE COAST OF PERU AND CHILE[1]

E-AN ZEN[2]
U. S. Geological Survey, Silver Spring, Maryland

ABSTRACT

The mineralogy and petrography of forty cores of marine bottom sediments from the Peru-Chile Trench area were studied by X-ray and microscopic techniques. Samples from each core were collected at intervals of 10 cm, or more frequently where visible lithologic variations occur. The $-1.3\,\mu$ fractions of many of these samples were also studied and the clay minerals identified by means of treatment with ethylene glycol and by heating to 200° and to 450°C.

The most common minerals in the cores are quartz, plagioclase, calcite, and the clay minerals kaolinite, chlorite, illite, and a mixed-layer clay predominantly montmorillonite. Halite and gypsum are important in many cores as results of dehydration of the cores. Volcanic glass, in various stages of devitrification, is extremely common in nearly all the cores; some samples are sufficiently abundant in glass to be called ash beds.

Among the less common minerals are aragonite, dolomite, rhodochrosite, potassic feldspar, glauconite, biotite, phillipsite, pyroxene, and amphibole. Chemically precipitated dolomite is found in one core at a water depth of 4600 meters. Besides dolomite, minerals which are at least partly authigenic are quartz, calcite, rhodochrosite, phillipsite, glauconite, and kaolinite. The observed mineral associations are given in a table.

The gross lithology of the cores includes sand, silt, mud, black mud, and calcareous and siliceous ooze. While large lithological variations exist between adjacent cores, within each core the lithology tends to be fairly uniform over the entire length.

The methods of identification of the 7–14 Å clay minerals are in an unsatisfactory state. The Bradley criteria are applicable to fine-grained, poorly crystalline chlorite, of relatively lower thermal stability than the well-crystallized chlorite to which the Brindley criteria apply. The very identification of a chlorite in a mineral mixture would thus be predicated on assumptions regarding the detailed nature of the material. The two sets of criteria, however, are not altogether contradictory; by a suitable combination it is possible in many cases not only to identify the chlorite but also to estimate its crystallinity. Most of the chlorites from the Peru-Chile Trench area satisfy the Bradley criteria.

Samples from the seaward side of the Peru-Chile Trench are uniformly fine mud. Samples from within the Trench are largely fine mud but include thin beds of silty to sandy material. Samples from the landward side of the Trench are heterogeneous in size as well as in mineralogical and chemical compositions. Although on the whole the near-shore samples tend to be most coarse-grained, there is no simple correlation between grain size and distance from the coast, nor between grain size and bottom topography. Sediment transport appears to be due largely to bottom currents, the existence of which is independently established by the discovery of graded bedding and cross-bedding in a number of the cores.

INTRODUCTION

During the winter months of 1955–1956, the research vessel *Atlantis*, of the Woods Hole Oceanographic Institution, under the joint leadership of B. Kummel, P. D. Trask, and the late H. C. Stetson, cruised the Pacific Ocean off the coast of Peru and northern Chile, covering the central part of the area of the Peru-Chile Trench. One of the principal objectives of the cruise was to collect bottom sediment samples from this tectonically active, but hitherto little studied area. Eighty-four Stetson type gravity cores, ranging in length from 1 foot to 8 feet, averaging about 5 feet, were collected from eight traverses. Seven of these traverses lie approximately at right angles to the shore line, spanning the Peru-Chile Trench; one traverse runs along the coast between Arica, Chile, and Callao, Peru.

The mineralogy of 14 of these cores has already been published (Zen, 1957); the present paper is a final report of this study, covering 26 other cores as well as some revisions and emendations of the earlier data. Although only about half of the cores in the

---

[1] Contribution no. 389 from the Department of Mineralogy and Petrography, Harvard University; no. 1036 from the Woods Hole Oceanographic Institution.

Manuscript received April 7, 1959.

[2] In the preliminary report (Zen, 1957) on this core, this mineral was not recognized. The following discussion corrects and supersedes that report.

collection have been examined, the attempted even distribution of the samples (fig. 1) and the nature of the results suggest that what is known may be fairly representative of the area as a whole.

The sediments from the Peru-Chile Trench area are of special interest for several reasons. The region is one of active tectonism and volcanic activity, and may well represent a typical eugeosynclinal belt of sedimentation. Much effort has gone into the study of ancient eugeosynclinal deposits, but more data from their supposed modern counterparts are desirable. The varied climatic conditions and source rocks on shore, coupled with the rugged land and submarine topography, as well as relative paucity of sediment data to date (Revelle, 1944, Ewing, Heezen, and Ericson, 1959, Worzel, 1959), make the study of the sediments in this region interesting.

For bed rock geology along the coastal region, the reader is referred to the works of Jenks (1946, 1956), Cristi (*in* Jenks, 1956), and Rüegg (1957). Unfortunately, hydrographic data on the coastal and near-shore waters are rather poor; Gunther's study (1936) of the surface hydrography is one published source. The bottom topography, on the other hand, has received some attention; a review of the literature was given by Zeigler, Athearn, and Small (1957), who also reported 14 bottom profiles across the Peru-Chile Trench from echo-sounding data collected by the *Atlantis* cruise, as well as data from the 1952 *Shellback* Expedition of the Scripps Institution of Oceanography. More recently, the *Downwind* Expedition of the Scripps Institution of Oceanography (Revelle, 1958) has further augmented the oceanographic and geologic data from the Peru-Chile Trench area.

METHOD OF STUDY

The sediment cores were stored in the plastic liners of the coring tubes plugged with cork or plastic stoppers. Despite the fact that they were stored in a high-humidity cabinet, many of the cores were partially or completely desiccated when opened for study. Because of original incomplete filling, and shrinkage during subsequent drying, some disturbance of the samples, before and during the opening of these cores, proved unavoidable. These are noted in the descriptive logs.

When a core was split open, the sediment was sliced longitudinally into two halves. The megascopic lithology was immediately logged and the approximate carbonate content tested with 6 N HCl. The core and log were photographed together. Samples were taken at roughly 10 cm intervals, or wherever a visible lithologic change occurs. The samples were air-dried for grinding and study.

The methods of preparation and study of both the bulk and the clay fractions of the samples, by X-ray and microscopic examinations, have been described elsewhere (Zen, 1957, 1959; Schmalz and Zen, in preparation). All X-ray work was done on a Norelco Geiger-counter diffractometer with Cu radiation and Ni filter. The clay-fractions were obtained by simple decantation of a suspension from standard cylinders at fixed time intervals, producing material with upper size limits whose effective settling diameter was calculated by Stokes' Law to be about 1.3 μ (Zen, 1959, p. 30). The clay-fractions were washed and dried on glass slides to produce maximum orientation of the platy minerals. Ethylene glycol was used for lattice expansion studies.

In a few instances, the existence of a mineral, such as rhodochrosite, is verified by X-ray fluorescence analysis, on a Norelco unit using LiF as analyzer.

The criteria used for the identification of various mineral phases have been discussed in earlier papers (Zen, 1957, 1959). Specific points requiring comment will be made under the sections on individual minerals.

DESCRIPTION OF THE CORES

The 40 cores studied include all seven traverses transverse to the Pacific coast, and are shown as solid circles in figure 1; the unopened cores are shown as open circles. The locations of the core stations were given by Zeigler and others (1957), who also discussed the probable errors due to navigational uncertainties. The depths of water, taken from the Scientist's Log Book of the cruise, are from echo soundings and have not been corrected for sound velocity in deep waters (see Zeigler and others, 1957, p. 240).

Not all of the samples have been specifi-

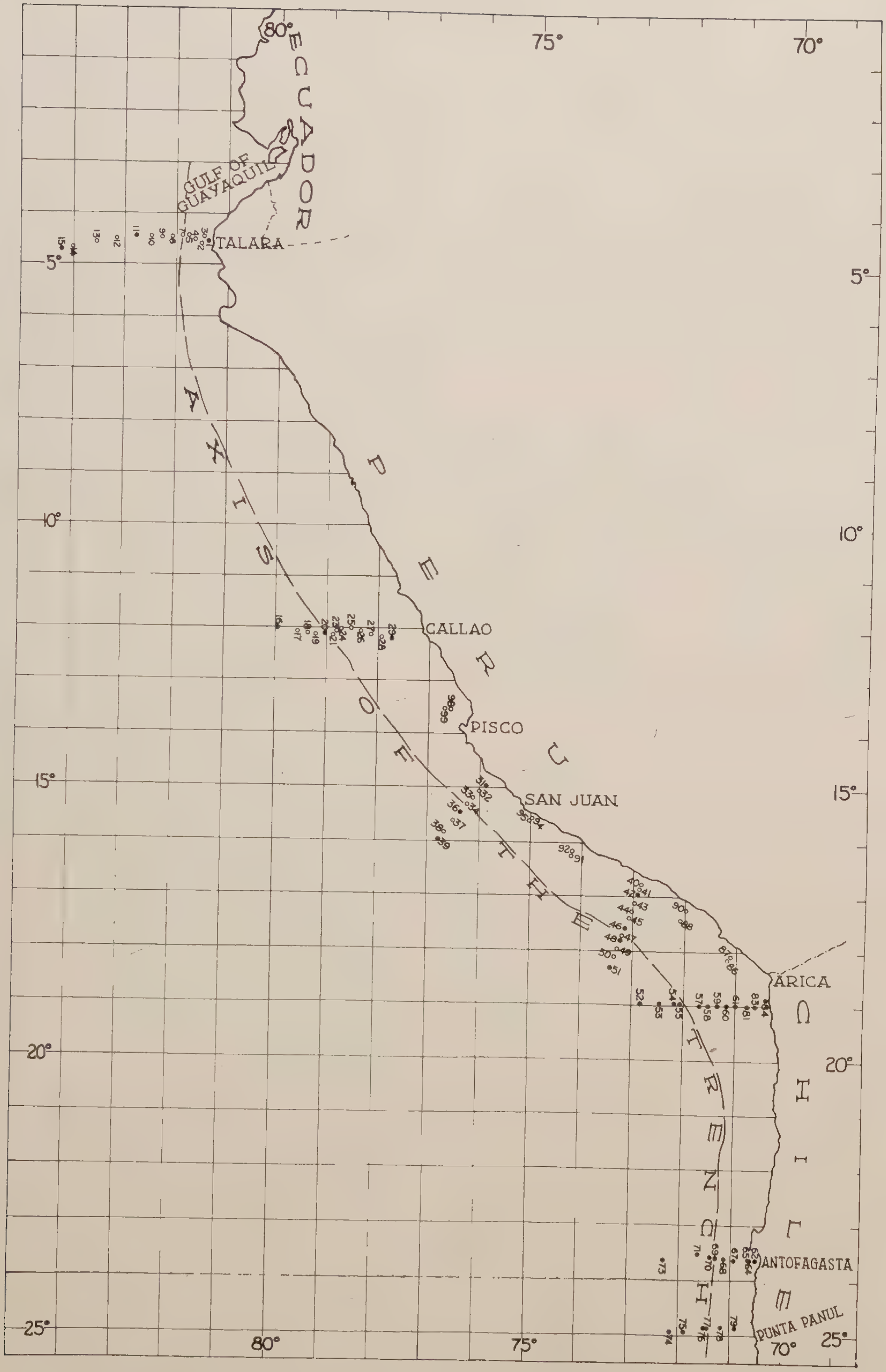
80°
75°
70°
ECUADOR
GULF OF GUAYAQUIL
TALARA
5°
5°
AXIS OF THE TRENCH
PERU
10°
10°
CALLAO
PISCO
15°
15°
SAN JUAN
ARICA
20°
20°
CHILE
ANTOFAGASTA
PUNTA PANUL
25°
25°
80°
75°
70°

FIG. 1.—Map showing the location of the 84 cores. Solid circles: cores have been studied
Open circles: cores have not been studied.

cally studied for the clay mineralogy of the $-1.3\ \mu$ fraction. Instead, for each core the X-ray diffraction results of the bulk samples were examined; the sample that appeared most interesting and worthy of detailed study was then prepared for the $-1.3\ \mu$ fractions. Conclusions drawn on the clay mineralogy, based on bulk samples, accord with those drawn on the $-1.3\ \mu$ fractions so consistently, that for routine identification of the mineral groups (for example, montmorillonite, chlorite), the bulk sample appears adequate

MINERALOGY

The detailed mineralogical data of the cores are presented in Table 1, and also in Table 2, where the mineralogy of each depth level corresponds to data from a single X-ray sample and therefore shows what minerals are actually found together. The individual minerals or mineral groups are considered below; considerations of their mutual relations, and possible implications on the environment of deposition or source material, will not be a subject of this paper.

Quartz

Quartz is an ubiquitous mineral in the cores studied, and is the single most abundant mineral in many of them. Its identification is relatively simple both by X-ray and by optical methods. In an oil immersion mount, however, much of the quartz can be seen to be angular fragments of apparently detrital origin, with no evidence for secondary overgrowth. Devitrification of volcanic glass in many of the samples also results in part in the formation of quartz. Quartz is rarely, if ever, found in the clay fraction of the samples with a maximum grain size of about $1.3\ \mu$

Plagioclase

Next to quartz, plagioclase feldspar is the most common mineral encountered in the cores. On the X-ray chart, its most intense line, at about 28° 2θ ($d=3.2$ Å), commonly, though not invariably, shows multiple peaks. If laboratory data on high-temperature plagioclase may be used, this multiplicity of peaks indicates an anorthitic component in the plagioclase in excess of about 30 percent by weight (Smith, 1956, p. 52). However, this multiplicity of peaks may be simply due to the superposition of peaks from plagioclase grains of different compositions and different lattice spacings.

Under the microscope, the albite-twinned, angular fragments of plagioclase can be easily recognized. These grains commonly give at least one index of refraction greater than 1.56, which indicates that the plagioclase is rather calcic. Occasionally, euhedral plagioclase grains can be found embedded in fresh to nearly fresh volcanic glass; more commonly these grains are embedded in a fine-grained material which is presumably devitrified glass. Much of the plagioclase grains probably were derived from such an origin. The grains are commonly fresh, showing little or no sign of alteration.

It is uncertain if plagioclase forms as a product of devitrification. One would expect such plagioclase to be relatively soda-rich (albitic); and if untwinned and in a fine-grained mixture, such a mineral would be difficult to identify.

Potassic Feldspar

The identification of potassic feldspar is considerably less certain than that of plagioclase in the present study. This mineral has not been recognized optically, and its identification rests solely on the presence of the strongest potassic feldspar line at 27.5° 2θ; this peak is commonly of low intensity on the X-ray chart and may be interfered with by lines from other minerals, such as the (111) of halite and the (110) of rutile. Where the potassic feldspar line is definite on the chart, however, it generally occurs in more than one, and commonly consecutive, depth levels in a given core.

Because of the nature of the material, it has not been possible to determine the specific nature of the potassic feldspar phase—that is, its detailed composition and whether it is triclinic or monoclinic in symmetry. It is also unknown if the grains are of detrital or authigenic origin.

Pyroxene and Amphibole

Pyroxene and/or amphibole, predominantly the latter, are commonly identified in the cores. Microscopic examination shows these to be relatively coarse, angular grains,

(*Text continued on page 522*)

TABLE 1.—*Lithology and mineralogy of the cores*

Core No.	Water depth (meters)	Depth in core (cm)	Description
1-1	825	0–7	Empty
		7–30	Brown to gray silty mud, with visible mica flakes. Faint layering due to size difference at 1 mm intervals. Weak, spotty HCl reaction. Predominantly angular quartz and feldspar. Abundant siliceous microfossils and rare glass
		30–34	Rusty brown layer. Moderate HCl reaction
		34–90	Blue-gray mud with mica flakes and broken shells. Rusty brown along borders of core and along cracks. Moderate HCl reaction. Mineralogy like 7–30 cm levels
11-1	3200	0–10	Empty
		10–144	Fine, olive-green clayey mud. No layering. Rare white round spots ½ mm across. Moderate HCl reaction above 35 cm level; vigorous below. Quartz is important. Abundant devitrified glass, diminishing in amount downward. Siliceous and calcareous fossils are very abundant
15-1	4047	0–23	Empty
		23–201	Fine, soft, plastic clayey mud. Mostly olive-green, with areas about ½ mm ×3 mm of brown color, above 44 cm and below 178 cm levels. Center of core tends to be blue-green with gradual color boundary. White spots, 1 mm in size, scattered uniformly in core. Vigorous HCl reaction. Calcite is important; quartz and plagioclase are subsidiary and partly detrital. Siliceous and calcareous microfossils
16-2	4650	0–8	Empty
		8–10	Fine clayey mud, light brown. No HCl reaction. Quartz is important (same is true throughout the core)
		10–20	Mixed light brown and olive-green clayey mud. No HCl reaction. Siliceous microfossils
		20–78	Light olive-green to green-gray mud, with irregular layering due to deeper coloration about 2 mm thick below 53 cm level. No HCl reaction
		78–90	Same, but yellow-olive color with fairly sharp contact
		90–110	Same, grading back to olive-gray
		110–137	Olive-gray mud, with irregular layering due to color variation to pink-gray, dark gray, or yellow-gray; otherwise same. Devitrified glass
		137–153	Yellow-brown mud, otherwise the same. Faint 2 mm layers of gray color. Rare fresh glass
		153–169	Gray to bluish gray mud, otherwise the same
20-2	5630	0–8	Empty
		8–12	Medium brown sand in muddy matrix. No HCl reaction. Quartzofeldspathic, with devitrified glass and siliceous microfossils
		12–17	Alternating 1–5 mm layers of olive-gray vs. dark brown mud, with a few thin streaks of pale, clean sand. No HCl reaction
		17–20	Dull buff chalky-looking layer with sharp contacts. No HCl reaction
		20–70	Olive-gray, hard, dense, uniform, clayey mud, with thin irregular brown streaks and bands 1–5 mm wide. Rare white spots 1 mm across. Grades down to dark brown, then to brown-olive, gradually becoming silty below 65 cm level. No HCl reaction. Rare glass
		70–76	Dark olive-brown silt, moderate HCl reaction
		76–82	2 mm streaks of clean sand in silt. Vigorous HCl reaction
		82–90	Sandy silt grades down into hard brown mud. None to moderate HCl reaction. Fresh glass and calcareous and siliceous fossils
		90–98	Grades down to brown fine sand. Vigorous HCl reaction
		98–105	Dark brown silty mud with sharp upper contact. Slight color variations at 5 mm intervals suggesting layering. Pass downward to fine, friable sand. No HCl reaction
		105–113	Brown sand, partly in mud matrix. Sand is friable where matrix is absent. Vigorous HCl reaction
		113–115	Thin layers of muddy silt vs. friable sand
		115–121	Friable fine sand. Vigorous HCl reaction
		121–126	Brown clayey silt. Vigorous HCl reaction
29-2	1075	0–6	Olive-green, hard, compact, silty sand, massive and uniform, without stratification. Numerous white shell fragments. Moderate HCl reaction. Largely quartzofeldspathic with siliceous microfossils
		6–119	Hard, compact, massive silty sand, light buff-brown, with cleavage flakes of feldspar (?). Rare tiny white spots scattered in interval between 71–87 cm levels. Moderate HCl reaction. Rare glass
31-3	225	0–12	Empty
		12–17	Dark olive-brown, homogeneous clayey mud. Weak HCl reaction. Largely microfossils, showing no X-ray pattern and optically isotropic, throughout the core
		17–23	Grades down from above through light brown silt to white, friable, sandy layer (2 cm). No HCl reaction
		23–42	Sharp contact above; fine brown clayey mud. No HCl reaction
		42–48	Grading down into yellowish white sandy layer (2 cm), with irregular bodies of brown mud. No HCl reaction
		48–62	Sharp upper contact; brown mud with light-colored sandy layers 1 mm thick, locally crossbedded. No HCl reaction
		62–77	Brown clayey mud. No HCl reaction
		77–90	Alternation of 1 mm layers of brown clayey and pale sandy layers, with planar beddings. No HCl reaction
		90–107	Brown clayey mud with occasional shell remains. Weak HCl reaction. Abundant quartz at 97 cm level
		107–115	Like 77–90 cm levels, but strongly crossbedded. Weak HCl reaction
		115–174	Brown mud, with thin white layers at irregular intervals; the latter type becoming rarer towards the bottom. No HCl reaction except locally
		174–183	Like 77–90 cm levels. Weak to no HCl reaction

TABLE 1.—*Lithology and mineralogy of the cores* (*continued*)

Core No.	Water depth (meters)	Depth in core (cm)	Description
36-3	4435	0–199	Deep olive-brown, clayey mud. Uniform textured, without visible grains. Occasional irregular patches varying in color from pale brown to dark brown. Rare white ovoids scattered throughout the core. No reaction with HCl except in depth intervals between 45 and 120 cm. Largely quartz and feldspar, with common devitrified glass and abundant fossils
39-3	2600	0–30	Brown, friable silt with scattered white and black spots. Vigorous HCl reaction. Largely calcite (organic remains). Abundant glass throughout the core
		30–36	Grades down to white silty loam, with sharp contact at the bottom. Moderate to weak HCl reaction. Largely plagioclase
		36–63	Brown silt with interspersed layers of white chalky silt in the upper part; otherwise same as 0–30 cm. Sharp contact at the bottom changing to
		63–90	Pale, chalky silt, with vigorous HCl reaction, grading down to
		90–185	Pure white chalk, without stratification. Vigorous HCl reaction
42-4	1152	0–40	Unconsolidated, medium sand. Massive and homogeneous, dark olive-green. Rare 1 mm laminae of white sand. Vigorous HCl reaction except for the top 10 cm. Largely quartz and feldspar, with partially devitrified glass
		40–80	Gradationally changes from above into olive-yellow color with local brown stain; otherwise no change in lithology. Vigorous HCl reaction, in part due to aragonitic shell fragments
		80–86	Gradationally changes from above into light gray, fine silt with dark green partings. Vigorous HCl reaction
46-4	5515	0–194	Pale buff-gray, fine, hard, uniform clayey mud, without visible textural variations, and only very faint suggestion of layering due to shades of gray at 1 mm intervals, within the following depth intervals: 30–36 cm; 62–67 cm. HCl reaction: moderate, 0–20 cm; none, 20–90 cm; moderate, 90–100 cm; none, 100–115 cm; moderate, 115–194 cm. Rare rusty spots and wisps throughout the length of the core. Predominantly quartz and feldspar, with glass and siliceous fossils Note: Bottom stopper lost on receipt of core. Core is completely dry and portions have moved relative to one another during handling
48-4	6146	0–14	Sticky, fine clayey mud. mostly olive to brown, with local black layers. No HCl reaction. Predominantly quartz and plagioclase, with abundant glass and microfossils, throughout the core
		14–16	Light brown, friable layer with oölitic texture. No HCl reaction
		16–80	Same as 0–14 cm interval; below 32 cm level largely olive-brown with faint, irregular layering due to color variation. No HCl reaction
		80–82	Yellowish olive, silty clay. No HCl reaction
		82–151	Same as 16-80 cm interval. No HCl reaction
51-4	4456	0–18	Empty
		18–80	Deep brown, plastic clayey mud, uniform and homogeneous, nonstratified, with rare white, tiny ovoids. Gradually becomes brownish gray towards the bottom. No HCl reaction. Largely quartz and feldspar, with microfossils and rare glass throughout the core
		80–91	Same as above, except that the mud is hard and non-plastic
		91–254	Brown plastic mud as above, gradually becoming olive-brown below 200 cm level. Very local HCl reaction
52-5	4278	0–12	Empty
		12–31	Reddish chocolate-brown fine clayey mud. Homogeneous and uniform, slightly mottled with deeper color. At 25 cm level there is a 1 cm layer of sooty-gray color. No HCl reaction. Quartz and feldspar predominate in the core
		31–76	Olive yellow-brown fine mud. Homogeneous, with irregular and vague layering due to grayer patches. No HCl reaction
		76–120	Same, with irregular and indistinct greenish brown patches, 2 mm–10 mm; rarely suggesting layering. No HCl reaction
		120–231	Same as 31–76 cm interval
53-5	4597	0–6	Empty
		6–93	Brownish red, sticky, clayey mud, no stratification. Black and buff as well as white streaks. Color becomes yellowish brown below 13 cm level. No HCl reaction. Largely quartz and feldspar
		93–103	Same, with olive-green brown irregular streaks, about 2 mm thick, approximately normal to the length of the core. Also spots like in interval 103–109 cm below, between 93 and 95 cm levels. No HCl reaction except the spots
		103–109	Hunk of pale olive, hard, cement-like, much pitted material, surrounded by brown mud, which also contains smaller pieces of the same, some forming 1 cm oval-shaped coatings on mud. Poor HCl reaction on this object (which is dolomite), none on the mud
		109–200	Reddish brown, fine, sticky mud, no stratification or any textural variation. No HCl reaction
54-5	6011	0–6	Empty
		6–45	Brown, fine clayey mud, with numerous angular insets of pale buff to nearly white color, 1–2 mm across, in random orientation; locally voids exist in the space among the insets. Insets constitute about $\frac{1}{3}$ of total bulk. No HCl reaction. Largely quartz in core
		45–66	Fine brown mud, massive, sticky and uniform. No HCl reaction
		66–82	Sharp contact with above, change to light yellow-brown mud. No textural change, but mud tends to crumble. No HCl reaction
		82–114	Buff brown mud with angular insets of pale color, generally 1 mm across but up to 3 mm, like between 6 and 45 cm levels. Patch of yellow, friable sand at 108 cm level. No HCl reaction
		114–119	Same as 82–114 cm levels, but with sooty black streaks
		119–162	Same as 82–114 cm levels; insets diminish in quantity downwards. No HCl reaction
		162–163	Layer of white angular "blocks," like inset material, up to 10 mm across. No HCl reaction. Largely material amorphous to X-ray
		163–178	Same as 119–162 cm levels, grading down to bright yellow mud, with white insets

TABLE 1.—*Lithology and mineralogy of the cores* (*continued*)

Core No.	Water depth (meters)	Depth in core (cm)	Description
55-5	6700	0–17	Empty
		17–58	Olive-gray medium sand (A), irregularly interlayered with olive-green silty clay mud (B). Sand is mostly quartz, but mica flakes may be seen. Poor to no HCl reaction, except where bulk of sample is B type. Largely quartz in core
		23	A
		28	A
		35–37	A plus B
		47–49	A plus B
		58–64	A, plus patches of B; sharp lower contact
		64–108	Same as 17–58 cm levels. B becomes dark olive towards bottom of section
		66–67	Finger of A
		78–79	A
		85–86	A
		91–92	A
		108–123	A and B in about equal amounts, in layers ½ cm to 2 cm thick, with sharp contacts
		123–125	Possible cross-bedding of A and B type of layers
		125–132	Same as 108–123 cm interval
		132–139	A and B mixed, no stratification
57-5	4106	0–60	Dull whitish green-gray mud, fine, compact, hard, with irregular thin films of a green color criss-crossing the sample at intervals of a few mms. No HCl reaction. Core is largely quartz and feldspar, with abundant glass partly devitrified, and microfossils
		60–62	Angular fragments of fine white silty matter in green argillaceous matrix. No HCl reaction
		62–118	Same as 0–60 cm levels
		118–138	Olive-brown, unconsolidated, well sorted sand with pale, argillaceous cement; sharp contacts. No HCl reaction
		138–175	Same as 62–118 cm levels
58-5	3110	0–13	Empty
		13–98	Olive drab, fine, massive silty mud, with rare visible grains of quartz (?). Rare white spots up to 2 mm across, and 2 mm fine, gray sand layers at 28 cm, 44 cm, and 46 cm levels. HCl reaction: none above 37 cm level, poor below 37 cm level; none on sand layers. Largely quartz and feldspar in core
		98–100	Gray, fine, well sorted medium sand, with sharp contacts on both sides. No HCl reaction
		100–129	Massive olive drab silty mud as above 98 cm level. No HCl reaction
		129–136	Faint color banding due to greenish vs. brownish olive layers at ½ mm apart. No HCl reaction
		136–155	Same as between 100 and 129 cm levels. No HCl reaction
		155–157	Well sorted sand with sharp contact, as between 98 and 100 cm levels. No HCl reaction
		157–187	Olive-brown fine silty mud as between 136 and 155 cm levels. No HCl reaction
		187–202	Same, but with whitish gray irregular and discontinuous layers 2 mm thick. No HCl reaction in mud, vigorous in white layers
59-5	2470	0–19	Empty
		19–31	Sticky, massive, dark olive brown clayey mud, with rare ½ mm white and buff spots. No HCl reaction. Largely quartz and feldspar in core
		31	1 mm layer of pale buff mud. Moderate HCl reaction
		31–77	Same as 19–31 cm interval, except with irregular streaks of buff and sooty black color approximating stratification. No HCl reaction
		77–166	Same massive mud, brown with dark charcoal brown streaks, but axial portion of the core is pale blue-brown. Abundant white spots between 77 and 84 cm levels. Moderate HCl reaction to 130 cm level, no HCl reaction below except for the white spots
		166–167	White, loamy, loose material with sharp contacts on both sides. No HCl reaction
		167–170	Same as between 77 and 166 cm interval
60-5	2268	0–11	Empty
		11–23	Light olive brown, slightly friable silty mud, with irregular stringers of lighter color about 1 mm. ×5 mm approximating layering. Rare white spots 1 mm across. No HCl reaction. Largely quartz and feldspar in core
		23–50	Same, becoming brown. Moderate HCl reaction
		50–58	Same, no HCl reaction
		58–73	Same, moderate HCl reaction
		73–95	Same, but pale stringers become more sharply defined as sharp, 1 mm beds at 1–5 mm intervals. Moderate HCl reaction
		95–129	Same, the two types of layers are dark brown vs. light olive brown in color, latter may not form continuous layers. Rare white spots. No HCl reaction except for the white spots
		129–143	Apparently same as above, but record disturbed due to loss of bottom stopper. No HCl reaction
61-5	1490	0–13	Empty
		13–40	Hard, massive green-gray siltstone. Rare visible cleavage flakes due to mica or feldspar. Rare white spots ½ mm across. No HCl reaction above 30 cm level, moderate to poor below. Largely quartz and feldspar in core
		40–120	Grade down to brown-gray and finer-grained; moderate HCl reaction above 80 cm level, poor to none below. Bright green, well-defined spots, about 2 mm across, at 103 cm level
		120–136	Gray-olive siltstone with faint layering due to color intensity variations, about 2 mm thick but uniform and persistent. HCl reaction: poor to none
81-5	1500	0–34	Olive-gray, massive, poorly sorted and loosely cemented medium sand, with rare reflecting cleavage flakes of mica or feldspar. No HCl reaction. Largely quartz and feldspar in core
		34–39	Friable sand, otherwise same as above
		39–40	Silty sand as above, but with crude parting into thin layers
		40–50	Same as 0–34 cm levels

TABLE 1.—*Lithology and mineralogy of the cores* (*continued*)

Core No.	Water depth (meters)	Depth in core (cm)	Description
83-5	1216	0–6	Empty
		6–108	Light olive-green fine silt, massive and uniform. Rare cleavage flakes of mica or feldspar. No HCl reaction on massive material; moderate on powdered material. Largely quartz and feldspar
84-5	933	0–76	Deep olive-brown, unconsolidated, non-clayey sand. Uniform, nonstratified. Scattered calcareous shell remains throughout. HCl reaction: moderate to weak. Largely quartz and feldspar in core, with abundant glass and microfossils
		76–156	Much like above, but with numerous small (about 2 mm × 4 mm) irregular light-colored patches scattered in the core, locally concentrated to suggest layering. No HCl reaction
62-6	79	0–30	Massive, olive colored, well-sorted unconsolidated sand, grains about 0.5 mm across. Scattered shells of complete or fragmentary gastropods and pelecypods, locally concentrating into layers. Vigorous HCl reaction. Largely calcite and feldspar, with glass and abundant fossils (calcite and aragonite) in core
		30–90	Same as above but with dark brown argillaceous layers interspersed, up to 2 cm thick, at irregular intervals
		90–122	Same as above, but the sand becomes finer-grained approaching silt; core well stratified by color variation (coarser, olive color vs. finer, brown color)
64-6	228	0–36	Empty
		36–54	Dense, compact, dark olive-green, silty mud (type A). Strong odor. Above 42 cm level full of shell fragments. Mottled appearance due to 1 mm white spots. At 47 cm level there is a ½ mm light olive-yellow silt layer with sharp contacts. Poor HCl reaction. Largely quartz and feldspar, with siliceous microfssils and glass
		54–60	Grades down to light olive brown, about ⅕ of bulk is white, discontinuous layers ½ mm × 3 mm, giving the core a ligniform texture (type B). Vigorous HCl reaction. Largely calcite, with siliceous microfossils
		60–66	Type A with sharp upper contact. Vigorous HCl reaction
		66–67	Type B
		67–81	Type A, with increasing proportion of type B towards the bottom
		81–84	Type A, with vigorous HCl reaction
		84–185	About 50% of bulk is largely continuous, sharply defined white fluffy layers like type B, less than 2 mm thick, interspersed in type A. Spacing of the former varies from 1 mm to 3 mm apart. Vigorous HCl reaction in Type A and poor to none in type B
		185–187	Type A only. Vigorous HCl reaction
		187–199	Same as between 84 and 185 cm interval. Vigorous HCl reaction
65-6	457	0–4	Empty
		4–72	Dark olive brown-gray, loose mixture of silt and sand. Silt has reflecting mica (?) flakes. About ⅓ to ½ of bulk consists of white, 1 mm "sand" grains, of foraminiferal tests. Massive, uniform; fossils are uniformly scattered in silt matrix. Rare 1 mm size gastropod shells. Vigorous HCl reaction. Largely calcite and feldspar in core
		72–119	Same, but color becomes paler brown olive except at 84–86 cm interval. Patches of fine silt at 79, 82, 84, 111, 113, and 116 cm levels. Vigorous HCl reaction
		119–135	Fairly rapid change downward to dark brown-gray color. Otherwise same as above. Vigorous HCl reaction
		135–147	Lighter color, otherwise same as above. Vigorous HCl reaction
		147–158	Darker and less friable than above, otherwise the same. Loose, light-colored patch at 152–154 cm interval. Vigorous HCl reaction
67-6	3036	0–18	Fine, homogeneous mud. Gray-tan on dry specimen. Some surface cracks have black coatings. Rare 1 mm white spots. No HCl reaction. Largely quartz and feldspar down to 58 cm level
		18–23	Dark gray-black sooty material, in granules 1 mm or less, mixed with mud granules of same size. No HCl reaction
		23–58	Same as 0–18 cm interval. No HCl reaction above 50 cm level; poor to moderate below.
		58–140	Same, color becomes pale tan. Vigorous HCl reaction. Largely quartz and calcite
68-6	5011	0–20	Buff, dense, dry mud with white spots less than 2 mm across, also irregular dark gray spots. No HCl reaction. Largely quartz and feldspar in core, with glass and siliceous microfossils
		20–23	Same, with dark brown to black coating along cracks. No HCl reaction
		23–24	Pellets of silty sand, 3 mm or less across, in brown mud matrix. No HCl reaction
		24–26	Same as 0–20 cm interval
		26–59	Homogeneous, buff-brown, somewhat friable silty mud, with reflecting cleavage flakes of some mineral. At 42 cm level there is a 2 mm layer of loose sand with sharp contacts. No HCl reaction
		59–77	Same, with irregular yellowish patches. No HCl reaction.
		77–92	White-buff mud with visible black specks and white spots. No HCl reaction
69-6	6950	0–12	Empty
		12–26	Hard, dense, buff-brown, dried clayey mud. Massive and homogeneous, with local patches of darker brown color. No HCl reaction. Largely quartz in core, with glass and siliceous microfossils
		26–34	Same, with vague 1–5 mm layering due to dark reddish brown color, with sharp but slightly irregular boundaries. No HCl reaction
		34–44	Same as 12-26 cm interval
		44–46	Yellow-buff, thin-bedded mud, bedding due to deep brown, ½ mm, sharp and planar layers. No HCl reaction
		46–177	Same as 34–44 cm interval; color gradually becoming olive gray below 80 cm level. No HCl reaction

TABLE 1.—*Lithology and mineralogy of the cores* (*continued*)

Core No.	Water depth (meters)	Depth in core (cm)	Description
70-6	6999	0–70	Fine, sticky, dark brown, homogeneous clayey mud with only occasional color variations to suggest layering. No HCl reaction. Largely quartz and feldspar in core, with variable amount of glass partly devitrified. Rare microfossils
		70–131	Gradual change from above: slowly becomes a clay-mud of steel gray color with the same texture. No HCl reaction
		131–134	Gray, friable, fine silt with gradational upper and sharp lower contacts. No HCl reaction
		134–138	Steel gray fine clayey mud as above 131 cm level. No HCl reaction
		138–141	Same as 131–134 cm interval with gradational upper and sharp lower contacts. No HCl reaction
		141–145	Olive gray-green clayey mud. No HCl reaction
71-6	5377	0–38	Empty
		38–96	Pale chocolate brown, fine, compact clayey mud, with stringers of gray color and patches of orange color. At 50, 58, and 70 cm levels there exist 1 mm layers of orange color below 3 mm layers of dark chocolate gray. No HCl reaction. Largely quartz and feldspar in core, with rare glass and with siliceous microfossils
		96–99	15 mm of friable orange mud with 2 mm of dark brown mud in the middle. Contacts sharp. No HCl reaction
		99–178	Deep chocolate brown, homogeneous and clayey mud. No HCl reaction
		178–182	Orange-brown friable mud, with gradual contacts. No HCl reaction. Largely quartz and rhodochrosite
		182–192	Same as 99–178 cm interval. No HCl reaction
73-6	4279	0–31	Empty
		31–107	Deep chocolate brown, sticky, clayey mud. Uniform and homogeneous, without stratification. Locally (67–72 cm) vaguely layered due to slight color differences, or motley-colored (78–88 cm). Color grades downwards into pale chocolate brown. No HCl reaction. Largely quartz in core, with glass and microfossils
		107–110	Yellowish brown silty mud, with sharp contacts. No HCl reaction
		110–279	Same as above 107 cm level, except that a 2 mm silty layer exists at 111 cm level. Color is predominantly chocolate brown near the top, grading downwards through yellow-brown to gray-brown. No HCl reaction
74-7	3968	0–98	Deep brown, fine, hard mud, with thin, faint layerings at 1–5 mm intervals due to color variations. HCl reaction: above 36 cm, none; 36–70 cm, moderate; 70–98 cm, none. Largely quartz and feldspar in core, with abundant glass and microfossils
		98–108	Same as above, with faint, irregular layers of buff mud. HCl reaction: moderate
		108–121	Same as 0–98 cm levels. HCl reaction: moderate
		121–141	Same as 98–108 cm levels. HCl reaction: moderate
		141–149	Same as 108–121 cm levels. HCl reaction: weak to none
		149–160	Same as 121–141 cm levels. HCl reaction: moderate to good
		160–173	Deep brown clayey mud with numerous fine, even layers of light buff mud. HCl reaction: vigorous
75-7	4700	0–23	Empty
		23–45	Chocolate brown, uniform, fine, compact clayey mud. Rare white spots scattered in core. No HCl reaction except the spots. Largely quartz and feldspar in core, with partly devitrified glass and siliceous microfossils
		45–64	Motley, pale chocolate vs. buff mud, otherwise same as above. Moderate to vigorous HCl reaction
		64–75	Buff, slightly loamy or chalky appearing mud with irregular upper contact. Vigorous HCl reaction
		75–127	Same as between 23 and 45 cm levels, with sharp upper contact. Irregular oval-shaped buff patches 1 cm across scattered in core. HCl reaction: none in chocolate brown mud, vigorous in buff patches
		127–140	Motley deep chocolate brown and pale chocolate patches, former occupying about ⅔ of the bulk. Rare white spots. Vigorous HCl reaction
		140–150	Same, with vague layering effect due to color contrast. Vigorous HCl reaction
		150–210	Same as 23–45 cm interval. Moderate HCl reaction above 187 cm level, none below
76-7	5669	0–6	Empty
		6–8	Dark brown mud, uniform and homogeneous (type A). No HCl reaction. Largely quartz and feldspar
		8–18	Same, with about equal amounts of irregular patches of fine, buff mud (type B); the two types in sharp contact. No HCl reaction. Largely feldspar and phillipsite
		18–30	Type A, with HCl reaction. Largely calcite
		30–35	Type B, with HCl reaction. Largely calcite with fresh glass
		35–40	Type A, with HCl reaction
		40–61	A and B in about equal amounts, forming layers or with B in irregular patches. HCl reaction
		61–70	Type A, with HCl reaction
		70–78	A and B in about equal amounts, with B in irregular patches. HCl reaction
		78–103	Type A, with HCl reaction. Largely feldspar and phillipsite
77-7	6218	0–13	Empty
		13–31	Pale purplish-tan mud, uniform in texture. Rare white spots. No HCl reaction. Largely quartz and feldspar in core, with siliceous microfossils and glass
		31–49	Same, becoming grayish white. No HCl reaction
		49–53	Irregular patches of dark gray sand with yellow sandy borders against buff-gray mud matrix. No HCl reaction
		53–96	Buff-gray mud as between 31 and 49 cm interval. No HCl reaction
		96–97	Dark gray loose sand, with yellow borders. No HCl reaction.
		97–164	Same as between 53 and 96 cm interval, with pockets of dark gray sand with yellow borders, at 139 cm level. No HCl reaction.

TABLE 1.—*Lithology and mineralogy of the cores* (*continued*)

Core No.	Water depth (meters)	Depth in core (cm)	Description
78-7	4042	0–10	Empty
		10–23	Buff-gray, massive and homogeneous silt. Moderate HCl reaction. Largely quartz and feldspar in core, with siliceous microfossils and partly devitrified glass
		23–24	3 mm layer of gray loose sand, with sharp lower and gradual upper contacts. Vigorou HCl reaction
		24–31	Buff olive, massive, muddy silt. Vigorous HCl reaction
		31–32	Gray loose sand
		32–90	Olive-gray, hard, massive and compact silt with mud matrix. Vigorous HCl reaction above 60 cm level, moderate between 60 and 85 cm levels, none below
		90	2 mm layer of loose sand
		90–106	Silty mud as between 32 and 90 cm interval, changing gradually to dense olive-brown clayey mud. Vague and irregular layering due to color intensity changes at 2–5 mm intervals. No HCl reaction
		106–150	Gradually becoming silty with visible reflecting specks of mineral grains. Dense, massive, olive-brown. No HCl reaction above 137 cm level, vigorous below
79-7	1856	0–2	Empty
		2–26	Olive-green, medium-fine, massive sand, with mud matrix. Local shell fragments. Vigorous HCl reaction. Quartz, feldspar and calcite dominate in core, with variable amounts of glass and microfossils
		26–30	Same as above, with 3–5 mm white sand layers at 3–5 mm distance apart.
		30–82	Same as 2–26 cm levels
		82–85	Gray unconsolidated, well-sorted sand, medium-coarse, without matrix material. Gradational upper, and sharp lower contacts. Fossils are chiefly foraminifera
		85–118	Fine brown clayey silt, uniform but for one pale, sandier layer between 94 and 96 cm levels. Visible quartz and mica grains rarely present
		118–131	Intimate interlayering of brown, muddy and white, sandy silt, grading down to uniform fine muddy silt
		131–138	Slightly coarser silt, same as above 118 cm level
		138–140	Same as between 82 and 85 cm levels; gradational upper and sharp lower contacts
		140–150	Same as above 138 cm level, with two thin sandy layers near the upper contact
		150–152	Same as between 138 and 140 cm levels; gradational upper and sharp lower contacts
		152–156	Same as above 150 cm level
		156–158	Same as between 150 and 152 cm levels; gradational upper contact

some of which are embedded in volcanic glass. It is probable that both these ferromagnesian minerals are completely derived from volcanic detritus. Part of the amphibole is dark brown and appears to be oxyhornblende.

Calcite

Calcite is a very common mineral in the cores. On the X-ray diffractometer, it is identified by the (10.4) reflection at 3.03 Å (29.5° 2θ); as a rule its presence is easily verified by optical examinations.

In many instances, the calcite can be definitely attributed to organic remains, either microfossils or fragments of larger forms; quite commonly, however, microscopic examination of the sample shows well-developed, discrete rhombs of calcite, or merely tiny highly-birefringent blebs. The origin of such material is much more in doubt. Finally, samples also exist which are identified as calcite on the basis of refractive indices but which are embedded in partly devitrified volcanic glass (Zen, 1959, p. 31). Such calcite is clearly inorganic and chemical in origin, formed during diagenesis.

The amounts of calcite in the cores are quite variable. In some samples, calcite occurs only as small, white, rounded spots in an otherwise calcite-free matrix. By and large, where it is the dominant mineral in a sample, the calcite can be definitely identified as organic in origin.

The detailed chemical composition of the calcite has not been studied in this survey work. Approximate X-ray data show that most of the calcite shows the (10.4) spacing very nearly that of pure $CaCO_3$.

There is no obvious correlation between the occurrence of calcite and other mineral phases in the samples studied.

Dolomite

Dolomite has been identified, in nearly all cases, by its X-ray diffraction pattern alone. A line at 2.89 Å (30.9° 2θ) is taken as indicative of dolomite. That the phase dolomite does in fact occur is demonstrated in two instances. In one, core 29-2, depth level 3 cm, a rhombohedral carbonate with $\omega \approx 1.67$ was found in an oil immersion mount and is taken to be the phase dolomite. A conclusive demonstration of dolo-

(*Text continued on page 531*)

TABLE 2.—*Microscopic and X-ray mineralogy of individual sediment samples*

Core no.	Depth in core (cm)	Minerals[1]														
		Qt	Pl	Ksp	Cal	Dol	Arag	Px-Amp	Mu	M.L.	Cl	K	K-Cl	Gyp	Gl	Others
1-1	7	x	x					x	x				x	x		
	16	x	x					x	x	x	x				x	
	25	x	x						x	x	x			x		
	35	x	x		?				x		x		x			
	47	x	x		x				x	x	x		x			
	56	x	x	?				x	x		x					
	64	x	x		x			x	x	x	x		x			
	73	x	x		x				x	x			x	x	x	
	82	x	x		x				x	x			x	x		
	90	x	x					x	x	x	x				x	
11-1	11	x	x						x	x					x	
	21	x	x		x				x	x	?		x			
	36	x	?		x				x	x	x					
	47	x	x		x				?	x	?		x			
	60	x	x		x				?	x	?					
	74	x	?		x				?	x	x					
	84	x	?		x				?	?						
	96	x	?		x					?						
	106	x	x		x					?						Olivine?
	116	x	x		x				x	x						
	128	x	x		x					?	?					
	139	x	x		x				x	x	x			x		
15-1	26	x	x		x					x	?				?	
	38	x	?		x				?	?						
	50	x			x					?						
	66	x			x											
	77	x			x											
	90	x	?		x					?				x		
	102	x			x											
	115	x			x				x		x					
	128	x	?		x				x	x						
	142	x	?		x					x						
	153	x			x				x							
	167	x			x											
	177	x	x		x				x	x	x					
	185	x			x							x		x		
	196	x	x		x				x	x			x			
16-2	9	x	x						x	x	x					
	18	x	x						x	x	x					
	32	x	x						x	x	x					
	44	x	x						x	x	x					
	55	x	x					x	x	x		?	?			
	68	x	x						x	x	x					
	79	x	x						x	x	x					
	90	x	x					x	x	x					x	
	101	x	x						x	x	x					
	113	x	x						x	x	x					
	125	x	x					x	x	?	x				?	
	135	x	x						?	x	x					
	140	x	x						x	x	?		x			
	149	x	x					x	?	x	?				x	
	160	x	x						x	x	x					
20-2	11	x	x					x	x			x			x	
	20	x	x		x			x	x	x	x					
	26	x	x					x	x	?	?	?	x			
	38	x	x						x	x	x				x	
	48	x	x						x	x	x					
	58	x	x					x	x	x		x		x		
	69	x	x		x			x	x	x	x			?	x	
	71	x	x		?			x	x	x		x				
	81	x	x		x			x	x		?			x		
	90	x	x		x			x	x	x	x			x	x	
	96	x	x		x			x	x		x			x		
	99	x	x					x	x	x	x	?	x			
	106	x	x					x	x		x				?	
	117	x	x		x			x	x	x		x		x		

[1] Abbreviations: Qt, quartz; Pl plagioclase; Ksp, potassic feldspar; Cal, calcite; Dol, dolomite; Arag, aragonite; Px, pyroxene; Amp, amphibole; Mu, illite; M.L., mixed-layer clay; Cl, chlorite; K, kaolinite; K-Cl, undifferentiated kaolinite and/or chlorite; Gyp, gypsum; Gl, glass.

x, mineral identified on bulk material; ?, identification is tentative; c, clay fraction mineralogy; s, several distinct phases present; s?, possibly several phases ;c?, tentative identification from clay-fraction study; *, one-layer montmorillonite.

TABLE 2.—*Microscopic and X-ray mineralogy of individual sediment samples* (*continued*)

Core no.	Depth in core (cm)	Minerals														
		Qt	Pl	Ksp	Cal	Dol	Arag	Px-Amp	Mu	M.L.	Cl	K	K-Cl	Gyp	Gl	Others
29-2	3	x	x		x	x		x	x	?	x			x		
	13	x	x		x			x	x	x	x			x		
	23	x	x		x			x	x		x	x		x		
	38	x	x		x			x	x		?	x		x		
	49	x	x		x			x	x		x	?		x	x	
	62	x	x		?			x	x	?	x	?		x		
	73	x	x	x	x			x	x		x	?		x	x	
	80	x	x		x				x	?	?		x			
	93	x	x		x			x	x	x	?	x		x	x	
	105	x	x		x			x	x	x	?		x	x		
	114	x	x		x			x	x	x				x	x	
31-3	14	x	?		x				?					?		
	19	x	?	?	x				?					?		
	22	x		x	x				?		?			?		
	27	x	x					x	x		x					
	31	x		?	?									x		
	38	x		?												
	42	x	?	?	x				?					x		
	49	x		?	x									x		
	59	x			x									x		
	61	x			x			x	x		?			?	?	
	67	x	x													
	78	x								?		x		x		
	86	x			x					?		?		x		
	97	x	x						x	?	x					
	114	x			x											
	124	x	x						x		x			x		
	138	x	x					x	x		x					
	149	x	x					x	x		x			x	x	Rhodochrosite?
	162	x	x						x		x					
	174	x	x		x				?		?			?		
	181	x			x									x		
36-3	7	x	x						x	?	x					
	20	x	x		?				x	?	x				?	
	30	x	x						x	?			x			
	33	x	x					x	x	?	x			x		
	46	x	x					x	x	?	x					
	57	x	x		x				x		x			x	x	
	67	x	x						x	x	x					
	70	x	x		x			x	x	x	x			x		
	82	x	x		x				x	?	x			x		
	98	x	x		x				x	?	x			x		
	107	x	x		x			x	x	?	x					
	114	x	x		x			x	x	?	x				x	
	128	x	x					x	x	x	x					
	146	x	x		x				x	x	x					
	157	x	x						x	?	x			x		
	168	x	x					x	x	x	x			x	x	
	179	x	x		x		?	x	x	x	x					
	190	x	x						x	x	x				x	
39-3	4	x	x		x				x		x	x				
	12	x	x		x				x		?	x			x	
	16	x	x		x			x	x	x	x					
	22	x	x		x				x	x	?	x	x			
	27	x	x		x			x	x		x					
	31	x	x		?			x	x						x	
	37	x	x		x			x	x		?	x				
	39	x	x		x			x	x							Biotite?
	46	x	x		x				x		x					
	55	x	x		x				x							
	64	x	x		x			x	x							
	70	x			x										x	
	78	x	x		x				x	x	x					
	88	x	x	?	x				x	?			?			
	99				x											
	115				x											
	125	x		?	x											
	135	x			x						x					Hematite?
	150	x			x											
	162	x			x											
	172	x			x					?						
	185	x			x											

TABLE 2.—*Microscopic and X-ray mineralogy of individual sediment samples* (*continued*)

Core no.	Depth in core (cm)	Minerals¹														
		Qt	Pl	Ksp	Cal	Dol	Arag	Px-Amp	Mu	M.L.	Cl	K	K-Cl	Gyp	Cl	Others
42-4	5	x	x		?			x	x		x				x	
	13	x	x		x			x	x				x		x	
	14	x	x					x	x			?	x		x	
	20	x	x		x			x	x		?		x		x	
	30	x	x		x			x	x				x		x	
	41	x	x		x			x	x			?	x		x	
	48	x	x		x			x	x		?		x		x	
	57	x	x		x			x	x				x	x	x	
	66	x	x		x			x	x				x		x	
	76	x	x		x			x	x		?		x		x	
	84	x	x		x			x	x			?		x	x	
46-4	1	x	x					x	xc	xcs	xc	xc	x	x	x	
	19	x	x					x	x	x	x	x				
	30	x	x						x		x	x				
	40	x	x						xc	xcs	xc	xc			x	
	52	x	x						x		?	x				
	64	x	x						xc	xcs	xc	xc			x	
	75	x	x						x	x	x	?				
	90	x	x						x		x	?				
	108	x	x		x			x	xc	xcs	xc	xc				
	124	x	x		x			x	x	x	x	?				
	140	x	x						x	x	x	?				
	153	x	x		?	?			x	x		x				
	166	x	x		?			x	x	x	?				x	
	179	x	x					x	x	x	?	x				
	190	x	x		?			x	xc	xcs	xc	c			x	Biotite
48-4	1	x	x					x	x		x				x	Biotite
	5	x	x					x	x		x				x	
	8	x	x					?	x	x	x				?	
	11	x	x					x	x	x	x				x	
	14	x	x					x	x		x				x	
	21	x	x					x	x	x	?	x			x	
	32	x	x					x	x	x	x	?	x			
	43	x	x					x	x	x	x			x		
	56	x	x					x	x	x	x	?	x			
	69	x	x						x		x					
	81	x	x						x	x	x			x		
	90	x	x						x	x	x					
	100	x	x						x		?	?	x			
	112	x	x		?				x		x				x	
	128	x	x					x	x		x	x	x		x	
	139	x	x						x		x					
	150	x	x						x		x	?	x			
51-4	18	x	x						x	x	x			x		
	30	x	x						x	x	x			x		
	42	x	x					x	x	x	x					
	56	x	x						x	x	x					
	62	x	x						x	x	x					
	80	x	x					x	x	x	x					
	96	x	x					x	x	x	x					
	105	x	x						x	x	?	x				
	119	x	x					x	x	x	x				x	
	130	x	x						x	x	x					
	145	x	x					x		x						
	158	x	x					x	x	x	x					
	175	x	x						x	?	x				x	Biotite?
	187	x	x						x	x	x	?				
	200	x	x						x	x						
	212	x	x							x						
	225	x	x						x	x						
	240	x	x						x	x	x					Olivine?
	253	x	x						x	x	?	x				
52-5	14	x	x						x	x			x			
	24	x	x						xc	xc	xc	xc				
	36	x	x						x	x			x			
	50	x	x						x	x	x	?	x			
	53	x	x						x	x			x			
	75	x	x						xc	xc	xc	?	x	x		
	90	x	x						x	x	x	?	x			
	107	x	x						x	x			x			
	119	x	x						x	x			x			
	130	x	x					x	xc	xc	xc	?	x			
	145	x	x						x	x			x			
	161	x	x						x	x			x			
	176	x	x						xc	xc	?	c	x			
	192	x	x						x	x			x	x		
	208	x	x						x	x	x		x			
	219	x	x						x	x			x			
	231	x	x						xc	xc	c	?				

TABLE 2.—*Microscopic and X-ray mineralogy of individual sediment samples* (*continued*)

Core no.	Depth in core (cm)	Minerals[1]														
		Qt	Pl	Ksp	Cal	Dol	Arag	Px-Amp	Mu	M.L.	Cl	K	K-Cl	Gyp	Gl	Others
53-5 (X-ray only)	7	x	x						xc	xc	xc	c	x			
	26	x	x	x					xc	xc	?	xc				
	41	x	x	x					x	x	x		x			Phillipsite?
	59	x	x						x		x					
	70	x	x					x	xc	xcs?	c	c				Phillipsite
	81	x	x						x	x		?				
	96	x	x						x	x	x					
	106	x	x			x		x	xc	cs?	xc	c				
	120	x	x						xc	xc	c	xc				
	133	x	x					x	x	x	?	x				
	146	x	x						x	x	?	x				
	155	x	x						xc	xc	xc	xc				
	171	x	x						x	x	x					
	188	x	x						x	x	x	?				
	199	x	x						x	x	x	?				
54-5 (X-ray only)	8	x	x						xc	xc	xc	xc				
	18	x	x					x	x	x	x	?				
	32	x	x					x	xc	xcs	xc	xc				
	42	x	x							x	x					
	50	x	x						xc	xc	c	xc				
	65	x	x						x	x	x	x				
	73	x	x						xc	xcs	xc	c				
	83	x	x						xc	xc	xc	c				
	86–88	x							?							
	94	x	x						xc	xc	c	c				
	108	x	x						x	x	?	x				
	114	x	x						xc	xcs	xc	c				
	126	x	x						x	x	x	?				
	136	x	x						x	x	x					
	149	x	x						x	xs	x	?				
	162	x														
	169	x	x						x	x	x					
	177	x	x						xc	xcs	c	xc				
55-5 (X-ray only)	23	x	x	?					xc	xcs	xc	c				
	32	x	x						x	x	x	?		x		
	45	x	x						x	x	x	?				
	55	x	x					x	xc	xcs	xc	c				
	63	x	x					x	x	x	?	x		x		
	77	x	x						xc	c	c?	c				
	89	x	x						x	x	x	?				
	99	x	x					x	x	x	x	?				
	106	x	x					x	xc	xcs	xc	c				
	115	x	x					x	x		x					
	130	x	x					x	xc	xc	xc	c				
	138	x	x	?				x	x	xs	x					
57-5	4	x	x						x	x			x	x		
	18	x	x					x	x	x	x				x	
	27	x	x						x	x	x	?	x	?		
	38	x	x						x	?	x			x		
	49	x	x					x	x	x	x					
	60	x	x						x		x				x	
	74	x	x						x		x					
	85	x	x						x	x	x	?		x		
	95	x	x					x	x	x	x			x	?	
	104	x	x					x	x	?	x					
	116	x	x						x	?	x	?	x	x		
	121	x	x					x	x		x			x		
	137	x	x					x			x			x		
	138	x	x						?	x	x			?	x	
	139	x	x						x	x	x				?	
	148	x	x						x		x	?				
	157	x	x						x		x			?		
	165	x	x					?	x		x				x	
	175	x	x						x	?	x					
58-5 (X-ray only)	16	x	x					x	x	x	?	x				
	36	x	x						x	x	?	x				
	53	x	x					x	x	x	?	x				
	65	x	x					x	x	x	?	x				
	76	x	x						x	xs	?	x				
	91	x	x						x	x	?	x		x		
	100	x	x					x	x	x	?	?		x		
	110	x	x						x	x	?	x		x		
	125	x	x					x	x	x	?	x				
	136	x	x						x	x	x	x				
	149	x	x					x	x	x	?	x				
	163	x	x						x	x	?	x				
	176	x	x						x	x	x	x				
	188	x	x						x	x	?	x		x		
	197	x	x						x	x	?	x		x		

TABLE 2.—*Microscopic and X-ray mineralogy of individual sediment samples* (*continued*)

Core no.	Depth in core (cm)	Minerals[1]														
		Qt	Pl	Ksp	Cal	Dol	Arag	Px-Amp	Mu	M.L.	Cl	K	K-Cl	Gyp	Gl	Others
59-5 (X-ray only)	25	x	x		x				x		x					x*
	36	x	x	?					x	x	x					
	49	x	x					x	x	x	x					
	61	x	x						xc	xc	xc	c				
	72	x	x					x	x	x	x					
	82	x	x		x				xc	xc	c?	xc				
	93	x	x		x				xc	xc	xc	xc				
	110	x	x		x				x	x	x	x				
	120	x	x		x				xc	xc	c?	c	x			
	132	x	x					x	xc	xcs?	c?	xc				
	142	x	x						xc	xc	c	xc				
	153	x	x						x	x	x	x				
	161	x	x					x	x	x	x					
	167	x	x				?	?		x						
	169	x	x						x	x	x					
60-5 (X-ray only)	12	x	x						xc	xc	xc	xc		x		
	28	x	x		x			x	x	x	?	x				
	36	x	x		x				x	x	?	x				
	49	x	x					x	x	x	x	?				
	57	x	x	?					x	x	x	?				
	71	x	x		x				xc	xc	xc?	c				
	80	x	x		x			x	xc	xc	xc	c				
	93	x	x		x				x	x	?	x				
	109	x	x						xc	xc	xc	c				
	120	x	x						xc	xc	c	xc				
	131	x	x					x	x	x	x	?		x		
	142	x	x	?				x	x	x	x	?				
61-5 (X-ray only)	14	x	x				?		x	x	x	x				
	26	x	x					x	x	x	?	x				
	35	x	x		x			x	x	x	x	x				
	48	x	x		x				x	x	?	x				
	62	x	x		x			x	x	x	?	x				
	71	x	x		x				x	x	?	x				
	86	x	x		x				x	x	?	x				
	95	x	x						x	x	x	x				
	103	x	?						?	?						Glauconite
	108	x	x		x				x	x	?	x				
	121	x	x		x			x	x	x	x	x				
	133	x	x						x	x	?	x		x		
81-5 (X-ray only)	1	x	x					x	x	x	?	x		x		
	11	x	x			?		x	x	x	?	x				
	22	x	x					x	x	x	?	x				
	35	x	x					x	x	?	x	x				
	46	x	x					x	x	x	?	x		x		
83-5 (X-ray only)	6	x	x					?	x	x	x	x				
	17	x	x						x	x	?	x		x		
	28	x	x		x			x	x	x	?	x		x		
	40	x	x		x			x	?	x	?	x		x		
	49	x	x	?	x				x	x	?	x				
	60	x	x		x			x	x	x	?	x				
	72	x	x		x				?	x	x	x		x		
	80	x	x		x				x	x	?	x				
	92	x	x		x				x	x	?	x		x		
	106	x	x		x			x	x	x	x	x		x		
84-5	10	x	x					x	?	x	?	?	x	x		
	20	x	x		x	?		x	x	x	x	?	x		x	
	32	x	x		?	?			x	x	x			x		
	41	x	x		?			x	x	x	?	x		x		
	51	x	x					x	?	x	x	?		x	x	
	58	x	x		x			x	x	x	x	?		x		
	71	x	x		?				x		?	x		x		
	80	x	x		x			x	x	?	x	?		x	x	
	91	x	x					x	x	x	x	?		x		
	104	x	x		x				x	x	x	?		x	x	
	117	x	x		x			x	x	x	x	?		x		
	130	x	x		x			x	x	x	x	?		x	x	
	142	x	x		x			x	x	x				x		
	155	x	x						x		x	?		x	x	

TABLE 2.—*Microscopic and X-ray mineralogy of individual sediment samples (continued)*

Core no.	Depth in core (cm)	Minerals¹														
		Qt	Pl	Ksp	Cal	Dol	Arag	Px-Amp	Mu	M.L.	Cl	K	K-Cl	Gyp	Gl	Others
62-6	2	x			x		x	x		?				x		
	11	x	x		x		x	x		?	x				x	
	21	x	x		x		x	x			x	?	x	x		
	31	x	x	?	x		?	x			?	x		x	?	
	40	x	x	x			x	x			x			x		
	49	x	x		x		x	x	x			x			x	
	60	x	x		x		x	x	x					x		
	68	x	x		x		x	x						?		
	79	x	x		x		x	x								
	90	x	x		x		x	x	x		x					
	101	x	x		x		x	x				x		x		
	110	x	x		x		x			?	x					
	121	x	x		x		x	x						x	?	
64-6	39	x	x					x	x	x	x			x	x	
	49	x	x		x			x	x		x					
	59	x			x			x	x		x	?				
	71	x	x		x			x	xc	c?	c?	c?				
	82	x	x		x			x	x	?	x	x				
	93	x	x		x			x			x	?	x			
	107	x	x			x	x	x	x		c?	x				
	104–112, dark	x	x		x	x	x	x	x		?	?	x		x	
	104–112, white	x	x		x	?	x	x		x			x			
	125	x	x		x	?	x	x	x		x			x		
	140	x	x		x	?	x	x	x	?	c?	c?		x		
	156	x	x		x	?	x		?	?	?	x				
	171 white	x	x		x	?	?	x								
	186 dark	x	x		x	?	?	x	xc	c?	c?	c?				
	196	x	x		x	?	x	x	x	?	?	x		x		
65-6 (X-ray only)	3	x	x		x			x	x	?	x	x				
	20	x	?		x			x	x	?	?	x				
	39	x	x		x		?	x	x	?	x	x				
	55	x	x		x			x	x		?	x				
	70	x	x		x			x	x	?	?	x				
	88	x	x		x			x	x	?	x	?				
	99	x	x		x			x	x	?	x	x		x		
	113	x	x		x			x	x	x	?	x				
	131	x	x		x			x	x	x	x	x		x		
	145	x	x		x	?		x	x		?	x				
	157	x	x		x			x	x	x	?	x		x		
67-6 (X-ray only)	1	x	x		?			x	xc	xc	xc	c?				
	10	x	x	?				x	x	x	x	?				
	22	x	x					x	x	x	x	?				
	36	x	x						xc	xc	xc	c?				
	49	x	x	?				x	xc	xc	xc	c?				
	64	x	x		x			x	x	x	x	?				
	79	x	x		x			x	x	x	x	?				
	89	x	x		x			x	xc	xc	xc	c?				
	105	x	x		x			x	x		x	x				
	116	x	x		x			x	x	x	x	x				
	127	x	x		x			x	xc	xc	xc	xc				
	139	x	x		x			x	x	x	x	?				
68-6	2	x	x					x	xc	xc	c	c?			x	Iron oxide?
	13	x	x					x	x	x	x	x				
	22	x	x					x	xc	xc	xc	xc				
	29	x	x					x	x	x		x				
	40	x	x					x	x	x	?	x				
	50	x	x		?			x	xc	xc	c	c?			x	
	60	x	x					x	x	x	?	x				
	71	x	x					x	xc	xc	xc	c?			x	
	81	x	x					x	x	x	?	x				
	91	x	x						xc	xc	c	c?			x	
69-6	14	x	x					x	x	x	x	x				
	28	x	x					x	xc	xc	xc	xc			x	
	40	x	x					x	x	x	x	?				
	45	x	x						xc	xc	xc	c?				
	56	x	x					x	xc	xc	xc	xc				Hematite?
	72	x	x					x	x	x	x	x				
	88	x	x					x	x	x	x	x				
	100	x	x					x	x	x	x	x			x	
	111	x	x					x	xc	xcs?	xc	xc				
	127	x	x					x	x	x	x	x				
	141	x	x					x	xc	xc	xc	xc			x	
	159	x	x						x	x	x	x				
	166	x	x						x	x	x	?			x	

TABLE 2.—*Microscopic and X-ray mineralogy of individual sediment samples (continued)*

Core no.	Depth in core (cm)	Minerals[1]														
		Qt	Pl	Ksp	Cal	Dol	Arag	Px-Amp	Mu	M.L.	Cl	K	K-Cl	Gyp	Gl	Others
70-6	9	x	x					x	xc	xc	c?	c?				
	16	x	x					x	xc	c?	xc	c?				
	29	x	x					x	x	x	x	x				Biotite Hematite?
	41	x	x					x	x	x	x	?				
	52	x	x					x	x	x	?	x	x			
	65	x	x					x	x	xc	x	c?				
	75	x	x					x	x	x	x	?			x	
	89	x	x					x	x	x	x	?				
	100	x	x					x	x	x	x	?				
	111	x	x					x	x	x	x	x			x	
	121	x	x					x	x		x	?				
	129	x	x					x	x	?	x					
	132	x	x					x	x	x	x	?			x	
	137	x	x						x	?	x	?				
	140	x	x		?			x	x		x	x			x	Biotite
	144	x	x						x		x	?			?	
71-6	38	x	x					x	x	x	x	x			x	
	50	x	x					x	x	x	?	x				
	73	x	x					x	xc	xc	xc	c?			x	
	80	x	x						x	x	?	x				
	92	x	x						x	x	x	x				
	98	x	x						c	xc	c	c	x	x		
	113	x	x					x		x	x	?				
	126	x	x					x	xc	xc	c	c?				
	138	x	x						x	x	?	x				
	150	x	x					x	xc	xc	c	c?			x	
	164	x	x					x	x	x	?	x				
	175	x	x						x	x	x	?	x			
	179	x	x						x	x	?	?				
	180	x	x						x	x	x	x	x		x	Rhodochrosite
	182	x	x					x	xc	c	c	c?	x			
	191	x	x						x	x	x	?			x	
73-6	37	x	x					x	x	?	x	x			x	
	51	x	x						x	x	x	?				
	69	x	x						xc	xc	xc	c				
	77	x	x						x	x	x				x	
	87	x	x						x	x	x					
	99	x	x					x	x	x	?	x				
	109	x	x						x	?	x	?			x	
	113	x	x						xc	xc	xc	c			x	Biotite
	125	x	x						x	?	x	?				
	140	x	x						x	x	x	?			x	
	150	x	x					?	x	x	x	?				
	165	x	x					x	xc	xc	c?	c				
	178	x	x					x	x	x	x	?				
	190	x	x						x	x	?	x				
	205	x	x						x	x	?	?	x			
	215	x	x					x	x	?	?	x				
	229	x	x					x	x	x	x	?			x	Olivine?
	240	x	x						x	x	x	?				
	251	x	x							x	x					
	264	x	x					x	x		x	?				
	279	x	x					x	x	x	x	?	x			
74-7	2–4	x	x		x			x	x	x	?		x		x	
	10–11	x	x		x			x	x	x	?		x	x	x	
	15-16	x	x						x	x	x	?		x		
	19–20	x	x					x	x	xs	?	?	x			
	22–23	x	x					x	x	?	x	?	x			
	39	x	x		x				x	?					x	
	48–51	x	x		x			x	x	x	x	?	x		x	
	59-61	x	x		x			x	x	x	x	?	x		x	
	70–72	x	x		x				x	x			x			
	87	x	x		x			x	x	x	x	?	x		x	
	103	x	x		x				x	?	x	?				
	139	x	x		x			x	x		x	?			x	
	141	x	x	x					x	x	x	?				
	158	x	x	?	x			x	x	x	x	?			x	
	171–173	x	x		x				x		x	?			x	

TABLE 2.—*Microscopic and X-ray mineralogy of individual sediment samples (continued)*

Core no.	Depth in core (cm)	Minerals[1]														
		Qt	Pl	Ksp	Cal	Dol	Arag	Px-Amp	Mu	M.L.	Cl	K	K-Cl	Gyp	Gl	Others
75-7	23	x	x					x	xc	xc	xc	c?			x	Epidote?
	25	x	x		x				x	x		x				
	49	x	x		x			x	x	x		x			x	Hematite?
	61	x	x		x				xc	xc	c?	c?				
	71	x	x		x			x	x	?		x			x	
	81	x	x		x				x	x		x				
	92	x	x					x		x		x				
	101	x	x						xc	xc	c?	xc			x	
	115	x	x						x	x		x				
	127	x	x		x			x	x	x	?	x			x	
	137	x	x		x			x		x		x				
	145	x	x		x			x	x	x		x			x	
	158	x	x						x	x	?	x				
	170	x	x		x			x		x	?	x				
	178	x	x		x			x	x	x		x			x	
	190	x	x		x			x	x	x		x				
	205	x	x					x	xc	c?	c?	xc			x	
76-7	8	x	x	x				x	xc	xc	xc	c?			x	Phillipsite
	17	x	x	?	?				x		x	?	x		x	Phillipsite
	26	x	x	?	x				c	c?			x			
	31	x	x		x				x	?	x	?			x	Phillipsite?
	39	x	x	?	x								x			
	50	x	x	x	x					x			x			Phillipsite
	61	x	x	x	x				x	x			x			
	81	x	x	x	x				x				x		x	
	90	x	x	x	x				x	x	x	x				
	100	x	x	x					x				?		x	Phillipsite
77-7	15	x	x					x	xc	xc	xc	c?			x	
	28	x	x					x	x	x	?	x		x		
	34	x	x					x	x	x	?	x				
	48	x	x					x	x	x	x	x			?	
	51	x	x					x	xc	xcs	c	c?		x		Zoisite?
	62	x	x					x	x	x	x	x				
	76	x	x					x	x	x	x	x				
	90	x	x					x	xc	xc	xc	xc				
	102	x	x					x	x	x	?	x				
	113	x	x						xc	xc	xc	c?				
	125	x	x					x	x	x	x	x			x	
	137	x	x						x	x	x	x				
	149	x	x						x	x	?	x				
	161	x	x					x	xc	xc	xc	c			x	Phillipsite?
78-7	11	x	x					x	xc	xc	xc	c?			x	
	20	x	x		x			x	xc	xc	xc	c?			x	
	24	x	x		x			x	x	x	x	x				
	32	x	x		x			x	x	x	x	x				
	46	x	x		x			x	x	x	x	x				
	57	x	x		x			x	x	x	x	x				
	70	x	x		x			x	xc	xc	c?	xc			x	
	82	x	x		x			x	x	x	x	?				
	92	x	x		?				xc	c	xc	xc			x	
	102	x	x					x	x	x	x	?				
	116	x	x					x	x	x	x	?				
	127	x	x					x	x	x	x	?				
	138	x	x		x			x	xc	xc	xc	c?			x	
	150	x	x		x			x	x	x	x	?				
79-7	3	x	x		x			x	xc	c	xc	c				
	17	x	x		x			x	x		x	?			x	
	27	x	x		x			x	x	x	x	?				
	38	x	x		x				x	x	?	?	x			
	53	x	x	?	x				x	x	x	x			x	Olivine?
	63	x	x		x			x	xc	xc	xc	c				
	68	x	x	?	x				x		x	x				
	80	x	x	?	x			x	x	x	?	x			x	
	84	x	x	?	x			x	x	?	?	x				
	90	x	x		x			x	x		?	x				
	102	x	x		x				x	x	x	?				
	112	x	x		x			x	x		?	x			x	
	120	x	x		x				x		x	x				
	129	x	x	?	x				x		x	x				
	133	x	x		x			x	xc	c	c	c?				
	139	x	x		x			x		x	x	?			x	
	147	x	x		x			?	x		x	?				
	156	x	x		x			x	x		?			x	x	

mite, however, is in core 53-5. At depth levels between 104 and 108 cms, the core consists of a single, pitted chunk of olive-gray, cement-like material that reacts weakly with 6 N HCl. At adjacent levels smaller pieces of similar material are found, at least part of which form fragile coatings, 1 mm thick, on the clayey mud which constitutes the bulk of the core. On the X-ray chart the carbonate gives unmistakable dolomite pattern; unfortunately, due to the presence of other phases it has not been possible to decide whether the dolomite is ordered or disordered "protodolomite" (Graf and Goldsmith, 1956, p. 184). The mineral association of this particular occurrence of dolomite is given in table 2. Aside from quartz and plagioclase, clay-fraction studies show the presence of illite, kaolinite, chlorite, and mixed-layer clay. An amphibole has also been found.

Aragonite

Aragonite has been found in a number of cores, exclusively on the basis of X-ray studies. Aragonite is always subsidiary in amount, and occurs only where abundant organic carbonate fragments obtain.

In general, for a given core at a given depth level, only one carbonate phase exists. Cores 62-6 and 64-6 are the salient exceptions. Core 62-6 has both calcite and aragonite, whereas 64-6 has, in addition, dolomite throughout most of its length. The problem of chemical equilibrium among the carbonates in the open ocean has been discussed elsewhere (Zen, in press); the prevalent one-carbonate mineral associations are consistent with, though by no means confirm, the hypothesis of the attainment of chemical equilibrium among the carbonates. However, aragonite is known to be metastable under surface conditions (Jamieson, 1953; MacDonald, 1956; Clark, 1957) and must be excluded in any equilibrium considerations.

Rhodochrosite

Rhodochrosite, the manganese carbonate, has been observed about the 180 cm level of core 71-6. It occurs in a layer about 4 cm thick. The bulk material is orange-brown in color, loamy and incohesive, and passes both upwards and downwards into the chocolate-brown clayey mud typical of the core. Rhodochrosite is recognized under the microscope by its index of refraction and high birefringence. Many crystals appear to be skeletal and subhedral.

The strong reflections at 24.3° 2θ (relative intensity 50) and 31.3° 2θ (relative intensity 100), corresponding to *d*-spacings of 3.66 Å and 2.86 Å, respectively, agree with the data for rhodochrosite (Brindley, ed., 1958, A.S.T.M. card no. 7-268). The value of ω, 1.76 ± 0.005, is too low for rhodochrosite; however, this value might be low due to difficulties in measuring the very fine-grained material. X-ray fluorescence analysis of the sample, using LiF analyzer, yields a strong $\mathrm{Mn}_{k\alpha_1}$ line at 62.9° 2θ.

The mineral association of the rhodochrosite-bearing layer is given in table 2; this consists of quartz, plagioclase, illite, kaolinite, chlorite, and mixed-layer clay dominantly montmorillonite. Clay-fraction studies on a sample from the 182 cm level, of similar material, yield these same clay minerals except possibly kaolinite. Optical examination of the sample shows the presence of volcanic glass.

Phillipsite

A mineral identified as phillipsite is found definitely in cores no. 76–7,[2] 53-5, and possibly in 77-7. The identification is based primarily on the X-ray diffraction pattern, with strong reflections at 7.14 Å and 4.10 Å (12.4° and 21.7° 2θ, respectively). The strongest reflection at 3.20 Å, corresponding to a 2θ value of 27.9°, unfortunately, interferes with plagioclase lines and is not useful. Table 3 gives a typical X-ray chart reading of a sample which contains much phillipsite.

Where identification is reported as "definite," the mineral has been verified by optical examination. In a typical sample, core 76–7, depth level 100 cm, phillipsite occurs as small, colorless, rectangular, euhedral, and untwinned crystals that are length-slow with $Z \wedge C \approx 29°$. The birefringence is very low, and $\beta \approx \gamma = 1.498 \pm 0.003$. According to Winchell and Winchell (1951, p. 343), this corresponds to a rather high calcium, therefore low-silica composition.

In some samples phillipsite is strongly indicated by the strong, sharp, and symmetrical 12.4° 2θ line, but presumably due to its

TABLE 3.—*X-ray chart of a typical phillipsite-containing sample*
Sample no.: 76-7-100

2θ, CuKα (uncorrected)	d, Å	Intensity (arb. scale)	Mineral
6.3	14.0	3	Chlorite? Mixed-layer clay?
8.8	10.0	9	Illite
10.8	8.19	8	Amphibole
12.4	7.14	55	Phillipsite
13.9	6.37	5	Feldspar
16.5	5.37	15	Phillipsite
17.9	4.96	22	Illite and phillipsite
20.8	4.27	7	Quartz
21.7	4.10	20	Phillipsite
21.9	4.06	32	Plagioclase
26.6	3.35	20	Quartz and illite
27.5	3.24	30	Potassic feldspar?
28.0	3.19	>100	Plagioclase and phillipsite
30.3	2.95	15	Plagioclase?
31.7	2.82	25	Halite
32.7	2.74	17	Phillipsite
33.4	2.68	20	Phillipsite

small amount and tiny grain size cannot be verified by optical means.

Phillipsite has been found with rather high frequency with potassic feldspar. Thus of the five samples definitely containing phillipsite, three also definitely have potassic feldspar, and one a questionable potassic feldspar. Of the three remaining questionable phillipsite samples, one contains potassic feldspar. Many phillipsite samples also contain calcite. As phillipsite is a hydrous calcium-potassium-aluminum silicate, the mutual relationships of these phases, plus illite and kaolinite, and possibly also the mixed-layer clays, constitute an interesting and relatively simple chemical system for study. This will be undertaken in a separate contribution.

The Phyllosilicates

The phyllosilicates that have been found in the Peru-Chile Trench cores include illite, chlorite, kaolinite, mixed-layer clays, glauconite, and biotite.

Illite, biotite, and glauconite.—Illite is used in the sense of Grim (1953, p. 35), and applies to all platy minerals which give a strong X-ray reflection at about 10 Å. It thus includes possible glauconite in the sample. Nagelschmidt (1937, p. 519) suggests the use of the (060) line to distinguish the dioctahedral from the trioctahedral micas, a criterion which Brown (*in* Brindley, 1951, p. 159) points out does not apply to glauconite. Moreover, the criterion is unsuitable for samples with minerals such as kaolinite and quartz with interfering diffraction lines (see, for example, Brindley and MacEwan, *in* Brindley, 1951, table XIV, 1, II). Nagelschmidt also suggests (1937, p. 519) that the relative weakness or absence of the 5 Å basal reflection is suggestive of trioctahedral micas. Most of the 10 Å micas from the cores show this relationship. However, this does not seem to be a reliable criterion, as prolonged grinding of natural, coarsely crystalline muscovite by the writer has resulted in the complete obliteration of the 5 Å line while the 10 Å line remains strong.

On the bulk and also the untreated $-1.3\ \mu$ samples, the 10 Å reflection of illite is commonly interfered with by lines from the mixed-layer clays. This interference shows up in the asymmetry of the line, with more abrupt high-angle dropoff. Fortunately, the relative amounts of these clays in the samples studied are such that the peak position of the illite lines can generally be determined without difficulty. This position can then be compared with that after glycol treatment; a lack of shift in the line position is used to ascertain the presence of illite.

As is discussed, the exact nature of the illite is difficult to establish although such information is crucial in any consideration on the origin of the minerals. Microscopically, identifiable micas, all or part of which may give an "illite" pattern by X-ray, belong to four descriptive categories.

1. Large laths of colorless mica which are optically identical with muscovite.
2. Large laths of mica which are pleochroic from yellow to brown. These are biotite grains, and are relatively rare. The occurrences have been noted in table 2. Most likely these laths represent detrital grains.
3. Tiny (about 5 μ or less), colorless, loose shreds, lath-shaped and invariably length-slow. Birefringence is moderate.
4. A phase that is optically much like the above, but is embedded within grains of volcanic glass in various stages of devitrification. Most of these grains are colorless, but

TABLE 4.—*Comparison of the (010) spacings of muscovite and glauconite*

Sample	(060), Å	(010), Å
Muscovite, source unknown (pegmatite material)	1.50(5)	9.03
Muscovite from slate, Castleton, Vt.	1.50(7)	9.04
Muscovite from slate, Castleton, Vt.	1.50(9)	9.05
Muscovite from slate, Castleton, Vt.	1.50(7)	9.04
Muscovite from Renssalaer, N. Y.	1.50(7)	9.04
Muscovite from slate, Hampton, N. Y.	1.50(8)	9.04
Glauconite, Hazel, N. J.	1.51(6)	9.10
Glauconite, Kent, England	1.51(3)	9.08
Glauconite, Birmingham, N. J.	1.51(4)	9.08
"Glauconite", core 61-5	1.51(2)	9.07

owing to the color of the glass the color of the grains may remain in doubt. The textural relations of the micaceous grains to the glass matrix is variable. For some relatively fresh grains, mica occurs near the grain-boundary of the glass which is otherwise quite fresh; with more advanced devitrification, however, mica may pervade the grains. In many samples, in fact, the only indications of the original glassy nature of the matrix are the enclosed phenocrysts of euhedral feldspar and/or amphibole.

Certainly both the first two types, and probably both the latter types as well, contribute to the 10 Å X-ray reflection. From the appearance of the material under the microscope, much of it may be dioctahedral mica closely akin to muscovite; however this is not a proven point. The existence of a colorless phlogopite, for instance, cannot be excluded.

As table 2 shows, only an extremely limited number of samples does not contain illite. It is found associated with every other mineral except possibly glauconite; the two minerals, however, cannot be easily differentiated by routine X-ray examination even if they do coexist.

Although many of the samples show, under the microscope, an olive-green, fine paste, the mineral glauconite has been definitely identified only in one sample. This is from core 61-5, at depth levels between 102 and 106 cms. The bulk of the core here is a brownish-gray, fine, homogeneous silt, with moderate HCl reactions; scattered through this material are a number of deep green, shapeless, very fine-grained patches, each 1–3 mm across. The boundaries with the matrix are sharp. X-ray examination shows that these green spots have, aside from small amounts of quartz and plagioclase which are also abundant in the matrix material, a very broad reflection centered at about 10 Å. This peak is little affected by heating to 440° C for $\frac{1}{2}$ hour; glycol saturation, however, shifts part of it to nearly 18 Å (4.9° 2θ), but peaks also exist at 14.3 Å, 12.6 Å, and 10.0 Å (6.2°, 7.0°, and 8.8° 2θ, respectively). The (060) line is broad and poorly resolved; its peak, however, is at 61.3° and corresponds to a (010) spacing of 9.1 Å. This mineral, or group of minerals, is identified as glauconite, as well as mixed-layer clays with important glauconite components. Finally, the "glauconite" sample also gives, on the X-ray fluorescence analyzer, an $\mathrm{Fe}_{k\alpha_1}$ line with its intensity 2.6 times[3] as strong as the matrix from an adjacent level has yielded.

The value of the (010) spacing of the glauconite, 9.1 Å, is intermediate between the trioctahedral micas like biotite and the dioctahedral aluminum micas like muscovite, but agrees with the (010) of undoubted glauconite. Table 4 gives the X-ray data on a number of muscovite and glauconite samples; for reference, the (010) of muscovite and phlogopite are given as 9.04 Å (Winchell and Winchell, 1951, p. 367) and 9.23 Å (Bragg, 1937, p. 213), respectively.

The enlargement of the (010) dimension of glauconite, as compared to muscovite, is

---

[3] This ratio has not been corrected for the non-linearity of the Geiger counter in the particular intensity range encountered. The more intense reflection should give a reading relatively too low and so the ratio is a minimum value.

TABLE 5.—*Procedure for the identification of chlorite*

Untreated sample	Code Ethylene glycol saturated	Heated to 350°C
7 Å (A)	Not affected (1)	Not affected (a)
	Shifted (2)	Disappeared (b)
		Diminished (c)
14 Å (B)	Not shifted (3)	Not affected (d)
	Shifted (4)	Disappeared (e)
		Shifted to 10 Å (f)

Scheme for Identification

A-no B-1-a:	Kaolinite
-b:	Chlorite ("Bradley")
-c:	Kaolinite+chlorite ("Bradley")
B-no A-4-f:	Mixed-layer clay
A-B-1-a-3-d:	Chlorite ("Brindley"). Kaolinite?
-e:	Kaolinite+chlorite ("Bradley")
-4-f:	Kaolinite+mixed-layer clay
-b-3-e:	Chlorite ("Bradley")
-4-e:	Mixed-layer clay+chlorite?
-f:	Mixed-layer clay+chlorite?
-c-3-e:	Kaolinite+chlorite ("Bradley")
-4-f:	Mixed-layer clay+chlorite?

None of the other combinations of the code, of which there are 36, have been observed.

presumably due to the substitution of Fe''' for Al in the dioctahedral positions. A similar relation in the (010) dimensions of beidellite and its ferric analog, nontronite, is reported by MacEwan (*in* Brindley, 1951, p. 106); the (010) increases in this instance from 8.95 Å for beidellite to 9.15 Å for nontronite.

Kaolinite.—The term kaolinite as used here is based virtually exclusively on X-ray records, and has been defined in an earlier paper (Zen, 1959, p. 31). As such, the name applies to any *ca.* 7 Å platy mineral whose basal reflection is not destroyed by heating to about 450° C. In some instances, the $-1.3\ \mu$ fractions show the (002) reflection at 24.9° 2θ which distinguishes it from chlorite, with its (004) reflection at 25.2°; however, this distinction is not always possible as the peaks may not be resolved. The term "kaolinite," as used here not only fails to differentiate the stacking polymorphs of the various phases in the kaolinite group, but also fails to distinguish such minerals as antigorite, amesite, or the "septechlorites" (Nelson and Roy, 1958, p. 708).

Kaolinite has been found with all the other minerals, including phillipsite and calcite. The only exception is a lack of association with glauconite; this may well be a sampling problem since glauconite was found but once. The phase-equilibrium relation of kaolinite and calcite has been considered elsewhere (Zen, 1959); relation between kaolinite and phillipsite, as well as other essential potassic phases, will be considered in a separate paper.

Chlorite.—The operational definition of chlorite, based on X-ray diffraction, has been set out before (Zen, 1959, p. 31). One practical difficulty in the identification of chlorite is the fact that there are two sets of criteria available (Brindley and Robinson, *in* Brindley, 1951; Bradley, 1954) which are not always mutually compatible. Brindley and Robinson based their criteria on relatively coarse, well-crystallized chlorite (Brindley, 1957, personal communication), whereas Bradley's criteria, based on the presumption of lower thermal stability of chlorite when heated in the open air, are more useful for fine-grained, poorly crystalline chlorite (Bradley, 1957, personal communication). Thus to establish the *existence* of the chlorite phase in a sample, one would have to assume first the nature of the chlorite one is dealing with. Fortunately, in practice the two sets of criteria can be combined to a large extent, and the adapted procedures are outlined by the scheme shown in table 5.

The origin of the two different types of chlorite is a matter for speculation. The "Brindley" chlorite always gives sharp and symmetrical basal reflections, in contrast to the "Bradley" chlorite which tends to give diffuse and broad basal peaks. These facts are consistent with their presumed state of crystallinity. One is tempted to correlate the "Brindley" chlorite with coarse, detrital flakes and the "Bradley" chlorite with authigenic material, although this point is not established. "Brindley" chlorite is much less common than the "Bradley" chlorite in the samples from the Peru-Chile Trench area. Chlorite as a group, but in particular the "Bradley" type, has been found with all other mineral phases identified in the core samples. It is unfortunate that nothing can be said of the detailed compositions of the chlorite samples from different mineral associations.

Mixed-layer clays and montmorillonite.—In the preliminary report (Zen, 1957), it was stated that montmorillonite is rare and mixed-layer clays not found in the Peru-Chile cores. Since the writing of that report, more detailed work on the $-1.3\ \mu$ fractions has shown this to be incorrect. Instead, mixed-layer clays turn out to be among the most common minerals in the core samples.

In an air-dried sample, most of the material shows a broad reflection between 6.0° and 7.5° 2θ (14.7 Å to 11.8 Å) but commonly centered about 6.5° (13.6 Å). Glycolation shifts this spectrum of reflections to a broad peak centered commonly around 5.3° (16.7 Å). The diffraction lines are unaffected by heating to around 200°C in open air for one hour, but collapse to about 10 Å upon heating to around 450°C for one-half hour in the open air.

The results of heat treatment indicate that the non-expanding layers are 10 Å material, perhaps muscovite-type layers. The results of glycolation show that, for much of the material, about 80 percent of the layers are expandable (Weaver, 1956, p. 206). Using this information, it is then possible to say that the untreated expandable layers have basal spacing of about 14 Å. The broadness of the lines, both in untreated and glycolated material, may indicate that a collection of mixed-layer material, with the 10 Å and 14 Å layers in variable proportions, exists in many of the samples. This accords with the observation of Weaver (1956, p. 210) on the clay mineralogy of some sedimentary rocks.

In many samples, for instance 53-5-120, the untreated $-1.3\ \mu$ fraction gives, in addition to the broad peak between 6.0° and 7.5° 2θ, a rather well-defined peak at 8.2° 2θ, or 10.8 Å. Using the migration chart of Brown and MacEwan (*in* Brindley, 1951), this might be interlayered 10 Å type with (a) 30% 12.4 Å type; (b) 20% 14 Å type; or (c) 15% 15.4 Å type. Glycolated samples yield a line at 13.4 Å; using Weaver's migration chart (1956, p. 206), the first choice is accepted.

As another example, specimen 54-5-114 gives, in addition to a broad peak between 6.0° and 7.0° 2θ, a peak at 7.6°. This peak is associated with a 5.7° peak for the glycolated sample, and is taken to be 55% 12.4 Å layers mixed with 10 Å type. In addition, a 5.7° peak of the untreated sample (15.5 Å) is taken to be nearly pure two-layer montmorillonite.

These are but a few typical examples; many other $-1.3\ \mu$ samples from different cores give similar results. It is clear that mixed-layer clays involving different types of layers occur, as well as those involving different proportions of the same types of layers.

The 12.4 Å layers may be attributed to one-layer hydration (Bradley, Grim, and Clark, 1937, p. 221), or may be due to Na or K adsorption (Weaver, 1956, p. 205). The 14 Å type layers may be due to Ca-adsorbed layers with octahedrally coordinated H_2O (MacEwan, *in* Brindley, 1951, p. 110), but may also be due to vermiculite layers. The 15.5 Å type is probably simple two-layer H_2O type.

Halite

Halite is a very common mineral in the core samples, and is easily identified by the (200) line at 31.8° 2θ on the X-ray chart. When very abundant, its (111) line at 27.5° 2θ interferes with the potassic feldspar line.

Halite is, without much doubt, the result of dehydration of the cores. It is weak to absent in highly permeable, sandy cores, but is especially important in cores made up largely of tests of microorganisms which offer many traps for water.

Gypsum

Gypsum is found in some cores, presumably as a phase resulting from the drying up of the entrapped sea water. The diagnostic line used on the X-ray chart is at 11.8° 2θ, which is destroyed by heating of the sample to 450°C.

Glass

Volcanic glass is, quantitatively, a very important phase in many of the core samples. Being non-crystalline, it is not recorded by X-ray diffraction; optical examination alone establishes its presence.

Volcanic glass occurs typically as angular to subrounded fragments, commonly mixed with the rest of the material but rarely (as in core 70-7 and 73-6) forming thin but nearly pure layers. The material is devitrified to different extents, as can be seen even in a single oil-immersion mount; it ranges from completely fresh and clean to completely altered material, the latter recognizable as devitrified glass only by the enclosed euhedral phenocrysts. The fresh material ranges in refractive indices from near 1.50 to 1.56 or more. Presumably this range reflects differences in chemical composition, from rhyolitic to basaltic glass (Wahlstrom, 1955, p. 288). The glass with low refractive index tends to be colorless, where even tiny fragments of those with high indices are commonly olive-green to olive-brown.

FOSSILS

No specific study has been made of the fossil records of the Peru-Chile cores. The brief notes below are observations incidental to the mineralogical studies.

The fossil remains can be conveniently divided into two groups: the calcareous forms and those which, under the microscope, are completely isotropic and which on the X-ray chart leave no record. This latter type is presumably composed of amorphous silica.

The calcareous fossils may be composed of aragonite, but much more commonly the carbonate is calcite. In fact, most of the calcite in the samples may be correlated with fossils. Megascopic fossils such as gastropod and pelecypod shells are fairly common, particularly in the coarser-grained, nearshore (landward of the Trench axis) material; more commonly, however, the fossils are microscopic, including abundant foraminifera. These occur in the fine mud as well as in the coarse material. Locally such material makes up nearly the entire core, as for example core 65-6, a substantial part of which is composed of 1 mm size foraminifera; and core 39-3, the lower portion of which is a white chalky deposit of globigerina ooze.

The siliceous fossils are extremely common in all the cores. These are always microscopic in size and commonly fragmentary.

SEDIMENTARY FEATURES

The sedimentary structures to be described in this section are necessarily rather small-scale phenomena, limited by the diameter of a core. It has not been possible to correlate such data as the spacing and nature of bedding from one core to another, partly from lack of information on the time-equivalence among the cores, and partly because of sparsity of cores compared to the size of the area covered.

Size Distribution

Quantitative study of the size distribution in the cores is being reported by P. D. Trask of the University of California and is outside the scope of this report. The following generalizations, based on the megascopic data of table 1, however, may be of interest.

West of the Peru-Chile Trench axis, the cores are uniformly of fine mud, the individual grains too small to be seen with the naked eye. Along the Trench axis, the material is mainly fine mud, but interlayering of seams of silty sand is quite common (cores 20-2, 55-5, 70-6, 77-7). These silty sands tend to be rather thin-bedded, each individual layer no more than a few inches thick, and commonly have sharp boundaries against the muddy matrix. Moreover, the sand is generally well-sorted, and either loosely cemented or uncemented.

Shoreward from the Trench axis, silty to sandy cores become much more prevalent. Although the most shoreward core of each traverse tends to be most sandy, the distribution of sand and silty mud does not seem to correlate simply with distance from shore along any given traverse. Either sand, or silt, or both, may also be interbedded with fine mud in a given core. Finally, between cores of relatively coarse material, fine clayey mud cores may occur. Core no. 59-5, for example, is fine mud throughout, and is located between a silty core no. 60-5 and a sandy-silty core 58-5. Likewise, core no. 67-6, of fine mud, is found between no 68-6, with silty material, and no. 65-6, of silt and sand. On the basis of available information (Zeigler and others, 1957, pp. 243–244), these patterns of distribution do not seem to be attributable to the bottom topography.

It would be interesting to know the mode of transport of the relatively coarse material into the axial portion of the Trench. Much of the coarse material consists of thin, clearly-defined beds of well-sorted material. Furthermore, coarse material is wanting seaward of the Trench axis. These facts indicate that bottom currents, rather than wind or surface currents, may be the dominant agent of transportation for sediments of this size range (see also Schmalz, 1958, p. 107). Unfortunately, data on deep-water currents in this area are lacking.

Bedding

Because the cores are extremely superficial samples of the sediments, large-scale bedding cannot be seen. Bedding, as it is observed, may be gradational or sharp, and individual beds range in thickness from a fraction of a millimeter on up.

Graded bedding has been found in a number of cores. Examples are core nos. 20-2, 31-3, 70-6, 78-7, and 79-7; the gradation is always "normal," the sandy beds possessing sharp bottom contacts but grading upward into fine mud. Perhaps the most striking instance of graded bedding is core no. 31-3, between levels 21 and 23 cms; here graded bedding is the result of size gradation of tests of siliceous microfossils. The graded bedding in this core, and in core no. 79-7, are well-sorted; the other examples show poor sorting, with gradation of the maximum grain sizes.

Cross-bedding has been found in two samples. One is core no. 31-3, depth levels 110–116 cms; the cross-bedding, with laminae about 1 mm thick, spanning the 6 cm interval, is due to interlayering of white siliceous microfossil tests and dark mud. The second, and more questionable, instance is core no. 55-5, depth levels 124–126 cms; "cross-bedding" is due to 1–2 mm layers of medium sand separated by dark, muddy partings. In both examples, the cross-bedding is normal in that the beds are tangent to the bottom and truncated at the top. Unfortunately, the orientation of the features in the horizontal plane is unknown, so that an interpretation cannot be made of the direction of bottom currents.

GEOLOGIC IMPLICATIONS

One of the clearcut results of this study is the variation of grain size with distance from the shore to the Trench axis, already described. It should be emphasized, however, that this seaward decrease in size is not necessarily true in detail, so that a core of fine sediment may in fact be found between two cores of coarser material; landward of the Trench axis local variations of sediment grain size span the entire size-range so far found.

Because of the relative sparsity of cores, as well as lack of three-dimensional control on the bottom topography, it is impossible to say how extensively the lithologic types persist. Although most of the cores are of fine mud, one is not justified in correlating them as one individual unit. The sedimentary types may be quite variable. Thus, upon diagenesis, core no. 31-3 may well become an impure chert bed; 36-3 a shale, and 39-3 in part a chalky limestone. Many of the cores will become fine-grained arkose, feldspathic sandstone, or subgraywacke; whereas at least one core, no. 1-1, which was a dark gray, hydrogen-sulfide smelling fine mud, that oxidized in a few days to a reddish-brown color, might well become a black shale deposit.

The cores tend to show little overall lithologic variation along their length, the common small-scale variations averaging out over the length of the core. Since the longest core is less than 10 feet, however, it is not possible to state what vertical changes there may be in the sediments as a whole. There are no data for estimating the thicknesses of the sedimentary columns in this area, on the basis of the present study.

The finding of volcanic glass in the sediments is of stratigraphic as well as petrologic interest. Glass fragments are so plentiful in many of the samples that the beds may well be termed ash deposits. Other samples, however, show admixture of quartz, carbonate (at least in part organic remains), and possibly other minerals in variable amounts, so that the resulting rocks might, when indurated and perhaps later metamorphosed, be expected to show mineral assemblages different from either greenstones on one hand and ordinary clastic shales on the other. A proper appreciation of the genesis of these beds is clearly essential to the interpretation of the geologic history from the sedimentary records, for areas of similar tectonic conditions.

The possible correlation of the mineralogy of the cores with the provenance areas has been studied by Schmalz (1958), to whose work the reader is referred.

ACKNOWLEDGEMENTS

I wish to thank Drs. E. H. Smith and C. O. Iselin, past Directors of the Woods Hole Oceanographic Institution, for their interest and administrative support which made this study possible. Professor B. Kummel, of Harvard University, initiated this program. His active interest in the work has been indispensable; this I am pleased to acknowledge with gratitude. Stimulating discussions on various phases of the work, with Kummel, as well as with Professors R. Siever and J. B. Thompson, Jr., of Harvard University, Professor R. F. Schmalz of the Pennsylvania State University, and Dr. W. F. Bradley of the Illinois Geological Survey, have helped my understanding of the problems. Siever and Schmalz also kindly read the manuscript and improved both its style and content. I must also record my indebtedness to the Faculty of the Division of Geological Sciences at Harvard University, who generously put at my disposal all the research facilities to enable me to carry out this study. Finally, it is a pleasant duty to acknowledge the able assistance of Mrs. Marilyn Anderson, who shared much of the drudgery of the experimental work with patience and never failing good cheer.

REFERENCES

BRADLEY, W. F., 1954, X-ray diffraction criteria for the characterization of chloritic material in sediments. *In* Clays and clay minerals, Publ. no. 327, Nat. Acad. Sci. and Nat. Res. Council. p. 324–334.

———, GRIM, R. E., AND CLARK, G. L., 1937, A study of the behavior of montmorillonite upon wetting: Zeit. Krist. v. 97, p. 216–222.

BRAGG, W. L., 1937, Atomic structure of minerals. Cornell University Press, Ithaca, New York. 292 p.

BRINDLEY, G. W., ed., 1951, X-ray identification and crystal structures of clay minerals: The Mineralogical Society, London. 345 p.

———, ed., 1958, X-ray powder data file. Am. Assoc. Testing Materials Spec. Publ. 48-G.

CLARK, S. P., JR., 1957, A note on calcite-aragonite equilibrium: Am. Mineralogist v. 42, p. 564–566.

EWING, M., HEEZEN, B. C., AND ERICSON, D. B., 1959, Significance of the Worzel deep sea ash: Nat. Acad. Sci. Proc. v. 45, p. 355–361.

GRAF, D. L., AND GOLDSMITH, J. R., 1956, Some hydrothermal syntheses of dolomite and protodolomite: Jour. Geology v. 64, p. 173–186.

GRIM, R. E., 1953, Clay mineralogy. McGraw-Hill Book Company, New York. 384 p.

GUNTHER, E. R., 1936, A report on oceanographical investigations in the Peru coastal current. *Discovery* Repts. v. 13, p. 107–276.

JAMIESON, J. C., 1953, Phase equilibrium in the system calcite-aragonite: Jour. Chem. Phys. v. 21, p. 1385–1390.

JENKS, W. F., 1946, Preliminary note on geologic studies of the Pacific slope in southern Peru: Am. Jour. Sci. v. 244, p. 367–372.

———, ed., 1956, Handbook of South American geology. Geol. Soc. America Mem. 65, New York. 378 p.

MACDONALD, G. J. F., 1956, Experimental determination of calcite-aragonite equilibrium relations at elevated temperatures and pressures: Am. Mineralogist, v. 41, p. 744–756.

NAGELSCHMIDT, G., 1937, X-ray investigation on clays, Pt. III: Zeit. Krist v. 97, p. 514–521.

NELSON, B. W., AND ROY, R., 1958, Synthesis of the chlorites and their structural and chemical constitution: Am. Mineralogist v. 43, p. 707–725.

REVELLE, R. R., 1944, Marine bottom samples collected in the Pacific Ocean by the *Carnegie* on its seventh cruise: Carnegie Inst. Wash. Publ. 556, Pt. 1, p. 1–180.

———, 1958, The *Downwind* expedition to the southeast Pacific (abs.) Am. Geophysical Union Trans. v. 39, p. 528.

RÜEGG, W., 1957, Geologie zwischen Cañete-San Juan 13°00′–15°24′ Südperu. Geologische Rundschau v. 45, p. 775–858.

SCHMALZ, R. F., 1958, A technique for quantitative modal analysis by X-ray diffraction and its application to modern sediments of the Peru-Chile Trench. Harvard University Thesis. 150 p.

———, AND ZEN, E. (in prep.), Quantitative modal analysis of sediments by X-ray diffraction.

SMITH, J. V., 1956, The powder patterns and lattice parameters of plagioclase feldspars. I. The soda-rich plagioclases: Mineralog. Mag. v. 31, p. 47–68.

WAHLSTROM, E. E., 1955, Petrographic mineralogy. John Wiley and Sons. New York. 408 p.

WEAVER, C. E., 1956, The distribution and identification of mixed-layer clays in sedimentary rocks: Am. Mineralogist v. 41, p. 202–221.

WINCHELL, A. N., AND WINCHELL, H., 1951, Elements of optical mineralogy. Part II. John Wiley and Sons. New York. 551 p.

WORZEL, J. L., 1959, Extensive deep sea sub-bottom reflections identified as white ash: Nat. Acad. Sci. Proc. v. 45, p. 349–355.

ZEIGLER, J. M., ATHEARN, W. D., AND SMALL, H., 1957, Profiles across the Peru-Chile Trench: Deep-Sea Research, vol. 4, p. 238–249.

ZEN, E., 1957, Preliminary report on the mineralogy and petrology of some marine bottom samples off the coast of Peru and Chile: Am. Mineralogist v. 42, p. 889–903.

———, 1959, Clay mineral-carbonate relations in sedimentary rocks: Am. Jour. Sci. v. 257, p. 29–43.

———, (in press), Carbonate equilibria in the open ocean and their bearings on the interpretation of ancient carbonate rocks: Geochim. et Cosmochim. Acta.

Contribution No. 1037

Reprint OIKOS 10:I 1959

NOTE ON STIMULATION OF CIRRIPEDE NAUPLII

BY

H. BARNES[1] and *MARGARET BARNES*

(The Marine Station, Millport and The Friday Harbor Laboratories,
University of Washington, Seattle)

The freshly deposited and newly fertilised egg masses of many cirripedes are present in the mantle cavity of the adult as a pair of distinct but very soft and somewhat globular masses; they quickly set to a rigid form that is determined largely by the shape of the mantle cavity itself. In some species (many Pedunculates) these egg lamellae are attached by a secretion to a fold in the lining of the adult mantle cavity—the so-called ovigerous fraena—while in other species (Operculates) they lie free. In neither case, as far as is known, is there any metabolic connection between lamellae and adult. The stiff form of the lamellae, their attachment when present and in the Operculates their transference while still soft to the base of the mantle cavity, all serve to prevent loss of the embryos through the opercular opening during incubation as a result of the normal cirral activity of the adult (DARWIN 1851). Depending upon the species each lamella may or may not be surrounded by a membrane that varies greatly in structure and appearance. Before the nauplii hatch this egg mass breaks down—a process that appears to be associated in a boreo-arctic species such *Balanus balanoides* (L.) with renewed vigorous feeding activities at the time of the spring diatom outburst (BARNES 1957).

The actual escape of the Stage I nauplius from the egg membrane appears to be purely mechanical in at least one species (BARNES 1955), rupture being effected by embryonic movement. This is supported by direct observations during hatching as well as by experimental work on the lamellae. For example, hatching is inhibited by respiratory poisons and the embryonic fluid is isotonic with the external medium. Direct microscopic observations on many other species, both Operculates and Pedunculates, indicate that rupture of the membrane by the movements of the embryo is a common feature of the group.

---

[1] Contribution No. 1037 from the Woods Hole Oceanographic Institution. This work was supported by a Research Fellowship from the Woods Hole Oceanographic Institution and a grant from the Office of Naval Research (Contract No. N.R. 165/142, Dr. D. L. Ray); these and leave of absence from the Scottish Marine Biological Association are gratefully acknowledged.

It has also been shown (Crisp 1956; Barnes 1957) that hatching is stimulated by the addition of extracts of adult bodies to sea water in which lamellae are suspended. Direct observations indicate that this accelerated hatching is in no way abnormal; the sequence of events is identical with that seen in the absence of added extracts. This fact, together with the speed of the effect, suggests that the process involves stimulation of the embryo rather than dissolution of any membranes. It was further demonstrated that the substance responsible for the stimulation is water soluble, relatively heat stable and, for several common species, non-specific.

It has now been shown that the active substance is dialysable. The supernatant obtained from homogenizing *B. balanoides* prosomas was dialysed against sea water for several days (with the addition of chloroform to prevent bacterial action). After blowing off the chloroform the residue was tested on groups of eggs (taken from ripe lamellae) by the technique previously described (Barnes 1957). The results (mean of five replicates) are shown in Table 1.

Table 1. Mean % nauplii hatching (5 replicates).

Sea water	45
Sea water and chloroform (removed)	43
Raw body extract	71
Dialysed body extract	49

It is evident that dialysis has removed most of the active principle. The above results were confirmed by dialysing into a small volume of sea water when the dialysate was found to be as active as the residue. The active principle may be assumed, therefore, to have a relatively low molecular weight.

It was previously stressed that the breakdown of the egg lamellae and the stimulation of hatching was closely associated with renewed and vigorous feeding of the adult and the moulting process was suggested as perhaps being related to the stimulation. It is, of course, conceivable that stimulation results from the presence of different concentrations of certain inorganic ions, e. g. potassium or calcium, in the body fluid from those present in sea water. The presence of neurosecretory cells in the central nervous system of a number of species of barnacles has recently been demonstrated (Barnes and Gonor, 1958) and the relation of this to moulting and other activities is being investigated. Now, the well known stimulatory effects of some of the substances involved in neurosecretion (Welsh 1955; Knowles and Carlisle 1956) when considered in relation to the known properties of the active principle in *B. balanoides* suggest that they may be involved; a substance such as 5-hydroxytryptamine could well be concerned. As an alternative approach to the problem a number of physiologically active substances have, therefore, been investigated with regard to their effect on the hatching process.

The species used was *B. nubilus* Darwin: this grows to a very large size—some 10 cm basal diameter—and a pair of lamellae from a single large individual is adequate for many tests. In this way uncertainties arising from the effects of different degrees of ripeness when many small lamellae have to be used, may to some extent be eliminated. The technique previously described was employed. Small well-washed pieces of egg lamellae were transferred to the test solutions made up in sea water contained in test tubes. Any nauplii hatching during manipulation were either pipetted off or neglected and a whole series was set up as quickly as possible to avoid any changes in the 'test' lamella itself. After gently mixing by a single inversion and then standing for five minutes, formalin was added and the number of free and unhatched nauplii subsequently counted. For *each* test substance at *each* strength five replicate tubes were used as well as five sea water controls (in the event that changes in normal hatching took place while the large number of tubes were being set up). Included in the test substance were compounds that might be expected to have stimulatory or depressant effects (other than known toxins) and others known to be physiologically active in various metabolic processes. The results are shown in Table 2.

It is evident from this table that many of the substances are, as would be expected, quite without effect on the release of nauplii. Indeed, only one substance, namely 5-hydroxytryptamine, has a very marked positive effect at the higher dilutions. (The depressant effect of γ-(indole-3)-n-butyric acid is to be noted). The presence of this and related substances in neurosecretory activities suggests that they may be effective in the stimulation obtained with prosoma extracts.

The question arises as to how far this stimulation—from whatever cause—is of importance to the animal under natural conditions. Viable nauplii will readily hatch when a ripe egg mass is transferred from the mantle cavity to sea water and indeed active and to all appearances fully viable nauplii of *B. balanoides* and other species have hatched from egg masses that have been developed *in vitro* outside the mantle cavity from the early stages of cleavage. A stimulus originating from any secretory or other substance in the adult is, therefore, not essential; nevertheless, it does not follow that such a substance may not be present and active, particularly when the metabolic activity of the adult is high. If it is believed that stimulation, either by body extract or physiologically active substances, has no significance under natural conditions then it may be considered that in this type of experiment one is merely using ripe embryos as a test animal in assaying active substances present in the adult.

Table 2. % Nauplii (*Balanus nubilus*) hatched with test substance. Mean of 5 replicates. Ripe egg lamellae used for all tests. Solution in contact for five minutes.

Substance	Concentrations			Control
	10^{-2} g/l	10^{-4} g/l	10^{-6} g/l	
5-hydroxytryptamine	*63*	*64*	*50*	34
γ-(indole-3)-n-butyric acid	*24*	*20*	*20*	41
D-tryptophane	30	37	23	39
Bufotenine	19	29	17	23
Acetylcholine	69	68	73	69
Adrenalin	33	46	31	37
γ-amino-butyric acid	34	–	–	34
Ethylamine	*19*	31	32	37
Leucamine HCl	*80*?	69	70	68
Nor-valamine HCl	65	64	70	63
Metrazol	57	55	48	55
α-ketoglutaric acid	62	50	50	52
DL-phenylalanine	47	54	53	47
L-glutamic acid	42	54	54	48
β-methyl-β-ethylglutarimide	44	43	53	44
Seramine HCl	49	47	48	49
L-tyrosine	*60*	48	46	37
α-ketobutyric acid	47	53	41	49
3-hydroxytyramine HCl	47	53	49	54
L-tryptophane	41	39	35	45
Tyramine HCl	35	47	34	27
Sarcosine HCl	*63*	52	52	46

However, it has also been shown that extracts of ripe nauplii accelerate hatching from ripe egg lamellae so the fact that nauplii may develop *in vitro* and out of contact with the adult does not necessarily rule out the existence of stimulation under natural conditions. It would be very difficult to demonstrate unequivocally that hatching was stimulated under natural conditions by an active principle (organic or inorganic) present in the embryo or surrounding fluid. Nevertheless, if this were the case it could be suggested that the initiation of movements of the nauplius within the egg membrane that eventually lead to the rupture of the latter results from a feed-back mechanism arising from stimulation by substances present in the ripe and fully developed embryo.

Summary

1. The egg masses of many cirripedes, at first soft, soon set to a pair of firm lamellae lying in the mantle cavity. This firmness ensures that they are not lost from the mantle cavity by the activity of the adult during the in-

cubation period. Before the nauplii hatch the egg masses break down, a process that is associated with the spring diatom increase in a boreo-arctic species such as *Balanus balanoides*.

2. The escape of the nauplius from the egg membrane appears from various lines of evidence to be purely mechanical. However, the hatching is stimulated by the addition of extracts of adult bodies. The active substance is relatively water soluble, heat stable, dialysable, and for many species non-specific.

3. The nature of this active substance is considered; the recent discovery of neurosecretory cells in certain cirripedes and the known stimulatory action of some substances associated with such cells suggested testing a number of physiologically active substances on the hatching process. Although this is no proof that it is involved in the stimulation by adult body extracts, 5-hydroxytryptamine was found to be very effective at high dilutions; many other substances were ineffective.

4. The question is considered as to how far this process is of significance under natural conditions. Since nauplii can be hatched from lamellae reared *in vitro* the presence of material from the adult is not essential. It may come from the ripe embryo. Such a process in the form of a feed-back mechanism could initiate the movements of the nauplius leading to its escape.

References

BARNES, H., 1955: The hatching process in some barnacles. Oikos, *6*, 114–123.

— 1957: Processes of restoration and synchronization in marine ecology; the spring diatom increase and the 'spawning' of the common barnacle *Balanus balanoides* (L.). Ann. Biol., *33*, 67–85.

— & J. J. GONOR, 1958. Neurosecretory cells in some cirripedes. Nature, Lond., *181*, 194 only.

CRISP, D. J., 1956: A substance promoting hatching and liberation of young in cirripedes. Nature, Lond., *178*, 263 only.

DARWIN, C. R., 1851: A monograph of the sub-class Cirripedia. Ray Soc., London, 400 pp.

KNOWLES, F. G. W. & D. B. CARLISLE, 1956: Endocrine control in the Crustacea. Biol. Rev., *31*, 396–473.

WELSH, J. H., 1955: "Neurohormones". Chapter III in 'The Hormones', Academic Press, New York.

OIKOS 10:I, Copenhagen 1959

Contribution No. 1038

[Reprinted from INSTITUTE OF MARINE SCIENCE, Vol. V, December, 1958]

Seasonal Growth of Benthic Marine Plants as Related to Environmental Factors in an Estuary[1]

JOHN T. CONOVER

Institute of Marine Science
The University of Texas
Port Aransas, Texas

Abstract

A study was made of the standing crops of 70 taxa of benthic marine plants and some physical, chemical, and biotic agents in a tidal estuary. Seasonal comparisons were made between plant growth and environmental factors from 1952 to 1954.

The standing crop of benthic marine plants was in excess of 4.0 kg. wet weight per square meter during July and August and less than 1.5 kg. in January. Temperature and illumination were variously associated with the maximum seasonal growth of those benthic plants studied. Some species, including *Cladophora gracilis* F. *tenuis*, *Enteromorpha linza*, E. *plumosa*, *Stilophora rhizoides*, and *Ulva lactuca* var. *latissima*, grew best under conditions of high insolation (over 500 gram calories per square centimeter per day) at moderate water temperatures (18° to 20° C.). Others, including *Agardhiella tenera*, *Enteromorpha compressa*, *Gracilaria verrucosa*, *Ruppa maritima* and *Zostera marina*, showed increased growth under diminished light intensities (less than 400 gram calories per square centimeter per day) at high water temperatures (over 24° C.). The low calculated seasonal yield of one group, including *Enteromorpha clathrata*, *E. intestinalis*, *Ectocarpus siliculosus*, *Gracilaria verrucosa*, *Polysiphonia novae-angliae*, *Punctaria plantaginea*, and *Scytosiphon lomentaria* was related to low concentrations of inorganic phosphate (less than 0.4 microgram atoms/liter P) in the spring (April and May) and nitrate (less than 0.2 microgram atoms/liter N) in the fall (October).

Forty-seven of the 70 taxa flourished in the tidal and brackish areas of the estuary. Sixteen of the 70, including *Chondrus crispus*, *Corallina officinalis*, *Enteromorpha linza*, *Gelidium crinale*, *Nemalion multifidum*, *Petalonia fascia*, *Polysiphonia nigrescens*, *P. novae-angliae*, *Punctaria plantagineae*, *Sargassum filipendula* and *Ulva lactuca* var. *rigida* were found only in normal sea water at the mouth of the estuary. The occurrence of some species, including *Ceramium rubrum* var. *proliferum*, *Ectocarpus siliculosus*, *Gracilaria verrucosa*, *Spyridia filamentosa* and *Stilophora rhizoides*, in the brackish water sloughs in January and February and their absence in low salinity water in March and April, suggested some relationship with either rising temperatures or changes in water density.

Six species of *Vaucheria*, found only in the marshland between neap and spring high water levels, were observed to fruit in winter and early spring but attained best vegetative growth in mid-summer. Fruiting periods of all six species were associated with spring tides.

A large portion of the benthic plant populations of the major basin of the estuary was observed to receive large additions of algal sporelings which first became established on coarse beach sediments and after some growth were wave-transported onto the silt-laden basin floor. These plants were still attached to small shells or pebbles. The effects of sedimentation, tidal currents, storm and hurricane winds, ice, and freezing are described. The aperiodic occurrences of some species in the area from 1952 through 1956 remain unexplained.

---

[1] Based on a dissertation presented to the faculty of the University of Michigan in partial fulfillment of the requirements for the Ph.D. degree. These studies were supported by Woods Hole Oceanographic Institution (Contribution number 1038) and The University of Texas.

Contents

ABSTRACT .... *Page* 97

INTRODUCTION 98

Review of Related Work

Acknowledgments

METHODS 103

Sampling

Measuring Plant Populations

Measuring Physical and Chemical Factors

SEASONAL HISTORIES OF THE PRINCIPAL BENTHIC MARINE PLANTS 108

Seasonal Periodicity of Growth in Great Pond

Comparison of Seasonal Growth in Great Pond with Growth Regimes in Other Latitudes

Local Distribution in the Estuary

Changes from One Year to the Next in Species Composition and Abundance

Overseason Persistence of Summer and Winter Species

Seasonal Periodicity in Reproduction

EFFECTS OF ENVIRONMENTAL FACTORS ON THE SEASONAL GROWTH OF BENTHIC PLANTS 120

Light, Temperature, and Seasonal Growth

Nitrate, Phosphate, and Seasonal Growth

Dissolved Oxygen and Growth

pH and Benthic Plant Growth

Physical Factors and the Distribution of Benthic Plants

Biotic Factors and Seasonal Growth

Storms, Extreme Temperatures, and Icing

Similarities and Differences in Successive Years

LITERATURE CITED 145

Introduction

The present investigation concerns seasonal periodicity in the growth and reproduction of larger aquatic plants in an estuary. In an early paper F. E. Fritsch (1906) stated that the seasonal phenomena eventually would be explored on a quantitative basis by estimating phytoproductivity, by measuring the important environmental features, and then by comparing these data in search of causal relationships. Fritsch's suggested program of study was proffered at a time when the science of ecology was quite new. Development of the proper methods was to take a number of decades. With remarkable early insight he perceived two kinds of seasonal change: regular periodic changes and irregular ones. Regular patterns he described as those recurring normally each year in seasonal sequence, while irregular changes had no fixed pattern of occurrence and could take place at any season.

Fritsch suggested that there were probably both direct and indirect forces in the environment which had an impact on periodicity in plants. Light and temperature he believed to be direct, while all others were indirect as part of a complex affecting the organism. This point of view has not changed essentially over the intervening 50 years.

The present study was undertaken to determine the relative importance of several environmental agents affecting events in the seasonal histories of the dominant, benthic, multicellular marine plants in a specialized marine habitat. The investigation was confined to a representative, relatively self-contained estuary, Great Pond, near Woods Hole on the southern shores of Cape Cod, Massachusetts (Fig. 1).

REVIEW OF RELATED WORK

Over the past 50 years most studies of the seasonal occurrence and growth of benthic marine plants have been descriptive. Excellent summaries of these descriptive studies are given by Funk (1927), J. Feldmann (1937, 1951), Fritsch (1945) and Bernatowicz (1952a). More recently a number of limited, quantitative studies have increased our knowledge of seasonal growth. Yet, as Blinks (1955) has pointed out, "Long term (seasonal or yearly) production of organic matter has not been studied as thoroughly in littoral algae as in algae of the open ocean."

Qualitative studies indicate that some plants grow throughout the year while others have dormant periods (Kylin, 1907). In Ceylon at approximately 8° N. Lat. maximum plant cover is believed to occur in spring followed by a decrease in summer with the minimum appearing in autumn (Svedelius, 1906). Some algal species in Swedish coastal waters show greatest vegetative growth in late winter and early spring (Printz, 1939). Rees (1934, 1935) found the peak vegetation cover for the coast of Wales to occur in mid-summer. Certain species, for example *Fucus vesiculosus* and *Ectocarpus siliculosus*, may show best growth in summer in polar seas but seem to exhibit maximum cover in winter in warm temperate waters (Knight and Parke, 1931). The benthic vegetation of Bermuda at 32° N. Lat. may be similar in its seasonal growth cycle to that reported for Ceylon (Bernatowicz, 1952a). Since all these studies are based upon visual estimates, the conclusions are questionable. These results can be confirmed only by using quantitative ecological techniques.

A few quantitative studies using such techniques have been made over the past 40 years. Early studies include those of Petersen (1912) and Boysen-Jensen (1941), who attempted standing crop estimates for *Zostera marina*. More recently, improved methods have shown that high growth rates generally occur during the spring in temperate waters. Dry weight increases in *Laminaria* (Black, 1950) and in *Ascophyllum nodosum* (Printz, 1950) indicate maximum growth for these species in the spring. Knight and Parke (1950) reported growth rates of 0.5 to 0.85 cm./week for *Fucus serratus* and *F. vesiculosus*. Estimates for *Macrocystis pyrifera* showed yields of several kg./M^2/yr. in the extensive kelp beds of California (Sargent and Lantrip, 1952). Annual yields up to 10 g./M^2/yr. have been reported for kelp in the coastal beds of Scottish waters (Inst. Sea Weed Res., 1953). Carpelan (in Blinks, 1955) gave spring and fall growth estimates in temperate seas ranging from 70 g./M^2/yr. dry weight for *Ulva* to 4.4 kg./M^2/yr. for blades of *Laminaria*. Blinks (1955) compared these values with the 0.5 g./M^2/yr. reported for phytoplankton. The red alga, *Iridophycus cornicopeae*, in a locality in Japanese waters, attained a maximum standing crop in the spring (Hasegawa and Fukuhara, 1956). Several workers have shown early spring growth maxima for *Porphyra*. Although these studies represent a commendable beginning, most have not included com-

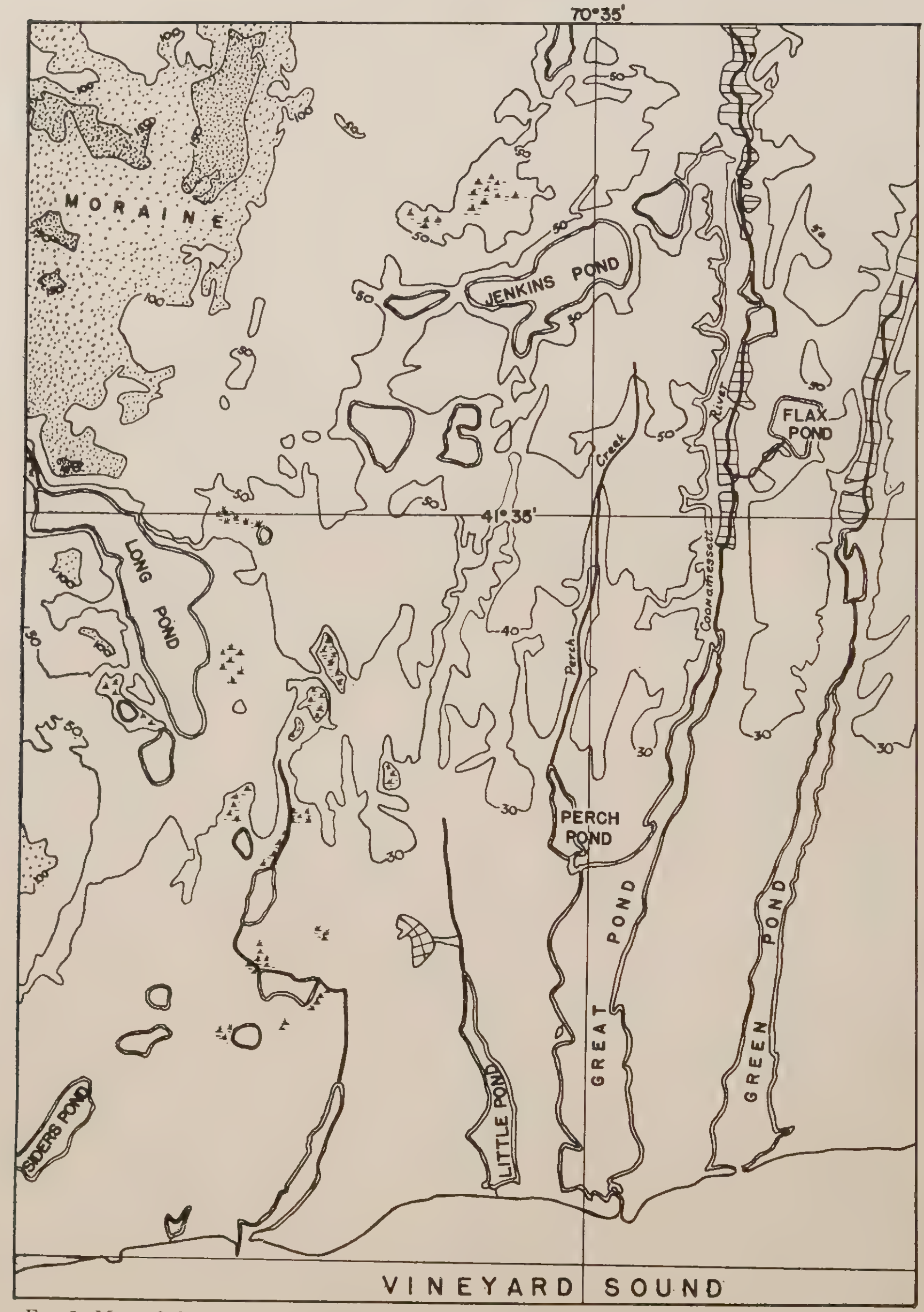
70°35'
MORAINE
100
150
50
JENKINS POND
FLAX POND
Coonamessett River
Creek
41°35'
LONG POND
Perch
40
30
PERCH POND
GREAT POND
GREEN POND
LITTLE POND
SIDERS POND
VINEYARD SOUND

Fig. 1. Map of Great Pond, Falmouth, Mass. after a U. S. Geological Survey Map showing the drainage basin and the Wisconsin Moraine. The rectilinear areas are cranberry bogs. Contour intervals are in feet. Only 30, 50, and 100 foot contours are drawn. One inch approximately equals one mile.

plete seasonal cycles of growth. Moreover, none of these studies have measured entire benthic plant communities.

The relationship between light and the seasonal growth of benthic marine plants is little understood even today. Reviews of work concerned with the subject appear in papers by Fogg (1953), Blinks (1955) and Holmes (1957). A review of important contributions which apply to the present study follows. Svedelius (1906) believed light was the major factor affecting growth at low latitudes. No investigator has confirmed these observations with quantitative ecological methods. In temperate seas growth optima were demonstrated for plants of low and high light intensity types in both fresh and salt water (Ehrke. 1929. 1931). Some kelps have been shown to attain higher standing crops at depth betwen 4 and 8 meters presumably due to the efficiency of the auxiliary pigments in green light. Walker (1952) found a reduction in the density of kelps at depths below 2 meters. perhaps related to the diminishing quality and intensity of light. In *Macrocystis pyrifera* the synthesis of sugars takes place mostly in the assimilatory tissues of the fronds at or near the surface (Sargent and Lantrip, 1952). Despite the evolution of special auxiliary pigments in red and brown algae, Blinks (1955) asserts that phytoproduction may always be highest at or near the surface in temperate seas. Some studies indicate that the uptake of carbon dioxide and hence the synthesis of organic matter by marine plants, may be limited by certain intensities of light (Holmes, 1957). Moreover, these so-called saturation values may vary from one species to another. Data cited by Holmes suggest that higher light intensities are required by a given plant for increases in photosynthesis than may be tolerated for maximum rates of cell division. These results suggest that various portions of the electromagnetic spectrum of energy from infra-red to ultra-violet may be affecting different phases of growth.

Temperature effects on growth concern still another aspect of radiant energy which governs biological processes. Gunter (1957), in his review of temperature and marine ecology, indicated the complexity of temperature studies. He stated, "Temperature is the most important single factor governing the occurrence and behavior of life. Temperature changes affect protoplasm directly and change the physical and biological environment as well." Attempts to correlate temperature with biological process have always been extremely difficult. Hedgpeth (1957) has given a summary of biological studies and principles including examples of benthic marine plant growth as related to temperature zonation. He considered temperature, with qualifications, as the most important single factor governing the distribution of life in the sea.

As early as 1851, W. H. Harvey considered temperature to be the major factor affecting plant growth and geographical distribution. Throughout its range from the Arctic to New Jersey, when water temperatures are between 3° and 6° C, *Ascophyllum nodosum* grows and produces oöspores (Setchell, 1920a, 1932). In arctic waters this temperature range occurs in midsummer but in southern New England and New Jersey these temperatures occur in midwinter. The behavior of this species is considered by Hedgpeth (1957) to be a good example in support of Hutchins' theory of temperature zonation. Setchell (1915, 1917, 1920a, 1920b) also developed an idea of temperature intervals and thermal zones. His concept was based upon 5° intervals of annual mean temperatures of a hemisphere along parallels of latitude, within which the broad distribution lines for benthic marine algae might be explained.

The study of growth rates has received some attention in more recent years. Klugh and Martin (1927) found the growth rates of some benthic algae decreased with depth and temperature. Laboratory experiments (Boyle and Doty, 1949) indicate that algal plants were killed more quickly at higher temperatures in dilute sea water than the control plants growing in normal sea water. Low killing temperatures for plants in brackish water were about the same as those for the controls in normal sea water. There is a dearth of information, apparently, relating temperature to seasonal growth rates or standing crops. Many quantitative accounts mention temperature as probably affecting seasonal growth without supporting data for these assumptions.

The role of nutrients in seasonal growth of benthic marine plants has been singularly neglected. Among the few observations is a suggestion by Rochford (1952) that the interstitial phosphate in the muds of the more saline portions of shallow tidal estuaries may be readily available to shallow-bedded species of benthic algae, such as *Gracilaria.* He also considered the same phosphorus source as directly benefiting beds of the rooted immergent marine phanerogams such as *Zostera marina.* Although he found high concentrations of both phosphorus and nitrogen in the muds of estuaries in areas with good plant cover, no proof was offered that the plants did benefit from the mud reservoir of nutrients. There is much evidence from freshwater studies (Gessner, 1955) that rooted aquatic plants utilize nutrients from bottom muds.

Blinks (1955) has postulated that in the cycle of plant growth and decay in littoral communities along open coasts, the reserves of carbon, nitrogen and phosphorus, and other constituents of protoplasm, may be in such ever present excess as to be causally related to the very high phytoproductivity of coastal areas. A thorough study of the nutrient requirements and relationships between seasonal growth and the nutrient concentrations in nature awaits investigation.

A review (Doty and Newhouse, 1954) of several phases of the effects of salinity dilution by freshwater indicates no quantitative growth measurements have been made. Species of benthic marine plants which are present or absent along a diluted sea water gradient series have been listed in a number of studies by Luther (1951a, 1951b) and Doty and Newhouse (1954). Fassett (1928) described the zonation of immergent as well as emergent marine phanerogams as related to salinity in a marsh. Hoffmann (1929) reported that many marine plants tend to have higher respiration rates when growing in brackish water. Such plants may use up organic matter in respiration more rapidly than they can synthesize it due to low salinities. Sterility has often been reported in benthic plants growing in dilute sea water (Häyren, 1940, Levring, 1940; and others). Further studies are needed to separate with certainty those effects produced by differences in salinity from those effects which depend upon nutrients, light and temperature. We also need to know the physiological explanation for various growth and developmental responses to differences in salinity.

The pattern of algal periodicity in some areas is modified by the absence of suitable habitats for attachment at the time of sporulation. Some studies show that texture of the substratum (roughness, and hardness) is more important than chemical composition of the rock minerals (J. Feldmann, 1937, 1951). The presence or absence of lithophytes is profoundly affected by suitability of the bottom type (Rees, 1934; Levring, 1940; and others). Moul (personal communication) believes there is a "condition factor" brought about by previous plant and animal occupants preparing a substratum for attached plants sporulated in the following season.

In the survey of communities of Great Pond, those environmental factors measured were the same ones suggested as important to benthic plants from previous studies. These included light, temperature, salinity, nutrients and the character of the substrate.

ACKNOWLEDGEMENTS

I am most grateful for the guidance of Dr. Wm. Randolph Taylor, major professor during the course of this investigation and for the encouragement and suggestions of Dr. Alfred C. Redfield regarding the field problems. Thanks are given to Dr. Madeline Pierce for assistance in the field work, to Dr. Howard T. Odum for stimulation during the final writing, to Dr. John C. Ayers for suggestions regarding the nutrient cycles, to Drs. Kenneth L. Jones, Chester A. Arnold, Frederick K. Sparrow and Frederick E. Smith for advice as members of my Ph.D. committee, to Drs. Edward Moul and Maxwell Doty for counsel on the field problems and to Drs. Doty and Butcher for copies of unpublished manuscripts.

Acknowledgement is given to members of the Woods Hole Oceanographic Institution who took part in a cooperative hydrological survey of Great Pond in 1954 as part of a series of related problems in estuarine ecology. Thanks are extended to the following for their help and for use of the 1954 Great Pond survey data: Mr. Nathaniel Corwin, Mr. Donald Foster, Mrs. Grace Creitz Fraser, Dr. Francis Richards, Dr. John Ryther and Mr. Ralph Vaccaro. Drs. John P. Barlow and E. M. Hulburt provided their 1950 Great Pond survey data. Dr. Bostwick Ketchum gave suggestions and data on Great Pond from the ecology course class records of the Marine Biological Laboratory. Messrs. William Athearn, Carlyle Hayes, Robert Lufborough and John Francis aided in the field in making current measurements, mapping, and taking cores of the bottom sediment of Great Pond. Dr. Wilbur Marx arranged for an aerial photograph of Great Pond. Dr. John Blum kindly made the identifications of the specimens of *Vaucheria*. Dr. Albert Bernatowicz permitted the writer to use unpublished data from his studies in Bermuda.

This survey was supported by the Woods Hole Oceanographic Institution by the award of a fellowship in 1953 and with facilities and equipment. The study was completed at The University of Texas Institute of Marine Science during the past year. The author is deeply grateful for the generous and untiring assistance of his wife.

Methods

SAMPLING

Sixteen transects were established, generally orientated at right angles to the long axis of the estuary. Each transect represented an area and was designated by a section number. Time of sampling did not exceed 30 hours for one complete circuit of all stations. In addition, eight hours were scheduled for water analysis every two weeks.

Quadrats were established along each transect. In the intertidal zones on the rock jetty, 25 cm^2 quadrats were used (Fig. 2). Initially, paired transects were established about 30 meters apart to check reproducibility in the major basin. During the season of prevailing moderate southeast winds, when the test pairs were studied, fairly good agreement was obtained. However, after the upstream transect of each pair had been abandoned, there was some suspicion that waves reached the bottom during storm periods, changing their distribution and density, diminishing homogeneity. Deposition on the shore was common during severe northeast, southwest or tropical storms.

FIG. 2. Map of Great Pond, Falmouth, Mass., with topography, environmental zones, area boundaries, sections, and locations of hydrographic stations.

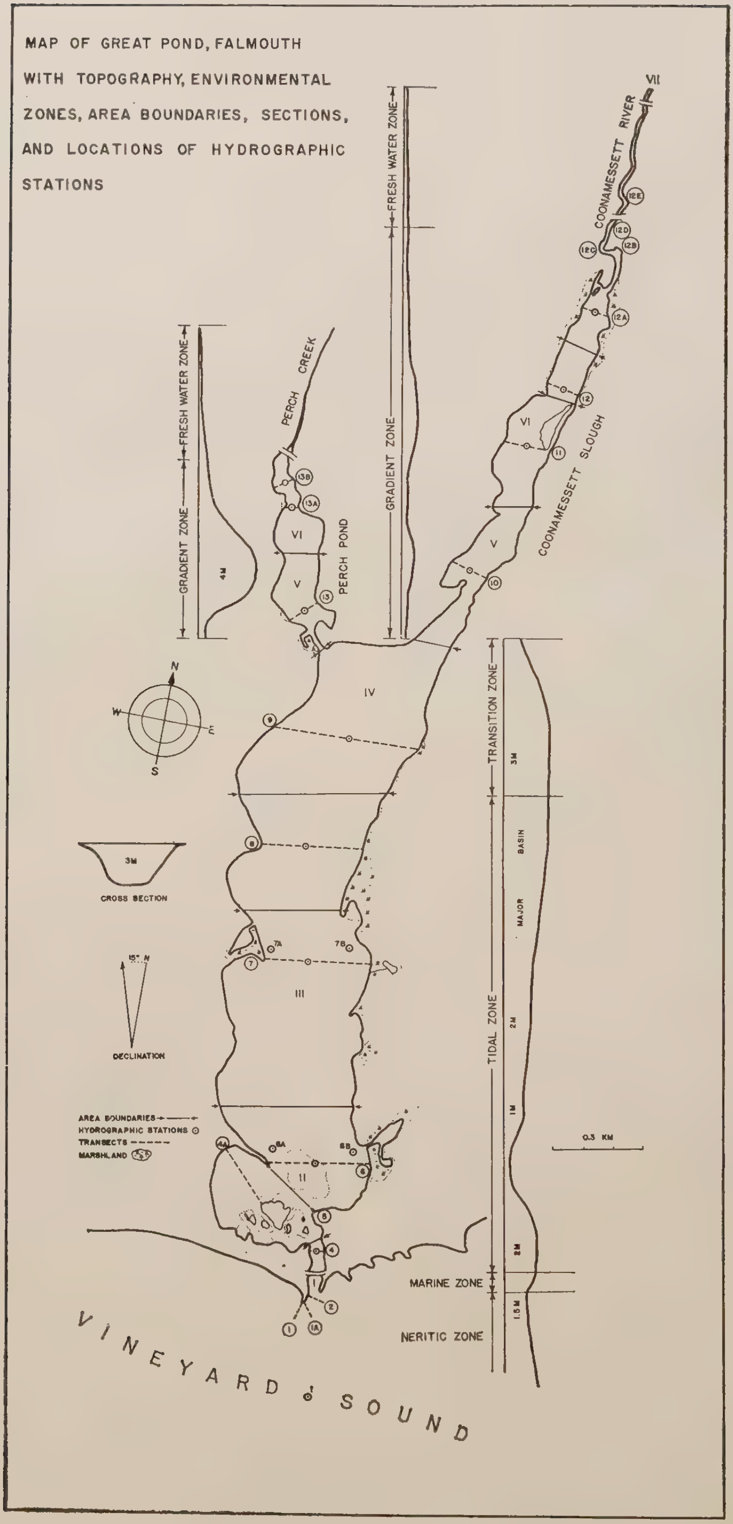

MAP OF GREAT POND, FALMOUTH WITH TOPOGRAPHY, ENVIRONMENTAL ZONES, AREA BOUNDARIES, SECTIONS, AND LOCATIONS OF HYDROGRAPHIC STATIONS

VII
COONAMESSETT RIVER
12E
12D
12C
12B
12A
12
11
10
VI
V
COONAMESSETT SLOUGH
FRESH WATER ZONE
GRADIENT ZONE
PERCH CREEK
PERCH POND
13B
13A
13
VI
V
FRESH WATER ZONE
GRADIENT ZONE
3M
N
W
E
S
IV
9
8
TRANSITION ZONE
3M
BASIN
MAJOR
3M
CROSS SECTION
15° N
DECLINATION
7A
7B
7
III
TIDAL ZONE
2M
1M
AREA BOUNDARIES
HYDROGRAPHIC STATIONS
TRANSECTS
MARSHLAND
0.5 KM
4A
6A
6B
6
II
5
4
I
2
1
1A
2M
MARINE ZONE
NERITIC ZONE
1.5M
VINEYARD SOUND

Hydrographic stations were established in 1952–53 at the centers of all transects except 4A and 5 (Fig. 2). Station 1 was located 0.4 km. offshore in the sound and station 12E in the fresh water portion of the Coonamessett River above State Highway 28.

MEASURING PLANT POPULATIONS

Plant populations were counted on each quadrat. The cover was estimated and sampled with a specially designed scoop, 25 cm.^{2} in capture area covered with one cm.^{2} mesh wire. The scoop was attached to a four-meter pole. A hooded, glass-bottom scanning box was fastened to the side of the skiff. Samples of plants observed through the scanning box were taken with the scoop, identified, measured, preserved, labeled, and retained for further study. Fortunately, during the seasons when the sea water was too chilly for skin-diving, the turbidity was generally low, permitting good visibility of the bottom particularly on cloudy days. In the summer months, when turbidity was high, skin-diving proved effective.

Observations at all stations except on the jetty were made from a 9-foot skiff with outboard motor. A 25 cm.^{2} grid of dural tubing was improvised to mark off quadrats on the jetty. A meter-square grid guide, made from two one-meter brass rods, crossed at right angles and brazed together at their centers was lowered on a line to the bottom to mark off the meter-square under-water quadrats.

Estimates of percentage cover were made using the "percentage cover guide" method explained in detail in Braun-Blanquet (1932). This method makes use of guides for three types of area cover: checkered, solid block, and asymetrical body figure grids. The percentage cover guide is first used to train the investigator's accuracy in estimating plant cover and later serves as a reminder. The writer made trial runs which proved to be reproducible within a 5 percent significance level at the low end of the scale and 10 percent at the upper end. Since detailed data also were recorded regarding thickness of an algal mat, estimates of area and volume of many populations could be computed from the measurements.

Cover estimates were first obtained in the field from an average of three grid counts per quadrat. These data were totaled for all quadrats on each transect.

An aerial photograph, taken by a U. S. Navy airplane on December 10, 1954, showed the presence of scattered patches of material on the bottom which were believed to be large clumps of algae. The patterns seen from above resembled the patterns developed in the cover surveys.

For each species average percentage cover for each section was obtained from the average for all quadrats on the transect. The average cover for the Great Pond estuary as a whole was determined by averaging the percentage cover on all transects.

To obtain wet weight estimates of the standing crop of each of the dominant species, plants were removed from square meter quadrats with one hundred percent cover. The excess water was removed from the plants by draining and air drying for one hour. The quadrat sample was then weighed. For each species the weight of plants at 100 percent cover was multiplied by percentage cover of the species to obtain an actual standing crop estimate for the quadrat.

The 26 species studied in detail represented over seven-eighths of the total benthic crop of plant material present in the estuary at any season. Hence, the instantaneous biomass for all species measured was considered a reasonable estimate of the apparent net plant production for each month of the survey.

Biotic surveys were run every week, but individual quadrats were visited once every two weeks. Water analyses were made monthly during 1952–53, but every fortnight during 1954. Detailed analyses were based on the 1954 data, while those for the previous year were used to interpret trends in the environment during the period of observations on the biota. Limitations of time prevented detailed synoptic analysis of physical, chemical and biological changes in 1952–53. In January and April of 1953 storm conditions prevented observations on all transects. However, the partial data are used. All data were transcribed to McBee "Keysort" punch cards.

MEASURING PHYSICAL AND CHEMICAL FACTORS

Salinity.—In 1952–53 salinity measurements were made with the aid of a precision-calibrated specific-gravity hydrometer. Salinity was determined from specific gravity readings by using the average of three readings per sample. Glass and temperature corrections were applied, and chlorinity and salinity values obtained from Knudsen's tables (Knudsen-Oxner, 1946).

Samples taken with a water sampler were placed in thrice-flushed 100 ml. glass-stoppered reagent bottles, sealed with petroleum jelly and inverted in storage. Measurements with the hydrometer were made the following day when all samples had reached room temperature. In 1954 all salinity samples were titrametrically determined by the Knudsen silver nitrate method (Knudsen-Oxner, 1946) and the values expressed in parts per thousand (‰).

Water Temperatures.—Water temperatures were recorded in both years with the aid of a −10° to +50° Centigrade (C.), partial immersion, guarded thermometer graduated in tenths of a degree. Both surface and bottom water temperatures were taken with the aid of a water sampler. Direct sunlight and exposure to cold winds were avoided during the readings.

Density.—Density of the estuarine water was obtained by converting salinity and temperature data at atmospheric pressure to *in situ* density using Knudsen's tables (Knudsen-Oxner, 1946). The results were expressed in Sigma-t Units (σ_t) obtained from density figures by moving the decimal three places to the right and dropping the initial 1: thus density 1.0260 gm./ml. = σ_t 26.0.

Dissolved Oxygen.—The standard Winkler method (Amer. Pub. Health Assoc. *et al.*, 1946, 1955) was used to determine the partial pressure of dissolved oxygen in sea water. Examination of results indicated amounts of ferrous and nitrate salts were not great enough to affect the accuracy of the method. The results were expressed in milliliters of dissolved oxygen per liter (ml./L.).

pH Measurements.—Measurements of pH were made within three hours after sampling with a Beckman Model G pH meter.

Total and Inorganic Phosphorus.—Inorganic phosphorus was determined by a modification of the Deniges colorimetric, stannous chloride method (Truog and Meyer, 1929; Amer. Pub. Health Assoc. *et al.*, 1955). The modifications were: (1) use of low-phosphate sea water for the preparation of standards to eliminate salt error and, (2) the use of a sea-going colorimeter, called the electric eye photometer (Ford, 1949). Total phosphorus was determined by a method after H. W. Harvey (1948) and the results expressed in microgram atoms of phosphorus per liter (μg-at P/L).

Nitrate and Nitrite.—Nitrite was determined according to a method first described by Ilosvay and later modified by Weston (1905). Nitrate was determined colorimetrically using a strychnine reduction method of H. W. Harvey (1948). In both instances, the results are expressed in microgram atoms of nitrogen per liter (μg-at.N/L.).

Titration Alkalinity.—The method used is described in the American Public Health Association water analysis manual (1946, 1955). Both phenolphthalein and methyl orange alkalinity were determined and the results expressed in hydrogen ion equivalents.

Illumination.—Photometric measurements using a Leitz camera photometer were made seasonally to determine the minimum and maximum transparencies which could be expected in the estuarine waters. Data kindly provided by the Epply Co. of Newport, R. I., measured with an Epply pyroheliometer, gave total radiation in Langleys or gram calories per square centimeter per day (gm.-cal./cm.^{2}/day).

Current Measurements.—Both velocities and directions of the surface and subsurface tidal currents of Great Pond were measured and the values plotted for analysis. For determining surface currents, a standard 60 cm. meteorological balloon was attached directly to a galvanized sheet iron cross. For mid-depth current estimates the cross was suspended from the balloon by a 1 meter length stainless steel wire. The balloon was inflated just enough to buoy up the cross but not enough to cause appreciable wind drag. By releasing a number of current crosses from a given line and keeping track of their positions with time, the direction and rate for each could be obtained. In addition, a line of a half dozen current crosses were released and followed to obtain an estimate of the overall ebb and flood tide circulation for interpretative purposes. One analysis was made during a period of moderate southwest prevailing wind direction and another during a period of a fresh north-northwest wind.

Water Sampler.—The sampler consisted of four 100 ml. glass-stoppered bottles strapped to a wooden platform and separated by a wooden cross. A centered, two-foot-long upright member supported a 400 ml. plastic overflow chamber stoppered at both ends. The platform was weighted with a keel of six pounds of lead. The four reagent bottles were fitted with rubber stoppers with a pair of holes in each to accommodate the plastic tubing which led from the first through the last bottle in a series and finally into an overflow cylinder. The inlet tubing extended to the bottom and the outlet tubing was inserted just into the top of each bottle. This arrangement permitted a flow of water to move in succession through each of the four bottles and, finally, to fill the overflow cylinder. Normally a thin-walled, rubber air-escape tube could be attached to the top of the overflow cylinder and brought above the surface of the water. A hose clamp could then be closed on the free end and the air-filled sample bottles stoppered and lowered in a rack to any desired level in the water column without filling from unwanted levels. Upon opening the hose clamp water pressure would force the air from the bottles, fill them with sea water and in turn fill the overflow cylinder. In shallow water or at the surface insufficient water pressure is developed to operate the apparatus. To speed up the process, a 4 meter thick-walled rubber tube was attached to the top of the overflow cylinder and terminated with a bicycle pump with inverted pump washer. This arrangement provided enough suction without creating cavitation to fill the sampler in 20 seconds at any depth.

The first bottle in the series received the greatest degree of flushing and its contents were used for oxygen determination. The second sample was used for pH and titration alkalinity, the third for phosphorus, nitrate and nitrite, and the fourth for salinities. The water in the overflow chamber was suitable for temperature measurements since flushing tended to bring the chamber to water temperature. During the 1954 survey, a weighted four liter glass pail, which could be filled at any level by pulling its stopper by an attached cord, was used to obtain water samples for all analyses except dissolved oxygen, pH, alkalinity and temperature. Samples for these were collected using the sampler described previously.

Data from Other Sources.—Precipitation, air temperatures and pressures as recorded at Nantucket Island, Massachusetts, were obtained from the U. S. Weather Bureau's climatological summaries, both national and regional.

Rochford's (1952) estuarine classification, based largely on salinity and bottom type, was used to characterize Great Pond. The zones, according to the system, are indicated in Table 1 and Figure 2. Great Pond estuary falls into Rochford's classification of systems dominated by "tidal zone" characteristics without seasonal shifts in the positions of the zones. Most of the habitats in Great Pond are exposed to marine rather than brackish influences.

TABLE 1

Hydrographic Zones in Great Pond Based Upon Differences in Salinity and Bottom Sediments

Zone	Sections	Stations	Bottom Types	Salinity ‰ Surface	Salinity ‰ Bottom
Neritic	none	1	coarse sand	28–31	30–32
Marine	I	4	coarse sand	28–31	29–31
Tidal	II, III	4A,6,6A,6B,7,7A,7B,8,8A,8B	firm sandy clayey silt	23–30	26–31
Transition	IV	9,9A,9B	soft silty sandy clay	12–30	20–31
Gradient	V, VI	10,11,12,12A,13,13A	soft silty sandy clay ooze	1–28	1–30
Fresh	VII	12E,13C	firm silty sand	<1	<1

Seasonal Histories of the Principal Benthic Marine Plants

SEASONAL PERIODICITY OF GROWTH IN GREAT POND

From a check list of 135 species or varieties of benthic marine plants observed in Great Pond, the preliminary *seasonal histories*[2] of 89 were studied, but only 70 of these were suitable for quadrat analysis. Of the 70 suitable taxa, 26 of the more common forms were measured for seasonal growth studies. In Table 2 data for presence, growth, periods of maximum growth, and dormancy are given for each species. The species prominent at any one season are listed with information concerning their distribution in various sections of the estuary.

In the yearly cycle of growth in Great Pond the largest number of species and the maximum rate of growth occurred during the spring (Fig. 3, Table 2). The maximum standing crop occurred between June and early September but was represented by fewer species. A rapid decline in cover and number of species followed in September and October. By mid-autumn the warm season vegetation had greatly diminished and was replaced by the winter vegetation beginning in early November.

---

[2] In some areas, species of benthic marine plants may give rise to either or both of the alternating generations such as the sporophyte and gametophyte. In a field study, observation is made only on those generations which are most conspicuous. The term seasonal history was suggested by Taylor to mean only that portion of the life-history that may occur in a given area. For many species only one of the two generations, usually the sporophyte, was observed during the survey. With many thallophytes, the sexual and asexual generations have different seasonal periods of occurrence (Knight and Parke, 1931).

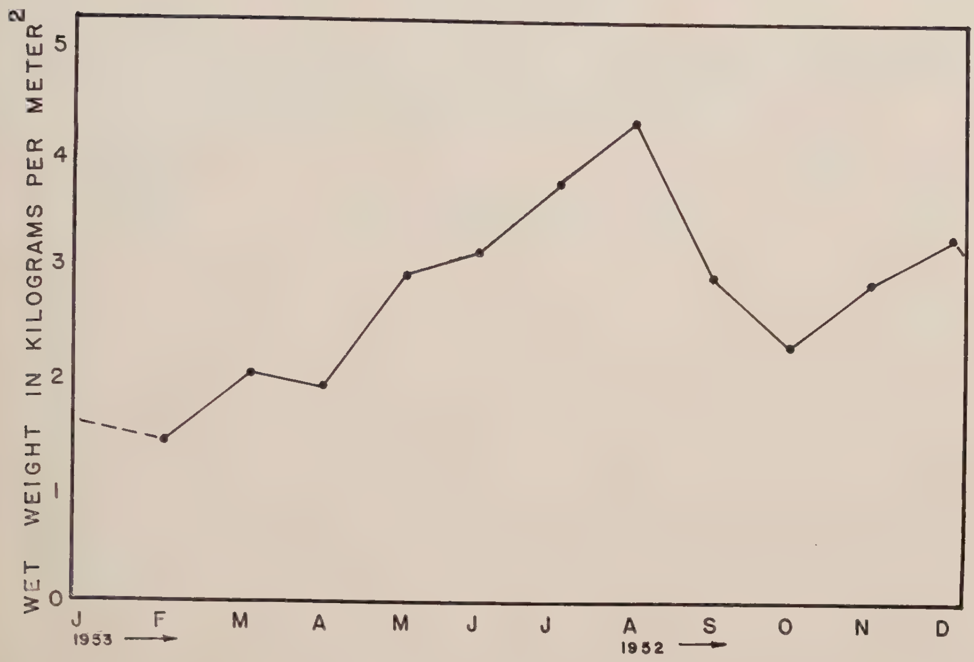

Fig. 3. Seasonal fluctuations in the total standing crop of benthic marine plants in Great Pond in 1952–53. Data are given in kilograms wet weight per square meter.

Table 2

Check List and Monthly Distribution of Benthic Plants in Great Pond, Mass. (after Taylor, 1957)
T = Trace Present; D = Dormant; G = Growth Indicated; M = Period of Maximum Standing Crop; ? = Uncertain.

	Months												Section of the Estuary which had maximum growth	Section of the Estuary which had minimum growth
	Sept.	Oct.	Nov.	Dec.	Jan.	Feb.	Mar.	Apr.	May	June	July	Aug.		
						AQUATIC PHANEROGAMS								
Ruppia maritima L.	G	D	D	D	D	D	D	G	G	G	M	G	3–5	2
Zostera marina L.	G	G	D	D	D	D	G	G	G	G	M	G	1–4	5
						XANTHOPHYTA								
Vaucheria thuretii Wor.	M	D	D	D	D	D	G	G	M	M	M	M	2–4	5
V. compacta	G	D	D	D	D	D	G	G	M	M	M	M	2–4	5
V. minuta Blum et Con.	G	D	D	D	D	D	G	G	M	M	M	M	2–4	5
V. coronata Nordst.	G	D	D	D	D	D	G	G	M	M	M	M	2–4	5
V. arcassonensis Dang.	G	D	D	D	D	D	G	G	M	M	M	M	2–4	5
V. intermedia Nordst.	G	D	D	D	D	D	G	G	M	M	M	M	2–4	5
						CHLOROPHYTA								
Ulothrix implexa Kütz.	....	....	....	....	....	....	G	G	G	....	....	....	6	....
Enteromorpha clathrata (Roth) J. Ag.	G	G	M	M	M	G	M	G	....	M	G	....	2–4	5,6
E. compressa (L.) Grev.	....	....	....	....	....	....	G	G	M	M	M	....	4,5	2,3
E. intestinalis (L.) Link	M	G	G	G	G	G	M	M	M	G	G	G	3,4	2,5
E. linza (L.) J. Ag.	M	M	G	G	G	G	M	G	M	G	M	G	1,2	3
E. plumosa Kütz.	M	G	G	M	....	....	....	G	M	G	G	G	3,4	5,6
E. torta (Mert.) Reinb.	....	....	....	....	....	....	M	G	G	M	G	G	2,3	4

TABLE 2—Continued

Check List and Monthly Distribution of Benthic Plants in Great Pond, Mass. (after Taylor, 1957) T = Trace Present; D = Dormant; G = Growth Indicated; M = Period of Maximum Standing Crop; ? = Uncertain.

	Months												Section of the Estuary which had maximum growth	Section of the Estuary which had minimum growth
	Sept.	Oct.	Nov.	Dec.	Jan.	Feb.	Mar.	Apr.	May	June	July	Aug.		
Monostroma oxyspermum (Kütz.) Doty	....	G	M	G	G	....	G	G	G	M	....	....	5,6	..
Ulva lactura L.	G	G	G	M	G	G	M	M	M	M	G	G	1–3	4,5
Ulva lactuca var. *latissima* (L.) De Cand.	M	M	G	G	G	G	G	G	M	M	M	G	4,5	2,3
Ulva lactuca var. *rigida* (C. Ag.) Le Jolis	M	M	G	G	G	G	G	G	M	M	M	G	1	..
Chaetomorpha aerea (Dillw.) Kütz.	G	G	G	G	G	G	G	M	M	M	G	G	1	..
C. linum (Müll.) Kütz.	G	G	G	G	....	....	M	M	G	G	....	....	5	3
Cladophora gracilis (Griff. ex Harv.) Kütz. F. *tenuis* Farl.	M	M	M	G	....	....	G	G	G	M	G	G	3,4	2,5,6
C. refracta (Roth) Kütz.	G	M	G	....	....	G	G	M	M	G	....	....	4–6	..
C. rudolphiana (C. Ag.) Harv.	....	....	....	....	....	....	G	G	G	G	G	G	4–6	..
Rhizoclonium riparium (Roth) Harv.	....	....	....	....	....	....	G	M	M	M	G	....	4–6	..
PHAEOPHYTA														
Ectocarpus confervoides (Roth) Le Jolis	M	M	?	?	G	G	?	G	M	?	?	...	2	4
E. siliculosus (Dillw.) Lyngb.	?	?	?	M	G	G	G	M	G	G	G	....	2	5
Giffordia mitchellae (Harv.) Hamel	G	M	M	G	?	G	G	?	M	G	?	G	1	2
Sphacelaria cirrosa (Roth) C. Ag.	M	M	G	....	....	....	G	G	M	M	G	....	1	2
Ralfsia verrucosa (Aresch.) J. Ag.	G	M	M	M	G	G	G	M	M	M	G	G	1	2
Leathesia difformis (L.) Aresch.	....	....	....	....	....	....	....	....	....	M	....	....	1	..
Acrothrix novaeangliae Taylor	....	....	....	....	....	....	....	....	M	G	....	....	2	..
Stilophora rhizoides (Ehrh.) J. Ag.	T	T	M	M	G	G	G	G	M	M	G	G	3,4	2,5
Desmarestia viridis (Müll.) Lamour.	....	....	....	....	....	....	M	M	G	G	....	....	2	1
Striaria attenuata (C. Ag.) Grev.	....	....	....	....	....	....	....	....	M	....	....	....	2	..
Petalonia fascia (Müll.) Kuntze	....	....	G	M	G	G	M	M	G	G	....	....	1	2
Punctaria latifolia Grev.	....	....	G	M	G	G	M	M	G	....	....	....	1	4
P. plantaginea (Roth) Grev.	....	....	G	G	G	G	M	M	G	G	....	....	1	..
Scytosiphon lomentaria (Lyngb.) J. Ag.	....	....	G	G	G	G	G	G	G	G	G	....	1,2	3,4
Dictyosiphon foeniculaceus var. *americanus* Coll.	....	....	....	....	....	....	M	M	M	G	....	....	2,3	4
Chorda filum (L.) Lamour.	....	....	....	....	....	....	M	M	G	....	....	....	1	2
Fucus spiralis L. (typical)	M	M	M	M	G	G	M	M	M	M	D	D	1	2,3
F. vesiculosus L.	M	M	M	M	G	G	M	M	M	M	D	D	1	2,3

TABLE 2—Continued

Check List and Monthly Distribution of Benthic Plants in Great Pond, Mass. (after Taylor, 1957)
T = Trace Present; D = Dormant; G = Growth Indicated; M = Period of
Maximum Standing Crop; ? = Uncertain.

	Months												Section of the Estuary which had maximum growth	Section of the Estuary which had minimum growth
	Sept.	Oct.	Nov.	Dec.	Jan.	Feb.	Mar.	Apr.	May	June	July	Aug.		
Sargassum filipendula C. Ag.	M	G	D	D	D	D	D	M	M	M	M	M	1	2
RHODOPHYTA														
Bangia fuscopurpurea (Dillw.) Lyngb.	....	....	....	....	G	M	M	G	....	....	....	....	1	4
Porphyra leucosticta Thur.	....	....	....	G	G	M	M	G	G	....	....	....	1	4
Nemalion multifidum (Web. et Mohr.) J. Ag.	....	....	....	T	T	T	....	....	G	M	T	....	1	..
Gelidium crinale (Turn.) Lamour.	M	G	....	....	....	....	....	....	G	M	M	M	1	..
Corallina officinalis L.	M	G	D	D	D	D	D	G	M	M	M	M	1	
Fosliella lejolisii (Rosen.) Howe	....	....	....	....	....	....	G	G	G	G	G	G	1,2	3,4
Agardhiella tenera (J. Ag.) Schm.	G	D	D	D	D	D	D	G	G	G	M	M	3,4	1,2,5
Hypnea musciformis (Wulf.) Lamour.	G	....	....	....	....	....	....	....	....	....	....	M	1	2
Gracilaria verrucosa (Huds.) Papenf.	M	M	G	G	G	G	G	M	M	M	M	M	2,3,4	1,5
Chondrus crispus (L.) Stackh.	M	G	G	D	D	D	D	G	M	M	M	M	1	
Champia parvula (C. Ag.) Harv.	G	....	....	....	....	....	....	....	M	M	M	G	1	2
Lomentaria baileyana (Harv.) Farl.	G	G	....	....	....	....	....	....	....	M	M	M	1,2,3	4,5
Callithamnion byssoides Arn.	....	....	M	G	G	G	M	G	G	G	....	....	1	2
Ceramium rubrum (Huds.) C. Ag.	M	M	M	D	D	D	M	G	G	G	G	G	1	2
C. rubrum var. *proliferum* Harv.	M	M	G	D	D	D	D	M	M	M	M	M	3	4
Griffithsia globulifera Harv.	G	G	....	....	....	....	....	....	....	....	....	G	1	2
Spyridia filamentosa (Wulf.) Harv.	M	D	D	D	D	D	G	G	G	M	M	M	2–4	1,5
Grinnellia americana (C. Ag.) Harv.	G	....	....	....	....	....	....	....	....	G	G	M	1,2	3
Dasya pedicellata (C. Ag.) C. Ag.	G	G	G	....	....	....	....	....	....	....	....	G	3	1,2
Bostrychia rivularis Harv.	....	....	....	....	....	....	....	....	....	....	M	M	4	5
Chondria baileyana (Mont.) Harv.	G	....	....	....	....	....	....	....	....	G	G	M	1,2	3
C. sedifolia Harv.	....	....	....	....	....	....	....	....	....	....	G	M	1	2
C. tenuissima (Good.)														
C· tenuissima (Good. et Woodw.) C. Ag.	....	....	....	....	....	....	....	....	....	....	G	M	1	2
Polysiphonia harveyi var. *arietina* (Bailey) Harv.	G	G	G	G	....	....	....	....	M	M	M	G	2	3–5
P. novae-angliae Taylor	G	G	G	G	G	G	G	G	M	M	G	G	1	..
P. denudata (Dillw.) Kütz.	M	D	D	D	D	D	G	G	G	G	G	M	3	4

The standing crop of winter vegetation (Fig. 3) was smaller than that of the spring and early summer. In the late spring period summer and winter vegetation elements were observed growing side by side (Figs. 4, 5, 6; Table 2). By May or June the winter populations had ceased active growth or had begun to disappear. Reproduction, however, continued until these populations disappeared in late May or June.

Thus the 1952–53 data show two distinct major sequences in the seasonal vegetation of Great Pond, a cold and a warm season group. There are two major periods of decline and decay; one in June to early August (death of the winter-spring populations) and another in late September and October (death of the summer populations). Both periods of decline represent a peak occurrence of epiphytes and animal grazers. There is also evidence for considerable bacterial activity. The end of the first period in early August is more noticeable when blades and stems of *Zostera* and *Ruppia* become detached and are driven up on the beaches by wave action. Here these plants decay and create a general nuisance to man. However, estimates show the amount of debris belonging to phanerogams in Great Pond to be less than one sixth of the total plant material present (Figs. 5, 7). Eel grass probably constitutes a much larger fraction of the plant communities on the coast where dense beds have returned since the great blight of the early thirties (Dexter, 1953).

Those species of benthic plants most common in the winter vegetation, with initial growth in November and December, included *Ectocarpus siliculosus, Petalonia fascia, Punctaria latifolia, P. plantagineae, Scytosiphon lomentaria,* and the perennial fucoids. New plants were produced sporadically all winter and spring by these species. By June

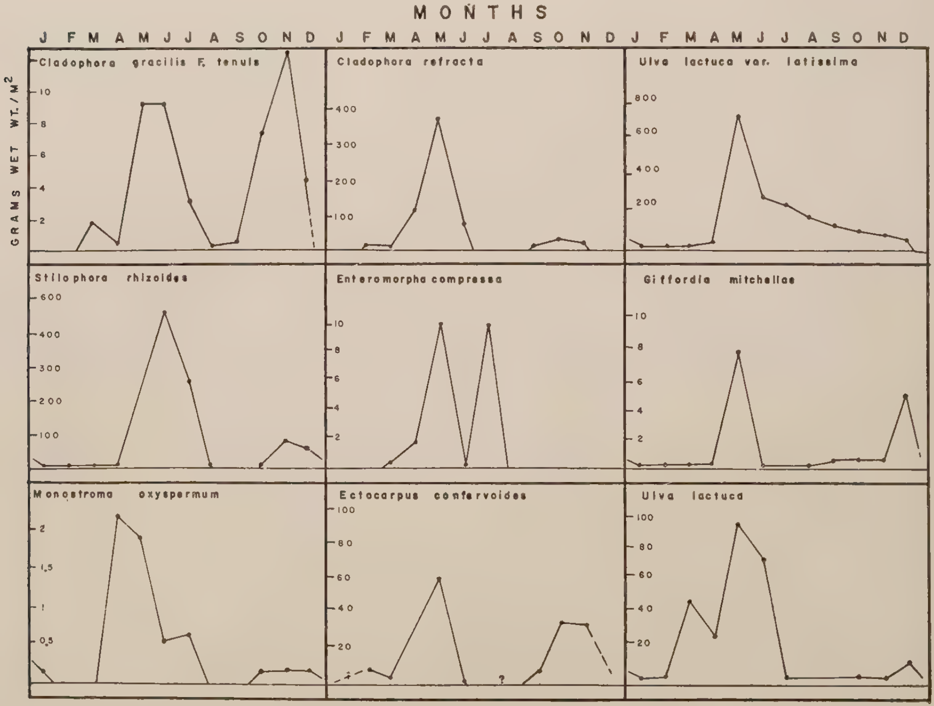

Fig. 4. Standing crops of some benthic plants dominant in the spring and fall periods in 1952–53. Data are given as grams wet weight per square meter.

growth was generally very limited and only certain dormant persistent forms carried these species through the warm summer and fall months. In midwinter, usually by January, *Bangia fuscopurpurea* and *Porphyra leucosticta* made their appearance and flourished for a few months. By May only an occasional plant remained.

The spring vegetation in Great Pond appeared in March but most of the plant species were waning or gone by May or June. The list of species included ephemeral, short-growing-season species such as *Acrothrix Novae-angliae, Chorda filum, Desmarestia viridis, Dictyosiphon foeniculaceus* var. *americanus, Stilophora rhizoides, Striaria attenuata,* and *Nemalion multifidum,* as well as various species of *Cladophora, Enteromorpha, Monostroma,* and *Ulva.* The greens usually reappeared or showed another increase in abundance in the fall period. The sea grasses, *Zostera marina* and *Ruppia maritima* showed initial growth in mid and late spring but did not reach their peak growth until summer. The summer plant populations included the sea grasses which began initial growth in late spring. The most common algae species among these were *Enteromorpha compressa, Ulva lactuca* and its two varieties, *Agardhiella tenera, Gracilaria verrucosa, Ceramium rubrum* var. *proliferum, Hypnea musciformis, Spyridia filamentosa,* and a number of species of *Dasya, Ceramium, Champia, Lomentaria* and *Polysiphonia.*

In the fall, there was a reappearance and renewed growth of some species which grew in the spring. The list includes mostly greens such as the various species of *Enteromorpha, Ulva, Cladophora,* and *Monostroma,* and the brown *Stilophora rhizoides.* Between September and November no really new additional species appeared in Great

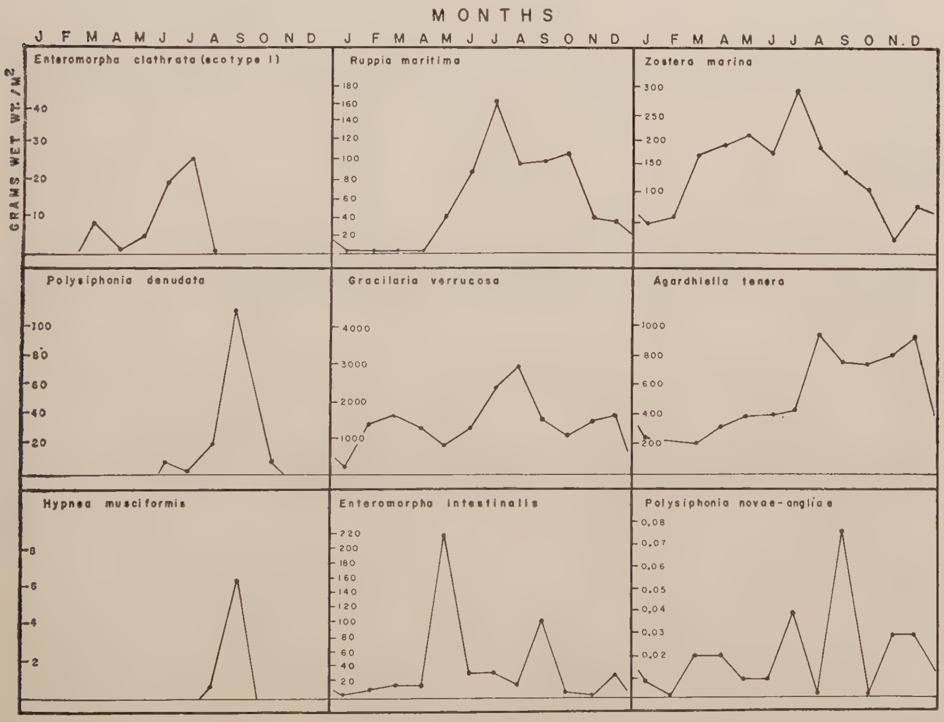

FIG. 5. Standing crops of some dominant species appearing in spring and summer, early spring through fall, and late spring through fall. Data are given in grams wet weight per square meter.

Pond. The winter plant communities generally appeared year after year, in late October along the coast and in early November in the estuaries.

For further details on the seasonal histories of benthic plants in Great Pond, see Table 2. The reader should be cautioned that these data represent measurements on the quadrats and do not include the occasional appearance in other parts of the estuary of other species. These seasonal histories are considered to be characteristic of an estuary rather than the open coastline.

COMPARISON OF SEASONAL GROWTH IN GREAT POND WITH GROWTH REGIMES IN OTHER LATITUDES

Great Pond, at Latitude 41° N., as indicated in this study, has two major groups of plants each with growth at different seasons. Polar and tropical seas each have one dominant group with one growing season. Seas of intermediate latitudes are believed to be populated by more or less mixtures of warm and cold climate species. A brief review of studies concerning seasonal growth of marine plant communities from polar seas to the tropics shows the intermediate nature of southern New England plant communities.

In the Arctic, above Latitude 60° N., visual estimates of benthic marine plant growth suggest that there is only one seasonal growth period. Apparently growth only occurs during the short summer interval. Yet, reproduction may occur at other times of the year in some species. A review of these studies may be found in Fritsch (1945).

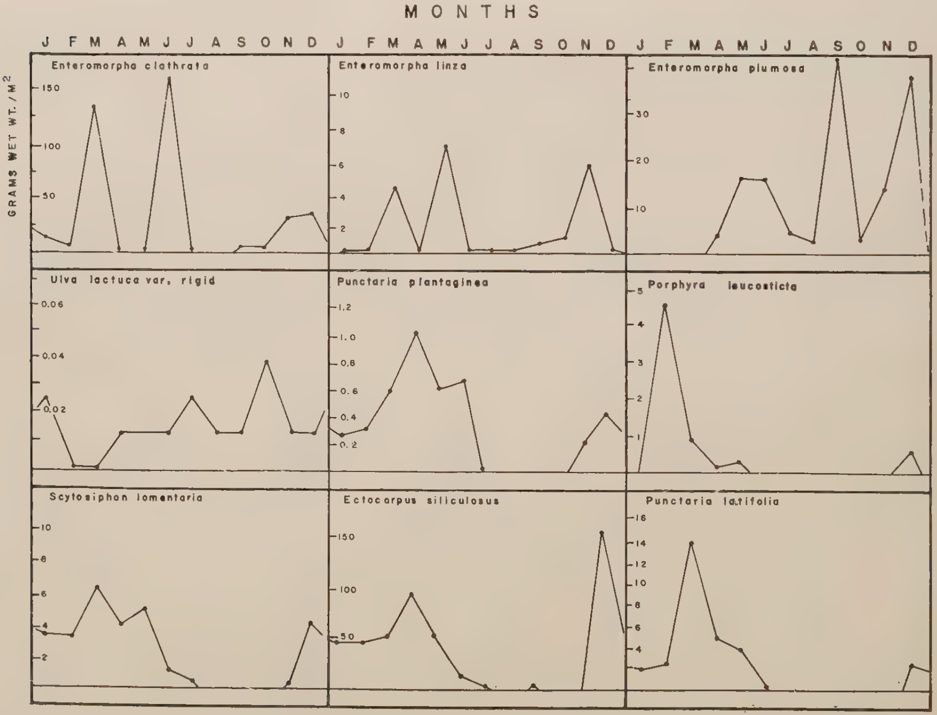

FIG. 6. Standing crops of some benthic plants seasonally dominant in the fall and winter period in 1952–53. Data are given in grams wet weight per square meter.

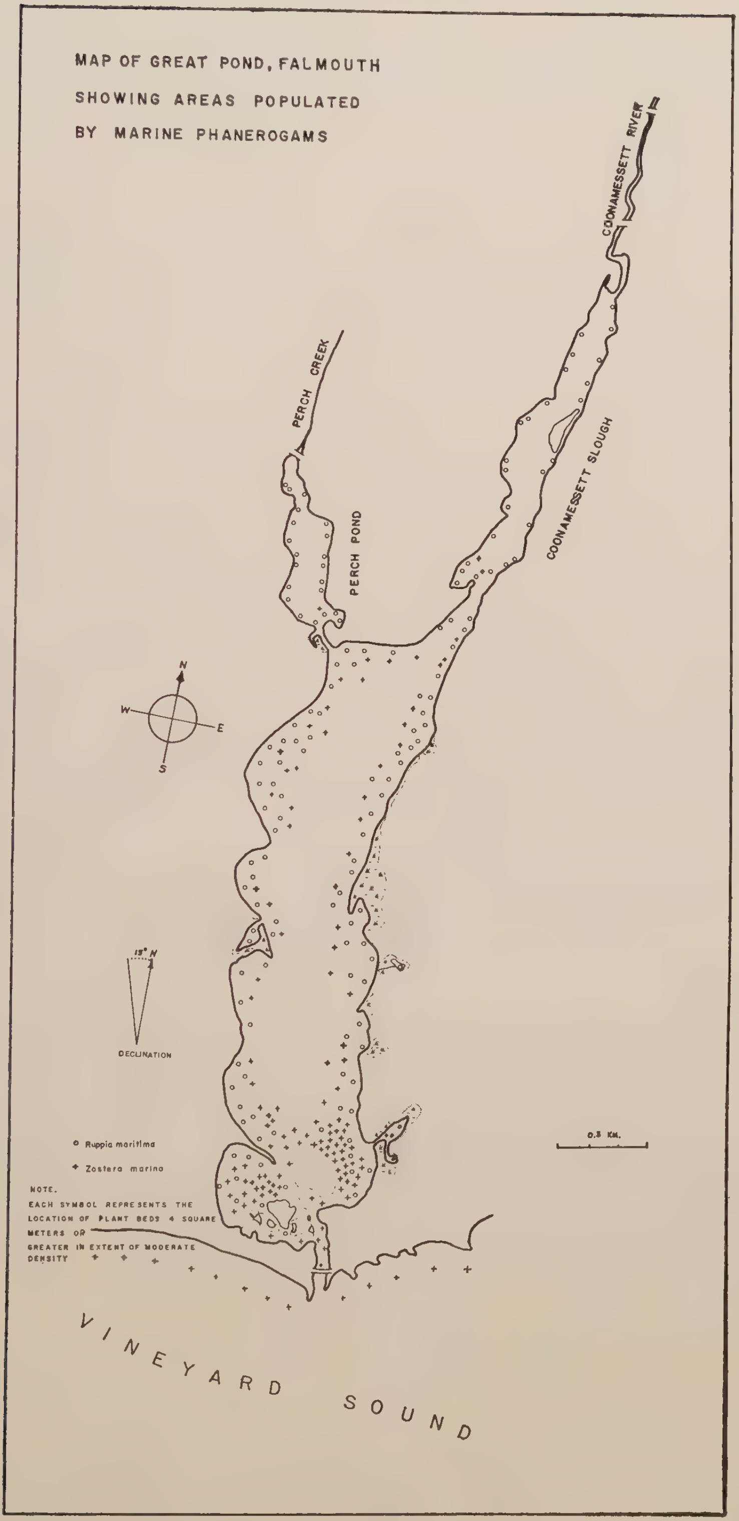
MAP OF GREAT POND, FALMOUTH
SHOWING AREAS POPULATED
BY MARINE PHANEROGAMS
COONAMESSETT RIVER
PERCH CREEK
PERCH POND
COONAMESSETT SLOUGH
N
W
E
S
15° N
DECLINATION
0.5 KM.
○ Ruppia maritima
+ Zostera marina
NOTE.
EACH SYMBOL REPRESENTS THE
LOCATION OF PLANT BEDS 4 SQUARE
METERS OR
GREATER IN EXTENT OF MODERATE
DENSITY
VINEYARD SOUND

Fig. 7. Map of Great Pond, Falmouth, Mass., showing areas populated by marine phanerogams.

In boreal waters, MacFarlane (1952) reported a predominance of spring growth for the important commercial kelps and in Irish moss along the coast of Nova Scotia. These quantitative data are for open coastal water rather than protected or estuarine situations. Bell (1927) and Bell and MacFarlane (1933) provided visual estimates of a less prominent summer-growth group. No information appears to be available on winter growth for the area.

Bermuda, at Latitude 32° N., has really only one major seasonal growth group and possibly two minor ones (Bernatowicz, 1950, 1952a, 1952b). Only three winter species, *Callithamnion corymbosum*, *Scytosiphon lomentaria*, and *Sphacelaria tribuloides*, grow in those waters. Six annuals with short growth seasons appear in the spring but the bulk of the vegetation persists the year around. The maximum growth period for most species is in May and June. Bernatowicz's data are for quiet, protected habitats and hence may be readily compared with the Great Pond data. Results of studies in the Mediterranean by Feldmann (1937) and Funk (1927, 1954) suggest a similar seasonal growth aspect to that reported from Bermuda.

According to an early report by Svedelius (1906) the tropics may have only one major seasonal growth period. Presumably growth is maximum in winter and early spring at Ceylon.

Local Distribution in the Estuary

Standing crop totals for the commonest species (Figs. 4, 5, 6, 7; Table 2) clearly indicated that in Great Pond the bottom of the entire major basin (transects 6 through 9, sections II-IV, Fig. 2) supported the largest accumulation of benthic marine plants. In comparison, the intertidal areas of both basin and riprap supported a relatively negligible amount. The "gradient" zone was scantly populated by attached plants which occurred on the few sandy shoals and on the embankments of the sloughs. Some species populations showed a seasonal change not only in growth but in their local distribution within the estuary. In the cooler months these species tended to populate more brackish water in the upper basin and in the sloughs. Other species showed no such change in distribution.

One example, *Stilophora rhizoides* (Fig. 8) was typical of species with changing distributions, whereas others such as *Petalonia fascia* showed no such change. *Stilophora rhizoides*, an annual (Fritsch, 1945), was found somewhere in the estuary, at least as an occasional plant, during all seasons of the year. There were two seasonal periods of marked abundance alternating with periods of scarcity. In November and December of 1952, the populations of this species occupied an area in the middle and upper portions of the major basin (sections III and IV, Figs. 2, 8). A few plants were found just inside the entrance to Perch Pond Slough (transect 13, section V, Fig. 2). By February, no plants were found in any of the quadrats and only an occasional one was found elsewhere in the estuary.

In April a significant reappearance of *Stilophora rhizoides* occurred just inside the mouth of the Coonamesset Slough (section V, transect 10, Figs. 2, 8). During May, the species became conspicuous over the central and upper portions of the major basin (sections III and IV, transects 7–9).

In June the population in the upper end of the basin was noticeably diminished (section IV, Figs. 2,8). In contrast an increase in abundance occurred at the seaward end of the estuary (sections II and III, including transects 6 and 7). By July the plants

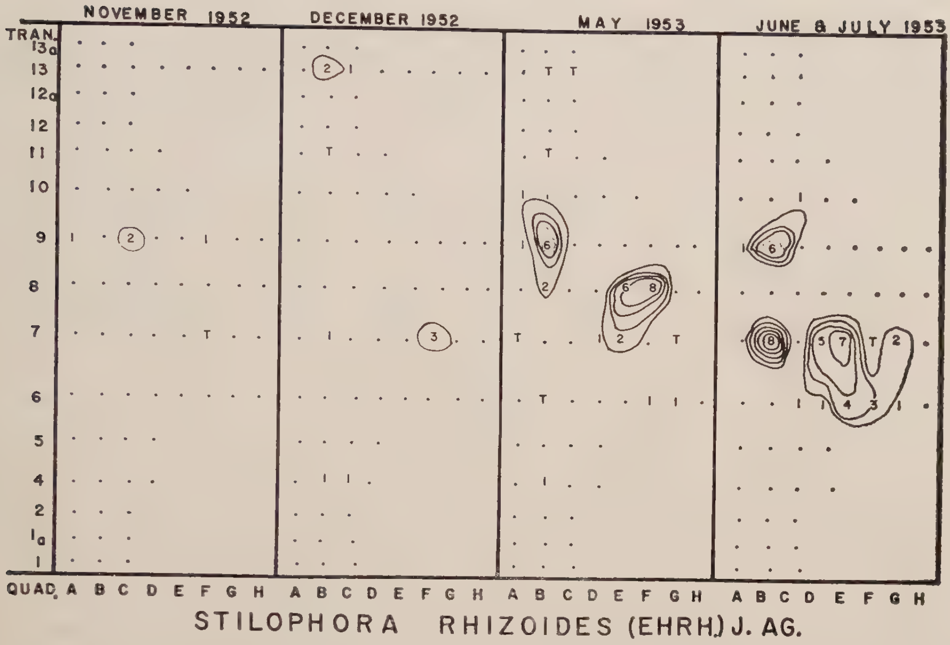

Fig. 8. Seasonal distribution and percent cover of *Stilophora rhizoides* in Great Pond in 1952–53. The graph shows transects 1 through 13 including transects in both sloughs. T indicates a trace. A dot indicates absence of plants. A number indicates the percentage cover of plants where 1=10 percent. Relative length of each transect is suggested by the length of each line of quadrats. Each dot on the riprap transects 1, 1A, and 2 represents four 25-centimeter-square quadrats. The number of quadrats is the sum of dots and numbers.

Species population isopleths indicate the plant's density in the estuary at four selected periods of the year. Isopleths are drawn at intervals: 15%, 30%, 45%, 60%, 75%, and 90%.

found at the upper end of the major basin in section IV were scarce, dying and heavily epiphytized. A fair abundance of somewhat healthier plants was found toward the lower end of the basin (section II, transect 6, Fig. 2). During August and September individual plants were rarely seen in the estuary and none within the measured quadrats. The few occasional plants found in late summer were in fairly saline habitats near the mouth of the estuary (section II, transect 6, Fig. 2). A similar history was found for *Gracilaria verrucosa* as shown in Figure 9.

Changes from One Year to the Next in Species Composition and Abundance

Since the present quantitative vegetation survey was begun in July of 1952 and terminated in August 1953, direct comparisons between 1952 and 1953 were possible for the months of June, July and August. Spot checks on some quadrats were made in 1954 and some cursory inspections at several seasons conducted in 1955 and 1956. Some species were either missing or had altered their positions in the economy of the estuary. Conspicuous by its absence was *Punctaria plantaginea* in the winters of 1954 and 1955. Not even an occasional plant appeared in or near the entrance of Great Pond. The species *Punctaria latifolia* was not nearly as abundant in 1954 and 1955 as the previous winter, 1952–53. Some *Zostera marina* beds failed to produce leaves in 1954–55 becoming less abundant. The sea grass, *Ruppia maritima,* showed a distinct increase in

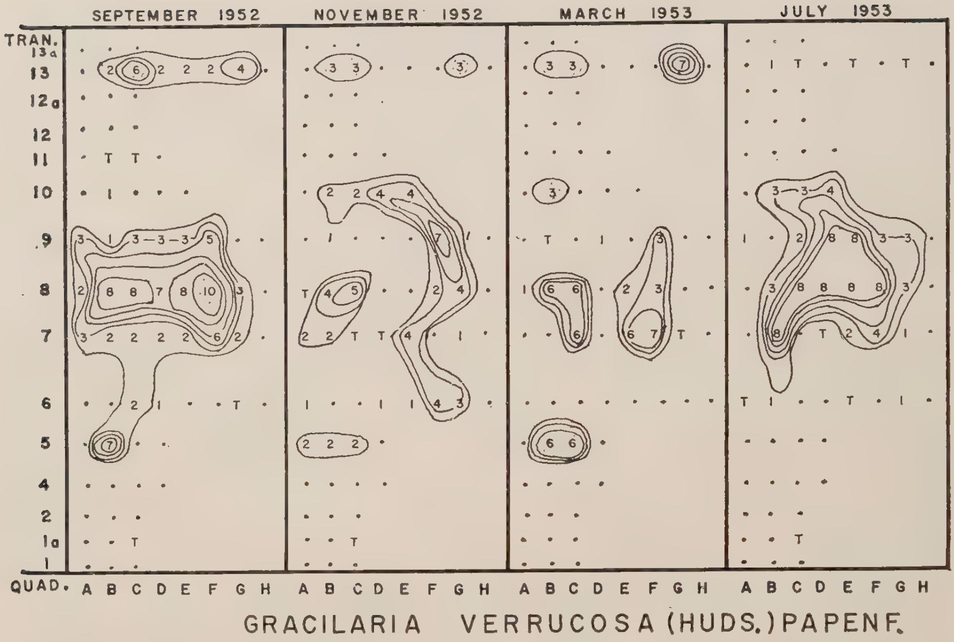

Fig. 9. Seasonal distribution and percentage cover of *Gracilaria verrucosa* in Great Pond in 1952–53. Isopleth interval is 15 percent. Legend is the same as for Figure 8.

1954–55 especially in areas occupied largely by Zostera in 1952–53. The species accumulating the largest biomass in Great Pond was *Gracilaria verrucosa.* This form was abundant in 1952, less abundant in 1953 and was further reduced in 1955. The alga, *Gelidium crinale,* absent for several years from the Woods Hole-Falmouth area, according to Taylor (personal communication), had appeared as a conspicuous but narrow intertidal zone 3 cm. wide on the jetty. By the winter and spring of 1955, very little of this population remained. In 1956, *Gelidium* seemed to be reclaiming ground lost in 1955 but diminished after the more severe winter of 1957. The species *Bostrychia rivularis* was first observed in July 1952. By the summer of 1956 no plants could be found anywhere in the estuary.

Overseason Persistence of Summer and Winter Species

An opportunity to study the winter persistence of some species was afforded during the seasonal growth survey. Branched basal portions of the previous season's thalli of *Gracilaria verrucosa,* which had persisted through the winter months, were observed to regenerate new, branched systems the following spring. During the winter period no intact, branched, basal portions of this species were observed along the exposed coast where holdfasts are commonly found. Dormant, branched portions of thalli may only occur in quiet, protected waters such as Great Pond.

In *Agardhiella tenera,* branched portions of the thallus likewise persisted over winter and in late spring produced new growth. In addition, small germlings of *Agardhiella* were found in late spring at the same time that regeneration was detected in the branched thalli of the previous growing season. The juvenile plants were seen only outside the estuary on pebbles and shells in the shoal water of Vineyard Sound. Apparently

Agardhiella over-winters as holdfast discs in coastal water and vegetatively in south shore tidal estuaries.

Solitary plants of *Nemalion multifidum*, an early summer annual, were observed in mid-winter attached to boulders below the intertidal zone. In contrast the early summer habitat was in the upper intertidal zone. Maximum luxuriance of this species occurred in late June. Unattached, branched portions of *Hypnea musciformis* were found in May apparently dormant, but viable, suggesting that these may regenerate after the winter. Some individuals of *Ceramium rubrum* passed the winter months mature, full-grown, and actively reproducing. The size and number of individuals were usually reduced suggesting very limited vegetative growth.

SEASONAL PERIODICITY IN REPRODUCTION

Some observations of a general nature were made on the occurrence of reproduction in the seasonal histories of some species of benthic plants. Generally, conspicuous reproductive structures such as those developed in the Rhodophyta and Phaeophyta are present throughout the period of maximum luxuriance and continue into the waning phase. In *Polysiphonia novae-angliae*, *P. denudata*, *Champia pravula* and *Agardhiella tenera*, both the gametophyte and the sporophyte were present during the season of active growth. An increase in population usually was paralleled by an increase in the number of individuals bearing reproductive structures. A correlation between growth and reproduction for some species was also found in Bermuda by Bernatowicz (1952a). Smith (1947) found a correlation between spring tides and sporulation in *Ulva lactuca*. Evidence for similar periodic sporulation was obtained in Great Pond. Measurements were made on juvenile plant populations of *Ceramium rubrum*, *Petalonia fascia*, *Sargassum filipendula* and *Scytosiphon lomentaria*. In the study of *Scytosiphon*, for example, the juvenile plants were measured on four 25-centimeter-square plots on different, closely associated, rock surfaces at about the same intertidal exposure. The plants were very uniform in height. Within each plot less than one third of the height measurements exceeded the standard error for all plots. This evidence suggests that nearly all plants in each plot germinated at about the same time. Over a period of 20 days, the mean height of juvenile plants in each plot increased uniformly as shown in Table 3. Older plants in all plots were significantly taller than the juveniles. Possibly the sexually mature plants in the population had responded to some rhythmic factor in the environment.

TABLE 3

The Mean Height of Juvenile Plants of *Scytosiphon Lomentaria* in Four Plots on a Jetty at Falmouth, Mass.
(Height in centimeters)

	Plot number			
	1	2	3	4
March 3	2.8	2.3	1.9	2.0
March 8	3.4	3.5	3.3	3.4
March 14	5.2	5.7	5.1	5.3
March 21	8.1	8.4	8.0	8.2

The study of the seasonal growth of benthic marine plants in Great Pond has provided measurements of a series of biological events. These events may be characteristic of other quiet water lagoons or estuaries in southern New England. The environmental factors causally related to these growth events are considered in the following chapter.

Effects of Environmental Factors on the Seasonal Growth of Benthic Plants

Those environmental influences which normally occur year after year may be separated from those which occur intermittently, irregularly, or rarely. Some of the regular influences found to be important are insolation, air and water temperatures, chemical properties of the water mass, tidal movements, the run-off waters from fresh-water streams, and the seasonal weather patterns of the region.

The irregular types of environmental influence include insolation in prolonged periods of clear skies, severe low temperatures, icing, unusual numbers of severe frontal storms, tropical hurricanes, prolonged emersion and immersion due to offshore or onshore winds, pollution by man, wholesale wasting diseases due to plant parasites (Dexter, 1953, Taylor, 1933) and unusually heavy grazing by a large year-class of some herbivorous animal (Lodge, 1948; Odum, 1953). During the course of the present survey, an evaluation of both regular and irregular factors was made.

Light, Temperature, and Seasonal Growth

The separate effects of light and temperature on plant growth may be provisionally separated in a field study since the annual temperature and light curves (Figs. 10, 11) show minima, maxima, rises and falls at different times. It is fully appreciated that interpretations of results are limited due to the many interacting variables on growth. These results reported here are thus tentative. Further experimental studies are needed to confirm the suggested relationships.

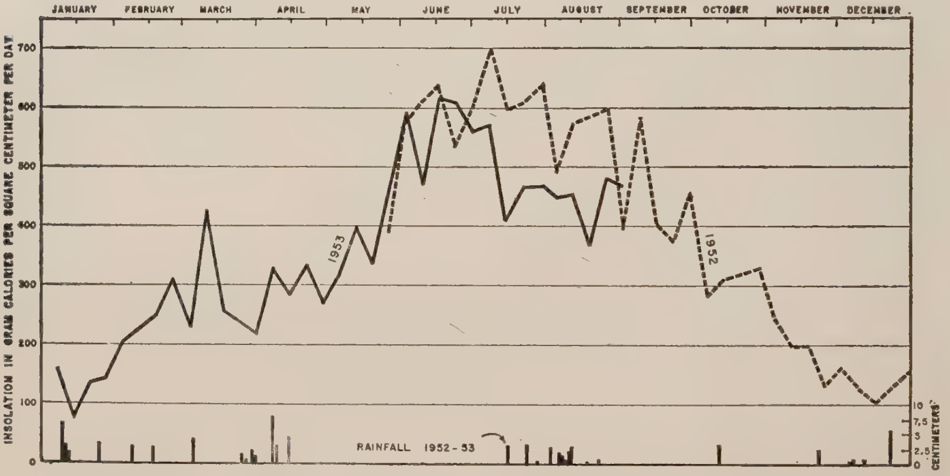

FIG. 10. Weekly average of total solar radiation at Newport, Rhode Island, 1952–53. The bar graph at the bottom of the figure indicates rainfall in centimeters.

Overall benthic plant production in Great Pond during 1952–53 indicates that the largest standing crop developed between June and September with the maximum in August (Fig. 3). The minimum plant biomass occurred in January and February. These maxima and minima are associated with the maxima and minima in temperature and insolation (Figs. 10, 11) suggesting that these two factors play the leading role in the seasonal growth of benthic plants in Great Pond.

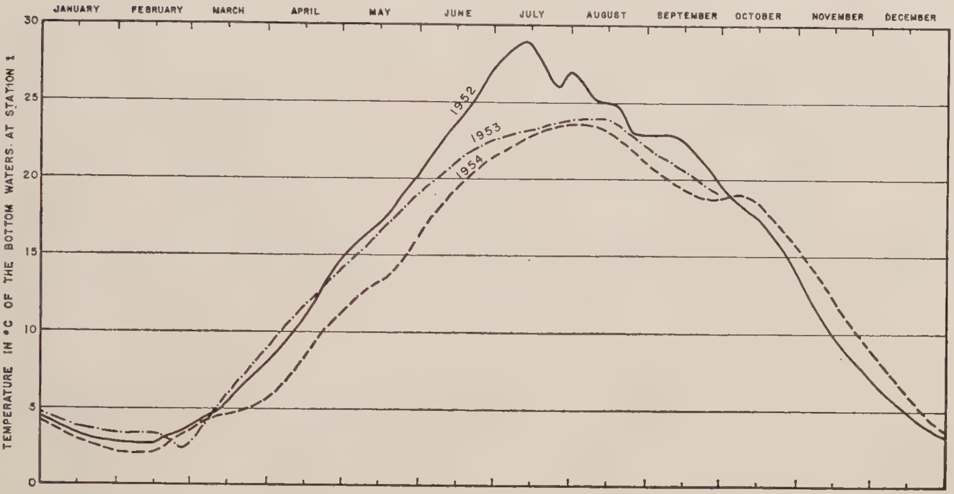

FIG. 11. Seasonal changes in the bottom water temperature in 1952–53 in the "neritic" zone (Figure 2) adjacent to Great Pond.

Late winter and early spring species including some short-growing-season ephemerals, (Fig. 6, Tables 2, 4) attained maximum population density in April and May and showed a marked reduction by June. Presumably these plants were adjusted for optimum net phytosynthesis at low temperatures and illumination. Plant species with maximum growth in the spring period were of two types. One showed irregular growth (see section on nutrients) through the season, i.e., *Enteromorpha compressa* (Fig. 4), while the other maintained a steady increase in growth, i.e. *Stilophora rhizoides* (Fig. 4). The latter type, growing in late spring (Table 5), is believed to be more dependent on light than temperature. Temperature effects are undoubtedly present. A more rapid weekly increase in light as compared with temperature supports this opinion (See Figs. 10, 11; compare the slopes of curves for April-June).

A different group of species attained maximum growth rates during June and early July (Fig. 5, Table 6) during the peak illumination period (Fig. 10). Other plants (Fig. 5, Table 7) grew best during the temperature maximum (Fig. 11) in August. These data suggest one group of species may be adapted for optimum net photosynthesis at maximal light and submaximal temperature while the latter group is adapted to maximal

TABLE 4

Standing Crops of Some Dominant Benthic Plants Occurring in Late Winter and Spring, 1952–53 (in Grams Wet Weight per Square Meter)

Species	March	April	May	June
Cladophora refracta	1.4	132.0	346.0	84.2
Enteromorpha clathrata	134.8	0.1	+	161.0
Enteromorpha intestinalis	17.9	12.9	228.0	30.8
Enteromorpha linza	4.3	0.0	6.9	0.0
Monostroma oxyspermum	0.0	2.2	1.9	0.5
Ectocarpus confervoides	6.4	?	62.0	2.4
Giffordia mitchellae	0.0	?	7.5	0.1
Ectocarpus siliculosus	49.5	93.9	49.5	8.9
Punctaria latifolia	14.0	5.4	3.9	0.1
Scytosiphon lomentaria	6.4	3.7	4.9	0.5
Ulva lactuca	48.2	22.6	98.7	77.2

temperature and submaximal light for this latitude. It should be pointed out that the few species listed in Table 6 are responsible for the largest fraction of the plant cover for the mid-summer period.

A small group of species, including plants with warm climate affinities, grew in Great Pond over September and into early October of 1952 (Tables 2, 8). The influence of light may have dominated other factors in its effect on growth. The fall off in light intensity was rather rapid in September and October (Fig. 10), but bottom water temperatures tended to fall more slowly (Fig. 11). There was a general reduction in standing crop of most species in the estuary in October (Figs. 3, 4, 5; Tables 2, 8) possibly associated,

TABLE 5

Standing Crops of Some Dominant Benthic Plants Occurring in the Late Spring Period, 1953
(in Grams Wet Weight per Square Meter)

Species	April	May	June	July	August
Cladophora gracilis f. *tenuis*	5.7	98.5	98.0	30.3	0.2
Enteromorpha intestinalis	12.9	228.0	30.8	33.2	13.1
Enteromorpha linza	0.0	6.9	0.0	0.0	0.0
Enteromorpha plumosa	3.8	16.7	16.3	4.6	3.0
Stilophora rhizoides	12.8	222.0	398.0	253.0	0.6
Ulva lactuca var. *latissima*	13.7	652.0	274.0	191.4	44.3

TABLE 6

Standing Crops of Some Dominant Benthic Plants Occurring in the Mid-Summer Period, 1952–53
(in Grams Wet Weight per Square Meter)

Species	April	May	June	July	August	September
Agardhiella tenera	350.0	124.0	406.0	464.0	989.0	785.0
Enteromorpha compressa	1.9	10.2	0.6	9.9	0.0	0.0
Gracilaria verrucosa	1,262.0	733.0	1,310.0	2,310.0	2,980.0	1,452.0
Ruppia maritima	+	35.4	34.0	161.0	96.9	98.5
Zostera marina	+	208.0	170.0	293.0	188.0	136.0

TABLE 7

Standing Crops of Some Dominant Benthic Plants Occurring in the Late-Summer Period, 1952–53
(in Grams Wet Weight per Square Meter)

Species	June	July	August	September	October
Enteromorpha intestinalis	30.80	33.20	13.10	107.00	6.74
Enteromorpha plumosa	16.30	4.57	3.02	47.30	2.38
Hypnea musciformis	0.00	0.00	0.35	6.91	0.00
Polysiphonia denudata	6.95	3.35	60.00	118.00	1.60
Polysiphonia novae-angliae	0.01	0.00	0.001	0.10	0.001

TABLE 8

Standing Crops of Some Dominant Benthic Plants Occurring in the Autumn Period
(in Grams Wet Weight per Square Meter)

Species	August	September	October	November	December
Cladophora gracilis f. *tenuis*	0.2	0.6	77.7	134.5	0.0
Cladophora refracta	0.0	22.7	41.1	29.3	0.0
Ectocarpus confervoides	?	9.3	30.6	29.7	?
Ulva lactuca	0.6	0.6	1.9	1.4	11.2
Monostroma oxyspermum	0.0	0.0	0.1	0.1	0.1

in part, with the decrease in light intensity. During the last two weeks of October bottom water temperatures dropped below 18° as the rate of cooling increased. Decreases in both temperature and light at this time may have accelerated the degradation of warm season plant populations.

A few plants, which grew in the spring, including *Cladophora gracilis* F. *tenuis*, *C. refracta*, *Enteromorpha clathrata*, *E. intestinalis*, *E. plumosa* and *Monostroma oxyspermum* (Figs. 4. 6; Tables 5. 8) showed renewed growth in the fall. Light intensities were similar in spring and fall during the periods of growth. Yet, water temperatures were several degrees higher in the fall for the same light intensity. Does this mean that light was the determining factor? Phytoproduction was much lower in the fall for these species populations. There is a possible explanation. In the spring light and temperature as well as photosynthesis and respiration were increasing. In the fall solar radiation and metabolism were decreasing.

In November, the species shown in Table 9 appeared to be dominant and by December had carpeted the estuary. Many of these cold season annuals had appeared along the open coast a week or two earlier. The difference in time of initial growth between estuary and coastal communities in 1952 may possibly be explained on the basis of the presence of higher temperatures (Fig. 12) within the estuary than along the coastal areas. By early November temperatures in both protected and exposed communities were below 18° C. The light intensity associated with early November (Fig. 10), the time of initial growth of these winter plant communities, was the same as that in March and April. Water temperatures in the spring period, however, were 5° C. lower (Fig. 11). Maximum growth was exhibited by these species in March and April (Fig. 6, Tables 2, 4). These data seem to indicate that the rôle of light was possibly more critical as related to growth than water temperature.

TABLE 9

Standing Crops of Some Dominant Benthic Plants Occurring in the Winter Period
(in Grams Wet Weight per Square Meter)

Species	November	December	January	February	March	April
Ectocarpus siliculosus	?	152.000	44.600	42.600	49.500	93.900
Punctaria latifolia	?	2.460	1.800	2.480	14.000	5.450
Punctaria plantaginea	0.184	0.390	0.265	0.265	0.604	1.050
Scytosiphon lomentaria	0.145	4.000	3.040	2.940	6.440	3.680

The only species which grew best during the winter temperature minimum in January and February of 1953, were *Bangia fuscopurpurea* and *Porphyra leucosticta* (Table 2). These plants grow well at or near freezing temperatures. The plants appeared while illumination increased from the winter minimum of less than 100 gm. cal./cm.^{2}/day on January 10th, 1953, to 300 gm. cal./cm.^{2}/day by mid February. Here is another example in which light intensity may have been more important than water temperatures. Many of the winter species present in Great Pond grow in summer in polar and boreal seas (See review by Fritsch, 1945). It is suggested from the above results that a study of boreal and polar benthic plant growth with respect to light and temperature may show the critical rôle of illumination at high latitudes.

NITRATE, PHOSPHATE AND SEASONAL GROWTH

From physiological studies (Gessner, 1955) it is known that the amounts of nitrate and phosphate available can regulate plant growth during periods of nutrient scarcity.

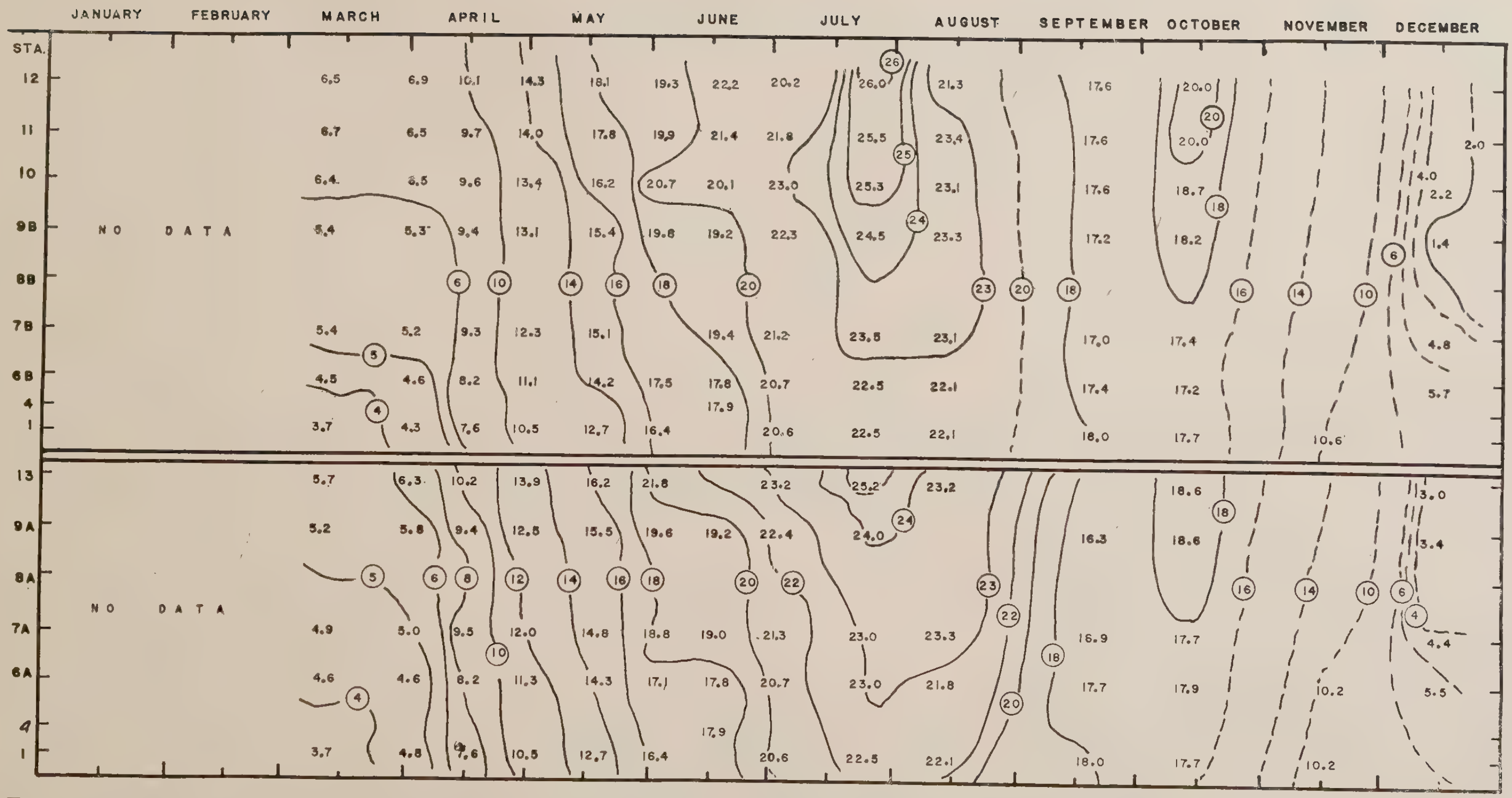

Fig. 12. Temperature in the bottom water of Great Pond, Falmouth in 1954 in degrees centigrade (C°).

In this and all subsequent frequency polygon projections of Great Pond data, two graphs are shown separated by a double line. The lower graph represents a section along the western side of the estuary including station 1 in Vineyard Sound and station 13 in Perch Pond Slough. The upper graph represents a section on the eastern side of the estuarine basin also including station 1 in the sound as well as stations 10 through 12 in the Coonamessett Slough. The two graphs provide a means of comparing the more swiftly moving tidal water of the eastern half of the basin with the more sluggish water of the western half.

Multicellular plants store large concentrations of nutrients in their extensive tissues (Vinogradov, 1953). In estuarine communities the available nutrients are in part supplied by regeneration from dead plants.

Evidence that nitrogen and phosphorus may limit growth in Cape estuaries is provided by a fertilization experiment (Pratt, 1950) conducted in Megansett estuary. Enriched fertilizer was dumped into the small embayment. Large excesses of nitrogen and phosphorus yielded blooms of phytoplankton, and masses of benthic plant growth fouled the shallow basin. Great Pond is like Megansett estuary with a similar geologic history.

In Great Pond there are low concentrations of nitrate (NO^3-N) and inorganic phosphate (PO^4-P) during the spring and fall periods (Fig. 13). One period of maximum nutrient salt regeneration *in situ* within the estuary occurs in August, and minor ones occur in late fall and in the spring (Fig. 13). The spread and reduction in abundance of many benthic plant species seems to follow changes of phosphorus in spring and nitrogen in the fall.

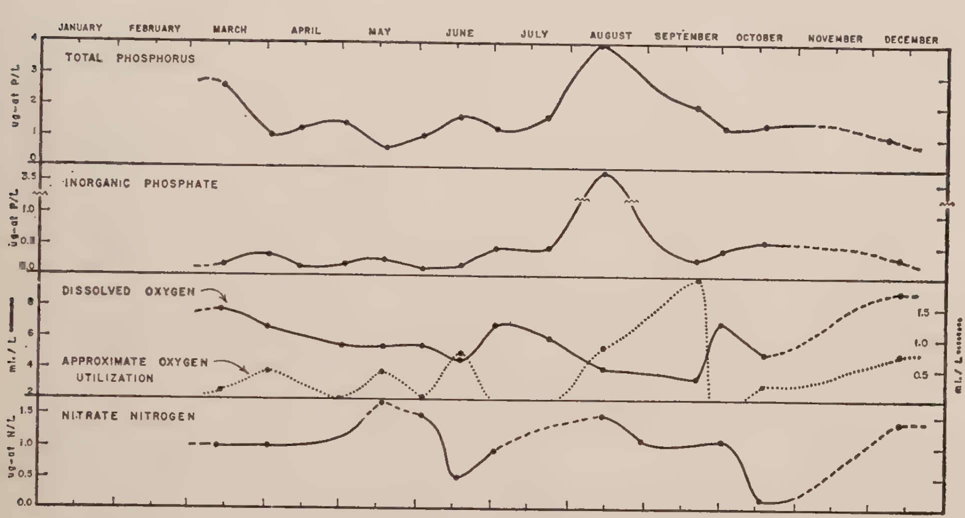

FIG. 13. Seasonal changes in total phosphorus, inorganic phosphate phosphorus, nitrate and dissolved oxygen in the bottom water of the "transition" zone (Figure 2) of Great Pond in 1954.

Data for the seasonal fluctuations in the nitrogen cycle in Great Pond (Fig. 13, 14, 15, 16) furnish some evidence that nitrate may have been low enough in the bottom water to affect the growth of benthic plants in October. Measurements of nitrogen in October indicate that less than 0.4 μg-at. N/L were present in those sections (II–IV, Fig. 2; Table 2) of Great Pond where phytoproduction was high in other seasons. Concentrations of nitrogen and phosphorus were considered low when amounts were near or at limiting levels for unicellular algae under laboratory conditions (Ketchum 1939). During October a number of species, many of them dominants, exhibited drastic reductions in standing crops (Figs. 3, 4, 5; Tables 2, 8). Many plants terminated growth. The possibility that light and temperature play an important rôle here was discussed earlier. No new additions to the benthic vegetation were observed in October. Only two species *Cladophora gracilis* f. *tenuis* and *Ulva lactuca* var. *rigida* increased in standing crop. There was a delay in the appearance of winter species within the estuary (Fig. 6,

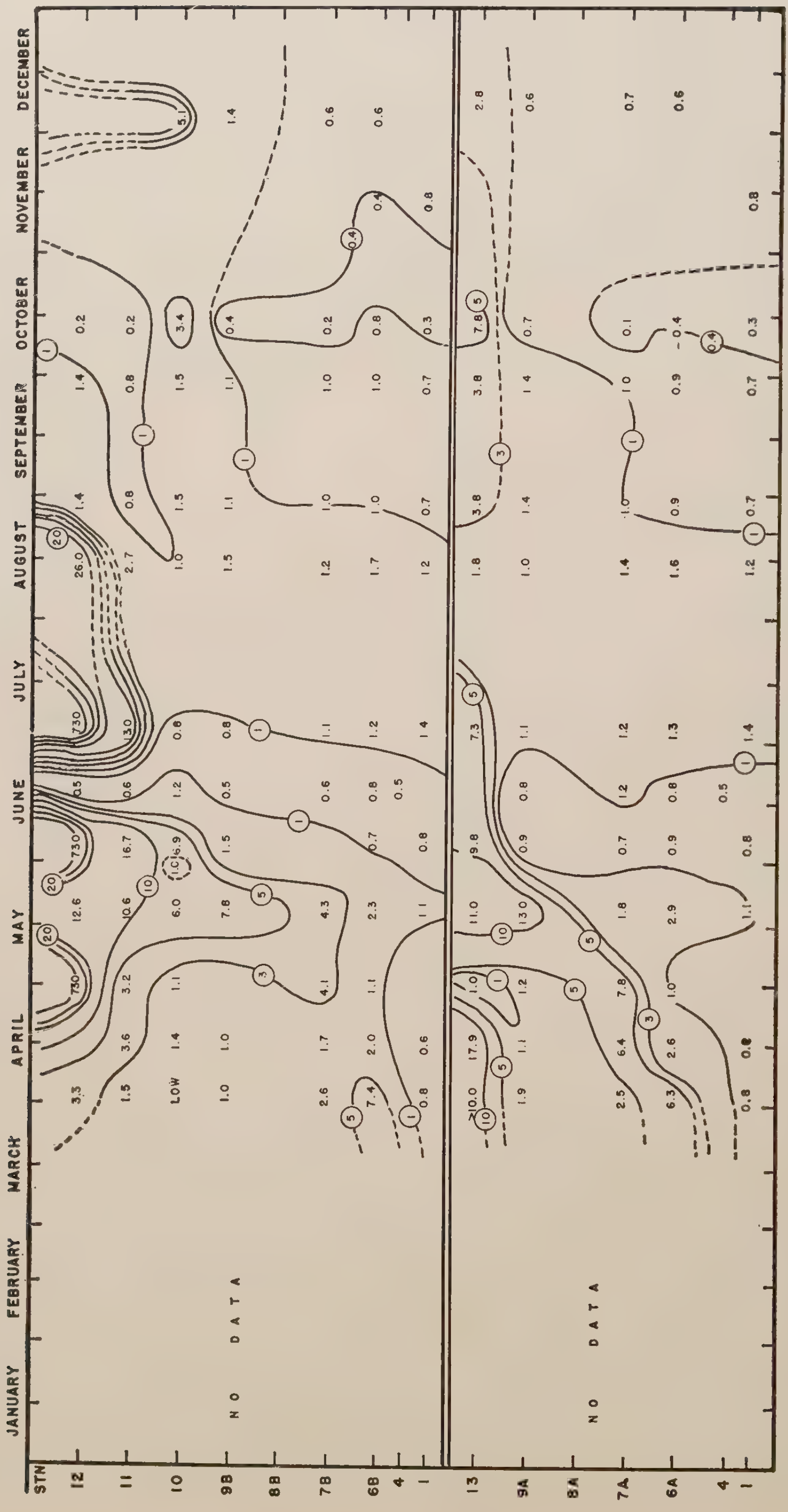

FIG. 14. The seasonal changes in nitrate in the bottom water of Great Pond in 1954, expressed in microgram atoms N/L. The two graphs shown are frequency polygons, described in detail in the legend for Figure 12.

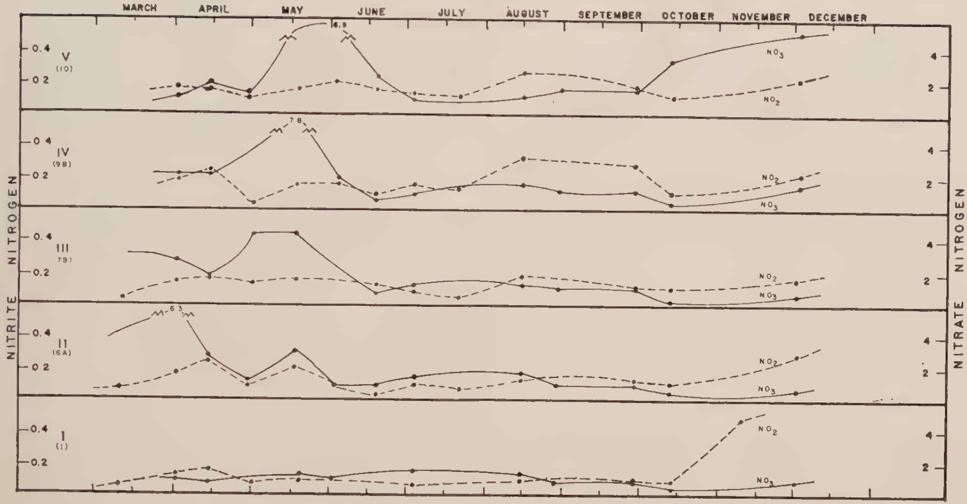

FIG. 15. Seasonal distribution of nitrite (NO_2) and nitrate (NO_3) in the bottom water of Great Pond by hydrographic sections (Figure 2) in 1954, expressed in microgram atoms N/L.

Table 4) mentioned earlier. All these responses may have been related to a nitrogen deficiency.

The seasonal changes in the phosphorus content for Great Pond are given in Figures 13, 17, 18, 19. The relatively low concentrations in spring and fall with possible limiting amounts of phosphorus in April and June suggest phosphorus as well as nitrogen may have limited growth in Great Pond.

Phosphorus concentrations are charted in Figures 17, 18, and 19. Diminished growth of benthic vegetation may be observed in Figures 4, 5, 6; Tables 4, 5. Species present in the spring first appeared in March, sustained diminished growth rates in April, but increased again in May. In April PO^4-P levels were less than 0.3 μg-at. P/L in the bottom water of the usually productive sections of the estuary (Fig. 2, sections II–IV). Another period of reduced standing crops for many of these and some additional species occurred in June. At this same time PO^4-P concentrations had decreased to low values. Not all species in the estuary were equally affected by the low supply of nutrient salts. Different species have different minimum nutrient requirements (see review by Ketchum, 1954). Unfortunately, there are few published data on the minimum nutrient requirements of attached marine plants (Feldmann, 1951).

During the winter months in 1952–53, when nutrient salts were in highest concentration, the six species of *Vaucheria* found in Great Pond marshes were in fruit (Table 2). When these species were still showing good vegetative growth in late summer to fall, nutrients were possibly near limiting levels. Whether the nutrient cycles in the marsh areas are similar to those in the basin is not known.

The largest supply of inorganic phosphate and nitrate (Figs. 13 through 19) occurred in the estuary within hydrographic sections II and IV (Fig. 2). These sections were also the scene of the highest plant production per unit area in the entire estuary (Fig. 9, Table 2). The sea grasses, *Ruppia maritima* and *Zostera marina* (Fig. 7), which represent an important part of the plant biomass in summer, are most abundant in these sections of the major basin of Great Pond. Since sections II and IV were the scene of marked tidal water exchanges (see current velocities, Fig. 20), more nutrients per unit

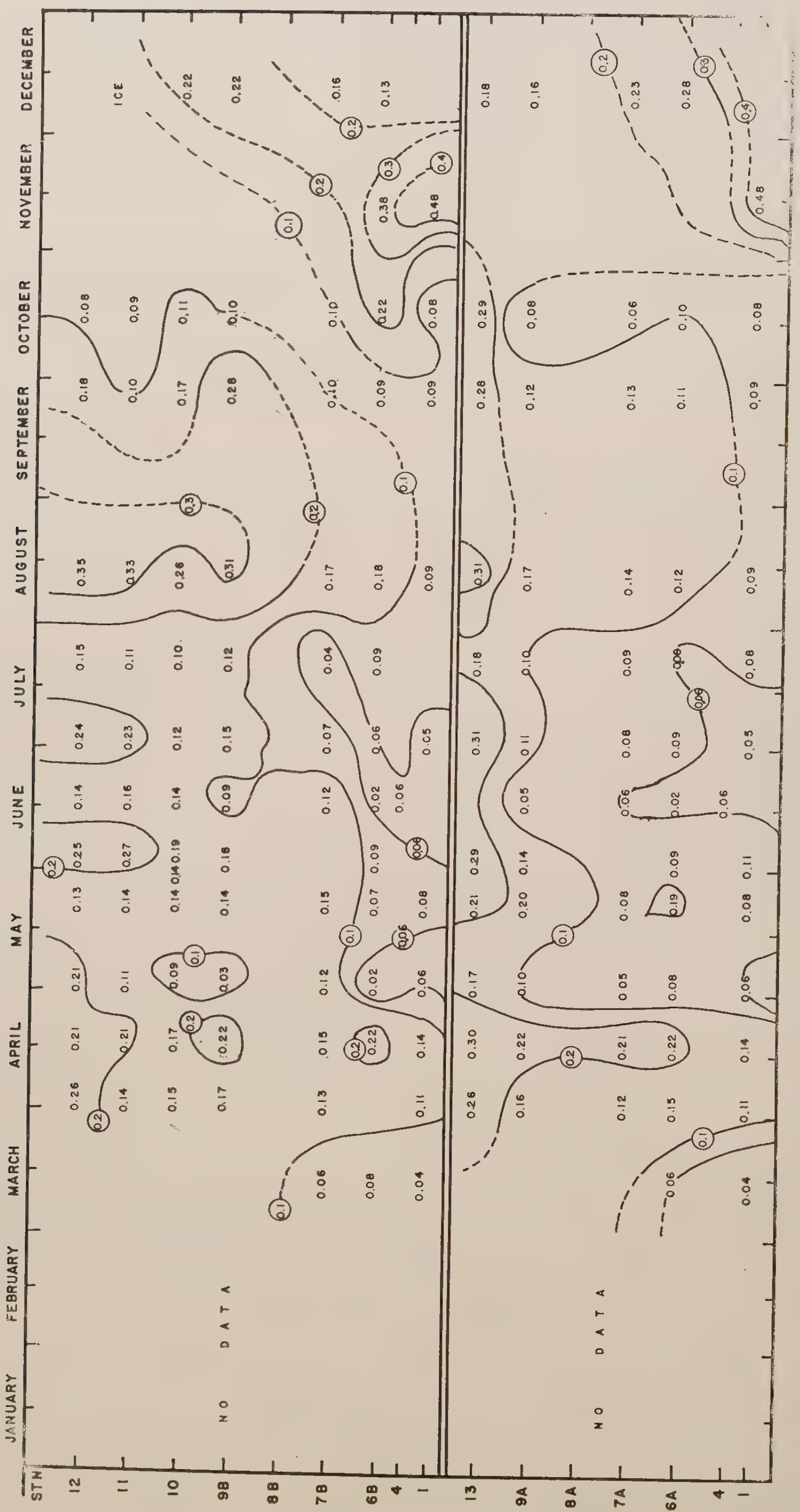

FIG. 16. The seasonal changes in nitrite in the bottom water of Great Pond in 1954, expressed in microgram atoms N/L. The two graphs are frequency polygons, described in detail in the legend for Figure 12.

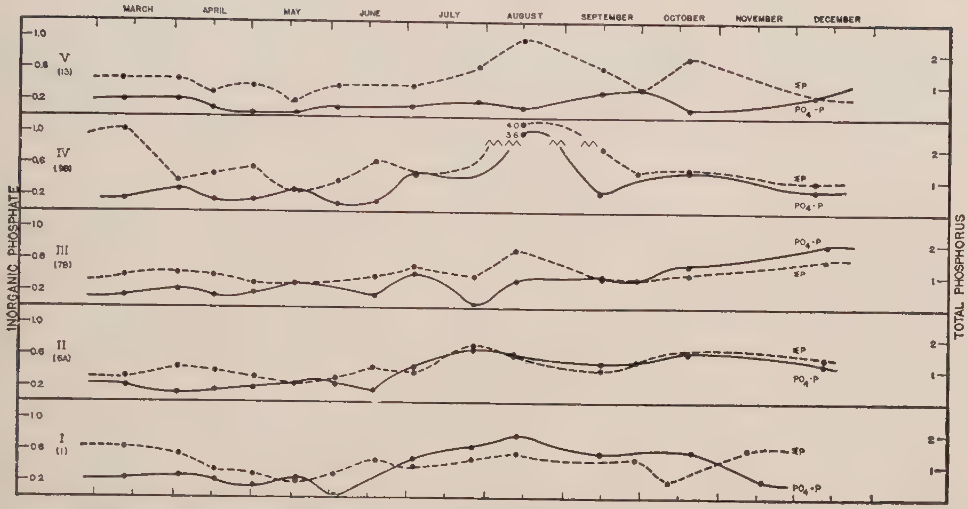

FIG. 17. Seasonal distribution of inorganic phosphate (PO_4–P) and total phosphorus (ΣP) in the bottom water by hydrographic sections (Figure 2) in Great Pond in 1954, expressed in microgram atoms P/L.

of time due to currents may have aided plant production in these areas (Gessner, 1952).

Thus the recycling of organic materials in Great Pond may occur primarily *in situ* possibly augmented by contributions from Vineyard Sound and terrestrial run-off. Hulburt (1956) did not include macroscopic benethic plants in his explanations for seasonal phosphorus changes in Great Pond. The nutrient limitations may help to explain why plant growth in Great Pond is limited and irregular.

DISSOLVED OXYGEN AND GROWTH

The effects of oxygen deficiency on benthic plant growth could not be observed in Great Pond since no anaerobic conditions were observed in the bottom water at any season. Oxygen data for 1952–53 and 1954 (Figs. 13, 21, 22) substantiate this conclusion. Ketchum (personal communication) did measure an oxygen deficit 0.0 ml. O_2/L in Great Pond immediately following a heavy rain storm. Such short term depletions may not seriously affect plant growth in an estuary with good transport and mixing. Reduced oxygen in the bottom water in some seasons was correlated with high growth rates and the regeneration cycles of nutrients.

PH AND BENTHIC PLANT GROWTH

The pH of the bottom water (Figs. 22, 23) may have had some direct influence on benthic plant growth especially in brackish water. Maximum growth occurred in the "tidal" zone (Fig. 2) of Great Pond where there was only a limited annual range of pH between 7.8 and 8.2. pH may affect plants by controlling the carbon dioxide state available for photosynthesis. The brackish waters exhibited pH extremes from 7.0 to 8.4. During the summer months growth rates (Fig. 23) were highest (Fig. 3) during periods of lower pH (7.8 usually). One explanation is that overall attrition and respiration may have exceeded photosynthesis during peak growth periods causing the pH to drop. It is also possible that the regeneration of nutrients during such periods may have stimulated growth in particular plants.

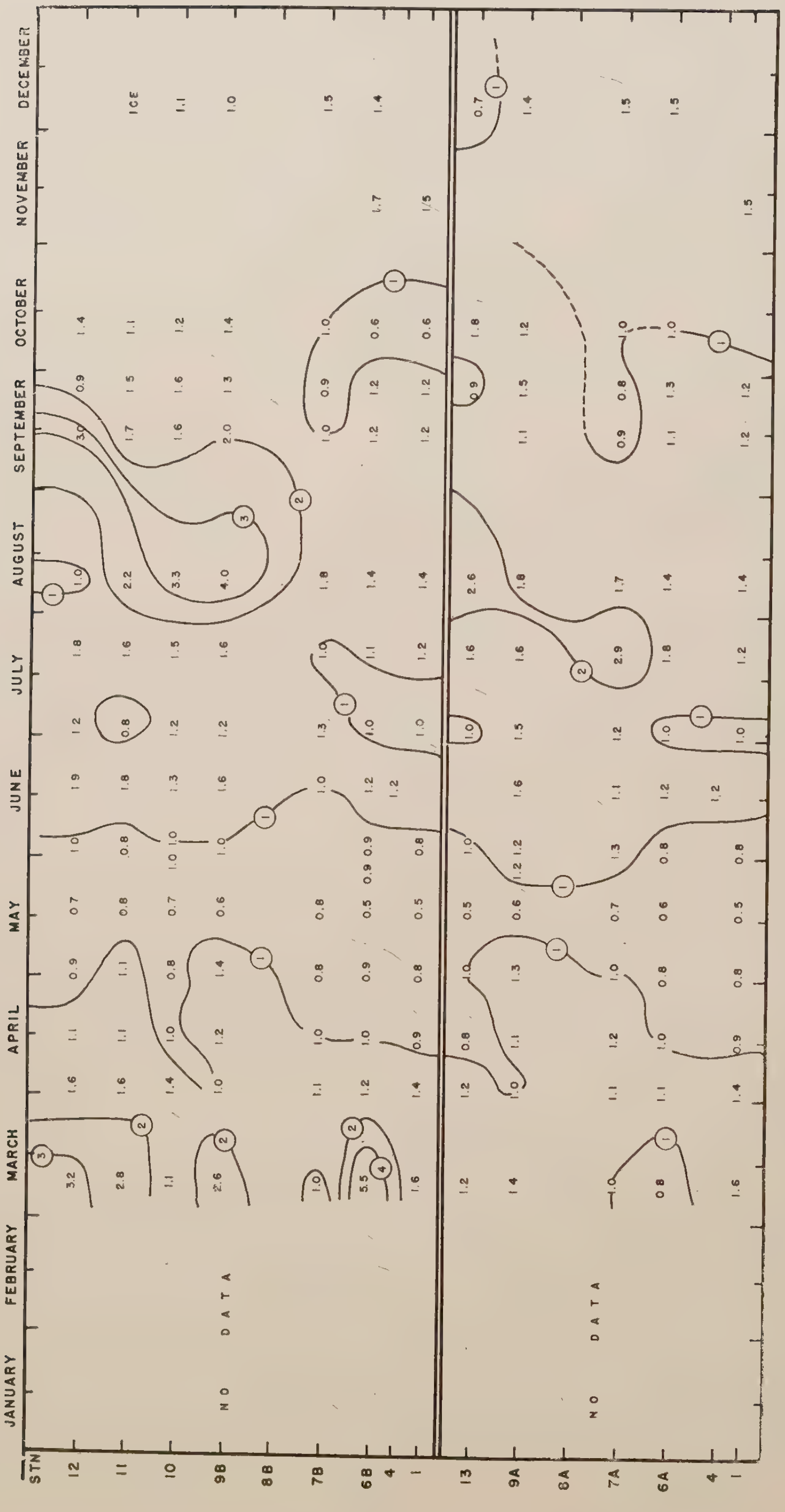

FIG. 18. The seasonal distribution of total phosphorus in the bottom water of Great Pond in 1954, expressed in microgram atoms P/L. The two graphs shown are frequency polygons, described in detail in the legend for Figure 12.

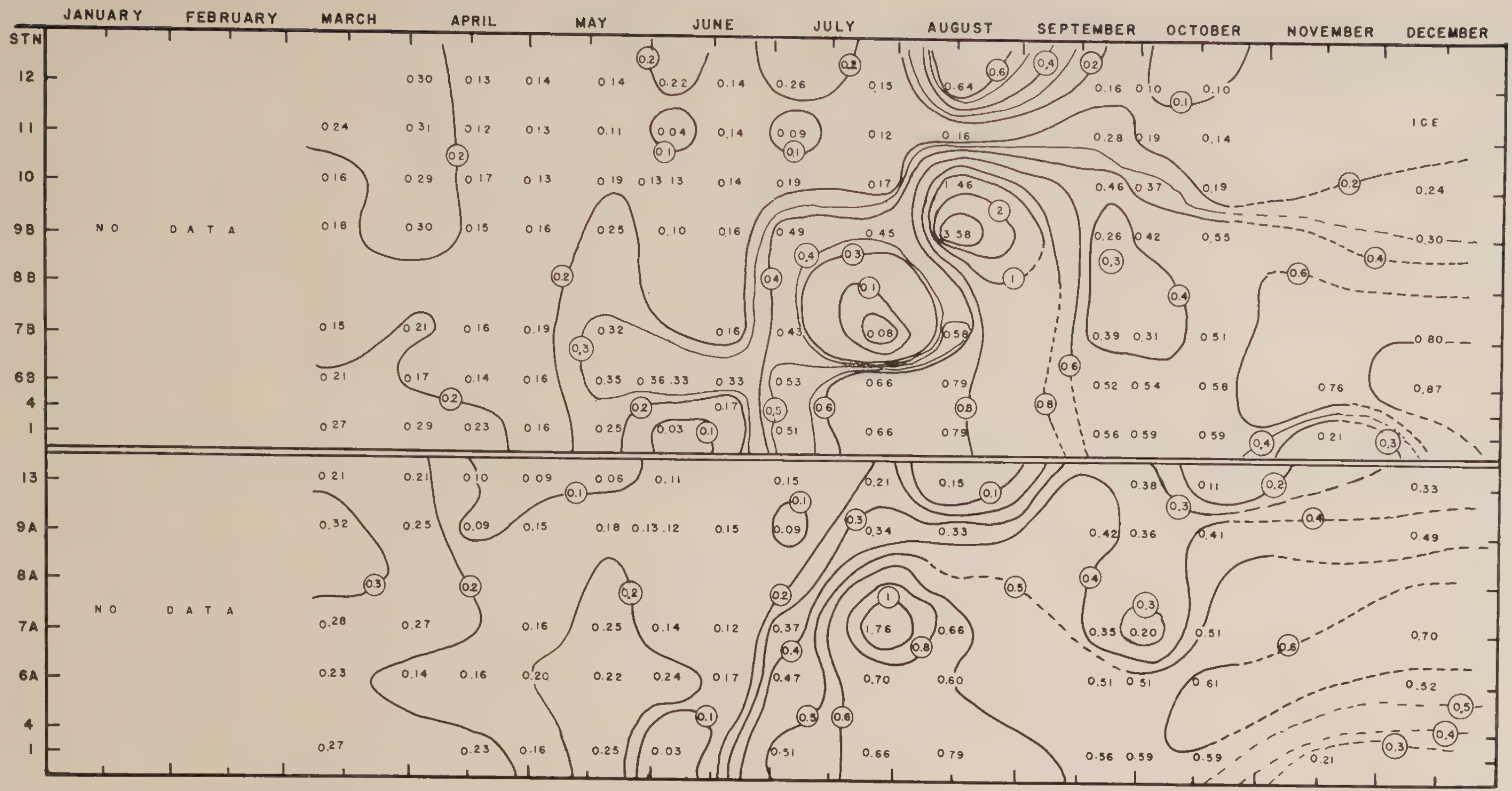

FIG. 19. The seasonal distribution of inorganic phosphate in the bottom water of Great Pond in 1954, expressed in Microgram atoms P/L. The two graphs are frequency polygons, described in detail in the legend for Figure 12.

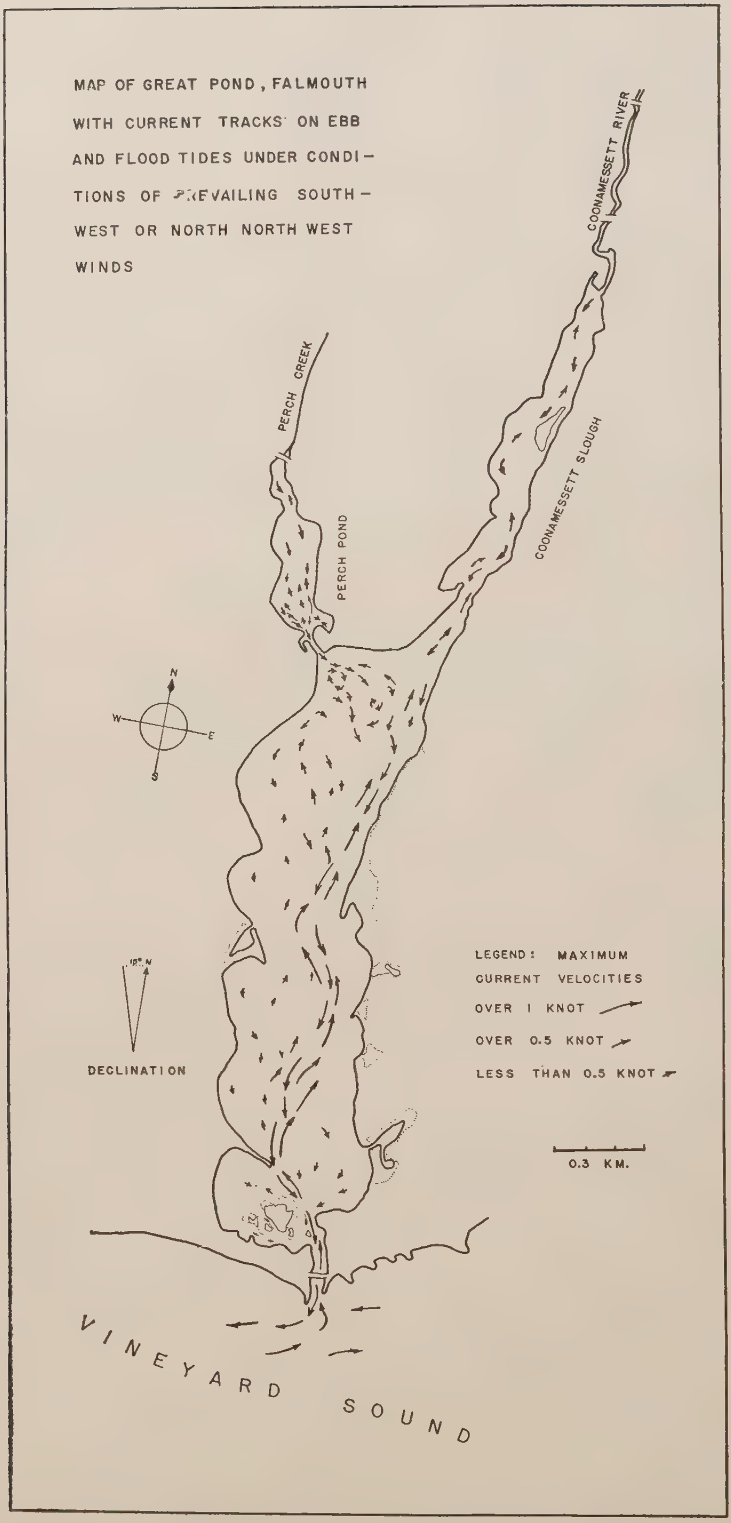
MAP OF GREAT POND, FALMOUTH
WITH CURRENT TRACKS ON EBB
AND FLOOD TIDES UNDER CONDI-
TIONS OF PREVAILING SOUTH-
WEST OR NORTH NORTH WEST
WINDS
COONAMESSETT RIVER
PERCH CREEK
PERCH POND
COONAMESSETT SLOUGH
N
W
E
S
15° N
DECLINATION
LEGEND: MAXIMUM
CURRENT VELOCITIES
OVER 1 KNOT
OVER 0.5 KNOT
LESS THAN 0.5 KNOT
0.3 KM.
VINEYARD SOUND

Fig. 20. Map of Great Pond, Falmouth with current tracks on ebb and flood tides under conditions of prevailing southwest or north northwest winds. Maximum current velocities are indicated by arrows.

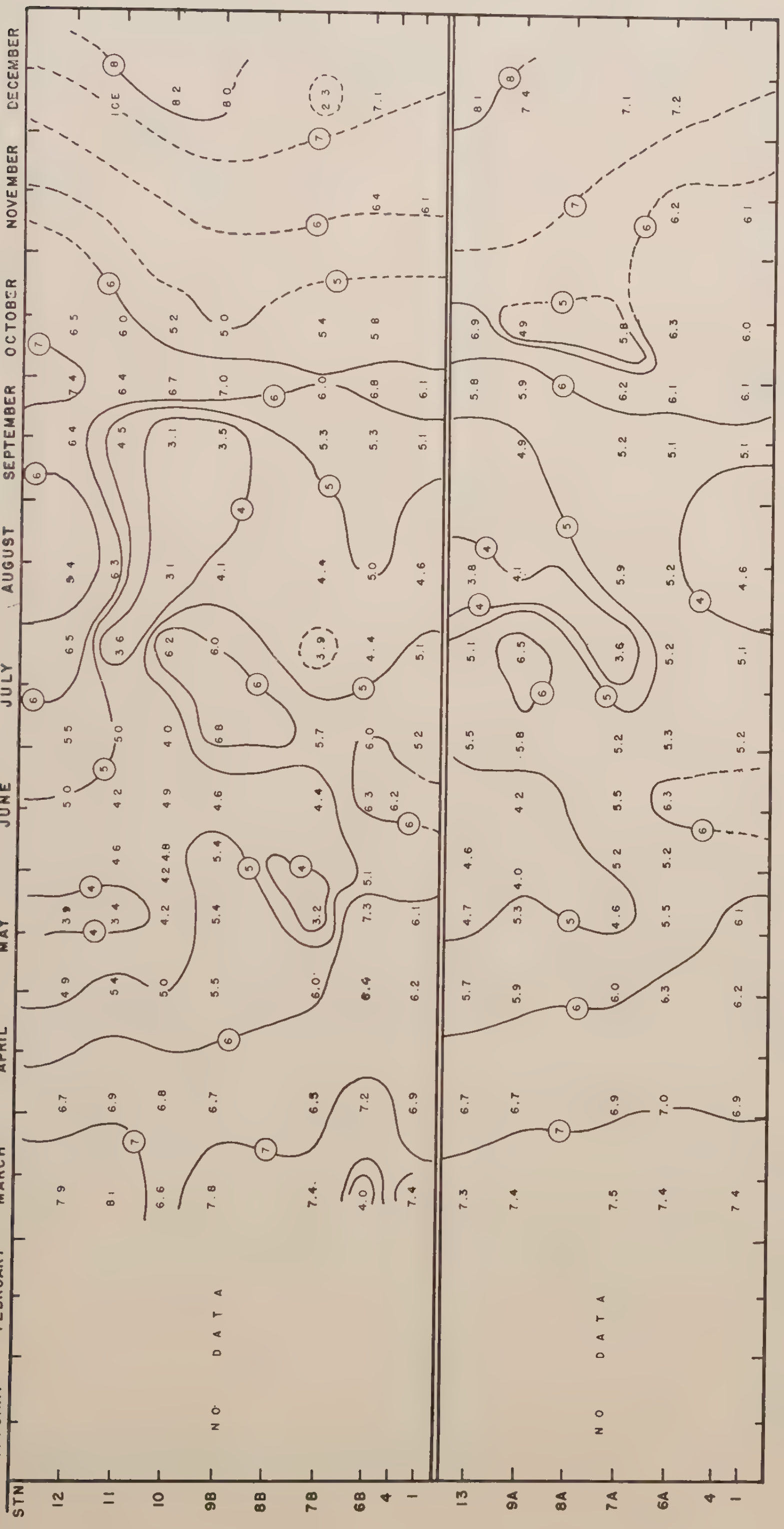

FIG. 21. The seasonal distribution of dissolved oxygen in the bottom water of Great Pond in 1954, expressed in milliliters per liter. The two graphs are frequency polygons, described in detail in the legend for Figure 12.

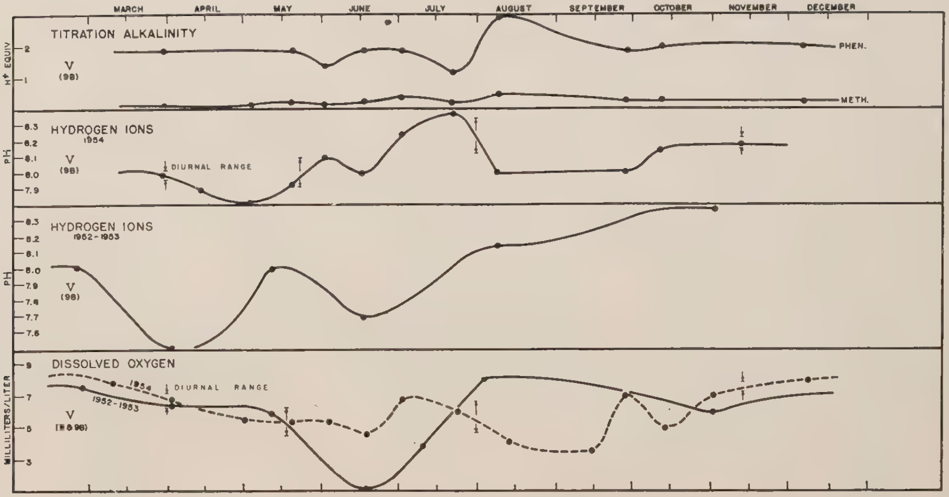

FIG. 22. Seasonal changes in titration alkalinity in 1954 and pH and dissolved oxygen in the bottom water of the "transition" zone of Great Pond in 1952–53 and 1954.

PHYSICAL FACTORS AND THE DISTRIBUTION OF BENTHIC PLANTS

Wave Action: When intense storms, occurring in the period from October through December, sweep over the estuary, waves have been observed to reach the bottom and to leave ripple marks. Poorly anchored benthic plants such as *Agardhiella tenera, Gracilaria verrucosa* and *Stilophora rhizoides* were transported a considerable distance as observed on several occasions. The occurrence of severe northeasterly storms has probably been largely responsible for the dense accumulation of algal beds within the arcs of the sand spits of the western shore. These arcs are also the scene of substantial changes in sedimentation during such storms.

The net movement of the poorly anchored species is mostly across the long axis of the estuary. Especially after a period of high winds, moribund plants of *Gracilaria* and *Agardhiella* were found in the sloughs. These plants, which presumably came from the major basin, differed from those which normally grow in the sloughs. Slough inhabiting plants have distinct modifications, such as short internodes and bushy habits.

Storms frequently separate the dying elements in the plant communities of the basin and collect them into windrows on the beach. This action tends to provide space for the younger, healthier plants in the habitat and at the same time aids in the recycling of nutrient salts.

Current: Paths taken by the flooding and ebbing tidal currents in Great Pond pass over areas abundantly populated by attached juvenile plants and by more fully developed algae attached to cobble. In Figure 24 are shown small areas where deposits of coarse sand cobble coincide with the tracks of tidal current (Fig. 20) near shore, and in narrow channels. Three explanations are offered for the abundance of the plants in the areas with currents. Active tidal currents probably transport a large number of viable spores over these areas from both neritic water and the estuary. Second, due to the constant movement of tidal water, more nutrient salts per unit of time are probably supplied to the plants in the path of the currents (Odum and Hoskin, 1957). Third, coarse sediments for attachment generally are present where water movements are

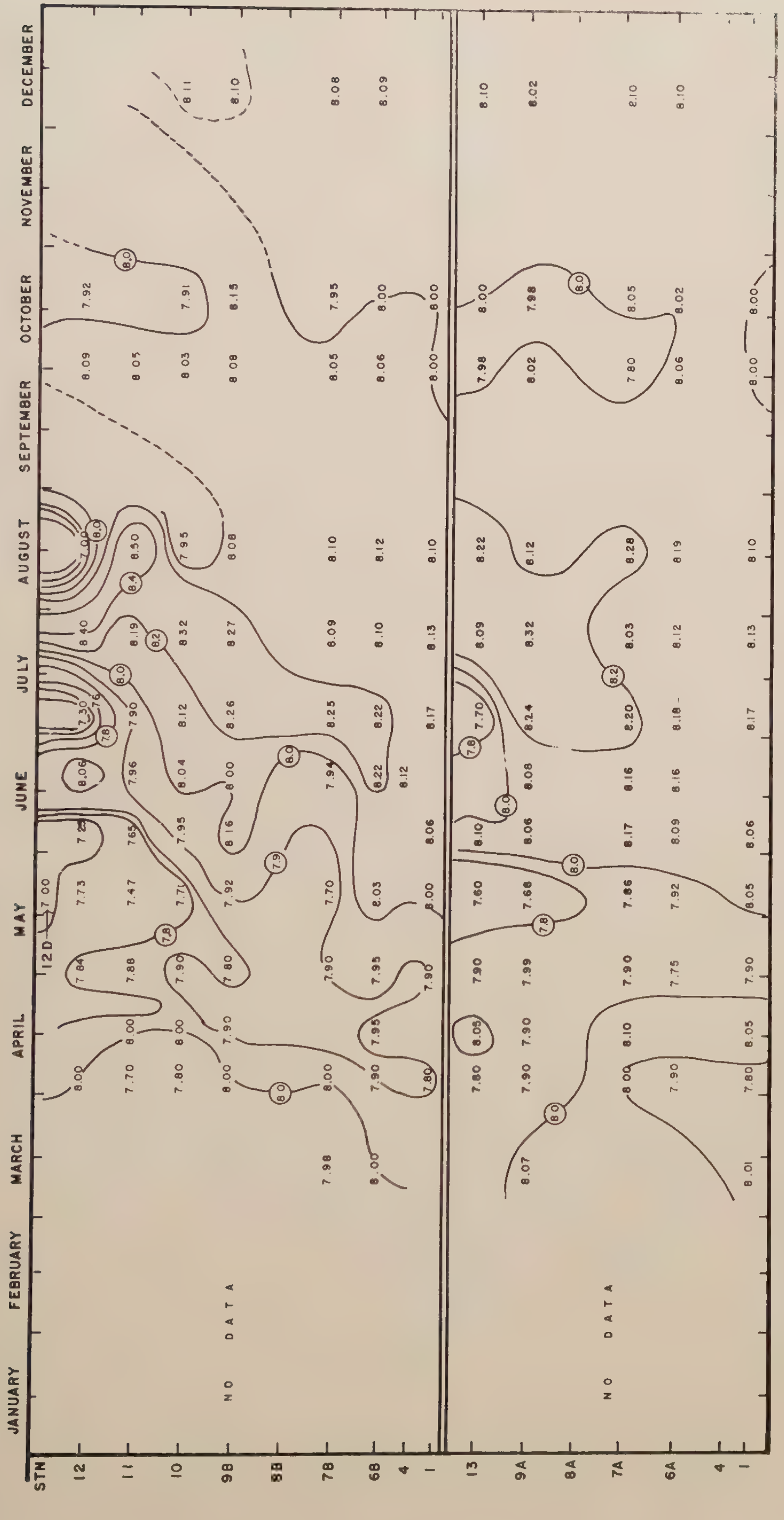

FIG. 23. The seasonal distribution of the pH of the bottom water of Great Pond in 1954. The two graphs are frequency polygons described in detail in the legend for Figure 12.

rapid. Such coarse sediments in Great Pond include large sand grains, pebble, cobble and boulder. These coarse materials probably were deposited by glacial outwash streams and are being eroded from the shoreline of the estuary. They are now very suitable for plant attachment.

Sedimentation: Butcher's data (Fig. 24) provide evidence for the development of sandy slopes strewn with pebble and shell on both shores, whereas the bottom is silt-covered. There is believed to be a correlation between the abundance of juvenile plants on the sandy shoals of the shoreline and the poorly anchored, well developed plants found on the basin floor. Poorly anchored, well developed plants growing in the major basin were nearly always attached to a sizeable sand grain, pebble or shell fragment. The cycle of events suggested by these findings starts with the attachment of spores and growth of juvenile plants on the coarse sediments of the sandy shoals. As these plants grow to some height, they are transported by wave action into deeper water where they accumulate in large masses. Eventually the algae die, after one or more seasons, and are cast upon the beach by wave action to decay. The decomposed plant debris releases nutrients for new growth. There is little doubt that this mechanism is quite necessary for the development of large accumulations of benthic plants on the basin floor.

Poor conditions for attachment, and rapid burial, are often brought on by the sedimentation of fine-grained materials in a "gradient" zone (Rochford, 1952). The fine silt enters the system in the run-off water, becomes flocculated by an electrolytic process and settles rapidly to the bottom of the sloughs. The rate of deposition is usually determined by the amount of salt present (Rochford, 1952). The soft, yielding sediments of the two sloughs (Fig. 24) are incapable of supporting attached plants. Thus, the survival of benthic plants on the slough bottom is improbable due to lack of a stable substratum. This is one reason that the floors of the two sloughs remain essentially barren of benthic plant life. Only the immediate banks and sandy shoreline slopes of the sloughs support attached algae and *Ruppia* beds.

Salinity: The effects of salinity on plants are variously related to other variables in a tidal estuary. Local distribution in estuarine water may be controlled by salinity and temperature (Luther 1951a, 1951b; Doty and Newhouse, 1954). Large changes in salinity require rather severe osmotic regulation in an organism (Sverdrup *et al.*, 1942). Certain benthic marine plants such as *Chondrus crispus, Corallina officinalis, Gelidium crinale, Nemalion multifidum, Petalonia fascia, Polysiphonia novae-angliae, Punctaria plantaginea, Ulva lactuca* var. *rigida* and others were never observed within the "tidal" or "gradient" zones of Great Pond (Figs. 2, 25) but established themselves only on the riprap along the open coast. In contrast, *Agardhiella tenera, Ectocarpus confervoides, E. siliculosus, Gracilaria verrucosa, Polysiphonia denudata, Porphyra leucosticia, Punctaria latifolia, Scytosiphon lomentaria, Spyridia filamentosa, Stilophora rhizoides* and others (Table 2) established themselves in the major basin of Great Pond and a few plants grew in the brackish water of the sloughs. In the colder months species including *Ectocarpus siliculosus, Punctaria latifolia* and *Stilophora rhizoides* were found in brackish water areas from which they were conspicuously absent in the spring. These plants were much less tolerant of low salinities at the relatively high water temperatures obtained in mid to late spring. Doty and Newhouse (1954) reported similar plant distributions in low salinity water when comparing summer and fall periods in the Oyster River. Due to a relatively uniform rainfall the year around (Table 10) seasonal (Fig.

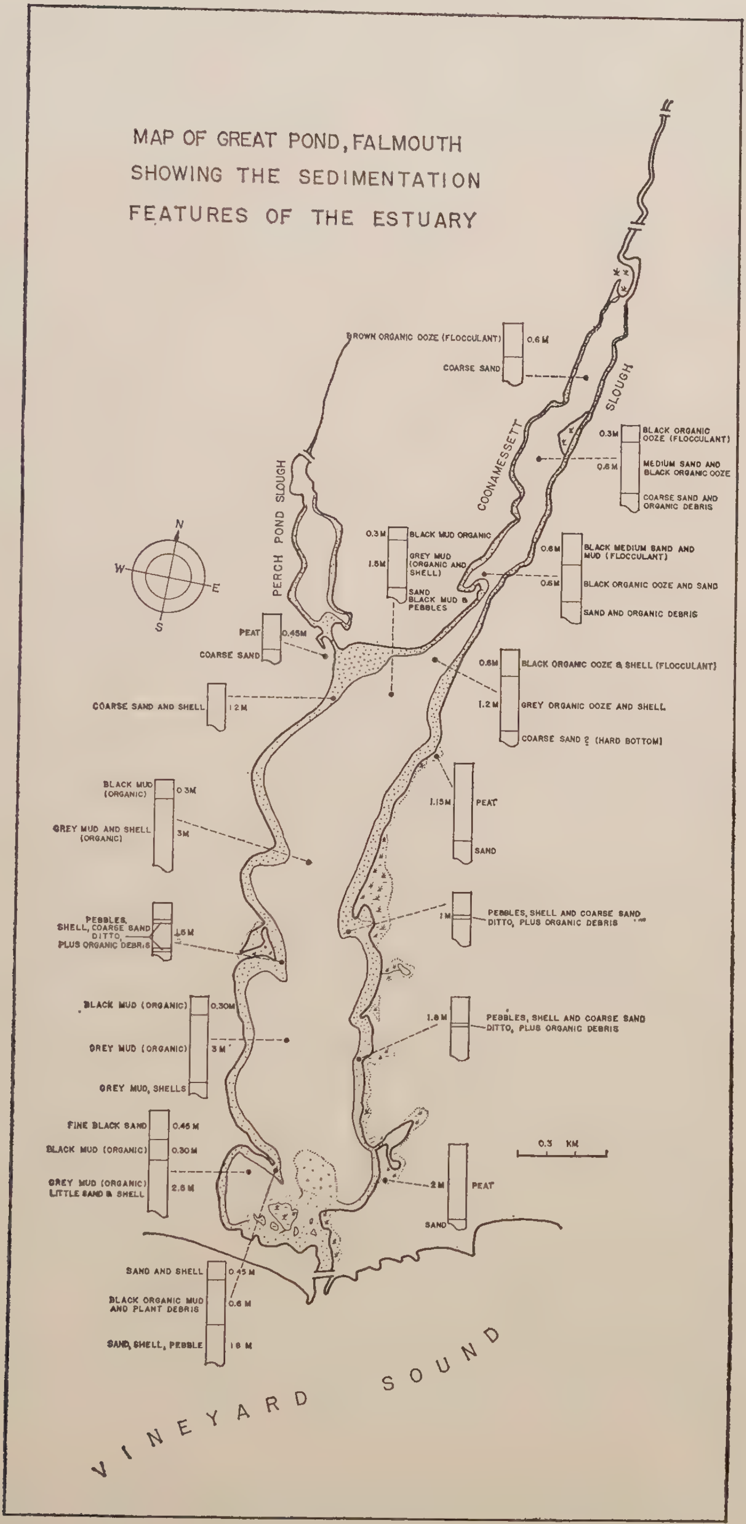
MAP OF GREAT POND, FALMOUTH
SHOWING THE SEDIMENTATION
FEATURES OF THE ESTUARY
N
W
E
S
PERCH POND SLOUGH
COONAMESSETT
SLOUGH
BROWN ORGANIC OOZE (FLOCCULANT)
0.6 M
COARSE SAND
0.3M
BLACK ORGANIC OOZE (FLOCCULANT)
0.6M
MEDIUM SAND AND BLACK ORGANIC OOZE
COARSE SAND AND ORGANIC DEBRIS
0.3 M
BLACK MUD ORGANIC
1.5M
GREY MUD (ORGANIC AND SHELL)
SAND BLACK MUD & PEBBLES
0.6M
BLACK MEDIUM SAND AND MUD (FLOCCULANT)
0.6M
BLACK ORGANIC OOZE AND SAND
SAND AND ORGANIC DEBRIS
PEAT
0.45M
COARSE SAND
COARSE SAND AND SHELL
1 2 M
0.6M
BLACK ORGANIC OOZE & SHELL (FLOCCULANT)
1.2 M
GREY ORGANIC OOZE AND SHELL
COARSE SAND ? (HARD BOTTOM)
BLACK MUD (ORGANIC)
0 3M
GREY MUD AND SHELL (ORGANIC)
3M
1.15M
PEAT
SAND
PEBBLES, SHELL, COARSE SAND
DITTO, PLUS ORGANIC DEBRIS
1.5M
1 M
PEBBLES, SHELL AND COARSE SAND
DITTO, PLUS ORGANIC DEBRIS
BLACK MUD (ORGANIC)
0.30M
GREY MUD (ORGANIC)
3 M
GREY MUD, SHELLS
1.8 M
PEBBLES, SHELL AND COARSE SAND
DITTO, PLUS ORGANIC DEBRIS
FINE BLACK SAND
0.45 M
BLACK MUD (ORGANIC)
0.30 M
GREY MUD (ORGANIC) LITTLE SAND & SHELL
2.6 M
0.3 KM
2 M
PEAT
SAND
SAND AND SHELL
0.45 M
BLACK ORGANIC MUD AND PLANT DEBRIS
0.6 M
SAND, SHELL, PEBBLE
1 8 M
VINEYARD SOUND

FIG. 24. Map of sediments of Great Pond based on unpublished data by Butcher.

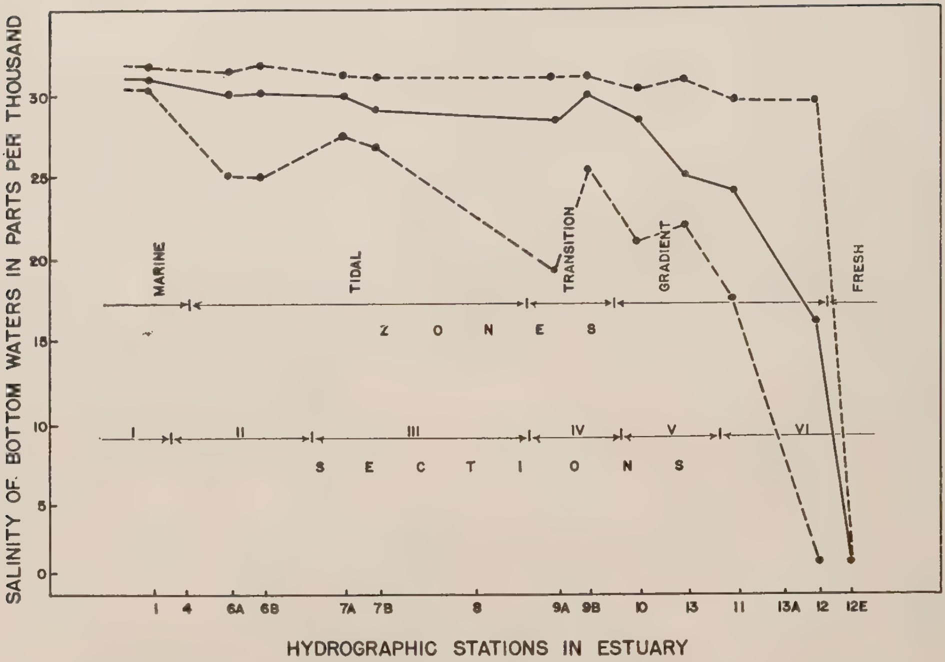

Fig. 25. The annual means and extremes of salinity of bottom water in Great Pond, Falmouth along the long axis of the estuary in 1952–53. Data are given in parts per thousand (0/00). The zones (after Rochford, 1952) and sections are those indicated in Figure 2. The anomalous extremes of decreased salinity at stations 6A and 6B are due to mixing of bottom water with surface water over a shoal sand bar at the seaward end of the basin (see Fig. 2).

Table 10

Monthly Precipitation in Centimeters for Nantucket Island, Massachusetts

	1952	1953	1954
January	16.0	20.9	13.0
February	20.5	13.7	6.0
March	11.6	15.8	6.7
April	6.6	21.4	9.8
May	8.2	4.7	9.2
June	1.7	0.5	1.8
July	0.4	14.9	2.9
August	14.9	8.0	12.2
September	1.9	11.5	12.7
October	5.1	11.1	3.3
November	5.2	19.9	11.4
December	12.1	10.0	16.2
Annual	104.2	152.4	105.2

26) and daily ranges (Barlow, 1956) in salinity were nearly the same in Great Pond. Temperatures (Fig. 12), however, varied widely with the season.

Where the dilution of sea water becomes too great, the normal growth of a species may not continue (Legendre, 1921). The sloughs are the last outpost for a few invading marine species of benthic algae and marine phanerogams and there is only a small total plant standing crop at all seasons (Fig. 7, Table 2). Considerable growths of *Enteromorpha clathrata, E. compressa, E. intestinalis, Monostroma oxyspermum* and *Ulva lactuca* var. *latissima* were found, but the two species *Enteromorpha linza* and *E. minima,*

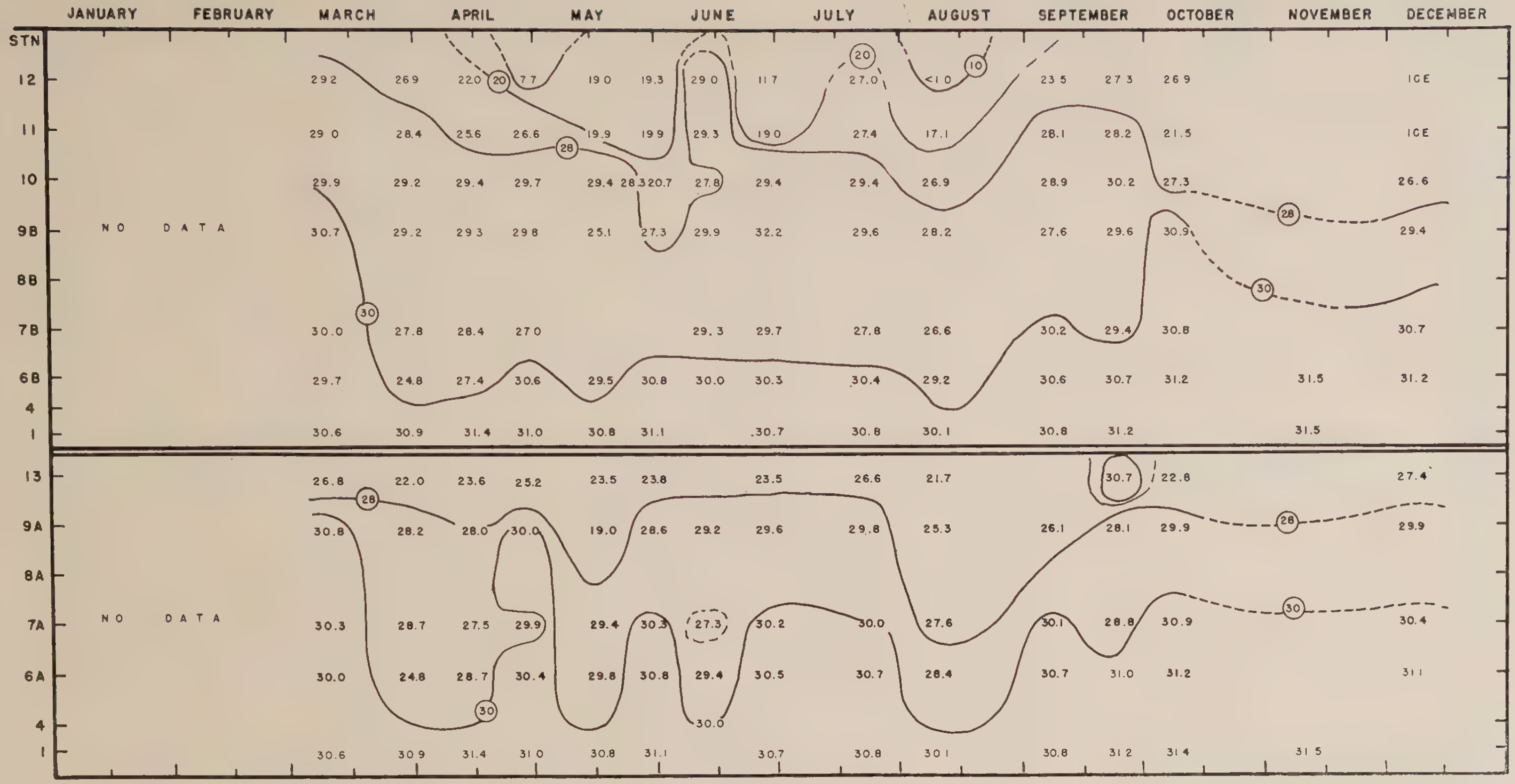

Fig. 26. The seasonal patterns of salinity in parts per thousand in the bottom water of Great Pond in 1954. For explanation of the coordinates see legend of Figure 12.

were never found in brackish water. Reduced salinities were characteristic of the "transition" zone (Figs. 25, 26; Table 2) yet the area supported a large portion of the total plant material in the estuary. Brackish water in the sloughs apparently greatly reduced growth and caused abnormal ties in some species of marine plants such as *Ceramium rubrum, Gracilaria verrucosa, Punctaria latifolia, Scytosiphon lomentaria* and *Spyridia filamentosa.*

There is evidence that some species of benthic marine plants remain sterile if they inhabit brackish water (Levring, 1940; Hayren, 1940, and others). In those sections of Great Pond where the mean salinity of the bottom water was below 26‰, sterility was common among the benthic algae. Probably the spores which arise on attached plants in brackish water come from plants in normal sea water habitats. Among the Phaeophyto no unilocular reproductive organs were observed in *Punctaria latifolia* or *Scytosiphon lomentaria.* The alga *Ectocarpus siliculosus,* appeared to be one of the few species in the division Phaeophyta which bore both unilocular and plurilocular reproductive structures in brackish water habitats. Nothing is known concerning the viability of the spores which this species produces in low salinity water.

The identity of specimens of *Ectocarpus siliculosus* found in the "gradient" zone may be open to question. The gametangia were more attenuated and elongated than in the typical form. Although plants of *Agardhiella tenera, Ceramium rubrum* var. *proliferum* and *Gracilaria verrucosa* grew in the "transition" and "gradient" zones (Figs. 2, 26), all specimens examined were sterile. The species, *Stilophora rhizoides,* could be separated into two morphological types in the "tidal" and "transitional" zones and the "gradient" zone respectively. The latter was smaller and finer branched. Both forms were induced to liberate swarmers in the laboratory suggesting that the species is capable of reproducing in brackish water.

Fruiting periodicity was studied in six species of marine *Vaucheria* (Blum and Conover, 1953). Fruiting occurred in several species from January through May soon after the occurrence of spring tides. Thus fruiting appeared to be related to prolonged immersion in water of much higher salinity than normal for the habitat.

Water Density: Whereas there seemed to be no clear-cut correlation between temperature or salinity alone and the seasonal occurrence of some benthic marine plants, there was a correlation between density and plant growth. Some plant species grew in brackish water habitats in winter but were absent from these areas by midspring and summer. Species which followed such a pattern included *Ectocarpus siliculosus, Gracilaria verrucosa* (Figs. 5, 6), *Punctaria latifolia, Scytosiphon lomentaria* and *Stilophora rhizoides* (Figs. 4, 6). These plants grew in brackish water as long as the water density (Fig. 27) was above 20 sigma-t units (1.020 gm./cc.), but disappeared from the sloughs when the density fell below 20 sigma-t units. In the major basin, where growth was not affected, the density ranged from 20.6 in winter to 24.5 sigma-t units in summer. In the sloughs the density ranged over the year from 12.0 in summer to 22.5 simga-t units in winter. From these results it would seem that density is correlated with growth in some seasons more than either temperature or salinity alone. Exactly why there is a correlation of density and growth is not known. Boyle and Doty (1949) believed that tolerances of marine algae to diluted sea water may decrease with increases in temperature. Since density is a function of temperature and salinity, the apparent correlation may be a matter of tolerance to low salinities at low temperatures.

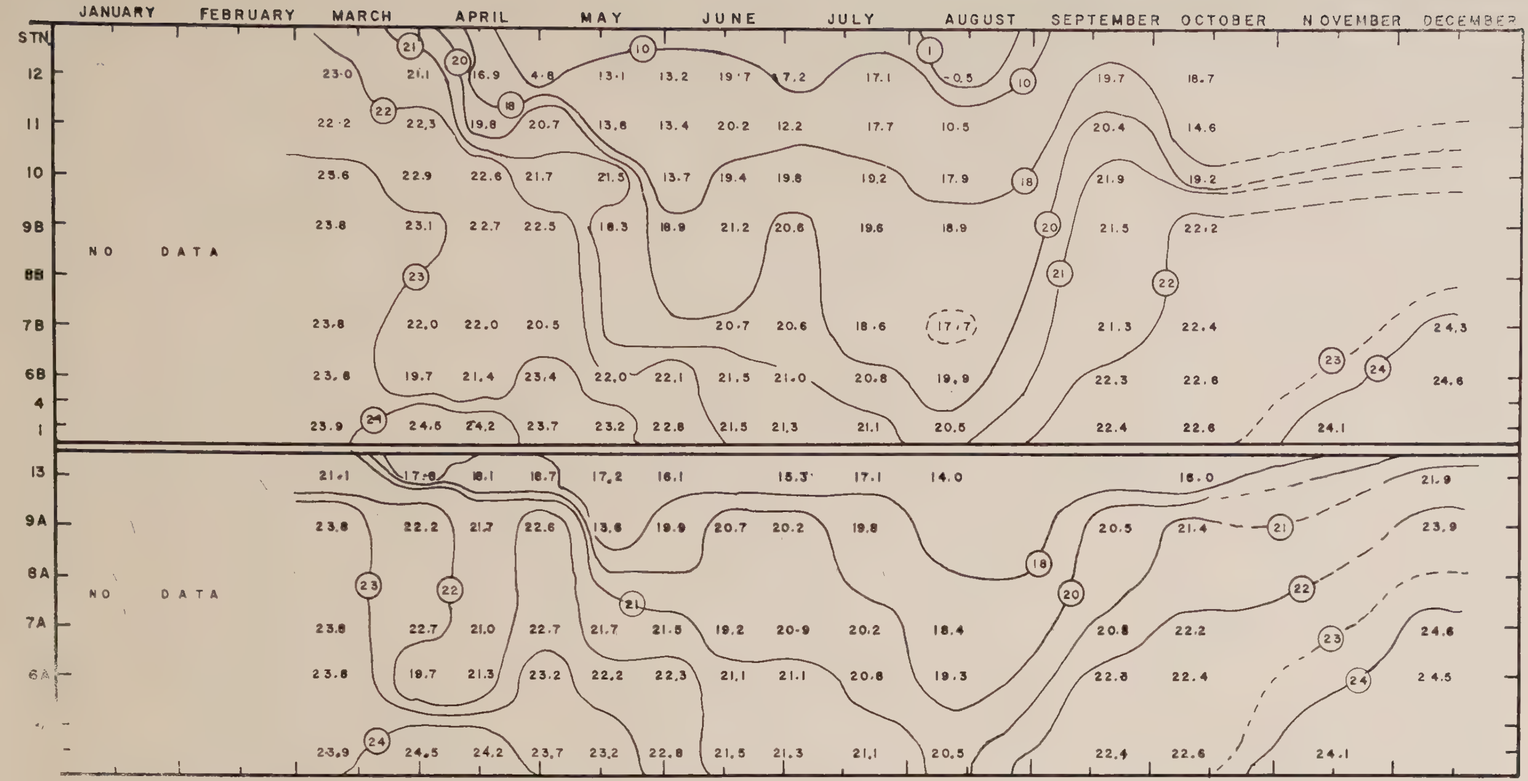

FIG. 27. Water density in sigma-t units in bottom water of Great Pond in 1954. The two graphs shown are frequency polygons, described in detail in the legend for Figure 12.

BIOTIC FACTORS AND SEASONAL GROWTH

Animal grazing apparently begins or takes place immediately after there is an initiation of phytoplankton growth (H. W. Harvey, 1955). With benthic marine plants in Great Pond, there is a period in early growth when grazing and epiphytism appear to be slight.

Immature plants of *Agardhiella tenera, Ceramium rubrum, Gracilaria verrucosa* and *Polysiphonia novae-angliae* were studied periodically to observe the relationship between growth and attack by other organisms. Very little grazing by the snails, *Bittium alternatum* or *Nassa obsoleta,* was witnessed. Only slight coverage by algal epiphytes was noted. On well developed plants about three weeks old many evidences of grazing were found, and epiphytes were noticeable with the unaided eye. Epiphytism and grazing were marked when the species populations had attained or passed their peak production levels.

Summer populations under conditions of high illumination and temperature were those most severely affected, but *Polysiphonia novae-angliae* showed attack by epiphytes and grazing early in its growth period. During the time of most active growth, attached plants in normal sea water did not seem to be seriously reduced by animal grazers. Observations on some marine plant species in both normal sea water and brackish water indicated that many more epiphytes had developed, and grazing by gastropods was far more intense on plants growing in more brackish water habitats than in normal sea water. Apparently, plants, whose optimum growth processes take place in normal sea water, are less able to resist attack and predation during early growth in a brackish environment.

Although morphological differences provide adequate grounds for establishing varieties in algae, other evidence may also be used. Seasonal growth data on varieties of *Ulva lactuca* provided evidence for a separation. In Great Pond *Ulva lactuca* var. *latissima* and *Ulva lactuca* var. *rigida* (Figs. 4, 6) exhibited dissimilar seasonal growth patterns.

STORMS, EXTREME TEMPERATURES AND ICING

Winds and Tropical Hurricanes: During the entire 1952–53 survey period water temperatures were mild (Fig. 11) and no violent storms (Fig. 10) were recorded. Thin sheets of ice formed on the sloughs only for a brief two-week period in February. According to the small deviation from the 62-year norm for the area (Table 10) rainfall in the survey years was fairly normal except in January and April, 1953. The illumination received in the summer of 1952 was somewhat above average. Measurements of standing crops of the dominant benthic marine plants during 1952–53 were believed to be representative for tidal estuaries on the Cape, according to sample surveys of several other estuaries along the southern coast of the peninsula. From June 1952 to August 1954 average climatic conditions prevailed in New England.

On August 31, 1954, a tropical hurricane swept over southern New England, bringing over 180 km. per hour wind velocity and 13 cm. of rainfall to the south Cape region. This storm was followed by a second one a week later. A series of salinity measurements were made in Great Pond to observe what had taken place (Table 11). Following the first hurricane, "Carol," the salinity of waters in Vineyard Sound increased only about 1‰ at the seaward end of the major basin. Then due to the heavy rainfall accompanying

Table 11

Salinity in Parts per Thousand in Great Pond Before and After Hurricanes “Carol” and “Edna”, September, 1954

(Figure 2) Stations	Level	July 23	Aug. 11	Aug. 31	Sept. 8	Sept. 11	Sept. 16	Sept. 27
6A	surface	30.6	27.1	Hurricane “Carol”	31.0	Hurricane “Edna”	30.5	31.0
	bottom	30.7	28.4		31.0		30.7	31.0
9A	surface	19.7	20.5		16.4		26.1	28.6
	bottom	29.7	25.3		30.0		26.1	28.1
10	surface	28.6	8.5		4.7		23.2	8.0
	bottom	29.4	26.9		27.0		28.9	30.1
1	surface	30.8	29.9		31.2		30.5	31.0
	bottom	30.8	30.1		31.2		30.8	31.2

the two storms, salinities decreased in the surface waters of the sloughs as the river discharge rate nearly doubled the normal amount for that season. These changes in salinity had little effect on the benthic vegetation according to a cursory examination. Precipitation in hurricanes had a greater effect on salinity than high storm tides. At any rate, such changes are quite temporary.

Wave action on the riprap disarranged the boulders, stripped most of the larger plants off the rocks and removed large amounts of the basin-inhabiting algae from Great Pond. In the summer of 1956 quadrat studies were made on transect 6 (section II, Fig. 2) to determine the fate of benthic plant populations. To all appearances the former luxuriance of the benthic vegetation had been restored.

Extreme Low Temperatures and Icing: In 1955, ice completely covered Great Pond to a depth of 7 cm. and persisted from January 20 through February 12. In 1956 icing conditions were even more severe. An ice sheet, which had a maximum thickness of 12 cm., remained for six weeks over the estuary. Inspection of the riprap at the mouth of the estuary showed ice-scouring had removed large quantities of *Chondrus crispus*, *Corallina officinalis* and *Fucus spiralis* but had done little damage to populations of *Fucus vesiculosus*. The latter occupies a sublittoral position on the riprap. Ice-scouring affected the attached plants on most Falmouth jetties during this period also, as large sheets of fringe-ice lined the shore. For the first time in nine years (records of the Woods Hole Oceanographic Institution), Buzzards Bay was covered by large sheets of ice which broke off during the thaw as large chunks passed through Woods Hole and entered Vineyard Sound.

The effect of low water temperatures and subsequent icing during this period also may have been responsible for the near extinction of *Gelidium crinale*. This species occupied a habitat in the intertidal belt where ice-scouring was severe. At this time the alga, *Bostrychia rivularis*, disappeared from section IV and could not be found anywhere in the estuary through the summer of 1956. The alga, *Punctaria plantaginea*, so abundant in the winter of 1952–53 did not appear along the Falmouth coastline in 1954 or the following winters through 1957. No explanation could be given for disappearance of a species that is found characteristically in arctic waters in a sublittoral habitat little affected by icing (Kjellman, 1883).

SIMILARITIES AND DIFFERENCES IN SUCCESSIVE YEARS

A question arises in a two-year study such as the present one in which the biotic survey was made one year and the hydrological survey the second year. Can one logically relate the biological data for 1952–53 to oceanographic data for 1954? Since some properties

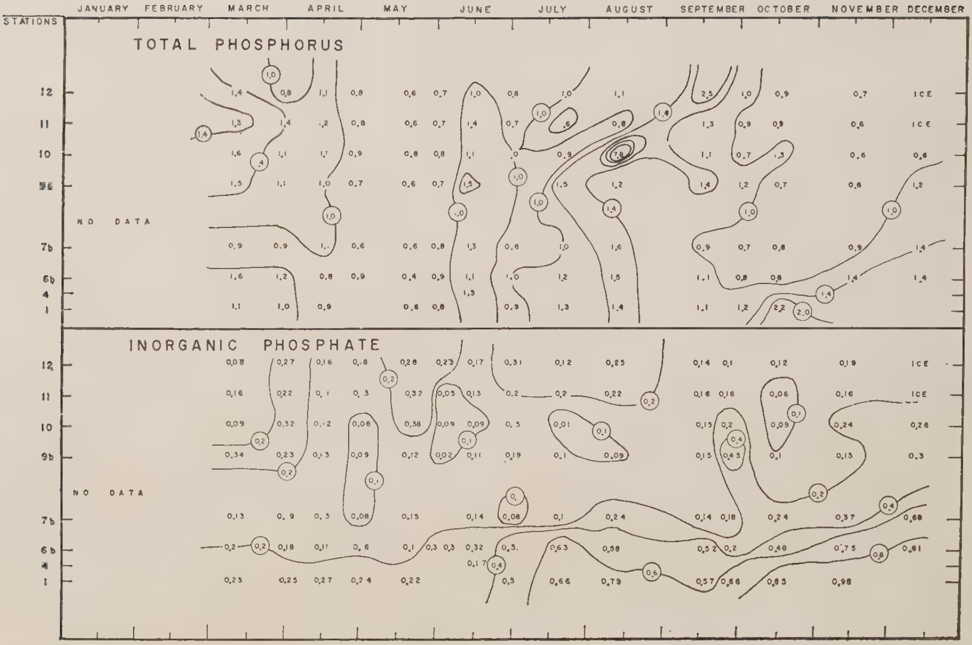

Fig. 28. Total phosphorus and inorganic phosphate in the surface water of Great Pond in 1954, expressed in microgram-atoms P/L. The two graphs shown are frequency polygons. Stations were located at the center in 1951 and along the eastern side of the pond in 1954. Refer to Figure 12.

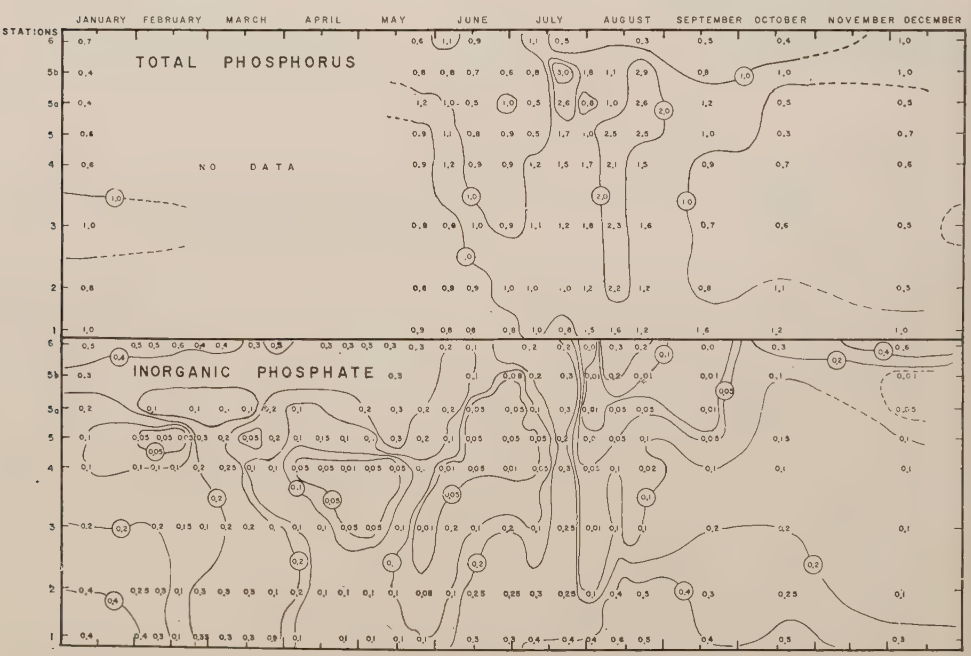

Fig. 29. Total phosphorus and inorganic phosphate in the surface water of Great Pond in 1950 (data after Hulbert), expressed in microgram atoms P/L. Compare these data with those of Figure 28 for 1954. The legend is the same as for Figure 28.

were measured in both years, a partial answer can be given. In Figure 22 dissolved oxygen and pH for 1952–53 and 1954 have been plotted. The same trends are present. There is also a close parallel between the 1950 and 1954 seasonal distribution of surface phosphorus. Data for 1950 are from Hulbert; Figures 28 and 29. Apparently the regular factors represented by the patterns of oxygen, pH, and phosphorus are repeated with similar amplitude from year to year.

The plant populations, however, are not exactly similar (See section on changes from year to year). It may be inferred that irregular factors and unusual departures are responsible for the changes in seasonal growth and reproduction of the plants from one year to the next.

LITERATURE CITED

American Public Health Association and American Water Works Association. 1946. Standard Methods for the Examination of Water and Sewage. 9th Ed. Lancaster, Pa., Lancaster Press, 286 pp.

American Public Health Association, American Water Works Association and Federal Sewage Industrial Wastes Association. 1955. Standard Methods for the Examination of Water, Sewage, and Industrial Wastes. 10th Ed. Baltimore, Md., Waverly Press, Ind., 522 pp.

Barlow, J. P. 1956. The hydrography of Great Pond, a tidal estuary. J. Mar. Res., 15(3): 193–203.

Bell, H. P. 1927. Seasonal disappearance of certain marine algae. Trans. N. S. Inst. Sci., 17(1): 1–5.

Bell, H. P. and C. MacFarlane. 1933. The marine algae of the maritime provinces of Canada, II. A Study of Their Ecology. Canad. J. Res., 9: 280–293.

Bernatowicz, Albert J. 1950. Seasonal aspects of the Bermuda algal flora. Pap. Mich. Acad. Sci., 36: 3–8.

————. 1952a. Seasonal changes in the marine algal flora of Bermuda. Univ. Mich., Ann Arbor, Mich. Dissertation Series Publ., 186 pp.

————. 1952b. Marine monocotyledonous plants of Bermuda. Bull. Mar. Sci. Gulf & Caribb., 2(1): 338–345.

Black, W. A. B. 1950. The seasonal variation in weight and chemical composition of the common British Laminariaceae. J. Mar. Biol. Ass. U. K., 29: 45–72.

Blinks, L. R. 1955. Photosynthesis and productivity of littoral marine algae. J. Mar. Res., 14(4): 363–373.

Blum, John L. and John T. Conover. 1953. New or noteworthy Vaucheriae from New England salt marshes. Biol. Bull., 105(3): 395–401.

Boyle, M. and M. S. Doty. 1949. The tolerance of stenohaline forms to diluted sea water. Biol. Bull., 97: 232.

Boysen-Jensen, B. 1941. Studies concerning the organic matter of sea bottoms. Rept. Danish Biol. Sta., 22: 5–39.

Braun-Blanquet, J. 1932. Plant Sociology. New York, McGraw Hill Book Co., 439 pp.

Dexter, R. W. 1953. Recession of eelgrass at Cape Ann, Mass., Ecology, 13(1): 229–231.

Doty, M. S. and J. Newhouse. 1954. The distribution of marine algae into estuarine waters. Amer. J. Bot., 41(6): 508–515.

Ehrke, Gerhard. 1929. Die Einwirkung der Temperatur und des Lichtes auf die Atmung und Assimilation der Meeresalgen. Planta, 9: 631–638.

————. 1931. Über die Wirkung der Temperatur und des Lichtes auf die Atmüng und Assimilation einiger Meeresund Süsswasser Algen. Planta, 13: 221–310.

Fassett, N. C. 1928. The vegetation of the estuaries of North Eastern North America. Proc. Bost. Soc. Nat. Hist., 39(3): 73–130.

Feldmann, Jean, 1937. Recherches sur la végétation marine de la méditerranée. La Côte des Alberes. Rev. Algol., 10: 1–339.

————. 1951. Ecology of marine algae, in Manual of Phycology. Waltham, Mass., Chronica Botanica Co.; pp. 313–334.

Fogg, G. E. 1953. The Metabolism of Algae. London, England, Methuen & Co. Ltd., ix + 149 pp.

Ford, Wm. L. 1949. Seagoing photoelectric colorimeter. Analyt. Chem., 22: 1431–1435.

Fritsch, F. E. 1906. Problems in aquatic biology with special reference to the study of algal periodicity. New Phytol., 5(7): 149–167.

————. 1945. The Structure and Reproduction of the Algae. Cambridge, England, Cambridge Univ. Press, Vol. II. xiv + 939 pp.

Funk, G. 1927. Die Algenvegetation des Golfs von Neapel nach Neueren Okologischen Untersuchungen. Pubbl. Staz. zool. Napoli, 7(Suppl.): 1–507.

————. 1954. Beitrage zur Kenntnis der Meeresalgen von Neapel. Pubbl. Staz. zool. Napoli, 25 (Suppl.): 1–178.

Gessner, Fritz. 1952. Der Druck in Seiner Bedeutung fur das Wachstum submesser Wasserpflanzen. Planta., 40: 391–402.

————. 1955. Hydrobotanik, die Physiologischen Grundlagen der Pflanzenverbreitung im Wasser. I. Energiehaushalt. Berlin, Germany, V.E.B. Deutscher Verlag der Wissenschaften, 517 pp.

Gunter, G. 1957. Temperature. Mem. geol. Soc. Amer., 67. Treatise on Marine Ecology and Paleoecology., 1: 159–184.

Harvey, H. W. 1948. The estimation of phosphate and total phosphorus in sea waters. J. Mar. Biol. Assoc. U.K., 27(2): 337–359.

————. 1955. The Chemistry and Fertility of Sea Waters. Cambridge, England, Univ. Press, vii + 224 pp.

Harvey, W. H. 1851. Nereis Boreali-Americana I. Melanospermeae. Smithson. Contr. Knowl. Pt. I, 3(4): 1–67.

Hasegawa, Y. and E. Fukuhara. 1956. On the seasonal and local variations in the weight of fronds. Bull. Hokkaido Reg. Fish. Res. Lab., 12: 29–39.

Häyren, E. 1940. Über die Meersalgen der Insel Hogland im Finischen Meerbusen. Acta, phytogeogr. suec., 13: 50–62.

Hedgpeth, J. W. 1957. Marine Biogeography. Mem. geol. Soc. Amer. 67. Treatise Marine Ecology and Paleontology, 1: 359–382.

Hoffmann, C. 1929. Die Atmung der Meeresalgen und ihre Beziehung zum Salzgehald. Jb. wiss. Bot., 71: 214–268.

Holmes, R. W. 1957. Solar Radiation, Submarine Daylight, and Photosynthesis. Mem. geol. Soc. Amer. 67. Treatise on Marine Ecology and Paleoecology, 1: 109–128.

Hulburt, E. M. 1956. Distribution of phosphorus in Great Pond, Massachusetts. J. Mar. Res., 15(3): 181–192.

Institute of Seaweed Research. 1953. Annual Report, 1953.

Ketchum, B. H. 1939. The development and restoration of deficiencies in the phosphorus and nitrogen composition of unicellular plants. J. cell. comp. Physiol., 13: 373–381.

————. 1954. Mineral nutrition of phytoplankton. Annu. Rev. Pl. Physiol., 5: 55–74.

Kjellman, F. R. 1883. Algae of the Arctic Sea. K. svenska Vetensk. Akad. Handl., N. F., 20(5): 1–349.

Klugh, A. B. and J. R. Martin. 1927. The growth-rate of certain marine algae in relation to depth of submergence. Ecology, 8: 221–231.

Knudsen, Martin (trans. by M. Oxner). 1946. The Determination of chlorinity by the Knudsen method (hydrographic tables by M. Knudsen). Woods Hole Oceanographic Institution, Woods Hole, Mass., 63 pp.

Knight, Margery and Mary W. Parke. 1931. Manx algae. Liverpool. Mar. Biol. Comm. Mem., 30: 1–155.

————. 1950. A biological study of *Fucus vesiculosis* L. and *F. serratus* L. J. Mar. Biol. Assoc. U.K., 29: 439–514.

Kylin, Harald. 1907. Studien über die Algen flora der Schwedischen Westküste. Akad. Afh. Upsala, 288 pp.

Legendre, R. 1921. Influence de la salinité de l'eau de mer sur l'assimilation chlorophyllienne des Algues. C. R. Soc. Biol., Paris, 85: 222–224.

Levring, Thor. 1940. Studien über die Algenvegetation von Belkinge Südschweden. Lund, Sweden, Akad. Abhandl., 178 pp.

Lodge, S. M. 1948. Algal growth in the absence of *Patella* on an experimental strip of foreshore, Port St. Mary, Isle of Man. Proc. Lpool. biol. Soc., 56: 78–83.

Luther, Hans. 1951. Verbreitung und Ökologie der hötheren Wasserpflanzen im Brackwasser der Ekenaesgegend in Suedfinnland. Teil I. Acta bot. fenn., 49: 1–232; 50: 1–370.

MacFarlane, C. 1952. A Survey of certain seaweeds of commercial importance in southwest Nova Scotia. Canad. J. Bot., 30: 78–97.

Odum, E. P. 1953. Fundamentals of Ecology. Philadelphia, W. B. Saunders Co., 384 pp.

Odum, H. T. and C. M. Hoskins. 1957. Metabolism of a laboratory stream microcosm. Publ. Inst. Mar. Sci. Univ. Tex., 4(2) : 115–133.

Petersen, C. G. J. 1912. Über Menge und Jahresproduktion der Bentospflanzen an den westuropaischen Küsten. Int. Rev. Hydrobiol, 5: 47–52.

Pratt, D. M. 1950. Experiments in the fertilization of a salt water pond. J. Mar. Res., 8(1) : 36–59.

Printz, H. 1939. Über die Kohlensäure Assimilation der Meeresalgen in verschiedenen Tiefen. Skr. norske Vidensk. Akad., 5: 1–272.

————. 1950. Seasonal growth and production of dry matter in *Ascophyllum nodosum*. Arh. norkse Vidensk. Akad., 4: 1–15.

Rees, T. K. 1934. Algal migration on the Gower coast. Proc. Swansea sci. Fld. Nat. Soc., 1: 235–239.

————. 1935. The Marine Algae of Lough Ine. J. Ecol., 23: 69–133.

Rochford, D. J. 1952. Studies in Australian estuarine hydrology. I. Introductory and comparative features. Aust. J. Mar. Fresh. Res., 2(1) : 1–116.

Sargent, M. and L. Lantrip. 1952. Photosynthesis, growth and translocation in giant kelp. Amer. J. Bot., 39: 99–107.

Setchell, W. A. 1915. The law of temperature connected with the distribution of the marine algae. Ann. M. bot. Gan., 2: 287–305.

————. 1917. Geographical distribution of the marine algae. Science, 45(1157) : 197–204.

————. 1920a. The temperature interval in the geographical distribution of marine algae. *Ibid.* 42 (1339) : 187–190.

————. 1920b. Stenothermy and zone invasion. Amer. Nat., 44: 385–397.

————. 1932. Macrocystis and its holdfasts. Univ. Calif. Publ. Bot., 16: 445–492.

Smith, G. M. 1947. On the reproduction of some Pacific coast species of *Ulva*. Amer. J. Bot., 34(2) : 80–87.

Svedelius, Nils. 1906. Über die Algenvegetation eines ceylonischen Korallenriffes. *in* Bot. Stud. till F. R. Kjellman. Upsala, pp. 184–220.

Sverdrup, H. W., M. W. Johnson, and R. H. Fleming. 1942. The Oceans, Their Physics, Chemistry and General Biology. New York, Prentice-Hall, Inc., x + 1087 pp.

Taylor, W. R. 1933. Epidemic among zostera colonies. Rhodora, 35: 186.

————. 1957. Marine algae of the northeastern coast of North America. 2nd. Ed. Univ. Mich. Sci. Ser., Ann Arbor, Mich., Univ. Mich. Press, viii + 509 pp.

Truog, E., and A. H. Meyer. 1929. Improvements in the Deniges colorimetric method for phosphorus and arsenic. Industr. Engng. Chem. (Anal.), 1: 136–139.

Vinogradov, A. P. (Trans. by J. Efron and J. K. Setlow). 1953. The Elementary Chemical Composition of Marine Organisms. New Haven, Conn., Mem. Sears Foundation Mar. Res. No. 2, xiv + 647 pp.

Walker, F. T. 1952. Sublittoral seaweed surveys: Dunbar to East Castle, East Scotland. J. Ecol., 40: 74–83.

Weston, R. S. 1905. Notes on the determination of nitrogen as nitrites in waters. J. Amer. Chem. Soc., 27: 281–282.

Contribution No. 1039

Reprinted from LIMNOLOGY AND OCEANOGRAPHY
Vol. IV, No. 4, October, 1959
Printed in U.S.A.

Light Adaptation by Marine Phytoplankton[1]

JOHN H. RYTHER
Woods Hole Oceanographic Institution

AND

DAVID W. MENZEL
Bermuda Biological Station

ABSTRACT

Photosynthesis-light intensity curves were obtained for natural phytoplankton populations in the Sargasso Sea from surface waters and from depths to which 10% and 1% of the surface light penetrated. In winter, when the water was isothermal and mixed to depths below the euphotic zone, phytoplankton from all three depths behaved like "sun" forms, becoming fully light saturated at 5000 foot candles. In summer, when the water and plankton were stratified, the surface plankton were similar to the winter plankton, those from the 1% light level behaved like "shade" plants, becoming light saturated below 1000 foot candles, those from the 10% light level were intermediate in their response to light. The effect of light adaptation on the calculation of primary production from chlorophyll and light is discussed.

INTRODUCTION

The distinction between plants which are adapted to living at high and low light intensities is a familar one. These so called "sun" and "shade", or "heliophillic" and "umbrophillic", forms have certain distinguishing characteristics which are usually, though not always, consistent. Thus, the "sun" forms normally contain less chlorophyll, photosynthesis becomes light saturated at higher intensities, and their assimilation number (photosynthesis per unit of chlorophyll) is frequently lower at all intensities. These characteristics are found in different species which inhabit different types of environment (*i.e.* desert vs. forests), in individuals of the same species conditioned respectively to high and low light intensities, and even in "sun" and "shade"adapted leaves of the same plant. A partial review of this subject may be found in Rabinowitch (1951).

Most of the known examples of these phenomena are restricted to the higher plants and macroscopic algae. There have been fewer studies of light adaptation by unicellular algae and, though the distinction is often assumed to exist, evidence is almost lacking for natural phytoplankton populations. Steemann Nielsen (1934) described species of the dinoflagellate genus *Ceratium* which were found characteristically in deep ocean waters (*i.e.* 100 meters), while others were found only at the surface. He termed these "shade" and "sun" species respectively, and compared the morphology of the "shade" forms with umbrophillic forest tree leaves. His observations on the distribution of these species were later confirmed by Graham and Bronikovsky (1944). Rodhe *et al* (1958) concluded that the phytoplankton in Lake Erken adapts seasonably to changing light conditions, the summer species being more typical of "sun" forms, the winter population being shade adapted and light inhibited at the surface even at the low intensities encountered in mid-December in Sweden (*i.e.* 15 g cal/cm^2/day as compared with 700 g cal/cm^2/day for clear summer days). One of the present authors (Ryther, 1956) obtained photosynthesis-light intensity curves for a variety of marine phytoplankton cultures. In general the green algae, the diatoms, and the dinoflagellates respectively become both saturated and inhibited at progressively higher light intensities. In this sense these three groups could be considered as "sun", "intermediate" and "shade" forms, though the distinction is ecologically meaningless since they frequently coexist in the same environment.

---

[1] Contribution No. 255 from the Bermuda Biological Station and Contribution No. 1039 from the Woods Hole Oceanographic Institution, under Contract No. AT(30-1)-2078 (U. S. Atomic Energy Commission) and with the partial support of NSF Grant G-3234.

Using natural surface phytoplankton populations Steeman Nielsen and Jensen (1957) made a series of photosynthesis-intensity curves during the *Galathea* expedition. Their curves for tropical ocean waters were extremely consistent and remarkably similar to the mean curve for all species examined in the culture experiments of Ryther described above. A similar series from the Tasman Sea in mid-summer, however, showed the phytoplankton to be more shade adapted, light saturation being reached at about 1,000 foot candles rather than the 2,000–2,500 foot candles for the tropical waters. Later studies by Steemann Nielsen and Hansen (1959) in the North Atlantic revealed that the surface plankton of this region were comparable to those of the Tasman Sea. However, samples from depths to which only 1% of the surface light penetrated (30–50m) showed quite different characteristics, becoming light saturated at intensities below 500 foot candles. These deeper organisms were described by Steemann Nielsen and Hansen as "shade plankton". In contrast to this, they found no differences in the light curves of phytoplankton from all depths sampled at the mouth of the Godthaab Fjord, where tidal currents caused a pronounced vertical mixing.

While the publication of Steemann Nielsen and Hansen was in press, the present authors were engaged in somewhat similar studies in the Sargasso Sea off Bermuda. The results which will be reported below will be largely a confirmation of the experiments described by the Danish scientists. However, they include more detailed ancillary data and are of particular interest because of the contrasting hydrographic conditions, the varying distributions of phytoplankton, and the resulting differences in the intensity and duration of light intensities to which the plants are exposed at different times of the year in these waters.

During the "winter" (November–April) the Bermuda offshore surface waters are isothermal and apparently well mixed to depths as great as 400 meters and always in excess of 150 meters. The chemical and biological properties of this mixed layer, including the phytoplankton, are very nearly homogeneous. For the rest of the year, the water is thermally stratified with a well developed, seasonal thermocline in the upper 25–50 meters. Under these conditions, the surface waters become nutrient impoverished and extremely poor in phytoplankton. However, a maximum of chlorophyll characteristically develops at a depth of 100–150 meters, just at the lower limit of the euphotic zone (1% of the surface radiation penetrates to about 100 meters in these waters). J. H. Steele and C. S. Yentsch (unpublished data) have recently investigated the causes of this chlorophyll peak, which appears to occur very commonly in other regions where the surface waters are thermally stratified. They proposed that this peculiar distribution results from a reduction in the rate of sinking of nutrient-deficient phytoplankton on encountering the richer water below the euphotic zone. The mathematical model which Steele developed to describe this phenomenon was substantiated by experimental evidence in which the settling rate of nutrient-deficient diatoms was greatly retarded by enriching the cultures.

Figure 1 shows vertical profiles of temperature and chlorophyll under typical unstratified ("winter") and stratified ("summer") conditions in the Sargasso Sea off Bermuda. While the rates of vertical circulation in winter are unknown, it seems reasonable to assume that the phytoplankton within the mixed layer would all be exposed to approximately the same average light conditions and would be circulated rapidly enough to prevent their being conditioned to the light intensity at any one depth. In

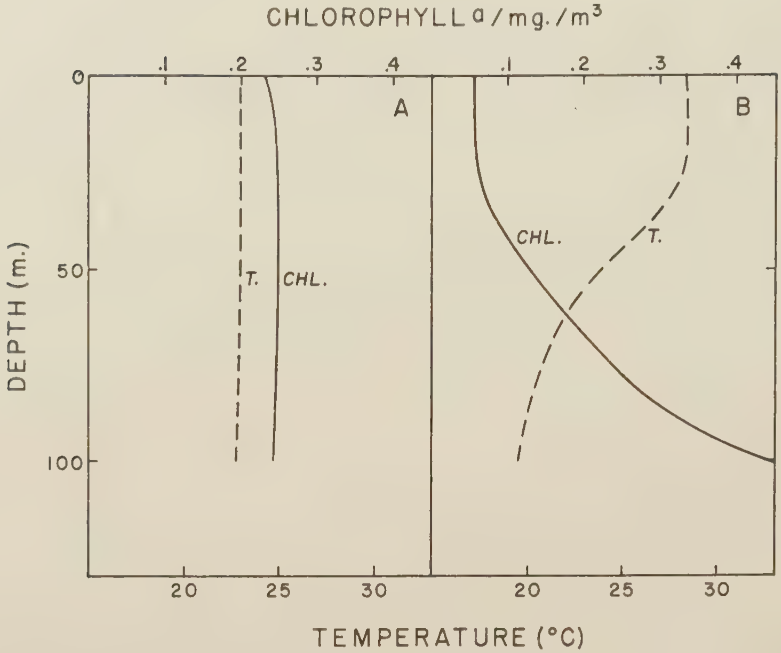

Fig. 1. Depth profiles of chlorophyll a (chl) and temperature (T) in November (A on left) and October (B on right) in the Sargasso Sea off Bermuda.

contrast to this, the vertical circulation in summer may be assumed to be negligible and the phytoplankton hence exposed for relatively long periods to the light conditions where they are found. These conditions provided an excellent opportunity to examine populations of the same species of phytoplankton held under extremely different natural illumination for evidence of a physiological light adaptation. Of particular interest was the comparison between the surface phytoplankton and that comprising the deep chlorophyll peak, and the comparison between summer "stratified" and winter "mixed" populations.

EXPERIMENTAL METHODS AND RESULTS

The experiments described below were carried out on November 14 and on October 4 and 15, 1958 when conditions were similar to those shown in Figures 1A and 1B respectively. Water was collected with a non-metallic sampler from the surface, 50 and 100 meters, where corresponding light intensities were equivalent to 100%, 10% and 1% of the incident surface radiation, as determined with a submarine photometer. Each sample was dispensed into a series of five 150 ml glass stoppered bottles to which were added approximately 15 μ curies of $C^{14}O_3^=$. The bottles were then placed in an incubator cooled with running surface water and covered with a series of neutral density filters which transmitted respectively 100%, 50%, 25%, 10% and 1% of the incident radiation. The experiments lasted for approximately four hours consisting of the two hours before and the two hours after solar noon. During this period, solar intensities are not only greatest but vary by only about 10% under clear skies. Solar radiation was recorded during the experimental periods with an Epply pyrheliometer, and the mean intensity received by the bottles was calculated for each experiment.

After exposure the contents of each bottle was filtered through an HA millipore filter. The filters were washed with 10 ml of 0.001 N HCl in a 3% NaCl solution, dried in a desiccator, and their radio-activity determined in a gas flow Geiger counter. The activity of each sample was taken as an index of relative photosynthesis.

The results of these experiments are shown

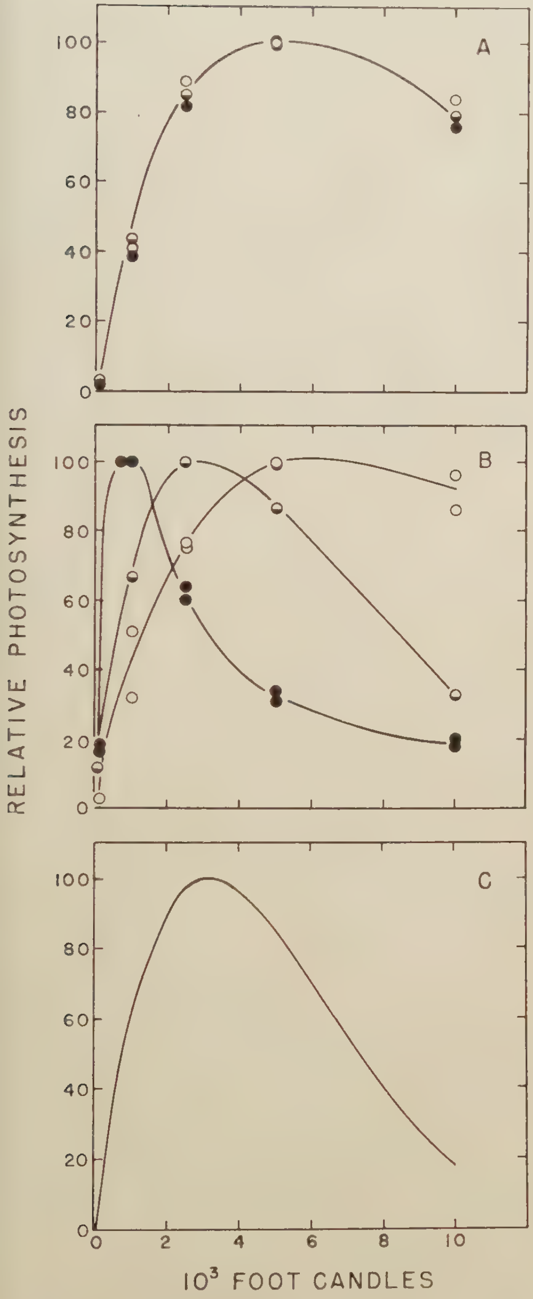

FIG. 2. Photosynthesis-light intensity curves of Sargasso Sea phytoplankton from depths to which 100% (open circles), 10% (half-filled circles) and 1% (filled circles) of the surface light penetrated in November (A top) and October (B center). C (bottom) is mean curve for phytoplankton cultures from Ryther (1956a).

in Figure 2; A being the series of curves from the three depths on November 15 when the water was mixed to below 100 meters, and B the similar curves on October 4 and 15 (two complete series on each day) when the water and plankton were stratified. Figure 2 C is the mean curve of all the experiments with cultures of marine phytoplankton as reported by Ryther (1956b).

Under the "winter" conditions, the phytoplankton at all depths within the euphotic zone showed the same relationship to light intensity. Surprisingly, the plants behaved as "sun" species, becoming fully light saturated at 5,000 foot candles, reaching half this value at 1,200 foot candles.

In October, three distinct curves were obtained with phytoplankton from the three depths. Those living in the surface waters, again acting as "sun" forms, behaved essentially the same as did the winter plankton from all depths. The phytoplankton collected from 50 meters (10% light) were intermediate in their response to light and their photosynthesis-intensity curve is almost identical to the average curve obtained with cultures (Figure 2 C). The plankton from 100 meters (1% light), on the other hand, behaved like "shade" plants, reaching light saturation below 1,000 foot candles.

DISCUSSION

The photosynthesis-light intensity curve obtained from algae cultures, reproduced in Figure 2 C, has been used in conjunction with chlorophyll concentration for calculating the natural rate of photosynthesis of marine phytoplankton (Ryther and Yentsch, 1957). This method assumes a constant assimilation number (photosynthesis per unit of chlorophyll at optimal light intensity) which is corrected for the natural light intensity from the ps-light curve, incident radiation, and submarine light penetration data.

This average curve obviously does not describe the behavior of the Sargasso Sea winter phytoplankton, which we have described as more typical of "sun" plants. However, a roughly bell shaped curve of this type, whether displaced to the right or left, is somewhat self-adjusting in that more or less photosynthesis at lower intensities is to some extent compensated by the reverse at higher intensities.

The curve in Figure 2 C is still a good average description of the behavior of phytoplankton within the whole euphotic zone in summer. However, the use of an average curve in this case would be quite misleading for it would result in the under estimation of photosynthesis both in the surface waters where intensities are high, and in deep waters where intensities are low. In other words, it does not take into consideration the light adaptation of both surface and deep plankton.

The broken curve in Figure 3 shows a hypothetical depth profile of daily photosynthesis in midsummer (820 langleys/day incident radiation), assuming a phytoplankton population evenly distributed with depth. This curve was calculated from Figure 2 C and actual radiation data as recorded at Newport, R. I. on June 17, 1954, and is a reproduction of Figure 5 in Ryther (1956b). The solid line in Figure 3 is a recalculation of the same profile using, in place of Figure 2 C, the three curves in Figure 2 B. As discussed above, daily photosynthesis at both the upper and lower limits of the euphotic zone is higher due to

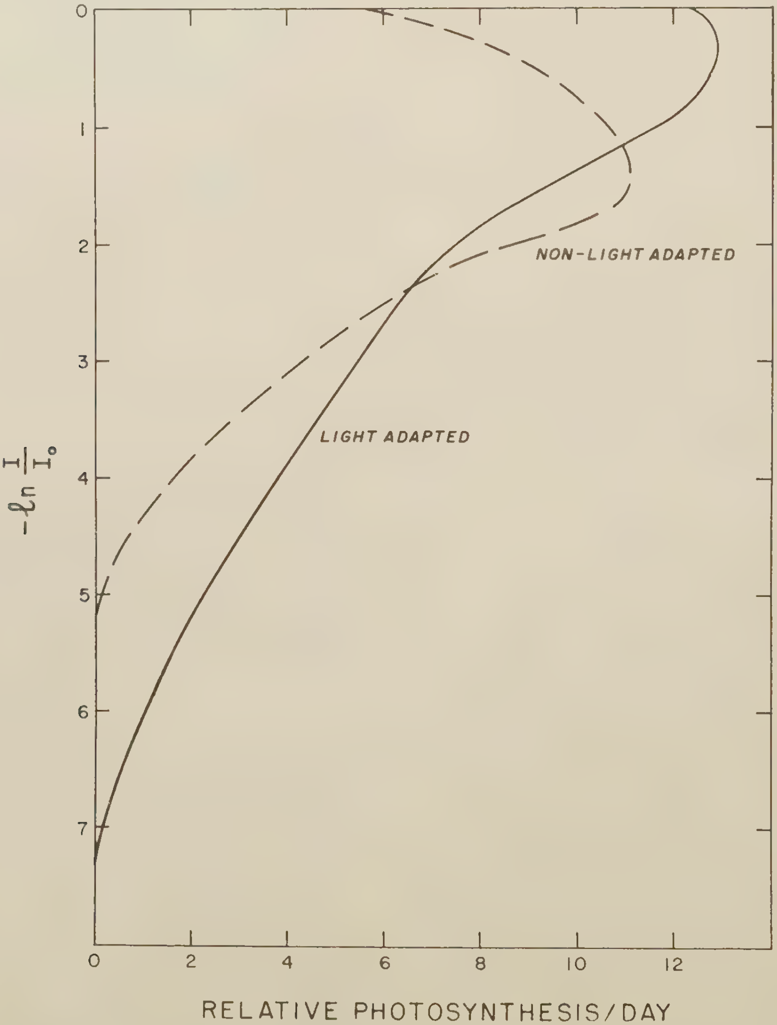

FIG. 3. Hypothetical depth profiles of daily photosynthesis by non light-adapted phytoplankton (calculated from Fig. 2 C) and light-adapted phytoplankton (calculated from Fig. 2 B).

light adaptation of the plants at these depths, while that at the intermediate depth remains nearly the same. The resulting daily rate of photosynthesis beneath a square meter of surface (*i.e.* the area of the curves in Figure 3) is some 30% greater for the light adapted algae. Under natural summer conditions, a greater discrepancy could be expected, since most of the phytoplankton occur near the lower limit of the euphotic zone (Figure 1B).

REFERENCES

Graham, H. W. and N. Bronikovsky (1944). The genus *Ceratium* in the Pacific and North Atlantic Oceans. Carnegie Inst. Wash. Publ. No. 565: 1-209.

Rabinowitch, E. I. (1951). Photosynthesis and related processes. Vol. II, Part I. Interscience Publishers, Inc., New York.

Rodhe, W.; R. A. Vollenweider; and A. Nauwerk (1958). The primary production and standing crop of phytoplankton. In, Perspectives in marine biology. A. A. Buzzati-Traverso, Ed., U. of California Press, Berkeley.

Ryther, J. H. (1956). Photosynthesis in the ocean as a function of light intensity. Limnol. & Oceanogr., **1:** 61–70.

Ryther, J. H. and C. S. Yentsch (1957). The estimation of phytoplankton production in the ocean from chlorophyll and light data. Limnol. & Oceanogr., **2:** 281–286.

Steemann Nielsen, E. (1934). Untersuchungen über die verbreitung, Biologie, und Variation der Ceratien im Sudlichen Stillen Ozean. Dana Rep. **4:** 1–67.

Steemann Nielsen, E. and E. A. Jensen (1957). Primary oceanic production. The autotrophic production of organic matter in the oceans. Galathea Rpts., **1:** 49–136.

Steemann Nielsen, E. and V. Kr. Hansen (1959). Measurements with the carbon-14 technique of the respiration rates in natural populations of phytoplankton. Deep Sea Res., **5:** 222–233.

Contribution No. 1043

Measurements of Bioluminescence off Monaco and Northern Corsica

BY

George L. CLARKE and Lloyd R. BRESLAU
*Harvard University, and Woods Hole Oceanographic Institution**

Measurements of underwater illumination made with the bathyphotometer in the Atlantic Ocean at depths down to 3750 m disclosed the presence of varying amounts of bioluminescence at all levels below those at which light penetrating from the surface interfered (Clarke & Wertheim, 1956; Clarke & Backus, 1956; and Clarke & Hubbard, 1959). The intensity of the brightest flashes was about 100,000 times the weakest light recorded as background illumination. Flashes occurred under different circumstances with frequencies of about 1 per minute up to more than 160 per minute. The duration of a flash, or a combination of flashes, ranged more than 10 sec to less than 0.2 sec. Wide variation in the frequency, duration, and intensity of flashing was observed at different depths, localities, and times of day. Similar findings in Pacific waters were reported by Boden and Kampa (1957) and Kampa and Boden (1957). Bioluminescence was recorded in the eastern Mediterranean by Boden and Kampa (1958) to a depth of about 200 m.

These observations indicated that bioluminescence is far commoner and in greater variety at various depths in the sea and perhaps plays a more significant role in the behavior of oceanic animals than previously supposed. Accordingly, the authors were particularly pleased to be invited by Commandant Jacques Cousteau, Director of the Oceanographic Institute, Monaco, to extend measurements to the deep regions of the Mediterranean off Monaco and northern Corsica during May and June 1958. Dr. and Mrs. Brian P. Boden, who were also scheduled to undertake an investigation from the Research Vessel *Calypso* during the same period, kindly shared the facilities of the ship with us. We

---

* Contribution N° 1043 from the *Woods Hole Oceanographic Institution.*

Bull. Inst. océanogr. Monaco, N° 1147, 24 juin 1959.

wish to express our appreciation not only to Commandant COUSTEAU but also to other members of the Oceanographic Institute and to the officers and crews of the *Calypso* and the *Winnaretta Singer* whose friendly cooperation made the successful completion of this work possible. We are also indebted to Miss Beatrice CROSBY for assistance in preparing this report. Our work was supported in part by funds from Research Grant N° 3838 of the U.S. National Science Foundation.

The observations recorded in this paper were carried out in May and June 1958 at five stations for which the positions and other pertinent data are given in Fig. 1 and Table 1. Stations A and B were located in the Villefranche canyon 8 to 14 miles south of Monaco. Stations C and D were in the deeper waters of the Ligurian Sea and Station E was in a different water mass to the east of Cap Corse. Observations made by the *Calypso* earlier in May showed that in the Ligurian Sea the temperature below 50 m departed but little from 13° C. Above this depth a sharp thermocline occurred, with surface temperatures ranging from 17.8° to 15.1° C.

The design and method of use of the bathyphotometer, as employed in this investigation, have been described by CLARKE and HUBBARD (1959). The calibration of the instrument was rechecked periodically. Measurements of the transparency of the water to daylight were made with the photometer window directed upwards. Observations intended primarily for the investigation of bioluminescence were made with the photometer reversed, that is, with the receiving window directed downward so that the effect of the light penetrating from the surface would be minimized. The instrument then recorded at each depth (1) the upward scattered light derived originally from the sunlight, skylight, moonlight, or starlight falling on the surface according to conditions and time of day, and (2) the bioluminescence from water beneath within a cone of 90°. Few, if any, flashes of luminescence are bright enough to be received from distances greater than 10 m and most probably come from much smaller distances (CLARKE & HUBBARD, 1959). Motion of the photometer, resulting from the roll of the ship or from rapid raising or lowering of the cable, would be expected to cause the instrument to strike nearby organisms or at least to produce turbulence in their vicinity. Either action would be likely to elicit a discharge from luminescent organisms within the volume of water affected. To the extent to which this is true the records show more luminescence than would occur in undisturbed water. When the photometer is quiet, naturally occurring luminescence is recorded; when it is agitated vigorously, the amount of luminescence revealed is probably maximal for this locality. With an approximately funiorm degree of agitation, as produced by the roll of the ship during the same weather conditions, or by reeling in or out at a constant speed or for a constant distance, the abundance of potentially luminescent organisms at different depths may be compared. As a supplementary study the luminescence camera described by BRESLAU and EDGERTON (1958) was also employed in an effort to photograph some of the animals producing luminescence at various depths.

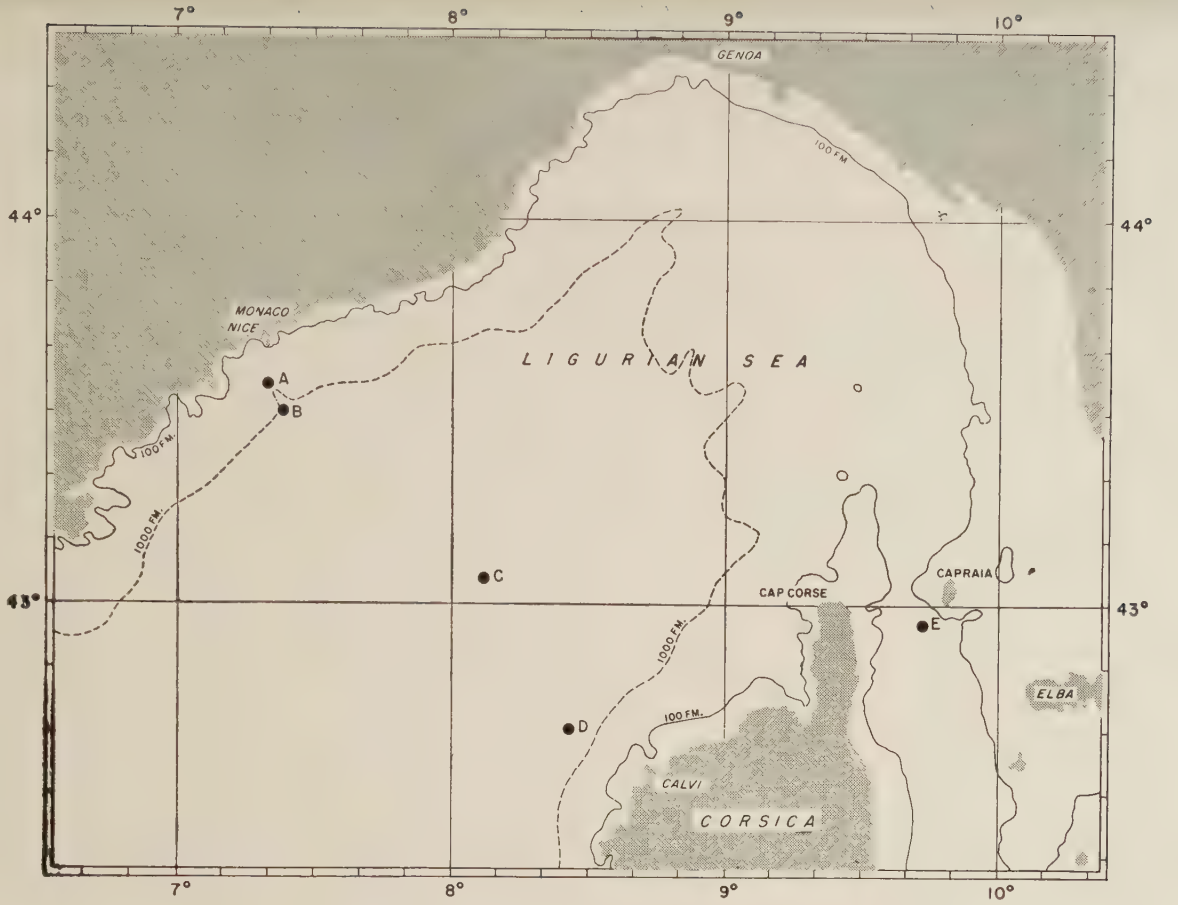
7°
8°
9°
10°
44°
43°
GENOA
100 FM
MONACO
NICE
LIGURIAN SEA
A
B
C
D
E
100 FM.
1000 FM.
CAP CORSE
CAPRAIA
ELBA
CALVI
CORSICA

FIG. 1. — Location of Stations occupied May 17 to June 8, 1958.

Table I

Summary of Station data

Station	Latitude	Longitude	Bottom Depth (meters)	Series	Figure	Date 1958	Time (European)	Sky	Sea	Wind
A	43°34'N	7°19'E	1400	2	3	May 17	1547-1647	Clear	1	0
				3	4	May 17-18	2350-0235	Clear, no moon	1	1
				7	5	May 20	0154-0402	Clear, no moon	0	1
B	43°30'	7°23'	1400-1960	15	6	June 7	1520-1842	Clear	1	1
				17	2	June 8	1120-1334	Clear	0	1
				18	7 & 8	June 8-9	24 Hours	Clear to cloudy	1	1
C	43°04'	8°07'	2560	10	9	May 22	0040-0202	Clear, no moon	2	3
D	42°40'	8°26'	2650	12	10	May 23	0945-1320	Scattered clouds	3	2
E	42°57'	9°43'	438	13	11	May 23	2209-2330	Clear, new moon	0	0

Transparency measurements made at Station B (Fig. 2) revealed a layer of clear water, with an average vertical extinction coefficient of k = .072, extending from the surface to a depth of about 80 m. Surface light was reduced to 1 % at 62 m and to 0.15 % at 80 m. Since the bathyphotometer is sensitive to the whole of the visible spectrum, part of the reduction of intensity was due to the rapid loss of light at the ends of the spectrum. Evidence that this effect was limited to the surface layers is provided by the fact that no significant change in the rate of light extinction occurred from 20 m to 80 m. In clear sea water radiation rather quickly becomes confined between 4300A and 5000A which is the region of greatest transparency and also of the greatest sensitivity of our photometer. Below 80 m the water was even more transparent with an extinction value of k = .035 for the stratum from 80 m to 350 m and of k = .029 from 350 m to 700 m. The transparency of the deeper water is thus one of the highest ever measured in the sea and approaches closely that of distilled water which was found to lie between k = .01 and k = .03 in the spectral region between 4359A and 4900A by Clarke & James (1939). In water with an extinction coefficient of k = .03 light is reduced by only 3 % for each meter traversed. At 600 m the ambient light of 2×10^{-5} μw/cm² was about 3×10^{-10} of the surface illumination. Jerlov and Piccard (1959) reported an extinction coefficient of k = .048 for the depth interval 100-300 m at a station 5 miles south of Capri.

Luminescent flashes greater than the ambient light, as received by the upward-directed photometer, first appeared on the record at 600 m. The ambient light values recorded below that depth are for the level of the illumination between individual flashes. As the daylight was further reduced at successively greater depths, weaker and weaker flashes could be detected, so that the total number recorded per unit time became greater. The intensities of the brightest flashes observed during this series of measurements at each depth are indicated by the broken horizontal lines. The dash-and-dot extension of the line at 700 m shows the intensity of the most intense flash observed at this depth during another measurement at this station.

The curve of light penetration indicates a lower rate of extinction below 700 m. The effect is probably not due to the occurrence of more transparent water but is almost certainly due to overlapping bioluminescent flashes in the background contributing a significant fraction to the ambient light at these depths. The illumination at 800 m was recorded as 2×10^{-7} μw/cm² or 3×10^{-12} of the surface intensity. If the same rate of extinction had continued below 700 m, the intensity of daylight at 800 m would have been about 6×10^{-8} μw/cm², or a little less than 10^{-12} of surface light. Individual flashes of luminescence were often more than 100 × the intensity of the background light and one was more than 10,000 × this value. No further reduction in the response of the instrument was observed below 800 m. The response probably represents the dark level of the instrument, but since this tends to drift, a portion of the value recorded below 800 m may have been due to background

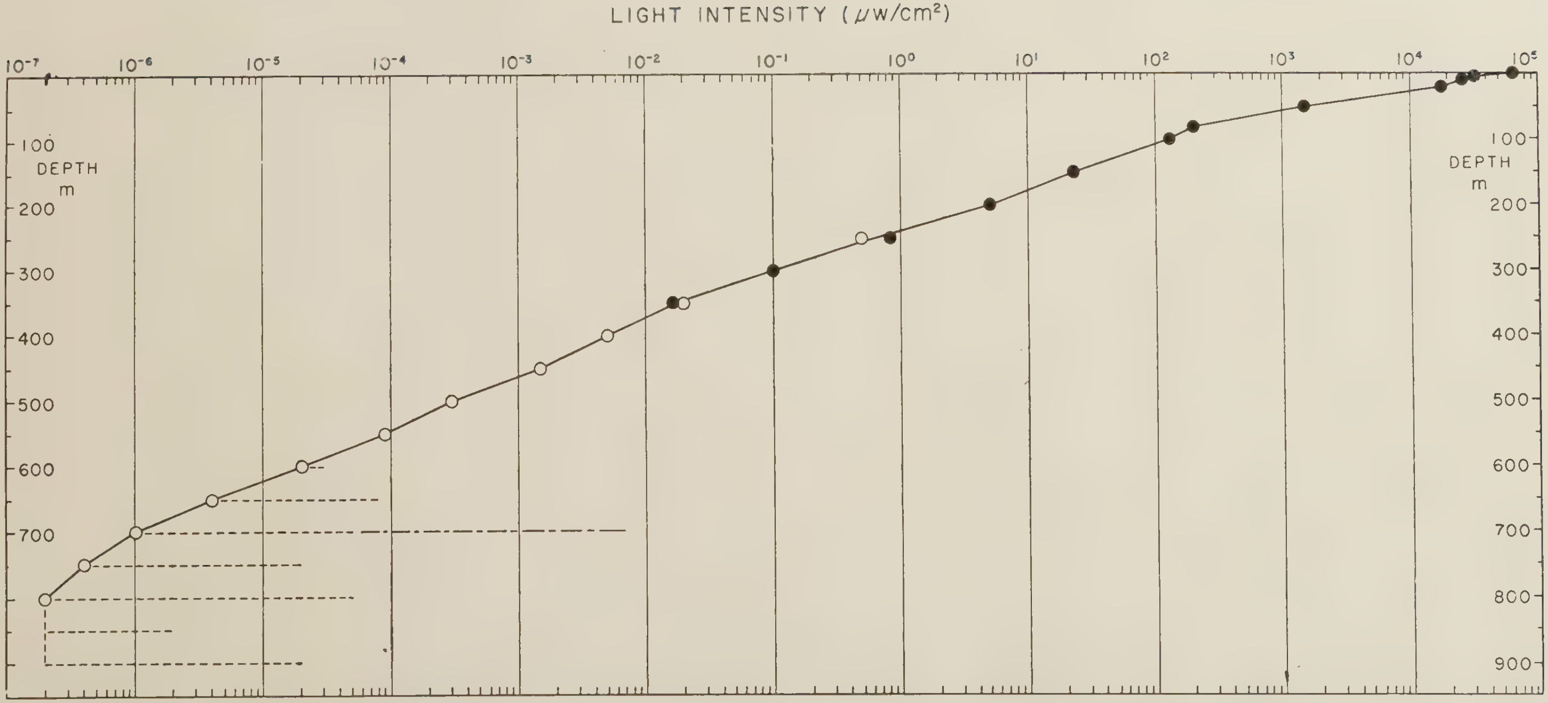

FIG. 2.—Relation between depth and light intensity (logarithmic scale) at Station B between 1120 and 1334 hours on June 8.

bioluminescence. Since the response of the instrument is logarithmic, slight drifts in dark level have only a trivial effect on the calibration values for higher intensities.

The studies of bioluminescence at Station A in the Villefranche canyon consisted of one daytime and two nighttime runs. Excerpts from the day series (Fig. 3) show that the first detectable luminescence occurred at 360 m where the upward scattered daylight received on the inverted photometer had an intensity of about 5×10^{-4} μw/cm², or about 2 ½ % of the downward passing light. Luminescent flashes appear as small peaks reaching 10^{-3} μw as a maximum. At a depth of 600 m the ambient light level had dropped below 10^{-6} μw/cm² and the largest number of flashes (64 in one minute) was observed. At 700 m the ambient light was reduced to less than 10^{-7} μw and at 800 m it had reached the dark level of the instrument which at this time was at about 10^{-8} μw. At 700, 800, 900 and 1200 m the number of flashes observed per minute was progressively less. The deepest of these records was made at a depth only 100 m or so above the bottom. During these observations the sun was very bright, the sea calm, and the ship steady.

During the following night, with the sea remaining calm, a second series of measurements from the surface to the same depth was carried out. Excerpts from this series (Figure 4) show that the ambient light between flashes diminished rapidly with increasing depth to a value of 10^{-6} μw at 100 m, and then more slowly to about 5×10^{-7} μw at 250 m. The drop to 1×10^{-7} μw at 500 m and the subsequent rise to somewhat greater values are probably due to the drift of the dark level of the instrument. These slight changes might also conceivably be due to differences in background light produced by many weak, overlapping flashes. The greatest amount of luminescence was observed at 50 m where single and multiple flashes occurred in profusion. Many fewer flashes occurred at 100 m and the discharges showed a periodicity of about 5 or 6 sec. Since this corresponds to the approximate period of the ship's roll, it is probable that the flashing was in large measure caused by the movement of the photometer. There was little change in the amount of luminescence from 100 to 200 m and only a slight reduction at levels down to 400 m (Table 2). Below that depth frequency of flashing diminished but rose to a secondary maximum at 700 m. The much lower number at 600 m than had been observed during the day may be accounted for by a movement of animals toward the surface at night.

Two days later a second night series was run at approximately the same locality. With a calmer sea the generally lower rate of flashing observed is probably accounted for by the reduced rolling of the ship and a consequent lessened movement of the photometer in the water. In order to test the degree to which agitation of the water by the photometer might influence the frequency of flashing, the arm of the crane, over which the wire leading to the photometer passed, was raised and lowered as rapidly as possible at designated times. This resulted in a vertical oscillation of the cable with amplitude of about 3 m in a period of about 12 sec. The effect of this agitation may be observed in the

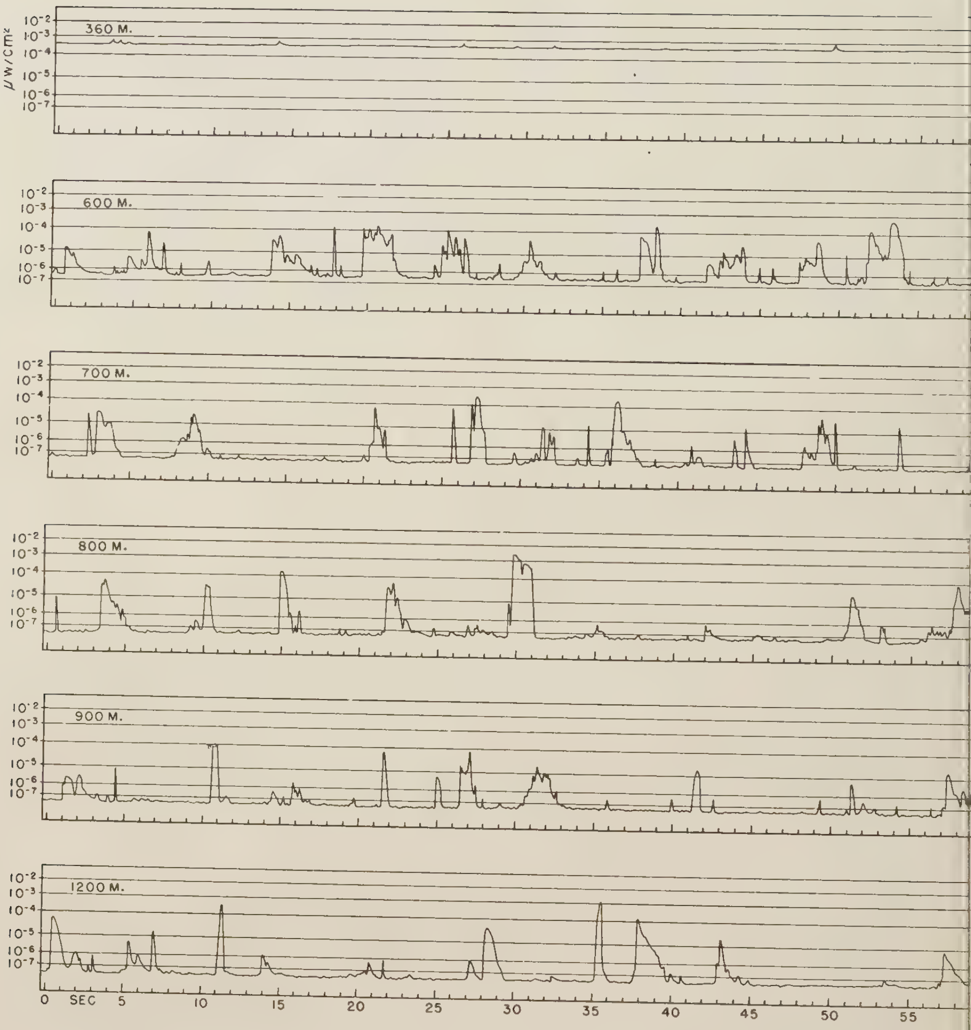

FIG. 3. — Sections of record at Station A May 17, 1547-1647 hrs, showing light received by inverted photometer at indicated depths. Bottom depth 1400 m.

strips of record, marked (AG) or (A) at 100 m, 800 m, and 1100 m (Fig. 5). In all cases the amount of luminescence was increased. At 1100 m, particularly, bursts of light flashes occurred about every 12 sec. However, added agitation did not cause a noticeable increase in the maximum brilliance of the flashes nor in the number of large flashes; its chief effect was to produce a larger number of the smaller flashes. The foregoing shows that each series of records must be interpreted in relation to the sea conditions and the consequent variation in the amount of agitation of the photometer. When different levels or localities are

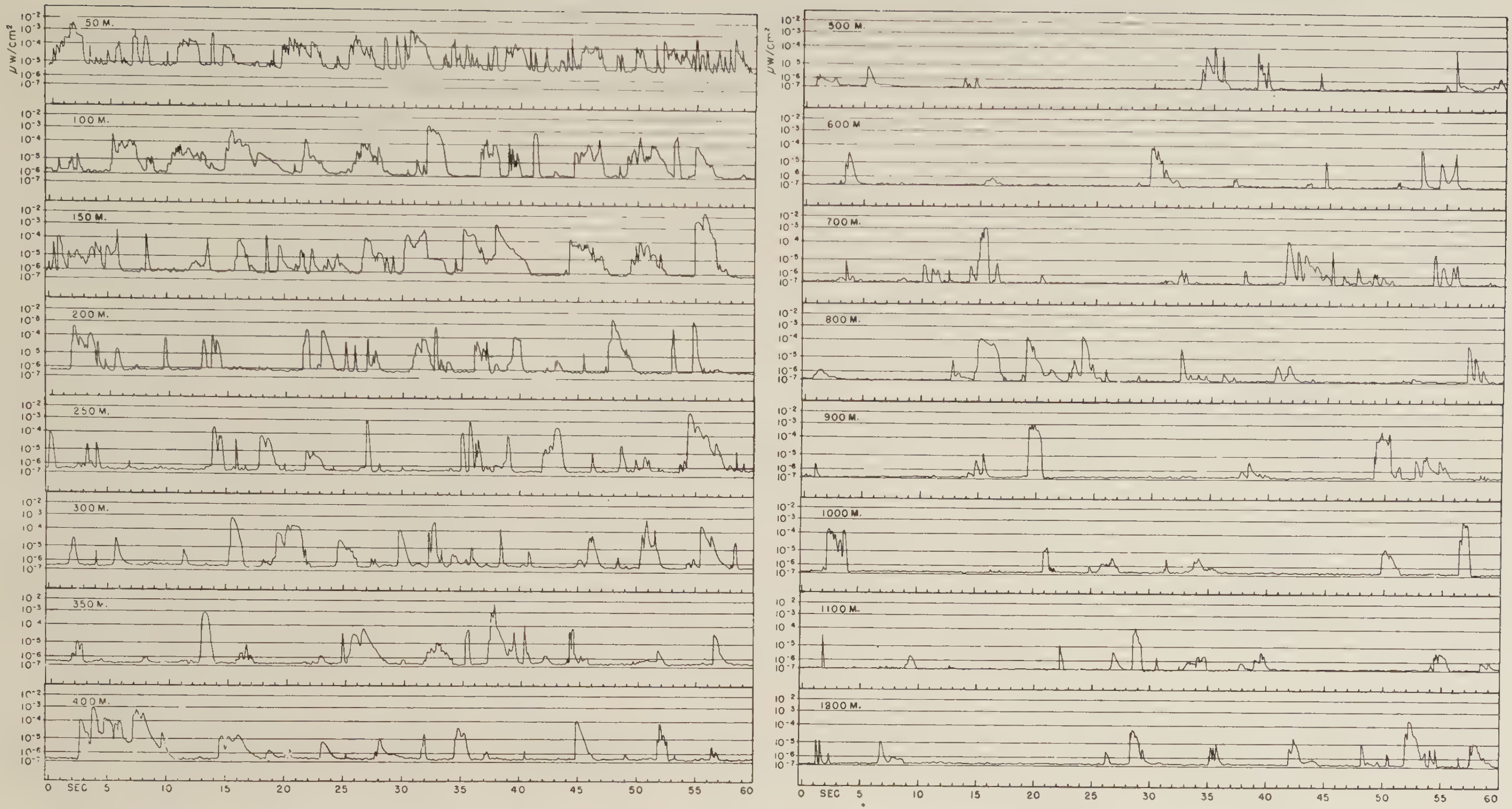

FIG. 4. — Sections of record at Station A, 2350 hrs, May 17, to 0235, May 18. Bottom depth 1400 m.

Table 2

Frequency distribution of flashes of indicated intensities.

Station A ; May 17-18, 1958 ; Time 2350-0235 hrs, Series 3.

Depth (Meters)	Number of flashes per minute					
	10^{-2} to 10^{-3} μw/cm²	10^{-3} to 10^{-4} μw/cm²	10^{-4} to 10^{-5} μw/cm²	10^{-5} to 10^{-6} μw/cm²	10^{-6} to 10^{-7} μw/cm²	Total
50	3	45	55	—	—	103
100	2	15	33	18	—	68
150	3	10	32	20	2	67
200	2	6	20	18	6	54
250	1	7	16	15	11	53
300	0	8	12	17	8	45
350	1	3	10	13	9	36
400	0	7	13	10	10	40
500	0	1	6	8	11	26
600	0	0	9	2	13	25
700	1	3	4	19	17	44
800	0	3	5	8	17	32
900	0	5	2	8	16	31
1000	0	5	5	8	11	29
1100	0	1	3	12	11	26
1200	0	1	8	15	13	37

to be compared, records should be used, as far as possible, which were made within a short period of time and under the same sea conditions. Variation in agitation due to slight changes in sea condition did not obscure the differences in luminescence at various levels in the present study. Thus when the records of May 17-18 are compared with those made May 20 without extra agitation, they show the same diminution in luminescence with increasing depth even though flashing was generally less on the latter occasion.

Observation of bioluminescence at Station B, about 5 miles farther offshore in the Villefranche canyon, embraced a daytime series at depths from 400 m to 1400 m and a 24-hour continuous record at 700 m. During the day series the intensity of the ambient light received by the inverted photometer dropped from 10^{-4} μw/cm² at 400m to about 4×10^{-8} μw at 700 m where it approached the dark level of the instrument (Fig. 6).

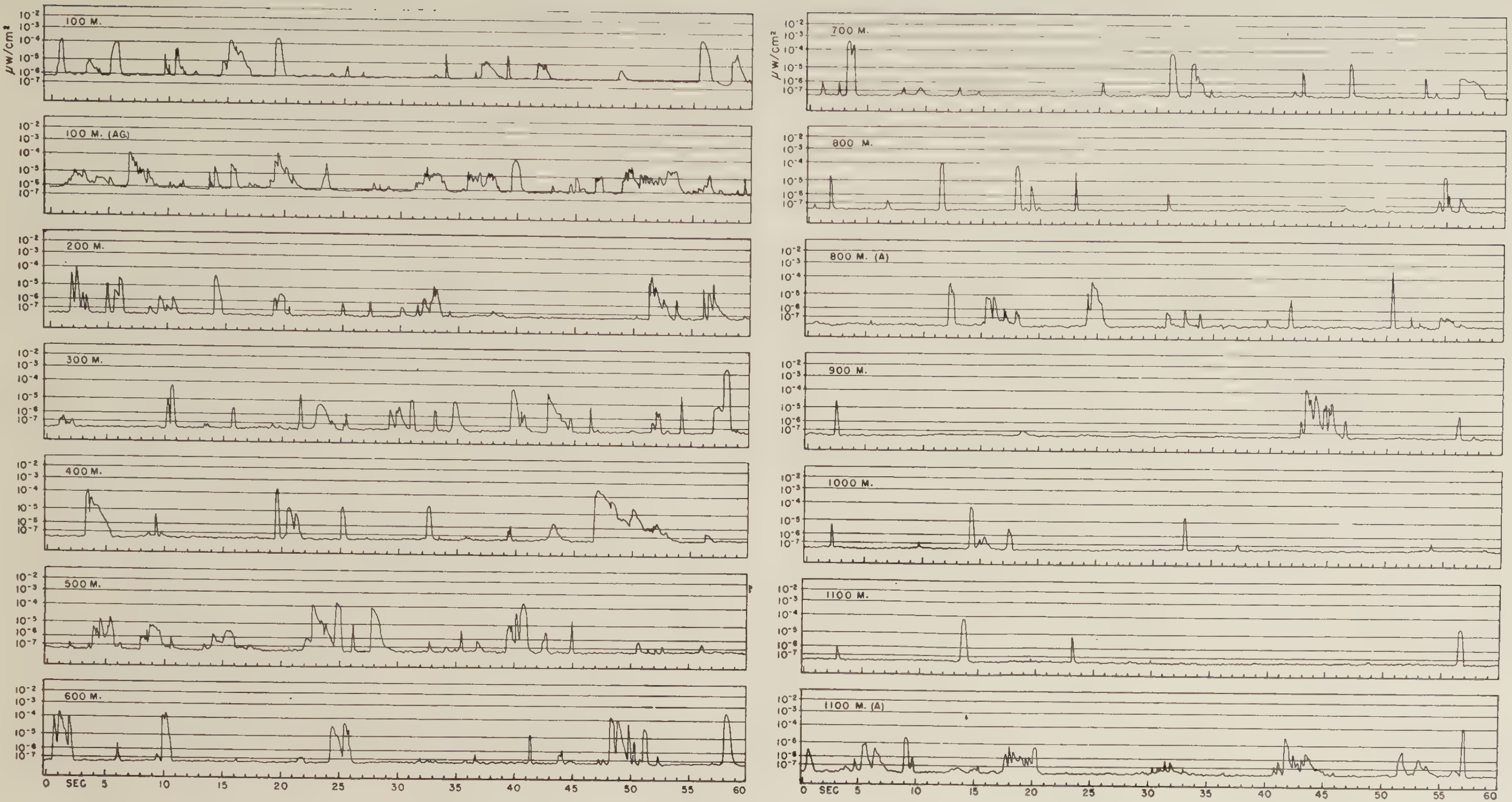

FIG. 5. — Sections of record at Station A, 0154-0402 hrs, May 20. Bottom depth 1400 m. AG or A = photometer agitated by raising and lowering crane.

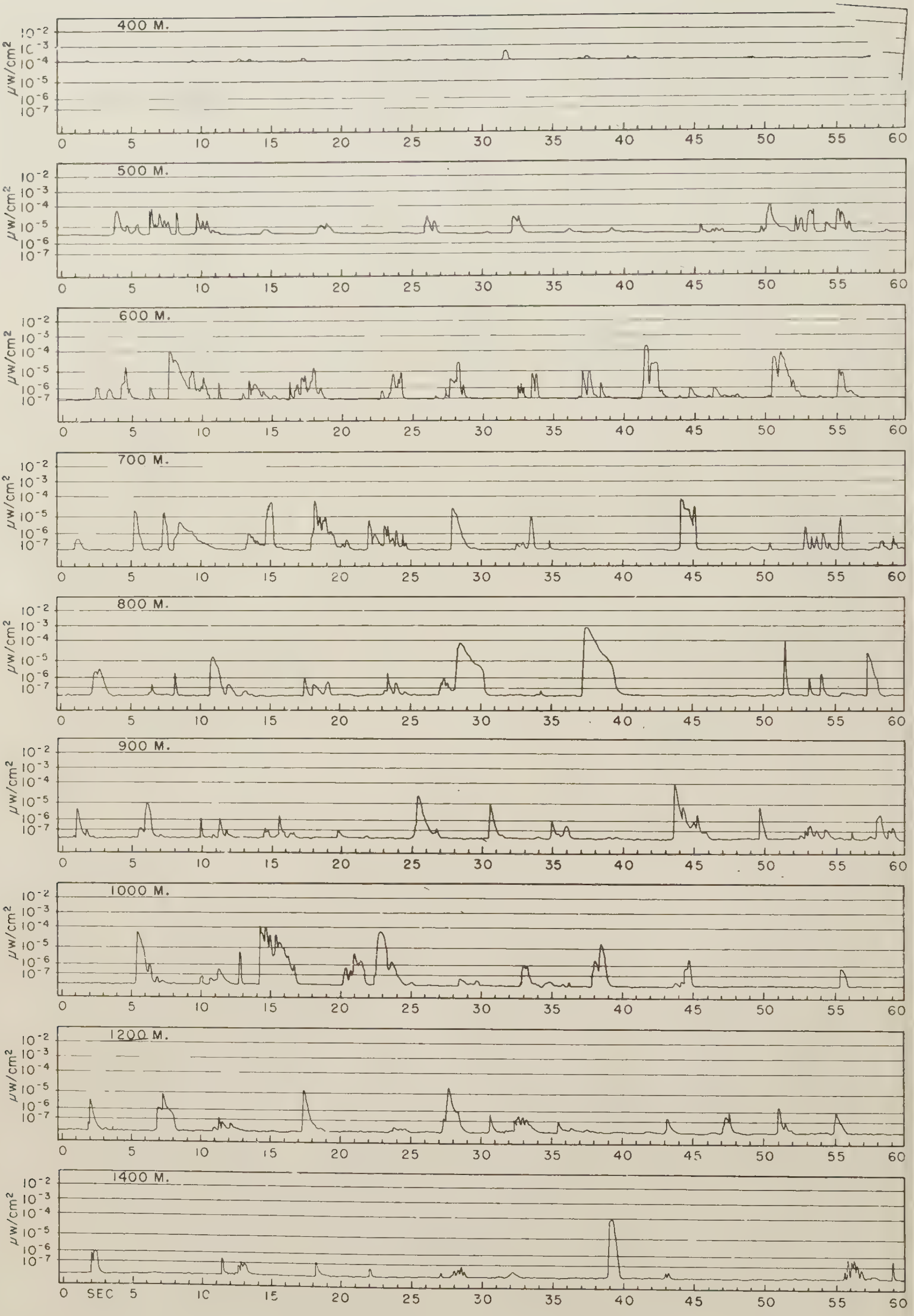

FIG. 6. — Sections of record at Station B, 1520-1842 hrs, June 7. Bottom depth 1880 m.

At successively greater depths the slight further drop in the position of the tracing between flashes was probably due to a drift in the dark level but it may also have been influenced by a reduction in background luminescence. It is of interest to compare the foregoing values for the ambient light received by the inverted photometer with those received by the upward-directed photometer which were made at the same station on the following day and have been presented in Fig. 2. Comparison is hindered by the fact that the latter series was made in the middle of the day whereas the former was carried out in the late afternoon and the fact that there was a ten-fold difference in the dark levels of the instrument. Subject to the attendant uncertainties, we found that the upward-passing light varied between 0.5 % and 3.0 % of the downward-passing light at the same level at depths ranging from 400 m to 700 m. The regular reduction of ambient light received by the inverted photometer at each level down to 600 indicates that this light is made up mostly of upward-scattered daylight. Probably some scattered daylight is included in the value at 700 m along with background luminescence but no upward light could be detected below that depth. Daylight was definitely detected by the upward-directed photometer at 700 m and probably contributed to the value obtained at 800 m.

The intensity of flashes observed at 400 m ranged between 10^{-4} and 10^{-3} μw/cm but no flashes brighter than 10^{-4} μw were recorded at 500 m and only occasional strong flashes occurred at other depths. The largest total number of flashes in one minute was found at 600 m which is the same depth at which the maximum was observed during the daylight series at Station A. Below 600 m the rate of flashing became progressively less; at 1400 m only one discharge brighter than 10^{-6} μw occurred during the sample minute of observation with relatively few smaller flashes.

The continuous 24-hour record of luminescence at 700 m began at 1400 hrs on June 8. No other observation in the present study nor in those previously reported, extended for more than about an hour at any one depth. The object was to determine the extent of variation at one place from minute to minute, from hour to hour, and from day to night. During the course of these observations the wind was light and the sea calm so that the *Winnaretta Singer*, which was used for the work at Station B only, drifted only slowly. Only once, after a drift of about 5 miles had occurred, at about 0500 hrs on June 9, was it necessary to reel the cable in and run the ship back to its original position. The record made at slow speed showed no important or consistent change during the whole period. Two 20-minute sections of the record, reproduced in Fig. 7, were selected as representing examples of the greatest amount of variability from minute to minute which was observed due presumably to brifting into and out of patches of luminescent organisms. Such possible fluctuation must be taken into account in comparing short records from one body of water with another. To minimize this source of error excerpts of records showing maximum luminescent activity have been used for comparison at each level and locality. In the present

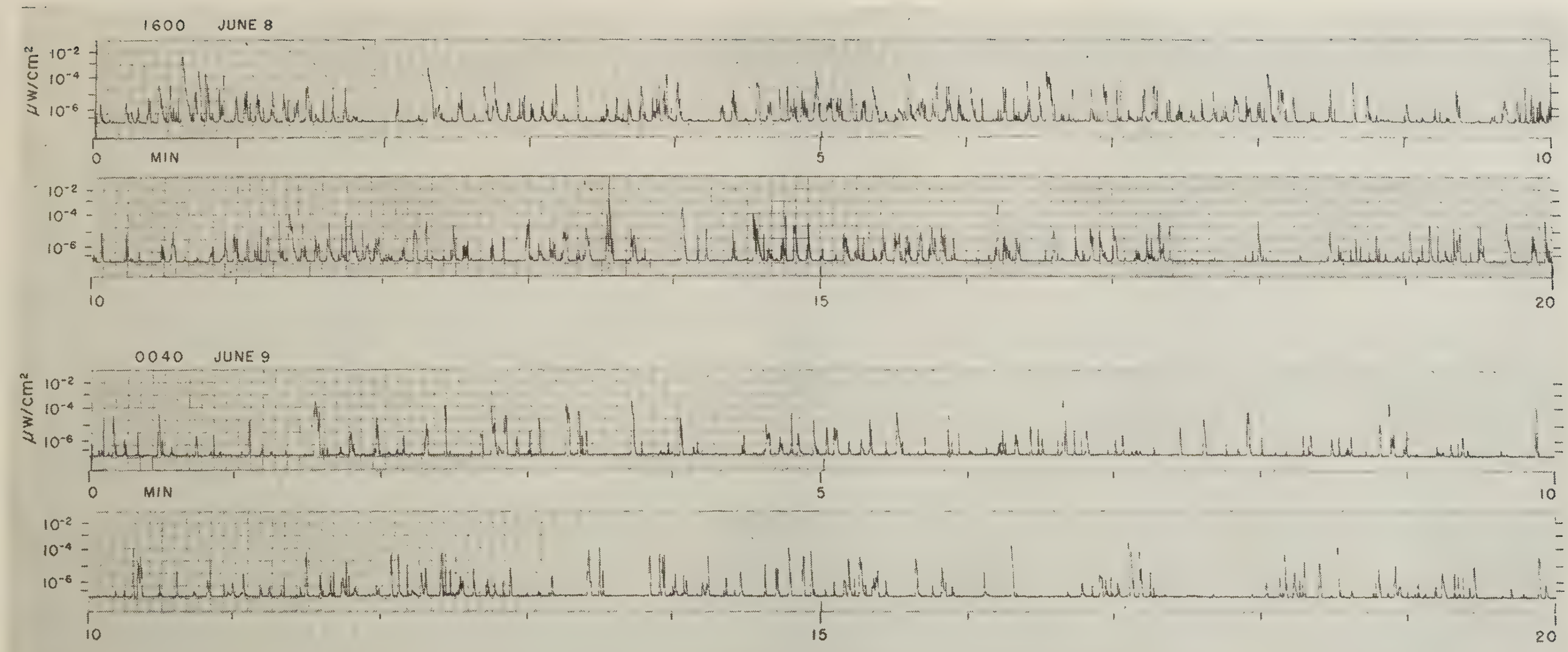

FIG. 7. — Two 20-minute continuous records at 700 m at slow speed of recorder at 1600 hrs on June 8 and at 0040 on June 9, with ship drifting in vicinity of Station B. Bottom depth varying from 1400 to 1960 m.

series at hourly intervals the recorder was switched for five minutes to the fast speed used in other series. Typical one-minute sections of these records from 1630 on June 8 to 0325 on June 9 are reproduced in Fig. 8. A variety of bright and weak flashes occurred in all sections. Considerable variation in total number occurred from hour to hour but no noticeable change was found when the sun disappeared at sunset (1925 hrs) or after dark that could be correlated with any significant diurnal vertical migration of planktonic or nektonic animals present.

Station C in the deep water midway between Monaco and Corsica was occupied in the middle of the night. A strong wind with moderate sea caused the ship to roll regularly and provided a uniform agitation of the photometer. The night was sufficiently dark, with no moon, so that detailed measurements of luminescence could be made at shallow depths, as well as at levels down to 700 m (Fig. 9). The effect of the ship's roll on luminescence was discernible at all depths although it was more pronounced at some levels than at others. At 1 m and 8.5 m a very large number of short flashes was observed superimposed upon background illumination penetrating from the surface and producing light fluctuating around an average value of about 10^{-4} μw/cm². At 8.5 m the amplitude of the flashes was slightly larger and the average illumination slightly lower. At 20 m the intensity of light between flashes dropped to 10^{-5} μw but at no depth down to this level did any flash or combination of flashes reach intensities greater than 10^{-3} μw. Quite a different picture was presented by the populations existing at 50 m and 75 m with many individual flashes exceeding 10^{-3} μw. The ambient light dropped below 10^{-5} μw at 50 m and below 10^{-6} μw at 75 m. The frequency of flashing reached its highest value at these levels (Table 3). Most of the flashes were of extremely short duration, in many instances so short that the descending trace of the recorder needle is indistinguishable from the rising trace for a good part of its length. At 100 m many fewer flashes were encountered and the number continued to drop off from this depth down to the limits of the observations at this station. However, the range of the intensity of the light flashes remained about the same from 50 m to 700 m.

Daytime measurements were made at Station D about 28 miles southeast of the previous station following a sharp storm in the early morning. Trouble was encountered with drift of the recorder response during this series, probably due to a bad connection which was subsequently detected and corrected. In the first section of the record made at 600 m relatively few flashes (20 in one minute) occurred above the ambient light level of less than 10^{-5} μw and the brightest flashes were less than 10^{-4} μw/cm² (Fig. 10). At 700 m only an occasional bright flash was obtained and at 800 m the scarcity of flashing was remarkable even though the ambient had been reduced to such a point that even weak flashes would have been recorded. An increase in the abundance of flashing animals occurred at 900 m and 1000 m (about 30 in one minute) but numbers fell again and a very sparse population was recorded at 1800 m, the greatest depth attained and about 850 m above the bottom.

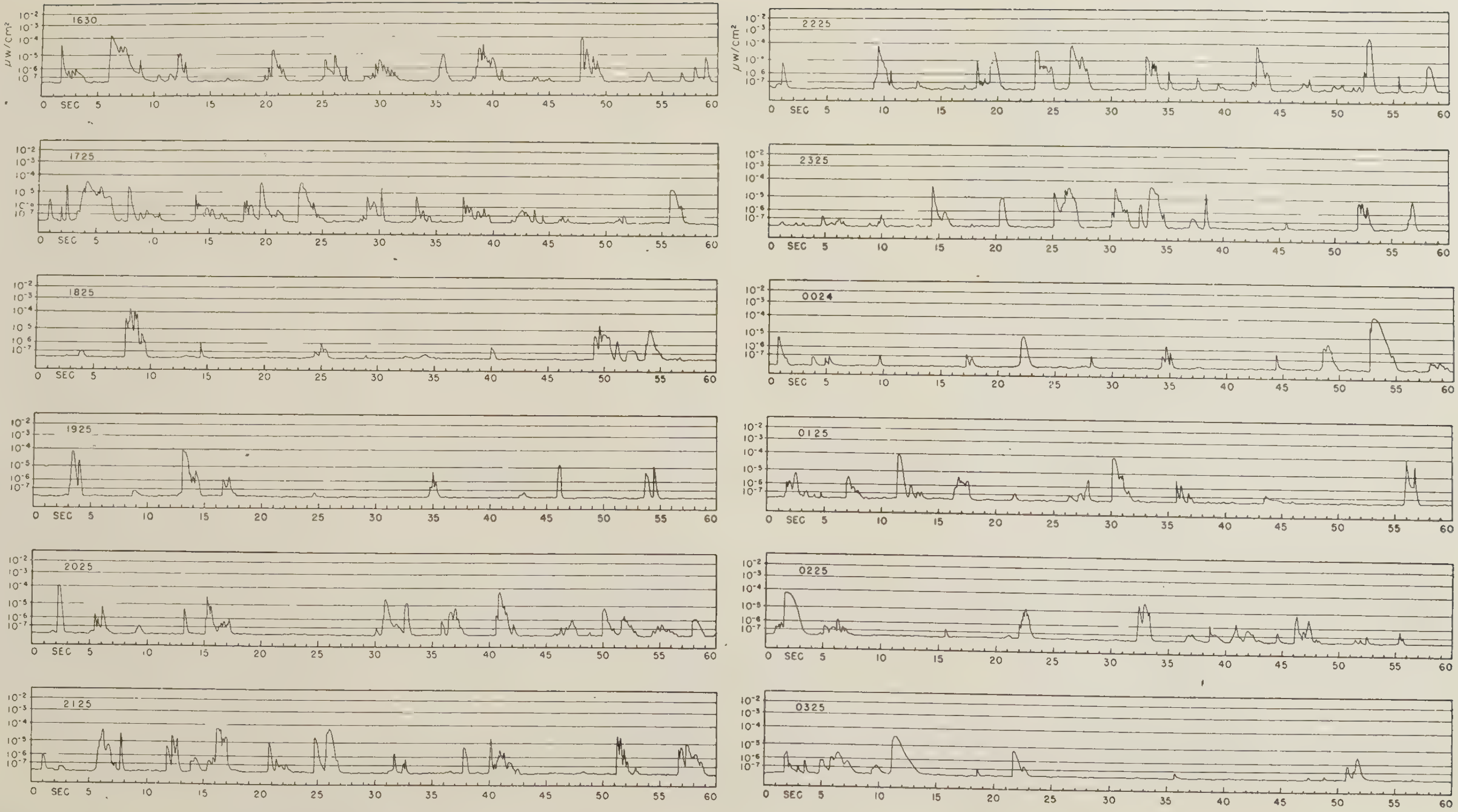

FIG. 8. — Sections at fast recorder speed of continuous record at 700 m at Station B on June 8-9 at the indicated hours.

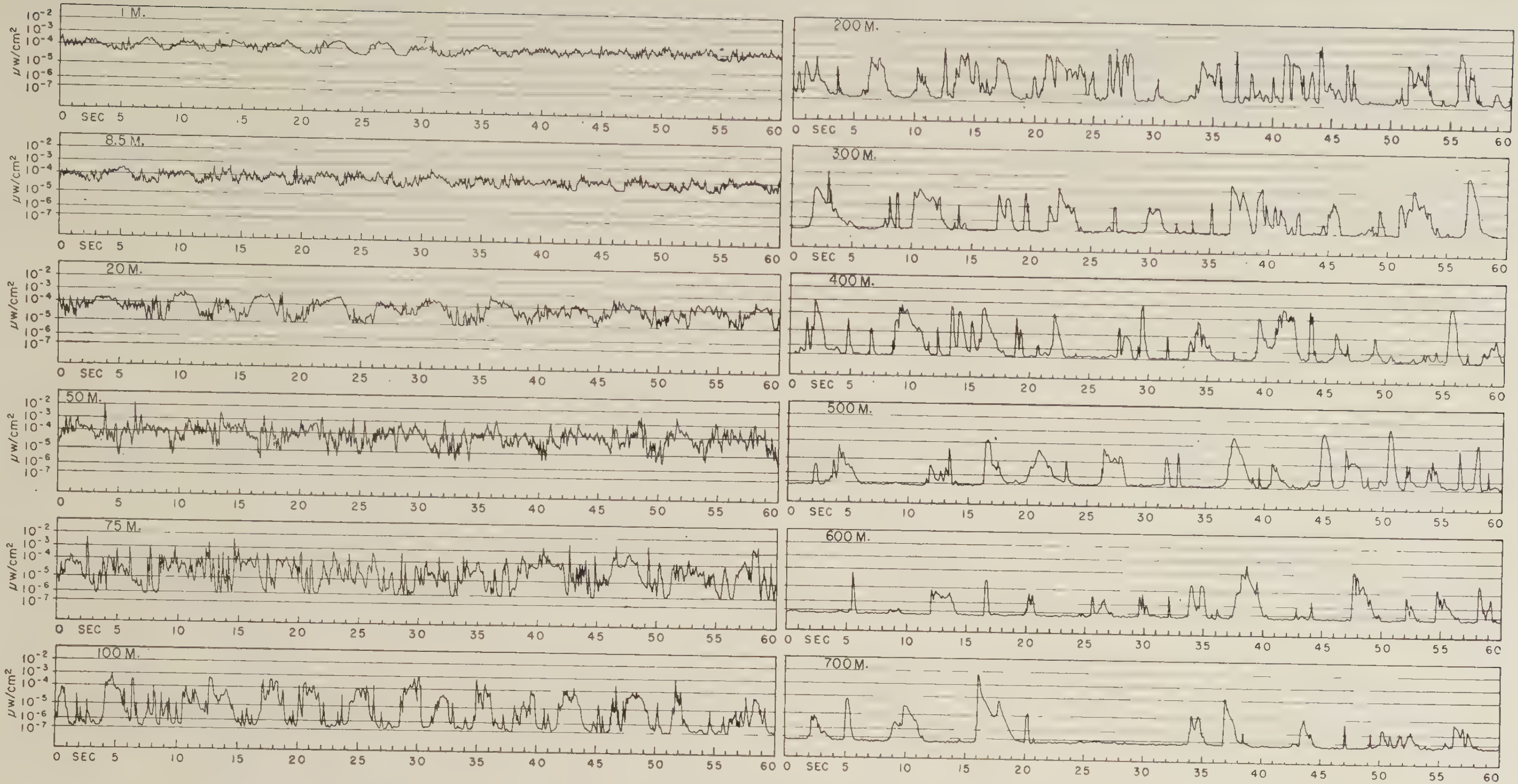

FIG. 9. — Sections of record at Station C, 0040-0202 hrs, May 22. Bottom depth 2560 m.

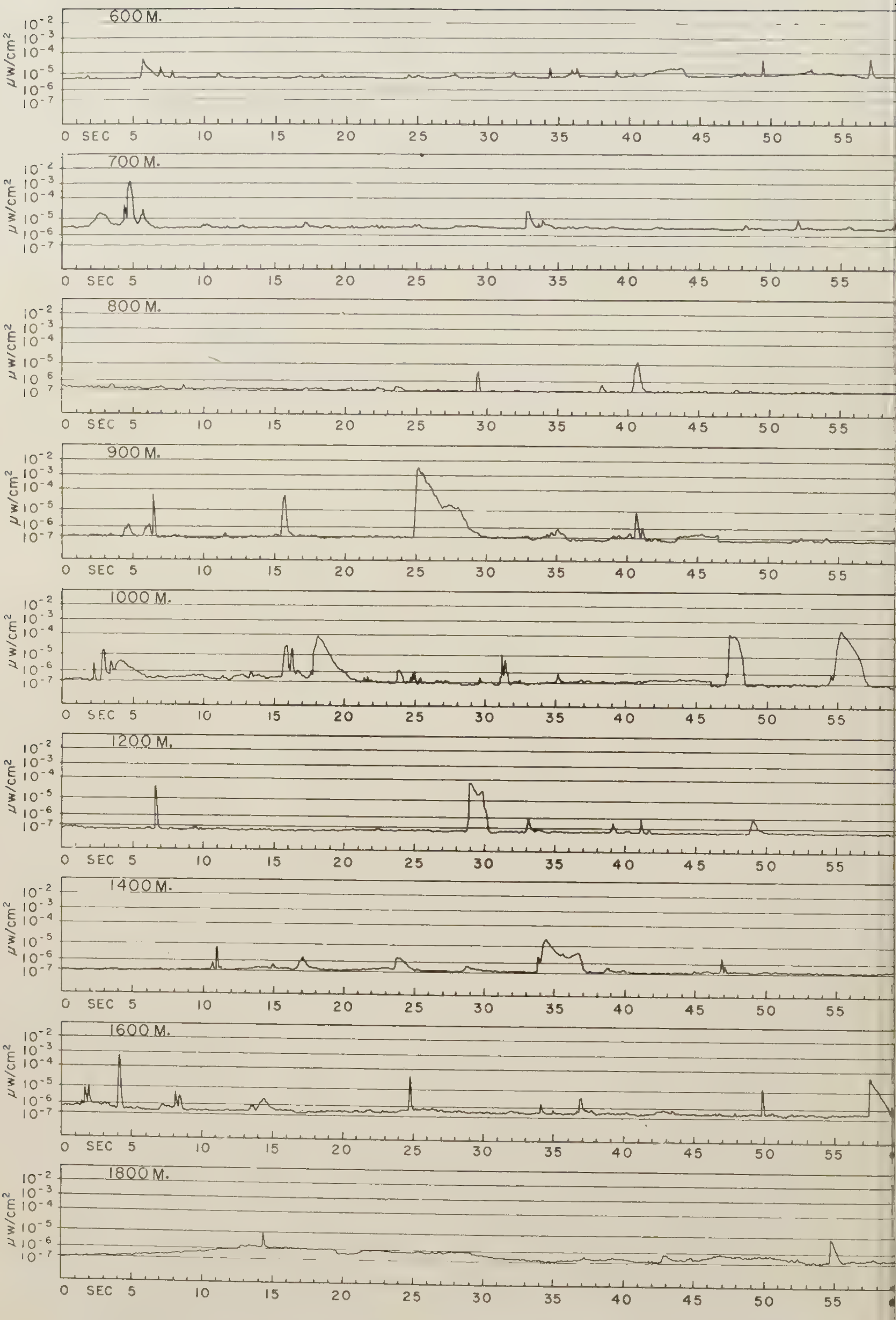

FIG. 10. — Sections of record at Station D, 0945-1320 hrs, May 23. Bottom depth 2650 m.

Table 3

Frequency distribution of flashes of indicated intensities.

Station C; May 21-22, 1958; Time 0040-0202 hrs, Series 10.

Depth (Meters)	Number of flashes per minute					
	10^{-2} to 10^{-3} μw/cm^2	10^{-3} to 10^{-4} μw/cm^2	10^{-4} to 10^{-5} μw/cm^2	10^{-5} to 10^{-6} μw/cm^2	10^{-6} to 10^{-7} μw/cm^2	Total
1	0	65	13	—	—	78
8.5	0	56	28	—	—	84
20	0	45	36	—	—	81
50	14	68	34	—	—	116
75	9	39	50	5	—	103
100	0	17	36	21	8	82
200	4	17	29	14	8	72
300	2	4	24	10	13	53
400	0	16	17	14	12	59
500	2	3	17	18	6	46
600	0	3	9	18	11	41
700	1	1	6	13	7	28

Since the sea was rough, with a great deal of ship motion, there was unquestionably more agitation of the photometer than on any previous day. Presumably, most, if not all, of the potentially luminescent animals near the photometer were stimulated and their flashing recorded on this occasion.

Station E was occupied during the night, with crescent moon, bright stars, very calm sea, and practically no ship roll. Observations were made from 25 m to 400 m in water that was 438 m deep. At each depth for which excerpts are presented, a record was made with the winch stopped, so that there was no agitation of the photometer (Fig. 11a). Immediately afterwards a second section of record was obtained with a standard amount of agitation produced by means of raising and lowering the crane (Fig. 11b). Comparing the two sets of records from the figures and from Table 4, it is seen that without agitation luminescence was scarce at 25 m but slightly more abundant at 50 m. Flashing reached a maximum at 100 m and then dropped to a minimum at 300 m. There is some indication of an increase in luminescence at greater depths

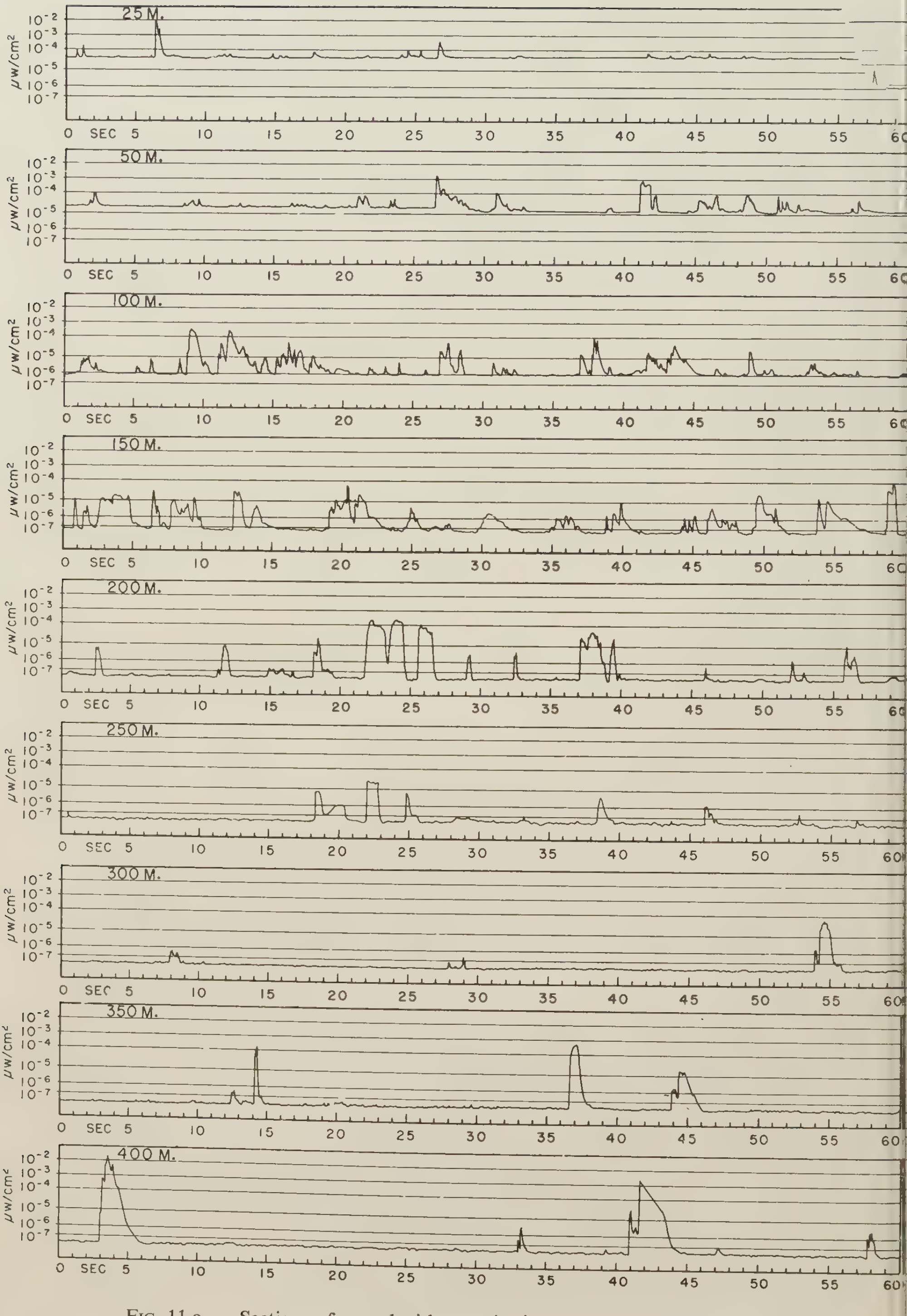

FIG. 11 a. — Sections of record with no agitation of the photometer at Station E, 2209-2330 hrs, May 23. Bottom depth 438 m.

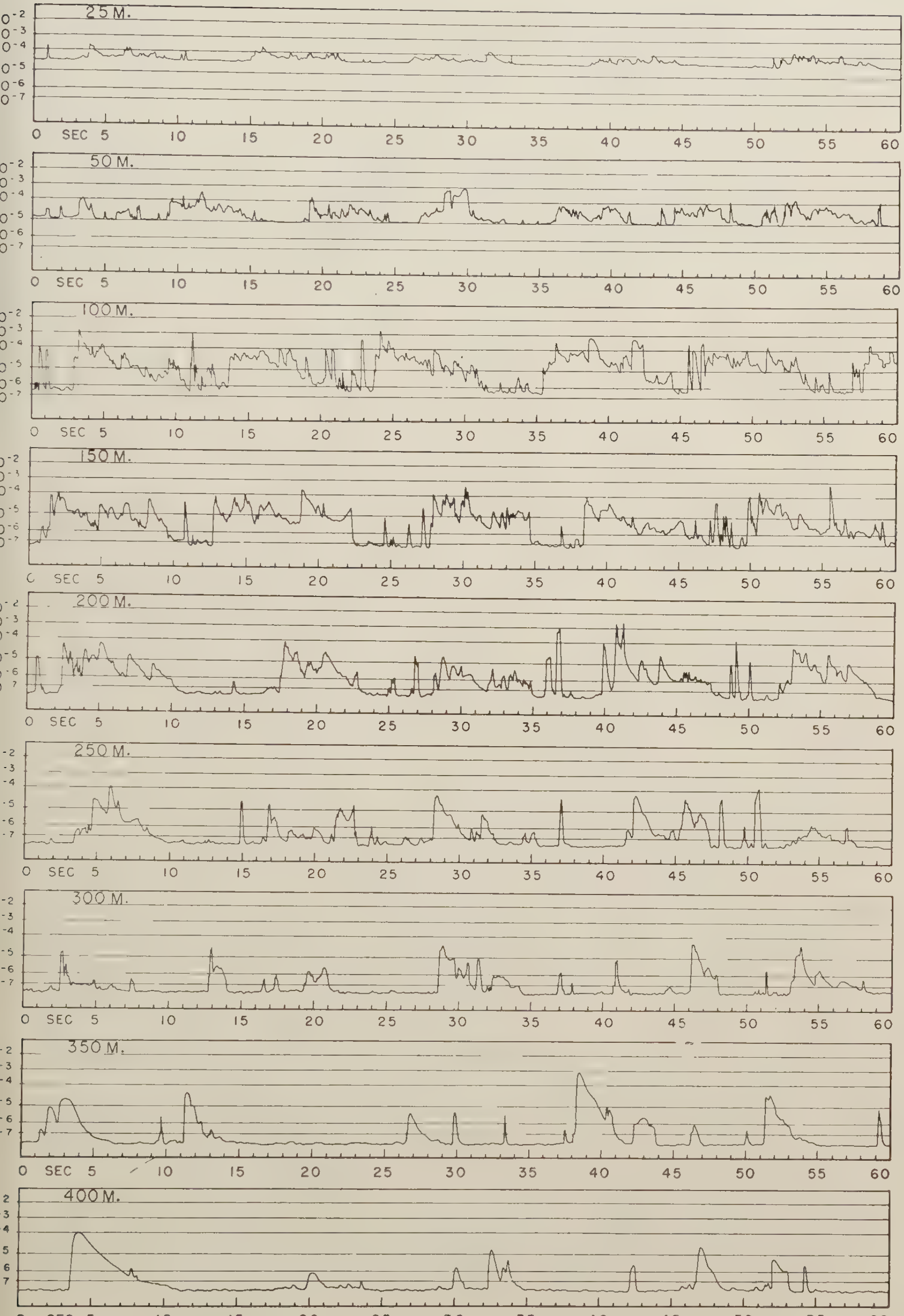

FIG. 11 b. — Sections of record with agitation produced by raising and lowering the crane at Station E, 2209-2330 hrs, May 23. Bottom depth 438 m.

Table 4

Frequency distribution of flashes of indicated intensities.

Station E ; May 23, 1958 ; Time 2209-2330 hrs ; Series 13.

N = No agitation, A = Agitation of photometer.

Depth (Meters)	Number of flashes per minute											
	10^{-2} to 10^{-3} $\mu w/cm^2$		10^{-3} to 10^{-4} $\mu w/cm^2$		10^{-4} to 10^{-5} $\mu w/cm^2$		10^{-5} to 10^{-6} $\mu w/cm^2$		10^{-6} to 10^{-7} $\mu w/cm^2$		Total	
	N	A	N	A	N	A	N	A	N	A	N	A
25	2	0	3	12	21	47	—	—	—	—	26	59
50	1	0	4	14	35	72	—	—	—	—	40	86
100	0	2	2	11	18	62	35	24	—	4	55	103
150	0	0	0	9	18	41	22	27	10	12	50	89
200	0	3	2	2	8	23	8	25	7	8	25	61
250	0	0	0	2	3	11	4	10	4	22	11	45
300	0	0	0	0	1	7	1	12	3	10	5	29
350	0	0	2	1	2	4	2	10	2	6	8	21
400	3	0	1	0	1	3	4	8	2	3	11	14

in respect to the larger flashes. Indeed, at 400 m the brightest flash ever recorded, over 10^{-2} $\mu w/cm^2$, was observed. Turning to the records made during periods of agitation, it is observed that more luminescence was recorded at each level, but that the picture of relative abundance, and of the type of luminescent flashing, remained essentially the same. Moderate luminescent activity occurred at 25 m with few large flashes. Maximum luminescence was again found at 100 m with the brightest flashes more intense than those at either 50 m or 25 m. At greater depths the number of flashes diminished but individual flashes were practically as intense as at shallower depths.

Further tests of the effect of agitation were made from the research vessel *Calypso* while she lay at the quay in Calvi Harbor during the evening of May 22 when there was no moon and a partly cloudy sky. The photometer was lowered in the inverted position to a depth of 5 m. None of the lights from the ship or from the shore shone directly into the water in the vicinity of the photometer but the sky was somewhat illuminated by the lights of the town. The record at A (Fig. 12), made when the cable was motionless, shows a number of flashes that occurred in the undisturbed water. At B the cable supporting the photometer was

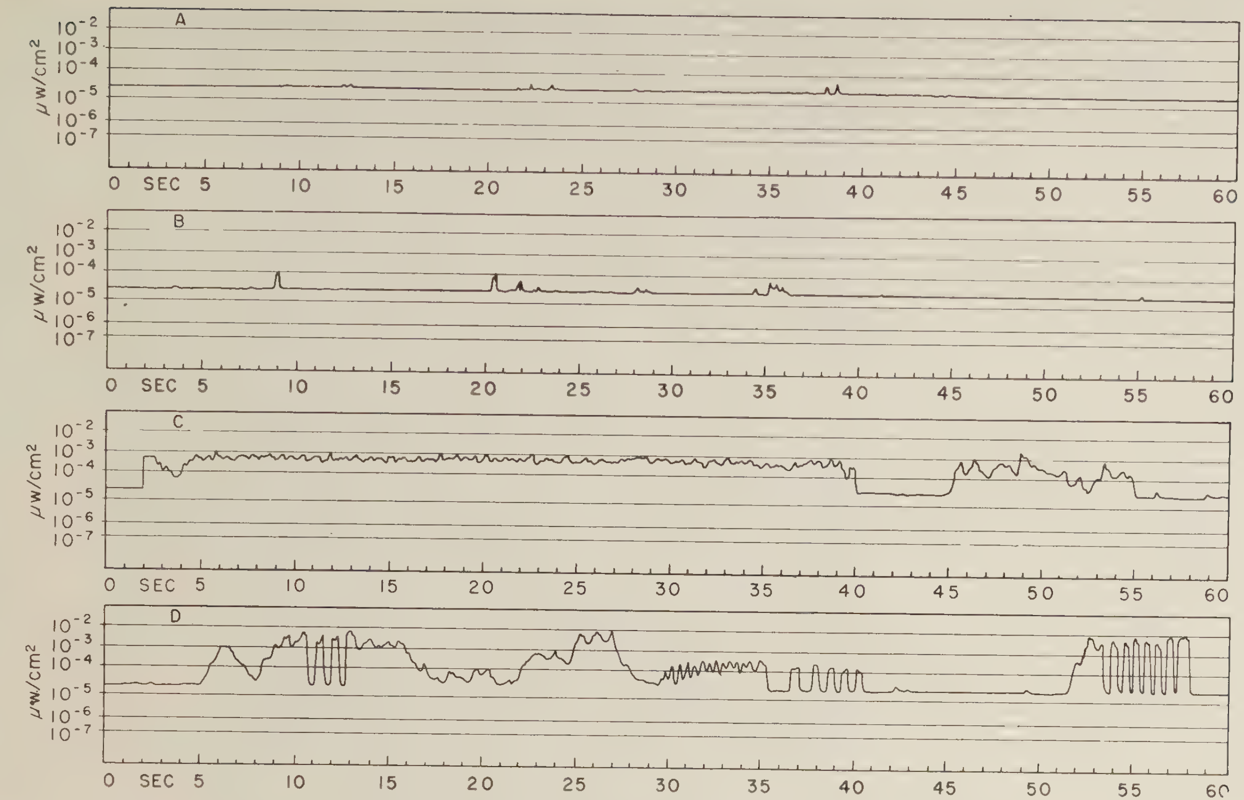

FIG. 12. — Records made in Calvi Harbor, 2100 hrs, May 22, at 5 m. A = no agitation, B = cable agitated at surface, C = photometer agitated by diver, D = water in front of the photometer window agitated by diver's hand.

shaken by hand at a point above the water. The remaining records were made while Dr. André LABAN, equipped with aqualung, examined the photometer as it hung in the same position in the water. At C the instrument itself was actively shaken by the diver and at D the diver's hand agitated the water in front of the photometer window with varying degrees of force. Moderate disturbance in the water raised the level of illumination to 10^{-3} $\mu w/cm^2$ and violent agitation produced flashes as bright as 10^{-2} μw. Dr. LABAN reported that small individual flashes could be seen in the undisturbed water and that strong agitation appeared to evoke the luminescence of many small organisms in such a way as to produce a glow in the water. These observations thus confirm our earlier suggestion that bright luminescence might be produced by many overlapping flashes as well as by large individual animals.

The luminescence camera (Fig. 13) was employed at a number of depths at the various stations. Since the original model was described (BRESLAU and EDGERTON, 1958), a scale and a watch about 2 cm in diameter have been added in the sensitive zone where they are photographed along with any animal present. The size of the animal as well as the time and,

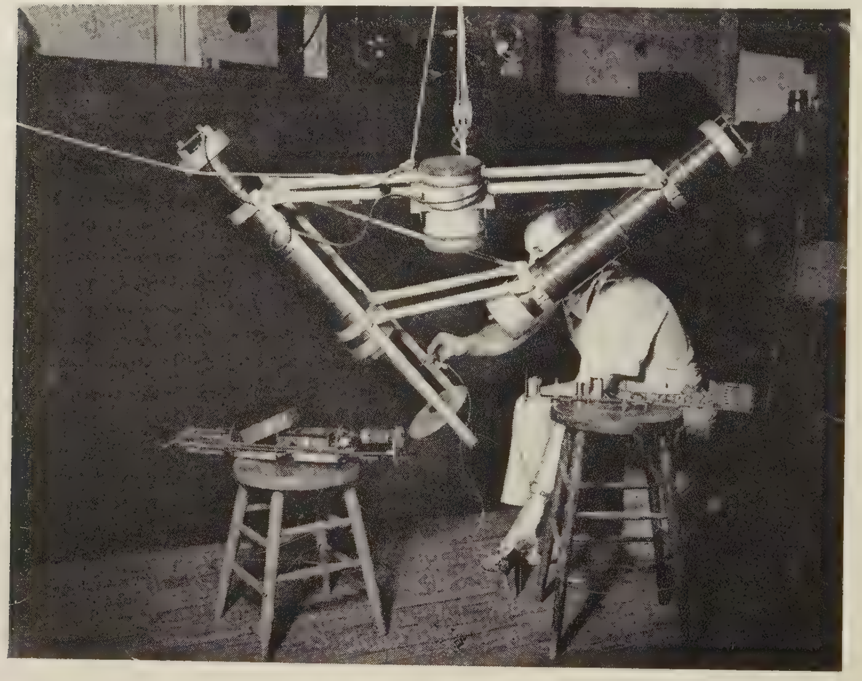

FIG. 13. — The Luminescence Camera in the laboratory with the inner parts o the photomultiplier detector and electronic flash unit (left) and the camera unit (right) removed from their housings. The junior author holds a test light in the sensitive region of the device.

from the log record, the depth at which the photograph was taken can thus be determined. After each exposure made by the discharge of the camera's electronic flash, the device is insensitive for a period of 5 sec during which recharging takes place and the film is wound to the next frame. Tests showed that the camera flash was not self-firing but was triggered only by an outside source of light, — that is, under operating conditions, by the flashes of one or more luminescent organisms in the sensitive zone. For the work at Station B the instrument was set at reduced sensitivity, at which luminescent intensities of 10^{-2} μw-cm^{2} (at the baffle) to 10^{-4} μw/cm^{2} (at the receiving window) were required to activate the camera; at all other stations full sensitivity was employed, at which flashes between 10^{-4} μW and 10^{-6} μw were sufficient to trigger the instrument.

A total of more than 1300 exposures was made by the luminescence camera during nine series of tests, but in only a few of them did objects larger than 1 cm appear in the photographs. The conclusion is drawn that at all the depths and localities studied in this investigation most of the luminescence is produced by organisms too small to be distinguishable in a photograph. Laboratory tests have shown that unicellular forms such as protozoans or dinoflagellates, which are unrecognizable by the unaided eye, can emit flashes bright enough to be seen or to trigger the camera. Two of the larger objects recognized as animals in the present study are shown in Figs 14 and 15 — the former is some type of cephalopod (only partly in the field of view), and the latter probably a pteropod. These animals may have activated the camera by their own light flashes, or they may have been accidentally in the sensitive zone at the time the instrument was triggered by the luminescence from other, unseen organisms.

Even though no recognizable photographs were obtained of the organisms which were chiefly responsible for the luminescence encountered in the present study, it is of interest to determine from the times shown by the watch the intervals between flashes which activated the camera at the different depths as the various stations. With the triggering device set at full sensitivity the average time between exposures varied from 24 sec (at 0219 hrs, May 22, Station C, at 50 m) to 11 min (at 0630 hrs, May 18, Station A, at 600 m). At reduced sensitivity the average time was usually much longer, as would be expected, and ranged from 1 to 108 min under various conditions at Station B. The differences agree generally with the variation in flashing rate and frequency recorded by the bathyphotometer under corresponding circumstances. The frequency distribution of the time intervals between flashes which triggered the camera under conditions of greatest luminescent activity (upper 100 m, Station C, 2310 hrs May 21 to 0519 hrs May 22) showed a mode at 20 sec and the great majority of intervals ranged between 10 and 40 sec. Thus it appears that the 5 sec recycle time of the camera had little effect on the interval between exposures.

The results from both the bathyphotometer and the camera observations show a considerable variation in bioluminescence among the

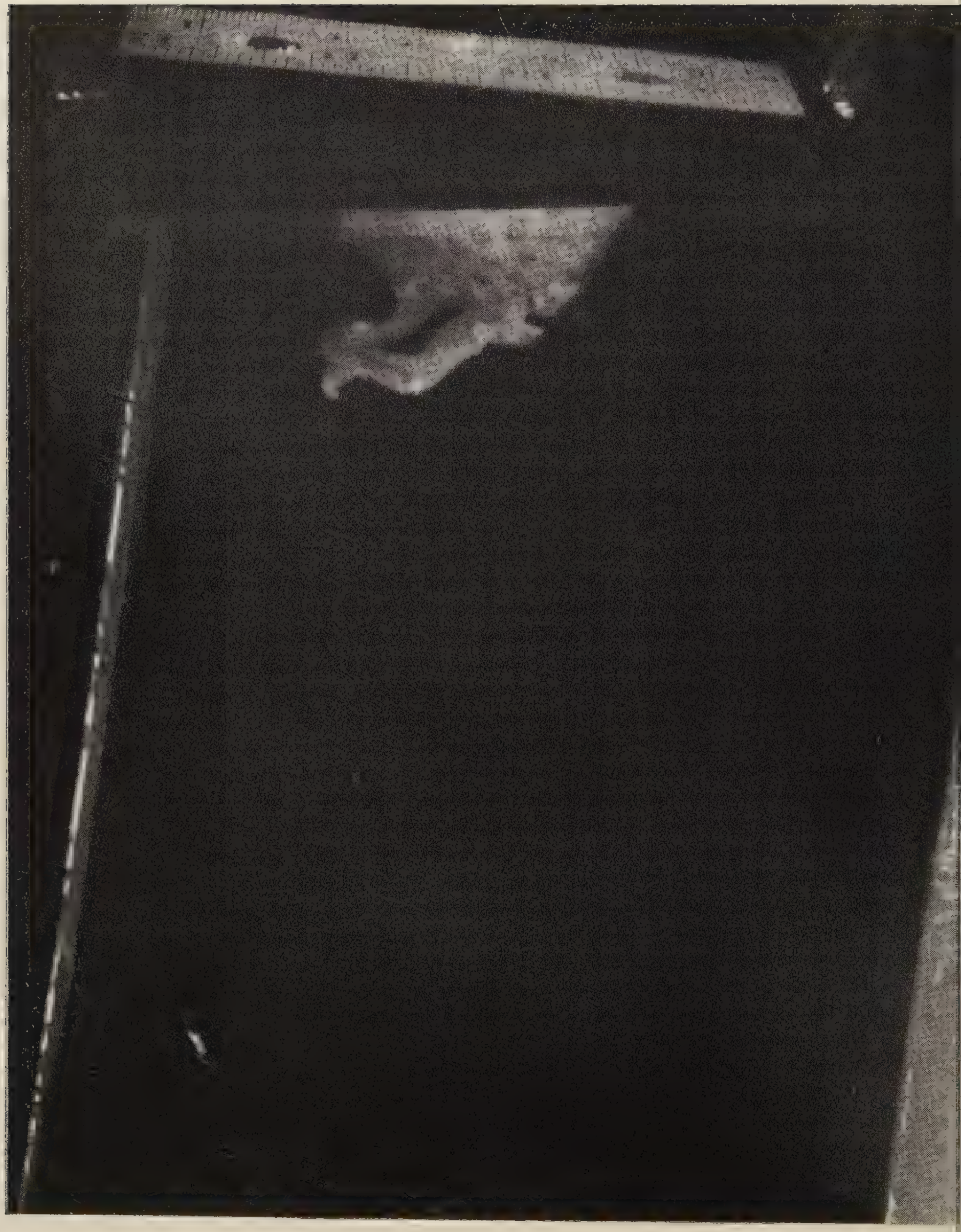

FIG. 14. — Photograph taken with the luminescence camera showing part of a cephalopod. A scale, in centimeters and inches, is in the field of view. Station B, June 10, time 0231 hrs. depth 10 m.

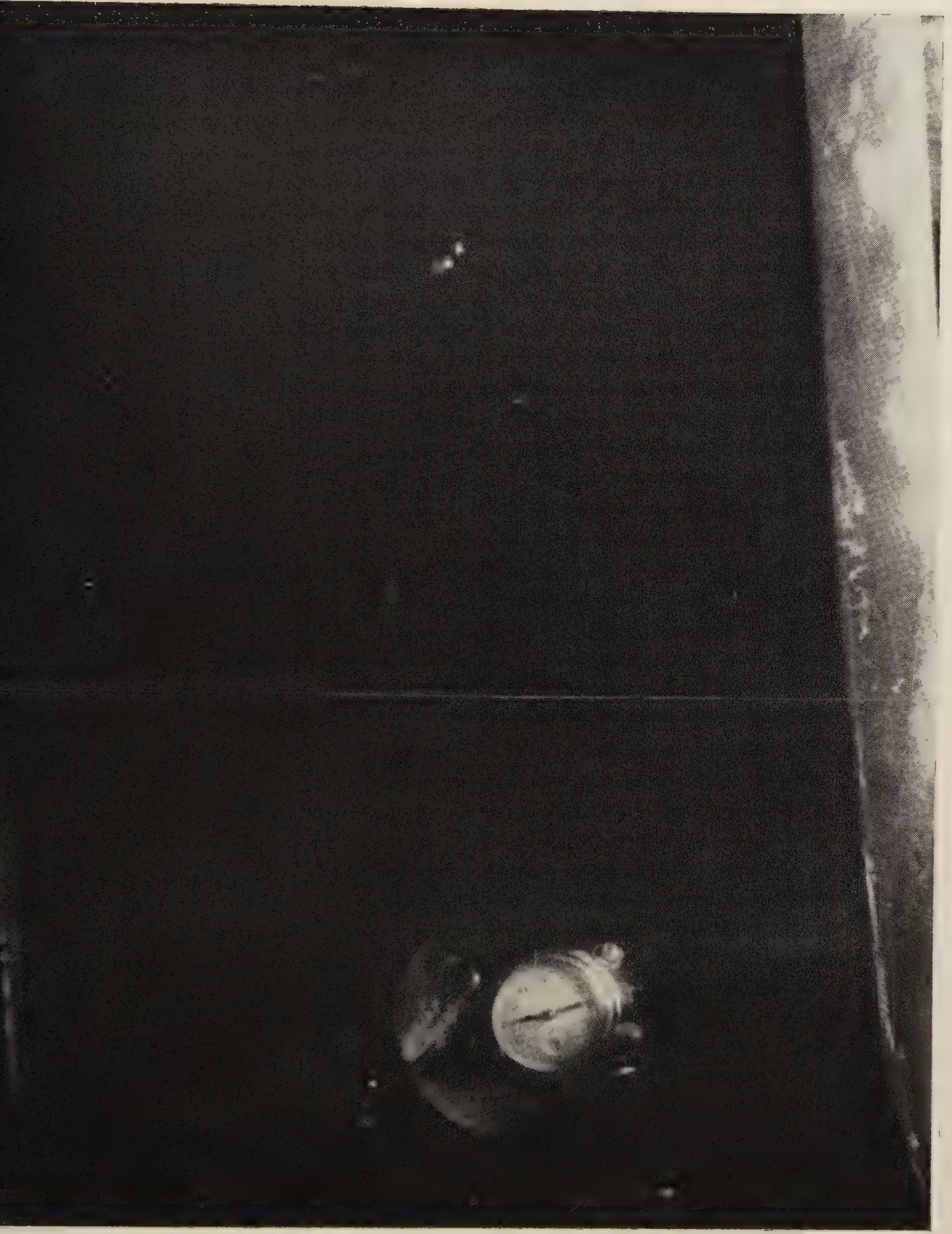

FIG. 15. — Photograph taken with the luminescence camera showing an animal, about 1 cm in diameter, probably a pteropod. Station B, June 10, time 0915 hrs. depth 600 m.

stations occupied in the present study and also between these and the localities investigated in the Atlantic. Among the Mediterranean stations made at night luminescent flashing reached its highest frequency at Station C in the middle of the Ligurian Sea where more than 40 flashes were observed per minute at all depths down to 600 m and more than 100 per minute were recorded at 50 and 75 m. At Station A in the Villefranche Canyon about the same rate of flashing was recorded at 50 m but luminescent activity dropped to a minimum at 600 m before rising to the secondary maximum at 700 m. To the east of Cap Corse at Station E the highest flashing rate was found at 100 m followed by a sharp reduction from about 200 m to 400 m. During the daytime the grestest amount of luminescence occurred at 600 m at both Stations A and B. At Station D the flashing rate was generally much less, but tended to increase to a maximum at 1000 m.

The observations thus indicate that luminescent organisms, like most planktonic forms, commonly exist in layers of abundance, the vertical positions of which differ with time and place. Such concentrations of animal life were observed in the Mediterranean by TREGOUBOFF (1958 a & b), DIETZ (1959), and others from the bathyscaph when the water was illuminated by daylight or by artificial light. Since our present study suggests rather strongly that most of the luminescence is produced by organisms too small to be photographed, these forms would also probably be too small to be recognized from the bathyscaph. Therefore, no exact correspondence between the depths of abundance for the two types of observations would be expected, unless some coordinating relation, such as that of prey and predator, could be demonstrated. Too few studies of relative luminescence from the bathyscaph with all lights extinguished have been reported for present comparison.

The frequency of flashing in the present study was considerably less than that reported by CLARKE & HUBBARD (1959) in the slope water several hundred miles off New York. In the latter investigation the number of flashes ranged from 60 to 118 per minute during the day and from 40 to 90 per minute during the night at depths of 600 m to 900 m. At night the maximum flashing rate (over 135 per min) was found at 100 m to 200 m. From 1000 m to 1700 m the frequency of flashing was generally over 35 per min both day and night, and on some occasions over 60 per min. These results agree with the known generally greater abundance of plankton in the slope water off the Atlantic coast as compared with the western Mediterranean. Interestingly enough a larger proportion of discharges brighter than 10^{-3} μw/cm^2 was recorded in the present study, mostly found in the upper 200 m, but otherwise the distribution of flash intensity was about the same in both areas. Not only was considerable light flashing observed at every locality and level investigated, but also the potentiality for much increased luminescence when the water is agitated, or disturbed by the movement of an animal, has been demonstrated. These findings coupled with the unusually high transparency of the water indicate the probable great importance of bioluminescence in the ecology of these areas of the Mediterranean.

SUMMARY

Investigation of underwater light conditions at five stations in the northern Mediterranean was undertaken from research vessels of the Oceanographic Institute, Monaco, using the improved bathyphotometer and the luminescence camera.

The transparency of the water was extremely great at all depths with minimum extinction coefficient of $k = .029$ found from 350 m to 700 m. Some evidence of daylight extended to 800 m.

Flashes of luminescent organisms were recorded by the inverted photometer at every depth investigated below the level at which scattered light from the surface interfered (below about 360 m.). Flashes ranged in intensity from over 10^{-2} μw/cm^2 (equivalent to the intensity of downward passing sunlight at a depth of about 350 m) down to the dark level of the instrument (10^{-7} to 10^{-8} μw/cm^2). The frequency of flashing varied from over 100 per minute at night at 50 m at stations off Monaco to less than 20 per minute at depths greater than 1000 m in the Ligurian Sea and greater than 200 m off Cap Corse. Extra agitation of the water produced by movement of the photometer caused a considerable increase in luminescence.

A 24-hour record made at 700 m in the Villefranche Canyon showed considerable variation in luminescence within intervals of a few minutes but no important change from day to night.

Since more than 1300 exposures made with the luminescence camera yielded only a few photographs of objects larger than 1 cm, evidence was obtained that most of the flashing is produced by very small organisms, such as dinoflagellates or protozoans.

The frequency of flashing was less than that previously observed in the Atlantic slope water off New-York but the intensity of the luminescence was as great or sometimes greater. Bioluminescence, both regularly occurring and potential, in conjunction with the very clear water, would thus appear to play a significant ecological role in these areas of the Mediterranean.

RÉSUMÉ

Des recherches sur la pénétration de la lumière du jour et sur la bioluminescence ont été entreprises à cinq stations en Méditerranée du Nord, à partir des navires de recherche de l'Institut océanographique de Monaco, en utilisant un bathyphotomètre perfectionné et une caméra à luminescence.

La transparence de l'eau était très grande à toutes les profondeurs avec un coefficient d'extinction minimum de $k = 0{,}029$ rencontré à une profondeur de 350 à 700 m. Des traces de lumière du jour pouvaient être discernées jusqu'à 800 m.

Des éclairs des organismes luminescents ont été enregistrés par le photomètre inversé à toutes les profondeurs étudiées au-dessous du niveau auquel interférait la lumière diffusée de la surface (au-dessous de 360 m). L'intensité des éclairs s'échelonnait depuis plus de 10^{-2} μw/cm^2 (équivalent à l'intensité des rayons du soleil dirigés vers le bas à une profondeur d'environ 350 m) jusqu'au niveau obscur de l'instrument (10^{-7} à 10^{-8} μw/cm^2). La fréquence des émissions enregistrées variait entre plus de 100 éclairs par minute, la nuit à une profondeur de 50 m, à la station au large de Monaco, et moins de 20 par minute à des profondeurs de plus de 1000 m dans la mer Ligurienne et de plus de 200 m au large du Cap Corse. Une agitation supplémentaire de l'eau provoquée par un mouvement du photomètre a provoqué un accroissement assez considérable de la luminescence.

Un enregistrement de 24 heures fait à une profondeur de 700 m dans le canyon de Villefranche a montré une variation considérable de la luminescence à des intervalles de quelques minutes, sans changement appréciable entre le jour et la nuit.

Plus de 1.300 clichés pris avec la caméra à luminescence n'ont donné que quelques photos d'objets de plus d'un centimètre; il paraît donc évident que la plupart des éclairs sont produits par de minuscules organismes tels que Dinoflagellés ou Protozoaires.

La fréquence des émissions des éclairs était inférieure à celle observée sur le versant atlantique, (« slope water ») au large de New-York, mais l'intensité de la luminescence était aussi grande, parfois même supérieure. La bioluminescence, tant régulière que potentielle, associée à une eau très claire, paraîtrait ainsi jouer un rôle écologique significatif dans ces régions méditerranéennes.

REFERENCES

Boden, B. P. and Kampa, E.M. 1957. Records of Bioluminescence in the ocean. *Pacific Science*, 2 : 229-235.

Boden, B. P. et Kampa, E. M. 1958. Lumière, bioluminescence et migrations de la couche diffusante profonde en Méditerranée occidentale. *Vie et Milieu*, Tome IX, fasc. 1, p. 1-10.

Breslau, L. R. and Edgerton, H.E. 1958 a. The Luminescence Camera. Unpublished Manuscript, Woods Hole Oceanographic Institution. Reference N° 58-14.

Breslau, L. R. and Edgerton, H.E. 1958 b. The Luminescence Camera. *Journal of the Biological Photographic Association* 26 : (2) p. 49-58.

Clarke, G. L. and Backus, R. H. 1956. Measurements of light penetration in relation to vertical migration and records of luminescence of deep sea animals. *Deep-Sea Res.*, 4 : 1-14.

Clarke, G. L. and Hubbard, C. J. 1959. Quantitative Records of the Luminescent Flashing of Oceanic Animals at Great Depths. *Limnology and Oceanography*, 4 : 163-180.

Clarke, G. L. and James, H. R. 1939. Laboratory analysis of the selective absorption of light by sea water. *J. Opt. Soc. Am.* 29 : 43-55.

Clarke, G. L. and Wertheim, G. K. 1956. Measurements of illumination at great depths and at night in the Atlantic Ocean by means of a new bathyphotometer. *Deep-sea Res.*, 3 : 189-205.

Dietz, R. S., 1959. 1100-meter dive in the bathyscaph *Trieste*. *Limnology and Oceanography*, 4 : 94-101.

Jerlov, N. G. and Piccard, J. 1959. Bathyscaph measurements of daylight penetration into the Mediterranean. *Deep-Sea Research*, 5 : 201-204.

Kampa, E. M. and Boden, B. P. 1957. Light generation in a sonic-scattering layer. *Deep-Sea Res.*, 4 (2) : 73-92.

Tregouboff, G. 1958 a. Prospection biologique sous-marine dans la région de Villefranche-sur-Mer au cours de l'année 1957. I. Plongées en bathyscaphe. *Bulletin de l'Institut océanographique*. Monaco, N° 1117.

Tregouboff, G. 1958 b. Le bathyscaphe au service de la planctonologie. *Annales de l'Institut océanographique*. 35 (4) : 327-341.

Contribution No. 1047

Deep-Sea Research, 1959, Vol. 6, pp. 60 to 64. Pergamon Press Ltd., London. Printed in Great Britain

SHORTER COMMUNICATION

The temperature correction of oceanic inorganic phosphorus analyses

DAVID A. McGILL, NATHANIEL CORWIN and BOSTWICK H. KETCHUM

(*Received* 10 *June* 1959)

Abstract—The colour intensity of the molybdate-blue complex in the analysis for inorganic phosphorus in sea-water increases 1·25 per cent per degree centigrade. The apparent phosphorus content of sea-water samples analysed in tropical regions may be erroneously high unless temperature is controlled or corrections are made. The effect of temperature correction on the agreement between total and inorganic phosphorus contents of Atlantic Ocean water is described. It is recommended that temperature corrections be included in future publications of data on the distributions of inorganic phosphorus.

INTRODUCTION

THE intensity of colour developed in the Deniges-Atkins method (1923) for the determination of phosphorus increases with temperature. ROBINSON and THOMPSON (1948) and WOOSTER and RAKESTRAW (1951) found increases in colour of about 1 per cent per degree C. HARVEY (1955) cites a value of 1·2 per cent per °C for the colour increment. In oceanographic studies of the distribution of phosphorus, considerable variation in the correct value may be expected if the temperature variation among the samples analysed is great. For this reason it has become customary to allow the samples to reach the ambient temperature before analysis, thus eliminating the effects of the large temperature variations between surface and deep water, which may be as much as 25–30°C in tropical and subtropical areas. WOOSTER and RAKESTRAW (1951) recommend a constant temperature water bath for this purpose. The temperature effect would also be eliminated if the standard and unknown solutions are at the same temperature during comparison (for visual estimation of colour) or calibration (for photometric determinations).

The temperature effect has commonly been neglected in oceanographic work, presumably because it has been assumed to be a small error in comparison with other inaccuracies of the method. During recent extensive determinations of the distribution of phosphorus in the Atlantic Ocean in connexion with observations made during the International Geophysical Year, we have found it essential to make temperature corrections for the inorganic phosphorus analyses made on shipboard. Correction was necessary because the calibration of the photometer, though repeated frequently, was performed when temperatures were about 20°C, whereas the analyses were performed at temperatures ranging up to 33°C in the tropics. The validity of the temperature correction is indicated by comparisons between the inorganic and total phosphorus.

METHODS

Inorganic phosphate was determined by the Deniges–Atkins method as described by WOOSTER and RAKESTRAW (1951). The colour developed by the molybdate-blue complex was measured in the photo-electric colorimeter (FORD, 1950) using a red light filter (Corning 2408) and a cell with a 29 cm light path for concentrations less than 1·0 μg A/l or a cell with a 9 cm light path for higher concentrations. Samples were analysed after they had been adjusted to the laboratory temperature on shipboard. The photometer was calibrated using standard solutions prepared with surface Sargasso sea-water. This water was nearly phosphate-free and the small residual phosphorus content was determined on blank samples.

Total phosphorus was determined by the Harvey method as modified by Ketchum *et al.* (1955), using a tube length of 29 cm in the photometer. The calibration was made by subjecting standards, prepared in Sargasso Sea-water, to the same procedure used for the unknowns.

OBSERVATIONS

The need for temperature correction first became apparent when the inorganic and total phosphorus concentrations in the deep water of the Atlantic Ocean were compared. The data were collected on Cruise 10 of the Research Vessel *Crawford* as part of our observations for the programme of the International Geophysical Year. In such comparisons, particulate or dissolved organic phosphorus is presumed to be present in the water when the total concentration significantly exceeds that of inorganic phosphorus. Consistently, however, in the deep water of tropical and sub-tropical regions, the inorganic concentration exceeded that of the total, a result which is theoretically impossible. It was apparent, therefore, that there was a consistent bias in our analytical results. Since the discrepancy was exaggerated in the tropics, where shipboard laboratory temperatures averaged about 30°C, the effect of correction for temperatures has been studied.

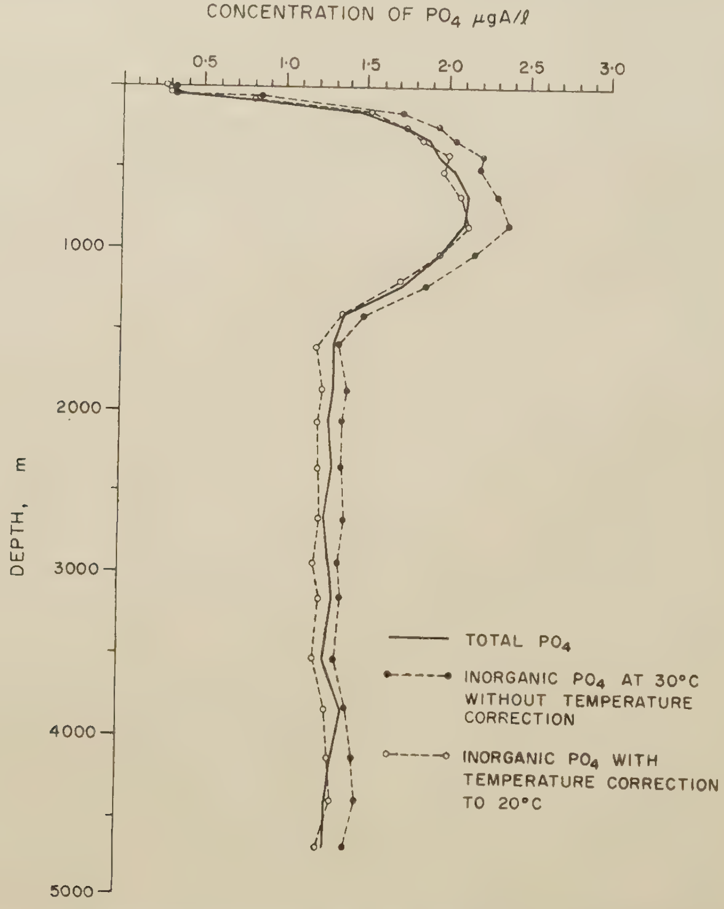

Fig. 1. Comparison of the apparent inorganic with the total phosphorus for a station in the tropical Atlantic. (*Crawford* Cruise 10, Station 168, Lat. 8°N, Long. 36°W).

The analyses for inorganic phosphorus were made on shipboard as soon as possible after collection, but after allowing ample time for the samples to come to laboratory temperature. The temperature of each sample was not recorded on this cruise, but periodically the ambient laboratory temperature was recorded. The excess in temperature over the calibration temperature (20°C) was used to correct the inorganic phosphorus concentrations. The correction applied was 1 per cent per °C in accordance with data of Robinson and Thompson (1948) and Wooster and Rakestraw (1951). Since the total phosphorus was determined in Woods Hole at the calibration temperature no correction for these was made.

An example of the effect of this correction on the apparent phosphorus at various depths is given in Fig. 1. These data are for *Crawford* Station 168 at 8°N, 36°W in the central Atlantic. The phosphorus analyses on shipboard were made at 30°C, and the corrected values are thus decreased by 10 per cent. The uncorrected inorganic phosphorus exceeded the total at all depths. Although the difference on individual samples is not statistically significant (Ketchum *et al.*, 1955), the consistency of the bias is apparent. Applying the temperature correction produced complete agreement in the layer of maximum concentration. In the deep waters this correction reduced the inorganic concentrations to values slightly less than the total.

As a further illustration of the effect of the temperature correction, the average inorganic and total phosphorus concentrations for samples collected at 2000 (± 150) m on four sections are compared in Table 1. This depth was selected to conform to Redfield's (1958) presentation of the global distribution of phosphorus. The standard deviations for these data include not only analytical variations but actual differences in geographical distribution. The uncorrected inorganic phosphorus concentrations exceeded the total in all cases, emphasizing again the consistency of the bias. The corrected inorganic phosphorus concentrations closely agree with the total in every section.

Table 1. Comparison of total and inorganic phosphorus in sea-water at 2000 m *depth in the Atlantic Ocean*

Section	*Number of Samples*	*Inorganic* $PO_4^{=}$ (*μg* A/l) *Uncorrected* *Mean*	*σ*	*Corrected* *Mean*	*σ*	*Total* P (*μg* A/l) *Mean*	*σ*
Western Atlantic Basin							
Bermuda–Dakar	6	1·35	0·080	1·27	0·068	1·27	0·057
8° 15′N	8	1·42	0·100	1·22	0·091	1·23	0·074
8° 15′S	11	1·55	0·040	1·36	0·036	1·36	0·052
15° 45′S	18	1·60	0·094	1·47	0·091	1·49	0·093
Eastern Atlantic Basin							
Bermuda–Dakar	6	1·46	0·088	1·37	0·088	1·39	0·069
8° 15′N	13	1·47	0·104	1·34	0·078	1·35	0·070
8° 15′S	15	1·53	0·117	1·36	0·035	1·42	0·088
15° 45′S	9	1·62	0·141	1·49	0·100	1·53	0·072

Table 2. Effects of temperature on the development of colour in the phosphorus analysis (9cm *tube for inorganic and* 29 cm *tube for total analysis*)

°C	*No. of samples*	*Average factor* *μg* A/l	*Standard deviation σ*
Inorganic analysis			
15·0°	10	$1·228 \times 10^{-2}$	$0·056 \times 10^{-2}$
23·5°	9	$1·110 \times 10^{-2}$	$0·036 \times 10^{-2}$
30·0°	9	$1·016 \times 10^{-2}$	$0·029 \times 10^{-2}$
Total Analysis			
15·0°	10	$0·874 \times 10^{-2}$	$0·058 \times 10^{-2}$
23·5°	8	$0·820 \times 10^{-2}$	$0·090 \times 10^{-2}$
30·0°	10	$0·793 \times 10^{-2}$	$0·070 \times 10^{-2}$

The effect of temperature on colour development has been redetermined using our photometer and methods. Complete calibrations were performed by adding inorganic phosphorus in concentrations of 0·5, 1·0, 1·5, 2·0 and 2·5 μg atoms per litre to Sargasso Sea-water. These samples were analysed after equilibration at temperatures of 15°, 23·5° and 30°C in constant temperature water baths. For each sample, a factor which relates each unit of the arbitrary scale of the photometer with microgramme atoms per litre was computed. The results are given in Table 2 and in Fig. 2.

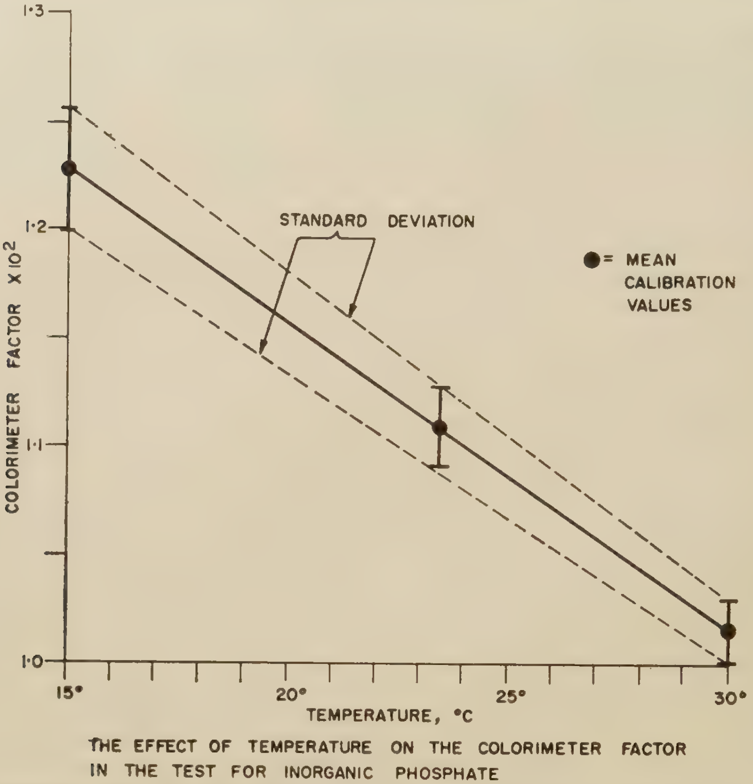

Fig. 2. Calibration for inorganic phosphorus analysis as a function of temperature. The dotted lines show the standard deviation.

The increased colour development, which produces a lower factor, corresponds to 1·25 per cent per degree centigrade. A similar set of calibrations was performed on the total phosphorus analysis at these same temperatures. The temperature correction in this method corresponds to 0·65 per cent per °C. As mentioned above, it has not been necessary to correct the total values because both calibration and analysis are performed at substantially the same temperature.

Table 3. Apparent phosphorus content of a sea-water sample to which 2·0 μg A/1 *of inorganic phosphorus was added.* (*For explanation see text*)

Temperature of analysis	*Uncorrected* μg A/1	*Corrected to* 20°C μg A/1	*Observed* μg A/1
15·0°	1·94	2·04	2·08
23·5°	2·14	2·07	2·04
30·0°	2·31	2·07	2·05

The validity of the temperature correction is further indicated by the data in Table 3 which compares the apparent phosphorus concentration of a sample analysed at these different temperatures and computed in three ways. The uncorrected values are obtained by computing the phosphorus content using the calibration factor measured at 20°C. This corresponds to the uncorrected values in Fig. 1. In the second column these values have been corrected to 20°C by application of the 1 per cent/°C correction, as was done with the *Crawford* data. In the final column the concentration is computed using the average calibration factor derived for the appropriate temperature. Both methods of correcting for temperature of analysis appear to be satisfactory.

CONCLUSIONS

To obtain correct values for inorganic phosphate measured at sea a temperature correction must be applied unless the colour development in standards and unknowns is measured at the same temperature. This was, of course, true when direct comparisons were made visually. The error may be considerable, however, when a photometer is used.

Several methods are available to eliminate this error. Samples can be placed in a constant temperature bath and brought to the calibration temperature, as suggested by WOOSTER and RAKESTRAW (1951). In the humid tropics, however, condensation on the walls of the absorption cell can give trouble unless the temperature is higher than is expected at any time during the cruise. Furthermore, on small ships and long cruises, available space may not permit this refinement. Another possibility is to include standards and to determine the calibration factor separately for each set of analyses. When large numbers of samples are to be analysed by a single chemist on the ship this is also impractical.

The simplest method for correcting for the effect of temperature involves calibrating the photometer at various temperatures, and using the appropriate calibration factor for the temperature of each sample at the time of analysis. From the calibration data in Table 2 and Fig. 2, a table of calibration factors at various temperatures, in 0·5°C intervals, was prepared for this purpose. The stability of the photometer and reagents can be checked during the cruise at any time regardless of temperature.

Temperature corrections have been applied to all of the inorganic phosphorus analyses collected by this Institution during the I.G.Y. For the earlier cruises, *Crawford* 10 and 16, a correction of 1 per cent/°C in excess of 20°C was applied. It was necessary to use the ambient air temperature in the laboratory for this purpose since on these cruises the temperature was not measured on each sample. For the later cruises, *Crawford* 22 and *Atlantis* 247, the calibration factor for the temperature of each sample has been used as described above. It is recommended that all inorganic phosphorus analyses made by photometer at sea be corrected in this way, or, if this is not done, that temperatures during calibration and analysis be recorded.

Woods Hole Oceanographic Institution
Woods Hole, Mass.

Contribution No. 1047 from the Woods Hole Oceanographic Institution. This work was supported in part by a research grant from the National Science Foundation.

REFERENCES

ATKINS W. R. G. (1923) The phosphate content of fresh and salt waters in its relationship to the growth of the algal plankton. I. *J. Mar. Biol. Assoc.* (*U.K.*) **13,** 119-150.
FORD W. L. (1950) Seagoing photoelectric colorimeter. *Anal. Chem.* **22,** 1431-1435.
HARVEY H. W. (1955) *The chemistry and fertility of sea waters.* C.U.P. 224 pp.
KETCHUM B. H., CORWIN N. and KEEN D. J. (1955) The significance of organic phosphorus determinations in ocean waters. *Deep-Sea Res.* **2,** 172-181.
REDFIELD A. C. (1958) The biological control of chemical factors in the environment. *Amer. Sci.* **46,** 205-221.
ROBINSON R. J. and THOMPSON T. G. (1948) The determination of phosphates in sea water. *J. Mar. Res.* **7,** 33-41.
WOOSTER W. S. and RAKESTRAW N. W. (1951) The estimation of dissolved phosphate in sea water. *J. Mar. Res.* **10,** 91-100.

Printed in Great Britain by The Salisbury Press Ltd,, Publicity House, Wilton Road, Salisbury, Wilts. (18731)

Contribution No. 1060

Sonderdruck aus der Deutschen Hydrographischen Zeitschrift. Ergänzungsheft Reihe B (4°), Nr. 3

A Note on the Constancy of the T/S Relationship in a Water Mass

By Karl E. Schleicher*

Summary. Nine repeated hydrographic series on F.F.S. „Anton Dohrn“ station no. 2548 (61° 54′ N, 23° 48′ W) on the 25–27 August 1958 show a maximum deviation in the T/S correlation of about $0.008^0/_{00}$ (a mean deviation of $\pm\ 0.003^0/_{00}$) which is very nearly within the limits of precision of the Woods Hole salinometer used on board. The facts (1) that the T/S curve shows no irregularities and (2) that the scatter of all the points is essentially random and is not dependent upon time, indicate the presence of only one water mass throughout the time period of observation.

Über die T/S-Beziehungen im Wasser (Zusammenfassung). Neun ozeanographische Wiederholungsserien wurden auf F.F.S. „Anton Dohrn“-Station Nr. 2548 (61° 54′ N, 23° 48′ W) in der Zeit vom 25.—27. August 1958 ausgeführt; sie zeigen eine Maximalabweichung von ungefähr $0{,}008^0/_{00}$ in der T/S-Beziehung (mittlere Abweichung $= \pm\ 0{,}003^0/_{00}$). Dieser Wert liegt sehr eng innerhalb der Genauigkeitsgrenzen des Woods Hole-Salzgehaltsmessers, der an Bord benutzt wurde. Die Tatsachen, daß 1. die T/S-Kurve keine Unregelmäßigkeiten aufweist und 2. die Streuung aller Punkte im wesentlichen zufällig ist und nicht von der Zeit abhängt, weisen auf das Vorhandensein nur einer Wasserart während der gesamten Beobachtungszeit hin.

Sur les relations TS dans une masse d'eau (Résumé). Des séries à neuf reprises, effectuées le 25—27 août 1958 à bord du navire explorateur de pêche «Anton Dohrn» à la station 2548 (61° 54′ N, 23° 48′ W), montrent une déviation maximum de $0{,}008^0/_{00}$ environ (déviation moyenne de $\pm 0{,}003^0/_{00}$) dans la relation TS. Ces valeurs sont très voisines des limites de précision du mesureur de salinité d'après le type de la Woods Hole Oceanographic Institution, utilisé à bord de l'«Anton Dohrn». Les faits que 1° la courbure TS ne montre pas d'irrégularités et que 2° l'écartement de tous les points est essentiellement fortuit et ne dépend pas du temps, indiquent la présence d'un seul type d'eau pendant toute la période d'observation.

The manœuvres of a research vessel during a *Dauerstation*, made primarily to measure the change in current with time over a particular area, also offer the opportunity to study the water mass at one location over a period of time. By repeating hydrographic stations one can obtain data for studying the change, if

---

Contribution No. 1060 from the Woods Hole Oceanographic Institution, Woods Hole, Mass., U.S.A.

any, in the salinity temperature relationship with time. The data from the repeated hydrographic stations on the *Dauerstation* (station no. 2548) of the F.F.S. „Anton Dohrn" cruise in the International Geophysical Year may be of special interest in so far as the salinities were determined by the conductivity method which is considerably more precise than the usual Knudsen titration method. The instrument used for determining the salinities on the „Anton Dohrn" was an improved model of the original Woods Hole salinometer described by K. E. Schleicher and A. Bradshaw [1956].

Ten hydrographic series were made during this *Dauerstation* at a location of 61° 54′ N, 23° 48′ W. The first two series were made five minutes apart and together covered a total depth of 1400 m. (series 1: 10 to 98 m., series 2: 147 to 1400 m.). The remaining, series 3 to 10, were made at 4 hours intervals, were limited to samples taken between approximately 400 and 1000 m. (Series 10 also had a sample at 277 m.) The total depth of water at this location was 1440 meters.

A plot of the resulting data of temperature versus salinity is presented in the accompanying graph. The points represented here are limited to those taken between 277 and 993 meters. A curve has been drawn through the points, determined by eye to be the best averaging line. The maximum salinity deviation from this line is $.008^0/_{00}$, the mean deviation being $\pm .003^0/_{00}$.

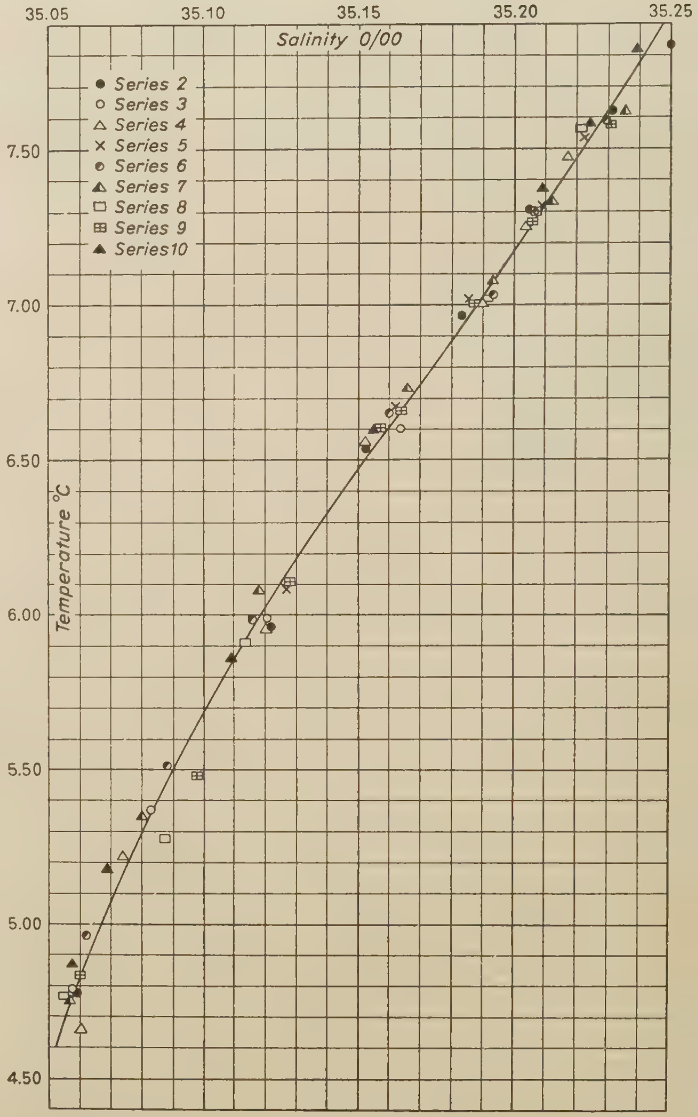

Fig. 21 T/S-diagram for repeated hydrographic series of F.F.S. „Anton Dohrn"-station no. 2548, cruise no. 3

From previous experience with the salinometer and from controlled laboratory experiments the overall precision of the instrument is considered to be about ± .005‰ (maximum deviation) and even better than this when the measurements are made close to each other in time as is the case of the samples discussed here. The scatter, obtained at this *Dauerstation*, is slightly more than might be expected from instrumental error alone. It can be seen also by use of the coded symbols that the scatter is fairly random and does not seem to be associated with the differences in time of the various series.

In view of this it is tempting to ask whether the scatter is, in part at least, a property of the water mass itself. However, there are other factors which may affect or determine the amount of scatter in this TS diagram such as the operation of the Nansen bottles and the handling of the samples from the time they are drawn from the Nansen bottle to the time they are introduced into the cells of the salinometer. These factors are practically impossible to evaluate quantitatively (at least without undertaking a rather elaborate controlled experiment) and therefore we cannot determine how much of the scatter is due to them. The contribution to the scatter of the errors involved in temperature measurement are considered to be negligible in view of the precision usually associated with such temperature measurements.

We must then be satisfied with the conclusion that the temperature-salinity relationship of the water mass in question is constant to at least the degree represented by the scatter of the points of the T/S diagram, and that part of this scatter is either due to the variability of the T/S relationship in the water mass or to experimental errors other than those associated with the salinometer.

Schrifttum

Schleicher, K. E., A. Bradshaw, 1956: A Conductivity Bridge for Measurement of the Salinity of Sea Water. J. Cons. int. Explorat. Mer 22, No. 1, 2.

Eingegangen im März 1959

Contribution No. 1061

Reprinted from BIOLOGICAL BULLETIN, Vol. 117, No. 3, pp. 594–600, December, 1959
Printed in U. S. A.

RESPIRATION AND ANAEROBIC SURVIVAL IN SOME SEA WEED-INHABITING INVERTEBRATES

WOLFGANG WIESER AND JOHN KANWISHER

Dept. of Zoology, Univ. of Vienna, Austria, and Woods Hole Oceanographic Institution, Woods Hole, Massachusetts

RESPIRATION AND ANAEROBIC SURVIVAL IN SOME SEA WEED-INHABITING INVERTEBRATES [1, 2]

WOLFGANG WIESER AND JOHN KANWISHER

Dept. of Zoology, Univ. of Vienna, Austria, and Woods Hole Oceanographic Institution, Woods Hole, Massachusetts

L. C. Beadle in a paper on the respiration in the African swampworm *Alma emini* (Beadle, 1957) showed that the waterlogged mats of *Cyperus papyrus* are devoid of oxygen most of the time and that all animals living in them have to be adapted to this situation one way or the other. The case of the swamps is certainly an extreme one, but there can be no doubt that wherever plants grow in water or are easily flooded, anaerobic conditions may prevail occasionally or quite regularly.

The large sea weeds growing along the open coasts seem to represent an exception to such a statement and might be regarded as the prototype of a well-aerated habitat. This is certainly true at high tide. At low tide, however, these sea weeds collapse, forming thick clumps within and under which water is trapped. In the night or on cloudy days respiration of the algae may exceed photosynthesis and the water, cut off from atmospheric circulation, will gradually lose its oxygen to the plants.

This, then poses an ecological problem which can be stated as follows: Does the oxygen content of the water trapped by emersed sea weeds ever fall to zero and if so, how do the animals living in the sea weeds cope with this situation?

MATERIAL AND METHODS

The work was carried out at the Woods Hole Oceanographic Institution, Woods Hole, Massachusetts. The water samples were taken from under clumps of emersed brown algae (*Fucus, Ascophyllum*) on July 13 and 14, 1959, by means of 5-cc. syringes which were stoppered with glass plugs, and analyzed in the laboratory with the gasometric water analyzer of Scholander (Scholander *et al.*, 1955). The sampling site was a flat piece of gravelly and rocky beach (Woods Hole Yacht Club) on which brown algae grew quite luxuriantly. All the samples came from the upper and the middle zone of the exposed algal belt. The tidal range at Woods Hole is 1.8–2.2 ft. The temperature within a clump of sea weeds measured 20° C. at one occasion.

Various animals living in the large brown sea weeds around the Woods Hole Oceanographic Institution were collected at high tide and their respiration and anaerobic survival studied. The respiration of nematodes and mites was measured by the Cartesian diver method as described by Holter and Linderstrøm-Lang (1943) and others. The divers used had a volume from 6.5 to 37.4 μl. and volume changes could be read to 0.001–0.006 μl. O_2/hr. The respiration of the

---

[1] Supported by NSF grant G-4813.

[2] Contribution no. 1061 from the Woods Hole Oceanographic Institution.

amphipods was measured by means of the volumetric micro- and macro-respirometer of Scholander (Scholander *et al.*, 1952). Respirometer runs were made at 10° C. and in the following diagram the respiration values are corrected to 20° C., the temperature at which the diver was run, by assuming a Q_{10} of 2. This value seems to be a reasonable—perhaps even too low—guess in the light of the data on the amphipod *Talorchestia* by Edwards and Irving (1943) as re-plotted by Rao and Bullock (1954).

Anaerobic survival was studied by putting the animals into a small amount of water in a Thunberg tube which then was evacuated and flushed with tank-nitrogen. Constant experimental conditions were maintained by putting a constant amount of water into the Thunberg tubes and by flushing each tube exactly 100 times. The evacuation of the Thunberg tubes was carried out at room temperature. Subsequently, the tubes were kept either in the refrigerator at approximately 2° C., or at 15° C., or in the laboratory which had a fairly constant temperature of 25° C. The behavior of the animals was studied either by observing them in the closed tube, or after a certain time had elapsed, by emptying them into a dish with normal sea water. The recovery time of nematodes and mites was defined as the time interval within which 75% of the animals used for one experiment had resumed movement.

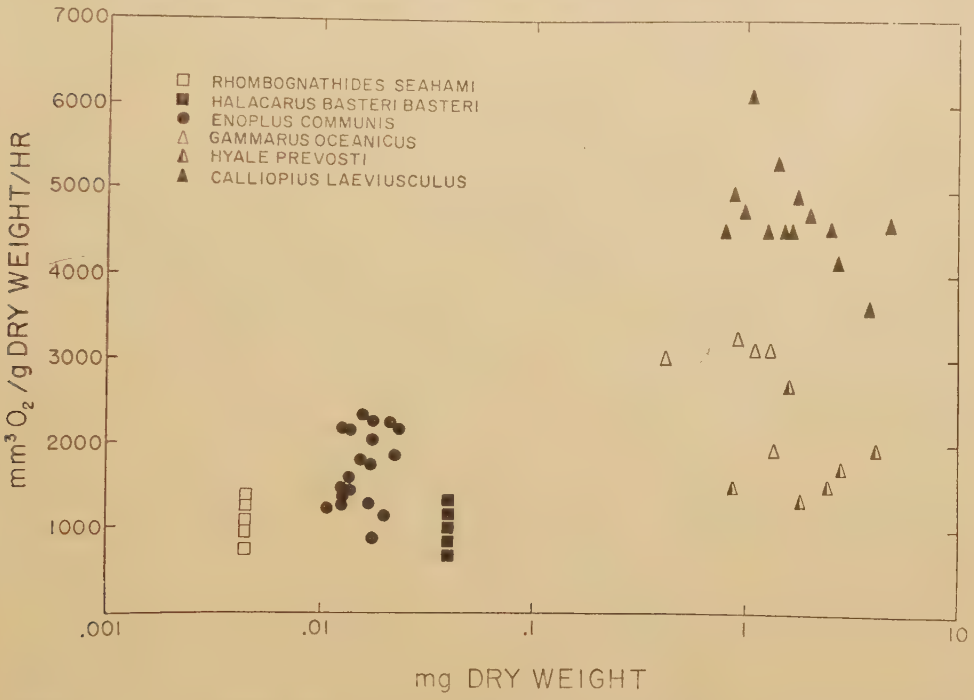

FIGURE 1. Oxygen consumption per gram dry weight of the six species of animals investigated. Each convention represents one experiment.

The dry weight of the nematodes was established by measuring volume and specific gravity as described elsewhere (Wieser, 1960). The dry/wet weight ratio

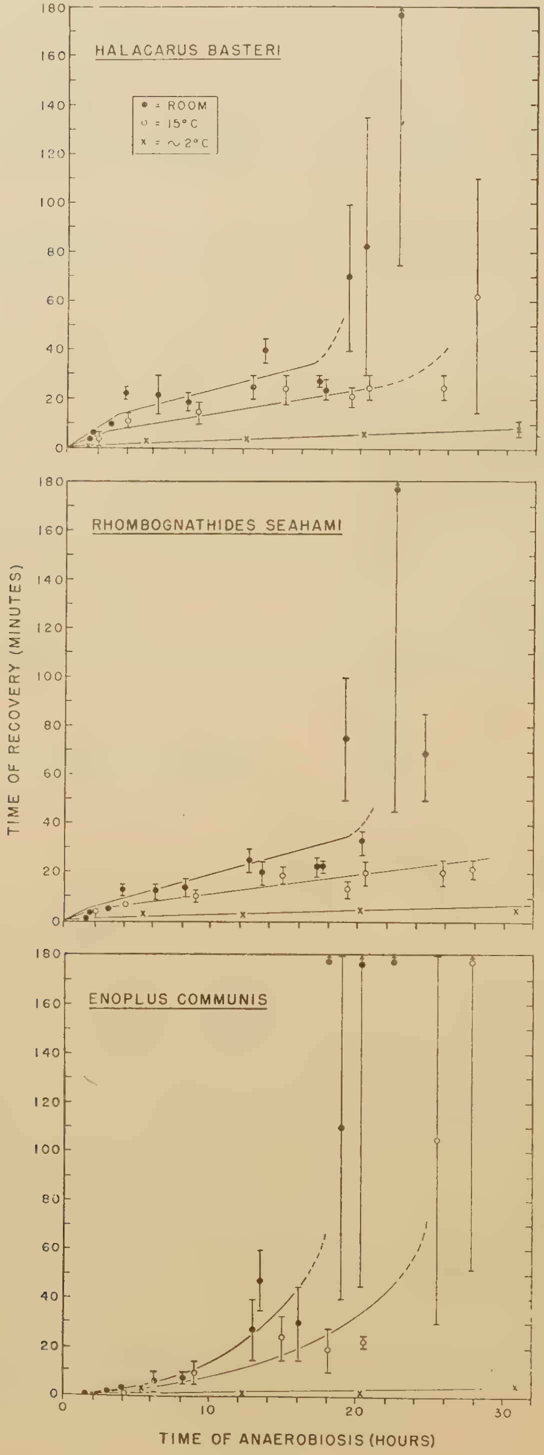
HALACARUS BASTERI
● = ROOM
○ = 15° C
x = ∼ 2° C
RHOMBOGNATHIDES SEAHAMI
ENOPLUS COMMUNIS
TIME OF RECOVERY (MINUTES)
TIME OF ANAEROBIOSIS (HOURS)
0
20
40
60
80
100
120
140
160
180
0
10
20
30

FIGURE 2.

was assumed to be 25% in all specimens. The mites were dried at 100° C. and weighed in batches on a "Misco" quartz helix (by Dr. R. Conover, W.H.O.I.). The dried amphipods were weighed individually on a torsion balance.

RESULTS

The water analyses gave the following results:

Sample no.:	1	2	3	4	5	6
Time:	10 P.M.		10 A.M.			
Ml. O_2/1 liter H_2O:	0.25	0.30	0.0	0.05	0.96	1.65

The night samples were taken exactly at low tide, the day samples 30–40 minutes after low tide on a cloudy day (illumination 1700 foot-candles). The oxygen content of saturated sea water at 20° C. and the local salinity (approximately 31‰) is 5.5 ml. O_2/1 liter H_2O (Sverdrup *et al.,* 1946).

For the measurement of respiration and anaerobic survival two groups of species were chosen; one, consisting of the nematode *Enoplus communis* and the sea mites (Halacaridae) *Rhombognathides seahami* and *Halacarus basteri basteri,* represented very small animals of low motility, unable to swim and without special respiratory organs. The other group consisted of three amphipod species, *Calliopius laeviusculus, Gammarus oceanicus* (identified by Dr. H. Werntz, Harvard University) and *Hyale prevosti,* representing medium-sized, very agile animals with good swimming capabilities and equipped with gills.

The respiratory rates per gram dry weight of the six species investigated are summarized in Figure 1. It is evident that if the size difference is taken into account (Zeuthen, 1947), the amphipods have a much higher metabolic rate than the other three species.

The two groups of species could also be distinguished in their reaction to anaerobic stress. Nematodes and mites, after the oxygen had been removed from the Thunberg tube, became paralyzed. From this state they recovered after they were put back into oxygenated water, provided that the time of anaerobic stress had not lasted too long. The recovery time as shown in Figure 2 is a function of the time of anaerobiosis and of the temperature at which the latter was spent. The three amphipods, however, remained active under anaerobic stress for a certain time and then died (Fig. 3). One could, of course, say that they, too, became paralyzed after a period of activity, but that the paralyzed state which preceded death was of extremely short duration. If an animal after readmission to normal conditions did not recover right away, it did not recover at all.

FIGURE 2. Relationship between time of anaerobiosis and time of recovery in the two halacarids (upper two diagrams) and the nematode. Each convention represents one experiment on a batch of animals. Range of variability in recovery time indicates beginning of movements in the first and in 75% of the animals in one batch. Recovery periods exceeding 180 minutes are characterized by an arrow and by a circle close to the upper abscissa of the diagram.

The survival period of one amphipod, *Calliopius laeviusculus,* was extremely short, certainly not more than 5 minutes at a temperature of 25° C. The other two species, *Gammarus oceanicus* and *Hyale prevosti,* did considerably better, the survival period ranging from about half an hour of anaerobic stress to about three hours. There was no clear-cut relationship between survival time and the size of the animals.

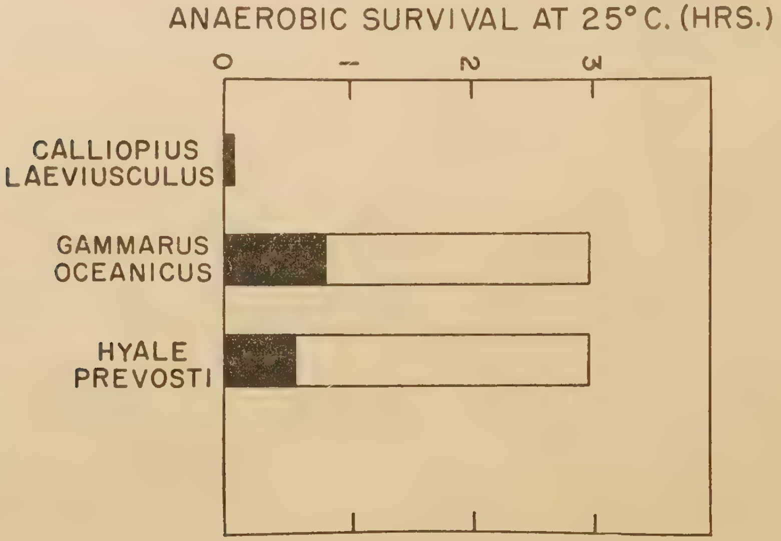

Figure 3. Survival under anaerobic conditions of the three species of amphipods studied. The black part of each column indicates the time of anaerobiosis *all* individuals survived, the white part indicates ranges of variability of survival time.

Discussion

The water analyses show plainly that animals living in the water trapped by large sea weeds at low tide may be subject to oxygen-free or almost oxygen-free conditions. Under extreme circumstances (very large clumps of algae, no light, high temperature) these conditions probably set in soon after the receding tide has uncovered the plants and may last for several hours. A drop in the oxygen content to 30% saturation value was found by Revelle and Emery (1958) in intertidal basins with algal growth at the bottom.

Animals living in sea weeds react in different ways to the movements of the tides. As shown previously (Wieser, 1952), some animals remain in the sea weeds all the time while others (in Plymouth, England, *e.g.* copepods and the amphipod *Stenothoe monoculoides*) leave their habitat with the receding tide and return to it with the rising tide. To the former group, obviously, belong slow-moving, non-swimming animals like the nematode and the mites studied in this paper. These species are adjusted to their environment by being able to withstand anaerobic conditions at 25° C. for at least 12 hours which, in an area with diurnal tides, is the theoretical maximum their habitat could remain emersed.

That paralysis during anaerobiosis is due to the accumulation of toxic metabolites within the body has been pointed out by von Brand (1946). Since the accumulation of metabolic substances is a temperature-dependent process, the close dependence of the rate of recovery from paralysis on the temperature at which the anaerobiotic period was spent (Fig. 2) could have been anticipated (see also Miller, 1957). Furthermore, the recovery time from anaerobiosis is a characteristic of each species. In the two halacarids, a linear relationship exists between the time of anaerobiosis and the time of recovery, up to the point at which the effects of asphyxiation become lethal and the curve expressing the relationship turns sharply upwards (Fig. 2). The slope of the linear portion of the curve is steep in the beginning and flattens out somewhat after 2–4 hours' application of anaerobic stress at room temperature. The points of inflection of the triphasic curve and the absolute values of recovery time, but not the slopes of the curves, are different in the two species of Halacaridae. However, the triphasic curve is well defined only for the experiments at room temperature. The 10-times larger species of *Halacarus* is more susceptible to the effects of asphyxiation than the species of *Rhombognathides*.

The relationship between time of anaerobiosis and time of recovery in the nematode *Enoplus communis* is an exponential one.

Kalmus (1942), in similar experiments, reported the recovery time to be different in different species and even mutants of *Drosophila*. In this genus, as in the halacarids over a certain period, a linear relationship between time of anaerobiosis and time of recovery was observed.

The second group of species, which consists of animals obviously able to leave and to repopulate the sea weeds at will, does not have to be adjusted for survival of anaerobic periods. The efficiency of receptor and locomotor organs of amphipods and related forms can always be considered as being sufficient to keep the animals in oxygenated water all the time. Accordingly *C. laeviusculus* has almost no resistance to the reduction of oxygen in its environment. The data in Figure 3 show that even five minutes of anaerobic conditions bring about the death of all members of this species, but the other two species of amphipods show some resistance. A related species of *Gammarus, G. duebeni,* is even known to occur on European coasts in rock pools and stagnant waters smelling of H_2S (Kinne, 1959).

The data of Figure 1 show that the least resistant amphipod, *C. laeviusculus,* has twice the oxygen consumption of the other two amphipod species. This might reflect the fact that the former species also leads a pelagic life, particularly in winter (Kunkel, 1918).

In a very general way it can be concluded that the nematode and the two halacarids in an anaerobic environment produce and deposit metabolic breakdown products which are toxic and cause paralysis. Up to a certain time, however, the tissues are not irreversibly injured by these breakdown products. The failure of *Calliopius laeviusculus* to endure even very short periods of de-oxygenation might be due either to its inability to gain sufficient energy under anaerobic conditions, or to the irreversibly harmful effects of even very small amounts of the breakdown products of anaerobic metabolism. The behavior of the remaining two amphipod species could be explained by assuming that either their energy or their excretory mechanisms function imperfectly under anaerobic conditions.

Summary

1. The water trapped by large brown sea weeds at low tide may become oxygen-free in the night or on cloudy days.

2. Slow-moving, non-swimming animals living in the sea weeds all the time (like nematodes and mites) are paralyzed by the removal of oxygen from the water, but they recover from this state if the period of anaerobic stress has lasted less than approximately 16 hours at 25° C. The relationship between time of anaerobiosis and time of recovery is temperature-dependent and a characteristic of each of the three species investigated (*Enoplus communis, Rhombognathides seahami, Halacarus basteri basteri*).

3. Agile animals, capable of leaving and repopulating the sea weeds with the tides, show a different reaction pattern. One of the amphipods investigated (*Calliopius laeviusculus*) did not survive even a few minutes of anaerobiosis, while the other two species (*Gammarus oceanicus, Hyale prevosti*) survived from about half an hour to three hours of anaerobiosis. The former species occasionally leads a pelagic life and has twice the respiratory rate of the latter two species.

LITERATURE CITED

Beadle, L. C., 1957. Respiration in the African swampworm, *Alma emini* Mich. *J. Exp. Biol.*, **34**: 1–10.

von Brand, T., 1946. Anaerobiosis in invertebrates. Biodynamica Monographs, no. 4, 328 pp. Biodynamica, Normandy, Mo.

Edwards, G. A., and L. Irving, 1943. The influence of season and temperature upon the oxygen consumption of the beach flea, *Talorchestia megalophthalma*. *J. Cell. Comp. Physiol.*, **21**: 183–189.

Holter, H., and K. Linderstrøm-Lang, 1943. On the Cartesian Diver. *C. R. Trav. Lab. Carlsberg. Sér. Chim.* (*Copenhagen*), **24**: 333–478.

Kalmus, H., 1942. Narcosis and asphyxiation in some species and mutants of *Drosophila*. *J. Exp. Biol.*, **19**: 238–254.

Kinne, O., 1959. Ecological data on the amphipod *Gammarus duebeni*. A Monograph. *Veröff. Inst. Meeresforsch. Bremerhaven*, **6**: 177–202.

Kunkel, B. W., 1918. The Arthrostraca of Connecticut. Connecticut Geol. Nat. Hist. Survey (Hartford), Bull. no. 26: 1–261.

Miller, J. A., 1947. Influence of temperature upon resistance to asphyxia. *In:* Influence of temperature on biological systems (F. H. Johnson, ed.) pp. 229–258. Amer. Physiol. Soc. Washington, D. C.

Rao, K. P., and T. H. Bullock, 1954. Q_{10} as a function of size and habitat temperature in poikilotherms. *Amer. Natur.*, **88**: 33–44.

Revelle, R., and K. O. Emery, 1958. Chemical erosion of beach rock and exposed reef rock. Geol. Surv. Professional Paper 260-T: 698–707. Washington, D. C.

Scholander, P. F., C. L. Claff, J. R. Andrews and D. F. Wallach, 1952. Microvolumetric respirometry. Methods for measuring O_2 consumption and CO_2 production by cells and enzymic reactions. *J. Gen. Physiol.*, **35**: 375–395.

Scholander, P. F., L. van Dam, C. L. Claff and J. W. Kanwisher, 1955. Micro gasometric determination of dissolved oxygen and nitrogen. *Biol. Bull.*, **109**: 328–334.

Sverdrup, H. U., M. W. Johnson and R. H. Fleming, 1946. The Oceans. Prentice-Hall, Inc., New York. Page 188.

Wieser, W., 1952. Investigations on the microfauna inhabiting sea weeds on rocky coasts. IV. *J. Mar. Biol. Assoc.*, **31**: 145–174.

Wieser, W., 1960. Benthic studies in Buzzards Bay. II. The Meiofauna. *Limnol. Oceanogr.* (in press).

Zeuthen, E., 1947. Body size and metabolic rate in the animal kingdom, with special regard to the marine micro-fauna. *C. R. Lab. Carlsberg, ser. Chim.*, **26**: 17–161.

Report for the year 1959

THE WOODS HOLE OCEANOGRAPHIC INSTITUTION
REPORT FOR THE YEAR
1959

PAGE

3 TRUSTEES

4 MEMBERS OF THE CORPORATION

6 HIGHLIGHTS OF 1959

13 DIRECTORS' REPORT

56 TREASURER'S REPORT
BALANCE SHEETS

CONTENTS

left:
Part of a group attending the Course for Industry given by the Institution.

middle:
The first International Oceanographic Congress was held August and September at the United Nations, New York City.

right:
The "Aries", recently acquired from Mr. R. J. Reynolds, after her arrival at the Institution.

below:
A special House Subcommittee on Oceanography, from Washington, hold a hearing in Woods Hole on the importance, support and future of the marine sciences.

hydrosphere

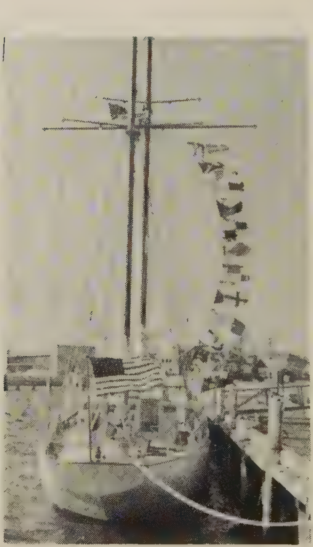

As of December 31, 1959 TRUSTEES

Henry B. Bigelow, Museum of Comparative Zoology, Cambridge 38, Massachusetts
L. O. Colbert, 4408 29th Street, N.W., Washington, D. C.
Marion Eppley, 510 Park Avenue, New York, New York
Alexander Forbes, 610 Harland Street, Milton, Massachusetts
Horace S. Ford, 77 Massachusetts Avenue, Cambridge 39, Massachusetts
A. G. Huntsman, 217 Indian Road, Toronto, Canada
Arnaud C. Marts, 521 Fifth Avenue, New York, New York
Lawrason Riggs, Riggs, Ferris and Geer, Room 1201, 74 Trinity Place, New York 6, New York
Harlow Shapley, Sharon Cross Road, Peterborough, New Hampshire
Henry L. Shattuck, 10 Milk Street, Boston, Massachusetts
Selman A. Waksman, Institute of Microbiology, Rutgers University, New Brunswick, New Jersey

Honorary Trustees

James S. Coles, Bowdoin College, Brunswick, Maine
Carl H. Eckart, Scripps Institution of Oceanography, La Jolla, California
Homer H. Ewing, Greenville, Wilmington 7, Delaware
Cecil H. Green, 338 Via del Norte, La Jolla, California
Milford R. Lawrence, Siders Pond Road, Falmouth, Massachusetts
Francis C. Welch, 73 Tremont Street, Boston, Massachusetts

Until 1963

Charles Francis Adams, Raytheon Company, 138 River Street, Waltham 54, Massachusetts
Columbus O'D. Iselin, Woods Hole Oceanographic Institution, Woods Hole, Massachusetts
Augustus P. Loring, Loring, Walcott Office, Inc., 35 Congress Street, Boston, Massachusetts
Albert E. Parr, American Museum of Natural History, Central Park West at 79th Street, New York, New York
Athelstan F. Spilhaus, Institute of Technology, University of Minnesota, Minneapolis 14, Minnesota
Alfred M. Wilson, Minneapolis-Honeywell Regulator Co., 2747 4th Avenue, South, Minneapolis 8, Minnesota

Until 1962

Harvey Brooks, Division of Applied Science, Harvard University, Cambridge 38, Massachusetts
Frank A. Howard, 30 Rockefeller Plaza, New York, New York
Robert R. Shrock, Department of Geology and Geophysics, Massachusetts Institute of Technology, Cambridge 39, Massachusetts
Edward H. Smith, Woods Hole, Massachusetts
Raymond Stevens, c/o Arthur D. Little, Inc., 30 Memorial Drive, Cambridge 42, Massachusetts
E. Bright Wilson, Jr., Department of Chemistry, Harvard University, Cambridge 38, Massachusetts

Until 1961

Detlev W. Bronk, The Rockefeller Institute of Medical Research, 66th Street and York Avenue, New York 21, N. Y.
Noel B. McLean, Edo Corporation, College Point 56, Long Island, N. Y.
Daniel Merriman, Bingham Oceanographic Laboratory, Yale University, New Haven, Connecticut
Emanuel R. Piore, International Business Machines Corp., 590 Madison Avenue, New York 22, New York
Alfred C. Redfield, Maury Lane, Woods Hole, Massachusetts
Gerard Swope, Jr., c/o International General Electric Co., 570 Lexington Avenue, New York, N. Y.

Until 1960

Edwin D. Brooks, Jr., P. O. Box 1135, Boston 3, Massachusetts
Mary Sears, Woods Hole Oceanographic Institution, Woods Hole, Massachusetts
Paul M. Fye, Woods Hole Oceanographic Institution, Woods Hole, Massachusetts

Ex Officio

Raymond Stevens, President of the Corporation, c/o Arthur D. Little, Inc., 30 Memorial Drive, Cambridge 42, Massachusetts
Henry B. Bigelow, Chairman of the Board of Trustees, Museum of Comparative Zoology, Cambridge 38, Massachusetts
Edwin D. Brooks, Jr., Treasurer, P. O. Box 1135, Boston 3, Massachusetts
Mary Sears, Clerk of the Corporation, Woods Hole Oceanographic Institution, Woods Hole, Massachusetts

Officers

MEMBERS OF THE CORPORATION

Charles Francis Adams, Raytheon Company, 138 River Street, Waltham 54, Massachusetts
Oliver Ames, III, "Edgewater", Beverly Farms, Massachusetts
Philip B. Armstrong, Medical Center of Syracuse, State University of New York, Syracuse, New York
Eric G. Ball, Harvard Medical School, Shattuck Street, Boston, Massachusetts
Henry B. Bigelow, Museum of Comparative Zoology, Cambridge 38, Massachusetts
Detlev W. Bronk, The Rockefeller Institute of Medical Research, 66th Street and York Avenue, New York 21, N. Y.
Edwin D. Brooks, Jr., P. O. Box 1135, Boston 3, Massachusetts
Harvey Brooks, Division of Applied Science, Harvard University, Cambridge 38, Massachusetts
George F. Carrier, Department of Mechanical Engineering, 211 Pierce Hall, Harvard University, Cambridge 38, Massachusetts
C. Lloyd Claff, Single Cell Research Foundation, Inc., 5 Van Beal Road, Randolph, Massachusetts
L. O. Colbert, 4408 29th Street, N.W., Washington, D. C.
Kenneth S. Cole, National Institutes of Health, Bethesda 14, Maryland
James S. Coles, Bowdoin College, Brunswick, Maine
Edward M. Douglas, West Chop, Massachusetts
Henry B. DuPont, Wilmington, Delaware
Ferdinand Eberstadt, 39 Broadway, New York 6, New York
Carl H. Eckart, Scripps Institution of Oceanography, La Jolla, California
Harrison P. Eddy, c/o Metcalf & Eddy, 1300 Statler Building, Boston, Massachusetts
Marion Eppley, 510 Park Avenue, New York, New York
Homer H. Ewing, Greenville, Wilmington 7, Delaware
Alexander Forbes, 610 Harland Street, Milton, Massachusetts
Horace S. Ford, 77 Massachusetts Avenue, Cambridge, Massachusetts
Paul M. Fye, Woods Hole Oceanographic Institution, Woods Hole, Massachusetts
John A. Gifford, 14 Wall Street, New York 5, New York
Cecil H. Green, 338 Via del Norte, La Jolla, California
Paul Hammond, Hammond, Kennedy & Legg Co., 230 Park Avenue, New York, N. Y.
Hudson Hoagland, Worcester Foundation for Experimental Biology, 222 Maple Avenue, Shrewsbury, Massachusetts
Frank A. Howard, 30 Rockefeller Plaza, New York, New York
Columbus O'D. Iselin, Woods Hole Oceanographic Institution, Woods Hole, Massachusetts
J. Seward Johnson, Cedar Lane Farm, Oldwick, New Jersey
Augustus B. Kinzel, Union Carbide Corporation, 30 East 42nd Street, New York 17, New York
Milford R. Lawrence, Siders Pond Road, Falmouth, Massachusetts
Alfred L. Loomis, Room 2420, 14 Wall Street, New York, New York
Augustus P. Loring, Loring, Walcott Office, Inc., 35 Congress Street, Boston, Massachusetts
Arnaud C. Marts, 521 Fifth Avenue, New York, New York
Robert E. McConnell, First National Bank, Hobe Sound, Florida
Noel B. McLean, Edo Corporation, College Point 56, Long Island, New York
Daniel Merriman, Bingham Oceanographic Laboratory, Yale University, New Haven, Connecticut
Henry S. Morgan, 2 Wall Street, New York, New York
Frank A. Pace, General Dynamics Corporation, 445 Park Avenue, New York 22, New York
Albert E. Parr, American Museum of Natural History, Central Park West at 79th Street, New York, New York
Sumner T. Pike, Lubec, Maine
Emanuel R. Piore, International Business Machines Corp., 590 Madison Avenue, New York 22, New York
Alfred C. Redfield, Maury Lane, Woods Hole, Massachusetts
George H. Richards, 68 Williams Street, New York, New York

Lawrason Riggs, Riggs, Ferris and Geer, Room 1201, 74 Trinity Place, New York 6, New York
William W. Rubey, U. S. Geological Survey, Washington 25, D. C.
Francis C. Ryder, 37 Larchwood Drive, Cambridge 39, Massachusetts
Mary Sears, Woods Hole Oceanographic Institution, Woods Hole, Massachusetts
Harlow Shapley, Sharon Cross Road, Peterborough, New Hampshire
Henry L. Shattuck, 10 Milk Street, Boston, Massachusetts
Robert R. Shrock, Department of Geology and Geophysics, Massachusetts Institute of Technology, Cambridge 39, Massachusetts
Edward H. Smith, Woods Hole, Massachusetts
Athelstan F. Spilhaus, Institute of Technology, University of Minnesota, Minneapolis 14, Minnesota
H. Burr Steinbach, Department of Zoology, University of Chicago, Chicago 37, Illinois
Raymond Stevens, c/o Arthur D. Little, Inc., 30 Memorial Drive, Cambridge 42, Massachusetts
Julius A. Stratton, Office of the Vice President and Provost, Massachusetts Institute of Technology, Cambridge 39, Massachusetts
Gerard Swope, Jr., c/o International General Electric Co., 570 Lexington Avenue, New York, New York
Selman A. Waksman, Institute of Microbiology, New Brunswick, New Jersey
Thomas J. Watson, Jr., International Business Machines Corporation, 590 Madison Avenue, New York 22, New York
Francis C. Welch, 73 Tremont Street, Boston, Massachusetts
Alfred M. Wilson, Minneapolis-Honeywell Regulator, 2747 4th Avenue South, Minneapolis 8, Minnesota
E. Bright Wilson, Jr., Department of Chemistry, Harvard University, Cambridge 38, Massachusetts

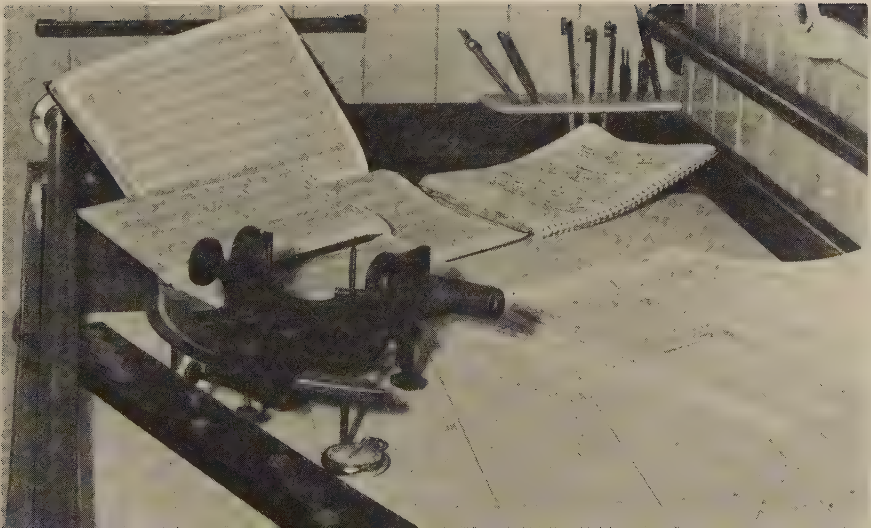

HIGHLIGHTS OF 1959

The multitude of technical problems presented by the oceans continues to stimulate and inspire scientists devoted to their solution. This has been a good year for oceanography in that the opportunities for oceanographers have expanded and the challenges of the ocean have been dramatically defined by a number of important events. As an introduction to the **"Annual Report"** of the Woods Hole Oceanographic Institution, a few of these important events are listed.

Two reports of national significance in oceanography were published early in the year. In January, Admiral Arleigh Burke officially approved the U. S. Navy's TENOC (Ten-Year Oceanographic) program. In February, the National Academy of Sciences released its report "Oceanography 1960-1970". National interest was aroused by these reports. A Special Subcommittee on Oceanography of the Committee of Merchant Marine and Fisheries of the House of Representatives started hearings in Washington where many oceanographers and Government representatives were heard. We were most pleased that the Subcommittee's Chairman, Representative George P. Miller (D.-Cal.), together with Congressmen James C. Oliver (D.-Me.), Gerald T. Flynn (D.-Wis.) and the representative for the 9th Massachusetts district, Hastings Keith (R.-Mass.), arranged to hold a hearing at Woods Hole in June. The Director and staff members presented statements followed by demonstrations and an inspection of facilities. The interest created by these reports and congressional hearings should develop sufficient support in oceanography so that we can realize many long-standing objectives and permit marine sciences to assume their proper role in technological development.

At the beginning of the year we received a fine gift from Mr. R. J. Reynolds in the form of his 93-foot ketch ARIES. The ship was brought to Woods Hole during some heavy March gales and was refitted with a minimum of damage to her yacht-like appearance to serve for a two-year period in the Bermuda area. It is worth noting that the ARIES has been used in a joint project with the National Institute of Oceanography of England, to study subsurface currents in the mid-ocean.

The CHAIN made her first long cruise in our service from April to August on extensive geophysical investigations in the Atlantic Ocean and the Mediterranean Sea. The ship has performed extremely well; the comfort of a larger ship is one that our sea-going staff—long used to cramped, uncomfortable quarters —readily has accepted. In November, we were able to take over the manning of the CHAIN with our officers and crew from the Military Sea Transportation Service which, under Captain Wallace S. Olivey, handled the vessel ably under her first year in our service. Altogether the ships of our fleet spent 865 days at sea in 1959 compared with 740 days in 1958. A simple breakdown into major research areas shows that during 1959 our oceanographers spent 2,231 man days at sea in the study of physical oceanography, chemistry and geology; 2,737 man days on underwater acoustics and geophysics and 566 man days on biology.

In a year in which so much of importance transpired, it is somewhat difficult to point to the outstanding event. Probably the first International Oceanographic Congress held at the United Nations, August 31 to September 12, was the highlight of 1959. The Director transferred the Institution's headquarters to New York for the Congress and together with 70 staff members met with the 1,200 oceanographers from around the world. The Congress itself was a resounding success which largely may be attributed to the hard work of Dr. Mary Sears who spent an immeasurable number of hours organizing this important occasion in the history of oceanography.

The CHAIN and the ATLANTIS were tied up at Pier #34 in New York, together with the overshadowing MIKHAIL LOMONOSOV of the Academy of Sciences, U.S.S.R., and the JOSIAH WILLARD GIBBS of the Hudson Laboratories. Nearly a thousand visitors from 27 countries came on board the ATLANTIS and the CHAIN.

Our summer fellowship program had its most successful year in the the history of the Institution. Twelve excellent Fellows were chosen from the 118 applicants applying from four countries. Ten of these were graduating seniors or graduate students and there were two postdoctoral fellows. A total of five students are currently doing year-round graduate research at Woods Hole. A summer course in "Theoretical Studies in Geophysical Fluid Dynamics" was supported by the National Science Foundation and was so successful that repeats in future summers are planned. The enthusiastic response to the course for industry in "Environmental Factors Influencing the Performance of Naval Weapons Systems", which was repeated in December, indicates the growing interest of American industry in oceanography. The public attention created by the report of The National Academy of Sciences' Committee on Oceanography seems to have had a direct influence on the interest of university students in this subject. For example, the number of students attending the introductory course in physical oceanography at the Massachusetts Institute of Technology was nearly twice that of previous years—some 23 persons; of this group four have elected to work toward advanced degrees in oceanography.

A final, and most significant, highlight of the year was the awarding to the Institution by the National Science Foundation of $3,000,000 for the construction of the first research ship to be built in the 1960-1970 program. We are greatly honored to receive this grant which enables us to replace the ATLANTIS with an equally fine ship, uniquely designed, as was the ATLANTIS, for oceanographic research. Design plans are proceeding well and it is anticipated that a very modern replacement should follow promptly the retirement of the ATLANTIS. The Development Program adopted by the Trustees in August has been greatly helped by this grant.

As of December 31, 1959 RESEARCH STAFF

ARNOLD B. ARONS, Associate in Physical Oceanography
Professor of Physics, Amherst College

WILLIAM D. ATHEARN, Research Associate in Geology

JOHN C. AYERS, Associate in Marine Biology
Associate Professor, Great Lakes Research Institute, and Associate Professor of Zoology, Department of Zoology, University of Michigan

RICHARD H. BACKUS, Marine Biologist

JOHN P. BARLOW, Associate in Marine Biology
Assistant Professor of Oceanography, Cornell University

LINCOLN BAXTER II, Research Associate in Physics

DAVID L. BELDING, Associate in Marine Biology
Professor of Bacteriology and Experimental Pathology (Emeritus), Boston University; Consultant, U. S. Fish & Wildlife Service

BRUCE BENSON, Associate in Physics
Associate Professor of Physics, Amherst College

HENRY B. BIGELOW, Associate in Oceanography
Professor of Zoology (Emeritus), Harvard University; Research Oceanographer, Museum of Comparative Zoology

DUNCAN C. BLANCHARD, Research Associate in Meteorology

BERT BOLIN, Associate in Meteorology
Director, Institute of Meteorology, University of Stockholm; Director, International Institute of Meteorology, Stockholm

VAUGHAN T. BOWEN, Geochemist
Lecturer in Zoology, Yale University

ALVIN L. BRADSHAW, Research Associate in Oceanography

ROBERT R. BROCKHURST, Research Associate in Physics

JOHN G. BRUCE, JR., Research Associate in Oceanography

KIRK BRYAN, JR., Research Associate in Meteorology

DEAN F. BUMPUS, Oceanographer

ELIZABETH T. BUNCE, Research Associate in Physics

ANDREW F. BUNKER, Meteorologist

CORNELIA L. CAREY, Associate in Marine Bacteriology
Associate Professor of Botany (retired), Barnard College

CHARLES E. CARVER, JR., Associate in Hydraulics
Associate Professor of Civil Engineering, University of Massachusetts

JOSEPH CHASE, Research Associate in Physical Oceanography

GEORGE L. CLARKE, Marine Biologist
Associate Professor of Zoology, Harvard University

NATHANIEL CORWIN, Research Associate in Chemistry

HERBERT C. CURL, JR., Research Associate in Marine Biology

WILLARD DOW, Electronics Engineer

RICHARD S. EDWARDS, Research Associate in Geophysics

W. MAURICE EWING, Associate in Geophysics
Professor of Geology, Columbia University; Director, Lamont Geological Observatory

ALAN J. FALLER, Research Associate in Meteorology

HARLOW G. FARMER, JR., Research Associate in Hydraulics

CHARLES J. FISH, Associate in Marine Biology
Professor of Marine Biology, University of Rhode Island; Director, Narragansett Marine Laboratory

DAVID H. FRANTZ, JR., Research Associate in Engineering

FREDERICK C. FUGLISTER, Physical Oceanographer

PAUL M. FYE, Chemist

MICHAEL GARSTANG, Research Associate in Meteorology

JOHN W. GRAHAM, Research Associate in Geology

DONALD R. GRIFFIN, Associate in Physiology
Professor of Zoology, Harvard University

ROBERT R. L. GUILLARD, Research Associate in Marine Biology

Bernhard Haurwitz, Associate in Meteorology
Professor of Astrogeophysics, University of Colorado

Earl E. Hays, Physicist

John B. Hersey, Geophysicist
Associate Professor of Oceanography, Massachusetts Institute of Technoolgy

Louis N. Howard, Associate in Mathematics
Associate Professor of Mathematics, Massachusetts Intitute of Technology

Edward M. Hulburt, Research Associate in Marine Biology

Columbus O'D. Iselin, Henry Bryant Bigelow, Oceanographer
Associate Professor of Physical Oceanography, Harvard University; Research Oceanographer, Museum of Comparative Zoology; Professor of Oceanography, Massachusetts Institute of Technology

Henry R. Johnson, Research Associate in Underwater Acoustics

John W. Kanwisher, Biophysicist

Bostwick H. Ketchum, Senior Oceanographer
Lecturer in Biological Oceanography, Harvard University

David D. Ketchum, Research Associate in Electronics

Sydney T. Knott, Jr., Research Associate in Engineering

Richard G. Leahy, Research Associate in Geology

Benjamin B. Leavitt, Associate in Marine Biology
Associate Professor of Biological Sciences, University of Florida

Joseph Levine, Research Associate in Meteorology

Joyce C. Lewin, Research Associate in Marine Biology

Joanne S. Malkus, Meteorologist

Willem V. R. Malkus, Physical Oceanographer
Professor of Oceanography, Massachusetts Institute of Technology

Frank J. Mather III, Research Associate in Oceanography

James W. Mavor, Jr., Associate in Applied Physics
Associate Professor of Mechanical Engineering, Northeastern University

William G. Metcalf, Physical Oceanographer

Arthur R. Miller, Physical Oceanographer

Robert L. Miller, Associate in Submarine Geology
Associate Professor, Qualitative Sedimentology, The University of Chicago

Raymond B. Montgomery, Associate in Physical Oceanography
Associate Professor of Oceanography, Chesapeake Bay Institute, The Johns Hopkins University

Hilary B. Moore, Associate in Marine Biology
Professor in Marine Biology and Assistant Director, Marine Laboratory, University of Miami

James M. Moulton, Associate in Marine Biology
Assistant Professor of Biology, Bowdoin College

Jerome Namias, Associate in Meteorology
Chief, Extended Forecast Section, U. S. Weather Bureau

A. Conrad Neumann, Research Associate in Sedimentary Geology

Geoffrey D. Nicholls, Associate in Geochemistry
Lecturer, Department of Geology, University of Manchester, Manchester, England

Daniel R. Norton, Associate in Chemical Oceanography
Research Chemist, Sprague Electric Co., North Adams, Massachusetts

Charles B. Officer, Jr., Associate in Geophysics
Associate Professor of Geology, Rice Institute

David M. Owen, Research Associate in Underwater Photography

Mary Alys Plunkett, Associate in Chemistry
Associate Professor of Chemistry, Vassar College

Alfred C. Redfield, Senior Oceanographer (Emeritus)
Professor of Physiology (Emeritus), Harvard University

Charles E. Renn, Associate in Engineering
Professor of Sanitary Engineering, School of Engineering, The Johns Hopkins University

Francis A. Richards, Associate in Chemical Oceanography
Associate Professor of Chemistry, Department of Oceanography, University of Washington, Seattle, Washington

William S. Richardson, Physical Chemist

Gordon A. Riley, Associate in Marine Physiology
Associate Director, Bingham Oceanographic Laboratory, Yale University

Helen M. Roberts, Associate in Mathematics
Assistant Professor of Mathematics, University of Connecticut

Allan R. Robinson, Associate in Physical Oceanography
Assistant Professor of Geophysics, Harvard University

F. Claude Ronne, Research Associate in Photography

John H. Ryther, Marine Biologist

Howard L. Sanders, Research Associate in Marine Biology

Harold E. Sawyer, Research Engineer

Irving I. Schell, Associate in Meteorology
Research Associate, Department of Geology, Tufts University

William E. Schevill, Associate in Oceanography
Research Associate in Zoology, Museum of Comparative Zoology, Harvard University

Karl E. Schleicher, Research Associate in Physics

William C. Schroeder, Ichthyologist
Associate Curator of Fishes, Museum of Comparative Zoology, Harvard University

Mary Sears, Planktonologist

Raymond Siever, Associate in Geology
Assistant Professor of Geology, Harvard University

Edward H. Smith, Associate in Oceanography
Development Office, The Cooper Union for the Advancement of Science and Art

Paul Ferris Smith, Associate in Physical Oceanography
Electronics Engineer, Rockefeller Institute for Medical Research

Floyd M. Soule, Associate in Physical Oceanography
Oceanographer, U. S. Coast Guard

Allard T. Spencer, Research Associate in Engineering

Edward A. Spiegel, Associate in Astrophysics
Assistant Professor of Astrophysics, University of California

Athelstan F. Spilhaus, Associate in Physical Oceanography
Dean, Institute of Technology, University of Minnesota

Melvin E. Stern, Research Associate in Physics

Henry M. Stommel, Physical Oceanographer
Professor of Oceanography, Massachusetts Institute of Technology

Edward D. Stroup, Associate in Physical Oceanography

Thomas T. Sugihara, Associate in Geochemistry
Associate Professor of Chemistry, Clark University

William H. Sutcliffe, Jr., Associate in Marine Biology
Director, Bermuda Biological Station for Research, Inc.

Parker D. Trask, Associate in Submarine Geology
Professor of Geological Engineering, University of California

Harry J. Turner, Jr., Marine Biologist
Lecturer in Zoology, University of New Hampshire

Ralph F. Vaccaro, Research Associate in Microbiology

George Veronis, Mathematician

Allyn C. Vine, Physical Oceanographer

Gordon H. Volkmann, Research Associate in Physical Oceanography

William S. von Arx, Physical Oceanographer
Professor of Oceanography, Massachusetts Institute of Technology

Arthur D. Voorhis, Research Associate in Physics

Robert G. Walden, Research Associate in Electronics

Edmond E. Watson, Associate in Physical Oceanography
Professor of Physics, Queen's University, Kingston, Ontario

Stanley W. Watson, Research Associate in Marine Bacteriology

Raymond Wexler, Associate in Meteorology
Allied Research Associates, Inc., Boston, Massachusetts

Geoffrey G. Whitney, Jr., Research Associate in Physical Oceanography

Alfred H. Woodcock, Oceanographer

George P. Woollard, Associate in Geophysics
Professor of Engineering Geology and Geophysics, University of Wisconsin

L. Valentine Worthington, Physical Oceanographer

Charles S. Yentsch, Research Associate in Marine Biology

John M. Zeigler, Research Associate in Marine Geology

ADMINISTRATIVE STAFF

Paul M. Fye	Director
Richard G. Leahy	Technical Assistant to the Director
James R. Mitchell	Administrative Assistant to the Director
Ronald A. Veeder	Development Program Manager
John McGilvray	Business Manager
Jan Hahn	Public Information
Norman T. Allen	Archivist
Harvey MacKillop	Controller
John F. Pike	Port Captain

DIRECTOR'S REPORT

The following summaries of our scientific achievements during the year have been compiled with the help of many staff members and the excellent editorial assistance of the Director's Technical Assistant. It is impossible to properly credit the work of each research investigation but appreciation is gratefully acknowledged for the technical work of our entire staff which is herewith recorded.

Respectfully submitted,

Paul M Fye

Paul M. Fye

Overall picture of the Woods Hole Oceanographic Institution and the National Institute of Oceanography "Atlantic Ocean Survey". Detail shows oceanographic positions and plots of the five cruises on which bathythermograph observations were obtained.

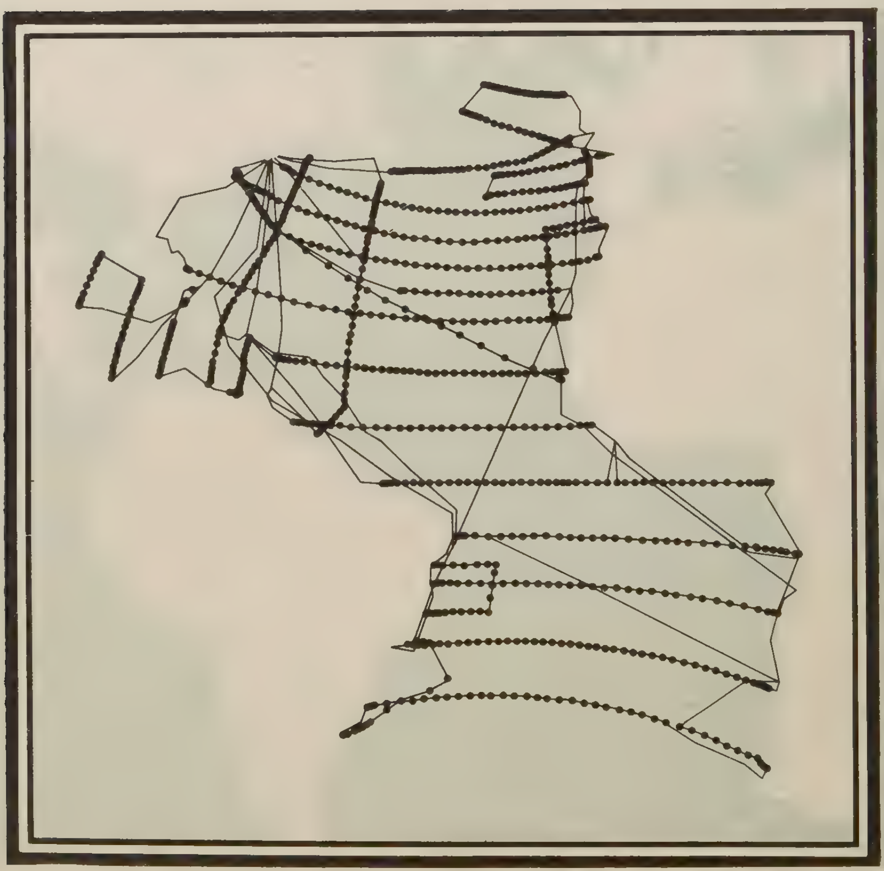

The Atlantic Ocean Atlas, describing the results of the survey will be published June 1960.

PHYSICAL OCEANOGRAPHY

During 1959 the Institution completed the International Geophysical Year field program. In the first seven months of the year, the final cruise under this project was carried out by the ATLANTIS. Four crossings of the Atlantic were completed, including a very long hydrographic section at 32° S latitude between Montevideo, Uruguay and Cape Town, South Africa. One other additional IGY hydrographic section across the Atlantic at 36° N latitude was made by the CHAIN. Computation and tabulation of the ATLANTIS data is now almost completed and when submitted to the International Geophysical Year Data Center will represent the formal termination of our cooperation in this program.

This participation has at one time or another involved a majority of the people working at the Institution, three of our research vessels and two research vessels from other countries. It has included research at the two Arctic Ocean ice stations, flights to sample atmospheric CO^2 along the Atlantic coastline from the equator to Newfoundland and mutual cooperation with uncounted foreign investigators including the crew of a Russian research vessel who collected water samples for a project in which we were involved. Twelve trans-Atlantic hydrographic cross sections were completed as well as four sections in the northeastern Atlantic, four sections in the Caribbean and several intensive hydrographic studies including the area to the west of the Strait of Gibraltar, as well as portions of the Mediterranean and Red Seas and the Gulf of Aden.

An analysis of the Atlantic data is in progress and the descriptive portion is being prepared for presentation in a hydrographic atlas of the Atlantic Ocean. This work is a major effort which should provide a fresh description of the Atlantic Ocean and be of value for many decades.

A north-south section from the northeast of Sable Island to the east of Bermuda was completed in June by the CRAWFORD. These and similar observations made from the CHAIN indicate that conditions in the northern Sargasso Sea are different from those considered to be normal. The thermocline at a number of stations was 300 meters shallower than expected and the temperatures of the upper layers were generally below normal values for that time of year. It has been suggested that this occurrence results from an intrusion of water from the east of the Sargasso Sea as indicated by the temperature—salinity relationships. The north—south CRAWFORD section also showed that there was almost no slope water. Although this was unexpected, not enough previous data were available from this area to exclude the possibility that this absence is not simply a seasonal occurrence. A further study of this problem is being made and it is hoped that the temperature records made by commercial ships on the North Atlantic run may prove helpful.

Studies of sea surface waves have continued to be based mainly on data collected by an instrumented tower in Buzzards Bay. Observations are made by measuring the wetted resistance of three vertical sensing wires which are suspended from the tower down through the sea surface. The wave height data from the individual waves in the array are transmitted by an FM radio link to the laboratory in Woods Hole where it is recorded and subsequently automatically printed on a punched tape which is designed to be fed directly into a computer for analysis. The analysis of these data will deal primarily with the directional spectrum, but it is also planned to make slope frequency measurements.

In addition to the neutrally buoyant float technique, developed by Dr. John Swallow of the National Institute of Oceanography, some other deep-water tracking devices such as parachute drogues were utilized for the direct measurement of currents during the past year. Comparisons of simultaneous measurements by different methods were generally satisfactory.

A remote recording thermograph, placed on the bottom at Browns Ledge last summer, was retrieved and its record analyzed. This experiment demonstrated the tidal influence on temperature at the instrument location and also showed that a persistent wind can cause advection throughout the water column.

An extensive use of neutrally buoyant deep current measuring floats was made in a long term study of the deep circulation around Bermuda. Using the ARIES, and later the ARIES and the CRAWFORD jointly, an anomalous patch of 18°C water was located and traced over a period of many weeks. Deep current measurements made beneath this 18° patch displayed no particular pattern. It was decided that the high velocities of 8 to 12 centimeters per second were not related to this water lens. The lens was defined chiefly by a dip in the isotherms extending to about 1000 meters. Measurements inside it showed a strong (1 knot) clockwise circulation following the isotherms quite closely. The lack of T-S anomalies and slightly higher oxygen values indicate the patch had a relatively local and fairly recent origin. The flushing of the reef waters at Bermuda is considered to be its most likely source. While the large majority of measurements showed a southerly or southwesterly set to the lens, measurements made at points as little as 30 miles apart showed no relationship to one another. Floats only 2 or 3 miles apart did, however, move in nearly the same direction and at comparable speeds. The predominant southerly set encountered in this area is at variance with present theoretical expectations for the deep ocean circulation.

The surface current measuring program also revealed an interesting feature. Ten drift bottles launched during the spring and summer off southern New England were recovered to the southward, some from points beyond Cape Hatteras. Previously, only two bottles launched off southern New England have ever been recovered south of Hatteras. This pronounced southeasterly drift of at least 5 miles a day along the mid-Atlantic seaboard during the month of September may be associated with a period of northeast winds which persisted in the region for over two weeks. The progress of cold coastal water around Cape Hatteras during this period was substantiated in the salinity and temperature data taken at the Diamond Shoal Lightship.

Research into the meanderings and pulsations of the Gulf Stream has shown that on the Blake Plateau in the offing of Onslow Bay, North Carolina, the course and speed of the current is also related to meteorological conditions. Variations in the course of the current have been related to the monthly, semimonthly, and daily tidal frequencies, and also are found to correlate with the synoptic motion of atmospheric low pressure systems leaving the continent by way of the Cape Hatteras storm track.

The lateral motions of the Gulf Stream associated with tidal frequencies range from 5 to 10 nautical miles, while those associated with the passage of meteorological disturbances over the area may be as much as 30 miles. Because these motions of the Gulf Stream have too high a frequency to be studied by traditional dynamic methods, it is of interest to develop methods which provide direct measurements of the time variation of the horizontal pressure gradients in the ocean. Several techniques are under trial or consideration both for shipboard use and for instrumentation on a system of anchored buoys.

Comparing "Atlantis" and "Meteor" Sections of the South Atlantic.

MATHEMATICS AND THEORETICAL OCEANOGRAPHY

A most successful venture was the presentation during the summer of 1959 of an eight weeks' course entitled "Theoretical Studies in Geophysical Fuild Dynamics". The course was supported by a grant from the National Science Foundation, and eight participants were selected from graduate and post-graduate applicants. Each participant was encouraged to formulate a tractable statement of a suitable problem so that he might continue his research upon returning to his own Institution. The introduction to the course concerned the fundamental theory of steady flow and fluid instability in rotating and non-rotating systems. Other topics covered were the statistical theories of turbulence and their applications to isotropic homogeneous fluid motions, conductive instability due to radative heat flux and the problems of wave motion. The course was so well received that it will be presented again during the summer of 1960.

One of the more interesting research projects of the group concerned a study of the instability of the Ekman viscous boundary layer on both theoretical and experimental terms. Preliminary results suggest a more direct coupling between the Ekman boundary layer and its associated geostropic flows than one would expect from experience with boundary layer phenomena in non-rotating systems. Another development is the formulation of a Rayleigh instability criterion for vertical heat and salt transfer. This discovery has possible implications in an understanding of the thermohaline circulation in the ocean. It has been shown that the actual distribution of salt in sub-tropical oceans is in principle very unstable which points out the necessity for finding some mechanism for maintaining the high surface salinities observed at sea. This question has stimulated several experimental and theoretical studies.

In the experimental studies, it was discovered that the salt convection occurs as long thin vertical columns of the sinking salt water, and intermediate rising columns of fresher water. These succeed in transferring salt vertically through the stable density gradient without a significant transfer of heat. It was further shown that small disturbances, such as very gentle stirring, can prevent the formation of convective elements and inhibit fallout of salt. Presumably something of a similar nature happens in the ocean because a widespread fallout of salt does not seem to prevail. A theoretical analysis of this steady columnar convective regime seems to account qualitatively for its main features.

Other studies undertaken by the group have included an analysis of water mass characteristics of the abyssal circulation of the world ocean. Using a numerical model on the observed data of deep temperature, salinity, radio-carbon, and heat flux through the bottom, it was considered possible to make some fairly definite statements about the composition and time-rates of formation of Pacific—Indian Ocean common water. This study is a generalization of normal water mass analysis. Future work may lead to further refinements and extensions of the method to other oceanographic areas.

Experimental studies of the field of motion produced by electrical forces were made in the hope that these might contribute to an understanding of non-linear fluid processes. Electrical measurements are technically simpler to make than direct thermal or force measurements. However, the problem of interpreting the electrical experiments is not simpler than for thermal studies so that these results are primarily of academic interest.

An estimate of the seasonal change of heat stored in a vertical column of water as a function of latitude and longitude in the North Atlantic has been dependent on the steadily increasing mass of data in the hydrographic file at the Institution. This study is based on the cumulative mean temperatures at standard depths obtained from a large number of bathythermograms. Because the study rests upon such a wealth of detailed information, comparison with the seasonal heat storage caluculated indirectly from meteorological data is particularly interesting. Taking averages for the entire North Atlantic between 20° and 55° N, the two types of estimates agreed within 15%.

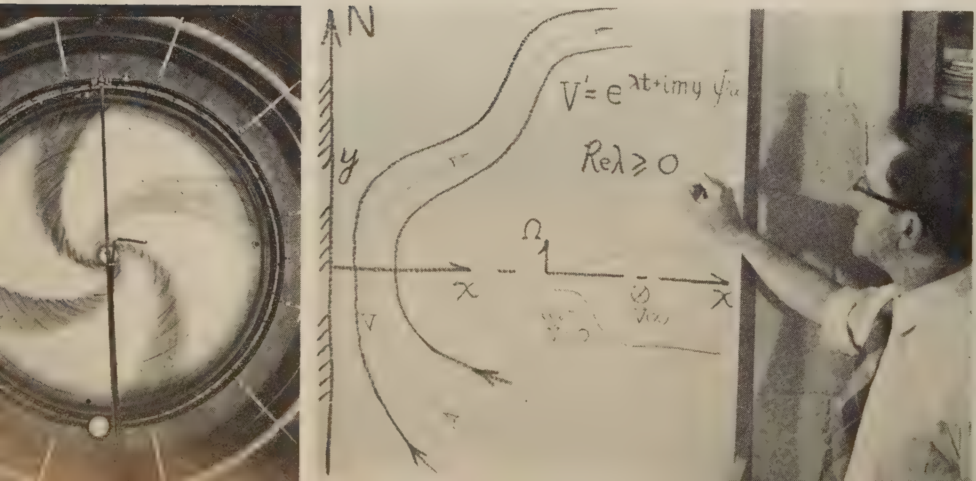

Theoretical
and Experimen
Studies in
Geophysical
Fluid Dynamics

MARINE METEOROLOGY

The interaction between the sea and the atmosphere is indeed a two-way street which, in a sense, merits a name such as "Meteorological Oceanography" as much as it does the familiar one of "Marine Meteorology". That the latter is now used may indicate man's rapid progress in learning about the effects of the sea on the atmosphere as compared to his slower pace in understanding the effects of air on the sea. Though some work on both is done at the Institution, it is the air above the sea which receives most attention. So much of marine meteorology is yet to be investigated that a wide range of attacks is feasible. The diversity of the work undertaken at the Institution gives some idea of the scope of the problem, and its pioneering status is suggested by the number of instruments developed or improved by Woods Hole investigators.

One of the longer-term research efforts in this field has been an investigation of the modification of air masses over the ocean. The analysis of the flux of heat and water vapor from the sea to the air as continental polar air masses travel southeastward from the United States' eastern coast into the tropics has been the basis for much of this. This work has required that special emphasis be placed on the development of instruments to observe the various atmospheric parameters required for the analysis of the problem and has resulted in an increasing refinement and elaboration of the instrumentation on the R4D airplanes. In particular, fast response temperature and liquid water content instruments proved to be very successful. Using these techniques, field work has been extended to the Atlantic trade wind areas over the ocean to the east of Trinidad. Associated with this has been an analysis of clear and cloudy areas near a cold front. This latter work was based on

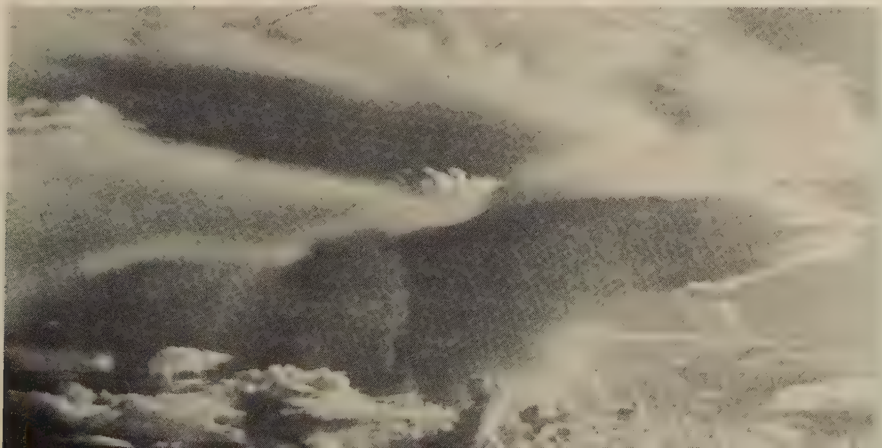

Tropical Cumulonimbus.

photographs made with specially modified cameras which were mounted in the nose of the aircraft.

The work on sea-salt nuclei has been progressing. It has included a continuation of an analysis of orographic rains in Hawaii in an effort to obtain a more complete understanding of the condensation process, and of the origin of the showers themselves. An improved design of the airborne flame spectrometer was completed and installed in the R4D. This instrument, which permits the sampling of atmospheric salt in much smaller parcels of air than was previously possible using the older slide collection techniques, was flown successfully off Trinidad in association with the heat flux measurements, and it is expected to provide unique information regarding the distribution of salt in the cloud region.

The study of the bursting of air bubbles at the sea surface has been continued and has verified the theory that by this process positively charged droplets are injected into the atmosphere. The electrical charge of these particles may not only influence the behavior of the particle within a cloud, but the sum total of these taken over all the nuclei in the cloud appears to give a net positive charge that has been transferred from the ocean to the atmosphere. The amount of charge as a function of bubble and drop size, bubble age and salinity of the water has also been determined. It has been shown to be dependent upon the circumstances under which the bubbles burst. An organic film on the surface of the water can diminish or even prevent the formation of the nuclei.

The tropics were the focus of an extensive analysis of heat balance. The methods utilized range from photographic observation of cloud development to the description of natural processes in terms of applied mathematical models. Convection, heat balance, hurricane energy and a description of cloud geometry were all subjects related to this problem which were studied by staff members and their associates at other Institutions. This work is being continued along many interesting lines, one of which is the investigation of the factors considered important in the inhibition of convection. This research is the offshoot of the concept of the bubble-like growth of cumulus clouds which was developed previously by various members of the Institution.

Meteorological instruments mounted on the R4D.

Detailed examination of the data for 1958 hurricane "Daisy" has indicated the importance of major cloud towers. Assuming reasonable sizes, buoyancies and entrainment rates, model calculation suggests that there should be no particular difficulty in getting penetration of these major towers into the stratosphere in such a hurricane. The good correlation of the theoretical prediction of the characteristics of such major clouds with the photographic measurement of towers in hurricane "Daisy" supports the proposed model. The development of these cloud towers under model conditions also implies updrafts of the order of 50 meters per second. These extreme rise rates have also been indirectly supported by radar and pilot balloon observations along the walls of the hurricane eye. The effect of high humidity conditions in hurricane rain areas reduces downdrafts and turbulence associated with the proximity of updraft and downdraft zones. Cloud towers forming under dryer, unstable conditions indicate that such zones could produce intense turbulence.

UNDERWATER ACOUSTICS

Our interests in the vertical migrations of organisms and in the scattering layer have been continued. Two techniques have been developed in an attempt to obtain photographs of the species involved. One of these involves immersing a sound transducer in the scattering layer and taking a picture when the organism which reflects the sound is expected to be in focus for the camera. The other operates by an automatically triggered camera which depends upon the luminescent flashing of the organism. In both cases successful photographs of either sound scattering or luminescent organisms have been obtained from the various depths in the sea. Broad-band acoustic observations of scattering layers were extended during the year to new localities in the eastern North Atlantic Ocean and in the Mediterranean Sea. These observations employ an explosion as the sound source and give information about sound-scatterers over a wide portion of the sound spectrum. Comparison of such observations from many widely-separated points should do much towards delineating the faunal provinces of the upper part of the high seas.

On a cruise in the deep water south of New England in August an echo-sounder and bathyphotometer were used to make observations of the vertical movement of scattering layers with respect to illumination, a continuation of the work begun three years ago.

It was possible to determine the approximate distribution of a special midwater sound scatterer which has come to our attention in recent years. This feature, popularly known as "Alexander's Acres", is composed of a larger or more numerous sound scatterer, judging from records, than is found in ordinary deep scattering layers. During the spring and summer, the scatterer was found to be almost continuously distributed in the ocean area from the latitude of New Jersey south to Cape Hatteras and from the 200-fathom curve offshore to the Gulf Stream. This feature perhaps represents an exploitable resource, and identification of the responsible organism is an early objective of the scattering layer program.

The National Science Foundation-supported investigation on various aspects of the natural history of whales and porpoises has continued, and particular emphasis has been placed on the production of sound by these animals and its relationship to their behavior. This work was pursued from the ASTERIAS, BEAR and CRAWFORD on cruises in local waters, to the Gulf of Maine and in the deep ocean south of New England. The newly-acquired Helio-Courier aircraft was also used in these investigations and has proved valuable for locating groups of whales and directing surface craft to them. Because of its low-speed characteristics and unobstructed view, this aircraft is excellent for aerial photography of cetaceans and other large sea animals.

Since their discovery in local waters a few years ago, observation of the rare North Atlantic right whale at the time of its springtime, northward migration has become an annual event. Over the period of several weeks in March and April of this year about 30 of these animals were observed in Vineyard Sound and Cape Cod Bay and first extensive recordings of their underwater sounds were made.

During the summer in deep water to the south of Woods Hole a little-known porpoise, ***Stenella styx,*** was extensively observed and the first positively identified recordings of the underwater sounds of this species were obtained.

The studies of the ocean as a medium for the transmission of sound have continued. The environmental factors which have received most attention in the past year are the sound velocity variations in the water and the shape and reflecting qualities of the bottom. These observations have been made at sea mainly from the CHAIN on a part of her Mediterranean cruise and on a series of cruises designed for just this purpose in the Woods Hole-Bermuda-Bahamas area.

The intricate velocity variations in the upper few hundred feet of the ocean have been ascertained indirectly by making detailed temperature observations with the thermistor chain. Sound transmission experiments conducted with the simultaneous determination of the thermal microstructure of the upper few hundred feet show that very small scale features, such as thin sound channels of only a few miles in length may have relatively large effects on sound transmission.

Last year our interest in direct measurements of the sound velocity of sea water was reported. This work was continued with the sound velocity meter developed at the National Bureau of Standards. It has been possible to compare for the first time sound velocity profiles made with this instrument with values computed from salinity, temperature and pressure data collected by classical oceanographic methods. This was done at 11 stations in the Mediterranean Sea on the cruise of the CHAIN. These comparisons indicate that there are discrepancies between the values directly observed with this instrument and those computed using Matthews' and Kuwahara's tables; the computed values being in general lower than those measured.

In spite of the success of direct sound velocity measurements, sound velocities based on temperature and salinity data continue

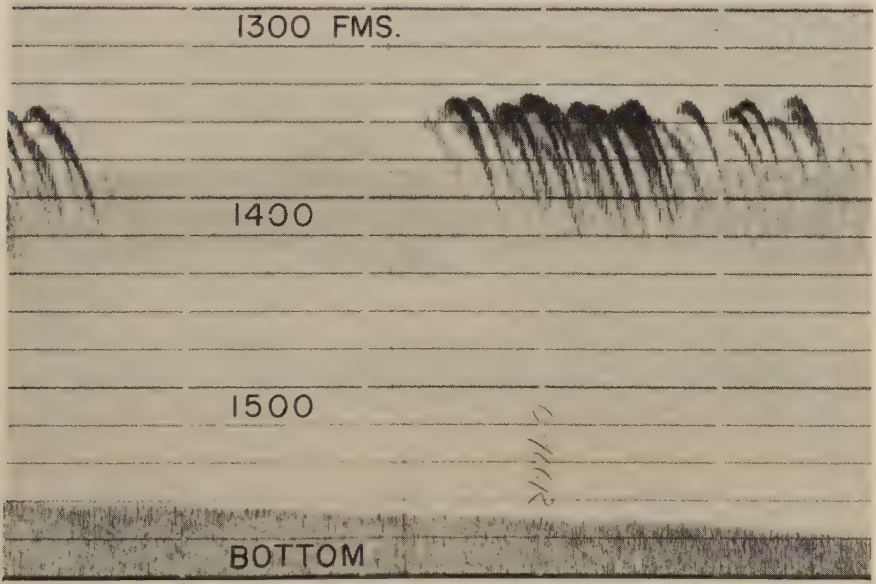

A fathometric record showing "Alexanders Acres" and scattering layers in deep water.

to be useful for underwater acousticians. Reports on the sound-velocity structure of the Mediterranean Sea and a restricted portion of the western North Atlantic have been prepared. Preliminary studies have also been made of the Arctic Ocean and parts of the Norwegian Sea.

Observations in local waters and theoretical work relevant to sound transmission problems were also carried. A number of interesting experiments were conducted from bottom-mounted towers in Buzzards Bay during the spring and fall in order to learn more about the stability of sound transmission paths. In one set of observations the fluctuations in intensity of a 600 cycle-per-second tone were recorded. It was evident from these data that surface waves cause changes in the phase and amplitude of the received sound. In another set, fluctuations of a repetitive spark source were determined. At ranges greater than a mile, large fluctuations in the intensity of the signals received were noted, and at a range of seven miles, the received sound was intermittent with a period of several minutes, much as in radio fading.

Installing the Buzzards Bay tower.

GEOPHYSICS AND SUBMARINE GEOLOGY

We have continued to examine the ocean bottom and the structure of the crust of the earth beneath the oceans by means of echo-sounding, seismic reflection, and seismic refraction techniques and have studied superficial processes on the ocean floor by means of bottom sampling with rock dredges, grab samplers and core sampling devices, as well as by underwater photography and echo-sounding. The most intensive and exciting events were a cooperative venture with several university laboratories of an area north of Puerto Rico in selecting a possible site for drilling a bore hole to the Mohorovicic discontinuity (the MOHOLE project of the National Academy of Sciences) and an extensive survey of the crustal structure in the Mediterranean Sea between the Côte d'Azur and Corsica. The latter project was carried out in collaboration with the Oceanographic Museum of Monaco and is a continuation of a seismic study of the Mediterranean Sea carried out by this Institution and the Lamont Geological Observatory in 1958. Other especially significant programs were the correlations of core samples with shallow sub-bottom echoes in deep water sediments of the Mediterranean, the application of the deep sonar pinger, originated by Edgerton and Cousteau for bottom photography, to monitoring deep coring operations and the recording of sub-bottom seismic reflection in deep water.

For several years we have been improving the resolution of our echo-sounders by shortening the length of the sound ping and by increasing the writing rate of the graphic recorders. Technical improvements in the recorders have allowed us to record with high resolution (pulse length 0.2 to 0.5 milli-second long and writing rates of about 150 inches per second) routinely from the CHAIN over many hundreds of miles in the North Atlantic and the Mediterranean. Several horizontally stratified sediment "ponds" have been found; two in the Mediterranean were surveyed in some detail. Cores were taken in "ponds" which are now being analyzed and compared with the echo evidence of stratification.

Several other bathymetric projects have been continued from previous years. The northern third of the Blake Plateau, surveyed in some detail over a period of six years when cruising across the area, is a nearly flat plain about a half mile deep lying between the Bahamas and Cape Hatteras. Its low relief seems from the earlier traverses to reflect deep-seated faulting. The principal patterns in this topography have been revealed as a result of several cruises in

1959. Several single seamounts of the North Atlantic were also examined in detail, as well as portions of the mid-Atlantic Ridge and the contact between the abyssal plain of the North Atlantic Basin and the foothills of the Ridge.

For the second successive year we have extended both geophysical and geological cruises to the Mediterranean. Emphasis was given to dredge sampling of the steepest slopes and coring in the basin areas. Sediments dredged on several rather steep slopes along the escarpment between the Peloponnesos and Crete were all terrigenous muds and clays. Rock fragments were found only in a deep gorge running through the Strait of Sicily; elsewhere only fine materials were recovered. Coring in basin areas produced several 25- to 30-foot cores and many more shorter ones. All were taken by a new method in which the lowering was wholly monitored by a sonar pinger attached to the heavy steel cable suspension of the coring apparatus. Echoes from the corer and the ocean floor are recorded on the ship, thus informing the observer of the success or failure of the operation while the apparatus is still on bottom. The short sound pulse bottom echoes of the pinger gave detailed sub-bottom information at the exact core location. A simple apparatus employing ultra-sonic (0.5 x 10^6 cps) pulses was subsequently used to measure sound velocity every two inches along the cores. In the one core that has been studied in detail the position of abrupt changes in sound velocity agree well with the sub-bottom echoes of the pinger and with changes from clay to sandy layers in the core. We are indebted to Dr. A. B. Wood of the Admiralty Research Laboratory in Great Britain for the loan of the ultra-sonic tranducers used for these sound velocity measurements.

The seismic profiler was also used for a short time to study the coastal shelf south of Cartagena, Spain, and in the Strait of Sicily. A third considerably more detailed survey was made in and to the northwest of the Strait of Messina. A model based on these data suggests the pattern of deposition in the channels leading northwestward from the Strait into the Tyrrhennian Sea. A brief study with a horizontal hydrophone array and explosives in the Balearic Basin suggests local occurrence of a thick horizontally-bedded sedimentary sequence.

By far the most intensive geophysical study was a series of long seismic-refraction profiles made from the CHAIN in cooperation with members of the Oceanographic Museum of Monaco on their ship WINNARETTA SINGER. Early results indicate that the sound velocity, slightly over 8000 meters/second, identified with the Moho is comparatively shallow—about 14 kilometers below sea level. This corroborates results from a nearby profile made in 1958. The two profiles are nearly perpendicular, thus reducing the possibility of a fortuitously high apparent velocity that could result from a profile across a basin structure.

For several years Institution seismographers have been accumulating information on local sediments and shallow bedrock structures in the inland waters near Woods Hole, in the Gulf of Maine, and on the continental shelf from New Jersey out across Georges Bank. In addition, the reconnaissance with the seismic profiler in Cape Cod Bay, on Georges Bank and on the continental shelf clearly demonstrates the potential of this reflection method for studying sediment structures.

Investigations ten years ago by the Institution and later confirmed by the Lamont Geological Observatory indicated that the earth's crust was very thin along the ridge just north of the Puerto Rico Trench. This is now of special interest to the National Academy of Sciences project for drilling a hole to the Mohorovicic discontinuity. In May and June a detailed pattern of seismic refraction profiles was completed in this area working with the Lamont Geological Observatory, the Agricultural and Mechanical College of Texas and the University of Miami. The seismographers are continuing to analyze the data which indicate a thickness of 10 kilometers from sea level down to the Moho. Other considerations such as probable weather and sea conditions and availability of proper drilling equipment may have as much to do with the final site selection as the thickness of the crust. Some members of the staff are being asked to consider the influence of weather, waves, and currents on the drilling operation.

On the long International Geophysical Year cruise of the ATLANTIS in the South Atlantic during the first half of the year, several long core and dredge samples were taken along a line 2,000 miles to the northeastward from the mouth of the Rio de la Plata off Montevideo to a feature known as the Bromley Plateau in the western Atlantic. The original concept was that sediments in the basin between the Plateau and the continental shelf off Montevideo would be formed as the result of a very slow rate of deposition and would show the effects of the submarine erosion of the Plateau to the eastward and of the introduction of weathered continental rock material from the westward as the result of the outflow of the Rio de la Plata. Instead, the discharge and transport of sediment by the Plata was found to be so great that this material was found all the way out to the flanks of the Bromley Plateau. The pattern of sedimentary deposition which was found fitted that which had been previously known for the western basin of the Atlantic from the latitude of the Amazon northward to the region of ice rafted sediments in the North Atlantic.

In October and November the ATLANTIS made a cruise along the northern coast of South America continuing the marine geological work of the previous year. Extensive related projects were also undertaken which will greatly enhance the value of the geological program. Venezuela and Colombia cooperated and their scientists were on board the ship during much of the time at sea.

In addition to the novel and effective use of echo-sounding techniques in coring, several purely mechanical advances have been made during this period. One of these, an improved core-barrel coupling, is a simple time-saving device which has been a great help to the operator. This coupling can be used with the older style of tubes as well as the new. It uses common nails driven into peripheral grooves in the coupling and the tube and combines great strength with ease of assembly.

Other changes were devised to enable the operator to obtain samples without contamination from hydrocarbons and to pre-

Photograph of the north wall of the Puerto Rico Trench in about 4000 fathoms of water using an Edgerton Stereo Camera.

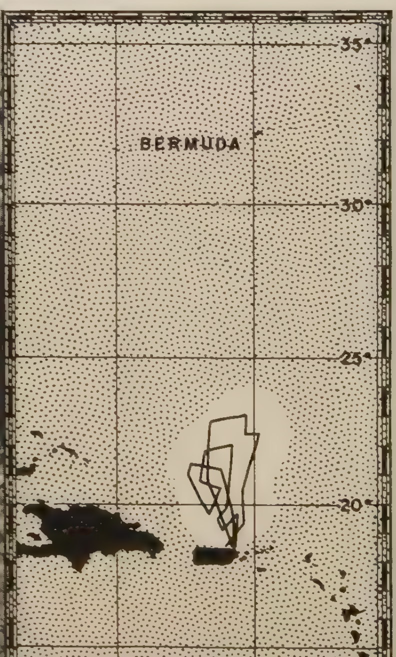

HOLE survey area.

serve the sample without loss of connate water. Contamination from oil and grease, usually used in preserving the apparatus, has heretofore prevented some important determinations of trace constituents. We have been searching for a preservative which prevents rust and corrosion, has a low coefficient of friction, is an "acceptable" contaminant, and is applicable to the inside of long tubes. A process in which nickel is chemically deposited upon steel has proven feasible and the appropriate parts of our coring gear have been nickel plated by this method.

An air operated hydraulic core extruder has been built and successfully used in the field. This consists of a completely portable device which is capable of exerting well-controlled pressures up to 2000 psi upon a free piston placed in the core tube. As the piston advances, sediment is extruded from the tube and sampled by the observer.

CHEMISTRY

Collection of large-volume water samples at sea has continued but at a much slower rate than in previous years. Most of the year's activities were devoted to laboratory investigations of analytical methods or to the analysis of previously obtained material. Our strontium-90 analytical method has been checked by using aliquots of strontium-90 from the National Bureau of Standards which were measured by a calibrated beta counting technique. In addition, several duplicate samples have now been analyzed, and the correspondence between these independently analyzed replicates is very satisfactory. The cerium analytical technique has been speeded up by modifications of several steps in the rare-earth procedure. This has not only provided more consistent and higher yields of cerium, but, at the same time, a complicated series of efficiency evaluations of each step in the procedure has permitted a realistic estimate of the overall confidence limits for the analysis of cerium-144 and promethium-147.

The tabulation of our strontium-90 profiles between latitudes 35°N and 16°S shows that the concentrations of this isotope between the 300 and 500 meter level is approximately 50% of the concentration at the surface. The isotope can also be detected to the 1100 meter level in this region. Rough integration of the vertical strontium gradient in such areas indicates that there is three to four times as much of this isotope below the 100 meter level as there is between the 100 meter level and the surface. Since the amount below 100 meters must be related to introduction times of two to four years ago, this distribution indicates a major and relatively rapid transport of water across the themocline. The complete understanding of this phenomenon is dependent upon an evaluation of the fallout of this isotope over the sea. Either our present model of stratospheric fallout or our evaluations of the efficiency of sampling by land stations must be reconsidered in order to bring the high strontium-90 levels in the ocean in line with our picture of the total strontium-90 path in the atmosphere and ocean.

The occurrence and constitution of several fossil pigments is being investigated. A comparison of their structure with that of the biological parent compounds will help us gain a better understanding of organic reactions in sediments. As one of a series of studies related to the organic chemistry of sea water which have just been initialed, foam fractionation is being examined as one of the potential tools for the enrichment of organic compounds from sea water. In several experiments a lowering of surface tension by 30% has been measured in the early foam fractions, indicating selective removal of the surface-active compounds. We intend to isolate and characterize the materials responsible for this effect.

A large volume water sampler.

MARINE BIOLOGY

Our effort of marine biology has continued to be concentrated in four main areas, all aimed at an understanding of the ecology of the populations in the oceans. These are the ecology, physiology and distribution of the phytoplankton; the feeding, migrations and distribution of the zooplankton; the dynamics and breeding cycles of sedentary bottom populations; and the life cycle and distribution of pelagic fishes, especially of sharks and rays. Closely associated with the phytoplankton work are the investigations of the distribution of essential nutrient chemicals in the water. These projects continue to be supported by Institution funds, by contracts with Atomic Energy Commission and with the Office of Naval Research and by several research grants from the National Science Foundation and from the National Institutes of Health.

The phenomena observed at sea raise questions which can only be answered by an experimental approach in the laboratory. Conversely, the results of the laboratory experiments under idealized conditions must, in turn, be tested under the conditions in nature to determine whether the results are of general application.

One part of the program has been designed to describe and to assist in our understanding of the phytoplankton cycle both in the inshore waters and in the Sargasso Sea. This included an evaluation of the various ways of measuring the photosynthesis or productivity of the phytoplankton crop, the distributions of chloropyll and other plant pigments, and the relationship of the photosynthesis of the phytoplankton to the essential fertilizing elements in the water. Contrary to our previous concepts, large seasonal and annual variations in primary production have been observed in the waters of the Sargasso Sea off Bermuda. It had generally been assumed that this area is one of rather uniform conditions throughout the year.

Until recently it was unfortunate that practically no species of oceanic phytoplankton had been grown in pure culture. Much of our fundamental physiological information about phytoplankton organisms was based on a few tough species which may have abnormal reactions and which might be considered the "weeds" of the sea. We now have nearly a hundred different species in pure cultures and a comparison of their physiology will show how variable their responses may be. Differences in the response of some species to temperature have already been established, but it is dependent upon future work to determine how these may be used to explain the distribution of the phytoplankton organisms in the sea.

Chlorophyll has long been used as an index of the amount of phytoplankton in the water and of the photosynthetic potential of the population. There have, however, been questions concerning the prevalence of "dead" chlorophyll which would be included in the determination but would not contribute to photosynthesis. With the acquisition of the Cary spectrophotometer it has been possible to begin an investigation of this problem. So far this study has indicated that chlorophyll decays very rapidly in the sea but that some of the breakdown products may indeed be included as active chlorophyll with the methods of determination now in use. The distribution and abundance of plants in the sea also has a profound affect on the color of the daylight which reaches various depths, and studies of the effects of the pigments themselves and of the particles and color of the water on the absorption have begun.

From our surveys of the phytoplankton populations at various locations between Woods Hole and Bermuda, it has been possible to relate the distribution of some species to temperature and salinity of the water. Less than a fifth of the species were associated with the extremes of temperature. However, most of the species in our populations are adjusted to a wide range of temperatures which indicates the rather small part played by temperature in seasonal succession of these species.

The nutrition of phytoplankton has also been examined both in the laboratory and in field. It has long been known that the physiology of cells deficient in an essential element such as phosphorous or nitrogen is different from that of normal cells, and we have suggested that such a deficiency would reduce the photosynthesis of the populations. While this has been easy to demonstrate in laboratory cultures, it is difficult to determine whether a population in nature is indeed deficient or not. One approach is to enrich the sample of seawater with known fertilizing elements and to determine the rate of photosynthesis before and after enrichment. This approach has demonstrated that in addition to nitrogen and phosphorus several trace elements such as iron and manganese may be limiting to photosynthesis.

One approach to the investigation of deficiences of actual populations is the use of radioisotopes to determine whether or not the cells assimilate these in excess amounts when they are made available. We have initiated experiments using radiophosporous to determine whether our natural populations at sea are deficient in this element. This has proved to be a powerful tool in laboratory experiments, but our studies of the natural populations have barely begun.

With direct chemical methods we are trying to determine the ways in which nitrogen deficiency of the natural population may affect the photosynthesis of these populations. The transformations of nitrogen in the sea are complex, and we have evidence that the plants may not only assimilate nitrogen compounds from the water but may transform them and produce some of the intermediate products of nitrogen metabolism. These observations may help to explain disturbances which have been difficult to understand on the basis of bacterial decomposition alone. The bacterial contributions to the transformation of the nitrogen compounds and of the effects of the phytoplankton population on these transformations is also being actively looked into.

In addition to the intimate relationship between phosphorus and the cycle of plant production in the ocean, this element may be used as a characteristic of water masses. For several years we have been obtaining samples for total phosphorus determinations on practically all of the hydrographic cruises that have left Woods Hole. We now have an extensive coverage of the western North Atlantic, and the data are being worked up to describe the distribution of phosphorus at all depths. Total and inorganic phosphorus determinations were also made on all stations occupied during the International Geophysical Year. These will provide a body of information unequalled in terms of nutrient distributions in both North and South Atlantic oceans.

Our zooplankton work is also a combination of laboratory and field investigations. Feeding experiments have concentrated on the copepod, *Calanus hyperboreus,* because of its large size and

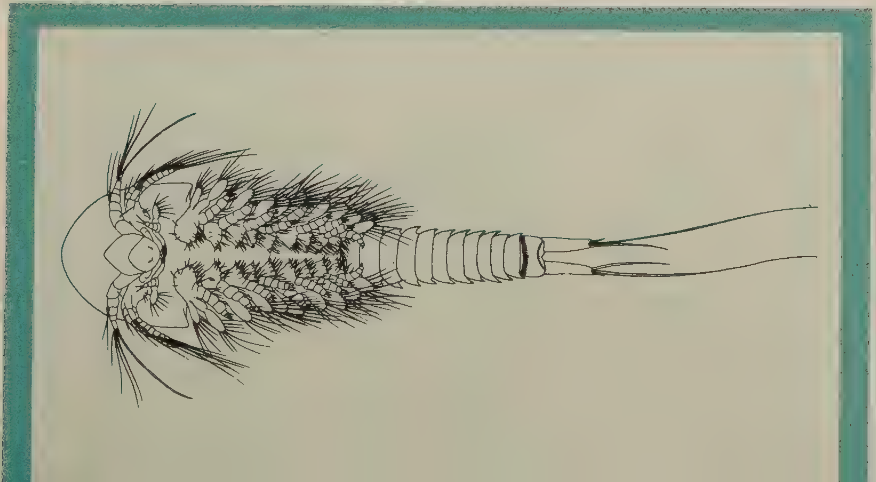

Hutchinsoniella macracantha
a living "fossil"
1/10" long,
from the bottom
of Buzzards Bay.

adaptability to laboratory conditions. Individuals of this species have been maintained for about a year under laboratory conditions where the life cycle seems to follow approximately the same sequence of events as occurs in nature. Although the life cycle has not yet been completed in culture, experimental animals have passed through most stages of their development in the laboratory.

In the laboratory, experiments on the dark and light adaptation of various arthropod eyes and on the responses to polarized light have been continued. If the crustaceans of the sea are, indeed, the organisms which determine the extent and timing of the vertical migrations, these results of dark adaptation will be invaluable in interpreting the results in the natural environment as will the investigations of the conditions of light in the sea. In clear waters various types of luminescent flashing were recorded at different depths, and some of the flashes biologically produced light were found to be a thousand times the intensity of the background light. Of particular interest was a survey of Bahia Fosforescente, Puerto Rico, where the light emitted by agitated water was found to be comparable to moonlight in intensity and over 100 times brighter than the bioluminescence outside the Bay.

Collections to ascertain the distribution of species of zooplankton at various locations between Woods Hole and Bermuda were continued. Dramatic changes in the population as one goes from the coastal waters through the slope water and the Gulf Stream to the Sargasso Sea continue, as in the past, to be impressive. It appears that the coastal waters are often dominated by one or two species of the zooplankton whereas in the Gulf Stream waters and in the Sargasso Sea several groups combined dominate the populations.

Skeletonema costatum an important diatom in New England coastal waters. Half the silicon dioxide cell wall is shown in an electron micrograph, magnified about 5,000 diameters.

The studies of the bottom communities have still been largely confined to the inshore, shallow areas. The types of organisms present in each community are determined not only by the character of the sediments but also by biological competition between the various species. Different types of sediment favor one method of feeding over another, and the character of the bottom population is determined by these differences. Deposit feeders were found to be prevalent in stable sandy sediments in intertidal environments, apparently because in these very shallow waters diatoms and dinoflagellates can grow directly on the sand. In contrast, deposit feeders are not common in sandy bottoms in deeper waters where plant growth is restricted.

The breeding cycle of various sedentary forms was determined in the laboratory. It has been found possible to stimulate both the development of the sexual cells and breeding by controlling temperature for several of the common species. Control of the breeding cycle will not only make it possible to have specimens in various stages of development at various times of year but might ultimately lead to the possibility of controlled genetic studies on marine organisms.

The collection of skates and rays trawled by the U. S. Fish and Wildlife Vessel OREGON chiefly along the Atlantic coast of Central America has continued. The preparation of a DANA report on a collection of sharks from the Atlantic, Pacific and Indian Oceans is also underway.

The life span and migrations of sailfish and marlin are now better known. This information has resulted from recapture of fish tagged in the western North Atlantic. For the first time trans-Atlantic migration of bluefin tuna has been established, and a heretofore unknown wintering ground of medium bluefin tuna in the Gulf Stream has been discovered. Data are now available to permit a revision of the taxonomy of the four western North Atlantic species of the genus *Seriola* and to make the first direct comparison of bluefin tuna populations from California, Spain and the western Atlantic.

INSTRUMENTATION

This year has seen the fruition of several of the instrument systems which have been under development at Woods Hole. The transponding radio buoy has been sent out for commercial manufacture and about eighteen have been bought for use as drifting current indicators and for radio-acoustic ranging. In addition to our own uses, four have been purchased by the Fisheries Research Board of Canada and four by the Scripps Institution of Oceanography. Because of this demand and an indicated increase in the use of these buoys in the near future, the design has been let out to another company for modification to increase reliability and ease of servicing. This will lead to a somewhat more expensive version which should be more adaptable to long term use.

With the acquisition of the ARIES for use in following the deep circulation by means of the Swallow float, the Electronics Department assisted by making much of the equipment needed for this work. In addition to the more usual equipment needed on any research vessel, navigation by means of Loran C was desired but receiving equipment was not available. A simple inexpensive set was developed which has provided this project with navigational control varying from a few yards in the Cape Hatteras area to about 250 yards in the vicinity of Bermuda. The ARIES is one of the few vessels in the world using this navigational system successfully. Also as part of the deep current program, an improved pinger was developed which provides a useful increase in range.

A 12 Channel FM telemetry system using a VHF radio link and recording on magnetic tape has been developed for the wave research program. During the late summer it was used from a tower installed in Buzzards Bay to record six channels of wave data and wind direction and speed. This equipment has provided the best records we have ever obtained for machine computation of surface wave power spectra and the first data for computation of directional spectra. An unfortunate accident in which the Buzzards Bay tower collapsed (apparently caused by a boat tying up to it) set back the work for about two months, but the equipment was used from a tower off the Florida coast this winter. In October a meeting was held at Woods Hole at which oceanographers from several laboratories accepted this telemetry system as a basic one for recording oceanographic data.

Now that the shipboard salinometer for measurement of the salinity of water samples brought up in Nansen bottles has become standard on our vessels, emphasis is being placed on development of a cable-lowered *in situ* salinometer. Conductivity cells of the electrode type and also the toroidal induction type are under development. As a necessary adjunct to this problem studies have been made of the effect of carbon dioxide and oxygen on conductivity and experiments have been started to improve the measurements of the pressure effect. These have become important due to the increased precision of the conductivity bridge salinometers themselves. If a conductivity type salinometer is used as an *in situ* meter, the effect of pressure on conductivity will have to be evaluated.

Another set of equipment which has been developed for use on the Texas Towers is a string of thermisters, one every ten feet, which is programmed to a digitizing system which punches paper in a form useful for machine computation. These data will be processed to obtain the spectra of internal waves and thermal noise.

A new method for the acquisition of data has been tried this year. This is the use of vertical instrument vehicles which are dropped free of the ship and carried to the bottom by weights. At the bottom or at a selected mid-depth the weights are released and the vehicle returns rapidly to the surface by means of its own buoyancy. The vehicle itself is a streamlined device 6 feet long and 2 feet in diameter, the upper half of which forms a tank holding 50 gallons of gasoline to provide buoyancy. Instruments are contained in pressure proof cases in the tail of the vehicle. A considerable number of tests were run to determine the action of the vehicle under various load conditions. Measurements of stability

Unattended (waxpaper) thermograph.

rmistor chain.

were also undertaken, and although oscillations with amplitudes in excess of 15° were encountered, the vehicle performed very successfully. Various ascent and descent rates were achieved using combinations of parachutes and weights, and it was found that pay loads of 50 lbs. weight in water could be achieved and still give ascent rates three times that of a standard hydrographic winch. Although most of the instrumentation used in the vehicle was designed to test its performance, instruments recording temperature and dissolved oxygen have also been used successfully at much higher data-acquisition rates than is currently possible with cable-lowered gear. These measurements were compared with similar observation taken by normal hydrographic techniques in the same area and clearly illustrated fine structure features which could not have been found by normal procedures.

It is well known that the method of computation of dynamic sections, now widely employed in the study of oceanic circulation, excludes measurements of the horizontal pressure gradients which remain unchanged with depth. While steady forces, such as the trade wind, acting over a period of several years will produce motions whose amplitude are strongly depth dependent, there is a spectrum of motion, almost independent of depth produced by such transient forces as intense storms. Methods for investigating these latter effects on a regional scale require either a network of sensitive piezometers to detect the time dependent changes of the slopes of the isobaric surfaces in the volume of the sea or some means for measuring the regional inclination of the sea surface.

An instrument for measuring the regional slope of the sea surface has been built for the latter purpose. It has sufficient angular resolution to measure regional tilts in the order of one part in a million. The errors caused by atmospheric refraction, surface waves and barometric pressure gradients are being studied from land stations. A sea-going version of this apparatus requires that a gyro-pendulum be constructed to provide an indication of the direction of local gravity at the ship's position to the same high order of accuracy as that of the tilt measurements. The gyro-pendulum problem poses serious technical difficulties. But the rate of improvement of these devices, which are integral parts of modern inertial and star tracking navigation systems, is sufficiently great to anticipate that the necessary accuracies may be obtained within the next decade.

FLEET OPERATIONS

Undoubtedly the most significant development related to our fleet during the year was the National Science Foundation's grant to the Institution of $3,000,000 for the construction of a new research vessel. As discussed elsewhere in this report, this grant is one of the utmost importance, not only for the Institution's future but for the future of American oceanography.

Three other important developments took place with respect to the Institution's fleet. In January the ARIES was acquired through the generosity of Mr. Richard J. Reynolds. She was taken over by the Institution in Hamilton, Bermuda, and after a very rough passage to Woods Hole, she was modified for oceanographic research. She returned to Bermuda in June and has been used there on a deep buoy tracking program ever since. This program is expected to continue throughout most of 1960.

In July the Institution purchased a five-passenger Helio-Courier light aircraft. This plane has been used on floats since her acquisition and in favorable weather can be landed in front of the Institution and beached at the end of Water Street near the Fish and Wildlife Service building. This capability contributes considerably to the convenience of using this plane and has proved a valuable asset in light of the cessation of railway transportation to the Cape area. This particular aircraft was chosen for its unusual flight characteristics. Automatic slots on the leading edges of the wings and other slow-speed design features allow the plane to be flown as slow as 30 knots. In even moderate winds this gives the plane almost helicopter-like hovering characteristics. On the other hand, a high performance engine, the automatic slots, and controllable flaps give it a short take-off distance and a cruising speed of 130 knots. As the wing design requires no bearing struts, these features combine to make the plane uniquely suitable for a number of projects, and the Helio will more than adequately replace our five-passenger Stinson.

The third major change in the status of the fleet was the Institution's take-over of the operation of the CHAIN from the Military Sea Transportation Service. The ceremonies took place on November 13th in the Bethlehem Steel Company yard in East Boston where the ship was docked for final conversion to oceanographic use.

The CHAIN was used almost continuously, being away from Woods Hole 210 days compared to 161 days for YAMACRAW and CHAIN combined in 1958. Most of these operations were in the western Atlantic, but in the early summer a three and one-half month cruise to the eastern Mediterranean was undertaken to further the earlier geophysical studies in the area by the ATLANTIS and YAMACRAW. On a portion of this cruise successful joint ship operations were carried out with French scientists from the Museum at Monaco. The CHAIN returned from this cruise in time to go to New York for the first International Oceanographic Congress which was held at the United Nations in early September. She tied up at a pier in the Hudson River with several other research vessels. All of the research vessels were open to those attending the Congress.

The ATLANTIS, on the other hand, began the year with an extensive seven month's cruise to the South Atlantic. This was the last International Geophysical Year cruise undertaken by the Institution and was delayed more than a year due to the 1958 difficulties with the ATLANTIS' main engine. The ship made four crossings of the Atlantic Ocean, including one long crossing at 32° South between Montevideo, Uruguay, and Cape Town, South Africa. The remainder of the ATLANTIS' operations were in the western North Atlantic; and, like the CHAIN, was sent to the International Oceanographic Congress in New York. The contrast in size between the 142-foot ATLANTIS and the 337-foot MIKHAIL LOMONOSOV of the U.S.S.R. was very striking.

R.V. Aries.

The CRAWFORD operated for most of the year in the western North Atlantic Ocean, and as a result of yard periods in the beginning and at the end of the year, put in fewer days at sea than during the heavy International Geophysical Year operations. In the late fall and early winter she operated out of St. George's, Bermuda, in association with the ARIES. The availability of two ships for the deep buoy tracking work and the superior speed and range of the CRAWFORD added considerably to this long-term program of deep current measurement.

As is generally the case, the BEAR operated out of Woods Hole for most of the year. In May and June, however, she took part in the well-publicized MOHOLE survey north of Puerto Rico. This work was done in conjunction with the VEMA of the Lamont Geological Observatory, the JOSIAH WILLARD GIBBS of the Hudson Laboratory and the HIDALGO of the Agricultural and Mechanical College, Texas. This multi-ship seismic survey was one of the first of this sort ever undertaken in this country. The use of multiple receiving ships had previously been attempted by the U.S.S.R. in the Black Sea.

Our DC3-type, Navy-supplied aircraft was used extensively by several investigators. Most of the operations were between Woods Hole and Bermuda, but several southern flights were made and one twenty-day flight in the Trinidad area was carried out in late fall. Scientific instrumentation on this aircraft has become increasingly refined, and the plane is becoming a more and more important tool for meteorological research.

Considering the year as a whole, the Institution's operations at sea increased considerably in 1959. In 1959 the fleet put in 864 days at sea compared to 741 in 1958, the highest year heretofore. This increase can be accounted for by the addition of the ARIES to the fleet.

The level of aircraft operations was comparable to that of last year, but the Institution's research staff has shown an increasing interest in obtaining the use of a four-engine airplane for use in mid-ocean and at high altitudes, and such a facility will have to be acquired in the near future.

N-4144D
WHOI

Helio Courier

With the ATLANTIS' projected retirement date only a year and a half in the future, the Ship Design Committee has been accelerating their activities in developing the specifications for her replacement. The general design characteristics arrived at by the Institution Ship Committee call for a vessel of approximately 175 feet overall length and a gross registered tonnange of 850 tons. By comparison, the ATLANTIS is 142 feet in overall length and has a gross registered tonnage of 293 tons. The new ship's surface speed is expected to be in excess of 12 knots and its range at sea at a 10 knot speed is estimated to be about 10,000 miles. Several special features are being considered, including a below-waterline bow observation chamber, a center well, active stabilization, specialized winches, cranes and hoisting equipment, and such laboratory features as a chemical bench, aquaria and large freezing facilities. In addition special consideration will be given to the acoustical characteristics of the vessel, and it is hoped that a very low noise level can be achieved for silent ship operation. A stabilized platform is also being considered for gravity measurements at sea and several specialized navigational aids are being planned. A high degree of maneuverability is also considered necessary and a bow propulsion unit for maneuvering is being studied. Thus our current progress in oceanography is symbolized by improvements in the research fleet.

ATLANTIS

Cruise No.	Dates	Areas of Operation	Days	Chief Scientist
247	31 Jan.—7 June	Woods Hole—South Africa	107	Miller
	10 Jun.—23 Jul.	South Africa—Woods Hole	39	Munns
248	27 Jul.—22 Aug.	Boston—Yard	27	
249	29 Aug.—13 Sept.	International Oceanographic Congress	16	
250	22 Sept.—27 Oct.	Bermuda Area	27	Bunce
251	4 Nov.—2 Dec.	Blake Plateau	25	Stetson
252	9 Dec.—25 Dec.	Bermuda Area	28	Swallow

CHAIN

Cruise No.	Dates	Areas of Operation	Days	Chief Scientist
4	12 Jan.—15 Feb.	Bermuda—Nassau	40	Hersey
5	9 Mar.—25 Mar.	Bermuda Area	9	Hersey
6	27 Mar.—3 Apr.	Shipyard and Sea Trials	8	
7	8 Apr.—18 May	Woods Hole—Cadiz, Spain	32	Worthington
	19 May—12 Jul.	Mediterranean	56	Hersey
	15 Jul.—17 Aug.	Spain—Woods Hole	34	Hays
8	29 Aug.—17 Sept.	International Oceanographic Congress	5	
9	22 Sept.—26 Oct.	Bermuda Area	34	Hersey
10	9 Nov.—	Boston, Yard for inventory WHOI takeover and conversion		

CRAWFORD

Cruise No.	Dates	Areas of Operation	Days	Chief Scientist
23	3 Feb.— 6 Feb.	Boston Yard	4	
24	25 Feb.—15 Mar.	Bermuda Area	17	Ryther, Curl, Ketchum
25	1 Apr.—21 Apr.	Boston Yard	21	
26	22 Apr.—24 Apr.	Shelf	3	Curl
27	18 May—28 May	Gulf Stream	9	Ketchum
28	10 Jun.—30 Jun.	Gulf Stream	19	Worthington, Bumpus
29	15 Jul.—30 Jul.	Shelf	16	Vine
30	4 Aug.— 7 Aug.	Shelf	4	Clarke
31	12 Aug.—18 Aug.	Shelf	7	Clarke
32	20 Aug.—25 Aug.	Shelf	6	Backus
33	21 Sept.—25 Sept.	Shelf	5	Bowen
34	6 Oct.—30 Oct.	Bermuda Area	22	Stommel
	5 Nov.—3 Dec.	Bermuda Area	25	Swallow
35	15 Dec.—20 Dec.	Bermuda—Woods Hole	6	Ketchum
36	23 Dec.—	Boston Yard		

ARIES

Cruise No.	Dates	Areas of Operation	Days	Chief Scientist
	19 Jan.—ARIES became property of WHOI at Bermuda.			
1	9 Mar.—16 Mar.	Bermuda—Woods Hole	8	
2	10 May—10 May	Local	1	Swallow
3	25 May—29 May	Fairhaven Yard	5	
4	4 Jun.—9 Jun.	Woods Hole—Bermuda	6	Swallow
5-16	20 Jun.—18 Nov.	Bermuda Area	103	Swallow
17-19	24 Nov.—13 Dec.	Bermuda Area	19	Volkmann
20	14 Dec.—	Bermuda, Yard		

BEAR

Cruise No.	Dates	Areas of Operation	Days	Chief Scientist
203-214	11 Feb.—1 May	Local	28	Frantz, Schevill, Day, Davis Fahlquist, Voorhis, Bunce
215	14 May—27 Jun.	North of Puerto Rico	42	Fahlquist
216-230	29 Jul.—18 Dec.	Local	67	Curl, Zeigler, Knott, Backus, Bunce, Voorhis, Athearn, Baxter, Conover
231	30 Dec.—	New Beford, wet storage		

PERSONNEL

The following persons were awarded grants, honoraria or fellowships during 1959:

Walter H. Adey	Massachusetts Institute of Technology
Robert A. Berner	Harvard University
Esteban Boltovskoy	Servicio de Hidrografia Naval, Buenos Aires, Argentina
John T. Conover	University of Texas
Dennis J. Crisp	Marine Biological Station, University College of North Wales, Anglesey
Philip G. Drazin	Massachusetts Institute of Technology
Erik Eriksson	Institute of Meteorology, University of Stockholm, Stockholm, Sweden
John S. Farlow, III	Johns Hopkins University
Stig Fonselius	Institute of Meterology, University of Stockholm, Stockholm, Sweden
Ernst Føyn	University of Oslo, Oslo, Norway
Michael Garstang	Florida State University
Ivan C. Getting	Harvard University
John G. Gille	Massachusetts Institute of Technology
Edward J. Green	Massachusetts Institute of Technology
Stina Gripenberg	Havforskingsinstitutet, Helsinki, Finland
Donald J. Hall	University of Michigan
Louis N. Howard	Massachusetts Institute of Technology
Sidney Hsiao	Department of Zoology & Entomology, University of Hawaii, Honolulu, Hawaii
Robert H. Kraichnan	New York University
Joseph Levine	Massachusetts Institute of Technology
William S. Maddux	Rutgers University
David A. McGill	Yale University
Christian Myers	George Washington High School, Alexandria, Virginia
Göte Östlund	Radioactive Dating Laboratory, Geological Survey of Sweden, Stockholm, Sweden
Thomas O. Phillips	Princeton University
Robert A. Phinney	Massachusetts Institute of Technology
John E. G. Raymont	The University, Southampton, England
John S. Reitzel	Harvard University
Herbert Riehl	University of Chicago
Allan R. Robinson	Harvard University
Philip Saffman	Cambridge University, England
Peter M. Saunders	Department of Meteorology, Imperial College of Science & Technology, London, England
Vincent J. Schaefer	Munitalp Foundation, Schenectady, New York
David H. Shonting	Massachusetts Institute of Technology
Theodore J. Smayda	University of Rhode Island
Edward A. Speigel	University of California
Edward D. Stroup	Johns Hopkins University
Lynn R. Sykes	Massachusetts Institute of Technology
B. Samuel Tanenbaum	Yale University
Aarno Voipio	Havforskingsinstitutet, Helsinki, Finland
Thomas F. Webster	Massachusetts Institute of Technology
Torbin Wolff	Universitets Zoologiske Museum, Copenhagen, Denmark
Georg Wüst	Institute für Meereskunde, Kiel, Germany

VISITORS

We were honored during the year by receiving visits from distinguished colleagues from other countries. Among these the following spent a considerable period of time:

Masateru Anraku	Faculty of Fisheries, Hokkaido University, Hokkaido, Japan
Moshe A. Avnimelech	Department of Geology, Hebrew University, Jerusalem, Israel
Esteban Boltovskoy	Servicio de Hidrographia Naval, Buenos Aires, Argentina
Francis Bernard	Zoologie Génerále, Faculté des Sciences, Université d'Alger, Algiers, Algeria
Michelle F. Bernard	Zoologie Génerále, Faculté des Sciences, Université d'Alger, Algiers, Algeria
Bert Bolin	International Meteorological Institute, Stockholm, Sweden
W. Brandhorst	Estacion de Biologia Marina, Universidad de Chile, Vina del Mar, Chile
J. D. Bromhall	Fisheries Research Unit, University of Hong Kong, Hong Kong, B.C.C.
Margarethe Brongersma-Sanders	Geologisch-Meteorologisch Laboratorium, Rijksuniversiteit te Leiden, Netherlands
Neil L. Brown	Commonwealth Scientific and Industrial Research Organization, Cronulla, Australia
H. O. Bull	Dove Marine Laboratory, Cullercoats, Northumberland, Great Britain
Tso-You Chu	National Taiwan University, Taiwan, National China
Carl W. Correns	Sedimentpetrographisches Institut, Göttingen, Germany
James Crease	National Institute of Oceanography, England
Dennis J. Crisp	Marine Biological Station, University College of North Wales, Anglesey
A. DeMaio	Istituto Universitario Naval Napoli, Naples, Italy
Ingvar Emilsson	Instituto Oceanografico, Universidade de Sao Paulo, Sao Paulo, Brasil
Erik Eriksson	Institute of Meteorology, Stockholm, Sweden
Stig Fonselius	Institute of Meteorology, Stockholm, Sweden
Ernst Føyn	University of Oslo, Oslo, Norway
Roland S. Glover	Oceanographic Laboratory, Scottish Marine Biological Association, Edinburgh, Scotland
Stina Gripenberg	Havforskningsinstitutet, Helsinki, Finland
Masayoshi A. Hatanaka	Tohôku University, Japan
Shoitiro Hayami	Geophysical Institute, Kyoto University, Japan
Hildegard Hass	Sedimentpetrographisches Institut, Göttingen, Germany
M. N. Hill	Department of Geodesy and Geophysics, Cambridge University, Great Britain

George F. Humphrey	Commonwealth Scientific and Industrial Research Organization, Cronulla, Australia
S. Ishiguro	Nagasaki Marine Observatory, Japan
Hideo Iwasaki	Tohôku University, Japan
Wolfgang Krauss	Institut für Meereskunde der Universität, Kiel, Germany
Anna M. Mani	Instrument Division, Meteorological Service of India
Maurice Menaché	Chef, Service Central d'Océanographic Physique, Office de la Recherche Scientifique et Technique Outre Mer, Paris, France
Sigeru D. Motoda	Faculty of Fisheries, Hokkaido University, Hokkaido, Japan
Masito Nakano	Meteorological Research Institute, Tokyo, Japan
Kurt W. Ockelmann	Marine Biological Laboratory, Helsingör, Denmark
Göte Östlund	Radioactive Dating Laboratory, Geological Survey of Sweden, Stockholm, Sweden
Ramon L. Perez-Mena	Ministry of Mines, Venezuela
H. Postma	Zoologisch Station, Den Helder, Holland
Claës G. H. Rooth	Institute of Meteorology, Stockholm, Sweden
Tadayoshi Sasaki	Scientific Research Institution, Tokyo, Japan
Peter M. Saunders	Department of Meteorology, Imperial College of Science and Technology, London, England
Hellmuth A. Sievers	Departamento de Navegacion e Hidrografia de la Armada, Valparaiso, Chile
Jens Smed	Bureau du Conseil International pour l'Exploration de la Mer, Charlottenlund Slot, Charlottenlund, Denmark
C. C. Stavropoulos	South African Council for Scientific and Industrial Research, Union of South Africa
Bernard Saint-Guily	Centre National de la Recherche Scientifique au Museum, Paris, France
Unnstein Stefansson	Fisheries Research Institute, Reykjavik, Iceland
John C. Swallow	National Institute of Oceanography, England
Paul Tchernia	Laboratoire d'Océanographie Physique au Museum, Paris, France
J. Verwey	Zoologisch Station, Buitenhaven 27, Den Helder, Holland
Aarno Voipio	Havforskningsinstitutet, Helsinki, Finland
K. H. Wedepohl	Sedimentpetrographisches Institut, Göttingen, Germany
John D. H. Wiseman	British Museum (N. H.) London, England
Torben Wolff	Universtets Zoologiske Museum, Copenhagen, Denmark
Georg Wüst	Institut für Meereskunde, Kiel, Germany

EMPLOYEES AND STAFF

The following personnel were in the employ of the Institution for the twelve-month period ending December 31, 1959.

Ethel B. Allen
Norman T. Allen
Nellie E. Anderson
Herbert A. Ashmore
William D. Athearn
Cyril Backus
Harold Backus
Jeanne M. Backus
Richard H. Backus
Rose L. Barbour
Joseph R. Barrett, Jr.
Elmer M. Barstow
Martin R. Bartlett
Lincoln Baxter, II
Edward R. Baylor
Henry G. Behrens
James S. Bercaw
Stanley W. Bergstrom
Robert Betterley
Duncan C. Blanchard
Ralph H. Bodman
George H. Boltz
Jane B. Boltz
Vaughan T. Bowen
Warren O. Bowman
Mabel D. Bradley
Alvin L. Bradshaw
Winfield S. Bray
Robert R. Brockhurst
Joseph C. Brown
Margaret Brown
John G. Bruce, Jr.
Kirk Bryan, Jr.
Edwin T. Bryant
John Q. Bumer
Dean F. Bumpus
Elizabeth T. Bunce
Andrew F. Bunker
Charles A. Burnham
John P. Cabral
John V. Cabral
Henry A. Cain
Sybil A. Campbell
Angelo Cangiamila
Ruth H. E. Carlson
Henri L. Caron
Alwyn L. Carter
David F. Casiles
James J. Cavanaugh
Constance W. Chadwick
Margaret A. Chaffee
Agnes C. Chalmers
Joseph Chase
John A. Christian
Edward H. Chute
David B. Clarke
George L. Clarke
William H. Clarkin
Arthur D. Colburn, Jr.
John W. Condon
William J. Conley
Robert J. Conover
Hans Cook
Nathaniel Corwin
Jerome M. Cotter
Brooks W. Coughlin
Marion W. Crocker
Porter A. Crouse
Elizabeth L. Curl
Herbert C. Curl, Jr.
Lee C. Davis
C. Godfrey Day
Joseph V. Day
Charles D. Densmore
Richard H. Dimmock
Willard Dow
William M. Dunkle, Jr.
Richard S. Edwards
Stanley N. Eldridge
Davis A. Fahlquist
Alan J. Faller
Harlow G. Farmer
Gregory Farnum
Sandra K. Ferguson
Alice H. Ferris
George A. Ferris
Frederick E. Fielden
Stanley O. Fisher
Richard A. Fitzgerald
Donald B. Foster
David H. Frantz
John G. Fraser
Frederick C. Fuglister
Paul M. Fye
Gloria S. Gallagher
Rosemary Gallagher
William F. Gallagher
Michael Garstang
Fred Gaskell
John W. Gates
Lambert C. Gates
Graham S. Giese
James E. Gifford
Barbara L. Gill
Norman Gingrass
Florence E. Glaeser
John W. Graham
Carlton W. Grant
Robert R. L. Guillard
Jan Hahn
Peter A. Hall
James E. Hanks
Kaleroy L. Hatzikon
Carlyle R. Hayes
Earl E. Hays
Helen C. Hays
John B. Hersey
George L. Hilton
Lloyd D. Hoadley
Harry L. Hodgkins
Sloat F. Hodgson
Alfred Hoffman
Roy Holmes
Paul M. Howe
Myron P. Howland, Jr.
Paul C. Howland
Edward M. Hulburt
Otis E. Hunt
Charles S. Innis, Jr.
Columbus O'D. Iselin
Delmar R. Jenkins
Alfred C. John
Barbara R. Johnson
Henry R. Johnson
Yolande A. Kahler
John W. Kanwisher
Willard E. Ketchen
Bostwick H. Ketchum
David D. Ketchum
Sydney T. Knott, Jr.
John A. Kostrzewa

Joseph L. Lambert
Anne E. Langenheim
Delia M. Lavin
Richard G. Leahy
Joseph Levine
Joyce C. Lewin
Robert R. Longyear
Thomas Lyon
Harvey MacKillop
Duane E. Maddux
Joanne S. Malkus
Willem V. R. Malkus
Ann Martin
George E. Martin
Frank J. Mather, III
Francis S. Matthews
Clement L. McCann, Jr.
Margaret E. McCloskey
Eileen M. McCormack
Joseph M. McElliott
John McGilvray
Florence K. Mellor
William G. Metcalf
Arthur R. Miller
Francis Minot
Juanita A. Mogardo
Wendell A. Mordy
Clayton B. Morehouse
Kenneth Morrison
Joseph C. Motta
Robert G. Munns
Eugene J. Mysona
A. Conrad Neumann
James S. Nicholson
Alice B. Nilsson
Mary Ortolani
Betty P. Ostiguy
David M. Owen
Michael Palmieri, Jr.
Gale G. Pasley, Jr.
Helen F. Phillips
Samuel F. Pierce
John F. Pike
John M. Pimental
Stanley E. Poole
Richard M. Pratt
William S. Richardson
Helen M. Roberts
Henry A. Rogers, Jr.
Mary D. Rogers
F. Claude Ronne
Nicholas A. Rosa
Lawrence Rose
John H. Ryther
James E. Salthouse
John D. Sandblom
Howard L. Sanders
Harold E. Sawyer
William E. Schevill
John L. Schilling
Karl E. Schleicher
Elizabeth H. Schroeder
William C. Schroeder
Mary Sears
Harry H. Seibert
Arnold G. Sharp
William J. Shields
William S. Shultz
Raymond Siever
Luther V. Slabaugh
Eloise M. Soderland
Otto Solberg
James H. Souza
Thomas A. Souza
Elizabeth C. Sparks
Allard T. Spencer
Charles E. Spooner
Robert J. Stanley
Richard Stansfield
Melvin E. Stern
Thomas R. Stetson
Raymond G. Stevens
Stephen L. Stillman
John W. Stimpson
Paul B. Stimson
Henry M. Stommel
Thomas T. Sugihara
Thomas O. L. Sutcliffe
Herman Tasha
Louis J. Tometich
Wendell K. Tripp
Harry J. Turner, Jr.
Ralph F. Vaccaro
Ronald A. Veeder
George Veronis
Allyn C. Vine
Gordon H. Volkmann
William S. von Arx
Carl R. von Dannenberg
Arthur D. Voorhis
Robert G. Walden
Jean D. Walker
William A. Watkins
Margaret E. Watson
Stanley W. Watson
Robert G. Weeks
Geoffrey G. Whitney, Jr.
Phillips B. Wilde
Charles H. Wilkins
George A. Williams
Edward Wilson
Esther N. Wilson
Asa S. Wing
Carleton R. Wing
Warren E. Witzell
Alfred H. Woodcock
Fred C. Woodward, Jr.
L. Valentine Worthington
Charles S. Yentsch
Javan D. York
John M. Zeigler

It should be noted that Dr. Max Blumer, an organic chemist, arrived in Woods Hole on 9 November 1959 to join the group working in geochemistry.

PUBLICATIONS

During 1959, sixty-three papers bearing contribution numbers were published. See Author, Subject-Locality, Taxonomic Index published in 1957 for a complete list through 1956.

No. 738 C. B. Officer. On some Offshore Seismic Refraction Profiles in the Cook Strait, Tasman Bay, and Golden Bay Areas of New Zealand. *N.Z. Jour. Geol. and Geophys.*, Vol. 2, No. 2, pp. 350-354. 1959.

No. 872 P. F. Scholander and John Krog. Countercurrent Heat Exchange and Vascular Bundles in Sloths. (Published in 1957). *Jour. Applied Physiol.*, Vol. 10, No. 3, pp. 405-411. 1957. (Not included in *Collected Reprints*).

No. 927 Malcolm S. Gordon. Osmotic and Ionic Regulation in Scottish Brown Trout and Sea Trout (*Salmo trutta L.*). *Jour. Exper. Biol.*, Vol. 36, No. 2, pp. 253-260. 1959.

No. 947 William C. Schroeder. The Lobster, *Homarus americanus*, and the Red Crab, *Geryon quinquedens*, in the Offshore Waters of the Western North Atlantic. *Deep-Sea Research*, Vol. 5, pp. 266-282. 1959.

No. 948 Susan I. Scholander and Joan T. Kanwisher. Latitudinal Effect on Respiration in Some Northern Plants. *Plant Physiol.*, Vol. 34, No. 5, pp. 574-576. 1959. (Not included in *Collected Reprints*).

No. 950 H. Barnes and Margaret Barnes. A Comparison of the Annual Growth Patterns of *Balanus balanoides* (L.) with Particular Reference to the Effect of Food and Temperature. *Oikos*, Vol. 10, No. 1, pp. 1-18. 1959.

No. 954 Bernhard Haurwitz, Henry Stommel and Walter H. Munk. On the Thermal Unrest in the Ocean. In: The Atmosphere and the Sea in Motion (The Rossby Memorial Volume), pp. 74-94. Rockefeller Institute Press, New York. 1959.

No. 956 John M. Zeigler, Carlyle R. Hayes and Sherwood D. Tuttle. Beach Changes during Storms on Outer Cape Cod, Massachusetts. *Jour. Geology*, Vol. 67, No. 3, pp. 318-336. 1959.

No. 961 Robert H. Gibbs, Jr., and Bruce B. Collette. On the Identification, Distribution, and Biology of the Dolphins, *Coryphaena hippurus* and *C. equiselis*. *Bull. Mar. Sci. Gulf and Carib.*, Vol. 9, No. 2, pp. 117-152. 1959.

No. 962 E-an Zen. Clay Mineral—Carbonate Relations in Sedimentary Rocks. *Amer. Jour. Sci.*, Vol. 257, pp. 29-43. 1959.

No. 964 Theodore J. Smayda. The Seasonal Incoming Radiation in Norwegian and Arctic Waters, and Indirect Methods of Measurement. *Jour. du Conseil*, Vol. 24, No. 2, pp. 215-220. 1959.

No. 967 Joanne S. Malkus and Georg Witt. The Evolution of a Convective Element: A Numerical Calculation. In: The Atmosphere and the Sea in Motion (The Rossby Memorial Volume), pp. 425-439. Rockefeller Institute Press, New York. 1959.

No. 971 Frances L. Parker and William D. Athearn. Ecology of Marsh Foraminifera in Poponesset Bay, Massachusetts. *Journ. Paleont.*, Vol. 33, No. 2, pp. 333-343. 1959.

No. 973 J. B. Hersey, Elizabeth T. Bunce, R. F. Wyrick, and F. T. Dietz. Geophysical Investigation of the Continental Margin between Cape Henry, Virginia, and Jacksonville, Florida. *Bull. Geol. Soc. Amer.*, Vol. 70, pp. 437-466. 1959.

No. 974 Melvin E. Stern. The Moving Flame Experiment. *Tellus,* Vol. 11, No. 2, pp. 175-179. 1959.

No. 975 Jack McLachlan and Guy C. McLeod. The Use of Conversion Factors for the Determination of the Concentration of Nutrients in Culture Media. *Limnol. and Oceanogr.,* Vol. 4, No. 2, pp. 218-219. 1959.

No. 980 G. D. Nicholls, Herbert Curl, Jr., and V. T. Bowen. Spectrographic Analyses of Marine Plankton. *Limnol. and Oceanogr.,* Vol. 4, No. 4, pp. 472-478. 1959.

No. 982 T. T. Sugihara, H. I. James, E. J. Troianello and V. T. Bowen. Radiochemical Separation of Fission Products from Large Volumes of Sea Water. Strontium, Cesium, Cerium, and Promethium. *Analyt. Chem.,* Vol. 31, No. 1, pp. 44-49. 1959.

No. 984 Charles S. Yentsch and John H. Ryther. Relative Significance of the Net Phytoplankton and Nanoplankton in the Waters of Vineyard Sound. *Jour. du Conseil,* Vol. 24, No. 2, pp. 231-238. 1959.

No. 985 G. Veronis. Cellular Convection with Finite Amplitude in a Rotating Fluid. *Jour. Fluid Mech.,* Vol. 5, Pt. 3, pp. 401-435. 1959.

No. 986 C. Godfrey Day. Oceanographic Observations, 1957, East Coast of the United States. *U. S. Fish and Wildlife Service, Spec. Sci. Rept.—Fisheries* No. 282, 123 pp. 1959. (Not included in *Collected Reprints*).

No. 987 Alan J. Faller and William S. von Arx. The Modeling of Fluid Flow on a Planetary Scale. *Proceedings of the Seventh Hydraulics Conference, Iowa Institute of Hydraulic Research,* pp. 53-72. 1959.

No. 988 John M. Zeigler. Origin of the Sea Islands of the Southeastern United States. *Geogr. Rev.,* Vol. 49, No. 2, pp. 221-237. 1959.

No. 989 Malcolm S. Gordon. Ionic Regulation in the Brown Trout *(Salmo trutta L.)*. *Jour. Exper. Biol.,* Vol. 36, No. 2, pp. 227-252. 1959.

No. 992 Elizabeth Schroeder, Henry Stommel, David Menzel and William Sutcliffe, Jr. Climatic Stability of Eighteen Degree Water at Bermuda. *Jour. Geophys. Res.,* Vol. 64, No. 3, pp. 363-366. 1959.

No. 993 Jack McLachlan. The Growth of Unicellular Algae in Artificial and Enriched Sea Water Media. *Canad. Jour. Microbiol.* Vol. 5, pp. 9-15. 1959.

No. 995 John C. Ayers. The Hydrography of Barnstable Harbor, Massachusetts. *Limnol. and Oceanogr.,* Vol. 4, No. 4, pp. 448-462. 1959.

No. 996 Edward R. Baylor. The Responses of Snails to Polarized Light. *Jour. Exper. Biol.,* Vol. 36, No. 2, pp. 369-376. 1959.

No. 997 Guy C. McLeod and Jack McLachlan. The Sensitivity of Several Algae to Ultraviolet Radiation of 2537 A. *Physiol. Plant.,* Vol. 12, pp. 306-309. 1959.

No. 999 C. B. Officer, J. I. Ewing, J. F. Hennion, D. G. Harkrider and D. E. Miller. Geophysical Investigations in the Eastern Caribbean: Summary of 1955 and 1956 Cruises. In: Physics and Chemistry of the Earth, Vol. 3, pp. 17-109. Pergamon Press, New York. 1959.

No. 1002 Harry J. Turner, Jr. and James E. Hanks. Infestation of *Pecten irradians* by *Polydora. The Nautilus,* Vol. 72, No. 4, pp. 109-111. 1959.

No. 1003 Allan Robinson and Henry Stommel. The Oceanic Thermocline and the Associated Thermohaline Circulation. *Tellus,* Vol. 11, No. 3, pp. 295-308. 1959.

No. 1004 Allan Robinson and Henry Stommel. Amplification of Transient Response of the Ocean to Storms by the Effect of Bottom Topography. *Deep-Sea Research,* Vol. 5, pp. 312-314. 1959.

No. 1008 Henry Stommel. Florida Straits Transports: June 1956 — July 1958. *Bull. Mar. Sci. Gulf and Carib.,* Vol. 9, No. 2, pp. 222-223. 1959.

No. 1010 Jack McLachlan and Charles S. Yentsch. Observations on the Growth of *Dunaliella euchlora* in Culture. *Biol. Bull.,* Vol. 116, No. 3, pp. 461-471. 1959.

No. 1011 John W. Graham. Metabolically Induced Precipitation of Trace Elements from Sea Water. *Science,* Vol. 129, No. 3360, pp. 1428-1429. 1959.

No. 1012 Joseph Levine. Spherical Vortex Theory of Bubble-Like Motion in Cumulus Clouds. *Jour. Meteorol.,* Vol. 16, No. 6, pp. 653-662. 1959.

No. 1013 John Kanwisher. Histology and Metabolism of Frozen Intertidal Animals. *Biol. Bull.,* Vol. 116, No. 2, pp. 258-264. 1959.

No. 1014 John Kanwisher. Polarographic Oxygen Electrode. *Limnol. and Oceanogr.,* Vol. 4, No. 2, pp. 210-217. 1959.

No. 1015 L. V. Worthington. The 18° Water in the Sargasso Sea. *Deep-Sea Research,* Vol. 5, pp. 297-305. 1959.

No. 1016 John H. Ryther. Potential Productivity of the Sea. *Science,* Vol. 130, No. 3376, pp. 602-608. 1959.

No. 1017 John W. Graham and Susan C. Cooper. Biological Origin of Manganese-rich Deposits of the Sea Floor. *Nature,* Vol. 183, pp. 1050-1051. 1959.

No. 1019 George L. Clarke and Charles J. Hubbard. Quantitative Records of the Luminescent Flashing of Oceanic Animals at Great Depths. *Limnol. and Oceanogr.,* Vol. 4, No. 2, pp. 163-180. 1959.

No. 1020 Richard Barakat. A Note on the Transient Stage of the Random Dispersal of Logistic Populations. *Bull. Math. Biophysics,* Vol. 21, pp. 141-151. 1959.

No. 1021 W. V. R. Malkus. Magnetoconvection in a Viscous Fluid of Infinite Electrical Conductivity. *Astrophys. Jour.,* Vol. 130, No. 1, pp. 259-275. 1959.

No. 1022 Carl E. Tschiegg and Earl E. Hays. Transistorized Velocimeter for Measuring the Speed of Sound in the Sea. *Jour. Acoust. Soc. Amer.,* Vol. 31, No. 7, pp. 1038-1039. 1959.

No. 1024 Patrick Butler. Palynological Studies of the Barnstable Marsh, Cape Cod, Massachusetts. *Ecology,* Vol. 40, No. 4, pp. 735-737. 1959. (Published posthumously).

No. 1025 Bert Bolin and Erik Eriksson. Changes in the Carbon Dioxide Content of the Atmosphere and Sea due to Fossil Fuel Combustion. In: The Atmosphere and the Sea in Motion (The Rossby Memorial Volume), pp. 130-142. Rockefeller Institute Press, New York. 1959.

No. 1026 John H. Ryther and R. R. L. Guillard. Enrichment Experiments as a Means of Studying Nutrients Limiting to Phytoplankton Production. *Deep-Sea Research,* Vol. 6, pp. 65-69. 1959.

No. 1027 Charles S. Yentsch and John H. Ryther. Absorption Curves of Acetone Extracts of Deep Water Particulate Matter. *Deep-Sea Research,* Vol. 6, pp. 72-74. 1959.

No. 1028 W. Mordy, Computations of the Growth by Condensation of a Population of Cloud Droplets. *Tellus,* Vol. 11, No. 1, pp. 16-44. 1959.

No. 1029 Irving I. Schell. On a Criterion of Representativeness of Sea Surface Temperature Data. *Bull. Amer. Meteorol. Soc.,* Vol. 40, No. 11, pp. 571-574. 1959.

No. 1030 J. S. Hart and Laurence Irving. The Energetics of Harbor Seals in Air and in Water with Special Consideration of Seasonal Changes. *Canad. Jour. Zool.,* Vol. 37, pp. 447-457. 1959.

No. 1032 Joseph Chase. Wind-Induced Changes in the Water Column along the East Coast of the United States. *Jour. Geophys. Res.,* Vol. 64, No. 8, pp. 1013-1022. 1959.

No. 1036 E-an Zen. Mineralogy and Petrography of Marine Bottom Sediment Samples off the Coast of Peru and Chile. *Jour. Sed. Petrol.,* Vol. 29, No. 4, pp. 513-539. 1959.

No. 1037 H. Barnes and Margaret Barnes. Note on Stimulation of Cirripede Nauplii. *Oikos,* Vol. 10, No. 1, pp. 19-23. 1959.

No. 1038 John T. Conover. Seasonal Growth of Benthic Marine Plants as Related to Environmental Factors in an Estuary. *Publ. Inst. Mar. Sci., Univ. Texas,* Vol. 5, pp. 97-147. 1959.

No. 1039 John H. Ryther and David W. Menzel. Light Adaptation by Marine Phytoplankton. *Limnol. and Oceanogr.,* Vol. 4, No. 4, pp. 492-497. 1959.

No. 1041 A. C. Redfield. Physical and Chemical Properties of Sea Water: Biological Considerations — The Fourth Phase. Conference held at Easton, Maryland, Sept. 4-5, 1958. *Nat. Acad. Sci. — Nat. Res. Council, Publ. 600,* pp. 101-112. 1959. (Not included in *Collected Reprints*).

No. 1043 George L. Clarke and Lloyd R. Breslau. Measurements of Bioluminescence off Monaco and Northern Corsica. *Bull. Inst. Océanogr., Monaco,* No. 1147, pp. 1-31. 1959.

No. 1047 David A. McGill, Nathaniel Corwin, and Bostwick H. Ketchum. The Temperature Correction of Oceanic Inorganic Phosphorus Analyses. *Deep-Sea Research,* Vol. 6, pp. 60-64. 1959.

No. 1048 C. Godfrey Day. Oceanographic Observations, 1958, East Coast of the United States. *U. S. Fish and Wildlife Service, Spec. Sci. Rept. — Fisheries* No. 318, 119, pp. 1959. (Not included in *Collected Reprints*).

No. 1060 Karl E. Schleicher. A Note on the Constancy of the T/S Relationship in a Water Mass. *Deutsche Hydrogr. Zeitschr.,* Vol. 12, No. 3 (Ergänzungsheft Reihe B (4°)), pp. 46-48. 1959.

No. 1061 Wolfgang Wieser and John Kanwisher. Respiration and Anaerobic Survival in some Sea Weed—Inhabiting Invertebrates. *Biol. Bull.,* Vol. 117, No. 3, pp. 594-600. 1959.

TREASURER'S REPORT FOR THE YEAR 1959

The accounts for the year 1959 have been audited by Lybrand, Ross Bros. & Montgomery.

The book value of endowment funds at December 31, 1959 was $3,400,922 of which $96,191 represented accumulated net gains from sales of investments. The market value of endowment assets on the same date, including real estate at book amount, was $5,150,329. Endowment fund investments and income received therefrom are summarized in Schedule D.

Income received on endowment assets was $188,639 for the year ended December 31, 1959, compared with $178,607 the previous year. Included in endowment income was $6,420 of real estate income representing a 5% return on this investment. The balance of real estate income, $7,949, was transferred to endowment assets to amortize cost of property. Endowment income represented a return on endowment fund assets of 3.7% at year-end market quotation, 5.5% on the book amount and 7.7% on the contributed amount of the endowment fund.

Endowment income was allocated for 1959 operating expenses at the rate of 5.5% of the book amount of original endowment funds, or $133,131. Of the balance of endowment income, $55,508, there was transferred to the income and salary stabilization reserve $54,683 and to unexpended balance of gifts from Oceanographic Associates as income from investment of life memberships $825.

A general review with our auditors of our method of accounting for plant items on the balance sheet has resulted in the institution of certain changes in the balance sheet presentation. These changes are detailed in the note on page 59 following the balance sheet. We believe these changes result in a balance sheet that more accurately reflects the funds invested in plant and the cash properly allocable to plant funds.

The details of unexpended balance of gifts and receipts for research, other than government, are shown in Schedule C. The income from Woods Hole Oceanographic Associates for the year amounted to $60,273, plus $2,380 net rebate of real estate taxes paid in 1956. Expenditures and allocations to specific projects amounted to $12,563, increasing the balance on hand from $89,918 at December 31, 1958 to $140,008 at December 31, 1959.

The Institution's 1959 contribution to the Woods Hole Oceanographic Institution's Employees Retirement Trust amounted to $83,871. The trust is administered by three trustees. The balance of the old Retirement Fund, administered by the Treasurer, amounted to $70,438 as at December 31, 1959. This balance consisted of amounts on deposit in sixteen savings bank accounts held in trust for ten members of the plan. No contributions to the Old plan were made in 1959. Interest totalling $2,297 was credited to the savings accounts during the year.

In the financial statements that follow it is interesting to note that for each dollar spent 79.7 cents was spent for direct costs of research activity, 14.1 cents for general and administration expenses and 6.2 cents for plant operation and miscellaneous. Administrative salaries amounted to only 5.4 cents of each dollar of total expense. Included in the 14.1 cents of general and administration expenses was 3.3 cents for staff benefits (group insurance, social security taxes, and contributions to retirement plan).

LYBRAND, ROSS BROS. & MONTGOMERY
ACCOUNTANTS AND AUDITORS

Woods Hole Oceanographic Institution
Woods Hole, Massachusetts

We have examined the balance sheet of Woods Hole Oceanographic Institution as at December 31, 1959 and the related statement of income, operating expenses and unappropriated general fund for the year then ended. Our examination was made in accordance with generally accepted auditing standards, and accordingly included such tests of the accounting records and such other auditing procedures as we considered necessary in the circumstances; however, it was not practicable to confirm receivables from United States Government departments, as to which we have satisfied ourselves by means of other auditing procedures.

In our opinion, the accompanying financial statements present fairly the position of Woods Hole Oceanographic Institution at December 31, 1959 and the results of its operations for the year then ended, on a basis consistent with that of the preceding year.

Boston, Massachusetts
April 8, 1960

Lybrand, Ross Bros. & Montgomery

BALANCE SHEET *As at December 31, 1959*

ASSETS

Endowment fund assets:		
Investments (Schedule D):		
Bonds (market quotations $1,703,716)		$1,836,255
Stocks (market quotations $3,290,728)		1,408,782
Real estate		120,470
		3,365,507
Cash		35,415
		3,400,922
Plant fund assets (note B):		
Laboratory plant and equipment		707,841
Vessels and equipment		812,998
Other property		161,541
Total plant		1,682,380
Advance to current funds		62,011
		1,744,391
Current fund assets:		
Cash		374,628
Marketable security		246
Accounts receivable:		
U. S. Government	$168,745	
Other	17,971	186,716
Unbilled costs on research contracts:		
U. S. Government	620,155	
Other	50,805	670,960
Supply inventories		28,967
Deferred charges		32,046
		1,293,563
Less advance from plant funds		62,011
		1,231,552
		$6,376,865

LIABILITIES

Endowment Funds:		
Unrestricted		$2,017,311
For upkeep of plant		419,420
Henry Bryant Bigelow Chair of Oceanography		2,000
Accumulated net gain on sale of investments		962,191
		3,400,922
Plant funds:		
Invested in plant		1,682,380
Unexpended:		
Fund for purchase and reconditioning of boat Aries		4,306
General plant and equipment reserve (note A)		57,705
		1,744,391
Current liabilities and funds:		
Accounts payable and accrued expenses		208,039
Contribution payable to employees' retirement plan and trust		83,871
Unexpended balances of gifts and grants for research:		
Government	$466,639	
Other (Schedule C)	163,265	629,904
General fund:		
Income and salary stabilization reserve	266,082	
Unappropriated	43,656	309,738
		1,231,552
		$6,376,865

The appended notes are an integral part of this balance sheet.

NOTES TO BALANCE SHEET

For the Year Ended December 31, 1959

A — General plant and equipment reserve was reclassified in 1959 from current funds. Changes in this fund were as follows:

Balance January 1, 1959		$244,084
Additions to reserve:		
Depreciation and amortization charged to operating expenses:		
In 1959		64,563
In prior years (credited directly to asset accounts in those years)		54,017
Proceeds from sale of Caryn in 1958 tranferred from fund for purchase and reconditioning of boat Aries		16,000
		378,664
Charges against reserve:		
Amount added to plant fund assets in 1959:		
Costs of Crawford reconditioning:		
Prior years	$238,274	
1959	9,985	
Cost of electronic equipment purchased in 1957	31,055	
Cost of Helio aircraft purchased in 1959	41,645	320,959
Balance December 31, 1959		$ 57,705

B — Since 1945 the Institution has provided for depreciation of plant assets other than vessels at annual rates of 2% on buildings and 5% to 33⅓% on equipment, carrying the amounts to general plant and equipment reserve.

STATEMENT OF INCOME OPERATING EXPENSES AND UNAPPROPRIATED GENERAL FUND

For the Year Ended December 31, 1959

Income:		
Receipts for sponsored research:		
For direct costs		$2,919,804
For indirect costs		692,791
Fees for use of facilities		98,166
		3,710,761
Endowment income (Schedule D)	$188,639	
Less amounts added to income and salary stabilization reserve ($54,683) and unexpended balance of gifts from Oceanographic Associates as income from investment of life memberships ($825)	55,508	133,131
Miscellaneous		17,433
Total income availed of		3,861,325
Operating expenses:		
Direct costs of research activity (Schedule A):		
Salaries and wages		1,125,539
Vessel operations		738,304
Materials and services		1,032,756
Travel		135,290
		3,031,889
Indirect costs:		
General and administration (Schedule B)	536,012	
Plant operation (Schedule B)	222,403	
Miscellaneous	11,717	770,132
Total operating expenses		3,802,021
Excess of income		59,304
Additions to plant from current funds — books and equipment purchased		36,766
		22,538
Unappropriated general fund, January 1, 1959		21,118
Unappropriated general fund, December 31, 1959		$ 43,656

SCHEDULE A

DIRECT COSTS OF RESEARCH ACTIVITY

For the Year Ended December 31, 1959

	Salaries and Wages	Vessel Operations	Materials and Services	Travel	Total
U.S. Government contracts	$1,057,926	$715,685	$ 956,413	$127,146	$2,857,170
Other sponsored research	23,028	670	35,269	3,667	62,634
Total direct costs of sponsored research.	1,080,954	716,355	991,682	130,813	2,919,804
Institution research	44,585	21,949	41,074	4,477	112,085
Total direct costs of research	$1,125,539	$738,304	$1,032,756*	$135,290	$3,031,889

* Includes grants and fellowships:

U. S. Government contracts	$ 11,025
Other sponsored research	8,750
Institution research	22,531
	$42,306

SCHEDULE B

GENERAL AND ADMINISTRATION EXPENSES AND EXPENSES FOR PLANT OPERATION

For the Year Ended December 31, 1959

GENERAL AND ADMINISTRATION		
General expenses:		
Staff benefits:		
Contributions to retirement plan		$ 83,871
Social security taxes		35,079
Group insurance		5,859
		124,809
Shop services		102,814
Housing, net		5,720
Administration expenses:		
Salaries and wages	$205,326	
Insurance, travel, supplies and other	97,343	302,669
		$536,012
PLANT OPERATION		
Salaries and wages		51,234
Provision for depreciation (credited to general plant and equipment reserve)		44,068
Other repair costs	25,695	
Heat, light and power	22,656	
Vessel design studies	57,452	
Other	21,298	127,101
		$222,403

SCHEDULE C

SUMMARY OF GIFTS AND RECEIPTS FOR RESEARCH

For the Year Ended December 31, 1959

	Unexpended Balance January 1, 1959	Received	Expended		Other Charges or (Credits)	Unexpended Balance December 31, 1959
			Direct Costs	Indirect Costs		
Bermuda Biological Station for Research		$ 12,839	$12,258	$ 581		
Commonwealth of Massachusetts — shellfish propagation		9,857	5,753	4,104		
Manufacture, sale, and calibration of instruments		22,762	23,697	7,970	($7,470) (a) (1,435) (b)	
Lou Marron science fund — pelagic fish studies	$ 386	500	886			
Massachusetts Institute of Technology — Institute for Atmospheric Research		2,713	1,917	796		
National Academy of Sciences — project Nobska		40	40			
Oceanographic Associates:						
Deuterium studies	51	1,000	645	236		$ 170
Fellowships		8,750	8,750			
Unappropriated	89,918	60,273 (9,750)			2,813 (c) (2,380) (d)	140,008
Research Corporation — instrument fund	2,687				(400) (e)	3,087
Sundry work for others		7,397	6,803	594		
Towns of Brookhaven and Islip, New York — Great South Bay survey	783	2,000	1,885	898		
Other gifts	5,000	15,000				20,000
	$98,825	$133,381	$62,634	$15,179	($8,872)	$163,265

(a) Charged to income.
(b) charged to other projects.
(c) Miscellaneous expenditures.
(d) Net rebate of real estate taxes paid in 1956.
(e) Sale of equipment.

SCHEDULE D

SUMMARY OF INVESTMENTS

As at December 31, 1959

	Book Amount	% of Total	Market Quotation	% of Total	Endowment Income
Bonds:					
U. S. Government	$ 460,615	13.69	$ 447,329	8.75	$ 10,323
Railroad	479,718	14.25	425,064	8.31	20,146
Public utility	392,368	11.66	360,197	7.04	17,499
Industrial	348,587	10.36	312,213	6.10	14,527
Financial and investment	154,967	4.60	158,913	3.11	8,305
Total bonds	1,836,255	54.56	1,703,716	33.31	70,800
Stocks:					
Preferred	252,508	7.50	223,363	4.37	12,470
Common:					
Public utility	371,138	11.03	846,028	16.54	26,833
Industrial	594,041	17.65	1,832,870	35.83	57,448
Miscellaneous	191,095	5.68	388,467	7.59	14,668
Total common stocks	1,156,274	34.36	3,067,365	59.96	98,949
Total stocks	1,408,782	41.86	3,290,728	64.33	111,419
Real estate	120,470	3.58	120,470*	2.36	6,420
Total investments .	$3,365,507	100.00	$5,114,914	100.00	$188.639

---

* At book amount.

List of Contributions

LIST OF CONTRIBUTIONS

FROM THE WOODS HOLE OCEANOGRAPHIC INSTITUTION

See Author, Subject-Locality, Taxonomic Indexes, published in 1957,
for a complete list through 1956.

No. 701. R. B. Montgomery. Convection of Heat. *Arch. Meteorol., Geoph. u. Bioklim.*, Ser. A, Meteorol. und Geoph., Bd. 7, pp. 125–132. 1954.

No. 702. Frank J. Mather III. Northerly Occurrences of Warm Water Fishes in the Western Atlantic. *Copeia*, No. 4, pp. 292–293. 1954.

No. 703. C. W. Newton. Analysis and Data Problems in Relation to Numerical Prediction. *Bull. Amer. Meteorol. Soc.*, Vol. 35, No. 7, pp. 287–294. 1954.

No. 704. George L. Clarke. Elements of Ecology. John Wiley & Sons, Inc., New York. 534 pp. 1954. (Not included in *Collected Reprints*).

No. 705. L. van Dam. On the Respiration in Scallops (Lamellibranchiata). *Biol. Bull.*, Vol. 107, No. 2, pp. 192–202. 1954.

No. 706. Joanne Starr Malkus and R. S. Scorer. The Erosion of Cumulus Towers. *Jour. Meteorol.*, Vol. 12, No. 1, pp. 43–57. 1955.

No. 707. Athelstan F. Spilhaus. Sea and Air Resources. *Geogr. Rev.*, Vol. 44, No. 3, pp. 346–351. 1954.

No. 708. Charles J. Fish and Mary Curtis Cobb. Noxious Marine Animals of the Central and Western Pacific Ocean. *U. S. Fish and Wildlife Service, Research Report* 36, 45 pp., 1954.

No. 709. P. F. Scholander, Warner E. Love and John W. Kanwisher. The Rise of Sap in Tall Grapevines. *Plant Physiol.*, Vol. 30, No. 2, pp. 93–104. 1955. (Not included in *Collected Reprints*).

No. 710. P. F. Scholander, L. van Dam and Susan I. Scholander. Gas Exchange in the Roots of Mangroves. *Amer. Jour. Bot.*, Vol. 42, No. 1, pp. 92–98. 1955.

No. 711. Duncan C. Blanchard. A Simple Method for the Production of Homogeneous Water Drops down to 1 Micron Radius. *Jour. Colloid Sci.*, Vol. 9, No. 4, pp. 321–328. 1954.

No. 712. John H. Ryther. Ecology of Autotrophic Marine Dinoflagellates with Refence to Red Water Conditions. In: The Luminescence of Biological Systems, F. H. Johnson, Edit., Publ. by Amer. Assoc. Adv. Sci., Washington, pp. 387–414. 1955.

No. 713. Henry Stommel. Serial Observations of Drift Currents in the Central North Atlantic Ocean. *Tellus*, Vol. 6, No. 3, pp. 203–214. 1954.

No. 714. Francis A. Richards. Oxygen in the Ocean. *Geol. Soc. Amer., Mem.*, 67, Vol. 1, Ch. 9, pp. 185–238. 1957.

No. 715. Harry J. Turner, Jr. and J. Arthur Posgay. Sixth Report on Investigations of the Shellfisheries of Massachusetts. *Com. Mass., Dept. Nat. Res., Div. Mar. Fish.*, pp. 1–74. 1953.

No. 716. Joanne Starr Malkus and Claude Ronne. On the Structure of Some Cumulonimbus Clouds which Penetrated the High Tropical Troposphere. *Tellus*, Vol. 6. No. 4, pp. 351-366. 1954.

No. 717. L. V. Worthington. A Preliminary Note on the Time Scale in North Atlantic Circulation. *Deep-Sea Research*, Vol. 1, pp. 244–251. 1954.

No. 718. Arthur R. Miller. Some Suggestions for more precise Loran Navigation. *Navigation*, Vol. 3, Nos. 1 and 2, pp. 23–29. 1951. (Included in *Collected Reprints* for 1953).

No. 719. Henry B. Bigelow and Isabel Pérez Farfante. Fishes of the Western North Atlantic. Lancelets. *Mem. Sears Found. Mar. Res.*, No. 1, Pt. 1, Ch. 1, pp. 1–28. 1948. (Not included in *Collected Reprints*).

No. 720. Henry B. Bigelow and William C. Schroeder. Fishes of the Western North Atlantic. Cyclostomes. *Mem. Sears Found. Mar. Res.*, No. 1, Pt. 1, Ch. 2, pp. 29–58. 1948. (Not included in *Collected Reprints*).

No. 721. Henry B. Bigelow and William C. Schroeder. Fishes of the Western North Atlantic. Sharks. *Mem. Sears Found. Mar. Res.*, No. 1, Pt. 1, Ch. 3, pp. 59–576. 1948. (Not included in *Collected Reprints*).

No. 722. Arthur H. Clarke, Jr. Some Mollusks from the Continental Slope of Northeastern North America. *Breviora, Mus. Comp. Zool.*, No. 40, 11 pp. 1954.

No. 723. C. W. Newton. Frontogenesis and Frontolysis as a Three-Dimensional Process. *Jour. Meteorol.*, Vol. 11, No. 6, pp. 449–461. 1954.

No. 724. Charles B. Officer. Southwest Pacific Crustal Structure. *Trans. Amer. Geophys. Union*, Vol. 36, No. 3, pp. 449–459. 1955.

No. 725. K. G. Wilson and A. B. Arons. Osmotic Pressures of Sea Water Solutions Computed from Experimental Vapor Pressure Lowering. *Sears Found., Jour. Mar. Res.*, Vol. 14, No. 2, pp. 195–198. 1955.

No. 726. Joanne Starr Malkus. On the Formation and Structure of Downdrafts in Cumulus Clouds. *Jour. Meteorol.*, Vol. 12, No. 4, pp. 350–354. 1955.

No. 727. Joanne Starr Malkus. The Effects of a Large Island upon the Trade-Wind Air Stream. *Quart. Jour. Roy. Meteor. Soc.*, Vol. 81, No. 350, pp. 538–550. 1955.

No. 728. Paul Ferris Smith. Further Measurements of the Sound Scattering Properties of Several Marine Organisms. *Deep-Sea Research*, Vol. 2, pp. 71–79. 1954.

No. 729. Willard Dow. Underwater Telemetering. *Deep-Sea Research*, Vol. 2, pp. 145–151 (erroneously dated 1954). 1955.

No. 730. John H. Ryther. Inhibitory Effects of Phytoplankton upon the Feeding of *Daphnia magna* with Reference to Growth, Reproduction, and Survival. *Ecology*, Vol. 35, No. 4, pp. 522–533. 1954.

No. 731. Charles B. Officer. A Deep-Sea Seismic Reflection Profile. *Geophysics*, Vol. 20, No. 2, pp. 270–282. 1955.

No. 732. Henry B. Bigelow and William C. Schroeder. Occurrence off the Middle and North Atlantic United States of the Offshore Hake *Merluccius albidus* (Mitchill) 1818, and of the Blue Whiting *Gadus (Micromesistius) poutassou* (Risso) 1826. *Bull. Mus. Comp. Zool.*, Vol. 113, No. 2, pp. 205–226. 1955.

No. 733. JOHN H. RYTHER. The Ratio of Photosynthesis to Respiration in Marine Plankton Algae and its Effect upon the Measurement of Productivity. *Deep-Sea Research*, Vol. 2, pp. 134–139 (erroneously dated 1954). 1955.

No. 734. DUNCAN C. BLANCHARD. Bursting of Bubbles at an Air-Water Interface. *Nature*, Vol. 173, p. 1048. 1954.

No. 735. JOSEPH CHASE. Winds and Temperatures in Relation to the Brood-Strength of Georges Bank Haddock. *Jour. du Conseil*, Vol. 21, No. 1, pp. 17–24. 1955.

No. 736. GRACE I. CREITZ and FRANCIS A. RICHARDS. The Estimation and Characterization of Plankton Populations by Pigment Analysis. III. A Note on the use of "Millipore" Membrane Filters in the Estimation of Plankton Pigments. *Sears Found., Jour. Mar. Res.*, Vol. 14, No. 3, pp. 211–216. 1955.

No. 737. CHARLES J. FISH. Preliminary Observations on the Biology of Boreo-Arctic and Subtropical Oceanic Zooplankton Populations. In: Symposium on Marine and Fresh-Water Plankton in the Indo-Pacific, Bangkok, Jan. 25–26, 1954, FAO-UNESCO, Sect. 1, No. 1, pp. 1–7, 1955. (Not included in *Collected Reprints*).

No. 738. C. B. OFFICER. On some Offshore Seismic Refraction Profiles in the Cook Strait, Tasman Bay, and Golden Bay Areas of New Zealand. *N.Z. Jour. Geol. and Geophys.*, Vol. 2, No. 2, pp. 350–354. 1959.

No. 739. WILLIAM G. METCALF. On the Formation of Bottom Water in the Norwegian Basin. *Trans. Amer. Geophys. Union*, Vol. 36, No. 4, pp. 596–600. 1955.

No. 740. ANDREW F. BUNKER. Turbulence and Shearing Stresses Measured over the North Atlantic Ocean by an Airplane-Acceleration Technique. *Jour. Meteorol.*, Vol. 12, No. 5, pp. 445–455. 1955.

No. 741. WILBUR MARKS and F. CLAUDE RONNE. Aerial Stereo-Photography and Ocean Waves. *Photogr. Engineering*, March 1955, pp. 107–110. 1955.

No. 742. MALCOLM S. GORDON. Summer Ecology of Oceanic Birds off Southern New England. *The Auk*, Vol. 72, pp. 138–147. 1955.

No. 743. CHARLES B. OFFICER. Geologic Interpretation of a Series of Seismic Reflection Profiles from Bermuda to the Continental Margins. *Deep-Sea Research*, Vol. 2, pp. 253–260. 1955.

No. 744. J. W. KANWISHER and GORDON VOLKMANN. A Scattering Layer Observation. *Science*, Vol. 121, No. 3134, pp. 108–109. 1955.

No. 745. IRVING I. SCHELL. Interrelations of Arctic Ice with the Atmosphere and the Ocean in the North Atlantic — Arctic and Adjacent Areas. *Jour. Meteorol.*, Vol. 13, No. 1, pp. 46–58. 1956.

No. 746. H. G. FARMER, W. MARKS, R. G. WALDEN and G. G. WHITNEY, JR. A Technique for Ocean Wave Measurements. In: Proc. First Conf., Ships and Waves, Oct. 1954, Counc. Wave Res. and Soc. Naval Arch. and Mar. Eng., pp. 11–32. 1955.

No. 747. DUNCAN C. BLANCHARD. Electrified Droplets from the Bursting of Bubbles at an Air-Sea Water Interface. *Nature*, Vol. 175, No. 4451, pp. 334–336. 1955.

No. 748. E. M. HULBURT. Distribution of Phosphorus in Great Pond, Massachusetts. *Sears Found., Jour. Mar. Res.*, Vol. 15, No. 3, pp. 181–192. 1956.

No. 749. F. C. FUGLISTER. Alternative Analyses of Current Surveys. *Deep-Sea Research*, Vol. 2, pp. 213–229. 1955.

No. 750. Gilbert L. Voss. The Cephalopoda Obtained by the Harvard-Havana Expedition off the Coast of Cuba in 1938–39. *Bull, Mar. Sci., Gulf and Caribbean*, Vol. 5, No. 2, pp. 81–115. 1955.

No. 751. Frank S. Essapian. Speed-Induced Skin Folds in the Bottle-Nosed Porpoise, *Tursiops truncatus*. *Breviora, Mus. Comp. Zool.*, No. 43, 4 pp., 9 Pls. 1955.

No. 752. John P. Barlow. Effect of Wind on Salinity Distribution in an Estuary. *Sears Found., Jour. Mar. Res.*, Vol. 15, No. 3, pp. 193–203. 1956.

No. 753. John P. Barlow. Physical and Biological Processes Determining the Distribution of Zooplankton in a Tidal Estuary. *Biol. Bull.*, Vol. 109, No. 2, pp. 211–225. 1955.

No. 754. Alan J. Faller. A Demonstration of Fronts and Frontal Waves in Atmospheric Models. *Jour. Meteorol.*, Vol. 13, No. 1, pp. 1–4. 1956.

No. 755. P. F. Scholander. Evolution of Climatic Adaptation in Homeotherms. *Evolution*, Vol. 9, No. 1, pp. 15–26. 1955.

No. 756. Hilary B. Moore. Variations in Temperature and Light Response within a Plankton Population. *Biol. Bull.*, Vol. 108, No. 2, pp. 175–181. 1955.

No. 757. A. H. Woodcock and W. A. Mordy. Salt Nuclei, Wind and Daily Rainfall in Hawaii. *Tellus*, Vol. 7, No. 3, pp. 291–300. 1955.

No. 758. Floyd M. Soule and J. E. Murray. Physical Oceanography of the Grand Banks Region and the Laborador Sea in 1954. *U. S. Coast Guard Bull.*, No. 40, pp. 79–168. 1955.

No. 759. Bostwick H. Ketchum, Nathaniel Corwin and D. Jean Keen. The Significance of Organic Phosphorus Determinations in Ocean Waters. *Deep-Sea Research*, Vol. 2, pp. 172–181. 1955.

No. 760. Dean F. Bumpus and E. Lowe Pierce. The Hydrography and the Distribution of Chaetognaths over the Continental Shelf off North Carolina. Pap. Mar. Biol. and Oceanogr., *Deep-Sea Research*, Suppl. to Vol. 3, pp. 92–109. 1955. (Included in *Collected Reprints* for 1955, Part II).

No. 761. A. H. Woodcock. Bursting Bubbles and Air Pollution. *Sewage and Industrial Wastes*, Vol. 27, No. 10, pp. 1189–1192. 1955.

No. 762. Gordon A. Riley. Review of the Oceanography of Long Island Sound. Pap. Mar. Biol. and Oceanogr., *Deep-Sea Research*, Suppl. to Vol. 3, pp. 224–238. 1955. (Included in *Collected Reprints* for 1955, Part II).

No. 763. Talbot H. Waterman. Polarization of Scattered Sunlight in Deep Water. Pap. Mar. Biol. and Oceanogr., *Deep-Sea Research*, Suppl. to Vol. 3, pp 426–434. 1955. (Included in *Collected Reprints* for 1955, Part II).

No. 764. E. M. Hulburt. The Phytoplankton of Great Pond, Massachusetts. *Biol. Bull.*, Vol. 110, No. 2, pp. 157–168. 1956.

No. 765. C. O'D. Iselin. Recent Advances in our Understanding of the Circulation Problem and their Implications. *Sears Found., Jour. Mar. Res.*, Vol. 14, No. 4, pp. 315–322. 1955.

No. 766. John C. Ayers. Population Dynamics of the Marine Clam, *Mya arenaria*. *Limnol. and Oceanogr.*, Vol. 1, No. 1, pp. 26–34. 1956.

No. 767. Edward M. Thorndike. Hydroscopes. *Trans. Amer. Geophys. Union*, Vol. 36, No. 3, pp. 470–472. 1955.

No. 768. A. H. Woodcock and D. C. Blanchard. Tests of the Salt-Nuclei Hypothesis of Rain Formation. *Tellus*, Vol. 7, No. 4, pp. 437–448. 1955.

No. 769. Wilbur Marks and Joseph Chase. Observation of the Growth and Decay of a Wave Spectrum. In: Interaction of Sea and Atmosphere. *Meteorol. Monogr.*, Vol. 2, No. 10, pp. 67–74. 1957.

No. 770. C.-G. Rossby and H. Egnér. On the Chemical Climate and its Variation with Atmospheric Circulation Pattern. *Tellus*, Vol. 7, No. 1, pp. 118–133. 1955.

No. 771. Stefan Machlup and J. B. Hersey. Analysis of Sound-Scattering Observations from Non-Uniform Distributions of Scatterers in the Ocean. *Deep-Sea Research*, Vol. 3, pp. 1–22. 1955.

No. 772. Bostwick H. Ketchum. Distribution of Coliform Bacteria and other Pollutants in Tidal Estuaries. *Sewage and Industrial Wastes*, Vol. 27, No. 11, pp. 1288–1296. 1955.

No. 773. Susan I. Scholander. Land Birds over the Western North Atlantic. *The Auk*, Vol. 72, pp. 225–239. 1955.

No. 774. Harvey R. Bullis, Jr. and F. J. Mather, III. Tunas of the Genus *Thunnus* of the Northern Caribbean. *Amer. Mus., Novitates*, No. 1765, 12 pp. 1956.

No. 775. Bostwick H. Ketchum and D. Jean Keen. The Accumulation of River Water over the Continental Shelf between Cape Cod and Chesapeake Bay. Pap. Mar. Biol. and Oceanogr., *Deep-Sea Research*, Suppl. to Vol. 3, pp. 346–357. 1955. (Included in *Collected Reprints* for 1955, Part II).

No. 776. Alfred C. Redfield. The Hydrography of the Gulf of Venezuela. Pap. Mar. Biol. and Oceanogr., *Deep-Sea Research*, Suppl. to Vol. 3, pp. 115–133. 1955. (Included in *Collected Reprints* for 1955, Part II).

No. 777. Harry J. Turner, Jr. How Clam Drills Capture Razor Clams. *The Nautilus*, Vol. 69, No. 1, pp. 20–22. 1955.

No. 778. J. W. Kanwisher. Freezing in Intertidal Animals. *Biol. Bull.*, Vol. 109, No. 1, pp. 56–63. 1955.

No. 779. Ruth D. Turner. Scaphopods of the *Atlantis* Dredgings in the Western Atlantic with a Catalogue of the Scaphopod Types in the Museum of Comparative Zoology. Pap. Mar. Biol. and Oceanogr., *Deep-Sea Research*, Suppl. to Vol. 3, pp. 309–320. 1955. (Included in *Collected Reprints* for 1955, Part II).

No. 780. E. Steemann Nielsen. The Production of Antibiotics by Plankton Algae and its Effect upon Bacterial Activities in the Sea. Pap. Mar. Biol. and Oceanogr., *Deep-Sea Research*, Suppl. to Vol. 3, pp. 281–286. 1955. (Included in *Collected Reprints* for 1955, Part II).

No. 781. W. T. Edmondson. Factors Affecting Productivity in Fertilized Water. Pap. Mar. Biol. and Oceanogr., *Deep-Sea Research*, Suppl. to Vol. 3, pp. 451–464. 1955. (Included in *Collected Reprints* for 1955, Part II).

No. 782. Henry C. Stetson. Patterns of Deposition at the Continental Margin. Pap. Mar. Biol. and Oceanogr., *Deep-Sea Research*, Suppl. to Vol. 3, pp. 298–308. 1955. (Included in *Collected Reprints* for 1955, Part II).

No. 783. Harry J. Turner, Jr. and Stanley Scher. Seventh Report on Investigations of the Shellfisheries of Massachusetts. *Com. Mass., Dept. Nat. Res., Div. Mar. Fish.*, 35 pp. 1954.

No. 784. Alfred C. Redfield. Preludes to the entrapment of organic matter in the sediments of Lake Maracaibo. In: Habitat of Oil. Amer. Assoc. Petrol. Geologists, June, 1958, pp. 968–981. 1958.

No. 785. Earl Barrett and Gunnar Brodin. The Acidity of Scandinavian Precipitation. *Tellus*, Vol. 7, No. 2, pp. 251–257. 1955.

No. 786. T. F. Goreau and V. T. Bowen. Calcium Uptake by a Coral. *Science*, Vol. 122, No. 3181, pp. 1188–1189. 1955.

No. 787. Henry B. Bigelow, William C. Schroeder and Stewart Springer. Three New Shark Records from the Gulf of Mexico. *Breviora, Mus. Comp. Zool.*, No. 49, 12 pp. 1955.

No. 788. Dean F. Bumpus. The Circulation over the Continental Shelf South of Cape Hatteras. *Trans. Amer. Geophys. Union*, Vol. 36, No. 4, pp. 601–611. 1955.

No. 789. Donald R. Griffin. Hearing and Acoustic Orientation in Marine Animals. Pap. Mar. Biol. and Oceanogr., *Deep-Sea Research*, Suppl. to Vol. 3, pp. 406–417. 1955. (Included in *Collected Reprints* for 1955, Part II).

No. 790. William C. Schroeder. Report on the Results of Exploratory Otter-Trawling along the Continental Shelf and Slope between Nova Scotia and Virginia during the Summers of 1952 and 1953. Pap. Mar. Biol. and Oceanogr., *Deep-Sea Research*, Suppl. to Vol. 3, pp. 358–372. 1955. (Included in *Collected Reprints* for 1955, Part II).

No. 791. L. V. Worthington. A New Theory of Caribbean Bottom-Water Formation. *Deep-Sea Research*, Vol. 3, pp. 82–87. 1955.

No. 792. C. O'D. Iselin. Coastal Currents and the Fisheries. Pap. Mar. Biol. and Oceanogr., *Deep-Sea Research*, Suppl. to Vol. 3, pp. 474–478. 1955. (Included in *Collected Reprints* for 1955, Part II).

No. 793. Barbara Lawrence and William E. Schevill. The Functional Anatomy of the Delphinid Nose. *Bull. Mus. Comp. Zool.*, Vol. 114, No. 4, pp. 103–151. 1956. (Not included in *Collected Reprints*).

No. 794. William S. Von Arx and W. S. Richardson. On the Fine-Structure of the Gulf Stream Front. *Deep-Sea Research*, Vol. 3, pp. 46–65. 1955.

No. 795. P. F. Scholander, L. van Dam, C. Lloyd Claff and J. W. Kanwisher. Micro Gasometric Determination of Dissolved Oxygen and Nitrogen. *Biol. Bull.*, Vol. 109, No. 2, pp. 328–334. 1955.

No. 796. Henry Stommel. Lateral Eddy Viscosity in the Gulf Stream System. *Deep-Sea Research*, Vol. 3 pp. 88–90. 1955.

No. 797. Irving I. Schell. Further Evidence of Dynamic Persistence and of its Application to Foreshadowing. *Jour. Meteorol.*, Vol. 13, No. 5, pp. 471–481. 1956.

No. 798. Nora Gladwin Fairbank. Methods and Preliminary Results in a Study of Minerals from the Eastern Gulf of Mexico. *Jour. Sed. Petrol.*, Vol. 26, No. 3, pp. 268–275. 1956.

No. 799. Henry Stommel, Arnold B. Arons and Duncan Blanchard. An Oceanographical Curiosity: the Perpetual Salt Fountain. *Deep-Sea Research*, Vol. 3, pp. 152–153. 1956.

No. 800. M. S. Gordon and Richard H. Backus. New Records of Labrador Fishes with Special Reference to those of Hebron Fjord. *Copeia*, No. 1, pp. 17–20. 1957.

No. 801. Floyd M. Soule and J. E. Murray. Physical Oceanography of the Grand Banks and the Labrador Sea in 1955. *U. S. Coast Guard Bull.*, No. 41, pp. 59–114. 1956.

No. 802. James M. Moulton and Richard H. Backus. Annotated References Concerning the Effects of Man-Made Sounds on the Movements of Fishes. *Dept. Sea and Shore Fish., Fish. Circ.*, Augusta, Maine, No. 17, 8 pp. 1955.

No. 804. W. V. R. Malkus. Outline of a Theory of Turbulent Shear Flow. *Jour. Fluid Mech.*, Vol. 1, Pt. 5, pp. 521–539. 1956.

No. 805. John Mackiewicz and Richard H. Backus. Oceanic Records of *Lasionycteris noctivagans* and *Lasiurus borealis*. *Jour. Mammalogy*, Vol. 37, No. 3, pp. 442–443. 1956.

No. 806. Allyn C. Vine. Oceanographic Instrumentation. *Science*, Vol. 122, No. 3173, pp. 748–751. 1955.

No. 807. P. F. Scholander and William E. Schevill. Counter-Current Vascular Heat Exchange in the Fins of Whales. *Jour. Appl. Physiol.*, Vol. 8, No. 3, pp. 279–282. 1955.

No. 808. E. Steemann Nielsen. The Interaction of Photosynthesis and Respiration and its Importance for the Determination of ^{14}C-Discrimination in Photosynthesis. *Physiologia Plantarum*, Vol. 8, pp. 945–953. 1955.

No. 809. Duncan C. Blanchard. The Supercooling, Freezing and Melting of Giant Waterdrops at Terminal Velocity in Air. Proceedings of the First Conference on the Physics of Cloud Precipitation Particles, Woods Hole, September 7–10, 1955. In: Artificial Stimulation of Rain, pp. 233–249. Pergamon Press Ltd., New York, London, Paris. 1957.

No. 810. Karl E. Schleicher and Alvin Bradshaw. A Conductivity Bridge for Measurement of the Salinity of Sea Water. *Jour. du Conseil*, Vol. 22, No. 1, pp. 9–20. 1956.

No. 811. G. W. Morgan. On the Wind-Driven Ocean Circulation. *Tellus*, Vol. 8, No. 3, pp. 301–320. 1956.

No. 812. Duncan C. Blanchard. Discussion of Raindrop Distributions made during Project Shower, Hawaii, 1954. Proceedings of the First Conference on the Physics of Cloud Precipitation Particles, Woods Hole, September 7–10, 1955. In: Artificial Stimulation of Rain, pp. 213–223. Pergamon Press Ltd., New York, London, Paris. 1957.

No. 813. R. W. Holmes. The Annual Cycle of Phytoplankton in the Labrador Sea, 1950–51. *Bull. Bingham Oceanogr. Coll.*, Vol. 16, Art. 1, 74 pp. 1956. (Not included in *Collected Reprints*).

No. 814. Richard H. Backus, Stewart Springer and Edgar L. Arnold, Jr. A Contribution to the Natural History of the White-Tip Shark, *Pterolamiops longimanus* (Poey). *Deep-Sea Research*, Vol. 3, pp. 178–188. 1956.

No. 815. William E. Schevill. *Lagenorhynchus acutus* off Cape Cod. *Jour. Mammalogy*, Vol. 37, No. 1, pp. 128–129. 1956.

No. 816. P. F. Scholander, L. van Dam and Theodore Enns. Nitrogen Secretion in the Swimbladder of Whitefish. *Science*, Vol. 123, No. 3185, pp. 59–60. 1956.

No. 817. Harold E. Edgerton and Lloyd D. Hoadley. Cameras and Lights for Underwater Use. *Jour. Soc. Motion Pict. and Television Eng.*, Vol. 64, pp. 345–350. 1955.

No. 818. P. F. Scholander, John W. Kanwisher and D. C. Nutt. Gases in Icebergs. *Science*, Vol. 123, No. 3186, pp. 104–105. 1956.

No. 819. John H. Ryther. Photosynthesis in the Ocean as a Function of Light Intensity. *Limnol. and Oceanogr.*, Vol. 1, No. 1, pp. 61–70. 1956.

No. 820. William S. von Arx. An Experimental Approach to Problems in Physical Oceanography. In: Progress in Physics and Chemistry of the Earth, Vol. 2, pp. 1–29. Pergamon Press Ltd., London, New York, Paris. 1957.

No. 821. George L. Clarke and Gunther K. Wertheim. Measurements of Illumination at Great Depths and at Night in the Atlantic Ocean by Means of a New Bathyphotometer. *Deep-Sea Research*, Vol. 3, pp. 189–205. 1956.

No. 822. P. F. Scholander. Hydrostatic Pressure in Coconuts. *Plant Physiol.*, Vol. 30, No. 6, pp. 560–561. 1955.

No. 823. John C. Ayers. A Dynamic Height Method for the Determination of Currents in Deep Lakes. *Limnol. and Oceanogr.*, Vol. 1, No. 3, pp. 150–161. 1956.

No. 824. Parker D. Trask. The *Atlantis* Marine Geological Expedition to Peru and Chile. *Nature*, Vol. 177, pp. 454–455. 1956.

No. 825. John H. Ryther. The Measurement of Primary Production. *Limnol. and Oceanogr.*, Vol. 1, No. 2, pp. 72–84. 1956.

No. 826. Robert L. Miller. Trend Surfaces: Their Application to Analysis and Description of Environments of Sedimentation. 1. The Relation of Sediment-Size Parameters to Current-Wave Systems and Physiography. *Jour. Geology*, Vol. 64, No. 5, pp. 425–446. 1956.

No. 827. Joanne Starr Malkus. On the Maintenance of the Trade Winds. *Tellus*, Vol. 8, No. 3, pp. 335–350. 1956.

No. 828. Alfred C. Redfield and Arthur R. Miller. Water Levels Accompanying Atlantic Coast Hurricanes. In: Interaction of Sea and Atmosphere. *Meteorol. Monogr.*, Vol. 2, No. 10, pp. 1–23. 1957.

No. 829. Arthur R. Miller. The Effect of Steady Winds on Sea Level at Atlantic City. In: Interaction of Sea and Atmosphere. *Meteorol. Monogr.*, Vol. 2, No. 10, pp. 24–31. 1957.

No. 830. Francis A. Richards and Ralph F. Vaccaro. The Cariaco Trench, an Anaerobic Basin in the Caribbean Sea. *Deep-Sea Research*, Vol. 3, pp. 214–228. 1956.

No. 831. David C. Nutt and Lawrence K. Coachman. The Oceanography of Hebron Fjord, Labrador. *Jour. Fish. Res. Bd., Canada*, Vol. 13, No. 5, pp. 709–758. 1956.

No. 832. William E. Schevill and Barbara Lawrence. Food-Finding by a Captive Porpoise (*Tursiops truncatus*). *Breviora, Mus. Comp. Zool.*, No. 53, 15 pp. 1956.

No. 833. A. F. Bunker. Turbulence Measurements in a Young Cyclone over the Ocean. *Bull. Amer. Meteorol. Soc.*, Vol. 38, No. 1, pp. 13–16. 1957.

No. 834. Richard H. Backus and J. B. Hersey. Echo-Sounder Observations of Midwater Nets and their Towing Cables. *Deep-Sea Research*, Vol. 3, pp. 237–241. 1956.

No. 835. Joseph Chase. The Bermuda-Azores High Pressure Cell. Its Surface Wind Circulation. *Miscelânea Geofísica*, Luanda, Angola, pp. 29–54. 1956. (In *Collected Reprints* for 1957).

No. 837. A. H. Woodcock. Dimorphism in the Portuguese Man-of-War. *Nature*, Vol. 178, No. 4527, pp. 253–255. 1956.

No. 838. E. M. Hulburt. The Taxonomy of Unarmored Dinophyceae of Shallow Embayments on Cape Cod, Massachusetts. *Biol. Bull.*, Vol. 112, No. 2, pp. 196–219. 1957.

No. 839. C. B. Officer, J. I. Ewing, R. S. Edwards and H. R. Johnson. Geophysical Investigations in the Eastern Caribbean: Venezuelan Basin, Antilles Island Arc, and Puerto Rico Trench. *Bull. Geol. Soc. Amer.*, Vol. 68, pp. 359–378. 1957.

No. 840. Francis A. Richards. On the State of our Knowledge of Trace Elements in the Ocean. *Geochimica et Cosmochimica Acta*, Vol. 10, No. 4, pp. 241–243. 1956.

No. 841. Henry R. Johnson, Richard H. Backus, J. B. Hersey and D. M. Owen. Suspended Echo-Sounder and Camera Studies of Midwater Sound Scatterers. *Deep-Sea Research*, Vol. 3, pp. 266–272. 1956.

No. 842. John H. Ryther. Interrelation between Photosynthesis and Respiration in the Marine Flagellate, *Dunaliella euchlora*. *Nature*, Vol. 178, pp. 861–862. 1956.

No. 843. Joanne Starr Malkus. Trade Cumulus Cloud Groups: Some Observations Suggesting a Mechanism of Their Origin. *Tellus*, Vol. 9, No. 1, pp. 33–44. 1957.

No. 844. Francis A. Richards. Some Current Aspects of Chemical Oceanography. In: Progress in Physics and Chemistry of the Earth, Vol. 2, pp. 77–128. Pergamon Press Ltd., London, New York, Paris. 1957.

No. 845. Henry Stommel. Florida Straits Transports, 1952–1956. *Bull. Mar. Sci., Gulf and Caribbean*, Vol. 7, No. 3, pp. 252–254. 1957.

No. 846. Henry Stommel. On the Determination of the Depth of No Meridional Motion. *Deep-Sea Research*, Vol. 3, pp. 273–278. 1956.

No. 847. Athelstan Spilhaus. Control of the World Environment. *Geogr. Rev.*, Vol. 46, No. 4, pp. 451–459. 1956.

No. 848. Henry B. Bigelow and William C. Schroeder. A Study of the Sharks of the Suborder Squaloidea. *Bull. Mus. Comp. Zool.*, Vol. 117, No. 1, pp. 1–150. 1957. (Not included in *Collected Reprints*).

No. 849. Duncan C. Blanchard. Electrically Charged Drops from Bubbles in Sea Water and their Meteorological Significance. *Jour. Meteorol.*, Vol. 15, No. 4, pp. 383–396. 1958.

No. 850. H. Walden and H. G. Farmer. Auswertung von Seegangsregistrierungen des Forschungsschiffes "Atlantis" mit dem "Ship-Borne Wave Recorder" sowie Vergleich mit entsprechenden Seegangsberechnungen aus den Windverhaltnissen (Hindcasting). *Deutsche Hydrogr. Zeitschrift*, Bd. 10, Heft 4, pp. 121–134. 1957.

No. 851. Allyn C. Vine, Some Trends in Oceanographic Instrumentation. *Proc. UNESCO Symp. Phys. Oceanogr.*, Tokyo, 1955: 49–52. 1597. (Not included in *Collected Reprints*).

No. 852. Francis A. Richards and Nathaniel Corwin. Some Oceanographic Applications of Recent Determinations of the Solubility of Oxygen in Sea Water. *Limnol. and Oceanogr.*, Vol. 1, No. 4, pp. 263–267. 1956.

No. 853. Irving I. Schell. On the Nature and Origin of the Southern Oscillation. *Jour. Meteorol.*, Vol. 13, No. 6, pp. 592–598. 1956.

No. 854. Richard H. Backus. Northern Record of the Snake Eel *Ophichthus gomesi* (Castelnau). *Copeia*, No. 1, p. 61. 1957.

No. 855. A. B. Arons and Henry Stommel. A β-Plane Analysis of Free Periods of the Second Class in Meridional and Zonal Oceans. *Deep-Sea Research*, Vol. 4, pp. 23–31. 1956.

No. 856. Gordon Volkmann, John Knauss and Allyn Vine. The Use of Parachute Drogues in the Measurement of Subsurface Ocean Currents. *Trans. Amer. Geophys. Union*, Vol. 37, No. 5, pp. 573–577. 1956.

No. 857. Richard H. Backus. Notes on Western North Atlantic Sharks. *Copeia*, No. 3, pp. 246–248. 1957.

No. 858. George L. Clarke and Richard H. Backus. Measurements of Light Penetration in Relation to Vertical Migration and Records of Luminescence of Deep-Sea Animals. *Deep-Sea Research*, Vol. 4, pp. 1–14. 1956.

No. 859. G. Veronis and Henry Stommel. The Action of Variable Wind Stresses on a Stratified Ocean. *Sears Found., Jour. Mar. Res.*, Vol. 15, No. 1, pp. 43–75. 1956.

No. 860. I. Friedman and A. H. Woodcock. Determination of Deuterium-Hydrogen Ratios in Hawaiian Waters. *Tellus*, Vol. 9, No. 4, pp. 553–556. 1957.

No. 861. J. I. Ewing, C. B. Officer, H. R. Johnson, and R. S. Edwards. Geophysical Investigations in the Eastern Caribbean: Trinidad Shelf, Tobago Trough, Barbados Ridge, Atlantic Ocean. *Bull. Geol. Soc. Amer.*, Vol. 68, pp. 897–912. 1957.

No. 862. James M. Moulton. Influencing the Calling of Sea Robins (*Prionotus* spp.) with Sound. *Biol. Bull.*, Vol. 111, No. 3, pp. 393–398. 1956.

No. 863. S. T. Knott and J. B. Hersey. Interpretation of High-Resolution Echo-Sounding Techniques and their Use in Bathymetry, Marine Geophysics, and Biology. *Deep-Sea Research*, Vol. 4, pp. 36–44. 1956.

No. 864. H. B. Moore and E. G. Corwin. The Effects of Temperature, Illumination, and Pressure on the Vertical Distribution of Zooplankton. *Bull. Mar. Sci., Gulf and Caribbean*, Vol. 6, No. 4, pp. 273–287. 1956.

No. 865. Richard S. Edwards and Francis A. Richards. A Bottom-Water Sampler. *Deep-Sea Research*, Vol. 4, pp. 65–66. 1956.

No. 866. M. S. Rutstein. Flooded Quarries for Experimental Work. *Trans. Amer. Geophys. Union*, Vol. 35, No. 5, pp. 688–690. 1957.

No. 867. Irving Friedman, Daniel R. Norton, Douglas B. Carter and Alfred C. Redfield. The Deuterium Balance of Lake Maracaibo. *Limnol. and Oceanogr.*, Vol. 1, No. 4, pp. 239–246. 1956.

No. 868. M. S. Gordon. Observations on Osmoregulation in the Arctic Char (*Salvelinus alpinus* L.). *Biol. Bull.*, Vol. 112, No. 1, pp. 28–33. 1957.

No. 869. Helen S. Vishniac. On the Ecology of the Lower Marine Fungi. *Biol. Bull.*, Vol. 111, No. 3, pp. 410–414. 1956.

No. 870. W. S. Wooster and Bostwick H. Ketchum. Transport and Dispersal of Radioactive Elements in the Sea. In: The Effects of Atomic Radiation on Oceanography and Fisheries. *Nat. Acad. Sci.-Nat. Res. Council, Publ.* No. 551, Chap. 4, pp. 43–51. 1957.

No. 871. Bostwick H. Ketchum. The Effects of the Ecological System on the Transport of Elements in the Sea. In: The Effects of Atomic Radiation on Oceanography and Fisheries. *Nat. Acad. Sci.-Nat. Res. Council, Publ.* No. 551, Chap. 5, pp. 52–59. 1957.

No. 872. P. F. Scholander and John Krog. Countercurrent Heat Exchange and Vascular Bundles in Sloths. *Jour. Applied Physiol.*, Vol. 10, No. 3, pp. 405–411. 1957. (Not included in *Collected Reprints*).

No. 873. Lawrence K. Coachman, E. Hemmingsen and P. F. Scholander. Gas Enclosures in a Temperate Glacier. *Tellus*, Vol. 8, No. 4, pp. 415–423. 1956. (Not included in *Collected Reprints*).

No. 874. J. B. Hersey. Electronics in Oceanography. In: Advances in Electronics and Electron Physics, Vol. 9, pp. 239–295. Academic Press, Inc., New York. 1957. (Not included in *Collected Reprints*.)

No. 875. Duncan C. Blanchard and A. H. Woodcock. Bubble Formation and Modification in the Sea and its Meteorological Significance. *Tellus*, Vol. 9, No. 2, pp. 145–158. 1957.

No. 876. Harry J. Turner, Carl J. George and Joseph H. Connell. Eighth Report on Investigations of the Shellfisheries of Massachusetts. *Com. Mass., Dept. Nat. Res., Div. Mar. Fish.*, 25 pp. 1955.

No. 877. Floyd M. Soule and J. E. Murray. Physical Oceanography of the Grand Banks Region and the Labrador Sea in 1956. *U. S. Coast Guard Bull.*, No. 42, pp. 35–100. 1957. (In *Collected Reprints* for 1958).

No. 878. J. W. Kanwisher and H. Leivestad. Thermal Regulation in Whales. *Norwegian Whaling Gazette*, No. 1, pp.1–5. 1957.

No. 879. P. F. Scholander and L. van Dam. Micro Gasometric Determination of Oxygen in Fish Blood. *Jour. Cell. and Comp. Physiol.*, Vol. 48, No. 3, pp. 529–532. 1956. No. 3, pp. 517–522. 1956.

No. 880. P. F. Scholander. Observations on the Gas Gland in Living Fish. *Jour. Cell. and Comp. Physiol.*, Vol. 48, No. 3, pp. 523–528. 1956.

No. 881. P. F. Scholander, L. van Dam and Theodore Enns. The Source of Oxygen Secreted into the Swimbladder of Cod. *Jour. Cell. and Comp. Physiol.*, Vol. 48, No. 3, pp. 517–522. 1956.

No. 882. H. L. Sanders. The Chepalocarida and Crustacean Phylogeny. *Syst. Zool.*, Vol. 6 No. 3, pp. 112–129. 1957.

No. 883. John C. Ayers and Roger Bachmann. Simplified Computations for the Dynamic Height Method of Current Determination in Lakes. *Limnol and Oceanogr.*, Vol. 2, No. 2, pp. 155–157. 1957.

No. 884. John M. Zeigler and F. C. Ronne. Time-Lapse Photography - - an Aid to Studies of the Shoreline. *Research Reviews*, Office of Naval Research, Washington, April, pp. 1–6. 1957.

No. 885. Shannon R. Torphy and John M. Zeigler. Submarine Typography of Eastern Channel, Gulf of Maine. *Jour. Geology*, Vol. 65, No. 4, pp. 433–441. 1957.

No. 886. Harry J. Turner and David L. Belding. The Tidal Migrations of *Donax variabilis* Say. *Limnol and Oceanogr.*, Vol. 2, No. 2, pp. 120–124. 1957.

No. 887. J. W. Kanwisher. Freezing and Drying in Intertidal Algae. *Biol. Bull.*, Vol. 113, No. 2, pp. 275–285. 1957.

No. 888. J. W. Kanwisher and Alfred Ebeling. Composition of the Swim-Bladder Gas in Bathypelagic Fishes. *Deep-Sea Research*, Vol. 4, pp. 211–217. 1957.

No. 889. A. H. Woodcock and A. T. Spencer, An Airborne Flame Photometer and its Use in the Scanning of Marine Atmospheres for Sea-Salt Particles. *Jour. Meteorol.*, Vol. 14, No. 5, pp. 437-447. 1957.

No. 890. Willem A. van Bergeijk and Emil Witschi. The Basila Papilla of the Anuran Ear. *Acta Anatomica*, Vol. 30, pp. 81–91. (Not included in *Collected Reprints*).

No. 891. P. F. Scholander, L. van Dam, J. W. Kanwisher, H. T. Hammel and M. S. Gordon. Supercooling and Osmoregulation in Arctic Fish. *Jour. Cell. and Comp. Physiol.*, Vol. 49, No. 1, pp. 5–24. 1957.

No. 892. P. F. Scholander and L. van Dam. The Concentration of Hemoglobin in Some Cold Water Arctic Fishes. *Jour. Cell. and Comp. Physiol.*, Vol. 49, No. 1, pp. 1–4. 1957.

No. 893. Charles S. Yentsch and John R. Ryther. Short-term Variations in Phytoplankton Chlorophyll and Their Significance. *Limnol. and Oceanogr.*, Vol. 2, No. 2, pp. 140–142. 1957.

No. 894. Richard H. Backus and Harold Barnes. Television-Echo-Sounder Observations by Midwater Sound Scatterers. *Deep-Sea Research*, Vol. 4, pp. 116-119. 1957.

No. 895. Robert G. Walden, David D. Ketchum and David H. Frantz, Jr. Buoy Telemeters Ocean Temperature Data. *Electronics*, McGraw-Hill Co., New York, Vol. 30, No. 6, pp. 164–167. 1957.

No. 896. Richard H. Backus. The Fishes of Labrador. *Bull. Amer. Mus. Nat. Hist.*, Vol. 113, Art. 4, pp. 273-337. 1957. (Not included in *Collected Reprints*).

No. 897. Harold Barnes. The Northern Limit of *Balanus balanoides* (L). *Oikos*, Vol. 8, No. 1, pp. 1–15. 1957.

No. 898. Charles S. Yentsch. A Non-Extractive Method for the Quantitative Estimation of Chlorophyll in Algal Cultures. *Nature*, Vol. 179, pp. 1302-1304. 1957.

No. 899. Henry Stommel and George Veronis. Steady Convective Motion in a Horizontal Layer of Fluid Heated Uniformly from Above and Cooled Non-Uniformly from Below. *Tellus*, Vol. 9, No. 3, pp. 401–407. 1957.

No. 900. Arthur R. Miller. The Effects of Winds on Water Levels on the New England Coast. *Limnol. and Oceanogr.*, Vol. 3, No. 1, pp. 1–14. 1958.

No. 901. Frank J. Mather III and Robert H. Gibbs. Distributional Records of Fishes from Waters off New England and the Middle Atlantic States. *Copeia*, No. 3, pp. 242–244. 1957.

No. 902. John H. Ryther and Charles S. Yentsch. The Estimation of Phytoplankton Production in the Ocean from Chlorophyll and Light Data. *Limnol. and Oceanogr.*, Vol. 2, No. 3, pp. 281-286. 1957.

No. 903. W. H. Sutcliffe, Jr. An Improved Method for the Determination of Preserved Plankton Volumes. *Limnol. and Oceanogr.*, Vol. 2, No. 3, pp. 295–296. 1957.

No. 904. Dean F. Bumpus. Surface Water Temperature along Atlantic and Gulf Coasts of the United States. *U. S. Fish and Wildlife Service, Spec. Sci. Rept. — Fisheries*, No. 214, 153 pp. 1957. (Not included in *Collected Reprints*).

No. 905. William D. Athearn. Comparisons of Clay from the Continental Shelf off Long Island with the Gardiners Clay. *Jour. Geology*, Vol. 65, No. 4, pp. 448–449. 1957.

No. 906. John H. Ryther and Charles S. Yentsch. Primary Production of Continental Shelf Waters off New York. *Limnol. and Oceanogr.*, Vol. 3, No. 3, pp. 327–335. 1958.

No. 907. Vaughan T. Bowen and T. T. Sugihara. Strontium 90 in North Atlantic Surface Water. *Proc. Nat. Acad. Sci.*, Vol. 43, No. 7, pp. 576–580. 1957.

No. 908. L. V. Worthington and William E. Schevill. Underwater Sounds Heard from Sperm Whales. *Nature,* Vol. 180, p. 291. 1957

No. 909. Jan Hahn. Oceanus Goes to the Bottom of the Sea. *Oceanus,* Vol. 5, Nos. 1 and 2, pp. 20–31. 1957.

No. 910. J. C. Swallow and L. V. Worthington. Measurements of Deep Currents in the Western North Atlantic. *Nature,* Vol. 179, pp. 1183–1184. 1957.

No. 911. G. C. McLeod. The Effect of Circularly Polarized Light on the Photosynthesis and Chlorophyll *a* Synthesis of Certain Marine Algae. *Limnol. and Oceanogr.,* Vol. 2, No. 4, pp. 360–362. 1957.

No. 912. Robert H. Gibbs, Jr. A Taxonomic Analysis of *Myctophum affine* and *M. nitidulum,* two Lantern-Fishes Previously Synonymized, in the Western North Atlantic. *Deep-Sea Research,* Vol. 4, pp. 230–237. 1957.

No. 913. E-an Zen. Preliminary Report on the Mineralogy and Petrology of Some Marine Bottom Samples off the Coast of Peru and Chile. *Amer. Mineralogist,* Vol. 42, pp. 889–903. 1957.

No. 914. James M. Moulton. Sound Production in the Spiny Lobster *Panulirus argus* (Latreille). *Biol. Bull.,* Vol. 113, No. 2, pp. 286–295. 1957.

No. 915. Joanne S. Malkus. On the Structure and Maintenance of the Mature Hurricane Eye. *Jour. Meteorol.,* Vol. 15, No. 4, pp. 337-349. 1958.

No. 916. G. G. Whitney, Jr. Factors Affecting the Accuracy of Thermometric Depth Determinations. *Jour. du Conseil,* Vol. 22, No. 2, pp. 167–173. 1957.

No. 917. Henry Stommel. A Survey of Ocean Current Theory. *Deep-Sea Research,* Vol. 4, pp. 149–184. 1957.

No. 918. Dean F. Bumpus. Oceanographic Observations 1956, East Coast of the United States. *U. S. Fish and Wildlife Service, Spec. Sci. Rept. — Fisheries,* No. 233, 132 pp. 1957. (Not included in *Collected Reprints*).

No. 919. John M. Zeigler, W. D. Athearn and H. Small. Profiles across the Peru-Chile Trench. *Deep-Sea Research,* Vol. 4, pp. 238–249. 1957.

No. 920. A. H. Woodcock. The Release of Latent Heat in Tropical Storms due to the Fall-Out of Sea-Salt Particles. *Tellus,* Vol. 10, No. 3, pp. 355-371. 1958.

No. 921. P. F. Scholander. Oxygen Dissociation Curves in Fish Blood. *Acta Physiol. Scand.,* Vol. 41, No. 4, pp. 340–344. 1957.

No. 922. Robert H. Gibbs, Jr. Preliminary Analysis of the Distribution of White Marlin, *Makaira albida* (Poey), in the Gulf of Mexico. *Bull. Mar. Sci., Gulf and Caribbean,* Vol 7, No. 4, pp. 360–369. 1957.

No. 923. Alfred C. Redfield. The Inadequacy of Experiment in Marine Biology. In: Perspectives in Marine Biology, Symposium held at Scripps Inst. of Oceanogr., Univ. Cal., March 24-April 2, 1956, pp. 17–23. Univ. California Press. 1958.

No. 924. Mary A. Plunkett. The Qualitative Determination of Some Organic Compounds in Marine Sediments. *Deep-Sea Research,* Vol. 4, pp. 259-262. 1957.

No. 926. Dean F. Bumpus, Joseph Chase, C. Godfrey Day, David H. Frantz, Jr., David D. Ketchum and Robert G. Walden. A new Technique for Studying Non-Tidal Drift with Results of Experiments off Gay Head, Mass., and in the Bay of Fundy. *Jour. Fish Bd., Canada,* Vol. 14, No. 6, pp. 931–944. 1957.

No. 927. Malcolm S. Gordon. Osmotic and Ionic Regulation in Scottish Brown Trout and Sea Trout (*Salmo trutta L.*). *Jour. Exper. Biol.*, Vol. 36, No. 2, pp. 253–260. 1959.

No. 928. H. Barnes and Margaret Barnes. The Rate of Development of *Balanus balanoides* (L.) Larvae. *Limnol. and Oceanogr.*, Vol. 3, No. 1, pp. 29–32. 1958.

No. 929. Theodore R. Folsom and Allyn C. Vine. On the Tagging of Water Masses for the Study of Physical Processes in the Oceans. In: The Effects of Atomic Radiation on Oceanography and Fisheries. *Nat. Acad. Sci.-Nat. Res. Council, Publ.* No. 551, Chap. 12, pp. 121–132. 1957.

No. 930. William S. von Arx. "Dister": A Displacement Sequence Stereoscope. *Jour. Meteorol*, Vol. 15, No. 2, pp. 230–231. 1958.

No. 931. William S. von Arx. Synoptic Photography. *Weather, Roy. Meteorol. Soc.*, London, pp. 179–197. 1958.

No. 932. Henry B. Bigelow and William C. Schroeder. Four New Rajids from the Gulf of Mexico. *Bull. Mus. Comp. Zool.*, Vol. 119, No. 2, pp. 201–233. 1958.

No. 933. G. Veronis. On the Transient Response of a β-plane Ocean. *Jour. Oceanogr. Soc., Japan*, Vol. 14, No. 1, pp. 1–5. 1958.

No. 934. William S. Richardson and Charles H. Wilkins. An Airborne Radiation Thermometer. *Deep-Sea Research*, Vol. 5, pp. 62–71. 1958.

No. 935. Joyce C. Lewin, R. A. Lewin and D. E. Philpott. Observations on *Phaeodactylum tricornutum*. *Jour. Gen. Microbiology*, Vol. 18, No. 2, pp. 420–426. 1958.

No 936. Joyce C. Lewin. The Taxonomic Position of *Phaeodactylum tricornutum*. *Jour. Gen. Microbiology*, Vol. 18, No. 2, pp. 427–432. 1958.

No. 937. H. Barnes. Temperature and the Life Cycle of *Balanus balanoides* (L.). In: Marine Boring and Fouling Organisms, pp. 234–245. Univ. Washington Press, Seattle. 1959. (Reprints not available for *Collected Reprints*, 1959).

No. 938. Harry J. Turner. The Effect of Nutrition on the Color of the Callus of *Polinices duplicatus*. *The Nautilus*, Vol. 72, No. 1, pp. 1–3. 1958.

No. 939. Henry Stommel, A. B. Arons and A. J. Faller. Some Examples of Stationary Planetary Flow Patterns in Bounded Basins. *Tellus*, Vol. 10, No. 2, pp. 179–187. 1958.

No. 940. Howard L. Sanders. Benthic Studies in Buzzards Bay. I. Animal-Sediment Relationships. *Limnol. and Oceanogr.* Vol. 3, No. 3, pp. 245–258. 1958.

No. 941. Dean F. Bumpus and C. Godfrey Day. Drift Bottle Records for the Gulf of Maine and Georges Bank, 1931–56. *U. S. Fish and Wildlife Service, Spec. Sci. Rept. — Fisheries*, No. 242, 61 pp. 1957.

No. 942. Frank J. Mather, III and Robert H. Gibbs, Jr. Distribution of the Atlantic Bigeye Tuna, *Thunnus obesus*, in the western North Atlantic and the Caribbean Sea. *Copeia*, 1958, No. 3, pp. 237–239. 1958.

No. 943. W. V. R. Malkus and G. Veronis. Finite Amplitude Cellular Convection. *Jour. Fluid Mech.*, Vol. 4, Pt. 3, pp. 225–260. 1958.

No. 944. J. B. Hersey and M. S. Rutstein. Reconnaissance Survey of Oriente Deep (Caribbean Sea) with a Precision Echo Sounder. *Bull. Geol. Soc. Amer.*, Vol. 69, pp. 1297–1304. 1958.

No. 945. Alan J. Faller. An Optical Method for the Measurement of Surface Waves in the Laboratory. *Trans. Amer. Geophys. Union*, Vol. 39, No. 4, pp. 716–720. 1958.

No. 946. Bostwick H. Ketchum, John H. Ryther, Charles S. Yentsch and Nathaniel Corwin. Productivity in Relation to Nutrients. *Rapp. et Proc.-Verb., Cons. Perm. Internat. Explor. de la Mer*, Vol. 144, pp. 132–140. 1958.

No. 947. William C. Schroeder. The Lobster, *Homarus americanus*, and the Red Crab, *Geryon quinquedens*, in the Offshore Waters of the Western North Atlantic. *Deep-Sea Research*, Vol. 5, pp. 266–282. 1959.

No. 948. Susan I. Scholander and Joan T. Kanwisher. Latitudinal Effect on Respiration in Some Northern Plants. *Plant Physiol.*, Vol. 34, No. 5, pp. 574–576. 1958. (Not included in *Collected Reprints*).

No. 949. H. Barnes and Margaret Barnes. Further Observations on Self-Fertilization in *Chthamalus* sp. *Ecology*, Vol. 39, No. 3, p. 550. 1958.

No. 950. H. Barnes and Margaret Barnes. A Comparison of the Annual Growth Patterns of *Balanus balanoides* (L.) with Particular Reference to the Effect of Food and Temperature. *Oikos*, Vol. 10, No. 1, pp. 1–18. 1959.

No. 951. Takashi Ichiye. A Theory of Vertical Structure of Density in the Ocean. *Jour. Oceanogr. Soc., Japan*, Vol. 14, No. 2, pp. 35–40. 1958.

No. 952. Takashi Ichiye. Tsunami Waves—What are known about them—How we have studied them. *The Port Engineer*, Calcutta, India, Vol. 7, No. 1, pp. 5–19 [1–14]. 1958.

No. 953. Henry Stommel. Letter to the Editors: The Abyssal Circulation. *Deep-Sea Research*, Vol. 5, pp. 80–82. 1958.

No. 954. Bernhard Haurwitz, Henry Stommel and Walter H. Munk. On the Thermal Unrest in the Ocean. In: The Atmosphere and the Sea in Motion (The Rossby Memorial Volume), pp. 74-94. Rockefeller Institute Press, New York. 1959.

No. 955. G. C. McLeod. Delayed Light Action Spectra of several Algae in Visible and Ultraviolet Light. *Jour. Gen. Physiol.*, Vol. 42, No. 2, pp. 243–250. 1958.

No. 956. John M. Zeigler, Carlyle R. Hayes and Sherwood D. Tuttle. Beach Changes during Storms on Outer Cape Cod, Massachusetts. *Jour. Geology*, Vol. 67, No. 3, pp. 318–336. 1959.

No. 957. James M. Moulton. The Acoustical Behavior of some Fishes in the Bimini Area. *Biol. Bull.*, Vol. 114, No. 3, pp. 357–374. 1958.

No. 958. Robert L. Miller and John M. Zeigler. A Model Relating Dynamics and Sediment Pattern in Equilibrium in the Region of Shoaling Waves, Breaker Zone, and Foreshore. *Jour. Geology*, Vol. 66, No. 4, pp. 417-441. 1958.

No. 959. Floyd M. Soule and R. M. Morse. Physical Oceanography of the Grand Banks Region and the Labrador Sea in 1957. *U. S. Coast Guard Bull.*, No. 43, pp. 81–131. 1958.

No. 960. James M. Moulton. A Summer Silence of Sea Robins, *Prionotus* spp. *Copeia* 1958, No. 3, pp. 234–235. 1958.

No. 961. Robert H. Gibbs, Jr., and Bruce B. Collette. On the Identification, Distribution, and Biology of the Dolphins, *Coryphaena hippurus*, and *C. equiselis*. *Bull. Mar. Sci. Gulf and Carib.*, Vol. 9, No. 2, pp. 117–152. 1959.

No. 962. E-an Zen. Clay Mineral—Carbonate Relations in Sedimentary Rocks. *Amer. Jour. Sci.*, Vol. 257, pp. 29–43. 1959.

No. 963. Takashi Ichiye. The response of a Stratified Bounded Ocean to Variable Wind Stresses. *Oceanogr. Mag.*, Tokyo, Japan, Vol. 10, No. 1, pp. 19–63. 1958.

No. 964. Theodore J. Smayda. The Seasonal Incoming Radiation in Norwegian and Arctic Waters, and Indirect Methods of Measurement. *Jour. du Conseil*, Vol. 24, No. 2, pp. 215–220. 1959.

No. 965. Theodore J. Smayda. Biogeographical Studies of Marine Phytoplankton. *Oikos*, Vol. 9, No. 2, pp. 158–191. 1958.

No. 967. Joanne S. Malkus and Georg Witt. The Evolution of a Convective Element: A Numerical Calculation. In: The Atmosphere and the Sea in Motion (The Rossby Memorial Volume), pp. 425–439. Rockefeller Institute Press, New York. 1958.

No. 968. Bostwick H. Ketchum and Vaughan T. Bowen. Biological factors determining the distribution of radio-isotopes in the sea. *Proc. 2nd Internat. Conference on the Peaceful Uses of Atomic Energy*, Geneva, Sept. 1–15, 1958, Vol. 18, pp. 429–433. 1958.

No. 969. Joanne Starr Malkus. On the Structure of the Trade Wind Moist Layer. *Papers in Physical Oceanography and Meteorology*, Vol. 13, No. 2, pp. 1–47. 1958. (Not included in *Collected Reprints*).

No. 970. Vaughan T. Bowen amd T. T. Sugihara. Marine Geochemical Studies with Fall-out Radioisotopes. *Proc. 2nd Internat. Conference on the Peaceful Uses of Atomic Engery*, Geneva, Sept. 1–15, 1958, Vol. 18, pp. 434–438. 1958.

No. 971. Francis L. Parker and William D. Athearn. Ecology of Marsh Foraminifera in Poponesset Bay, Massachusetts. *Journ. Paleont.*, Vol. 33, No. 2, pp. 333– 343. 1959.

No. 972. Charles S. Yentsch and Ralph F. Vaccaro. Phytoplankton Nitrogen in the Oceans. *Limnol. and Oceanogr.*, Vol. 3. No. 4, pp. 443–448. 1958.

No. 973. J. B. Hersey, Elizabeth T. Bunce, R. F. Wyrick, and F. T. Dietz. Geophysical Investigation of the Continental Margin between Cape Henry, Virginia, and Jacksonville, Florida. *Bull. Geol. Soc. Amer.*, Vol. 70, pp. 437–466. 1959.

No. 974. Melvin E. Stern. The Moving Flame Experiment. *Tellus*, Vol. 11, No. 2, pp. 175–179. 1959.

No. 975. Jack McLachlan and Guy C. McLeod. The Use of Conversion Factors for the Determination of the Concentration of Nutrients in Culture Media. *Limnol. and Oceanogr.*, Vol. 4, No. 2, pp. 218–219. 1959.

No. 976. Alfred C. Redfield. The Biological Control of Chemical Factors in the Environment. *Amer. Scientist*, Vol. 46, No. 3, pp. 205–222. 1958.

No. 977. C. Godfrey Day. Surface Circulation in the Gulf of Maine Deduced from Drift Bottles. *Fish. Bull.* 141, *U. S. Fish and Wildlife Service, Fish. Bull.*, Vol. 58, pp. 443–472. 1958.

No. 978. John H. Ryther, Charles S. Yentsch and Ralph F. Vaccaro. The Dynamics of a Diatom Bloom. *Biol. Bull.*, Vol. 115, No. 2, pp. 257–268. 1958.

No. 979. A. T. Spencer and D. C. Blanchard. A Portable Raindrop Recorder for semi-Continuous Determination of Size Distributions. *Trans. Amer. Geophys. Union.* Vol. 39, No. 5, pp. 853–857. 1958.

No. 980. G. D. Nicholls, Herbert Curl, Jr., and V. T. Bowen. Spectrographic Analyses of Marine Plankton. *Limnol. and Oceanogr.*, Vol. 4, No. 4, pp. 472–478. 1959.

No. 981. Takashi Ichiye. On Convective Circulation and Density Distribution in a Zonally Uniform Ocean. *Oceanogr. Mag.*, Tokyo, Japan, Vol. 10, No. 1, pp. 97–135. 1958.

No. 982. T. T. Sugihara, H. I. James, E. J. Troianello and V. T. Bowen. Radiochemical Separation of Fission Products from Large Volumes of Sea Water. Strontium, Cesium, Cerium, and Promethium. *Analyt. Chem.*, Vol. 31, No. 1, pp. 44–49. 1959.

No. 983. P. F. Scholander. Counter Current Exchange: A Principle in Biology. *Hvalrådets Skrifter*, No. 44, 24 pp. Oslo. 1958.

No. 984. Charles S. Yentsch and John H. Ryther. Relative Significance of the Net Phytoplankton and Nanoplankton in the Waters of Vineyard Sound. *Jour. du Conseil*, Vol. 24, No. 2, pp. 231–238. 1959.

No. 985. G. Veronis. Cellular Convection with Finite Amplitude in a Rotating Fluid. *Jour. Fluid Mech.*, Vol. 5, Pt. 3, pp. 401-435. 1959.

No. 986. Godfrey C. Day. Oceanographic Observations, 1957, East Coast of the United States. *U. S. Fish and Wildlife Service, Spec. Sci. Rept. — Fisheries*, No. 282, 123 pp. 1959. (Not included in *Collected Reprints*).

No. 987. Alan J. Faller and William S. von Arx. The Modeling of Fluid Flow on a Planetary Scale. *Proceedings of the Seventh Hydraulics Conference*, Iowa Institute of Hydraulic Research, pp. 53–72. 1959.

No. 988. John M. Zeigler. Origin of the Sea Islands of the Southeastern United States. *Geogr. Rev.*, Vol. 49, No. 2., pp. 221–237. 1959.

No. 989. Malcolm S. Gordon. Ionic Regulation in the Brown Trout (*Salmo trutta L.*). *Jour. Exper. Biol.*, Vol. 36, No. 2, pp. 227–252. 1959.

No. 992. Elizabeth Schroeder, Henry Stommel, David Menzel and William Sutcliffe, Jr. Climatic Stability of Eighteen Degree Water at Bermuda. *Jour. Geophys. Res.*, Vol. 64, No. 3, pp. 363-366. 1959.

No. 993. Jack McLachlan. The Growth of Unicellular Algae in Artificial and Enriched Sea Water Media. *Canad. Jour. Microbiol.*, Vol. 5, pp. 9–15. 1959.

No. 994. Gilbert L. Voss. The Cephalopods Collected by the R/V Atlantis during the West Indian Cruise of 1954. *Bull. Mar. Sci., Gulf and Caribbean*, Vol. 8, No. 4, pp. 369–389. 1958.

No. 995. John C. Ayers. The Hydrography of Barnstable Harbor, Massachusetts. *Limnol. and Oceanogr.*, Vol. 4, No. 4, pp. 448–462. 1959.

No. 996. Edward R. Baylor. The Responses of Snails of Polarized Light. *Jour. Exper. Biol.*, Vol. 36, No. 2, pp. 369–376. 1959.

No. 997. Guy C. McLeod and Jack McLachlan. The Sensitivity of Several Algae to Ultraviolet Radiation of 2537 Å. *Physiol. Plant.*, Vol. 12, pp. 306–309. 1959.

No. 998. H. Barnes. Regarding the Southern Limits of *Balanus balanoides* (L.). *Oikos*, Vol. 9, No. 2, pp. 139–157. 1958.

No. 999. C. B. Officer, J. I. Ewing, J. F. Hennion, D. G. Harkrider and D. E. Miller. Geophysical Investigations in the Eastern Caribbean: Summary of 1955 and 1956 Cruises. In: Physics and Chemistry of the Earth, Vol. 3, pp. 17-109. Pergamon Press Ltd., New York. 1959.

No. 1001. L. R. Breslau and H. E. Edgerton. The Luminescence Camera. *Jour. Biol. Photogr. Assoc.*, Vol. 26, No. 2, pp. 49–58, 1958.

No. [illegible] Harry J. Turner, Jr. and James E. Hanks. Infestation of *Pecten irradians* by *Polydora*. The Nautilus, Vol. [illegible], No. 4, pp. [illegible]. [illegible].

No. [illegible] Allan R. Robinson and Henry Stommel. The Oceanic Thermocline and the Associated Thermohaline Circulation. *Tellus*, Vol. 11, No. 3, pp. 295–308. 1959.

No. [illegible] Allan Robinson and Henry Stommel. Amplification of Transient Response of the Ocean to Storms by the Effect of Bottom Topography. *Deep-Sea Research*, Vol. 5, pp. 312–314. 1959.

No. [illegible] Bert Bolin. On the Use of Tritium as a Tracer for Water in Nature. *Proc. 2nd Internat. Conference on the Peaceful Uses of Atomic Energy*, Geneva, Sept. 1–13, 1958, Vol. 18, pp. 336–343. 1958. (In *Collected Reprints* for 1958).

No. [illegible] [illegible]. [illegible] Tropical Storm [illegible]. *Bull. Mar. Sci. Gulf and Caribbean*, Vol. 9, No. 1, pp. [illegible]. 1959.

No. [illegible] Jack McLachlan and Charles S. Yentsch. Observations on the Growth of *Dunaliella euchlora* in Culture. *Biol. Bull.*, Vol. 116, No. 3, pp. 461–471. 1959.

No. [illegible] John W. Graham. Metabolically Induced Precipitation of Trace Elements from Sea Water. *Science*, Vol. 129, No. [illegible], pp. [illegible]. 1959.

No. [illegible] Joseph Levine. Spherical Vortex Theory of Bubble-Like Motion in Cumulus Clouds. *Jour. Meteorol.*, Vol. 16, No. 6, pp. 653–662. 1959.

No. [illegible] John Kanwisher. Histology and Metabolism of Frozen Intertidal Animals. *Biol. Bull.*, Vol. 116, No. 2, pp. [illegible]. 1959.

No. [illegible] John Kanwisher. Polarographic Oxygen Electrode. *Limnol. and Oceanogr.*, Vol. 4, No. 2, pp. [illegible]. 1959.

No. [illegible] L. V. Worthington. The 18° Water in the Sargasso Sea. *Deep-Sea Research*, Vol. 5, pp. [illegible]. 1959.

No. [illegible] John H. Ryther. Potential Productivity of the Sea. *Science*, Vol. 130, No. [illegible], pp. [illegible]. 1959.

No. [illegible] John W. Graham and Susan C. Cooper. Biological Origin of Manganese-rich Deposits of the Sea Floor. *Nature*, Vol. 183, pp. [illegible]. 1959.

No. [illegible] George L. Clarke and Charles J. Hubbard. Quantitative Records of the Luminescent Flashing of Oceanic Animals at Great Depths. *Limnol. and Oceanogr.*, Vol. 4, No. 2, pp. [illegible]. 1959.

No. [illegible] [illegible]. A Note on the Transient Stage of the Random Dispersal of Logistic Populations. *Bull. Math. Biophysics*, Vol. 21, pp. [illegible]. 1959.

No. [illegible] W. V. R. Malkus. Magnetoconvection in a Viscous Fluid of Infinite Electrical Conductivity. *Astrophys. Jour.*, Vol. 130, No. 1, pp. 259–275. 1959.

No. [illegible] [illegible] and Earl E. Hays. Transmissometer Velocimeter for Measuring the Speed of Sound in the Sea. *Jour. Acoust. Soc. Amer.*, Vol. 31, No. 7, pp. [illegible]. 1959.

No. [illegible] [illegible]. [illegible] Studies of the Barnstable Marsh, Cape Cod, Massachusetts. [illegible], Vol. [illegible], No. [illegible], pp. [illegible]. [illegible]. (Published posthumously).

No. [illegible] Bert Bolin and Erik Eriksson. Changes in the Carbon Dioxide Content of the Atmosphere and Sea due to Fossil Fuel Combustion. In: *The Atmosphere and the Sea in Motion*. The Rossby Memorial Volume, pp. [illegible]. Rockefeller Institute Press, New York. 1959.

No. 1026. John H. Ryther and R. R. L. Guillard. Enrichment Experiments as a Means of Studying Nutrients Limiting to Phytoplankton Production. *Deep-Sea Research*, Vol. 6, pp. 65–69. 1959.

No. 1027. Charles S. Yentsch and John H. Ryther. Absorption Curves of Acetone Extracts of Deep Water Particulate Matter. *Deep-Sea Research*, Vol. 6, pp. 72–74. 1959.

No. 1028. W. A. Mordy. Computations of the Growth by Condensation of a Population of Cloud Droplets. *Tellus*, Vol. 11, No. 1, pp. 16–44. 1959.

No. 1029. Irving I. Schell. On a Criterion of Representativeness of Sea Surface Temperature Date. *Bull. Amer. Meteorol. Soc.*, Vol. 40, No. 11, pp. 571–574. 1959.

No. 1030. J. S. Hart and Laurence Irving. The Energetics of Harbor Seals in Air and in Water with Special Consideration of Seasonal Changes. *Canad. Jour. Zool.*, Vol. 37, pp. 447–457. 1959.

No. 1032. Joseph Chase. Wind-Induced Changes in the Water Column along the East Coast of the United States. *Jour. Geophys. Res.*, Vol. 64, No. 8, pp. 1013–1022. 1959.

No. 1036. E-an Zen. Mineralogy and Petrography of Marine Bottom Sediment Samples Off the Coast of Peru and Chile. *Jour. Sed. Petrol.*, Vol. 29, No. 4, pp. 513–539. 1959.

No. 1037. H. Barnes and Margaret Barnes. Note on Stimulation of Cirripede Nauplii. *Oikos*, Vol. 10, No. 1, pp. 19–23. 1959.

No. 1038. John T. Conover. Seasonal Growth of Benthic Marine Plants as Related to Environmental Factors in an Estuary. *Publ., Inst. Mar. Sci.*, Univ. Texas, Vol. 5, pp. 97–147. 1959.

No. 1039. John H. Ryther. Light Adaptation by Marine Phytoplankton. *Limnol. and Oceanogr.*, Vol. 4, No. 4, pp. 492–497. 1959.

No. 1041. A. C. Redfield. Biological Considerations — The Fourth Phase Conference on Physical and Chemical Properties of Sea Water, Easton, Maryland, Sept. 4–5, 1958. *Nat. Acad. Sci. — Nat. Res. Council, Publ.* 600, pp. 101–112. 1959. (Not included in *Collected Reprints*).

No. 1043. George L. Clarke and Lloyd R. Breslau. Measurements of Bioluminescence off Monaco and Northern Corsica. *Bull. Inst. Océanogr. Monaco*, No. 1147, pp. 1–31. 1959.

No. 1047. David A. McGill, Nathaniel Corwin and Bostwick H. Ketchum. The Temperature Correction of Oceanic Inorganic Phosphorus Analyses. *Deep-Sea Research*, Vol. 6, pp. 60–64. 1959.

No. 1048. Godfrey C. Day. Oceanographic Observations, 1958, East Coast of the United States. *U. S. Fish and Wildlife Service, Spec. Sci. Rept. — Fisheries*, No. 318, 119 pp. 1959. (Not included in *Collected Reprints*).

No. 1060. Karl E. Schleicher. A Note on the Constancy of the T/S Relationship in a Water Mass. Die Expeditionen von F. F. S. "Anton Dohrn" und V. F. S. "Gauss" im Internationalen Geophysikalischen Jahr 1957/1958. *Deutsche Hydrogr. Zeitschr.*, Ergänzungsheft, Reihe B (4°), No. 3, pp. 46–48. 1959.

No. 1061. Wolfgang Wieser and John Kanwisher. Respiration and Anaerobic Survival in some Sea Weed — Inhabiting Invertebrates. *Biol. Bull.*, Vol. 117, No. 3, pp. 594–600. 1959.

No. 1075. H. Barnes and Margaret Barnes. The Effect of Temperature on the Oxygen Uptake and Rate of Development of the Egg-Masses of Two Common Cirripedes, *Balanus balanoides* (L.) and *Pollicipes polymerus* J. B. Sowerby. *Kieler Meeresforschung*, Bd. 15, pp. 242–251. 1959. (Reprints not available for *Collected Reprints*, 1959).

No. 1124. Robert L. Miller and John M. Zeigler. A Study of the Relation between Dynamics and Sediment Pattern in the Zone of Shoaling Wave, Breaker, and Foreshore. *Ecologae Geol. Helv.*, Vol. 51, No. 3, pp. 542–551. 1958. (Not included in *Collected Reprints*).